Tokyo Medical and Dental University
Global Center of Excellence (GCOE) Program
International Research Center for Molecular Science in Tooth and Bone Diseases

東京医科歯科大学　グローバルCOEプログラム

歯と骨の分子疾患科学国際教育研究拠点

平成23年度 実績報告書

東京医科歯科大学

ご挨拶

グローバルCOEプログラムは、我が国の文部科学省による大学院教育の高度化の為の競争的資金であり、優れた大学院を世界のトップ拠点としてさらに発展させることを目標とするもので、大学院教育研究の一層の充実を図り、世界最高水準の研究基盤の元での世界をリードする総合的な人材育成を図るために、国際的に卓越した研究拠点の形成を支援するシステムとして設定されています。特にその重点は国際的競争力のある大学づくりの推進です。「歯と骨の分子疾患科学の国際教育研究拠点-デント・メドミクスのインテリジェンスハブ-」をタイトルとする本拠点は、平成20年度の医学の領域で採択され、平成22年度の中間評価においても、医学領域の14件のグローバルCOE拠点中のトップランクの2拠点の1つとして評価を受け、平成23年度においても、これを反映する支援を受けてグローバルCOE活動が展開されました。

“歯と骨の分子疾患科学の国際教育研究拠点”を課題とする本GCOEプログラムにおいては、英語の発表と討論に基づく客観的な評価によって選抜した若手研究者や、選抜した大学院生を重点的に教育するプログラムを実行し、平成20年度から平成23年度までに発展的な成果を挙げつつあります。このプログラムは、歯と骨の領域における新時代の大学院教育システムとして、特に博士課程大学院生に対する経済的支援を行うと共に、若手研究者が自立した環境で活躍出来る機会を設定しており、国際PIシャペロンやAISS（アドバンスト・I・スーパースチューデント）としての若手研究者が、その能力を十分に発揮できる環境整備を行い、国際的に活躍する若手を育成しています。本プログラムについては、国際競争力を強化する為に、審査・評価体制として外国人レフリーによる審査が採用され、歯と骨の領域の国際的な研究者による世界的な競争力を重視する観点に基づく英文資料を用いた審査が実施されています。さらに、本プログラムにおいては、平成20年度より平成23年度まで毎年の歯と骨の領域の世界的なリーダーであるトップの研究者のsite visitによる国際アドバイザリーと外部評価を行い、これによる国際的な視点からも高い評価が与えられています。

将来的には、歯と骨の歯学・医学において学術の急速な発展による専門家・細分化に対応する深い専門性を持つと共に、一方で新たな学問分野として急速な科学技術のイノベーションに対応できるフレキシビリティーの高い、幅広い応用力を持つ人材の養成を目標として更なる活動が続けられています。本、歯と骨の教育研究拠点は既に、世界的に活躍する多数の若手を輩出し、欧米の一流研究室での研究者や欧米の若手とトップレベルで競合する人材、さらにはアジアの指導者となって活躍しており、国際的な人材育成を推進しています。

歯学・医学においては、国際性を涵養し、大学院教育・研究を活性化することがより強く求められています。歯と骨のグローバルCOE研究拠点は、これまでの教育研究実績を更に高め、新たな国際性の高い実力のある若手研究者の育成と将来性の高い大学院生を育てることをその目標に掲げ、その実現がなされています。大学全体としての取り組みの一環として、歯と骨の伝統ある本学の先輩方の業績に基づき、新しい領域を開拓しつつ、未来の国際的指導者を育成する場としてのグローバルCOEの今後の展開が望まれており、平成23年度においてもその目標に向い、学長はじめ理事の先生方のリーダーシップの下に、事業推進担当者の先生方の不断のご尽力により、報告書に示されております本拠点の活動が達成されました。今度とも、皆様の一層のご支援をお願い申し上げます。

野田　政樹
Masaki Noda

東京医科歯科大学

平成23年度

グローバルCOEプログラム実績報告書

歯と骨の分子疾患科学の国際教育研究拠点

専攻等名

医歯学総合研究科器官システム制御学系専攻・口腔機能再構築学系専攻・生体支持組織学系専攻
顎顔面頸部機能再建学系専攻・先端医療開発学系専攻・生体環境応答学系専攻・疾病生命科学研究部
生体材料工学研究所・難治疾患研究所

野田　政樹 Masaki Noda
拠点リーダー／医歯学総合研究科・器官システム制御学系専攻・教授
分子薬理学／医学博士・歯学博士

拠点形成統括および先端硬組織分子再建科学の研究

田上　順次 Junji Tagami
医歯学総合研究科・口腔機能再構築学系専攻・教授
齲蝕制御学／歯学博士

先端硬組織分子再建科学

高柳　広 Hiroshi Takayanagi
医歯学総合研究科・生体支持組織学系専攻・教授
分子情報伝達学／医学博士

硬組織分子喪失病態学

森田　育男 Ikuo Morita
医歯学総合研究科・顎顔面頸部機能再建学系専攻・教授
分子細胞機能学／薬学博士

先端硬組織分子再建科学

小村　健 Ken Omura
医歯学総合研究科・口腔機能再構築学系専攻・教授
顎口腔外科学／医学博士

硬組織疾患ゲノム科学

春日井　昇平 Shohei Kasugai
医歯学総合研究科・口腔機能再構築学系専攻・教授
インプラント・口腔再生医学／歯学博士

先端硬組織分子再建科学

須田　英明 Hideaki Suda
医歯学総合研究科・口腔機能再構築学系専攻・教授
歯髄生物学／歯学博士

先端硬組織分子再建科学

和泉　雄一 Yuichi　Izumi
医歯学総合研究科・生体支持組織学系専攻・教授
歯周病学／歯学博士

硬組織分子喪失病態学

柳下　正樹 Masaki Yanagisita
医歯学総合研究科・生体支持組織学系専攻・教授
硬組織病態生化学／医学士

先端硬組織分子再建科学

山口　朗 Akira Yamaguchi
医歯学総合研究科・口腔機能再構築学系専攻・教授
口腔病理学／医学博士

先端硬組織分子再建科学

森山　啓司 Keiji Moriyama
医歯学総合研究科・顎顔面頚部機能再構築学系専攻・教授
顎顔面矯正学／医学博士

硬組織分子喪失病態学

大川　淳 Atsushi Okawa
医歯学総合研究科　先端医療開発学系専攻・教授
整形外科学／医学博士

先端硬組織分子再建科学

宮坂　信之 Nobuyuki Miyasaka
医歯学総合研究科・生体環境応答学系専攻・教授
膠原病・リウマチ内科学／医学博士

硬組織分子喪失病態学

宗田　大 Takeshi Muneta
医歯学総合研究科・生体支持組織学系専攻・教授
運動器外科学／医学博士

先端硬組織分子再建科学

稲澤　譲治 Johji Inazawa
難治疾患研究所・教授
分子細胞遺伝学／医学博士

硬組織疾患ゲノム科学

三木　義男 Yoshio Miki
難治疾患研究所・教授
分子遺伝／医学博士

硬組織疾患ゲノム科学

石野　史敏 Fumitoshi Ishino
難治疾患研究所・教授
エピジェネティクス／理学博士

硬組織疾患ゲノム科学

澁谷　浩司 Hiroshi Shibuya
医歯学総合研究科・器官システム制御学系専攻・教授
分子細胞生物学／理学博士

硬組織基礎生命科学

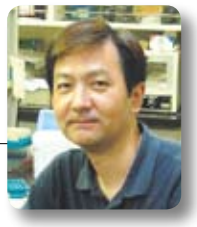

小川　佳宏 Yoshihiro Ogawa
医歯学総合研究科・器官システム制御学系専攻・教授
分子代謝医学／医学博士

硬組織基礎生命科学

水島　昇 Noboru　Mizushima
医歯学総合研究科・器官システム制御学系専攻・教授
細胞生理学／医学博士

硬組織分子喪失病態学

中川 一路 Ichiro　Nakagawa
医歯学総合研究科・口腔機能再構築学系専攻・教授
細菌感染制御学／歯学博士

硬組織分子喪失病態学

四宮　謙一 Kenichi Shinomiya
医歯学総合研究科・先端医療開発学系専攻・非常勤講師
脊椎・脊髄神経外科学／医学博士、横浜市立みなと赤十字病院・院長

先端硬組織分子再建科学

秋吉　一成 Kazunari Akiyoshi
生体材料工学研究所・素材研究部門・非常勤講師
有機材料学／工学博士、京都大学 大学院工学研究科高分子化学・教授

先端硬組織分子再建科学

萩原　正敏 Masatoshi Hagiwara
疾患生命科学研究部・高次生命制御研究部門・非常勤講師
形質発現制御学／医学博士、京都大学 大学院医学研究科形態形成機構学・教授

硬組織基礎生命科学

国際PIシャペロン、AISS・QAISS

Takuya Notomi, Ph.D.

（納富拓也）
Research Assistant Professor
Department of Molecular Pharmacology

Alireza Sadr, D.D.S., Ph.D.

Research Assistant Professor
Department of Cariology and Operative Dentistry

Masatsugu Oh-hora, M.D., Ph.D.

（大洞将嗣）
Research Associate Professor
Department ofCell Signaling

Iimura Tadahiro, D.D.S., Ph.D.

（飯村忠浩）
Research Associate Professor
Department of Oral Pathology

Naoto Haruyama, D.D.S., Ph.D.

（春山　直人）
Research Associate Professor
Department of Maxillofacial Orthognathics

Hideyuki Iwai, M.D., Ph.D.

（岩井秀之）
Research Assistant Professor
Department of Medicine & Rheumatology

Kunikazu Tsuji, M.D., Ph.D.

（辻邦和）
Research Assistant Professor
Department of Orthopedic Surgery

Lee Jiyoung, Ph.D.

（李知英）
Research Assistant Professor
Department of Epigenetics

Naoki Sawada, M.D., Ph.D.

（澤田直樹）
Research Assistant Professor
Department of Molecular Medicine and Metabolism

Patricia Makishi

Dept. of Cariology and Operative Dentistry
「レジンセメントと象牙質界面における
ナノリーケージについて」

許　ジン
（Xu Jing）
歯髄生物学
視床下部性神経ペプチドによる
中枢性骨代謝制御機構の解明
Uncovering the molecular mechanism of central control of bone remodeling by hypothalamic neuropeptides

Reena Rodriguez

Dept. of Oral Impltantology & Regenerative Dental Medicine
「Epigallocatechin-3-gallate 含有Gelatin Hydrogelを
用いた骨再生に関する研究」

則武　加奈子

Kanako Noritake
Dept. of Oral Impltantology & Regenerative Dental Medicine
「スーパーGBR膜「ハイドロゲルシート」の開発」

郝　佳
（Hao Jia）
インプラント・口腔再生医学　hydeoxyapatiteコーティングインプラント埋入時にZoledronic Acidを局所投与した際の骨形成に与える影響と細菌接着について
Bacterial adhesion and bone formation effect of Zoledronic Acid immobilized hydroxyaptite implants

Paksinee Kamolratanakul

Dept. of Molecular Pharmacology
「ナノゲルscaffoldを用いたEP4アゴニストとBMPの
骨再生能に関する研究」

中川　朋美

Tomomi Nakagawa
Dept. of Molecular Pharmacology
「悪性黒色腫の骨の転移における転写因子Cizの
役割の解明」

鈴木　尋之

Hiroyuki suzuki
Dept. of Maxillofacial Orthognathics
「可溶型fibroblast growth factor receptor2（FGFR2）の
頭蓋冠縫合部早期癒合症に対する治療効果」

Erik Idrus

Dept. of Cell Signaling
「RANKL刺激によるNFATc1制御遺伝子と
microRNAの同定」

Gamaralalage Amodini Rajakaruna

Dept. of Periodontology
「歯周病とバージャー病の関連の解明」

藤田　浩二

Koji Fujita
Dept. of Orthopaedic and Spinal Surgery
「Vitamin Eの骨代謝に対する影響について」

木原　翼

Tasuku Kihara
Oral pathology
骨芽細胞分化と骨再生におけるCCN3の役割
The role of CCN3 in osteoblast differentiation and bone regeneration

古田　繭子

Mayuko Furuta
分子細胞遺伝学（Molecular Cytogenetics）
新たなRNA創薬に寄与する癌制御性microRNAの機能的スクリーニング
Exploration of novel tumor-suppresive microRNAs using functional genomics-assisted approach

安藤　彰子

Akiko Ando
バイオイメージングを用いた歯周組織幹細胞の同定
Identification of periodontal stem cells by bio-imaging approaches

Bharti Pariksha
歯周病学
歯周治療が全身の炎症に与える影響
Effect of Periodontal Treatment on systemic inflammation.

辻　香織

Kaori Tsuji
顎顔面矯正学
Zinc finger 型転写因子POKEMONの破骨細胞における役割の解明
Investigation of the role of zinc finger transcription factor, POKEMON in osteoclasts

許　レン
XU Ren
整形外科（Orthopaedic and Spinal Surgery）
視床下部性神経ペプチドによる中枢性骨代謝制御機構の解明
Uncovering the molecular mechanism of central control of bone remodeling by hypothalamic neuropeptides

周　夢宇

Zhou Mengyu
歯髄生物学（Pulp Biology and Endodontics）
歯根形成のメカニズム-SCAP（根尖部幹細胞）からの象牙芽細胞およびセメント芽細胞分化に関与する因子の解明
The mechanisms of root formation- Elucidation of the signaling molecules on odontoblast and cementoblast differentiation from SCAP

Smriti Aryal A. C

分子薬理学（Molecular Pharmacology）
細胞骨格による骨代謝制御の分子機構 -Nckの骨の細胞機能調節に於ける役割の解明-
Molecular Mechanisms Underlying Cytoskeletal Regulation of Bone Metabolim-Role of Nck Proteins in Bone Cell Function-

Chokechanachaisakul Uraiwan

歯髄生物学（Pulp Biology and Endodontics）
ラットを用いた歯髄生物学
Rat's pulp biology

Kunawarote Sitthikorn

う蝕制御学
う蝕象牙質に対する接着性能の改良
Improve Bond strength to Caries-affected dentin

Ilnaz Hariri

う蝕制御学
高度に石灰化した接着界面構造の作成と機械的性質の評価
Generation of hyper mineralized adhesive Interface and study on its mechanical properties

AL-BARI MD. ABDUL ALIM

分子情報伝達学（Cell Signaling）
破骨細胞分化を制御するphosphatidylinositol-3,4,5-trisphosphate結合タンパク質の同定と機能解析
Identification and analysis of phosphatidylinositol-3,4,5-trisphosphatebinding proteins（PIP_3BPs）that regulate osteoclast differentiation

古市　祥子

Akiko Furuichi
インプラント・口腔再生医学
酸素ナノバブル水の骨組織における生体活性評価
Evaluation for the biologically activity of oxygen nano bubbles solution（OXNB）

Hamid Nurrohman

う蝕制御学（Cariology and Operative Dentistry）
人口口腔装置を用いたバイオフィルムによるう蝕形成後の”Super Dentin”のナノ構造解析
The effect of collagenolytic inhibitors on the quality of acid-base resistant zone in dentin

Chui Chanthoeun

歯周病学（Periodontology）
歯周組織の除菌のための新しい治療様式の開発:LEDと光感受性色素を用いた抗菌的光線力学療法の効果に関する基礎的研究
Development of a New Treatment Modality for Periodontal Disinfection: Basic Study on the Effect of Antimicrobial Photodynamic Therapy using the Combination of an LED
light Source and a Photosensitizing Dye

Samir Kumar Pal

口腔病理学（Oral Pathology）
口腔扁平上皮癌による骨破壊におけるThrombospondin-1の役割
The Role of Thrombospondin-1（TSP-1）in Bone Destruction by Oral Squamous Cell Carcinoma

Hoi　Chin　Hew

遺伝子応用医学
新規プロラインキナーゼC（PKC）アポトーシス標的分子Evi-1の同定
Identification of Evi － 1 as a novel PKC Apoptosis Regulatory Target

村松　智輝

Tomoki Muramatsu
分子細胞遺伝学（Molecular Cytogenetics）
食道扁平上皮癌の発生・進展におけるYAP増幅・発現亢進の分子病理学的意義
Significance of YAP amplification/overexpression in the pathogenesis of esophageal squamous cell carcinoma

鈴木　允文

Suzuki Takafumi
歯周病学
骨吸収を引き起こす咬合性外傷の分子機構について解析する-TRPV4の役割-
Molecular mechanism underlying occlusal trauma, induced-bone loss Role of TRPV4

宮嶋　大輔

Daisuke Miyajima
顎顔面外科（分子薬理）
骨代謝における負のMCSFシグナルによる新制御機構の解析 -Dok　アダプター分子による破骨細胞制御と骨粗鬆症-
Novel Insights into Negative Molecular Regulation of MCSF Signaling in Bone Metabolism -Function of Dok Adaptor Molecules in Osteoclasts and Osteoporois -

Atukorallaya Devi Sewvandini Atukorala

硬組織構造生物学
咽頭鰓弓および咽頭鰓発生への外胚葉上皮の関わり
Tracing the fate of ectoderm during the pharyngeal arch development

Kandakar Abu Shameem Md. Saadat

分子発生学
RB/E2F経路の制御と骨肉腫形成過程におけるDRIL1の役割
The Role of DRIL1in the Regulation of RB/E2F Pathway and Tumorigesis of Osteosarcoma

関根　由莉奈

高次生命科学
ナノゲル　リポソーム複合体ハイブリッドゲルの設計と医療応用
Design and Application of Hydrid Hydrogels with Nanogel-coated Liposomes complex

馬　成山

(Ma Chengshan)
整形外科学
骨リモデリングにおける中枢神経制御の経路
A Novel Central-Control Pathway of Bone Remodeling

妻沼　有香

歯周病学
歯根膜細胞シートのインプラント両方への応用
Application of periodontal ligament cell sheet for implant therapy.

Bhargava Suhas Srilatha

インプラント・口腔再生医学
Y-TZPジルコニアの表面処理が骨芽細胞と線維芽細胞に及ぼす影響
Surface modified Y-TZP Zirconia: its effect on osteoblasts and fibroblasts in vitro

MD ABDULLA AL MASUD KHAN

硬組織薬理学
TNFαとRANKLアンタゴニストであるW9ペプチドの骨形成における役割
A Role of TNF- α and RANKL antagonist peptide W9 on osteogenesis

滝沢　文彦

発生発達病態学
マクロファージToll-like receptor 4シグナルにおける細胞内カルシウムおよびTransient Receptor potential Vanilloid 2の役割の解析
Role of intracellular calcium and Transient Receptor potential Vanilloid 2 in macrophage Toll-like receptor 4 signaling

白　樺

Bai Hua
Dept. of Moleclurar Cytogenetics
「ヒト癌におけるオートファジー関連遺伝子LC3Av1遺伝子の機能解析」

Bakhsh, Turki Abdulsalam A.

う蝕制御学
コンポジットレジン接着界面の長期的な挙動について、SS-OCTを用いた定量的評価
SS-OCT as a new tool for long term quantitative evaluation on the resin-dentin interface in a bonded restoration

Warunee Pluemsakunthai

インプラント・口腔再生医学
ウサギ頭蓋骨欠損モデルにおける改良PRF含有αTCPの骨再生における有用性の検討
The effect of platelet rich fibrin (PRF) preparation with Alpha-tricalcium phosphate (α -TCP) enhance bone regeneration in rabbit calvarium

森田　淳平

顎顔面矯正学
可溶型線維芽細胞成長因子受容体2を用いたアペール症候群の新規治療方法の開発 - アペール症候群表現型の救済 -
The development of novel treatment for Apert syndrome by a soluble form of FGFR2-Rescue of Apert phenotypes

Bijaya Baobam

細菌感染制御学
オートファジーおよび免疫応答におけるA群レンサ球菌認識機構の解析
Molecular analysis of recognition mechanisms of Group A Streptococcus in autophagic degradation system and immune responses

山田　梓

歯周病学
ヒト歯根膜幹細胞の骨芽細胞/セメント芽細胞分化を誘導する因子の探索
The search of factoers inducing osteoblastic/cementoblastic differentiation in human Periodontal Ligament Stem Cells

南原　弘美

歯周病学
歯周病原細菌によるWnt5a遺伝子発現機構の解析
The modulation of Wnt5a expression by periodontopathic bacteria

中根　綾子

小児歯科学
慨定量的in situ　蛍光イメージングによる骨細胞の慨日リズムの可視化と、成長発達過程におけるその機能解析
Quantitative in situ fluorescent imaging approach for functional dynamics of osteocytes through circadian oscillation during growth and development

Nurmaa Dashzeveg

バイオ情報学
骨肉腫におけるP53によって誘導されるアポトーシス関連遺伝子の解析
Discovery of pro-apoptotic genes induced by p5 3 in osteosarcoma

荻田　真弓

歯周病学
ヒト歯根膜細胞におけるレーザー照射およびサイトカイン刺激によるhuman-beta-defensin（HBDs）発現の探査
The expression of HBDs by laser irradiation, various cytokines and bacterial components in human PDL cells

山口　佑季

バイオ情報学
哺乳類の特徴的形質における哺乳類特異的遺伝子群の役割
The role of mammalian specific genes in mammalian characteristics

大上　えりか
顎顔面外科学
口腔扁平上皮癌が生産する破骨細胞性骨吸収制御因子の同定
Identification of osteoclastic bone resorption regulatory factors produced by oral squamous cell carcinoma

湯浅　将人
整形外科学
デキサメタゾン併用によるBone morphogenetic protein による骨形成に対する有効性の検討
The efficiency of bone formation by BMP with dexamethasone

宮部　斉重
膠原病・リウマチ内科学
関節リウマチ病態形成におけるLPA/LPA受容体、ATXの関与
Pathogenic roles of LPA/LPA receptors and ATX on the rheumatoid arthritis

山田　剛史
整形外科学
骨髄由来間葉系細胞（MSC）の質 - 骨形成抑制因子の同定 -
The significance of the quality of the human bone marrow mesenchymal cells（hBMMCs）in the bone formation

Rojbani Hisham Khalifa
インプラント・口腔再生医学
ブラッククミン（Nigella　Sativa）の骨再生における効果の検討
Effect of Nigella Sativa on Bone Formation

チェン康
（Chang Kang）
インプラント・口腔再生医学　歯科用インプラント周囲骨における直流電流装置を用いた骨形成促進作用に関する研究
A direct current device for accelerating bone formation in tissues surrounding a dental implant.

Osama Zakaria
インプラント・口腔再生医学
異なる表面性状を有する歯科用インプラント周囲骨における電気的刺激を用いた骨形成促進作用に関する研究
Electrical stimulation for accelerationing Peri-implant bone formation of different implant surfaces

岩崎　陽平
分子薬理学
骨に対するPTH作用におけるCB2の調節作用の解析 - 骨細胞集団および中枢神経系の骨量調節における連関の解明 -
Analysis of regulatory effect of CB2 to thePTH effect to Bone.- Relevance of Bone Cell Assembly（BCA）and Central Nervous System（CNS）in the maintenance of bone-

長谷川　久紀
膠原病・リウマチ内科学
関節リウマチ（RA）の新規治療標的となるmicroRNAの探究
Identification of microRNA as a new therapeutic target for rheumatoid arthritis.

福田　真
膠原病・リウマチ内科学
関節リウマチ病態形成におけるFROUNTの関与
Pathogenic roles of FROUNT on Rheumatoid Arthritis

佐藤　潔
顎口腔外科学
口腔扁平上皮癌の顎骨浸潤における癌関連線維芽細胞の役割
Roles of carcinoma-associated fibroblasts in bone invasion by oral squamous cell carcinoma

Marwa Madi
インプラント・口腔再生医学
インプラント周囲炎を誘発させた状態における、HA薄膜スパッタリングインプラントと、他の表面性状インプラントの比較
Experimental periimplantitis at HA sputtered coated implants in comparison to other surface treatments

渡辺　千穂
顎顔面矯正学
骨代謝におけるRNA stabitlityの機能解析
Functional analysis of RNA stability in bone metabolism

細矢　匡
膠原病・リウマチ内科学
TEAM1-TREM1-Ligand 相互作用修飾による自己免疫疾患の新規治療法の開発
Development of new treatment of autoimmune diseases by modifying interaction between TREM1 and TREM-Logand

徐　成
（Cheng Xu）
整形外科学
骨形成におけるmicroRNAの役割
Role of microRNA in bone formation

木村　直樹
膠原病・リウマチ内科学
腫瘍による筋炎発症のメカニズムの解析
Analysis of cancer-associated autoimmune myosis

Prasansuttiporn Taweesak
う蝕制御学
次亜塩素酸ナトリウム処置後象牙質に対するrosmarinic acidの接着強さ及び耐久性への影響
Effect of rosmarinic acid on bond strength and bond longevity to NaOCL-treated dentin.

Adorno Quevedo Carlos Gabriel
歯髄生物学
ラット歯髄の慢性炎症後にみられるリンパ管新生
Lymphangiogenesis in the rat dental pulp following induced chronic inflammation

安岡　潤一
高次生命科学
カチオン性ナノゲルによる新規核酸デリバリーシステム
Novel nucleic acid Delivery Systems by Cationic Nanogel

鈴木　晶子

膠原病・リウマチ内科学
マウス膠原病モデルの病態における体液調整因子の働きを明らかにする。
The role of circulating plasma volume regulation factors in murine arthritis and myositis model

土戸　優志

高次生命科学
新規ナノゲルによるタンパク質デリバリー
Protein Delivery by Novel Nanogel

宮原　宇将

インプラント・口腔再生医学
ナノゲルを用いた骨再生に関する研究
A research on bone regeneration by using Nanogel

Thitthaweerat Suppason
う蝕制御学
次亜塩素酸ナトリウムとロスマリン酸の失活歯への接着強さと長期接着耐久性に及ぼす影響
Influence of NaOCIand rosmarinic acid on bond strength and long-term bond durability in endodontically treated tooth

Md.Sofiqul Islam

う蝕制御学
フラボノイドによる、象牙質コラーゲン保護と脱灰象牙質の再石灰効果 - 新しい根面蝕歯 -
治療アプローチ
Flavonoid Reserves Dentin Collagen and Promotes human Root Dentin Lesion Re-mineralization in vitro

Gerardo Jose Joves Mendez

う蝕制御学
塩化カルシウム・フッ素含有ボンディングシステムを用いた歯質接着界面の強化
Reinforcement of adhesive interface using a CaCl2/fluoride-incorporated bonding system

芦垣　紀彦

歯周病学
歯周病原細菌が慢性腎不全を悪化させる病因の解析
Periodontal bacteria aggravate chronic renal failure by subtotal nephrectomy in mice

Paveenarat Aukkarasongsup
顎顔面矯正学
低酸素状態下のマウス歯根幕細胞におけるペリオスチン遺伝子発現制御メカニズムの解析：低酸素応答領域の同定とHIF－1経路関わり
Analysis of periostion gene expression in mouse periodontal ligament cells under hypoxia: identification of HRE and HIF-1 pathway

渡辺　高

顎顔面外科学
in situ蛍光イメージング解析による、骨の分化・再生におけるRunk2タンパク細胞内動態の新規調節機構の解析
Investigation of novel subcelular bynamics of Runx2 during bone differentiation and regeneration by in situ fluorescent imaging analysis

坂野　若詠
う蝕制御学
新規象牙質接着システムの開発及び評価について
Developing resin composite restoration with adhesive system

Rumana Khanom
口腔病理学
シグナル分子としてのケラチン17が癌の骨浸潤に果たす役割の解析
The functional role of leratin 17 as a signaling molecule in bone invasion of oral cancer

Duarte Puerto Carolina Lizeth
顎顔面矯正学
磁気制御されたRelaxin と　BMP-2ナノ粒子を用いた骨縫合の拡大
Sutural Expansion Assisted With Magnetically Controlled Site Specific Relaxin and BMP-2 Nanoparticles

于　淼
(Yu Miao)
インプラント・口腔再生医学
尾部懸垂マウスを用いた、骨再生におけるメカニカルストレスの関与に関する研究
The role of mechanical stress in bone regeneration using tail suspension mice

上園　将慶
顎顔面矯正学 低浸襲かつ早期に骨接合する新規矯正用デバイスの開発
Development of minimally invasive and rapidly osseointegratable orthodontic devices

Amir Nazari

う蝕制御学
う蝕脱灰象牙質を高度石灰化組織へと変化させるための再石灰化技術の創造
Developing a Dentin Remineralising Method（DRM）to Transform Carious Demineralised Dentin into Hypermineralised Substrate

Gombo Bolortuya

Dept. of Pulp Biology and Endodontics
「インテグリン発現を評価することによる象牙芽細胞の成熟とシグナル伝達に対する低出力レーザー療法の効果」

伊達　佑生

Yuki Date
Dept. of Oral Impltantology & Regenerative Dental Medicine
「歯根発生に関する因子の同定」

大城　暁子
健康推進歯学
FDC-SPの口腔内組織での機能
The roles of FDC-SP in oral tissues

Aslam Al Mehdi

Dept. of Periodontology
「歯周疾患は動脈疾患の進行に重要なリスクファクターとなる」

松本　力

Tsutomu Matsumoto
口腔病理学
矯正的歯の移動における骨細胞の役割
The role of osteocyte in orthodontic tooth movement

Wayakanon Praween

分子細胞機能学（Cellular Physiological Chemistry）
アニュラーギャップジャンクションの形成機構
The Mechanisms of Annular Gap Junction Formation

青井　陽子
Yoko Aoi
Dept. of Cellular Physiological Chemistry
「低酸素下におけるサイトカイン産生変動機序～メチル化の関与」

下田　麻子
Asako Shimoda
有機材料（Organic materials）
ナノゲル架橋ハイドロゲルによるタンパク質デリバリー
Design of Nanogel-assembled hydrogel for protein delivery

高橋　治子
Haruko Takahashi
有機材料（Organic materials）
Polysaccharide nano-ball を用いた新規ナノキャリアの開発
Design of Funtional Polysaccharide nano-ball as new nanocarrier

半場　秀典
う蝕制御学
Creating “acid resistant enamel” : de- /re-mineralization methods

馬　騰
分子発生学
Effect of p53 activating chemical compounds on p53 phosphorylation and p53-mediated apoptosis in osteosarcoma and oral squamous cell carcinoma

島田　泰如
顎口腔外科学
Molecular pathogenesis of Keratocystic Odontogenic Tumors

Zayar Lin
インプラント・口腔再生医学
Application of oral mucosal fibroblasts as a source of cell-mediated bone regeneration therapy

葉　暢暢
歯周病学
Periodontal disease and preterm low birth weight The cross reaction between antibodies of periodontal pathogens and β2GPI

Dawud Abduweli
硬組織構造生物学
Pharyngeal Dentition of Medaka: Tooth Replacement and Stem Cell Niche

白川　純平
顎口腔外科学
Stem Cell G0/G1 Control for Bone Formation by Molecular Link between Mechanical Stimulation and PTHR Signaling

Suphanantachat Supreda
歯周病学
Determination of gene expression profile during cementogenesis using next generation sequencing system

カハル　アブラ
運動器外科学
Roles of BMP-7 in joint homeostasis

小野　岳人
分子情報伝達学
Elucidating effects of inflammatory responses on bone system

顧　潔
歯髄生物学
Analysis of receptive mechanism and recognition in the CNS of pulpal sensation

瀧本　昇陽
歯髄生物学
Regulation of inflammation and induction of regeneration in the dental pulp by MMP-3

吉崎　正子
顎顔面矯正学
Investigation on inhibitory effects of soluble Apert FGFR2-nanogel complex on premature fusion of cranial sutures

Mandurah, Mona Mohammad M.
う蝕制御学
Study on evaluation of sclerotic dentin–resin interface using SS-OCT and nanoindentation

山下　優
インプラント・口腔再生医学
In Vivo Study in a Rat Calvarial Defect Model on the application of combined PRF Membrane with Novel GBR of Cholesterol-bearing Pullulan Nanogel Scaffold for increased bone regeneration

Lodha Ena
う蝕制御学
Enhancement of bleaching action and reminerralization using iontophoresis

Rajapakshe Mudiyanselage Anupama Rasadari Rajapakshe
硬組織病態生化学
Histological observation of the inflamed gingival tissue at the site of periodontitis.

Mohd Haidil Akmal Bin Mahdan
う蝕制御学
Effect of long term water strage and thermal cycling on bonding durability in crown and root canal dentin in vitro

Thanatvarakorn Ornnicha
う蝕制御学
Comparative Study on Effect of Long-term Artificial Saliva Immersion and Acid Challenge on the Dentin Permeability Reduction by Two Desensitizers

横山　和佳
膠原病・リウマチ内科学
Pathogenic Roles of CCL25/CCR9 on Rheumatoid Arthritis

松尾　祐介
膠原病・リウマチ内科学
Identification of the origin of pathogenic fibroblast-like synoviocytes in murine arthritis

中里　洋子
膠原病・リウマチ内科学
Analysis of cancer-associated autoimmune myositis

Maheswari Kuppusamy
インプラント・口腔再生医学
Periosteal elevation in rat calvarium using different Titanium mesh

東京医科歯科大学
歯と骨の分子疾患科学の国際教育研究拠点

グローバルCOEプログラム活動概要

1. 目的・必要性

東京医科歯科大学は“歯”と“骨”の疾患科学において世界的な拠点であること特徴とする。本拠点形成の目的は、世界で最も高年齢化の進行する我国にあって、人々が生きるために必須の“歯”と“骨”の分子疾患科学について、21世紀COEの成果を発展的に継承し、世界最先端の研究を展開して、合わせて次世代を担う国際的に活躍する若手研究者を養成する世界でも類のない国際教育研究拠点を形成することである。

2. 人材育成計画

(1) 国際PIシャペロン（PI-Chaperon（PIC））制度

国際PIシャペロン（PIC）制度とは、国際公募により選抜され、国際的に活躍する自立した研究者を目指す（Principal Investigator）、シャペロン型（大学院生を指導し共に研究する）のPostDoc終了後の（PDは採用しない）若手研究者育成制度である。さらに挑戦的な学際領域を開拓して（Prime Innovation）未来の領域を作り上げ、国際的に競争力のある創造性豊かなプロジェクトを遂行する（Project with Imagination）ことの3つのPIをキーワードとする若手研究者を育成するシステムである。英語のインタビューにより、全て外部より採用する。またGrant Writing等の指導ではGrant査読者やStudy Section担当者による教育を含め国際的視点でのトレーニングを行う。

(2) アドバンスト・I・スーパースチューデント（AI-SS）制度

アドバンスト・I・スーパースチューデントとは選抜され重点的な大学院教育と経済支援を受け、国際的に発展する力をつけるスーパースチューデント（SS）である。21世紀COEにおいては、本拠点は重点教育・経済支援の対象となるSS制度を創出し、優れた大学院生の教育、育成を達成した。本拠点においては、これを発展させ，(i) 国際的に活躍する（International），(ii) 国際的に大学院生同士で相互に切磋琢磨する（Interactive），(iii) 個性の輝く（Individual Identity）の“3つのI”をキーワードとする指導的人材の育成を目指す新制度を創設する。新たに、(1) 国際教育としての国際メンター制度、(2) 国際“Interactive”プログラムによる、一流の大学院であるUCSF、ハーバード大（米国）トロント大（カナダ）における大学院の教育（学生発表会）に参加し、海外拠点の大学院生との交流ならびに現地海外教員による教育を受け、(3) 個を伸ばす国際教育プログラムとして国際コンティニュエータープログラム（AISS-ICP）などを自ら選択しつつ教育を創造する。医歯学系大学院留学生数は全国一位だが更に海外の若手のリクルート、キャリアパスの担当部を其々設置して強化する。

3. 研究活動計画

拠点の研究においては、歯と骨の疾患領域における世界最高レベルの研究として硬組織の喪失と形成に関わる疾患のメカニズムならびにその診断・治療基盤研究を推進する。具体的研究目的は以下の3点である。即ち、【研究目的1】歯と骨の喪失に至る疾患の分子病態成立のメカニズムの解明、【研究目的2】歯と骨の先進的再建の為の治療法の基盤研究の推進、【研究目的3】歯と骨の疾患の統合的機能情報研究の推進である。これらの有機的融合により新たな歯と骨の疾患分子の統合研究（デントメドミクス）を創成する。この目的のために、歯学部、医学部、難治疾患研究所、生体材料工学研究所、研究部の五つの部局が横断的体制をとり、個々の先進研究をさらに発展させるとともにこれらを合わせた新領域のイノベーションを推進する。

4. 組織構成

学部・研究所を越えた横断的体制をとり、先進研究をさらに発展させる。

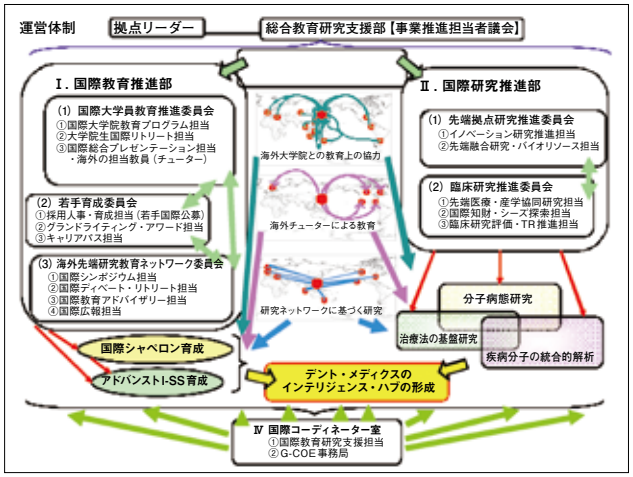

5. 中間評価結果（文部科学省発表2011年1月7日）

「グローバルCOEプログラム」（平成20年度採択拠点）中間評価について

http://www.mext.go.jp/a_menu/koutou/globalcoe/1301052.htm

グローバルCOEプログラム　平成20年度採択拠点中間評価結果一覧（総括評価内訳）

【医学系】

現行の努力を継続することによって、当初目的を達成することが可能と判断されるとされた12件に選ばれ、更にこの中で特に秀れた2件として評価された。

拠点番号	拠点プログラム名	機関名
F07	歯と骨の分子疾患科学の国際教育研究拠点	東京医科歯科大学

専攻等名	拠点リーダー名	連携先機関名（※）	特に優れている拠点12件中2件
医歯学総合研究科器官システム制御学系専攻	野田政樹		◎

グローバルCOE プログラム 平成20年度採択拠点中間評価【特に優れている拠点】概要

【医学系】

F07「歯と骨の分子疾患科学の国際教育研究拠点」
東京医科歯科大学医歯学総合研究科器官システム制御学系専攻

特に人材育成面において、国際PI シャペロン教員やアドバンスト・I・スーパースチューデントなどユニークなシステムが立ち上がり、世界の著名大学の教員をメンターに採用するなどメンター制度も効率的に活用され、若手研究者育成に大変優れた成果があがっている。

また、毎週1 回の国際総合プレゼンテーション、海外のトップ研究者を招く海外研究者講演会、国際シンポジウムの開催などが積極的、生産的になされるとともに、海外の先端的研究者による国際外部評価会など、拠点の活動に対する評価システムをうまく構築しており、教育にかなりの努力が払われている。

研究活動においても、世界トップレベルの業績が得られ、基礎的研究の実績のみならず、臨床研究活動も進展している。

運営面では、大学及び拠点リーダーの強いリーダーシップの下で精力的に拠点が運営され、国際化に向けた取組みも盛んで、歯科と医科の融合もうまくなされている。

6. 国際外部評価会

実施日

2012.1.26

歯と骨のGCOE国際外部評価会
International Advisory Review

EVALUATION FORM（7名回答）

【評価者】

Thomas John Martin
Emeritus Professor of Medicine, University of Melbourne, Australia
John Holt Fellow St. Vincent's Institute of Medical Research
Post Appointments

Henry Kronenberg
Director, Endocrine Division Massachusetts General Hospital, USA

Erwin F. Wagner
Vice-Director and Director of the BBVA Foundation – CNIO Cancer Cell Biology Programme, CNIO, Madrid, Spain

Gerard Karsenty
Member, College of CSR Reviewers, NIH
Professor and Chair, Department of Genetics and Development, College of Physicians and Surgeons, Columbia University Center, USA

Benjamin Alman
Interim Director, Toronto Musculoskeletal Centre (Extradepartmental Unit), Medicine,
Faculty of, University of Toronto, Toronto, Ontario, Canada

Naoyuki Takahashi
Director and Professor, Institute for Oral Science, Matsumoto

Dental University
Dean and Professor, Graduate School of Oral Medicine, Matsumoto Dental University, Nagano, Japan

Shigeaki Kato
Professor, Director, Research Center for Epigenetic Diseases Institute of Molecular and Cellular Biosciences The University of Tokyo

A . Overall Evaluation on the Global COE Program

1. Overall evaluation on the Global COE program activities

Excellent	Good	Fair	Poor	N/A
7				

2. Research

2-1. Evaluation on the researches in the Global COE program

Excellent	Good	Fair	Poor	N/A
7				

2-2. Collaboration within the Global COE program

Excellent	Good	Fair	Poor	N/A
5	2			

2-3. Clinical aspects of the Global COE program

Excellent	Good	Fair	Poor	N/A
6	1			

3. Education

3-1. Efforts to promote young scientists in the Global COE program

Excellent	Good	Fair	Poor	N/A
6	1			

3-2. International collaborative efforts

Excellent	Good	Fair	Poor	N/A
5	1			1

4. Management

4-1. Administrative structure of the Global COE program (Excellent, Good, Fair, Poor)

Excellent	Good	Fair	Poor	N/A
7				

4-2. Is the budget of the Global COE program spent efficiently?

Excellent	Good	Fair	Poor	N/A
5	1			1

5. Perspective

Will the GCOE program contribute to the future development of the bone and tooth field?

Excellent	Good	Fair	Poor	N/A
7				

7. 国際教育活動

歯と骨のGCOEの大学院生（AISS/QAISS）による海外活動リスト

2012年2月14日 University of Toronto　Research Day
参加者：Gamaralalage Amodini Rajakaruna, Takehito Ono

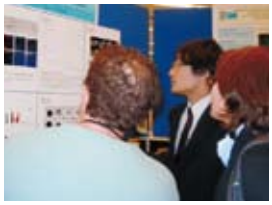

2012年2月15日　University of Torontoでの大学院生・Takehito Ono（AISS）によるレクチャー

2011年10月13日　UCSF Research Day
参加者：Azusa Yamada, Khandakar Abu Shameem Md.Saadat

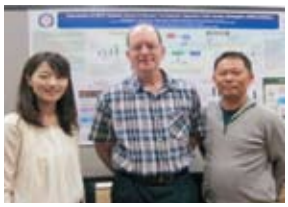

2011年10月14日　UCSF　Research Dayでの大学院生・Azusa Yamada（QAISS）によるレクチャー

2011年4月13日　Harvard Dental School Research Day
参加者：Daisuke Miyajima, Smriti Aryal AC, MD ABDULLAAL MASUD KHAN

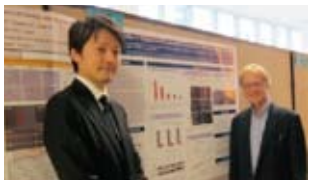

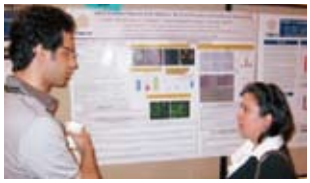

2011年4月13日　Harvard Dental School Research Day での大学院生・MD ABDULLAAL MASUD KHAN（AISS）によるレクチャー

2011年8月31日　Dr. Mark I. Ryderとのディスカッション

2011年8月11日　Dr. David E. Birkとの個別ディスカッション

2012年1月23日　Dr. T. John Martinとのラボミーティング

2012年1月23日
Dr. Gerard Karsenty

2012年1月23日　Dr. Henry Kronenberg

2012年1月23日　Dr. Benjamin Alman

2012年1月26日　大学院生の研究発表

8. 総合プレゼンテーション

参加者　教授60名を含む1,536名参加　学生評価　Excellent ＆ Good率　平均　94%（全22回分）［アンケート数1,045件］

ポスター	プレゼンテーションタイトル	日　付
	第96回「変形性関節症関連遺伝子の機能解析」	2012年3月5日
	第95回「新規関節炎治療薬の開発-新規メカニズムの解明を含めて」	2012年2月20日
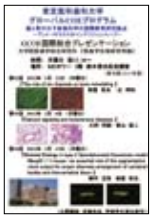	第94回『２型脊椎肋骨異骨症モデルマウスの骨格形成における病因論 - 分節時計の出力は椎体と椎間の正しい交互配置に必須である - 』	2012年2月13日
	第93回『カルシウムシグナルと自己免疫疾患』	2012年2月6日
	第92回『イオンチャンネルと骨代謝機構』	2012年1月12日
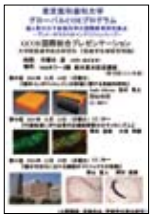	第91回『歯の石灰化における細胞外マトリックスの役割』	2011年12月19日
	第90回『代謝疾患に伴う血管内皮機能障害の分子メカニズム』	2011年11月21日
	第89回『歯科コンポジットレジンの評価に関する革新的研究』	2011年11月14日
	第88回「生殖幹細胞の樹立と卵子形成の試験官内再構築」	2011年11月7日
	第87回「比較ゲノム解析に基づくレンサ球菌属の外来性遺伝子獲得と進化機構の解析」	2011年10月24日
	第86回「オートファジーによる細胞内分解の役割と制御機構」	2011年10月17日
	第85回「常在細菌の管理による疾患予防の新しい取り組み」	2011年9月26日
	第84回「WntシグナルにおけるIQGAP1の役割」	2011年9月12日
	第83回「半月板再生モデルからみた半月板機能の維持の重要性」	2011年9月5日
	第82回「IL-6阻害療法が教えてくれたものとは?」	2011年6月20日
	第81回「力学的刺激と矯正学的歯の移動」	2011年6月6日

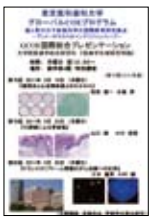	第80回「トランスクリプトーム情報のがん治療への応用」	2011年5月30日
	第79回「口腔癌による骨破壊」	2011年5月23日
	第78回「歯周炎と心血管疾患とのかかわり」	2011年5月16日
	第77回「骨の造成に何が必要か?」	2011年5月9日
	第76回「下顎再建の現況」	2011年4月18日
	第75回「破骨細胞分化制御と骨免疫学」	2011年4月11日

平成23年度　総合プレゼンテーション　出席者・アンケート集計

平成23年度	H23/4/11～H24/3/5	参加者						The quality of content						The method of the presentations was						Overall evaluation of your attitude (effort,motivation and commitment)					
		教授	シャペロン・コーディネーター	学生日本人	学生外国人	一般	合計	Excellent (%)	Good (%)	Excellent & Good (%)	回収枚数	Excellent	Good	Excellent (%)	Good (%)	Excellent & Good (%)	回収枚数	Excellent	Good	Excellent (%)	Good (%)	Excellent & Good (%)	回収枚数	Excellent	Good
1	第75回	4	7	26	23	10	70	84%	16%	100%	44	37	7	84%	14%	98%	44	37	6	77%	20%	98%	44	34	9
2	第76回	4	5	22	26	8	65	60%	30%	91%	43	26	13	65%	26%	91%	43	28	11	65%	23%	88%	43	28	10
3	第77回	2	6	29	37	12	86	83%	14%	97%	63	52	9	84%	13%	97%	63	53	8	81%	14%	95%	63	51	9
4	第78回	4	5	23	35	9	76	75%	24%	98%	55	41	13	64%	31%	95%	55	35	17	69%	25%	95%	55	38	14
5	第79回	3	6	21	39	7	76	89%	11%	100%	56	50	6	88%	11%	98%	56	49	6	84%	13%	96%	56	47	7
6	第80回	4	8	23	38	14	87	72%	24%	97%	58	42	14	71%	24%	95%	58	41	14	71%	22%	93%	58	41	13
7	第81回	5	5	22	40	7	79	85%	13%	98%	53	45	7	79%	17%	96%	53	42	9	77%	21%	98%	53	41	11
8	第82回	5	3	25	36	12	81	89%	11%	100%	55	49	6	89%	11%	100%	55	49	6	84%	15%	98%	55	46	8
9	第83回	4	6	21	37	12	80	87%	12%	98%	52	45	6	85%	13%	98%	52	44	7	81%	17%	98%	52	42	9
10	第84回	3	6	20	32	8	69	76%	19%	94%	54	41	10	72%	20%	93%	54	39	11	74%	19%	93%	54	40	10
11	第85回	2	3	14	31	12	62	64%	32%	95%	44	28	14	48%	43%	91%	44	21	19	55%	39%	93%	44	24	17
12	第86回	3	3	18	18	15	57	97%	3%	100%	31	30	1	94%	3%	97%	31	29	1	90%	10%	100%	31	28	3
13	第87回	3	6	23	31	5	68	62%	30%	92%	50	31	15	52%	34%	86%	50	26	17	48%	36%	84%	50	24	18
14	第88回	2	7	24	32	3	68	62%	30%	92%	50	31	15	60%	28%	88%	50	30	14	58%	32%	90%	50	29	16
15	第89回	2	6	24	32	11	75	78%	18%	96%	49	38	9	73%	22%	96%	49	36	11	71%	20%	92%	49	35	10
16	第90回	2	6	23	29	8	68	84%	14%	98%	44	37	6	82%	16%	98%	44	36	7	80%	16%	95%	44	35	7
17	第91回	2	9	29	29	6	75	69%	29%	98%	45	31	13	69%	27%	96%	45	31	12	62%	33%	96%	45	28	15
18	第92回	1	4	16	23	6	50	74%	20%	94%	35	26	7	69%	23%	91%	35	24	8	63%	29%	91%	35	22	10
19	第93回	2	6	18	33	2	61	80%	20%	100%	44	35	9	82%	18%	100%	44	36	8	80%	18%	98%	44	35	8
20	第94回	1	5	13	29	6	54	88%	13%	100%	32	28	4	91%	9%	100%	32	29	3	91%	9%	100%	32	29	3
21	第95回	1	4	17	32	3	57	81%	21%	102%	43	35	9	63%	35%	98%	43	27	15	67%	33%	100%	43	29	14
22	第96回	1	5	19	31	16	72	67%	27%	93%	45	30	12	64%	20%	84%	45	29	9	62%	24%	87%	45	28	11
	合計	60名	121名	470名	693名	192名	1536名																		

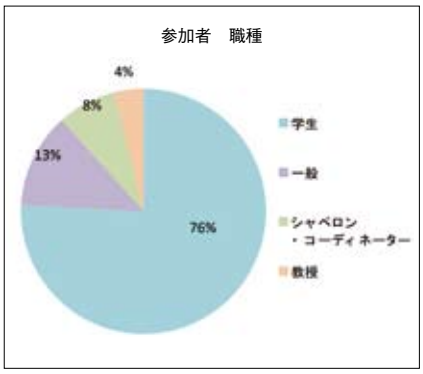

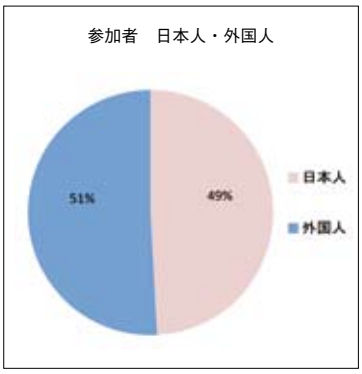

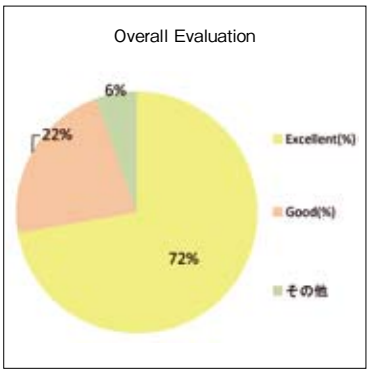

平均 (Overall evaluation)

Excellent (%)	Good (%)	その他
72%	22%	6%

開催回数　22回

アンケート回収枚数　1,045枚

出席者数　教授60名を含む1,536名

学生評価　Excellent ＆ Good率　平均　94%

9. 国際シンポジウム

ポスター	タイトル	講演者	日　付
	第6回グローバルCOE国際シンポジウム “ Molecular Control of Bone Remodeling 骨リモデリングの分子機構 ”	T. John Martin、Gerard Karsenty Henry Kronenberg Erwin Wagner、Benjamin Alman 加藤　茂明、高橋　直之 今泉　和則、田中　栄 妻木　範行、竹田　秀 西村　栄美、浅原　弘嗣　　他	2012年 1月23日～25日

大山学長と国際シンポジウム講演者（2012年1月23日）

Dr. Martin

Dr. Karsenty

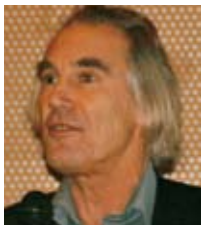
Dr. Wagner

Dr. Kronenberg

Dr. Alman

Dr. Takahashi

Dr. Imaizumi

Dr. Tanaka

Dr. Tsumaki

Dr. Kato

Dr. Martin

Ephrin-B2 and Ephb4 signaling in bone remodeling

Thomas John Martin, M.D.
St Vincent's Institute of Medical Research, Melbourne, Australia

The ephrin/Eph receptor tyrosine kinases are critical for many tissue-remodeling processes including cellular migration, angiogenesis and axon guidance. Through direct cell contact, ephrin ligands bind to multiple Eph receptors, resulting in either forward or reverse signaling. Osteoclast differentiation in vitro has been shown to be inhibited by ephrin-B2 reverse signaling (1). In studies of differentiating osteoblasts in vitro we have shown that blockade of ephrin-B2 / EphB4 signaling inhibits late stages of osteoblast differentiation in vitro, but in contrast, enhances the production of RANKL (2, 3). Furthermore, treatment with parathyroid hormone (PTH) was found to rapidly enhance ephrin-B2 expression by osteoblasts in vitro and in bone in vivo . For these reasons the present work addresses the role of ephrin-B2 / EphB4 signaling within the osteoblast lineage

In order to study the role of ephrin-B2 / EphB4 signaling in PTH anabolic action, we treated mice for 1 month with daily PTH, with and without soluble EphB4 (sEphB4) as an ephrin-B2/EphB4 receptor blocker. Treatment with sEphB4, with or without PTH, increased formation of osteoblasts that produce less osteoid and mineralized bone. This impairment of osteoblast differentiation is consistent with in vitro effects of ephrinB2 / blockade, and with the phenotype that we find in osteoblast – specific ephrin-B2 knockout mice. Most strikingly though, treatment of mice with sEphB4 and PTH together resulted in conversion of the PTH anabolic effect to a resorptive response, with bone loss due to increased osteoclast numbers and surface in bone. In confirmation of this, sEphB4 in co-cultures of calvarial osteoblasts with marrow or spleen cells in vitro enhanced osteoclast formation in response to PTH or to other stimuli, including 1,25 - dihydroxyvitamin D. Co-treatment of calvarial osteoblasts with sEphB4 and either PTH or 1,25 - dihydroxyvitamin D also substantially enhanced production of RANKL mRNA by mouse calvarial osteoblasts. The enhancing effect of receptor blockade on osteoclast formation might result either from increased RANKL production resulting from receptor blockade, or from sEphB4 preventing the ephrin-B2 reverse signaling in precursors that has been shown to limit osteoclast differentiation (1).

The findings indicate that, as in several other tissues, ephrin/Eph signaling is likely to play important roles in bone remodeling, through actions both within the osteoblast lineage to enhance late stages of osteoblast differentiation, and by communicating to the hemopoietic lineage to restrict osteoclast formation. The increased resorption resulting from ephrin-B2 / EphB4 receptor blockade needs assessment in view of the interest in EphB4 signaling as a target for anti-cancer treatment.

1. Zhao C et al. Bidirectional ephrinB2-EphB4 signaling controls bone homeostasis. Cell Metab. 4:111-121 (2006).
2. Allan EH et al. EphrinB2 regulation by PTH and PTHrP revealed by molecular profiling in differentiating osteoblasts. J Bone Miner Res. 23:1170-1181 (2008).
3. Martin TJ et al. Communication Between EphrinB2 and EphB4 Within the Osteoblast Lineage. Adv Exp Med Biol. 658:51-60 (2010).

1

Dr. Karsenty

miR-34s regulate proliferation and osteoblast differentiation in the mouse

Jianwen Wei, and Gerard Karsenty, M.D., Ph.D.
Department of Genetics & Development,
College of Physicians and Surgeons, Columbia University,
New York, NY 10032, USA

A screen to identify microRNA's preferentially expressed in osteoblasts and which affect their proliferation and/or differentiation, identified members of the miR-34 family as regulators of these processes. In vivo, osteoblast-specific gain- and loss-of-function experiments revealed that miR-34s affect skeletogenesis during embryonic development, and bone mass accrual after birth through two complementary cellular and molecular mechanisms. First, they inhibit osteoblast proliferation by suppressing Cyclin D1, CDK4, and CDK6 accumulation. Second, they inhibit terminal differentiation of osteoblasts,through mechanism that will be presented at the meeting. These results identify a specific family of microRNA involved in bone formation in vivo, and a specific genetic pathway by which these miRNAs regulate osteoblast differentiation.

13

Dr. Wagner

Functions of FOS/AP-1 proteins in bone development and beyond

Erwin F. Wagner, Ph.D.
BBVA Foundation-CNIO Cancer Cell Biology Program,
Spanish National Cancer Centre (CNIO), Melchor Fernandez Almagro,
3, E-28029 Madrid, Spain

We have been defining the specific functions of various Fos proteins, e.g. c-Fos, Fra-1 and Fra-2 in bone development and disease using gain-of-function and loss-of-function experiments in mice. Recent experiments also employ inducible bone-specific expression and loss-of-expression of Fos/AP-1 members employing a Tet-regulated switchable expression system.

The role of c-Fos as a differentiation-specific transcription factor for osteoclasts, the bone resorbing cells, is well established, whereas the functions of Fra-1 and Fra-2 are less well understood. It appears that Fra-1 mainly controls matrix gene expression, whereas Fra-2 was shown to be important for chondrocyte differentiation (1). Moreover, Fra-2 is essential for postnatal mouse development and the maintenance of bone mass. Mutant newborns are osteopenic and display giant osteoclasts (2). On the other hand, transgenic mice over-expressing Fra-2 have increased bone mass and pulmonary fibrosis (3). Mechanistically, Fra-2 controls osteoblast differentiation through direct regulation of osteocalcin and collagen 1a2 expression (4). Interestingly, mice expressing Fra-2 specifically in osteoblasts display beyond the bone phenotype also a metabolic disorder with increased osteocalcin and decreased adiponectin secretion. Recent unpublished data demonstrate that ectopic expression of Fra-2 in osteoblasts leads to an inflammatory phenotype with macrophage infiltrates in lung, liver and spleen. We are currently investigating the underlying molecular mechanisms of the metabolic phenotype and the role of inflammation in these novel mouse models.

(1) Wagner EF, Eferl R (2005) Fos/AP-1 proteins in bone and the immune system. Immunol Rev. 208, 126-40.
(2) Bozec A, Bakiri L, Hoebertz A, Eferl R, Schilling AF, Komnenovic V, Scheuch H, Priemel M, Stewart CL, Amling M, Wagner EF (2008) Nature 454, 221-225.
(3) Eferl R, Hasselblatt P, Rath M, Popper H, Zent R, Komnenovic V, Idarraga M-H, Kenner L, Wagner EF (2008) PNAS 105, 10525-10530.
(4) Bozec A , Bakiri L., Jimenez M., Schinke T., Amling M., Wagner EF (2010) J Cell Biol 190, 1093-1106.

77

Dr. Kronenberg

PTHrP regulates chondrocyte differentiation in the growth plate by modulating the activity of HDAC4

Henry Kronenberg, M.D., Ph.D.
Endocrine Unit, Massachusetts General Hospital and
Harvard Medical School, Boston, MA 02114, USA

Parathyroid hormone-related protein (PTHrP) regulates growth plate chondrocytes by activating the PTH/PTHrP receptor in chondrocytes; this activation leads to a delay in differentiation of proliferating chondrocytes to hypertrophic chondrocytes. These activities have been demonstrated through the use of a series of knockout and transgenic mice. But the molecular mechanism whereby PTHrP slows differentiation of chondrocytes has remained incompletely understood. Recently, Lassar's group (Kozhemyakina E et al, Mol. Cell. Biol. 29:5751 (09)) has demonstrated that, in cultured primary chondrocytes and in a chondrocyte cell line, PTHrP activates protein kinase A (PKA) and then PKA activates protein phosphatase (PPase) 2A. This PPase 2A then dephosphorylates histone deacetylase 4 (HDAC4), allowing movement of HDAC4 into the nucleus. HDAC4 then binds to and blocks the activity of MEF2c, the transcription factor crucial for driving chondrocyte hypertrophy.

We have now performed a series of experiments in vivo to determine whether HDAC4 mediates the actions of PTHrP in the fetal mouse growth plate. We first confirmed that HDAC4 knockout mice have a growth plate phenotype that resembles that of the PTHrP knockout mouse. In both the sternum (previously reported by Olson's group) and the long bones, the HDAC4 knockout mouse has accelerated chondrocyte hypertrophy that does resemble that of the PTHrP knockout, though it is somewhat milder. Like the PTHrP heterozygous knockout mouse, the HDAC4 heterozygous knockout mouse has no phenotype in the growth plates of the limb. We examined the phenotype of mice doubly heterozygous for both PTHrP and HDAC4. These mice demonstrated accelerated hypertrophy. Since each heterozygous mouse separately had no phenotype, this result argues that PTHrP and HDAC4 act on the same pathway to control chondrocyte hypertrophy.

We next examined a model of PTHrP overexpression in the growth plate. These mice, constructed by Weir and Broadus, use the collagen II promoter to drive overexpression of PTHrP in chondrocytes. These mice have only proliferating chondrocytes and no hypertrophic chondrocytes in their limb growth plates, and, consequently, no osteoblasts or marrow space. In this background we generated HDAC4 heterozygous and homozygous mice. Heterozygosity for HDAC4 in the setting of PTHrP overexpression led to the appearance of a small number of hypertrophic and prehypertrophic chondrocytes. Remarkably, homozygosity for HDAC4 in the presence of PTHrP overexpression led to fairly normal bone formation. The resultant tibia is WT in length and contains a growth plate with hypertrophic chondrocytes and associated adjacent intermembranous cortical and trabecular bone, along with a primary spongiosa. Nevertheless, if HDAC4 were the only mediator of PTHrP action, then the combination of PTHrP overexpression and HDAC4 knockout should have had a phenotype identical to that of the HDAC4 knockout. In fact, though, the proliferative and hypertrophic layers of the growth plate were larger than in the HDAC4 knockout and the amount of bone in the primary spongiosa was increased. These findings suggest that HDAC4 is not the sole mediator of the actions of PTHrP. We are currently exploring the possibility that other HDACs in the HDAC4 family may also mediate the actions of PTHrP. Nevertheless, these studies strongly suggest that the hypothesis of Lassar is relevant to the actions of PTHrP in vivo.

21

Dr. Alman

Beta-catenin in mesenchymal progenitors: from neoplasia to repair

Benjamin Alman, M.D.
Department of Surgery and Department of Lab Medicine and Pathobiology
University of Toronto Division of Orthopaedics and Program in
Developmental and Stem Cell Biology Hospital for Sick Children Toronto,
Ontario, Canada

Beta-catenin is a critical mediator in the canonical Wnt signaling cascade. When an appropriate Wnt ligand is present, the protein is stabilized, and binds to members of the Tcf transcription factor family, regulating gene expression in a cell type specific manner. We found that beta-catenin is mutated in the locally invasive mesenchymal soft tissue tumor aggressive fibromatosis (also called desmoid tumor), and generated a series of genetically modified mice in which we could study beta-catenin function in mesenchymal cells. During cutaneous wound repair, beta-catenin is transcriptionally active in mesenchymal dermal cells and regulates the number of mesenchymal cells that accumulate during the proliferative phase of wound repair and ultimately scar size. In wound repair, beta-catenin is regulated by interactions with extracellular matrix components, through an integrin-mediated process. Similar to the situation in wound repair, beta-catenin is also transcriptionally active during fracture repair. Beta-catenin levels need to be precisely regulated to allow the differentiation of undifferentiated mesenchymal cells to an osteochondral progenitor during fracture repair. Once the cells become osteochondral progenitors, beta-catenin enhances osteoblast formation. Beta-catenin stabilization maintains undifferentiated mesenchymal cells in a less differentiated state. During repair, it is transiently activated by either growth factors or by interactions with the immature extracellular matrix. In neoplasia, mutations cause constitutive activated, resulting in an uncontrolled proliferation of immature mesenchymal cells. Pharmacologic agents to modulate beta-catenin can be used to alter undifferentiated mesenchymal cell behavior and might be used to treat tumors and disorders of bone and skin repair. Initial pre-clincial studies provide evidence to support this notion.

Dr. Takahashi

Osteoclast precursors in vivo

Naoyuki Takahashi, Ph.D.
Division of Hard Tissue Research, Institute for Oral Science,
Matsumoto Dental University

Osteoclasts, bone-resorbing cells, develop from the monocyte/macrophage lineage under the control of osteoblast-lineage cells (osteoblasts). Osteoblasts express two cytokines essential for osteoclastogenesis: receptor activator of nuclear factor- κ B ligand (RANKL) and macrophage colony-stimulating factor (M-CSF). Osteoblasts also produce osteoprotegerin (OPG), a soluble decoy receptor for RANKL, which blocks osteoclastogenesis by inhibiting RANKL-RANK (RANKL receptor) interaction. Osteoclast precursors expressing RANK and M-CSF receptor (M-CSFR) differentiate into osteoclasts through interaction with osteoblasts. Although it is well established that osteoclasts are formed under the strict regulation of osteoblasts, little is known about characteristics of osteoclast precursors in vivo. We have examined characteristics and behaviors of osteoclast precursors in vivo for these five years.

(1) Distribution of osteoclast precursors determines the site of osteoclastogenesis.

Using RANKL$^{-/-}$ mice and M-CSF-deficient op/op mice, we examined how the site for osteoclastogenesis is determined. When RANKL was injected into RANKL$^{-/-}$ mice or M-CSF into op/op mice, osteoclasts were formed in the correct site in bone but not in soft tissues in those mutant mice. Osteoclasts induced by RANKL and M-CSF injection were always detected in the vicinity of osteoblasts. These results suggest that, besides RANKL and M-CSF, an unknown osteoblast-derived factor(s) is involved in the determination of the correct site for osteoclast formation (Endocrinology 147:3366, 2006). In the next experiment, we identified osteoclast precursors in vivo, and name them "cell cycle-arrested quiescent osteoclast precursors (QOPs)" (J Cell Biol 184:541, 2009). QOPs differentiate into osteoclasts without cell cycle progression in response to RANKL and M-CSF. QOPs localized in bone in RANKL$^{-/-}$ mice, suggesting that the distribution of QOPs determines the correct site for osteoclastogenesis. QOPs were fate-determined cells, and they were detected in blood as well as bone marrow (J Bone Miner Res, in press). Circulating QOPs settled down into the correct site in bone. Osteoblasts appear to be involved in homing of QOPs in bone, because QOPs were detected in near osteoblasts in bone.

(2) Spleen acts as a reservoir of QOPs in M-CSF deficient op/op mice.

Osteoclasts induced by M-CSF administration in op/op mice were derived from QOPs (J Cell Biol 184:541, 2009), suggesting that QOPs exist in op/op mice. Then we investigated where QOPs of op/op mouse would exist. We surprisingly found that QOPs existed in not bone but spleen in op/op mice, and spleen acts as their reservoir of osteoclast precursors in those mice. IL-34, a newly discovered M-CSFR ligand, was highly expressed in the vasculature in spleen but not bone in op/op mice, suggesting a role for IL-34 in the splenic generation of QOPs. Splenectomy blocked M-CSF-induced osteoclastogenesis in op/op mice. Osteoclasts appeared in aged op/op mice with up-regulated IL-34 expression in spleen and bone. Splenectomy also blocked the age-associated appearance of OCs. These results suggest that IL-34 plays pivotal roles in maintaining the splenic reservoir of QOPs, and M-CSFR signaling is necessary for generation of QOPs.

(3) Wnt5a-Ror2 signaling plays a role in up-regulation of RANK expression in QOPs.

The expression level of RANK by QOPs detected in spleen is much weaker than that detected in bone. This suggests that the expression of RANK in QOPs must be enhanced in bone. We recently found that osteoblasts up-regulated RANK expression in QOPs through Wnt noncanonical signaling. Wnt signals are divided into two pathways: β- catenin-dependent canonical and β- catenin-independent noncanonical pathways. Impairment of canonical Wnt signaling causes bone loss in arthritis and osteoporosis; however, it is unclear how noncan onical Wnt signaling regulates bone resorption. We showed that Wnt5a-Ror2 signaling between osteoblasts and osteoclast precursors enhanced osteoclastogenesis. Osteoblasts express Wnt5a, while osteoclast precursors express Ror2. Wnt5a$^{-/-}$, and Ror2$^{-/-}$ mice exhibited impaired osteoclastogenesis. Osteoclast precursor-specific Ror2$^{-/-}$ and osteoblast-specific Wnt5a$^{-/-}$ mice similarly exhibited impaired osteoclastogenesis. Wnt5a-Ror2 signals enhanced RANK expression in osteoclast precursors by activating JNK and recruiting c-Jun on the RANK promoter, thereby enhancing RANKL-induced osteoclastogenesis. Thus, Ror2-mediated up-regulation of RANK in QOPs occurs in bone, and this is an essential step for osteoclastogenesis.

I would like to describe how differentiation of osteoclast precursors is regulated in vivo in this symposium.

Dr. Imaizumi

The roles of unfolded protein response in differentiation of osteoblasts and chondrocytes

Kazunori Imaizumi, Ph.D.
Department of Biochemistry, Graduate School of Biomedical Sciences,
Hiroshima University

Eukaryotic cells can adapt to endoplasmic reticulum (ER) dysfunction by producing diverse signals from the ER to the cytosol or nucleus. These signalling pathways are collectively known as the unfolded protein response (UPR). The canonical branches of the UPR are mediated by three ER membrane-bound proteins: PERK, IRE1 and ATF6. These ER stress transducers basically play important roles in cell survival after ER stress. Recently, novel types of ER stress transducers that share a region of high sequence similarity with ATF6 have been identified, Luman, OASIS, BBF2H7, CREBH, and CREB4 (Asada et al., J. Biochem., 2011). Despite their structural similarities with ATF6, differences in activating stimuli, tissue distribution and response element binding indicate specialized functions of each member on regulating the UPR in specific organs and tissues. Among these, we identified OASIS and BBF2H7, and have investigated the functions of these ER stress sensors in osteogenesis and chondrogenesis.

【OASIS】

OASIS is a member of the CREB/ATF family and has a transmembrane domain and a bZIP (basic leucine zipper) domain. OASIS is processed by regulated intramembrane proteolysis (RIP) in response to ER stress, and is highly expressed in osteoblasts (Kondo et al., Nature Cell Biol., 2005). OASIS(-/-) mice exhibited severe osteopenia, involving a decrease in type I collagen in the bone matrix and a decline in the activity of osteoblasts, which showed abnormally expanded rough ER, containing of a large amount of bone matrix proteins (Murakami et al., Nature Cell Biol., 2009). We identified the gene for type 1 collagen, Col1a1, as a target of OASIS, and demonstrated that OASIS activates the transcription of Col1a1 through an unfolded protein response element (UPRE)-like sequence in the osteoblast-specific Col1a1 promoter region. Moreover, expression of OASIS in osteoblasts was induced by BMP2 (bone morphogenetic protein 2), the signalling of which is required for bone formation. Additionally, RIP of OASIS was accelerated by BMP2 signalling, which causes mild ER stress. Our studies show that OASIS is critical for bone formation through the transcription of Col1a1 and the secretion of bone matrix proteins, and they reveal a new mechanism by which ER stress-induced signalling mediates bone formation.

【BBF2H7】

BBF2H7 (BBF2 human homologue on chromosome 7) is also an ER-resident basic leucine zipper transcription factor, and is preferentially expressed in chondrocytes (Kondo et al., Mol. Cell. Biol., 2007). We generated BBF2H7 (-/-) mice to assess the in vivo function of BBF2H7. The mice showed severe chondrodysplasia and died by suffocation shortly after birth because of an immature chest cavity (Saito et al., Nature Cell Biol., 2009). The cartilage showed a lack of typical columnar structure in the proliferating zone and a decrease in the size of the hypertrophic zone, resulting in a significant reduction of extracellular matrix proteins. Interestingly, proliferating chondrocytes showed abnormally expanded rough ER, containing aggregated type II collagen (Col2) and cartilage oligomeric matrix protein (COMP). We identified Sec23a, which encodes a coat protein complex II component responsible for protein transport from the ER to the Golgi, as a target of BBF2H7. BBF2H7 N-terminus directly bound to a CRE-like sequence in the promoter region of Sec23a to activate its transcription. When Sec23a was introduced to BBF2H7 (-/-) chondrocytes, the impaired transport and secretion of cartilage matrix proteins was totally restored, indicating that by activating protein secretion the BBF2H7-Sec23a pathway has a crucial role in chondrogenesis. Our findings provide a new link by which ER stress is converted to signalling for the activation of ER-to-Golgi trafficking.

【Conclusion】

The UPR signalling was originally found as an evading system from cellular damage in acute ER perturbation. However, recent advances have revealed that UPR signalling provides important for regulating cellular physiology. During differentiation from mesenchymal stem cells to mature osteoblasts or chodrocytes, ER stress occurs in immature osteoblasts. The ER stress is very mild and does not cause cell death. Although the detailed mechanisms of why ER stress occurs during osteoblast differentiation remains unclear, it is possible that when the switch for production of bone or cartilage matrix is pressed at the stage of differentiation, nascent protein is delivered in amounts that exceed the capacity of the ER. Such an event may serve as a trigger for mild ER stress conditions (physiological ER stress). OASIS and BBF2H7 are activated by this physiological ER stress. The UPR signalling mediated by OASIS or BBF2H7, including promoting transcription of matrix proteins and activating secretory machinery, is essential for conversion of undifferentiated cells to professional secretory cells such as osteoblasts or chondrocytes.

Dr. Tanaka

Segregation of the pro-apoptotic and anti-resorptive functions of risedronate

Sakae Tanaka, M.D., Ph.D.
Department of Orthpaedic Surgery, Faculty of Medicine,
The University of Tokyo

Bisphosphonates (BPs), stable analogs of pyrophosphate, strongly inhibit bone resorption and have been used to treat various diseases driven by increased bone resorption, such as postmenopausal osteoporosis, Paget's disease and tumor bone metastases. Although BPs are poorly absorbed from the intestine, they are quickly deposited on the bone surface once absorbed. The acidic environment produced by osteoclasts (OCs) reduces the ability of BPs to chelate Ca2+ and releases BPs from the bone surface, and BPs are then ingested into OCs by endocytosis. It was speculated that BPs concentration reaches as high as 0.1-1 mM in the resorption lacuna.

BPs are divided into two groups according to the structure of the side chains, a nitrogen-containing type (N-BPs) and a non nitrogen-containing type. The difference in the structures results in different BP mechanisms of action for anti-resorbing activity. Non nitrogen-containing BPs are reported to act through the intracellular accumulation of non-hydrolyzable ATP analogs that exert cytotoxic effects on OCs, while N-BPs inhibit the mevalonate pathway and prevent the post-translational prenylation of small GTP-binding proteins such as Ras, Rho, Rac and Cdc42. Previous studies have demonstrated that small G proteins control the differentiation, apoptosis, cytoskeletal organization and vesicular trafficking of OCs. Therefore, the anti-resorptive properties of N-BPs can be exhibited by inducing OC apoptosis, altering the OC cytoskeleton or affecting OC vesicular and membrane trafficking. Recently, it was reported that N-BPs suppress the bone-resorbing activity of OCs independently of apoptosis. In addition, Weinstein et al. demonstrated that bone biopsy specimens from patients with long-term alendronate administration exhibited an increased OC number in proportion to the accumulated amount of alendronate. These observations have led to the notion that the anti-resorptive function of N-BPs is regulated through a different signaling pathway than their pro-apoptotic function.

This study aimed to distinguish the molecular mechanisms regulating the pro-apoptotic function and anti-resorptive function of N-BP's using risedronate (RIS) as a model. We previously reported that the proapoptotic BH3-only protein Bim plays a crucial role in the OC apoptosis induced by cytokine deprivation. We analyzed the effect of RIS in bim-/- mice and normal mice in vivo, and tried to elucidate whether or not the anti-resorptive effect of RIS in vivo is through the induction of OC apoptosis.

RIS (0.01 mg/kg body weight) or normal saline was subcutaneously injected into14-week-old bim-/- and wild type (WT) mice once a day for 14 days. Next day after the final injection, the mice were sacrificed and were analyzed radiologically, biochemically and histologically. Histological analysis of proximal tibial metaphysis showed that OC apoptosis induced by RIS was prominently suppressed in bim-/- mice compared to WT mice as determined by TUNEL staining. However, RIS treatment induced increase in bone mass and decrease in serum type I collagen crosslinks at the comparable levels in both bim-/- and WT mice (Figure). RIS treatment induced about 50% increase in OC number per bone perimeter in WT mice as compared to untreated mice, while RIS-induced increase in OC number was not observed in bim-/- mice. Giant OCs detached from bone surfaces were similarly observed in both bim-/- and WT mice in response to RIS treatment.

These results suggested that anti- resorptive effect of RIS in vivo is due to other mechanism than induction of OC apoptosis.

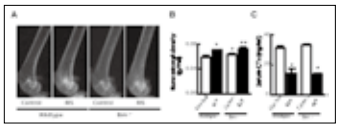

Figure: Representative radiography images of the distal femur of 14 weeks male Bim-/- and wildtype mice + RIS treatment for 14 days. B, Bone mineral density (BMD) of the distal femur in the Bim-/- and wildtype mice + RIS treatment. *p<0.05 versus the untreated wildtype mice and **p<0.05 versus the untreated Bim-/- mice C, The serum concentration of type I collagen crosslinks (CTx-I) in Bim-/- and wildtype mice. *p<0.01 versus the untreated mice.

Dr. Tsumaki

Direct induction of chondrogenic cells from a mouse dermal fibroblast culture

Noriyuki Tsumaki, M.D., Ph.D.
Center for iPS Cell Research and Application,
Kyoto University, Japan

The repair of cartilage injury with hyaline cartilage remains a challenging clinical problem. Articular cartilage damage sometimes heals with fibrocartilage, which is different from hyaline cartilage. Fibrocartilage is a type of scar tissue that expresses types I and II collagen. In contrast, hyaline cartilage does not express type I collagen. When aiming to induce hyaline chondrogenic cells directly from dermal fibroblasts, in addition to the activation of cartilage-specific matrix genes, eliminating the expression of type I collagen is needed for the generation of hyaline cartilage. Otherwise, the presence of type I collagen impairs the cartilage extracellular matrix architecture, which leads to the formation of fibrocartilage. The generation of induced pluripotent stem cells has provided a tool for reprogramming dermal fibroblasts to an undifferentiated state by the ectopic expression of reprogramming factors (c-Myc, Klf4, Sox2 and Oct3/4). We hypothesized that the transduction of dermal fibroblasts with the combination of a part of reprogramming factors and chondrogenic factors may produce chondrogenic cells, and therefore carried out experiments to try and prove this theory.

To select cells that could acquire a chondrogenic phenotype, we generated transgenic mice bearing β-geo (fusion gene of β-galactosidase and neomycin-resistant genes) linked to the cartilage-specific promoter and enhancer sequences of the type XI collagen α2 chain gene (Col11a2). We prepared dermal fibroblasts from adult Col11a2-β geo transgenic mice. We transduced Col11a2-β geo dermal fibroblasts with various combinations of reprogramming factors and chondrogenic factors, and continued the culture in the presence of G418. After examining various combinations of factors, we found the retroviral expression of two reprogramming factors (c-Myc and Klf4) and one chondrogenic factor (SOX9) to induce G418-resistant cells from Col11a2-β geo mouse dermal fibroblasts. G418-resistant cells showed a polygonal morphology and stained positively for alcian blue. We picked up cells and established cell lines.

The induced cells expressed marker genes for chondrocytes such as the type II collagen gene, aggrecan gene and link protein gene. On the other hand, the induced cells did not express marker genes for fibroblasts such as the type I collagen α1 chain gene and type I collagen α2 chain gene. A bisulfite sequencing analysis revealed the promoter regions of type I collagen α1 and α2 chain genes to be highly methylated in induced cells, whereas those in parental mouse dermal fibroblasts were hypomethylated. These results suggest that type I collagen genes were silenced in induced cells.

The transplantation of induced cells into the subcutaneous spaces of nude mice revealed that there were two types of cells: namely, chondrogenically reprogrammed cells and partially reprogrammed intermediate cells. Chondrogenically reprogrammed cells generated stable homogenous hyaline cartilage-like tissue when subcutaneously injected into nude mice. No tumors formed thereafter for 4 months. Hyaline cartilage-like tissue expressed type II collagen, but not type I collagen. These results suggest that these induced cells are chondrogenic. On the other hand, partially reprogrammed intermediate cells expressed type I collagen and produced tumors when injected into nude mice. A histological analysis showed these tumors to be fibrous and not teratomas. Tumors appeared to develop because of the persistent the expression of c-Myc and Klf4 transgenes.

The induced chondrogenic cells did not undergo a pluripotent state during induction from a dermal fibroblast culture, as time-lapse observations did not detect any GFP reporter expression during the induction from dermal fibroblasts prepared from transgenic mice in which GFP is inserted into the Nanog locus. These results suggest that the chondrogenic cells induced by this approach are theoretically free from the risk of teratoma formation which is associated with the cells prepared through the generation of iPS cells followed by redifferentiation into the target cell type.

The dox-inducible induction system demonstrated that induced cells are able to respond to a chondrogenic medium by expressing endogenous Sox9 and maintain a chondrogenic potential after the substantial reduction of transgene expression due to the withdrawal of dox. These results suggest that the persistent expression of c-Myc, Klf4 and SOX9 transgenes was not necessary for the maintenance of induced chondrogenic cells. It is therefore ideal to induce chondrogenic cells by the transient expression of these factors without the integration of the vectors into the genome. This approach could therefore, in the future, potentially lead to the successful production of hyaline cartilage directly from skin, without going through pluripotent stem cell stage, and therefore be applicable to the field of regenerative medicine.

Dr. Kato

A Y chromosome gene, Uty, defines sexual dimorphism in skeletal phenotype

Shigeaki Kato, Ph.D.
Institute of Molecular and Cellular Biosciences,
The University of Tokyo

Males have higher bone mass and larger skeletal size than females. Such gender-specific bone phenotype has considered to be generated by the actions of sex steroid hormones. However, an uncharacterized Y chromosome gene is assumed as a significant factor to form gender-specific bone phenotype from clinical observations of patients mutated in the GCY (Growth Controlling region on the Y chromosome).

To reveal the biological functions of Y chromosome gene in skeletal systems, we ablated mouse Uty (Ubiquitously transcribed tetratricopeptide repeat gene, Y chromosome) gene, whose human ortholog is located in the GCY. Using a Cre/loxP system and two step ES gene-targeting methods that are potent to low efficiency of homologous recombination in Y chromosome, successfully, Uty gene was genetically disrupted for the first time among the Y chromosome genes. Uty knockout mice ($Uty^{X/L}$) exhibited short stature with shortened trunk and long bones like wild-type (WT) female littermates, while no endocrine disturbance was detected. In $Uty^{X/L}$, the thickness of growth plates, especially at proliferative zone, was significantly reduced when compared with that of WT male littermates. As expected, primary cultured chondrocytes from $Uty^{X/L}$ showed decreased proliferative ability with increased expression of Col10a1, a marker of hypertrophic chondrocytes. These results suggest that Uty regulates male skeletal length by controlling cartilage development. Since Uty bears a JmjC domain, we assumed Uty function as an epigenetic regulator. In a co-immunoprecipitation assay, Uty was found to associate with Runx2 and Hdac4, the key factors in chondrocytes differentiation. Consistently, Uty was potent to repress transcriptional activity of Runx2 in an OSE-luc assay. A ChIP assay showed that these factors were recruited to the Runx2 target gene (Col10a1) promoter. Moreover, recruitment of Hdac4 was reduced and several histone modifications of Col10a1 promoter were altered in $Uty^{X/L}$ chondrocytes.

Thus, these findings suggest that Uty is a negative regulator for Runx2 by recruiting a transcriptional co-repressor HDAC4, expressed at hypertrophic chondrocytes, and thereby facilitates cartilage development. Taken together, the present study has uncovered a molecular basis of gender-specific cartilage development.

10. 新聞記事

2011年(平成23年)12月13日 火曜日 朝日新聞

痛むひざ半月板再生

東京医科歯科大、臨床研究へ

幹細胞採り注射

一度傷つくと再生が難しいひざの半月板を、自分のひざの滑膜という組織からとった幹細胞で再生させる治療法を、東京医科歯科大の関矢一郎教授（軟骨再生学）が開発し、来年4月にも臨床研究を始める。

半月板損傷は、全国に250万人という変形性膝関節症につながる。歩きづらいひざの痛みに苦しむ患者には朗報になりそうだ。

半月板は関節軟骨に挟まれた軟骨組織で、クッションの役目をする。加齢などすり切れると、縫い合わせて補強したりするが、手術できない場合も多い。新しい治療法では、患者のひざの状態を内視鏡で確認するとき、半月板の近くにある滑膜の一部を採取。2週間培養して増やした幹細胞を、注射器で半月板の損傷部に移植して再生させる。同大で3年間で20人ほどの患者を対象に臨床研究を行ったあと、他の病院にも広げて臨床試験を行う。

幹細胞を使う再生医療では骨髄の幹細胞がよく使われるが、お年寄りでは採りにくいことがある。

関矢教授は、同じ手法でひざの関節軟骨の再生治療をしている。2008年以降、滑膜幹細胞を移植して半年以上たった18人のうち14人で軟骨が再生していることが確認された。14人は移植の翌日には松葉杖で、6週間後には自力で歩けるようになったという。半月板でも同じペースでの回復を見込む。「まずは、従来の手術のみで治癒させるのが難しい半月板の断裂を対象にしたい」といい、当面は手術とセットで行う。

軟骨の再生医療に詳しい京都大学iPS細胞研究所の戸口田淳也教授（整形外科）は「滑膜は手術前に通常行う検査で採れるのが利点。ひざの動きに耐えうる強度を確保することが大事で、うまくいけば画期的な治療になる」と話す。半月板の損傷に悩むスポーツ選手も多く、昨年のサッカーW杯で活躍した本田圭佑選手やプロ野球阪神の城島健司選手らがいる。（下司佳代子）

ひざの構造

関節軟骨 滑膜 ひざ 半月板

朝日新聞

2011年（平成23年）12月13日 火曜日

経済6・8面
国際11・13面
金融情報16・17面
文化18面
小説18面／生活22・25面
スポーツ26・27面
囲碁・将棋30面
地域32・33面
TV・ラジオ29・30・40面

朝日新聞大阪本社
発行所〒530-8211大阪市北区中之島3-2-4
電話06-6231-0131 www.asahi.com

朝日新聞

2011年(平成23年)10月17日 月曜日

骨粗鬆症 仕組み一部解明

運動しないと骨が弱くなるのは、交感神経と骨を結ぶたんぱく質の働きが原因だと、東京医科歯科大の野田政樹教授らのチームが明らかにした。このたんぱく質を抑えられれば、骨粗鬆症の安価な治療薬ができる可能性があるという。

チームは、マウスに薬を与えて交感神経を刺激すると「オステオポンチン」というたんぱく質が増えて骨が減り、オステオポンチンがないマウスでは交感神経を刺激して活性化させても骨が減らないことを実験で確かめた。研究成果は米科学アカデミー紀要（電子版）に掲載された。

11. 海外研究者等招聘講演会

ポスター	タイトル	講演者	日　付
	第225回Bone Biology Seminar 第52回グローバルCOE海外研究者講演会共催 「Study of OsteocyteLacunarProperties by 3D X-Ray Microscopy」	Dr. Donald B. Kimmel, D.D.S., Ph.D.	2012年3月02日
	第51回グローバルCOE海外研究者講演会 「Clinical Dental Medicine 2020」	Dr. NairnWilson	2011年11月18日
	第50回グローバルCOE海外研究者講演会 「Distinct impact of anti-B cell directed therapy on B cell subsets」	Dr. Thomas Dörner	2011年12月12日
	第11回骨免疫セミナー 第49回グローバルCOE海外研究者講演会共催 「Nonapoptotic role of Fas-Fas ligand system in bone」 「RANKL, osteoclast differentiation and osteoimmunology」	Dr. Ana Marusic, M.D., Ph. D. Dr. Yongwon Choi, Ph.D.	2011年11月17日
	大学院特別講義 第48回グローバルCOE海外研究者講演会共催 「Digital Dentistry with CAD/CAM and Cone Beam Computed Tomography and their Applications in Implantology」	Dr. Andreas F. Bindl Dr. Lutz Ritter	2011年10月11日
	第47回グローバルCOE海外研究者講演会 「Role of transglutaminase-enzymes and matrix stabilization in bone formation and maintainance of adult bone mass」	Dr.Mari T. Kaartinen	2011年9月26日
	第46回グローバルCOE海外研究者講演会 「New Developments in Research Funding and Grant Review in the United States」	Dr. MarkI. Ryder	2011年8月31日
	第224回 Bone Biology Seminar 第45回グローバルCOE講演会共催 「Regulation of tendon extracellular matrix assembly.」	Dr. David E. Birk, Ph.D.	2011年8月11日

	第44回グローバルCOE海外研究者講演会 「Clinically Unsolved Problems Related to Osteoporosis and Bone Atrophy in OrthopaedicSurgery」	大川　淳	2011年6月27日
	第223回 Bone Biology Seminar 第43回グローバルCOE講演会共催 「Drug Development for Osteoporosis」	Dr. Arthur C. Santora Ⅱ	2011年6月20日

12. イノベーション研究活動推進

【2011年度】

実施日：2011年9月5日、9月6日

プロジェクト1
研究代表者：歯周病学　和泉　雄一
共同研究者：野田　政樹
研究課題名：歯周炎における硬組織代謝に与える神経性炎症の役割について

プロジェクト2
研究代表者：分子細胞遺伝　稲澤　譲治
共同研究者：分子薬理学　野田　政樹、
顎口腔外科学　小村　健、
顎顔面矯正学　森山　啓司、
膠原病・リウマチ内科学　宮坂　信之、
分子遺伝学　三木　義男、
整形外科学 大川　淳
研究課題名：難治性硬組織疾患の病態オミックス先端拠点研究

プロジェクト3
研究代表者：歯髄生物学　須田　英明
共同研究者：運動器外科学　宗田　大
研究課題名：歯髄・歯肉組織由来の間葉幹細胞による歯槽骨・顎骨再生

プロジェクト4
研究代表者：硬組織病態生化学　柳下　正樹
共同研究者：歯周病学　和泉　雄一
研究課題名：歯周組織炎症部位におけるスフィンゴシン-1-リン酸シグナルの役割

プロジェクト5
研究代表者：口腔病理学 山口　朗
共同研究者：分子情報伝達学 高柳　広
研究課題名：光メージングと分子生物学の融合によるオステオネットワークの解明を目指したフロンティア研究拠点

プロジェクト6
研究代表者：歯周病学　和泉　雄一
共同研究者：細菌感染制御学　中川　一路
研究課題名：口腔メタバイオーム解析による骨・歯周組織破壊因子の同定

13. 国際PIシャペロンの活動

●2011年7月5日

国際PIシャペロン競争的研究費審査

1位　大洞将嗣（分子情報伝達学）、2位　飯村忠浩（口腔病理学）、3位　岩井秀之（膠原病・リウマチ内科学）

●2011年11月24日

国際PIシャペロンフォーラム

●2012年1月26日

国際外部評価会での研究発表

14. 大学院生採用面接評価　複数教員による英語（年次）面接と評価　優秀賞受賞者

●第Ⅵ期（2011年4月～）

1位　Most Excellent Award 辻香織

2位　Excellent Award 古田繭子

3位　Excellent Award宮嶋大輔

第Ⅵ期　AISS採用面接　点数分布

評価点数	全体平均　70.33	該当者数
91 – 100	○	1
86 – 90	○○	2
81 – 85	○○○○○	5
76 – 80	○○○○○○○○○○	10
71 – 75	○○○○○○○	7
66 – 70	○○○○○○○○○○○○○○○○	16
61 – 65	○○○○○○○○○○	10
56 – 60	○○○○○	5
51 – 55	○○○○	4
46 – 50		0
合　計		60

●第Ⅶ期（2011年10月～）

1位　Most Excellent Award 小野岳人

2位　Excellent Award　Smriti Aryal A.C.

3位　Excellent Award　山田梓

第Ⅶ期　AISS採用面接　点数分布

評価点数	全体平均　71.51点	該当者数
81 – 100	○○	2
76 – 80	○○○	3
71 – 75	○○○○○○○○○○○○	12
66 – 70	○○○○○○○○○○○○	12
61 – 65	○○○○○○○	7
56 – 60	○○○	3
合　計		39

●第Ⅷ（2012年4月～）

1位　Most Excellent Award 川崎真希理

2位　Excellent Award　中里洋子

3位　Excellent Award　葉暢暢

第Ⅷ期　AISS採用面接　点数分布

評価点数	全体平均　73.07点	該当者数
81 – 85	○○○○○○○○	8
76 – 80	○○○○○○○○○○	10
71 – 75	○○○○○○○○○○○○○○○	15
66 – 70	○○○○○○○○○	9
61 – 65	○○○	3
56 – 60	○○○○	4
51 – 55	○	1
合　計		50

15. プレゼンテーション型　英語クラス

開催日

Student Instruction：
2011年4月25日、5月30日、6月27日、7月25日、8月25日、9月26日、10月31日、11月28日、2012年2月20日、3月12日
Staff Instruction：2011年12月19日、2012年1月16日
Instructor：Mr. Kevin Cleary（本学准教授）
参加者：28名

16. 歯と骨のGCOE　受賞リスト

田上　順次

・First place outstanding paper award, Sadr A, Bartakova S, Parchar P, Hariri I, Nazari A, Shimada Y, Tagami J, Sumi Y.
Adhesion of Flowable Composite in Class I Cavities: Combination of SS-OCT Imaging and Microtensile Bond Strength. The 4th International Conference on Adhesive Dentistry, Seoul, Korea, April 15-17, 2011.
・The first place outstanding poster, IAD, 2011, Islam MS, Hiraishi N, Otsuki M, Tagami. Effect of Hesperidin Incorporation into the Primer of a Self-etching Adhesive on Micro Tensile Bond Strength to Dentin. The 4th International Congress on Adhesive Dentistry, Korea, April 15-17, 2011.

高柳　広

・The 3rd Joint Conference of the International Bone & Mineral Society and the European Calcified Tissue Society, IBMS-BONE Herbert A. Fleisch Award　平成23年5月9日
・中島　友紀
1st Bio-Rheumatology International Congress (BRIC2011), Poster Presentation Award 平成23年11月
・古賀　貴子
第29回日本骨代謝学会、優秀演題賞　平成23年7月29日
・辻　香織
The 59th Annual meeting of Japanese Association for Dental Research
The Hatton Award 2012 Finalist of Japanese Association for Dental Research

小村　健

・佐藤　潔, 坂本　啓, 栢森　高, 山口　朗: 第53回歯科基礎医学会総会　優秀ポスター賞　2011年10月1-2日　岐阜市「口腔扁平上皮癌による骨破壊予防療法の開発」

須田　英明

・西原良治（指導　鈴木規元、石村瞳）.スーパーエンドα、βを用いた根管充填の速度および充填率に関する研究.D4研究体験実習学生発表会　歯学科長賞,2010年9月25日.

和泉　雄一

・Nanbara H, Travel Award. Wnt5a expression by Porphyromonas gingivalis LPS via NF- κ B and STAT1. The 10th World Congress on Inflammation, Paris, 2011.6.25-29.
・坪川正樹.第23回日本レーザー歯学会総会・学術大会優秀発表賞.光干渉断層画像診断法（OCT)による歯肉縁下歯石の検出.第23回日本レーザー歯学会総会・学術大会.大阪,2011.12.3-4.

森山　啓司

・小林起穂、ヴァイスティネン・ロッタ、ライス・デビッド、森山啓司. Runx2・発現抑制によるGli3Xt-J/Xt-Jマウス頭蓋冠縫合部早期癒合症発症の予防効果. 第70回日本矯正歯科学会＆第4回国際会議・優秀発表賞、名古屋、平成23年10月17－20日.
・出井彩乃、宮本順、高田潤一、小野卓史、森山啓司.口輪筋訓練における口輪筋筋活動および血流量の同時計測の有用性. 第70回日本矯正歯科学会＆第4回国際会議・優秀発表賞、名古屋、平成23年10月17－20日.
・湊亜紀子、宮本順、小野卓史、誉田栄一、倉林亨、森山啓司. 舌触覚刺激に対する2点弁別および大脳皮質賦活パタンにおける習慣性咀嚼側の関与. 第70回日本矯正歯科学会＆第4回国際会議・優秀発表賞、名古屋、平成23年10月17－20日.

・松本力、山口朗、森山啓司. 矯正学的歯の移動における骨細胞の役割. 第70回日本矯正歯科学会＆第4回国際会議・優秀発表賞、名古屋、平成23年10月17－20日.
・川久保直美、小野卓史、宮本順、誉田栄一、倉林亨、森山啓司. 咬みしめに伴う上肢筋の促通とそれに同期した脳賦活パタンfMRIを用いた研究. 第70回日本矯正歯科学会＆第4回国際会議・優秀発表賞、名古屋、平成23年10月17－20日.

宮坂　信之

・溝口史高.第55回日本リウマチ学会総会・学術集会.ポスター賞。神戸.2011年7月18日
・溝口史高.第39回日本臨床免疫学会総会・学術集会.優秀演題賞。東京.2011年9月17日
・岩井秀之.第39回日本臨床免疫学会総会・学術集会.優秀演題賞。東京.2011年9月17日
・岩井秀之.The 4th East Asian Group of Rheumatology. Young Investigator award Tokyo. 2011年10月15日.
・平田真哉　.第39回日本臨床免疫学会総会・学術集会.優秀演題賞。東京.2011年9月17日

宗田　大

・堀江雅史
Implantation of Allogenic Synovial Stem Cells Promotes Meniscal Regeneration in a Rabbit Meniscal Defect Model
東京医科歯科大学整形外科同門会　研究奨励賞2011年12月23日
・Toshifumi Watanabe; Michael Conditt; Scott Banks; Stefan Kreuzer; Kevin Leffers; Takeshi Muneta; Jennifer Jones
Deep Flexion Kinematics With Robotic Modular Knee Arthroplasty
International Society For Technology in arthroplasty (ISTA) 2011
Best poster award
Brugge　2011/9/20-23

稲澤　譲治

・春木茂男（大学院医歯学総合研究科博士課程平成21年度卒業）が第12回田中道子がん研究奨励賞を受賞.
・村松智輝が平成22年度「難治疾患の研究」を重点課題とする研究助成に採択.
・小野宏晃が平成22年度大学院生・若手研究者研究発表会で大学院生部門1位（ベストプレゼンテーション賞）を受賞.
・本田尚三が平成22年度大学院生・若手研究者研究発表会で大学院生部門2位を受賞.
・村松智輝が平成22年度大学院生・若手研究者研究発表会で難治疾患研究賞を受賞.
・古田繭子が平成22年度大学院生・若手研究者研究発表会で萌芽賞を受賞.
・古田繭子が東京医科歯科大学グローバルCOE（GCOE）スーパースチューデント（SS）研究発表で優秀賞「Excellent Award」を受賞.
・井上純が川野小児医学奨学財団の研究助成に採択.
・村松智輝が平成23年度東京医科歯科大学大学院学生研究奨励賞を受賞.
・古田繭子が文部科学省科学研究費新学術領域研究がん研究分野の特性等を踏まえた支援活動・平成23年度日仏がんワークショップの公募に採択.（フランスに派遣）

小川　佳宏

・菅波孝祥　日本肥満学会学術奨励賞「肥満の脂肪組織における慢性炎症の分子機構の解明と医学応用」
・伊藤美智子　日本肥満学会若手研究奨励賞「NASHの発症・進展と脂肪組織炎症ー新しいNASHモデル・MC4R欠損マウスを用いてー」
・小川佳宏　日本糖尿病・肥満動物学会研究賞「糖尿病・肥満における慢性炎症の分子機構に関する研究」

水島　昇

・平成23年11月 武田医学賞受賞（科学新聞　2011.10.07）

17. Research Day

●国際的トップ大学Research Dayへ派遣

Harvard University

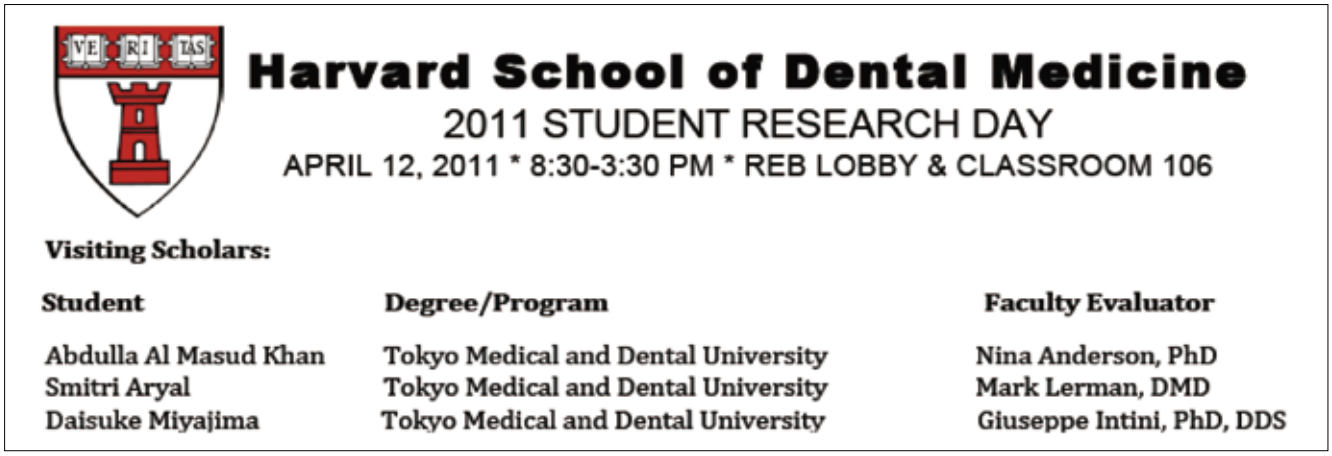

Harvard School of Dental Medicine

2011 STUDENT RESEARCH DAY

APRIL 12, 2011 * 8:30-3:30 PM * REB LOBBY & CLASSROOM 106

Visiting Scholars:

Student	Degree/Program	Faculty Evaluator
Abdulla Al Masud Khan	Tokyo Medical and Dental University	Nina Anderson, PhD
Smitri Aryal	Tokyo Medical and Dental University	Mark Lerman, DMD
Daisuke Miyajima	Tokyo Medical and Dental University	Giuseppe Intini, PhD, DDS

University of California San Francisco

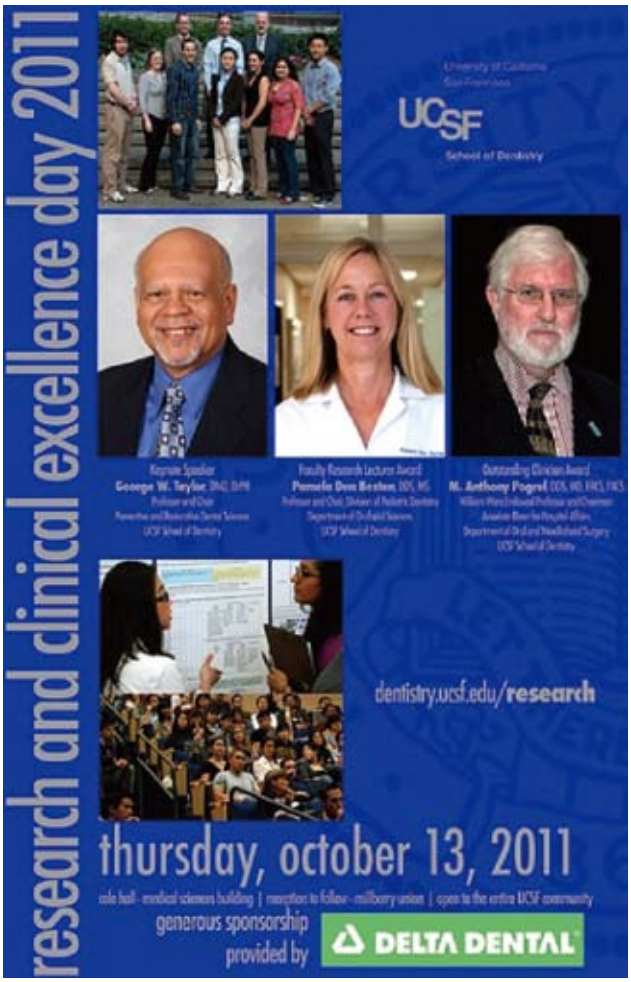

University of Toronto

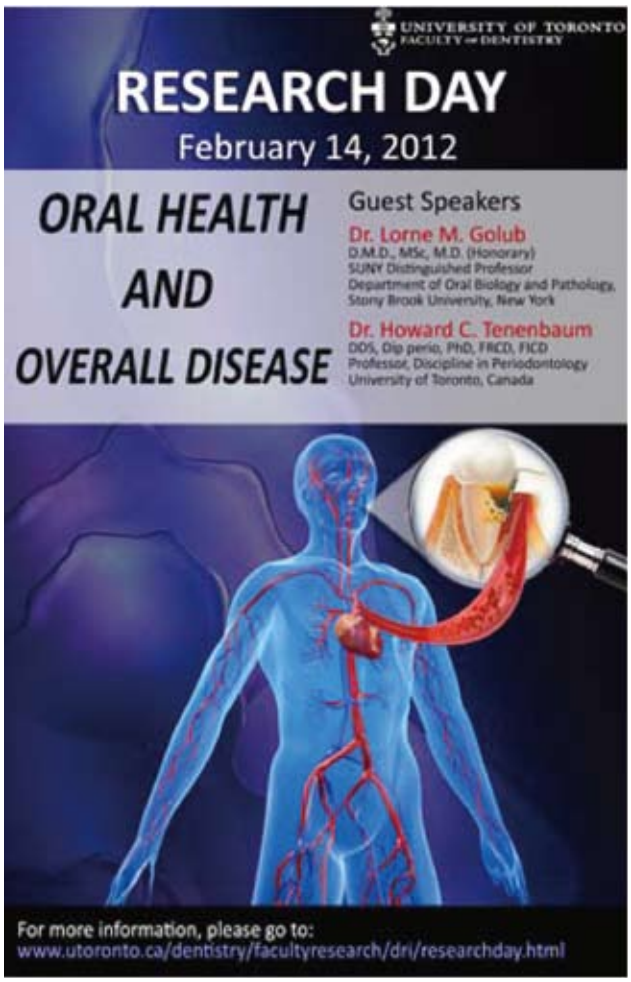

Harvard School of Dental Medicine

2011 STUDENT RESEARCH DAY

APRIL 12, 2011 * 8:30-3:30 PM * REB LOBBY & CLASSROOM 106

8:30-9:30 AM **BREAKFAST**
8:45-9:00 **Welcome and Introductions**

Student	Degree/Program	Faculty Evaluator
9:00-9:30 AM		
Soulafa Almazrooa	DMSc/Oral Medicine	Giuseppe Intini, PhD, DDS
Athbi Alqareer	DMSc/Orthodontics	Xiuping Wang, MD, DMD
Wendy Cohen	MMSc/Orthodontics	Elona Hart, PhD
Jyoti/Dangi	MMSc/Dental Public Health/Oral Epidemiology	Nina Anderson,PhD
Sirena Hsieh	MMSc/Orthodontics	Mark Lerman, DMD
Zainab Khan	DMSc/Oral Biology	Vicki Rosen, PhD
Peter Ok	MMSc/Endodontics	Dorothy Pazin, PhD
9:30-10:00 AM		
Vinicius Rodrigues	DMSc/Periodontology	Dorothy Pazin, PhD
Tina Vani	MMSc/Endodontic	Elona Hart, PhD
Hessam Rahimi	DMSc/Orthodontics	Mark Lerman, DMD
Siamak Abai	MMSc/Prosthodontics	Donald Giddon, DMD,PhD
Rita Han	MMSc/Prosthodontics	Nina Anderson, PhD
Jennifer Hong	MMSc/Endodontics	Vicki Rosen, PhD
Jason Outlaw	DMSc/Oral Biology	Giuseppe Intini, PhD, DDS
Sattheesh Elangovan	DMSc/Periodontology	Nalaka Jayaratne, DMD, PhD
10:00-10:30 AM		
Visiting Scholars:		
Ashkan Saadi	Fellow, Oralfacial Pain	Donald Giddon, DMD, PhD
Abdulla Al Masud Khan	Tokyo Medical and Dental University	Nina Anderson, PhD
Smitri Aryal	Tokyo Medical and Dental University	Mark Lerman, DMD
Daisuke Miyajima	Tokyo Medical and Dental University	Giuseppe Intini, PhD, DDS
Amerlie Yi	GPR, Cambridge Health Alliance	Elona Hart, PhD
Joshua Lee	GPR, Cambridge Health Alliance	Xiuping Wang, MD, DMD
Mashid Bahadoran	GPR, Cambridge Health Alliance	Dorothy Pazin, PhD
10:30-11:00		
Daniel Bienstock	DMD 2011	Donald Giddon, DMD, PhD
Yuliya Kostenko	DMD 2011	Nina Anderson, PhD
Tracy Pogal-Sussman	DMD2011	Vicki Rosen, PhD
Judith Rosenbloom	DMD 2011	Giuseppe Intini, PhD, DDS
Elliot Saperstein	DMD 2011	Dorothy Pazin, PhD
Preetha Thomas	DMD 2011	Mark Lerman, DMD
Kimberly Whippy	DMD 2011	Xiuping Wang, MD, DMD
Duy Do	DMD 2012	Elona Hart, PhD

18. リトリート

【日程】

1月23日（月曜日）

10：00-12：00　海外研究者とのディスカッション

・Dr. Henry Kronenberg
（担当：森山教授、学生28名）

・Dr Jack Martin
（担当：高柳教授、学生22名）

・Dr. Benjamin Alman
（担当：山口教授、学生17名）

・Dr. Gerard Karsenty
（担当：野田教授、学生17名）

16：00-16：30　ポスターセッションⅠ（28演題）

18：30-　懇親会

1月24日（火曜日）

15：00-15：30　ポスターセッションⅡ（26演題）

1月25日（水曜日）

14：30-15：00　ポスターセッションⅢ（26演題）

18:00-　ポスター優秀者発表

【場所】

東京医科歯科大学　M＆Dタワー2階　ホワイエ

【ポスター発表　優秀者】

1位

Samir Kumar Pal
"The Role of Thrombospondin-1(TSP-1) in Bone Destruction by Oral squamous cell carcinoma"

2位

馬騰
"Inability of p53-Reactivating compounds Nutlin-3 and RITA to overcome p5 3 resistance in tumor cells deficient for p53Ser46 phosphorylation"

渡辺高
"Changes in Subcellular Localization of osteoblast specific transcriptional factors during bone development, revealed by 3-dimensional fluorescence morphometry"

Dawud Abduweli
"3D approaches for stem cell niches in medaka pharyngeal dentition"

3位

松本力
"The role of osteocyte during orthodontic tooth movement"

Rajakaruna Gamaralalage Amodini
"Localization of Porphyromonas gingivalis and Tannerella forsythia in Gingival and Subgingival Granulation Tissues Using Novel Monoclonal Antibodies"

小野岳人
"Effects of the immune system on bone regeneration after drill-hole injury"

Kahaer Abula
"BMP7 is prerequisite for postnatal joint homeostasis"

森田淳平
"The development of novel treatment for Apert syndrome by a soluble form of FGFR2 - Rescue of Apert phenotypes"

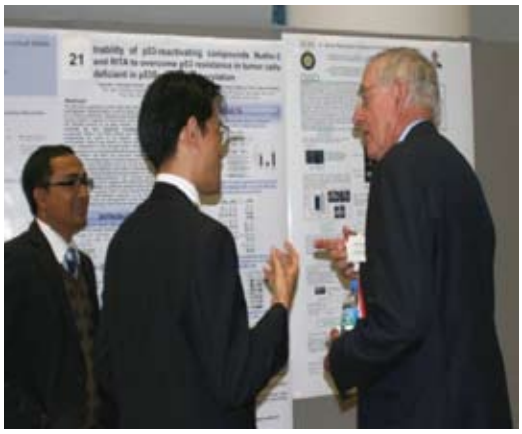
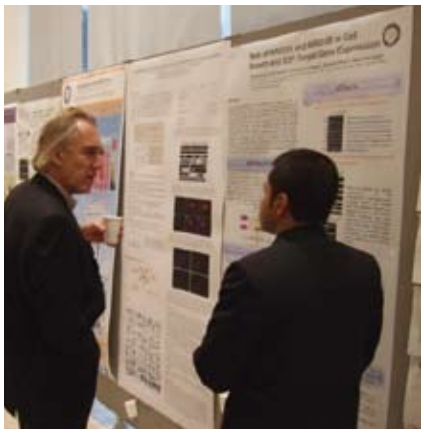

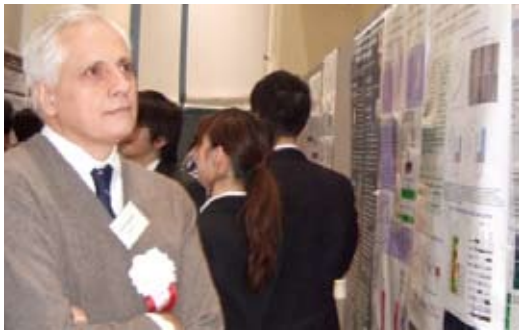

Poster Session

Retreat 2012

Poster No.	Day	Name	Grade	Title
1	day 1	Gamaralalage Amodini Rajakaruna	4	Localization of Porphyromonas gingivalis and Tannerella forsythia in Gingival and Subgingival Granulation Tissues Using Novel Monoclonal Antibodies
2	day 2	Takashi Watanabe	4	Changes in Subcellular Localization of osteoblast specific transcriptional factors during bone development, revealed by 3-dimensional fluorescence morphometry
3	day 3	Cheng Kang	3	Effects of low − intensity pulsed ultrasound stimulation on bone healing in a rat calvarial defect model
4	day 1	Zhou Mengyu	3	The multiple function of periostin in teeth development ,aging,and dentin repair of mice.
5	day 2	Dawud Abduweli	2	3D approaches for stem cell niches in medaka pharyngeal dentition.
6	day 3	Jyunpei Shirakawa	2	Both the PTH-induced and fluid-flow induced osteoblast proliferation are associated with up-regulation of CyclinD1 and expression
7	day 1	Ma Chengshan	2	A Novel Central-Control Pathway of Bone Remodeling
8	day 2	Takehito Ono	1	Effects of the immune system on bone regeneration after drill-hole injury
9	day 3	Wayakanon Praween	4	The Role of C-terminus of Cx43 in Gap Junction Plaque Internalization
10	day 1	Kahaer Abula	1	BMP7 is prerequisite for postnatal joint homeostasis
11	day 2	Hidenori Hamba	4	Quantitative Measurement of Enamel Lesion Using Micro-computed tomography and Micro-radiography
12	day 3	Yoko Nakazato	1	Role of interferon-gamma and interleukin 4 in C protein-induced myositis
13	day 1	Daisuke Miyajima	4	Profilin1 regulates sternum development and endochondral bone formation
14	day 2	Xu Ren	3	Uncovering the molecular mechanism of Semaphorin 3a on the bone remodeling
15	day 1	Samir Kumar Pal	3	The Role of Thrombospondin-1(TSP-1) in Bone Destruction by Oral squamous cell carcinoma
16	day 2	Cheng Xu	2	The function of the circadian clock on bone resorption
17	day 3	Bakhsh, Turki Abdulsalam A.	3	Non-invasive Evaluation of Dental Composite Failure using SS-OCT
18	day 2	Zayar Lin	2	Application of Oral Mucosa Fibroblasts as a source of Cell-Mediated Bone Regeneration Therapy
19	day 3	Akiko Suzuki	2	Analysis of the role of PI3K in murine myositis model
20	day 1	Takafumi Suzuki	4	TRPV4 is a regulator of calcium oscillation under mechanical stress in differentiating osteoblasts
21	day 2	Ma Teng	4	" Inability of p53-Reactivating compounds Nutlin-3 and RITA to overcome p5 3 resistance in tumor cells deficient for p53Ser46 phosphorylation"
22	day 1	Md. Abdulla Al Masud Khan	3	A Bone Resorption Inhibitor Promotes Bone Formation
23	day 2	Jyunpei Morita	3	The development of novel treatment_for Apert syndrome by a soluble form of FGFR2__- Rescue of Apert phenotypes
24	day 3	Koyo Takimoto	3	Regulation of Pulpal Inflammation by MMP-3
25	day 1	Ye Changchang	2	The role of periodontal bacteria on antiphospholipid syndrome and preterm low birth weight
26	day 3	Rumana Khanom	2	Expression of basal cell keratin 15 and keratin 19 in oral squamous neoplasms represents diverse pathophysiologies
27	day 1	Tsutomu Matsumoto	4	the role of osteocyte during orthodontic tooth movement
28	day 2	Aslam Al Mehdi	4	Histological and SEM Analysis of root cementum following irradiation with Er:YAG and CO2 lasers
29	day 3	Bharcgava Suhas Srilatha	4	Effect of sandblasting different ceramic abrasives on mechanical properties of zirconia
30	day 1	Chiho Watanabe	3	Cnot3, a regulator of a mRNA stability, is involved in the maintenance of the bone mass

Poster No.	Day	Name	Grade	Title
31	day 2	Yasuyuki Shimada	3	Genetic Etiology of Keratocystic Odontogenic Tumor
32	day 3	Yuka Tsumanuma	3	Comparison of different tissue-derived stem cell sheets for periodontal regeneration in a canine 1-wall defect model
33	day 1	Shin Fukuda	2	Agonist for cannabinoid receptor 2 (CB2) ameliorates murine collagen-induced arthritis
34	day 2	Warunee Pluemsakunthai	2	Understanding of Platelet-Rich Fibrin
35	day 3	Duarte Puerto Carolina Lizeth	2	Suture expansion assisted with magnetically controlled Relaxin loaded liposones
36	day 1	Khan Abu Shameem Md. Saadat	4	Role of ARID3A and ARID3B in Cell Growth and E2F-Target Gene Expression
37	day 2	Bharti Pariksha	4	Periodontal treatment with topical antibiotics improves glycemic control in association with elevated serum adiponectin in patients with type 2 diabetes mellitus
38	day 1	Erika Ohue	4	CXCL2 is a regulatory factor for osteoclastic bone resorption synthesized by oral squamous cell carcinoma
39	day 3	Yuki Matsushita	3	The role of CCN3 in osteoblast differentiation and bone regeneration
40	day 2	Marwa Madi	3	Ligature-induced peri-implantitis around bioactive coated implants. An experimental study in dogs
41	day 3	Prasansuttiporn Taweesak	3	Effect of reducing agents on bond strength to NaOCl-treated dentin
42	day 1	Masako Yoshizaki	2	Investigation on inhibitory effects of soluble FGFR2-nanogel complex on premature fusion of cranial sutures
43	day 2	Jyunichi Yasuoka	2	Constitution of proteo-liposome using cell-free protein synthesis system
44	day 3	Suphanantachat Supreda	2	The existence and role of C-kit positive population in human periodontal ligament stem cells
45	day 1	Kiyoshi Sato	4	RANKLs synthesized by both oral squamous cell carcinoma and stromal cells participate in osteoclastic bone resorption
46	day 2	Thanatvarakorn Ornnicha	1	In vitro evaluation of a newly formulated calcium phosphates desensitizing material - durability after long term immersion in artificial saliva-
47	day 3	Hamid Nurrohman	4	Hydroxyapatite crystal protection against acid-attack beneath resin-dentin interface with four adhesives: TEM and crystallography evidence.
48	day 1	Nurmaa Dashzeveg	2	Discovery of pro-apoptotic genes induced by p53 in osteosarcoma
49	day 2	Al-Bari Md. Abdul Alim	4	Lysosomal function is important for osteoclast differentiation and function
50	day 3	Tsuyoshi Yamada	3	The significance of the quality of the human bone marrow mesenchymal cells (hMSCs) in the bone formation
51	day 1	Rajapakshe Mudiyanselage Anupama Rasadari Rajapakshe	2	Lysosome associated membrane protein-2 (LAMP-2) involvement in the stimulation dependent RANKL release from mouse osteoblastic cells
52	day 2	Tomoki Muramatsu	3	Establishment and characterization of a spontaneous metastatic model using a human pancreatic cancer cell line, Panc1.
53	day 3	Yu Miao	2	The study of Zr alloy as biomedical material
54	day 1	Gu Jie	1	Analysis of Receptive Mechanism and Recognition in the CNS of Pulpal Sensation
55	day 2	Yusuke Matsuo	1	Identification of the lineage of _pathogenic fibroblast-like synoviocytes (FLS) _in rheumatoid arthritis
56	day 3	Chokechanachaisakul Uraiwan	4	Artificial dental pulp exposure injury up-regulates mitogen-activated protein kinase 13 and 14 in rat central nervous system
57	day 1	Kaori Tsuji	4	Stage-specific functions of LRF in the transcriptional control of osteoclast development
58	day 3	Ilnaz Hariri	4	Effects of Structural Orientation on Local Refractive Indices of Human Enamel and Dentin by Optical Coherence Tomography
59	day 3	Mayuko Furuta	3	Functional genomics-assisted approach identifies candidates for tumor-suppressive microRNAs in hepatocellular carcinoma.

Poster No.	Day	Name	Grade	Title
60	day 1	Yoshishige Miyabe	3	Autotaxin and lysophosphatidic acid receptors: potential target molecules in new therapies for rheumatoid arthritis
61	day 2	Thitthaweerat Suppason	3	Effect of waiting interval in chemical activation mode of dual-cure one-step adhesives on bonding to root canal dentin
62	day 3	Naoki Kimura	2	Proinflammtory muscle fiber regeneration in autoimmune myositis
63	day 1	Md.Sofiqul Islam	2	Effect of Hesperidin Incorporation into the Primer of a Self-etching Adhesive on Micro Tensile Bond Strength to Dentin
64	day 2	Chui Chanthoeun	3	Bactericidal effect of a-PDT using high power blue LED and red dye agent on Porphyromonas gingivalis
65	day 3	Yurina Sekine	3	Preparation of Lipid Nanotubes for Construction of Micro Bio Device
66	day 1	Norihiko Ashigaki	2	Periodontal Pathogens Deteriorated survival Rate after Subtotal Nepherctomy in Mice
67	day 2	Gerardo Jose Joves Mendez	2	Artificial caries affected dentin model for bonding studies.
68	day 3	Yuji Tsuchido	2	Protein-crosslinked Nanogel for Biomedical Applications
69	day 1	Smriti Aryal A. C.	3	Nck, actin cytoskeleton protein maintains bone remodeling by regulating osteoblast and osteoclast
70	day 2	Masayoshi Uezono	2	Bone Forming Capability Around Novel Subperiosteal Anchorage Device for Orthodontic Treatment
71	day 3	Yuki Yamaguchi	2	Analysis of Dlk1-Dio3 imprinted region in adult somatic cell lineage
72	day 1	Yu Yamashita	2	Absorption Rate of Platelet Rich Fibrin in a Rat Study Model.
73	day 2	Mayumi Ogita	2	Proteomoc analysisi of protein components in human gingival fibroblast following low-level Er:YAG laser irradistion
74	day 3	Mandurah, Mona Mohammad M.	2	optical and mechanical charecterization of sclerotic dentin of attrition teeth by the use of SS-OCT and nanoindentation techneque
75	day 1	Azusa Yamada	3	Expression of WNT related genes in human periodontal ligament cells during osteogenic differentiation
76	day 2	Mohd Haidil Akmal Bin Mahdan	2	BOND STRENGTH OF HEMA-FREE & HEMA CONTAINING SELF ETCH ADHESIVES UNDER PULPAL PRESSURE
77	day 3	Maheswari Kuppusamy	1	PERIOSTEAL ELEVATION IN RAT CALVARIUM USING DIFFERENT TITANIUM MESHES
78	day 1	Tadashi Hosoya	2	Mechanisms of inflammatory mediators suppression in rheumatoid synovial fibroblast by CDK4/6 inhibition."
79	day 2	Lodha Ena	2	Effect of functional monomers on Dentin demineralization.
80	day 1	Waka Yokoyama	1	Interaction between CCL25 and CCR9 might play important roles in the pathogenesis of rheumatoid arthritis

Important information.

From the next lecture series we would like to evaluate your understanding of the lectures every week as this course would be certified as one of formal lectures of the university. Please express your opinion and submit both the following questionnaire including your short comments on the contents of lecture at the end of each lecture:

Questionnaire

1. The name of the lecturer.
2. Your name and department.
3. Evaluation of the lecture

   The quality of the content of the lecture was

   (excellent, good, average, relatively poor, poor)

   The method of the presentations was

   (excellent, good, average, relatively poor, poor)

   Overall evaluation of your attitude (effort, motivation and commitment).

   (excellent, good, average, relatively poor, poor)

4. Your comments or questions to the lecturer.

   破骨細胞の分化や、それに関わる病気など
   多くの分子がでてきたが、図やグラフを用いて
   とてもくわしく説明してくださり興味深く
   聴講することができた。
   サイトカインなどとても複雑なものに対する
   研究アプローチの良い勉強になった。

Prof. F. Ishino, the GCOE Committee on International Education Programs

Prof. I. Morita, the GCOE Committee on Development of Young Scientists

Important information.

From the next lecture series we would like to evaluate your understanding of the lectures every week as this course would be certified as one of formal lectures of the university. Please express your opinion and submit both the following questionnaire including your short comments on the contents of lecture at the end of each lecture:

Questionnaire

1. The name of the lecturer.
2. Your name and department.
3. Evaluation of the lecture

The quality of the content of the lecture was

(excellent, good, average, relatively poor, poor)

The method of the presentations was

(excellent, good, average, relatively poor, poor)

Overall evaluation of your attitude (effort, motivation and commitment).

(excellent, good, average, relatively poor, poor)

4. Your comments or questions to the lecturer.

Thank you for enlighting us that the emerging concept of the osteoimmune system. That means the osteoblastogenesis and osteoclastogenesis are very related to each other.
I would like to know that such as anti-Rankl therapy can inhibit the bone resorption but meanwhile. If it also can promote the bone formation or not?

Prof. F. Ishino, the GCOE Committee on International Education Programs

Prof. I. Morita, the GCOE Committee on Development of Young Scientists

Questionnaire

1. The name of the presenter

   Miyajima Daisuke, Smriti Aryal A.C.,MD ABDULLA AL MASUD KHAN

2. Your name and department.

3. Questions and Comment to the presenter

Miyajima Daisuke

Harvard と UCSF との違いを中心に話してもらって、より興味深かった。研究室によるのかもしれないが、Harvard の雰囲気は UCSF に比べると日本に近いのかなという印象を受けた。

Smriti Aryal A.C.

Poster presentation での実際のやりとりを、詳しく述べてくれて面白かった。その場の状況がよく分かった。Harverd の在籍者が Asia 系の人が多いということを聞いて、驚いた。

MD ABDULLA AL MASUD KHAN

3者3様で Harderd の research day の報告をしていたが、MASUD さんは、Lecture の内容を中心に話してくれて、興味深かった。研究に役立つアドバイスが得られたのは、彼が一番多かった印象であった。

平成23年度

GCOEプログラム 実績報告書

CONTENTS

野田　政樹（分子薬理学分野）…… 36
田上　順次（う蝕制御学分野）…… 48
高柳　広（分子情報伝達学分野）…… 82
森田　育男（分子細胞機能学分野）…… 106
小村　健（顎口腔外科学分野）…… 120
春日井 昇平（インプラント・口腔再生医学分野）…… 144
須田　英明（歯髄生物学分野）…… 156
和泉　雄一（歯周病学分野）…… 178
柳下　正樹（硬組織病態生化学分野）…… 196
山口　朗（口腔病理学分野）…… 206
森山　啓司（顎顔面矯正学分野）…… 228
大川　淳（整形外科学分野）…… 250
宮坂　信之（膠原病・リウマチ内科学分野）…… 266
宗田　大（運動器外科学分野）…… 296
稲澤　譲治（分子細胞遺伝学分野）…… 324
三木　義男（分子遺伝分野）…… 348
石野　史敏（エピジェネティクス分野）…… 362
澁谷　浩司（分子細胞生物学分野）…… 374
小川　佳宏（分子代謝医学分野）…… 388
水島　昇（細胞生理学分野）…… 402
中川　一路（細菌感染制御学分野）…… 426

分子薬理学分野

野田 政樹

医歯学総合研究科・器官システム制御学系専攻
分子薬理学・教授

1）研究の課題名

主題1：骨芽細胞制御機構の解析

骨のリモデリングにおいては根幹となる骨形成を担う骨芽細胞の制御の機構を明らかにする必要がある。骨芽細胞の制御に関わる全身性の因子と局所性の因子のそれぞれにおける分子メカニズムはなお十分には明らかでない。そこで骨芽細胞の制御のメカニズムの解析を行い、分子の機能を明らかにすることは今後の新たな治療を開発する上でも基盤となる。したがって骨芽細胞の生体における制御についての検討を行い、beta adrenergic receptorのシグナルならびに細胞外基質の蛋白の相互作用の存在することを明らかにした（Proceedings of the National Academy of Sciences of the United States of America 2011）。また、nanogel によるBMPに基ずく骨量の制御を解析した結果、微小量BMPに対しPGEの受容体EP4の選択的顎にストが が骨形成の上で有用であることが明らかとなった。（Arthritis Rheum 2011）。

主題2：DOKに基づく破骨細胞の機能制御に関わる研究

骨吸収する破骨細胞はそのsignal制御に関わるレベルが骨量の決定に関わる。従って、シグナル制御のメカニズムの解明が課題となる。のメカニズムの解析として Dok-1 ならびにDok-2 がシグナルの伝達の上で、その担い手の一つであることを明らかにした（Journal of Cellular Physiology 2011）。

主題3：幹細胞による骨形成と骨吸収の共役に関わるメカニズム

骨のリモデリングにおいては、その形成および吸収のバランスが制御されるが、この平衡を担う分子の機構はまだなお十分に明らかではない。骨量の制御メカニズムの中で幹細胞による形成は重要である。Constitutively active pth/pthrp receptorが骨の幹細胞制御に関わる役割を明らかにした
（Journal of Cellular Physiology 2011）

2）

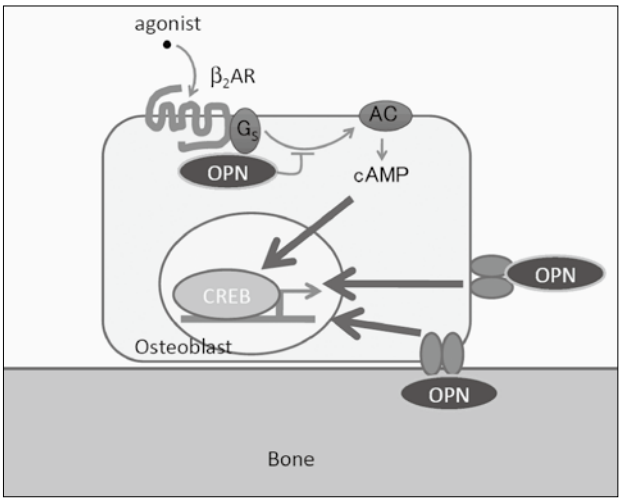

3）発表の研究内容についての英文要約

Bone mass is the important factor for the QOL as fractures in elder people deteriorate locomoter function and even affects life expectancy. Bone mass level is dependent on mechanism maintained by bone formation andbone resorption.With respect to bone resorption and bone formation, wehave identified that beta adrenergic receptor function is under the regulation of osteopontin. Osteopontin is a ECM protein and cytokine and has beenknown for its role, in the maintenance of bone mass. However, we identified that osteopontin is present in cells as well as outside the cells to be an regulatory factor in the mass of bone with respectto sympathetic tone dependent bone mass regulation. We have further identified nanogel to be supportive for EP4A and BMP induced bone formation as well. Furthermore, bone resorption analysis identified Dok-1 and 2 to be novel signaling factor for bone resorption.

4）本事業に関連して世界的な研究拠点形成に向けて、以下の点で改善・整備等されたこと

A（研究拠点体制）

若手教員ならびに これまでに選抜されたAISS大学院

生による研究体制が整えられた。

B（研究教育環境）

事業推進担当者ならびにシャペロンによる総合プレゼンテーションによる教育研究環境が整えられた。

C（人材確保）

国際公募による若手研究者が選抜された大学院生を教育するなど、優秀な人材が確保された。

D（人材育成）

若手研究者ならびに大学院生の中で英語による選抜で優れた者を選抜し、教育する体制が整えられた。

E（国際化）

大学院生が国際的に成果を発信しGCOEの中で国際的な研究者との交流に基づく活動が行われた。

5）GCOE事業を推進するに当たって力を入れた点

歯と骨の領域の世界最高水準の研究を推進する為に若手教育を中心としつつ、事業推進担当者同士の研究体制がInnovation研究費によって整えられると共に選抜大学院生と共に研究を推進する体制が整えられた。

6）英文原著論文

1. Masashi Nagao, Timothy Feinstein, Youichi Ezura, Tadayoshi Hayata, Takuya Notomi, Yoshitomo Saita, Ryo Hanyu, Hiroaki Hemmi, Yayoi Izu, Shu Takeda, Kathryn Wang, Susan Rittling, Tetsuya Nakamoto, Kazuo Kaneko, Hisashi Kurosawa, Gerard Karsenty, David Denhardt, Jean-Pierre Vilardaga, Masaki Noda. Sympathetic control of bone mass regulated by osteopontin. Proceedings of the National Academy of Sciences of the United States of America; 108（43）：17767-72, 2011
2. Kamolratanakul P, Hayata T, Ezura Y, Kawamata A, Hayashi C, Yamamoto Y, Hemmi H, Nagao M, Hanyu R, Notomi T, Nakamoto T,Amagasa T, Akiyoshi K, Noda M. Nanogel-based scaffold delivery of prostaglandin E（2）receptor-specific agonist in combination with a low dose of growth factor heals critical-size bone defects in mice. Arthritis Rheum; 63（4）：1021-33, 2011
3. Hiroaki Hemmi, Neeha Zaidi, Bei Wang, Ines Matos, Christopher Fiorese, Ashira Lubkin, Lori Zbytnuik, Koji Suda, Kenneth Zhang, Masaki Noda, Tsuneyasu Kaisho, Ralph M. Steinman, and Juliana Idoyaga. Treml4, an Ig superfamily member, mediates presentation of several antigens to T cells in vivo, including protective immunity to HER2 protein. The Journal of Immunology; Epub ahead of print 2011
4. Nagao M, Saita,Y, Hanyu,R, Hemmi H, Notomi T Hayata T, Nakamoto T, Kaneko K, Kurosawa H, Ishii S, Ezura Y, Noda M. Schnurri-2 deficiency counteracts against bone loss induced by ovariectomy. Journal of Cellular Physiology;226：573-578, 2011
5. Kawamata A, Inoue A, Miyajima D, Hemmi H, Mashima R, Hayata T, Ezura Y, Amagasa T, Yamanashi Y, Noda M. Dok-1 and Dok-2 deficiency induces osteopenia via regulation of osteoclasts. Journal of Cellular Physiology; 226（12）：3087-93, 2011
6. Seo Sachiko, Nakamoto Tetsuya, Takeshita Masataka, Suzuki Takahiro, Ichikawa Motoshi, Noda Masaki, Ogawa Seishi, Honda Hiroaki, Oda Hideaki, Kurokawa Mineo. Cas-L regulates myeloid cell motility and suppresses progression of leukemia induced by p210Bcr/Abl. Cancer Science; 102（12）：2109-2117, 2011
7. Hanyu R, Hayata T, Nagao M, Saita Y, Hemmi H, Notomi T, Nakamoto T, Schipani E, Knonenbery H, Kaneko K, Kurosawa H, Ezura Y, Noda M. Per-1 is a specific clock gene regulated by parathyroid hormone（PTH）signaling in osteoblasts and is functional for the transcriptional events induced by PTH. Journal of Cellular Biochemistry;112：433-438, 2011
8. Kondo H, Ezura Y, Nakamoto T, Hayata T, Notomi T, Sorimachi H, Takeda S, Noda M. MURF1 deficiency suppresses unloading-induced effects on osteoblasts and osteoclasts to lead to bone loss. Journal of Cellular Biochemistry; 112（12）：3525-30, 2011
9. Morishita M, Ono N, Miyai K, Nakagawa T, Hanyu R, Nagao M, Kamolratanakul P, Notomi T, Rittling SR, Denhardt DT,Kronenberg HM, Ezura Y, Hayata T, Nakamoto T, Noda M. Osteopontin deficiency enhances parathyroid hormone/parathyroid hormone related peptide receptor（PPR）signaling-induced alteration in tooth formation and odontoblastic morphology. Tissue and Cell; 43：196-200, 2011
10. Yumoto K, Nifuji A, Rittling SR, Tsuchiya Y, Kon S, Uede T, Denhardt DT, Hemmi H, Nakamoto T, Notomi T, Hayata T, Ezura Y, Noda M. Osteopontin Deficiency Suppresses TNF-alpha-Induced Apoptosis in Chondrocytes. Cartilage; in press, 2011
11. Yayoi Izu, Yoichi Ezura, Fumitaka Mizoguchi, Aya Kawamata, Tetsuya Nakamoto, Kazuhisa Nakashima, Tadayoshi Hayata, Hiroaki Hemmi, Paolo Bonaldo, Masaki Noda. Type VI collagen deficiency induces osteopenia with distortion of osteoblastic cell morphology. Tissue and Cell; 44（1）：1-6, 2012
12. Ono N, Nakashima K, Schipani E, Hayata T, Ezura Y, Soma K, Kronenberg HM, Noda M. Constitutively active pth/pthrp receptor specifically expressed in osteoblasts enhances bone formation induced by bone marrow ablation. Journal of Cellular Physiology; 227（2）：408-15, 2012

7）特許取得、特許申請

野田政樹
　抗オステオポンチン抗体及びその用途/
　ANTI-OSTEOPONTIN AND USE THEREOF
秋吉一成、野田政樹
　骨形成促進物質とナノゲルを含有する骨形成用生体材料
　平成23年10月21日

8）平成24年3月までの自己評価

研究成果としては新たな骨量制御に関わる神経系とOPN分子の相互作用ならびに破骨細胞の機能制御に関わるDokを見出し、またこれらの関係を維持する為のメカニズムや幹細胞制御の機構が見出された。

また教育体制、研究体制がグローバルCOEの拠点として整えられたことが評価される。

9）学会発表（英文）

1. Ryo Hanyu, Masashi Nagao, Yoshitomo Saita, Hisashi Kurosawa, Kauzo, Kaneko, Masaki Noda, Anabolic action of PTH signaling on bone activated expression of a clock gene, Per-1, The 1st International Academy of Sportology, Tokyo, Japan, March 5, 2011
2. Masashi Nagao, Timothy N. Feinstein, Jan-Pierre Vilardaga, Masaki Noda, Sympathetic control of bone mass regulated by osteopontin, The 93rd Annual Meeting & Expo, Boston, MA, USA, June 4-7, 2011
3. Tadayoshi Hayata, Yoichi Ezura, Makoto Asashima, Ryuichi Nishinakamura, Masaki Noda, Inactivation of Dullard in the mouse limb and sternum displays reatrdatio of ossification in sdeletogenesis, KEY Forum in Developmental Biology and Regenerative Medicine-Supported by Global COE and IMEG, Kumamoto University, Kumamoto, Japan, September 8-9, 2011
4. Yoichi Ezura, Tadayoshi Hayata, Tetsuya Nakamoto, Takuya Notomi, Ichiro Sekiya, Takeshi Muneta, Masaki Noda, Identification of the Differentially Methylated Promoter and Intronic CpG Sites in the Human Synovium and Bone Marrow Derived Mesenchymal Stem Cells, The 33rd Annual Meeting of American Society for Bone and Mineral Research, San Diego, CA, USA, September 16 - 20, 2011
5. Tetsuya Nakamoto,Takayuki Motoyoshi, Makiri Kawasaki, Tomomi Sakuma, Tadayoshi Hayata, Yoichi Ezura, Masaki Noda, Molecular Mechanism of CIZ Actions to Exacerbate Inflammation in Serum-induced Arthritis Based on Formation of Positive Feedback Loop with IL-1 Beta, The 33rd Annual Meeting of American Society for Bone and Mineral Research, San Diego, CA, USA, September 16 - 20, 2011
6. Tadayoshi Hayata, Yoichi Ezura, Makoto Asashima, Ryuichi Nishinakamura, Masaki Noda, Dullard Is a Novel Common Negative Regulator of BMP Signaling in Osteoblasts and Chondrocytes Acting at Smad1 Level Independently of Caveolae-Proteasome Pathway, The 33rd Annual Meeting of American Society for Bone and Mineral Research, San Diego, CA, USA, September 16 - 20, 2011
7. Takuya Notomi, Miyuki Kuno, Yoichi Ezura, Masaki Noda, Opto-Functional Control of Intracellular RANKl Transport/Secretion in Osteoblasts to Enhance Coupling With Osteoclasts Based on Photo-Energy Conversion of Molecularly-Engineered Channel-Rhodopsin , The 33rd Annual Meeting of American Society for Bone and Mineral Research, San Diego, CA, USA, September 16 - 20, 2011
8. Masashi Nagao, Timothy N. Feinstein, Yoichi Ezura, Tadayoshi Hayata, Takuya Notomi, Yositomo Sait, Ryo Hanyu, Hiroaki Hemmi, Yayoi Izu, Shu Takeda, Kathryn X. Wang, Susan Rittling, Tetsuya Nakamoto, Kazuo Kaneko, Hisashi Kurosawa, Gerald Karsenty, David T. Denhardt, Jean-Pierre Vilardaga, Masaki Noda, Sympathetic Control of Bone Mass Regulated By Osteopontin, The 33rd Annual Meeting of American Society for Bone and Mineral Research, San Diego, CA, USA, September 16 - 20, 2011
9. Tomomi Sakuma, Tetsuya Nakamoto, Hiroaki Hemmi, Takuya Notomi, Tadayoshi Hayata, Yoichi Ezura, Teruo Amagasa, Masaki Noda, Role of CIZ in Melanoma Activity for Metastasis, The 33rd Annual Meeting of American Society for Bone and Mineral Research, San Diego, CA, USA, September 16 - 20, 2011
10. Smriti Aryal A.C , Kentaro Miyai, Tadayoshi Hayata, Yoichi Ezura, Takuya Notomi, Tetsuya Nakamoto, Tony Pawson, Shigeaki Kato, Masaki Noda, Nck, Actin Cytoskeleton Protein, Supports Osteoblastic Bone Increment and Suppresses Osteoclastic Bone Loss, The 33rd Annual Meeting of American Society for Bone and Mineral Research, San Diego, CA, USA, September 16 - 20, 2011
11. Daisuke Miyajima, Tadayoshi Hayata, Takafumi Suzuki, Yoichi Ezura, Tetsuya Nakamoto, Takuya Notomi, Teruo Amagasa, Ralph T Böttcher, Reinhard Fässler, Masaki Noda, Conditional Profilin1 Deficiency in Multiple Cell Linages of Mesenchyme Origin Based on Prx1-Cre System Severely Disrupts Axial and Appendicular Skeletal Development, The 33rd Annual Meeting of American Society for Bone and Mineral Research, San Diego, CA, USA, September 16 - 20, 2011
12. Suzuki T, Notomi T, Miyajima D, Ezura Y, Nakamoto T, Hayata T, Mizuno A, Suzuki M, Mizoguchi F, Izumi Y, Noda M , TRPV4 Deficiency Suppresses Fluid Flow Induced Activation of Calcium Oscillation in a Manner

Dependent on Osteoblastic Differentiation, The 33rd Annual Meeting of American Society for Bone and Mineral Research, San Diego, CA, USA, September 16 - 20, 2011

13. Chiho Watanabe, Masahiro Morita, Yoichi Ezura, Tetsuya Nakamoto, Tadayoshi Hayata, Hiroaki Hemmi, Takuya Notomi, Keiji Moriyama, Tadashi Yamamoto, Masaki Noda, Cnot3, a Crucial Factor of mRNA Stability, Controls Osteoblastic Differentiation, The 33rd Annual Meeting of American Society for Bone and Mineral Research, San Diego, CA, USA, September 16 - 20, 2011
14. Makiri Kawasaki, Tetsuya Nakamoto, Takuya Notomi, Tadayoshi Hayata, Yoichi Ezura, Masaki Noda, Expression of Ift88, a Cilia Component Gene, is Under Temporal Regulation Along with the Differentiation of Chondrocytic Cell Line ATDC5, The 33rd Annual Meeting of American Society for Bone and Mineral Research, San Diego, CA, USA, September 16 - 20, 2011

10）学会発表（和文）

1. 佐久間朋美、中元哲也、宮井健太郎、辺見弘明、納富卓也、早田匡芳、江面陽一、天笠光雄、野田政樹 悪性黒色腫細胞の転移におけるCIZの促進的作用第65回NPO法人日本口腔科学会学術集会　4月21日-22日, 2011　東京、日本
2. 宮嶋大輔、天笠光雄、野田政樹　四肢－胸郭間葉系細胞におけるProfilin1欠失マウスは重度骨格形成不全を示す　Profilin1-deficient mice in limb-thoracis mesenchyme exhibit severe defects in skeletal development　第56回（社）日本口腔外科学会総会・学術大会　10月21日-23日, 2011　大阪　日本

11）外部資金の獲得状況

グローバルCOE プログラム

研究題目：歯と骨の分子疾患科学の国際教育研究拠点－デント・メドミクスのインテリジェンスハブ－

代表：野田政樹

2008年－2012年

研究費　281,811 千円（2011年度分）

日本学術振興会研究費補助金（萌芽）

研究題目：顎骨形成促進への新戦略の分子機構研究

代　　表：野田政樹

期　　間：2011-2012年

研 究 費：280万円

12）特別講演、招待講演

2011年

・野田政樹：米国細胞生物学会　2011年12月

演題：Control of Osteoblastic Function via Local and Central Mechanisms

13）主催学会

GCOE 国際シンポジウム・ワークショップ

14）新聞

2011年10月17日

骨粗鬆症　仕組み一部解明　朝日新聞

2011年10月19日

骨粗しょう症　原因物質を解明　日経産業新聞

2011年10月21日

運動刺激ないと骨委縮　関与分子の機能を特定　科学新聞

2011年10月25日

寝たきり等での骨萎縮　原因タンパクを特定

日本歯科新聞

15）GCOE総合講義のサマリー

骨の形成は局所因子と全身性因子の相互作用に基づく。この分子機構は細胞内および細胞外基質の分子が内分泌系および神経系の制御の総和として理解される。

16）教室、分野や講座の准教授、講師、助教、特別研究員、ポスドク、指導を受けた大学院生の名前

准 教 授	江面　陽一
助　　教	早田　匡芳
特任講師	中元　哲也（国際コーディネーター）
特任講師	納富　拓也（国際PI シャペロン）
大学院生	○宮嶋　大輔
	○鈴木　允文
	○渡辺　千穂
	○Smriti Ayral A. C.
	○白川　純平
	守屋　秀一
	川崎　真希理

○はAISS

The Science News 科学新聞
2011年（平成23年）10月21日（金曜日） 第3361号

運動刺激ないと骨萎縮 関与分子の機能を特定

東京医歯大 骨粗鬆症治療法開発期待

東京医科歯科大学難治疾患研究所分子薬理学分野・グローバルCOEプログラム「歯と骨の分子疾患科学国際教育研究拠点」の野田政樹教授、江面陽一准教授の研究グループは、ピッツバーグ大学、順天堂大学、ラトガース大学との共同研究で、骨の折れやすくなる病気〝骨粗鬆症〟を起こす、運動や重力刺激がないと骨の減る現象（廃用性骨萎縮）の原因が交感神経の骨芽細胞作用を仲介するオステオポンチン（OPN）によることを突き止めることに成功した。

骨粗鬆症が寝たきりや無重力の状態で急速に進行すること、また反射性交感神経性ジストロフィーにおける骨萎縮など、交感神経と骨との関わりが知られているが、骨の量の減少が交感神経の亢進のもとにいかに働くかという仕組みがわからなかった。このため、廃用性骨萎縮に対する有効な治療法は現在も見いだされていなかった。研究グループは、寝たきりによる廃用性骨萎縮が交感神経系のブロッカーにより抑制され、また同時に骨芽細胞の細胞外基質であるOPNの欠失が廃用性骨萎縮を抑止することを観察し、この知見に基づき、寝たきり等による廃用性骨萎縮の交感神経系の作用において、OPNがその仲介をなす重要な分子であることがわかった。この発見により、OPNに対する抑止薬の開発を含め、廃用性骨萎縮に関わる治療への道が開かれたとしている。

今後、日本で急増している骨粗鬆症の中でも特に、循環器疾患ならびに神経系疾患等による、運動機能低下に伴う廃用性骨萎縮に対する病態のさらなる解明と新規治療法への開発が期待できるとしている。

日経産業新聞 2011年（平成23年）10月19日（水曜日）

骨粗しょう症

原因物質を解明

東京医科歯科大 マウスで実験

東京医科歯科大学の野田政樹教授らは、骨粗しょう症のうち、運動をしない時や無重力時に骨が減少する「廃用性骨萎縮」の原因物質を突き止めた。この原因物質をなくしたマウスで実験したところ、骨が減らないことを確認した。骨の減少時にはこの原因物質が増殖しており、発生を抑える治療薬の開発へと研究を進める考えだ。

順天堂大学、米コロンビア大学などとの共同研究による成果。廃用性骨萎縮に関与していたのは、オステオポンチン（OPN）と呼ぶ物質で、人間の体内では骨と細胞をつなぐ役割を担う。

通常のマウスとOPNをなくしたマウスを用意し、人工ホルモンの「イソプロテレノール」を与えて交感神経を刺激したところ、通常のマウスで骨の減少がみられた。一方、OPNをなくしたマウスでは、骨の減少がみられなかった。交感神経がOPNを増加させ、骨を減少させているという。

野田教授によると、足が不自由になって寝たきりになると、人間は多大なストレスを受ける。このストレスが交感神経を刺激。OPNが増加して、骨の減少を進行させているとみられ、体を動かさないと骨が減る仕組みが分かったという。

OPNは骨粗しょう症以外の病気とも関係する。がん細胞は自らOPNを作り出し、OPNががんの転移を促していることが既に明らかになっている。

朝日新聞
2011年（平成23年）10月17日 月曜日

骨粗鬆症 仕組み一部解明

運動しないと骨が弱くなるのは、交感神経と骨を結ぶたんぱく質の働きが原因だと、東京医科歯科大の野田政樹教授らのチームが明らかにした。このたんぱく質を抑えられれば、骨粗鬆症（こつそしょうしょう）の安価な治療薬ができる可能性があるという。

チームは、マウスに薬を与えて交感神経を刺激すると「オステオポンチン」というたんぱく質が増えて骨が減り、オステオポンチンがないマウスでは交感神経を刺激して活性化させても骨が減らないことを実験で確かめた。研究成果は米科学アカデミー紀要（電子版）に掲載された。

日本歯科新聞
2011年（平成23年）10月25日（火曜日）

寝たきり等での骨萎縮

原因タンパクを特定

東医歯大 野田教授らの研究で

寝たきりによる骨萎縮の原因は、交感神経の骨芽細胞作用を仲介するタンパク質「オステオポンチン（OPN）」にあるー。東京医科歯科大学難治疾患研究所分子薬理学分野（野田政樹教授）のグローバルCOEプログラム「歯と骨の分子疾患科学国際教育研究拠点」の研究グループが、順天堂大学と、米国のピッツバーグ大学、ラトガース大学、コロンビア大学の3大学と共同研究で骨と神経を結ぶ分子の機能を明らかにした。OPNを制御することで骨萎縮を防げることが示された。

これまで、寝たきりや無重力の状態で骨粗鬆症が進行することや、反射性交感神経ジストロフィーにおける骨萎縮など、神経と骨の関わりは知られていた。しかし、骨減少のメカニズムが分からなかったために、有効な治療法が見いだせなかった。

野田教授らは、寝たきり等で起こる廃用性骨萎縮が交感神経系のブロッカーにより抑制され、同時に骨芽細胞の細胞外基質OPNの欠失が廃用性骨萎縮を抑止することを観察。

マウスを使った実験で、「OPN欠失が交感神経による骨量減少および骨形成低下を抑制する」や、「抗OPN抗体で骨減少が抑えられる」、「細胞内信号伝達物質サイリックAMPをOPNが制御する」、「OPNは交感神経の細胞制御を調節する」ことなどを発見。廃用性骨萎縮の交感神経系の作用においてOPNが重要な仲介分子であることが判明した。

野田教授はこれらの発見の意義について「OPNに対する抑止薬の開発を含め、廃用性骨萎縮に関わる治療への道が開かれた。研究をさらに発展させることで、日本で急速に増加している骨粗鬆症の中でも特に、循環器疾患や神経系疾患等の全身性疾患による運動機能低下に伴う廃用性骨萎縮病態の解明と治療法開発が期待できる」と説明する。

Sympathetic control of bone mass regulated by osteopontin

Masashi Nagao[a,b,c,1], Timothy N. Feinstein[d,1], Yoichi Ezura[a,c,e,f], Tadayoshi Hayata[a,c], Takuya Notomi[a,c], Yoshitomo Saita[b], Ryo Hanyu[a,b,c], Hiroaki Hemmi[a,c,g], Yayoi Izu[a], Shu Takeda[c], Kathryn Wang[h], Susan Rittling[i], Tetsuya Nakamoto[a,c], Kazuo Kaneko[b], Hisashi Kurosawa[b], Gerard Karsenty[j], David T. Denhardt[h], Jean-Pierre Vilardaga[d,2], and Masaki Noda[a,c,e,f,g,2]

[a]Department of Molecular Pharmacology, Medical Research Institute, and [c]Global Center of Excellence Program, International Research Center for Molecular Science in Tooth and Bone Diseases, Tokyo Medical and Dental University, 1-5-45 Yushima, Bunkyo-ku, 113-8510 Tokyo, Japan; [b]Department of Orthopedics, School of Medicine, Juntendo University, 2-1-1 Hongo, Bunkyo-ku, 113-8421 Tokyo, Japan; [g]Medical Top Track Program, Medical Research Institute, Tokyo Medical and Dental University, 1-5-45 Yushima, Bunkyo-ku, 113-8510 Tokyo, Japan; [h]Department of Cell Biology and Neuroscience, Rutgers, The State University of New Jersey, Piscataway, NJ 08701; [i]Forsyth Institute, Boston, MA 02115; [j]Department of Genetics and Development, College of Physicians and Surgeons, Columbia University, New York, NY 10032; [e]Advanced Bone and Joint Science Program, Tokyo Medical and Dental University, 1-5-45 Yushima, Bunkyo-ku, 113-8510 Tokyo, Japan; [f]Hard Tissue Genome Research Center, Tokyo Medical and Dental University, 1-5-45 Yushima, Bunkyo-ku, 113-8510 Tokyo, Japan; and [d]Laboratory for GPCR Biology, Department of Pharmacology and Chemical Biology, School of Medicine, University of Pittsburgh, Pittsburgh, PA 15261

Edited by Harvey Cantor, Dana-Farber Cancer Institute, Boston, MA, and approved September 8, 2011 (received for review June 13, 2011)

The sympathetic nervous system suppresses bone mass by mechanisms that remain incompletely elucidated. Using cell-based and murine genetics approaches, we show that this activity of the sympathetic nervous system requires osteopontin (OPN), a cytokine and one of the major members of the noncollagenous extracellular matrix proteins of bone. In this work, we found that the stimulation of the sympathetic tone by isoproterenol increased the level of OPN expression in the plasma and bone and that mice lacking OPN (OPN-KO) suppressed the isoproterenol-induced bone loss by preventing reduced osteoblastic and enhanced osteoclastic activities. In addition, we found that OPN is necessary for changes in the expression of genes related to bone resorption and bone formation that are induced by activation of the sympathetic tone. At the cellular level, we showed that intracellular OPN modulated the capacity of the β2-adrenergic receptor to generate cAMP with a corresponding modulation of cAMP-response element binding (CREB) phosphorylation and associated transcriptional events inside the cell. Our results indicate that OPN plays a critical role in sympathetic tone regulation of bone mass and that this OPN regulation is taking place through modulation of the β2-adrenergic receptor/cAMP signaling system.

osteoporosis | G protein-coupled receptor | osteoblast

Bone formation and bone resorption require a tight regulation of the two facets of bone metabolism: new bone deposition by osteoblasts and bone resorption by osteoclast cells. Pathologic bone loss and bone accumulation disorders are nearly always caused by dysregulation of this balance, either toward bone accumulation (e.g., osteopetrosis) or bone loss (e.g., osteopenia or osteoporosis). The most common disorder of bone loss, osteoporosis, contributes to a high fracture risk and challenges quality of life and longevity of affected populations such as the elderly and postmenopausal women (1). Osteoporosis can also develop after prolonged inactivity or weightless space travel because of the loss of mechanical stress stimuli that promote anabolic bone remodeling and inhibit resorption (2–4). Unlike bone loss from unloading and inactivity, postmenopausal osteoporosis is characterized by both an increase in bone formation as well as a relatively greater increase in bone resorption, and bone deterioration therefore proceeds more slowly. The primary regulators of bone metabolism include hormones such as parathyroid hormone (PTH) and parathyroid hormone-related protein (PTHrP), inflammatory and anti-inflammatory cytokines, and the sympathetic tone of the nervous system, which regulates bone mass through neurotransmitters such as epinephrine and norepinephrine via innervation of bone cells (5, 6). As in the case of disuse (unloading) osteoporosis, bone loss through the sympathetic tone is characterized by stimulation of bone resorption and suppression of bone formation (7). Conversely, inhibition of the sympathetic tone by β-blockers suppresses unloading-induced bone loss by suppressing bone resorption and enhancing bone formation (8). Nonetheless, the mechanism by which the sympathetic tone regulates bone catabolism remains largely unknown.

Osteopontin (OPN), a major member of the noncollagenous extracellular matrix secreted by osteoblasts and a cytokine involved in proliferation, apoptosis, and inflammatory signaling, has been implicated in bone remodeling after mechanical stress (9). Indeed, OPN-deficient mice show both increased deposition and reduced resorption of bone after unloading (10–12). In terms of the control of bone metabolism, the OPN-KO phenotype therefore phenocopies treatment with β-blockers. Here, we hypothesize that OPN serves as a molecular link between the sympathetic tone and bone metabolism. Using a combination of mouse KO studies and cell-based assays, we find that intracellular OPN acts by modulating activity of the β2-adrenergic receptor (β2AR), a G protein-coupled receptor (GPCR) expressed in osteoblasts and involved in regulation of bone resorption in response to the activity of sympathetic nerves (7). This study thus suggests that intracellular OPN links bone to the sympathetic tone via regulation of the β2AR signaling cascade.

Results

OPN is necessary for bone loss mediated by a sympathomimetic ligand. To determine whether the sympathetic nervous system influences expression of OPN, we measured the level of circulating OPN after injection of isoproterenol (ISO), a sympathomimetic ligand, or saline vehicle into the peritoneum of mice of two different strains. ISO treatment increased plasma OPN in both 129sv mice (Fig. 1*A*) and C57BL/6 mice (Fig. 1*B*). This increase originated, at least in part, from bone, where an increase in OPN mRNA expression was also detected in response to ISO (Fig. 1*C*).

MEDICAL SCIENCES

Author contributions: M. Nagao, T.N.F., J.-P.V., and M. Noda designed research; M. Nagao, T.N.F., Y.E., T.H., T. Notomi, Y.S., R.H., H.H., Y.I., and J.-P.V. performed research; S.T., K.W., S.R., T. Nakamoto, K.K., H.K., G.K., and D.T.D. contributed new reagents/analytic tools; J.-P.V. and M. Noda analyzed data; and J.-P.V. and M. Noda wrote the paper.

The authors declare no conflict of interest.

This article is a PNAS Direct Submission.

[1]M. Nagao and T.F. contributed equally to this work.

[2]To whom correspondence may be addressed. E-mail: noda.mph@mri.tmd.ac.jp or jpv@pitt.edu.

This article contains supporting information online at www.pnas.org/lookup/suppl/doi:10.1073/pnas.1109402108/-/DCSupplemental.

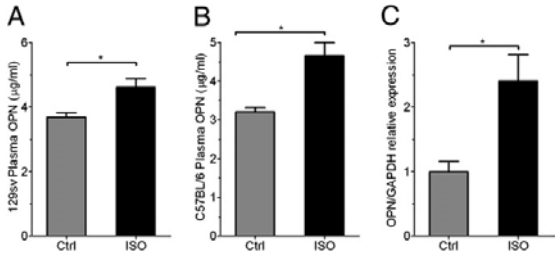

Fig. 1. ISO treatment up-regulates OPN levels in bone and circulation. (*A* and *B*) OPN protein expression in circulation for both 129sv (*A*) and C57B/L6 (*B*) mice in response to ISO treatment. (n = 3–4 per group, $*P < 0.05$.) (*C*) OPN mRNA expression in bone in vivo in response to ISO treatment, normalized to GAPDH mRNA expression. Results are in arbitrary units as mean ± SEM of n = 4 ($*P < 0.05$).

We next examined bone structure and bone mass after injection of ISO into OPN-deficient (OPN-KO) and WT mice. Microcomputed tomography (μCT) analyses of long bone showed a reduction in crowdedness of trabecular bone after ISO injection in WT mice (Fig. 2 *A* vs. *B*) but not in OPN-KO mice (Fig. 2 *C* vs. *D*). Quantification indicated that ISO significantly reduced bone mass [bone volume/tissue volume (BV/TV)] and trabecular number in WT mice, whereas ISO injection into OPN-KO mice had no effect (Fig. 2 *E* and *G*). ISO treatment also enhanced the levels of trabecular separation (Fig. 2*F*) and trabecular spacing (Fig. 2*H*) in WT but not in OPN-KO mice. This observation was not limited to long bone because similar effects were observed in vertebrae (Fig. 2 *I–L*), where ISO significantly reduced BV/TV in WT but not in OPN-KO mice (Fig. 2*M*). As was the case with long bone, OPN deficiency also reduced the effect of ISO on structural parameters in vertebral bone such as trabecular number (Fig. 2*O*), trabecular separation (Fig. 2*N*), and trabecular spacing (Fig. 2*P*). Thus, OPN is necessary for ISO-induced bone loss in both vertebral and long bones. ISO treatment increased OPN expression in cultured bone, indicating that the catabolic effect of ISO on bone is most likely mediated by direct control of OPN expression (Fig. S1).

Sympathetic nervous tone requires OPN to increase osteoclast activity and to decrease osteoblast activity. We next examined whether OPN mediates ISO-induced bone resorption by increasing osteoclastic activity, decreasing osteoblast activity, or both. Administration of ISO in WT mice increased both histomorphometric and biochemical parameters of bone resorption, including the number of osteoclasts, the levels of bone surface covered by tartrate-resistant acid phosphatase-positive ($TRAP^+$) cells (osteoclast surface per bone surface) (Fig. 3 *A–D*), and urine levels of deoxypyridinoline, a marker of systemic bone destruction that reflects collagen degradation mediated by osteoclastic activity

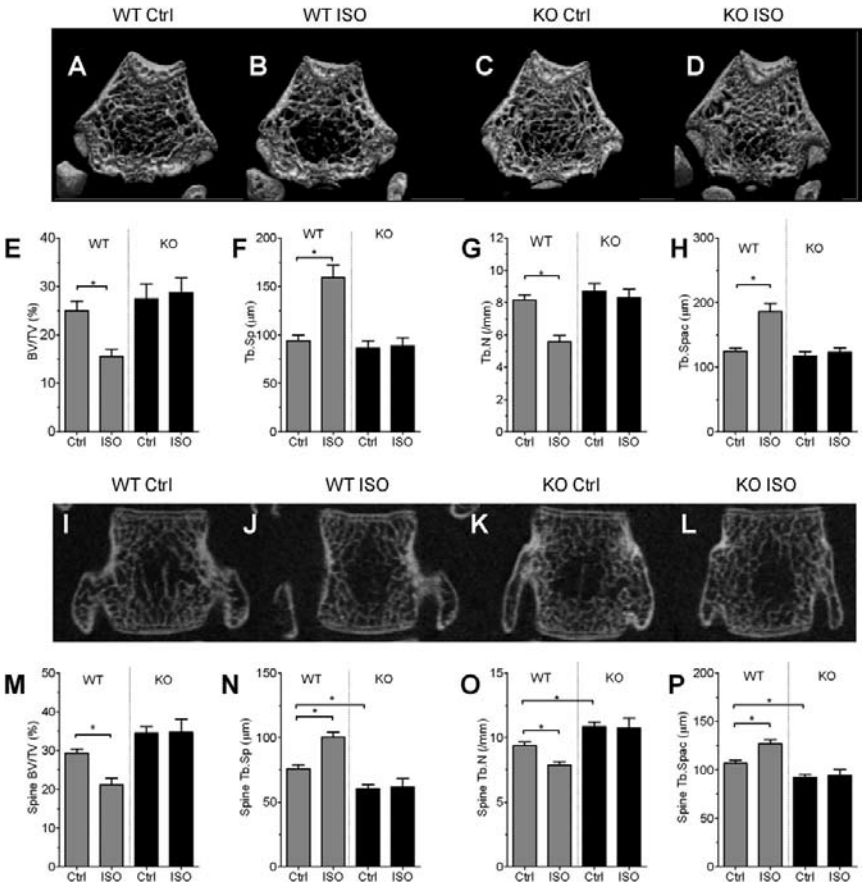

Fig. 2. OPN deficiency suppresses ISO-induced bone loss. (*A–D*) Representative 3D-μCT images of the distal metaphyseal regions of femora in vehicle (*A* and *C*) and ISO treatment (*B* and *D*) groups of WT (*A* and *B*) and OPN-KO (*C* and *D*) mice. (*E–H*) Bone parameters measured from data shown in *A–D*. (*E*) BV/TV. (*F*) Trabecular separation (Tb.Sp). (*G*) Trabecular number (Tb.N). (*H*) Trabecular spacing (Tb.Spac). Data represent the mean ± SEM of n = 7–8 mice per group ($*P < 0.05$). (*I–L*) Representative 2D-μCT images of vertebrae in mice treated with vehicle (*I* and *K*) and ISO treatment (*J* and *L*) groups of WT (*I* and *J*) and OPN-KO (*K* and *L*) mice. (*M–P*) Bone parameters measured from data shown in *I–L*. (*M*) BV/TV. (*N*) Trabecular separation (Tb.Sp). (*O*) Trabecular number (Tb.N). (*P*) Trabecular spacing (Tb.Spac). Data represent the mean ± SEM of n = 7–8 mice per group ($*P < 0.05$).

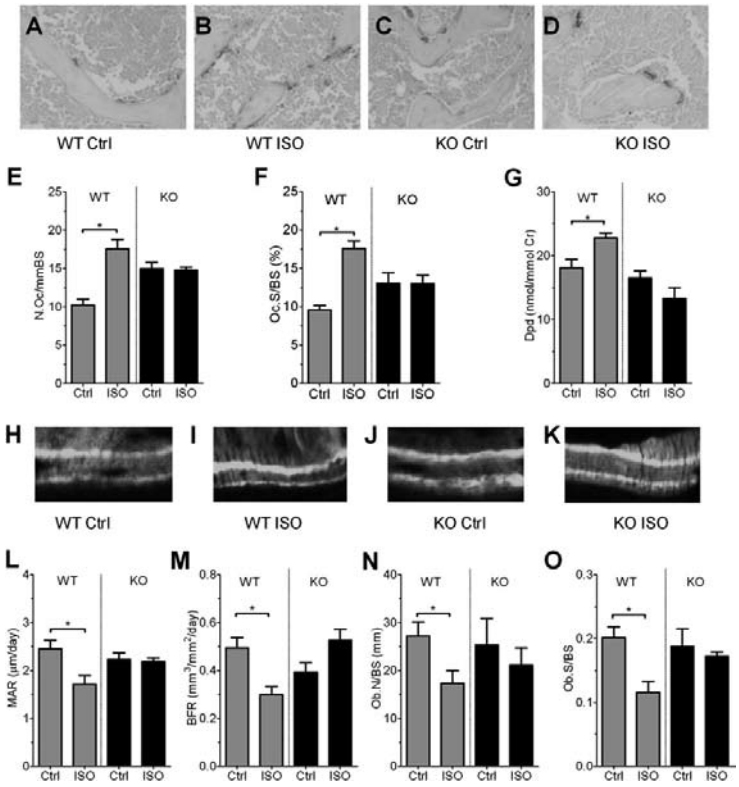

Fig. 3. OPN control of the inhibitory effect of ISO on bone remodeling. (*A–D*) Secondary trabecular regions of the epiphyses of tibiae were examined for osteoclasts based on TRAP staining in vehicle (*A* and *C*) and ISO treatment (*B* and *D*) groups of WT (*A* and *B*) and OPN-KO (*C* and *D*) mice. (*E–G*) Parameters of osteoclast activity. Number of osteoclasts per bone surface (N.Oc/BS) (*E*), osteoclast surface per bone surface (Oc.S/BS) (*F*), and urinary deoxypyridinoline (Dpd) (*G*) excretion levels are shown. Bars represent the mean ± SEM of n = 5–9 mice per group (*$P < 0.05$). (*H–K*) Bone formation activity was evaluated in vivo as described in *Materials and Methods*. Calcein bands were visualized to obtain dynamic histomorphometric parameters. (*L–O*) Parameters of osteoblast activity. Levels of mineral apposition rate (MAR) (*L*), bone formation rate (BFR) (*M*), osteoblast number (Ob.N/BS) (*N*), and osteoblast surface (Ob.S/BS) (*O*) are shown. Bars represent the mean ± SEM of n = 5 mice per group (*$P < 0.05$).

(Fig. 3 *A*, *B*, and *E–G*, gray bars). OPN deficiency suppressed the stimulatory effect of ISO on all parameters of bone resorption (Fig. 3 *C–G*, black bars). However, the slightly higher osteoclast number and osteoclast surfaces in OPN-KO compared with WT mice at baseline ($P < 0.01$) could hide some but not all of the changes that would be caused by ISO injection (e.g., Fig. 3 *E* and *F*). Despite the uncertainty in differentiating the effect of ISO injection and OPN deficiency on osteoclast number and surface, the data indicate without ambiguity that OPN is necessary for ISO-induced increases in systemic bone resorption activity.

We next compared osteoblastic activity in WT and OPN-KO mice treated with ISO. The basal level of mineral apposition rate (MAR), a parameter that reflects individual osteoblast-mediated bone formation, was similar in WT and OPN-KO mice (Fig. 3 *H*, *J*, and *L*, control). After ISO treatment, the MAR level in WT mice decreased significantly; this decrease was not observed in OPN-KO mice (Fig. 3 *K* and *L*). The bone formation rate was decreased by ~40% in response to ISO in WT but not in OPN-KO mice (Fig. 3*M*), paralleling the decrease of MAR. Osteoblast number per bone surface and osteoblast surface per bone surface were suppressed by ISO in WT but not in OPN-KO mice (Fig. 3 *N* and *O*). These data indicate that sympathetic nervous tone requires OPN to decrease bone mass both by way of increased osteoclast activity and by decreased osteoblast activity.

OPN is necessary for sympathetic tone-associated osteoclast development in vitro. Given the stimulatory effect of ISO on osteoclast activity of WT mice, we next examined whether OPN regulates osteoclast development by the sympathetic tone. To this end, we used bone marrow cells taken from mice after injection of saline vehicle or ISO and cultured in the presence of vitamin D_3 (10 nM) and dexamethasone (100 nM). ISO treatment in vivo resulted in an increase in $TRAP^+$ cells in bone marrow cultures from WT mice (Fig. 4*A*, gray bars, $P < 0.05$), reflecting a higher osteoclastic activity. In contrast, OPN deficiency did not statistically increase baseline osteoclast number ($P = 0.075$) but did prevent ISO-induced enhancement of osteoclast development in cultured bone marrow cells from ISO-treated mice (Fig. 4*A*, black bars). These data indicate that OPN directly mediates the development of osteoclasts in response to increased sympathetic activity.

OPN is necessary for sympathetic tone-induced gene expression in bone. To examine the effects of OPN deficiency on the sympathetic tone-induced changes in gene expression in bone cells in vivo, we compared mRNA from bones of mice treated with either vehicle or ISO. ISO injections increased the mRNA level of TRAP (Fig. 4*B*), a representative osteoclast marker, and conversely reduced the basal level of Runx2, an important transcription factor for osteoblastogenesis, in WT mice but not in

MEDICAL SCIENCES

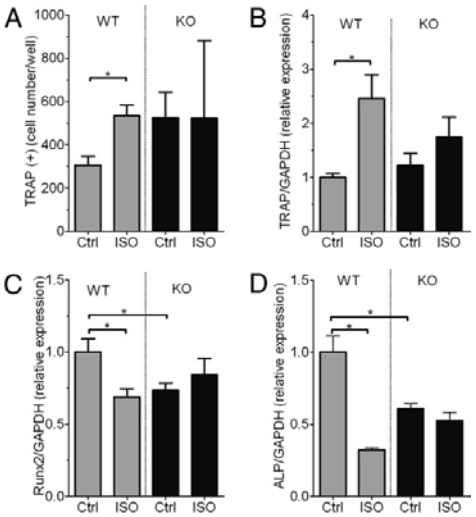

Fig. 4. OPN deficiency suppresses ISO-induced osteoclast development and changes in mRNA expression. (*A*) Bone marrow cells obtained from WT and OPN-KO mice treated with ISO or saline vehicle (Ctrl) were cultured in the presence of vitamin D and dexamethasone to determine osteoclast development ($TRAP^+$ multinucleated cells). Bars represent the mean ± SEM of $n = 5$ mice per group (*$P < 0.05$). (*B–D*) Gene expression in bone samples from WT and OPN-KO mice. Expression of TRAP (*B*), Runx2 (*C*), and alkaline phosphatase (ALP) (*D*), all normalized to GAPDH mRNA expression, in bone samples from WT and OPN-KO mice. Results are expressed in arbitrary units as mean ± SEM of $n = 5$–6 per group (*$P < 0.05$).

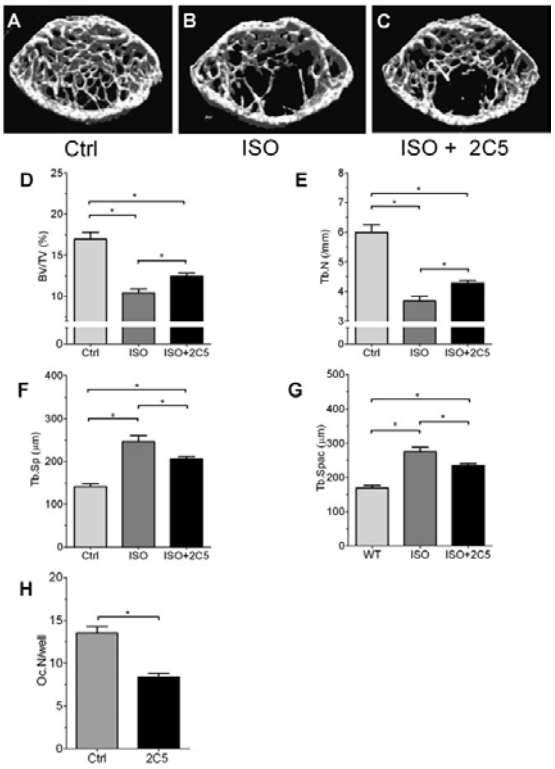

Fig. 5. Effects of neutralizing antibody against OPN on ISO-induced bone loss. (*A–C*) μCT analyses of WT proximal tibiae treated with or without 2C5. (*D–G*) Structural parameter analysis of the tibiae. (*D*) BV/TV. (*E*) Trabecular number (Tb.N). (*F*) Trabecular separation (Tb.Sp). (*G*) Trabecular spacing (Tb.Spac). (*H*) In vitro reduction of osteoclast development by anti-OPN antibody, 2C5 (*$P < 0.05$).

OPN-KO mice (Fig. 4 *B* and *C*). ISO also induced suppression of alkaline phosphatase transcripts in WT mice to a significantly greater degree than in OPN-KO mice (Fig. 4*D*). These observations indicate that OPN is necessary for changes in the expression of genes related to bone resorption and bone formation that are induced by activation of the sympathetic tone.

Extracellular and intracellular OPN contribute to bone mass regulation by ISO. Given that OPN can act as an extracellular cytokine and as an intracellular signaling molecule (13, 14), we next used a specific and neutralizing anti-OPN monoclonal antibody (named 2C5) to differentiate the extra- and intracellular actions of OPN (13). In WT mice, treatment with 2C5 weakly attenuated (by less than 25%) the reduction of bone mass (BV/TV) induced by ISO (Fig. 5 *A–D*). This small attenuation of ISO-induced alteration in bone architectural parameters was also observed in trabecular bone number (Fig. 5*E*). The effect of ISO on the enhancement of trabecular separation and trabecular spacing was also weakly attenuated by 2C5 (Fig. 5 *F* and *G*). These modest attenuations contrast with the strong inhibitory effect of 2C5 in the number of osteoclasts in monolayer culture (Fig. 5*H*), indicating that the antibody effectively neutralized extracellular OPN. These results indicate that circulating OPN contributes only part of the protein's regulatory effect on bone metabolism.

Intracellular OPN regulates transcriptional events mediated by the β2AR. Given that activation of β2AR in osteoblasts contributes to bone remodeling (7), we next tested whether OPN directly regulates β2AR signaling. We addressed this hypothesis by using several lines of experiment.

We first examined whether depletion of OPN by siRNA (as shown in Fig. S2) influences the capacity of ISO to stimulate cAMP production in MC3T3-E1 cells. To do so, we measured the time course of ISO-mediated cAMP production in individual cells with a FRET-based biosensor, epac-CFP/YFP, which has been previously described (15). In this assay, a single cell under study is continuously superfused with either control buffer or ligand. This condition thus excludes the existence of secreted extracellular OPN. Addition of ISO (10 μM) caused a fast increase in cAMP similar to that induced by forskolin (10 μM) (Fig. 6*A*). After this increase, the cAMP response was rapidly desensitized, even in the continuous presence of the ligand, consistent with previous reports (16, 17) (Fig. 6*A*, *Left*, control). The time course of cAMP generation was longer in cells depleted of OPN, and the integrated cAMP response for 30 min was significantly increased ($P < 0.01$) (Fig. 6*A*, si-OPN and bar graph). Conversely, overexpression of OPN (Fig. S2) reduced cAMP generation in response to ISO (10 μM) (Fig. 6*A*, *Right*, OPN). Blockade of secreted OPN action by exposing cells to a neutralizing OPN antibody did not affect the cAMP response to ISO (Fig. S3), thus suggesting that the effect of OPN overexpression is likely mediated by intracellular OPN. A slight but significant increase in basal cAMP was also observed in the absence of OPN expression (Fig. S4). Altogether, these data suggest that intracellular OPN does regulate cAMP production mediated by β2AR. Given that the absence of OPN had no effect on the capacity of forskolin (10 μM) to produce a maximal cAMP response, these data indicated that OPN modulates the time course of cAMP response by acting at the level of the receptor and/or the stimulatory G protein (G_S) rather than the adenylate cyclase effector molecule. Pull-down experiments did not indicate

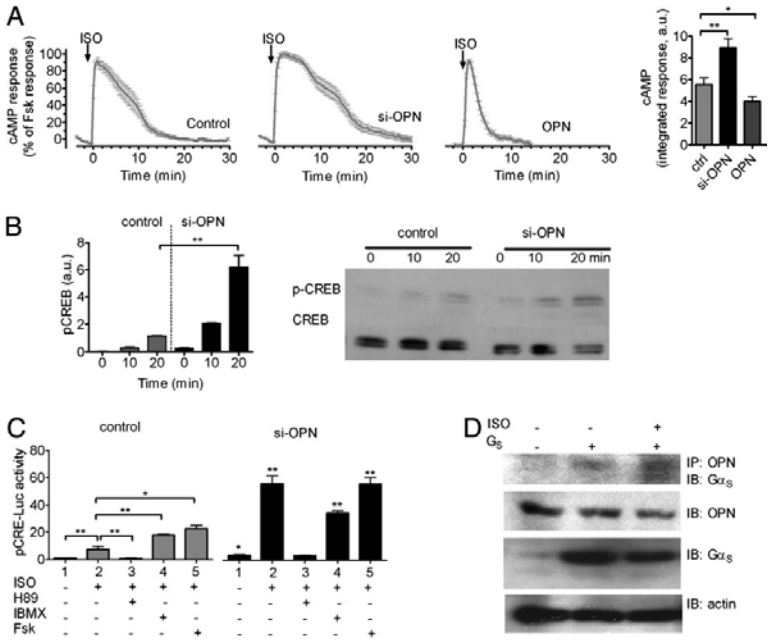

Fig. 6. OPN control of β2AR signaling. (*A*) Averaged cAMP responses mediated by ISO. cAMP induction over a 30-min time course was monitored by FRET changes from MC3T3 osteoblastic cells transiently expressing epac-CFP/YFP alone (control, *Left*) or in combination with si-OPN (*Center*) or overexpressing OPN (*Right*). Bars represent the average cAMP responses determined by measuring the area under the curve from 0 to 30 min for cAMP. Data represent the mean ± SEM of $n = 15$ (ctrl), $n = 28$ (si-OPN), and $n = 34$ (OPN). (*$P < 0.01$, **$P < 0.05$). (*B*) Western blot analyses of CREB phosphorylation in control and OPN-depleted MC3T3 cells in response to 10 μM ISO. Bars represent the mean ± SEM of $n = 3$ (**$P < 0.01$). (*C*) CRE-Luc activity (pCRE-Luc) in control cells (control) and cells transfected with si-OPN in response to 10 μM ISO with or without H89, IBMX, or forskolin (Fsk). siRNA for OPN enhanced the ISO-induced increase in the levels of luciferase activity, and H89, a PKA inhibitor, suppressed the enhancement. Bars represent the mean ± SEM of $n = 4$ (*$P < 0.05$, **$P < 0.01$). (*D*) Coimmunoprecipitation of GαS and OPN. Cells transfected with GαS in combination with Gβ1γ2 (G_S) and empty vector were challenged with carrier or with 10 μM ISO. OPN was immunoprecipitated with Sepharose beads conjugated to anti-C25 monoclonal antibody, and $G\alpha_S$ was detected with a polyclonal antibody against GFP ($n = 4$). IP, immunoprecipitation; IB, immunoblot detection.

association between OPN and the receptor but rather supported the existence of transient complexes of OPN and $G\alpha_S$ (Fig. 6*D*). However, detection of this complex required the use of a membrane-permeant cross-linker, dithiobis(succinimidyl) propionate, indicating a transient and potentially weak interaction. A low baseline interaction was detected when OPN and G_S were coexpressed, possibly reflecting constitutive interaction of a small fraction of OPN. Altogether, these data support a physical proximity of OPN to G_S inside the cell and suggest a role for intracellular OPN in regulating cAMP production mediated by the β2AR/G_S system.

We next tested whether OPN influences the downstream signaling of β2AR. To do so, we measured β2AR-mediated phosphorylation of a cAMP-dependent transcription factor called cAMP-response element binding (CREB) protein as well as transcription of genes controlled by the CRE regulatory element in MC3T3-E1 cells. ISO stimulated CREB protein phosphorylation to a moderate degree in control cells and to a significantly greater degree in cells depleted of OPN (Fig. 6*B*). This enhanced capacity of ISO to simulate CREB activity in the absence of OPN correlates with the effect of OPN on cAMP generation in the same cells (Fig. S5, *Left*). Similarly, depletion of OPN increased the changes in CRE-dependent gene expression as measured by a luciferase-based CRE reporter (CRE-Luc) (Fig. S5). Consistent with the involvement of the cAMP/PKA signaling pathway in the transcriptional regulation induced by ISO, no enhancement of ISO-induced luciferase activity was observed when OPN-specific siRNA transfected (si-OPN) cells were pretreated with H89, a specific PKA inhibitor (Fig. 6*C*, black bars, lane 2 vs. 3). Isobutylmethylxanthine (IBMX), an inhibitor of cAMP-specific phosphodiesterases, increased ISO-induced luciferase activity (Fig. 6*C*, gray bars, lane 2 vs. 4), and depletion of OPN increased luciferase activity still further (Fig. 6*C*, gray bar in lane 4 vs. black bar in lane 4). Forskolin, a direct activator of adenylate cyclases, had a similar effect (Fig. 6*C*, gray bar in lane 5 vs. black bar in lane 5). We further confirmed a role for OPN in regulating downstream signaling by β2AR in a mesenchymal cell line (C2C12; Fig. S6, lane 2 vs. lane 4). OPN thus inhibits CRE transcription in at least two different osteoblastic lineage cells. Interestingly, si-OPN alone slightly enhanced CRE-Luc activity in the absence of ISO in osteoblasts, similar to the increased baseline cAMP levels described above (Fig. 6*C*, gray bar in lane 1 vs. black bar in lane 1). Altogether, these data show that OPN inhibits both immediate and downstream signaling by β2AR and that OPN acts by interacting with G_S rather than with the receptor itself.

Discussion

Genetic studies have shown that the sympathetic nervous system controls bone mass by regulating local bone remodeling (7, 8). However, mechanisms that link the nervous system and bone metabolism remain poorly understood. Based on results obtained with genetic, physiological, and cell-based assays, we propose that OPN plays a key role in linking the sympathetic tone and the

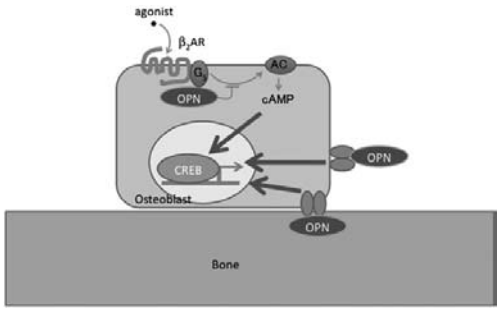

Fig. 7. Model of regulation of β2AR signaling by OPN. Our data suggest that intracellular OPN regulates β2AR signaling in osteoblasts by interacting with G_S to reduce the time course of cAMP production and CRE-dependent transcription activity to ultimately reduce bone mass. Extracellular OPN is also involved in regulation of bone cells by activation of CD44/integrin family of receptors.

MEDICAL SCIENCES

regulation of bone loss by regulation of cAMP signaling by the β2AR. First, sympathetic tone enhances OPN mRNA and protein levels in circulation and bone cells. Second, OPN is required for influence of the sympathetic tone on two aspects of bone metabolism, increased catabolic activity by osteoclasts and reduced anabolic activity by osteoclasts, resulting in decreased in bone mass. Third, OPN depletion enhances the capacity of β2AR agonists to stimulate cAMP production, CREB protein phosphorylation, and CRE-dependent luciferase activity in cultured mouse osteoblasts, whereas OPN overexpression has the inverse effect. It is notable that loss of OPN slightly increased basal cAMP as well as CRE-Luc activity even in the absence of agonist treatment. This observation would suggest that OPN reduces both ligand-dependent and -independent signaling by β2AR. The influence of OPN on bone metabolism is therefore at least partially attributable to direct regulation of β2AR signaling at the cellular level. These characteristics would make OPN a key player in the regulation of bone mass by the sympathetic tone. Given that OPN has an inhibitory effect on adrenergic receptors, the up-regulation of OPN expression in bone by the sympathetic tone could represent a unique feedback pathway to influence metabolic responses not only to agonists of the β2AR but also to other receptors.

Secreted OPN acts as a cytokine by binding extracellular domains of cell-surface receptors such as CD44 and $\alpha v\beta_3$ (18). Recent reports indicate that OPN is also present in the intracellular compartment, where it can act as a signaling molecule or a scaffold (13, 19, 20). With a perfusion system and a FRET-based cAMP assay, we were able to assess the action of OPN inside the cell. Given that OPN function is also detected inside the cell, it is therefore possible that intracellular as well as secreted OPN regulate ISO-induced cAMP signaling (Fig. 7). Thus, we have identified a functional interaction between the β2AR/G_S system and OPN that might modulate bone mass.

Materials and Methods

Animals. OPN-deficient male mice were produced as described (12). The original chimeric mice were backcrossed with 129 S1 mice to generate 129 mixed-background mice. Animals were backcrossed to the 129 strain to obtain isogenic mice. β2AR-deficient mice in the C57BL/6 background were produced as described (21). All animals were housed under controlled conditions at 25 °C on a 12-h light/12-h dark cycle. Experiments were approved by the animal welfare committee of the Tokyo Medical and Dental University. Mice were killed by overdose of pentobarbital.

FRET-Based cAMP Assay in Live Cells. This assay was performed with individual cells as previously described (22). In brief, cells plated on glass coverslips coated with poly-D-lysine and maintained in FRET buffer were placed on a Nikon Ti-E or Zeiss Axiovert 200 inverted microscope equipped with an oil-immersion 60 N.A. 1.49 plan-apo objective and a dichroic beam splitter to allow simultaneous recording of CFP and YFP fluorescence channels (DualView2; Photometrics or TILL Photonics). The emission fluorescence intensities were determined at 535 ± 15 nm (YFP) and 480 ± 20 nm (CFP) with a beam splitter DCLP of 505 nm. The FRET ratio for single experiments was corrected according to Eq. **1**:

$$Ratio\left(\frac{F_{YFP}}{F_{CFP}}\right)=\frac{F_{YFP}^{ex436/em535}-a\times F_{CFP}^{ex436/em480}-b\times F_{YFP}^{ex500/535}}{F_{CFP}^{ex436/em480}} \quad [1]$$

where $F_{YFP}^{ex436/em535}$ and $F_{CFP}^{ex436/em480}$ represent, respectively, the emission intensities of YFP (recorded at 535 nm) and CFP (recorded at 480 nm) upon excitation at 436 nm; *a* and *b* represent correction factors for the bleed-through of CFP into the 535-nm channel (*a* = 0.35) and the cross-talk attributable to the direct YFP excitation by light at 436 nm (*b* = 0.06). $F_{YFP}^{ex500/em535}$ represents the emission intensity of YFP (recorded at 535 nm) upon direct excitation at 500 nm and was recorded at the beginning of each experiment. Note that bleed-through of YFP into the 480-nm channel was negligible. For each measurement, changes in fluorescence emissions attributable to photobleaching were subtracted. To ensure that CFP- and YFP-labeled molecule expression were similar in examined cells, we performed experiments in cells displaying comparable fluorescence levels.

The means of FRET experiments were calculated according to Eq. **2**, which normalizes for different expression levels of CFP and YFP molecules:

$$N_{FRET}=\frac{F_{YFP}^{ex436/em535}-a\times F_{CFP}^{ex436/em480}-b\times F_{YFP}^{ex500/em535}}{\sqrt{F_{CFP}^{ex436/em480}\times F_{YFP}^{ex500/em535}}} \quad [2]$$

Note that, in the epac-CFP/YFP, the F_{CFP}/F_{YFP} ratio decreases upon generation of cAMP, but it is represented as a positive signal for convenience.

More details are included in *SI Materials and Methods*.

Statistical Evaluation. Data are expressed as mean ± SEM for all values. Statistical significance of the differences was evaluated based on Student's *t* test or two-way ANOVA.

ACKNOWLEDGMENTS. This work was supported by Grants-in-Aid 18109011, 18659438, 18123456, and 20013014 from the Japanese Ministry of Education (Global Center of Excellence Program, International Research Center for Molecular Science in Tooth and Bone Diseases), grants from the Japan Space Forum (to M. Noda), and National Institutes of Health Award R01DK087688 (to J.-P.V.).

1. Kanis JA, et al. (2003) The components of excess mortality after hip fracture. *Bone* 32: 468–473.
2. Lanyon L, Skerry T (2001) Postmenopausal osteoporosis as a failure of bone's adaptation to functional loading: a hypothesis. *J Bone Miner Res* 16:1937–1947.
3. Ehrlich PJ, Lanyon LE (2002) Mechanical strain and bone cell function: a review. *Osteoporos Int* 13:688–700.
4. Noda M, ed (2011) *Mechanosensing Biology* (Springer, Tokyo).
5. Raisz LG (2005) Pathogenesis of osteoporosis: concepts, conflicts, and prospects. *J Clin Invest* 115:3318–3325.
6. Karsenty G (2006) Convergence between bone and energy homeostases: leptin regulation of bone mass. *Cell Metab* 4:341–348.
7. Elefteriou F (2008) Regulation of bone remodeling by the central and peripheral nervous system. *Arch Biochem Biophys* 473:231–236.
8. Kondo H, et al. (2005) Unloading induces osteoblastic cell suppression and osteoclastic cell activation to lead to bone loss via sympathetic nervous system. *J Biol Chem* 280: 30192–30200.
9. Denhardt DT, Noda M, O'Regan AW, Pavlin D, Berman JS (2001) Osteopontin as a means to cope with environmental insults: regulation of inflammation, tissue remodeling, and cell survival. *J Clin Invest* 107:1055–1061.
10. Ishijima M, et al. (2001) Enhancement of osteoclastic bone resorption and suppression of osteoblastic bone formation in response to reduced mechanical stress do not occur in the absence of osteopontin. *J Exp Med* 193:399–404.
11. Ishijima M, et al. (2002) Resistance to unloading-induced three-dimensional bone loss in osteopontin-deficient mice. *J Bone Miner Res* 17:661–667.
12. Rittling SR, et al. (1998) Mice lacking osteopontin show normal development and bone structure but display altered osteoclast formation in vitro. *J Bone Miner Res* 13:1101–1111.
13. Shinohara ML, Kim JH, Garcia VA, Cantor H (2008) Engagement of the type I interferon receptor on dendritic cells inhibits T helper 17 cell development: role of intracellular osteopontin. *Immunity* 29:68–78.
14. Cantor H, Shinohara ML (2009) Regulation of T-helper-cell lineage development by osteopontin: the inside story. *Nat Rev Immunol* 9:137–141.
15. Nikolaev VO, Bünemann M, Hein L, Hannawacker A, Lohse MJ (2004) Novel single chain cAMP sensors for receptor-induced signal propagation. *J Biol Chem* 279:37215–37218.
16. Violin JD, et al. (2008) β2-adrenergic receptor signaling and desensitization elucidated by quantitative modeling of real time cAMP dynamics. *J Biol Chem* 283:2949–2961.
17. Feinstein TN, et al. (2011) Retromer terminates the generation of cAMP by internalized PTH receptors. *Nat Chem Biol* 7:278–284.
18. Wang KX, Denhardt DT (2008) Osteopontin: role in immune regulation and stress responses. *Cytokine Growth Factor Rev* 19:333–345.
19. Diao H, et al. (2004) Osteopontin as a mediator of NKT cell function in T cell-mediated liver diseases. *Immunity* 21:539–550.
20. Shinohara ML, Kim HJ, Kim JH, Garcia VA, Cantor H (2008) Alternative translation of osteopontin generates intracellular and secreted isoforms that mediate distinct biological activities in dendritic cells. *Proc Natl Acad Sci USA* 105:7235–7239.
21. Chruscinski AJ, et al. (1999) Targeted disruption of the β2 adrenergic receptor gene. *J Biol Chem* 274:16694–16700.
22. Ferrandon S, et al. (2009) Sustained cyclic AMP production by parathyroid hormone receptor endocytosis. *Nat Chem Biol* 5:734–742.

う蝕制御学分野

田上 順次

医歯学総合研究科・口腔機能再構築学系専攻
齲蝕制御学・教授

1）研究課題名

光照射器が可視光応答型酸化チタン光触媒を用いた歯の漂白に及ぼす影響

Effect of light units on tooth bleaching with visible-light activating titanium dioxide photocatalyst

近年、可視光応答型酸化チタン光触媒（VL-TiO2）と過酸化水素を含むオフィスブリーチングのための新しい漂白材（TiON in office、ジーシー製）が開発された。本研究では、牛歯変色歯モデルを作製し、これを用いて、異なる光源がTiON in officeの漂白効果に及ぼす影響について検討を行った。

牛歯に対して煮出した紅茶を染色液として、変色歯モデルを作製した。次いでオフィスブリーチング材（TiON in office）を用いて業者の指示にしたがって漂白操作を行った。その際、ハロゲン照射器（CoBee、CB群、900 mW/cm2、ジーシー製）、または、LED照射器（G-Light、ジーシー製）を用いた。G-Lightは7個の青色LEDと1個の青紫色LEDから成り、本研究では本器を改造して、青色と青紫色LEDが点灯するモード（GL-BV群、650mW/cm2）、および、青色LEDのみが点灯するモード（GL-B群、600 mW/cm2）を用いた。漂白前と漂白後の測色値の差ΔL、Δa、および、Δbを求め、さらに色差値（ΔE）を算出した。いずれの実験群においても、漂白効果が認められ、処置回数を増すごとに、その効果は顕著となっていくのが目視で確認された。漂白処置を繰り返すにしたがって、L*値は増加し、a*値とb*値は減少した。それに伴いΔLおよびΔEは増加した。牛歯変色歯モデルにおいて、LED照射器の青色と青紫色照射光は、VL-TiO2含有漂白材を用いた漂白で、より高い漂白効果を示した。照射器の波長分布は、漂白効果に影響を及ぼすことが明らかとなった。

接着によるSuper Toothの生成とその構造解析

Creation of Super Tooth by adhesion and analysis of its structure

接着材料の歯質接着性の向上とともに、ボンディング材の性能評価は、単に接着強さを比較する時代から、ボンディング材の質を問う時代へとシフトしている。これまで象牙質に対する接着メカニズムについては、Nakabayashiらの樹脂含浸層（ハイブリッド層）の理論が広く認められている。しかし、修復物周囲の二次う蝕の発生について詳しく検討すると、接着により象牙質との界面に樹脂含浸層を形成する接着性修復物では二次う蝕は生じないことがわかってきた。臨床的には今でもコンポジットレジンの二次う蝕と診断されるケースは多いものの、これは修復物周囲に生じた初発う蝕（一次う蝕）と二次う蝕とを判別する明確な診断基準が存在しないためと思われる。

わが国では接着システムの高性能化と簡略化が進み、2ステップのセルフエッチングシステムの開発から、最近ではさらに最近では1ステップのセルフエッチングシステム（あるいはオールインワンシステム）が主流となっている。このセルフエッチングシステムを象牙質に接着させた場合、人工的にう蝕を作製して接着界面を観察すると、樹脂含浸層の直下にはう蝕抵抗性を示すもう一つの層が存在することがわかった。この層はヒドロキシアパタイトの結晶を含み、象牙質と類似構造を示す。この層は、セルフエッチングシステムを接着材として使った時にのみ形成され、リン酸エッチングでは認められず、接着によって強化された象牙質と考えるもできるため、これをSuper Dentinと呼んでいる。Super Dentinの形成機序については、接着材に含まれる機能性モノマーやフッ化物などが重要な働きを示すことがわかってきた。セルフエッチングシステムを用いた接着によるSuper Dentinの形成によって、従来の樹脂含深層の形成による「歯を守る」という考え方から、より接着的に「歯を強化する」という接着の活用が検討されるようになってきた。

レジンコーティング法の臨床応用

Clinical application of the resin coating technique

インレーなどの間接修復は、う蝕が広範囲に及ぶ場合が対象であるが、これまで窩洞形成後に露出した象牙質の取り扱いが問題になってきた。すなわち、間接法においては露出した象牙質面は直ちに封鎖されるのではなく、印象採得され、次回来院時まで仮封されるのである。この間、仮封材の封鎖性の悪さから仮封材の脱落は、よく経験するところであり、それによって象牙質は口腔内に露出して、外部からの物理的・化学的な刺激やプラークの付着に伴う細菌の侵入などの様々な刺激に晒される危険性がある。レジンコーティング法では、窩洞形成を終了した時点で、窩洞内面を直ちにボンディングシステムとフロアブルレジンとを用いてコーティングして封鎖する。セルフエッチングシステムを用いて象牙質表面に接着すればSuper Dentinが形成され、象牙質が強化でき、これによって治療期間を通して患者に痛みを与えないだけでなく、レジンセメントと象牙質との接着力や修復物辺縁の封鎖性の向上も期待できる。インレー窩洞に対するコーティングでは、象牙質に対する接着性の向上を最優先に考えており、ボンディングシステムとフロアブルレジンの組み合わせによるコーティングを推奨している。しかし、これではかなり厚みのあるコート層が形成されるため、クラウンの支台歯に対するコーティングとしては厚くなりすぎて扱いづらい。最近ではかなり薄いコーティング層を形成できる材料も市販されており、クラウンの支台歯のコーティングに適している。最近ではこの薄膜コーティング材料を健全歯質に応用して歯質を強化することを目的としたコーティングについても検討している。すなわち、薄膜コーティングを露出根面に応用することによって、根面う蝕を抑制でき、新しい予防的修復材料の開発の可能性について検討中である。

破折歯の接着再植に関する研究

Study on vertical root fracture reconstruction

う蝕、歯周病の原因が明らかになり、メンテナンスが進んできた今日、これらの疾患を予防することによって歯を失う割合が少なくなってきた一方、歯根破折を原因とする歯の喪失が注目されている。最近の調査では全国の歯科医院における抜歯理由の約11%が歯根破折によるものと報告されている。とくに破折によって抜歯に至るのは生活歯に比べて、失活歯の割合が高い。歯根破折の発生には、何らかの外力が加わることによってまず歯根に亀裂が生じ、それが破折線となって最終的に歯根破折に至るプロセスをたどる。歯根破折に至った症例においても、それを接着を用いて適切に対応し、歯の延命につなげることが本研究の目的である。接着再植を想定して作製した抜去歯の歯根破折モデルに対して、各種接着材を使用して、接着したのち、試料を水中に長期保管し、その接着耐久性について微小引っ張り接着試験により検討した。その結果、接着材料によってその耐久性は異なり、2ステップセルフエッチングシステムを用いた場合に、安定した接着耐久性を示した。

マイクロCTを用いた歯の脱灰、再石灰化に関する研究

Micro CT analysis on demineralization/remineralization of tooth

従来のTMR法では、歯や骨などの硬組織の形態学的研究において、試料を切削して試料を作製する必要があったが、マイクロCTでは、非破壊による検査が可能であり、高解像度の立体像を得ることができる。しかし、マイクロCTを用いる場合、その障壁となる線質硬化（ビームハードニング）と呼ばれる偽像（アーチファクト）が生じることが知られている。我々は、各種フィルターと画像解析ソフトを併用することによりこの問題を解決し、歯質のミネラルの観察の標準法として用いられるTMRと同等の画像解析が可能であることが分かった。我々は、マイクロCTを用いてエナメル質及び象牙質表層の脱灰および再石灰化の変化を経時的に観察することをこころみた。CPP-ACPは、再石灰化に対して有効であることが報告されているが、これをエナメル質表面に塗布した場合の効果についてマイクロCTを用いて検討した。その結果、CPP-ACPペーストの歯質脱灰抑制効果が認められ、さらにCPP-ACPにフッ化物を配合したペーストによいてよりその効果が高いことが分かった。

う蝕象牙質に対するレジンの接着性能の改良

Improvement of bonding to caries-affected dentin

う蝕罹患象牙質に対するレジンの接着性能が低下する原因としては、特にう蝕罹患象牙質の無機成分量に低下および結晶構造の変化、管間象牙質中の水分量の増加、象牙質コラーゲン性状の変化などが考えられている。特に、Self-etch接着システムでは健全象牙質とのスミヤー層構造・成分の違いも原因のひとつとして考えられる。すなわち、う蝕罹患象牙質スミヤー層における有機成分比率の増加により、健全象牙質のスミヤー層と比べ溶解・除去されにくく、レジンモノマーの象牙質への浸透を妨げている可能性がある。

これまでの研究により6%NaOCl水溶液を応用し、う蝕罹患象牙質スミヤー層表層の有機成分を除去したところ、Self-etch接着システムのう蝕罹患象牙質に対する接着性能を向上させることが可能であることが判明した。しかしながら、酸化効果を持つNaOCl水溶液で長時間、処理した場合、レジンの重合反応（酸化-還元反応）を阻害してしまい、健全象牙質に対するレジンの接着性能が低下した。そこで、NaOCl水溶液処理後に抗酸化剤（還元剤）による処理を追加することを試み、第一歩として健全象牙質を用いて、酸化剤の種類およびその処理時間に関し、検討を行った。

さらにNaOCl水溶液は、口腔内での使用に関し安全性に関し問題を有しているので、有機質溶解作用を示すが安全性の高い弱酸性次亜塩素酸機能水の応用を試みることとし、健全象牙質を用いて、濃度および処理時間に関する検討を行った。その結果をもとに、う蝕象牙質に対する接着強さ試験を行ったところ、弱酸性次亜塩素酸機能水ではSelf-etch接着システムにおける健全象牙質への接着性能に対する影響は少なく、NaOCl水溶液より短時間の使用で、う蝕罹患象牙質に対するSelf-etch接着システムの接着性能の向上効果が発現することが示唆された。

コンポジットレジンの接着強さに及ぼす残存象牙質厚さの影響

The Effect of RDT on Resin Composite Bond Strength to the Dentin

レジンの接着強さは、平坦面の象牙質被着体に対して評価されることが多いが、残存象牙質厚さが少ないとレジンの象牙質への接着強さが低下することが報告されている。そこで本研究では、各種ボンディングシステムを使用したレジンの接着強さに及ぼす残存象牙質厚さの影響について検討した。ヒト抜去大臼歯の咬合面エナメル質を削除し、600番のシリコンカーバイドペーパーで仕上げした象牙質平坦面を作製した。3種の接着システム;Clearfil Mega Bond、Single Bond、Clearfil Tri-S Bondを用い業者指示に従い処理した後、Z-100のレジンを3x5x2mm（C-factor=0.3）に築盛し、実験用ハロゲンランプ電圧可変光照射器（GC）を用い、出力600 mW/cm^{2}で40秒間光照射を行い重合硬化させた。37℃暗所水中に24時間保管後、試料中央部から長軸方向に、約1 mm^{2}の試片を切り出した。これら試片の残存象牙質厚さ（RDT）を測定した後、試片の両端を試験装置にシアノアクリレートで接着し、これをEZ testに装着して、クロスヘッドスピード1mm/minで微小引張り接着強さ（μ-TBS）を測定した。接着強さはRDTにより、1〜4 flatの4群に分けた。1 flat：RDT< 2 mm、2 flat：2 ≦ -<3 mm、3 flat：3 ≦-< 4 mm、4 flat：≧ 4 mm。その結果、全ての群でClearfil Mega Bondが最も高い接着強さを示した。Clearfil Mega Bondの接着強さはRDTと相関があり、Single Bondの接着強さはRDTの影響を受けず、Clearfil Tri-S Bondの接着強さはRDTが2mm未満の場合のみ低下することが明らかとなった。

レジンの象牙質接着強さへ及ぼすRDTの影響は、ボンディングシステムにより異なる傾向を示すことが判明した。

窩洞内各面に対するコンポジットレジンの接着強さ

The Resin Composite Bond Strength to the Different Cavity Wall

コンポジットレジンの接着強さは、平坦面の象牙質被着体に対して評価されることが多く、窩洞内各面に対するレジンの接着強さについての報告はほとんど認められない。そこで本研究では、2種のボンディングシステムを使用したレジンの接着強さに及ぼす窩洞内象牙質各面の影響について検討した。ヒト大臼歯の咬合面エナメル質を削除した、象牙質平坦面に3x 5x 2 mmのI級窩洞を形成した。この窩洞に2種のセルフエッチングシステム、Clearfil Mega BondとClearfil Tri-S Bondを用い製造者指示に従い処理した後、処理面にZ100のレジンを填塞した。実験用ハロゲンランプ電圧可変光照射器を用い、出力600 mW/cm^{2}で40秒間光照射を行いレジンを重合硬化させた。37℃暗所水中に24時間保管後、窩底と窩壁のレジン-象牙質界面に垂直に、界面の面積約0.9 mm^{2}の試片を切り出した。これら試片の両端を試験装置にシアノアクリレートで接着させ、EZ testに装着して、クロスヘッドスピード1mm/minで微小引張り接着強さ（μ-TBS）を測定した。その結果、窩洞内面に対するClearfil Mega Bondの接着強さは、窩底、窩壁共にClearfil Tri-S Bondより有意に高い接着強さを示した。また、Clearfil Mega Bondでは、窩底面、窩壁面に対する接着強さに有意差は認められなかったが、Clearfil Tri-S Bondでは、窩底面におけるレジンの接着の方が窩壁面より有意に低い接着強さを示した。

コンポジットレジン修復物の接着強さは、窩洞内の部位、接着システムの影響を受けることが判明した。

コンポジットレジンの接着強さに及ぼす象牙細管の影響

The Effect of Dentin Location on the Composite Bond Strength to the Dentin

コンポジットレジンの接着強さは、平坦面の象牙質被着体に対して評価されることが多いが、その平坦面被着体のほとんどは咬合面象牙質であり、象牙質側壁面に対するレジンの接着強さについての報告はほとんど認められない。そこで本研究では、2種ボンディングシステムを使用したレジンの接着強さに及ぼす象牙細管の影響について検討した。ヒト大臼歯の咬合面エナメル質を削除した、象牙質平坦面に3x 5x 2 mmのI級窩洞を形成した後、窩洞形成後に側壁周囲の壁を取除いた窩底平坦面試料を作製した。この窩底平坦面と側壁平坦面を2種の接着システム、Clearfil Mega Bond、Single Bond を用い製造者指示に従い処理した後、処理面にZ100のレジンを3 x 5 x 2 mmに築盛した。実験用ハロゲンランプ電圧可変光照射器を用い、出力600 mW/cm^{2}で40秒間光照射を行いレジンを重合硬化させた。37℃暗所水中に24時間保管後、レジン-象牙質界面に垂直に、界面の面積約1 mm^{2}の試片を切り出した。これら試片の両端を試験装置にシアノアクリレートで接着させ、EZ testに装着して、クロスヘッドスピード1mm/minで微小引張り接着強さ（μ-TBS）を測定した。その結果、象牙質側壁平坦面に対するClearfil Mega Bondの接着強さが全ての群で最も高い接着強さを示した。側壁平坦面に対する接着強さは、Clearfil Mega Bond、Single Bond共に、窩底平坦面に対する接着強さより有意に高かった。

コンポジットレジン修復物の接着強さは、象牙質の部位、象牙細管走行の影響を受けることが判明した。

コンポジットレジン修復のSS-OCTを用いた辺縁封鎖性評価

Assessment of marginal adaptation of composite restoration using SS-OCT

光干渉断層計（Optical Coherence Tomography, OCT）は、生体の断層画像を非侵襲的に得ることができ、歯科臨床における導入が期待される。今回、抜去歯にI級窩洞を形成し、コンポジットレジン修復を行い、OCTを用いて辺縁の様相を調査した。OCT画像における輝度変換部分に画像処理を行い、ギャップの検知を試みた。また、コンポジットレジン修復の3D画像を構築し、修復物内面の適合状態を評価した。

3D画像から2次元のOCT画像を抽出し、dBユニット表示された窩洞周囲のグレースケールの変化を画面上のピクセル毎に調査し、その明るさの変化をイメージングソフトウエアにより解析した結果、窩洞の外形ならびに充填されたコンポジットレジンの様相を立体的に再現することができ、また3D画像の任意の部位から得られた断層画像において、窩洞周囲にみられる輝度の上昇は、接着界面に発生したギャップであることが確認できた。OCTから得られたコンポジットレジン修復物の3D画像を用いることにより、修復物の総体的な適合性の評価を、効率的に行うことができた。このようなギャップは光照射を行った直後の重合収縮によって生じることがものと推察され、今後さらに検討していく予定である。

SS-OCT による歯の脱灰の定量評価

Quantitative analysis of tooth demineralization using SS-OCT

エナメル質ならびに象牙質を、所定の期間脱灰処理を行った後、OCTによる観察を行った。OCT画像におけるdBユニットの輝度変換のプロファイルを獲得した後、脱灰処理を行った試片から薄切研磨標本を作製し、Transversal Microradiography（TMR）法によってミネラル密度を定量的に測定し、比較した。

脱灰処理を行ったエナメル質では、乾燥状態から得られたプロファイルと湿潤状態から得られたプロファイルの交点における深さを基準としたところ、TMRにおける脱灰深さとの高い相関が得られた。一方、脱灰象牙質では、エナメル質ほど高い相関ではないものの、脱灰前と脱灰後のプロファイルの交点における深さを基準としたところ、TMRにおける脱灰深さとの有意な相関を得ることができた。

エナメル質ならびに象牙質の脱灰部から得られたOCT画像は、TMRによる定量的評価と有意な相関がみられた。したがって、OCTによるう蝕の診断は、極めて精度の高いものであることがわかった。再石灰化処理を行ったエナメル質ならびに象牙質においても一定の相関が得られるものと思われ、臨床における再石灰化治療の、非破壊的評価の実現に期待を抱かせる結果となった。

POs-Caおよびフッ素配合ガム咀嚼後のエナメル質初期う蝕の再石灰化効果

Effects of a chewing gum containing POs-Ca and fluoride on remineralization and crystallization of enamel subsurface lesions in situ

POs-Ca（リン酸オリゴ糖カルシウム）およびフッ素配合ガム咀嚼後のエナメル質初期う蝕の再石灰化効果について検証した。すなわち、被験者36名を3群に分け，エナメル質初期う蝕サンプルを取り付けた口腔内装置を装着した状態で,Controlガム,POs-Ca 配合ガム, POs-Ca・茶フッ素配合ガムのいずれかを二重盲検下にて1回2粒1日3回14 日間摂取させ、TMR、広角X線分析お

よび微小硬さ試験を用いて再石灰化効果を検討した.さらに、飛行時間二次イオン質量分析計（Time-of-flight secondary ion mass spectrometer：TOF-SIMS）を用い,POs-Ca およびフッ素配合ガム咀嚼後のエナメル初期う蝕最表層部におけるフッ素分布についてイオン質量分析を行った.その結果、POs-Caおよびフッ素配合ガムを摂取することにより、エナメル質初期う蝕の再石灰化が促進されること,さらにミネラル密度回復は,ハイドロキシアパタイト結晶量の回復である可能性を示唆した.微小硬さ回復率は, POs-Ca ガムでは17.4 ± 4.3%,POs-Caおよびフッ素配合ガムでは31.3 ± 2.2%を各々示し,両群間において有意差を認めた（$p<0.05$）.さらに,TOF-SIMS画像より,POs-Ca およびフッ素配合ガム咀嚼後の再石灰化部において, 脱灰部では認められないフッ素分布が観察された.以上より, in situ環境下,短期間フッ素配合ガム摂取において、ガム由来フッ素がエナメル質初期う蝕最表層部に取り込まれ,同最表層部の微小硬さ変化に影響を及ぼす可能性が示唆された。

Acid base resistant zone の精査と改質

Assessment and improvement of Acid-base resistant zone

象牙質接着界面において歯質を強化している層、すなわちアシッドベースレジスタントゾーンの存在が確認されている。これまでのところ様々な接着剤を用いた際の形態の変化や、長期保存における耐久性などは少しずつ解明されてきたが、実際にどのような構造になっているかまた、どうすればより良いAcid base resistant zoneが作れるのかといったことは不明なままである。これらを受けて、ラマン分析やTOF-SIMS、TEMなどを用い、それぞれの材料におけるAcid base resistant zoneの分析や微小構造の観察が行われている。また、接着剤の特性を活かし歯質をより強化できるよう、新たな製品の開発や実験を行っている。これまでのところ樹脂含浸層とは異なり、Acid base resistant zone内には多くのカルシウムの存在が確認されており、より歯質の成分に近い層であることが分かっている。また接着操作に加えて、歯質に有利なカルシウムやリンなどの成分を補充することで、より安定して強固なAcid base resistant zoneを作り出すことが出来ることもわかっている。

マイクロCTによる光重合型コンポジットレジンの重合収縮挙動の評価

Evaluation of resin composite polymerization by three dimensional micro-CT imaging

コンポジットレジンの重合時に発生する重合収縮は避けられない事象である。歯質と修復物との間の接着界面にギャップやマイクロリーケージクを引き起こし、術後疼痛、細菌侵入による二次う蝕や歯髄炎の原因となることが考えられる。従来から化学重合型レジンは重合時、窩洞の中心方向に向かって収縮し、光重合型コンポジットレジンは光の照射方向に収縮すると考えられてきた。これらの重合収縮時における挙動は有限要素法やレーザースペクトル法により研究、解析されているが、重合に伴う収縮の挙動を直接観察できる手法は少ない。本実験ではコンポジットレジンで作られた疑似一級窩洞に、実験用に試作したコンポジットレジンを充填し、光照射前と光照射後の試作コンポジットレジンをマイクロCTにより撮影し収縮挙動の解析を行った。X線造影性のないコンポジットレジン、SOLARE（A3、GC）に疑似一級窩洞を作成し、実験用試作コンポジットレジン（A3、トクヤマデンタル）をセラミックプライマー（クラレメディカル）とメガボンド（クラレメディカル）を塗布した窩洞に充填した。続いて光照射（D-LUX2000、DENTRADE）前、光照射後それぞれに、試料の3D画像をマイクロCT（SMX100CT、島津製作所）にて撮影した。得られた3D画像よりマーカーとなるフィラーを専用ソフト（ラトックシステムエンジニアリング）を使って抽出し、窩洞内の全てのマーカーフィラーの重合前、重合後の座標を測定する。

象牙質接着性材料の基礎的研究とその臨床応用

Fundamental analysis and clinical application of dentin adhesives

ワンステップボンディング材は親水性であることが知られており、その親水性から吸水することが知られている。象牙質接着の耐久性には吸水によるボンディング材の劣化が影響を与えると考えられ、またワンステップボンディング材には乾燥後も溶媒が残存し、重合率を低下させその機械的強度を低下させることが判明した。また溶媒の除去には一般的にエアブローを用いて行われるが、ボンディング層が薄膜化し接着界面にかかる応力を適度に分散できることができない可能性がある。エアブローを必要としない溶媒を含まないボンディングシステムや、疎水性接着システムは吸水の影響が少なく機械的強度も高いため、経時的に安定した機械的性質を持ちレジン―象牙質接着の耐久性を向上させるものと今後期待される。ボンディング層の機械的性質と接着性能との関係を明らかにし、溶媒を含有しないボンディングシステムや疎水性のボンディ

ングシステムがどのように接着耐久性に寄与するか接着界面破壊様相の動的挙動の3次元的解析を行う。

歯の組織学的構造とミネラル密度の違いによる屈折率の研究

Refractive index of human tooth in relation to structural orientation and mineral content.

本研究の目的は、エナメル質と象牙質に存在するエナメル小柱と象牙細管の組織学的構造による光学特性の違いをOCT（optical coherence tomography）を使用して明らかにすることである。天然歯から様々な角度（エナメル小柱に対し水平又は矢状断、象牙細管に対し水平、矢状、斜走断）で切り出された歯牙を使って、OCTから得られた画像と実際の距離より屈折率（n）を計算した。それと同時にOCTから得られる位置信号と歯牙の構造による光学的特性の関係についても計算を行った。エナメル質とは違い、象牙質における屈折率とOCTから得られる信号パターンは象牙質の部位によって大きく変化し、その変化は象牙細管の存在が大きく関わっていることが判明した。一方エナメル質内ではOCTの信号強度の減弱は緩やかである。これら結果から得られる結論は、光と歯牙硬組織の関係をより理解することに大変重要であると思われる。また我々は、歯牙の屈折率とTMR（transverse microradiography）から得られた健全、脱灰歯牙のミネラル量、又はエナメル質と象牙質の再石灰化の関係を研究し、OCTの信号強度の減弱が歯牙のミネラル量と結晶性に強く依存していることが判明した。

歯牙硬組織と生体材料のナノメカニカル特性の評価

New strategy of nanomechanical characterization of dental hard tissue and biomaterials

我々は歯牙硬組織の微小時間おける機械的微小変化を、ナノインデンテーション法（nanoindentation）により検証を行ってきた。この実験方法は従来から行われている引っ張り試験のような破壊試験に比べ、従来では得られなかった有用な情報を得ることができる。そこで今回、歯牙の脱灰層、再石灰化層や歯牙硬組織と歯科材料の接着界面などの極めて薄い界面付近を、ナノインデンテーション法の微小マッピング法を使って検証を行った。本実験により健全歯質やリン酸エッチングやエッチアンドリンスのボンディングシステムによって処理された界面に比べ、セルフエッチング型のボンディングシステムを使って処理された界面は形態的にも機械的にも優れていることが明らかになった。我々のナノインデンテーション法を使った実験方法により、従来から提唱されてきた樹脂含浸層と、スーパーエナメルやスーパーデンティンといった考え方を比較検討する為の、十分な根拠を得ることができる。

セルフエッチボンディング材への照射光量における直接光およびコンポジットレジン透過間接光が象牙質接着性能に及ぼす影響

The influence of light intensities irradiated directly and indirectly through resin composite to self-etch adhesives on dentin bonding

ボンディングレジンの重合率に大きく影響を与える要因の一つに照射光量がある。ボンディング材は塗付後に直接、また充填したコンポジットレジンを透過し間接的にと二度の照射をうける。直接照射される光量が減弱すると、ボンディング材の機械的強度が下がることは報告されているが、1ステップ接着システムでは、間接的に照射される光量がその親水性のボンディングレジンと疎水性のコンポジットレジンの共重合にも影響を与えることが考えられ、2ステップ接着システムより接着接合界面に大きな影響が出るのではないかと考えられた。そこで、2ステップ接着システム（Clearfil SE Bond（SE））と2種類の1ステップ接着システム（Clearfil S^3 Bond（TS）、Bond Force（BF））において、照射光量を350 mW/cm^2と600 mW/cm^2とに変化させて、直接光およびコンポジットレジン透過間接光が象牙質接着性能に及ぼす影響について微小引張り接着強さ試験を用い検討し、さらに象牙質接合界面の形態学的観察を行った。コンポジットレジンは透過性の異なるClearfil Photo Core（PC）とClearfil Majesty OA2 shade（MJ）とを比較した。これより、SEは同条件下でBF、TSより有意に高い接着強さを示し、全ての接着材においてPC/600 mW/cm^2群はMJ/600 mW/cm^2群より高い接着強さを示した。SEとBFでは、PC/350 mW/cm^2群がMJ/600 mW/cm^2群より高い接着強さを示した。各群中MJ/350 mW/cm^2群が最も低い接着強さを示した。また、破壊形態分析ではほぼ全ての試料において混合破壊が観察された。走査顕微鏡を用いた界面観察ではすべての群においてボンディング層と象牙質界面でナノリーケージが観察され、BF/MJ/350 mW/cm^2群では加えてボンディング層とコンポジットレジン界面においてもナノリーケージが観察され、2層の共重合が阻害されていたことが窺えた。材料により異なるものの、高い象牙質接着強さを得るには直接ボンディング材に照射される光量だけでなく、間接的にコンポジットレジンを透過して照射された光量も重要な役

割を担っていることが判明した。

HEMA含有およびHEMA非含有1ステップ接着材の吸水および最大引っ張り強さの長期評価

Long-term evaluation of water sorption and ultimate tensile strength of HEMA-containing/-free one-step self-etch adhesives

近年、臨床上の簡便さから1ステップセルフエッチングシステムの接着材が広く臨床に用いられている。1ステップセルフエッチングシステムは、エッチング、プライミングおよびボンディングという3つのステップを一度に行うため、酸性接着性モノマー、親水性・疎水性モノマー、フィラー、水および有機溶媒が一つの容器に混合されている。1ステップセルフエッチングシステムの接着材は重合後も高い親水性を示し、2ステップ接着システムのボンディング材などと比べ、重合硬化後も高い吸水性を示すことまた吸水によりその機械的性質は乾燥状態に比べ低下することが報告されている。それゆえ、ボンディング材の長期的な吸水量の多寡はその機械的性能に影響を与え、ひいては象牙質接着耐久性に影響を与えることが推測される。親水性モノマーのひとつであるHEMAは、象牙質のぬれを良好にし、象牙質接着強さの向上に寄与すること、さらに1ステップセルフエッチングシステムにおいては相分離の防止という役割を担っていることが報告されている。一方、レジンポリマー鎖の中に分散したpoly-HEMAは親水性を示し、重合後の吸水を促すことが知られている。しかし、長期水中浸漬がHEMA含有およびHEMA非含有1ステップセルフエッチングシステムの接着材の吸水性および機械的性能を検討した報告はない。そこで本研究では、長期水中浸漬がHEMA含有およびHEMA非含有1ステップセルフエッチングシステムの接着材の硬化体の吸水率およびその最大引っ張り強さ（UTS）におよぼす影響について検討を行った結果、HEMA含有1ステップセルフエッチングシステムは経時的な吸水率の増加を示し、UTSの低下を示した。またHEMA非含有1ステップセルフエッチングシステムは吸水率、UTSともに360日水中浸漬による影響を受けなかった。

2級コンポジットレジン修復におけるエナメル質と象牙質に対する窩洞適合性と微小引張り強さ

Contemporary adhesives：marginal adaptation and microtensile bond strength of class II composite restorations

直接法による2級コンポジットレジン修復は、接着技術の向上、ミニマルインターベンション、審美的要求の点から臨床において広く行われるようになっている。しかし、修復物周囲からの着色や2次カリエスは再治療の大きな原因となっている。そこで本研究では、4種類の接着システムを用いて2級コンポジットレジン修復を行い、隣接面エナメル質と象牙質への窩洞適合性と接着強さに及ぼす影響について検討した。

窩洞適合性において、エナメル質では、すべての材料において95.4%以上の連続マージンが観察され、各材料間に有意差は認められなかった（$p>0.05$）。一方、象牙質では60.2%から84.8%の連続マージンが認められ、Clearfil SE Bond と Clearfil Tri-S Bond は、Adper Scotchbond Multi PurposeとAdper Scotchbond 1 XTより有意に多い連続マージンが認められた（$p<0.05$）。微小引張り接着強さにおいて、Adper Scotchbond Multi Purpose、Adper Scotchbond 1 XT、Clearfil SE Bond、Clearfil Tri-S Bondはそれぞれエナメル質に対して、40.5、37.3、30.8、23.2 MPa、象牙質に対して37.7、33.0、37.3、29.0 MPaの接着強さを示した。接着システムの違いはエナメル質に対する窩洞適合性に影響を及ぼさないが、象牙質に対してはエッチ＆リンスシステムと比較してセルフエッチシステムの優れた窩洞適合性が得られた。Adper Scotchbond Multi Purposeは、エナメル質と象牙質に対して最も高い接着強さが得られた。Clearfil SE Bondは、象牙質に対して最も安定した接着強さが得られ、エナメル質に対しても良好な接着強さが得られた。

二次う蝕に対する強アルカリ電解水の影響について

An in vitro study to assess the efficacy of OH- ion superadded alkali-ion water in inhibiting caries and secondary caries.

近年、人工的にバイオフィルムを形成させる人工口腔装置（Oral Biofilm Reactor; OBR）を用いた、in vitro二次う蝕形成モデルが報告された。このモデルは、短期間（7日間）でもエナメル質とCR境界面に二次う蝕の形成が報告されており、in vitroにおける二次う蝕の発生に関連した研究に寄与したと言える。本研究では、上記モデルを活用し、う蝕予防効果が期待されるアルカリ性電解水（AW）を用いて、二次う蝕進行抑制効果を検証した。AWは、水道水を電気分解する事で生成される高濃度水酸化物イオン（OH-）を含有する塩基性還元水である。胃腸障害や消化不良等へ効能を示す健康機能水としてすでに飲用されているが、近年の研究により、う蝕バイオフィルムの主要構成要素であるグルカンを溶解

することが報告された。これまでグルカンは、水酸化ナトリウム溶液（NaOH）などの強塩基性試薬に溶解することは知られていたが、口腔内での使用は危険を伴うため、避けられてきた。一方で、菌に焦点を当てた従来の抗菌剤や消毒剤では、熟成されたバイオフィルム内部への浸透殺菌力の低減や、長期投与による口腔内への影響等が懸念されてきた。そこで、NaOH等と同様に塩基性を示し、且つ、安全性の高いAWを応用してう蝕バイオフィルムを溶解し、う蝕・二次う蝕予防進行抑制効果を図ることを考えた。従って、本研究では、二次う蝕モデルを使用し形成した人工二次う蝕に、pHの異なる3種類のAWを作用させたときの二次う蝕進行抑制効果を、蛍光顕微鏡観察を用いた画像解析により検証した。

SS-OCTを用いた脱灰象牙質の再石灰化度の推定（TMRとの比較）

Estimation of dentin lesion remineralization by SS-OCT in comparison with TMR

人工的に作製した脱灰象牙質を各期間再石灰化し、その期間ごとにSS-OCT（Swept Source Optical Coherence Tomography）にて病変の断層画像を取得し、一方で同一病変のTMR（Transverse Microradiography）画像から再石灰化の進行度（脱灰深さ、ミネラル損失量など）を計測し、両者の比較からSS-OCTにて再石灰化の進行度が推定できるかどうかを検討すること。表面研磨した牛歯根象牙質を18日間脱灰し、これらを6群に分けそれぞれ一定期間（2〜11週間）再石灰化させた（以下、サンプル）。同時に、SS-OCT（HSL-2000®, Santec）にて、脱灰前後と再石灰化後の断層画像を取得した。同画像にて、脱灰前線と推察される輝度変化の境界（boundary）が観察されたので、サンプル表面からそこまでの深さを計測した。また画像解析ソフトを用いてSS-OCT画像の断層プロファイル（輝度dB vs深さ）を作成し、ミネラル溶出量と推定される面積値の差（ΔR=Rdemin - Rremin ; R：dB × boundaryまでの深さの積分値）も算出した。一方、再石灰化の終了後、サンプルからTMR用の薄切片を作製し、病変のデジタル画像を取得後、解析ソフトにて脱灰パラメータ（脱灰深さ、脱灰量：ΔZ）を算出した。こうして得られたOCT情報（boundary深さ、断層プロファイル）と脱灰パラメータとの相関性を検討した。OCT画像で推定された脱灰深さ（boundary深さ）とTMR解析で得られた脱灰深さとの間に統計的に有意な相関性を認めた。2）ΔR値とΔZとの間にも同様に有意な相関性を認めた。3）再石灰化後において多様な断層プロファイルが認められ、脱灰深さや再石灰化表層の形成や厚さと関連するような「特徴（ピークや屈曲点など）」は確認できなかった。

クロルヘキシジン含有・歯科接着剤の抗菌性、接着耐久性の研究

The effect of chlorhexidine to improve dentin bond durability

医薬用殺菌薬のクロルヘキシジンは、口腔粘膜への非侵襲的修復治療に一般に用いられるが、これをグラスアイオノマーセメントに混合した抗菌活性を有する歯科材料の臨床への応用が試みられている。さらにこのクロルヘキシジンは歯質接着性の長期耐久性劣化を遅延する働きが報告されている。劣化原因として象牙質基質から放出されるMMP（Matrix Metalloproteinases）の存在が指摘されているが、クロルヘキシジンはジンククロライド、ドキシサイクリンと並び、MMP阻害剤として、歯科修復への使用が注目されている（J Dent Res 2004;83：216-21）。感染象牙質の残存細菌を減らす効果と共に、接着界面での象牙質コラーゲンの劣化を抑制させる効果を備えるクロルヘキシジンを付加した歯科材料は、臨床において、一般レジン修復をはじめ、レジンセメント、歯内治療での根充レジンシーラーに応用が期待される。本研究ではクロルヘキシジン含有の接着性歯科材料の、クロルヘキシジンの放出、付加に伴う物性の変化、殺菌効果、象牙質コラーゲンの劣化抑制効果を検討し、長期接着性への影響を包括的にとらえ、臨床応用の可能性を評価する。

ヘスペリジンによるヒト歯根面象牙質脱灰後のコラーゲンの保護と、再石灰化への影響

Effect of Hesperidins on stabilization of collagen and remineralization of dentin Lesion

歯質 象牙質は70%が無機質（ヒドロキシアパタイト）、20%が有機物（膠原繊維（コラーゲン繊維）と非膠原性タンパク質）からなり、う蝕のメカニズムを考える上で、酸による無機質の脱灰抑制とあわせて、有機質の保護を考慮しなければならない。近年、有機質の保護が確立できれば、これを足場にしてう蝕脱灰部の再石灰化が有意に起こると考えられている。フラボノイド（flavonoid）は天然に存在する安全性の高い有機化合物群で，少量でも抗酸化作用を有し、天然の架橋剤としてコラーゲンを保護すると報告されている。本研究では天然フラボノイドのヘスペリジンを歯質象牙質に作用させ、う蝕の進行への影響を評価した。方法：象牙質う蝕モデルとし

てpHを調整した脱灰、再石灰溶液にて8日間保存した。この間、象牙質にヘスペリジンン溶液にて一日2時間作用させた。最終脱灰量、コラーゲン崩壊度を定量分析し、x線を用いたミネラルプロファイル測定による脱灰部の分析を行った。また同じフラボノイドのグレープシード抽出物と、う蝕予防に使用されるクロロヘキシジンとの効果を比較検討した。結果考察：ヘスペリジン群は有意に脱灰量、コラーゲン崩壊度を抑制していた。脱灰部の分析を行った結果、表層のみならず、やや深部まで再石灰化が見られた。これらの結果より、ヘスペリジンは、う蝕の脱灰抑制、再石灰化促成に何らかの効果があることが分かった。作用メカニズムは、今後さらなる研究が必要だが、う蝕の発生また進行をコントロールするうえで、生体に安全なフラボノイドは有効な薬理作用を持つと予測され、将来の治療薬と期待される。

口腔粘膜から遊走する異なる4つの樹状細胞亜群における異なる共刺激分子発現と遊走特性

Differential expression of co-signal molecules and migratory properties in four distinct subsets of migratory dendritic cells from the oral mucosa

樹状細胞（DC）の共刺激分子発現やサイトカイン産生は、所属リンパ節（RLN）に遊走するDCの抗原提示能に多大な影響を与える。粘膜は、皮膚と同様に最前線に位置し生体防御機能を発揮している。口腔粘膜は、免疫応答を誘導する舌下ワクチンや免疫寛容を誘導する舌下免疫療法で、抗原塗布部位として使用されているが、口腔粘膜に存在するDCの特性についてはあまりよくわかっていない。本研究では、抗原を捕捉後RLNに遊走するDCを4つのサブセットに分類し、その経時的遊走能の変化と共刺激分子発現を検討した。RLNに遊走する口腔粘膜DCは、CD11C. CD207, CD103, CD326, CD11b の表現型から、F1（CD11c^{hi}CD207-粘膜下樹状細胞（SMDC））, F2（CD11c$^{int/lo}$CD207-新規リクルートSMDC）, CD103^{+} F3（CD11c$^{int/lo}$CD207^{+} レジデントSMDC）, CD103- F3（ランゲルハンス細胞、LC）の4サブセットに分類できた。CD207^{+} SMDCは、CD103の発現によりLCと区別することができた。F1 DCは最も早く遊走し、CD86, CD273, CD274を高く発現していた。これに対して、CD103^{-} およびCD103^{+} F3 DC共に、遅れての遊走が認められ、CD103^{-} LCでは、共刺激分子発現誘導は制限されていた。F1 SMDCとF3 LCでは、遊走時期と共刺激分子発現の違いから、異なる役割を担っていることが示唆された。

2）

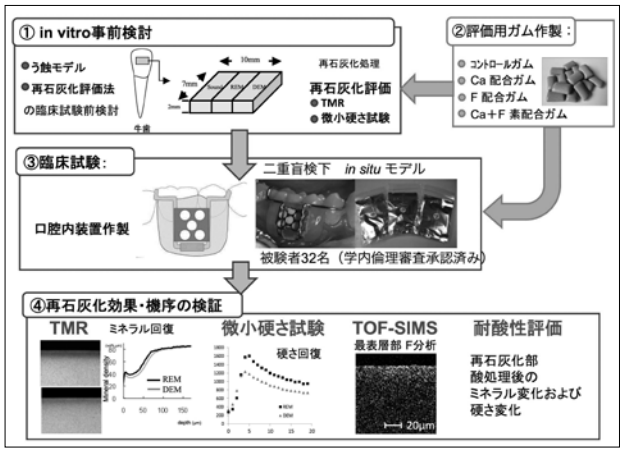

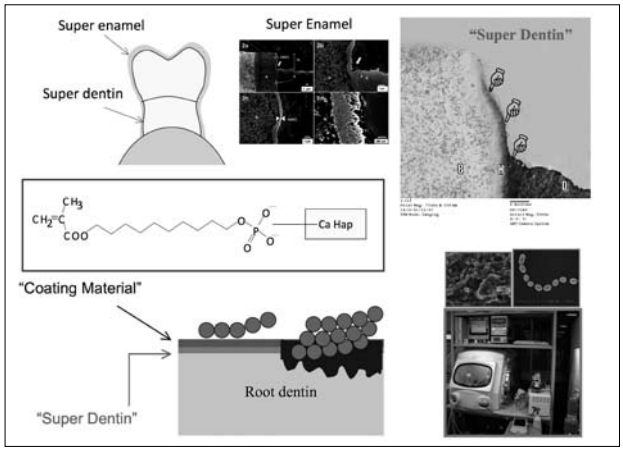

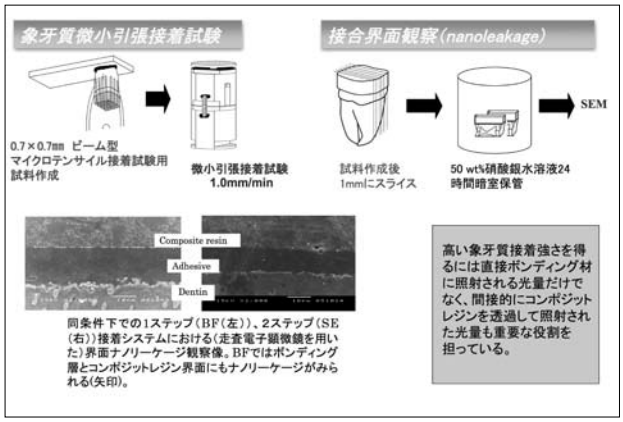

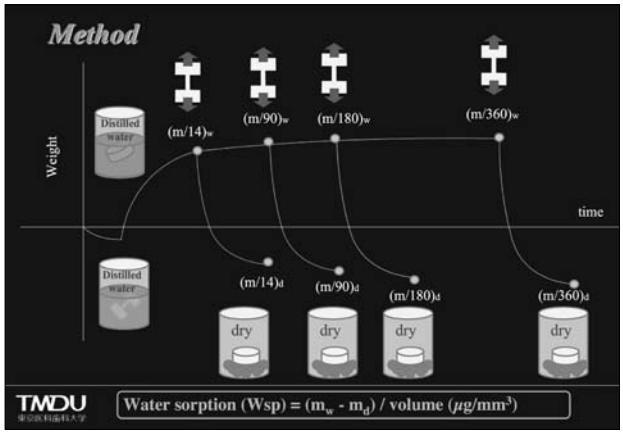

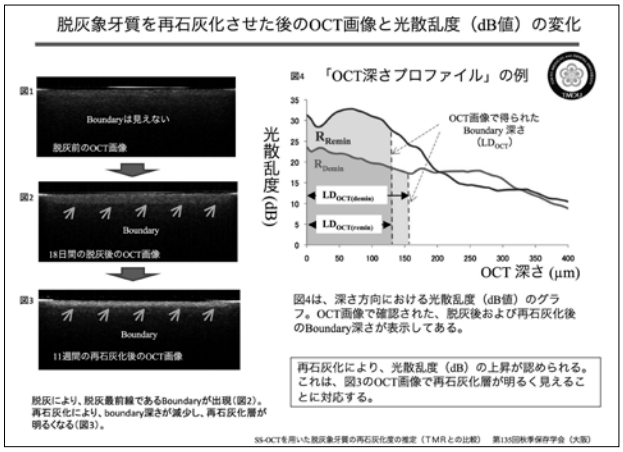
脱灰象牙質を再石灰化させた後のOCT画像と光散乱度（dB値）の変化
図1
Boundaryは見えない
脱灰前のOCT画像
図2
Boundary
18日間の脱灰後のOCT画像
図3
Boundary
11週間の再石灰化後のOCT画像
脱灰により、脱灰最前線であるBoundaryが出現（図2）。再石灰化により、boundary深さが減少し、再石灰化層が明るくなる（図3）。
図4 「OCT深さプロファイル」の例
光散乱度（dB）
OCT画像で得られたBoundary深さ（LD_OCT）
OCT 深さ（μm）
図4は、深さ方向における光散乱度（dB値）のグラフ。OCT画像で確認された、脱灰後および再石灰化後のBoundary深さが表示してある。
再石灰化により、光散乱度（dB）の上昇が認められる。これは、図3のOCT画像で再石灰化層が明るく見えることに対応する。
SS-OCTを用いた脱灰象牙質の再石灰化度の推定（TMRとの比較） 第135回秋季保存学会（大阪）

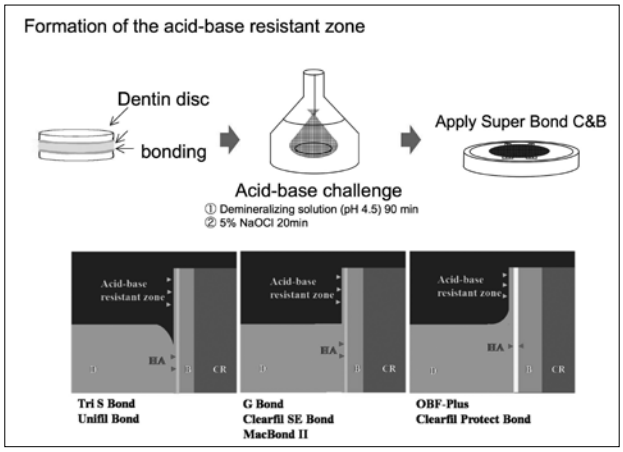
Formation of the acid-base resistant zone
Dentin disc
bonding
Apply Super Bond C&B
Acid-base challenge
① Demineralizing solution (pH 4.5) 90 min
② 5% NaOCl 20min
Acid-base resistant zone
HA
CR
Tri S Bond
Unifil Bond
G Bond
Clearfil SE Bond
MacBond II
OBF-Plus
Clearfil Protect Bond

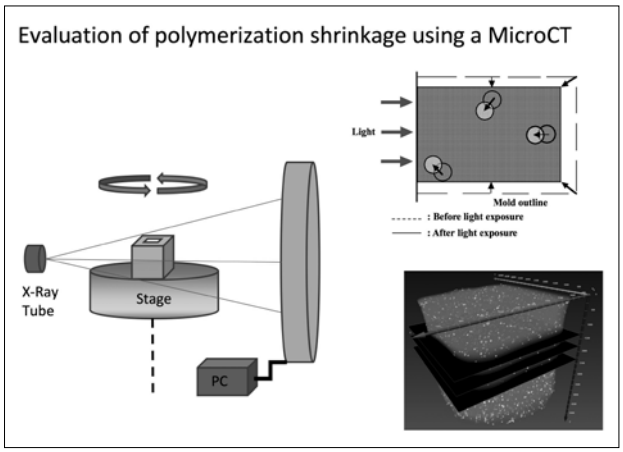
Evaluation of polymerization shrinkage using a MicroCT
Light
Mold outline
: Before light exposure
: After light exposure
X-Ray Tube
Stage
PC

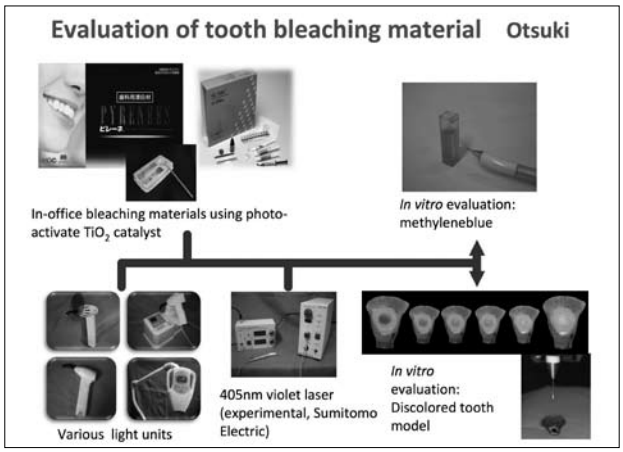
Evaluation of tooth bleaching material Otsuki
In-office bleaching materials using photo-activate TiO2 catalyst
In vitro evaluation: methyleneblue
Various light units
405nm violet laser (experimental, Sumitomo Electric)
In vitro evaluation: Discolored tooth model

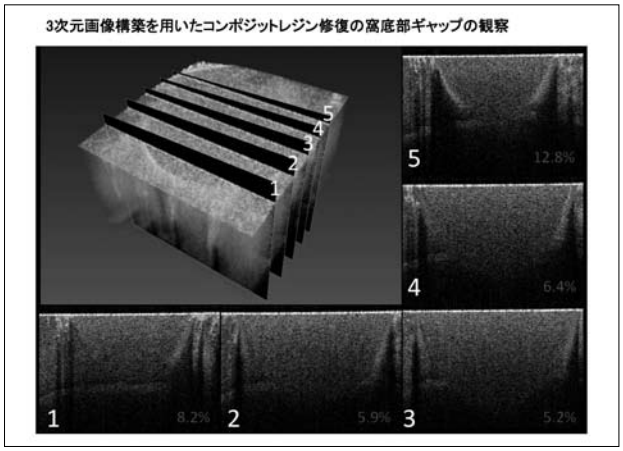
3次元画像構築を用いたコンポジットレジン修復の窩底部ギャップの観察
1
2
3
4
5
8.2%
5.9%
5.2%
6.4%
12.8%

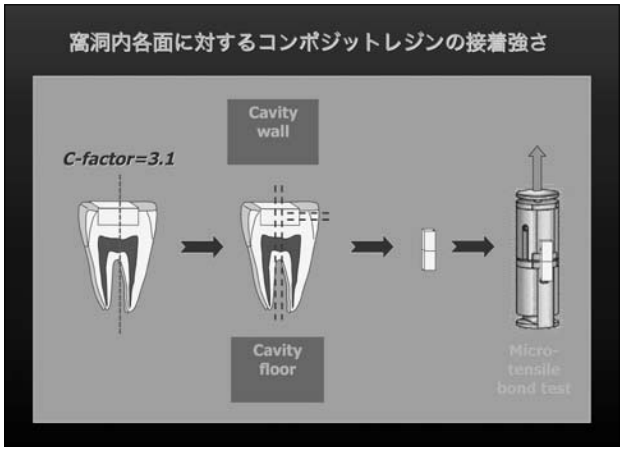
窩洞内各面に対するコンポジットレジンの接着強さ
C-factor=3.1
Cavity wall
Cavity floor
Micro-tensile bond test

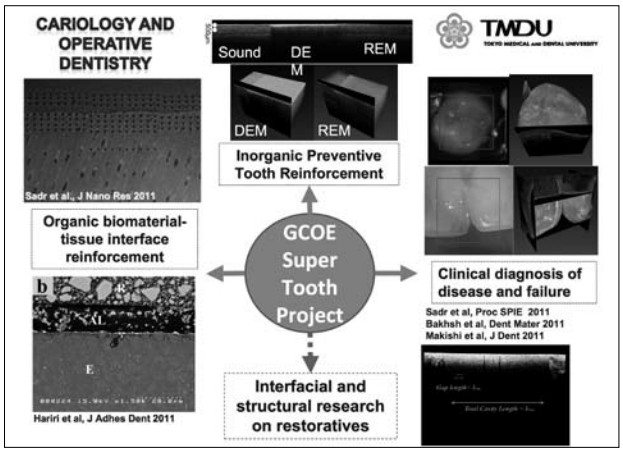
CARIOLOGY AND OPERATIVE DENTISTRY
TMDU
Sound
DEM
REM
Inorganic Preventive Tooth Reinforcement
Sadr et al., J Nano Res 2011
Organic biomaterial-tissue interface reinforcement
Hariri et al, J Adhes Dent 2011
GCOE Super Tooth Project
Clinical diagnosis of disease and failure
Sadr et al, Proc SPIE 2011
Bakhsh et al, Dent Mater 2011
Makishi et al, J Dent 2011
Interfacial and structural research on restoratives

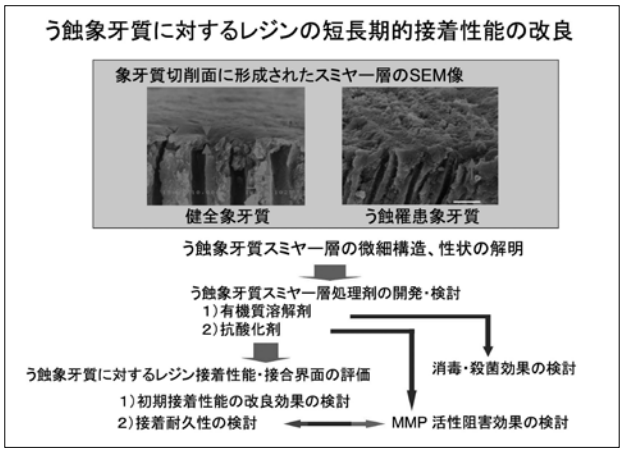
う蝕象牙質に対するレジンの短長期的接着性能の改良
象牙質切削面に形成されたスミヤー層のSEM像
健全象牙質
う蝕罹患象牙質
う蝕象牙質スミヤー層の微細構造、性状の解明
う蝕象牙質スミヤー層処理剤の開発・検討
1）有機質溶解剤
2）抗酸化剤
消毒・殺菌効果の検討
う蝕象牙質に対するレジン接着性能・接合界面の評価
1）初期接着性能の改良効果の検討
2）接着耐久性の検討
MMP 活性阻害効果の検討

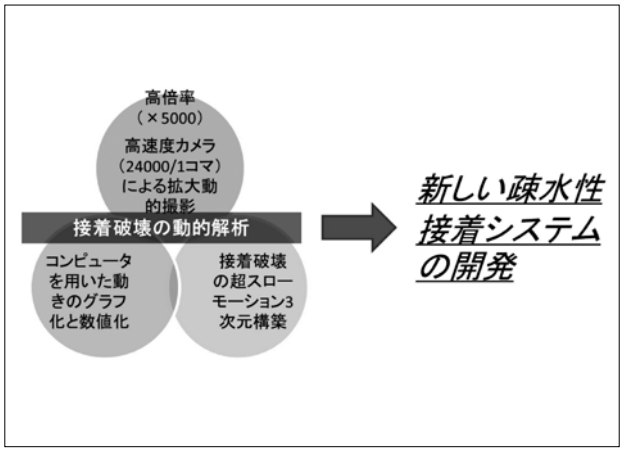

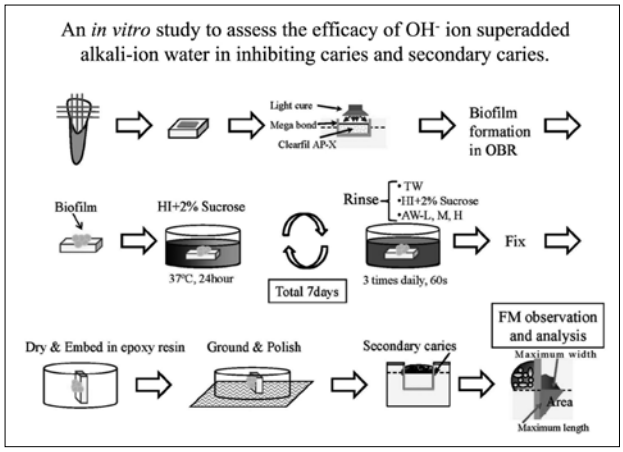

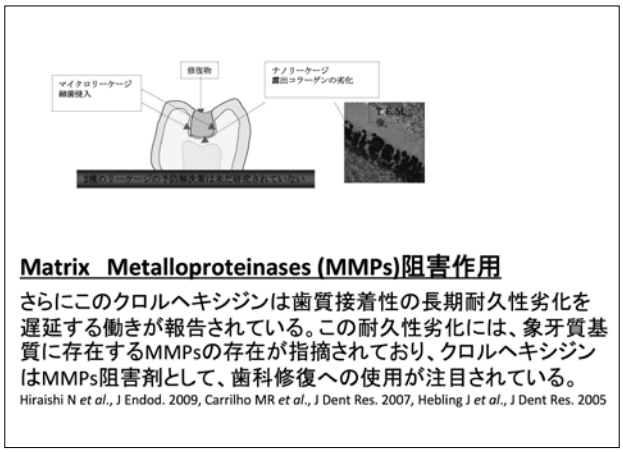

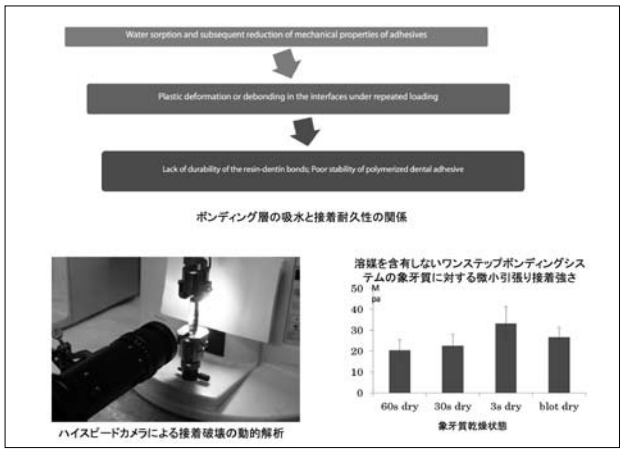

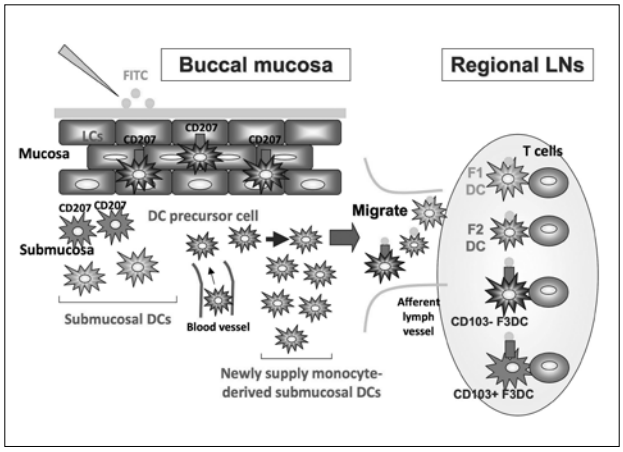

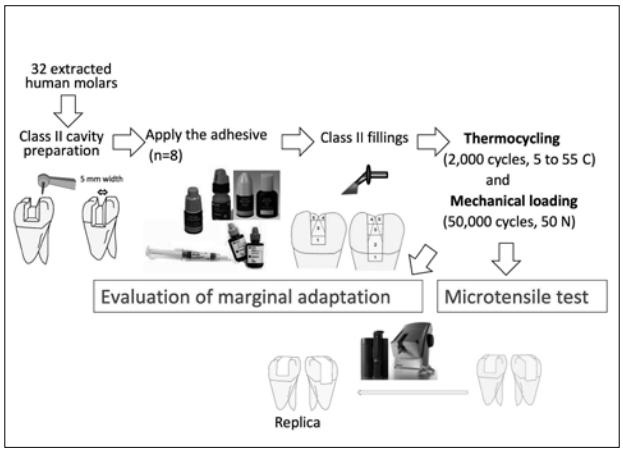

3）発表の研究内容についての英文要約

Effect of light units on tooth bleaching with visible-light activating titanium dioxide photocatalyst

This study evaluated the influence of different light sources on the efficiency of an office bleaching agent containing visible-light activating titanium dioxide photocatalyst（VL-TiO2）using an artificial discoloration tooth model. Extracted bovine teeth were stained by black tea. The CIE L*a*b* values were measured before and after nine consecutive treatments by the VL-TiO2-containing bleaching agent（TiON in Office, GC, Tokyo, Japan）. A halogen light unit（CB; CoBee, GC）or an LED unit（G-light, GC）with two modes（blue and violet：GL-BV, blue：GL-B）were used to activate the bleaching agent in three groups（n=8）. Brightness（ΔL）and color difference（ΔE）increased as bleaching repeated in all groups. Two-way ANOVA showed that both number of treatments and light sources significantly affected ΔE（$p<0.05$）. GL-BV showed better bleaching effect than GL-B. In measurement of irradiation spectra, CB showed a wide spectrum（380-530nm）, GL-B had a sharp peak at 470nm and GL-BV showed an additional peak at 405nm. It was concluded that the light source influenced the efficiency of the tooth bleaching with VL-TiO2.

Creation of Super Tooth by adhesion and analysis of its structure

The presence of an acid-base resistant zone (ABRZ) below the hybrid layer has been documented with self-etching adhesive systems in an artificial secondary caries attack. When ultrastructure of the ABRZ is assessed by SEM and TEM observations, formation of the ABRZ is considered to be due to the monomer penetration potential and fluoride release in the adhesive systems. Natural dentin has a limited potential to resist an acid attack of secondary caries; however, the ABRZ does not purely consist of dentin in morphology, it is rather a combination of dentin and the adjacent hybrid layer. Therefore, the reinforced dentin has been called ''Super Dentin'' bearing the ability to prevent primary and secondary caries. Recently, the evidence of the acid-base resistant enamel, so-called "Super Enamel" has also been confirmed. Formation of "Super Enamel/Dentin" is strongly influenced by the structural formulae of the functional monomer in the adhesive systems.

Clinical application of the resin coating technique

The purpose of this study was to evaluate the effect of resin coating and occlusal loading on microleakage of class II ceramic restorations. Molars were prepared for an MOD inlay and were divided into two groups : non-coated) ; and resin-coated, in which the cavity was coated with a combination of a dentin bonding system (Clearfil Protect Bond) and a flowable resin composite (Clearfil Majesty Flow) . Ceramic inlays were fabricated using the CAD/CAM technique (CEREC 3) and cemented with resin cement (Clearfil Esthetic Cement) . After 24 h of water storage, the specimens were divided into two subgroups : unloaded or loaded with an axial force of 80 N for 250,000 cycles. The teeth were sectioned bucco-lingually at the restorations. Tandem scanning confocal microscopy (TSM) was used for evaluation of microleakage. Loading did not have a significant effect on microleakage in either the resin-coated or non-coated group. Resin coating significantly reduced microleakage regardless of loading. Non-coated dentin showed extensive leakage, whereas resin-coated dentin showed decreased leakage. Resin coating with a combination of a dentin-bonding system and a flowable resin composite may be indicated prior to impression-taking when restoring teeth with CAD/CAM ceramic inlays in order to reduce microleakage at the tooth–resin interface.

Study on vertical root fracture reconstruction

Root fractures frequently occur in endodontically treated teeth. The treatment of vertical root fracture in a single-rooted tooth is usually extraction. A method involving intentional extraction followed by rotational replantation of tooth fragments bonded with adhesive resin cement has been proposed as a new treatment modality for complete vertical root fracture. Therefore the present study was designed to evaluate a dual cure composite core material along with different dentin adhesive systems as a reconstruction method of root fragments in a model complete vertical root fracture. The durability of adhesion between root fragments was tested for one year in water storage. The mean μTBS of the three different adhesive system-composite groups to root dentin demonstrated that the two step self-etch adhesive system, Clearfil SE Bond accomplished significantly higher μTBS than the rest of the adhesive system groups, Tokuyama Bond Force and Clearfil DC Bond regardless of water immersion period ($p<0.05$) .

Micro CT analysis on demineralization / remineralization of tooth

The study evaluated the effects of casein phosphopeptide-amorphous calcium phosphate (CPP-ACP) and CPP-ACP with 900 ppm fluoride (CPP-ACPF) pastes on inhibition of enamel demineralization over time, using micro-CT. The specimens were each treated by one of the following agents : deionized water; CPP-ACP paste; CPP-ACPF paste; and NaF solutions. After treatment, the specimens were immersed in a demineralizing solution (pH 4.5) for 24, 72, and 120 h. Mean mineral loss (ML) and lesion depth (LD) were determined from mineral density profiles obtained using micro-CT. ML values in all the treatment groups were significantly smaller than those in the control group after 72 and 120 h of demineralization ($p < 0.05$) . ML values in CPP-ACPF and NaF solution groups were significantly smaller compared to CPP-ACP group after 72 h ($p < 0.05$) . LD values in the CPP-ACPF and all the NaF solutions groups were significantly smaller compared to the control group after 120 h ($p < 0.05$) . The application of CPP-ACP or CPP-ACPF pastes to sound enamel surfaces resulted in inhibition of enamel demineralization, and a better effect was noted for the latter paste. Quantitative assessment using polychromatic micro-CT demonstrated to be useful for detecting mineral density changes.

Pretreatment effect of mildly acidic hypochlorous acid on adhesion to caries-affected dentin using a self-etch adhesive

Caries-affected dentin is covered with a thicker and organically enriched smear layer than normal dentin. This may affect the demineralization ability and the infiltration of self-etch adhesives, thus reducing the efficacy of bonding to caries-affected dentin. This study evaluated the adhesion of a two-step self-etching adhesive to normal and cariesaffected dentin after pretreatment with mildly acidic hypochlorous acid (HOCl) solutions. We used a microtensile bond strength (μ TBS) test to compare the μ TBS of Clearfil SE Bond to either caries-affected dentin or to

normal dentin, after pretreatment for 5 s with one of three solutions（806 mM NaOCl, or 0.95 or 1.91 mM HOCl）. The μ TBS of the self-etch adhesive was significantly lower to caries-affected dentin than to normal dentin. Pretreatment with 0.95 mM HOCl improved the μ TBS of the self-etch adhesive to caries-affected dentin, but there was no significant difference compared with normal dentin. On the other hand, pretreatment with 806 mM NaOCl or 1.91 mM HOCl did not demonstrate a significant improvement in the μ TBS to caries-affected dentin. None of the pretreatments demonstrated a negative effect on adhesion to normal dentin.

The Effect of RDT on Resin Composite Bond Strength to the Dentin

The purpose of this study was to evaluate the effect of remaining dentin thickness（RDT）on resin composite bond strength to the flat dentin surfaces using various adhesive systems. The occlusal enamel was ground to expose a flat dentin surfaces and finished of human molars. Each specimen was restored with one of three adhesives：Clearfil SE Bond, Single Bond or Clearfil Tri-S Bond; followed by buildup（3x5x2 mm, C-factor=0.3）of resin composite using Z100. After 600mW/cm^2 for 40s light-curing, teeth were stored in the dark for 24 hours in water. The teeth were sectioned perpendicularly to flat dentin obtaining approximately 1 mm^2 beams. All specimens remaining dentin thickness（RDT）was measured. The micro-tensile bond strength（μTBS）was determined. Data were separating four group; 1 flat：RDT< 2 mm、2 flat：2 ≦-<3 mm、3 flat：3 ≦-< 4 mm、4 flat：≧ 4 mm. RDT ≧4mm group using Clearfil Mega Bond showed highest μTBS in all data. Resin composite bond strength to different RDT flat dentin was affected by adhesive system.

The Resin Composite Bond Strength to the Different Cavity Wall

The purpose of this study was to evaluate the effect of cavity wall on resin composite bond strength to the dentin using two adhesive systems. The occlusal enamel of human molars was ground to expose a flat dentin surfaces and finished with carbide paper. Box-form occlusal cavities, 3 mm wide, 5 mm long, 2 mm deep（C-factor=3.1）, were prepared on flat dentin surfaces of human molars. Each specimen was restored with one of two self-etching adhesive systems：Clearfil Mega Bond or Clearfil Tri-S Bond; followed by bulk filling using Z100 resin composite. After 600mW/cm^2 for 40s light-curing, teeth were stored in the dark for 24 hours in water maintained at 37 degrees centigrade. Specimen was cut perpendicular to cavity floor and cavity wall obtaining beams having cross-sectional areas of approximately 0.9 mm^2. The micro-tensile bond strength（μTBS）was determined. The bond strength of resin composite to a cavity dentin was affected by wall part and bonding system used.

The Effect of Dentin Location on the Composite Bond Strength to the Dentin

The purpose of this study was to evaluate the effect of dentinal tubule orientation on resin composite bond strength to floor and wall using various adhesive systems. Box-form occlusal cavities 3 x 5 x 2 mm were prepared on flat dentin surfaces of human molars. After that walls of cavities were removed in order to make flat dentin floors and walls for bonding. Each specimen was restored with one of two adhesives：Clearfil Mega Bond or Single Bond; followed by build up using Z100 resin composite. After 600mW/cm^2 for 40s light-curing, teeth were stored in the dark for 24 hours in water maintained at 37 degrees centigrade. Specimen was cut parallel to floor or wall obtaining approximately 1 mm^2 beams. The micro-tensile bond strength（μTBS）to flat dentin floor or wall specimen, was determined. Clearfil Mega Bond bond strength to dentin wall group showed highest bond strength in all group. Clearfil Mega Bond and Single Bond showed significantly higher μ-TBS to dentin wall compared with that of dentin floor group. Bonding to dentin floor and wall was affected by dentin location and dentin tubule orientation.

Non-invasive quantification of resin-dentin interfacial gaps using SS-OCT

Polymerization shrinkage of light-cured dental composites may result in gap formation at the tooth-restoration interface; non-destructive assessment and monitoring of these defects are important. Three dimensional imaging of a composite restoration can help in clinical decision making by the dentist. The aim of this study is to assess the tooth-restoration interface using 3D images obtained from swept source optical coherence tomography（SS-OCT）and to confirm the findings with confocal laser scanning microscope（CLSM）. Cross-sectional images of restoration-tooth interfaces were chosen from the constructed 3D images of composite restoration; Area fraction of pixels with high brightness values at the interfacial zone was then calculated using digital image analysis software. A significant positive linear correlation was found between stained and non-stained SS-OCT images. It was concluded that 3D imaging by SS-OCT can be considered as a non-invasive technique for fast detection of gaps at the restoration interface, with or without a staining solution.

Quantitative analysis of enamel and dentin demineralization using SS-OCT

This study aimed to investigate whether swept source optical coherence tomography（SS-OCT）could estimate the lesion depth and mineral loss quantitatively without the

use of polarization sensitivity, and to examine a relationship between OCT data and transverse microradiography (TMR) lesion parameters. Bovine enamel and dentin specimens were demineralized for experimental periods, following SS-OCT observation and TMR analysis were performed. The OCT images showed "boundaries," suggesting the lesion front. Integrated dB values before and after the demineralization and their difference were calculated from the lesion surface to the corrected depth of boundary. The interaction point of SS-OCT signal profile obtained from demineralized enamel with and without moisture showed significant correlation with the deminaralized depth from TMR analysis. In case of dentin, OCT also could estimate the lesion depth and mineral loss as significant, but moderate correlations in the lesion parameters were found between SS-OCT and TMR. The OCT showed a potential for quantitative estimation of lesion depth and mineral loss with enamel and dentin lesions.

Effects of a chewing gum containing POs-Ca and fluoride on remineralization and crystallization of enamel subsurface lesions in situ

The aim of this study was to assess the effect of a chewing gum containing POs-Ca and fluoride on remineralization of enamel subsurface lesions. Thirty-six volunteer subjects wore appliances with insets of bovine enamel with subsurface demineralized lesions. For 14 days the subjects chewed one of the three chewing gums (control, POs-Ca, POs-Ca + F). After each treatment period, the insets were removed from the appliance, and then subjected to laboratory tests; mineral level was determined by TMR, and hydroxyapatite (HAp) crystallites were assessed by synchrotron radiation wide-angle X-ray diffraction (WAXRD). Chewing POs-Ca and POs-Ca + F gums resulted in 21.9 ± 10.6 and 26.3 ± 9.4 (mean ± SD) percentage mineral recovery, which was significantly higher than that of placebo gum (15.0 ± 11.4) ($p < 0.05$). Chewing POs-Ca + F gum resulted in 24.9 ± 5.4 (mean ± SD) percentage HAp crystallites recovery, which was significantly higher compared to POs-Ca (16.0 ± 4.1%) or placebo (11.1 ± 4.8%) gums ($p < 0.05$). Addition of POs-Ca to the chewing gum resulted in significant remineralization of enamel subsurface lesions in situ.

Assessment and improvement of Acid-base resistant zone

Previous studies showed the existence of acid base resistant zone beneath the hybrid layer. Fluoride in adhesives could reinforce the dentin-adhesive interface and make the acid base resistant zone strong than normal dentin. In terms of durability of this layer, after 3 or 6 months the shape did not change. However the acid base resistant zone without fluoride has been attacked after storing and reduced its width. On the other hand, the effects of the fluoride and calcium containing solution apply onto tooth surface before bonding were showed on micro tensile bond strength test and acid base resistant zone observation. The application of the solution didn't affect bond strength and did make good effect on acid base resistant zone.

Evaluation of resin composite polymerization by three dimensional micro-CT imaging.

Light-cured composites undergo shrinkage during polymerization. The aim of this study was to evaluate regional shrinkage within a light-cured composite during polymerization by microcomputed tomography and mechanical properties by nanoindentation in bonded or non-bonded class-I cavity. The magnitude and direction of regional polymerization shrinkage depends on boundary conditions, depth and conversion degree. Polymerization shrinkage effect is most significant at the deepest part of the cavity. The application of micro-CT combined with sophisticated image analysis is a novel approach to investigate shrinkage mechanisms of dental composites.

Fundamental analysis and clinical application of dentin adhesives

The newly developed relatively hydrophobic one-step adhesive system bonded to dentin, compared with commercially available one-step adhesives was evaluated. Flat coronal dentin surfaces of extracted third human molars were prepared. One-step adhesive systems, MTB-200 (Kuraray Medical Inc.), Clearfil S3 Bond (Kuraray) and Bond Force (Tokuyama Corp.) were applied to the dentin surfaces according to the manufacturer's instructions. A hybrid resin composite (Clearfil AP-X, Kuraray) was used for the coronal build-up. After storage in water for 24h, the specimens were vertically sectioned into slabs that were trimmed to hourglass shapes and subjected to micro-tensile bond testing (μTBS). The data were statistically analyzed using a one-way ANOVA and Dunnett T3 test (a=0.05). Results : Values are in MPa ± S.D. (n=10). Groups identified by the different superscript letter are significantly different ($p<0.05$). The failure mode of bonded specimens of each adhesive was observed by hi-speed camera.

The influence of light intensities irradiated directly and indirectly through resin composite to self-etch adhesives on dentin bonding

This study was designed to evaluate effects of light-irradiated intensities directly and indirectly through resin composites to one- and two-step self-etch adhesives on dentin bonding. One-step (Clearfil S^3 Bond; TS, Bond Force; BF) or two-step (Clearfil SE Bond; SE) self-etch adhesives was applied to dentin surface. The adhesive agent was

light-cured with light-intensity of 350 or 600 mW/cm^2, and then resin composite with different colors (translucent or opaque shade) was filled and light-cured with the same light-intensity as the bonding procedure. After 24 h water storage, bond strengths to dentin were determined using μ TBS test. For the 600 and 350 mW/cm^2 groups, translucent shade resin obtained higher μ TBS than opaque shade resin. Using SE and BF, the 350 mW/cm^2 group in translucent shade resin was higher μ TBS than the 600 mW/cm^2 group in opaque shade resin, while TS showed no different μ TBS between them.

Long-term evaluation of water sorption and ultimate tensile strength of HEMA-containing/-free one-step self-etch adhesives

The objective of this study was to evaluate the water sorption (Wsp) and ultimate tensile strength (UTS) of one-step self-etch adhesives after long-term water-storage. Three HEMA-containing one-step self-etch adhesives (Bond Force (BF), Clearfil S (3) Bond (S3) and OptiBond All-In-One (OP)), and one HEMA-free one-step self-etch adhesive, G Bond (GB) was used. After the solvents of each adhesive were evaporated, polymerised adhesive disks and dumbbell-shaped specimens of thirty-two each were prepared and divided into four groups of 14-, 90-, 180- and 360-day water-storage. After immersion in water for the designated storage periods, the disks were subjected to measurement of Wsp, and the dumbbell-shaped specimens were subjected to measurement of UTS. The data were statistically analysed using a two-way ANOVA and Bonferroni test. Wsp of BF, S3 and OP increased over time, whereas for GB, there were no significant differences in Wsp among all the storage periods. Wsp of GB was lower than those of BF, S3 and OP in each period. The UTS of BF, S3 and OP decreased over time, whereas for GB, there were no significant differences in UTS among all storage periods. The highest UTS was initially seen in BF>GB=S3=OP, and after 360-day water-storage, seen in BF=GB>OP=S3.

Contemporary adhesives：marginal adaptation and microtensile bond strength of class II composite restorations

The marginal adaptation (in terms of % continuous margin) and microtensile bond strength (μTBS) of the enamel and dentin of direct class II composite restorations were evaluated.

32 class II cavities were prepared with one proximal box limited within the enamel and one proximal box extending into the dentin. The teeth (n=8/group) were restored with：Adper Scotchbond Multi Purpose (SMPP), Adper Scotchbond 1 XT (S1XT), Clearfil SE Bond (CSEB), or Clearfil Tri-S Bond (CTSB) and incrementally placed composite restorations. Marginal adaptation was evaluated by SEM. The teeth were sectioned and trimmed to obtain specimens for μTBS testing. All adhesive systems exhibited continuous margins with enamel of over 95.4%, whereas continuous margins with dentin ranged from 60.2 to 84.8%. The mean μ TBSs [MPa] for enamel were 40.5 (SMPP), 37.3 (S1XT), 30.8 (CSEB) and 23.2 (CTSB), and for dentin, they were 37.7 (SMPP), 33.0 (S1XT), 37.3 (CSEB) and 29.0 (CTSB). The self-etch adhesive systems showed excellent marginal adaptation to dentin. SMPP provided the highest bond strength to both enamel and dentin, whereas CSEB was the most predictable adhesive for dentin and an acceptable adhesive for enamel.

The effect of chlorhexidine to improve dentin bond durability

The activities of endogenous collagenase and gelatinase derived from demineralized dentin are thought to induce the degradation of bonded dentin matrix in the hybrid layer. Therefore, the application of some specific MMP inhibitors which can suppress dentin collagenolytic and gelatinolytic activities should be considered in clinical procedure. Chlorhexidine (CHX) is a broad-spectrum anti- microbial agent used widely in the treatment of oral diseases. Its antibacterial efficacy is com-parable to that of sodium hypochlorite. Recently, CHX has been found to have desirable MMP- inhibition properties even at low concentrations. In this project, we examine that application of CHX before use of adhesives has no influence on the short-term bonding strength. Moreover the long term durability of dentin adhesives is investigated.

Effect of Hesperidins on stabilization of collagen and remineralization of dentin Lesion

The aim of this study to evaluate the effect of hesperidin on：

1) Prevent dentin collagen breakdown.
2) Enhance the dentin remineralization .
3) Inhibit the progression of caries formation

Although the mechanism of dentin caries has not been well established, the de/re-mineralizing process would be regulated through the interactions of mineral contents with the condition of exposed collagen matrix. It was reported that stability of dentin matrix can be achieved by the use of hesperidin, a citrus flavonoid, because of its effect of collagen cross-linkers. We observe the effect of hesperidin in vitro bovine and human dentin collagen and de/re-mineralization and compare with that of grape seed, epigallocate- chin gallate and chlorhexidine.

Degradation of collagen during the pH cycling is determined using the chloramine T method by estimating hydroxyproline content from degraded collagen. Dissolved calcium ion is measured by means of an atomic absorption

spectroscopy. The mineral loss and lesion depth is examined using transverse microradiography.

Effect of Natural Cross-linkers Incorporation in the Primer of a Self-Etch Adhesive on Resin-Dentin Bond Strength

The use of cross-linking agents such as tannic acid has been found not only to lower the rate of enzymatic degradation of collagen thus enhancing the resin-dentin bond strength but also increased the mechanical properties of dentin . Hesperidin was found to resist collagen degradation and arrest demineralization on bovine root dentin. The objectives of this study are to evaluate the effect of hesperidin inclusion into the primer of a self-etch adhesive system and compare it with the effect of other compounds. We examine that incorporation of cross-linker improve the initial bond strength to dentin, and addition of cross-linker improve the micro-mechanical properties of resin-dentin interface. Further we study whether the long term durability of dentin bond would be improved when hesperidin can be incorporated into self-etching primers.

Estimation of dentin lesion remineralization by SS-OCT in comparison with TMR

Ultimate gaol of this study is to develop a quantitative diagnostic system for monitoring de-/ remineralization in root caries lesion. So the purpose of this in vitro study was to examine relationship between SS-OCT（Swept Source Optical Coherence Tomography）cross-sectional image information and TMR（transverse microradiography）lesion parameters（lesion depth, mineral loss）using artificially produced root caries lesions which were remineralized for 2-11 weeks. This study demonstrated that the OCT image showed a clear“boundary”, looked brighter due to back-scattering, which corresponded to the lesion front confirmed by TMR analysis. The“boundary depth”, from lesion surface to the“boundary”, was decreased by remineralization period over time. Statistically significant correlation was found between the“boundary depth”and actual lesion depth determined by TMR. Similar correlation was noted between integrated reflective intensity（dB × μ m）and mineral loss.

Differential expression of co-signal molecules and migratory properties in four distinct subsets of migratory dendritic cells from the oral mucosa

Variations in co-signal ligand expression and cytokine production greatly influence the antigen-presenting properties of migrating DCs in regional lymph nodes（RLNs）. We investigated DCs migrating from the oral mucosa using CD326 and CD103 antigens for discriminate $CD207^{+}$ Langerhans cells（LCs）from $CD207^{+}$ submucosal DCs（SMDCs）. We identified four distinct oral mucosal DC（OMDC）subsets, $CD11c^{hi}CD207\text{-}CD103\text{-}CD326^{int}CD11b^{hi}$（F1; resident $CD11b^{hi}$ SMDCs）, $CD11c^{int/lo}CD207\text{-}CD103\text{-}CD326^{lo}CD11b^{int/hi}$（F2; newly recruited blood-derived SMDCs）, $CD11c^{int/lo}CD207^{+}CD103^{+}CD326^{int/hi}CD11b^{lo}$（$CD103^{+}$ F3; resident $CD207^{+}$ SMDCs）, and $CD11c^{int/lo}CD207^{+}CD103\text{-}CD326^{int/hi}CD11b^{lo}$（CD103- F3; resident LCs）. F1 DCs migrated rapidly after fluorescein isothiocyanate（FITC）painting and expressed notably high levels of CD86, CD273, and CD274 at an earlier time point. In contrast, CD103-LCs expressing the highest levels of the epithelial cell adhesion molecule CD326 accounted for a minor subset at the earlier time point, but increased slowly with $CD103^{+}CD207^{+}$ SMDCs. However, their expression of CD86, CD273, and CD274 was very limited. The delayed migration and limited induction of co-signal ligands suggest that roles of OMLCs are distinct from those of the other three DC subsets. The identification of distinct subsets of OMDCs in RLNs may benefit efforts to determine the functional specialization of each subset in T cell responses against orally administrated antigens.

4）本事業に関連して世界的な研究拠点形成に向けて、以下の点で改善・整備等されたこと

A（研究拠点体制）

ペンシルバニア大学歯学部（米国）、ジョージア医科大学歯学部（米国）、カンピナス大学歯学部（ブラジル）、アレキサンドリア大学歯学部（エジプト）、テヘラン大学歯学部（イラン）、King's College of London 歯学部（英国）、ミュンヘン大学歯学部（ドイツ）、モンペリエ大学歯学部（フランス）、ブルノ大学歯学部（チェコ共和国）、国際カトリック大学（スペイン）、マヒドン大学歯学部（タイ）、チュラロンコン大学歯学部（タイ）、チェンマイ大学歯学部（タイ）、シドニー大学歯学部（オーストラリア）、香港大学歯学部（中国）、西安第4軍医大学（中国）、延世大学歯学部（韓国）、岡山大学歯学部（日本）との間で外国人研究者の受入れ、共同研究の継続および新たな立ち上げを行った。内外の歯科器材メーカー8社と、器材の共同開発のための企画の立ち上げ、情報交換のための会議を行った。

B（研究教育環境）

各種研究設備の整備のため、獲得した外部資金や企業との委託研究による資金を充てた。分野内で調達できないものについては学外の施設の利用を推進した。特にOCTの実用化に向けて、試作機を導入して臨床評価を開始した。

C（人材確保）

外部資金により複数の特任教員を雇用し、特に歯の脱

灰と再石灰化に関する研究と、抗MMP物質の根面う蝕の抑制効果に関する研究に取り組む学生の指導の強化および研究の推進を図った。さらに外国人研究者も多く受け入れて、大学院生と共同で研究をおこなわせることで、相互の能力開発を図った。特任教員による指導により大学院学生が国際学会で優秀発表賞を受賞した。

D（人材育成）

多くの学生を国際学会に派遣して研究発表させて、多くの研究者と討論させる機会を提供した。各研究グループと定期的なミーティングを行い、研究内容に関する議論の場を多く持つよう心掛けた。学会発表に際しては、すべての演者にリハーサルを義務付けて、分野の教員、学生全員により、プレゼンテーションの内容、形式についての改善を行った。学生及び若手教員が内外の学会で学術賞を受賞した。

E（国際化）

国際学会だけでなく、海外での臨床家向けのプログラムにおいても講演を積極的に行い、現在臨床に携わる歯科医師にも当教室の研究成果を普及し、新たな留学生確保のための情報提供も行った。大学院生の約40%が留学生という状況を最近5年間維持している。東アジア東南アジアだけでなく、中東からの学生も増加し、新たな国際ネットワーク形成が確立しつつある。特に母国政府の奨学金を受給する学生の受け入れが進んでいる。大学院向けの講義は長年英語で行ってきており、外国人留学生、研究者が活動しやすい環境を整備している。米国の臨床家向けのUSCの卒後研修プログラムで、講演の機会を得て、本プログラムの成果を普及することができた。

5）GCOE事業を推進するに当たって力を入れた点

・外部資金は決して十分とはいえないが、複数の特任教員を雇用して、これまでに十分な研究指導、推進ができなかった領域をカバーした。
・国際学会での研究発表の機会を多く提供できるよう、外部資金の獲得に努めている。
・研究拠点としてのアピールのため、臨床的なテーマのプログラムにおいても多くの講演、研究発表を行い、研究成果の臨床への貢献をアピールするよう心掛けた。

6）英文原著論文

1. ◎Aoki K, Kitasako Y, Ichinose S, Burrow MF, Ariyoshi M, Nikaido T, Tagami J. Ten-year observation of dentin bonding durability of 4-MATE/MMA-TBB resin cements – a SEM and TEM study. Dent Mater J 30（4）：438-447, 2011
2. Aramaki O, Chalermsarp N, Otsuki M, Tagami J, Azuma M. Differential expression of co-signal molecules and migratory properties in four distinct subsets of migratory dendritic cells from the oral mucosa. Biochem Biophys Res Commun 413（3）：407-413, 2011
3. ◎Bakhsh TA, Sadr A, Shimada Y, Tagami J, Sumi Y. Non-invasive quantification of resin-dentin interfacial gaps using optical coherence tomography：validation against conforcal microscopy. Dent Mater 27（9）：915-25, 2011
4. ◎Bakhsh TA, Sadr A, Shimada Y, Khunkar S, Tagami J, Sumi Y. Relationship between Non-destructive OCT Evaluation of Resins Composites and Bond Strength in a Cavity. Proc SPIE 8208（in press）.
5. ◎Bakry AS, Takahashi H, Otsuki M, Yamashita K, Tagami J. CO2 Laser Improves 45S5 Bioglass Interaction with Dentin. J Dent Res 90（2）：246-50, 2011
6. ◎Bakry AS, Tamura Y, Otsuki M, Kasugai S, Ohya K, Tagami J. Cytotoxicity of 45S5 bioglass paste used for dentine hypersensitivity treatment. J Dent 39（9）：599-603, 2011
7. ◎Cho E, Sadr A, Inai N, Tagami J. Evaluation of resin composite polymerization by three dimensional micro-CT imaging and nanoindentation. Dent Mater 27（11）：1070-8、2011
8. ◎Emamieh S, Sadr A, Ghasemi A, Torabzadeh H, Akhavanzanjani V, Tagami J. Effects of solvent drying-time and water storage on ultimate tensile strength of adhesives. J Inves Clin Dent（in press）
9. ◎Fujii M, Kitasako Y, Sadr A, Tagami J. Roughness and pH changes of enamel surface induced soft drinks in vitro-applications of stylus profilometry, focus variation 3D scanning microscopy and micro pH sensor. Dent Mater J 30（3）：404-410, 2011
10. ◎Hamba H, Nikaido T, Inoue G, Sadr A and Tagami J. The effects of CPP-ACP with sodium fluoride on inhibition of bovine enamel demineralization：a quantitative assessment using micro-computed tomography. J Dent. 39（6）：405-13, 2011
11. ◎Hariri I, Sadr A, Shimada Y, Tagami J, Sumi Y. Effects of structural orientation of enamel and dentin on light attenuation and local refractive index：an optical coherence tomography study. J Dent（in press）
12. ◎Hariri I, Shimada Y, Sadr A, Ichinose S, Tagami J. The Effects of Aging on Shear Bond Strength and Nanoleakage Expression of an Etch-and-Rinse Adhesive on Human Enamel and Dentin. J Adhes Dent（in press）
13. ◎Hariri I, Sadr A, Shimada Y, Nakashima S, Sumi Y, Tagami J. Relationship between Refractive Index and Mineral Content of Enamel and Dentin Using SS-OCT

and TMR. Proc SPIE 8208（in press）.
14. ◎Hayati F, Okada A, Kitasako Y, Tagami J, Matin K. An artificial biofilm-induced secondary caries model for in vitro studies. Aust Dent J 56（1）：40-7, 2011
15. ◎Ichikawa C, Nikaido T, Inoue G, Sadr A, Tagami J. Ultra-morphologies of the dentin acid-base resistant zone of two-step self-etching systems after long-term storage in water. J Adhes Dent（in press）
16. ◎Jamleh A, Sadr A, Nomura N, Yahata Y, Ebihara A, Hanawa T, Tagami J, Suda H. Nano-indentation testing of new and fractured nickel-titanium endodontic instruments. Int Endod J（in press）
17. ◎Kishi A, Otsuki M, Sadr A, Ikeda M, Tagami J. Effect of light units on tooth bleaching with visible-light activating titanium dioxide photocatalyst. Dent Mater J 30（5）：723-729, 2011
18. ◎Kitasako Y, Tanaka M, Sadr A, Hamba H, Ikeda M, Tagami J. Effects of a chewing gum containing phosphoryl oligosaccharides of calcium（POs-Ca）and fluoride on remineralization and crystallization of enamel subsurface lesions in situ. J Dent 39（11）：771-779, 2011
19. ◎Kitayama S, Nasser NA, Pilecki P, Wilson RF, Nikaido T, Tagami J, Watson TF, Foxton RM. Effect of resin coating and occlusal loading on microleakage of class II computer-aided design/computer-aided manufacturing fabricated ceramic restorations：a confocal microscopic study. Acta Odontol Scand 69（3）：182-192, 2011
20. ◎Kunawarote S, Nakajima M, Foxton RM, Tagami J. Pretreatment effect of mildly acidic hypochlorous acid on adhesion to caries-affected dentin using a self-etch adhesive. Eur J Oral Sci 119（1）：86-92, 2011
21. ◎Kuribayashi M, Kitasako Y, Matin K, Sadr A, Shida K, Tagami J. Intraoral pH measurement of carious lesions with qPCR of cariogenic bacteria to differentiate caries activity. J Dent（in press）
22. ◎Makishi P, Shimada Y, Sadr A, Tagami J, Sumi Y. Non-destructive 3D imaging of composite restorations using optical coherence tomography：marginal adaptation of self-etch adhesives. J Dent 39（4）：316-25, 2011
23. ◎Natsume Y, Nakashima S, Sadr A, Shimada Y, Tagami J, Sumi Y. Estimation of lesion process in artificial root caries by swept source optical coherence tomography in comparison to transverse microradiography. J Biomed Opt 16（7）：071408, 2011
24. ◎Nikaido T, Chikawa C, Li N, Takagaki T, Sadr A ,Yoshida Y, Suzuki K, Tagami J. Effect of functional monomers in all-in-one adhesive systems on formation of enamel/dentin acid-base resistant zone. Dent Mater J 30（5）：576-582, 2011
25. ◎Nurrohman H, Nikaido T, Sadr A, Takagaki T, Kitayama S, Ikeda M, Waidyasekera K, Tagami J. Long-term regional bond strength of three MMA-based adhesive resins in simulated vertical root fracture. Dent Mater J. 30（5）：655-663, 2011
26. Oyanagi T, Tagami J, Matin K. Potentials of Mouthwashes in Disinfecting Cariogenic Bacteria and Biofilms Leading to Inhibition of Caries. The Open Dent J（in press）
27. ◎Prasansuttiporn T, Nakajima M, Kunawarote S, Foxton RM, Tagami J. Effect of reducing agents on bond strength to NaOCl-treated dentin. Dent Mater 27（3）：229-234, 2011
28. ◎Sadr A, Nikaido T, Takagaki T, Hariri I, Nazari A, Tagami J. Ultra-morphological and Nanomechanical Characterization of Reinforced Enamel and Dentin by Self-etch Adhesives：The Super Tooth. J Nano Res（in press）
29. ◎Seki N, Nakajima M, KishikawaR, HosakaK, Foxton RM, TagamiJunji. The influence of light intensities irradiated directly and indirectly through resin composite to self-etch adhesives on dentin bonding. Dent Mater J 30（3）：315-322, 2011
30. Senawongse P, Pongprueksa P, Hannirattisai C, Sumi Y, Otsuki M, Shimada Y, Tagami J. Non-destructive assessment of cavity wall adaptation of class V composite restoration using swept-source optical coherence tomography. Dent Mater J 30（4）：517-22, 2011
31. ◎Shinoda Y, Nakajima M, Hosaka K, Otsuki M, Foxton RM, Tagami J. Effect of smear layer characteristics on dentin bonding durability of HEMA-free and HEMA-containing one-step self-etch adhesives. Dent Mater J 30（4）：501-510, 2011
32. ◎Shinoki.T, Kato J, Otsuki M, Tagami J. Effect of cavity preparation with Er：YAG laser on marginal integrity of resin composite restorations. Asian Pac J Dent 11（1）：19-25, 2011
33. ◎Takahashi M, Nakajima M, Hosaka K, Ikeda M, Foxton RM, Tagami J. Long-term evaluation of water sorption and ultimate tensile strength of HEMA-containing/-free one-step self-etch adhesives. J Dent 39（7）：506-12, 2011
34. ◎Takahashi R, Nikaido T, Tagami J, Hickel R, Kunzelmann KH. Contemporary adhesives：marginal adaptation and microtensile bond strength of class II composite restorations. Am J Dent（in press）
35. ◎Tanno K, Hiraishi N, Otsuki M, Tagami J. Evaluation of cavity adaptation of low-shrinkage composite resin. Asian Pac J Dent 11（1）：27-33, 2011
36. ◎Tsai Y-L, Nakajima M, Wang C-Y, Foxton RM, Lin C-P, Tagami J. Influence of etching ability of one-step self-etch adhesives on bonding to sound and non-carious cervical sclerotic dentin. Dent Mater J 30（6）：941-947, 2011

37. ◎Uchida R, Matin K, Tagami J. An in vitro study to assess the efficacy of OH- ion superadded alkali-ion water in inhibiting caries and secondary caries. Asian Pac J Dent 11：1-8, 2011.
38. ◎Sadr A, Nakashima S, Shimada Y, Tagami J, Sumi Y. Longitudinal assessment of subsurface artificial root caries lesions by optical coherence tomography in comparison with transverse microradiography. Proc SPIE 8208（in press）.

7）総説ならびに著書

［総説］

（英文）

1. Nakajima M. Kunawarote S, Prasansuttiporn T, Tagami J. Bonding to caries-affected dentin. Japanese Dental Science Review 47（2）：102-114, 2011
2. Nikaido T, Inoue G, Takagaki T, Waydeasekera K, Iida Y, Shinohara SM, Sadr A, Tagami J. New strategy to create "Super Dentin" using adhesive technology; Reinforcement of adhesive-dentin interface and protection of tooth structures. Japanese Dental Science Review 47：31-42, 2011

（イタリア語）

1. Nikaido T, Inoue G, Takagaki T, Waydeasekera K, Li N, Sadr A, Tagami J. La strategia del "Super Dente"：il rafforzamento dentina/smalto grazie alla tecnologia self-etching. ildentistamodemo（in press）

（和文）

1. 井上剛、田上順次.接着材料としてのセルフアドヒーシブレジンセメントの効果。日本歯科理工学会誌、30（3）150-153、2011
2. 島田康史、有吉芽生、今井加奈子、マキシパトリシア、吉岡俊彦、田上順次、角保徳.光干渉断層計（OCT）を利用した非破壊断層画像診断.日本歯科理工学会雑誌30（1）：21-24.2011
3. 島田康史.微小剪断接着試験の基礎理論と測定法.接着歯学 29（2）：98-102、2011.
4. 趙 永哲、須永昌代、田上順次、木下淳博.歯科診療室-講義室間のインターネット同時中継によるライブ講義システムの開発と評価.日本歯科理工学会誌 30（3）：158-160、2011

［著書］

1. 田上順次.粘接性复合樹脂修复体臨床指南 zhanjiexing fuheshuzhi xiufuti linchuang zhinan . 人民軍医出版社　印次2011年1月
2. 田上順次.歯科の疫学調査における歯科疾患の診断基準並びに客対数に関する研究.厚生労働科学研究費助成金地域医療基盤開発推進研究事業.平成22年度総括・分担研究報告書.2011年3月
3. 田上順次.日常臨床で必ず使える コンポジットレジン修復の一手.クインテッセンス出版株式会社 YEAR BOOK 2011.2011年1月10日
4. 田上順次.コンポジットレジンによる歯冠審美修復の未来（前編）.日本歯科評論.別刷.通刊822号　vol.71 no.5. 2011年5月
5. 石川 烈 編 大槻昌幸、田上順次、Er：YAGレーザーの基礎と臨床、211ページ、2011年

8）平成23年度までの自己評価

GCOE開始以来、これまでの研究成果の臨床への応用、普及に努め、Super Dentin, Super Enamel を含む Super Tooth の創出に関する論文を7編、OCTに関する論文を8編発表した。その他歯質接着の領域で、接着耐久性の向上、新材料の開発などに関する論文などを含めて、40報の英文論文を発表した。Super Toothの概念、OCTによる新しいう蝕診断法の普及のため、国内外で講演を行い、研究者だけでなく、オピニオンリーダーとされる臨床家に情報提供することができた。特に、OCTについては臨床応用可能な試作機を製作し、倫理審査委員会の承認を得て、臨床評価を開始するに至った。

これらの成果は国際的にも評価されつつあり、23年度中の外国人研究者の受け入れは8名である。大学院博士課程には外国人留学生としてあらたに6名を受け入れた。うち2名は母国の奨学金受給者でさらに2名は国費（文部科学省）留学生で、優秀な留学生を確保することができた。

分野での教育研究の環境整備のため、外部資金の獲得に努め、科学研究費のほか、受託研究、奨学寄附金などを得ることができた。これらの資金により、2名の特任教員を昨年から継続して雇用することができた。これらの特任教員とともに行った研究は学会でも高く評価され、学術賞を受賞している。

学生、若手教員とも総じて優れた成果を挙げ、内外での発表の経験を積み、各個人の存在感も大きくなっている。教室員が各種学術プログラムで特別講演やシンポジストとして、招待されることも増加している。

9）和文原著論文

1. 田上順次,千田彰,大槻昌幸,二階堂徹,中島正俊,友田篤臣,山田三良,河合利浩.可視光応答型酸化チタン光

触媒を含む漂白材（ティオノフィス）の臨床評価.日歯保存誌 54（2）：131-141、2011

2. 吉川孝子, WATTANAWONGPITAK N, 趙　永哲, 田上順次. コンポジットレジンの接着強さに及ぼす残存象牙質厚さの影響. 日本歯科保存学雑誌 54（6）：442447、2012
3. 吉川孝子, WATTANAWONGPITAK N, 田上順次. 窩洞内各面に対するコンポジットレジンの接着強さ. 日本歯科保存学雑誌（印刷中）、2012
4. 吉川孝子, WATTANAWONGPITAK N, 田上順次. コンポジットレジンの接着強さに及ぼす象牙細管の影響. 日本歯科保存学雑誌（印刷中）、2012

10）学会発表（英文）

1. Aksornmuang J, Nakajima M, Senawongse P, Tagami J. Effect of C-factor and resin volume on the bonding to root canal with and without fibre post insertion. The 4th International Congress on Adhesive Dentistry, Oral, Seoul, Korea, April 15-17, 2011
2. ◎Islam MS, Hiraishi N, Otsuki M, Tagami . Effect of Hesperidin Incorporation into the Primer of a Self-etching Adhesive on Micro Tensile Bond Strength to Dentin. The 4th International Congress on Adhesive Dentistry. Poster and Oral, Korea, Date：April 15-17, 2011
3. ◎Sadr A, Bartakova S, Parchar P, Hariri I, Nazari A, Shimada Y, Tagami J, Sumi Y. Adhesion of Flowable Composite in Class I Cavities：Combination of SS-OCT Imaging and Microtensile Bond Strength. 4th, IAD, Seoul, Oral, April 15-17, 2011
4. ◎Prasansuttiporn T, Nakajima M, Foxton RM, Tagami J. Scrubbing effect of self-etching adhesives on bond strength to NaOCl-treated dentin. The 4th International Congress on Adhesive Dentistry, Oral, Seoul, Korea, April 15-17, 2011
5. ◎ Yoshikawa T, Wattanawongpitak N, Cho E, Tagami J. Effect of Remaining Dentin Thickness on Bond Strength. The 4th International Congress on Adhesive Dentistry, Oral, Seoul, April 15-17, 2011
6. Sadr A. Ultra-morphological and Nanomechanical Characterization of Reinforced Enamel and Dentin by Self-etch Adhesives：The Super Tooth, 7th International Conference on Diffusion in Solids and Liquids, June 24, 2011, Algarve, Portugal.
7. Hamba H, Nikaido T and Tagami J. Quantitative micro-computed tomography for investigation of enamel de/remineralization：Creation of “Super enamel” The 1st Tri-University Consortium, Oral, Bangkok, Thailand, August 4-5, 2011
8. Sadr A, Shimada Y, Tagami J, Sumi Y. Innovative Composite Evaluation Method：Cavity Adaptation Combined with Bond Strength. 59th, JADR, Hiroshima, Poster, October 8-9, 2011
9. Bakhsh TA, Sadr A, Shimada Y, Sumi Y, Tagami J. Composite Failure Assessment in Different Filling Techniques using SS-OCT. 59th, JADR, Hiroshima, Poster, October 8-9, 2011
10. Hamba H, Nikaido T, Nakashima S, Sadr A and Tagami J. Quantitative Measurement of Enamel Lesion Using Micro-computed tomography and Micro-radiography. Academy of Dental Materials, Poster, Bahia, Brazil, October 13-15, 2011
11. ◎ Islam MS, Hiraishi N, Otsuki M, Tagami J. Effect of Incorporation of Hesperidin in a Self-etching Primer on Dentin Bond Strength. 135th, The Japanese Society of Conservative Dentistry, Oral, Osaka, October 20-21, 2011.
12. ◎ Yoshikawa T, Wattanawongpitak N, Cho E, Tagami J. Effect of Remaining Dentin Thickness on Bond Strength. The 4th International Congress on Adhesive Dentistry, Oral, Seoul, April 15-17, 2011.
13. ◎ Takahashi R, Nikaido T, Tagami J. Contemporary adhesives：marginal adaptation and microtensile bond strength of class II composite restorations, 13th, Joint-Scientific Meeting of KACD and JSCD, Poster, Soul, November 11-13, 2011
14. ◎ Sadr A, Nakashima S, Shimada Y, Tagami J, Sumi Y. Longitudinal assessment of subsurface artificial root caries lesions by optical coherence tomography in comparison with transverse microradiography. Lasers in Dentistry XVIII, SPIE Photonics West, San Francisco, Oral, January 21-26, 2012
15. ◎Bakhsh TA, Sadr A, Shimada Y, Khunkar S, Tagami J, Sumi Y. Relationship between Non-destructive OCT Evaluation of Resins Composites and Bond Strength in a Cavity. Lasers in Dentistry XVIII, SPIE Photonics West, San Francisco, Oral, January 21-26, 2012
16. ◎Hariri I, Sadr A, Shimada Y, Nakashima S, Sumi Y, Tagami J. Relationship between Refractive Index and Mineral Content of Enamel and Dentin Using SS-OCT and TMR. Lasers in Dentistry XVIII, SPIE Photonics West, San Francisco, Poster, January 21-26, 2012

11）学会発表（和文）

1. 鷹佐知子, マティン カイルール, 小柳岳大, 田上順次. 次亜塩素酸電解水による歯科用切削バーの短時間での殺菌効果について. 第134回日本歯科保存学会春季学術大会、浦安、2011年6月9、10日
2. 木島峯雄, 木島武尊, 横瀬敏志, 大槻昌幸、田上順次. 新しいタイプの歯周病治療（第10報）- レーザーとプロポリスを用いて歯槽骨の造成 -. 第134回日本歯科保

存学会春季学術大会、浦安、2011年6月9,10日
3. サダルアリレザ、マンドゥラモナ、田上順次.ナノインデンテーションを用いた深い窩洞でフロアブルレジンベースの評価に関する検討.第134回日本歯科保存学会春季学術大会、浦安、2011年6月9、10日
4. 田中美由紀、北迫勇一、池田正臣、田上順次.唾液分泌量および唾液緩衝能と最大咬合圧の関連性第.134回日本歯科保存学会春季学術大会、千葉、2011年6月9、10日
5. Thitthaweerat Suppason、坂野若詠、中島正俊、田上順次.ワンステップデュアルキュア接着システムにおける化学重合硬化の放置時間が根管象牙質への接着強さに及ぼす影響について.第134回日本歯科保存学会学術大会,浦安、2011年6月9、10日.
6. 中嶋省志、島田康史、夏目悠子、角保徳、サダルアリレザ、田上順次. SS-OCTを用いた象牙質脱灰病変（表層下脱灰）の経時観察と定量評価の試み.第134回日本歯科保存学会春季学術大会、浦安、2011年6月9、10日
7. ナザリアミル、サダルアリレザ、田上順次、島田康史、角保徳. SS-OCTを用いたⅠ級窩洞における各種フローアブルレジンの接着界面の考察.第134回日本歯科保存学会春季学術大会、浦安、2011年6月9、10日
8. Bakry A、大槻昌幸、田上順次.第134回　日本歯科保存学会春季学術大会.浦安.2011年6月9,10日
9. 平石典子, 曽野良平, ISLAM MD.SOFIQU, 大槻昌幸, 田上順次, 高塚勉. ヘスペリジンによる牛歯根面象牙質の脱灰抑制、再石灰化効果-新しい根面齲蝕予防のアプローチ　第I34回日本歯科保存学会春季学術大会、千葉、6月9-10日、2011.
10. マンドゥラモナ、サダルアリレザ、田上順次、島田康史、角保徳. SS-OCTとナノインデンテーション法による硬化象牙質の光学的ならびに機械的特性.第134回日本歯科保存学会春季学術大会、浦安、2011年6月9、10日
11. 島田康史、田上順次、角保徳.学生実習におけるコンポジットレジン修復のSS-OCTを用いた断層画像評価.第30回日本歯科医学教育学会総会および学術大会、東京、2011年、7月15、16、17日
12. 藤巻太一朗、中島正俊、坂野若詠、有吉芽生、大竹志保、駒田亘、吉田恵一、池田正臣、三浦宏之、荒木孝二、田上順次.台湾歯科学生臨床模擬実習コンテスト参加への取り組み.第30回日本歯科医学教育学会総会・学術大会および記念大会、東京、2011年7月16、17日
13. 大槻昌幸、田上順次、河合利浩、千田 彰.歯の明度とオフィスホワイトニングの効果に各種因子が及ぼす影響.第22回日本歯科審美学会学術大会.奈良.2011年10月8、9日
14. サダルアリレザ、田上順次、島田康史、角保徳.OCTを用いたⅠ級窩洞のフローアブルレジンベースのリアルタイム2次元断層画像撮影.第135回日本歯科保存学会秋季学術大会、大阪、2011年10月20、21日
15. 平石典子、大槻昌幸、田上順次.STD-NMR法を用いたコラーゲンモデルと接着性モノマー相互作用の分析.第135回日本歯科保存学会秋季学術大会.2011年10月20,21日
16. 北迫勇一、池田正臣、小林隆嗣、田中智子、釜阪寛、Alireza Sadr、田上順次. エナメル質初期う蝕最表層部におけるPOs-Caおよびフッ素配合ガム咀嚼後の微小硬さ変化ならびにフッ素分布. 日本歯科保存学会2011年度秋季学術大会、大阪、2011年10月20,21日
17. 中嶋省志、島田康史、夏目悠子、角保徳、サダルアリレザ、田上順次.SS-OCTを用いた脱灰象牙質の再石灰化度の測定.第135回日本歯科保存学会秋季学術大会、大阪、2011年10月20、21日
18. 半場秀典,井上剛,二階堂徹,田上順次.新規歯面処理材によるエナメル質表層下脱灰病変の再石灰化効果.第135回日本歯科保存学会秋季,大阪,2011年10月20,21日
19. 平石典子,大槻昌幸, 田上順次. STD-NMR法を用いたコラーゲンモデルと 接着性モノマー相互作用の分析.第I35回日本歯科保存学会、大阪、10月20-21日、2011.
20. Thitthaweerat Suppason、中島正俊、田上順次.ワンボトル・セルフエッチボンディング材を応用した新規デュアルキュアレジンコアシステム（MTB-200/NDC-100）の根管壁象牙質に対する接着性能.第135日本歯科保存学会学術大会,大阪、2011年10月20、21日
21. 吉川孝子、Nipaporn Wattanawongpitak、趙永哲、田上順次. レジンの象牙質接着強さに及ぼす残存象牙質厚さの影響について.第135回日本歯科保存学会秋季学術大会、大阪、2011年10月20、21日
22. 島田康史、大槻昌幸、田上順次、角保徳.学生実習にて行ったコンポジットレジン修復のSS-OCTによる評価.第76回口腔病学会学術大会、東京、2011年12月9、10日
23. 袁 楊、Kong Kalyan、大槻昌幸、田上順次.油分の付着がセルフエッチングタイプ接着材の象牙質接着

に及ぼす影響.第30回日本接着歯学会学術大会.函館.2012年1月21,22日.

24. 吉峰斉昭、サダルアリレザ、島田康史、田上順次、角保徳.OCTを用いた低収縮性コンポジットレジンの光照射前後の適合に対する画像診断.第30回日本接着歯学会学術大会、函館、2012年1月21、22日
25. 中川寿一、サダルアリレザ、島田康史、中嶋省志、田上順次、角保徳.脱灰エナメル質におけるレジン浸透材のSS-OCT観察.第30回日本接着歯学会学術大会、函館、2012年1月21、22日
26. 和田郁美、島田康史、サダルアリレザ、中嶋省志、田上順次、角保徳.クサビ状欠損のSS-OCTによる断層画像診断.第30回日本接着歯学会学術大会、函館、2012年1月21、22日

12）受賞

First place outstanding paper award, Sadr A, Bartakova S, Parchar P, Hariri I, Nazari A, Shimada Y, Tagami J, Sumi Y. Adhesion of Flowable Composite in Class I Cavities：Combination of SS-OCT Imaging and Microtensile Bond Strength. The 4th International Conference on Adhesive Dentistry, Seoul, Korea, April 15-17, 2011.

The first place outstanding poster, IAD, 2011, Islam MS, Hiraishi N, Otsuki M, Tagami. Effect of Hesperidin Incorporation into the Primer of a Self-etching Adhesive on Micro Tensile Bond Strength to Dentin. The 4th International Congress on Adhesive Dentistry, Korea, April 15-17, 2011.

13）外部資金の獲得状況

受託研究

研究題目：リン酸化オリゴ糖カルシウムの歯の再石灰化効果に関する研究
代表：田上　順次
期間：平成20年―平成24年
研究費総額：1454万円

委託研究

研究題目：口腔内プローブを用いた光干渉断層計（OCT）の臨床応用
代表：田上　順次
研究費総額：150万円

委託研究

研究題目：近赤外光・レーザーを用いた新たな歯科疾患診断・治療用機器の開発に関する研究
代表：田上　順次
研究費総額：600万円

科学研究費補助金、基盤B

研究題目：光干渉断層計の歯冠修復領域への応用
代表：田上　順次
期間：平成23年―平成25年
研究費総額：832万円

科学研究費補助金、 挑戦的萌芽

研究題目：コラーゲンの高分子修飾と高密度石灰化ハイブリッドSuper Dentinの誘導形成
代表：田上　順次
期間：平成23年―平成24年
研究費総額：106万円

科学研究費補助金、基盤C

研究題目：歯の漂白の評価のための変色歯モデルと評価システムの開発
代表：大槻 昌幸
期間：平成21―平成24年
研究費総額：405万円

科学研究費補助金、基盤C

研究題目：レジン修復物の重合収縮応力緩和と接着性能同時向上効果を有する臨床技法の開発
代表：吉川　孝子
期間：平成22年―平成24
研究費総額：322万円

科学研究費補助金、基盤C

研究題目：非侵襲的トモグラフィーを用いた修復物の欠陥と二次う蝕の精密画像診断
代表：島田　康史
期間：平成21年―平成23年
研究費総額：470万円

科学研究費補助金、基盤C

研究題目：クロルヘキシジン含有・歯科接着剤の抗菌性、接着耐久性の研究
代表：平石 典子
期間：平成22年―平成24年
研究費総額：500万円

平成23年度8020研究推進

研究題目：根面う蝕に関与する唾液中のバイオマーカーの加齢による変化
代表：平石 典子
期間：平成22年―平成23年
研究費総額：80万円

科学研究費補助金、若手B

研究題目：アシッドベースレジスタントゾーンの精査

と改質
代表：井上　剛
期間：平成22年―平成25年
研究費総額：300万円

科学研究費補助金、若手研究B
研究題目：光干渉断層画像診断法の歯科臨床への応用
代表：岸川　隆蔵
期間：平成21年―平成23年
研究費総額：310万円

科学研究費補助金、若手研究B
研究題目：周波数掃引光コヒーレンストモグラフィーの信号強度と歯硬組織の特性の関連性
代表：サダル　アリレザ
期間：平成22年―平成24年
研究費総額：200万円

科学研究費補助金、若手研究B
研究題目：マイクロCTによる光重合型コンポジットレジンの重合収縮挙動の観察の研究
代表：趙　永哲
期間：平成23年―平成25年
研究費総額：182万円

科学研究費補助金、若手研究B
研究題目：3次元動的解析法を用いた疎水性接着システムの開発
代表：保坂　啓一
期間：平成23年―平成25年
研究費総額：382万円

14）特別講演、招待講演、シンポジウム

1. 田上順次.「百歳まで歯を守る知恵と技術」.市民フォーラム.岡山大学創立五十周年記念館.2011年2月6日
2. 田上順次.The 4th International Congress on Adhesive Dentistry Symposium：How to evaluate bonding?
「Micro-tensile, micro-shear or conventional test?」基調講演、Hotel Millennium Hiltonソウル、2011年4月16日
3. 田上順次.「Esthetic restorations supported with innovations technologies」特別講演、協力関係検討の打ち合わせ、マサリク大学医学部口腔科学科、2011年5月6日
4. 田上順次.「OCTの歯科保存領域への応用」講演.日本医用歯科機器学会.大阪歯科大学　天満橋学舎（附属病院）.2011年7月31日
5. 田上順次.CU-TMDU Young Researchers' Meeting出席、チュラロンコン大学歯学部CU-TMDU Research and Education Collaboration Center、2011年8月3日
6. 田上順次.「Promotion interdisciplinary international projects and educating research-oriented health care professionals」講演、The 1st Tri-University Consortium on Oral Science and Education, Chulalongkorn-Peking-Tokyo Medical and Dental University、チュラロンコン大学歯学部Than Phu Ying Petchara Auditorium、2011年8月4日
7. 田上順次.「人生は短い、今何をすべきか」三重高等学校OB.三重中学校・三重高等学校創立50周年記念講演会.三重高等学校第一体育館.2011年10月28日
8. 田上順次.「メタルフリーを成功に導く接着材とその使い方」コメンテーター.日本接着歯学会2011年度シンポジウム「-メタル?メタルフリー?それが問題だ!-」.鹿児島大学鶴陵会館.2011年9月4日
9. 田上順次.「コンポジットレジンが実現する究極のMI」講演.第22回日本歯科審美学会学術大会シンポジウム3.奈良県新公会堂.2011年10月9日
10. Sadr A. Innovative research on the characterization of dental restorative composite materials, 89th Open Session of Tooth and Bone GCOE, IRCMSTBD, Tokyo Medical and Dental University, November 14, 2011.
11. 田上順次.「Dental education in Japan and TMDU」及び「Innovations in adhesive dentistry and aesthetic dentistry」講演、マサリク大学医学部口腔科学科、2011年12月12日

15）主催学会

第132回 日本歯科保存学会春季学術大会、2010年6月4、5日、熊本

16）新聞、雑誌、TV報道

TV

1. 報道1.田上順次.TBS「カラダのキモチ―聞かぬは一生の損!? 歯医者さんが語る!歯の全て―」出演.2011年3月6日.
http：//topicsnow.blog7 2.fc2.com/blog-entry-1 3 3 6.html
2. 田上順次.TBS「カラダのキモチ―聞かぬは一生の損!? 歯医者さんが語る!歯の全て―」出演.2011年6月19日.

http：//topicsnow.blog7 2.fc2.com/blog-entry-1 3 3 6.html

3. 田上順次.NHK BSプレミアム「アインシュタインの眼」出演．2011年9月14日.
http：//www.nhk.or.jp/einstein/archive/1110.html

17）GCOE総合講義

＜第89回GCOE国際総合プレゼンテーション＞

日時：平成23年3月28日

演題：Various approach to create the super tooth

演者：Junji Tagami GCOE lecture

Through the studies of dentin bonding, a new dentin structure that showed more resistant to the acid and base attacks than normal dentin. This acid-base resistant dentin is observed adjacent to the hybrid layer only when the self-etching type adhesives are applied. We named this new dentin layer as the " Super Dentin".
The mechanism of creating the Super Dentin is still unclear, however, the penetration of the adhesive resin monomer to the dentin under the demineralization front by self etching effect must be necessary. Plausible chemical modification of dentin with the adhesive resin monomers is expected.
The Super Dentin is believed to be very effective to prevent the recurrent caries at the dentin margin, as well as improvement of dentin bond durability.
The dentin bond durability was also improved by adhesive resins that can release fluoride ion. Clearfil SE Protect, which is consisted of the anti-bacterial self-etching primer and fluoride releasing bond, showed stable dentin bonding even after a long period storage in water. Also, the material exhibited the thicker Super Dentin creation than the materials without fluoride release.
Evidence of creation of the "Super Enamel" is also published（Li Na et al., 2010）.
The Super Tooth including Super Dentin and Super Enamel is a concept of a dental therapy to improve the chemical and mechanical properties of natural teeth and lesion or defect of tooth for providing the natural and healthy dentition for the whole life longevity of the people. Applications of fluoride, restorative materials, anti-matrix metalloproteinases（MMPs）, calcium phosphate are considered to contribute to create the Super Tooth.

日時：平成23年11月14日（月）

演題：『歯科コンポジットレジンの評価に関する革新的研究』

演者：Sadr Alireza

Innovative research on the characterization of dental restorative composite materials
This lecture aimed to give an overview of the current treatments provided for caries using direct restorative materials, and discuss the relationship between clinical success of these materials with the ongoing research in the field. As a part of the Super Tooth GCOE project we are working on new method to explore most clinically relevant tests for laboratory evaluation of dental restoratives.
Using advanced tomographic imaging systems such as OCT, in combination with micro-computed tomography and conventional tests. We show that a combination of the imaging methodology and microtensile bond-strength in cavity for testing of restorative materials can be a meaningful test method. We also present real-time tomographic imaging of adaptation of dental composite during placement, polymerization and post-polymerization under OCT, to discuss various approaches that the manufacturers have taken to address the polymerization shrinkage issue. Collectively this lecture concludes that rate of modulus development in the gel-phase dominates volumetric shrinkage effects in stress generation of composites, and that super-filled composites may encounter some adaptation issues other than shrinkage. Moreover, compositional incompatibilities of simplified adhesives remain unsolved as of today. Adaptation and adhesion are still research priorities in restorative dentistry; dental composites research must orient towards multiaspect and combinatory testing in clinically relevant cavities, establishing new testing standards. Our OCT methodology uniquely offers time-resolved analysis of defect formation and propagation in dental composites, shedding light on the mechanisms of failure.

18）教室、分野や講座の准教授、講師、助教、特別研究員、ポスドク、指導を受けた大学院生の名前

准教授	大槻　昌幸
准教授	佐々木　好幸
講師	二階堂　徹
	中島　正俊
助教	吉川　孝子
	島田　康史
	北迫　勇一
	岸川　隆蔵
	井上　剛
	趙　永哲
	保坂　啓一
	高垣　智博
	原田　直子

GCOE

特任講師　Alireza SADR
特任講師　中嶋　省志
特任助教　平石　典子
日本学術振興会特別研究員　Ahmed BAKRY
JICA日本研修員　Patricia MAKISHI
大学院4年　荒牧　音
高井　智行
田中　美由紀
矢作　智花
小柳　岳大
夏目　悠子
坪根　真子
田野　絵里
○半場　秀典
神原　啓介
Hamid NURROHMAN
Amir NAZARI
Sitthikorn KUNAWAROTE
○Ilnaz HARIARI
大学院3年　今井　加奈子
今村　友美
鵜鷹　佐知子
丸藤　伊織
桐原　大
栗林　恵美
坂野　若詠
美田　瞳
○Taweesak PRASANSUTTIPORN
大学院2年　Gerardo Jose JOVES Mendez
田中　梓
貝ノ瀬　公典
Mona Mohammad MANDURA
Md. Sofiqul ISLAM
中川　寿一
Haidil Akmal MAHDAN
Ena LODHA
Suppason THITTHAWEERAT
○Turki A BAKHSH
大学院1年　松井　七生子
和田　郁美
上杉　有美子
吉峰　斉昭
太嶋　恵美
永井　茂之
Mohannad NASSAR
Ornnicha　THANATVARAKORN
Alaa TURKISTANI
Teerapong MAMANEE
Sahar Jameel KHUNKAR
喬　華（キョウ　カ）

○はAISS

JOURNAL OF DENTISTRY 39 (2011) 405–413

available at www.sciencedirect.com

ScienceDirect

journal homepage: www.intl.elsevierhealth.com/journals/jden

Effects of CPP-ACP with sodium fluoride on inhibition of bovine enamel demineralization: A quantitative assessment using micro-computed tomography

H. Hamba [a,b], *T. Nikaido* [a,*], *G. Inoue* [a], *A. Sadr* [b], *J. Tagami* [a,b]

[a] *Cariology and Operative Dentistry, Department of Restorative Sciences, Graduate School of Medical and Dental Sciences, Tokyo Medical and Dental University, 1-5-45, Yushima, Bunkyo-ku, Tokyo 113-8549, Japan*

[b] *Global Center of Excellence (GCOE) Program, International Research Center for Molecular Science in Tooth and Bone Diseases at Tokyo Medical and Dental University, Tokyo, Japan*

ARTICLE INFO

Article history:
Received 11 November 2010
Received in revised form
21 February 2011
Accepted 18 March 2011

Keywords:
CPP-ACP
Demineralization
Enamel
Fluoride
Longitudinal analysis
Micro-CT

ABSTRACT

Objectives: The present study evaluated the effects of casein phosphopeptide-amorphous calcium phosphate (CPP-ACP) and CPP-ACP with 900 ppm fluoride (CPP-ACPF) pastes on inhibition of enamel demineralization over time, using polychromatic micro-computed tomography (micro-CT).

Methods: Enamel blocks were prepared from bovine teeth. The specimens were each treated by one of the following agents, 30 min daily for 7 days: deionized water (negative control); CPP-ACP paste; CPP-ACPF paste; and NaF solutions (positive controls) (90, 900, and 9000 ppm F). After treatment, the specimens were immersed in a demineralizing solution (pH 4.5) for 24, 72, and 120 h. Mean mineral loss (ML) and lesion depth (LD) after each period were determined from mineral density profiles obtained using micro-CT.

Results: ML values in all the treatment groups were significantly smaller than those in the control group after 72 and 120 h of demineralization ($p < 0.05$, two-way ANOVA and *t*-test with Bonferroni correction). ML values in CPP-ACPF and NaF solution groups were significantly smaller compared to CPP-ACP group after 72 h ($p < 0.05$). LD values in the CPP-ACPF and all the NaF solutions groups were significantly smaller compared to the control group after 120 h ($p < 0.05$). The 9000 ppm F group showed the lowest nominal ML and LD values.

Conclusions: The application of CPP-ACP or CPP-ACPF pastes to sound enamel surfaces resulted in inhibition of enamel demineralization, and a better effect was noted for the latter paste. Quantitative assessment using polychromatic micro-CT demonstrated to be useful for detecting mineral density changes.

© 2011 Elsevier Ltd. All rights reserved.

1. Introduction

Enamel is the hardest substance in human body. Continuous balanced demineralization and remineralization are natural dynamic processes in enamel.[1] If the balance is interrupted and demineralization process dominates, it may eventually lead to the development of caries lesions in enamel and dentine.

In a neutral environment, the hydroxyapatite crystals of enamel are in a dynamic equilibrium with calcium and phosphate ions.[2] Demineralization is caused by acids which

* *Corresponding author*. Tel.: +81 3 5803 5483; fax: +81 3 5803 0195.
E-mail address: nikaido.ope@tmd.ac.jp (T. Nikaido).

0300-5712/$ – see front matter © 2011 Elsevier Ltd. All rights reserved.
doi:10.1016/j.jdent.2011.03.005

have intrinsic or extrinsic sources; some acids are produced when certain bacteria colonize on the tooth surface and metabolize carbohydrates, and some are introduced into the mouth as a part of food or drinks. The demineralization can be reverted if the pH is neutralized and there are sufficient bioavailable calcium and phosphate ions in the immediate environment.[3]

As the "Minimal Intervention" concept[4] becomes widely spread, various products with tooth surface protection, anti-cariogenic or remineralizing effects attract an increasing attention. Casein phosphopeptides (CPP) containing the cluster sequence -Ser(P)-Ser(P)-Ser(P)- Glu-Glu- have been reported to bind amorphous calcium phosphate, forming small clusters of casein phosphopeptide-amorphous calcium phosphate (CPP-ACP), thereby stabilizing calcium phosphates in solution.[5,6] CPP-ACP is reported to promote remineralization through release of free calcium and phosphate ions by several studies; Reynolds et al.,[5,7] Poggio et al.,[8] and Oshiro et al.[9] reported that the paste was effective against enamel demineralization.

Historically, the effectiveness of topical sodium fluoride (NaF) as a cariostatic agent has been established well, and professional topical NaF applications are commonly used to arrest the progression of active caries. Reynolds et al. suggested that products containing CPP-ACP with NaF (CPP-ACPF) might be superior in reducing caries risk, when compared to CPP-ACP,[7] whilst Pulido et al.[10] and Kumar et al.[11] found a slight more demineralization with CPP-ACPF compared to fluoridated paste applied without CPP-ACP.

Non-destructive techniques for evaluation of mineral content enable long-term assessment of effects of the remineralizing agents on enamel. Micro-computed tomography (micro-CT) imaging provides a unique opportunity to capture three-dimensional (3D) architectural information from samples. Micro-CT has been frequently used in the experiments exploring mineral density and structure of mineral tissues, like bones and teeth.[12–14] The technique is also a promising method to assess demineralization or remineralization in enamel or dentine.[15–19] Micro-CT systems are mainly classified into two types; synchrotron radiation micro-CT that can produce parallel monochromatic X-ray beams,[20] and commercial or desktop micro-CT that can produce polychromatic X-rays.[18] Where the polychromatic X-ray source is used, quantitative determination of mineral density requires correction of beam-hardening artifacts, especially in high mineral density tissues such as enamel.

Although micro-CT bears the advantage of obtaining 3D information non-destructively when compared to the destructive two-dimensional (2D) techniques such as transversal microradiography (TMR),[21–23] few studies have to date employed this technique to quantitatively evaluate the effects of preventive agents on enamel.

Therefore, the aim of this study was to utilize polychromatic micro-CT for quantitative and non-destructive assessment of the effects of CPP-ACP and CPP-ACPF pastes on prevention of enamel demineralization over time. The null hypotheses were that: CPP-ACP would have no preventive effect on enamel demineralization, and that CPP-ACPF would have no additional benefits for prevention of demineralization compared to CPP-ACP.

2. Materials and methods

2.1. *Specimen preparation*

A flow chart of the procedures in the present study is shown in Fig. 1. Eight extracted, non-damaged permanent bovine incisors were stored frozen until experiment. The teeth were thoroughly cleaned and washed under running water to remove all adherent soft tissues. Specimens were prepared by cutting the teeth into 3 mm × 5 mm × 3 mm enamel–dentine blocks using a low-speed diamond saw (Isomet, Buehler, Lake Bluff, IL, USA) under water as a coolant. Each incisor was sectioned into 6 blocks to give a total of 48 specimens.[24] The enamel surfaces were ground flat with 600–2000-grit silicon carbide papers (Fuji Star, Sankyo Rikagaku, Saitama, Japan) under running water. The surfaces were then covered by a nail varnish (CO11, Revlon, New York, NY, USA) leaving a window (2 mm × 4 mm) exposed on the polished enamel surface of each specimen. In order to set a reference landmark for micro-CT scans, a hole (1.0 mm in diameter, 0.5 mm in depth) was made at the side of each specimen by a diamond bur (440SS ISO # 010, Shofu, Kyoto, Japan).

2.2. *Specimen treatments*

The 48 specimens were distributed to six treatment groups as shown in Table 1: (a) deionized water (Milli-Q water, Millipore, Billerica, MA, USA) as a negative control; (b) CPP-ACP paste

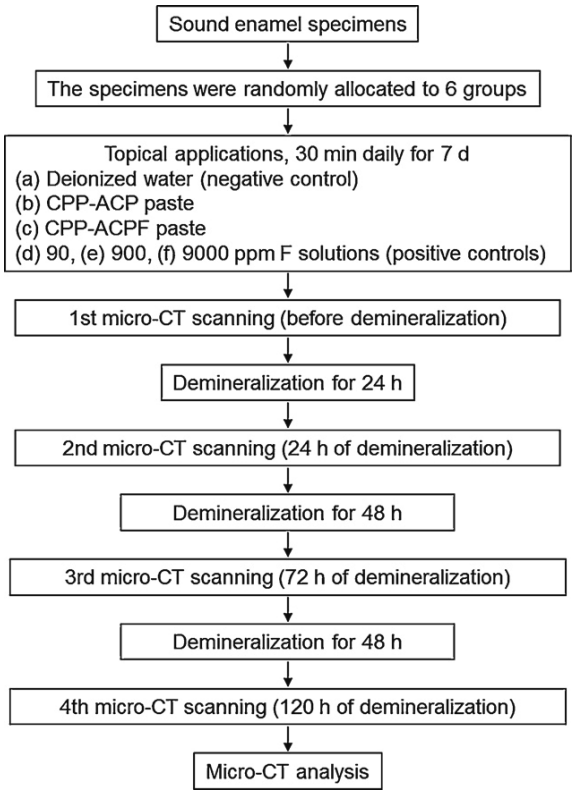

Fig. 1 – Flow chart of the study experimental design.

Table 1 – Treatment groups.

Group	Product	Active ingredients	Manufacturer	Lot no.
Deionized water	Milli-Q water	–	Millipore, Billerica, MA, USA	–
CPP-ACP	Tooth Mousse	10% CPP-ACP	GC, Tokyo, Japan	071004V
CPP-ACPF	Tooth Mousse Plus	10% CPP-ACP, 900 ppm F as NaF	GC, Tokyo, Japan	071018V
90 ppm F	NaF solution[a]	90 ppm F as NaF	Wako, Osaka, Japan	–
900 ppm F		900 ppm F as NaF		
9000 ppm F		9000 ppm F as NaF		

CPP-ACP: calcium phosphopeptide-amorphous calcium phosphate, NaF: sodium fluoride.
[a] Solutions were prepared by deionized water

(CPP-ACP) (Tooth Mousse, GC, Tokyo, Japan); (c) CPP-ACP with 900 ppm F paste (CPP-ACPF) (Tooth Mousse Plus, GC); and NaF solutions with different concentrations as positive controls adjusted at (d) 90 ppm F; (e) 900 ppm F; or (f) 9,000 ppm F as NaF (NaF, Wako, Osaka, Japan) by adding deionized water. Suspensions and solutions were prepared at a dilution of 1:3 (paste or solution: deionized water) for treatments according to the procedure described by a previous study.[11] The suspensions and solutions were thoroughly stirred and mechanically agitated for 1 min by means of a vortex mixer (MF-71, TGK, Tokyo, Japan). The specimens were immersed in the suspension (or the solution) at 37 °C continuously for 30 min daily for 7 days. At other times during the treatment period, the specimens were stored in deionized water in the incubator at 37 °C. After each treatment, the specimens were rinsed-off using a mild air–water spray for 15 s, and returned to the storage medium. The suspensions and solutions were refreshed every day.

2.3. *Demineralization*

The demineralizing solution contained 2.2 mM $CaCl_2$, 2.2 mM KH_2PO_4 and 50 mM acetic acid adjusted at pH 4.5 with 10 M KOH according to a previous study.[25] Each specimen was individually immersed in 10 ml of the demineralizing solution at 37 °C, and continuously stirred by a magnetic stirrer. The specimens were removed from the solution after 24, 72, and 120 h of demineralization for micro-CT scanning. At 24 and 72 h, the specimens were returned into the demineralizing solution after scanning. The demineralizing solution was also refreshed every day.

2.4. *Micro-CT scanning*

A bench-top micro-CT system (InspeXio SMX-90CT, Shimadzu, Kyoto, Japan) was used to evaluate the mineral density of the specimens. The micro-CT system can generate polychromatic X-rays with a cone-beam geometry. A 0.2-mm-thick brass (Cu–Zn) filter was installed in the beam path to reduce beam-hardening effect, as suggested by Jennings[26]. The specimen was mounted on a computer-controlled turntable, which synchronized the rotation and the axial shift. The nominal isotropic resolution of the setup was 10 μm, with an integration time of 400 s. The scanning was performed in the offset CT scanning mode, with the specimen being rotated 360° at rotation steps of 0.6°. The tube voltage was 90 kV at a current of 109 μA. The distance from X-ray source to the sample was 11 mm, and that from X-ray source to the detector was 283 mm. The sample was mounted so that the X-ray beam was perpendicular to the treated enamel surface. In order to avoid drying of the specimen during scanning, a wet wiper roll was placed on top of the specimen during the scanning.

For the purpose of mineral density calibration, a series of mineral reference phantoms (Phantoms, Ratoc System Engineering, Tokyo, Japan) were scanned prior to specimen scanning. Three phantoms were used; two hydroxyapatite disks (0.60 and 0.80 $g_{HAp}\,cm^{-3}$) and a pure aluminum wire 0.9 mm in diameter (1.55 $g_{HAp}\,cm^{-3}$), which were scanned using the same setup and parameters as for the tooth specimens.

Each of the 48 specimens in this study was scanned 4 times during the experiment; at the baseline (before demineraliza-

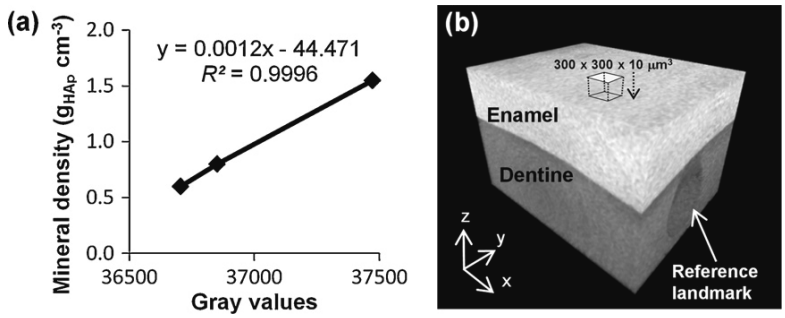

Fig. 2 – (a) Mineral density calibration curve based on 16-bit gray values obtained from the mineral reference phantoms (linear regression, $R^2 > 0.9996$). (b) Three-dimensional CT image of a sound enamel–dentine block with a hole as a reference landmark. Each density label for measurement of mineral density was set through enamel surface in a volume of interest (VOI) of 300 μm × 300 μm × 10 μm, at the center of demineralization window.

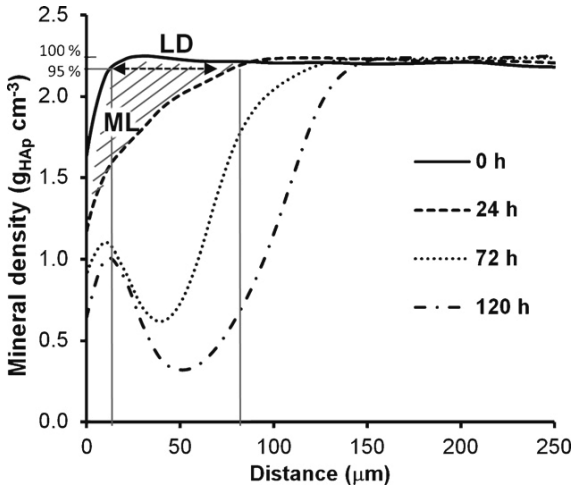

Fig. 3 – Graph showing the 3D mineral density profiles of the positive control, with the distance in x-axis (μm) and mean mineral density values (g_{HAp} cm^{-3}) in y-axis, before demineralization and after 24, 72, and 120 h of demineralization. The mean mineral loss (ML) (g_{HAp} cm^{-3} μm) and lesion depth (LD) (μm) at each demineralization time were calculated from the mineral density profiles.

tion) and after 24, 72, and 120 h of demineralization. In total, 192 scans were carried out for the specimens.

2.5. *Data analysis*

The data in each scan were acquired as 250 images in 16-bit TIFF format, and used to reconstruct a 3D image stack from the 2D images, with a resolution of 512 × 512 pixels and an isotropic volumetric pixel (voxel) size of 10 μm by a 3D analysis software (TRI/3D-BON, Ratoc System Engineering), which was used for visualization and quantitative volumetric measurements. CT values were converted into mineral density values (g_{HAp} cm^{-3}) using a linear calibration curve based on the gray values obtained from the mineral reference phantoms (linear regression, $R^2 > 0.9996$) as illustrated in Fig. 2a. A noise reducing median filter was applied to the data, and the background was removed by excluding those pixels with a CT value lower than the zero mineral density value according to the calibration curve (Fig. 2b). In order to compare changes in each enamel lesion, 3D data images from the same sample acquired at different times had to be aligned and registered into one coordinate system. The rendered 3D volumes were manually translated and rotated in the software to visually match the baseline image which served as the reference. The features on each image used for the matching process were the sound enamel surface, specimen edges and reference landmarks (holes made by a bur on dentine) (Fig. 2b). The assessment was performed in a volume of interest (VOI) of 300 μm × 300 μm × 1000 μm, at the center of demineralization window (Fig. 2b). Mean mineral density values (MD) were calculated in the VOI at each 10 μm depth. MD profile in each specimen was obtained by plotting the MD against the depth.

Mean mineral loss (ML) (g_{HAp} cm^{-3} μm) and lesion depth (LD) (μm) after each demineralization period were calculated from the MD profiles; with the reference point of the depth axis (0 μm) set at the axial position of the sound enamel surface at baseline (Fig. 3). ML on each specimen was calculated from the MD profiles by subtracting the area under the curve at each demineralization time from the area before demineralization, as shown in Fig. 3. LD was recorded as the depth of the region where the mineral content reached 95% of the maximum mineral density.[22] These calculations were performed by importing the MD and depth data into a spreadsheet software package (Microsoft Excel 2007 for Windows, Microsoft, Redmond, WA, USA).

2.6. *Statistical analysis*

The ML and LD results were expressed as means and standard deviations. The collected values were statistically analyzed using two-way analysis of variance (ANOVA) with demineralization time and treatment as factors, and *t*-test with Bonferroni correction. All statistical tests were performed with a computerized statistical program (SPSS for Windows Ver. 11, SPSS, Chicago, IL, USA). The significance level of all tests was set at $\alpha = 0.05$.

3. Results

3.1. *Micro-CT analysis*

Typical 3D images of the control group are shown in Fig. 4. The baseline group represents sound enamel–dentine blocks

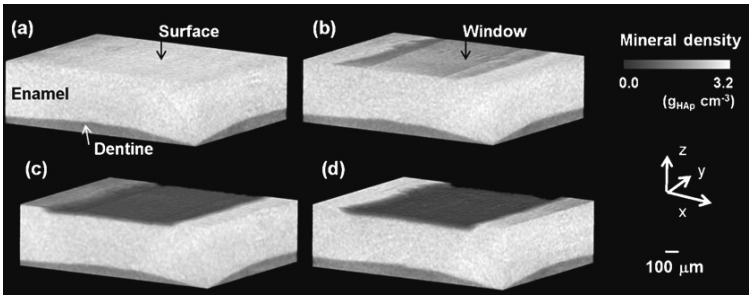

Fig. 4 – Typical 3D images of enamel–dentine blocks in the deionized water group as negative control. The same specimens scanned before demineralization (a) and after 24 (b), 72 (c), and 120 (d) h of demineralization. Mineral density values (g_{HAp} cm^{-3}) are assigned to gray values by the 3D analysis software.

(Fig. 4a), and changes after 24, 72, and 120 h of demineralization (Fig. 4b–d) can be observed. Mineral density values at the enamel surface decreased gradually with demineralization time.

3.2. *Mean mineral density profiles*

MD profiles for each experimental group in the present study are indicated in Fig. 5. All groups showed identical profiles at the baseline (before demineralization). The MD profiles of the negative control group (a) after demineralization clearly showed mineral loss, with gradual decrease of mineral density at the surface resembling erosive loss. In the CPP-ACP group (b), the profiles followed a similar pattern as those of the negative control group, whilst in the CPP-ACPF group (c), the mineral profiles was similar to that of 90 ppm F group (d) at all demineralization times. On the other hand, the specimens treated with NaF solutions (positive controls) showed some extent of resistance against demineralization; the 9000 ppm F group (f) showed the least pronounced changes in the profile, followed by the 900 and 90 ppm F groups (e, d) after 24 h of demineralization. A surface zone with a higher mineral content

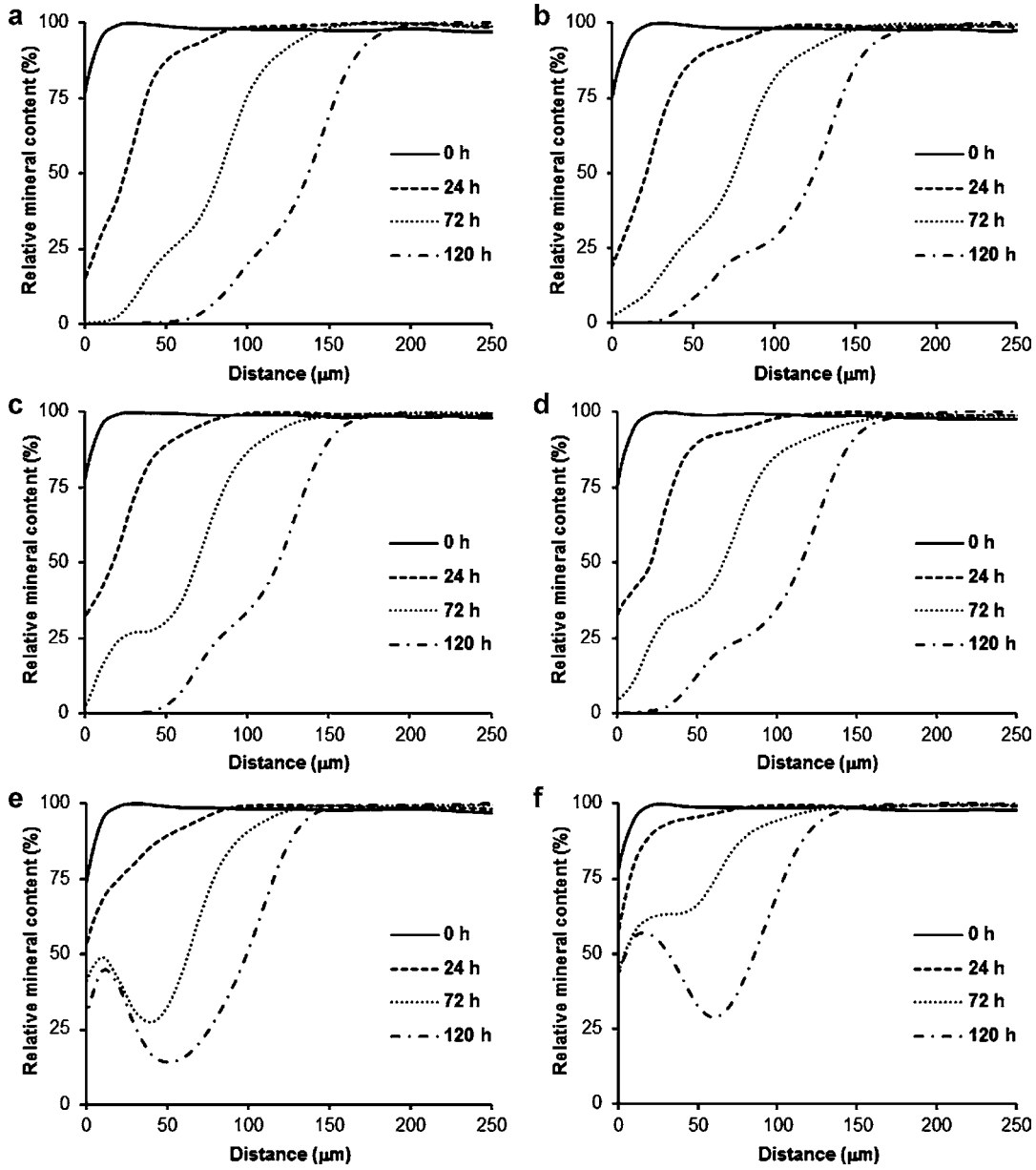

Fig. 5 – Mean mineral density profiles for each experimental group. Graphs show the mean mineral density profiles with the distance in *x*-axis (μm) and relative mineral content (%) in *y*-axis, before demineralization and after 24, 72, and 120 h of demineralization in the deionized water (a), CPP-ACP (b), CPP-ACPF (c), 90 ppm F (d), 900 ppm F (e), and 9000 ppm F (f) groups.

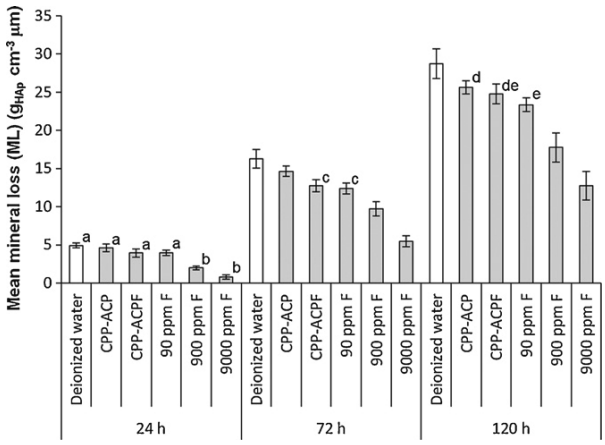

Fig. 6 – Mean mineral loss (ML) (g_{HAp} cm^{-3} μm) for each experimental group. Results are expressed as means and standard deviations (SD). Same lower case letters indicate no significant differences amongst the values ($p > 0.05$).

compared to the lesion body was clearly observed in the profiles of the 900 and 9000 ppm F groups after 72 and 120 h.

3.3. *Mean mineral loss and lesion depth*

The ML and LD values of each group calculated from the MD profiles are shown in Figs. 6 and 7, respectively. Two-way ANOVA revealed significant effects for both factors of demineralization time and treatment (ML: $p < 0.005$, LD: $p < 0.001$ for both), and a significant interaction between the two factors ($p < 0.001$). Multiple comparisons with t-test with Bonferroni correction within each group revealed significant differences in ML and LD between different demineralization times ($p < 0.05$).

After 24 h, no significant differences were found in ML amongst the control, CPP-ACP, CPP-ACPF, and 90 ppm F groups ($p > 0.05$). However, ML in both 900 and 9000 ppm F groups were significantly smaller than that in the negative control group ($p < 0.05$). After 72 h, significant differences were found in ML amongst all the groups ($p < 0.05$) except for the CPP-ACPF and 90 ppm F groups ($p > 0.05$). After 120 h, there were no significant differences either between the CPP-ACP and CPP-ACPF groups, or between the CPP-ACPF and 90 ppm F groups ($p > 0.05$).

As for the LD, after 24 h and 72 h, the 9000 ppm F group showed significantly different values compared to all other groups ($p < 0.05$). After 72 h, there were significant differences between the 900 ppm F group and all the other groups, except for the CPP-ACPF group ($p < 0.05$). After 120 h, LD in all the treatment groups was significantly smaller than the negative control group, except for the CPP-ACP group. The 900 and 9000 ppm F groups showed significantly different LD with all the other groups ($p < 0.05$).

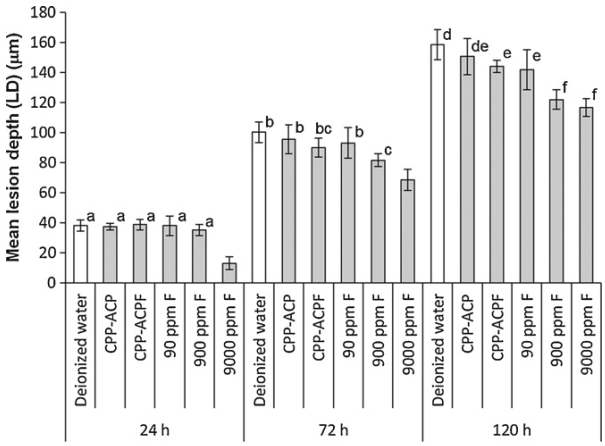

Fig. 7 – Mean lesion depth (LD) (μm) for each experimental group. Results are expressed as means and standard deviations (SD). Same lower case letters indicate no significant differences amongst the values ($p > 0.05$).

4. Discussion

Bovine teeth were used in the present study as they are easy to obtain, show less variability in composition compared to human teeth,[27] and have large caries-free enamel surfaces. It has been suggested that the use of a continuous exposure in the acidic environment, as in the present study, would simulate a severe case scenario of demineralization, magnifying the effects of each treatment on enamel.[24] Bovine enamel is more porous than human enamel resulting in more rapid progress of erosive lesions.[28] Moreover, grinding and polishing of enamel surfaces would expose a more porous subsurface, rendering the enamel more susceptible to acid attacks.[29] Deionized water was used as the medium for negative control treatment since in our pilot study, seven days storage in deionized water did not result in changes detectable by micro-CT.

Mineral quantification by means of X-ray absorption has been known since 1940s.[30] TMR has been considered as the "gold standard" technique for the determination of mineral content and caries lesion depth.[22,31] However, specimen preparation in this method is destructive and time consuming, requiring a thin slice of the hard tissue (<100 μm in enamel and <200 μm in dentine). Micro-CT can obtain 3D images and MD profiles non-destructively from a bulk of the specimen without preparing thin slices. Artifacts resulted from preparing thin sections could be removed, and the 3D reconstruction enables evaluation of any desired location on the scanned specimen.[32] A recent report concluded that micro-CT has the potential to substitute TMR for in vitro studies on dental caries.[33]

On the other hand, a number of artifacts intrinsic to the technique may hinder optimal quantitative use of micro-CT. In this regard, it was suggested that quantitative evaluation of dental hard tissues by micro-CT required the use of appropriate metal filters[34] and mineral reference phantoms.[35] Beam-hardening effect is one of these artifacts caused by the polychromatic nature of the X-ray beam used in the computed tomography. In short, the low energy photons are eliminated from the beam at a faster rate than the higher energy levels. Consequently, the X-ray beam becomes more penetrating, or

harder, as it traverses through matter. Beam-hardening leads to an apparent higher attenuation near the periphery of an otherwise homogeneous sample material.[26,36,37] Beam-hardening artifacts can be reduced by filtering out the low-energy radiation or pre-hardening the beam using attenuating metal filters (aluminum, copper or brass).[26,34] In the present study, we used a 0.2-mm-thick brass (Cu–Zn) filter. According to our pilot investigation, the 0.2-mm-brass filter diminished beam-hardening effect better than aluminum filters alone for an enamel substrate with a high mineral density.

For the purpose of mineral density determination, a system of calibration standards also known as mineral reference phantoms was used in the present study.[18,35,38-40] The strong linear regression of the mineral density calibration curve and its reproducibility demonstrated validity of the mineral determination technique and the experiment setup, in line with findings of a previous study.[40,41]

In order to quantitatively compare the preventive effects of the newly introduced products, NaF solutions with three different concentrations were used to serve as the positive controls in the present study. There is convincing evidence that NaF treatment provides preventive effect against demineralization, possibly through the precipitation of fluoridated apatite by a low concentration of fluoride ion in solution during demineralization.[42] The fluoride ion may be released from calcium fluoride (CaF_2) or CaF_2-like deposits formed by fluoride products on the treated enamel. In more detail, rate of the precipitation of fluoridated apatite is proportional to the ion concentration; an increased ion concentration increases degree of saturation with respect to fluorapatite.[43,44] It has also been reported that NaF is most effective when applied in a solution, and the ion concentration in the solution affects the efficacy of the treatment to prevent erosive demineralization.[29,45] The present results reconfirmed the dose-response effect of NaF on inhibition of enamel demineralization. This dose-response effect also indicated that the present micro-CT measurement conditions were suitable for the present study.

Several studies have reported that CPP-ACP has a protective effect on erosive loss and demineralization of enamel.[8,46,47] In the present study, the CPP-ACP paste showed a comparatively modest preventive effects on enamel demineralization. A significant inhibition of mineral loss was observed after 72 and 120 h of demineralization.

Reynolds et al.[10,46] showed that remineralization potential of CPP-ACP was improved when used in combination with NaF. It was also reported that the fluoride containing paste showed an improved inhibition potential, when compared to CPP-ACP alone, particularly with regard to early mineral loss.[11,48] In the present study, the CPP-ACPF and 90 ppm F groups showed very similar profile patterns with no statistical difference in ML or LD at any periods. In the profiles of the 900 and 9000 ppm F groups, the formation of a subsurface layer after 72 and 120 h was clearly observed. This finding suggested that in both groups, the fluoride ions were effectively incorporated into enamel and exerted the mechanism of action mentioned above. Moreover, the superficial zone with some increased resistance against demineralization could be observed after 72 h in the CPP-ACPF and 90 ppm F groups, although a distinct peak in MD was not detected.

In contrast to the fluoride containing groups, an erosion type demineralization with no distinct border between surface and subsurface was observed in the negative control group. Significant difference in ML between CPP-ACP and CPP-ACPF groups disappeared after 120 h. This result might reveal that the enamel surface reinforced by the fluoride in CPP-ACPF had been already dissolved by 120 h of demineralization under the conditions of the current experiment.

The CPP-ACPF paste, which contained 900 ppm F, was expected to show an effect close to the 900 ppm F solution. However, the effect of treatment with CPP-ACPF was similar to that of 90 ppm F solution. It should be noted that CPP-ACPF was applied in the form of a paste, which could have a lower penetration to enamel surface, compared to the NaF solution. Meanwhile, the extent of penetration of the fluoride ions into the enamel was not clearly characterized in the present study. It has been argued that NaF could potentially interact with the ACP and precipitate. On the other hand, it was suggested that the development of the CPP carrier for calcium and phosphate (as CPP-ACPF) greatly improved this problem, presumably as nanocomplexes.[43,49]

Further research using CPP-ACP and CPP-ACPF pastes with different approaches as preventive treatments using a model simulating the oral conditions with natural saliva and dental plaque as an *in situ* model are needed. Mechanisms of inhibition of demineralization by CPP-ACPF warrant further examination.

In short, it was suggested that polychromatic micro-CT scanning could provide various range of mineral density changes occurring in demineralization. The null hypotheses of this study must be rejected as according to mineral loss results, the application of CPP-ACP on sound enamel surfaces could increase resistance to demineralization. In addition, the application of CPP-ACPF had some additional benefits in comparison to CPP-ACP. Clinically, the use of CPP-ACPF paste as a daily homecare product can be beneficial to inhibition of demineralization.

5. Conclusions

The application of CPP-ACP or CPP-ACPF pastes to sound enamel surfaces showed inhibitory effect on enamel demineralization, and a better effect was noted for the latter paste. Quantitative assessment using polychromatic micro-CT demonstrated to be useful for detecting mineral density changes occurring in enamel demineralization.

Acknowledgements

The authors thank Dr. N. Nango of Ratoc System Engineering for helpful discussion of micro-CT results and Dr. M. Ikeda of School of Dental Technologists, Tokyo Medical and Dental University for help with the statistical analysis.

This work was supported by the grant from the Japanese Ministry of Education, Global Center of Excellence (GCOE) program, ''International Research Center for molecular Science in Tooth and Bone Diseases''.

GC corp. (Tokyo, Japan) provided the Tooth Mousse and Tooth Mousse Plus.

Conflict of interest

The authors state no conflict of interest.

REFERENCES

1. Huang TT, Jones AS, He LH, Darendeliler MA, Swain MV. Characterisation of enamel white spot lesions using X-ray micro-tomography. *Journal of Dentistry* 2007;**35**:737–43.
2. Silverstone LM, Hicks MJ, Featherstone MJ. Dynamic factors affecting lesion initiation and progression in human dental enamel. II. Surface morphology of sound enamel and carieslike lesions of enamel. *Quintessence International* 1988;**19**:773–85.
3. Barbour ME, Parker DM, Allen GC, Jandt KD. Enamel dissolution in citric acid as a function of calcium and phosphate concentrations and degree of saturation with respect to hydroxyapatite. *European Journal of Oral Sciences* 2003;**111**:428–33.
4. Tyas MJ, Anusavice KJ, Frencken JE, Mount GJ. Minimal intervention dentistry—a review. FDI Commission Project 1–97. *International Dental Journal* 2000;**50**:1–12.
5. Reynolds EC. The prevention of sub-surface demineralization of bovine enamel and change in plaque composition by casein in an intra-oral model. *Journal of Dental Research* 1987;**66**:1120–7.
6. Cross KJ, Huq NL, Palamara JE, Perich JW, Reynolds EC. Physicochemical characterization of casein phosphopeptide-amorphous calcium phosphate nanocomplexes. *Journal of Biological Chemistry* 2005;**280**:15362–9.
7. Reynolds EC, Cai F, Cochrane NJ, Shen P, Walker GD, Morgan MV, *et al.* Fluoride and casein phosphopeptide-amorphous calcium phosphate. *Journal of Dental Research* 2008;**87**:344–8.
8. Poggio C, Lombardini M, Dagna A, Chiesa M, Bianchi S. Protective effect on enamel demineralization of a CPP-ACP paste: an AFM in vitro study. *Journal of Dentistry* 2009;**37**: 949–54.
9. Oshiro M, Yamaguchi K, Takamizawa T, Inage H, Watanabe T, Irokawa A, *et al.* Effect of CPP-ACP paste on tooth mineralization: an FE-SEM study. *Journal of Oral Science* 2007;**49**:115–20.
10. Pulido MT, Wefel JS, Hernandez MM, Denehy GE, Guzman-Armstrong S, Chalmers JM, *et al.* The inhibitory effect of MI paste, fluoride and a combination of both on the progression of artificial caries-like lesions in enamel. *Operative Dentistry* 2008;**33**:550–5.
11. Kumar VL, Itthagarun A, King NM. The effect of casein phosphopeptide-amorphous calcium phosphate on remineralization of artificial caries-like lesions: an in vitro study. *Australian Dental Journal* 2008;**53**:34–40.
12. Stock SR, Barss J, Dahl T, Veis A, Almer JD. X-ray absorption microtomography (microCT) and small beam diffraction mapping of sea urchin teeth. *Journal of Structural Biology* 2002;**139**:1–12.
13. Stock SR, Vieira AE, Delbem AC, Cannon ML, Xiao X, Carlo FD. Synchrotron microcomputed tomography of the mature bovine dentinoenamel junction. *Journal of Structural Biology* 2008;**161**:162–71.
14. Zhou XZ, Zhang G, Dong QR, Chan CW, Liu CF, Qin L. Low-dose X-irradiation promotes mineralization of fracture callus in a rat model. *Archives of Orthopaedic and Trauma Surgery* 2009;**129**:125–32.
15. Kinney JH, Balooch M, Haupt Jr DL, Marshall SJ, Marshall Jr GW. Mineral distribution and dimensional changes in human dentin during demineralization. *Journal of Dental Research* 1995;**74**:1179–84.
16. Anderson P, Elliott JC, Bose U, Jones SJ. A comparison of the mineral content of enamel and dentine in human premolars and enamel pearls measured by X-ray microtomography. *Archives of Oral Biology* 1996;**41**:281–90.
17. Davis GR, Wong FS. X-ray microtomography of bones and teeth. *Physiological Measurement* 1996;**17**:121–46.
18. Wong FS, Elliott JC, Davis GR, Anderson P. X-ray microtomographic study of mineral distribution in enamel of mandibular rat incisors. *Journal of Anatomy* 2000;**196**: 405–13.
19. Efeoglu N, Wood D, Efeoglu C. Microcomputerised tomography evaluation of 10% carbamide peroxide applied to enamel. *Journal of Dentistry* 2005;**33**:561–7.
20. Dowker SE, Elliott JC, Davis GR, Wilson RM, Cloetens P. Synchrotron x-ray microtomographic investigation of mineral concentrations at micrometre scale in sound and carious enamel. *Caries Research* 2004;**38**:514–22.
21. Ten Bosch JJ, Angmar-Mansson B. A review of quantitative methods for studies of mineral content of intra-oral caries lesions. *Journal of Dental Research* 1991;**70**:2–14.
22. Arends J, ten Bosch JJ. Demineralization and remineralization evaluation techniques. *Journal of Dental Research* 1992;**71**. Spec No. 924–28.
23. White DJ, Faller RV, Bowman WD. Demineralization and remineralization evaluation techniques—added considerations. *Journal of Dental Research* 1992;**71**. Spec No. 929–33.
24. Ablal MA, Kaur JS, Cooper L, Jarad FD, Milosevic A, Higham SM, *et al.* The erosive potential of some alcopops using bovine enamel: an in vitro study. *Journal of Dentistry* 2009;**37**:835–9.
25. ten Cate JM, Duijsters PP. Alternating demineralization and remineralization of artificial enamel lesions. *Caries Research* 1982;**16**:201–10.
26. Jennings RJ. A method for comparing beam-hardening filter materials for diagnostic radiology. *Medical Physics* 1988;**15**:588–99.
27. Nakamichi I, Iwaku M, Fusayama T. Bovine teeth as possible substitutes in the adhesion test. *Journal of Dental Research* 1983;**62**:1076–81.
28. Arends J, Christoffersen J, Ruben J, Jongebloed WL. Remineralization of bovine dentine in vitro The influence of the F content in solution on mineral distribution. *Caries Research* 1989;**23**:309–14.
29. Ganss C, Klimek J, Schwarz N. A comparative profilometric in vitro study of the susceptibility of polished and natural human enamel and dentine surfaces to erosive demineralization. *Archives of Oral Biology* 2000;**45**:897–902.
30. Thewlis J. The structure of teeth as shown by X-ray examination, Medical Research Council Special Report Series 1940:238.
31. Inaba D, Takagi O, Arends J. A computer-assisted videodensitometric method to visualize mineral distributions in in vitro and in vivo formed root caries lesions. *European Journal of Oral Sciences* 1997;**105**:74–80.
32. Damen JJ, Exterkate RA, ten Cate JM. Reproducibility of TMR for the determination of longitudinal mineral changes in dental hard tissues. *Advances in Dental Research* 1997;**11**: 415–9.
33. Lo EC, Zhi QH, Itthagarun A. Comparing two quantitative methods for studying remineralization of artificial caries. *Journal of Dentistry* 2010;**38**:352–9.

34. Meganck JA, Kozloff KM, Thornton MM, Broski SM, Goldstein SA. Beam hardening artifacts in micro-computed tomography scanning can be reduced by X-ray beam filtration and the resulting images can be used to accurately measure BMD. *Bone* 2009;**45**:1104–16.
35. Schwass DR, Swain MV, Purton DG, Leichter JW. A system of calibrating microtomography for use in caries research. *Caries Research* 2009;**43**:314–21.
36. Chen CY, Chuang KS, Wu J, Lin HR, Li MJ. Beam hardening correction for computed tomography images using a postreconstruction method and equivalent tissue concept. *Journal of Digital Imaging* 2001;**14**:54–61.
37. Kovacs M, Danyi R, Erdelyi M, Fejerdy P, Dobo-Nagy C. Distortional effect of beam-hardening artefacts on microCT: a simulation study based on an in vitro caries model. *Oral Surgery Oral Medicine Oral Pathology Oral Radiology & Endodontics* 2009;**108**:591–9.
38. Clementino-Luedemann TN, Kunzelmann KH. Mineral concentration of natural human teeth by a commercial micro-CT. *Dental Materials Journal* 2006;**25**:113–9.
39. Nazarian A, Snyder BD, Zurakowski D, Muller R. Quantitative micro-computed tomography: a non-invasive method to assess equivalent bone mineral density. *Bone* 2008;**43**:302–11.
40. Burghardt AJ, Kazakia GJ, Laib A, Majumdar S. Quantitative assessment of bone tissue mineralization with polychromatic micro-computed tomography. *Calcified Tissue International* 2008;**83**:129–38.
41. Neves Ade A, Coutinho E, Vivan Cardoso M, Jaecques SV, Van Meerbeek B. Micro-CT based quantitative evaluation of caries excavation. *Dental Materials* 2010;**26**:579–88.
42. Bartlett DW, Smith BG, Wilson RF. Comparison of the effect of fluoride and non-fluoride toothpaste on tooth wear in vitro and the influence of enamel fluoride concentration and hardness of enamel. *British Dental Journal* 1994;**176**:346–8.
43. Barkvoll P, Rolla G, Lagerlof F. Effect of sodium lauryl sulfate on the deposition of alkali-soluble fluoride on enamel in vitro. *Caries Research* 1988;**22**:139–44.
44. Ogard B, Seppa L, Rolla G. Professional topical fluoride applications—clinical efficacy and mechanism of action. *Advances in Dental Research* 1994;**8**:190–201.
45. Attin T, Deifuss H, Hellwig E. Influence of acidified fluoride gel on abrasion resistance of eroded enamel. *Caries Research* 1999;**33**:135–9.
46. Ranjitkar S, Kaidonis JA, Richards LC, Townsend GC. The effect of CPP-ACP on enamel wear under severe erosive conditions. *Archives of Oral Biology* 2009;**54**: 527–32.
47. Panich M, Poolthong S. The effect of casein phosphopeptide-amorphous calcium phosphate and a cola soft drink on in vitro enamel hardness. *Journal of the American Dental Association* 2009;**140**:455–60.
48. Reynolds EC. Remineralization of enamel subsurface lesions by casein phosphopeptide-stabilized calcium phosphate solutions. *Journal of Dental Research* 1997;**76**:1587–95.
49. Cochrane NJ, Saranathan S, Cai F, Cross KJ, Reynolds EC. Enamel subsurface lesion remineralisation with casein phosphopeptide stabilised solutions of calcium, phosphate and fluoride. *Caries Research* 2008;**42**:88–97.

分子情報伝達学分野

高柳　広

医歯学総合研究科・生体支持組織学系専攻
分子情報伝達学・教授

1）研究の課題名

骨代謝制御ネットワークの解明：

Elucidation of novel regulatory mechanisms in bone metabolism

研究内容

骨代謝は、骨自身だけではなく他臓器や組織の恒常性維持にも重要である事が明らかにされている。本研究は骨代謝制御ネットワークを、骨を構成する個々の細胞間から最終的に全身の組織、臓器レベルで解明する。この実現の為に、研究内容は3つの項目から構成されている。A）骨構成細胞に発現する遺伝子・タンパク質の網羅解析;B）コンディショナル遺伝子改変マウスを用いた骨代謝制御遺伝子の機能解析; C）骨による全身性制御機構の解明である。本年度はこれらの成果を3本の論文としてまとめ、Nature Medicine誌に2本発表することができた。1）骨細胞だけを特異的に蛍光発色させる遺伝子（EGFP）を導入した改変マウスを作出し、世界に先駆け、高純度の骨細胞を単離培養することに成功した。さらに、骨や骨髄に含まれる細胞集団の中で、骨細胞が最もRANKLを発現しており破骨細胞を育てる能力に優れていることを見出し、骨細胞だけでRANKL遺伝子が破壊されるマウスは重篤な大理石骨病を発症することを発見した。興味深いことに、この大理石骨病は、生後直ぐには発症しておらず、成長に伴いその病状が悪化する。この表現型は、成長に伴い外界から受けるメカニカルストレスを骨細胞が感受し、RANKLを発現することが原因であると考えられた。2）破骨細胞が分泌する神経軸索ガイダンス分子の一つ、Sema4Dが骨芽細胞に作用して骨形成を抑制することを見出した。破骨細胞はSema4Dを特異的かつ高レベルに産生し、骨芽細胞にはSema4D受容体Plexin-B1が発現していた。Sema4DはPlexin-B1を介して、small-GTPase RhoAの活性化を亢進させ、骨形成を阻害した。Sema4d及びPlexin-B1欠損マウスはともに、骨芽細胞数と骨形成の増加による顕著な骨量増加を呈した。また、dominant negative型のRhoA を骨芽細胞特異的に発現するRhoA DNOBマウスも同様な骨形成亢進による骨量増加を示し、Sema4D-Plexin-B1-RhoAシグナルが生体内で必須の骨形成抑制機構を担っていることが明らかにした。本研究は、Sema4Dが骨リモデリングにおいて新たなカップリング因子として機能し、骨形成を促進させる薬剤開発の重要なターゲットとなりうることを示唆する重要な知見を提供する。

拠点内イノベーション研究

研究の題目

光メージングと分子生物学の融合によるオステオネットワークの解明を目指したフロンティア研究拠点

New frontier of osteonetwork research by combinational approaches of optical imaging and molecular biology

研究内容

骨のホメオスタシスは骨芽細胞による骨形成と破骨細胞による骨吸収のバランスで維持されており、これらの細胞系の分化・機能の制御機構を明らかにすることは骨生物学の大きな目標の一つである。近年では、骨組織に埋もれている骨細胞の機能が注目され、骨リモデリングにおける骨細胞、骨芽細胞、破骨細胞間の相互作用の解明も重要な研究課題となっている。また、骨組織の内部には、骨芽細胞、骨細胞、破骨細胞以外に間葉系幹細胞、造血・免疫系細胞、血管系細胞、脂肪細胞などの多くの細胞系が混在しているため、骨髄環境に存在する多くの細胞系の相互作用を明らかにすることも重要課題となっている。さらに、骨組織のホメオスタシスは、ホルモン、メカニカルストレスなどのバイオモデュレーターにより骨の外部から入力された刺激で制御されているので、骨組織と骨外の臓器・組織との相互作用を解析することも重要となる。

このように臓器としての骨組織の重要性は広がりつつあり、骨組織のホメオスタシスを生物学的に理解するには、

これら多くの細胞系の動的な相互作用を明らかにすることが極めて重要である。本研究グループでは、骨内外の細胞間の緊密なコミュニケーションをオステネットワークという新たな骨生物学のパラダイムとして捉え、ネットワークを構成する分子・細胞群を統合的かつ動的に解析することにより、骨をさらに深く理解することを目標とする。具体的には、骨組織に対する光イメージングの応用と遺伝子改変マウス作製を含めた網羅的分子生物学のテクニックを有機的に結合させ、研究を推進する。これら異分野として発展しつつある2つの先端科学的なアプローチを統合し、オステオネットワーク構成分子群の同定とその機能解明にチャレンジする。

2）

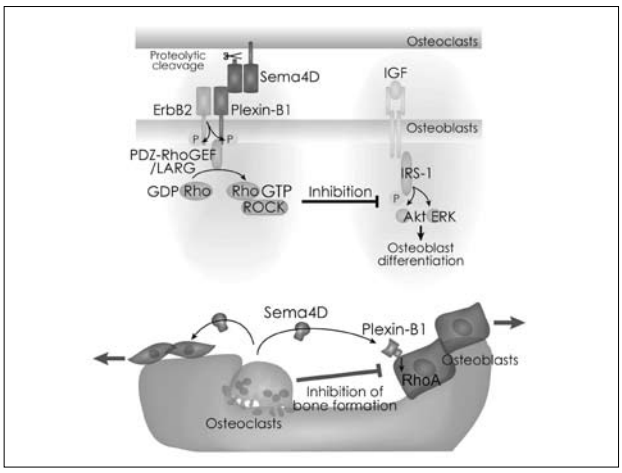

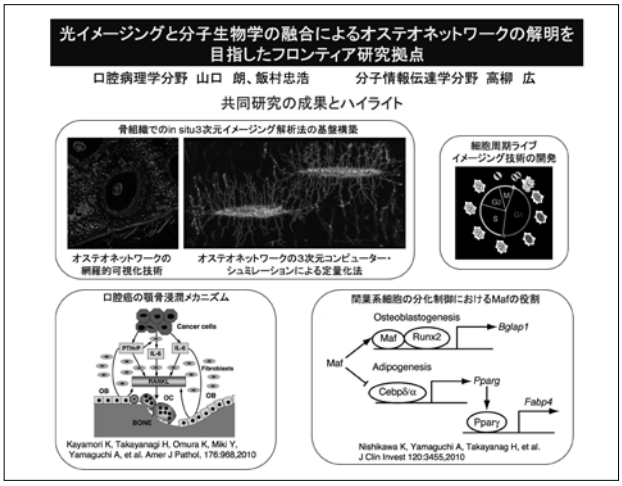

3）発表の研究内容についての英文要約

1）Osteocytes embedded in bone have been postulated to orchestrate bone homeostasis by regulating both bone-forming osteoblasts and bone-resorbing osteoclasts. We find here that purified osteocytes express a much higher amount of receptor activator of nuclear factor-κB ligand（RANKL）and have a greater capacity to support osteoclastogenesis in vitro than osteoblasts and bone marrow stromal cells. Furthermore, the severe osteopetrotic phenotype that we observe in mice lacking RANKL specifically in osteocytes indicates that osteocytes are the major source of RANKL in bone remodeling in vivo.

2）Most of the currently available drugs for osteoporosis inhibit osteoclastic bone resorption, whereas there are few drugs which promote osteoblastic bone formation. It is thus becoming increasingly important to identify the factors which regulate bone formation. We found that osteoclasts express semaphorin 4D（Sema4D）, known as an axon guidance molecule, which potently inhibits bone formation. The binding of Sema4D to its receptor Plexin-B1 on osteoblasts resulted in the activation of the small GTPase RhoA, which inhibited bone formation by suppressing insulin-like growth factor-1（IGF-1）signaling and by modulating osteoblast motility. The Sema4d$^{-/-}$ mice, Plxnb1$^{-/-}$ mice and the mice expressing a dominant-negative RhoA specifically in osteoblasts exhibited an osteosclerotic phenotype due to augmented bone formation. Notably, anti-Sema4D antibody treatment significantly prevented bone loss in a model of postmenopausal osteoporosis. Thus, Sema4D has emerged as a new therapeutic target for the discovery and development of bone-increasing drugs.

3）Bone homeostasis is maintained by a dynamic balance between bone resorption by osteoclasts and bone formation by osteoblasts. Since excessive osteoclast activity is implicated in pathological bone resorption, understanding the mechanism underlying osteoclast differentiation, function and survival is of both scientific and clinical importance. Osteoclasts are monocyte/macrophage lineage cells with a short life span that undergo rapid apoptosis, the rate of which critically determines the level of bone resorption in vivo. However, the molecular basis of rapid osteoclast apoptosis remains obscure. Here we report the role of a BH3-only protein, Noxa（encoded by the Pmaip1 gene）, in bone homeostasis using Noxa-deficient mice. Among the Bcl-2 family members, Noxa was selectively induced during osteoclastogenesis. Mice lacking Noxa exhibit a severe osteoporotic phenotype due to an increased number of osteoclasts. Noxa deficiency did not have any effect on the number of osteoclast precursor cells or the expression of osteoclast-specific genes, but led to a prolonged survival of osteoclasts. Furthermore, adenovirus-mediated Noxa overexpression remarkably reduced bone loss in a model of inflammation-induced bone destruction. This study reveals Noxa to be a crucial regulator of osteoclast apoptosis, and may provide a molecular basis for a new therapeutic approach to bone

diseases.

4) Cell fate determination is tightly regulated by transcriptional activators and repressors. Leukemia/lymphoma-related factor（LRF; encoded by Zbtb7a）, known as a POK family transcriptional repressor, is induced during the development of bone-resorbing osteoclasts, but the physiological significance of LRF in bone metabolism and the molecular mechanisms underlying the transcriptional regulation of osteoclastogenesis by LRF have not been elucidated. Here we show that LRF negatively regulates osteoclast differentiation by repressing nuclear factor of activated T cells c1（NFATc1）induction in the early phase of osteoclast development, while positively regulating osteoclast-specific genes by functioning as a coactivator of NFATc1 in the bone resorption phase. The stage-specific distinct functions of LRF were demonstrated in two lines of conditional knockout mice in which LRF was deleted in the early or late phase of osteoclast development. Thus, this study shows that LRF plays stage-specific distinct roles in osteoclast differentiation, exemplifying the delicate transcriptional regulation at work in lineage commitment.

4）本事業に関連して世界的な研究拠点形成に向けて、以下の点で改善・整備等されたこと

A（研究拠点体制）

他分野（特に免疫学）の学外研究者との協力し、世界的な成果を責任著者として3本の論文を発表できた。さらに学内共同研究の成果を論文として発表した。

B（研究教育環境）

GCOE AISS学生の博士号取得に向けた確実な研究指導を行った結果、GCOE AISS学生1名が博士号を取得し、残る3名のうち1名は論文revision中であり、2名は論文投稿に向け順調に研究を進めている。

C（人材確保）、D（人材育成）

昨年度に比べ、国内外から他分野に精通したポスドク、大学院生、技術補佐員をさらに増員し、学際的環境下で骨代謝研究を推進できる環境を整備した。

E（国際化）

海外において多数の講演を行った。さらに当研究室では、海外からのポスドクが常時研究に参画しており、ラボ内セミナーでの公用語は英語としている。

5）GCOE事業を推進するに当たって力を入れた点

GCOEシンポジウムや国際学会を積極的に活用して、世界の一線級の研究者と意見交換を行い、世界トップレベルの研究を意識した研究推進を行った。本年度も引き続き、GCOE拠点内にとどまらず東京医科歯科大学や他大学の研究者と広く密接な連携を行うことで、各分野の先端的な発想を自分の研究領域と融合させ、研究成果として結実させることを心がけた。

6）英文原著論文

◎1. Negishi-Koga T, Shinohara M, Komatsu N, Bito H, Kodama T, Friedel RH, Takayanagi H. Suppression of bone formation by osteoclastic expression of semaphorin 4D.
Nat Med., 17（11）：1473, 2011

◎2. Nakashima T, Hayashi M, Fukunaga T, Kurata K, Oh-hora M, Feng JQ, Bonewald LF, Kodama T, Wutz A, Wagner EF, Josef M. Penninger JM, Takayanagi H. Evidence for osteocyte regulation of bone homeostasis through RANKL expression.
Nat Med., 17（10）：1231, 2011

3. Kuroda S, Yamazaki M, Abe M, Sakimura K, Takayanagi H, Iwai Y. Basic leucine zipper transcription factor, ATF-like（BATF）regulates epigenetically and energetically effector CD8 T-cell differentiation via Sirt1 expression.
Proc Natl Acad Sci USA., 108（36）：14885, 2011

4. Barrow AD, Raynal N, Andersen TL, Slatter DA, Bihan D, Pugh N, Cella M, Kim T, Rho J, Negishi-Koga T, Delaisse JM, Takayanagi H, Lorenzo J, Colonna M, Farndale RW, Choi Y, Trowsdale J. OSCAR is a collagen receptor that costimulates osteoclastogenesis in DAP12-deficient humans and mice.
J Clin Invest., 121（9）：3505, 2011

5. Kamitani-Kawamoto A, Hamada M, Moriguchi T, Miyai M, Saji F, Hatamura I, Nishikawa K, Takayanagi H, Hotoshi S, Ikehara K, Hosoya T, Hotta Y, Takahashi S, Kataoka K. MafB interacts with Gcm2 and regulates parathyroid hormone expression and parathyroid development.
J Bone Miner Res., 26（10）：2463, 2011

◎6. Idrus E, Nakashima T, Wang L, Hayashi M, Okamoto K, Kodama T, Tanaka N, Taniguchi T, Takayanagi H. The Role of the BH3-only Protein Noxa in Bone Homeostasis.
Biochem Biophys Res Commun., 410（3）：620, 2011

◎7. Tsuji K, Negishi-Koga T, Sumiya E, Kukita A, Kato S, Maeda T, Pandolfi PP, Moriyama K, Takayanagi H. Stage-specific functions of LRF in the transcriptional control of osteoclast development.
Proc Natl Acad Sci USA., in press

7）総説ならびに著書

（英文）

1. Takayanagi H.
   Introduction to the special issue "The interaction among bone, immunology and vascular biology".
   Inflammation and Regeneration, 399-403（5ページ）, 2011
2. Nakashima T, Takayanagi H.
   Osteoimmunology：the effect of Inflammation on bone.
   Inflammation and Regeneration, 404-412（9ページ）, 2011
3. Kazuo Okamoto and Hiroshi Takayanagi
   Osteoclasts and interleukin-17-producing helper T cells in rheumatoid arthritis
   Arthritis：Pathophysiology, Prevention and Therapeutics, 75-89（15ページ）, 2011
4. Kazuo Okamoto and Hiroshi Takayanagi
   Osteoclasts in arthritis and Th17 development
   International Immunopharmacology, 543-548（6ページ）, 2011
5. Kazuo Okamoto and Hiroshi Takayanagi
   Regulation of bone by the adaptive immune system in arthritis
   Arthritis Research & Therapy, 219（1ページ）, 2011
6. Kazuo Okamoto and Hiroshi Takayanagi
   Potential molecular targets for suppressing Th17 development
   Inflammation and Regeneration, 354-360（7ページ）, 2011

（和文）

1. 中島友紀、高柳広：破骨細胞分化と骨免疫学
   CLINICAL CALCIUM、1843-1852（10ページ）、2011
2. 中島友紀、高柳広：RANKLシグナルと骨免疫学
   CLINICAL CALCIUM、1131-1140（10ページ）、2011
3. 中島友紀、高柳広：免疫系と破骨細胞
   細胞工学、250-258（9ページ）、2011
4. 中島友紀、高柳広：骨免疫学から見た生物学的製剤療法と新展開
   骨粗鬆症治療、53-59（7ページ）、2011
5. 中島友紀、高柳広：骨を作りか変える指令細胞の発見
   整形外科、50（1ページ）、2011
6. 根岸-古賀貴子、高柳広：「骨粗鬆症に対する抗体療法」
   医学のあゆみ、730-737（8ページ）、2011
7. 小松紀子、高柳広：骨免疫学と関節炎動物モデル
   CLINICAL CALCIUM、117-124（8ページ）、2011
8. 岡本一男、高柳広：Th17細胞と転写制御因子IκBζ
   生物の科学　遺伝、78-82（5ページ）、2011
9. 岡本一男、高柳広：Th17細胞分化に必須の転写制御因子IκBζ
   医学のあゆみ、803-804（2ページ）、2011
10. 岡本一男、高柳広：転写制御因子IκBζを標的としたTh17細胞制御
    最新医学、287-292（6ページ）、2011
11. 岡本一男、高柳広：転写制御因子IκBζによるTh17細胞分化制御
    Frontiers in Rheumatology & Clinical Immunology、53-57（5ページ）、2011
12. 西川恵三、高柳広：新着論文解説2;Mafは加齢に伴う間葉系細胞分化の運命決定に関与し、骨芽細胞分化を促進する
    O.li.v.e. －骨代謝と生活習慣病の連関－、35-39（5ページ）、2011
13. 中島友紀、高柳広：骨免疫学からみたRA治療の新展開
    最新医学、2012年2月号発行予定
14. 篠原正浩、高柳広：骨免疫学
    炎症と免疫、2012年2月号発行予定
15. 篠原正浩、高柳広：骨免疫学の最前線
    腎と骨代謝、2012年発行予定（季刊）

8）特許取得、特許申請

1. 発明の名称：CaMK阻害ペプチドおよびこれを含有するCaMK阻害剤（特願番号：2011－017295）

発明者：西川喜代孝、高橋美帆、西村浩輝、高柳広、尾藤晴彦
出願日：2011年1月28日
出願人：学校法人　同志社大学、国立大学法人　東京医科歯科大学

2. 発明の名称：骨形成促進剤（特願番号：2011－108642）

発明者：高柳広、古賀貴子
出願日：2011年5月13日
出願人：国立大学法人　東京医科歯科大学

9）平成23年度までの自己評価

本年度は、骨に埋め込まれた状態で存在する骨細胞を高純度で単離する方法を確率し、さらに骨細胞が発現するRANKLが破骨細胞の分化を制御し、骨の恒常性維持において重要な役割を果たすことを発見した。また、神経軸索ガイダンス因子Sema4Dが破骨細胞に、その受容体Plexin-B1が骨細胞に発現し、RhoAを活性化させる事によって骨形成を阻害する事を明らかにし、遺伝子改変マウスの解析からSema4D-Plexin-B1-RhoAシグナルが生体内で必須の骨形成抑制機構を担っていることを明

らかにした。これらに加えて、BH3モチーフだけを持つNoxaが破骨細胞の生存を制御し、Noxa欠損マウスは骨粗鬆症を呈することを明らかにした。以上、本年度は骨と免疫系が密接に関与している事を多数発見でき、主著論文3本（うち2本はNature Medicine誌）と共著論文3本、計6本の論文として発表した。また本年度は、これまでに行われた各骨構成細胞の網羅的なトランスクリプトーム解析やプロテオーム解析によって同定した骨代謝系と免疫系に関わる有望な候補遺伝子のコンディショナル遺伝子改変マウスの解析を進めた。その結果、現在2本の論文が投稿中である。その他の遺伝子改変マウスの解析もさらに進め、骨と免疫の相互作用の解明に取り組む予定である。

10）学会発表（英文）

◎Authors：Takako Negishi-Koga.
Title：Bone remodeling regulated by osteoclast-derived Semaphorin 4D.
32nd The Japanese Society of Inflammation and Regeneration（JCIR）and The Asia-Pacific Federation of Inflammation and Regeneration（APFIR）
Oral Presentation
Kyoto Japan, 2011 June 3

◎Authors：Tomoki Nakashima.
Title：Regulation of bone remodeling by osteoclastogenesis.
7th Meeting of Bone Biology Forum
Oral Presentation
Shizuoka, 2011 August 21

◎Authors：Masahiro Shinohara, Hiroshi Takayanagi.
Title：Class IA Phosphatidylinositol 3-kinases regulates osteoclastic bone resorption.
33th Annual Meeting of the American Society for Bone and Mineral Research
Poster Presentation
San Diego USA, 2011 September 18

◎Authors：Takako Negishi-Koga, Masahiro Shinohara, Hiroshi Takayanagi.
Title：Protection of bone loss by targeting semaphorin 4D expressed by osteoclasts.
33th Annual Meeting of the American Society for Bone and Mineral Research
Poster Presentation
San Diego USA, 2011 September 16, 17

◎K. Tsuji, T. Koga, K. Moriyama and H. Takayanagi.
The Transcriptional Repressor LRF Regulates Osteoclastogenesis.
The 59th Annual meeting of Japanese Association for Dental Research
Oral and Poster Presentation
Hiroshima, 2011 October 7-9

◎Authors：Tomoki Nakashima, Hiroshi Takayanagi.
Title：The crucial role of osteocyte-derived RANKL in bone homeostasis.
2nd Tokyo-Shanghai Workshop on Rheumatology
1st Bio-Rheumatology International Congress
（BRIC2011）, 8th GARN Meeting
Oral Presentation
Chiba, 2011 November 13

11）学会発表（和文）

著者名：根岸 - 古賀貴子、篠原正浩、高柳広
演題名：セマフォリン4Dを介した破骨細胞による骨形成抑制制御
学会名：第29回日本骨代謝学会学術集会
大阪、平成23年7月28日

著者名：辻香織
演題名：Zinc finger型転写因子LRFの破骨細胞における役割の解明
学会名：先端歯学スクール2011
三浦、平成23年9月1日

著者名：古賀貴子、篠原正浩、高柳広
演題名：神経軸索ガイダンス因子Sema4Dによる骨形成抑制機構
学会名：第34回日本分子生物学会
横浜、平成23年12月15、16日

著者名：Abdul Alim Al-Bari、篠原正浩、永井裕介、高柳広
演題名：Lysosomal function is important for osteoclast differentiation and function
学会名：第34回日本分子生物学会
横浜、平成23年12月15日

著者名：篠原正浩、永井裕介、中村正樹、田中栄、高柳広
演題名：PI3K-Akt経路はPlekhm1のリン酸化を介して破骨細胞の骨吸収を制御する
学会名：第33回日本分子生物学会年会
神戸、平成22年12月10日

12）受賞

高柳　広

The 3rd Joint Conference of the International Bone & Mineral Society and the European Calcified Tissue Society, IBMS-BONE Herbert A. Fleisch Award
平成23年5月9日

中島　友紀

1st Bio-Rheumatology International Congress（BRIC2011）, Poster Presentation Award
平成23年11月

古賀　貴子

第29回日本骨代謝学会、優秀演題賞
平成23年7月29日

辻　香織

The 59th Annual meeting of Japanese Association for Dental Research
The Hatton Award 2012 Finalist of Japanese Association for Dental Research

13）外部資金の獲得状況

（独）科学技術振興機構（JST）　戦略的創造研究推進事業（ERATO型研究）　平成21年度発足

研究題目：ERATO　高柳オステオネットワークプロジェクト
代表：高柳　広
期間：平成21年度～平成26年度
研究費総額：169,900万円

文部科学省科学研究費補助金　挑戦的萌芽研究

研究題目：骨代謝を制御するカップリング因子の同定と機能解析
代表：中島　友紀
期間：平成21年度～平成23年度
研究費総額：320万円

文部科学省科学研究費補助金　若手研究（A）

研究題目：破骨細胞特異的システムの解明—歯の革新的保存法の確立を目指して
代表：篠原　正浩
期間：平成22年度～平成24年度
研究費総額：2,186万円

特定領域　公募研究

研究題目：T系列細胞系列群の分化・機能におけるカルシウム流入制御機構の解明
代表：大洞　将嗣
期間：平成22年度～平成23年度
研究費総額：960万円

（独）科学技術振興機構（JST）　戦略的創造研究推進事業（さきがけ）「炎症の慢性化機構の解明と制御」

研究題目：イオンバランス破綻による自己免疫疾患の重症化機構の解明
代表：大洞　将嗣
期間：平成23年度～平成25年度
研究費総額：4,000万円

文部科学省科学研究費補助金　若手研究（A）

研究題目：炎症応答と骨破壊の両プロセスを包括して制御できる炎症性骨破壊治療法の確立
代表：岡本　一男
期間：平成23年度～平成25年度
研究費総額：2,130万円

文部科学省科学研究費補助金　基盤研究（C）

研究題目：末梢免疫寛容成立におけるカルシウムシグナルの役割の解明
代表：大洞　将嗣
期間：平成23年度～平成25年度
研究費総額：410万円

文部科学省科学研究費補助金　挑戦的萌芽研究

研究題目：メタボリックシンドロームにおける破骨細胞の機能解析
代表：篠原　正浩
期間：平成23年度～平成24年度
研究費総額：290万円

文部科学省科学研究費補助金　挑戦的萌芽研究

研究題目：細菌感染症におけるIL-17/IL-22産生制御機能の解明
代表：岡本　一男
期間：平成23年度～平成24年度
研究費総額：290万円

文部科学省科学研究費補助金　特別研究員奨励費

研究題目：RANK/RANKLシグナルの新規機能の解明
代表：高柳　広
期間：平成22年度～平成23年度
研究費総額：300万円

文部科学省科学研究費補助金　特別研究員奨励費

研究題目：溶骨性疾患と加齢における骨の恒常性におけるB細胞の役割の解明
代表：高柳　広
期間：平成23年度～平成24年度
研究費総額：160万円

文部科学省科学研究費補助金　特別研究員奨励費
研究題目：急性免疫反応における破骨細胞・骨芽細胞の意義
代表：寺島　明日香
期間：平成23年度～平成25年度
研究費総額：750万円

公益財団法人　持田記念医学薬学振興財団
研究題目：カルシウムシグナルを介した自己免疫疾患における胚中心形成機構の解明
代表：大洞　将嗣
期間：平成22年度～平成23年度
研究費総額：300万円

基礎研究支援プロジェクト　（中外製薬）
研究題目：骨リモデリング制御因子の同定とその機能解析
代表：中島　友紀
期間：平成22年度～平成26年度
研究費総額：1,000万円

ブリストル・マイヤーズ関節リウマチ研究助成（ブリストル・マイヤーズ）
研究題目：関節リウマチに伴う骨破壊の制御機構の解明　滑膜バイオロジーの創成
代表：中島　友紀
期間：平成23年度～平成25年度
研究費総額：1,000万円

公益財団法人　興和生命科学振興財団　研究助成
研究題目：骨構成細胞が産生する生理活性物質の探索と機能解明
代表：篠原　正浩
期間：平成23年度～平成24年度
研究費総額：100万円

公益財団法人　アステラス病態代謝研究会　研究助成金
研究題目：感染症リスクを提言できる自己免疫疾患治療法の確立
代表：岡本　一男
期間：平成23年度～平成24年度
研究費総額：100万円

14）特別講演、招待講演、シンポジウム

高柳広

1. Swiss Society for Allergology and Immunology Annual Congress 2011.3.18, Lugano, Switzerland
2. International PhD Program in Immunology, Cell Biology and Biochemistry 2010-2011 Lecture course, Institute for Research in Biomedicine 2011.3.21, Bellinzona, Switzerland
3. 第84回日本内分泌学会学術総会 2011.4.22、神戸
4. 4th New York Skeletal Biology and Medicine Meeting 2011.4. 28, New York, USA
5. Lecture in Symposium 4, 3rd Joint Meeting of the ECTS and IBMS 2011.5.9, Athens, Greece
6. Meet the Professor Session, 3rd Joint Meeting of the ECTS and IBMS, 2011.5.10 Athens, Greece
7. The 13th International TNF Conference 2011.5. 18, Awaji Island, Japan
8. 日本分子生物学会　第11回春期シンポジウム 2011. 5.26、石川
9. Bone inflammation and regeneration; sponsored symposium by the Japanese Society of Inflammation and Regeneration, 10th World Congress on Inflammation 2011.6.26, Paris, France
10. 第55回日本リウマチ学会総会・学術集会、第20回国際リウマチシンポジウム、アニュアルコースレクチャー 2011.7.17、神戸
11. 第55回日本リウマチ学会総会・学術集会、第20回国際リウマチシンポジウム、ランチョンセミナー 2011.7.18、神戸
12. 第55回日本リウマチ学会総会・学術集会、第20回国際リウマチシンポジウム、シンポジウム2 2011.7.19、神戸
13. 第29回日本骨代謝学会学術集会、シンポジウム3 2011.7.28、大阪
14. IOF Regionals – 2nd Asia-Pacific Osteoporosis and Bone Meeting being held in Conjunction with the ANZBMS Annual Scientific Meeting and JSBMR 2011.9.5, Gold Coast, Australia
15. 第39回日本臨床免疫学会総会 2011.9.15、東京
16. 第84回日本生化学会大会 2011.9.23、京都
17. 4th National Congress of Osteoporosis 2011.10.28, Antalya, Turkey
18. ACR Basic Research Conference：Bone Pathophysiology in Inflammatory and Rheumatic, the 2011 ACR/ARHR Annual Scientific Meeting 2011.11.4, Chicago, IL USA
19. Bio-Rheumatology International Congress

2011.11.15、東京
20. 第40回日本免疫学会総会・学術集会
2011.11.27、千葉
21. 第40回日本免疫学会総会・学術集会
2011.11.28、千葉

中島友紀

・第55回日本リウマチ学会、シンポジウム
2011年7月18日、神戸
・第1回Chiba Bone and Mineral Metabolism Research Meeting、招待講演
2011年10月13日、千葉
・第48回日本リハビリテーション医学会、シンポジウム
2011年11月2日、千葉
・第5回骨・軟骨フロンティア、招待講演
2011年11月19日、東京

古賀貴子

・32th The Japanese Society of Inflammation and Regeneration（JCIR）and The Asia-Pacific Federation of Inflammation and Regeneration（APFIR）
2011 June 3, Kyoto

岡本一男

・第20回東京免疫フォーラム、招待講演
2011年2月22日、東京

15）主催学会

第7回骨免疫ワークショップ
2011年11月25日、東京

16）新聞、雑誌、TV報道

1. Toshio Matsumoto：Molecular and Cell Biology
IBMS BoneKEy. 8（11）, 457-466（2011）doi：10.1138/20110538（Epub）
2. Lauren Martz：SEMA4D in osteoporosis
SciBx. 4（45）, doi：10.1038/scibx.2011.1255（EPub）
3. Emma Leah：Bone：Finding that osteoclasts repel osteoblast activity through Sema4D reveals novel target for bone-boosting therapies
Nat Rev Rheumatol. 7, 681（2011）
4. Rachel David：Development：Osteoblasts and osteoclasts keep in touch
Nat Rev Mol Cell Biol. 12, 767（2011）
5. Xu Cao：Targeting osteoclast-osteoblast communication
Nat Med. 17, 1344-46（2011）
6. Serge Ferrari：Bone Modeling, Remodeling, and Repair
IBMS BoneKEy. 8（10）, 428-432（2011）doi：10.1138/20110534（Epub）
7. David Killock：Osteocyte RANKL in bone homeostasis：a paradigm shift?
Nat Rev Rheumatol. 7, 619（2011）
8. Carol Wilson：Osteocytes, Rankl and bone loss
Nat Rev Endocrinol. 7, 693（2011）
9. 時事通信 2011.9.12;
骨を維持する司令塔＝内部細胞の機能確認-治療応用期待・東京医科歯科大など
10. 日本産業新聞2011. 9. 13;マウスで分離成功
11. 朝日新聞　2011.9.13　骨新生の「司令塔」を特定
12. 日経産業新聞　2011.9.13
東京医科歯科大マウスで分離成功
13. 日本歯科新聞　2011.9.20
骨リモデリング　“指令細胞”を発見
～東医歯大の高柳教授ら　骨疾患研究に期待～
14. 科学新聞　2011.9.23　骨の作りかえ『骨細胞』が指令
15. 日本経済新聞、（2011年10月24日）
16. 化学工業日報　（2011年10月24日）
17. 日経バイオテクONLINE（2011年10月24日
18. 産経新聞、（2011年11月4日）
19. 共同通信電子版ニュース
20. Nature Japan 特集記事：
骨に埋め込まれた骨細胞を単離。骨による全身の生体系制御システムの解明を目指す
http：//www.natureasia.com/japan/jobs/tokushu/detail.php?id=1015
BoneKEy：URL; http：//osteoimmunology.com/gazo/bonekey_ntbm_nov2011.tiff
21. 科学技術振興機構HP：
http：//www.jst.go.jp/pr/announce/2 0 1 1 1 0 2 4/index.html
22. ERATOブログ：
http：//mirai2wkwk.jugem.jp/?eid=109http：//mirai2wkwk.jugem.jp/?eid=109http：//mirai2wkwk.jugem.jp/?eid=109http：//mirai2wkwk.jugem.jp/?eid=109

17）教室、分野や講座の准教授、講師、助教、特別研究員、ポスドク、指導を受けた大学院生の名前

准教授	本郷　敏雄
特任准教授	大洞　将嗣
助教	篠原　正浩
	中島　友紀
	岡本　一男
	春宮　　覚
客員助教	古賀　貴子

特別研究員　　末松　綾子
Matteo Guerrini
寺島　明日香
Lynette Danks
ポスドク　　林　　幹人
永井　祐輔
住谷　恵里子
指導を受けた大学院生
○Erik Idrus、
○武智　香織、
○Abdul Alim Al-Bari、
○小野　岳人

○はAISS

18）GCOE活動についての感想、コメント、改善を望む点

シャペロン教官以外にも、ポスドク研究者の配置を増員できることが望ましい。病理組織作成と解析、ノックアウトマウス作成、トランスクリプトーム・プロテオーム解析、セルソーティング等にあたって、専門の技術補佐員の増員、あるいは共同研究施設と専属の技術員による管理・支援があると有益である。

ARTICLES

nature medicine

Suppression of bone formation by osteoclastic expression of semaphorin 4D

Takako Negishi-Koga[1–3], Masahiro Shinohara[1,3], Noriko Komatsu[1,3], Haruhiko Bito[4], Tatsuhiko Kodama[5], Roland H Friedel[6] & Hiroshi Takayanagi[1–3,7]

Most of the currently available drugs for osteoporosis inhibit osteoclastic bone resorption; only a few drugs promote osteoblastic bone formation. It is thus becoming increasingly necessary to identify the factors that regulate bone formation. We found that osteoclasts express semaphorin 4D (Sema4D), previously shown to be an axon guidance molecule, which potently inhibits bone formation. The binding of Sema4D to its receptor Plexin-B1 on osteoblasts resulted in the activation of the small GTPase RhoA, which inhibits bone formation by suppressing insulin-like growth factor-1 (IGF-1) signaling and by modulating osteoblast motility. *Sema4d*$^{-/-}$ mice, *Plxnb1*$^{-/-}$ mice and mice expressing a dominant-negative RhoA specifically in osteoblasts showed an osteosclerotic phenotype due to augmented bone formation. Notably, Sema4D-specific antibody treatment markedly prevented bone loss in a model of postmenopausal osteoporosis. Thus, Sema4D has emerged as a new therapeutic target for the discovery and development of bone-increasing drugs.

© 2011 Nature America, Inc. All rights reserved.

Bone is continuously renewed by a process called bone remodeling, in which the resorption phase is followed by the reformation phase[1–4]. Each of these phases and also the transition between them requires a fine regulation by humoral factors or molecules mediating the communication among bone cells. Typically these factors are either secreted by the bone cells, expressed on the membrane of the bone cells or released from the bone matrix[1,2,5–7]. For example, transforming growth factor-β (TGF-β) and IGF released during bone resorption are known to stimulate bone formation[2,5], thus being called 'classical' coupling factors. Despite a wealth of *in vitro* data on other candidate molecules that are crucial for osteoclast-osteoblast communication[6], *in vivo* evidence has been lacking.

Axon-guidance molecules are widely expressed outside the nervous system, where they control cell migration, the immune response, tissue development and angiogenesis[8–13]. Recent studies have suggested that axon-guidance molecules, such as the semaphorins and ephrins, are involved in the cell-cell communication that occurs between osteoclasts and osteoblasts[14–18]. Here we provide genetic evidence for the role of Sema4D derived from osteoclasts in the regulation of bone formation through its receptor Plexin-B1, which is expressed by osteoblasts.

RESULTS

Osteoclast-derived Sema4D inhibits bone formation

To gain insight into the involvement of axon guidance molecules in bone remodeling, we performed a comprehensive expression analysis of the semaphorin, ephrin, netrin and slit gene families in osteoclasts and osteoblasts in mice. We observed high expression of *Sema4d* in osteoclasts, but not in osteoblasts (**Fig. 1a** and **Supplementary Fig. 1a**). *Sema4d* expression increased during receptor activator of nuclear factor-κB ligand (RANKL)-induced osteoclastogenesis. The Sema4D induction was markedly reduced in nuclear factor of activated T cells c1–knockout cells (**Supplementary Fig. 1b**).

The elevated expression of Sema4D in the osteoclast lineage led us to analyze its function in the skeletal system using *Sema4d*$^{-/-}$ mice. Bone volume and trabecular thickness were significantly greater in *Sema4d*$^{-/-}$ mice as compared to wild-type mice (**Fig. 1b**). The three-point bending test showed that bone strength was greater in the *Sema4d*$^{-/-}$ mice (**Fig. 1b**). Bone morphometric analyses revealed that both the osteoblast surface and bone formation rate markedly increased (**Fig. 1c**, **Supplementary Fig. 1c** and **Supplementary Table 1**), whereas the parameters for osteoclastic bone resorption were normal in the *Sema4d*$^{-/-}$ mice (**Fig. 1d**), suggesting an osteosclerotic phenotype. *In vitro* osteoclastogenesis in *Sema4d*$^{-/-}$ cells was also normal (**Supplementary Fig. 1d**,**e**). These results suggest that the high-bone-mass phenotype in the *Sema4d*$^{-/-}$ mice was caused by an increase in bone formation activity by osteoblasts, even though Sema4D is expressed exclusively by osteoclasts.

We performed an adoptive transfer of bone marrow cells including osteoclast precursor cells. Wild-type mice engrafted with Sema4D-deficient bone marrow cells had a high bone mass, whereas *Sema4d*$^{-/-}$ mice engrafted with wild-type bone marrow cells had a normal bone

[1]Department of Cell Signaling, Graduate School of Medical and Dental Sciences, Tokyo Medical and Dental University, Tokyo, Japan. [2]Japan Science and Technology Agency, Exploratory Research for Advanced Technology, Takayanagi Osteonetwork Project, Tokyo, Japan. [3]Global Center of Excellence Program, International Research Center for Molecular Science in Tooth and Bone Diseases, Tokyo, Japan. [4]Department of Neurochemistry, Graduate School of Medicine, The University of Tokyo, Tokyo, Japan. [5]Laboratory for Systems Biology and Medicine, Research Center for Advanced Science and Technology, The University of Tokyo, Tokyo, Japan. [6]Department of Neurosurgery, Mount Sinai School of Medicine, New York, New York, USA. [7]Centre for Orthopaedic Research, School of Surgery, The University of Western Australia, Perth, Western Australia, Australia. Correspondence should be addressed to H.T. (taka.csi@tmd.ac.jp).

Received 24 June; accepted 22 August; published online 23 October 2011; doi:10.1038/nm.2489

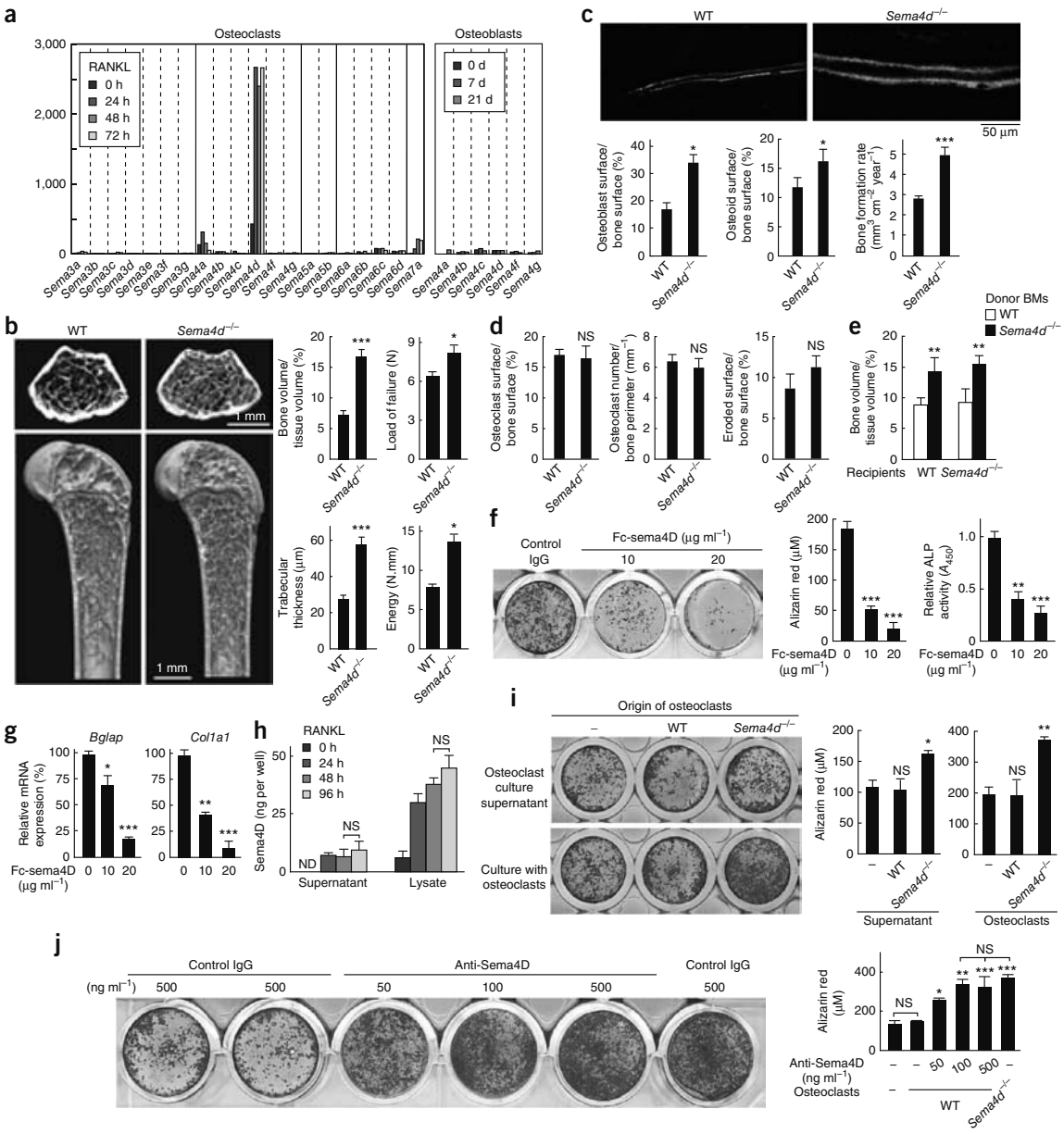

Figure 1 Inhibition of bone formation by osteoclast-derived Sema4D. (**a**) Genome-wide screening of mRNA for the semaphorin family proteins during differentiation of osteoclasts and osteoblasts. (**b**) Microcomputed tomography (μCT) of the proximal femur of the wild-type (WT) and *Sema4d*$^{-/-}$ mice (top left, axial view of the metaphyseal region; bottom left, longitudinal view). Bone volume and trabecular thickness were determined by μCT analysis (middle). Maximum load to failure and energy resorption were determined by the three-point bending test (right). (**c**) Bone formation, as observed by calcein double labeling at an interval of 4 d (top) and the parameters for osteoblastic bone formation, as determined by bone morphometric analysis (bottom). (**d**) The parameters for osteoclastic bone resorption, as determined by bone morphometric analysis. (**e**) Bone volume after adoptive transfer of wild-type or *Sema4d*$^{-/-}$ bone marrow cells (BMs) to wild-type (left) and *Sema4d*$^{-/-}$ (right) mice. (**f**) Effect of Fc-sema4D on bone nodule formation. Left, Alizarin red staining; middle, amount of alizarin red; right, effect of Fc-sema4D on ALP activity. (**g**) Effect of Fc-sema4D on the mRNA expression of *Bglap* and *Col1a1*. (**h**) The amount of Sema4D in the osteoclast supernatant and the cell lysate during osteoclast differentiation. The amount of Sema4D was analyzed using bone-resorbing osteoclasts 96 h after RANKL stimulation. (**i**) Effect of osteoclast culture supernatant or coculture with osteoclasts on bone nodule formation. Left, Alizarin red staining; right, amount of the alizarin red. (**j**) Effect of antibody to Sema4D (anti-Sema4D) on bone formation in wild-type osteoblasts cocultured with wild-type or *Sema4d*$^{-/-}$ osteoclasts. Left, Alizarin red staining; right, amount of alizarin red. $^{*}P < 0.05$; $^{**}P < 0.01$; $^{***}P < 0.005$; NS, not significant; ND, not detected. Error bars show s.e.m.

© 2011 Nature America, Inc. All rights reserved.

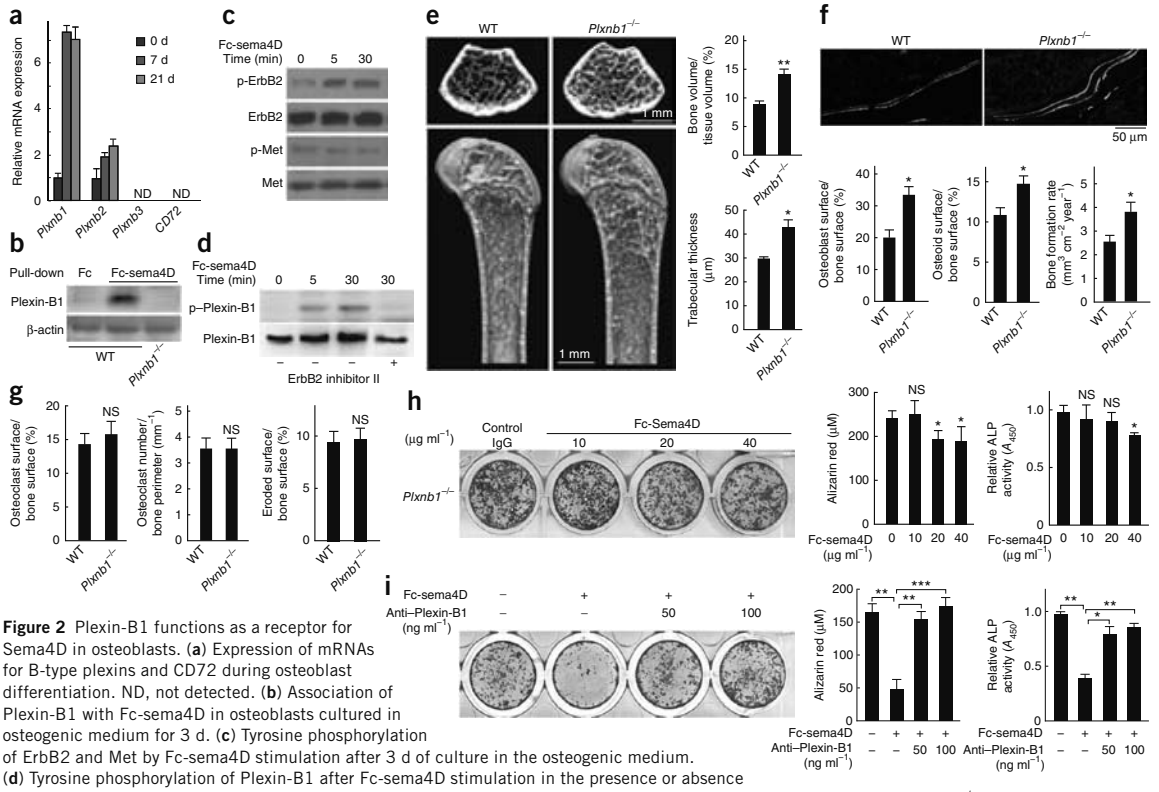

Figure 2 Plexin-B1 functions as a receptor for Sema4D in osteoblasts. (**a**) Expression of mRNAs for B-type plexins and CD72 during osteoblast differentiation. ND, not detected. (**b**) Association of Plexin-B1 with Fc-sema4D in osteoblasts cultured in osteogenic medium for 3 d. (**c**) Tyrosine phosphorylation of ErbB2 and Met by Fc-sema4D stimulation after 3 d of culture in the osteogenic medium. (**d**) Tyrosine phosphorylation of Plexin-B1 after Fc-sema4D stimulation in the presence or absence of 30 μM of an ErbB2 inhibitor (ErbB2 inhibitor II). (**e**) Microcomputed tomography of the femur of wild-type (WT) and *Plxnb1*$^{-/-}$ mice (see **Fig. 1b** legend for the details). (**f**) Bone formation, as observed by calcein double labeling and the parameters for osteoblastic bone formation determined. (**g**) The parameters for osteoclastic bone resorption were determined by bone morphometric analysis. (**h**) Effect of Fc-sema4D on bone formation in *Plxnb1*$^{-/-}$ osteoblasts. Left, bone nodule formation; middle, amount of alizarin red; right, ALP activity. (**i**) Effects of the antibody to Plexin-B1 (anti–Plexin-B1) on bone formation in Fc-sema4D–treated osteoblasts. Left, bone nodule formation; middle, the amount of alizarin red; right, ALP activity. $^{*}P < 0.05$; $^{**}P < 0.01$; $^{***}P < 0.005$; NS, not significant; ND, not detected. Error bars show s.e.m.

© 2011 Nature America, Inc. All rights reserved.

mass (**Fig. 1e**), showing that the bone phenotype in the *Sema4d*$^{-/-}$ mice resulted from a defect in hematopoietic lineage cells including osteoclasts. Consistent with this, there was no obvious increase in the bone nodule formation of *Sema4d*$^{-/-}$ calvarial cells in the absence of osteoclasts (**Supplementary Fig. 1f–h**). These results suggest that the Sema4D expressed by osteoclasts inhibits osteoblastic bone formation and is a mediator of osteoclast-osteoblast communication.

To observe the inhibitory effect of Sema4D on osteoblasts, we added soluble Sema4D fused with the IgG1 Fc region (Fc-sema4D)[19] to the calvarial cells cultured under osteogenic conditions. Addition of Fc-sema4D suppressed bone nodule formation, alkaline phosphatase (ALP) activity and the expression of osteoblastic marker genes such as osteocalcin (*Bglap*) and type I collagen (*Col1a1*) in a dose-dependent manner (**Fig. 1f,g**). There was no difference in the number of mesenchymal stem cells and osteoblast precursor cells in bone marrow between wild-type and *Sema4d*$^{-/-}$ mice (**Supplementary Fig. 2**).

Although Sema4D is a transmembrane protein, it is proteolytically cleaved into a soluble form upon cellular activation[9,20]. We did detect soluble Sema4D in the osteoclast culture supernatant, but only a small portion was released as a soluble form, regardless of the osteoclast maturation stage (**Fig. 1h**), suggesting that membrane-bound Sema4D has a larger role in suppression of bone formation. To examine the contribution of osteoclast-derived Sema4D to the regulation of bone formation, we cultured calvarial cells in the presence of osteoclast culture supernatant or cultured osteoclasts. The addition of culture supernatant of the wild-type osteoclasts to calvarial cells or coculturing calvarial cells with wild-type osteoclasts did not influence bone nodule formation, ALP activity or the expression of osteoblastic marker genes; in contrast, these processes were markedly enhanced by either the culture supernatant of the *Sema4d*$^{-/-}$ osteoclasts or the coculture with the *Sema4d*$^{-/-}$ osteoclasts (**Fig. 1i** and **Supplementary Fig. 3a–d**). Consistent with this, bone formation in the presence of wild-type osteoclasts was increased by Sema4D-specific antibody in a dose-dependent manner (**Fig. 1j** and **Supplementary Fig. 3e–g**). We concluded that osteoclasts generate factors promoting bone formation[1,5], which is obvious only in the absence of Sema4D, but osteoclast-derived Sema4D has a dominant effect that antagonizes this bone-forming activity. Collectively, the evidence shows that osteoclasts suppress bone formation through the expression of Sema4D.

Plexin-B1 recognizes Sema4D and inhibits bone formation

To identify the Sema4D receptors expressed by osteoblasts, we analyzed the mRNA expression of B-type plexins and CD72, which are known to be Sema4D receptors preferentially expressed in nonlymphoid and lymphoid cells, respectively[9,21]. Plexin-B1 expression was markedly induced

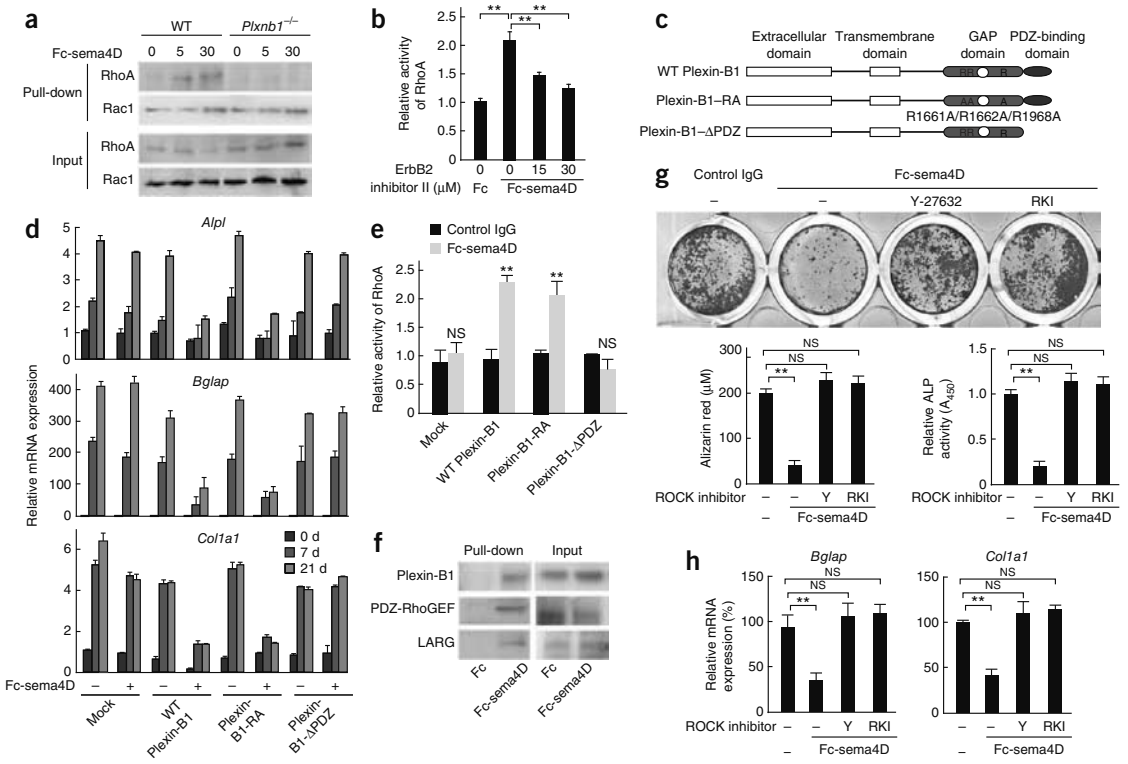

Figure 3 Inhibition of bone formation by the Sema4D–Plexin-B1–RhoA axis. (**a**) Amount of the GTP-bound form and total level of RhoA and Rac1 in wild-type (WT) and *Plxnb1*$^{-/-}$ osteoblasts cultured in osteogenic medium for 3 d. A pull-down assay was performed with GST-RBD (for RhoA) and GST-PAK1 (for Rac1) coupled to glutathione-Sepharose, followed by immunoblotting with antibody to RhoA (anti-RhoA) and antibody to Rac-1 (anti-Rac1), respectively. (**b**) Effect of the ErbB2 inhibitor on Fc-sema4D-induced RhoA activation in calvarial osteoblasts. (**c**) Schematic of wild-type Plexin-B1, a Plexin-B1-RA mutant harboring a mutation in the GAP domain (R1661A/R1662A/R1968A) and a truncated mutant of Plexin-B1 lacking the PDZ-binding domain (ΔPDZ). (**d**,**e**) Effect of retroviral expression of wild-type Plexin-B1 and the Plexin-B1 mutants in Fc-sema4D–treated *Plxnb1*$^{-/-}$ osteoblasts. The mRNA expression of *Alpl*, *Bglap* and *Col1a1* (**d**) and RhoA activation (**e**) were examined. (**f**) Association of Rho-specific GEFs, PDZ-RhoGEF and LARG with Plexin-B1 in osteoblasts. (**g**) Effect of the ROCK inhibitors Y-27632 and RKI on bone nodule formation in Fc-sema4D–treated osteoblasts. Top, Alizarin red staining; bottom left, amount of alizarin red; bottom right, ALP activity. (**h**) Effect of the ROCK inhibitors Y-27632 and RKI on mRNA expression of *Bglap* and *Col1a1*. $^{**}P < 0.01$; NS, not significant. Error bars show s.e.m.

© 2011 Nature America, Inc. All rights reserved.

during osteoblast differentiation (**Fig. 2a**), but not during osteoclast differentiation (data not shown). The induction of Plexin-B1 in osteoblasts was much higher than that of Plexin-B2, and Plexin-B3 and CD72 were almost undetectable (**Fig. 2a**). A pull-down experiment using Fc-sema4D indicated that Sema4D physically interacted with Plexin-B1 (**Fig. 2b**). Plexin-B1 forms a receptor complex with either erythroblastic leukemia viral oncogene homolog 2 (ErbB2) or hepatocyte growth factor receptor (Met), depending on the cell type[22]. Binding of Sema4D to Plexin-B1 results in the phosphorylation of the kinase (ErbB2 or Met) and Plexin-B1 (ref. 23). In osteoblasts, expression of ErbB2 was higher than that of Met (**Supplementary Fig. 4a**), and Sema4D stimulation induced the phosphorylation of ErbB2, but not Met (**Fig. 2c**). Sema4D induced the phosphorylation of Plexin-B1, and this phosphorylation was substantially lowered in the presence of the ErbB2 inhibitor (**Fig. 2d**), suggesting that Plexin-B1 functions as a receptor for Sema4D and ErbB2 serves as an associating kinase in osteoblasts.

Similar to *Sema4d*$^{-/-}$ mice, *Plxnb1*$^{-/-}$ mice had a high bone mass due to an increase in osteoblastic bone formation, and there was no obvious abnormality in osteoclastic bone resorption (**Fig. 2e–g** and **Supplementary Fig. 4b**,**c**). Fc-sema4D at 10 μg ml^{-1} did not inhibit bone formation in *Plxnb1*$^{-/-}$ osteoblasts but did cause strong inhibition in wild-type osteoblasts (**Fig. 2h** and **Supplementary Fig. 4d**), and the Plexin-B1–specific antibody effectively suppressed the inhibitory effect of Fc-sema4D on bone formation in wild-type cells (**Fig. 2i** and **Supplementary Fig. 4e**). In addition, similar to the *Sema4d*$^{-/-}$ osteoclasts, wild-type osteoclasts promoted bone formation in the *Plxnb1*$^{-/-}$ osteoblasts (**Supplementary Fig. 4f–h**). These results indicate that Plexin-B1 is mainly responsible for the osteoblast recognition of Sema4D. *Plxnb1*$^{-/-}$; *Sema4d*$^{-/-}$ mice, however, had a higher bone mass than did *Plxnb1*$^{-/-}$ mice (**Supplementary Fig. 5**), and a high concentration of Fc-sema4D slightly inhibited bone formation in *Plxnb1*$^{-/-}$ cells (**Fig. 2h** and **Supplementary Fig. 4d**), suggesting that the effect of Sema4D is partly mediated by other receptors, such as Plexin-B2.

RhoA mediates Sema4D-Plexin-B1 signaling in osteoblasts

The semaphorin-plexin system regulates cell morphology and migration by modulation of actin cytoskeletal rearrangement, primarily via Rho family small GTPases[23]. The amount of GTP-bound, activated form

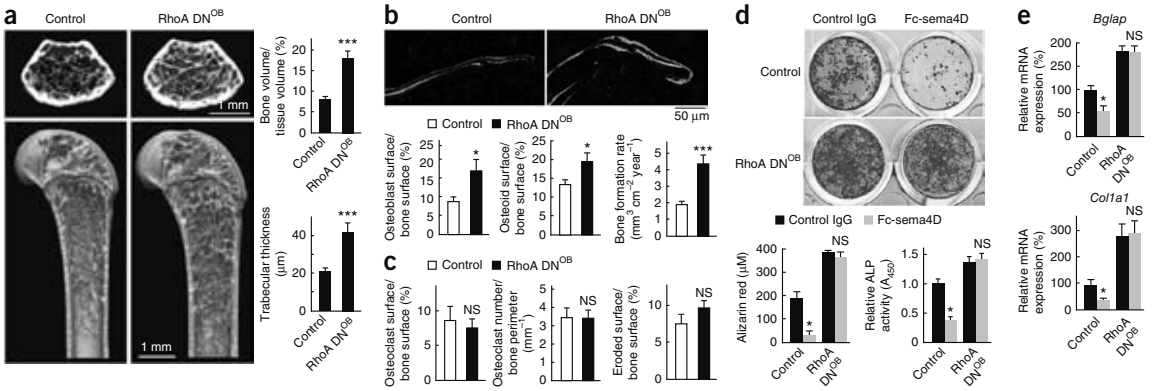

Figure 4 Osteoblas-spec st-specific loss of function of Rho GTPase leads to an osteosclerotic phenotype. (**a**) Microcomputed tomography of the femur in control and RhoA DN^{OB} mice (see **Fig. 1b** legend for the details). (**b**) Bone formation, as observed by calcein double labeling and the parameters for osteoblastic bone formation determined. (**c**) Parameters for osteoblastic bone formation and osteoclastic bone resorption, as determined by bone morphometric analysis. (**d**) Effect of Fc-sema4D on bone formation in calvarial cells derived from RhoA DN^{OB} mice. Top, alizarin red staining; bottom left, amount of alizarin red; bottom right, ALP activity. (**e**) Effect of Fc-sema4D on the mRNA expression of *Bglap* and *Col1a1*. $^{*}P < 0.05$; $^{***}P < 0.005$; NS, not significant. Error bars show s.e.m.

of RhoA in Sema4D-treated osteoblasts was notably lower in *Plxnb1*$^{-/-}$ cells as compared to wild type cells, whereas the level of GTP-bound Rac1 was not affected after Fc-sema4D stimulation (**Fig. 3a**). In addition, Sema4D-induced RhoA activation was reduced in the presence of an ErbB2 inhibitor (**Fig. 3b**). Adenoviral introduction of constitutively active RhoA (RhoA-V14) suppressed bone nodule formation in calvarial cells, whereas dominant-negative RhoA (RhoA-N19) promoted it (**Supplementary Fig. 6a–c**), suggesting that RhoA selectively mediates the inhibitory effect of Sema4D–Plexin-B1 on bone formation.

Plexin-B1 has two small GTPase regulatory domains, a GTPase-activating protein (GAP) domain and a PDZ-binding domain that binds Rho guanine nucleotide exchange factor (GEF)[24–27]. We generated two Plexin-B1 mutants: Plexin-B1-ΔPDZ, which is unable to activate RhoA[27], and Plexin-B1-RA, which does not elicit the GTPase activity of R-Ras[24] (**Fig. 3c**). We stimulated *Plxnb1*$^{-/-}$ calvarial cells overexpressing these mutants with Fc-sema4D and examined the effect on osteoblast differentiation. The inhibitory effect of Fc-sema4D on the mRNA expression of *Alpl* (encoding ALP), *Bglap*

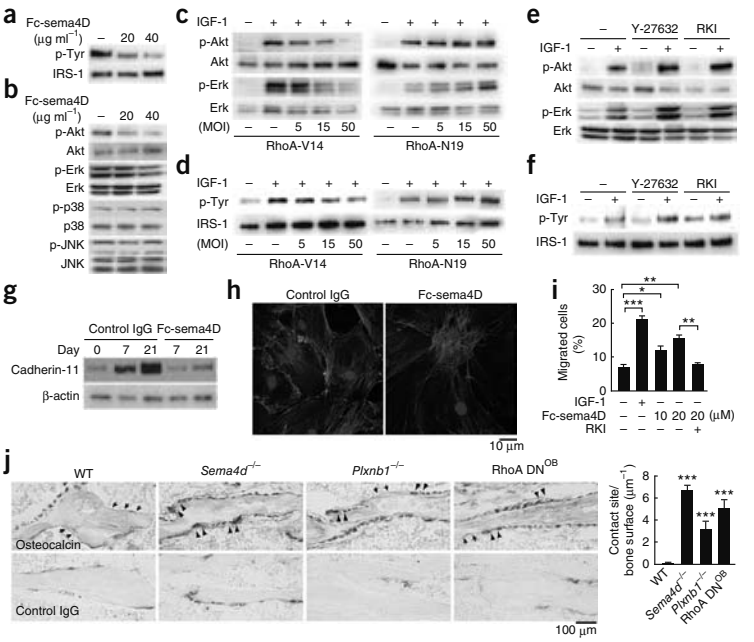

Figure 5 The mechanism of Sema4D–Plexin-B1–RhoA-mediated regulation of bone formation. (**a**) Effect of Fc-sema4D on the phosphorylation of IRS-1 during osteoblast differentiation. (**b**) Effect of Fc-sema4D on the phosphorylation of Akt, Erk, p38 and JNK during osteoblast differentiation. (**c**) Effect of constitutively active RhoA (RhoA-V14) or dominant-negative RhoA (RhoA-N19) on IGF-1–induced phosphorylation of Akt and Erk. MOI, multiplicity of infection. (**d**) Effect of RhoA-V14 or RhoA-N19 on IGF-1–induced phosphorylation of IRS-1. (**e**) Effect of the ROCK inhibitors Y-27632 and RKI on IGF-1–induced phosphorylation of Akt and Erk. (**f**) Effect of ROCK inhibitors on IGF-1–induced phosphorylation of IRS-1. (**g**) Effect of Fc-sema4D on the expression of cadherin-11 during osteoblast differentiation. (**h**) Immunofluorescence staining of cadherin-11 in osteoblasts. (**i**) Migration of osteoblasts in the presence of Fc-sema4D and the effect of RKI on Sema4D-induced cell motility. IGF-1 (100 ng ml^{-1}) was used as a positive control. (**j**) The spatial distribution of osteoblasts and osteoclasts on the bone surface of wild-type (WT), *Sema4d*$^{-/-}$, *Plxnb1*$^{-/-}$ and RhoA DN^{OB} mice. Osteoblasts and osteoclasts were detected as osteocalcin-positive (brown) and TRAP-positive cells (magenta), respectively. The osteoblast surface lies a certain distance from the osteoclast surface; arrows indicate the intervening quiescent surfaces. The number of sites in which osteoblasts are located within a 50-nm distance of osteoclasts (indicated by the arrowheads) were counted. $^{*}P < 0.05$, $^{**}P < 0.01$, $^{***}P < 0.005$. Error bars show s.e.m.

© 2011 Nature America, Inc. All rights reserved.

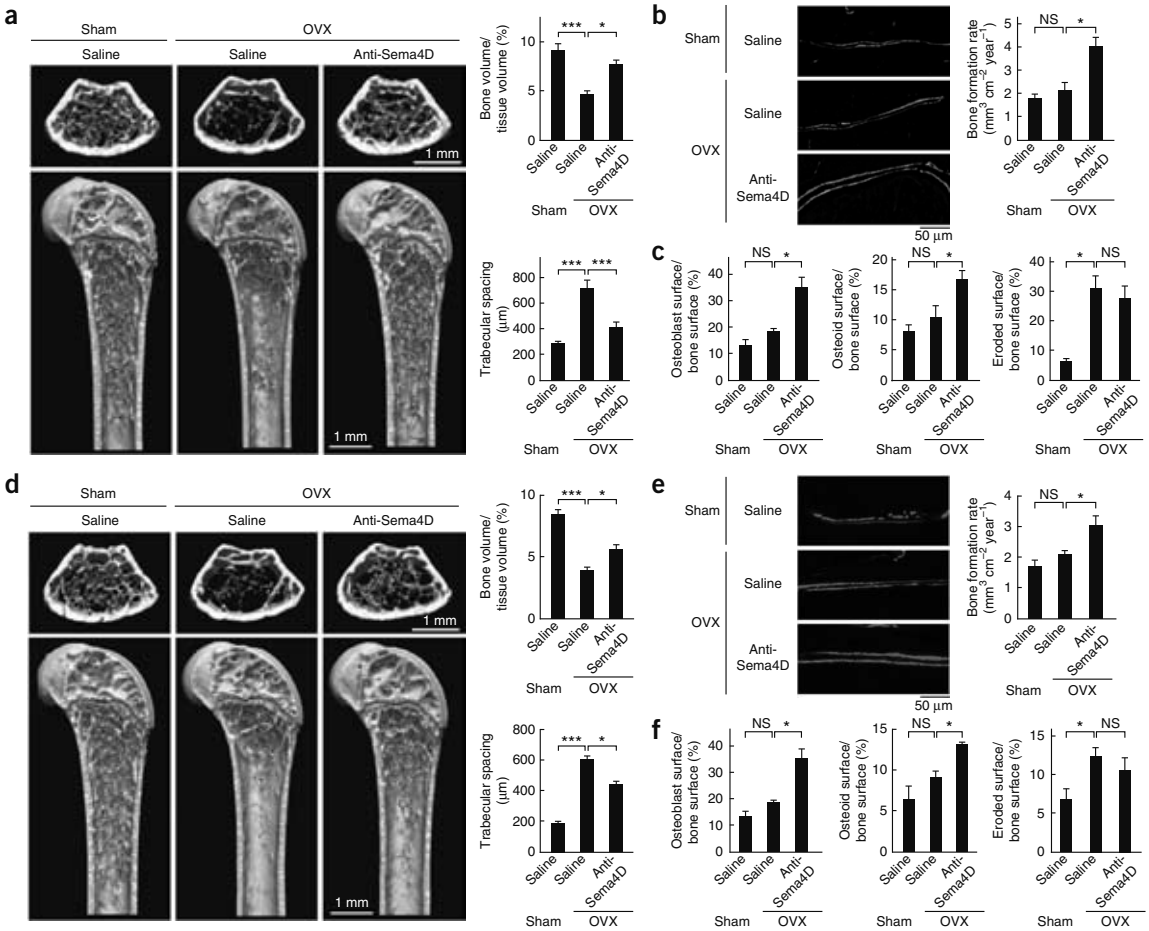

Figure 6 The bone-increasing effect of Sema4D–Plexin-B1 blockade. (**a**–**c**) The prophylactic effect of anti-Sema4D on ovariectomy (OVX)-induced bone loss. OVX mice were injected weekly with anti-Sema4D or saline from day 3 to week 8 after surgery. (**d**–**f**) The therapeutic effect of anti-Sema4D on OVX-induced bone loss. After 6 weeks of surgery, OVX mice were injected with anti-Sema4D or saline every 3 d for 3 weeks. In **a** and **d**, microcomputed tomography of the femur of the sham-operated (Sham), OVX and anti-Sema4D–treated OVX mice is shown (left; see **Fig. 1b** legend for the details). Bone volume and trabecular spacing were determined by microcomputed tomography analysis (right). In **b** and **e**, bone formation is shown by calcein double labeling and the bone formation rate. In **c** and **f**, the parameters for osteoblastic bone formation and osteoclastic bone resorption were determined by morphometric analysis using the tibia of mice. $^{*}P < 0.05$; $^{***}P < 0.005$; NS, not significant. Error bars show s.e.m.

© 2011 Nature America, Inc. All rights reserved.

and *Col1a1* in *Plxnb1*$^{-/-}$ cells was recovered by the overexpression of Plexin-B1-RA as well as wild-type Plexin-B1, but not by Plexin-B1-ΔPDZ (**Fig. 3d**), concomitantly with the restoration of RhoA activity (**Fig. 3e**). Plexin-B1 is known to bind two RhoGEFs, PDZ-RhoGEF (Arhgef11) and LARG (Arhgef12), through the PDZ-binding domain[25–27]. Osteoblasts expressed these RhoGEFs (**Supplementary Fig. 6d**), which interacted with Plexin-B1 (**Fig. 3f**), suggesting that these RhoGEFs are involved in the RhoA activation by Sema4D. RhoA activates various downstream effector molecules, including Rho-associated protein kinase (ROCK), whose inhibition, in turn, suppressed the inhibitory effect of Fc-sema4D on bone formation (**Fig. 3g**,**h**). These results suggest that the RhoA-ROCK pathway mediates the inhibition of bone formation by Sema4D.

We generated mice expressing dominant-negative RhoA specifically in osteoblasts (RhoA DN^{OB} mice) by crossing CAT-RhoA DN transgenic mice[28] with α1(I)-Cre transgenic mice[29]. RhoA DN^{OB} mice had a high bone mass due to enhanced osteoblastic bone formation, which recapitulates the bone phenotype of the *Sema4d*$^{-/-}$ and *Plxnb1*$^{-/-}$ mice (**Fig. 4a–c** and **Supplementary Fig. 6e**,**f**). Fc-sema4D did not inhibit bone formation in calvarial cells derived from RhoA DN^{OB} mice (**Fig. 4d**,**e**), indicating that RhoA regulates bone formation *in vivo* and may be a crucial mediator of bone mass modulation by Sema4D–Plexin-B1 signaling.

Sema4D controls osteoblast differentiation and migration via RhoA

What are the mechanisms by which Sema4D inhibits bone formation in osteoblasts? The RhoA-ROCK pathway mediates the phosphorylation of IRS-1, which is involved in IGF-1 signaling during embryogenesis[30]. In calvarial cells, Sema4D stimulation reduced the tyrosine phosphorylation of IRS-1 at the tyrosine residue required

for Akt and mitogen-activated protein kinase activation (**Fig. 5a**). Fc-sema4D reduced phosphorylation of Akt and extracellular signal-regulated kinase (Erk) in a dose-dependent manner, but not of p38 or JNK (**Fig. 5b**). The adenoviral introduction of RhoA-V14 reduced the IGF-1-induced phosphorylation of Akt and Erk, whereas either overexpression of RhoA-N19 or ROCK inhibitors markedly increased the phosphorylation of Akt and Erk as well as the tyrosine residue of IRS-1 (**Fig. 5c–f**). These results indicate that Sema4D-induced RhoA activation suppresses osteoblast differentiation at least in part through an attenuation of IGF-1 signaling.

Binding of Sema4D to the Plexin-B1–ErbB2 receptor complex is known to stimulate cell motility through RhoA activation[22]. In osteoblastic cells, Sema4D stimulation decreased the expression of cadherin-11 at the cell-cell contact region (**Fig. 5g,h**), suggesting that Sema4D stimulates cell motility through an impairment of cell-cell adhesion, which in turn results in the reduction in bone-forming activity. To test this hypothesis, we examined the effect of Sema4D on osteoblast motility. A Boyden chamber assay showed that Fc-sema4D induced an acceleration of spontaneous migration of osteoblasts, which was inhibited by a ROCK inhibitor (**Fig. 5i**), suggesting that Sema4D-induced RhoA activation promotes osteoblast motility.

In bone tissue, the osteoblast surface lies at certain distance from the osteoclast surface, and there is usually an intervening quiescent surface in between (**Fig. 5j**). It remains unclear how the quiescent surface is maintained, but it is possible that osteoclasts produce a molecule(s) that stimulates osteoblast motility and guides the osteoblasts to a proper site. In *Sema4d*$^{-/-}$ mice, as well as *Plxnb1*$^{-/-}$ and RhoA DN^{OB} mice, there were few quiescent surfaces, and we observed a cluster of osteoblasts in close proximity to bone-resorbing osteoclasts (**Fig. 5j**). Thus, osteoclast-derived Sema4D is required for the proper localization of osteoblasts and the maintenance of a quiescent surface.

Together, these data suggest that osteoclasts are involved in the spatial regulation of bone remodeling through Sema4D, which inhibits osteoblast differentiation in the proximity of osteoclasts and repels osteoblasts by increasing their motility.

Therapeutic effect of an antibody to Sema4D on bone loss

To test whether inhibition of Sema4D would be a useful approach to the treatment of osteoporosis, we examined the effect of a Sema4D-specific antibody on bone loss in an ovariectomized mouse model of postmenopausal osteoporosis. Ovariectomized 7-week-old mice were treated prophylactically with a weekly intravenous injection of the antibody starting 3 d after ovariectomy and continuing for 8 weeks, or osteopenic mice (6 weeks after ovariectomy) were therapeutically injected with the antibody once every 3 d for 3 weeks. Injection of the Sema4D-specific antibody was protective against bone loss after ovariectomy by promoting osteoblastic bone formation without affecting osteoclastic bone resorption in both prophylactic and therapeutic treatments (**Fig. 6** and **Supplementary Fig. 7**). Sema4D-specific antibody effectively increased bone formation in human osteoblastic cells in coculture with human osteoclasts or osteoclast supernatant (**Supplementary Fig. 8**). Along with the effect of Plexin-B1–specific antibody (**Fig. 2i** and **Supplementary Fig. 4e**), these results suggest that the blocking Sema4D–Plexin-B1interaction is a new and potentially effective strategy for increasing bone formation in humans.

DISCUSSION

The semaphorins have been implicated in repulsive axon guidance events in the developing nervous system. However, they are also widely expressed outside the nervous system and mediate diverse biological processes including organogenesis, vascularization, the immune response and tumor progression[31–35]. The semaphorins have also been suggested to be involved in the regulation of bone remodeling[15,16,18,36], although this function has not been clearly demonstrated *in vivo* in loss-of-function genetic models.

Sema4D, also known as CD100, was first identified in immune cells and has been extensively investigated in the immune system. Sema4D, constitutively expressed in T cells, regulates the activation of B cells[19] and dendritic cells[37] and inhibits monocyte migration[38]. In contrast to Sema3 family members, the function of Sema4D as an axon guidance cue has been less well understood, but a recent study provided genetic evidence that Sema4D positively regulates the migration of neurons during cortical development[39].

Bone remodeling is a cycle consisting of three phases: the initiation of bone resorption by osteoclasts; the transition into new bone formation by osteoblasts; and the synthesis of new bone and then termination[6]. In the initial phase, osteoblastic bone formation in the immediate vicinity of bone-resorbing osteoclasts or osteoblast recruitment to the bone resorption site needs to be suppressed until osteoclastic bone resorption is accomplished. The Sema4D expressed by osteoclasts may function as an inhibitor of bone formation in this phase by suppressing osteoblast differentiation and modulating osteoblast motility. Classically, coupling factors released during bone resorption activate bone formation, but the concept can be extended to include osteoclast-osteoblast communicating factors. These factors do not necessarily link bone resorption to formation but may dissociate formation from resorption, thus being crucial for specific phases in bone remodeling. In this study, we showed that osteoclasts control osteoblast localization through Sema4D regulation of osteoblast differentiation and motility, suggesting that Sema4D acts as a guidance molecule for bone cell positioning, which is analogous to the function of semaphorins in axon guidance.

We showed that the binding of Sema4D to Plexin-B1 results in the activation and autophosphorylation of ErbB2, which phosphorylates Plexin-B1. RhoA is subsequently activated by RhoGEFs including PDZ-RhoGEF and LARG, which associate with Plexin-B1. RhoA-ROCK inhibits the phosphorylation of IRS-1, which is the crucial step in IGF-1 signaling favoring osteoblast differentiation. Thus, we concluded that Sema4D inhibits osteoblast differentiation by RhoA activation.

Although the detailed mechanisms by which Sema4D regulates osteoblast motility remain obscure, we found that cadherin-11 expression was decreased by Sema4D stimulation. Cadherin-11 is a specific component of the osteoblast cell-cell adhesion machinery[40], and downregulation of cadherin-11 may be related to the higher osteoblast motility observed after Sema4D treatment. Consistent with this, mice lacking cadherin-11 show osteopenia, indicating that cadherin-11 is a positive regulator of bone formation[40]. Further study will be needed to understand the detailed function of cadherin-11 in Sema4D-mediated regulation of bone formation.

We confirmed that the Sema4D-specific antibody promotes bone formation in the coculture system of human osteoclasts and osteoblasts, suggesting that Sema4D is an auspicious therapeutic target in the treatment of human osteopenic disease (**Supplementary Fig. 8**). In the bone loss associated with inflammatory and neoplastic diseases, a decrease in bone formation is observed in addition to the enhanced osteoclastic bone resorption[41,42]. As Sema4D is expressed in T cells and certain types of cancer cells, Sema4D produced by these cell types may contribute to this reduction in bone formation. Intermittent parathyroid

© 2011 Nature America, Inc. All rights reserved.

hormone treatment is the only currently available strategy that has been demonstrated to increase bone formation. A Sost-specific antibody under development has attracted attention as a potential new bone-increasing agent among candidate strategies[43], and now the suppression of the Sema4D–Plexin-B1–RhoA signaling axis holds promise as a strategy for the design of new therapeutic approaches to bone and joint diseases, including osteoporosis, rheumatoid arthritis and bone tumors.

METHODS

Methods and any associated references are available in the online version of the paper at http://www.nature.com/naturemedicine/.

Note: Supplementary information is available on the Nature Medicine website.

ACKNOWLEDGMENTS

We are grateful to G. Karsenty (Columbia University), K. Kobayashi (Fukushima Medical University School of Medicine), A. Kumanogoh (Osaka University) and T. Kitamura (The University of Tokyo) for kindly providing α(1)I-Cre mice, CAT-RhoA DN mice, recombinant Fc-sema4D protein, and the retrovirus vectors and Plat-E cells, respectively. We also thank E. Sumiya, A. Suematsu, Y. Kunisawa, T. Ando, K. Okamoto, T. Nakashima, M. Oh-hora, M. Hayashi, A. Terashima, Y. Nagai and H. Negishi for discussion and assistance. This work was supported in part by a grant for the Exploratory Research for Advanced Technology, Takayanagi Osteonetwork Project from the Japan Science and Technology Agency, Grant-in-Aid for Young Scientist A, Grant-in-Aid for Challenging Exploratory Research and Grant-in-Aid for JSPS Fellows from the Japan Society for the Promotion of Science, a grant for the Global Center of Excellence Program from the Ministry of Education, Culture, Sports, Science and Technology of Japan, and grants from the Ichiro Kanehara Foundation, the Uehara Memorial Foundation and the Naito Foundation.

AUTHOR CONTRIBUTIONS

T.N.-K. performed most of the experiments, interpreted the results and prepared the manuscript. M.S. performed the molecular analysis of the regulation of bone formation by RhoA and contributed to the GTPase analysis and manuscript preparation. N.K. performed the FACS analysis. H.B. generated adenoviruses and contributed to data interpretation. T.K. conducted the GeneChip analysis. R.H.F. generated *Plxnb1*$^{-/-}$ mice and contributed to data interpretation. H.T. directed the project and wrote the manuscript.

COMPETING FINANCIAL INTERESTS

The authors declare no competing financial interests.

Published online at http://www.nature.com/naturemedicine/.
Reprints and permissions information is available online at http://www.nature.com/reprints/index.html.

© 2011 Nature America, Inc. All rights reserved.

1. Martin, T.J. & Sims, N.A. Osteoclast-derived activity in the coupling of bone formation to resorption. *Trends Mol. Med.* **11**, 76–81 (2005).
2. Hayden, J.M., Mohan, S. & Baylink, D.J. The insulin-like growth factor system and the coupling of formation to resorption. *Bone* **17**, 93S–98S (1995).
3. Hattner, R., Epker, B.N. & Frost, H.M. Suggested sequential mode of control of changes in cell behaviour in adult bone remodelling. *Nature* **206**, 489–490 (1965).
4. Takahashi, H., Epker, B. & Frost, H.M. Resorption precedes formative activity. *Surg. Forum* **15**, 437–438 (1964).
5. Tang, Y. *et al.* TGF-β1–induced migration of bone mesenchymal stem cells couples bone resorption with formation. *Nat. Med.* **15**, 757–765 (2009).
6. Matsuo, K. & Irie, N. Osteoclast-osteoblast communication. *Arch. Biochem. Biophys.* **473**, 201–209 (2008).
7. Parfitt, A.M., Mundy, G.R., Roodman, G.D., Hughes, D.E. & Boyce, B.F. A new model for the regulation of bone resorption, with particular reference to the effects of bisphosphonates. *J. Bone Miner. Res.* **11**, 150–159 (1996).
8. Larrivée, B., Freitas, C., Suchting, S., Brunet, I. & Eichmann, A. Guidance of vascular development: lessons from the nervous system. *Circ. Res.* **104**, 428–441 (2009).
9. Suzuki, K., Kumanogoh, A. & Kikutani, H. Semaphorins and their receptors in immune cell interactions. *Nat. Immunol.* **9**, 17–23 (2008).
10. Tran, T.S., Kolodkin, A.L. & Bharadwaj, R. Semaphorin regulation of cellular morphology. *Annu. Rev. Cell Dev. Biol.* **23**, 263–292 (2007).
11. Huber, A.B., Kolodkin, A.L., Ginty, D.D. & Cloutier, J.F. Signaling at the growth cone: ligand-receptor complexes and the control of axon growth and guidance. *Annu. Rev. Neurosci.* **26**, 509–563 (2003).
12. Dickson, B.J. Molecular mechanisms of axon guidance. *Science* **298**, 1959–1964 (2002).
13. Tamagnone, L. & Comoglio, P.M. Signalling by semaphorin receptors: cell guidance and beyond. *Trends Cell Biol.* **10**, 377–383 (2000).
14. Irie, N. *et al.* Bidirectional signaling through ephrinA2-EphA2 enhances osteoclastogenesis and suppresses osteoblastogenesis. *J. Biol. Chem.* **284**, 14637–14644 (2009).
15. Sutton, A.L. *et al.* Semaphorin 3B is a 1,25-dihydroxyvitamin D_3-induced gene in osteoblasts that promotes osteoclastogenesis and induces osteopenia in mice. *Mol. Endocrinol.* **22**, 1370–1381 (2008).
16. Takegahara, N. *et al.* Plexin-A1 and its interaction with DAP12 in immune responses and bone homeostasis. *Nat. Cell Biol.* **8**, 615–622 (2006).
17. Zhao, C. *et al.* Bidirectional ephrinB2-EphB4 signaling controls bone homeostasis. *Cell Metab.* **4**, 111–121 (2006).
18. Delorme, G., Saltel, F., Bonnelye, E., Jurdic, P. & Machuca-Gayet, I. Expression and function of semaphorin 7A in bone cells. *Biol. Cell* **97**, 589–597 (2005).
19. Kumanogoh, A. *et al.* Identification of CD72 as a lymphocyte receptor for the class IV semaphorin CD100: a novel mechanism for regulating B cell signaling. *Immunity* **13**, 621–631 (2000).
20. Elhabazi, A., Delaire, S., Bensussan, A., Boumsell, L. & Bismuth, G. Biological activity of soluble CD100. I. The extracellular region of CD100 is released from the surface of T lymphocytes by regulated proteolysis. *J. Immunol.* **166**, 4341–4347 (2001).
21. Tamagnone, L. *et al.* Plexins are a large family of receptors for transmembrane, secreted, and GPI-anchored semaphorins in vertebrates. *Cell* **99**, 71–80 (1999).
22. Swiercz, J.M., Worzfeld, T. & Offermanns, S. ErbB-2 and Met reciprocally regulate cellular signaling via plexin-B1. *J. Biol. Chem.* **283**, 1893–1901 (2008).
23. Kruger, R.P., Aurandt, J. & Guan, K.L. Semaphorins command cells to move. *Nat. Rev. Mol. Cell Biol.* **6**, 789–800 (2005).
24. Oinuma, I., Ishikawa, Y., Katoh, H. & Negishi, M. The Semaphorin 4D receptor Plexin-B1 is a GTPase activating protein for R-Ras. *Science* **305**, 862–865 (2004).
25. Driessens, M.H., Olivo, C., Nagata, K., Inagaki, M. & Collard, J.G. B plexins activate Rho through PDZ-RhoGEF. *FEBS Lett.* **529**, 168–172 (2002).
26. Perrot, V., Vazquez-Prado, J. & Gutkind, J.S. Plexin B regulates Rho through the guanine nucleotide exchange factors leukemia-associated Rho GEF (LARG) and PDZ-RhoGEF. *J. Biol. Chem.* **277**, 43115–43120 (2002).
27. Swiercz, J.M., Kuner, R., Behrens, J. & Offermanns, S. Plexin-B1 directly interacts with PDZ-RhoGEF/LARG to regulate RhoA and growth cone morphology. *Neuron* **35**, 51–63 (2002).
28. Kobayashi, K. *et al.* Survival of developing motor neurons mediated by Rho GTPase signaling pathway through Rho-kinase. *J. Neurosci.* **24**, 3480–3488 (2004).
29. Dacquin, R., Starbuck, M., Schinke, T. & Karsenty, G. Mouse α1(I)-collagen promoter is the best known promoter to drive efficient Cre recombinase expression in osteoblast. *Dev. Dyn.* **224**, 245–251 (2002).
30. Sordella, R. *et al.* Modulation of CREB activity by the Rho GTPase regulates cell and organism size during mouse embryonic development. *Dev. Cell* **2**, 553–565 (2002).
31. Gomez, C. *et al.* Expression of Semaphorin-3A and its receptors in endochondral ossification: potential role in skeletal development and innervation. *Dev. Dyn.* **234**, 393–403 (2005).
32. Soker, S., Takashima, S., Miao, H.Q., Neufeld, G. & Klagsbrun, M. Neuropilin-1 is expressed by endothelial and tumor cells as an isoform-specific receptor for vascular endothelial growth factor. *Cell* **92**, 735–745 (1998).
33. Behar, O., Golden, J.A., Mashimo, H., Schoen, F.J. & Fishman, M.C. Semaphorin III is needed for normal patterning and growth of nerves, bones and heart. *Nature* **383**, 525–528 (1996).
34. Sekido, Y. *et al.* Human semaphorins A(V) and IV reside in the 3p21.3 small cell lung cancer deletion region and demonstrate distinct expression patterns. *Proc. Natl. Acad. Sci. USA* **93**, 4120–4125 (1996).
35. Kitsukawa, T., Shimono, A., Kawakami, A., Kondoh, H. & Fujisawa, H. Overexpression of a membrane protein, neuropilin, in chimeric mice causes anomalies in the cardiovascular system, nervous system and limbs. *Development* **121**, 4309–4318 (1995).
36. Koh, J.M. *et al.* Association study of semaphorin 7a (sema7a) polymorphisms with bone mineral density and fracture risk in postmenopausal Korean women. *J. Hum. Genet.* **51**, 112–117 (2006).
37. Kumanogoh, A. *et al.* Requirement for the lymphocyte semaphorin, CD100, in the induction of antigen-specific T cells and the maturation of dendritic cells. *J. Immunol.* **169**, 1175–1181 (2002).
38. Delaire, S. *et al.* Biological activity of soluble CD100. II. Soluble CD100, similarly to H-SemaIII, inhibits immune cell migration. *J. Immunol.* **166**, 4348–4354 (2001).
39. Hirschberg, A. *et al.* Gene deletion mutants reveal a role for semaphorin receptors of the plexin-B family in mechanisms underlying corticogenesis. *Mol. Cell. Biol.* **30**, 764–780 (2010).
40. Di Benedetto, A. *et al.* N-cadherin and cadherin 11 modulate postnatal bone growth and osteoblast differentiation by distinct mechanisms. *J. Cell Sci.* **123**, 2640–2648 (2010).
41. Diarra, D. *et al.* Dickkopf-1 is a master regulator of joint remodeling. *Nat. Med.* **13**, 156–163 (2007).
42. Matsumoto, T. & Abe, M. TGF-β-related mechanisms of bone destruction in multiple myeloma. *Bone* **48**, 129–134 (2011).
43. Yadav, V.K. *et al.* Pharmacological inhibition of gut-derived serotonin synthesis is a potential bone anabolic treatment for osteoporosis. *Nat. Med.* **16**, 308–312 (2010).

ONLINE METHODS

Mice and analysis of the bone phenotype. Generation of *Sema4d*$^{-/-}$, *Plxnb1*$^{-/-}$, CAT-RhoA DN and α(1)I-Cre mice was as previously described[28,29,44,45]. *Sema4d*$^{-/-}$ mice (RBRC no. 00753) were provided by the RIKEN BioResource Center. All mice were backcrossed with C57BL/6 mice more than eight times, born in the expected Mendelian ratio without apparent developmental abnormalities, and maintained under specific-pathogen–free conditions. All mouse experiments were approved by the Institutional Animal Care and Use Committee of Tokyo Medical and Dental University and conformed to relevant guidelines and laws. The femurs and tibiae of 12-week-old female mice ($n \geq 8$) were subjected to three-dimensional microcomputed tomography and histomorphometric analysis, respectively, as previously described[46]. Bone mechanical strength testing was performed using a three-point bending method, as previously described[47].

Cell culture. We described the *in vitro* osteoclast differentiation method previously[48]. The *in vitro* osteoblast differentiation method was also as previously described[49]. Briefly, cells derived from calvaria were cultured in osteogenic medium (50 μM ascorbic acid, 10 nM dexamethasone and 10 mM β-glycerophosphate) and subjected to an analysis of the activity and mRNA expression of ALP (encoded by *Alpl*) (after 7 d), bone nodule formation and the expression of osteoblastic marker genes such as *Bglap* and *Col1a1* (after 21 d). Bone nodule formation was quantified as described[50]. Recombinant Sema4D (Fc-sema4D) (20 μg, unless otherwise indicated), neutralizing antibodies against Sema4D (BMA-12, MBL)[19,51] or Plexin-B1 (N-18, Santa Cruz)[52], or the ROCK inhibitors Y-27632 (10 μM, Calbiochem) and RKI (5 μM, Calbiochem), were added every 3 d. In **Figure 1i**, calvarial cells were cultured in osteoclast culture supernatant, which was collected from the culture of the wild-type and *Sema4d*$^{-/-}$ osteoclast precursor cells 2 d after RANKL stimulation. For the coculture of osteoblasts with osteoclasts, wild-type and *Sema4d*$^{-/-}$ osteoclasts were isolated by trypsinization 2 d after RANKL stimulation. Isolated osteoclasts (1×10^5 cells per well in a 24-well plate) were added every 3 d.

Immunoblot analysis. For the pull-down assay using Fc-sema4D, cell lysates were incubated with Fc-sema4D (500 ng) and analyzed by immunoblotting with antibodies to Plexin-B1, PDZ-RhoGEF and LARG. For analysis of the effect of Sema4D on intracellular signaling, calvarial cells were stimulated with Fc-sema4D after 3 d of culture in the osteogenic medium. Cells were stimulated with IGF-1 (10 nM, Sigma-Aldrich) after serum starvation for 8 h after 3 d of culture. Cells were pretreated with 30 μM of an ErbB2 inhibitor II (Santa Cruz), 10 μM Y27632 or 5 μM RKI for 1 h before stimulation with Fc-sema4D or IGF-1. Phosphorylation of Plexin-B1, Met, ErbB2 and IRS-1 was detected with a phosphotyrosine-specific antibody after immunoprecipitation with the specific antibodies. The antibodies used are listed in **Supplementary Table 2**.

Detection of RhoA activation. The pull-down assay to detect GTPase activity was performed as described[53]. Briefly, calvarial cells were cultured in the osteogenic medium for 3 d followed by incubation in serum-free α-MEM for 8 h, and then stimulated with Fc-sema4D. Cells were collected at the indicated time points and cell lysates were subjected to an incubation with 2 μg of GST-RBD (for RhoA) and GST-PAK1 (for Rac1) coupled to glutathione-Sepharose, followed by immunoblotting with RhoA-specific and Rac1-specific antibodies, respectively. For the ELISA of RhoA activity (**Fig. 3b**,**e**), GTP-bound RhoA was detected by G-LISA (Cytoskeleton) according to the manufacturer's protocol. To examine the effect of ErbB2, cells were pretreated with ErbB2 inhibitor II for 1 h before Fc-sema4D stimulation.

Ovariectomy-induced bone loss. This model of osteoporosis induced by ovariectomy has been described[54]. Briefly, 7-week-old female mice were ovariectomized or sham operated. More than eight mice were examined in each group. For the analysis of the prophylactic effect of the Sema4D-specific antibody, ovariectomized mice were intravenously injected with 20 μg of Sema4D-specific antibody (MBL) or saline via the tail vein weekly from day 3 to week 8 after surgery. To analyze the therapeutic effect of the Sema4D-specific antibody, after 6 weeks of surgery, we started an injection of the same amount of Sema4D-specific antibody and continued the injection every 3 d for 3 weeks. All of the mice were killed and subjected to microcomputed tomography and histomorphometric analyses 8 weeks (prophylactic model) or 9 weeks (therapeutic model) after surgery.

Motility assay. Cell migration was assessed using a modified Boyden chamber assay, as described[55]. Osteoblasts (3×10^4 cells) were added to the upper chamber. IGF-1 (100 ng ml^{-1}) or Fc-sema4D was added to the lower chamber. After 4 h, the cells that migrated to the lower surface of the membrane were counted. To analyze the effect of the ROCK inhibitor on Sema4D-induced cell motility, cells were pretreated with 5 μM RKI for 1 h and added to the upper chamber.

Statistical analysis. All data are expressed as the mean ± s.e.m. ($n = 5$). Statistical analyses were performed using the Student's *t* test analysis of variance followed by the Bonferroni test when applicable. Results are representative examples of more than four independent experiments.

Additional methods. Detailed methodology is described in the **Supplementary Methods**.

44. Shi, W. *et al.* The class IV semaphorin CD100 plays nonredundant roles in the immune system: defective B and T cell activation in CD100-deficient mice. *Immunity* **13**, 633–642 (2000).
45. Friedel, R.H. *et al.* Gene targeting using a promoterless gene trap vector ("targeted trapping") is an efficient method to mutate a large fraction of genes. *Proc. Natl. Acad. Sci. USA* **102**, 13188–13193 (2005).
46. Nishikawa, K. *et al.* Maf promotes osteoblast differentiation in mice by mediating the age-related switch in mesenchymal cell differentiation. *J. Clin. Invest.* **120**, 3455–3465 (2010).
47. Kim, S. *et al.* Stat1 functions as a cytoplasmic attenuator of Runx2 in the transcriptional program of osteoblast differentiation. *Genes Dev.* **17**, 1979–1991 (2003).
48. Takayanagi, H. *et al.* Induction and activation of the transcription factor NFATc1 (NFAT2) integrate RANKL signaling in terminal differentiation of osteoclasts. *Dev. Cell* **3**, 889–901 (2002).
49. Koga, T. *et al.* NFAT and Osterix cooperatively regulate bone formation. *Nat. Med.* **11**, 880–885 (2005).
50. Gregory, C.A., Gunn, W.G., Peister, A. & Prockop, D.J. An Alizarin red-based assay of mineralization by adherent cells in culture: comparison with cetylpyridinium chloride extraction. *Anal. Biochem.* **329**, 77–84 (2004).
51. Okuno, T. *et al.* Roles of Sema4D-plexin-B1 interactions in the central nervous system for pathogenesis of experimental autoimmune encephalomyelitis. *J. Immunol.* **184**, 1499–1506 (2010).
52. Regev, A., Goldman, S. & Shalev, E. Expression of plexin-B1 in the mouse ovary and its possible role in follicular development. *Fertil. Steril.* **84** (suppl 2), 1210–1219 (2005).
53. Shinohara, M. *et al.* Nox1 redox signaling mediates oncogenic Ras-induced disruption of stress fibers and focal adhesions by down-regulating Rho. *J. Biol. Chem.* **282**, 17640–17648 (2007).
54. Shinohara, M. *et al.* Tyrosine kinases Btk and Tec regulate osteoclast differentiation by linking RANK and ITAM signals. *Cell* **132**, 794–806 (2008).
55. Sotobori, T. *et al.* Bone morphogenetic protein-2 promotes the haptotactic migration of murine osteoblastic and osteosarcoma cells by enhancing incorporation of integrin 1 into lipid rafts. *Exp. Cell Res.* **312**, 3927–3938 (2006).

© 2011 Nature America, Inc. All rights reserved.

doi:10.1038/nm.2489

Stage-specific functions of leukemia/lymphoma-related factor (LRF) in the transcriptional control of osteoclast development

Kaori Tsuji-Takechi[a,b,c], Takako Negishi-Koga[a,b,d], Eriko Sumiya[a,b,d], Akiko Kukita[e], Shigeaki Kato[f], Takahiro Maeda[g,1], Pier Paolo Pandolfi[g], Keiji Moriyama[b,c], and Hiroshi Takayanagi[a,b,d,h,2]

[a]Department of Cell Signaling, Graduate School of Medical and Dental Sciences, Tokyo Medical and Dental University, Bunkyo-ku, Tokyo 113-8549, Japan; [b]Global Center of Excellence Program, International Research Center for Molecular Science in Tooth and Bone Diseases, Bunkyo-ku, Tokyo 113-8549, Japan; [c]Department of Maxillofacial Orthognathics, Graduate School of Medical and Dental Sciences, Tokyo Medical and Dental University, Bunkyo-ku, Tokyo 113-8549, Japan; [d]Takayanagi Osteonetwork Project, Japan Science and Technology Agency, Exploratory Research for Advanced Technology, Bunkyo-ku, Tokyo 113-8549, Japan; [e]Department of Microbiology, Faculty of Medicine, Saga University, Saga-shi, Saga 849-8501, Japan; [f]Institute of Molecular and Cellular Biosciences, Graduate School of Medicine, University of Tokyo, Bunkyo-ku, Tokyo 113-0032, Japan; [g]Cancer Genetics Program, Beth Israel Deaconess Cancer Center, Department of Medicine and Pathology, Beth Israel Deaconess Medical Center, Harvard Medical School, Boston, MA 02215; and [h]Centre for Orthopaedic Research, School of Surgery, University of Western Australia, Nedlands, WA 6009, Australia

Edited by Laurie H. Glimcher, Weill Cornell Medical College, New York, NY, and approved January 4, 2012 (received for review October 6, 2011)

Cell fate determination is tightly regulated by transcriptional activators and repressors. Leukemia/lymphoma-related factor (LRF; encoded by *Zbtb7a*), known as a POK (POZ/BTB and *Krüppel*) family transcriptional repressor, is induced during the development of bone-resorbing osteoclasts, but the physiological significance of LRF in bone metabolism and the molecular mechanisms underlying the transcriptional regulation of osteoclastogenesis by LRF have not been elucidated. Here we show that LRF negatively regulates osteoclast differentiation by repressing nuclear factor of activated T cells c1 (NFATc1) induction in the early phase of osteoclast development, while positively regulating osteoclast-specific genes by functioning as a coactivator of NFATc1 in the bone resorption phase. The stage-specific distinct functions of LRF were demonstrated in two lines of conditional knockout mice in which LRF was deleted in the early or late phase of osteoclast development. Thus, this study shows that LRF plays stage-specific distinct roles in osteoclast differentiation, exemplifying the delicate transcriptional regulation at work in lineage commitment.

Osteoclasts are responsible for both physiological and pathological bone resorption, and an accurate understanding of the molecular mechanisms of osteoclast differentiation is thus crucially important for the development of therapeutic strategies against bone and joint diseases (1–3). Receptor activator of nuclear factor-κB (NF-κB) ligand (RANKL) is an essential cytokine that induces the differentiation of monocyte/macrophage lineage cells into osteoclasts in the presence of macrophage colony-stimulating factor (M-CSF) (2, 3). RANKL promotes osteoclastogenesis through the induction and autoamplification of the key transcription factor nuclear factor of activated T cells c1 (NFATc1), which transcriptionally regulates most of the osteoclast-specific genes required for the bone resorbing activity, including *Ctsk* (encoding cathepsin K), *Mmp-9*, and *Clcn7* (encoding chloride channel 7) (3–6). The autoamplification of NFATc1 is a hallmark event in the early phase of osteoclast development, in which NFATc1 is preferentially recruited to its own promoter, thus enabling the autoamplification of expression (3, 7, 8). To achieve efficient NFATc1 autoamplification, transcription factors such as NF-κB and c-Fos are required. Osteoclast differentiation is negatively regulated by the transcription factors IFN regulatory factor-8 (IRF-8), v-maf musculoaponeurotic fibrosarcoma oncogene family protein B (MafB), and B-cell lymphoma 6 (Bcl-6), mainly through the inhibition of NFATc1 activity and expression (9–11). Thus, NFATc1 expression is controlled by a delicate balance between positive and negative transcriptional regulators during osteoclastogenesis.

Leukemia/lymphoma-related factor (LRF, also called Pokemon: POK erythroid myeloid ontogenic factor), which is encoded by the *Zbtb7a* gene, is a member of the POK (POZ/BTB and *Krüppel*) family of transcriptional repressors (12, 13). LRF is involved in the oncogenesis of T- and B-cell lymphoma, prostate, breast, non–small-cell lung, and ovarian cancers (14–18). LRF exerts its oncogenic effect by suppressing the expression of the tumor suppressor genes *Arf* and *Rb* (14, 19). LRF is implicated not only in oncogenesis, but also in diverse biological processes such as cell survival and lineage fate decisions in hematopoietic cells (20–22).

In the skeletal system, osteoclast-derived zinc finger (OCZF), a rat homolog of LRF, was originally identified as an osteoclast-specific protein in a screening performed with monoclonal antibodies (23). Recently, mice overexpressing LRF in osteoclasts were shown to exhibit an osteoporotic phenotype due to the increased number of osteoclasts (24). However, the physiological function of LRF in bone remodeling has not been demonstrated, because global deletion of LRF results in embryonic lethality (14). Thus, we investigated the function of LRF in osteoclastogenesis by disrupting *Zbtb7a* at the early and late stages of osteoclast differentiation using *Mx1*- and *Ctsk-Cre* mice, respectively. The distinct phenotypes of the two conditional knockout mice revealed that LRF plays certain stage-specific roles in the transcriptional program of osteoclast development.

Results

Physiological and Ectopic Expression of LRF During Osteoclastogenesis. We examined the expression and localization of the LRF protein during osteoclastogenesis. LRF was only slightly expressed in osteoclast precursor cells, but was markedly induced in bone marrow-derived monocyte/macrophage precursor cells (BMMs) stimulated with RANKL (Fig. S1*A*). LRF accumulated in the nuclei as BMMs underwent differentiation into osteoclasts (Fig. S1*B*), suggesting that it has a role in gene regulation. To examine the effect of the ectopic expression of LRF at the early and late stages of osteoclast differentiation, we infected BMMs at distinct time points with a retroviral vector carrying the *Zbtb7a* gene (pMX-LRF-IRES-EGFP). When BMMs were infected with the LRF-expressing retrovirus, the formation of tartrate-resistant acid phosphatase (TRAP)-positive multinucleated cells (MNCs) was significantly

Author contributions: K.T.-T., T.N.-K., and H.T. designed research; K.T.-T. performed research; A.K., S.K., T.M., and P.P.P. contributed new reagents/analytic tools; K.T.-T., T.N.-K., E.S., and K.M. analyzed data; and H.T. wrote the paper.

The authors declare no conflict of interest.

This article is a PNAS Direct Submission.

[1]Present address: Hematology Division, Brigham and Women's Hospital, Harvard Medical School, 1 Blackfan Circle, Boston, MA 02115.

[2]To whom correspondence should be addressed. E-mail: taka.csi@tmd.ac.jp.

This article contains supporting information online at www.pnas.org/lookup/suppl/doi:10.1073/pnas.1116042109/-/DCSupplemental.

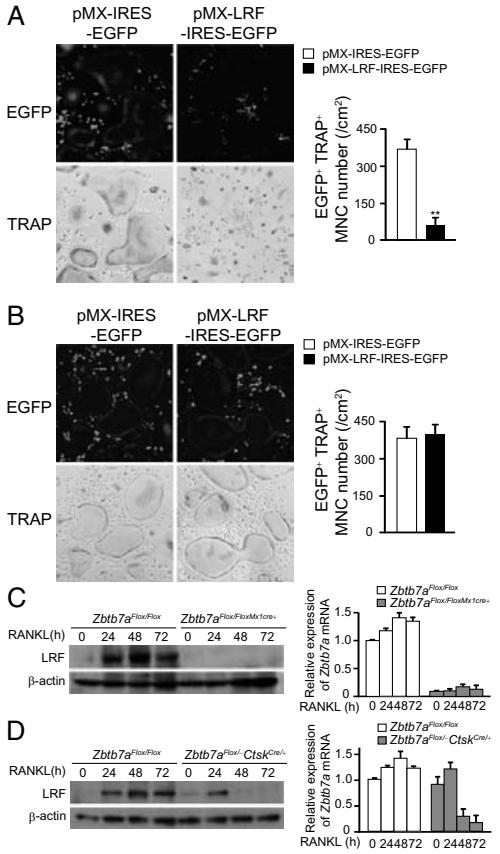

Fig. 1. Effect of ectopic expression of LRF on osteoclastogenesis and generation of two types of stage-specific conditional knockout mice. (*A*) Effect of retroviral expression of LRF at an early stage of osteoclastogenesis. TRAP$^+$ multinucleated cells were counted among the EGFP$^+$ (infected) cells. (*B*) Effect of retroviral expression of LRF at a late stage of osteoclastogenesis. (*C*) Expression of LRF at the protein (*Left*) and mRNA level (*Right*) in *Zbtb7a*$^{Flox/Flox}$ and *Zbtb7a*$^{Flox/FloxMx1cre+}$ cells during osteoclastogenesis. (*D*) Expression of LRF at the protein (*Left*) and mRNA level (*Right*) in *Zbtb7a*$^{Flox/Flox}$ and *Zbtb7a*$^{Flox/-}$*Ctsk*$^{Cre/+}$ cells during osteoclastogenesis. $^{**}P < 0.01$.

impaired in the EGFP$^+$ cells (Fig. 1*A*). However, this suppressive effect was not observed when the cells had been stimulated with RANKL for 2 d before the retroviral infection and the survival of the mature osteoclasts was not influenced by this ectopic expression of LRF in the late stage of osteoclast development (Fig. 1*B* and Fig. S2). These results suggest that LRF negatively regulates osteoclast differentiation at the early but not the late stage of osteoclastogenesis. It has been reported (24), however, that overexpression of LRF under the *Ctsk* promoter results in a prolonged survival of osteoclasts. These inconsistent in vitro results suggest that in vivo loss-of-function studies will be required for a clear understanding of the physiological function of LRF.

Differentiation Stage-Specific Disruption of LRF. To explore the physiological role of LRF in the osteoclast lineage, we investigated LRF conditional knockout mice. Because LRF exerted stage-specific effects in vitro, we generated two types of LRF conditional knockout mice, *Zbtb7a*$^{Flox/FloxMx1cre+}$ (20) and *Zbtb7a*$^{Flox/-}$*Ctsk*$^{Cre/+}$ mice, by crossing *Zbtb7a*$^{Flox/Flox}$ with *Mx1-Cre* transgenic mice and *Zbtb7a*$^{Flox/-}$ with *Ctsk-Cre* knock-in (*Ctsk*$^{Cre/+}$) mice, respectively. In the *Zbtb7a*$^{Flox/FloxMx1cre+}$ mice, the *Zbtb7a* gene is deleted upon polyinosinic-polycytidylic acid (poly I:C) treatment in various cell types, including immature hematopoietic cells, which allowed us to examine the effect of LRF depletion at the very early stage of osteoclast development. In fact, the expression of both the LRF protein and mRNA was undetectable at the stage of osteoclast precursor cells (time 0) in the *Zbtb7a*$^{Flox/FloxMx1cre+}$ cells (Fig. 1*C*). In the *Zbtb7a*$^{Flox/-}$*Ctsk*$^{Cre/+}$ mice, the *Zbtb7a* gene was deleted at the later stage of osteoclast lineage cells expressing cathepsin K. We found the LRF expression level in *Zbtb7a*$^{Flox/-}$*Ctsk*$^{Cre/+}$ cells to be markedly decreased at 48 and 72 h after RANKL stimulation (Fig. 1*D*).

Increased Osteoclast Number and Low Bone Mass in *Zbtb7a*$^{Flox/FloxMx1cre+}$ Mice. We analyzed the bone phenotype of *Zbtb7a*$^{Flox/FloxMx1cre+}$ mice, which had received poly I:C injection at the age of 21 d. The bone volume and the trabecular number were significantly reduced and trabecular separation was increased in the *Zbtb7a*$^{Flox/FloxMx1cre+}$ mice (Fig. 2*A* and Fig. S3*A*), without any changes in cortical thickness and bone mineral density (Fig. S4). Bone morphometric analysis indicated an increase in the osteoclast number and eroded surface (Fig. 2 *B* and *C*), but the parameters for osteoblastic bone formation were normal in the *Zbtb7a*$^{Flox/FloxMx1cre+}$ mice (Fig. S3 *B* and *C*). Wild-type mice engrafted with bone marrow cells derived from the *Zbtb7a*$^{Flox/FloxMx1cre+}$ mice also exhibited a low bone mass phenotype (Fig. S5). These results indicate that the low bone mass phenotype in the *Zbtb7a*$^{Flox/FloxMx1cre+}$ mice is caused by hematopoietic cells including osteoclast precursor cells. Thus, LRF in osteoclast precursor cells negatively regulates the osteoclast number in vivo.

Enhanced Osteoclastogenesis and NFATc1 Expression by the Deletion of LRF in Osteoclast Precursor Cells. We examined osteoclast differentiation in *Zbtb7a*$^{Flox/FloxMx1cre+}$ BMMs stimulated with RANKL in the presence of M-CSF. Because the number of T and B cells in the bone marrow differed between the *Zbtb7a*$^{Flox/Flox}$

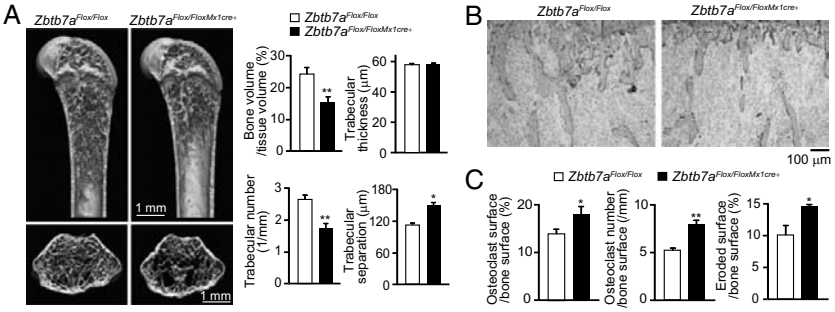

Fig. 2. Osteoporotic phenotype of *Zbtb7a*$^{Flox/FloxMx1cre+}$ mice. (*A*) Images of the proximal femurs of the control (*Zbtb7a*$^{Flox/Flox}$) and *Zbtb7a*$^{Flox/FloxMx1cre+}$ mice (*Upper*, longitudinal view; *Lower*, axial view of the metaphyseal region) and the parameters on microcomputed tomography (μCT) analysis. (*B*) Histological analysis of the proximal tibiae of the control and *Zbtb7a*$^{Flox/FloxMx1cre+}$ mice (TRAP staining). (*C*) Parameters for osteoclastic bone resorption determined by bone morphometric analysis. $^{*}P < 0.05$, $^{**}P < 0.01$.

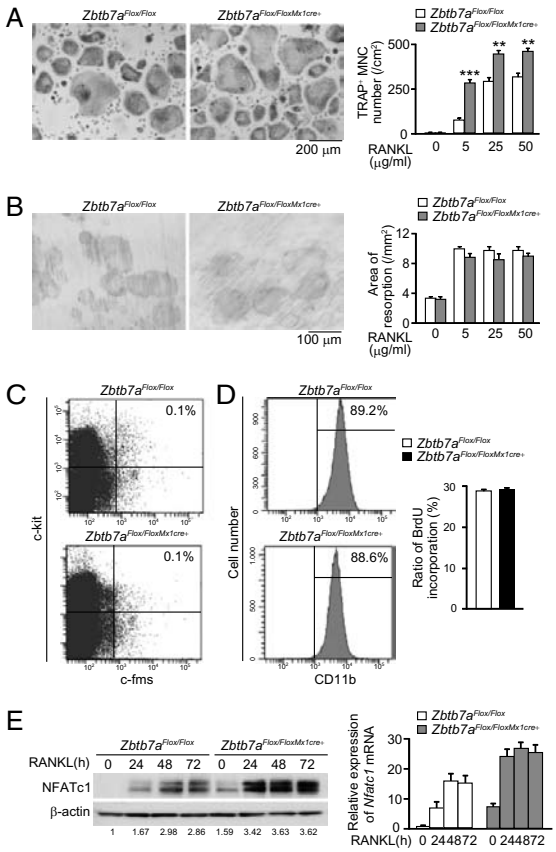

Fig. 3. LRF suppresses the early stage of osteoclast differentiation through inhibition of NFATc1 expression. (*A*) Osteoclast differentiation of the control (*Zbtb7a*$^{Flox/Flox}$) and *Zbtb7a*$^{Flox/FloxMx1cre+}$ cells (*Left*). TRAP$^+$ multinucleated cells (TRAP$^+$ MNC) were counted (*Right*). (*B*) Bone-resorbing activity of mature osteoclasts derived from the control and *Zbtb7a*$^{Flox/FloxMx1cre+}$ BMMs. (*C*) The percentage of c-kit$^+$c-fms$^+$ cells in the CD11b$^{lo/-}$CD3ε$^-$B220$^-$ population in the bone marrow of the control and *Zbtb7a*$^{Flox/FloxMx1cre+}$ mice. (*D*) Proportion of CD11b$^+$ osteoclast precursor cells (*Left*) and the BrdU incorporation (*Right*) in the control and *Zbtb7a*$^{Flox/FloxMx1cre+}$ BMMs. (*E*) NFATc1 expression at the protein (*Left*) and mRNA level (*Right*) in the control and *Zbtb7a*$^{Flox/FloxMx1cre+}$ cells during osteoclastogenesis. $^{**}P < 0.01$, $^{***}P < 0.005$.

and *Zbtb7a*$^{Flox/FloxMx1cre+}$ mice (20), we sorted and cultured CD4$^-$CD8$^-$B220$^-$ cells in the presence of M-CSF for 2 d, which were then used as BMMs. The TRAP$^+$ MNC number was markedly increased in the *Zbtb7a*$^{Flox/FloxMx1cre+}$ cells compared with the control cells (Fig. 3*A*), but there was a slight decrease in bone resorbing activity in *Zbtb7a*$^{Flox/FloxMx1cre+}$ osteoclasts when the same number of mature osteoclasts were seeded (Fig. 3*B*). Therefore, the increase in bone resorption in the *Zbtb7a*$^{Flox/FloxMx1cre+}$ mice was caused by the increased number of osteoclasts, not by an increase in their activity. To examine the influence of abnormalities of T or B cells on osteoclastogenesis, we analyzed osteoclast formation after depleting the T or B cells from bone marrow cells. Depletion and reconstitution of either T or B cells did not affect osteoclastogenesis in *Zbtb7a*$^{Flox/FloxMx1cre+}$ cells, suggesting that LRF functions in a cell-autonomous manner (Fig. S6). We examined the ratio of the osteoclast precursor cells among the bone marrow cells. The percentage of c-kit$^+$c-fms$^+$ cells in the CD11b$^{lo/-}$CD3ε$^-$B220$^-$ population (25) was comparable between the control and *Zbtb7a*$^{Flox/FloxMx1cre+}$ mice, indicating that the proportion of osteoclast precursor cells in the non-T non-B cells in the bone marrow was unchanged (Fig. 3*C*). In addition, there was no significant difference in the number or proliferation rate of CD11b$^+$ cells cultured in the presence of M-CSF for 2 d (Fig. 3*D*).

In *Zbtb7a*$^{Flox/FloxMx1cre+}$ cells, the induction of NFATc1 expression was accelerated at both the protein and mRNA levels (Fig. 3*E*). It is noteworthy that the expression of NFATc1 was detected even in the absence of RANKL stimulation (Fig. 3*E*), suggesting that LRF inhibits osteoclastogenesis through a suppression of NFATc1 expression. These results demonstrate that LRF deficiency in osteoclast precursor cells results in enhanced osteoclast differentiation by promoting NFATc1 expression without affecting the generation of osteoclast precursor cells.

Increased Bone Mass in *Zbtb7a*$^{Flox/-}$*Ctsk*$^{Cre/+}$ Mice. Unlike the *Zbtb7a*$^{Flox/FloxMx1cre+}$ mice, the *Zbtb7a*$^{Flox/-}$*Ctsk*$^{Cre/+}$ mice were shown to have an increased trabecular bone volume and trabecular number (Fig. 4*A* and Fig. S7*A*). Bone morphometric analysis indicated a marked decrease in the eroded surface, which is a bone resorption marker, but there was no significant difference in either the osteoclast number or surface (Fig. 4 *B* and *C*). There was no obvious abnormality in the parameters for osteoblastic bone formation, such as the bone formation rate or osteoblast surface (Fig. S7 *B* and *C*). These results suggested that the high bone mass phenotype of the *Zbtb7a*$^{Flox/-}$*Ctsk*$^{Cre/+}$ mice was caused by a decrease in osteoclastic bone-resorbing activity.

We obtained bone marrow cells from the *Zbtb7a*$^{Flox/-}$*Ctsk*$^{Cre/+}$ mice and subjected them to an in vitro osteoclast formation and bone resorption assay on dentine. RANKL induced a comparable number of TRAP$^+$ MNCs in the control and *Zbtb7a*$^{Flox/-}$*Ctsk*$^{Cre/+}$ cells (Fig. 5*A*), but the number and area of the resorption pits were markedly decreased in *Zbtb7a*$^{Flox/-}$*Ctsk*$^{Cre/+}$ osteoclasts, even though the same number of osteoclasts were seeded (Fig. 5*B*). The impaired bone resorption activity in *Zbtb7a*$^{Flox/-}$*Ctsk*$^{Cre/+}$ osteoclasts may be explained by the decrease in the mRNA expression

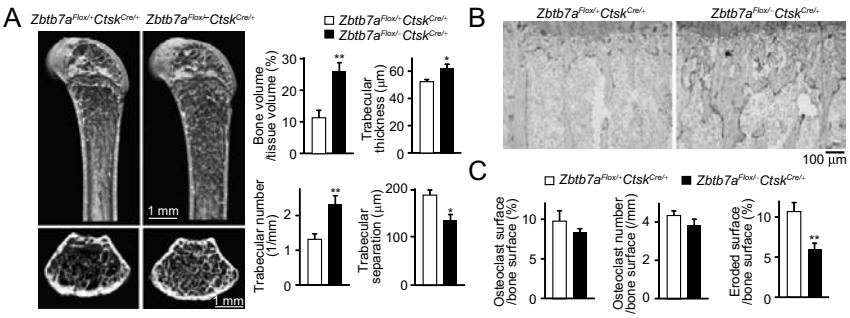

Fig. 4. Increased bone mass in *Zbtb7a*$^{Flox/-}$*Ctsk*$^{Cre/+}$ mice. (*A*) Images of the proximal femurs of the control (*Zbtb7a*$^{Flox/+}$*Ctsk*$^{Cre/+}$) and *Zbtb7a*$^{Flox/-}$*Ctsk*$^{Cre/+}$ mice (*Upper*, longitudinal view; *Lower*, axial view of the metaphyseal region) and the parameters on μCT analysis. (*B*) Histological analysis of the proximal tibiae of the control and *Zbtb7a*$^{Flox/-}$*Ctsk*$^{Cre/+}$ mice (TRAP staining). (*C*) Parameters for osteoclastic bone resorption determined by bone morphometric analysis. $^*P < 0.05$, $^{**}P < 0.01$.

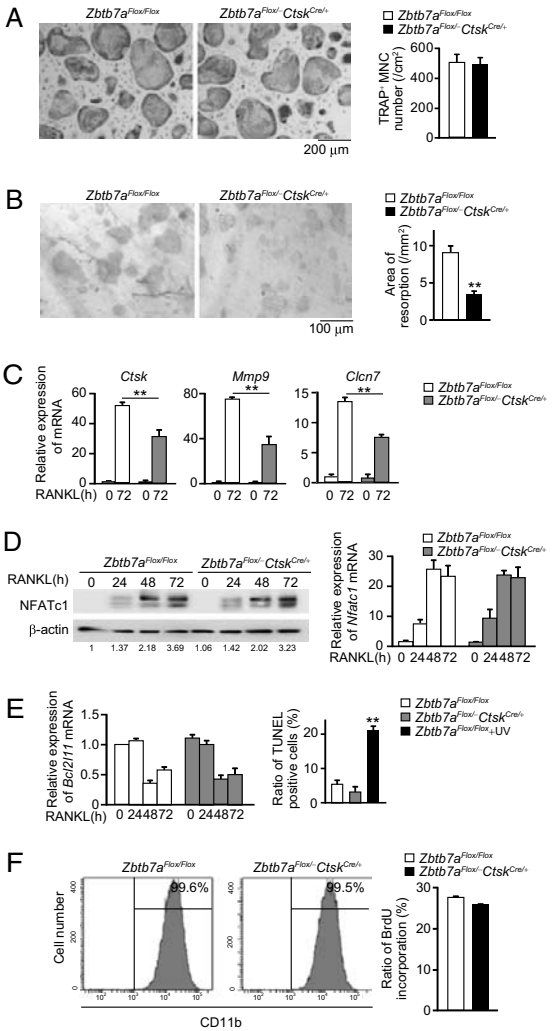

Fig. 5. LRF promotes the bone resorption activity of mature osteoclasts. (*A*) Osteoclast differentiation of the control (*Zbtb7a*$^{Flox/Flox}$) and *Zbtb7a*$^{Flox/-}$*Ctsk*$^{Cre/+}$ cells (*Left*). TRAP$^+$ MNCs were counted (*Right*). (*B*) Bone-resorbing activity of mature osteoclasts derived from the control and *Zbtb7a*$^{Flox/-}$*Ctsk*$^{Cre/+}$ BMMs. (*C*) Expression of osteoclast-specific genes in the control and *Zbtb7a*$^{Flox/-}$*Ctsk*$^{Cre/+}$ cells during osteoclastogenesis. (*D*) NFATc1 expression at the protein (*Left*) and mRNA (*Right*) in the control and *Zbtb7a*$^{Flox/-}$*Ctsk*$^{Cre/+}$ cells during osteoclastogenesis. (*E*) Expression of *Bcl2l11* (*Left*) and the apoptosis rate (*Right*) in the control and *Zbtb7a*$^{Flox/-}$*Ctsk*$^{Cre/+}$ cells 48 h after RANKL stimulation. (*F*) Proportion of CD11b$^+$ cells (*Left*) and BrdU incorporation (*Right*) in control and *Zbtb7a*$^{Flox/-}$*Ctsk*$^{Cre/+}$ cells 48 h after RANKL stimulation. $^{**}P < 0.01$.

of the genes required for bone resorption including *Ctsk*, *Mmp9*, and *Clcn7* may influence (Fig. 5*C*), although we cannot rigorously rule out the other possibilities. The NFATc1 induction was observed to be equal in the control and *Zbtb7a*$^{Flox/-}$*Ctsk*$^{Cre/+}$ cells (Fig. 5*D*), consistent with the result indicating the normal formation of TRAP$^+$ MNCs (Fig. 5*A*). LRF suppresses erythroblast apoptosis by inhibiting the expression of the proapoptotic protein Bim (encoded by *Bcl2l11*) (21). Bim also regulates osteoclast apoptosis (26), but there was no increase in Bim expression or the apoptosis rate in *Zbtb7a*$^{Flox/-}$*Ctsk*$^{Cre/+}$ cells (Fig. 5*E*). There was no significant difference in the number or the proliferation rate between the control and *Zbtb7a*$^{Flox/-}$*Ctsk*$^{Cre/+}$ cells 48 h after RANKL stimulation (Fig. 5*F*). Although LRF overexpression reportedly led to prolonged osteoclast survival in a gain-of-function study (24), these results in a loss-of-function study suggest that LRF expression at the late stage of osteoclastogenesis is not required for the survival of osteoclast lineage cells, but is instead essential for bone resorption activity.

Positive and Negative Regulation by LRF. Previous studies demonstrated that IRF-8, MafB, and Bcl-6 potently inhibit the expression and function of NFATc1 (9–11). However, the expression of such antiosteoclastogenic factors was not reduced in *Zbtb7a*$^{Flox/FloxMx1cre+}$ cells (Fig. S8*A*), raising the possibility that LRF directly inhibits NFATc1 expression at an early stage of osteoclastogenesis. A computational search on the upstream sequence of the transcription start site of the *Nfatc1* gene revealed that several LRF-binding sites (14) were located in the promoter region required for the NFATc1 autoamplification (Fig. 6*A*). In contrast, a smaller number of LRF-binding sites were found in the promoters of genes expressed in mature bone-resorbing osteoclasts, such as *Ctsk*, *Calcr*, *Mmp9*, and *Clcn7*, all of which are known to be transcriptional targets of NFATc1 (Fig. 6*A* and Fig. S8*B*).

LRF physically interacted with NFATc1 in the late phase of osteoclastogenesis (Fig. S8*C*). NFATc1 coimmunoprecipitated with full-length LRF and a mutant, ΔZF-LRF, which lacks the zinc finger domain required for DNA binding, but not with a mutant, ΔPOZ-LRF, lacking the POZ domain (Fig. 6*B*). Thus, LRF interacts with NFATc1 through the POZ domain. LRF suppressed the activation of the *Nfatc1*-P1 promoter by NFATc1 and this suppression was also observed without NFATc1 overexpression (Fig. 6*C*). ΔZF-LRF failed to suppress the *Nfatc1*-P1 promoter activity enhanced by NFATc1, suggesting that LRF acts as a transcriptional repressor by binding to the promoter through its zinc finger domain (Fig. 6*C*). Indeed, LRF resided at the proximal *Nfatc1* promoter before RANKL stimulation, but not in the late phase of differentiation (Fig. 6*D*). Previous reports showed that LRF binds to a corepressor complex composed of histone deacetylases (HDACs), *N*-CoR and SMRT through the POZ domain (19, 27). At the early stage of osteoclastogenesis, HDAC1, HDAC2, HDAC3, *N*-CoR, SMRT, and B-CoR were recruited to the *Nfatc1* promoter, but the recruitment of most of these components, if not all, was severely impaired in the LRF deficiency (Fig. 6*D*). The expression of Jmjd3, which is reported to be a histone demethylase regulating osteoclastogenesis (28), was not altered by the LRF expression (Fig. S8*D*). These results suggest that LRF repressed transcriptional activity of NFATc1 by recruiting a corepressor complex (Fig. 6*E*).

LRF was associated with the promoters of genes expressed by mature osteoclasts including *Ctsk* and *Calcr* in the late phase of differentiation (Fig. 6*D*). Activation of these promoters by NFATc1 was further enhanced by the expression of LRF as well as ΔZF-LRF (Fig. 6*C*), but not by the expression of ΔPOZ-LRF. There were four and eight NFAT-binding sites, but only two and no LRF-binding sites, in the *Ctsk* and *Calcr* promoter regions examined here, respectively (Fig. 6*A*). These results suggest that LRF functions as a transcription coactivator by binding to NFATc1 through its POZ domain in the regulation of genes required for bone resorbing activity, and this activity is not dependent on the direct DNA binding of LRF through the zinc finger domain.

Discussion

This study revealed that mice lacking LRF in osteoclast precursor cells exhibit an osteoporotic phenotype due to an increased osteoclast number, whereas mice lacking LRF in cells in the more advanced stage of osteoclastogenesis have an increased bone mass due to impaired osteoclastic bone resorption. LRF

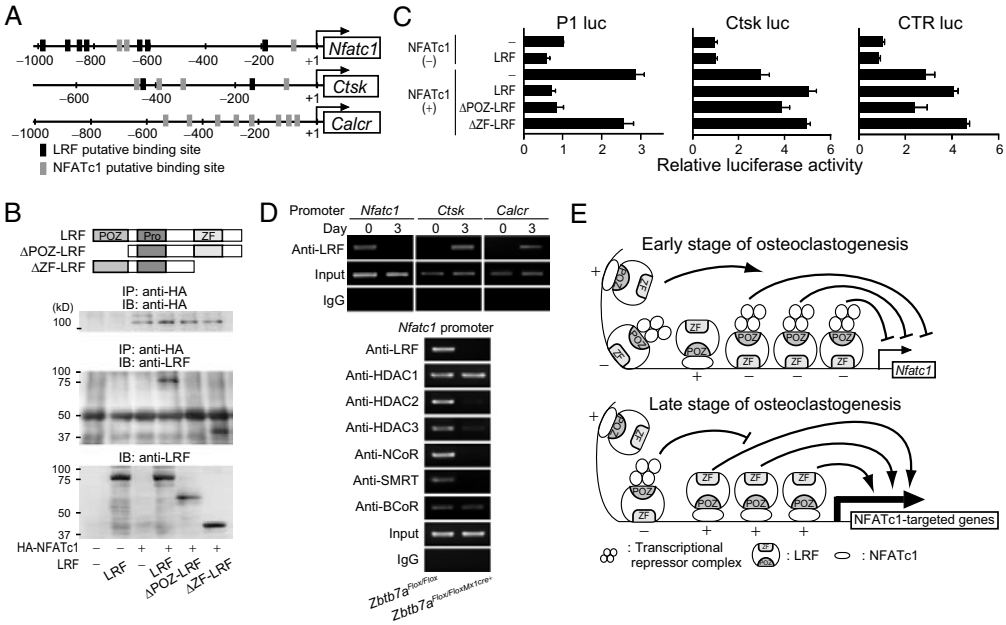

Fig. 6. Possible mechanism for the biphasic role of LRF in osteoclastogenesis. (*A*) Schematic view of the putative promoter regions in osteoclast-specific genes. The binding sites of LRF and NFAT on the 5′flanking region of the genes are shown as black and green rectangles, respectively. (*B*) Physical interaction between NFATc1 and LRF or its truncated mutants. Schematic illustration of LRF, ΔPOZ-LRF, and ΔZF-LRF (*Upper*). IP, immunoprecipitation; IB, immunoblot. (*C*) Effect of LRF and its truncated mutants on the NFATc1-mediated activation of the *Nfatc1* (P1 luc), *Ctsk* (Ctsk luc), and *Calcr* (CTR luc) promoters. (*D*) Recruitment of LRF to the promoters of the *Nfatc1*, *Ctsk*, and *Calcr* genes at early (day 0) and late (day 3) stages of osteoclastogenesis (*Upper*). Recruitment of corepressors to the *Nfatc1* promoter in *Zbtb7a*$^{Flox/FloxMx1cre+}$ BMMs (*Lower*). (*E*) Working model for the stage-specific functions of LRF during osteoclastogenesis. At the early stage of osteoclast development, LRF blocks NFATc1 expression by acting as a transcriptional repressor. At the late stage of osteoclastogenesis, LRF acts as a coactivator of NFATc1 to promote the expression of genes required for the bone-resorbing activity of osteoclasts.

thus plays a biphasic role in the transcriptional regulation of osteoclastogenesis: LRF represses osteoclast differentiation by acting as a transcriptional repressor of the *Nfatc1* gene in the early phase of osteoclast development and promotes bone resorption, at least in part, by acting as a coactivator of NFATc1 in controlling the genes required for the bone-resorbing activity of osteoclasts. The phenotype caused by the gene deletion in the early phase could be influenced by the deletion in the late phase that inevitably occurs, but the LRF deletion in the early phase resulted in a very high expression of NFATc1, which sufficiently functions even without cooperation with LRF. LRF regulates B versus T lymphoid lineage fate decision in the bone marrow through inhibiting the Notch pathway (20). Because Notch signaling is known to repress osteoclastogenesis (29), it is unlikely that LRF inhibits osteoclast differentiation through suppression of Notch function. Recent studies showed that LRF positively regulates transcription by the specific recognition of its DNA-binding sequence (18, 30, 31). It remains to be determined how LRF exerts positive and negative effects on the activity of each promoter, but it is interesting to note that the relative number of LRF- and NFAT-binding sites is markedly different between the promoters that are respectively inhibited and activated by LRF (Fig. 6*A* and Fig. S8*B*). Because the negative regulation by LRF is dependent on DNA binding and positive regulation is dependent on the interaction with NFATc1, it is reasonable to hypothesize that LRF functions as a repressor when the promoter contains a large number of LRF-binding sites and as an activator when the promoter contains considerably more NFAT- than LRF-binding sites (Fig. 6*E*).

Cell lineage commitment is strictly controlled so as to maintain the homeostasis of the biological systems of multicellular organisms. To this end, the cell differentiation program is tightly regulated by multiple signaling pathways, and negative feedback regulation is extremely important to avoid excessive cell differentiation. The negative regulators of osteoclastogenesis IRF-8, MafB, and Bcl-6, are highly expressed in the early phase of development, but the expression is blocked by various repressors, including Blimp-1, as the development proceeds (32). Unlike other antiosteoclastogenic factors, LRF is expressed at a relatively low level in osteoclast precursor cells, but it is induced during osteoclastogenesis, ultimately coming to function as a positive regulator of different target genes. The unique stage-specific regulation of osteoclastogenesis by LRF reveals an intricate transcriptional network in bone homeostasis and may provide a novel molecular basis for therapeutic strategies against bone and joint diseases.

Materials and Methods

Mice and Analysis of the Bone Phenotype. The generation of *Zbtb7a*$^{Flox/Flox}$, *Mx1-Cre* transgenic (003556; The Jackson Laboratory), and *Ctsk-Cre* knock-in (*Ctsk*$^{Cre/+}$) mice was previously described (20, 33). All of the animal experiments were approved by the institutional animal care and use committee and conformed to relevant guidelines and laws. All mice were backcrossed with C57BL/6 mice more than six times and maintained under specific pathogen-free conditions. For the induction of Cre recombinase expression in hematopoietic stem cells, poly I:C (Invitrogen) was administered into mice, as described, with minor modifications (34). Briefly, *Zbtb7a*$^{Flox/Flox}$ and *Zbtb7a*$^{Flox/FloxMx1cre+}$ mice were injected intraperitoneally with 0.25 mL of 1 mg mL^{-1} poly I:C every other day starting at postnatal day 21 for a total of three doses. The femurs of 9-wk-old male *Zbtb7a*$^{Flox/FloxMx1cre+}$ mice (n = 8), 12-wk-

old female *Zbtb7a*$^{Flox/-}$*Ctsk*$^{Cre/+}$ mice ($n = 8$), and their littermate controls were subjected to 3D microcomputed tomography (μCT) analysis. The tibiae of these mice were subjected to histomorphometric analysis. The methods for μCT and histomorphometric analyses were previously described (35).

In Vitro Assays for Osteoclast Differentiation and Function. The methods for in vitro osteoclast differentiation and bone resorption assay were previously described (36). Briefly, bone marrow cells cultured with 10 ng mL^{-1} M-CSF (R&D Systems) for 2 d were used as BMMs, which were further cultured with 50 ng mL^{-1} (unless otherwise indicated) of RANKL (Peprotech) in the presence of M-CSF (10 ng mL^{-1}) for 3 d. For the analysis of osteoclastogenesis in the *Zbtb7a*$^{Flox/FloxMx1cre+}$ cells, CD4^{-}CD8^{-}B220^{-} cells isolated using an AutoMACS cell separator were cultured in the presence of M-CSF for 2 d and used as BMMs. For the bone resorption assay, the osteoclasts generated on collagen-coated dishes were harvested 3 d after RANKL stimulation by trypsinization and cultured for 2 d on dentin slices (Wako) in the presence of indicated concentrations of RANKL. The resorbed areas were measured using an image analyzing software, ImageJ (NIH Image).

Statistical Analysis. Each series of experiments was repeated at least three times. All data are expressed as the mean ± SEM ($n = 5$). Statistical analysis was performed using Student's *t* test and ANOVA followed by a Bonferroni test when applicable.

Detailed procedures for the immunofluorescence staining, the retroviral gene transfer, immunoblot, and immunoprecipitation analyses, the quantitative PCR analysis, the flow cytometric analysis, the luciferase reporter gene assay, and the ChIP assay are described in *SI Materials and Methods*.

ACKNOWLEDGMENTS. We thank T. Kitamura and M. Matsumoto for kindly providing the retroviral vectors and Plat-E cells, and the reporter plasmid pCtsk-luc, respectively; and M. Shinohara, N. Komatsu, A. Terashima, T. Ando, Y. Kunisawa, Y. Ogihara, and A. Suematsu for discussion and technical assistance. This work was supported in part by a grant from Exploratory Research for Advanced Technology, Takayanagi Osteonetwork Project from Japan Science and Technology; a Grant-in-Aid for Scientific Research B; a Grant-in-Aid for Young Scientist A; a Grant-in-Aid for Challenging Exploratory Research from the Japan Society for the Promotion of Science; and a grant from the Global Center of Excellence Program from the Ministry of Education, Culture, Sports, Science and Technology of Japan.

1. Karsenty G, Wagner EF (2002) Reaching a genetic and molecular understanding of skeletal development. *Dev Cell* 2:389–406.
2. Teitelbaum SL, Ross FP (2003) Genetic regulation of osteoclast development and function. *Nat Rev Genet* 4:638–649.
3. Takayanagi H (2007) Osteoimmunology: Shared mechanisms and crosstalk between the immune and bone systems. *Nat Rev Immunol* 7:292–304.
4. Takayanagi H, et al. (2002) Induction and activation of the transcription factor NFATc1 (NFAT2) integrate RANKL signaling in terminal differentiation of osteoclasts. *Dev Cell* 3:889–901.
5. Matsumoto M, et al. (2004) Essential role of p38 mitogen-activated protein kinase in cathepsin K gene expression during osteoclastogenesis through association of NFATc1 and PU.1. *J Biol Chem* 279:45969–45979.
6. Song I, et al. (2009) Regulatory mechanism of NFATc1 in RANKL-induced osteoclast activation. *FEBS Lett* 583:2435–2440.
7. Asagiri M, et al. (2005) Autoamplification of NFATc1 expression determines its essential role in bone homeostasis. *J Exp Med* 202:1261–1269.
8. Negishi-Koga T, Takayanagi H (2009) Ca^{2+}-NFATc1 signaling is an essential axis of osteoclast differentiation. *Immunol Rev* 231:241–256.
9. Zhao B, et al. (2009) Interferon regulatory factor-8 regulates bone metabolism by suppressing osteoclastogenesis. *Nat Med* 15:1066–1071.
10. Kim K, et al. (2007) MafB negatively regulates RANKL-mediated osteoclast differentiation. *Blood* 109:3253–3259.
11. Miyauchi Y, et al. (2010) The Blimp1-Bcl6 axis is critical to regulate osteoclast differentiation and bone homeostasis. *J Exp Med* 207:751–762.
12. Davies JM, et al. (1999) Novel BTB/POZ domain zinc-finger protein, LRF, is a potential target of the *LAZ-3/BCL-6* oncogene. *Oncogene* 18:365–375.
13. Maeda T, Hobbs RM, Pandolfi PP (2005) The transcription factor *Pokemon*: A new key player in cancer pathogenesis. *Cancer Res* 65:8575–8578.
14. Maeda T, et al. (2005) Role of the proto-oncogene *Pokemon* in cellular transformation and *ARF* repression. *Nature* 433:278–285.
15. Apostolopoulou K, et al. (2007) Gene amplification is a relatively frequent event leading to *ZBTB7A* (*Pokemon*) overexpression in non-small cell lung cancer. *J Pathol* 213:294–302.
16. Aggarwal A, et al. (2010) Expression of leukemia/lymphoma-related factor (LRF/POKEMON) in human breast carcinoma and other cancers. *Exp Mol Pathol* 89:140–148.
17. Aggarwal H, et al. (2011) Expression of leukemia/lymphoma related factor (LRF/Pokemon) in human benign prostate hyperplasia and prostate cancer. *Exp Mol Pathol* 90:226–230.
18. Jiang L, et al. (2010) Overexpression of proto-oncogene FBI-1 activates membrane type 1-matrix metalloproteinase in association with adverse outcome in ovarian cancers. *Mol Cancer* 9:318.
19. Jeon BN, et al. (2008) Proto-oncogene FBI-1 (Pokemon/ZBTB7A) represses transcription of the tumor suppressor *Rb* gene via binding competition with Sp1 and recruitment of co-repressors. *J Biol Chem* 283:33199–33210.
20. Maeda T, et al. (2007) Regulation of B versus T lymphoid lineage fate decision by the proto-oncogene LRF. *Science* 316:860–866.
21. Maeda T, et al. (2009) LRF is an essential downstream target of GATA1 in erythroid development and regulates BIM-dependent apoptosis. *Dev Cell* 17:527–540.
22. Sakurai N, et al. (2011) The LRF transcription factor regulates mature B cell development and the germinal center response in mice. *J Clin Invest* 121:2583–2598.
23. Kukita A, et al. (1999) Osteoclast-derived zinc finger (*OCZF*) protein with POZ domain, a possible transcriptional repressor, is involved in osteoclastogenesis. *Blood* 94:1987–1997.
24. Kukita A, et al. (2011) The transcription factor FBI-1/OCZF/LRF is expressed in osteoclasts and regulates RANKL-induced osteoclast formation in vitro and in vivo. *Arthritis Rheum* 63:2744–2754.
25. Jacquin C, Gran DE, Lee SK, Lorenzo JA, Aguila HL (2006) Identification of multiple osteoclast precursor populations in murine bone marrow. *J Bone Miner Res* 21:67–77.
26. Akiyama T, et al. (2003) Regulation of osteoclast apoptosis by ubiquitylation of proapoptotic BH3-only Bcl-2 family member Bim. *EMBO J* 22:6653–6664.
27. Liu CJ, et al. (2004) Leukemia/lymphoma-related factor, a POZ domain-containing transcriptional repressor, interacts with histone deacetylase-1 and inhibits cartilage oligomeric matrix protein gene expression and chondrogenesis. *J Biol Chem* 279:47081–47091.
28. Yasui T, et al. (2011) Epigenetic regulation of osteoclast differentiation: possible involvement of Jmjd3 in the histone demethylation of *Nfatc1*. *J Bone Miner Res* 26:2665–2671.
29. Bai S, et al. (2008) NOTCH1 regulates osteoclastogenesis directly in osteoclast precursors and indirectly via osteoblast lineage cells. *J Biol Chem* 283:6509–6518.
30. Zu X, et al. (2011) Pro-oncogene *Pokemon* promotes breast cancer progression by upregulating *survivin* expression. *Breast Cancer Res* 13:R26.
31. Choi WI, et al. (2008) Proto-oncogene FBI-1 (Pokemon) and SREBP-1 synergistically activate transcription of fatty-acid synthase gene (FASN). *J Biol Chem* 283:29341–29354.
32. Nishikawa K, et al. (2010) Blimp1-mediated repression of negative regulators is required for osteoclast differentiation. *Proc Natl Acad Sci USA* 107:3117–3122.
33. Nakamura T, et al. (2007) Estrogen prevents bone loss via estrogen receptor α and induction of Fas ligand in osteoclasts. *Cell* 130:811–823.
34. Aliprantis AO, et al. (2008) NFATc1 in mice represses osteoprotegerin during osteoclastogenesis and dissociates systemic osteopenia from inflammation in cherubism. *J Clin Invest* 118:3775–3789.
35. Nishikawa K, et al. (2010) Maf promotes osteoblast differentiation in mice by mediating the age-related switch in mesenchymal cell differentiation. *J Clin Invest* 120:3455–3465.
36. Shinohara M, et al. (2008) Tyrosine kinases Btk and Tec regulate osteoclast differentiation by linking RANK and ITAM signals. *Cell* 132:794–806.

分子細胞機能学分野

森田 育男

医歯学総合研究科・顎顔面頸部機能再建学系専攻
分子細胞機能学・教授

1）研究の課題名

血管新生の制御機構の解明及び再生医療への応用

Optimized method for outgrowth endothelial progenitor cells in culture

血管新生は、多くの疾患と関係しているが、褥瘡、心筋梗塞、創傷治癒、バージャー病、閉塞性動脈硬化症などは、血管新生を促進することにより治療が可能となる病気であり、一方、固形腫瘍、関節リウマチ、動脈硬化、加齢黄斑変性、糖尿病性網膜症、炎症などは、血管新生を抑制することにより治癒、もしくは改善効果が得られる疾患である。一方、組織移植においては、移植された組織への酸素、栄養の供給のための血管新生が必須とされている。

しかし血管促進物質の全身投与によるガン増殖、転移の可能性や炎症の悪化の可能性、また組織移植への応用を考え、局所でのアプリケーションを行うため、印刷技術を応用した全く新しい概念のもとでの血管形成術を考案した。本方法により、自由なパターンの血管をin vitroで作成することが可能となり、この体外で作成した血管を生体内に移植し、血流改善効果が期待できるようになった。さらに、血管内皮細胞前駆細胞を臍帯血、抹消血から単離、増殖することが可能になった。

骨形成、骨吸収機構の解明

The effects of polyunsaturated fatty acids and their metabolites on osteoclastogenesis in vitro

骨代謝には骨形成と骨吸収のcouplingが必須であるが、これまでの研究は骨芽細胞による破骨細胞形成に焦点が当てられていた。しかし、骨のリモデリングを考えた場合、骨細胞―骨芽細胞のシグナルおよび、骨芽細胞―破骨細胞のシグナルが重要であることが考えられる。そこで、そのシグナルの解明を行っている。また、従来、当研究室では破骨細胞形成における接着分子の役割に関し多くの研究を行ってきたが、本年度はそれらに関しても研究を行い、脂肪酸が破骨細胞形成に与える影響について検討した。

炎症ならびに組織再生のメカニズム

The involvement of DNA and histone methylation in the repression of IL-1 β -induced MCP-1 production by hypoxia.

炎症局所や固形ガンの中心部における低酸素状態は、病態の進展に重要な各種サイトカイン・ケモカインの産生を調節している。しかし、これまでのサイトカインネットワークの構築に関する研究は通常の酸素分圧で行われており、炎症局所を反映していない。この低酸素下のケモカイン産生を担う転写因子はHIF-1だけでなく、NF-κBが重要な役割を果たしているが、我々はクロマチン構造そのものが低酸素における転写調節に重要であることをHDAC阻害剤を用いて明らかにしてきた。そこで、本研究では低酸素による種々のケモカイン産生の調節におけるケモカインのプロモータ領域へのNF-κB/HDACを含むタンパク複合体の結合の重要性を明らかにすることを目的としている。そこで、このタンパク複合体を同定するとともに、低酸素による変動を調べた。このことは、従来の概念とは異なる新しいタイプの抗炎症薬の開発に貢献できるものと期待している。

2）

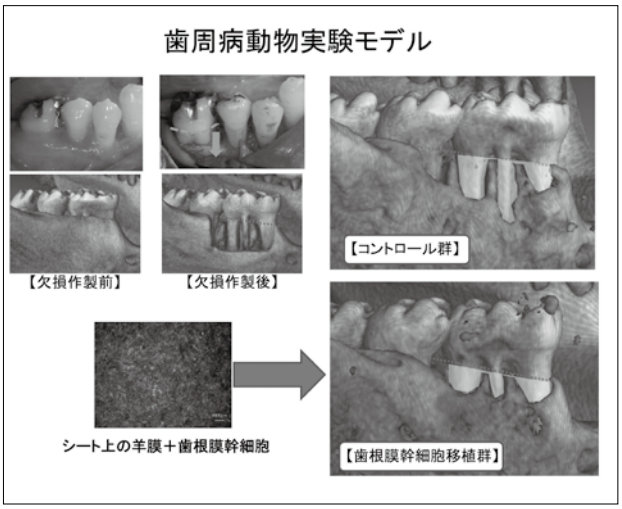

3）発表の研究内容についての英文要約

Optimized method for outgrowth endothelial progenitor cells in culture

Outgrowth endothelial progenitor cells（OECs）are expected to be useful for regenerative medicine as a source of blood vessel. However it has been studied intensively about their properties and functions, the feasibility of reliable acquirement remains unclear. This study was aimed to find out the optimized method to obtain OECs from human umbilical cord blood（hUCB）. We isolated mononuclear cells from hUCB and examined OEC colony formation rate（OEC-CFR）in various conditions based on following four points：1, cell density, 2, pre-selection of CD45 $^{(-)}$ cells, 3, culture medium and 4, influence of cryopreservation. OEC-CFR was 0.250 colony/ 5 × 107 CD45 $^{(-)}$ cells and dependent on the initial cell density. OEC-CFR of total mononuclear cells was about 0.347 colony/ 5 × 10^7 cells. This result suggested that pre-selection of CD45 $^{(-)}$ cells was not necessary to obtain OEC. Supplementation of EGM2-MV（endothelial basal medium-2）with culture medium caused to increase in OEC-CFR. Furthermore, we could obtain at least one colony from total mononuclear cells of each sample after cryopreservation, though OEC-CRF was decreased in compared to that from fresh cells. Flow cytometric analysis and immunocytochemistry showed that isolated OECs expressed CD31, CD34, CD73, CD146, CD144 and CD309. We confirmed tube formation of OEC on matrigel by confocal microscopy. In this study, we proposed the optimized method for isolation of OECs. This method can be useful for clinical use of OECs.

The effects of polyunsaturated fatty acids and their metabolites on osteoclastogenesis in vitro

Bone homeostasis is maintained by active remodeling through the balance between resorption（by osteoclasts）and synthesis（by osteoblasts）. In this study,weexamined the effects of polyunsaturated fatty acids（PUFAs）and their metabolites on sRANKL-induced differentiation of bone marrow-derived macrophages（BMMs）into osteoclasts in vitro. Docosahexaenoic acid（DHA）strongly inhibited osteoclastogenesis; however, dihomo--linolenic acid（DGLA）, arachidonic acid（AA）and eicosapentaenoic acid（EPA）enhanced it. The enhancement effect of PUFAs on osteoclastogenesis was mediated predominantly by cyclooxygenase（COX）products, because the effect was inhibited by a COX inhibitor. It was also found that COX products of PUFAs, prostaglandin E1, E2, and E3, clearly increased in osteoclastogenesis. The inhibitory effect of DHA on osteoclastogenesis was reversed by treatment with a lipoxygenase（LOX）inhibitor. Furthermore, resolvin D1, a LOX product of DHA, significantly inhibited osteoclastogenesis. Quantitative analysis of specific mRNA levels revealed that DHA-mediated attenuation of osteoclastogenesis might be due to a decrease in DC-STAMP expression. These results suggested that the effect of DHA on osteoclastogenesis is, at least in part, mediated by lipoxygenase products. This study showed a distinct mechanism of the effect of PUFAs on osteoclastogenesis and will provide evidence for therapeutic treatment with DHA in osteoporotic patients.

The involvement of DNA and histone methylation in the repression of IL-1 β -induced MCP-1 production by hypoxia.

Hypoxia is a microenvironmental pathophysiologic factor commonly associated with tumors and tissue inflammation. We previously reported that hypoxia repressed IL-1 β -induced monocyte chemoattractant protein-1（MCP-1）expression. The purpose of this study was to investigate the mechanisms involved in the repression of MCP-1 expression under hypoxia. Treatment of HeLa cells with 5-aza-dC, an inhibitor of DNA methylation, abolished the repression of IL-1 β -induced MCP-1 expression by hypoxia. A detailed study of the methylation of CpGs sites using bisulfite-sequencing PCR and 5-methylcytosine immunoprecipitation showed that hypoxia induced DNA methylation in both the enhancer and promoter regions of MCP-1in IL-1 β -treated cells. Next, we analyzed histone methylation within the MCP-1 promoter and enhancer regions. The level of H3K9 di-methylation, a mark of gene repression, in both promoter and enhancer regions was increased by hypoxia in IL-1 β -treated cells. Our findings suggest that changes in the methylation status of CpGs, as well as histone 3 methylation, may represent a critical event in transcriptional repression of IL-1 β -induced MCP-1 expression by hypoxia. Therefore, DNA methylation is associated with not only epigenetic gene silencing, but also with transient transcriptional repression.

4）本事業に関連して世界的な研究拠点形成に向けて、以下の点で改善・整備等されたこと

A（研究拠点体制）

大学として、研究拠点となるべく、研究と産学連携を一体化して推進できるよう、研究・産学連携機構を構築した。

B（研究教育環境）

バイオリソースの将来利用を可能とする包括同意の仕組みや個人情報・遺伝情報の保護と管理の体制などを早急に整備し、安全性を担保した盤石の体制でバイオリソースの物理的資源とファーマコゲノミクス情報を含む医療情報データベースを統合化した医療イノベーション推進のインフラの構築のため、疾患バイオリソースセンターを設立した。

C（人材確保）

若手の優秀な研究者・教育者を確保する目的で、テニュアトラック制を導入し、国際公募により、優秀な人員を確保した。

D（人材育成）

大学院改革を推進し、医歯学総合研究科と生命情報科学教育部を統合し、医歯学総合研究科医歯科学専攻、生命理工学専攻に改編した。本改革に伴い各専攻の学位授与方針等を議論し直し、博士課程の医歯学系においては、世界の第一線で活躍し得る研究者・指導者を養成すること、生命理工系においては高い専門性と倫理観を有し次世代の同分野の人材育成に貢献できる者、先端的技術開発を通して、医療・バイオ産業界の発展に貢献できる者等を養成することとした。本研究科はこれらの能力を修得した者に対して学位を授与することを学生のみならず、社会に対しても明確に示していくこととしている。

5）英文原著論

1. Kakutani S, Ishikura Y, Tateishi N, Horikawa C, Tokuda H, Kontani M, Kawashima H, Sakakibara Y, Kiso Y, Shibata H, Morita I. Supplementation of arachidonic acid-enriched oil increases arachidonic acid contents in plasma phospholipids, but does not increase their metabolites and clinical parameters in Japanese healthy elderly individuals：a randomized controlled study. Lipids Health Dis. 10（1）：241, 2011
2. ◎Aoi Y, Nakahama KI, Morita I, Safronova O.　The involvement of DNA and histone methylation in the repression of IL-1 β -induced MCP-1 production by hypoxia.　Biochem. Biophys.Res.Commun 414, 252-258, 2011
3. Kato K, Morita I. Acidosis environment promotes osteoclast formation by acting on the last phase of preosteoclast differentiation：A study to elucidate the action points of acidosis and search for putative target molecules. Eur J Pharmacol, 663（1-3）：27-39, 2011
4. Moriyama M, Ohno-Matsui K, Hayashi K, Shimada N, Yoshida T, Tokoro T, Morita I. Topographic Analyses of Shape of Eyes with Pathologic Myopia by High-Resolution Three-Dimensional　Magnetic Resonance Imaging.　Ophthalmology, 118（8）：1626-37, 2011
5. Wang J, Ohno-Matsui K, Nakahama KI, Okamoto A, Yoshida T, Shimada N, Mochizuki M, Morita I. Amyloid β Enhances Migration of Endothelial Progenitor Cells by Upregulating CX3CR1 in Response to Fractalkine, Which May Be Associated With Development of Choroidal Neovascularization.　Arterioscler Thromb Vasc Biol. 31（7）：e11-18, 2011
6. ◎Tsugawa J, Komaki M, Yoshida T, Nakahama K, Amagasa T, Morita I., Cell-printing and transfer technology applications for bone defects in mice.　J Tissue Eng Regen Med　5（9）：695-703, 2011
7. ◎Shirakihara T, Horiguchi K, Miyazawa K, Ehata E, Shibata T, Morita I, Miyazono K, Saitoh M. TGF-b regulates isoform switching of FGF receptors and epithelial-mesenchymal transition. EMBO J 30（4）：783-789, 2011
8. Nakamura M, Soya T, Hiratai R, Nagai A, Hashimoto K, Morita I, Yamashita K. .Endothelial cell migration and morphogenesis on silk fibroin scaffolds containing hydroxyapatite electret. J Biomed Mater Res A.（In press）
9. ◎Komaki M, Iwasaki K, Arzate H, Sampath Narayanan A, Izumi Y, Morita I.　Cementum protein 1（CEMP1）induces a cementoblastic phenotype and reduces osteoblastic differentiation in periodontal ligament cells. J Cell Physiol. in press

6）総説ならびに著書

1. 山口　朗、森田育男.研究水準　概観.我が国における歯科医学の現状と国際比較2010年度版.先端歯学国際教育ネットワーク、歯学連携ネットワークを活用した口腔からQOL向上を目指す研究. 10頁.新潟大学.2011年
2. 森田育男　血管生物学辞典（監修：佐藤靖史、森田育男、高倉伸幸、小室一成）アラキドンサン代謝物、103～105、2011
3. 森田育男　血管生物学辞典（監修：佐藤靖史、森田育男、高倉伸幸、小室一成）血管再建、178～179、2011

7）特許取得、特許申請

カナダ

特許出願番号：2541513
特許第2541513
特許出願日：2004年10月15日
特許承認日：2011年2月1日
特許の名称：人工細胞組織の作成方法、及びそのための基材
発明者：　森田育男、中村真人、三宅秀之、服部秀志、小林弘典、栗原正彰
特許出願人：大日本印刷

日　本

特許　第4836355
特許承認日：平成23年11月18日
発名の名称：細胞含有シート
発明者：森田育男、小林暁子、服部秀志、黒田正敏

特許出願人：東京医科歯科大学、大日本印刷

8）平成23年度までの自己評価

研究担当理事として、本学の研究環境の整備、人材育成、組織改革に取り組んできた。その中で、本G-COEに関しても、若手育成の立場から、特にシャペロン教員に対し、知的財産の講義、キャリアパスなどをともに考えてきた。その意味から、自分としては、高い評価をしている。

9）学会発表（英文）

1. Safronova O, Morita I. Hypoxia represses mRNA synthesis via HDAC3 sependent inhibition of P-TEFr elongation complex activity. DAVOS CONGRESS, OXYGEN-Hypoxia Research Conference Davos 2010, January 8-12, 2011
2. Akiyama M, Nakahama K, Li X, Takeda S, Morita I. Involvement of adhesion molecules in osteoclastogenesis. 穐山雅子、李　香蘭、竹田　省、中浜健一、森田育男.破骨細胞分化における接着分子の関与.第84回日本生化学会.京都.2011年9月21～24日
3. Oshima-Sudo N, Yoshida T, Akahori T, Komaki M, Nakahama K, Abe M, Morita I. Vascular regeneration using cell-printing system. Symposium56 Nanobiotchnology in vascular medicine, The 19th Annual Meeting of the Japanese Vascular Biology and Medicine Organization, The 1st Asia-Pacific Vascular Biology Meeting, Tokyo, December 8-10, 2011
4. Safronova O, Morita I. Hypoxia inhibits P-TEFb elongation complex by HDAC3-dependent deacetylation of Cdk9 and Cyclin T1. 2-c）function of Molecules and complexes/分子・複合体の機能、Transcription/転写.第34回日本分子生物学会年会.2011年12月13～16日

10）学会発表（和文）

須藤乃里子、久保田俊郎、森田育男.臍帯血と臍帯由来細胞を利用した生体外における毛細血管の作成.優秀演題賞候補プログラム.第63回日本産婦人科学会学術講演会.大阪.2011年8月29～31日

11）外部資金の獲得状況

科学研究費補助金、挑戦的萌芽研究

研究題目：組織細胞工学を用いた細胞多層化および血管導入法の開発と応用
代表：森田育男
分担：中浜健一、小牧基浩
期間：H22-23
研究費総額：280万円

科学研究費補助金、基盤研究（A）

代表：秋吉一成
分担：森田育男
研究題目：ナノゲルを基盤とした新規ドラッグデリバリーシステムの開発
期間：H22～H24

科学研究費補助金、基盤研究（C）

代表：安部まゆみ
分担：森田育男
研究題目：核蛋白ピグペンの血管新生促進作用の機序の解明と血管新生制御への応用
期間：H23-24
研究費総額：180万円

科学研究費補助金、基盤研究（C）

代表：穐山雅子
分担：森田育男、中浜健一
研究題目：ドコサヘキサエン酸による破骨細胞分化抑制機序の解明
期間：H23-25
研究費総額：390万円

科学研究費補助金、挑戦的萌芽研究

代表：大野京子
分担：森田育男
研究題目：アミロイドβを標的とした加齢黄斑変性・緑内障の早期診断・治療に向けた新規戦略法

科学研究費補助金、基盤研究（C）

代表：久保田俊朗
分担：森田育男
研究題目：自己組織を利用した欠損組織修復と血流回復を目指した新規新生児外科治療戦略
期間：H22～H24

科学研究費補助金、基盤研究（B）

代表：大野京子
分担：森田育男
研究題目：加齢黄斑変性発症の四次元時空的解明と分子標的治療の確立
期間：H22～H24

12）特別講演、招待講演、シンポジウム

1. 森田育男（副学長、理事・研究担当）.講演.脂質メディエーターの生理作用.サントリー（株）.東京.2011年2月16日
2. 森田育男.座長.シンポジウム4.血管新生.第32回日本炎症・再生医学会、合同開催：1st Meeting of Asian

Federation of Inflammation and Regeneration：APFIR2011.京都.2011年6月2～3日

3. 森田育男、須藤乃里子、吉田　朋子、小牧　基浩、中浜　健一、安部まゆみ.新規血管再生法に用いるヒト血管内皮前駆細胞、血管内皮細胞、平滑筋細胞の単離・培養法及び性質について.シンポジウム4.血管新生.第32回日本炎症・再生医学会、合同開催：1st Meeting of Asian Federation of Inflammation and Regeneration：APFIR2011.京都.2011年6月2～3日
4. 森田育男、森尾郁子、川口陽子.口演.歯科医学における大学院教育改善への取り組みとその評価.口演発表1　卒前専門基礎教育、卒前臨床実習、大学院教育（シミュレーション教育、歯科医学研究、歯科医療・口腔ケア・ヘルスプロモーション）.第30回歯科医学教育学会総会・学術大会および記念大会.東京.2011年7月15～17日
5. 森田育男.講演.基礎・臨床融合型教育を目指して.
   須藤乃里子.講演.分娩廃棄物を利用した再生医療-臨床から基礎研究へ、そして臨床応用に向けて.
   学術活性化委員会企画　トランスレーショナルリサーチの重要性.第63回日本産科婦人科学会学術講演会.大阪.2011年8月30日
6. 森田育男.特別講演.眼疾患治療の基礎的研究.ネバナックR懸濁性点眼液0.1%発売記念学術講演会in大阪.大阪.2011年9月18日

13）主催学会

The 1st Asia Pacific Vascular Biology Meeting 2011
12/8～10, Tokyo

14）教室、分野や講座の准教授、講師、助教、特別研究員、ポスドク、指導を受けた大学院生の名前

教　授　森田　育男
准教授　中浜　健一
助　教　加藤　幸太郎
特任助教　穐山　雅子
非常勤講師　藤田　浩（都立墨東病院・輸血科）
長谷（徳島）　貴子
安部　まゆみ（上武大学・看護学部）
大学院生　青井　陽子（～3月）
○Praween Wayakanon
渡辺　毅
派遣大学院生　王　紀英（眼科学）
島田典明（眼科学）
滝　敦子
（発達病態小児科学）（～3月）
須藤（大島）　乃里子
（生殖機能協関学）（～3月）
橋田　之彦（顎顔面外科）（4月～）
高宅　花織
（インプラント・口腔再生医学）
（4月～）
秦野　雄（循環器制御内科学）
（4月～）
本多　泉（生殖機能協関学）
（4月～）
許　博文（先端倫理医科学開発学）
（4月～）
特別研究学生　李　香蘭（順天堂大学）
輿石　太郎（順天堂大学）（～3月）
修　士　星野　優子
武田　真樹
卒論生　鈴木　南美（口腔保健学科）（～3月）
事務補佐員　吉田　美登里

GCOE

特任教員　Olga Safronova
SS大学院生　青井陽子（～3月）
須藤乃里子（～3月）
長岡亮介（～3月）
○Praween Wayakanon（4月～）

寄付講座　ナノメディスン（DNP）

准教授　小牧　基浩
助　教　岩崎　剣吾
研究員　田中　裕一
研究員　横山　尚毅
派遣大学院生　木村　康之（歯周病学）

○はAISS

Amyloid β Enhances Migration of Endothelial Progenitor Cells by Upregulating CX3CR1 in Response to Fractalkine, Which May Be Associated With Development of Choroidal Neovascularization

Jiying Wang, Kyoko Ohno-Matsui, Ken-ichi Nakahama, Aikou Okamoto, Takeshi Yoshida, Noriaki Shimada, Manabu Mochizuki, Ikuo Morita

Objective—Deposits that accumulate beneath retinal pigment epithelium, called drusen, are early signs of age-related macular degeneration (AMD). We have shown that amyloid β (Aβ) is present in drusen, and Aβ may be involved in AMD development. We have also shown that endothelial progenitor cells (EPCs) may contribute to the development of choroidal neovascularization (CNV). Thus, the purpose of this study was to investigate the role played by CX3CR1, a chemokine receptor, in EPC migration and CNV formation.

Methods and Results—EPCs collected from human umbilical cords were found to express higher levels of CX3CR1 than human umbilical vein endothelial cells, and exposure of EPCs to Aβ caused further upregulation of CX3CR1. This upregulation was decreased by blocking fractalkine, a ligand of CX3CR1. Exposure of EPCs to fractalkine increased their migration, but pretreatment with Aβ enhanced the migration. The fractalkine-induced EPC migration was more inhibited by EPCs derived from $CX3CR1^{-/-}$ mice than wild-type mice. The area of laser-induced CNV was significantly smaller in wild-type mice that received bone marrow transplantation from $CX3CR1^{-/-}$ mice than in those that received transplantation from wild-type mice.

Conclusion—These data suggest that Aβ enhances EPC migration through the upregulation of CX3CR1. This upregulation might play a role in development of CNV. **(*Arterioscler Thromb Vasc Biol*. 2011;31:e11-e18.)**

Key Words: angiogenesis ■ cell physiology ■ vascular biology ■ age-related macular degeneration ■ endothelial progenitor cells

Age-related macular degeneration (AMD) is the leading cause of irreversible vision decrease in the elderly worldwide.[1–4] The decrease of vision results from geographical atrophy or choroidal neovascularization (CNV) in the macula of the eye. During the development of CNV, new vessels develop from the choroidal vessels and penetrate the thick matrix of the Bruch membrane and pass into the avascular subretinal space.

Among the earliest signs of AMD are subretinal extracellular deposits, known as drusen, which accumulate beneath the retinal pigment epithelium (RPE).[5] Epidemiological studies have shown that the presence of many discrete or confluent drusen significantly increases the risk of developing CNV.[6,7]

We have found that amyloid β (Aβ) peptides are present in drusen, and we have suggested that their presence is the primary stimulus for the development of AMD.[8] The Aβ peptides vary in length from 39 to 43 amino acid residues and are produced by the sequential proteolytic processing of precursors of amyloid proteins.[9] Interestingly, Aβ is the main component of the senile plaques found in the brains of Alzheimer's patients.[9–11] The results of our study on senescent neprilysin gene-disrupted mice that lack the Aβ-degrading enzyme showed that there was a significant increase in the deposition of Aβ in the subretinal space.[8] This is relevant to this study because these mice developed several characteristics of human eyes at the early stage AMD, although they did not develop CNV spontaneously.

The exact mechanism of how CNV develop from drusen has not been determined. The results of recent studies have provided evidence that endothelial progenitor cells (EPCs) may be major contributors to the development of CNV.[12–17] For example, experiments on laser-induced CNV in chimeric C57Bl/6 mice with bone marrow transplantation from green

Received on: August 31, 2010; final version accepted on: April 18, 2011.

From the Department of Ophthalmology and Visual Science (J.W., K.O.-M., T.Y., N.S., M.M.) and Section of Cellular Physiological Chemistry (K.-i.N., I.M.), Tokyo Medical and Dental University, Tokyo, Japan; Department of Obstetrics and Gynecology, Jikei University School of Medicine, Tokyo, Japan (A.O.).

Drs Wang and Ohno-Matsui contributed equally to this work.

Correspondence to Kyoko Ohno-Matsui, MD, Department of Ophthalmology and Visual Science, Tokyo Medical and Dental University, 1-5-45 Yushima, Bunkyo-ku, Tokyo 113, Japan. E-mail k.ohno.oph@tmd.ac.jp

© 2011 American Heart Association, Inc.

Arterioscler Thromb Vasc Biol **is available at http://atvb.ahajournals.org** **DOI: 10.1161/ATVBAHA.110.215517**

Downloaded from http://atvb.ahajournals.org/ at TOKYO IKA SHIKA UNIV LIB on March 19, 2012

fluorescent protein–transgenic mice showed that 50% to 60% of the endothelial cells of the CNV were green fluorescent protein positive.[14] In addition, cells expressing the EPC marker AC133 were present in surgically excised CNV of human patients.[17] EPCs are considered to play significant roles in neovascularization elsewhere, such as in the hindlimb ischemia model in mice, by enhancing invasion of blood vessels into the matrix through the expression of protease cathepsin L.[18]

EPCs were first described by Asahara et al in 1997,[19] and recent studies have shown that the capacity of EPCs to invade into the matrix was higher than that of mature endothelial cells.[18,20] Basire et al[21] reported that EPCs express higher levels of urokinase-type plasminogen activator and its receptor than human umbilical vein endothelial cells (HUVECs). In addition, Urbich et al[18] reported that protease cathepsin L is expressed more strongly in EPCs than in mature endothelial cells, and cathepsin L is essential for matrix degradation and invasion by EPCs in vitro. We have recently shown that the cathepsin L expressed by EPCs is critical for the development of CNV in a mouse model of CNV.[22]

The migration of EPCs into the subretinal space requires their mobilization from the bone marrow into the bloodstream and subsequent recruitment from the choroidal circulation into the subretinal space. Although the molecular pathways leading to the mobilization of EPCs from the bone marrow are not fully known, earlier studies demonstrated that several humoral factors, such as vascular endothelial growth factor,[23,24] erythropoietin,[25] adiponectin,[23] and stromal cell–derived factor-1α[26] trigger the release of EPCs. It is known that the factors that contribute to the recruitment of EPCs are different for different diseases.[27]

CX3CR1 is a pertussis toxin–sensitive 7-transmembrane G protein-coupled receptor expressed on human natural killer cells, monocytes, Th1 $CD4^+$ cells, $CD8^+$ T cells, mast cells,[28] and lymphoid organ-derived endothelial cells.[29] Fractalkine, also designated CX3CL1, is the sole ligand of CX3CR1,[30] and the secreted form of fractalkine has potent chemotactic activity. You et al[31] reported that bovine retinal capillary endothelial cells express both fractalkine and CX3CR1. Immunostaining of human retinal tissue showed that the expression of fractalkine was strong in Müller glial cells, ganglion cells, and RPE.[32] In addition, an intravitreous injection of antifractalkine antibody decreased the retinal angiogenesis in the oxygen-induced retinopathy model,[31] suggesting that CX3CR1 and fractalkine play important roles in ocular angiogenesis.

Recent studies[33–36] have shown an association between the sequence variation/expression of CX3CR1 and AMD. Combadière et al[34] demonstrated that retinal microglia express CX3CR1 and that an impairment of cell migration caused by CX3CR1 polymorphisms increases the risk of AMD. They suggested that the CX3CR1-dependent accumulation of subretinal microglia evoked cardinal features of AMD and also suggested a role of microglial cells in the pathogenesis of AMD. However, the role played by CX3CR1 in the migration of EPCs has not been examined.

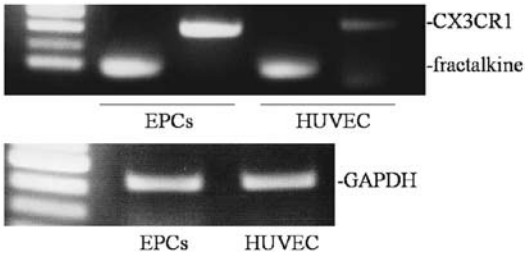

Figure 1. Real-time PCR to determine whether fractalkine and CX3CR1 are expressed in cultured human RPE cells, HUVECs, and EPCs. The cDNAs were synthesized from 2 μg of total RNA, and the reaction products were subjected to PCR amplification (35 cycles) with specific primers for human fractalkine and CX3CR1. Product sizes of amplified products were 68 bp for fractalkine and 163 bp for CX3CR1. GAPDH was used as an internal control.

Thus, the purpose of this study was to investigate what role CX3CR1 plays in the migration of EPCs and subsequent CNV formation.

Materials and Methods

EPCs were isolated from human cord blood or mouse abdominal artery blood. The expression of CX3CR1 was measured by immunocytochemistry, quantitative real-time polymerase chain reaction (PCR), and Western blot. EPC migration was examined using a modified Boyden chamber assay. Laser-induced CNV areas were compared between wild-type mice that received bone marrow transplantation from wild-type mice and those that received transplantation from $CX3CR1^{-/-}$ mice. Total cell numbers of leukocytes and EPCs in abdominal artery blood were compared between wild-type mice and $CX3CR1^{-/-}$ mice. The proliferative capacities of wild-type mice- and $CX3CR1^{-/-}$ mice-derived EPCs were also examined. Detailed materials and methods are given in the Supplemental Data, available online at http://atvb.ahajournals.org.

Results

CX3CR1 Expression Is Constitutively Higher in EPCs Than in HUVECs

The results of PCR demonstrated that the mRNAs of fractalkine and CX3CR1 were constitutively expressed in EPCs and in HUVECs (Figure 1). PCR also showed that the expression of the mRNA of CX3CR1 by EPCs was 46.7±6.5 times higher than its expression by HUVECs (Figure 2A). Fluorescence microscopy revealed that the proteins of CX3CR1 were expressed in both EPCs and HUVECs (Figure 2B). Consistent with the PCR results, the fluorescence intensity of CX3CR1 was markedly higher in EPCs than in HUVECs (Figure 2B).

Exposure to Aβ_{1-40}, Tumor Necrosis Factor-α, Interleukin-1β, and Fractalkine Upregulates CX3CR1 Expression in EPCs and HUVECs

Earlier studies showed that proinflammatory cytokines upregulate the CX3CR1 gene expression in HUVECs,[37] but there have been no reports of the expression and regulation of the CX3CR1 gene in EPCs. The PCR results showed that stimulation by Aβ_{1-40}, tumor necrosis

Downloaded from http://atvb.ahajournals.org/ at TOKYO IKA SHIKA UNIV LIB on March 19, 2012

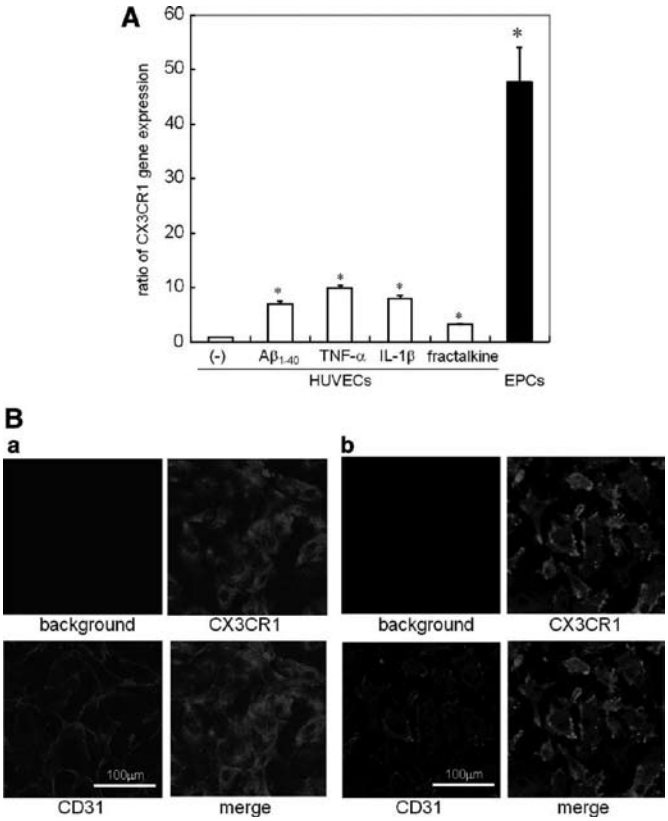

Figure 2. Expression of the mRNA of CX3CR1 in HUVECs and effect of $A\beta_{1-40}$, fractalkine, and pro-inflammatory cytokines. A, Real-time PCR analysis of the cDNA of CX3CR1 prepared from RNA isolated from HUVECs and EPCs in the presence or absence of $A\beta_{1-40}$ peptide (HCl form; 25 μmol/L), TNF-α (10 ng/mL), IL-1β (10 ng/mL), and fractalkine (100 ng/mL) for 24 hours. The levels of the mRNA of treated HUVECs and nontreated EPCs are shown as a ratio to that of nontreated HUVECs, and the average of 3 samples (±SEMs) are plotted. Data are from 5 independent experiments. *$P<0.05$ vs nontreated HUVECs. B, Immunostaining for CD31 (red) and CX3CR1 (green) in cultured EPCs and HUVECs. Left (a), HUVECs. Right (b), EPCs. Scale bars=100 μm.

factor-α (TNF-α), interleukin-1β (IL-1β), or fractalkine induced a significant increase in the expression of CX3CR1 in HUVECs (Figure 2A). However, the mRNA levels of the CX3CR1 gene in treated HUVECs were much lower than CX3CR1 mRNA levels of EPCs without any stimuli (Figure 2A). Also, $A\beta_{1-40}$, TNF-α, IL-1β, and fractalkine caused a significant increase in the expression of CX3CR1 mRNA in EPCs (Figure 3). Western blot analysis showed an increase in the synthesis of the CX3CR1 protein in human EPCs treated with $A\beta_{1-40}$, TNF-α, IL-1β, or fractalkine compared with nontreated EPCs (Supplemental Figure I).

Neutralization of TNF-α, IL-1β, and Fractalkine Partially Blocks $A\beta_{1-40}$-Induced CX3CR1 Upregulation in EPCs

To determine whether the $A\beta_{1-40}$-induced CX3CR1 upregulation in EPCs is regulated by TNF-α, IL-1β, or fractalkine, we examined the change in the level of the mRNA of CX3CR1 when EPCs were treated with neutralizing antibodies against TNF-α, IL-1β, or fractalkine by PCR. $A\beta_{1-40}$ induced a 2.66±0.05-fold increase of CX3CR1 mRNA expression compared with nontreated EPCs, whereas its reverse peptide $A\beta_{40-1}$ (the same amino acids but in reverse sequence) had no effect (Figure 3).

After confirming that the upregulation of CX3CR1 mRNA by TNF-α, IL-1β, or fractalkine was completely blocked by the addition of the neutralizing antibodies, we examined whether the neutralization of these factors affected the expression of the mRNA of CX3CR1 in EPCs. Neutralization of TNF-α, IL-1β, or fractalkine significantly reduced the $A\beta_{1-40}$-induced upregulation of CX3CR1 mRNA to 1.87±0.11-fold, 2.09±0.08-fold, and 2.11±0.27-fold that of the nontreated control cells, respectively. Combined neutralization of TNF-α, IL-1β, or fractalkine significantly reduced $A\beta_{1-40}$-induced CX3CR1 upregulation; however, it did not completely block the upregulation to the level of nontreated controls (still 1.45±0.12-fold that of nontreated control cells).

$A\beta_{1-40}$ Enhances Fractalkine-Induced Migration of EPCs

CX3CR1 has been shown to be associated with both the migration and adhesion of leukocytes in response to fractalkine.[28] Thus, the high expression of CX3CR1 in EPCs and the further upregulation by Aβ suggest the possibility that EPC migration may be mediated by CX3CR1. Cell migration analyses using Boyden chamber assays showed that fractalkine induced a migration of human EPCs in a dose-dependent manner. The pretreatment of EPCs with $A\beta_{1-40}$ significantly enhanced fractalkine-induced migration of EPCs, whereas $A\beta_{40-1}$ had no effect (Figure 4A).

Downloaded from http://atvb.ahajournals.org/ at TOKYO IKA SHIKA UNIV LIB on March 19, 2012

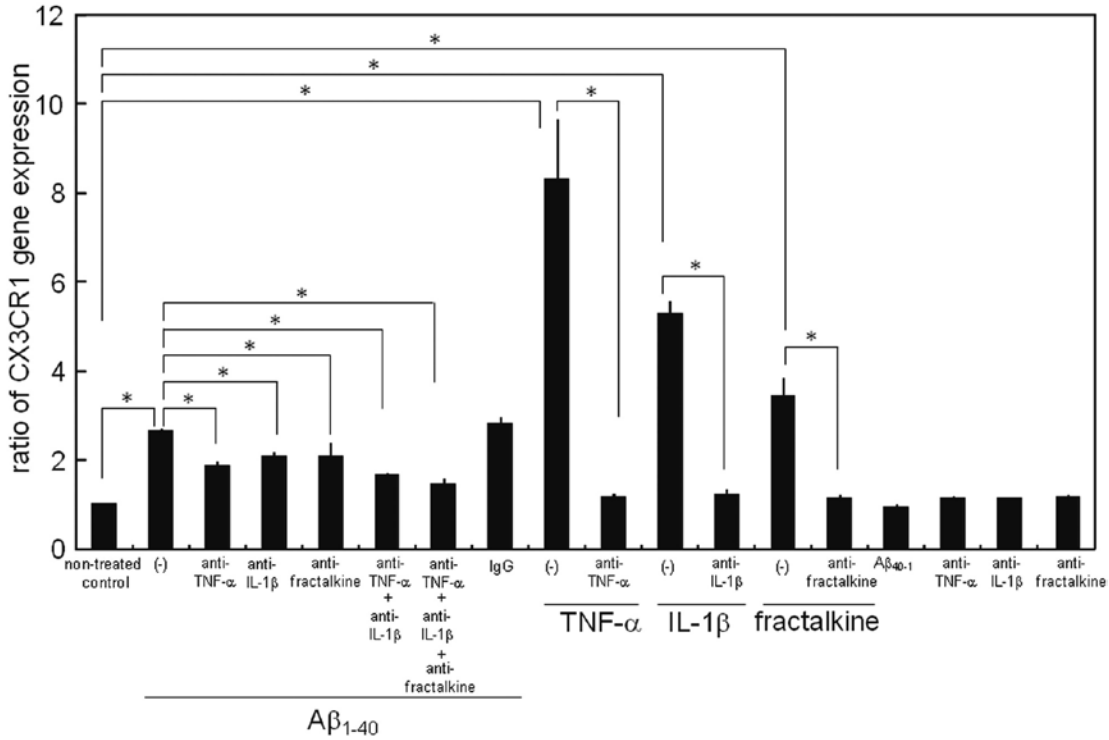

Figure 3. Expression of the CX3CR1 mRNA in EPCs is increased by $A\beta_{1-40}$, fractalkine and proinflammatory cytokines, and the effects of neutralizing antibodies. EPCs were stimulated with 25 μmol/L $A\beta_{1-40}$ peptide (HCl form; 25 μmol/L), IL-1β (10 ng/mL), TNF-α (10 ng/mL), or fractalkine (100 ng/mL) for 24 hours. In some experiments, neutralizing antibodies against human IL-1β (10 μg/mL), TNF-α (1 μg/mL), fractalkine (20 μg/mL), or normal goat IgG (2.5 μg/mL) were also used. The average of 3 samples±SEMs is plotted. *$P<0.05$. Data are from 5 independent experiments.

Fractalkine-Induced Cellular Migration Is Abolished in EPCs Derived From CX3CR1$^{-/-}$ Mice

EPCs derived from CX3CR1$^{-/-}$ mice and wild-type mice were also used in Boyden chamber assays to investigate the role of CX3CR1 in EPC migration. Our results showed that mouse recombinant fractalkine induced the migration of EPCs derived from wild-type mice in a dose-dependent manner, and pretreatment with $A\beta_{1-40}$ significantly enhanced the migration as shown in human EPCs. However, no obvious cell migration or enhancement of migration by $A\beta_{1-40}$ pretreatment was detected in EPCs derived from CX3CR1$^{-/-}$ mice even after stimulation by 200 ng/mL fractalkine (Figure 4B). In contrast, IL-1β, another well-known stimulator of migration of monocytes, was capable of inducing migration of EPCs derived from both wild-type mice and CX3CR1$^{-/-}$ mice (Supplemental Figure II).

Transplantation of CX3CR1$^{-/-}$ Mouse-Derived Bone Marrow Cells Inhibits CNV

To determine the contribution of CX3CR1 from bone marrow–derived cells to the development of CNV, we transplanted bone marrow cells from CX3CR1$^{-/-}$ mice or wild-type mice into wild-type mice as described.[22] One month after the transplantation, a laser-induced CNV was produced. Seven days after laser irradiation, the CNV area in wild-type mice that received bone marrow transplantation from CX3CR1$^{-/-}$ mice was significantly smaller ($1.44\pm0.23\times10^4$ μm^2) than that of wild-type mice that received a bone marrow transplantation from wild-type mice ($8.84\pm1.36\times10^4$ μm^2; $P<0.0001$, Figure 5 and Supplemental Figure III).

CX3CR1 Deficiency Does Not Affect Homing of Bone Marrow–Derived Cells

We compared the numbers of leukocytes and EPCs in wild-type and CX3CR1$^{-/-}$ mice. The results showed that there was no significant difference in the number of leukocytes between CX3CR1$^{-/-}$ mice ($1.61\pm0.13\times10^7$/mL; n=3) and age-matched wild-type mice ($1.55\pm0.30\times10^7$/mL; n=3; $P=0.753$, Supplemental Figure IVA). Also, there was no significant difference in the number of EPCs in the peripheral blood between CX3CR1$^{-/-}$ mice (1272±280/mL; n=3) and wild-type mice (1363±532/mL; n=3; $P=0.8065$, Supplemental Figure IVB).

Fractalkine or $A\beta_{1-40}$ Does Not Affect Proliferation of EPCs

Finally, we examined whether $A\beta_{1-40}$ or fractalkine/CX3CR1 signaling affected the proliferative potential of

Downloaded from http://atvb.ahajournals.org/ at TOKYO IKA SHIKA UNIV LIB on March 19, 2012

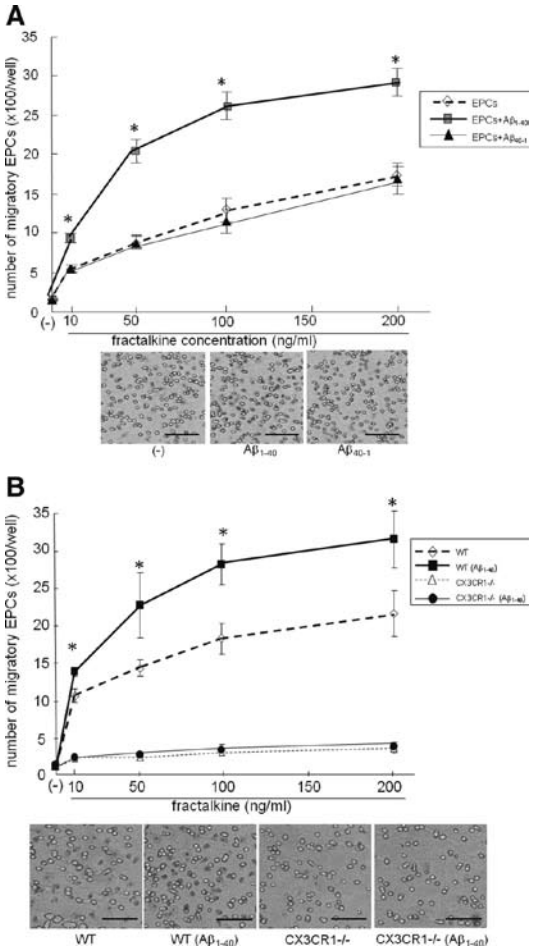

Figure 4. A, Effects of Aβ_{1-40} pretreatment on fractalkine-mediated migration of EPCs. Isolated EPCs that had been cultured in serum-free medium supplemented with or without Aβ_{1-40} (25 μmol/L) or Aβ_{40-1} (25 μmol/L) for 16 hours were harvested, washed, resuspended in 1% fetal calf serum (FCS, HyClone, Utah) EBM-2 medium (2×10^5 cell/mL suspensions). Cells were then placed on a polycarbonate membrane (8-μm pore size) in a modified Boyden chamber and were exposed for 6 hours to migratory stimulus in the lower chamber (10 to 200 ng/mL of fractalkine supplemented with 1% FCS EBM-2 medium). At the end of treatment, cells on the lower part of the membrane were stained with hematoxylin and counted. Data represent means±SDs for duplicate samples (upper panel). Dotted line shows the migration of EPCs without pretreatment. The bold line shows the migration of EPCs that were pretreated with Aβ_{1-40}, and the thin line shows the migration of EPCs pretreated with Aβ_{40-1}. Each condition was examined at least 6 times, and the experiments were repeated at least 3 times. *$P<0.05$ vs nontreated EPCs. Lower panels show representative images of migrated cells in the Boyden chamber assay by fluorescence digital microscopy (KEYENCE VB6000, Olympus, Tokyo). Scale bars=500 μm. B, Effects of Aβ pretreatment on fractalkine-induced cell migration in EPCs derived from CX3CR1$^{-/-}$ mice and wild-type mice (WT). Isolated EPCs from CX3CR1$^{-/-}$ mice and wild-type mice that had been cultured in serum-free medium supplemented with or without Aβ_{1-40} (25 μmol/L) or Aβ_{40-1} (25 μmol/L) for 16 hours were harvested, washed, and resuspended in 1% FCS EBM-2 medium (2×10^5 cell/mL suspensions). EPCs were then placed on a polycarbonate membrane (8-μm pore size) in a modified Boyden chamber and were exposed for 6 hours to migratory stimulus in the lower chamber (10 to 200 ng/mL of fractalkine supplemented with 1% FCS EBM-2 medium). The thin line shows the migration of EPCs derived from CX3CR1$^{-/-}$ mice that were pretreated with Aβ_{40-1}, and the thin dotted line shows the migration of EPCs from CX3CR1$^{-/-}$ mice without pretreatment. The bold line shows the migration of EPCs from wild-type mice that were pretreated with Aβ_{1-40}, and the bold dotted line shows the migration of EPCs from wild-type mice without pretreatment. Each condition was examined 6 times, and the experiments were repeated at least 3 times. *$P<0.05$ vs EPCs without Aβ_{1-40} treatment. Lower panels show representative images of migrated cells in the Boyden chamber assay by fluorescence digital microscopy (KEYENCE VB6000). Scale bars=500 μm.

EPCs (Supplemental Figure IVC). There was no significant difference in the number of EPCs among nontreated cells (1153±245; n=3), fractalkine-treated cells (1151±274; n=3), Aβ_{1-40} treated cells (1149±152; n=3), and cells treated with both Aβ_{1-40} and fractalkine (1155±202; n=3).

Discussion

Our results showed that EPCs expressed levels of CX3CR1 that were 46.7 times higher than those of HUVECs, and exposure to Aβ_{1-40} caused a further upregulation of CX3CR1 in EPCs. Because CX3CR1 is involved in the migration of various kinds of cells, including leukocytes,[28,38] monocytes/macrophages,[39] and lymphocytes,[40] we hypothesized that EPCs have a much higher potential to stimulate migratory activity than mature endothelial cells. In addition, we hypothesized that Aβ_{1-40} will enhance this activity. To the best of our knowledge, a regulation of the CX3CR1 expression in EPCs has not been reported. The EPCs used in our study were early EPCs, which we characterized earlier.[41] These early EPCs expressed endothelial cell-specific markers, such as VE cadherin or CD31, and no previous studies have shown that they produce such high levels of CX3CR1. A recent study reported that late EPCs (or outgrowth endothelial cells [OECs]) also play a significant role in AMD. Thill et al[42] isolated OECs from peripheral blood of AMD patients, and they showed that patients with neovascular AMD had a 5.1-fold higher number of OECs than subjects without AMD. To combine the results of the present study with those of Thill et al,[42] we believe that both early EPCs and OECs are important for the development of AMD, although they probably play different roles.

The earlier studies had shown that proinflammatory cytokines, such as IL-1β, IL-6, interferon-γ, and TNF-α are important modulators of CX3CR1 expression in various types of cells,[37,43–46] and the modulations take place through phosphatidylinositol 3-kinase and nuclear factor-κB signaling pathways.[43] Among the proinflammatory cytokines, IL-1β and TNF-α have been shown to be present in human CNV tissues,[47,34] and the results of this study showed that TNF-α and IL-1β upregulated the CX3CR1 expression in EPCs as reported in other cell types.[48,49] In addition, fractalkine, the sole ligand of CX3CR1, upregulated the CX3CR1 expression in EPCs. There has not been an article that reported an upregulation of CX3CR1 by fractalkine in an autocrine manner in any type of cells; however, in light of the facts that

Downloaded from http://atvb.ahajournals.org/ at TOKYO IKA SHIKA UNIV LIB on March 19, 2012

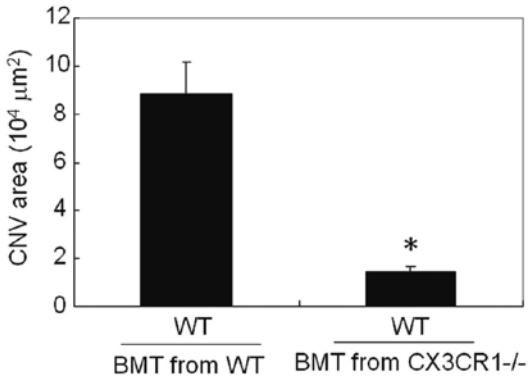

Figure 5. Comparison of areas with laser-induced CNV in the choroidal flat mounts between wild-type mice that received transplantation of bone marrow cells (BMT) from wild-type mice (n=9) and wild-type mice that received BMT from CX3CR1$^{-/-}$ mice (n=6). *$P<0.01$ vs the CNV area in the wild-type mice that received BMT from wild-type mice.

fractalkine activates nuclear factor-κB signaling in smooth muscle cells[43,50] and that TNF-α and IL-1β induced an upregulation of CX3CR1 in EPCs (Figure 3), it is reasonable that fractalkine upregulates the CX3CR1 expression in EPCs. It is also possible that the fractalkine-induced upregulation of CX3CR1 in EPCs is through TNF-α or IL-1β produced by $A\beta_{1-40}$-stimulated EPCs because EPCs produce TNF-α and IL-1β when stimulated by $A\beta_{1-40}$ (data not shown). This autocrine mechanism might be a specific feature of endothelial cells because they are the only cell types that express both CX3CR1 and fractalkine (Figure 3).

The $A\beta_{1-40}$-induced upregulation of CX3CR1 in EPCs was significantly decreased by neutralizing antibodies against TNF-α, IL-1β, and fractalkine. This would indicate that the $A\beta_{1-40}$-induced upregulation of CX3CR1 in EPCs is partly due to an autocrine mechanism that affects the release of cytokines or fractalkine from EPCs. However, even a combination of neutralizing antibodies against TNF-α, IL-1β, and fractalkine did not completely block the $A\beta_{1-40}$-stimulated upregulation of CX3CR1 in EPCs. Thus, we suggest the possibility that some other mechanisms might also contribute to the $A\beta_{1-40}$-induced upregulation of CX3CR1 in EPCs. This needs further investigation.

The results of the cell migration analyses showed that fractalkine induced EPC migration, and pretreatment of EPCs with $A\beta_{1-40}$ significantly enhanced the migration. However, fractalkine failed to induce the migration of EPCs derived from CX3CR1$^{-/-}$ mice, and Aβ did not enhance fractalkine-induced migration of EPCs derived from CX3CR1$^{-/-}$ mice (Figure 4B). These results suggest that CX3CR1 plays a critical role in EPC migration, and Aβ enhances the EPC migration through an upregulation of CX3CR1.

Macrophages and microglia have been observed in human CNV tissues,[34,47] and Greaves et al[51] reported that macrophages express fractalkine. In addition, human RPE cells constitutively express the mRNA of fractalkine, and they also secret a soluble form of fractalkine as determined by ELISA (data not shown). The expression of fractalkine by the RPE cells was upregulated by TNF-α and IL-1β (data not shown). We recently showed that $A\beta_{1-40}$ increased the expression of TNF-α and IL-1β in macrophages and microglia.[52] Taken together, these findings suggest that macrophages/microglia, as well as cytokine-stimulated RPE cells, are the major cells that produce soluble fractalkine and attract EPCs to the subretinal space.

Finally, to clarify the role of CX3CR1 in EPCs in the development of CNV, we performed bone marrow transplantation experiments. Because CX3CR1 is expressed by some ocular microglia,[34] we transplanted bone marrow EPCs to eliminate the possibility that the effects were due to resident cells expressing CX3CR1. Thus, cells from CX3CR1$^{-/-}$ mice whose bone marrow–derived cells lacked CX3CR1 were transplanted. The results showed that the CNV area was significantly smaller in wild-type mice that received bone marrow transplantation from CX3CR1$^{-/-}$ mice than in wild-type mice that received bone marrow transplantation from wild-type mice. In the laser-induced CNV model, more than 65% of vascular endothelial cells within the CNV were of bone marrow origin.[14] Because neprilysin-deficient mice do not develop CNV despite the subretinal deposition of Aβ, this mouse model was not used to examine the effect of bone marrow transplantation from CX3CR1$^{-/-}$ mice.

There was no difference in the number of leukocytes and EPCs in the peripheral blood of CX3CR1$^{-/-}$ mice and wild-type mice (Supplemental Figure IVA and IVB). In addition, fractalkine or $A\beta_{1-40}$ did not induce a proliferation of EPCs (Supplemental Figure IVC). Combining these data with the results of cell migration analysis that demonstrated that the fractalkine-induced EPC migration was lower in EPCs derived from CX3CR1$^{-/-}$ mice than in EPCs derived from wild-type mice (Figure 4B), we suggest that the absence of CX3CR1 in bone marrow–derived EPCs reduced the CNV development. This was probably because of a reduction in the migration of EPCs to the subretinal space.

In conclusion, we have shown that EPCs constitutively express significantly higher levels of CX3CR1 than HUVECs, and Aβ causes a further upregulation of CX3CR1 in EPCs. Boyden chamber assays showed that fractalkine induces EPC migration in a dose-dependent manner, and Aβ enhances the fractalkine-induced migration of EPCs. In the laser-induced CNV model, the CNV area was significantly smaller in wild-type mice that received bone marrow transplantation from CX3CR1$^{-/-}$ mice than in mice that received bone marrow transplantation from wild-type mice. Overall, our results suggest an important role for the Aβ-regulated CX3CR1 in EPC migration and in subsequent CNV development. Thus, therapy targeting the fractalkine/CX3CR1 axis might be useful for treating the CNV in AMD.

Acknowledgments

We thank Prof Duco Hamasaki for critical discussion and final manuscript revision.

Sources of Funding

This work was supported by the Japan Society for the Promotion of Science (Grants 22390322 and 21659399).

Downloaded from http://atvb.ahajournals.org/ at TOKYO IKA SHIKA UNIV LIB on March 19, 2012

Disclosures

None.

References

1. Sommer A, Tielsch JM, Katz J, Quigley HA, Gottsch JD, Javitt JC, Martone JF, Royall RM, Witt KA, Ezrine S. Racial differences in the cause-specific prevalence of blindness in east Baltimore. *N Engl J Med*. 1991;325:1412–1417.
2. Attebo K, Mitchell P, Smith W. Visual acuity and the causes of visual loss in Australia: the Blue Mountains Eye Study. *Ophthalmology*. 1996;103: 357–364.
3. VanNewkirk MR, Weih L, McCarty CA, Taylor HR. Cause-specific prevalence of bilateral visual impairment in Victoria, Australia: the Visual Impairment Project. *Ophthalmology*. 2001;108:960–967.
4. Oshima Y, Ishibashi T, Murata T, Tahara Y, Kiyohara Y, Kubota T. Prevalence of age related maculopathy in a representative Japanese population: the Hisayama study. *Br J Ophthalmol*. 2001;85:1153–1157.
5. Green WR, Harlan JB. Histopathologic features. In: Berger J, Fine S, Maguire M, eds. *Age-Related Macular Degeneration*. St. Louis, MO: Mosby; 1999:81–154.
6. Mukesh BN, Dimitrov PN, Leikin S, Wang JJ, Mitchell P, McCarty CA, Taylor HR. Five-year incidence of age-related maculopathy: the Visual Impairment Project. *Ophthalmology*. 2004;111:1176–1182.
7. Bressler SB, Maguire MG, Bressler NM, Fine SL. Relationship of drusen and abnormalities of the retinal pigment epithelium to the prognosis of neovascular macular degeneration: the Macular Photocoagulation Study Group. *Arch Ophthalmol*. 1990;108:1442–1447.
8. Yoshida T, Ohno-Matsui K, Ichinose S, Sato T, Iwata N, Saido TC, Hisatomi T, Mochizuki M, Morita I. The potential role of amyloid β in the pathogenesis of age-related macular degeneration. *J Clin Invest*. 2005;115:2793–2800.
9. Vassar R, Bennett BD, Babu-Khan S, Kahn S, Mendiaz EA, Denis P, Teplow DB, Ross S, Amarante P, Loeloff R, Luo Y, Fisher S, Fuller J, Edenson S, Lile J, Jarosinski MA, Biere AL, Curran E, Burgess T, Louis JC, Collins F, Treanor J, Rogers G, Citron M. β-Secretase cleavage of Alzheimer's amyloid precursor protein by the transmembrane aspartic protease BACE. *Science*. 1999;286:735–741.
10. Takasugi N, Tomita T, Hayashi I, Tsuruoka M, Niimura M, Takahashi Y, Thinakaran G, Iwatsubo T. The role of presenilin cofactors in the γ-secretase complex. *Nature*. 2003;422:438–441.
11. Haass C, Selkoe DJ. Soluble protein oligomers in neurodegeneration: lessons from the Alzheimer's amyloid β-peptide. *Nat Rev Mol Cell Biol*. 2007;8:101–112.
12. Csaky KG, Baffi JZ, Byrnes GA, Wolfe JD, Hilmer SC, Flippin J, Cousins SW. Recruitment of marrow-derived endothelial cells to experimental choroidal neovascularization by local expression of vascular endothelial growth factor. *Exp Eye Res*. 2004;78:1107–1116.
13. Espinosa-Heidmann DG, Caicedo A, Hernandez EP, Csaky KG, Cousins SW. Bone marrow-derived progenitor cells contribute to experimental choroidal neovascularization. *Invest Ophthalmol Vis Sci*. 2003;44: 4914–4919.
14. Espinosa-Heidmann DG, Reinoso MA, Pina Y, Csaky KG, Caicedo A, Cousins SW. Quantitative enumeration of vascular smooth muscle cells and endothelial cells derived from bone marrow precursors in experimental choroidal neovascularization. *Exp Eye Res*. 2005;80:369–378.
15. Sengupta N, Caballero S, Mames RN, Timmers AM, Saban D, Grant MB. Preventing stem cell incorporation into choroidal neovascularization by targeting homing and attachment factors. *Invest Ophthalmol Vis Sci*. 2005;46:343–348.
16. Tomita M, Yamada H, Adachi Y, Cui Y, Yamada E, Higuchi A, Minamino K, Suzuki Y, Matsumura M, Ikehara S. Choroidal neovascularization is provided by bone marrow cells. *Stem Cells*. 2004;22:21–26.
17. Sheridan CM, Rice D, Hiscott PS, Wong D, Kent DL. The presence of AC133-positive cells suggests a possible role of endothelial progenitor cells in the formation of choroidal neovascularization. *Invest Ophthalmol Vis Sci*. 2006;47:1642–1645.
18. Urbich C, Heeschen C, Aicher A, Sasaki K, Bruhl T, Farhadi MR, Vajkoczy P, Hofmann WK, Peters C, Pennacchio LA, Abolmaali ND, Chavakis E, Reinheckel T, Zeiher AM, Dimmeler S. Cathepsin L is required for endothelial progenitor cell-induced neovascularization. *Nat Med*. 2005;11:206–213.
19. Asahara T, Murohara T, Sullivan A, Silver M, van der Zee R, Li T, Witzenbichler B, Schatteman G, Isner JM. Isolation of putative progenitor endothelial cells for angiogenesis. *Science*. 1997;275:964–967.
20. Bagley RG, Walter-Yohrling J, Cao X, Weber W, Simons B, Cook BP, Chartrand SD, Wang C, Madden SL, Teicher BA. Endothelial precursor cells as a model of tumor endothelium: characterization and comparison with mature endothelial cells. *Cancer Res*. 2003;63:5866–5873.
21. Basire A, Sabatier F, Ravet S, Lamy E, Mialhe A, Zabouo G, Paul P, Gurewich V, Sampol J, Dignat-George F. High urokinase expression contributes to the angiogenic properties of endothelial cells derived from circulating progenitors. *Thromb Haemost*. 2006;95:678–688.
22. Shimada N, Ohno-Matsui K, Iseki S, Koike M, Uchiyama Y, Wang J, Yoshida T, Sato T, Peters C, Mochizuki M, Morita I. Cathepsin L in bone marrow-derived cells is required for retinal and choroidal neovascularization. *Am J Pathol*. 2010;176:2571–2580.
23. Mobius-Winkler S, Hollriegel R, Schuler G, Adams V. Endothelial progenitor cells: implications for cardiovascular disease. *Cytometry A*. 2009; 75:25–37.
24. Khakoo AY, Finkel T. Endothelial progenitor cells. *Annu Rev Med*. 2005;56:79–101.
25. Heeschen C, Aicher A, Lehmann R, Fichtlscherer S, Vasa M, Urbich C, Mildner-Rihm C, Martin H, Zeiher AM, Dimmeler S. Erythropoietin is a potent physiologic stimulus for endothelial progenitor cell mobilization. *Blood*. 2003;102:1340–1346.
26. Salcedo R, Wasserman K, Young HA, Grimm MC, Howard OM, Anver MR, Kleinman HK, Murphy WJ, Oppenheim JJ. Vascular endothelial growth factor and basic fibroblast growth factor induce expression of CXCR4 on human endothelial cells: in vivo neovascularization induced by stromal-derived factor-1α. *Am J Pathol*. 1999;154:1125–1135.
27. Jones CP, Pitchford SC, Lloyd CM, Rankin SM. CXCR2 mediates the recruitment of endothelial progenitor cells during allergic airways remodeling. *Stem Cells*. 2009;27:3074–3081.
28. Imai T, Hieshima K, Haskell C, Baba M, Nagira M, Nishimura M, Kakizaki M, Takagi S, Nomiyama H, Schall TJ, Yoshie O. Identification and molecular characterization of fractalkine receptor CX3CR1, which mediates both leukocyte migration and adhesion. *Cell*. 1997;91:521–530.
29. Crola Da Silva C, Lamerant-Fayel N, Paprocka M, Mitterrand M, Gosset D, Dus D, Kieda C. Selective human endothelial cell activation by chemokines as a guide to cell homing. *Immunology*. 2009;126:394–404.
30. Bazan JF, Bacon KB, Hardiman G, Wang W, Soo K, Rossi D, Greaves DR, Zlotnik A, Schall TJ. A new class of membrane-bound chemokine with a CX3C motif. *Nature*. 1997;385:640–644.
31. You JJ, Yang CH, Huang JS, Chen MS, Yang CM. Fractalkine, a CX3C chemokine, as a mediator of ocular angiogenesis. *Invest Ophthalmol Vis Sci*. 2007;48:5290–5298.
32. Silverman MD, Zamora DO, Pan Y, Texeira PV, Baek SH, Planck SR, Rosenbaum JT. Constitutive and inflammatory mediator-regulated fractalkine expression in human ocular tissues and cultured cells. *Invest Ophthalmol Vis Sci*. 2003;44:1608–1615.
33. Tuo J, Smith BC, Bojanowski CM, Meleth AD, Gery I, Csaky KG, Chew EY, Chan CC. The involvement of sequence variation and expression of CX3CR1 in the pathogenesis of age-related macular degeneration. *FASEB J*. 2004;18:1297–1299.
34. Combadière C, Feumi C, Raoul W, Keller N, Rodéro M, Pézard A, Lavalette S, Houssier M, Jonet L, Picard E, Debré P, Sirinyan M, Deterre P, Ferroukhi T, Cohen SY, Chauvaud D, Jeanny JC, Chemtob S, Behar-Cohen F, Sennlaub F. CX3CR1-dependent subretinal microglia cell accumulation is associated with cardinal features of age-related macular degeneration. *J Clin Invest*. 2007;117:2920–2928.
35. Yang X, Hu J, Zhang J, Guan H. Polymorphisms in CFH, HTRA1 and CX3CR1 confer risk to exudative age-related macular degeneration in Han Chinese. *Br J Ophthalmol*. 2010;94:1211–1214.
36. Chan CC, Tuo J, Bojanowski CM, Csaky KG, Green WR. Detection of CX3CR1 single nucleotide polymorphism and expression on archived eyes with age-related macular degeneration. *Histol Histopathol*. 2005;20: 857–863.
37. Moon SO, Kim W, Sung MJ, Lee S, Kang KP, Kim DH, Lee SY, So JN, Park SK. Resveratrol suppresses tumor necrosis factor-α-induced fractalkine expression in endothelial cells. *Mol Pharmacol*. 2006;70:112–119.
38. Fong AM, Robinson LA, Steeber DA, Tedder TF, Yoshie O, Imai T, Patel DD. Fractalkine and CX3CR1 mediate a novel mechanism of leukocyte capture, firm adhesion, and activation under physiologic flow. *J Exp Med*. 1998;188:1413–1419.
39. Ishida Y, Gao JL, Murphy PM. Chemokine receptor CX3CR1 mediates skin wound healing by promoting macrophage and fibroblast accumulation and function. *J Immunol*. 2008;180:569–579.
40. Muehlhoefer A, Saubermann LJ, Gu X, Luedtke-Heckenkamp K, Xavier R, Blumberg RS, Podolsky DK, MacDermott RP, Reinecker HC. Frac-

Downloaded from http://atvb.ahajournals.org/ at TOKYO IKA SHIKA UNIV LIB on March 19, 2012

talkine is an epithelial and endothelial cell-derived chemoattractant for intraepithelial lymphocytes in the small intestinal mucosa. *J Immunol*. 2000;164:3368–3376.
41. Mukai N, Akahori T, Komaki M, Li Q, Kanayasu-Toyoda T, Ishii-Watabe A, Kobayashi A, Yamaguchi T, Abe M, Amagasa T, Morita I. A comparison of the tube forming potentials of early and late endothelial progenitor cells. *Exp Cell Res*. 2008;314:430–440.
42. Thill M, Strunnikova NV, Berna MJ, Gordiyenko N, Schmid K, Cousins SW, Thompson DJ, Csaky KG. Late outgrowth endothelial progenitor cells in patients with age-related macular degeneration. *Invest Ophthalmol Vis Sci*. 2008;49:2696–2708.
43. Chandrasekar B, Mummidi S, Perla RP, Bysani S, Dulin NO, Liu F, Melby PC. Fractalkine (CX3CL1) stimulated by nuclear factor κB (NF-κB)-dependent inflammatory signals induces aortic smooth muscle cell proliferation through an autocrine pathway. *Biochem J*. 2003;373:547–558.
44. Nanki T, Imai T, Nagasaka K, Urasaki Y, Nonomura Y, Taniguchi K, Hayashida K, Hasegawa J, Yoshie O, Miyasaka N. Migration of CX3CR1-positive T cells producing type 1 cytokines and cytotoxic molecules into the synovium of patients with rheumatoid arthritis. *Arthritis Rheum*. 2002;46:2878–2883.
45. Fujimoto K, Imaizumi T, Yoshida H, Takanashi S, Okumura K, Satoh K. Interferon-γ stimulates fractalkine expression in human bronchial epithelial cells and regulates mononuclear cell adherence. *Am J Respir Cell Mol Biol*. 2001;25:233–238.
46. Valdivia-Silva JE, Franco-Barraza J, Silva AL, Pont GD, Soldevila G, Meza I, García-Zepeda EA. Effect of pro-inflammatory cytokine stimulation on human breast cancer: implications of chemokine receptor expression in cancer metastasis. *Cancer Lett*. 2009;283:176–185.
47. Oh H, Takagi H, Takagi C, Suzuma K, Otani A, Ishida K, Matsumura M, Ogura Y, Honda Y. The potential angiogenic role of macrophages in the formation of choroidal neovascular membranes. *Invest Ophthalmol Vis Sci*. 1999;40:1891–1898.
48. Imaizumi T, Yoshida H, Satoh K. Regulation of CX3CL1/fractalkine expression in endothelial cells. *J Atheroscler Thromb*. 2004;11:15–21.
49. Apostolakis S, Krambovitis E, Vlata Z, Kochiadakis GE, Baritaki S, Spandidos DA. CX3CR1 receptor is up-regulated in monocytes of coronary artery diseased patients: impact of pre-inflammatory stimuli and renin-angiotensin system modulators. *Thromb Res*. 2007;121:387–395.
50. Barlic J, Zhang Y, Murphy PM. Atherogenic lipids induce adhesion of human coronary artery smooth muscle cells to macrophages by up-regulating chemokine CX3CL1 on smooth muscle cells in a TNFα-NFκB-dependent manner. *J Biol Chem*. 2007;282:19167–19176.
51. Greaves DR, Häkkinen T, Lucas AD, Liddiard K, Jones E, Quinn CM, Senaratne J, Green FR, Tyson K, Boyle J, Shanahan C, Weissberg PL, Gordon S, Ylä-Hertualla S. Linked chromosome 16q13 chemokines, macrophage-derived chemokine, fractalkine, and thymus- and activation-regulated chemokine, are expressed in human atherosclerotic lesions. *Arterioscler Thromb Vasc Biol*. 2001;21:923–929.
52. Wang J, Ohno-Matsui K, Yoshida T, Shimada N, Ichinose S, Sato T, Mochizuki M, Morita I. Amyloid-β up-regulates complement factor B in retinal pigment epithelial cells through cytokines released from recruited macrophages/microglia: another mechanism of complement activation in age-related macular degeneration. *J Cell Physiol*. 2009;220:119–128.

Downloaded from http://atvb.ahajournals.org/ at TOKYO IKA SHIKA UNIV LIB on March 19, 2012

顎口腔外科学分野

小村　健

医歯学総合研究科・口腔機能再構築学系専攻
顎口腔外科学・教授

1）研究の課題名

1.「唇顎口蓋裂患者の顎裂部への骨移植術における多血小板血漿併用による骨吸収の抑制」

「Reduction of bone resorption by the application of platelet-rich plasma（PRP）in bone grafting of the alveolar cleft」

唇顎口蓋裂患者の顎裂部骨移植術において自家腸骨海綿骨移植に多血小板血漿（PRP）を併用した効果についてX線学的に検討した。自家骨移植でPRPを併用したPRP併用群14例、自家骨のみの対照群7例を対象として、術後1年までの経時的な移植部のアルミ当量値を算出して骨密度の評価を行い、移植部の幅径と高さにおける骨吸収率を評価した。顎裂骨移植にPRPを併用すると形態が保持され骨吸収を抑制したが、骨密度を有意に増加させる効果はなかった。

2.「癌抑制遺伝子型microRNA miR-218はmTORと複合体を形成するRictorを標的分子とし、口腔癌においてAktのリン酸化を抑制する」

「The tumor suppressive microRNA miR-218 targets the mTOR component Rictor and inhibits AKT phosphorylation in oral cancer」

（本研究は、東京医科歯科大学大学院医歯学総合研究科顎口腔外科学分野、東京医科歯科大学硬組織疾患ゲノムセンターおよび東京医科歯科大学大学院医歯学総合研究科分子細胞遺伝学分野の共同研究である）

機能性低分子RNAであるmicroRNA（miRNA）は、癌の発生や進展過程の分子機序に深く関与することが明らかにされている。本研究では、腫瘍特異的DNA過剰メチル化により発現抑制される新規癌抑制遺伝子型miRNA（TS-miRNA）の単離・同定を目指して、口腔扁平上皮癌（OSCC）細胞株での機能的スクリーニングとDNAメチル化解析ならびに発現解析を組み合わせた絞り込みによって、327種類のmiRNA配列からmiR-218とmiR-585を新規TS-miRNAとして同定した。さらにmiR-218はRictorを標的分子とし、OSCCにおいてAktのSer-473リン酸化を抑制することによって細胞増殖を負に制御していることを明らかにした。

3.「EGFRとSGLT1の共発現は口腔扁平上皮癌の組織学的分化度に関連する」

「Coexpression of SGLT1 and EGFR is associated with tumor differentiation in oral squamous cell carcinoma」

（本研究は、東京医科歯科大学大学院医歯学総合研究科顎口腔外科学分野、東京医科歯科大学硬組織疾患ゲノムセンターおよび東京医科歯科大学大学院医歯学総合研究科口腔病理学分野の共同研究である）

EGFRの強発現は 化学療法、放射線療法に抵抗性を示し、浸潤や転移、予後の悪化をもたらすため、化学療法の標的となる。しかしそのキナーゼ活性を標的とした治療薬の奏効率は20%程度である。SGLT1は、グルコースの細胞内移入に関与する分子であるが、EGFRはキナーゼ活性とは無関係にSGLT1を安定化させてグルコースを細胞内に取り入れる。本研究では、口腔扁平上皮癌におけるSGLT1とEGFRの発現を検討し、臨床病理学的特徴との関連を明らかにした。舌扁平上皮癌の切除標本を用いて免疫組織染色で検討したところ、SGLT1とEGFRは、有意に高い関連をもって共発現していた（P = 0.016）。さらに、腫瘍の組織学的分化度が低いほど共発現がみられたことから、SGLT1とEGFRの共発現は腫瘍の分化の過程に関与することが示唆された。

2)

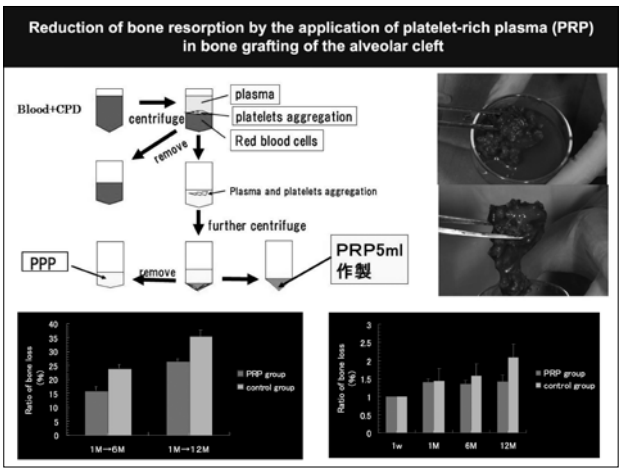

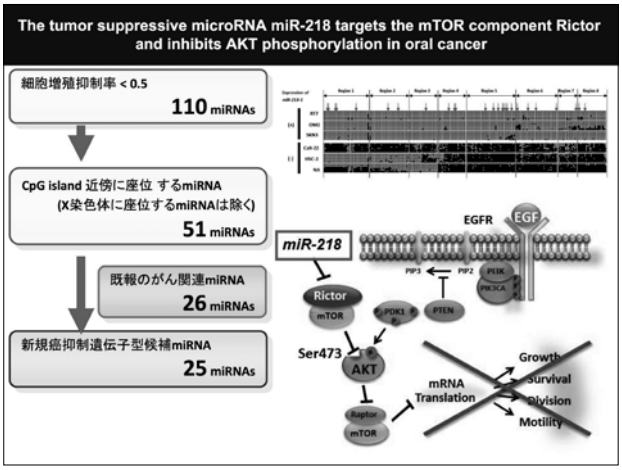

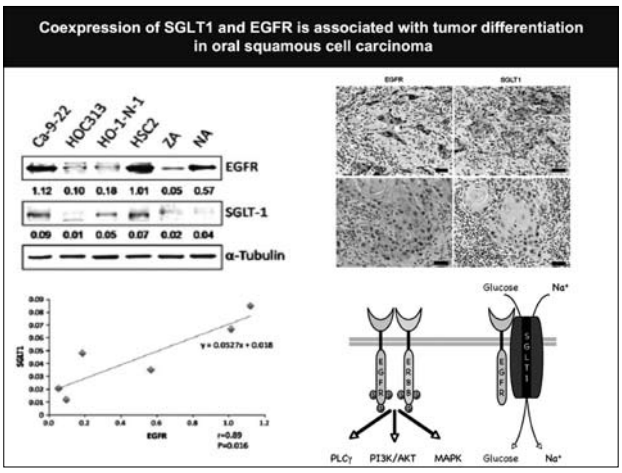

3）発表の研究内容についての英文要約

1.「Reduction of bone resorption by the application of platelet-rich plasma（PRP）in bone grafting of the alveolar cleft」

We evaluated the effectiveness of platelet-rich plasma（PRP）on the regeneration of autogenous cancellous bone and marrow grafted in the alveolar cleft. Twenty patients with alveolar clefts were examined; 6 were the control group and received cancellous bone and marrow grafts without PRP, while the remaining 14 comprised the PRP group and received grafts with PRP. Prior to surgery, 50 ml of blood was withdrawn and 5 ml of PRP gel produced through centrifugal separation. The bone graft mixed with PRP was then packed into the alveolar cleft. Postoperative bone density was assessed as the aluminium-equivalent value on occlusal X-ray films in a qualitative analysis. Quantitative evaluation of regenerated bone was made with computed tomography and panoramic radiographs at 1 month, 6 months and 1 year after surgery. Satisfactory bone bridging formation was observed in all patients without any complications. The bone density of the PRP group was lower than that of the control group at 1 week, but the same after 1 month. The added PRP reduced the resorption of regenerated bone postoperatively. Autogenous cancellous bone grafting with PRP, which significantly reduces postoperative bone resorption, is a reliable technique for alveolar bone grafting of cleft patients.

2.「The tumor suppressive microRNA miR-218 targets the mTOR component Rictor and inhibits AKT phosphorylation in oral cancer」

We profiled tumor suppressive microRNAs（miRNAs）that are silenced by DNA hypermethylation in oral squamous cell carcinoma（OSCC）using a functionbased screening approach. This approach employed a cell proliferation assay for 327 synthetic miRNAs in two OSCC cell lines. Among the 110 miRNAs identified in this set that exhibited inhibitory properties, we compared DNA methylation and expression status in a wider panel of OSCC cell lines and primary tumor tissues, resulting in the identification of miR-218 and miR-585 as functionally significant miRNA genes that are frequently silenced in OSCC by DNA hypermethylation. Ectopic expression of miR-218 and miR-585 in OSCC cells lacking
endogenous expression reduced cell growth in part through caspase-mediated apoptosis. Notably, miR-218 reduced levels of the rapamycin-insensitive component of mTOR, Rictor, in a manner associated with a suppression of Akt S473 phosphorylation. Together our findings define miR-585 as a tumor suppressive function that is often epigenetically silenced in OSCC, and they identify Rictor as a novel target of miR-218, suggesting that
activation of the mTOR-Akt signaling pathway induced by Rictor contributes centrally to oral carcinogenesis.

3.「Coexpression of SGLT1 and EGFR is associated with tumor differentiation in oral squamous cell carcinoma」

Overexpression of epidermal growth factor receptor（EGFR）is associated with resistance to chemotherapy and radiotherapy, advanced tumor stage, invasion, metastasis and poor prognosis in malignant tumors. Sodiumglucose

co-transporter 1（SGLT1）is a membrane protein that mediates the transport of glucose across cellular membranes. EGFR physically associates with and stabilizes SGLT1 to promote glucose uptake into cancer cells through a kinase-independent process. The purpose of this study was to investigate the coexpression of SGLT1 and EGFR and its relationships with clinicopathological features in oral squamous cell carcinoma（OSCC）. SGLT1 and EGFR were detected in all OSCC cell lines, and the expression levels of SGLT1 were significantly correlated with those of EGFR. Pearson product–moment correlation coefficient of SGLT1 and EGFR was 0.89（P = 0.016）. The immunohistochemical study using the surgical specimens in 52 patients with tongue SCC also showed a significant correlation between SGLT1 and EGFR. Moreover, SGLT1/EGFR expression was inversely related to tumor differentiation among the 5 clinicopathological factors（P = 0.004）. SGLT1/EGFR coexpression might be required in the de-differentiation of OSCC, but further study is needed to clarify the implication of these proteins in the manifestation of malignancy and clinical significance.

4）本事業に関連して世界的な研究拠点形成に向けて、以下の点で改善・整備等されたこと

A（研究拠点体制）

硬組織領域における教育、研究、臨床について優れた実績を上げるため、平成15年度より開始の21世紀COEプログラム「歯と骨の分子破壊と再構築のフロンティア」において形成した研究基盤をさらに発展させ、一方、特別教育研究経費による「先端硬組織疾患ゲノム・ナノサイエンス統合プロジェクト」との密なる連携を図りつつ、口腔扁平上皮癌などの口腔外科学領域における悪性腫瘍を中心とした硬組織疾患のテーラーメイド医療の実現とともに、トランスレーショナル・リサーチへの発展を視野にいれた研究を展開している。

B（研究教育環境）

教育・研究基盤をさらに発展させ、基礎医・歯学分野から臨床分野までの融合型国際教育研究拠点の強化・拡大を図ることによって、博士課程学生に優れた教育環境・プログラムを提供し、国内外の研究機関とも連携して“国際的創造型科学者”の育成を目指す。

C（人材確保）

基礎医・歯学分野から臨床分野までの様々な情報・技術交流を目指し、学外研究所等との大学院生・教員の相互的な派遣・受け入れの体制を整備し、基礎研究、臨床研究の両分野について先端的かつ十分な知識と技術を持つ人材の確保に取り組んでいる。

D（人材育成）

顎顔面疾患におけるテーラーメイド医療の実現とQOLの向上をも目指したトランスレーショナル・リサーチを推進することによって、基礎医・歯学分野から臨床・応用医学分野までを両立させた“国際的創造型科学者”を養成する。

E（国際化）

国際的な情報交換と技術交流を目指し、タイなどのアジア各国からの留学生を大学院生として受け入れて研究を遂行し、相互の発展に寄与している。

5）GCOE事業を推進するに当たって力を入れた点

臨床情報を具備した口腔扁平上皮癌症例の外科切除試料の系統的な収集と本学のバイオリソースセンターにおける保存を視野に入れつつ、これらの臨床検体を用いた網羅的発現解析によって口腔扁平上皮癌の頸部リンパ節転移診断モデルを構築するとともに、口腔扁平上皮癌細胞株での網羅的ゲノム・エピゲノム解析などにより新規口腔癌抑制遺伝子を単離・同定し、口腔扁平上皮癌における遺伝子変異の同定などについても明らかにすべく研究を推進してきた。また、先端硬組織疾患ゲノム・ナノサイエンス統合プロジェクトとの密接な学内連携のもと、これらのバイオリソースを用いた分子・細胞・組織・個体すべてのレベルにおける分子メカニズムの解明、顎顔面疾患の新たな診断から外科的治療法の開発を目指した系統的研究基盤の整備をすすめている。

6）英文原著論文

1. Sakamoto K, Aragaki T, Morita KI, Kawachi H, Kayamori K, Nakanishi S, Omura K, Miki Y, Okada N, Katsube KI, Takizawa T, Yamaguchi A：Down-regulation of keratin 4 and keratin 13 expression in oral squamous cell carcinoma and epithelial dysplasia：a clue for histopathogenesis. Histopathology. 58（4）531-542, 2011（Mar）
2. Cao Y, Zhang L, Ritprajak P, Tsushima F, Youngnak-Piboonratanakit P, Kamimura Y, Hashiguchi M, Azuma M. Immunoregulatory molecule B7-H1（CD274）contributes to skin carcinogenesis. Cancer Res. 71（14）：4737-4741, 2011（Jul）
3. Mochizuki Y, Omura K, Kayamori K, Sakamoto K, Shimamoto H, Yamaguchi A：Küttner's tumor of the sub-mandibular gland associated with fibrosclerosis and follicular hyperplasia of regional lymph nodes：a case report. J Med Case Reports. 29;5（1）：121, 2011（Mar）
4. Isobe K, Morita KI, Omura K：Enucleation and

repeated dredging treatment for a large ameloblastic fibroma in growing young patient：Report of a case with difficult treatment planning. Asian J Oral Maxillofac Surg. Available online 5 March 2011 Asian J Oral Maxillofac Surg. 23（2）96-98, 2011（May）
5. Harada H, Omura K, Mogi S, Okada N：Cementoblastoma arising in the maxilla of an 8-year-old boy：a case report. Int J Dent. 2011：384578, 2011（May）
6. Marukawa E, Oshina H, Iino G, Morita K, Omura K：Reduction of bone resorption by the application of platelet-rich plasma（PRP）in bone grafting of the alveolar cleft. J Craniomaxillofac Surg. 39（4）：278-83, 2011（Jun）
7. ◎ Uesugi A, Kozaki K, Tsuruta T, Furuta M, Morita K, Imoto I, Omura K, Inazawa J：The Tumor Suppressive MicroRNA miR-218 Targets the mTOR Component Rictor and Inhibits AKT Phosphorylation in Oral Cancer. Cancer Res. 71（17）：5765-78, 2011（Sep）
8. Mochizuki Y, Omura K, Nakamura S, Harada H, Shibuya H, Kurabayashi T：Preoperative predictive model of cervical lymph node metastasis combinating fluorine-18 fluorodeoxyglucose positron-emission tomography/computerized tomography findings and clinical factors in patients with oral or oropharyngeal squamous cell carcinoma. Oral Surg. Oral Med. Oral Pathol. Oral Radiol. Endod. in press.
9. ◎ Hanabata Y, Nakajima Y, Morita KI, Kayamori K, Omura K：Coexpression of SGLT1 and EGFR is associated with tumor differentiation in oral squamous cell carcinoma. Odontology. 2011 May 24. [Epub ahead of print]

7）総説ならびに著書

1. 佐藤　潔、栢森　高、小村　健、山口　朗：【骨代謝疾患治療における生物学的製剤の現状と将来への可能性】IL-6の骨代謝に対する作用. 骨粗鬆症治療 10（1）20-24, 2011　（2011.01）
2. 小村　健：口腔環境と摂食・嚥下障害. 今日の治療指針　私はこう治療している 2011 1317-1318頁　医学書院　2011年1月
3. 小村　健：BRONJに対する手術　その適応と方法. 口腔外科ハンドマニュアル ‘11 34-41頁　クインティセンス出版 2011年5月
4. 小村　健：口腔粘膜・舌の腫瘍. MB Derma 186：47-53, 2011.
5. 小村　健：癌・前癌病変の手術. 口腔外科専門医マニュアル　日本口腔外科学会編　196-209頁　医歯薬出版 2011年9月
6. 小村　健（分担執筆）：口腔顎顔面外科学専門用語集　日本口腔外科学会編　医歯薬出版　2011年9月

8）平成23年度までの自己評価

口腔扁平上皮癌などの口腔外科学領域における悪性腫瘍を中心とした硬組織領域における教育、研究、臨床については世界的にトップレベルの優れた実績を上げ、一方、特別教育研究経費による「先端硬組織疾患ゲノム・ナノサイエンス統合プロジェクト」との密なる連携を図りつつ、テーラーメイド医療の実現をめざしたトランスレーショナル・リサーチが展開できた。

9）和文原著論文

1. 花畑泰子：口腔扁平上皮癌におけるEGFRとSGLT1の発現解析. 口腔病学会雑誌　78（1）12-18, 2011.
2. 大迫利光, 小村　健, 原田浩之, 栢森　高：下唇粘膜部に発生した筋上皮癌の1例. 日本口腔科学会雑誌 60（4）：330-336, 2011.
3. 小村　健：唾液腺腫瘍の外科療法. 日本口腔腫瘍学会誌　23（3）：73-81, 2011.
4. 小林正治, 齊藤　力, 小村　健, 原田　清, 橋本賢二, 加納浩之, 高田佳之：顎矯正手術におけるポリ-L-乳酸/ポリ-D-乳酸/ポリグリコール酸生体吸収性骨接合材の臨床評価. 日本顎変形症学会雑誌 21（4）：238-243, 2011.
5. 富岡寛文, 小村　健：舌背に発生した平滑筋腫性過誤腫の1例. 日本口腔外科学会雑誌 57（11）606-609, 2011.
6. 富岡寛文, 小村　健, 原田浩之, 生田　稔：当科受診前に外科処置が行われた歯肉癌症例の検討.頭頸部癌 37（1）18-23, 2011.
7. 菊池　剛, 森田圭一, 樺沢勇司, 小村　健：Le Fort I型骨切り術後に生じた皮下気腫の1例. 日本口腔外科学会雑誌　57（3）124-127, 2011.
8. 平井秀明, 三澤常美, 小村　健, 河西八郎：下顎の歯性感染症から継発した多発性頭蓋内膿瘍の1例. 日本口腔外科学会雑誌 57（3）114-118, 2011.
9. 田中香衣, 小村　健, 原田浩之, 生田　稔, 白木理美：ベーチェット病患者の舌背部に発生した扁平上皮癌の1例. 日本口腔外科学会雑誌57（5）319-323, 2011.
10. 須田里香, 澤井俊宏, 小村　健：診断に苦慮した下顎智歯部に発生した歯周嚢胞の1例. 日本口腔診断学会雑誌 24（2）201-205, 2011.
11. 釘本琢磨, 島本裕彰, 小村　健：副耳下腺多形腺腫再発例の経頬法手術による治療経験. 日本口腔腫瘍学

会誌 23（2）33-40, 2011.

12. 松本佳奈子：自家蛍光可視化装置による口腔前癌病変ならびに口腔癌の検出. 口腔病学会雑誌78（2）：73-80, 2011.
13. 三澤常美, 松浦孝典, 樋口佑輔, 河西八郎, 平賀幸弘, 黄　淳一, 霜村真一：舌扁平上皮癌一次治療症例（117例）の治療成績. 山梨県立中央病院年報　37：1-5, 2011.

10）学会発表（英文）

1. Marukawa E, Takahashi Y, Hatakeyama I, Omura K：Evaluation of changes in the bone volume after sinus floor augmentation with autogenous bone and β-TCP. 4th International Conference advanced digital technology in head & neck reconstruction. May 5-8 2011. Freiburg, Germany　ポスター
2. Kabasawa Y, Sato M, Kikuchi T, Sato Y, Omura K. Three-Dimensional Evaluation of Nasal Morphological Changes after Le Fort Ⅰ Osteotomy：Comparison by Incision Lines of Le Fort Ⅰ Osteotomy. Advanced Digital Technology in Head and Neck Reconstruction May 5-8, 2011, Freiburg, Germany　口演
3. Shimamoto M, Harada H, Omura K：Mandibular reconstruction using vascularized　scapular osteocutaneous flap. 3rd World Congress of the International Academy of Oral Oncology. July 15-17, 2011, Singapore　口演
4. Maruoka Y, Kanaya F, Hoshino A, Iimura T, Imai H, Otsuka R, Ueha S, Fujioka K, Katsuragawa Y, Shimbo T, Mimori A, Yamazaki T, Manome Y, Moriyama K, Omura K, Matsushima K, Yamamoto K：Study of relations between progressive / idiopathic condylar resorption and impaired bone / cartilage metabolism associated with chemokine receptor disorder. The 20th International Conference on Oral and Maxillofacial Surgery, 1-4 November, 2011. Santiago, Chile　ポスター

11）学会発表（和文）

1. 森田圭一, 田口貴英, 島田泰如, 樺沢勇司, 小村　健：当科における角化嚢胞性歯原性腫瘍に対する治療. 第29回日本口腔腫瘍学会総会　2011年1月27-28日　熊本市　口演
2. ◎望月裕美, 中村　伸, 小村　健, 原田浩之, 中島雄介, 生田　稔, 島本裕彰, 森田圭一, 富岡寛文, 田中香衣, 金親あや乃, 渋谷　均：口腔扁平上皮がん頸部リンパ節転移の術前診断における18FDG-PETの有用性の検討. 第29回日本口腔腫瘍学会総会　2011年1月27-28日　熊本市　口演
3. 島本裕彰, 小村　健, 原田浩之, 中島雄介, 生田　稔, 富岡寛文, 田中香衣, 金親あや乃, 平井秀明, 釘本琢磨, 大迫利光, ラッシャタムカヤナーン　プラディット：当科における口腔多発癌症例の検討. 第29回日本口腔腫瘍学会総会　2011年1月27-28日　熊本市　ポスター
4. 持田薫利, 根岸綾子, 工藤雅範, 石井良昌：下唇に発生した神経鞘腫の1例. 第29回日本口腔腫瘍学会総会 2011年1月27-28日　熊本市 ポスター
5. 原田浩之, 小村　健, 中山秀樹, 平木昭光, 篠原正徳, 吉濱泰斗：口腔扁平上皮癌における術前TS-1・放射線同時併用療法の臨床第Ⅱ相試験. 第29回日本口腔腫瘍学会総会　2011年1月27-28日　熊本市 口演
6. ラッシャタームカヤナン　プラディット, 小村　健, 原田浩之, 島本裕彰, 大迫利光： Sequential bilateral tongue reconstruction in multiple oral squamous cell carcinoma：A case report. 第29回日本口腔腫瘍学会総会　2011年1月27-28日　熊本市　ポスター
7. 高橋幸伸, 丸川恵理子, 猪俣謙次, 小村　健：イヌ顎骨欠損におけるβ-リン酸三カルシウム/コラーゲン複合体の骨補填材としての検討. 第10回日本再生医療学会総会　2011年3月1-2日　東京　口演
8. 山本信祐, 島本裕彰, 岡田憲彦, 小村　健：頬部に生じた多形腺腫由来癌の1例. 第65回日本口腔科学会総会　2011年4月21-22日　東京　ポスター
9. 望月裕美,　中村　伸,小村　健,原田浩之,中島雄介,生田　稔,島本裕彰,森田圭一,富岡寛文,田中香衣,金親あや乃,渋谷　均：口腔扁平上皮がん転移リンパ節の[18F]FDG-PE/CTの診断精度と病理組織学的所見との関連性の検討.　第65回日本口腔科学会総会 2011年4月21-22日　東京　口演
10. 森田圭一, 根岸綾子, 今泉史子, 小村　健：片側性唇顎口蓋裂患者における顎矯正手術の必要性の予測. 第35回日本口蓋裂学会総会 2011年5月25-26日　新潟市　口演
11. 高原楠旻,樺沢勇司,佐藤　昌,菊池　剛,佐藤百合子,小村　健：顎矯正手術後に生じた進行性下顎頭吸収の1例. 第21回日本顎変形症学会総会　2011年6月16－17日　東京　ポスター
12. 佐藤百合子, 佐藤　昌, 菊池　剛, 樺沢勇司, 小村　健：下顎枝矢状分割術後の歯髄内血流動態および歯髄知覚に関する臨床的研究. 第21回日本顎変形症学会総会　2011年6月16－17日　東京　口演
13. 樺沢勇司, 佐藤　昌, 菊池　剛, 佐藤百合子, 小村　健：Le Fort Ⅰ型骨切り術後の鼻形態変化に対する

三次元的検討-Le Fort I 型骨切り術の切開線による比較. 第21回日本顎変形症学会総会　2011年6月16－17日　東京　口演

14. 森田圭一, ルシャタムカヤヌント・プラディット, 松川　祥, 小村　健：口腔がんにおけるFADDゲノム増幅. 第35回日本頭頸部癌学会　2011年6月9-10日　名古屋市　口演
15. 富岡寛文, 望月裕美, 金親あや乃, 田中香衣, 島本裕彰, 生田　稔, 中島雄介, 原田浩之, 小村　健：口腔扁平上皮癌における対側頸部リンパ節転移症例の検討. 第35回日本頭頸部癌学会　2011年6月9-10日　名古屋市　口演
16. 原田浩之, 小村　健, 中島雄介, 生田　稔, 島本裕彰, 富岡寛文, 田中香衣, 金親あや乃, 釘本琢磨, 大迫利光：口底扁平上皮癌の臨床病理学的検討. 第35回日本頭頸部癌学会　2011年6月9-10日　名古屋市　口演
17. 中島雄介, 花畑泰子, 森田圭一, 柏森　高, 小村　健：口腔扁平上皮癌におけるEGFRおよびSGLT1の発現解析. 第35回日本頭頸部癌学会　2011年6月9-10日　名古屋市　ポスター
18. 向山　仁,櫻井仁亨,曽我千恵子,瀬戸弘美,小笠原利枝,磯崎　淳,藤井由貴,黒田俊也：緩和ケア病棟入棟患者の全身症状, 口腔症状, 口腔関連QOLの評価-第8回日本口腔ケア学会　平成23年6月18日　東京　口演
19. 工藤雅範, 根岸綾子, 持田薫利, 石井良昌：咽頭・下顎骨周囲膿瘍に起因した重症ガス壊疽敗血症に対し集学的治療を行った1例.第20回日本有病者歯科医療学会総会　2011年6月26日　東京
20. 工藤雅範, 根岸綾子, 松本佳奈子, 持田薫利, 大久保亜耶, 石井良昌：上顎洞に充満した上顎洞内反乳頭腫の1例.第191回日本口腔外科学会関東地方会　2011年7月9日　横浜市　口演
21. 桜井仁亨, 向山　仁：低形成急性骨髄性白血病の経過中に出現した形質細胞肉芽腫の1例.　第191回日本口腔外科学会関東地方会　2011年7月9日　横浜市　口演
22. 鉄村明美,樺沢勇司,佐藤　昌,高　楠旻,川元龍夫, 小村　健,倉林　亨：顎関節MRIにおける矯正装置の影響.日本歯科放射線学会第213回関東地方会・第31回北日本地方会・第19回合同地方会　2011年7月9日　新潟市　口演
23. 向山　仁,櫻井仁亨,曽我千恵子,瀬戸弘美,小笠原利枝,磯崎　淳,藤井由貴,黒田俊也：緩和ケア病棟入棟患者のSTAS-J症状版, PPIおよび口腔症状の評価- 第16回日本緩和医療学会学術大会, 平成23年7月30日　札幌市　口演
24. 津島文彦, 桜井仁亨, 佐藤　昌, 栗林悠里, 吉本光洋, 小村　健：口腔扁平苔癬を疑い病理組織学的に上皮異形成と診断された症例の検討. 第21回日本口腔粘膜学会総会　2011年9月24-25日　鹿児島市　口演
25. 桜井仁亨, 津島文彦,佐藤　昌, 吉本光洋,小村　健：口腔扁平苔癬117例の臨床的検討　－長期予後に関する検討－. 第21回日本口腔粘膜学会総会　2011年9月24-25日　鹿児島　口演
26. 佐藤　潔, 坂本　啓, 栢森　高, 山口　朗：口腔扁平上皮癌による骨破壊予防療法の開発. 第53回歯科基礎医学会総会 2011年10月1-2日　岐阜市　ポスター
27. Uesugi A, Kozaki K, Tsuruta T, Furuta F, Imoto I, Omura K, Inazawa J：Functional screening of tumor-suppressive microRNAs silenced by DNA hypermethylation in oral cancer. 7 0th Annual Meeting of the Japanese Cancer Association. October 3-5 2011. Nagoya, Japan　口演
28. 森田圭一, 小村　健：顎骨立体モデルを用いて作製した顎矯正手術における上顎位置決め用スプリント. 第56回社団法人日本口腔外科学会総会 2011年10月21-23日　大阪市　口演
29. 釘本琢磨, 富岡寛文, 原田浩之, 小村　健：　PGAシート併用頬脂肪体有茎移植による口腔上顎洞瘻孔閉鎖術の経験. 第56回社団法人日本口腔外科学会総会 2011年10月21-23日　大阪市　口演
30. 小村　健, 島本裕彰, 富岡寛文, 田中香衣, 中島雄介, 原田浩之：Scapular osteofascioadipose flapによる下顎再建. 第56回社団法人日本口腔外科学会総会 2011年10月21-23日　大阪市　口演
31. 佐藤　昌,樺沢勇司,佐藤百合子,高　楠旻,小村　健：カントを伴う顔面非対称症例の馬蹄形骨切り併用上下顎骨移動術の術後安定性の検討.第56回社団法人日本口腔外科学会総会 2011年10月21-23日　大阪市　口演
32. 工藤雅範, 根岸綾子, 松本佳奈子, 持田薫利, 大久保亜耶, 石井良昌：1歳女児の下顎骨折に対し非観血的整復術を施行した1例.第56回社団法人日本口腔外科学会総会2011年10月21-23日　大阪市　口演
33. 工藤雅範, 小村　健, 根岸綾子, 松本佳奈子, 持田薫利, 大久保亜耶, 石井良昌：顎下腺部に発生した類表皮嚢胞の1例.第56回社団法人日本口腔外科学会総会 2011年10月21-23日　大阪市　口演
34. 丸川恵理子, 高橋幸伸, 畠山一朗, 小村　健：非培

養自己骨髄細胞とβ-TCPを用いた骨再生療法への実験的検討. 第56回社団法人日本口腔外科学会総会 2011年10月21-23日　大阪市　口演

35. 望月裕美,　中村 伸,小村 健,原田浩之,渋谷 均,倉林亨：[18F]FDG-PET/CTによる口腔癌頸部リンパ節転移診断の検討.　第51回日本核医学会学術総会 2011年10月27-29日　つくば市　ポスター
36. 森田圭一, 吉本光洋, 松川　祥, 小村　健：口腔白板症におけるFADDゲノム増幅. 第49回日本癌治療学会総会　2011 年10月27-29日　名古屋市　口演
37. 釘本琢磨, 森田圭一, 小村　健：　含嗽による剥離細胞を用いた口腔がん検出法. 第49回日本癌治療学会総会 2011年10月27-29日　名古屋市　口演
38. 望月裕美,小村 健,平井秀明,釘本琢磨,大迫利光,田口貴英：SAPHO症候群が疑われた慢性下顎骨骨髄炎の1例. 第45回日本口腔科学会関東地方部会　2011年11月19日　東京　口演
39. 森田圭一, 島田泰如, 小村　健：Gorlin 症候群19 例の臨床症状と角化嚢胞性歯原性腫瘍の治療. 第56回日本人類遺伝学会・第11回東アジア人類遺伝学会 共同大会 2011年11月9-12日　千葉市　口演
40. 高原楠旻,佐藤　昌,森田圭一,小村　健：過去5年間における口腔感染症Ⅲ～Ⅴ群の臨床的検討.第45回日本口腔科学会関東地方部会　2011年11月19日　東京　口演
41. 畠山一朗, 丸川恵理子, 高橋幸伸, 小村　健：イヌ抜歯窩での歯槽堤保存における乏血小板血漿（platelet poor plasma; PPP）と多血小板フィブリン（platelet rich fibrin; PRF）の効果. 第3回多血小板血漿（PRP）療法研究会　2011年11月20日　大阪市　口演
42. 丸川恵理子, 小村　健, 和泉雅一：歯根完成歯の移植におけるエムドゲインゲルと自家骨移植の有用性に関する検討.第11回日本外傷歯学会総会・学術大会 2011年11月26 - 27日　札幌市　口演
43. 畠山一朗, 丸川恵理子, 高橋幸伸, 小村　健：自己フィブリンゲルの抜歯窩歯槽堤保存法への応用に関する実験的検討.　第15回日本顎顔面インプラント学会総会・学術大会 2011年12月3-4日　千葉市　口演
44. 丸川恵理子, 小村　健, 和泉雅一：歯根完成歯の移植へのエムドゲインゲルと自家骨移植の応用に関する臨床的検討.第76回口腔病学会学術大会　2011年12月9-10日　東京　口演
45. 吉本光洋, 森田圭一, 小村　健：口腔白板症におけるFADDゲノム増幅検出法. 第76回口腔病学会学術大会　2011年12月9-10日　東京　口演
46. 松下善彦, 樺沢勇司, 佐藤　昌, 菊池　剛, 佐藤百合子, 木村　敦, 小村　健：当科における過去10年間の顎変形症手術に関する検討. 第76回口腔病学会学術大会　2011年12月9-10日　東京　口演
47. 工藤雅範, 松本佳奈子, 大久保亜耶, 石井良昌：習慣性転倒による顔面外傷が発見の契機となった頭蓋骨内髄膜腫の1例.第192回日本口腔外科学会関東地方会　2011年12月10日　東京　口演
48. 大久保亜耶, 工藤雅範, 松本佳奈子, 石井良昌：異時的に発生した両側舌癌の1例.第192回日本口腔外科学会関東地方会　2011年12月10日　東京　口演
49. 中川　聡,島本裕彰,高　楠旻,小村　健：顎下部に発生した静脈石の1例.第192回日本口腔外科学会関東地方会　2011年12月10日　東京　口演

12）受賞

1. 佐藤　潔, 坂本　啓, 栢森　高, 山口　朗：第53回歯科基礎医学会総会　優秀ポスター賞　2011年10月1-2日　岐阜市　「口腔扁平上皮癌による骨破壊予防療法の開発」

13）外部資金の獲得状況

1. 日本学術振興会科学研究費補助金・基盤研究C

「ナノサイズパーティクルを用いた口腔癌レセプターターゲティングDDSの開発」

研究代表者：中島雄介

期間：平成22-24年度

平成22年	直接経費	1,300,000円
	間接経費	390,000円
平成23年	直接経費	1,100,000円
	間接経費	330,000円
平成24年	直接経費	800,000円
	間接経費	240,000円

2. 日本学術振興会科学研究費補助金・基盤研究C

「組織弾性イメージングを用いた舌扁平上皮癌における術前治療効果の判定」

研究代表者：原田浩之

期間：平成23-25年度

平成23年	直接経費	2,300,000円
	間接経費	690,000円
平成24年	直接経費	1,700,000円
	間接経費	510,000円
平成25年	直接経費	100,000円

間接経費　　30,000円

3. 日本学術振興会科学研究費補助金・若手研究B

「自己血漿と骨髄間葉系幹細胞を併用したハイブリッドマテリアルによる骨再生療法の検討」

研究代表者：丸川恵理子

期間：平成23-25年度

平成23年　直接経費　1,700,000円

　　間接経費　　510,000円

平成24年　直接経費　1,400,000円

　　間接経費　　420,000円

4. 日本学術振興会科学研究費補助金・若手研究B

「11q13.3領域遺伝子増幅と口腔がんストレス応答骨破壊機構」

研究代表者：森田圭一

期間：平成23-24年度

平成23年　直接経費　1,900,000円

　　間接経費　　570,000円

平成24年　直接経費　1,400,000円

　　間接経費　　420,000円

5. 日本学術振興会科学研究費補助金・若手研究B

「ビスフォスフォネート長期投与による骨髄炎モデルの確立とその骨代謝機構に対する解明」

研究代表者：今泉史子

期間：平成20-23年度

平成20年　直接経費　1,400,000円

　　間接経費　　420,000円

平成21年　直接経費　　900,000円

　　間接経費　　270,000円

平成22年　直接経費　　500,000円

　　間接経費　　150,000円

平成23年　直接経費　　500,000円

　　間接経費　　150,000円

6. 日本学術振興会科学研究費補助金・若手研究B

「パラフィン包埋組織からのプロテオーム解析による新規口腔がんマーカーの開発」

研究代表者：根岸綾子

期間：平成22-23年度

平成22年　直接経費　1,600,000円

　　間接経費　　480,000円

平成23年　直接経費　1,400,000円

　　間接経費　　420,000円

7. 日本学術振興会科学研究費補助金・若手研究B

「新規免疫療法の確立を目指した口腔癌患者に誘導されている多能性免疫担当細胞の解析」

研究代表者：田中香衣

期間：平成21-24年度

平成21年　直接経費　　700,000円

　　間接経費　　210,000円

平成22年　直接経費　　700,000円

　　間接経費　　210,000円

平成23年　直接経費　　700,000円

　　間接経費　　210,000円

平成24年　直接経費　　800,000円

　　間接経費　　240,000円

8. 共同研究費　オリンパス株式会社

「機能性生体材料の顎口腔外科分野での応用検討」

研究代表者：小村　健

平成22年1月4日～平成24年9月30日

研究費：7,350,000円　　直接経費　6,681,819円

9. 武田科学振興財団研究助成金

自己血漿と骨髄間葉系幹細胞を併用したハイブリッドマテリアルによる骨再生療法の検討

2011年7月22日から2年

直接経費　3,000,000円　研究代表者　丸川恵理子

14）特別講演，招待講演，シンポジウム

シンポジウム

1. 小村　健：唾液腺腫瘍の外科治療　第29回日本口腔腫瘍学会総会　2011年1月28日　熊本市
2. 森田圭一，小村　健：口腔癌における診断マーカー探索．第4回硬組織疾患ゲノムセンターシンポジウム　2011年1月31日　東京

講　演

1. 小村　健：市民のための安心・安全な口腔管理 -口腔がん早期発見を目指して「口腔がん治療の現況と展望」．東京都歯科医師会　平成22年度 学術講演会・学術教育研修会　2011年2月6日　東京
2. 小村　健：「口腔癌治療の現況と展望」．山梨県がん診療連携拠点病院連絡協議会　がん医療従事者研修会　2011年2月18日　甲府市
3. 小村　健：口腔顎顔面外傷の診断と治療．日本外傷歯学会認定医研修セミナー　2011年6月12日　東京
4. 小村　健：「当科における下顎再建の現況」．横浜市大口腔外科同門会　特別講演　2011年7月3日　横浜市
5. Omura K： Mandibular fracture. -anatomy, biomechanics and surgical approach- AO CMF principal Course, Nagoya 2011年7月14日 名古屋市

6. Omura K：Regenerated medicine in jaw bone. AO CMF principal Course, Nagoya 2011年7月17日 名古屋市
7. 小村　健：ミニレクチャー　口腔外科医に必要な頸部郭清術の基礎. 第56回　日本口腔外科学会総会 2011年10月23日　大阪
8. 小村　健：下顎再建の現状. 第6回山口県口腔癌研究会　特別講演　2011年11月11日　宇部市

15）主催学会

1. 第8回 紹介医のための口腔外科セミナー　2011年11月6日　東京

16）新聞、雑誌、TV報道

1. 小村　健：治療歯の根が残っている． 暮らしと健康 第66巻8号　75頁
2. 原田浩之：口腔扁平上皮癌に対する術前S-1・放射線同時併用療法. Medical Tribune Vol44,No15 11頁 2011年4月14日

17）教室、分野や講座の准教授、講師、助教、特別研究員、ポスドク、指導を受けた大学院生の名前

助教授　原田　浩之
講　師　中島　雄介
　　櫻井　仁亨
助　教　樺沢　勇司
　　島本　裕彰
　　丸川　恵理子
　　佐藤　　昌
　　田中　香衣
　　富岡　寛文
硬組織疾患ゲノムセンター特任講師
　　森田　圭一
大学院生　釘本　琢磨
　　○佐藤　　潔
　　高橋　幸伸
　　吉本　光洋
　　大迫　利光
　　○島田　泰如
　　畠山　一朗
　　松川　　祥
　　田口　貴英
　　山本　信祐
　　高橋　由貴子
　　○白川　純平
　　木村　　敦
　　プラディット・ルシャタムカヤヌント
　　高原　楠旻

○はAISS

Published OnlineFirst July 27, 2011; DOI:10.1158/0008-5472.CAN-11-0368

Cancer Research

Molecular and Cellular Pathobiology

The Tumor Suppressive MicroRNA *miR-218* Targets the mTOR Component *Rictor* and Inhibits AKT Phosphorylation in Oral Cancer

Atsushi Uesugi[1,5], Ken-ichi Kozaki[1,3], Tomohiko Tsuruta[1], Mayuko Furuta[1,2], Kei-ichi Morita[4,5], Issei Imoto[1], Ken Omura[2,4,5], and Johji Inazawa[1,2,3]

Abstract

The incidence of oral squamous cell carcinoma (OSCC) is rising rapidly in developed countries, posing a growing challenge due to the poor management of this type of malignancy at present. In this study, we profiled tumor suppressive microRNAs (miRNAs) that are silenced by DNA hypermethylation in OSCC using a function-based screening approach. This approach employed a cell proliferation assay for 327 synthetic miRNAs in two OSCC cell lines. Among the 110 miRNAs identified in this set that exhibited inhibitory properties, we compared DNA methylation and expression status in a wider panel of OSCC cell lines and primary tumor tissues, resulting in the identification of *miR-218* and *miR-585* as functionally significant miRNA genes that are frequently silenced in OSCC by DNA hypermethylation. Ectopic expression of *miR-218* and *miR-585* in OSCC cells lacking endogenous expression reduced cell growth in part through caspase-mediated apoptosis. Notably, *miR-218* reduced levels of the rapamycin-insensitive component of mTOR, Rictor, in a manner associated with a suppression of Akt S473 phosphorylation. Together our findings define *miR-585* as a tumor suppressive function that is often epigenetically silenced in OSCC, and they identify *Rictor* as a novel target of *miR-218*, suggesting that activation of the mTOR-Akt signaling pathway induced by Rictor contributes centrally to oral carcinogenesis. *Cancer Res; 71(17); 5765–78. ©2011 AACR.*

Introduction

MicroRNAs (miRNAs) are an abundant class of endogenous, small, non-coding RNAs, the products of which are small single-stranded RNAs of 19 to 22 nucleotides with a primary role in posttranscriptional silencing generally through binding to the 3′-UTR of protein-coding transcripts, in turn triggering mRNA degradation or translational repression (1). In human cancers, the expression of miRNAs is generally downregulated in malignant tissues compared with the corresponding non-malignant tissues (2, 3), suggesting the deregulation of miRNA expression and the contribution of miRNAs to the multistep processes of carcinogenesis either as oncogenes or as tumor-suppressor genes (TSG; refs. 4, 5). Among various epigenetic mechanisms of cancer-related gene-silencing, DNA hypermethylation of CpG sites within CpG-islands is known to lead to the inactivation of many TSGs (6) and several tumor-suppressive miRNAs (TS-miRNAs; ref. 7). In fact, DNA methylation-mediated downregulation of miRNAs by proximal CpG-islands has been described by a number of groups including ours (8–10).

Oral cancer, predominantly oral squamous cell carcinoma (OSCC), is the most common head and neck neoplasm, affecting approximately 270,000 people worldwide in 2002 (11). In Japan, OSCC is relatively common, accounting for more than 5,500 deaths in 2003 (12). The carcinogenesis, including OSCC (13), is considered to arise through the progressive accumulation of multiple genetic abnormalities, which may impair the functions of oncogenes or TSGs that play a crucial role in the development of this disease. In addition, evidence has emerged that epigenetic mechanisms, such as altered DNA methylation patterns, play a significant role in the silencing of TSGs and contribute to malignant transformation during oral carcinogenesis (14).

In this study, we identified and characterized TS-miRNAs frequently silenced by DNA hypermethylation in OSCC and their targets using function-based screening with a cell proliferation assay for 327 synthetic miRNAs and a series of sequential analyses of DNA methylation and expression in OSCC cell lines and primary tumors. The function-based

Authors' Affiliations: [1]Department of Molecular Cytogenetics, Medical Research Institute and School of Biomedical Science; [2]Global Center of Excellence (GCOE) Program for International Research Center for Molecular Science in Tooth and Bone Diseases; [3]Department of Genome Medicine; [4]Department of Advanced Molecular Diagnosis and Maxillofacial Surgery, Hard Tissue Genome Research Center; and [5]Department of Oral and Maxillofacial Surgery, Tokyo Medical and Dental University, Tokyo, Japan

Note: Supplementary data for this article are available at Cancer Research Online (http://cancerres.aacrjournals.org/).

Corresponding Author: Johji Inazawa, Department of Molecular Cytogenetics, Medical Research Institute, Tokyo Medical and Dental University, 1-5-45 Yushima, Bunkyo-ku, Tokyo 113-8510, Japan. Phone: 03-5803-5820; Fax: 03-5803-0244; E-mail: johinaz.cgen@mri.tmd.ac.jp

doi: 10.1158/0008-5472.CAN-11-0368

©2011 American Association for Cancer Research.

Downloaded from cancerres.aacrjournals.org on January 6, 2012
Copyright © 2011 American Association for Cancer Research

Published OnlineFirst July 27, 2011; DOI:10.1158/0008-5472.CAN-11-0368

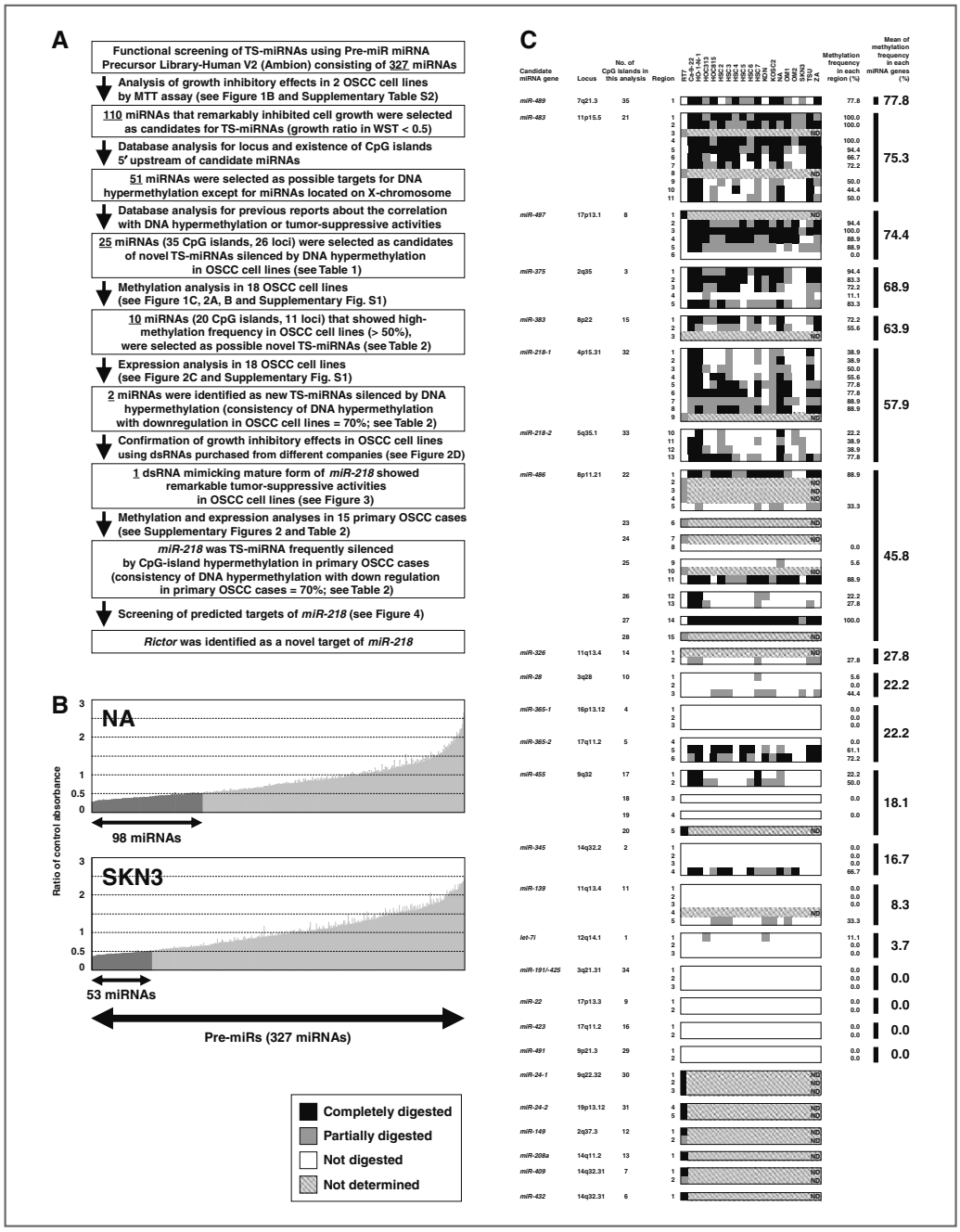

Downloaded from cancerres.aacrjournals.org on January 6, 2012
Copyright © 2011 American Association for Cancer Research

Published OnlineFirst July 27, 2011; DOI:10.1158/0008-5472.CAN-11-0368

screening presented in this paper is a powerful tool for exploring a large number of double-stranded RNAs (dsRNAs) having tumor-suppressive effects, including TS-miRNAs and siRNAs, as therapeutic agents for several types of cancer cells directly (15, 16). Through this approach, 2 epigenetically silenced TS-miRNAs in OSCC, *miR-218* and *miR-585*, which are located within the intron of *SLIT2* and *SLIT3*, respectively, and a novel target of *miR-218*, *Rictor*, were identified in our study. This study is the first to show clearly that the tumor-suppressive activity of *miR-585* is epigenetically silenced in OSCC and that *miR-218* targets *Rictor* inducing the activation of a TOR-Akt signaling pathway.

Materials and Methods

Cell lines and primary tumor samples

Derivations of and culture conditions for cell lines were reported previously (17). OSCC cell lines were authenticated in our previous studies of array-CGH analyses (17). RT7, human oral keratinocytes immortalized by TERT and human papillomavirus (HPV) type 16 E6/E7 oncogenes, was kindly provided by Dr N. Kamata (Hiroshima University Faculty of Dentistry, Japan). To analyze the restoration of genes, cells were cultured with or without 10 μmol/L of 5-aza 2′-deoxycytidine (5-aza-dCyd) for 5 days. A total of 15 frozen primary samples were obtained from OSCC patients treated at Tokyo Medical and Dental University with written consent from each patient in the formal style and after approval by the local ethics committee.

Transfection with synthetic miRNAs and siRNAs

A total of 10 nmol/L of dsRNA mimicking human mature miRNAs or control nonspecific miRNA (Ambion; Thermo Scientific Dharmacon), and 20 nmol/L of target-specific siRNAs for *PIK3CA* (Dharmacon) and *Rictor* (Invitrogen) or their control nonspecific siRNA were transfected individually into OSCC cells using Lipofectamine RNAiMAX (Invitrogen). The numbers of viable cells were assessed by the colorimetric water-soluble tetrazolium salt (WST) assay (Cell counting kit-8; Dojindo Laboratories). The cell cycle was evaluated by a fluorescence-activated cell sorting (FACS) analysis as described elsewhere (17).

Methylation analysis

Each of gene and CpG-island was searched miRBase database (release April 17, 2011; ref. 18), UCSC Genome Browser on Human February 2009 Assembly (hg19; ref. 19) and PubMed (20). The combined bisulfite restriction analysis (COBRA) and the bisulfite-sequencing analysis, using primer sets designed to amplify regions of interest (Supplementary Table S1), were done as described elsewhere (8).

Real-time reverse transcription-PCR

Real-time reverse transcription PCR (RT-PCR) was done as described elsewhere (8).

miRNA target predictions, Western blotting, and luciferase activity assay

Predicted targets for miRNAs and their target sites were analyzed using Microcosm Targets (21), miRanda (22), and TargetScan (23). Anti-caspase-3, anti-cleaved caspase-3, anti-cleaved PARP, anti-Akt, anti-phospho-Akt (Ser-473), anti-Rictor (Cell Signaling Technology) and anti-PIK3CA (Upstate Biotechnology) rabbit polyclonal antibodies were used in Western blotting. Luciferase constructs were made by ligating oligonucleotides containing the 3′-UTR target sites downstream of the luciferase gene in the pMIR-REPORT luciferase vector (Ambion). Luciferase activity was measured as described elsewhere (8).

Statistical analysis

Differences between subgroups were tested with the Mann–Whitney *U* test.

Results

Function-based screening of TS-miRNA in OSCC cell lines

To identify TS-miRNAs in OSCC, we first examined 327 synthetic miRNAs mimicking human mature miRNAs by function-based screening in 2 OSCC cell lines, NA and SKN3. The strategy used and partial results obtained are shown in Figure 1A. Since the proliferation-inhibitory effect was made an index for the rating of tumor-suppressive activity in our function-based screening, relative cell growth ratios in Figure 1B and Supplementary Table S2 indicate effects of each synthetic miRNA on cell growth 5 days after transfection. In this first screening, 110 miRNAs, including known TS-miRNAs, such as *miR-34* (24), *miR-124* (9, 25), *miR-193a* (8), and *miR-491* (15), showed remarkable inhibitory effects on cell growth (relative growth ratio < 0.5). Then we selected novel miRNAs with CpG-islands in the region 5′ upstream or around these genes and excluded miRNAs previously reported to correlate with DNA hypermethylation and their tumor-suppressive activity among 110 miRNAs by means of database analyses. From the first screening, 25 mature sequences of miRNAs emerged as candidates for new TS-miRNAs silenced by DNA hypermethylation in OSCC cell lines (Table 1).

Figure 1. Strategy employed and results of a function-based screening of TS-miRNAs in OSCC cell lines. A, strategy used for the identification of epigenetically silenced TS-miRNAs in OSCC. B, result of function-based screening of TS-miRNAs in NA and SKN3 cells using Pre-miR miRNA Precursor Library-Human V2 (Ambion). Cells (1.0×10^4/well) were inoculated onto 24-well plates. Following 24 hours of incubation, 10 nmol/L of 327 dsRNA mimicking mature miRNA or control nonspecific miRNA was transfected individually into cells. The numbers of viable cells 5 days after transfection were evaluated by the WST assay in duplicate. Relative cell growth ratios were then calculated by normalization of each result to the cell numbers in control cells transfected with nonspecific miRNA (see Supplementary Table S2). The lower solid arrow indicates the 327 miRNAs examined. The top and middle closed arrows indicate 98 miRNAs and 53 miRNAs which showed marked growth inhibitory effects in NA and SKN3 cells, respectively (growth ratio < 0.5). C, summary of the DNA methylation status of CpG-islands around 25 mature sequences of miRNAs located at 26 loci including 35 CpG-islands in 18 OSCC cell lines and RT7 as a control determined by COBRA. PCR products used for COBRA were digested with *Bst*UI, *Taq*I, or *Hha*I, and electrophoresed (see Figure 2A and B, Tables 1, 2, Supplementary Fig. S2, Supplementary Table S1, and data not shown). Black, gray, white, and striped boxes indicate complete, partial, and no digestion by restriction enzymes, and not determined, respectively.

Downloaded from cancerres.aacrjournals.org on January 6, 2012
Copyright © 2011 American Association for Cancer Research

Published OnlineFirst July 27, 2011; DOI:10.1158/0008-5472.CAN-11-0368

Table 1. Summary of 25 miRNAs (35 CpG islands, 26 loci) selected as candidates for novel TS-miRNA silenced by DNA hypermethylation in function-based screening using OSCC cell lines and Pre-miR miRNA Precursor Library - Human V2 (Ambion)

Number of candidate miRNAs	miRNAs	miRNA genes	Locus	Host genes	Clustered miRNAs	Number of CpG island in this analysis	Distance of CpG island from the most 5′ mature miRNA sequence	Methylation frequency (total %)
1	*hsa-let-7i*	*hsa-let-7i*	12q14.1	-	-	1	0	3.7
2	*hsa-miR-345*	*hsa-miR-345*	14q32.2	-	-	2	523	16.7
3	*hsa-miR-375*	*hsa-miR-375*	2q35	-	-	3	0	68.9
4	*hsa-miR-365*	*hsa-miR-365-1*	16p13.12	-	*miR-193b*	4	6067	22.2
		hsa-miR-365-2	17q11.2	-	*miR-193a*	5	15,053	
5	*hsa-miR-432**	*hsa-miR-432*	14q32.31	-	*miR-337/665/431/433/127/432/136*	6	960	ND
6	*hsa-miR-409-3p*	*hsa-miR-409*	14q32.31	-	*miR-409-5p(miR-485/453/154/496/377/541/412/369/410/656)*	7[a]	0	ND
7	*hsa-miR-409-5p*	*hsa-miR-409*	14q32.31	-	*miR-409-3p(miR-485/453/154/496/377/541/412/369/410/656)*	7[a]	0	ND
8	*hsa-miR-497*	*hsa-miR-497*	17p13.1	-	*miR-195*	8	4,060	78.7
9	*hsa-miR-22*	*hsa-miR-22*	17p13.3	*C17orf92*	-	9	1,924	0.0
10	*hsa-miR-28*	*hsa-miR-28*	3q28	*LPP*	-	10	53,4218	22.2
11	*hsa-miR-139*	*hsa-miR-139*	11q13.4	*PDE2A*	-	11	27,049	8.3
12	*hsa-miR-149*	*hsa-miR-149*	2q37.3	*GPC1*	-	12	0	ND
13	*hsa-miR-208a*	*hsa-miR-208a*	14q11.2	*MYH6*	-	13	1,482	ND
14	*hsa-miR-326*	*hsa-miR-326*	11q13.4	*ARRB1*	-	14	15,995	27.8
15	*hsa-miR-383*	*hsa-miR-383*	8p22	*SGCZ*	-	15	61,6781	63.9
16	*hsa-miR-423*	*hsa-miR-423*	17q11.2	*CCDC55*	-	16	87	0.0
17	*hsa-miR-455*	*hsa-miR-455*	9q32	*COL27A1*	-	17	54,692	18.1
						18	53,696	
						19	53,192	
						20	41,346	
18	*hsa-miR-483*	*hsa-miR-483*	11p15.5	*IGF2*	-	21	3,513	75.3
19	*hsa-miR-486-5p*	*hsa-miR-486*	8p11.21	*ANK1*	-	22	235,315	45.8
						23	215,510	
						24	167,723	
						25	136,850	
						26	106,530	
						27	65,110	
						28	41,230	
20	*hsa-miR-491*	*hsa-miR-491*	9p21.3	*KIAA1797*	-	29	31,468	0.0

(*Continued on the following page*)

Downloaded from cancerres.aacrjournals.org on January 6, 2012
Copyright © 2011 American Association for Cancer Research

Published OnlineFirst July 27, 2011; DOI:10.1158/0008-5472.CAN-11-0368

Table 1. Summary of 25 miRNAs (35 CpG islands, 26 loci) selected as candidates for novel TS-miRNA silenced by DNA hypermethylation in function-based screening using OSCC cell lines and Pre-miR miRNA Precursor Library - Human V2 (Ambion) (Cont'd)

Number of candidate miRNAs	miRNAs	miRNA genes	Locus	Host genes	Clustered miRNAs	Number of CpG island in this analysis	Distance of CpG island from the most 5′ mature miRNA sequence	Methylation frequency (total %)
24	*hsa-miR-24*	*hsa-miR-24-1*	9q22.32	*C9orf3*	*miR-23b/27b*	30	0	ND
		hsa-miR-24-2	19p13.12	-	*miR-23a/27a*	31	6,050	
21	*hsa-miR-218*	*hsa-miR-218-1*	4p15.31	*SLIT2*	-	32	273,030	57.9
		hsa-miR-218-2	5q35.1	*SLIT3*	*miR-585*	33	532,170	
22	*hsa-miR-191**	*hsa-miR-191*	3q21.31	*DALRD3*	*miR-425-3p*	34[a]	184	0.0
23	*hsa-miR-425-3p*	*hsa-miR-425*	3p21.31	*DALRD3*	*miR-191**	34[a]	659	0.0
25	*hsa-miR-489*	*hsa-miR-489*	7q21.3	*CALCR*	*miR-653*	35	90,755	77.8

[a]Same CpG islands.
NOTE: These data were searched miRBase database (release April 17, 2011), UCSC Genome Browser on Human February 2009 Assembly (hg19) and PubMed.

Methylation and expression analyses of candidates in OSCC cell lines

Next, we explored the DNA methylation status of 35 CpG-islands around 25 miRNAs located at 26 loci in a panel of 18 OSCC cell lines and a normal counterpart, RT7, an immortalized human oral keratinocyte line, by COBRA (Fig. 1C). Since multiple copies of some mature miRNAs, as listed in Table 1, are transcribed from different loci, the number of mature forms of miRNAs is smaller than the number of genomic loci. In COBRA, on the basis of a comparison of mean values of methylation frequencies in each region examined, frequent DNA hypermethylation (>50% of OSCC lines) was found in only 6 of 25 miRNAs, that is, *miR-218*, *miR-375*, *miR-383*, *miR-483*, *miR-489*, and *miR-497*, although CpG-island hypermethylation on/around these miRNAs was also detected in RT7. We next investigated the consistency in the correlation between DNA methylation status in each region of these 6 miRNA genes by COBRA and their expression patterns in 18 OSCC cell lines and RT7 by TaqMan real-time RT-PCR (Table 2), and found that values were higher in some regions of *miR-218-1* (50.0%–77.8%) and *miR-375* (100%) than other miRNA genes (0%–56.3%; Fig. 1A–C and Supplementary Fig. S1A–C). *miR-218-1* and *miR-218-2* are located at 4p15.31 and 5q35.1 within the intron of *SLIT2* and *SLIT3*, respectively (Fig. 2A and B). Interestingly, *miR-585*, together with *miR-218-2*, is also located within the intron of *SLIT3*, and the expression patterns of *miR-218* and *miR-585* were similar to those of *SLIT2* and *SLIT3*, respectively (Fig. 2B and C); note that the percentage of OSCC cell lines with significant downregulation of *miR-218*, *miR-585*, *SLIT2*, *SLIT3*, and *miR-375* expression (<0.5-fold) was 44.4% (8/18), 55.6% (10/18), 61.1% (11/18), 77.8% (14/18), and 100% (18/18), respectively (Fig. 2C and Supplementary Fig. 1C). To determine the relationship between DNA hypermethylation in CpG-islands on/around *miR-218-1*, *miR-218-2*, and *miR-375* and the downregulation of gene expression, we treated OSCC cell lines with 5-aza-dCyd, observing a remarkable restoration of the expression levels of these miRNAs and their host genes in 55.6% (10/18), 44.4% (8/18), 33.3% (6/18), 61.1% (11/18), and 100% (18/18) of OSCC cell lines, respectively (Fig. 2C and Supplementary Fig. 1D). Consistent with these results, CpG-island hypermethylation was also confirmed by bisulfite-sequencing in the OSCC lines lacking the expression of those candidate miRNAs, but not in RT7 and the cell lines expressing these miRNAs (Fig. 2A and B and Supplementary Fig. 1E). These results strongly suggest that DNA hypermethylation of CpG sites within CpG-islands on/around these genes deregulates their expressions in OSCC cell lines.

Confirmation of dsRNA-induced growth inhibition in OSCC cell lines

To confirm the growth inhibitory effects of *miR-218*, *miR-585*, and *miR-375* in the function-based screening, we used 2 synthetic miRNAs purchased from Ambion and Thermo Scientific Dharmacon to take into consideration the off-target effects of dsRNAs. The ectopic expression of these miRNAs in OSCC cell lines lacking their expressions by the transient transfection of dsRNA was evaluated by TaqMan real-time RT-PCR analysis (data not shown). Consistent with the results of the function-based screening (Supplementary Table S2), restoration of

Downloaded from cancerres.aacrjournals.org on January 6, 2012
Copyright © 2011 American Association for Cancer Research

Published OnlineFirst July 27, 2011; DOI:10.1158/0008-5472.CAN-11-0368

Table 2. Correlation between DNA hypermethylation status in each region of these 6 miRNA genes by COBRA and their expression patterns in OSCC cell lines and primary cases by quantitative real-time RT-PCR analysis

miRNAs	miRNA genes	Regions in COBRA	OSCC cell lines: Methylation frequency (%)[a]		OSCC cell lines: Consistency of methylation with down-regulation (%)[b]		Primary OSCC cases: Methylation frequency (%)[a]		Primary OSCC cases: Consistency of methylation with downregulation (%)[b]	
hsa-miR-489	*hsa-miR-489*	1	77.78	14	0.00	0	-		-	
hsa-miR-483	*hsa-miR-483*	1	100.00	18	16.67	3	-		-	
		2	100.00	18	16.67	3	-		-	
		3	ND		-		-		-	
		4	100.00	18	16.67	3	-		-	
		5	94.44	17	17.65	3	-		-	
		6	66.67	12	16.67	2	-		-	
		7	72.22	13	15.38	2	-		-	
		8	ND		-		-		-	
		9	50.00	9	22.22	2	-		-	
		10	44.44	8	-		-		-	
		11	50.00	9	11.11	1	-		-	
hsa-miR-497	*hsa-miR-195/497*	1	ND		-		-		-	
		2	94.44	17	47.06	8	-		-	
		3	100.00	18	50.00	9	-		-	
		4	88.89	16	50.00	8	-		-	
		5	88.89	16	56.25	9	-		-	
		6	0.00	0	-	0	-		-	
hsa-miR-375	*hsa-miR-375*	1	88.89	16	100.00	16	-		-	
		2	83.33	15	100.00	15	-		-	
		3	72.22	13	100.00	13	-		-	
		4	11.11	2	-		-		-	
		5	83.33	15	100.00	15	-		-	
hsa-miR-383	*hsa-miR-383*	1	72.22	13	7.69	1	-		-	
		2	55.56	10	10.00	1	-		-	
		3	ND		-		-		-	
hsa-miR-218	*hsa-miR-218-1*	1	38.89	7	-		20.00	3/15	100.00	3/3
		2	38.89	7	-		13.33	2/15	100.00	2/2
		3	50.00	9	77.78	7	6.67	1/15	100.00	1/1
		4	55.56	10	70.00	7	6.67	1/15	100.00	1/1
		5	77.78	14	50.00	7	53.33	8/15	75.00	6/8
		6	77.78	14	57.14	8	73.33	11/15	81.82	9/11
		7	88.89	16	50.00	8	66.67	10/15	80.00	8/10
		8	88.89	16	50.00	8	93.33	14/15	85.71	12/14
		9	ND		-		-		-	
	hsa-miR-585/218-2	10	22.22	4	-		13.33	2/15	100.00	2/2
		11	38.89	7	-		13.33	2/15	100.00	2/2
		12	38.89	7	-		6.67	1/15	100.00	1/1
		13	77.78	14	50.00	7	0	0/15	-	-
hsa-miR-486-5p	*hsa-miR-486*	1	88.89	16	31.25	5	-		-	
		2	ND		-		-		-	
		3	ND		-		-		-	
		4	ND		-		-		-	

(*Continued on the following page*)

Downloaded from cancerres.aacrjournals.org on January 6, 2012
Copyright © 2011 American Association for Cancer Research

Published OnlineFirst July 27, 2011; DOI:10.1158/0008-5472.CAN-11-0368

Table 2. Correlation between DNA hypermethylation status in each region of these 6 miRNA genes by COBRA and their expression patterns in OSCC cell lines and primary cases by quantitative real-time RT-PCR analysis (Cont'd)

miRNAs	miRNA genes	Regions in COBRA	OSCC cell lines: Methylation frequency (%)[a]		OSCC cell lines: Consistency of methylation with down-regulation (%)[b]		Primary OSCC cases: Methylation frequency (%)[a]	Primary OSCC cases: Consistency of methylation with downregulation (%)[b]
		5	33.33	6	-		-	-
		6	ND		-		-	-
		7	ND		-		-	-
		8	0.00	0	0.00	0	-	-
		9	5.56	1	-		-	-
		10	ND		-		-	-
		11	88.89	16	31.25	5	-	-
		12	22.22	4	-		-	-
		13	27.78	5	-		-	-
		14	100.00	18	27.78	5	-	-
		15	ND		-		-	-
hsa-miR-326	*hsa-miR-326*	1	ND		-		-	-
		2	27.78	5	-		-	-
hsa-miR-28	*hsa-miR-28*	1	5.56	1	-		-	-
		2	0.00	0	-		-	-
		3	44.44	8	-		-	-
hsa-miR-365	*hsa-miR-365-1*	1	0.00	0	-		-	-
		2	0.00	0	-		-	-
		3	0.00	0	-		-	-
	hsa-miR-365-2	4	0.00	0	-		-	-
		5	61.11	11	54.55	6	-	-
		6	72.22	13	53.85	7	-	-
hsa-miR-455	*hsa-miR-455*	1	22.22	4	-		-	-
		2	50.00	9	44.44	4	-	-
		3	0.00	0	0.00	0	-	-
		4	0.00	0	0.00	0	-	-
		5	ND		-		-	-
hsa-miR-345	*hsa-miR-345*	1	0.00	0	0.00	0	-	-
		2	0.00	0	0.00	0	-	-
		3	0.00	0	0.00	0	-	-
		4	66.67	12	0.00	0	-	-
hsa-miR-139	*hsa-miR-139*	1	0.00	0	-		-	-
		2	0.00	0	-		-	-
		3	0.00	0	-		-	-
		4	0.00		-		-	-
		5	33.33	6	-		-	-
hsa-let-7i	*hsa-let-7i*	1	11.11	2	-		-	-
		2	0.00	0	-		-	-
		3	0.00	0	-		-	-
hsa-miR-191/ miR-425-3p*	*hsa-miR-191/miR-425*	1	0.00	0	-		-	-
		2	0.00	0	-		-	-
		3	0.00	0	-		-	-

(*Continued on the following page*)

Downloaded from cancerres.aacrjournals.org on January 6, 2012
Copyright © 2011 American Association for Cancer Research

Published OnlineFirst July 27, 2011; DOI:10.1158/0008-5472.CAN-11-0368

Table 2. Correlation between DNA hypermethylation status in each region of these 6 miRNA genes by COBRA and their expression patterns in OSCC cell lines and primary cases by quantitative real-time RT-PCR analysis (Cont'd)

miRNAs	miRNA genes	Regions in COBRA	OSCC cell lines: Methylation frequency (%)[a]		OSCC cell lines: Consistency of methylation with down-regulation (%)[b]	Primary OSCC cases: Methylation frequency (%)[a]	Primary OSCC cases: Consistency of methylation with downregulation (%)[b]
hsa-miR-22	*hsa-miR-22*	1	0.00	0	-	-	-
		2	0.00	0	-	-	-
hsa-miR-423	*hsa-miR-423*	1	0.00	0	-	-	-
		2	0.00	0	-	-	-
hsa-miR-491	*hsa-miR-491*	1	0.00	0	-	-	-
		2	0.00	0	-	-	-
hsa-miR-24	*hsa-miR-24*	1	ND		-	-	-
		2	ND		-	-	-
		3	ND		-	-	-
hsa-miR-149	*hsa-miR-149*	1	ND		-	-	-
		2	ND		-	-	-
hsa-miR-208a	*hsa-miR-208a*	1	ND		-	-	-
hsa-miR-409-3p/ miR-409-5p	*hsa-miR-409*	1	ND		-	-	-
		2	ND		-	-	-
*hsa-miR-432**	*hsa-miR-432*	1	ND		-	-	-

[a]Frequency of cell lines or primary cases, in which DNA hypermethylation were detected by COBRA.
[b]Frequency of cell lines or primary cases, in which downregulation was consistent with DNA hypermethylation.
ND, not done.

miR-218 expression significantly reduced cell growth in the OSCC cell lines tested (Fig. 2D). In addition, a growth inhibitory effect of *miR-585* was clearly detected in Dharmacon product, whereas Ambion product of dsRNA mimicking *miR-585* was not on the market and could not be examined. In our *in vitro* analysis, tumor-suppressive functions of *miR-218* and *miR-585* were confirmed. Ambion product of dsRNA mimicking *miR-375* induced growth inhibition whereas Dharmacon product facilitated cell proliferation in both OSCC cell lines, and so *miR-375* was excluded from candidates in this study.

Methylation and expression analyses of *miR-218* and *miR-585* in primary OSCCs

To determine whether the CpG-island hypermethylation of *miR-218-1/SLIT2* and *miR-218-2/miR-585/SLIT3* also occurs in primary OSCCs in a tumor-specific manner, the correlation between DNA methylation status and the expression patterns of these genes in 15 primary OSCCs and corresponding non-cancerous oral mucosae was examined using COBRA and TaqMan real-time RT-PCR assay, respectively. In COBRA, the frequency of tumor-specific DNA hypermethylation in regions of *miR-218-1* and *miR-218-2/miR-585* was 6.7% to 93.4% and 6.7% to 13.3%, respectively, in primary OSCCs (Table 2, Supplementary Fig. 2A). Although the frequency of aberrant methylation at these CpG-islands was relatively low in primary tumors, expression levels of *miR-218* and *miR-585* in tumors as compared with paired normal oral mucosae were markedly reduced in 73.3% (11/15) and 66.7% (10/15) of primary OSCCs, respectively (< 0.5-fold expression, Supplementary Fig. 2B), and the consistency was comparatively high in these regions of *miR-218-1* (75.0%–100%) and *miR-218-2/miR-585* (100%). Although *miR-218* expression had been reported to be specifically reduced in HPV-positive cell lines and tissues (26), all of OSCC cell lines and primary samples examined in this study were confirmed the negative HPV-status by genomic PCR (Supplementary Fig. S3). Thus, our results suggest that *miR-218* and *miR-585* are most likely TS-miRNAs frequently silenced through tumor-specific DNA hypermethylation in OSCC.

Tumor-suppressive effects of ectopic *miR-218* and *miR-585* expression on the growth of OSCC cell lines

We examined tumor-suppressive effects of *miR-218* and *miR-585* on HSC-2 and NA (Fig. 3A and B). Restoration of the expression of these miRNAs significantly reduced cell growth in both cell lines tested. Since a large number of transfectants were rounded and floating compared with the control counterpart at 5 days after transfection, we conducted a FACS analysis and a Western blotting for caspase-mediated apoptosis using

Downloaded from cancerres.aacrjournals.org on January 6, 2012
Copyright © 2011 American Association for Cancer Research

Published OnlineFirst July 27, 2011; DOI:10.1158/0008-5472.CAN-11-0368

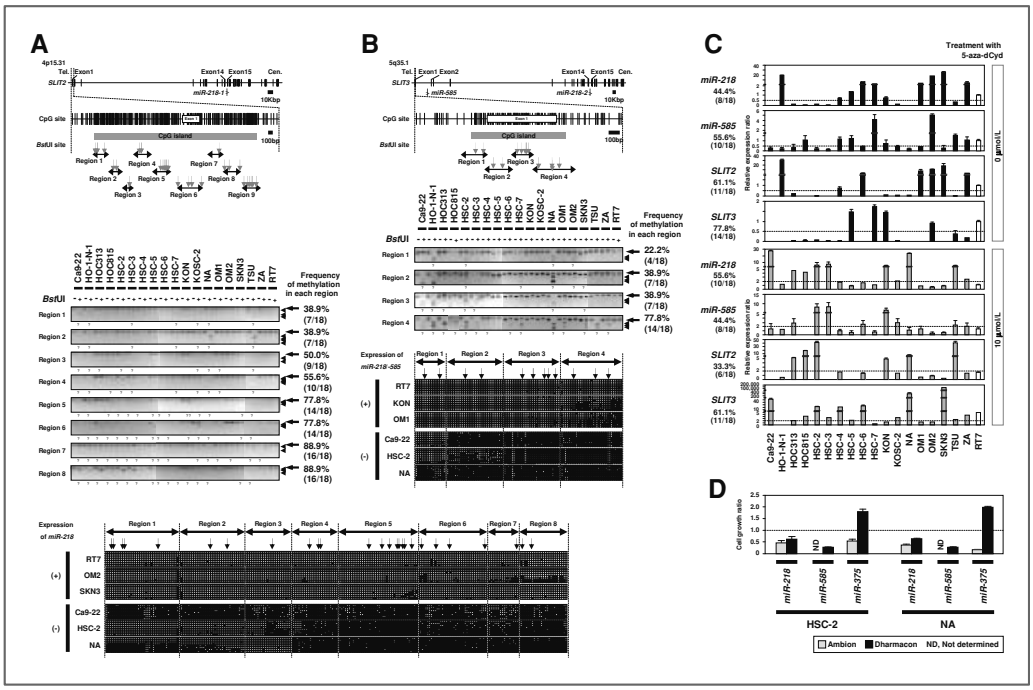

Figure 2. Correlation between methylation and expression of *miR-218* and the host genes *SLIT2* and *SLIT3* in OSCC cell lines. A and B, methylation analysis for *miR-218-1/SLIT2* (A) and *miR-218-2/SLIT3* (B). Top, these maps show intronic miRNAs, host genes, CpG-islands, CpG sites, and PCR products used for COBRA and bisulfite sequencing. White boxes, exons of *SLIT2* and *SLIT3*; gray box, CpG-island; closed arrows, PCR products (primers, Supplementary Table S1); vertical tick marks, CpG sites; vertical arrows, restriction enzyme sites. Middle, results of COBRA in 18 OSCC cell lines and RT7. Arrows, unmethylated alleles; arrowheads, methylated alleles; stars, samples with significant restricted fragments from methylated alleles. The presence of restriction enzyme processing is indicated with a plus or minus sign above the results of COBRA. Bottom, bisulfite sequencing of RT7 and representative OSCC cell lines with (+) or without (−) *miR-218* expression in PCR products examined by COBRA. Horizontal bars with arrowheads, PCR product; vertical arrows, restriction enzyme sites. Open and filled squares represent unmethylated and methylated CpG sites respectively, and each row represents a single clone. C, TaqMan real-time RT-PCR analysis for *miR-218*, *miR-585*, *SLIT2*, and *SLIT3* in 18 OSCC cell lines and RT7. Top, expression levels of intronic miRNAs and host genes were based on the amount of target message relative to *RNU6B* and *GAPDH*, respectively, to normalize the initial input of total RNA. Bar graphs show the ratio of the expression level in each cell line to that in RT7. Bottom, restoration of the expression of these genes after treatment with 10 μmol/L 5-aza-dCyd for 5 days in 18 OSCC cell lines. Bar graphs show the ratio of the expression level in treated cells to that in untreated cells. D, confirmation of tumor-suppressive activities of 3 candidate miRNAs in HSC-2 and NA cells using dsRNAs purchased from different companies (Ambion and Dharmacon). The numbers of viable cells 5 days after transfection with 10 nmol/L of dsRNAs were assessed by WST assay. Bar graphs show the growth ratio of cell numbers in *miR-218*-, *-375*-, and *-585*-transfectants relative to those in control-transfectants. Each point represents the mean of triplicate determinations (bars, SD).

both cell lines 72 hours after the transfection. In the FACS analysis, the effect of *miR-218* on the cell cycle in HSC-2 cells was weak while the accumulation of NA cells in the G_2/M phase was observed in *miR-218*-transfectants. Overexpression of *miR-585* induced the accumulation of cells in the G_2/M phase and sub-G_1 phase in the HSC-2 and NA cell lines, respectively. However, the Western blotting showed that ectopic expression of *miR-218* and *miR-585* remarkably increased protein levels of caspase3, cleaved caspase3 and cleaved PARP in both cell lines (Fig. 3C), *miR-218*- and *miR-585*-induced reductions of cell growth in these OSCC cell lines were not inhibited by caspase inhibitors (Supplementary Fig. S4A). In contrast, the G_2/M cell-cycle arrest was not confirmed by Western blotting for the phosphorylation status of Cdc2 and Chk1 in these transfectants (Supplementary Fig. S4B). These results, consistent with the previous report of *miR-218*-inducing apoptosis *in vitro* (27), suggest that *miR-218* and *miR-585* induce a reduction in cell growth at least in part through caspase-mediated apoptosis, whereas the cause of the cell death except the apoptosis in these transfectants remains unclear.

Screening of predicted targets for *miR-218* and *miR-585* in OSCC cell lines

While 5 genes of *EGFR*-coamplified and overexpressed protein (*ECOP*), *IκBs kinase* (*IKK*-β), *LIM* and *SH3 protein 1* (*LASP1*), *paxillin* (*PXN*), and *Robo1* have also been reported as direct targets of *miR-218* (28–32), the percentage of OSCC cell lines with notable upregulation of these genes (>2-fold expression) was 50.0% (9/18), 38.9% (7/18), 44.4% (8/18), 16.7% (3/18), and 11.1% (2/18), respectively (Fig. 4A). In addition, we also

Downloaded from cancerres.aacrjournals.org on January 6, 2012
Copyright © 2011 American Association for Cancer Research

Published OnlineFirst July 27, 2011; DOI:10.1158/0008-5472.CAN-11-0368

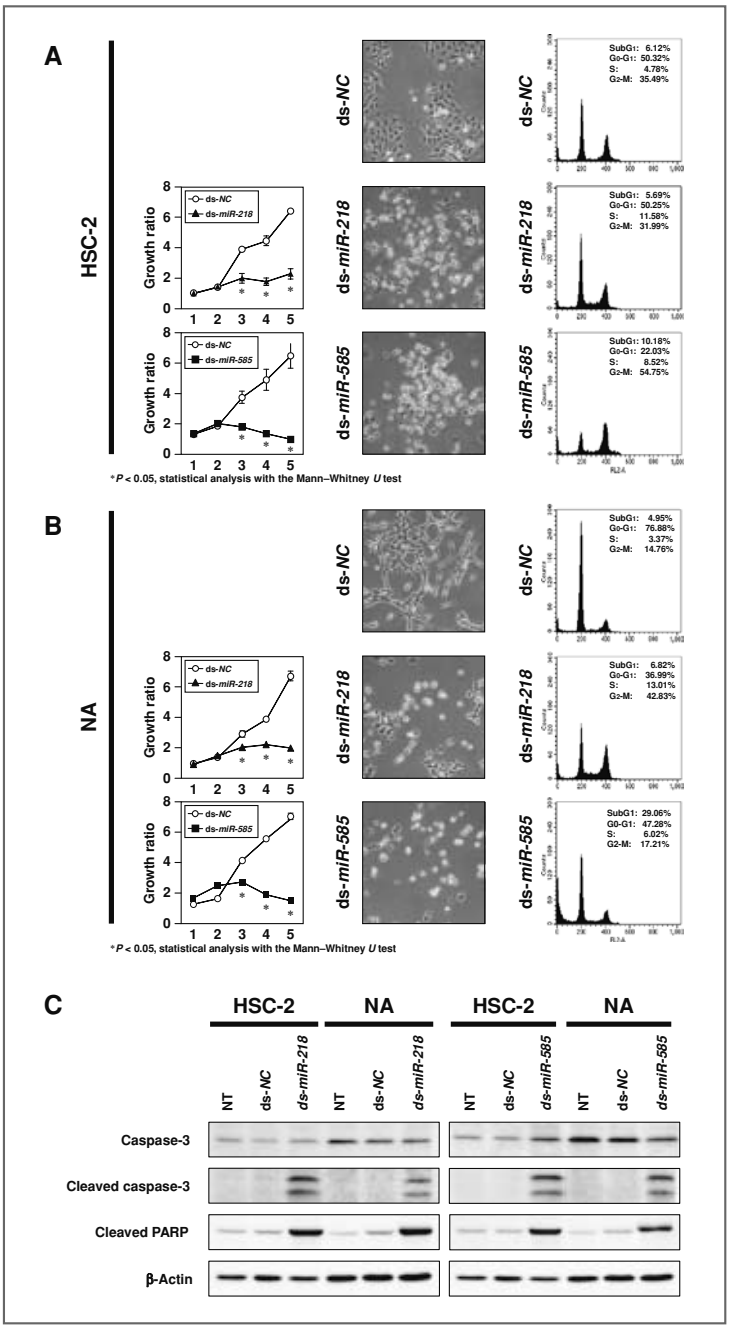

Figure 3. Tumor-suppressive effects of *miR-218* and *miR-585* on OSCC cell lines, HSC-2 and NA, lacking their expression. A and B, growth curves, phase-contrast micrographs, and results of FACS analysis in HSC-2 (A) and NA (B) cells in which 10 nmol/L of dsRNA mimicking *miR-218* or *miR-585*, or control nonspecific miRNA (ds-*NC*) was transfected. The numbers of viable cells after transfection were assessed by WST assay. Each data point represents the mean of triplicate determinations (bars, SD) in these experiments. Phase-contrast micrographs show OSCC cell lines cultured for 5 days after transfection. The size of the population in each phase of the cell cycle as assessed by FACS using OSCC cell lines 72 hours after transfection. C, the results of Western blotting of caspase3, cleaved caspase3, and cleaved PARP in HSC-2 and NA cells 48 hours after the transfection of each dsRNA.

Downloaded from cancerres.aacrjournals.org on January 6, 2012
Copyright © 2011 American Association for Cancer Research

Published OnlineFirst July 27, 2011; DOI:10.1158/0008-5472.CAN-11-0368

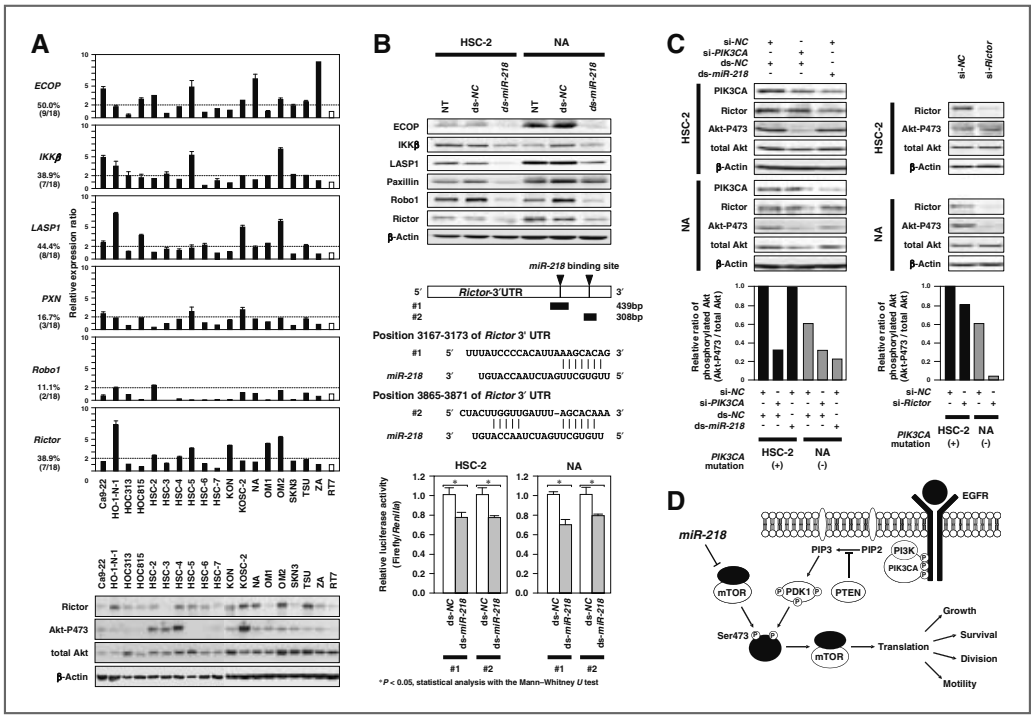

Figure 4. Identification and characterization of Rictor as a novel target of *miR-218*. A, expression analyses of 5 reported targets and one predicted target, *Rictor*, in 18 OSCC cell lines and RT7 using TaqMan real-time RT-PCR (top), and Western blotting (bottom). Expression levels of transcripts of these targets were based on the amount of target message relative to *GAPDH* to normalize the initial input of total RNA. Bar graphs show the ratio of the expression level in each cell line to that in RT7. B, identification of Rictor as a novel target of *miR-218*. Top, the results of Western blotting of 5 reported targets and Rictor in HSC-2 and NA cells 48 hours after the transfection of dsRNA mimicking *miR-218* or control nonspecific miRNA (ds-*NC*). Middle, putative binding sites of *miR-218* in the 3′-UTR region of *Rictor*. These sites were analyzed using Microcosm Targets (21), miRanda (22), and TargetScan (23). Bottom, luciferase assays of HSC-2 and NA cells 48 hours after cotransfection of pMIR-REPORT luciferase vectors containing a 3′-UTR target site of *Rictor* for *miR-218*, dsRNA mimicking *miR-218*, or control nonspecific miRNA, and pRL-CMV internal control vector. C, effects of *miR-218* on Akt activation in OSCC cell lines with/without mutant forms of *PIK3CA* by Western blotting. Both cell lines, HSC-2 with *PIK3CA* mutation and NA without a genetic alteration of *PIK3CA*, *EGFR*, or *PTEN*, had been shown to be activated their PI3K–Akt signaling pathway (see Figure 4A; ref. 34). Top, the results of Western blotting in HSC-2 and NA cells 48 hours after transfection of dsRNA mimicking *miR-218*, control nonspecific miRNA, *PIK3CA*-specific siRNA, *Rictor*-specific siRNA, or control nonspecific siRNA (si-*NC*). To determine the increased phosphorylation of Akt protein at Ser-473, levels of total Akt protein in same samples were evaluated. Bottom, relative Akt activities in these transfectants. The quantification of each protein band in the result of Western blotting was done using LAS-3000 with MultiGauge software (Fuji film). The amount of phosphorylated Akt was normalized versus that of total Akt. Bar graphs show the ratio of the Akt activities in ds-*miR-218*-, si-*PIK3CA*-, and si-*Rictor*-transfectants relative to those in control transfectants. D, schema of the negative regulation of the mTORC2-dependent Akt signaling pathway by *miR-218* in OSCC.

confirmed that their protein levels were decreased in *miR-218*-transfectants compared with their control counterparts (Fig. 4B).

To explore novel oncogenic targets of *miR-218* and *miR-585* in OSCC cell lines, we used the algorithms, MicrocosmTargets, miRanda, and TargetScan, and selected *rapamycin-insensitive companion of mTOR* (*Rictor*) as *miR-218*-targets and *jun B proto-oncogene* (*JunB*) as *miR-585*-targets. The expression of *Rictor* or *JunB* was frequently upregulated in 38.9% (7/18) and 44.4% (8/18) of OSCC cell lines, respectively, compared with RT7 (>2-fold expression; Fig. 4A and Supplementary Fig. S5A). In Western blotting of Rictor and JunB, their protein levels were markedly reduced in *miR-218*- and *miR-585*-transfectants, respectively, compared with their control counterparts (Fig. 4B and Supplementary Fig. S5B). To further determine whether the predicted target sites of *miR-218* and *miR-585* in the 3′-UTR of mRNAs of *Rictor* and *JunB*, respectively (Fig. 4B and Supplementary Fig. S5C), were responsible for the translational regulation by dsRNA mimicking these miRNAs, we next conducted luciferase assays with vectors containing these 3′-UTR target sites downstream of the luciferase reporter gene. In this analysis, we observed a statistically significant reduction of luciferase activity in a vector containing the target site of *Rictor*, but not *JunB* (Fig. 4B and Supplementary Fig. S5D). These findings, together with the results of Western blotting, suggest *Rictor* and *JunB* to be a

Downloaded from cancerres.aacrjournals.org on January 6, 2012
Copyright © 2011 American Association for Cancer Research

Published OnlineFirst July 27, 2011; DOI:10.1158/0008-5472.CAN-11-0368

novel direct target of *miR-218* and an indirect target of *miR-585*, respectively. Therefore, we focused on *Rictor* as the most likely target of *miR-218*, and conducted further analyses to explore the underlying molecular mechanisms of oral carcinogenesis.

Rictor, together with the mammalian target of rapamycin (mTOR) kinase, forms mTOR complex 2 (mTORC2), and the Rictor-mTOR complex directly regulates the phosphorylation of Akt at Ser-473, resulting in cell growth (33). We have previously reported that the phosphorylation of Akt at Ser-473 and Thr-308 was markedly increased in a HSC-2 cell line harboring a missense mutation in the *PIK3CA* gene, A3140G in exon 20, corresponding to the amino acid change H1047R (34). Interestingly, although NA cells without a genetic alteration of *PIK3CA*, *EGFR*, or *PTEN* also showed phosphorylated Akt, it has been unknown why the phosphorylation increased in this cell line. The phosphorylation status of Akt at Ser-473 in 18 OSCC cell lines and RT7 were shown in Figure 4A. To investigate whether Rictor might be associated with growth inhibitory effects of *miR-218* in OSCC cells, we analyzed the phosphorylation of Akt and cell proliferation in HSC-2 and NA cells transfected with or without dsRNAs mimicking *miR-218* or specific siRNAs for *Rictor* and *PIK3CA* (Fig. 4C). The treatment with *PIK3CA*- or *Rictor*-specific siRNA significantly inhibited cell growth in HSC-2 and NA cells whereas we found no noticeable differences in cell growth ratio of each transfectant in both cell lines (Supplementary Fig. S6). In Western blotting, the marked inhibition of the phosphorylation of Akt at Ser-473 in HSC-2 cells was observed in the treatment of RNA interference of *PIK3CA*, but not in restoration of *miR-218* expression and knockdown of *Rictor* expression, suggesting that phosphatidylinositol 3-kinase (PI3K) seems mainly to regulate the phospho-Akt activation in HSC-2 cells with a mutant form of *PIK3CA*. On the other hand, a notable reduction in the phosphorylated Akt was detected in NA cells at 48 hours after the transient transfection of dsRNAs mimicking *miR-218* or specific siRNA for *Rictor* compared with specific siRNA for *PIK3CA*, suggesting Akt to be significantly activated and phosphorylated by the TOR-Akt signaling pathway, not PI3K-Akt signaling pathway in NA cells without a mutant form of *PIK3CA*, *EGFR*, or *PTEN*. Our results clearly showed that *miR-218* acts as a suppressor of the TOR-Akt signaling pathway, independently of the PI3K-Akt signaling pathway, in OSCC (Fig. 4D).

Discussion

Here, we clearly identified *miR-218* and *miR-585* as TS-miRNAs silenced through tumor-specific DNA hypermethylation in oral cancer and characterized *miR-218* targeting *Rictor* and inhibiting the phosphorylation of Akt at Ser-473 in a OSCC cell line without a mutant form of *PIK3CA*, *EGFR*, or *PTEN*. In this study, we carried out function-based screening using 327 dsRNAs mimicking mature miRNAs to identify TS-miRNAs having remarkable inhibitory effects on the growth of OSCC cell lines, although expression-based and DNA methylation-based screening had been successfully done previously in OSCC (8) and hepatocellular carcinoma (9), respectively. Since several known TS-miRNAs, such as *miR-34* (24), *miR-124* (9, 25), *miR-193a* (8), and *miR-491* (15), were actually identified through this approach, function-based screening would be suitable for exploring dsRNAs, including miRNAs and siRNAs, as therapeutic agents for several types of cancer cells. The tumor-suppressive function of candidate miRNAs eventually identified in this screening was reevaluated using 2 kinds of dsRNA purchased independently to take account of off-target effects, known to complicate the interpretation of phenotypic effects in gene-silencing experiments using siRNAs (35).

We consider that the hypermethylation of CpG-islands on/around miRNA genes a good marker to explore novel epigenetically silenced TS-miRNAs, similar to classic TSGs in several types of cancer, and have already reported *miR-137*, *miR-193a*, *miR-124*, and *miR-203* as epigenetically silenced TS-miRNAs (8, 9). In this study, a second screening, combining DNA methylation and expression analyses in a panel of OSCC cell lines, resulted in the identification of *miR-218* and *miR-585* as prime candidates for TS-miRNAs silenced by DNA hypermethylation in OSCC. Our study is the first to show that *miR-218* and *miR-585* were frequently silenced by DNA hypermethylation in OSCC. This miRNA gene is located at 4p15.31 (*miR-218-1*) and 5q35.1 (*miR-218-2*) in introns of 2 host genes, *SLIT2* and *SLIT3*, respectively, and *miR-585*, together with *miR-218-2*, is also located within the intron of *SLIT3* at 5q35.1. Copy number losses at these loci and the downregulated expressions of *miR-218*, *SLIT2*, and *SLIT3* were reported in some types of cancer (36) although we found no homozygous loss in these regions in our previous studies of genomewide copy-number aberrations in 39 OSCC cell lines by array-CGH analyses (17, 37). Frequent epigenetic inactivation of *SLIT2* and *SLIT3* was also described in several cancers (38, 39). Although, in our study, the expression levels of these miRNAs and their host genes were remarkably restored in OSCC cell lines treated with 5-aza-dCyd, it was reported that the treatment of this inhibitor of DNA methylation did not reactivate the downregulated expression of *SLITs* in cervical cancer (40), suggesting a complex mechanism of inactivation in *Slits* in some types of cancers. Very recently, the downreguration of *miR-218* and its inhibitory effects on cell proliferation and invasion have been shown in several types of cancer, including HPV-positive cell lines and tissues (26–29, 31, 32, 36, 41), and in the present study, we confirmed the tumor-suppressive functions and the mechanism of action of this miRNA in OSCC. Regarding *miR-585*, however, this is the first report that this is a novel TS-miRNA frequently silenced by tumor-specific DNA hypermethylation in OSCC, suggesting a crucial role, similar to *miR-218*, in human cancers.

In this study, we successfully identified a possible direct target of *miR-218*, *Rictor*, although *ECOP*, *IKK-β*, *LASP1*, *PXN*, and *Robo1* have also been reported as direct targets of this miRNA. Since ECOP and IKK-β are components of the NF-κB pathway, our findings of caspase-mediated apoptosis in cells overexpressing *miR-218* strongly support early reports of a correlation between *miR-218* and targets (28, 29). LASP1, PXN, and Robo1 are known to be associated with cell adhesion, mobility, and migration, and their overexpression induced by *miR-218* suppression seem to enhance tumor invasion and

Downloaded from cancerres.aacrjournals.org on January 6, 2012
Copyright © 2011 American Association for Cancer Research

Published OnlineFirst July 27, 2011; DOI:10.1158/0008-5472.CAN-11-0368

metastasis (30–32). Interestingly, although Slit-Robo signaling has been described to facilitate tumor cell migration, Robo1 targeted by *miR-218* is known to be a receptor for Slit which is the host gene of *miR-218* and shown to form a negative feedback loop involving Slit, *miR-218*, and Robo1 (27, 32). In our expression analysis, the percentage of OSCC cell lines with remarkable downregulation of *miR-218*, *miR-585*, *SLIT2*, and *SLIT3* (< 0.5-fold), expression was 44.4% (8/18), 55.6% (10/18), 61.1% (11/18), and 77.8% (14/18), respectively, whereas that with notable upregulation of these genes (>2-fold expression) was 38.9% (7/18), 11.1% (2/18), 33.3% (6/18), and 0% (0/18), respectively. Since the biological and functional significances of Slits-*miR-218*-Robo signaling in cancer remains largely unknown, further study is needed for the characterization of this signaling.

Rictor is a component of the mTOR-containing complex mTORC2, which directly regulates the phosphorylation of Akt at Ser-473 (33). Knockdown of *Rictor* or *mTOR* in colon cancer was shown to inhibit cancer cell proliferation *in vitro* and tumor formation *in vivo* (42), and the selective requirement of Rictor for the development of prostate cancer induced by a loss of *Pten* in mice was shown (43). These results including our findings strongly support the notion that the silencing of *miR-218* through the hypermethylation of CpG-islands around this miRNA is likely to be an important mechanism of carcinogenesis and cancer progression at least partly involving the activation of mTORC2-Akt signaling in OSCC. In this study, we analyzed the effects of *miR-218* on the phosphorylation of Akt using 2 representative OSCC cell lines; HSC-2, with a missense mutation in the *PIK3CA* gene and activated PI3K-Akt signaling pathway, and NA, without genetic alterations of *PIK3CA*, *EGFR*, or *PTEN* (34). Although it has been unknown why the phosphorylation of Akt is increased in NA cells, our findings clearly showed *miR-218* to act as a suppressor of the TOR-Akt signaling pathway, independently of the PI3K-Akt signaling pathway, in OSCC, and that the activation of this signaling pathway through methylation-mediated silencing of *miR-218* may contribute to the pathogenesis of OSCC.

In conclusion, we described here the identification of 2 TS-miRNAs, *miR-218* and *miR-585*, frequently silenced by DNA hypermethylation in OSCC, using function-based screening and a series of sequential analyses. Moreover, we identified *Rictor* as a potential target of *miR-218*, suggesting that the epigenetic silencing of *miR-218* and consequent activation of the TOR-Akt signaling pathway induced by the overexpression of *Rictor* contribute to oral carcinogenesis, and that targeting *miR-218* may provide a novel strategy for the treatment of OSCC, although further studies *in vivo* will be needed to confirm that dsRNA mimicking *miR-218* can act as a TS-miRNA.

Disclosure of Potential Conflict of Interest

No potential conflicts of interest were disclosed.

Acknowledgments

We thank Ayako Takahashi and Rumi Mori for technical assistance.

Grant Support

This study was supported in part by Grant-in-Aid for Scientific Research (A), (B), and (C), and Scientific Research on Priority Areas and Innovative Areas, and a Global Center of Excellence (GCOE) Program for International Research Center for Molecular Science in Tooth and Bone Diseases from the Ministry of Education, Culture, Sports, Science, and Technology, Japan; a Health and Labour Sciences Research Grant by the Ministry of Health, Labour and Welfare, Japan; and a grant from the New Energy and Industrial Technology Development Organization (NEDO).

The costs of publication of this article were defrayed in part by the payment of page charges. This article must therefore be hereby marked *advertisement* in accordance with 18 U.S.C. Section 1734 solely to indicate this fact.

Received February 8, 2011; revised June 20, 2011; accepted July 13, 2011; published OnlineFirst July 27, 2011.

References

1. Ambros V. The functions of animal microRNAs. Nature 2004;431:350–5.
2. Miska EA. How microRNAs control cell division, differentiation and death. Curr Opin Genet Dev 2005;15:563–8.
3. Lu J, Getz G, Miska EA, Alvarez-Saavedra E, Lamb J, Peck D, et al. MicroRNA expression profiles classify human cancers. Nature 2005;435:834–8.
4. Esquela-Kerscher A, Slack FJ. Oncomirs - microRNAs with a role in cancer. Nat Rev Cancer 2006;6:259–69.
5. Osada H, Takahashi T. MicroRNAs in biological processes and carcinogenesis. Carcinogenesis 2007;28:2–12.
6. Herman JG, Baylin SB. Gene silencing in cancer in association with promoter hypermethylation. N Engl J Med 2003;349:2042–54.
7. Chuang JC, Jones PA. Epigenetics and microRNAs. Pediatr Res 2007;61:24R–9R.
8. Kozaki K, Imoto I, Mogi S, Omura K, Inazawa J. Exploration of tumor-suppressive microRNAs silenced by DNA hypermethylation in oral cancer. Cancer Res 2008;68:2094–105.
9. Furuta M, Kozaki K, Tanaka S, Arii S, Imoto I, Inazawa J. miR-124 and miR-203 are epigenetically silenced tumor-suppressive microRNAs in hepatocellular carcinoma. Carcinogenesis 2009;31:766–76.
10. Iorio MV, Piovan C, Croce CM. Interplay between microRNAs and the epigenetic machinery: An intricate network. Biochim Biophys Acta 2010;1799:10–2.
11. Parkin DM, Bray F, Ferlay J, Pisani P. Global cancer statistics, 2002. CA Cancer J Clin 2005;55:74–108.
12. Nomura K, Sobue T, Nakatani H, Maehara M, Kiryu Y, Tsukuma H, et al. The Editorial Board of Cancer Statistics in Japan. Number of deaths and proportional mortality rates from malignant neoplasms by site in Japan (2003). Cancer Statistics in Japan 2005;36–9. Available from:http://www.ncc.go.jp/en/statistics/index.html.
13. Scully C, Field JK, Tanzawa H. Genetic aberrations in oral or head and neck squamous cell carcinoma (SCCHN): 1. Carcinogen metabolism, DNA repair and cell cycle control. Oral Oncol 2000;36:256–63.
14. Ha PK, Califano JA. Promoter methylation and inactivation of tumour-suppressor genes in oral squamous-cell carcinoma. Lancet Oncol 2006;7:77–82.
15. Nakano H, Miyazawa T, Kinoshita K, Yamada Y, Yoshida T. Functional screening identifies a microRNA, miR-491 that induces apoptosis by targeting Bcl-X(L) in colorectal cancer cells. Int J Cancer 2010;127:1072–80.
16. Levy C, Khaled M, Iliopoulos D, Janas MM, Schubert S, Pinner S, et al. Intronic miR-211 assumes the tumor suppressive function of its host gene in melanoma. Mol Cell 2010;40:841–9.
17. Suzuki E, Imoto I, Pimkhaokham A, Nakagawa T, Kamata N, Kozaki K, et al. PRTFDC1, a possible tumor-suppressor gene, is frequently

Downloaded from cancerres.aacrjournals.org on January 6, 2012
Copyright © 2011 American Association for Cancer Research

Published OnlineFirst July 27, 2011; DOI:10.1158/0008-5472.CAN-11-0368

silenced in oral squamous-cell carcinomas by aberrant promoter hypermethylation. Oncogene 2007;26:7921–32.
18. Available from miRBase database (Release 17 April 2011): http://www.mirbase.org/index.shtml.
19. Available from UCSC Genome Browser on Human February 2009 Assembly (hg19): http://genome.ucsc.edu/cgi-bin/hgGateway.
20. Available from PubMed: http://www.ncbi.nlm.nih.gov/pubmed.
21. Available from MicrocosmTargets:http://www.ebi.ac.uk/enright-srv/microcosm/htdocs/targets/v5/.
22. Available from miRanda: http://microrna.sanger.ac.uk/sequences/index.shtml.
23. Available from TargetScan http://www.targetscan.org/.
24. He L, He X, Lowe SW, Hannon GJ. microRNAs join the p53 network–another piece in the tumour-suppression puzzle. Nat Rev Cancer 2007;7:819–22.
25. Pierson J, Hostager B, Fan R, Vibhakar R. Regulation of cyclin dependent kinase 6 by microRNA 124 in medulloblastoma. J Neurooncol 2008;90:1–7.
26. Martinez I, Gardiner AS, Board KF, Monzon FA, Edwards RP, Khan SA. Human papillomavirus type 16 reduces the expression of microRNA-218 in cervical carcinoma cells. Oncogene 2008;27:2575–82.
27. Alajez NM, Lenarduzzi M, Ito E, Hui AB, Shi W, Bruce J, et al. MiR-218 suppresses nasopharyngeal cancer progression through downregulation of survivin and the SLIT2-ROBO1 pathway. Cancer Res 2011;71:2381–91.
28. Gao C, Zhang Z, Liu W, Xiao S, Gu W, Lu H. Reduced microRNA-218 expression is associated with high nuclear factor kappa B activation in gastric cancer. Cancer 2010;116:41–9.
29. Song L, Huang Q, Chen K, Liu L, Lin C, Dai T, et al. miR-218 inhibits the invasive ability of glioma cells by direct downregulation of IKK-beta. Biochem Biophys Res Commun 2010;402:135–40.
30. Chiyomaru T, Enokida H, Kawakami K, Tatarano S, Uchida Y, Kawahara K, et al. Functional role of LASP1 in cell viability and its regulation by microRNAs in bladder cancer. Urol Oncol 2010[Epub ahead of print].
31. Wu DW, Cheng YW, Wang J, Chen CY, Lee H. Paxillin predicts survival and relapse in non-small cell lung cancer by microRNA-218 targeting. Cancer Res 2010;70:10392–401.
32. Tie J, Pan Y, Zhao L, Wu K, Liu J, Sun S, et al. MiR-218 inhibits invasion and metastasis of gastric cancer by targeting the Robo1 receptor. PLoS Genet 2010;6:e1000879.
33. Hresko RC, Mueckler M. mTOR.RICTOR is the Ser473 kinase for Akt/protein kinase B in 3T3-L1 adipocytes. J Biol Chem 2005;280:40406–16.
34. Kozaki K, Imoto I, Pimkhaokham A, Hasegawa S, Tsuda H, Omura K, et al. PIK3CA mutation is an oncogenic aberration at advanced stages of oral squamous cell carcinoma. Cancer Sci 2006;97:1351–8.
35. Svoboda P. Off-targeting and other non-specific effects of RNAi experiments in mammalian cells. Curr Opin Mol Ther 2007;9:248–57.
36. Davidson MR, Larsen JE, Yang IA, Hayward NK, Clarke BE, Duhig EE, et al. MicroRNA-218 is deleted and downregulated in lung squamous cell carcinoma. PLoS One 2010;5:e12560.
37. Nakamura E, Kozaki K, Tsuda H, Suzuki E, Pimkhaokham A, Yamamoto G, et al. Frequent silencing of a putative tumor suppressor gene melatonin receptor 1 A (MTNR1A) in oral squamous-cell carcinoma. Cancer Sci 2008;99:1390–400.
38. Dallol A, Da Silva NF, Viacava P, Minna JD, Bieche I, Maher ER, et al. SLIT2, a human homologue of the Drosophila Slit2 gene, has tumor suppressor activity and is frequently inactivated in lung and breast cancers. Cancer Res 2002;62:5874–80.
39. Dickinson RE, Dallol A, Bieche I, Krex D, Morton D, Maher ER, et al. Epigenetic inactivation of SLIT3 and SLIT1 genes in human cancers. Br J Cancer 2004;91:2071–8.
40. Narayan G, Goparaju C, Arias-Pulido H, Kaufmann AM, Schneider A, Durst M, et al. Promoter hypermethylation-mediated inactivation of multiple Slit-Robo pathway genes in cervical cancer progression. Mol Cancer 2006;5:16.
41. Li X, Shen Y, Ichikawa H, Antes T, Goldberg GS. Regulation of miRNA expression by Src and contact normalization: effects on nonanchored cell growth and migration. Oncogene 2009;28:4272–83.
42. Roulin D, Cerantola Y, Dormond-Meuwly A, Demartines N, Dormond O. Targeting mTORC2 inhibits colon cancer cell proliferation *in vitro* and tumor formation *in vivo*. Mol Cancer 2010;9:57.
43. Guertin DA, Stevens DM, Saitoh M, Kinkel S, Crosby K, Sheen JH, et al. mTOR complex 2 is required for the development of prostate cancer induced by Pten loss in mice. Cancer Cell 2009;15:148–59.

Downloaded from cancerres.aacrjournals.org on January 6, 2012
Copyright © 2011 American Association for Cancer Research

インプラント・口腔再生医学分野

春日井 昇平

医歯学総合研究科・口腔機能再構築学系専攻
インプラント・口腔再生医学・教授

1）研究の課題名

①インプラント治療に関連した組織再生に関する研究

Tissue regenerations related to dental implant treatment

歯科インプラント治療（以下インプラント治療）は歯が欠損した場合の確実な治療法となっており、治療を希望する患者数も増加している。しかし、インプラント埋入予定部位に十分な骨が存在しない場合には治療が困難であり、インプラント埋入前あるいは埋入時に骨造成をおこなう必要がある。現在自家骨移植が骨造成のゴールドスタンダードであるが、採取骨量に限界があることと、採取部位への侵襲が問題であり、効果的で、低侵襲で、簡便な骨造成法が求められている。Guided Bone Regeneration（GBR）は、遮断膜で骨再生のスペースを確保するユニークな手法であり、臨床応用されている。現在、非吸収性のPTFE膜、吸収性のコラーゲン膜あるいはPLGA膜が臨床で使用されている。これらの膜に比較してより効果的で安全性の高い2つの遮断膜を開発した。第一の膜はbeta-TCPを含有するゼラチン膜であり、この膜は骨再生を促進する様々なシグナル分子DDSのためのキャリアーとして適している。第二の膜は、多糖のプルランにコレステロールの側鎖が付いた分子から構成されるナノゲル膜であり、この膜も骨再生を促進する様々なシグナル分子DDSのためのキャリアーと適している。これらの膜をラットの頭蓋骨の骨欠損部に適用し、その有効性について放射線学的および組織学的に検討し、これら二つの膜が従来の膜に比較して骨再生を著しく促進することを確認した。さらに、骨膜下に遮断膜を置き、この遮断膜を徐々挙上するExpansible-GBR（EGBR）という新規の垂直的骨造成法を開発した。臨床において垂直的骨造成は極めて困難であるが、EGBRはそれを解決する臨床的手法となる可能性が高い。

②インプラント周囲組織の診断方法とインプラント周囲炎の治療法に関する研究

Diagnosis of peri-implant tissue and treatment to peri-implantitis

インプラント治療は確実な治療法となっているが、天然歯と比較して粘膜との結合が弱いため感染を起こしやすい。インプラント治療の広がりに伴って、インプラント周囲の炎症が起きてインプラント周囲骨が吸収するインプラント周囲炎の増加が大きな問題となっている。インプラント周囲炎を早期に発見するための診断法と、その診断によってどのような治療を選択するかのDecision Treeが、現在存在しない。我々は、一定の深さまでプローブを挿入するために必要な力を測定することが、インプラント周囲組織の診断に有効であることを明らかにした。またインプラント周囲炎治療法のDecision Treeを確立し、発表した。我々は、我々の提案するインプラント周囲炎治療法のDecision Treeが、世界スタンドードとなると考えている。

③生体親和性を向上させたインプラントの開発

Development of highly biocompatible dental implant

チタン製のスクリュー型のインプラントが現在世界中で広く使用されている。早期に骨に結合し、インプラント周囲炎に罹り難いインプラントが理想的である。我々は、骨と親和性の高いハイドロキシアパタイトを1-2μmで薄膜コーティングしたインプラントを開発し、このインプラントの臨床での有効性と安全性を確認した。このインプラントは早期に骨結合が得られる利点があるが、ハイドロキシアパタイトコーティングしたインプラントはインプラント周囲炎に罹患し易く進行が著しいと信じられている。イヌを用いてインプラント周囲炎の実験をおこない、このインプラントがインプラント周囲炎に対して従来のチタン製のインプラントと同程度であり、インプラント周囲炎に罹っても進行が遅いことが明らかになった。実際にこのインプラントを用

いて治療をおこなった患者を既に８年間追跡調査しているが、インプラント周囲炎に罹患したケースはまだ存在しない。

現在、ジルコニア（酸化ジルコニウム）は白色のセラミックで強度が大きいので、インプラントの上部に接続するアバットメントあるいは冠の材料として近年広く用いられている。しかし、靱性が弱いことが問題であり、ジルコニアのアバットメントや冠が破折することがあることは、臨床的に大きな問題である。我々はジルコニウム合金を開発し、この合金の表面にジルコニア（酸化ジルコニウム）が形成されることを明らかにした。この合金は生体親和性が高く、靱性が高く、表面が白色であるためインプラント、アバットメント、冠の材料としての応用が可能であり、歯科に革命を起こす素材であると考えている。

2）

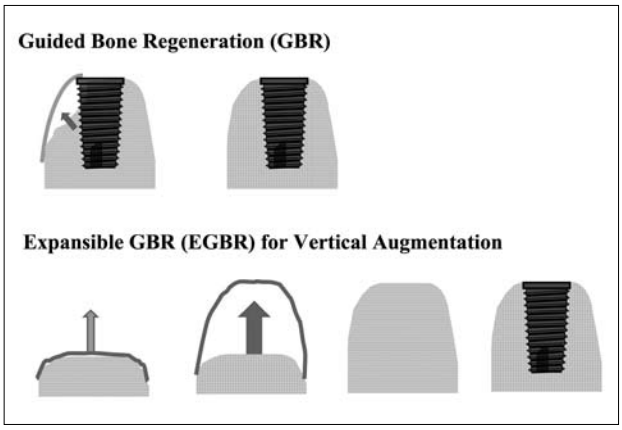

3）発表の研究内容についての英文要約

① **Tissue regenerations related to dental implant treatment**

Guided Bone Regeneration（GBR）is a unique clinical technique in which a barrier membrane provides a space for bone regeneration. Currently, non-resorbable PTFE membrane, resorbable collagen membrane and PLGA membrane have been clinically used; however, these membranes have some clinical problems. We developed two barrier membranes with more effectiveness and safe compared to the current membranes. The first membrane is gelatin membrane containing beta-TCP powder, which is potential for DDS material for signal molecules stimulating bone regeneration. The second membrane is nano-gel membrane consisting polysaccharide and cholesterol side chain, which is also potential for delivering some signal molecules stimulating bone regeneration. These membranes were applied on the parietal bone defects of rats stimulating bone regeneration extensively compared the commercially available ones. Furthermore, we developed expansible GBR（EGBR）for vertical bone augmentation in which the barrier membrane was place under the periosteum and gradually elevated. Clinically vertical bone augmentation is still challenging; however, EGBR can solve this clinical problem in the future.

② **Diagnosis of peri-implant tissue and treatment to peri-implantitis）**

Peri-implantitis, inflammation and bone loss around the implant, is a great clinical problem; however, there is no precise way to examine the tissue around the implant. In addition, there is no decision tree to choose modalities for peri-implantitis. We found that measuring the force to insert the probe into the sulcus of the implant was effective for examining the tissue around the implant and we proposed the decision tree based on the diagnosis to choose modalities for peri-implantitis. We believe that our decision tree would be a world standard.

③ **Development of highly biocompatible dental implant**

Titanium screw type implant is widely used. An implant binding to bone quickly and being resistant to implantitis would be ideal. We have developed an implant coated with thin hydroxyapatite（1-2 μ m）and reported effectiveness and safety of this implant. We found that the progression of implantitis of this implant is similar to the current titanium implants in dog experiments. We follow up the patients treated with this implant for 8 years and we have never observed any peri-implantitis around this implant.

We have developed an alloy containing zirconium, which surface is oxidized showing white color. The surface of this oxidized layer is zirconium, which is biocompatible ceramic and used as the materials for abutment and crown. However, zirconium is fragile and fractured clinically. Our new alloy will be able to solve this problem, which would be an evolution in clinical dentistry.

4）本事業に関連して世界的な研究拠点形成に向けて、以下の点で改善・整備等されたこと

A（人材確保）

海外からの大学での研究希望の増加が著しい

B（人材育成）

大学院修了者で、海外からの留学生は母国（タイ、ミャンマー、中国、台湾、ヨルダン）に帰って、教育と臨床と研究の指導的立場に立つケースが多い。また、海外の研究室のポスドク（香港大学、イエテボリ大学）のポジションを得た大学院修了者が２名いた。

C（国際化）

現在研究室の大学院生の半数が外国人留学生であり、研究室の急激な国際化が進んでいる。

5）GCOE事業を推進するに当たって力を入れた点

臨床での問題点を明確にして、その問題解決に繋がる研究をおこなうことを心掛けています。

6）英文原著論文

1. Fueki K, Igarashi Y, Maeda Y, Baba K, Koyano K, Akagawa Y, Sasaki K, Kuboki T, Kasugai S, Garrett NR. Factors related to prosthetic restoration in patients with shortened dental arches：a multicentre study. Journal of Oral Rehabilitation 38（7）：525-32, 2011
2. Hudieb MI, Wakabayashi N, Kasugai S. Magnitude and direction of mechanical stress at the osseointegrated interface of the microthread implant. Journal of Periodontology 82（7）：1061-70, 2011
3. Noritake K, Kuroda S, Nyan M, Ohya K, Tabata Y, Kasugai S. Development of a New Barrier Membrane for Guided Bone Regeneration：an in Vitro and in Vivo study J Oral Tissue Engineering 9（2）53-63, 2011
4. Hao J, Kuroda S. Ohya K. Bartakova S, Aoki H. Kasugai. S. Enhanced osteoblast and osteoclast responses to a thin film sputtered hydroxyapatite coating. Journal of Materials Science：Materials in Medicine. 22：1489-1499, 2011
5. Rodriguez R, Kondo H, Nyan M, Hao J, Miyahara T, Ohya K, Kasugai S, Implantation of green tea catechin α-tricalcium phosphate combination enhances bone repair in rat skull defects. Journal of Biomedical Material Research：Part B Applied Biomaterials 98B（2）：263-71, 2011
6. Ozeki M, Kuroda S, Kon K, Kasugai S, Differentiation of bone marrow stromal cells into osteoblasts in a selfassembling peptide hydrogel：in vitro and in vivo studies. J Biomater Appl 25（7）：663-84, 2011
7. Rojbani H, Nyan M, Ohya K, Kasugai S. Evaluation of the osteoconductivity of α-tricalcium phosphate, β-tricalcium phosphate, and hydroxyapatite combined with or without simvastatin in rat calvarial defect. Journal of Biomedical Materials Research：Part B Applied Biomaterials 98（4）：488-98, 2011
8. Bakry AS, Tamura Y, Otsuki M, Kasugai S, Ohya K, Tagami J. Cytotoxicity of 45S5 bioglass paste used for dentine hypersensitivity treatment. Journal of Dentistry 39（9）：599-603, 2011
9. Oshima M, Mizuno M, Imamura A, Ogawa M, Yasukawa M, Yamazaki H, Morita R, Ikeda E, Nakao K, Takano-Yamamoto T, Kasugai S, Saito M, Tsuji T. Functional tooth regeneration using a bioengineered tooth unit as a mature organ replacement regenerative therapy. PLoS One. 6（7）：e21531, 2011
10. Nyan M, Tsutsumi Y, Oya K, Doi H, Momura N, Kasugai S, Hanawa T. Synthesis of novel oxide layers on titanium by combination of sputter deposition and micro-arc oxidation techniques. Dental Material Journal 30（5）：754-61, 2011
11. Munakata M, Tachikawa N, Honda E, Shiota M, Kasugai S. Influence of menopose on mandibular bone quantity and quality in Japanese women receiving dental implants. Archives of Osteoporosis 6（1-2）：51-57, 2011
12. Murakami I, Murakami Y, Kopp CD, Palacci P, Kasugai S. Panoramic Implant Notation System--a method to denote implant positions and prosthodontic modalities. Journal of Prosthodontic Research 56（1）：65-9, 2012
13. Date Y, Yokoyama Y, Kondo H, Kuroda S, Ohya K, Ota MS, Iseki S, Kasugai S. Restricted expression of chromatin remodeling associated factor Chd3 during tooth root development. Journal of Periodontal Research 47（2）：180-187, 2012
14. Zakaria O. Madi M. Kasugai S. Induced osteogenesis using a new periosteal distractor. Journal of Oral and Maxillofacial Surgery 70（3）：225-34, 2012
15. Zakaria O. Kon K. Kasugai S. Evaluation of a biodegradable novel periosteal distractor：Journal of Biomedical Materials Research：Part B - Applied Biomaterials 100（3）：882-9, 2012
16. Miyahara T. Nyan M. Shimoda A. Yamamoto Y, Kuroda S. Shiota M. Akiyoshi K. Kasugai S. Exploitation of a novel polysaccharide nanogel cross-linking membrane for guided bone regeneration（GBR）J Tissue Engineering and Regenerative Medicine in press
17. Rungsiyanont S, Dhanesuan N, Swasdison S, Kasugai S. Regeneration of bone- and tendon/ligament-like tissues induced by gene transfer of bone morphogenetic protein-12 in a rat bone defect. J Biomater Appl. in press

7）平成23年度までの自己評価

インプラントの国際学会（Academy of Osseointegration, AO）の学術大会で2009年、2010年、2012年（本年3月）とClinical Innovationのセッションで3度Best Presentation Awardを受賞した。同一の研究室が3度受賞することはAOの歴史で初めてであり、大きな賞賛を受けた。また、春日井は2011年スウェーデン政府が多額の研究助成をおこなっているイエテボリ大学バイマテリアルの研究室の外部評価委員の委託を、スウェーデン政府より受けた。このことは、我々がおこなってきた研究が国際的に評価されていることを示している。

8）和文原著論文

山口葉子,塩田真,長尾浩史,宗像源博,立川敬子,春日井昇平. 単独植立インプラントのアバットメントが破折した1

症例.日本顎顔面インプラント学会誌.10（2）：69-73, 2011

9）学会発表（英文）

1. Pluemsakunthai W. Kuroda S. Shimokawa H. Kasugai S. The Effect of Platelet-Rich Fibrin Preparation with Alpha-Tricalcium Phosphate in Rabbit Calvarium　3rd GCOE Retreat Program, February 1-2, 2011, Tsukuba, Japan
2. Kuroda S. Nakata H. Noritake K. Hao J. Kasugai S. Interference in PPAR γ and transgene for Osterix stimulate osteogenesis in adipocytes. The International Congress of Oral Implantologists. Las Vegas, Nevada, USA. February 10-12, 2011.
3. Noritake K. Kuroda S. Nyan M. Atsuzawa Y. Kasugai S Development of an Ideal GBR Membrane for Enhanced Bone Healing　ICOI Winter Symposium February, 2011 Las Vegas, Nevada
4. Pluemsakunthai W. Kuroda S. Shimokawa H. Noritake K. Hao J. Miyahara T. Kasugai S. The Dissolution of Platelet Rich Fibrin and Platelet Derived Growth Factor Release Evaluation.（ICOI Winter Symposium, February 10-12, 2011, Las Vegas, USA）
5. Yamaguchi Y. Shiota M. Ahn K. Nagao H. Kasugai S. Analysis of Abutment Fracture on the Single Standing Implant. International Dental Materials Congress 2011. Eun-Myung Auditorium, Yonsei Univ. Seoul, Republic of Korea. 5月27-29. 2011.
6. Pluemsakunthai W. Kuroda S. Shimokawa H. Kasugai S. New Analysis of Platelet-Rich Fibrin Resorption and Platelet Derived Growth Factor Extraction Tri-University Consortium, June 3-6, 2011, Bangkok, Thailand
7. Miyahara T. Pluemsakunthai W. Nyan M. Shimoda A. Kobayashi H. Shimizu Y. Fujimori T. Shiota M. Akiyoshi K. Kasugai S Novel exploitation of polysaccharide nanogel cross-linking membrane for GBR European Association for Osseointegration 20th Annual Scientific Meeting October 12-15 2011 Skalkotas Hall Athens Greece
8. Yamamoto M. Shiota M. Kon K. Munakata M. Fuchigami K. Kasugai S. Dimensional assessment of crestal approached sinus augmentation with composite graft Annual Scientific Meeting of the European Association of Osseointegration. 13-15 October 2011, Athens, Greece
9. Kon K. Takahashi E. Ozeki M. Shimogisi M. Shiota M. Kasugai S. Oral bisphosphonate-related osteonecrosis of the jaw with dental implant; A single case report. Annual Scientific Meeting of the European Association of Osseointegration. 13-15 October 2011, Athens, Greece
10. Pluemsakunthai W. Kuroda S. Shimokawa H. Noritake K. Hao J. Miyahara T. Lin Z. Kasugai S. Platelet-Rich Fibrin Evaluation for Osteogenesis Annual Scientific Meeting of the European Association of Osseointegration. 13-15 October 2011, Athens, Greece
11. Nakata H. Kuroda S. Hao J. Yamamoto M. Kasugai S. Modification of culture into osteogenic or keratogenic differentiation from subcutaneous adipose-derived stem cells in vitro Annual Scientific Meeting of the European Association of Osseointegration. 13-15 October 2011, Athens, Greece

10）受賞

1. Akira Takebayashi. “Best presentation award in clinical innovation” Academy of Osseointegration 27th Annual Meeting 2011年3月1-3日
2. Takayuki Miyahara. “EAO travel Grants 2011” European Association for Osseointegration 20th Annual Scientific Meeting 2011年10月12-15日

11）外部資金の獲得状況

1. 日本学術振興会科学研究費補助金　挑戦的萌芽研究 上顎洞底挙上のためのX線透過性吸収性材料の開発 研究代表者：春日井昇平　平成22-24年　総額：260万円
2. 日本学術振興会科学研究費補助金　挑戦的萌芽研究 立体培養脂肪細胞による骨再生へのチャレンジ　研究代表者：黒田真司　平成23-25年　総額：280万円
3. 日本学術振興会科学研究費補助金　若手研究（B）「新規開発遅延型吸収性ナノゲルメンブレンを用いた骨増生における有効性の評価」研究代表：小林裕史　平成22-23年　総額：260万円
4. 厚生労働科学研究費　実験的再生歯の臨床応用に関する研究（分担研究者：春日井昇平）平成21-23年　総額：1,945万円
5. 受託研究　人工歯根（デンタルインプラント）による顎位安定と身体バランスの維持に関する研究（国立大学法人筑波大学）受託研究者：黒田真司　平成22-24年　総額：1,636万円

12）特別講演、招待講演、シンポジウム

1. 春日井昇平.骨造成に必要なもの　シンポジウム「骨の再生医療」 第65回口腔科学会学術大会 2011.4.21-22　タワーホール船堀　東京
2. Kasugai S. Bone augmentation in dental implant treatment：What is really required for bone augmentation? Korean Academy of Periodontology 2011.5.21 Kyongpook National University, Daegu, Korea

3. Kasugai S. Key for bone augmentation：Making regenerative space and encouraging endogenous key players. Internation Society of Blood-derived Biomaterials（ISBB）Taipei Workshop 2011.7.7-8 Yang-Ming University, Taipei, Taiwang
4. 春日井昇平.成功するインプラント治療：診査・診断・治療計画の重要性.東京都歯科医師会生涯研修 2011.7.31　東京医科歯科大学　東京
5. Pluemsakunthai W, Kuroda S, Shimokawa H, Kasugai S. New analysis of platelet rich fibrin resorption and platelet derived growth factor extraction. Tri-University Consortium on Oral Science and Education 2011.8.4-5 Chulalongkorn University, Bangkok, Thailand
6. Kasugai S. Keys for bone augmentation. Tri-University Consortium on Oral Science and Education 2011.8.4-5 Chulalongkorn University, Bangkok, Thailand
7. 春日井昇平.インプラントにおける再生医療について.嵌植義歯研究所講演会　2011.8.28　嵌植義歯研究所、仙台
8. 春日井昇平.歯科インプラント治療と再生医療の関わり.日本先端歯科研究所講演会　2011.9.10　日本先端歯科研究所、東京
9. 春日井昇平.ミューワンHAインプラント：簡便で良好な予後.Implant CAD/CAM Meeting 2011.11.12 横浜パシフィコ、横浜
10. Kasugai S. Keys for bone augmentation：Respecting endogenous key players and space for regeneration. Korean Association of Dental Sciences 2011.11.24 Yonsei University, Seoul, Korea
11. 春日井昇平.Keys for bone augmentation.新潟大学医歯学総合研究科大学院セミナー　2012.2.3
12. 春日井昇平.骨造成への新しいアプローチ：骨再生のための鍵を考える.玉川歯科医師会　2012.2.4

13）主催学会

1. 春日井昇平　第2回バイオインテグレーション学会 2012.1.29　東京医科歯科大学　東京（大会長：春日井昇平
2. 春日井昇平　第31回日本口腔インプラント学会関東・甲信越支部学術大会 2012.2.11-12 新宿京王プラザホテル　東京（大会長：春日井昇平）

14）教室、分野や講座の准教授、講師、助教、特別研究員、ポスドク、指導を受けた大学院生の名前

准教授	塩田　真
講師	立川　敬子
助教	黒田　真司
	宗像　源博
医員	山口　葉子
	中田　秀美
	作山　葵
	小林　裕史
	中村　貴弘
	今　一裕
	則武　加奈子（10月～）
	佐藤　大輔（～9月）
大学院生	木村　純一（～3月）
	伊達　佑生（～3月）
	宮原　宇将（～3月）
	Rojbani Hisham Khalifa（～3月）
	○郝　佳（～3月）
	○Rodoriguez Reena
	○Bhargava Srilatha
	秋野　徳雄
	永山　友子
	藤井　政樹
	古市　祥子
	Zakaria Osama
	高　尚
	下岸　将博
	○陳　康
	湯川　健、
	○Madi Marwa Ibrahim、
	山本　麻衣子
	高宅　香織
	Zayar Lin
	干　淼
	○Pluemsakunthai Warunee
	山下　優
	楠本　雄生（4月～）
	三田　稔（4月～）
	濱田　泰治（4月～）
	前田　大樹（4月～）
	宮坂　宗充（4月～）
	キム　ユキョン（4月～）

○はAISS

JOURNAL OF TISSUE ENGINEERING AND REGENERATIVE MEDICINE
J Tissue Eng Regen Med (2011)
Published online in Wiley Online Library (wileyonlinelibrary.com) **DOI:** 10.1002/term.475

RESEARCH ARTICLE

Exploitation of a novel polysaccharide nanogel cross-linking membrane for guided bone regeneration (GBR)

Takayuki Miyahara[1,4]*, Myat Nyan[1,4], Asako Shimoda[2,4], Yuka Yamamoto[2], Shinji Kuroda[1], Makoto Shiota[1], Kazunari Akiyoshi[2,3,4] and Shohei Kasugai[1,4]
[1]*Oral Implantology and Regenerative Dental Medicine, Tokyo Medical and Dental University, Japan*
[2]*Organic Biomaterials Institute of Biomaterials and Bioengineering, Tokyo Medical and Dental University, Japan*
[3]*Department of Polymer Chemistry, Graduate School of Engineering, Kyoto University, Japan*
[4]*Global Centre of Excellence (GCOE) Programme, International Research Centre for Molecular Science in Tooth and Bone Diseases, Tokyo Medical and Dental University, Japan*

Abstract

Cholesterol-bearing pullulan (CHP) nanogel is a synthetic degradable biomaterial for drug delivery with high biocompatibility. Guided bone regeneration (GBR) is a bone augmentation technique in which a membrane is used to create and keep a secluded regenerative space. The purpose of the present study was to evaluate the effects of the novel CHP nanogel membrane in GBR. Thirty-six adult Wistar rats were used and bilaterally symmetrical full-thickness parietal bone defects of 5 mm diameter were created with a bone trephine burr. Each defect was covered with the collagen membrane or the CHP nanogel membrane or untreated without any membrane. The animals were sacrificed at 2, 4 and 8 weeks and analysed radiologically and histologically. Furthermore, after incubating human serum with CHP nanogel or collagen, the amount of PDGF in the serum was measured using ELISA. New bone formation in terms of bone volume was higher in the nanogel group than in the control or collagen groups at 2 and 4 weeks. At 8 weeks, both membrane groups showed higher bone volumes than the control group. Notably, the newly-formed bone in the bone defect in the nanogel group was uniform and histologically indistinguishable from the original bone, whereas in the collagen group the new bone showed an irregular structure that was completely different from the original bone. After incubating with CHP nanogel, the amount of PDGF in the serum decreased significantly. CHP nanogel GBR membrane favourably stimulated bone regeneration, in which a unique characteristic of CHP nanogel, the storage of endogenous growth factors, was likely implicated. Copyright © 2011 John Wiley & Sons, Ltd.

Received 8 February 2011; Revised 14 June 2011; Accepted 5 July 2011

Keywords **guided bone regeneration; biomaterials; bone regeneration; acryloyl group-modified cholesterol-bearing pullulan (CHPOA); morphometric analysis; radiology; membrane; animal experiments**

1. Introduction

Dental rehabilitation of totally or partially edentulous patients with dental implants has become a routine treatment modality in recent decades, with reliable long-term results (Albrektsson *et al*., 1981, 1986; van Steenberghe, 1989; van Steenberghe *et al*., 1990; Lindquist *et al*., 1996; Buser *et al*., 1997; Arvidson *et al*., 1998; Lekholm *et al*., 1999; Brocard *et al*., 2000; Leonhardt *et al*., 2002). However, local conditions of the alveolar ridge, bone volume and bone quality, affect the long-term prognosis. Guided tissue regeneration (GTR) (Nyman *et al*., 1982, 1990) was originally developed for the treatment of periodontal defects and then the same concept was later applied to bone regeneration, which is called guided bone regeneration (GBR) (Dahlin *et al*., 1989). Vertical and horizontal bone augmentation with GBR has been

* *Correspondence to: T. Miyahara, Oral Implantology and Regenerative Dental Medicine, Tokyo Medical and Dental University, 1-5-45 Yushima, Bunkyo-ku, Tokyo 113–8549, Japan. E-mail: miyahara.irm@tmd.ac.jp*

Copyright © 2011 John Wiley & Sons, Ltd.

applied to improve alveolar ridge deformities (Buser *et al*., 1993; Simion *et al*., 1996; Urban *et al*., 2009). In GBR procedures, the barrier membrane keeps the bone regeneration space and it also prevents the invasion of fibrous connective tissue, resulting in new bone formation under the membrane.

Several different membranes, including non-resorbable and resorbable membranes, have been developed and clinically used in GBR. Resorbable membranes have been generally preferred because the second surgery for its removal was unnecessary, rendering the procedure less invasive to patients. Biomaterials such as collagen or copolylactic/glycolic acid (PLGA) have been developed as degradable GBR membranes. Since collagen is an animal-derived material, the risk of unknown infection is undeniable and an unfavourable immune response occurs in some patients (Charriere *et al*., 1989; Keefe *et al*., 1992; Lynn *et al*., 2004).

Although PLGA is a completely synthetic material, it will gradually produce acids, inducing inflammatory responses. These disadvantages are not clearly noticed clinically; however, developing more biocompatible synthetic GBR membrane is beneficial.

Hydrophobized polysaccharide, such as cholesterol-bearing pullulan (CHP), is a unique material for drug delivery systems (DDSs) (Akiyoshi *et al*., 1998, 1999, 2002, Akiyoshi, 2006). Cholesterol-bearing pullulan (CHP) self-aggregates to form a monodisperse and stable hydrogel nanoparticle, in which the domains of the associated cholesterol groups of CHP provide cross-linking points in a non-covalent manner (Figure 1). The size and density of the hydrogel nanoparticle can be controlled by changing the degree of substitution of the cholesterol groups of CHP. During that substitution process, it can incorporate growth factors and act as a molecular chaperone. We have reported that delivering prostaglandin E1 with CHP nanogel stimulates wound healing in rats (Kobayashi *et al*., 2009). In this previous study it was surprising to find that CHP nanogel alone enhanced wound healing. Therefore, the barrier membrane containing CHP nanogel may have great potential as a GBR membrane. The purpose of the present study was to evaluate the effectiveness of the novel bioabsorbable CHP nanogel cross-linking membrane as a GBR membrane.

2. Materials and methods

2.1. Collagen membrane

A bioabsorbable membrane made of collagen (Koken Tissue Guide®, Japan) was used. This material was combined with bovine collagen derived from dermis tissue and bovine insoluble collagen derived from tendon (9:1). It was freeze-dried and cross-linked with the addition of hexamethylenediisocyanate (HMDIC). The collagen membranes were cut into circles with a diameter of approximately 6 mm.

2.2. Nanogel cross-linking membrane

CHP was synthesized as reported previously (Akiyoshi *et al*., 1996). Acryloyl group-modified cholesterol-bearing pullulan (CHPOA) nanogel was synthesized by the reaction of 2-(acryloyloxy)-ethyl isocyanate (AOI) and CHP. CHPOA nanogel solution (40.5 μl, 26.7 mg/ml) in Dulbecco's phosphate-buffered saline (PBS; pH 7.4) and 5.4 μl DMSO were mixed and kept at 4 °C for 24 h. This CHPOA nanogel solution and 8.1 μl solution of PEG-SH in PBS (481.8 mg/ml) were mixed at the ratio of thiol groups to acryloyl groups, which was 1:1. Then 13 μl of the mixture was placed between two glass slides coated with Parafilm® for 4 h at 37 °C under humidified conditions, to form a membrane-shaped hydrogel. The diameter and thickness of the nanogel membrane was 6 and 0.4 mm, respectively. The prepared membrane was applied to bone defects of experimental animals within 24 h.

2.3. Animal experiments

The animal experiments in the present study were approved by the Committee of Animal Experiments, Tokyo Medical and Dental University.

2.4. Surgical procedures

Thirty-six adult male Wistar rats, 16 weeks old, were used and divided into three groups. Prior to the experiment, the overall health of each rat was monitored for 2 weeks. The rats were kept in a standard cage (Tokiwa, Japan) in an experimental animal room at 22 ± 3 °C at 40–60% humidity and 1 atm, on 6:00–20:00 light, fed a standard laboratory diet (CE-2 CLEA Japan Inc.) and given sterilized water. The animals were anaesthetized with a combination of ketamine (40 mg/kg)–xylazine (5 mg/kg). In addition, approximately 0.4 ml local anaesthesia with lidocaine–HCl containing epinephrine 1/80 000 (2% Xylocain, Astra Japan Ltd, Fujisawa Pharmaceutical Co. Ltd, Osaka, Japan) was injected at the surgical site. A cutaneous flap was created by making a mid-sagittal incision through the skin, which was raised from the forehead. The periosteum was incised and elevated to expose the calvarial bone on both sides of the midline. Two symmetrical, full-thickness bone defects with outer diameter of 5 mm were created with a bone trephine burr (Tele Components Co., Germany) under continuous saline irrigation. The defects were covered with CHP nanogel cross-linking membrane or collagen membrane or without any membrane. The animals were sacrificed under chloroform anaesthesia at 2, 4 and 8 weeks after the surgery and analysed radiologically and histologically.

2.6. Radiographic evaluation

The calvariae were dissected out and fixed in neutral 10% formalin and then analysed using micro-CT (μCT; InspeXio, Shimadzu Science East Corp., Tokyo, Japan) to measure the bone volume in the defect area.

Copyright © 2011 John Wiley & Sons, Ltd.

DOI: 10.1002/term

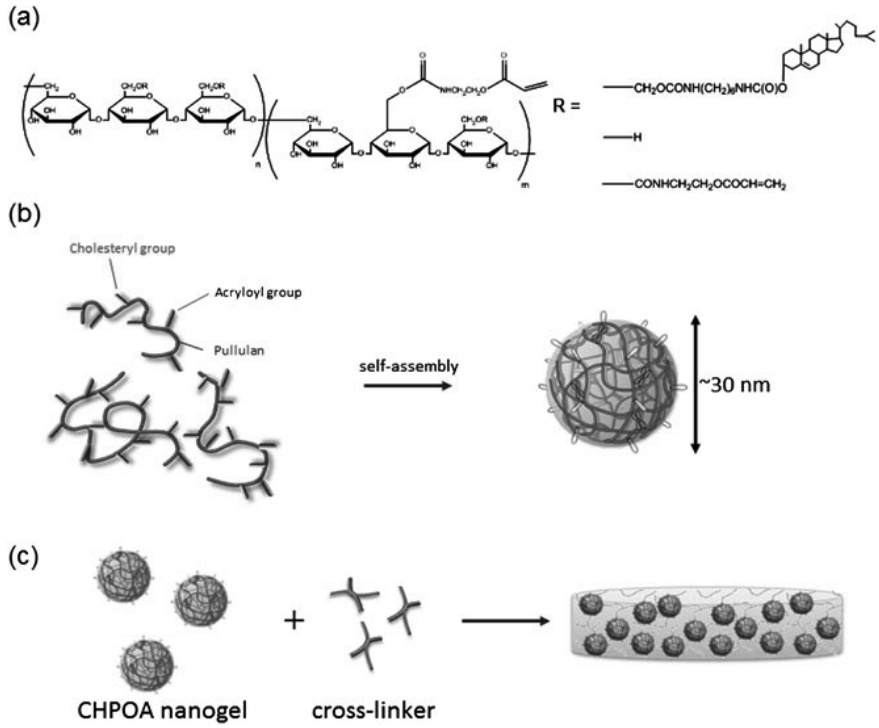

Figure 1. Scheme of acryloyl group-modified cholesterol-bearing pullulan (CHPOA). (A) Chemical structure of CHPOA nanogel. (B) Schematic illustration of CHPOA. (C) Schematic illustration of CHPOA nanogel cross-linking hydrogel (CHPOA–PEGSH)

2.7. Histological analysis

After radiographic analysis the calvariae were decalcified in 5% formic acid for 2 weeks. The specimens were dehydrated in ascending grades of ethanol, embedded in paraffin and sectioned 5 μm thick in the sagittal direction with a microtome. The sections were stained with haematoxylin and eosin (H&E).

2.8. PDGF concentration after incubating serum with materials, ELISA

Whole blood (50 ml) was obtained from the arm vein of a healthy, non-smoker male donor aged 34 years. After being stored overnight in a glass tube at room temperature, serum was prepared. The serum was incubated in three different combinations: serum alone, serum with collagen membrane and serum with nanogel membrane. The diameter of both membranes was 6 mm. These combinations were prepared in Eppendorf-type 1.5 ml vials and incubated for 3 h at room temperature. Then, PDGF-BB concentration in the serum was measured using an ELISA kit (Human PDGF-BB ELISA Kit, Ray Bio®, Ray Biotech Inc., Norcross, GA, USA) according to the manufacturer's instructions.

2.9. Statistical analysis

Data, apart from the ELISA result, were first analysed by one-way ANOVA. When this analysis suggested a significant difference between groups, the data were further analysed by Tukey *post hoc* multiple comparison tests, using SPSS software (v 11.5, SPSS, Chicago, IL, USA). For ELISA assay, statistical evaluation was performed with Student's *t*-tests (SPSS v 11.5). $p < 0.05$ was considered to be statistically significant.

3. Results

3.1. Radiographical images

Post-operative soft tissue healing was similar in all three groups without any membrane exposure in both membrane groups. The radiographical images of all the groups at 2, 4, and 8 weeks are presented in Figure 2. In the control group, newly formed bone could be seen only at the surrounding edge of the defect. In the collagen membrane group, part of the membrane appeared to be calcified, whereas in the CHP nanogel membrane group newly formed bone could be observed in almost the entire defected area. The surface of new bone in the CHP

Copyright © 2011 John Wiley & Sons, Ltd.

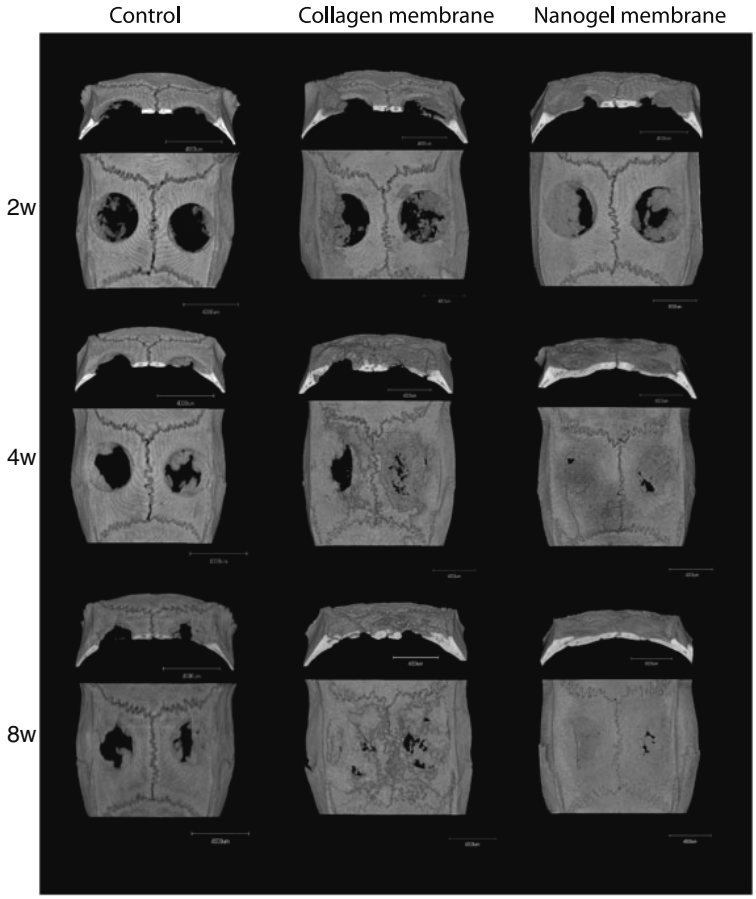

Figure 2. Cross-sectional micro-CT images of the bone defects at 2, 4 and 8 weeks

nanogel group was smooth; however, that in the collagen group was irregular. Volume of the newly formed bone is shown in Figure 3. New bone volume in the defect area in CHP nanogel group was highest at 2 and 4 weeks. At 8 weeks there was no statistical difference of newly-formed bone volume between the collagen and CHP nanogel groups. Newly-formed bone volume in the control group was lowest at the three time points.

3.2. Histological images

Histological images are presented in Figure 4. Corresponding to the radiographical images, new bone formation in CHP nanogel was prominent at 2 and 4 weeks compared with the other two groups. Notably, newly-formed bone in the CHP nanogel group was mature bone containing less connective tissue (Figure 4c, f, i, l),

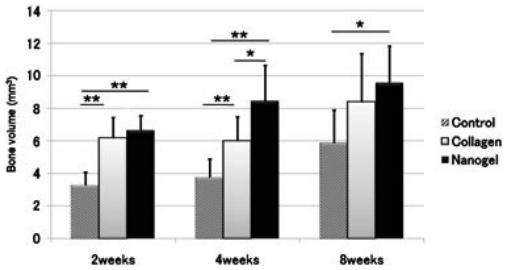

Figure 3. Bone volume in the defects at 2, 4 and 8 weeks. The data were obtained with micro-CT analysis. *$p < 0.05$, **$p < 0.01$

Copyright © 2011 John Wiley & Sons, Ltd.

J Tissue Eng Regen Med (2011)
DOI: 10.1002/term

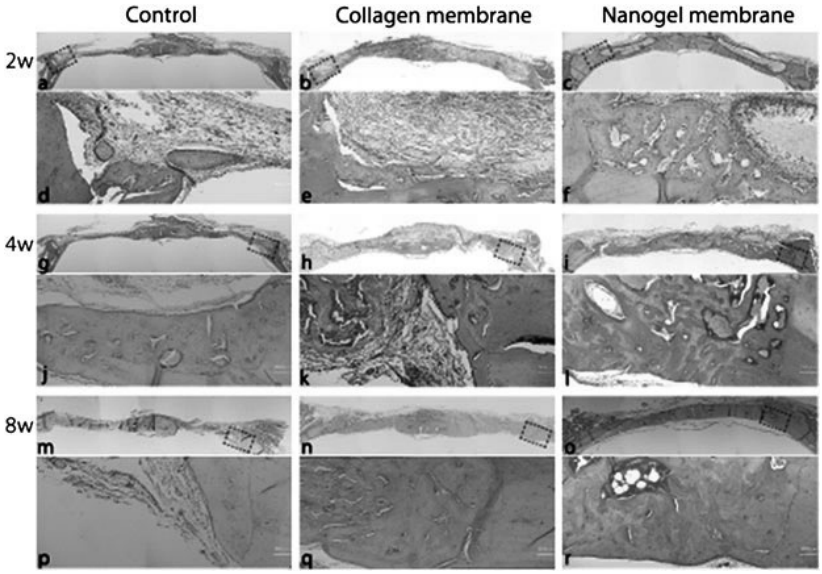

Figure 4. Histological images at 2, 4 and 8 weeks. High-magnification images of the parts of low-magnified images are presented; H&E staining

whereas in the collagen group less mature irregular bone was observed (Figure 4b, e, h, k). In addition, in the CHP nanogel group new bone formation occurred under the membrane, while it was observed both inside and under the membrane in the collagen group.

3.3. PDGF concentration after incubating serum with materials, ELISA

After incubating serum with the membranes, PDGF-BB concentration in the serum was measured. PDGF-BB concentration in the serum was the lowest when the serum was incubated with CHP nanogel membrane (Table 1), suggesting that CHP nanogel membrane trapped PDGF-BB in the material.

4. Discussion

The principle of GBR was originally explored for bone augmentation of the alveolar process in conjunction with oral implant therapy (Dahlin *et al.*, 1988; Buser *et al.*, 1993; Simion *et al.*, 1996; Urban *et al.*, 2009). In GTR and GBR, a membrane is used to keep regenerative space, preventing the invasion of the unfavourable surrounding tissue. The concept of tissue engineering is to provide the three key players to the regenerative site: cells, signal molecules and scaffolds; it is obvious that in both GTR and GBR, cells, signal molecules and scaffolds are endogenous. The progenitor cells are derived from the tissue facing the regenerative site, not from the tissue separated by a membrane. Signal molecules from activated platelets, such as PDGF and TGF-β, initially work for proliferation and differentiation of osteogenic cells. As scaffolds, fibrin initially plays important roles in regeneration. Collagen and other extracellular matrices are produced by the cells in the regenerative space and they work as scaffolds. Thus, GTR and GBR are characterized as encouraging endogenous regenerative ability by providing a space for regeneration.

In the present study, a bone defect model of rat calvaria was used to evaluate two types of GBR membrane. Although bone regeneration in the internal bone defect is different from external bone augmentation in GBR, the potential of the material for GBR membrane could be evaluated in the internal bone defect model of the present study. The present bone defect of 5 mm diameter did not heal spontaneously at 8 weeks when the defect was left without a membrane. The proliferation of undesired soft tissues in the bone defect interrupts the proliferation of bone forming cells from the periphery of the defect (Dahlin *et al.*, 1988; Kostopoulos *et al.*, 1994; Hämmerle *et al.*, 1995). Any material with some degree of biocompatibility can work as GTR or GBR membrane. Methyl

Table 1. PDGF concentration in the serum after incubating with collagen membrane or CHP nanogel membrane

	Mean ± SD (pg/ml)	
Serum	164.0 ± 5.0	*
Serum + collagen	163.3 ± 4.7	*
Serum + nanogel	151.9 ± 6.7	

*$p < 0.05$, significantly different from one another.

Copyright © 2011 John Wiley & Sons, Ltd.

cellulose was initially used as a GTR membrane. Polytetrafluoroethylene (PTFE), polyglycolic and polylactic acids (PLGA) and collagen have been clinically applied as GBR membranes (Bunyaratavej and Wang, 2001). Furthermore, other materials, such as chitin/chitosan and alginate, have also been investigated as GBR membranes (Eun-Jung Lee *et al*., 2009). Our previous studies demonstrated the high biocompatibility of CHP nanogel (Kobayashi *et al*., 2009), which is one of the required properties for wound dressing and also for GBR membranes. Compared with the other materials, the uniqueness of CHP nanogel is to trap hydrophobic and hydrophilic molecules inside. Since CHP nanogel contains > 90% of water, the water in the gels would be exchanged for tissue exudates. After incubating in serum for the ELISA assay, the colour of the nanogel changed into yellow, similar to the colour of the serum. PDGF is synthesized mainly by megakaryocytes and is stored in the α-granules of platelets. When platelets are activated, PDGF is released. *In vitro*, PDGF-AA and PDGF-BB enhance the proliferation of multiple types of bone cells, including both osteoblast and osteoclast lineages (Hadjidakis and Androulakis, 2006; Zhang *et al*., 1998). Although long-term exposure to PDGF reduces alkaline phosphatase activity and mineralization (Hsieh and Graves, 1998), application of PDGF stimulates regeneration of periodontal tissue and bone (Nevins *et al*., 2009).

In our previous study, CHP nanogel alone stimulated wound healing in rats (Kobayashi *et al*., 2009) and we speculated that CHP nanogel stored endogenous growth factors in wound exudates. In the present study, the decrease in the amount of PDGF-BB in the serum was small but significant after incubating the serum with CHP nanogel membrane. The result of the ELISA assay indicated that CHP nanogel membrane has an ability to store PDGF-BB. It is also possible that CHP nanogel membrane would store not only PDGF-BB but also other growth factors produced at the regenerative site. In addition to PDGF-BB, TGF-β, VEGF and FGF are also produced in and around the bone defects. It is likely that after storing growth factors at the regenerative site, CHP nanogel membrane would gradually release these growth factors during membrane degradation; in other words, it is reasonable to conclude that CHP nanogel membrane works as signal molecule attractant and reservoir at the regenerative site.

In the present study, both collagen and CHP nanogel membrane stimulated bone regeneration compared to the control, in which no membrane was applied. The amount of newly-formed bone at the early time point and the quality of the bone in the CHP nanogel group were superior to that of the collagen group. The character of the CHP nanogel membrane, storing and releasing endogenous growth factors, could partly explain this difference. In the histological images, bone was formed under the membrane in the CHP nanogel group, whereas it was formed both inside and under the membrane in the collagen group. In the μCT images we also observed the irregular surface of the regenerated bone facing the membrane in the collagen group. It is plausible that the collagen membrane used in the present study worked not only as a barrier membrane of GBR but also as a scaffold for bone regeneration.

CHP nanogel consists of pullulan and cholestesterol. Pullulan is a polysaccharide industrially prepared from starch and its medical application has been approved. CHP nanogel has already been used clinically for delivering insulin (Akiyoshi *et al*., 1998), interleukin 12 (Shimizu et al., 2008) and cancer antigen (Kageyama *et al*., 2008); in these studies, CHP nanogel did not exert any adverse effect. Therefore, CHP nanogel is an extremely safe material. The uniqueness of CHP nanogel is that it can incorporate growth factors and acts as a molecular chaperone. Thus, CHP nanogel is an ideal material for delivering growth factors. We have delivered BMP2 with CHP nanogel to the parietal bone of mice and observed new bone formation (Hayashi *et al*., 2009). In addition to growth factors, CHP nanogel can incorporate small biologically active molecules. Using CHP nanogel we have also delivered prostaglandin E agonist and prostaglandin E1 to bone and skin wounds, respectively, and reported the stimulation of bone and skin regeneration (Kobayashi *et al*., 2009; Kamolratanakul *et al*., 2011). The present study demonstrated that CHP nanogel membrane alone stimulated bone regeneration; however, delivering biologically active molecules, such as BMP and prostaglandin E1, with CHP nanogel would be effective and promising in bone regeneration (Hayashi *et al*., 2009). Although CHP nanogel membrane is promising as a GBR membrane, we have to solve the following two points before applying this membrane in GBR clinically. First, the membrane should be stable for a long time at room temperature. In the present study, CHP nanogel membrane was prepared within 24 h before the surgical application. It would be possible to make CHP nanogel membrane durable for a long storage period, because we observed that dried CHP nanogel membrane was also effective in the same bone defect model (authors' unpublished data). Second, enhancement of mechanical strength of the membrane is absolutely required. The present CHP nanongel membrane is strong enough to cover over a relatively small bone defect; however, it is obviously too weak to be applied for vertical or horizontal bone augmentation. Combining CHP nanogel membrane with biodegradable polymer would solve this problem.

5. Conclusion

The present results indicate that novel CHP nanogel crosslinking membrane would be potentially effective as a GBR membrane.

Acknowledgements

We greatly appreciate the help of Dr Tomoko Nagayama, Dr Jia Hao, Dr Reena Rodriguez, Dr Warunee Pluemsakunthai and Dr

Copyright © 2011 John Wiley & Sons, Ltd.

Hisham Rojbani with animal experiments and Dr Toshimitsu Yamamoto with histomorphometric analysis. This work was supported by Grants-in-Aid for GCOE Research and for Exploratory Research from the Ministry of Education, Culture, Sports, Science and Technology, Japan (Grant Nos 22791925, 22659355).

References

Albrektsson T, Branemark PI, Hansson HA, *et al*. 1981; Osseointegrated titanium implants. Requirements for ensuring a long-lasting, direct bone-to-implant anchorage in man. *Acta Orthop Scand* **52**: 155–170.

Albrektsson T, Zarb G, Worthington P, *et al*. 1986; The long-term efficacy of currently used dental implants: a review and proposed criteria of success. *Int J Oral Maxillofac Implants* **1**: 11–25.

Arvidson K, Bystedt H, Frykholm A, *et al*. 1998; Five-year prospective follow-up report of the Astra Tech Dental Implant System in the treatment of edentulous mandibles. *Clin Oral Implants Res* **9**: 225–234.

Akiyoshi K, Taniguchi I, Fukui H, *et al*. 1996; Hybrid nanoparticle formed by self-assembly of hydrophobized polysaccharide: stabilization of adriamycin by complexation. *Eur J Pharm Biopharm* **42**: 286–290.

Akiyoshi K, Kobayashi S, Shichibe S, *et al*. 1998; Self-assembled hydrogel nanoparticle of cholesterol-bearing pullulan as a carrier of protein drugs: complexation and stabilization of insulin. *J Control Release* **54**: 313–320.

Akiyoshi K, Sasaki Y, Sunamoto J. 1999; Molecular chaperone-like activity of hydrogel nanoparticles of hydrophobized pullulan: thermal stabilization with refolding of carbonic anhydrase B. *Bioconjug Chem* **10**: 321–324.

Akiyoshi K, Maruichi N, Kohara M, *et al*. 2002; Amphiphilic block copolymer with a molecular recognition site: induction of a novel binding characteristic of amylose by self-assembly of poly(ethylene oxide)-block-amylose in chloroform. *Biomacromolecules* **3**: 280–283.

Akiyoshi K. 2006; Nanogel engineering and chaperone engineering. *Nippon Rinsho* **64**: 215–220.

Buser D, Dula K, Belser U, *et al*. 1993; Localized ridge augmentation using guided bone regeneration. 1. Surgical procedure in the maxilla. *Int J Periodont Restor Dent* **13**: 29–45.

Buser D, Mericske-Stern R, Bernard JP, *et al*. 1997; Long-term evaluation of non-submerged ITI implants. Part 1: 8-year life table analysis of a prospective multi-center study with 2359 implants. *Clin Oral Implant Res* **8**: 161–172.

Brocard D, Barthet P, Baysse E, *et al*. 2000; A multicenter report on 1022 consecutively placed ITI implants: a 7-year longitudinal study. *Int J Oral Maxillofac Implants* **15**: 691–700.

Bunyaratavej P, Wang HL. 2001; Collagen membranes: a review. *J Periodontol* **72**: 215–229.

Charriere G, Bejot M, Schnitzler L, *et al*. 1989; Reactions to a bovine collagen implant. Clinical and immunological study in 705 patients. *J Am Acad Dermatol* **21**: 1203–1208.

Dahlin C, Linde A, Gottlow J, *et al*. 1988; Healing of bone defects by guided tissue regeneration. *Plast Reconstr Surg* **81**: 672–676.

Dahlin C, Sennerby L, Lekholm U, *et al*. 1989; Generation of new bone around titanium implants using a membrane technique: an experimental study in rabbits, *Int J Oral Maxillofac Implants* **4**: 19–25.

Hadjidakis DJ, Androulakis II. 2006; Bone remodeling. *Ann NY Acad Sci* **1092**: 385–396.

Hayashi C, Hasegawa U, Saita Y, *et al*. 2009; Osteoblastic bone formation is induced by using nanogel-crosslinking hydrogel as novel scaffold for bone growth factor. *J Cell Physiol* **220**: 1–7.

Hämmerle CH, Fourmousis I, Winkler JR, *et al*. 1995; Successful bone fill-in late peri-implant defects using guided tissue regeneration: a short communication. *J Periodontol* **66**: 303–308.

Hsieh SC, Graves DT. 1998; Pulse application of platelet-derived growth factor enhances formation of a mineralizing matrix while continuous application is inhibitory. *J Cell Biochem* **69**: 169–180.

Keefe J, Wauk L, Chu S, *et al*. 1992; Clinical use of injectable bovine collagen: a decade of experience. *Clin Mater* **9**: 155–162.

Kostopoulos L, Karring T, Uraguchi R. 1994; Formation of jawbone tuberosities by guided tissue regeneration: an experimental study in the rat. *Clin Oral Implants Res* **5**: 245–253.

Kobayashi H, Katakura O, Morimoto N, *et al*. 2009; Effects of cholesterol-bearing pullulan (CHP)-nanogels in combination with prostaglandin E1 on wound healing. *J Biomed Mater Res B Appl Biomater* **91**: 55–60.

Kageyama S, Kitano S, Hirayama M, *et al*. 2008; Humoral immune responses in patients vaccinated with 1–146 HER2 protein complexed with cholesteryl pullulan nanogel. *Cancer Sci* **99**(3): 601–607.

Kamolratanakul P, Hayata T, Ezura Y, *et al*. 2011; Nanogel-based scaffold delivery of prostaglandin E_2 receptor (EP4) specific agonist in combination with low dosage of growth factor heals critical size bone defect. *Arthritis Rheum* **63**: 1021–1033.

Lindquist LW, Carlsson GE, Jemt T. 1996; A prospective 15-year follow-up study of mandibular fixed prostheses supported by osseointegrated implants. Clinical results and marginal bone loss. *Clin Oral Implants Res* **7**: 329–336.

Lekholm U, Gunne J, Henry P, *et al*. 1999; Survival of the Branemark implant in partially edentulous jaws: a 10-year prospective multicenter study. *Int J Oral Maxillofac Implants* **14**: 639–645.

Leonhardt A, Grondahl K, Bergstrom C, *et al*. 2002; Long-term follow-up of osseointegrated titanium implants using clinical, radiographic and microbiological parameters. *Clin Oral Implants Res* **13**: 127–132.

Lee EJ, Shin DS, Kim HE, *et al*. 2009; Membrane of hybrid chitosan–silica xerogel for guided bone regeneration. *Biomaterials* **30**: 743–750.

Lyn AK, Yannas IV, Bonfield W. 2004; Antigenicity and immunogenicity of collagen. *J Biomed Mater Res B Appl Biomater* **71**: 343–354.

Nyman S, Lindhe J, Karring T, *et al*. 1982; New attachment following surgical treatment of human periodontal disease. *J Clin Periodontol* **9**: 290–296.

Nyman S, Lang NP, Buser D, *et al*. 1990; Bone regeneration adjacent to titanium dental implants using guided tissue regeneration: a report of two cases. *Int J Oral Maxillofac Implants* **5**: 9–14.

Nevins M, Garber D, Hanratty JJ, *et al*. 2009; Human histologic evaluation of anorganic bovine bone mineral combined with recombinant human platelet-derived growth factor BB in maxillary sinus augmentation: case series study. *Int J Periodont Restor Dent* **29**: 583–591.

Simion M, Scarano A, Gionso L, *et al*. 1996; Guided bone regeneration using resorbable and nonresorbable membranes: a comparative histologic study in humans. *Int J Oral Maxillofac Implants* **11**: 735–742.

Shimizu T, Kishida T, Hasegawa U, *et al*. 2008; Nanogel DDS enables sustained release of IL-12 for tumor immunotherapy. *Biochem Biophys Res Commun* **367**: 330–335.

Urban IA, Jovanovic SA, Lozada JL. 2009; Vertical ridge augmentation using guided bone regeneration (GBR) in three clinical scenarios prior to implant placement: a retrospective study of 35 patients 12 to 72 months after loading. *Int J Oral Maxillofac Implants* **24**: 502–510.

van Steenberghe D. 1989; A retrospective multicenter evaluation of the survival rate of osseointegrated fixtures supporting fixed partial prostheses in the treatment of partial edentulism. *J Prosthet Dent* **61**: 217–223.

van Steenberghe D, Lekholm U, Bolender C, *et al*. 1990; Applicability of osseointegrated oral implants in the rehabilitation of partial edentulism: a prospective multicenter study on 558 fixtures. *Int J Oral Maxillofac Implants* **5**: 272–281.

Zhang Z, Chen J, Jin D. 1998; Platelet-derived growth factor (PDGF)-BB stimulates osteoclastic bone resorption directly: the role of receptor beta. *Biochem Biophys Res Commun* **251**: 190–194.

Copyright © 2011 John Wiley & Sons, Ltd.

歯髄生物学分野

須田 英明

医歯学総合研究科・口腔機能再構築学系専攻
歯髄生物学・教授

1）研究の課題名

Pulp Biology Field

1. MEPEのC末断片は象牙芽細胞の分化を抑制する

Differentiation of odontoblasts is negatively regulated by MEPE via its C-terminal fragment

Matrix extracellular phosphoglycoprotein（MEPE）は細胞外マトリックスタンパクの一つで、主に石灰化組織に発現している。本研究の目的はMEPEの歯髄における局在を調べ、さらにその機能について検討することである。生後3日のWistarラット歯髄において、石灰化途上にある象牙芽細胞にMEPEは強く発現していた。象牙芽細胞株OLCにMEPEを強制発現あるいは発現抑制したところ、分化がそれぞれ抑制および促進された。MEPEは細胞内において合成された後、N末とC末に切断されるが、N末はOLCの分化に影響が無かったのに対し、RGD配列を有するC末はOLCの分化を抑制した。MEPEは象牙芽細胞の分化において、象牙質形成あるいはホメオスタシスを保つ上で重要な働きをしていると推察された。

2. MEPEはFurinにより活性化され、歯髄細胞の接着を促進する

MEPE activated by Furin promotes pulpal cell adhesion

Matrix extracellular phosphoglycoprotein（ MEPE ）は骨芽細胞、骨細胞、象牙芽細胞に発現が認められ、骨および象牙質代謝に重要な役割を担っている。このMEPEが活性化されるためには、翻訳後修飾が重要である。本研究は、furinによりMEPEの146R↓147部が切断され、RGD配列を含む切断されたC末が象牙芽細胞の接着に重要なことを本研究は明らかにした。

3. 未分化間葉系のKusaA1細胞の骨芽細胞分化は転写調節制御因子であるRbpjにより促進する

Osteogenic differentiation of mouse mesenchymal progenitor cell, Kusa-A1 is promoted by mammalian transcriptional repressor Rbpj

未分化間葉系の幹細胞は多様な細胞への分化が可能であるが、そのメカニズムはいまだ不明である。我々はNotchの主用な核内メディエーターであるRbpj（recombination signal-binding protein for immunoglobulin kappa j region）が骨芽細胞分化に関与していうる事を報告する。Rbpjを強制発現させたKusa-A1細胞は、in vitro、in vivoともに骨芽細胞分化が促進していた。また、RbpjはRunx2およびOse2のプロモーター活性を増加させた。以上の結果より、Rbpjは骨芽細胞分化において重要な働きをしていることが示唆された。

4. 歯髄細胞におけるNotchシグナル関連因子の発現と歯髄細胞分化にともなう発現変動

Expression of Notch signalling-related genes in normal and differentiating rat dental pulp cells

Notchは胎生期のみならず成体においても様々な組織の分化、機能に重要な働きを担っている。Hey1はNotchの重要な転写調節因子であるが、今回、歯髄細胞におけるHey1の発現動態について検討した。Wistarラット歯髄より得られた歯髄細胞を石灰化誘導条件で培養すると、象牙芽細胞特異的なマーカーであるDentin sialophosphoprotein発現が増加する一方、Hey1の発現は抑制された。このことから、Hey1を介するNotchシグナルは歯髄細胞の象牙芽細胞への分化を負の方向へ制御している可能性が示唆された。

5. ラット実験的根尖性歯周炎の進展におけるカテプシンK阻害剤の抑制効果

カテプシンKは破骨細胞に発現し、骨吸収において重要な役割を果たしている。カテプシンK阻害剤であるNC-2300（日本ケミファ）は、新たに開発された関節リウマチ

の治療薬であり、関節リウマチモデルにおいて、関節の骨破壊ばかりでなく炎症反応も抑制することが報告されている。本研究の目的は、ラットに実験的に誘発した根尖性歯周炎のモデルを用い、根尖性歯周炎の進展におけるNC-2300の抑制効果を検討することである。ラット下顎第一臼歯を露髄後、抜髄し、口腔内に開放することにより根尖性歯周炎を誘発した。露髄開放時よりNC-2300を1日2回経口投与した。21日後に屠殺して下顎臼歯を周囲の顎骨ごと摘出し、左側はマイクロCT撮影により根尖病変の大きさを測定した後、組織学的に検討した。右側は、根尖周囲の病変部を根尖とともに一塊として摘出し、RNA抽出後、リアルタイムPCRにて起炎症性サイトカインの発現量を測定した。マイクロCTによる評価の結果、NC-2300投与群における根尖病変の大きさは、コントロール（非投与）群と比較して有意に小さかった。また、組織学的検討により、コントロール群においては多数の破骨細胞が根尖周囲の歯槽骨上に観察され、活発な骨吸収が行われている像が認められたのに対し、NC-2300群では破骨細胞は認められるものの、その数および密度は有意に少なかった。MHC class II分子発現マクロファージの密度も、NC-2300群ではコントロール群に比べ有意に少なかった。病変中の炎症性サイトカイン発現を比較したところ、NC-2300投与群においてはIL-1αおよびIL-6の発現が有意に抑制されていた。以上の結果より、NC-2300の投与によって、破骨細胞におけるカテプシンK阻害作用による骨吸収抑制に加えて、炎症性サイトカインの発現が減少することにより破骨細胞形成が抑制され、その結果として根尖周囲の骨吸収が抑制された可能性が示唆された。

6. 歯根膜機械受容神経線維の応答性に対する歯髄の炎症性変化の影響

歯根膜に分布する求心神経は三叉神経の末梢枝であり，解剖学的な神経終末形態は自由神経終末とルフィニ神経終末様神経終末である。特に後者は機械的刺激に対して応答する歯根膜機械受容器としての機能的意義を有している。これまでの研究により，歯髄と歯根膜の両者をその分岐した枝が同時に支配している神経線維が存在することも示されている。他方，象牙質の口腔内への露出による外来刺激や，初期う蝕による細菌学的刺激に対して歯髄が反応し，可逆性歯髄炎の状態に陥る。この状態が適切な処置が施されないままに放置されると，歯髄内には軸策反射によって神経原性炎症が惹起され，ついには根尖孔を介して歯根膜内にも波及することになる。細菌感染などの刺激が歯髄に加わった場合に生ずる不可逆性歯髄炎の場合には，この過程がより顕著に現れるものと考えられる。

ところで，広義の歯髄疾患を対象とした根管治療の過程で，強い自発痛あるいは咬合痛のような臨床症状が消退した後にも，打診に対して軽度の痛みや違和感が残存して，この症状が軽快するのに長期間を要する症例に遭遇することがある。この病態の背景には，歯髄除去療法による根尖孔付近での歯髄神経求心線維の切断，感染根管を有する歯の根尖部での炎症性化学物質による歯根膜求心神経線維への刺激，あるいは根管処置時における根尖孔外への器具突出に伴う刺激に起因する根尖部歯周組織の炎症性変化や神経線維の機械的傷害など，種々の要因が考えられる。しかし，歯髄の初期の病的変化に伴う，歯根膜に分布する神経線維の活動性の変化を神経生理学的に明らかにした研究は，これまでに報告されていない。

本研究においては，動物を用いた実験系を構築し，歯髄の炎症性変化に伴う歯根膜機械受容神経線維の応答性の変化を，単一神経線維の応答性を指標に観察して神経生理学的に検索することを目的とした。

7. マスタードオイル歯髄適用により誘発された感作視床内の神経-免疫系の相互作用

Neuron-immune interactions in the sensitized thalamus induced by mustard oil application to rat molar pulp.

ラット歯髄へのマスタードオイル適用は視床ニューロンの活動性を増強させる，すなわち感作が生じる。ニューロンの活動性の記録，免疫組織化学的分析，並びに分子生物学的分析を，この視床の変化に関係する機構を解明するために実施した。マスタードオイル適用後，視床MD核のニューロンの応答性が増強した。MD核にMK-801を投与すると，一度増強したヌーロン活性は減少した。NMDA型受容器のサブユニット2D、GFAP，並びに抗原提示細胞関連遺伝子のmRNAはマスタードオイルを歯髄適用後10分時において対側視床で亢進した。しかし，拮抗薬の投与後10分時にはこれらは減少した。OX6を発現しているマイクログリア及びGFAPを発現しているアストロサイト数は，マスタードオイル歯髄適用後60分までその数が増加することは無かった。

8. 実験的歯髄病変由来の根分岐部病変の成立に関与するToll-like receptorと抗原提示細胞関連分子の遺伝子発現の増加

Increased gene expression of Toll-like receptors and antigen presenting cell-related molecules in the onset of experimentally induced furcation lesions of endodontic origin in rat molars

歯髄の炎症により惹起された根分岐部の炎症の初期の免疫病理学的機構は未だ十分に解明されていない。抜髄後開放したラット臼歯の分岐部歯根膜内のToll-like recepotors（TLRs）に対する免疫組織化学的および量的遺伝子発現分析を実施した。根分岐部歯根膜内のTLRならびに抗原提示細胞関係分子のmRNA発現レベルは抜髄後開放した臼歯周囲において有意に亢進した。同部位の免疫組織化学ではTLR発現細胞が分岐部直下の歯根膜内に分布していることを明らかにした。

9. 歯髄・歯肉組織由来の間葉幹細胞による歯槽骨・顎骨再生

【GCOE拠点内における異なる分野のInnovationを確立する研究】

Reconstruction of alveolar bone from mesenchymal stem cells derived from dental pulp and gingiva

ヒトおよびラットの歯髄および歯肉において間葉系幹細胞分画が存在し、これらの細胞をスフェロイド形成させることにより、骨芽細胞マーカーおよび象牙芽細胞マーカーの発現が増加することが明らかになった。さらに、これらを歯髄内および骨窩洞内にいれることで、組織再生を行うことが可能であると思われ、現在研究を遂行中である。

Endodontic Field

10. 歯科用コーンビームCTにおけるモーションアーチファクトの影響

Effect of motion artifact on cone-beam CT images

歯科用コーンビームCT（CBCT）撮影中の患者の体動が画像に与える影響を検討するための研究を行った.実験には1軸移動ステージを用い,撮影中に1度だけ試料を水平方向に移動させ,照射時間37秒でCBCT（ファインキューブ,吉田製作所）撮影した.ブタ下顎骨を試料とした実験では,撮影したCBCT画像を5名の歯科医師が評価した.結果は,試料の移動距離が0.126 mm以下の条件では,対照と有意差が認められなかったが,0.25mm以上の条件では有意に画質が低下した.また,エックス線照射開始6,12,18秒後に移動した群では,対照と比較して有意に画質が低下したが,24,30秒後に移動した群では,対照と統計学的に有意差は認められなかった.このことから今回の実験条件では,被写体の0.25 mm以上の移動によりCBCT画像が劣化した.また,同じ0.25 mm移動を行った場合においても,移動する時期により画質への影響が異なることが示された.次に,形が規格化されたアルミニウム円柱ファントムを用い同様の実験を行った.直径2,3,5 mmのアルミニウム製円柱を試料とし,鉛直に立てた状態でCBCT撮影を行い,軸位断像を観察した.エックス線照射開始18秒後に移動した場合には,移動した試料の大きさ,形態は保持され,移動前と移動後の2つの円が,移動距離分だけ離れた位置に重ね合わせた画像として観察された.エックス線照射開始12,18秒後に移動した場合,断面が2つの円の重なりに近い形態として観察されたが,6,24,30秒後では,外形が1つの円に近い形態であった.対照およびエックス線照射開始18秒後以外の条件では,円の濃度は一様ではなく,部分的に濃淡が認められた.以上の結果からCBCT撮影中の被写体の移動距離および時期がCBCT画像に影響することが結論された.

11. 新規ねじりファイルの相変態挙動と曲げ特性

Phase transformation behavior and bending property of newly twisted nickel–titanium endodontic instruments

近年,NiTiファイルの新しい加工法である,ねじり加工を用いたTwisted File（TF）が開発された.本研究の目的は,TFの相変態挙動と曲げ特性の関連性を調べることである.材料として,先端径0.30 mm,0.06 テーパーのTFと,対照としてK3を用いた.相変態挙動については示差走査熱量測定（DSC）を行い,相変態温度をDSC曲線より算出した.曲げ特性について片持ち梁式曲げ試験法を用い,37 ℃温度条件下で,負荷過程における曲げ荷重を評価した.相変態温度の比較にはStudent’s t-testを,曲げ荷重についてはMann–Whitney U-testを用い,有意水準5 %で統計学的に解析した.その結果,TFの相変態温度はK3より有意に高く,曲げ荷重は弾性領域と超弾性領域ともにK3より有意に低かった.熱処理をともなったねじり加工は,相変態温度の上昇と,より優れた柔軟性に寄与しているかもしれない.

12. レジン系根管充填用材料の根管封鎖性について

Root canal sealing ability of resin-based root canal sealer

近年様々な種類のレジン系根管充填用シーラーが開発および販売されている.しかしながら,レジン系根管充填用シーラー使用に際して推奨される根管形成方法や根管充填方法についてはいまだ意見が統一されていない.そこで,本研究では各種根管形成および根管充填方法におけるレジン系根管充填用材料の根管封鎖性について比較検討を行った.シングルポイント根管充填およびmatched taperd シングルポイント根管充填を行った被験歯に対して色素浸透試験を行った.その結果,シングルポイント根管充填を行った群では他群と比較して有意に

多い色素漏洩を示した.また,水平断面像の観察においては,シングルポイント根管充填を行った群では,全ての断面において最も多いシーラー占有面積を認めた.本研究の結果,レジン系根管充填用シーラーではシーラー占有量の少なくなる充填方法が推奨されることが示唆された.

13. 歯科用レーザー使用時における眼球への安全性

Safety of dental Laser use under microscopes to eyes

本研究の目的はレーザー用防護眼鏡またはフィルターおよび歯科用顕微鏡を介するレーザー光の透過エネルギーを検討することにより、レーザー使用時の眼球への安全性について考察することである。実験にはNd：YAGレーザー、Er：YAGレーザー、半導体レーザーの3種類の歯科用レーザーを用いた。実験1では、各レーザーの導光用ファイバーまたはチップ先端とレーザー用サーモパイル吸収ヘッドとの距離を5cmとし、吸収ヘッドに各種防護眼鏡を固定、パワーメーターで200mJ, 10pps, 10sの条件にて透過エネルギーを測定した（n=3）。防護眼鏡は、Nd：YAGレーザー用、Er：YAGレーザー用、半導体レーザー用、および防塵眼鏡の4種類を使用し、レーザー光の直接照射をコントロールとした。実験2では、実験1で使用した各種防護眼鏡の特性を変えずに平板化し、専用防護フィルターを作成した。レーザー光の透過エネルギーについて、各レーザーにおける眼球に対する最大許容露光量（MPE, IEC60825-1）を基準として比較検討した。その結果、実験1では各レーザーに対する専用防護眼鏡を使用した場合、全てのレーザーにおいて透過エネルギーは0になった。しかし、Nd：YAGレーザー照射時は専用防護眼鏡以外で、また半導体レーザー照射時は専用防護眼鏡およびNd：YAGレーザー用防護眼鏡以外で、透過エネルギーはMPEを超える値となった。
実験2では各レーザーに対する専用防護フィルターを使用した場合、全てのレーザーにおいて防護フィルターの位置に関わらず透過エネルギーは0になった。 他の防護眼鏡の使用や裸眼では、MPEを超える透過エネルギーが眼球に到達し、障害が生じる可能性がある。本実験条件下では、顕微鏡下でのレーザー使用の際、専用防護眼鏡の位置が接眼レンズ前でも対物レンズ後でも透過エネルギーが0となり、レーザーは顕微鏡下でも安全に使用できると思われた。したがって、対物レンズに防護フィルターを装着して散乱光を遮断できれば、専用防護眼鏡の代替としうる可能性がある。

14. レーザー照射による象牙質の歪

Dentin strain induced by Laser irradiation

歯科治療において歯根破折が注目されており、象牙質の歪が影響する可能性が考えられている。レーザー照射時における歪に関する報告はほとんどないため、本研究ではEr：YAGレーザーおよびNd：YAGレーザーを注水および非注水に分けて根管内照射を行い、その歪と温度変化について検討した。歪変化はストレインゲージを用いて、また温度変化は熱電対を用いてそれぞれ根尖部に設置して計測した。レーザー照射は1Wの条件で5秒間照射した。今回の結果では注水下Er：YAGレーザー照射群はNd：YAGレーザー群に比較して有意に小さな象牙質の歪および温度変化を示し、両レーザー群ともに注水された群は非注水の群よりも歪変化は小さい結果となった。熱により発生する歪としてはエネルギーを吸収した歯牙組織の熱膨張が考えられる。また注水による冷却は両レーザーに生じる歪を減少させた。

熱の発生は歪変化に対し大きな影響を与えると考えられ、各歯根象牙質の異なる形態や構造や性質や歯根破折に対する耐久性は異なると考えられるものの、より大きな歪は微小歯根破折のより大きな危険性につながると考えられる。レーザーに応じて注水、照射条件等を制御することの必要性が示唆された。

15. 逆根管充填材により誘発される象牙質の歪みと破折に関する研究

Dentin strain and fracture propagation caused by retrofilling materials

歯根端切除術の際には、逆根管充填窩洞を形成し充填を行う。NTAは現在最も推奨される逆根管充填材であり、その良好な封鎖性は硬化膨張によるものとされている。しかしその反面、膨張により象牙質に歪みが生じ歯根破折が誘発される懸念がある。本研究の目的歯、MTAを用いた逆根管充填により誘発される象牙質のゆがみを測定し、歯根破折の発生を調査することである。30本のヒト抜去前歯に根管形成およびガッタパーチャによる根管充填を行い、根尖部3mmを切除した。注水下あるいは無注水で超音波チップにより逆根管充填窩洞を形成し、Super EBAあるいはMTAにて充填した。根尖1/3に貼付した歪みゲージを用いて、逆根管充填材により生じたひずみを計測した。また、SEMにて破折の有無を観察した。平均最大歪みは、Super EBA と比較し有意にMTAで大きかった。破折は無注水群で散見された。逆根管充填材は、直接的に破折を生じてはいなかったが、逆根管充填窩洞形成により生じた破折線を促進していた。逆根管充填材と象牙壁間の間隙は、MTAで最小だった。本研究結果は、逆根管充填窩洞形成中に適切な冷却がなされないと、逆根管充填剤微小破折の危険性があることを示唆している。

16. 超音波吸引洗浄法の開発

Development of the negative pressure irrigation method

全根管系を機械的に根管形成することは不可能である.臨床的に成功するためには,改良された洗浄法が不可欠である.次亜塩素酸ナトリウム水溶液は,有機質溶解作用および殺菌性が高く最良の根管洗浄剤として良く知られている.次亜塩素酸ナトリウム水溶液を用いての,根尖孔近くの陽圧の洗浄は非常に危険である.最近,次亜塩素酸ナトリウム水溶液の根尖歯周組織への注入による,重篤な障害の症例を多くの学会誌で見ることができる.より良くより安全な洗浄として,陰圧による洗浄が選択されるべきである.我々は新しい陰圧洗浄法として超音波吸引洗浄法（UAT）を開発した.UATでは,吸引針自体が超音波振動し,洗浄効果を上げるとともに吸引針の詰まりを防止することができる.

UATの利点は,

・根尖部根管を洗浄出来る最も安全な方法である.

・デブリ除去効果が様々な洗浄法の中で最も高い.

2)

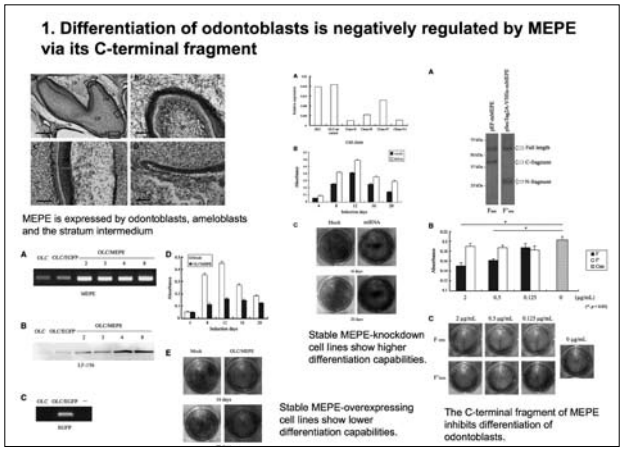

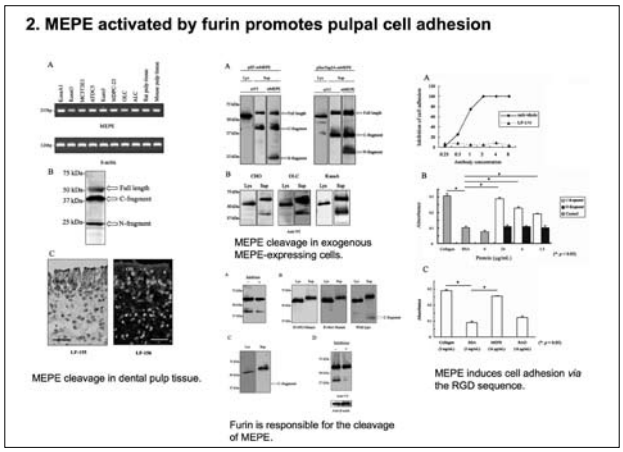

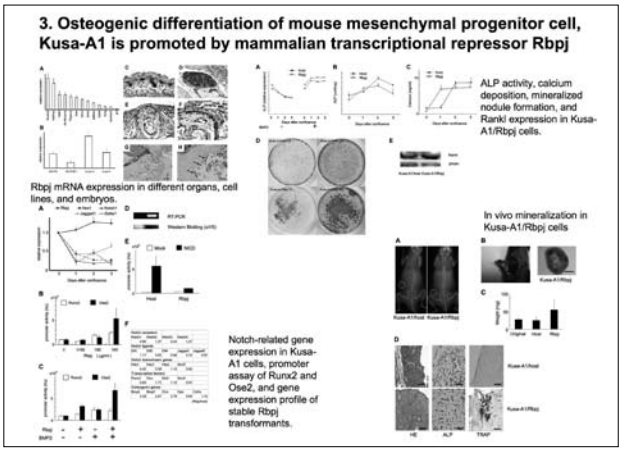

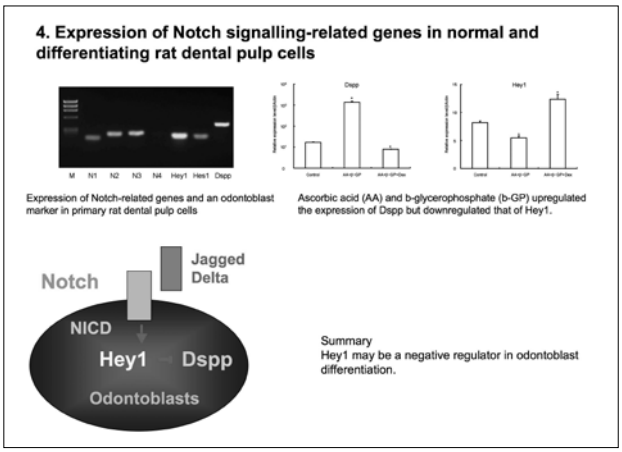

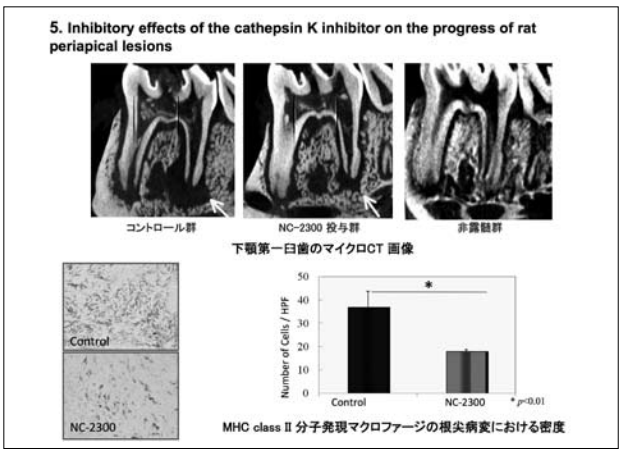

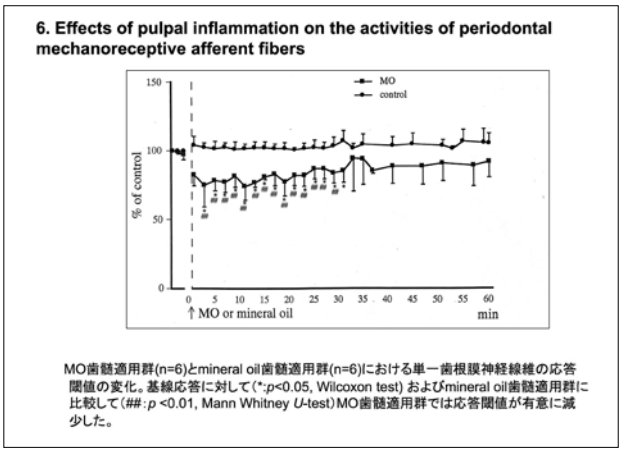

7. Neuron-immune interactions in the sensitized thalamus induced by mustard oil application to rat molar pulp.

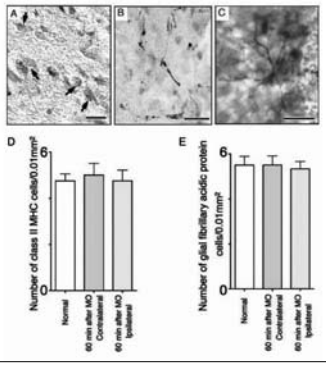

8. Neuron-immune interactions in the sensitized thalamus induced by mustard oil application to rat molar pulp.

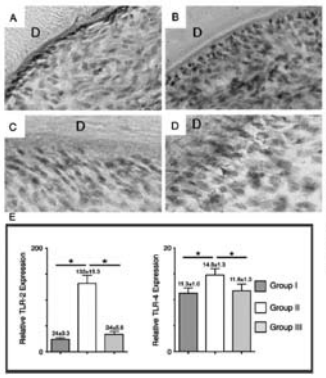

Immunohistochemistry and gene expression analysis of TLR-2 and TLR-4 at the furcal region of the PDL. (A-D) Representative images of (A) TLR-2 in group 1 (untreated control; original magnification, 20), (B) TLR-2 in group 2 (unsealed pulpotomy; original magnification, 20), (C) TLR-4 in group 1 (original magnification, 40), and (D) TLR-4 in group 2 (D: dentin; original magnification, 40). (E) Real-time polymerase chain reaction analysis of TLR-2 and TLR-4 relative messenger RNA expression in the furcal PDL tissue in each group. Data presented from real-time polymerase chain reaction experiments reflect the expression level of TLR-2 or TLR-4 normalized by glyceraldehyde 3-phosphate dehydrogenase (mean and standard error of the mean, n = 4 in each group). The single asterisks stand for $p < 0.05$ (Tukey test).

9. GCOE拠点内における異なる分野のInnovationを確立する研究提案

歯髄・歯肉組織由来の間葉幹細胞による歯槽骨・顎骨再生

Reconstruction of alveolar bone by mesenchymal stem cells derived from dental pulp and gingiva

研究目的:
近年、顎骨の再建の需要が高まっているが、そのための細胞ソースとして、歯髄、歯肉組織由来の間葉幹細胞の使用を検討し、その臨床的な応用手法の確立を目指す。

研究手法:
ヒトおよびラット歯肉、歯髄由来のコロニー形成細胞を継代(P2-4)後、下記解析を行う。

FACSによる細胞表面抗原の解析
SCIDマウスに実験的に作成した骨欠損への移植
SCIDマウスへの象牙質との移植
移植細胞の遺伝子プロファイル解析

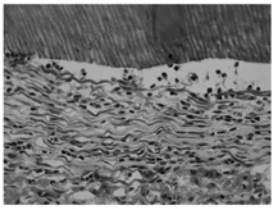

図:ラット歯髄細胞を象牙質とともにSCIDマウス皮下に移植した。3週後に歯髄様の組織が観察された。

10. Effect of moving distance

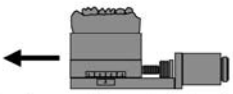

Sample mounted on a motorized x-axis stage

Clinical case

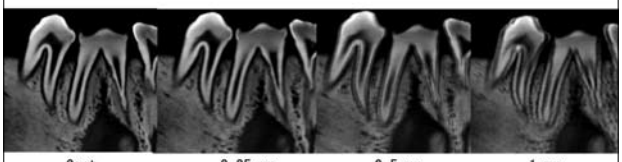

Cont. 0.25 mm 0.5 mm 1 mm

11. Phase transformation behavior and bending property of newly twisted nickel–titanium endodontic instruments

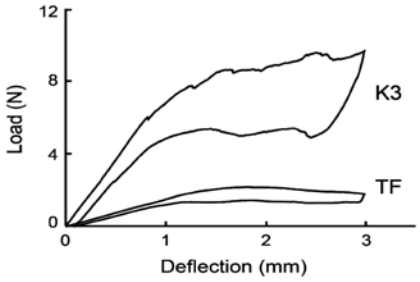

12. Root canal sealing ability of resin-based root canal sealer

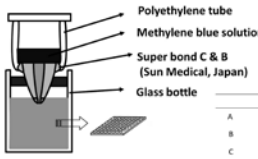

	Taper of prepare	Sealer	Point	Obturation method
A	.10	MetaSEAL™ (Parkell, USA)	.02 GP	SC
B	.06 (.06 ProFile®)	MetaSEAL™	.02 GP	SC
C	.06 (.06 ProFile®)	MetaSEAL™	.06 GP	SC

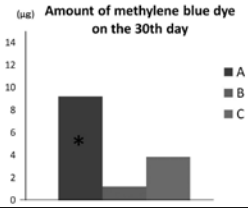

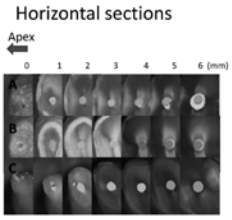

13. Safety of dental Laser use under microscopes to eyes

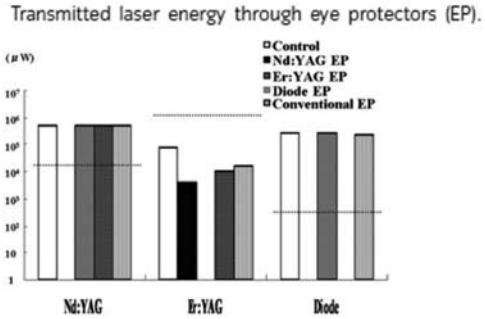

14. Dentin strain induced by Laser irradiation

Mean maximum root surface strain produced by each laser irradiation with and without water cooling.

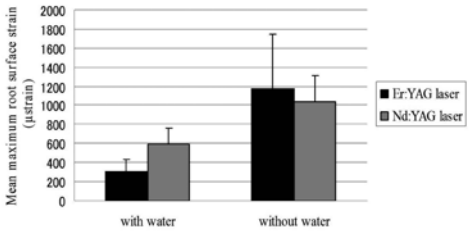

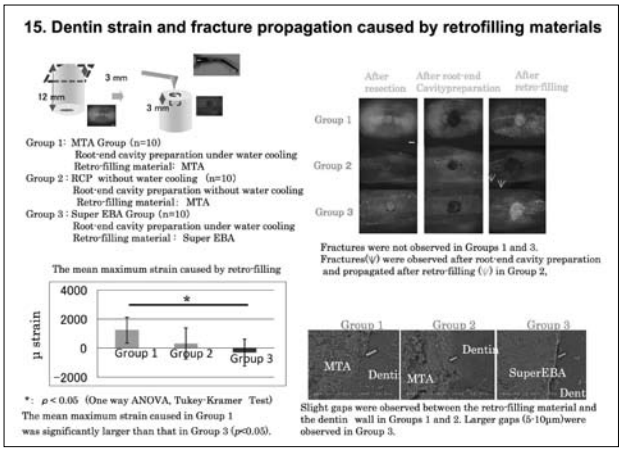

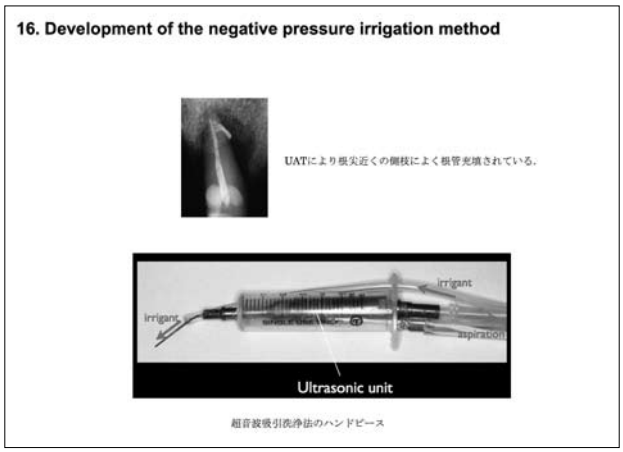

3）発表の研究内容についての英文要約

1. Differentiation of odontoblasts is negatively regulated by MEPE via its C-terminal fragment

Matrix extracellular phosphoglycoprotein（MEPE）is an extracellular matrix protein that is mainly expressed in mineralizing tissues, including the dental pulp. The purposes of this study were to clarify the localization of MEPE in the tooth germ and to investigate the roles of MEPE in the differentiation of odontoblasts. The immunohistochemical staining in the tooth germ of the upper first molars of male Wistar rats（postnatal day 3）revealed that MEPE was mainly localized in odontoblasts during dentinogenesis. Stable MEPE-overexpressing and MEPE-knockdown cell lines, which were established in odontoblast-lineage cells（OLCs）, showed lower and higher differentiation capabilities, respectively. Eukaryotic proteins of the N-terminal fragment of MEPE produced in HEK cells had no effect on the differentiation of OLCs, whereas the C-terminal fragment containing an RGD sequence inhibited their differentiation. These results indicated that the C-terminal fragment of MEPE containing an RGD sequence, cleaved in odontoblasts, appeared to be the active form of MEPE, which may play important roles in dentinogenesis and pulpal homeostasis by keeping the odontoblasts in immature condition.

2. MEPE activated by furin promotes pulpal cell adhesion

Matrix extracellular phosphoglycoprotein（MEPE）is predominantly expressed in osteoblasts, osteocytes, and odontoblasts and plays key biological roles in bone and dentin metabolism. Posttranslational modifications are essential for its activation. This study tested the hypothesis that MEPE is activated through proteolytic processing by furin in dental pulp. MEPE was present in three sizes, 1 full-length and 2 cleaved fragments; the cleavage site was 146R ↓ 147. The proprotein convertase family, particularly furin, was a candidate enzyme. Introducing a substitution at the cleavage
site inhibited hydrolysis, but there was no cleavage of MEPE expressed in furin-deficient LoVo cells. Therefore, furin is a strong candidate for the proteolytic cleavage of MEPE. The C-terminal cleavage product promoted cell adhesion via its RGD
motif. These results indicate that proteolytic processing by furin may activate MEPE during its secretion from odontoblasts and may play important roles in dentinogenesis and pulpal homeostasis.

3. Osteogenic differentiation of mouse mesenchymal progenitor cell, Kusa-A1 is promoted by mammalian transcriptional repressor Rbpj

Pluripotent mesenchymal stem cells possess the ability to differentiate into many cell types, but the precise mechanisms of differentiation are still unclear. Here, we provide evidence that Rbpj（recombination signal-binding protein for immunoglobulin kappa j region）protein, the primary nuclear mediator of Notch, is involved in osteogenesis. Overexpression of Rbpj promoted osteogenic differentiation of mouse Kusa-A1 cells in vitro and in vivo. Transient transfection of an Rbpj expression vector into Kusa-A1 cells
upregulated promoter activities of Runx2 and Ose2. Enhanced osteogenic potentials including high alkaline phosphatase activity, rapid calcium deposition, and increased calcified nodule formation, were observed in established stable Rbpj-overexpressing Kusa-A1（Kusa-A1/Rbpj）cell line. In vivo mineralization by Kusa-A1/Rbpj was promoted compared to that by Kusa-A1 host cells. Histological findings revealed that expression of Rbpj was primarily observed in osteoblasts. These results suggest that Rbpj may play essential roles in osteoblast differentiation.

4. Expression of Notch signalling-related genes in normal and differentiating rat dental pulp cells

Notch signalling is of fundamental importance to various

processes during embryonic development and in adults. The possible role of Hey1, an important Notch signalling component, in odontoblast differentiation was evaluated in this study. Primary cultured dental pulp cells, derived from upper incisors of 5-week-old Wistar rats, were placed in a-modification of Eagle' s minimal essential medium supplemented with 10% Fetal Bovine Serum (FBS), and ascorbic acid (AA) and b-glycerophosphate (b-GP), with or without dexamethasone, and cultured on dishes coated with collagen type IA for 7 days.
Conventional and real-time Polymerase Chain Reaction (PCR) was performed to determine the expression of Notch-related genes and dentin sialophosphoprotein as a marker of odontoblast differentiation. Dentin sialophosphoprotein and Hey1 expression was significantly increased and decreased in the presence of AA + b-GP compared with controls, respectively. These findings suggest that Hey1 may be a negative regulator in odontoblast differentiation.

5. Inhibitory effects of the cathepsin K inhibitor on the progress of rat periapical lesions

In this study, we investigated the inhibitory effects of the cathepsin K inhibitor (NC-2300) on the progress of rat periapical lesions. The periapical lesions were induced experimentally in the rat first lower molars, and NC-2300 was administrated orally in the experimental group. In the micro CT and the histological analyses, the size of the periapical lesion and the number and the density of osteoclasts and MHC class II molecules-expressing macrophages in the experimental group were significantly small compared to the control group. The expression of pro-inflammatory cytokines (IL-1 α and IL-6) in the experimental group was also significantly suppressed compared to the control group. These results suggest that NC-2300 may inhibit not only the cathepsin K activation in the osteoclasts, but also the osteoclastgenesis which is induced by the inflammatory cytokines, resulting that the bone resorption in the periapical lesion was suppressed.

6. Effects of pulpal inflammation on the activities of periodontal mechanoreceptive afferent fibers

Response properties of periodontal single afferents were investigated in cats with inflammatory irritant-induced pulpitis. A deep dentin cavity was prepared on the right mandibular canine in order to apply an inflammatory agent and small fiber excitant, allyl-isothiocyanate (mustard oil : MO), and single afferents innervating the canine periodontal mechanoreceptor were dissected out from the mandibular nerve bundle by examining impulse responses while applying mechanical stimuli to the tip of the crown. Evoked impulses by mechanical stimuli were increased in number for one hour with MO application to the pulp when compared with those with mineral oil. The mechanoreceptive thresholds of single nerve fibers were decreased after the MO application to the pulp when compared with those with mineral oil. These results suggest that the alteration of responses in the periodontal afferent fiber, or the peripheral sensitization, can be produced by MO-induced pulpal inflammation probably due to the axon reflex mechanism in the furcating branches of nerve fibers innervating both the tooth pulp and periodontal ligament.

7. Neuron-immune interactions in the sensitized thalamus induced by mustard oil application to rat molar pulp.

The application of mustard oil to the rat dental pulp induced neuronal activation or the sensitization in thalamus. The neuronal responsiveness recording, immunohistochemistry, and molecular biological analysis were performed to address the mechanisms involved in these thalamic changes. After mustard oil application, neuronal responsiveness was increased in the mediodorsal (MD) nucleus. When MK-801 was applied to the MD nucleus, the enhanced responsiveness was decreased. N-methyl D-aspartate receptor subunit 2D, glial fibrillary acidic protein (GFAP), and antigen-presenting cell-related gene mRNAs in the contralateral thalamus were up-regulated at 10 minutes after mustard oil application, but were down-regulated within 10 minutes after the antagonist application. OX6 expressing microglia and GFAP-expressing astrocytes did not increase until 60 minutes after mustard oil application.

8. Increased gene expression of Toll-like receptors and antigen presenting cell-related molecules in the onset of experimentally induced furcation lesions of endodontic origin in rat molars

Early immunopathologic mechanisms behind pulp infection-induced furcal inflammation have not been well understood. The immunohistochemical and quantitative gene expression analysis for toll-like receptors (TLRs) were conducted in the furcal periodontal ligament (PDL) of rat molars subjected to unsealed pulpectomy. Messenger RNA expression levels of TLRs and the antigen presenting cell (APC) -related molecules in the furcal PDL were significantly up-regulated in teeth with unsealed pulpectomy. Immunohistochemistry for unsealed pulpotomized teeth revealed that TLRs-expressing cells were predominantly distributed within the PDL beneath the furcal dentin.

9. Reconstruction of alveolar bone from mesenchymal stem cells derived from dental pulp and gingival

We have successfully identified the mesenchymal stem cell population in the human dental pulp and gingival. We separated the mesenchymal stem cell population in the rat dental pulp and gingiva, and tried to transplant into SCID

mouse with dentin subcutaneously. Transplanted pulpal stem cells survived on the dentin for 3 to 6 weeks.

Endodontic Field

10. Effect of motion artifact on cone-beam CT images

We have conducted a study to determine the effect of motion artifact on cone-beam CT images. The specimen was moved horizontally by a motorized x-axis stage. The CBCT images were taken using CBCT（Fine Cube, Yoshida, Japan）. The exposure time was 37 seconds. One mandibular jaw of the pig was used in exp. 1. Five dentists individually assessed the CBCT images. Under the conditions of this study, it was revealed that the sample motion of 0.25 mm and over deteriorated visibility of the anatomical structure. Our data indicate that the time of sample moving affects on the image quality. Cylindrical phantom made of aluminum, diameter of 2, 3, 5mm were used and the CBCT axial images were assessed in exp. 2. When the moving timing was 18 seconds after starting X-ray exposure, the shape and size of the samples were well maintained, and two circles in each image showed a moving distance. We conclude that the magnitude and timing of sample movement significantly affects the quality of CBCT images.

11. Phase transformation behavior and bending property of newly twisted nickel–titanium endodontic instruments

Recently, a new manufacturing process was developed to create a nickel–titanium（NiTi）endodontic instrument named the Twisted File（TF）. The aim of this study was to investigate the relationship between phase transformation behavior and bending property of NiTi endodontic instruments manufactured by a twisting process. The phase transformation behavior and bending property of Twisted Files（TF; SybronEndo, Orange, CA, USA）and K3（SybronEndo）with.06 taper and size 30 tip were investigated. K3 was used as control group. Phase transformation behavior was estimated by differential scanning calorimetry（DSC）. Transformation temperatures were calculated from the DSC curve. Bending load of the instruments was measured by cantilever-bending test at 37 °C. Student' s t-test was used to compare DSC data of the two groups and Mann–Whitney U-test was used to detect the difference of the bending load values between TF and K3（$P = 0.05$）. The phase transformation temperatures of TF were significantly higher（$P < 0.05$）than those of K3. The bending load values were significantly lower for TF than that of K3（$P < 0.05$）, both in the elastic and super-elastic ranges. The new method of manufacturing NiTi instruments by twisting coupled with heat treatment might contribute to the increased phase transformation temperatures and superior flexibility.

12. Root canal sealing ability of resin-based root canal sealer

In recent years obturating sealers has been developed based on dentin adhesion. However, there has no information that which condensation method provides good sealing ability with resin based root canal sealers. The aim of this study was to evaluate factors influencing the sealing ability of resin based root canal sealers. The teeth were prepared and obturated with single condensation method or matched tapered single condensation method using resin based root canal sealers. Then, dye penetration test was done and horizontal sections were made. The images of the horizontal sections were taken by a digital microscope, and sealer occupancy in the root canal was evaluated. The amount of leaked dye in single condensation method group was significantly more than that in the other experimental groups（$p< 0.05$）. In the images of horizontal sections, single cone method group showed the highest sealer occupancy at all levels. It was suggested that sealer occupancy may influence the root canal sealing ability of resin based root canal sealers.

13. Safety of dental Laser use under microscopes to eyes

The purpose of this study was to investigate the transmissivity of various types of lasers through the microscope with and without eye protectors. Nd：YAG laser, Er：YAG laser, and diode laser were irradiated to a power meter through laser eye protectors or a microscope. In control experiment, three lasers were irradiated directly or through eye protectors to the power meter positioned at a distance of 5 cm from the fiber tip or the contact tip. In main experiment, the fiber tip was positioned from the objective lens surface of the microscope. The power meter was placed behind the eyepieces. Matched eye protectors for each laser were placed in front of the objective lens or between the eyepieces and the power meter. The results obtained were as follows：No transmitted laser energy was detected when matched eye protectors were used. Mismatched eye protectors were not effective to shut out laser energy, especially for Nd：YAG and diode lasers. Little or no transmitted laser energy was detected through the microscope even when no eye protectors were used. It was concluded that we could use laser devices safely with the dedicated laser eye protectors in clinical situations, although under a microscope.

14. Dentin strain induced by Laser irradiation

The purpose of this study was to investigate the strain and temperature change in dentin induced by laser irradiation of human root canals with or without water cooling.

Twenty-eight palatal roots of extracted human maxillary first molars were used. The strain indentin was measured using strain gauges fixed on the apical third of the buccal root surface. The temperature change of the root dentin was monitored using thermocouples embedded into dentin near the apex. The root canal was irradiated with Er：YAG or Nd：YAG laser at an output of 1 W（100 mJ, 10 pps）for 5 s. The tip of the irradiation fiber was located 2.0 mm from the root apex. With water cooling,the mean maximum strain induced by Er：YAG laser was significantly lower than that by Nd：YAG laser（P< 0.05）. However, without water cooling, no significant difference between the two lasers（P> 0.05）was found. The results suggest that the strain induced by Er：YAG laser irradiation in dentin with water cooling may be minimal, but there still might be a risk of root micro fracture if cooling is not sufficient.

15. Dentin strain and fracture propagation caused by retrofilling materials

The purpose of this study was to investigate the kinetics of dentin strain and fracture propagation caused by retrofilling materials. Thirty roots of extracted human anterior teeth were prepared and laterally condensed with gguttapercha,. Then a 3 mm of the root end was resected. Root-end cavities were prepared using an ultrasonic device（high power setting）with or without water cooling. The cavities were dried and filled with Super EBA or MTA. Strain of dentin caused by the retrofilling materials was measured using strain gauges mounted on the apical third of the root surface., Finally presence or absence of fracture was examined by microscopy and SEM.　The mean maximum strain caused by MTA was significantly larger than that by Super EBA（p<0.05）. In Microscopic observation, fractures were found in some samples of the ultrasonic group without water cooling, Although fractures were not caused by retorofilling materials, some fracture lines caused by root-end cavity preparation were propagated by retrofilling materials. In SEM observations, minimal gaps were observed between the retorofilleng material and the dentin wall in MTA group. The results suggest that there might be a risk of micro root fracture propagation by retro -filling materials if cooling is inefficient during root-end preparation.

16. Development of the negative pressure irrigation method

Total root canal systems cannot be mechanically prepared. For a clinical　success, improved irrigations are inevitable. Sodium hypochlorite is well known as a best irrigant for its high organic substance dissolving and microorganisms killing actions. With sodium hypochlorite, positive pressure irrigation near the apical foramen is too dangerous. Recently, we can find a lot of serious injury cases on journals caused by sodium hypochlorite injection to the surrounding tissue. For a better and safer irrigation, negative pressure irrigations should be selected. We could developed a new negative pressure irrigation system, ultrasonic aspiration technique（UAT）. In UAT, aspiration needle itself ultrasonically vibrates. This ultrasonic vibration can enhance irrigation action and prevent needle choke.

The advantages of the UAT are：

- Safest irrigation method that can irrigate apical canals.
- Removal of debris is highest among various irrigation methods.

4）本事業に関連して世界的な研究拠点形成に向けて、以下の点で改善・整備等されたこと

A（研究拠点体制）

グローバルな視点に立って、歯学の中でも歯髄生物学および歯内療法学の発展に寄与できる研究を行うことのできるよう研究の環境整備を進めている。そのため、幅広く研究領域をカバーするとともに、それぞれの領域で先端的な研究を行うことができるよう、専任の指導教官を配備している。指導教員にはその領域において世界の第一線で活躍できる知識および経験を備えていることが求められる。

B（研究教育環境）

大学院生には、常に臨床と研究の接点を見失うことのないよう、週に最低3コマの診療コマが与えられている。また、専任の指導教官は個別に研究指導を行い、研究遂行上問題が生じた場合にはすぐに対応できる環境が整えられている。

C（人材確保）

大学院を終了した後に教室に残り、研究を続けることができるよう、大学院終了時に医員として大学に残ることが出来るように配慮している。医員は病院職員として臨床業務に携わるが、時間を有効に活用し研究業務に当たることが可能である。

D（人材育成）

研究課題を自ら考えて、それを解明するための実験系を遂行できる人材の育成に力をいれている。そのために、研究の内容について指導者と突っ込んだ話し合いを行い、自らの考えをきちんとまとめることができるよう指導している。

E（国際化）

海外からの留学生も多くいることから、各研究グループのセミナーおよび医局のセミナー用のスライドは原則英語にしている。また、当教室で行う大学院講義はスラ

イド、講義ともに英語で行っている。

5）GCOE事業を推進するに当たって力を入れた点

本事業を推進するにあたり、世界的な研究拠点づくりとのことから海外の研究機関との情報交換および人材交流に力を入れている。アメリカ、カナダ、イギリス、韓国、中国、タイなどの研究機関と現在交流を持っている。

6）英文原著論文

1. ◎H.G. Wang, N. Kawashima, T. Iwata, J. Xu, S. Takahashi, T. Sugiyama, H. Suda, MEPE Activated by Furin Promotes Pulpal Cell Adhesion, Jouranal of Dental Research 90（4）：529-534, 2011.
2. XM. Hou, Y. Yahata, Y. Hayashi, A. Ebihara, T. Hanawa and H. Suda, Phase transformation behaviour and bending property of twisted nickel–titanium endodontic instruments, International Endodontic Journal 44（3）：253-258, 2011.
3. A. Ebihara, Y. Yahata, K. Miyara, K. Nakano, Y. Hayashi and H. Suda, Heat treatment of nickel–titanium rotary endodontic instruments：effects on bending properties and shaping abilities, International Endodontic Journal 44（9）：843-849, 2011.
4. ◎G. Bolortuya, A. Ebihara, S. Ichinose, S. Watanabe, T. Anjo, C. Kokuzawa, H. Saegusa, N. Kawashima and H. Suda, Initial fibroblast attachment to Erbium：YAG laser-irradiated dentine, International Endodontic Journal 44（12）：1134-1144, 2011.
5. ◎Chokechanachaisakul U, Yamanaka Y, Kaneko T,Katsube K,　Kobayashi H, Okiji T, Suda H, Gene expression analysis of resident macrophages in lipopolysaccharide-stimulated rat molar pulp, Journal of Endodontics 37（9）：1258-1263, 2011.
6. Kaneko M, Kaneko T,Kaneko R. Chokechanachaisakul U, Kawamura J, Sunakawa M, Okiji T, Suda H, The role of N-methyl-D-aspartate receptor subunits in the rat thalamic mediodorsal nucleus during central sensitization, Brain Research 1371：16-22, 2011.
7. Adorno CG, Yoshioka T, Suda H, Crack initiation on the apical root surface caused by three different nickel-titanium rotary files at different working lengths, Journal of Endodontics 37（4）：522-5, 2011.
8. T. Yoshioka, I. Kikuchi, C. Adorno, H. Suda, Periapical bone defects of root filled teeth with persistent lesions evaluated by cone-beamcomputed tomography, International Endodontic Journal 44（3）：245-252, 2011.
9. T. Kaneko, H. Sakaue, T. Okiji, H. Suda, Clinical management of dens invaginatus in a maxillary lateral incisor with the aid of cone-beam computed tomography – a case report, Dental Traumatology27（6）：478-483, 2011.
10. Kaneko T, Okiji T, Kaneko R, Suda H, Nor JE, Laser-capture microdissection for factor Ⅷ-expressing endothelial cells in cancer tissues, Methods Mol Biol 755：395-403, 2011.
11. A. Jamleh, A. Sadr, N. Nomura, Y. Yahata, A. Ebihara, T. Hanawa, J. Tagami and H. Suda, Nano-indentation testing of new and fractured nickel-titanium endodontic instruments, International Endodontic Journal（in press）.
12. ◎Gombo B, Ebihara A, Ichinose S, Watanabe S, Anjo T, Kokuzawa C, Saegusa H, Kawashima N, Suda H, Effects of Dentin Surface Modifications Treated with Er：YAG and Nd：YAG laser Irradiation on Fibroblast Cell Adhesion, Photomedicine and laser surgery（in press）.
13. Curriculum Designs for Dental Students：a Brief Comparison between Dental Schools in China and Japan, Sun H, Kawashima N, et.al., Jouranal of Dental Education, in press.

7）総説ならびに著書

1. 須田英明, 南里嶽仁
   連載開始にあたって
   歯界展望（医歯薬出版）, 117（2）, 1, 2011
2. 八幡祥生, 須田英明
   基礎と臨床の架け橋として
   東京医科歯科大学生体材料工学研究所60周年記念誌, 日経BPコンサルティング1,1, 2011
3. 須田英明
   X歯髄疾患の治療法
   歯内治療学 第4版（医歯薬出版）4, 1, 2011
4. 須田英明
   ガッタパーチャに代わる新しい根管充填材について
   Dr.Martin Tropeの講演から ENDOで臨床を大きく変えよう!歯科治療の根幹ENDOで天然歯を守る（クインテッセンス出版）1, 4, 2011
5. 須田英明
   第36章　歯内療法に用いられる薬物
   現代歯科薬理学 第5版（医歯薬出版）5, 18, 2011
6. 須田英明, 海老原新
   "歯内療法におけるEr：YAGレーザーの臨床
   歯根端切除" Er：YAGレーザーの基礎と臨床（第一歯科出版）1, 8, 2011

8）平成23年度までの自己評価

世界の中心としての研究拠点を構築していくにあたり、各指導教員および大学院生あるいはポスドクが一体となっ

て研究活動に邁進する環境を整備する必要があるが、その整備が十分に行われていない。指導教員は自らの研究を行うと共に指導している大学院生の研究を補助し、さらに臨床、教育、雑務に従事せざるをえず、あまりの多忙に研究に対する熱意が薄れがちである。その一つの解決策として、他分野との共同研究を行うことが考えられる。共同研究を行うことにより、多方面からのアプローチが行えると共に、研究の効率化を進めることも可能となると期待される。

9）和文原著論文

1. 須田　英明
   透析患者の象牙質知覚過敏症、う蝕および歯髄疾患
   臨床透析27（6）：657-662, 2011
2. 森田一三, 武部純, 金村清孝, 石橋寛二, 須田英明, 福田仁一, 中垣晴男, 末瀬一彦
   歯科衛生士国家試験客観式多肢選択試験成績と養成校実技実習成績との相関
   日本歯科衛生士教育学会1（1）：16-26, 2011
3. 岡野友宏, 新井嘉則, 伊藤公一, 須田英明, 西堀雅一, 槇宏太郎, 朝田芳信, 林孝文
   歯科診療における歯科用コーンビームCTの基礎的・臨床的評価
   日歯医学会誌, 2011
4. 須田英明
   わが国における歯内療法の現状と課題
   日本歯内療法学会雑誌 32（1）：1-10, 2011
5. 渡辺聡, 三枝英敏、安生智朗、海老原新、須田英明
   根管照射用チップを用いたEr：YAGレーザー照射による象牙質切削の基礎的検討
   日本レーザー歯学会誌20（2）：74-80, 2011
6. 八幡祥生, 山内隆守, 海老原新, 須田英明
   複雑な根管を呈する下顎小臼歯の歯内治療 - 歯科用実体顕微鏡とコーンビームCTの有用性 -
   日本歯内療法学会雑誌33（in press）

10）学会発表（英文）

1. Chokechanachaisakul U, Yamanaka Y, Kaneko T, Katsube K, Kobayashi H, Okiji T, Suda H, A new method of culturing rat dental pulo tissue, IADR/AADR/CADR 89th General Session and Exhibition, poster, San Diego, 2011.03.16-19.
2. Ikeda H, Suda H , Regulatory Capacity of Volume and Form of Human Odontoblasts, IADR/AADR/CADR 89th General Session and Exhibition, oral, San Diego, 2011.03.18.
3. Li Y, Ikeda H, Suda H, Measurement of Functional Space for Fluid Movement in Dentinal Tubules, IADR/AADR/CADR 89th General Session and Exhibition, poster, San Diego, 2011.03.18.
4. R.Wadachi, H.Suda, Root canal treatment of oculo-fasio-cardio-dental（OFCD）syndrome, AAE, poster, San Antonio, 2011.04.13-16.
5. Yahata Y, Miyara K, Jamleh AO, Hayashi Y, Ebihara A, Suda H, Change of fatigue property of Ni-Ti rotary instruments through heat treatment, AAE, poster, San Antonio, 2011. 04.13-16.
6. Nakano K, Ebihara A, Ishimura H, Suda H , A survey on cone-beam computed tomography in endodontics, AAE, poster, San Antonio, 2011.04.13-16.
7. Suda H, Diagnosis and management of vertical root fracture, 16th Scientific Meeting of APEC 14th Annual Congress of the IAE, oral, Iran, 2011.04.20-22.
8. Kawashima N, Suzuki N, SudaH, Mechanisms of Bone Destruction in the Periapical Lesions and Its Regulation, K, 16th Scientific Meeting of APEC 14th Annual Congress of the IAE, oral, Iran, 2011.04.20-22.
9. Chokechanachaisakul U, Kanreko T, Yamanaka Y, Sunakawa M, Okiji T, Suda H Immuno-laser Capture Microdissection of Macrophages from Rat Tissue Calture Model, The Japanese Society of Microscopy 2011, Fukuoka, 2011.05.16-18.
10. Ikeda H, Li Y, Suda H, Response to mechanical deformation of human odontoblasts, Symposium on oral neurophysiology and molecular biology, Marseille, 2011.07.26.
11. Watanabe S, Kokuzawa C, Gomb B, Saegusa H, Ebihara A, Kobayashi C, Suda H, Dentin strain produced by root-end cavity preparation using Er：YAG laser, ESE, oral, Rome, 2011.09.15-17.
12. ◎Takahashi S, Kawashima N, Katsube K, Sugiyama T, Suda H, Shh and Wnt Signaling in Ameloblast Differentiation, ESE, poster, Rome, 2011.09.15-17.
13. ◎ Kawashima N, Xu J, Suzuki N, Zhou M, Takimoto K, Koizumi Y, Yamamoto M, Takahashi S, Sugiyama T, Suda H, Mineralization of Odonotoblastic-Lineage Cells Was Accelerated by Enhanced Expression of Mef2c, ESE, poster, Rome, 2011.09.15-17.
14. Chokechanachaisakul U, Kanreko T, Yamanaka Y, Kaneko R,Sunakawa M, Okiji T, Suda H, Immuno-laser Capture Microdissection of ED2 Expressing Resident Macrophages in Rat Molar Pulp, 第52回日本組織細胞科学会, poster, Ishikawa, 2011.09.24-25.
15. Chokechanachaisakul U, Kaneko T, Yamanaka Y, Kaneko R, Sunakawa M, Okiji T, Suda H, Immune-LCM of Resident Macrophages in Cultured Dental Pulp Tissues, The 10th China-Japan Joint Seminar on Histochemistry and Cytochemistry, poster, Beijing,

2011.10.21-24.

16. Sunakawa M, Suda H, Treatment of Teeth with "Neuropathic Pain" after Endodontic：Treatment. Report of Three Cases, 2011 Autumn Scientific Meeting of KACD（136th）and 13th Joint-Scientific Meeting of KACD-JSCD 2011, oral, Seoul , 2011.11.12.
17. Chokechanachaisakul U, Kaneko T, Sunakawa M, Okiji T, Suda H, Artificial Dental Pulp Exposure Injury Up-regulates Mitogen-activated Protain Kinase 13 and 14 in Rat Central Nervous System, 2011 Autumn Scientific Meeting of KACD（136th）and 13th Joint-Scientific Meeting of KACD-JSCD 2011, poster, Seoul, 2011.11.12.
18. Jamleh A, Sadr A, Nomura N, Yahata Y, Ebihara A, Hanawa T, Tagami J, Suda H, Nanoindentation of NiTi endodontic instruments after cyclic fatigue, 2011 Autumn Scientific Meeting of KACD（136th）and 13th Joint-Scientific Meeting of KACD-JSCD 2011, poster, Seoul, 2011.11.12.
19. ◎Kawashima N, Takimoto K, Koizumi K, Yamamoto M, Zhou M, Suzuki N, Nakashima M, H Suda, Down-regulation of Inflammatory Mediator Synthesis from macrophages by MMP3, 2011 Autumn Scientific Meeting of KACD（136th）and 13th Joint-Scientific Meeting of KACD-JSCD 2011, poster, Seoul, 2011.11.12.
20. Suzuki N, Kawashima N, Suda H, Mechanisms of Bone Destruction and its Regulation in the Periapical Lesions, 2011 Autumn Scientific Meeting of KACD（136th）and 13th Joint-Scientific Meeting of KACD-JSCD 2011, poster, Seoul, 2011.11.12.
21. Gombo B, Ebihara A, Kawashima N, Watanabe S, Anjo T, Saegusa H, Kokuzawa C, Suda H, Evaluation of fibroblast cell adhision to dentin modifications teated with Er：YAG and Nd：YAG laser irradiation, Japanese Society for Laser Dentistry, oral, Osaka, 2011.12.01.

11）学会発表（和文）

1. 竹田淳志, 須田英明, 大林尚人, 倉林亨
   歯科用コーンビームCTにおけるモーションアーチファクトの影響
   日本歯科放射線学会第212回関東地方会, 口頭, 東京, 2011.01.22
2. 辺見浩一, 川島伸之, 須田英明, 鈴木孝尚, 山下直也, 立花克郎, 中島美砂子
   ナノバブルを併用した新しい根管洗浄法に関する基礎的研究
   超音波分子診断治療研究会, 口頭, 福岡, 2011.03.05
3. 瀧本晃陽, 川島伸之, 小泉悠, 山本弥生子, 中島美砂子, 須田英明
   LPS刺激下におけるマクロファージの炎症性メディエーター産生に対するMMP-3の影響　日本炎症・再生医学会, ポスター, 京都, 2011.06.02
4. 坂上斉, 吉岡俊彦, 小松恵, 石村瞳, 海老原新, 須田英明
   mineral trioxide aggregateおよび接着性材料を用いた根管充填におけるコロナルリーケージの評価
   日本歯科保存学会, 口頭, 舞浜, 2011.06.09
5. 宮良香菜, 八幡祥生, 海老原新, 須田英明, 塙隆夫
   新型ニッケルチタンファイルPROFILE® VORTEX™の曲げ特性および相変態挙動
   日本歯科保存学会, ポスター, 舞浜, 2011.06.09
6. 和達礼子, 須田英明
   瘻孔を有する根尖性歯周炎の患歯の同定におけるComputed Tomographyの有用性
   日本歯科保存学会, ポスター, 舞浜, 2011.06.09
7. 吉岡俊彦, 小松恵, 坂上斉, 石村瞳, 海老原新, 島田康史, 田上順次, 須田英明
   OCTの歯根破折線の検出精度について
   日本歯科保存学会, 口頭, 舞浜, 2011.06.09
8. 辺見浩一, 川島伸之, 須田英明, 鈴木孝尚, 山下直也, 立花克郎, 中島美砂子
   低濃度次亜塩素酸溶液にナノバブルを併用した新しい根管洗浄法の開発
   日本歯科保存学会, ポスター, 舞浜, 2011.06.10
9. 朴　錦丹, 石村　瞳, 小林　千尋, 須田　英明, 吉岡隆知
   新しく開発された根管模型における電気的根管長測定器の測定精度について
   日本歯科保存学会, ポスター, 舞浜, 2011.06.10
10. 須田英明, 大谷啓一, 佐藤田鶴子, 伊藤公一, 森田章介, 中川寛一
    歯痛に対する非ステロイド性消炎鎮痛薬（NSAIDs）の鎮痛効果-標準的評価方法の検討
    日本歯科薬物療法学会, 口頭, 幕張, 2011.06.25
11. 吉岡俊彦, 石村瞳, 海老原新, 須田英明
    歯根破折歯の非破壊的観察-マイクロフォーカスCTとSS-OCT
    日本歯内療法学会, ポスター, 長崎, 2011.07.30
12. 小松　恵, 吉岡俊彦, 石村瞳, 海老原新, 須田英明
    歯科用CBCTを用いた根尖病変の三次元的評価
    日本歯内療法学会, ポスター, 長崎, 2011.07.30
13. 池田英治, 須田英明
    交流イオン導入法を用いたヒトエナメル質の物質透過性促進
    日本電電気泳動学会総会, 口頭, 横浜, 2011.10.12

14. 川島伸之, 周夢宇, 須田英明, 工藤 明, 勝部憲一
ペリオスチンによる骨芽細胞分化制御
日本歯科保存学会, 口頭, 大阪, 2011.10.20
15. 山本弥生子, 川島伸之, 須田英明
単層培養法と三次元培養法における歯髄細胞の象牙芽細胞分化について
日本歯科保存学会, ポスター, 大阪, 2011.10.20
16. 池田英治, 李穎, 須田英明
象牙細管内の動水力学的水圧に対する象牙芽細胞膜の歪みについて
日本歯科保存学会, 口頭, 大阪, 2011.10.21
17. 竹田淳志, 池田英治, 小林千尋, 須田英明
根管長測定可能な学生実習用顎模型の改良
日本歯科保存学会, ポスター, 大阪, 2011.10.21
18. 石村　瞳, 小松　恵, 吉岡　俊彦, 八幡　祥生, 吉岡隆知, 須田　英明
新型エアスケーラーを用いた根管内水酸化カルシウム材の除去について
日本歯科保存学会, ポスター, 大阪, 2011.10.21
19. 小松　恵, 吉岡俊彦, 坂上斉, 石村瞳, 海老原新, 須田英明
歯科用CBCTを用いた根尖病変の三次元的評価
日本歯科保存学会, 口頭, 大阪, 2011.10.21
20. 鶴田潤, 須永昌代, 川島伸之, 木下淳博, 須田英明, 森尾郁子
ビデオ会議システムを応用した国際大学院セミナー（TMDU-CU）について
口腔病学会, 口頭, 東京, 2011.12.10
21. 吉岡俊彦, 白金由紀子, 石村瞳, 海老原新, 須田英明
OCTを用いた根管の観察
口腔病学会, 口頭, 東京, 2011.12.10

12）受賞

1. 西原良治（指導　鈴木規元、石村瞳）.スーパーエンドα、βを用いた根管充填の速度および充填率に関する研究.D4研究体験実習学生発表会　歯学科長賞,2010年9月25日.

13）外部資金の獲得状況

1. 科学研究費補助金、基盤研究（B）
研究題目：Gap-junctionを介した象牙芽細胞複合体の電気的・化学的細胞間連絡の解析
代表：池田英治　分担：須田英明
期間：平成20年-平成24年
研究費総額：1220万円

2. 科学研究費補助金、基盤研究（B）
研究題目：歯髄細胞の分化におけるシグナルネットワークの新しいパラダイムの構築と臨床への展望
代表：川島伸之
期間：平成22年-平成25年
研究費総額：1475万円

3. 科学研究費補助金、若手研究（B）
研究題目：エナメル芽細胞におけるShhおよびBmpシグナルのクロストークと歯の再生への展望
代表：高橋里美
期間：平成21年-平成23年
研究費総額：374万円

4. 科学研究費補助金、若手研究（B）
研究題目：エンドドンティックマイクロサージェリーにおけるレーザー応用の有用性の検討
代表：三枝英敏
期間：平成21年-平成23年
研究費総額：300万円

5. 科学研究費補助金、挑戦的萌芽
研究題目：歯髄細胞および骨芽細胞の三次元培養におけるシグナルネットワークの解析と臨床的展開
代表：川島伸之
期間：平成22年-平成24年
研究費総額：260万円

6. GCOE拠点内研究費、
研究題目：
代表：須田英明・宗田大　分担：川島伸之
期間：平成23年
研究費総額：136万円

7. 科学研究費補助金、萌芽研究
研究題目：多光子励起顕微鏡法と膜電位感知タンパク解析法を用いた歯髄リンパ網の研究
代表：池田英治
期間：平成22年-平成23年
研究費総額：150万円

8. 科学研究費補助金、若手研究（B）
研究題目：合金組成および熱処理がニッケルチタンファイルに与える影響
代表：八幡祥生
期間：平成22年-平成23年
研究費総額：300万円

9. 科学研究費補助金、若手研究（B）
研究題目：破折を起こしにくい次代の歯内療法へのレー

ザー応用の有用性の検討
代表：渡辺聡
期間：平成22年-平成24年
研究費総額：300万円

10. 科学研究費補助金、若手研究（B）
研究題目：歯科用CTを用いた歯内療法の画像診断学の確立
代表：中野生和子
期間：平成22年-平成23年
研究費総額：240万円

11. 科学研究費補助金、若手研究（B）
研究題目：接着性根管充填材応用による垂直性歯根破折の挙動およびその予防
代表：花田隆周
期間：平成22年-平成24年
研究費総額：300万円

12. 長寿医療研究委託費、21指-8
研究題目：近赤外光・レーザー等を用いた新たな歯科疾患診断・治療用機器の開発に関する研究
代表：角保徳　分担：須田英明
期間：平成21年-平成23年
研究費総額：500万円

13. 長寿医療研究委託費、21指-7
研究題目：歯髄幹細胞を用いた象牙質・歯髄再生医療によるう蝕・歯髄疾患等のための治療技術の開発
代表：中島美砂子　分担：川島伸之
期間：平成21年-平成24年
研究費総額：150万円

14. 先端医療開発特区補助金
研究題目：歯髄幹細胞を用いた象牙質・歯髄再生医療によるう蝕・歯髄疾患等のための治療技術の開発
代表：中島美砂子　分担：川島伸之
期間：平成21-25年
研究費総額：2982万円

15. 科学研究費補助金、若手研究（B）
研究題目：ナノバブルを応用した新しい根管洗浄システムの開発とその臨床応用
代表：辺見浩一
期間：平成23-24
研究費総額：220万円

16. 科学研究費補助金、若手研究（B）
研究題目：サーマルサイクル後の水硬性仮封材の強度、辺縁漏洩への消毒液の影響
代表：東　春生
期間：平成23-24
研究費総額：280万円

17. 厚生労働科学研究費補助金　地域医療基盤開発推進研究事業
研究題目：比較・分析による歯科関連職種における国家試験の在り方
代表：須田英明
期間：平成23
研究費総額：200万円

18. 寄付金（ネオ製薬株式会社）
期間：平成23
研究費総額：100万円

14）特別講演、招待講演、シンポジウム

1. Kawashima N, Suzuki N, SudaH, Mechanisms of Bone Destruction in the Periapical Lesions and Its Regulation, K, 16th Scientific Meeting of APEC 14th Annual Congress of the IAE, oral, Iran, 2011.04.20-22.
2. Suda H, Diagnosis and management of vertical root fracture, 1 6th Scientific Meeting of APEC 1 4th Annual Congress of the IAE, oral, Iran, 2011.04.20-22.
3. Suzuki N, Kawashima N, Suda H, Mechanisms of Bone Destruction and its Regulation in the Periapical Lesions, 2011 Autumn Scientific Meeting of KACD（136th）and 13th Joint-Scientific Meeting of KACD-JSCD 2011, poster, Seoul, 2011.11.12.
4. Suda H, 香港大学歯学部 香港大学歯学部試験外部評価, 香港大学歯学部, 香港, 中国2011.06.21-24.
5. Suda H, Visual Information for Endodontic Treatmen, 中華牙医学會学術大会, 中山医科大学大慶キャンパス, 台中, 台湾, 2011.08.26-28.

15）教室、分野や講座の准教授、講師、助教、特別研究員、ポスドク、指導を受けた大学院生の名前

准教授　小林　千尋
　　砂川　光宏（感染対策歯科治療部 兼任）
講　師　竹田　淳志
　　池田　英治
助　教　海老原　新
　　川島　伸之
　　松本　宏之（感染対策歯科治療部 兼任）

和達　礼子
鈴木　規元
石村　　瞳

ポスドク（医員）
八幡祥生（H23.12月まで）
渡辺　　聡
中野　生和子（3月まで）
東　　春生
山内　隆守
辺見　浩一
新井　淳子（H23.4月から）

大学院生　Adrno Quevedo Carlos Gabriel
（H23.3月まで）
○許婧（H23.10月まで）
河村　　隼
小泉　　悠
石澤　千鶴子
坂上　　斉
○Bolortuya Gombo
吉岡　俊彦
○Uraiwan Chokechanachaisakul
瀧本　晃陽
○周　　夢宇
○李　　顥
小松　　恵
宮良　香菜
山本　弥生子
朴　　錦丹（H23.4月から）
ジャムレー（H23.4月から）
Salima Arkin（H23.4月から）
○顧潔（H23.4月から）

○はAISS

RESEARCH REPORTS
Biological

H.G. Wang[1], N. Kawashima[2,3]*, T. Iwata[4], J. Xu[2], S. Takahashi[2], T. Sugiyama[5], and H. Suda[2,3]

[1]Department of Operative Dentistry and Endodontics, School of Stomatology, Fourth Military Medical University, China; [2]Pulp Biology and Endodontics, Graduate School; [3]GCOE Program, International Research Center for Molecular Science in Tooth and Bone Diseases, Tokyo Medical & Dental University, 1–5-45, Bunkyo-ku, Tokyo 113–8549, Japan; [4]Institute of Advanced Biomedical Engineering and Science, Tokyo Women's Medical University, Japan; and [5]Department of Biochemistry, School of Medicine, Akita University, Japan; *corresponding author, kawashima.n.endo@tmd.ac.jp

J Dent Res 90(4):529-534, 2011

MEPE Activated by Furin Promotes Pulpal Cell Adhesion

ABSTRACT

Matrix extracellular phosphoglycoprotein (MEPE) is predominantly expressed in osteoblasts, osteocytes, and odontoblasts and plays key biological roles in bone and dentin metabolism. Post-translational modifications are essential for its activation. This study tested the hypothesis that MEPE is activated through proteolytic processing by furin in dental pulp. MEPE was present in three sizes, 1 full-length and 2 cleaved fragments; the cleavage site was 146R↓147. The proprotein convertase family, particularly furin, was a candidate enzyme. Introducing a substitution at the cleavage site inhibited hydrolysis, but there was no cleavage of MEPE expressed in furin-deficient LoVo cells. Therefore, furin is a strong candidate for the proteolytic cleavage of MEPE. The C-terminal cleavage product promoted cell adhesion *via* its RGD motif. These results indicate that proteolytic processing by furin may activate MEPE during its secretion from odontoblasts and may play important roles in dentinogenesis and pulpal homeostasis. *Abbreviations*: MEPE, matrix extracellular phosphoglycoprotein; PTM, post-translational modifications; OLC, odontoblast-lineage cells.

KEY WORDS: MEPE, post-translational modifications, proteolytic cleavage, furin, dental pulp cells.

DOI: 10.1177/0022034510391057

Received February 23, 2010; Last revision June 4, 2010; Accepted June 7, 2010

A supplemental appendix to this article is published electronically only at http://jdr.sagepub.com/supplemental.

© International & American Associations for Dental Research

INTRODUCTION

Matrix extracellular phosphoglycoprotein (MEPE) was first isolated by expression screening of a tumor cDNA library to identify genes up-regulated in the tumors of patients with oncogenic hypophosphatemic osteomalacia (Rowe *et al*., 2000). MEPE seems to be crucially involved in mineralization, but its exact role as a regulator of mineralization and the mechanisms underlying this function remain controversial.

Many studies have revealed the effects of MEPE on mineralization. MEPE expression was markedly increased in fully differentiated osteoblasts (Argiro *et al*., 2001) and promoted regeneration and skeletogenesis of long bones (Lu *et al*., 2004). Furthermore, a synthetic peptide of residues 242–264 of human MEPE called Dentonin or AC-100, which includes the RGD and SGDG motifs, stimulates new bone formation (Hayashibara *et al*., 2004; Nagel *et al*., 2004). This peptide also enhances dental pulp stem cell proliferation *in vitro* (Liu *et al*., 2004) and initiates pulp healing in response to injury (Six *et al*., 2007). In contrast, some have reported that MEPE inhibits mineralization. For example, MEPE was highly expressed in tumor-induced osteomalacia (Rowe *et al*., 2000; Quarles, 2003; Bresler *et al*., 2004) and in Hyp mice, a murine model for X-linked hypophosphatemia (S Liu *et al*., 2005). MEPE expression was observed only in immature odontoblasts, and it was down-regulated during odontoblastic differentiation (MacDougall *et al*., 2002; H Liu *et al*., 2005). A mouse model with targeted deletion of *MEPE* showed increased bone formation and bone mass (Gowen *et al*., 2003).

MEPE shares molecular similarities with several dentin-bone extracellular matrix RGD-containing phosphoglycoproteins, including dentin sialophosphoprotein, osteopontin, dentin matrix protein 1 (DMP1), and bone sialoprotein (Fisher and Fedarko, 2003). These non-collagenous proteins are believed to play key biological roles in the formation and mineralization of bone and/or dentin. Their functions are largely dependent on the nature and extent of post-translational modifications (PTM), including phosphorylation, glycosylation, and proteolytic processing. Proteolytic processing is particularly important in inducing the active forms of various proteins. DMP1 was proteolytically processed by PHEX enzyme or bone morphogenetic protein-1/Tolloid-like proteinases (Qin *et al*., 2003, 2004; Steiglitz *et al*., 2004).

The aims of this study were to evaluate the expression pattern of MEPE in dental pulp, the mechanisms involved in the PTM of MEPE in dental pulp cells and tissues, and the function of proteolytic fragments of MEPE in dentinogenesis.

Downloaded from jdr.sagepub.com at TOKYO IKASHIKA UNIVERSITY on January 13, 2012 For personal use only. No other uses without permission.

© 2011 International & American Associations for Dental Research

MATERIALS & METHODS

Construction of Expression Vectors and Mutants, Real-time PCR

The open reading frame of the mouse MEPE cDNA, with or without signal peptides, was subcloned into the eukaryotic expression vector pEF-Dest51 (pEF-mMEPE) or pSecTag2A with a V5His tag (pSecTag2A-V5His-MEPE), respectively. The cDNAs for the mouse MEPE mature peptide, C-terminal fragment (residues 18–146) and N-terminal fragment (residues 147–433), were subcloned into the prokaryotic expression vector pDEST17. MEPE R145G and R146A mutants in the pEF-mMEPE construct and mutant G176A (RGD→RAD) in the pDEST17-mMEPE construct were created by site-directed mutagenesis. MEPE mRNA expression was determined by real-time PCR with specific primers in several cell lines and in primary cells from rat dental pulp, periodontal ligament, and gingiva (Appendix Tables 1 and 2).

Transfection, Transient Expression, and Western Blotting Analysis

Odontoblast-lineage cells (OLC) (Arany *et al*., 2006) and several other types of cells were transfected with the MEPE expression vectors, and the conditioned medium was harvested for SDS-PAGE. Western blotting was performed with the primary antibodies, including anti-V5 (1:5000), anti-mMEPE (LF-156 & LF-155, 1:1000; kind gifts from Dr. L.W. Fisher), and anti-β-actin (1:1000).

Protein Production, Amino Acid Sequencing, Production of Antibody, and Cell Adhesion Assay

The eukaryotic MEPE protein was produced on a large scale by HEK293F cells. Sequencing of the C-terminal fragment was performed by the Edman degradation method. The full-length, C- and N-terminal fragments, and mutant G176A MEPE proteins were expressed in *Escherichia coli*. The full-length protein was used to produce the polyclonal antibody. All the proteins were tested by cell adhesion assay, while collagen I was used as a positive control and BSA as a negative control.

Immunohistochemical Staining

Dental pulp tissues of upper incisors from male Wistar rats (6-wks old) were fixed with 4% paraformaldehyde for 12 hrs at 4ºC. Immunohistochemical staining with anti-mMEPE antibody (LF-155, 1:250) was performed on frozen sections. Immunoreactivity was detected by the ABC method, and the color reaction was developed with DAB. The nucleus was counterstained by methyl green. For immunofluorescence with anti-mMEPE antibody (LF-156, 1:250), Alexa Fluor™ 594 conjugated goat anti-rabbit IgG (1:1000, Invitrogen, Carlsbad, CA, USA) was applied as a secondary antibody, and 4′,6′-diamidino-2-phenylindole (DAPI, 300 nM, Invitrogen) was used for nuclear staining. Based on the literature and our data, LF-156 recognizes full-length, N- and C-terminal fragments of MEPE protein, while LF-155 reacts only against the C-terminal fragment. Adult rat tibia was used as positive control and liver as negative control. All animal experiments were performed in accordance with the Animal Guidelines of Tokyo Medical and Dental University.

Statistical Analysis

All data are represented as means ± standard error. Statistical significance was determined by an unpaired Student's *t* test, and a p value of < 0.05 was considered statistically significant. Additional information on MATERIALS & METHODS can be found in the Appendix.

RESULTS

Cleavage of MEPE in Dental Pulp Tissue

RT-PCR revealed MEPE expression in mouse and rat dental pulp tissues. MEPE was ubiquitously expressed in hard-tissue-forming cells, including osteoblastic cells (Kusa-A1, Kusa-O, and MC3T3E1), chondroblastic cells (ATDC5, Kum5), odontoblast-lineage cells (OLC) and MDPC-23, and ameloblast-lineage cells (ALC) (Fig. 1A). In addition, high and low levels of MEPE expression were observed in rat dental pulp cells and in periodontal ligament cells, respectively. However, MEPE expression was below the detectable level in gingival cells (Appendix Fig. 1). Three forms of MEPE protein, 50, 38, and 25 kDa, were identified in the rat pulp tissue (Fig. 1B). The mature MEPE peptide is a 417-amino-acid secreted peptide with a calculated molecular mass of 44,247 Da. As a result of glycosylation, MEPE in rat dental pulp tissue migrated as an approximately 50-kDa protein in SDS-PAGE under reducing conditions. The 38- and 25-kDa proteins expressed in dental pulp tissue were truncated forms of MEPE, suggesting that MEPE is processed in dental pulp tissue. The similar staining patterns of LF-156 (anti all kinds of fragments of MEPE) and LF-155 (anti C-terminal fragment) suggested that the localization of full-length MEPE and its fragments should be similar (Fig. 1C).

Cleavage of MEPE in Exogenous MEPE-expressing Cells

After transfection of pEF-mMEPE, exogenous expression of the MEPE protein was observed in the cell lysate and the supernatant. Western blotting revealed 3 bands at 58, 45, and 22 kDa in the supernatant and a single band at 55 kDa in the cell lysate. The 58-kDa band, containing a 5-kDa V5-His tag, was full-length MEPE, while the 45-kDa band, containing a 5-kDa V5-His tag, was the C-terminal cleavage product of MEPE. The 28-kDa band, also containing a 5-kDa V5-His tag, was identified as the N-terminal cleavage product of MEPE. This cleavage was widely observed in protein-expression cell lines, and in odontoblastic and osteoblastic cell lines (Figs. 2A, 2B). The size of the full-length MEPE in the supernatant was slightly larger than that in the cell lysate, which may be caused by cell-specific PTM, such as phosphorylation or glycosylation, during secretion. The size of the full-length natural MEPE in the pulp tissues was about 10 kDa less than that of MEPE artificially synthesized with pEF-mMEPE. Most of this size discrepancy was due

Downloaded from jdr.sagepub.com at TOKYO IKASHIKA UNIVERSITY on January 13, 2012 For personal use only. No other uses without permission.

© 2011 International & American Associations for Dental Research

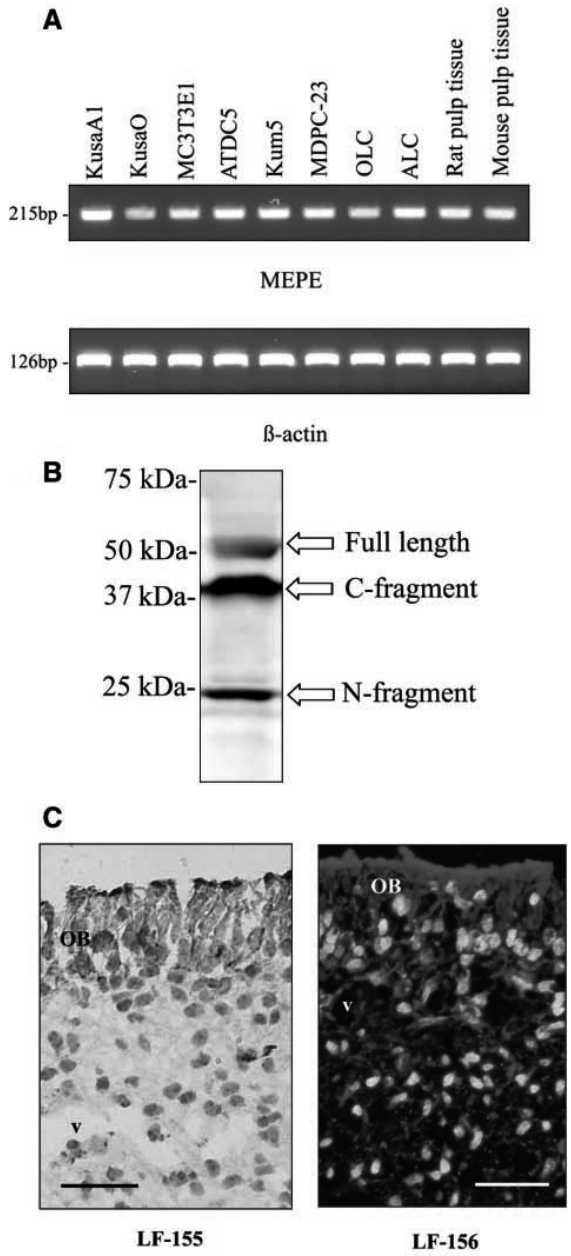

Figure 1. MEPE cleavage in dental pulp tissue. **(A)** MEPE is ubiquitously expressed in osteoblastic (Kusa-A1, Kusa-O, and MC3T3E1), chondroblastic (ATDC5, Kum5), odontoblastic (OLC, MDPC-23), and ameloblastic (ALC) cell lines and in mouse and rat dental pulp tissues. **(B)** Three forms of MEPE protein, 50, 38, and 25 kDa, were identified in rat pulp tissue by Western blotting analysis with anti-MEPE antibody. The 50-kDa protein was the full-length mature peptide, while the lower-molecular-weight proteins were truncated forms of MEPE. **(C)** Detection of MEPE in mature pulp tissue by two types of anti-MEPE antibody, LF-155 and LF-156. The staining pattern with LF-156, which recognizes all fragments of the MEPE protein, was similar to that of LF-155, which recognizes only the C-terminal fragment. The nucleus was counterstained with methyl green or 4′,6′-diamidino-2-phenylindole.

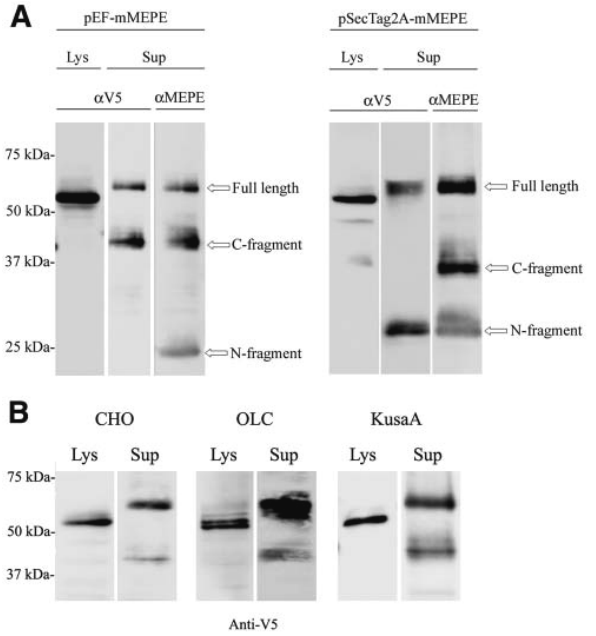

Figure 2. MEPE cleavage in exogenous MEPE-expressing cells. **(A)** Cleavage of MEPE was detected after transient expression in HEK293 cells with either pEF-mMEPE (contains the C-terminal V5-His tag) or pSecTag2A-V5His-MEPE (contains the N-terminal V5-His tag). For pEF-mMEPE, 3 bands at 58, 45, and 22 kDa appeared in the supernatant, and a single band at 55 kDa was observed in the cell lysate. The 58-kDa band, containing a 5-kDa V5-His tag, was full-length MEPE. The 45-kDa band, containing a 5-kDa V5-His tag, was the C-terminal cleavage product of MEPE. For pSecTag2A-V5His-MEPE, the cleaved products were similar, and the 28-kDa band containing the 5-kDa V5-His tag was identified as the N-terminal cleavage product of MEPE. The size of the full-length MEPE in the supernatant was slightly different from that in the lysate, which may be due to post-translational modifications such as phosphorylation or glycosylation, which occurred before secretion of MEPE. **(B)** The cleavage was widely observed in various cell lines. The full-length and C-terminal fragments of MEPE were observed in pEF-mMEPE-transiently transfected CHO cells, and in odontoblastic (OLC) and osteoblastic (Kusa-A1) cell lines. The bar represents 20 μm. OB = odontoblast, v = blood vessel, Lys = lysate, Sup = supernatant, αV5 = anti-V5, αMEPE = anti-MEPE.

to the addition of the 5-kDa V5-His tag to the expression vector, but some PTM may also be responsible for the difference in size of the artificially synthesized MEPE.

Proprotein Convertase is Involved in the Cleavage of MEPE

Amino acid sequencing of the C-terminal fragment (Appendix Fig. 2) revealed the sequence to be ^{147}STHYL, indicating that MEPE was cleaved at the ^{146}R↓^{147}S site. Several proteases, including Arg-C protease, clostripain, trypsin, cathepsin B, and proprotein convertases, may be responsible for the cleavage of MEPE. Arg-C protease, clostripain, and trypsin are serine proteases, while cathepsin B is a cysteine protease. To test these proteases, we added a protease inhibitor cocktail, which inhibits

Downloaded from jdr.sagepub.com at TOKYO IKASHIKA UNIVERSITY on January 13, 2012 For personal use only. No other uses without permission.

© 2011 International & American Associations for Dental Research

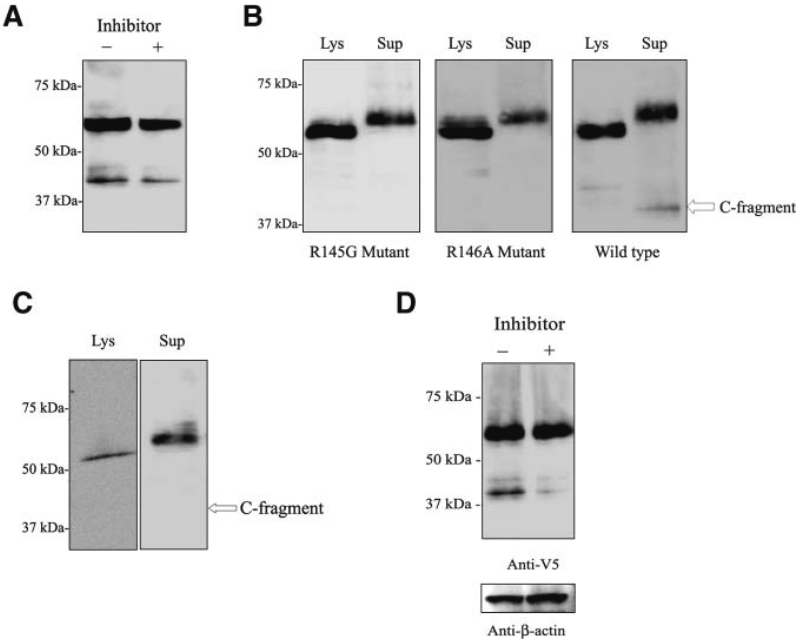

Figure 3. Furin is responsible for the cleavage of MEPE. **(A)** A protease inhibitor cocktail, which inhibits serine, cysteine, and metalloproteases, was added to the culture medium of Cos-7 cells. Protein production was inhibited, but cleavage still occurred, which excluded the 4 candidate proteases, Arg-C proteinase, clostripain, trypsin, and cathepsin B. **(B)** The R145G and R146A mutants were resistant to cleavage. Compared with the wild–type form, the 40-kDa C-terminal fragment was not detected after transfection. **(C)** In LoVo cells (furin-deficit human colon cancer cell line), there was no cleavage of MEPE after transfection and transient expression. **(D)** Cleavage of MEPE was effectively blocked by the furin-specific inhibitor in Cos-7 cells. Lys = lysate, Sup = supernatant.

serine, cysteine, and metalloproteases, to the culture medium for Cos-7 cells. Cleavage was not inhibited, which excluded these 4 proteases (Fig. 3A).

Only the full-length protein was detected in the conditioned medium after transient expression of either the R145G mutant or the R146A mutant, indicating that they were resistant to cleavage (Fig. 3B). ^{145}R and ^{146}R were clearly important for protease activity, which is consistent with the recognition site of proprotein convertases. The rule for recognition by proprotein convertases is (Arg/Lys)-(X)n-Arg (n = 0, 2, 4, or 6). For MEPE, the cleavage occurred at PRARR ↓STHYL for rat MEPE, and RQTRR ↓STHYL for mouse MEPE (n = 0). These results are consistent with the conclusion that proprotein convertases are involved in MEPE cleavage.

The mammalian proprotein convertase family is composed of 7 members, and, based on previous reports (Akamatsu *et al.*, 1999, 2000), furin and PACE4 are candidates. In LoVo cells, a human colon carcinoma cell line that lacks enzymatically active furin due to the presence of mutations in both alleles of the furin gene, MEPE was not cleaved after transfection and transient expression (Fig. 3C). Furthermore, cleavage of MEPE was effectively blocked by a furin-specific inhibitor in Cos-7 cells (Fig. 3D). RT-PCR showed that furin was expressed in all of the cell types used in this experiment, except LoVo cells. In contrast, PACE4 expression was detected in all of these cell lines, including LoVo cells (Appendix Fig. 3). Therefore, the expression of furin is consistent with the expression and cleavage of MEPE. These results indicate that furin is responsible for MEPE cleavage.

MEPE-induced Cell Adhesion *via* the RGD Sequence

The full-length eukaryotic protein (F_{HEK}) dose-dependently promoted the attachment of OLCs. Two μg/mL of protein showed activity similar to that of collagen I (Appendix Fig. 4A). In the antibody neutralization test, the antibody to the full-length prokaryotic protein ($F_{E.coli}$) dose-dependently neutralized cell adhesion on plates coated with 100 μL of F_{HEK} at 2 μg/mL. Two μg/mL of this antibody neutralized 100% of cell adhesion. However, the LF-156 antibody raised against a partial sequence of MEPE (CSREKVKGGVEHAGRAG & CSKHTKHTRQTRRSTHGG) showed no effect on the neutralization of protein activity (Fig. 4A). The antibody against full-length MEPE did not abrogate cell binding to collagen I (Appendix Fig. 4B). The C-terminal fragment of prokaryotic protein containing the RGD motif ($C_{E.coli}$) promoted cell adhesion, while the N-terminal fragment of prokaryotic protein ($N_{E.coli}$) did not (Fig. 4B). The G176A mutant (RGD→RAD) of prokaryotic protein ($RAD_{E.coli}$) did not promote cell adhesion, even at 16 μg/mL (Fig. 4C). These results indicate that MEPE promotes cell adhesion *via* the RGD sequence.

DISCUSSION

We revealed that MEPE was synthesized and secreted by odontoblasts, suggesting that MEPE plays roles in dentinogenesis and in the physiology of pulp tissue. In oral tissue, MEPE was highly expressed in dental pulp cells, but its expression was low in periodontal ligament cells and scant in gingival tissues. These results suggest that MEPE tends to be expressed in hard tissues and hard-tissue-related cells, and this indicates MEPE may be involved in the process of mineralization, as either a positive or a negative regulator.

Three forms of MEPE are found in pulp cells and tissues, with significantly different molecular masses: the full-length protein, and N-terminal and C-terminal cleavage products. The small and large MEPE components present in pulp tissues corresponded to the N-terminal and C-terminal fragments, respectively, and they were generated by cleavage between 146R and 147S. We found that the enzyme responsible for the cleavage of

Downloaded from jdr.sagepub.com at TOKYO IKASHIKA UNIVERSITY on January 13, 2012 For personal use only. No other uses without permission.

© 2011 International & American Associations for Dental Research

MEPE at this site is furin, which is a ubiquitously expressed proprotein convertase. To date, 7 members of the proprotein convertase family have been identified in mammalian species, namely, furin, PC2, PC1/PC3, PC4, PACE4, PC5/PC6, and LPC/PC7/PC8/SPC7 (Nakayama, 1997). They have been shown to be responsible for the conversion of precursors of peptide hormones, neuropeptides, and many other proteins into their biologically active forms (Nakayama, 1997). For example, furin can initiate BMP activity by direct endoproteolytic cleavage. Cleavage at the upstream site regulates the activity and signaling range of mature BMP-4 (Nakayama, 1997; Cui *et al*., 1998; Degnin *et al*., 2004). In rats, furin is widely expressed at all stages of dentinogenesis, from embryonic day 20.5 to post-natal day 14 (Akamatsu *et al*., 2000). Analysis of our data suggests that furin processes MEPE and that the active C-terminal fragments can be produced *in vitro*. Therefore, furin is a strong candidate enzyme for processing of active fragments of MEPE; however, this study does not exclude the possibility of other MEPE-processing enzymes.

The effects of the matrix are primarily mediated by integrins, a family of cell-surface receptors that attach cells to the matrix and mediate mechanical and chemical signals from the matrix. These signals regulate the activities of cytoplasmic kinases, growth factor receptors, and ion channels, and control the organization of the intracellular actin cytoskeleton (Giancotti and Ruoslahti, 1999). Binding between the RGD and integrins may trigger downstream signaling pathways through mediators such as FAK and ERK to regulate cell adhesion, migration, proliferation, and differentiation (Giancotti and Ruoslahti, 1999; Plow *et al*., 2000; Altroff *et al*., 2001). The cell adhesion test showed that the MEPE protein could induce cell adhesion *via* the RGD motif, which is located in the C-terminal cleavage product. MEPE may form part of the scaffold bridge between osteoblasts or odontoblasts and the extracellular matrix to regulate crystal growth. Therefore, in dental tissue, the C-terminal cleavage product is the active form of MEPE, which can promote cell adhesion through the RGD sequence.

In conclusion, the results of this study indicate that MEPE is cleaved by furin into 2 fragments during its secretion by odontoblasts. The C-terminal cleavage product, *via* the RGD motif, is an active fragment that promotes cell adhesion. Proteolytic processing is required for the activation of MEPE in dental pulp, and may play important roles in dentinogenesis.

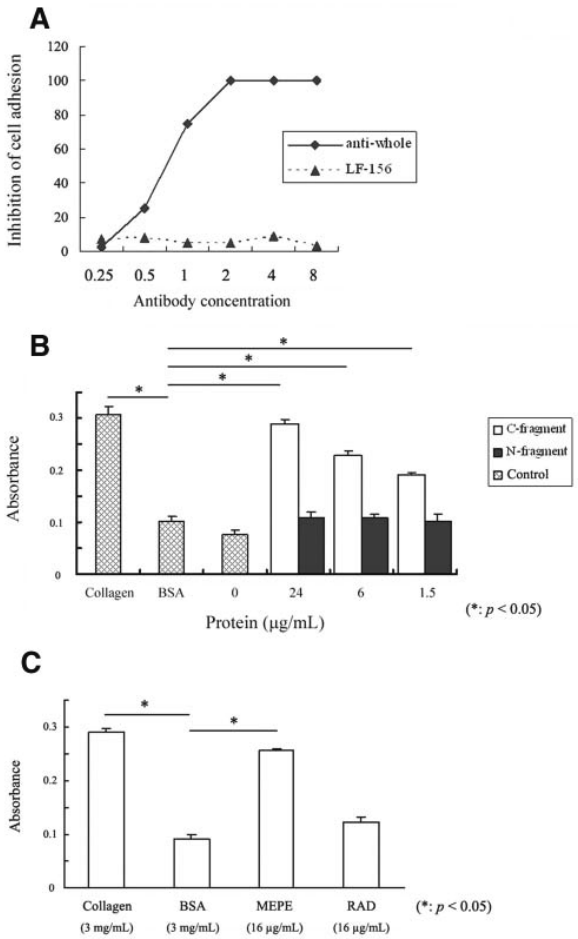

Figure 4. MEPE induces cell adhesion *via* the RGD sequence. **(A)** In the antibody neutralization test, the antibody against the full-length prokaryotic protein ($F_{E.coli}$) dose-dependently neutralized cell adhesion on plates coated with 100 μL of F_{HEK} at 2 μg/mL, and 2 μg/mL of the antibody could neutralize 100% of cell adhesion. However, the LF-156 antibody, which was raised against the partial sequence of MEPE (CSREKVKGGVEHAGRAG & CSKHTKHTRQTRRSTHGG), showed no effect on neutralization of protein activity. **(B)** The C-terminal fragment protein containing the RGD motif produced by *E. coli* ($C_{E.coli}$) promoted cell adhesion, while the N-terminal fragment protein produced by *E. coli* ($N_{E.coli}$) did not. **(C)** The G176A mutant (RGD→RAD) protein produced by *E. coli* ($RAD_{E.coli}$) did not promote cell adhesion at 16 μg/mL. *$p < 0.05$ compared with the control group (BSA).

ACKNOWLEDGMENTS

We greatly appreciate the contributions of Dr. Larry W. Fisher (NIDCR, Bethesda, MD, USA), Professor Wenli Yan (Fourth Military Medical University, China), and Professor James P. Simmer (University of Michigan, Ann Arbor, USA). The work was supported by a Japan-China Sasakawa Medical Fellowship, by Grants-in-Aids from the JSPS (Nos. 22390357 and 22659343 to N.K.; and No. 21791838 to S.T.), and by grants from the NSFC (No. 30901674 to H.W.).

REFERENCES

Akamatsu T, Matsuda Y, Tsumura K, Tada J, Parvin MN, Kanamori N, *et al*. (1999). Subtilisin-like proprotein convertase PACE4 (SPC4) is a candidate processing enzyme of bone morphogenetic proteins during tooth formation. *Dev Dyn* 216:481-488.

Akamatsu T, Matsuda Y, Tsumura K, Tada J, Parvin MN, Wei W, *et al*. (2000). Highly regulated expression of subtilisin-like proprotein convertase PACE4 (SPC4) during dentinogenesis. *Biochem Biophys Res Commun* 272:410-415.

Altroff H, van der Walle CF, Asselin J, Fairless R, Campbell ID, Mardon HJ (2001). The eighth FIII domain of human fibronectin promotes integrin alpha5beta1 binding via stabilization of the ninth FIII domain. *J Biol Chem* 276:38885-38892.

Downloaded from jdr.sagepub.com at TOKYO IKASHIKA UNIVERSITY on January 13, 2012 For personal use only. No other uses without permission.

© 2011 International & American Associations for Dental Research

Arany S, Nakata A, Kameda T, Koyota S, Ueno Y, Sugiyama T (2006). Phenotype properties of a novel spontaneously immortalized odontoblast-lineage cell line. *Biochem Biophys Res Commun* 342:718-724.

Argiro L, Desbarats M, Glorieux FH, Ecarot B (2001). MEPE, the gene encoding a tumor-secreted protein in oncogenic hypophosphatemic osteomalacia, is expressed in bone. *Genomics* 74:342-351.

Bresler D, Bruder J, Mohnike K, Fraser WD, Rowe PS (2004). Serum MEPE-ASARM-peptides are elevated in X-linked rickets (HYP): implications for phosphaturia and rickets. *J Endocrinol* 183:R1-R9.

Cui Y, Jean F, Thomas G, Christian JL (1998). BMP-4 is proteolytically activated by furin and/or PC6 during vertebrate embryonic development. *EMBO J* 17:4735-4743.

Degnin C, Jean F, Thomas G, Christian JL (2004). Cleavages within the prodomain direct intracellular trafficking and degradation of mature bone morphogenetic protein-4. *Mol Biol Cell* 15:5012-5020.

Fisher LW, Fedarko NS (2003). Six genes expressed in bones and teeth encode the current members of the SIBLING family of proteins. *Connect Tissue Res* 44(Suppl 1):33-40.

Giancotti FG, Ruoslahti E (1999). Integrin signaling. *Science* 285:1028-1032.

Gowen LC, Petersen DN, Mansolf AL, Qi H, Stock JL, Tkalcevic GT*, et al*. (2003). Targeted disruption of the osteoblast/osteocyte factor 45 gene (OF45) results in increased bone formation and bone mass. *J Biol Chem* 278:1998-2007.

Hayashibara T, Hiraga T, Yi B, Nomizu M, Kumagai Y, Nishimura R*, et al*. (2004). A synthetic peptide fragment of human MEPE stimulates new bone formation *in vitro* and *in vivo*. *J Bone Miner Res* 19:455-462.

Liu H, Li W, Gao C, Kumagai Y, Blacher RW, DenBesten PK (2004). Dentonin, a fragment of MEPE, enhanced dental pulp stem cell proliferation. *J Dent Res* 83:496-499.

Liu H, Li W, Shi S, Habelitz S, Gao C, DenBesten P (2005). MEPE is downregulated as dental pulp stem cells differentiate. *Arch Oral Biol* 50:923-928.

Liu S, Brown TA, Zhou J, Xiao ZS, Awad H, Guilak F*, et al*. (2005). Role of matrix extracellular phosphoglycoprotein in the pathogenesis of X-linked hypophosphatemia. *J Am Soc Nephrol* 16:1645-1653.

Lu C, Huang S, Miclau T, Helms JA, Colnot C (2004). MEPE is expressed during skeletal development and regeneration. *Histochem Cell Biol* 121:493-499.

MacDougall M, Simmons D, Gu TT, Dong J (2002). MEPE/OF45, a new dentin/bone matrix protein and candidate gene for dentin diseases mapping to chromosome 4q21. *Connect Tissue Res* 43:320-330.

Nagel DE, Khosla S, Sanyal A, Rosen DM, Kumagai Y, Riggs BL (2004). A fragment of the hypophosphatemic factor, MEPE, requires inducible cyclooxygenase-2 to exert potent anabolic effects on normal human marrow osteoblast precursors. *J Cell Biochem* 93:1107-1114.

Nakayama K (1997). Furin: a mammalian subtilisin/Kex2p-like endoprotease involved in processing of a wide variety of precursor proteins. *Biochem J* 327(Pt 3):625-635.

Plow EF, Haas TA, Zhang L, Loftus J, Smith JW (2000). Ligand binding to integrins. *J Biol Chem* 275:21785-21788.

Qin C, Brunn JC, Cook RG, Orkiszewski RS, Malone JP, Veis A*, et al*. (2003). Evidence for the proteolytic processing of dentin matrix protein 1. Identification and characterization of processed fragments and cleavage sites. *J Biol Chem* 278:34700-34708.

Qin C, Baba O, Butler WT (2004). Post-translational modifications of sibling proteins and their roles in osteogenesis and dentinogenesis. *Crit Rev Oral Biol Med* 15:126-136.

Quarles LD (2003). FGF23, PHEX, and MEPE regulation of phosphate homeostasis and skeletal mineralization. *Am J Physiol Endocrinol Metab* 285:E1-E9.

Rowe PS, de Zoysa PA, Dong R, Wang HR, White KE, Econs MJ*, et al*. (2000). MEPE, a new gene expressed in bone marrow and tumors causing osteomalacia. *Genomics* 67:54-68.

Six N, Septier D, Chaussain-Miller C, Blacher R, DenBesten P, Goldberg M (2007). Dentonin, a MEPE fragment, initiates pulp-healing response to injury. *J Dent Res* 86:780-785.

Steiglitz BM, Ayala M, Narayanan K, George A, Greenspan DS (2004). Bone morphogenetic protein-1/Tolloid-like proteinases process dentin matrix protein-1. *J Biol Chem* 279:980-986.

Downloaded from jdr.sagepub.com at TOKYO IKASHIKA UNIVERSITY on January 13, 2012 For personal use only. No other uses without permission.

© 2011 International & American Associations for Dental Research

歯周病学分野

和泉 雄一

医歯学総合研究科・生体支持組織学系専攻
歯周病学・教授

1）研究の課題名

新たな歯周組織再生法の開発と歯周病・全身疾患の関連性およびそのメカニズムに関する研究

Study on the development of novel therapy for periodontal tissue regeneration and the association between periodontal and systemic diseases and its mechanism.

歯周病によって破壊された歯周組織を再生することは歯周治療の最終ゴールである。細胞シートによる再生療法が注目されている。今回、ビーグル犬に作製した1壁性の骨欠損に対して3つの由来の異なる細胞シート（歯根膜細胞、骨膜細胞、骨髄細胞）とβ-TPC/コラーゲン複合体を移植し、再生能について比較検討した。その結果、歯根膜細胞由来の細胞シートが最も再生能が高く、加えて神経線維の再生が認められた。

循環器系疾患が関連する機序については、いまだ不明な点が多い。腹部大動脈瘤病変ではマトリックスメタロプロテイナーゼ（MMP）の上昇が認められ、腹部大動脈瘤患者の動脈瘤病変から、高率で歯周病原細菌が検出されている。そこで、歯周病原細菌感染が腹部大動脈瘤の進行に与える影響を検討することとした。マウスの腹部大動脈に塩化カルシウムを塗布することにより大動脈瘤を誘導した。マウスにPorphyromonas gingivalisを投与し、大動脈瘤誘導4週後に解析した。P. gingivalisを感染させた群では、未感染群と比較して動脈拡張が有意に亢進していた。免疫組織学的解析から、P. gingivalis感染させた群で動脈瘤組織でのT細胞、マクロファージ、MMP-2の増加が観察された。培養した脾細胞にP. gingivalisで刺激したところ、細胞増殖とMMP-2産生が促進した。結論として、P. gingivalis感染がMMPの発現上昇を誘導して腹部大動脈瘤形成を促進することが示された。

唾液中の抗菌ペプチド（LL-37/hCAP-18）レベルと歯周病の重症度との関連性を検討した。加えて、4つの歯周病原性細菌の存在有無および喫煙と関連するコチニンレベルが本抗菌ペプチド産生における寄与度合いを検索した。歯周病の重症化に伴い抗菌ペプチドレベルは正の相関を示し、抗菌ペプチドの産生が歯周病原性細菌の感染に起因することが確認された。一方、抗菌ペプチドレベルとコチニンレベルは逆相関を示したことから、長期の喫煙により、自然免疫において重要な働きを示す本ペプチドが余り産生されず、歯周病のリスクが高まることが示唆された。

2）

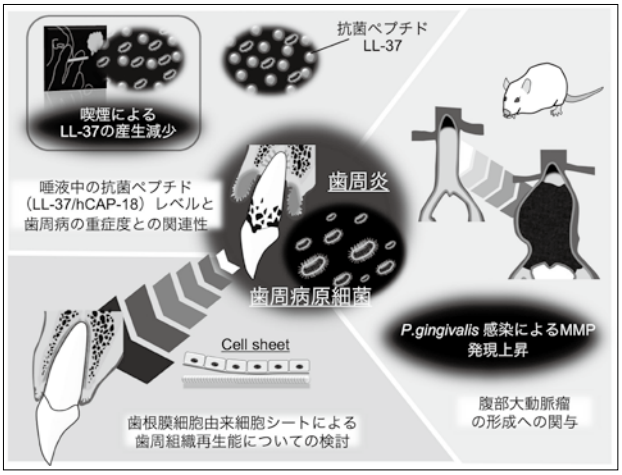

3）発表の研究内容についての英文要約

Cell sheet tissue engineering is a unique technique in tissue regeneration, with cell sheets harvested from temperature responsive culture dishes. To compare the potential of different cell sheets obtained from three kinds of mesenchymal tissues (e.g., periodontal ligament (PDL) tissue, iliac bone marrow, and alveolar periosteum) in a canine severe periodontal defect model (one-wall intrabony defect), PDL cell sheets combined with β-TCP/collagen induced true periodontal regenerations and neutral fibers. PDL cell should prove the most suitable cell source for periodontal regeneration.

Abdominal aortic aneurysm (AAA) is a common and

lethal disorder, and MMPs are highly expressed in AAA lesions. To analyze the influence of periodontopathic bacteria on AAA dilatation, challenge with Porphyromonas gingivalis can accelerate, or even initiate, the progression of experimental AAA through the increased expression of MMPs.

LL-37/hCAP-18 is an antibacterial peptide involved in the human innate immune defense system. To assess relationship between salivary LL-37 levels and clinical severity in chronic periodontitis and the impact of the following factors on LL-37 production：periodontopathic bacteria and salivary cotinine levels, salivary LL-37 level was positively correlated with severe periodontal destruction and LL-37 production was apparently associated with periodontopathic bacterial infection. The negative correlations between salivary LL-37 and cotinine levels also suggest that smoking or long-term exposure to environmental tobacco smoke can lead to lower LL-37 levels and increased risk of periodontitis.

4）本事業に関連して世界的な研究拠点形成に向けて、以下の点で改善・整備等されたこと

A（研究拠点体制）

米国UCSFのMark Ryder教授およびタイ国Khon Kaen大学のNawarat W Charoen歯学部長との研究協力体制を継続している。

B（研究教育環境）

大学院講義を英語で実施し、英語に親しむ環境の構築に努めた。ソニーとの研究協力関係を樹立した。

C（人材確保）

12人がAISSに採用された。大学院生を新規に4名受け入れた。

D（人材育成）

新人教育に力を入れ、研究面ではMark Ryder教授と研究討議を行い大学院生の指導をお願いした。

E（国際化）

1）第41回グローバルCOE海外研究者講演会（Dr. Neil S. Norton. Review of anatomic features using cone beam CT imaging. 2011.2.28）を主催した。

2）第48回グローバルCOE海外研究者講演会（Dr. Andreas F. Bindl and Dr. Lutz Ritter. Digital dentistry with CAD/CAM and cone beam computed tomography and their applications in implantology. 2011.10.11）を主催した。

3）日本学術振興会の論博事業に参画し、タイからの留学生を受け入れた。

5）GCOE事業を推進するに当たって力を入れた点

若い研究者に出来る限り国際化の意識を植え付けるように努めた。海外での研究発表を積極的に推進している。

6）英文原著論文

1. ◎Akiyama F, Aoki A, Miura-Uchiyama M, Sasaki KM, Ichinose S, Umeda M, Ishikawa I, Izumi Y. In vitro studies of the ablation mechanism of periodontopathic bacteria and decontamination effect on periodontally diseased root surfaces by erbium：yttrium-aluminum-garnet laser. Lasers Med Sci 26（2）：193-204, 2011.
2. ◎Aoyama N, Suzuki J, Wang D, Ogawa M, Kobayashi N, Hanatani T, Takeuchi Y, Izumi Y,Isobe M. Porphyromonas gingivalis promotes murine abdominal aortic aneurysms via matrix metalloproteinase-2 induction. J Periodont Res 46：176-183, 2011.
6. Chokechanachaisakul U, Kaneko T, Yamanaka Y, Kaneko R, Katsube K, Kobayashi H, Nör JE, Okiji T, Suda H. Gene expression analysis of resident macrophages in lipopolysaccharide-stimulated rat molar pulps. J Endodont 37（9）：1258-1263, 2011.
7. ◎Ebe N, Hara-Yokoyama M, Iwasaki K, Iseki S, Okuhara S, Podyma-Inoue KA Terasawa K, Watanabe A, Akizuki T, Watanabe H, Yanagishita M, Izumi Y. Pocket epithelium in the pathological setting for HMGB1 release. J Dent Res 90（2）：235-40. 2011.
8. ◎Ishihata K, Wakabayashi N, Wadachi J, Akizuki T, Izumi Y, Takakuda K, Igarashi Y. Reproducibility of pocket depth measurement by experimental periodontal probe incorporating optical fiber sensor. J Periodontol 2011 May 16. [Epub ahead of print]
9. ◎Himeno-Ando A, Izumi Y, Yamaguchi A, Iimura T. Structural differences in the osteocyte network between the calvaria and long bone revealed by three-dimensional fluorescence morphometry, possibly reflecting distinct mechano-adaptations and sensitivities. Biochem Biophys Res Commun 2011 Dec 16. [Epub ahead of print]
10. ◎Katagiri S, Nitta H, Nagasawa T, Izumi Y, Kanazawa M, Matsuo A, Chiba H, Miyazaki S, Miyauchi T, Nakamura N, Oseko F, Kanamura N, Ando Y, Hanada N, Inoue S. Reduced masticatory function in non-elderly obese Japanese adults. Obesity Research and Clinical Practice 5（4）：e279-286, 2011.
11. ◎Kobayashi C, Yaegaki K, Calenic B, Ishkitiev N, Imai T, Ii H, Aoyama I, Kobayashi H, Izumi Y, Haapasalo M. Hydrogen sulfide causes apoptosis in human pulp stem cells. J Endod 37（4）：479-84, 2011.
12. ◎Tanaka K, Iwasaki K, Fegali K, Komaki M, Ishikawa

I, Izumi Y. Comparison of characteristics of periodontal ligament cells obtained from outgrowth and enzyme-digested culture methods. Archs Oral Biol 56：380-388, 2011.

13.◎Tsumanuma Y, Iwata T, Washio K, Yoshida T, Yamada A, Takagi R, Ohno T, Lin K, Yamato M, Ishikawa I, Okano T, Izumi Y. Comparison of different tissue-derived stem cell sheets for periodontal regeneration in a canine 1-wall defect model. Biomaterials 32（25）：5819-5825, 2011.

14. Wang H, Watanabe H, Ogita M, Ichinose S, Izumi Y. Effect of human beta-defensin-3 on the proliferation of fibroblasts on periodontally involved root surfaces. Peptides 32（5）：888-894, 2011

15. ◎Aoyama N, Suzuki J, Ogawa M, Watanabe R, Kobayashi N, Hanatani T, Yoshida A, Ashigaki N, Izumi Y, Isobe M. Clarithromycin suppresses the periodontal bacteria-accelerated abdominal aortic aneurysms in mice. J Periodontal Res（in press）

16. Belal MH, Watanabe H, Ichinose S, Ishikawa I.Effect of PDGF-BB combined with EDTA gel on adhesion and proliferation to the root surface. Odontology（in press）

17. ◎Bharti P, Katagiri S, Nitta H, Nagasawa T, Kobayashi H, Takeuchi Y, Izumiyama H, Uchiyama I, Inoue S, Izumi Y. Periodontal treatment with topical antibiotics improves glycemic control in association with elevated serum adiponectin in patients with type 2 diabetes mellitus. Obesity Research and Clinical Practice（in press）

18. Hamaya R, Ogawa M, Kobayashi N, Suzuki J, Itai A, Nagai R, Isobe M. A novel IKK inhibitor prevents progression of restenosis after arterial injury in mice. Int Heart J（in press）

19. ◎Takahashi M, Chen Z, Watanabe K, Kobayashi H, Nakajima T, Kimura A, Izumi Y. Toll-like receptor 2 gene polymorphisms associated with aggressive periodontitis in Japanese. Open Dentistry Journal（in press）

20. ◎Takeuchi Y, Nagasawa T, Katagiri S, Kitagawara S, Kobayashi H, Koyanagi T, Izumi Y. Salivary levels of antibacterial peptide（LL-37/hCAP-18）and cotinine in periodontitis patients. J Periodontol（in press）

7）総説ならびに著書

総　説

1. Izumi Y, Aoki A, Yamada Y, Kobayashi H, Iwata T, Akizuki T, Suda T, Nakamura S, Wara-Aswapati N, Ueda M, Ishikawa I. Current and future periodontal tissue engineering. Periodontol 2000. 56（1）：166-87, 2011.

2. Pang P, Andreana S, Aoki A, Coluzzi D, Obeidi A, Olivi G, Parker S, Rechmann P, Sulewski J, Sweeney C, Swick M, Yung F. Laser energy in oral soft tissue applications. J Laser Dent 2011;18（3）：123-131.

3. 和泉雄一, 荒川真一, 南原弘美. 国際歯科ニュース：歯周炎と早産・低体重児出産との関わりに関する最近の話題. 日本歯科医師会雑誌, Vol.63, No.12, 72（1314）-74（1316）. 2011. 3.

4. 青木　章,Verica Aleksic,岩崎剣吾,渡辺　久,安孫子宜光,石川　烈,和泉雄一.低出力Er：YAGレーザーの生物学的効果.日レ医誌32（1）：64-70, 2011.

5. 青木　章,水谷　幸嗣,谷口陽一,和泉雄一.歯周治療—歯周ポケット治療におけるEr：YAGレーザーの効果とそのエビデンス.歯界展望117（3）：468-474, 2011.

6. 青木　章,Chanthoeun Chui,竹内康雄,江黒　徹,吉野敏明,田中真喜,和泉雄一. 光を用いた新しい抗菌治療法の歯周治療への応用—a-PDTによる光化学殺菌.デンタルダイアモンド36（9）：64-69, 2011,7月号.

7. 青木　章.Er：YAGレーザーを用いた非外科的外科的歯周ポケット治療のエビデンス.第13回Er：YAGレーザー臨床研究会事後抄録（東京,東京国際フォーラム,2010.8.8.）,pp.1-14. Er：YAGレーザー臨床研究会ホームページhttp：//www2.er-yag.gr.jp/.

8. 荒川真一.オゾンナノバブル水・酸素ナノバブル水—基礎的特質と臨床応用—
東京歯科同窓会雑誌　172、28-36, 2011

9. 和泉雄一.歯周治療とEr：YAGレーザー.第13回Er：YAGレーザー臨床研究会事後抄録（東京,東京国際フォーラム,2010.8.8.）,pp.1-39. Er：YAGレーザー臨床研究会ホームページhttp：//www2.er-yag.gr.jp/.

10. 和泉雄一,片桐さやか.生活習慣病としての歯周病
特集「生活習慣病における骨と歯」
The Bone 25（4）;421-425：2011

11. 和泉雄一, 秋月達也, 芦垣紀彦. インプラント周囲炎におけるPTMキットの臨床応用. デンタルエコー（松風歯科クラブ学術誌）. 株式会社松風, 東京, vol.166, p2-5, 2011.

12. 和泉　雄一,荒川真一.ストレスと歯周炎.国際歯科ニュース 日歯医師会誌 Vol. 64, No.8, 65-67, 2011.

13. 江黒　徹,青木　章,水谷幸嗣,Aristeo A. Takasaki,簗瀬武史,和泉雄一,勝海一郎. 歯科インプラント治

療におけるEr：YAGレーザーの応用.日レ医誌32(1)：48-54, 2011.
14. 片桐さやか, 和泉雄一. FORUM「合併症Ⅱ-歯周病」第1回　歯周病の原因と治療.
プラクティス 第28巻第1号：14-17, 2011.
15. 片桐さやか, 和泉雄一. FORUM「合併症Ⅱ-歯周病」第2回　糖尿病と歯周病の相互作用.
プラクティス第28巻第2号：117-119, 2011.
16. 片桐さやか, 和泉雄一. FORUM「合併症Ⅱ-歯周病」第3回　糖尿病治療と歯周治療の影響.
プラクティス第28巻第3号：239-241, 2011.
17. 竹内康雄,和泉雄一.中性電解機能水の歯周治療への応用.日本歯科理工学会雑誌 30（1）：13-16, 2011.
18. 谷口陽一,青木章,水谷幸嗣,和泉雄一.レーザーと歯周治療—歯周外科治療におけるEr：YAGレーザーの臨床応用と今後の展望,光アライアンス 22（9）：22-26, 2011.
19. 津久井　明, 渡辺　久. 上皮下結合組織移植術による根面被覆へのEr：YAGレーザーの応用.
日レ歯誌 22（1）：29-32, 2011.
20. 水谷幸嗣,青木章,石川烈,和泉雄一.歯周治療へのEr：YAGレーザーの応用.日レ医誌32（1）：39-47, 2011.
21. 吉野敏明,田中真喜,青木　章,和泉雄一.“光”を用いた殺菌治療：抗菌光線力学療法 歯周治療におけるフォトダイナミックセラピーの基礎と臨床-.ザ・クインテッセンス30（8）：140-149（1806-1815）, 2011.
22. 渡辺　久.臨床のヒント　歯周治療の長期予後について.東京医科歯科大学　歯科東京同窓会報170号：7-13, 2011.
23. 渡辺　久.歯周組織と歯石の管理へのレーザーの応用.特集「レーザー治療の現状」日歯理工誌 30 (6)：361-364, 2011.

著　書

1. Ishikawa I, Aoki A. Chapter 70（b）: Recent Advances in Surgical Technology, Lasers in periodontics. In: Newman MG, Takei HH, Klokkevold PR, Carranza FA（eds）, Carranza's Clinical Periodontology, 11th Edition and its electric version on website, Elsevier, pp.605-607, 2011.
2. 青木　章,水谷幸嗣,渡辺　久,石川　烈,和泉雄一.石川烈編,Er：YAGレーザーの基礎と臨床,4.歯周治療におけるEr：YAGレーザーの臨床—骨外科治療.第一歯科出版,東京,p.127-134, 2011.
3. 青木　章,内山真子,小田　茂,木下淳博,和泉雄一.石川烈編,Er：YAGレーザーの基礎と臨床,4.歯周治療におけるEr：YAGレーザーの臨床—軟組織治療.第一歯科出版,東京,p.107-113, 2011.
4. 青木　章,永井茂之,篠木　毅.安全対策および安全管理.和泉雄一,青木　章,石川　烈編集　歯周治療・インプラント治療におけるEr：YAGレーザーの使い方.医学情報社,東京　2011,24-27.
5. 青木　章,小田　茂,石川　烈.歯石除去と根面のデブライドメント.和泉雄一,青木　章,石川　烈編集　歯周治療・インプラント治療におけるEr：YAGレーザーの使い方.医学情報社,東京　2011,38-41.
6. 青木　章,穐山文彦,石川　烈.歯周病原細菌の殺菌と無毒化効果.和泉雄一,青木　章,石川　烈編集　歯周治療・インプラント治療におけるEr：YAGレーザーの使い方.医学情報社,東京　2011,42-45.
7. 青木　章,水谷幸嗣,小田　茂,和泉雄一.歯周ポケット治療.和泉雄一,青木　章,石川　烈編集　歯周治療・インプラント治療におけるEr：YAGレーザーの使い方.医学情報社,東京　2011,46-50.
8. 青木　章,Aristeo A. Takasaki,松山智子,和泉雄一.インプラント治療における応用.和泉雄一,青木　章,石川　烈編集　歯周治療・インプラント治療におけるEr：YAGレーザーの使い方.医学情報社,東京　2011,61-68.
9. 青木　章,和泉雄一,石川　烈.エピローグ：課題と展望.和泉雄一,青木　章,石川　烈編集　歯周治療・インプラント治療におけるEr：YAGレーザーの使い方.医学情報社,東京　2011,136-138.
10. 青木　章,澤辺正規,江尻健一郎,渡辺　久.低出力照射による生物学的効果.和泉雄一,青木　章,石川　烈編集　歯周治療・インプラント治療におけるEr：YAGレーザーの使い方.医学情報社,東京　2011,69-72.
11 青木　章,谷口陽一,竹内康雄,和泉雄一. フォトダイナミックセラピーの歯周炎・インプラント周囲炎への応用.和泉雄一,申基喆,二階堂雅彦,松井徳雄編集,インプラント時代の歯周マネジメント-確かな機能回復の成果を得るために,デンタルダイアモンド増刊号,デンタルダイアモンド社,東京,pp.187-189, 2011.
12 秋月達也, 斎田寛之, 和泉雄一. 1基本的な歯周治療の進め方. インプラント時代の歯周マネジメント 確かな機能回復の成果を得るために DENTAL DIAMOND増刊号. 株式会社デンタルダイヤモンド

社, 東京, p14-21, 2011.
13. 秋月達也, 和泉雄一. 第3編 ものづくり技術を生かした再生医療の臨床応用 第1章 再生誘導スペース確保のためのバイオマテリアル—歯周組織再生誘導法（GTR法）. ものづくり技術からみる再生医療-細胞研究・創薬・治療-. 株式会社シーエムシー出版, 東京, 2011.
14. 和泉　雄一,荒川　真一.第3章　天然歯との共存　総論、伊藤　隆利/編集代表、長期経過症例から学ぶ　成功するインプラント治療戦略　補綴臨床別冊、九州インプラント研究会（KIRG）p128-131, 2011.
15. 石川　烈,青木　章.Er：YAGレーザーの特性.和泉雄一,青木　章,石川　烈編集　歯周治療・インプラント治療におけるEr：YAGレーザーの使い方.医学情報社,東京　2011,13-16.
16. 和泉雄一,青木 章,石川 烈編著.歯周治療・インプラント治療におけるEr：YAGレーザーの使い方.医学情報社,東京,140 pages, 2011.
17. 和泉雄一.プロローグ：レーザーとは.和泉雄一,青木章,石川　烈編集　歯周治療・インプラント治療におけるEr：YAGレーザーの使い方.医学情報社,東京 2011,7-8.
18. 和泉雄一,青木　章.歯周治療やインプラント治療におけるレーザーの応用.和泉雄一,青木　章,石川　烈編集　歯周治療・インプラント治療におけるEr：YAGレーザーの使い方.医学情報社,東京　2011,9-12.
19. 江黒　徹,谷口陽一.伝送系とコンタクトチップ.和泉雄一,青木　章,石川　烈編集　歯周治療・インプラント治療におけるEr：YAGレーザーの使い方.医学情報社,東京　2011,17-20.
20. 小柳達郎,竹内康雄, 和泉雄一. 歯周病原細菌とインプラント周囲炎の原因菌の比較.デンタルダイヤモンド増刊号 インプラント時代の歯周マネジメント,デンタルダイヤモンド社,東京.p.63, 2011.
21. 丸山裕昭,穐山文彦,安藤嘉則,青木　章.石川烈編,Er：YAGレーザーの基礎と臨床,4.歯周治療におけるEr：YAGレーザーの臨床—デブライドメント後の照射歯根面の変化と処理法および除菌効果.第一歯科出版,東京,p.121-126, 2011.
22. 水谷幸嗣,和泉雄一.フラップレス骨整形.和泉雄一,青木　章,石川　烈編集　歯周治療・インプラント治療におけるEr：YAGレーザーの使い方.医学情報社,東京　2011,95-98.
23. 水谷幸嗣,青木　章,和泉雄一.歯肉色素沈着症.和泉雄一,青木　章,石川　烈編集　歯周治療・インプラント治療におけるEr：YAGレーザーの使い方.医学情報社,東京　2011,32-37.
24. 水谷幸嗣,青木　章,石川　烈.フラップ手術.和泉雄一,青木　章,石川　烈編集　歯周治療・インプラント治療におけるEr：YAGレーザーの使い方.医学情報社,東京　2011,51-56.
25. 水谷幸嗣,青木章,Aristeo A. Takasaki,石川烈,和泉雄一. 石川烈編,Er：YAGレーザーの基礎と臨床,4.歯周治療におけるEr：YAGレーザーの臨床—Er：YAGレーザーによる歯石除去と歯周ポケット治療.第一歯科出版,東京,p.114-120, 2011.
26. 鷲尾薫、葭田敏之、妻沼有香、岩田隆紀、岡野光夫、石川烈. 自己歯根膜細胞シートを用いた歯周病治療. 治療（10月号）南山堂 93（10）：2130-2135, 2011.
27. 渡辺　久、和泉雄一：7.軟組織治療.和泉雄一、青木章、石川　烈編集　歯周治療・インプラント治療におけるEr：YAGレーザーの使い方、医学情報社、東京　2011,28-31.
28. 渡辺　久、吉野敏明、和泉雄一：13.骨外科処置.和泉雄一、青木　章、石川　烈編集　歯周治療・インプラント治療におけるEr：YAGレーザーの使い方、医学情報社、東京　2011,57-60.
29. 渡辺 久,谷口陽一,石川 烈,和泉雄一.石川烈編,Er：YAGレーザーの基礎と臨床,4歯周治療におけるEr：YAGレーザーの臨床—歯周外科への応用.第一歯科出版,東京,p.135-137, 2011.

翻　訳

1. 南原弘美,荒川真一,和泉雄一.新鮮抜歯窩へ埋入したインプラント周囲の骨リモデリング（翻訳）Int J Periodont Rest Dent 日本語版. 2011; 19（1）：46-52.
2. 小柳達朗,荒川真一,和泉雄一.歯周疾患罹患歯歯根表面へのCarisolv適用効果に関する走査型電子顕微鏡法を用いたIn Vitro研究（翻訳）Int J Periodont Rest Dent 日本語版. 2011; 19（2）：79-83.
3. 南原弘美,荒川真一,和泉雄一.歯周疾患様症状を呈した歯肉扁平上皮癌（翻訳）Int J Periodont Rest Dent 日本語版. 2011; 19（2）：84-87.
4. 早雲彩絵,荒川真一,和泉雄一.スクリュースプレッディング：技術的考察と症例報告（翻訳）Int J Periodont Rest Dent 日本語版. 2011; 19（3）：39-43.
5. 南原弘美,荒川真一,和泉雄一.ツーピースジルコニ

アインプラントの臨床的および組織学的パイロット評価（翻訳）Int J Periodont Rest Dent 日本語版. 2011; 19（3）：52-58.

6. 小柳達朗,荒川真一,和泉雄一.脱タンパクウシ骨と生体吸収性コラーゲン膜を用いた歯槽堤増大術：トモデンシトメトリック（断層濃度測定)、組織学的、組織形態計測学的解析
（翻訳）Int J Periodont Rest Dent 日本語版. 2011; 19（4）：33-41.
7. 荒川真一：オーラルヘルスアトラス　世界の口腔健康関連地図　Roby Beaglehole, Jon Crail. 監訳　神原正樹、井上　孝、訳　日本歯科医師会学術交流委員会　財団法人　口腔保健協会　2011年1月28日　第1版　第1刷
8. 池田裕一、荒川真一、和泉雄一.　組換えヒト血小板由来成長因子BBとウマ由来骨ブロックを併用した水平的歯槽堤増大術：臨床研究と組織学的研究（翻訳）Int J Periodont Rest Dent 日本語版. 2011; 19（5）：58-63.
9. 池田裕一、荒川真一、和泉雄一.　上顎歯槽堤の水平的再建におけるヒト新鮮凍結骨移植の臨床的,組織学的評価（翻訳）Int J Periodont Rest Dent 日本語版. 2011; 19（6）：76-84.

8）特許取得、特許申請

荒川真一：欧州特許出願及び米国特許出願（H23.5）（1）欧州：TMDU整理番号：P06-061P-EP
発明の名称：組織の殺菌又は消毒用製剤　出願番号：07849809.4　（2）　米国：TMDU整理番号：P06-061P-US発明の名称：　同上出願番号：12/518974　発明の名称：組織の殺菌又は消毒用製剤 出願番号：12/518,974　貴学整理番号：P06-061P-US 弊所整理番号：TMDP0803F-US

9）平成23年度までの自己評価

今年度の研究課題についてはほぼ予定通りの進行を示している。また、研究拠点体制作りでは、タイのKhon Kaen大学のNawarat W Charoen歯学部長とのコラボレーションが順調に進んでいる。

10）和文原著論文

塩山秀裕, 水谷幸嗣,須田智也,田中敬子, 青山典生, 藤原-高橋　香, 秋月達也,竹内康雄,小林宏明,木下淳博,小田　茂,和泉雄一.エムドゲイン®ゲルを用いた先進医療「歯周外科治療におけるバイオ・リジェネレーション法」の治療成績.日歯保存誌 印刷中

11）学会発表（英文）

1. ◎Nanbara H, Wara-aswapati N, Yoshida Y, Nagasawa T, Yashiro R, Bando Y, Kobayashi H, Boch J.A, Izumi Y. Wnt5a expression by Porphyromonas gingivalis LPS via NF-κB and STAT1. The 10th World Congress on Inflammation, Paris, France,2011.6.25-29.
2. ◎Tsumanuma Y, Iwata T, Washio K, Yoshida T, Yamada A, Yamato M, Ishikawa I, Okano T, Izumi Y. Comparison of different tissue-derived stem cell sheets for periodontal regeneration in a canine 1-wall defect model. The 10th World Congress on inflammation. Paris, France, 2011.6.25-29.
3. ◎Yamada A, Izumi Y, Iwata T, Yamato M, Ishikawa I, Okano T. Expression of WNT
related gene in human periodontal ligament cells during osteogenic differentiation.
The 10th World Congress on Inflammation, Paris, France,2011.6.25-29.
4. Watanabe H, Hagiwara S, Izumi Y. A randomized control trial of Mastic usage in the periodontal treatment. 9th APSP（2011.9.9, Hong Kong）
5. ◎Chui C, Aoki A, Takeuchi Y, Sasaki Y, Abiko Y, Izumi Y. Bactericidal effect of a-PDT using high power blue LED and red dye agent on Porphyromonas gingivalis. The 97th annual meeting of the American Academy of Periodontology, Miami Beach, USA, Nov 12-15, 2011.
6. ◎Kobayashi N,　Suzuki J, Ogawa M, Aoyama N, Hanatani T, Ashigaki N, Yoshida A, Isobe M, Izumi Y. Infection of periodontal bacteria enhances neointimal formation through monocyte chemotactic protein-1 in mice.　American Academy of Periodontology 97th Annual Meeting, November 12-16, 2011. Miami, USA
7. ◎Kobayashi N,　Suzuki J, Ogawa M, Aoyama N, Hanatani T, Ashigaki N, Yoshida A, Hirata Y, Nagai R, Izumi Y, Isobe M.　A Periodontal Pathogen Promotes Neointimal Formation after Arterial Injury through Toll-Like Receptor-2 Signaling.　American Heart Association Scientific Sessions 2011, November 12-16, 2011. Orlando, USA.
8. ◎Kobayashi N,　Suzuki J, Ogawa M, Aoyama N, Hanatani T, Ashigaki N, Yoshida A, Izumi Y, Isobe M. Relationship between Periodontal Bacteria and Arterial Injury.　第28回国際心臓研究学会日本部会（ISHR）2011年12月2-3日、東京
9. ◎Ashigaki N,　Suzuki J, Ogawa M, Watanabe R, Aoyama N, Kobayashi N Hanatani T, Ashigaki N, Yoshida A, Izumi Y, Isobe M.　Periodontal Pathogens Deteriorated Survival Rate after Subtotal Nephrectomy in Mice. 第28回国際心臓研究学会日本部会（ISHR）

2011年12月2-3日、東京

12）学会発表（和文）

1. 谷口陽一,青木 章,水谷幸嗣,竹内康雄,小田 茂, 和泉雄一.高ヘルツEr：YAGレーザー によるインプラント体粗造面の最適デブライドメント出力の検討.日本口腔インプラント学会 第30回関東甲信越支部学術大会（2011. 2.12-13. 横浜）
2. 江黒 徹,青木 章,鈴木貴規,淺井潤彦,簗瀬武史.インプラント2次手術におけるEr：YAGレーザーを用いた無麻酔下でのソフトティッシュマネージメント.日本口腔インプラント学会—第30回 関東甲信越支部学術大会,（2011. 2.12-13. 横浜）
3. 小柳達郎,竹内康雄,丸山緑子,小田茂,和泉雄一.16S rRNA gene clone library法を用いたインプラント周囲炎細菌叢の解析.日本口腔インプラント学会 第30回関東甲信越支部学術大会,（2011. 2.12-13. 横浜）
4. 妻沼有香, 岩田隆紀, 鷲尾薫, 葭田敏之, 山田梓, 大和雅之, 石川烈, 岡野光夫, 和泉雄一.イヌ1壁性欠損モデルを用いた歯周組織再生における異なる組織由来細胞シートの比較. 第10回日本再生医療学会総会（2011.3.1-2. 東京）
5. 山田 梓・岩田隆紀・葭田敏之・大和雅之・石川 烈・岡野光夫・和泉雄一. ヒト歯根膜細胞の骨芽細胞分化におけるWNT関連遺伝子発現. 第10回日本再生医療学会総会（2011.3.1-2. 東京）
6. 高橋香, 藤田理恵子, 三浦紫陽子, 戸野倉雅美, 田熊大祐, 馬場亮, 松木薗麻里子, 難波直, 笹原沙衣子, 鴇田真弓, 市橋弘章, 伊藤寛恵, 佐藤雅美, 高畠正義, 文原千尋, 藤野浩子, 小暮啓介, 押田智枝, 片桐さやか, 藤田桂一.日本獣医内科学アカデミー/日本獣医臨床病理学会/日本獣医皮膚科学会 2011年大会 （2011. 3. 11-13. 横浜）
7. Kobayashi N, Suzuki J, Ogawa M, Aoyama N, Hanatani T, Ashigaki N, Yoshida A, Izumi Y, Isobe M. A periodontal pathogen promotes neointimal formation after arterial injury with enhanced expression of matrix metalloproteinase-2. 第76回日本循環器学会学術集会 2011年3月16-18日、福岡
8. 南原弘美, Nawarat Wara-aswapati, 長澤敏行, 吉田安宏, 矢代麗子, 坂東由記子, 小林宏明, Jason A. Boch, 和泉雄一. ヒト単球系細胞THP-1における歯周病原細菌刺激によるWnt5a遺伝子発現について.第54回日本歯周病学会春季学術大会（2011.5.27-28. 博多）
9. Almehdi Aslam, 青木 章,谷口陽一,澤辺正規,江尻健一郎,Chui Chantouen, 佐藤郁文.片桐さやか, 和泉雄一.Analysis of Root Cementum Alteration following Er：YAG Laser Irradiation.第54回日本歯周病学会春季学術大会（2011. 5.27-28. 福岡）
10. ラジャカルナ ガマララギアモヂイニ,内田佳介,梅田 誠,古川あすか,和泉雄一,江石義信.新規に開発したモノクロナール抗体を用いた病的歯肉組織中の歯周病原細菌の検出と局在.第54回 日本歯周病学会春季学術大会（2011. 5.27-28. 福岡）
11. 小柳達郎, 坂本光央, 竹内康雄, 丸山緑子, 大熊盛也, 和泉雄一. 16S rRNA gene clone library法を用いたインプラント周囲炎細菌叢の解析.第54回 日本歯周病学会春季学術大会（2011. 5.27-28. 福岡）
12. 宗像源博,作山 葵,立川敬子,竹内康雄,石渡正浩,和泉雄一,春日井 昇平.インプラント周囲炎を生じた患者に対する細菌学的検討.第54回日本歯周病学会 春季学術大会（2011. 5.27-28. 福岡）
13. 竹内康雄,竹内まや.慢性歯周炎患者に再生療法を適応した一症例.第54回日本歯周病学会春季学術大会（2011. 5.27-28. 福岡）
14. 渡辺 香.広汎型中等度慢性歯周炎の一症例 第54回日本歯周病学会春季学術大会（2011. 5.27-28. 福岡）
15. 大西英知,荒川真一,中島琢磨,和泉雄一. 歯周炎患者由来歯肉溝滲出液がTannerella forsythia FDFに与える影響. 第54回日本歯周病学会春季学術大会（2011. 5.27-28. 福岡）
16. 秋月達也,小田 茂,渡辺 隆. Miller Class Ⅱの歯肉退縮の患者にエンベロープテクニックを用いて結合組織移植を行った一症例. 第54回春季日本歯周病学会学術大会（2011.5.26-28. 福岡）
17. 由利啓子,秋月達也,小田 茂,十川裕子,難波佳子,足達淑子,和泉雄一. 患者のモチベーションの維持と継続的な口腔衛生指導の重要性を認識した重度慢性歯周炎の一症例. 第54回春季日本歯周病学会学術大会（2011.5.26-28. 福岡）
18. 岩崎剣吾,小牧基浩,木村康之,和泉雄一,森田育男.細胞培養による歯根膜幹細胞の血管平滑筋細胞様変化について.第54回春季日本歯周病学会学術大会（2011.5.26-28. 福岡）
19. 小牧基浩,岩崎剣吾,木村康之,和泉雄一,森田育男.骨髄細胞はマウス歯周組織欠損に動員される.第54回春季日本歯周病学会学術大会（2011.5.26-28. 福岡）

20. 木村康之,小牧基浩,岩崎剣吾,和泉雄一,森田育男.Caイオン刺激によりセメント質タンパクCEMP-1の発現上昇について.第54回春季日本歯周病学会学術大会（2011.5.26-28. 福岡）
21. 小田　茂,須田智也,青山典生,遠藤圭子,小原由紀,近藤圭子,荒木孝二,和泉雄一.東京医科歯科大学歯学部歯学科・口腔保健学科合同クリニカルケース検討授業―歯周治療症例を通じてのチーム歯科医療理解への試みー.第54回春季日本歯周病学会学術大会（2011.5.26-28. 福岡）
22. 伊藤　弘,関野　愉,村樫悦子,井口一美,橋本修一,沼部幸博,佐々木　大輔,八重柏　隆,國松和司,高井英樹,目澤 優,小方頼昌,渡辺　久,萩原さつき,和泉雄一,廣島佑香,木戸淳一,永田俊彦.歯肉溝滲出液（GCF）を用いた歯周病罹患部位の診断と治療効果のモニタリングの有用性 -歯周病迅速診断キット開発に向けて-第一報. 第54回春季日本歯周病学会学術大会（2011.5.26-28. 福岡）
23. 坪川正樹,青木　章,佐藤郁文,谷口陽一,江尻健一郎,澤辺正規,水谷幸嗣, 秋月達也, 小田　茂, 角　保徳, 和泉雄一.光干渉断層画像診断法（OCT）の歯周組織診断への応用- 歯石の検出.第134回日本歯科保存学会春期学術大会（2011. 6. 10-11. 舞浜,千葉）
24. 千ヶ崎乙文,梅田誠,青木章,竹内康雄,青山典生,池田裕一,鈴木允文,和泉雄一,佐々木好幸,水谷幸嗣,石川烈.歯周病原細菌の検出と歯周病罹患状況の横断的研究. 第134回日本歯科保存学会春期学術大会（2011. 6. 10-11. 舞浜,千葉）
25. 渡辺　久,萩原さつき,和泉雄一.新機能性食品の口腔衛生およびブレスケアへの臨床応用. 第134回日本歯科保存学会春期学術大会（2011. 6. 10-11. 舞浜,千葉）
26. 鈴木允文,納富拓也,溝口史高,宮嶋大輔,早田匡芳,中元哲也,江面陽一,和泉雄一,野田政樹.TRPV4はメカニカルストレス下での骨芽細胞におけるカルシウムイオン流入を延長する. TRPV4 induce prolonged calcium influx in osteoblast under mechanical stress. 第29回日本骨代謝学会学術集会（2011.7.28-30. 大阪）
27. 早雲彩絵,荒川真一,眞野喜洋,和泉雄一. オゾンナノバブル水の歯周治療への応用. 第12回口腔機能水学会（2011. 7. 30-31. 東京）
28. 荒川真一,早雲彩絵,眞野喜洋,和泉雄一. オゾンナノバブル水（NBW3）の殺菌効果と安全性について.第12回口腔機能水学会（2011. 7. 30-31. 東京）
29. 青山典生,鈴木淳一,小川真仁,小林奈穂,花谷智哉,芦垣紀彦,吉田明日香,渡辺　亮,和泉雄一,磯部光章.Toll-like receptor-2 plays a role in the periodontal bacteria-induced abdominal aortic aneurysms（歯周病原細菌感染を伴う腹部大動脈瘤の進行にはToll様受容体-2が関わる）.第75回日本循環器学会学術集会（2011.8.3-4. 横浜）
30. 三島昭宏,水野光春,高橋啓至,藤井俊秀,南部敏之,沼部幸博,渡辺　久,和泉雄一.歯周基本治療に対する歯周組織の反応性の予測について-新規歯周組織検査薬「PTMキット」を用いたAST測定―.第4回日本口腔検査学会（2011. 8. 27-28. 東京）
31. 杉澤　満、荒川　真一. インプラント周囲炎におけるPCR法を用いた症例の検討. 第14回　先進インプラント医療学総会・学術大会（2011. 9. 11. 東京）
32. ◎チュイ・チャントゥーン,青木　章,竹内康雄,佐々木好幸,安孫子宜光,和泉雄一.Bactericidal effect of a-PDT using high power blue LED and red dye agent on Porphyromonas gingivalis.第54回秋季日本歯周病学会学術大会（2011.9.24. 下関）
33. 小林宏明,木下淳博,須永昌代,片桐さやか,青山典生,渡辺久,和泉雄一.歯周ポケット測定訓練用顎模型に関する研究　―歯周病外来歯科医師と歯学部学生での評価―第54回秋季日本歯周病学会学術大会（2011.9.24. 下関）
34. 須永昌代,木下淳博,小林宏明,和泉雄一.術者目線のオリジナル3Dムービー作成・供覧システムの歯周外科講義への応用と評価.第54回秋季日本歯周病学会学術大会（2011.9.24. 下関）
35. 伊藤　弘,関野　愉,村樫悦子,井口一美,橋本修一,沼部幸博,佐々木　大輔,八重柏　隆,國松和司,高井英樹,目澤 優,小方頼昌,渡辺　久,萩原さつき,和泉雄一,廣島佑香,木戸淳一,永田俊彦.歯肉溝滲出液（GCF）を用いた歯周病罹患部位の診断と治療効果のモニタリングの有用性 -歯周病迅速診断キット開発に向けて-第二報. 第54回秋季日本歯周病学会学術大会（2011.9.24. 下関）
36. 芦垣紀彦,鈴木淳一,小川真仁,青山典生,小林奈穂,花谷智哉,吉田明日香,磯部光章,和泉雄一.歯周病原細菌感染は慢性腎臓病マウスの生存率を悪化させる.第54回秋季日本歯周病学会学術大会（2011.9.24. 下関）
37. 伊藤　弘,沼部幸博,関野　愉,村樫悦子,井口一美,戸円智幸,橋本修一,佐々木大輔,八重柏　隆,國松和司,高井英樹,目澤 優,小方頼昌,渡辺　久,萩原さつき,

和泉雄一,廣島佑香,木戸淳一,永田俊彦.歯肉溝滲出液（GCF）を用いた歯周病罹患部位の診断と治療効果のモニタリングの有用性 -歯周病迅速診断キット開発に向けて-（第三報）. 第134回 日本歯科保存学会 秋季学術大会（2011. 10. 20-21. 大阪）

38. 青山典生,鈴木淳一,和泉雄一,磯部光章.ドキシサイクリンによる歯周病原細菌感染を伴う腹部大動脈瘤拡張の抑制.第134回日本歯科保存学会 秋季学術大会（2011. 10. 20-21. 大阪）
39. 江部典子,横山三紀,寺澤和恵,柳下正樹,和泉雄一.酪酸による酸化ストレス誘導時に放出されるHMGB1の解析.第134回日本歯科保存学会 秋季学術大会（2011. 10. 20-21. 大阪）
40. 坪川正樹, 青木 章, 谷口陽一, 澤辺正規, 江尻健一郎,秋月達也, 小田 茂, 水谷幸嗣, 角 保徳, 和泉雄一.光干渉断層画像診断法（OCT）による歯肉縁下歯石の検出.第23回日本レーザー歯学会総会・学術大会.大阪,2011.12.3-4.
41. 谷口陽一,青木 章,澤辺正規, 江尻健一郎,和泉雄一.歯周組織再生治療におけるEr：YAGレーザーの応用：症例報告.第23回日本レーザー歯学会総会・学術大会.大阪,2011.12.3-4.
42. 津久井 明,渡辺 久.Er：YAGレーザーによる根面被覆（上皮下結合組織移植）への臨床応用.第23回日本レーザー歯学会総会・学術大会.大阪,2011.12.3-4.
43. 宮崎英隆,金 舞,加藤純二,渡辺 久,根岸明秀,横尾聡.超音波ガイド下で組織内レーザー照射法を行った舌静脈奇形の1例.第23回日本レーザー歯学会総会・学術大会.大阪,2011.12.3-4.
44. Kobayashi N, Suzuki J, Ogawa M, Hirata Y, Nagai R, Izumi Y, Isobe M. Periodontal bacteria infection enhances neointimal formation through monocyte chemotactic protein-1 in mice. 第19回日本血管生物医学会学術集会 2011年12月8-10日、東京
45. 小林宏明,木下淳博,須永昌代,和泉雄一.歯周ポケット測定訓練用顎模型に関する研究—歯周病外来歯科医師と歯学部生でのプロービングー. 第76回口腔病学会 （2011.12.8-9. 東京）
46. 春田千裕,小林宏明,笠間健嗣,和泉雄一.ヒト歯根膜細胞におけるTRPV1を介したアナンダマイドの骨代謝への影響.第76回口腔病学会 （2011.12.8-9. 東京）
47. 妻沼有香, 岩田隆紀, 鷲尾薫, 葭田敏之, 山田梓, 大和雅之, 石川烈, 岡野光夫, 和泉雄一. 歯根膜細胞シートによる歯周組織再生療法の実現に向けて. 日本歯周病学会関東9大学・日本臨床歯周病学会関東支部合同研修会（2012.2.11. 東京）

13）受賞

1. Nanbara H, Travel Award. Wnt5a expression by Porphyromonas gingivalis LPS via NF- κ B and STAT1. The 10th World Congress on Inflammation, Paris, 2011.6.25-29.
2. 坪川正樹.第23回日本レーザー歯学会総会・学術大会優秀発表賞.光干渉断層画像診断法（OCT）による歯肉縁下歯石の検出.第23回日本レーザー歯学会総会・学術大会.大阪,2011.12.3-4.

14）外部資金の獲得状況

1. 和泉雄一（代表）,小林宏明,岩崎剣吾,秋月達也,長澤敏行（分担）：器官形成シグナルのコントロールを基盤にした歯周病に対する新規治療戦略. 科学研究費補助金,基盤研究（B）平成21～23年度.
2. 梅田 誠（代表）：血管系疾患に関与する歯周病原細菌の特定と検証.科学研究費補助金,基盤研究（C）21592621 平成21～23年度.
3. 梅田 誠（分担）,井上芳徳（代表）：動脈疾患における歯周病の関与と血小板凝集の影響について.科学研究費補助金,基盤研究（C）22591399-1 平成22～24年度.
4. 荒川真一（代表）：歯周病原細菌由来FDFの細胞への影響及び歯周炎病態への関与の解析. 科学研究費補助金,基盤研究（C）21592620 平成21～23年度.
5. 青木 章（代表）,小林宏明,竹内康雄,秋月達也,水谷幸嗣（分担）：光エネルギーを
応用した歯周炎およびインプラント周囲炎の革新的治療法・予防法の開発.科学研究費補助金 基盤研究（C）22592308 平成22～24年度.
6. 小林宏明（代表）：歯周炎疾患進行におけるTGF betaを起点としたTh17制御メカニズムの解析.科学研究費補助金,若手研究（B） 平成22～23年度.
7. 竹内康雄（代表）：歯周炎・インプラント周囲炎細菌叢の総合的解析と弱アルカリ水による治療効果. 科学研究費補助金,若手研究（B）21792110 平成21～23年度.
8. 秋月達也（代表）：石灰化歯根膜シートと人工ペプチドを使用した歯周組織再生. 科学研究費補助金,若手研究（B）23792465 平成23～25年度.
9. 片桐さやか（代表）：糖尿病患者の血管新生緑内障

における歯周病由来抗 cardiolipin抗体の役割. 科学研究費補助金,若手研究（B）平成23～24年度.

10. 須田智也（代表）：Wntシグナルを介したβ - カテニンによる歯周組織細胞接着機構の解析.科学研究費補助金,若手研究（B）227922081平成22～23年度.
11. 江部　典子（代表）：歯周炎における酸化ストレス条件下でのTrx1とTxnipの役割の解析　科学研究費補助金,研究活動スタート支援 23890058平成23～24年度.
12. 津野顕子（分担）,新保卓郎（代表）：高齢者や易感染患者への抗菌光線力学的療法を用いた新たな口腔ケアの手法の開発と評価.厚生労働省平成21～23年度国際医療研究開発費
13. 山田　梓（代表）：日本学術振興会　特別研究員（DC2）「ヒト歯根膜細胞の骨芽細胞分化におけるWNT関連遺伝子発現」（平成23～24年度）
14. 和泉雄一：新規ビスフォスフォネート歯周病治療薬の局所投与試験.
    受託研究.昭和薬品化工株式会社　（平成21～24年度）
15. 和泉雄一,渡辺　久：歯周病迅速診断キットの開発に向けた歯肉溝滲出液（GCF）成分を用いた歯周病罹患部位の診断と治療効果のモリタリングの有用性に関する研究II. 依託研究　日本歯科医師会（平成23～24年度）
16. 荒川真一：オゾンナノバブル水 含嗽における口腔内細菌数の確認　共同研究　オリンパス株式会社（平成22年～23年度）
17. 和泉雄一,片桐さやか：糖尿病・肥満患者における口腔に関する多施設疫学研究
    8020推進財団：8020研究事業　平成23年度
18. 和泉雄一,秋月達也：クルクミン含有食品摂取による歯周病改善効果の臨床研究.
    奨学寄付金.株式会社セラバリューズ　平成23年度

15）特別講演、招待講演、シンポジウム

1. 和泉雄一：歯周病と糖尿病　その深い関係　-医科歯科連携の必要性、第1回糖尿病医科
   歯科連携のための研修会、(2011.2.13. 横浜)
2. 和泉雄一：現代歯周治療のスタンダード、徳島大学歯学部同窓会平成22年度卒後研修セミナー、(2011.2.20. 徳島)
3. 和泉雄一：天然歯とインプラント、平成23年度九州インプラント研究会、(2011.4.17. 熊本)
4. 和泉雄一：歯周病と心血管系疾患、第10回日本旅行医学会　旅行医学のトピック3、(2011.4.22.　東京)
5. 和泉雄一：再生歯科医療ガイダンス、再生歯科医療～現代から未来へ～Regenerative Strategy、東京医科歯科大学歯科同窓会創立80周年記念講演、(2011.5.15. 東京)
6. 和泉雄一：歯周炎と心血管疾患とのかかわり、第78回GCOE国際総合プレゼンテーション、(2011.5.16. 本学)
7. 和泉雄一：歯周治療の進め方と歯周外科治療、2011年度日本インプラント臨床研究会、(2011.5.21. 東京)
8. 和泉雄一：糖尿病の隠れた黒幕―それは歯周病!-医科歯科連携の必要性―、市民の健康と医療のシンポジウム　～歯周病と糖尿病について～、川口市民公開講座、(2011.6.5. 川口)
9. Yuichi Izumi：Periodontal Treatment and Periodontal Tissue Regeneration、Buerger Disease Forum in Chiang Mai 2011、(2011.6.18. Chiang Mai)
10. 和泉雄一：口とカラダの不思議な関係　～歯科の立場から～、第17回口腔保健シンポジウム、(2011.7.9. 大阪)
11. 和泉雄一：糖尿病と歯周病―その密接な関係　―医科歯科連携の必要性―、平成23年度歯科専門職研修会、(2011.7.10. 富山)
12. 和泉雄一：歯周病と全身の健康との関わり、平成23年度感染管理担当者ブロック別研修会、(2011.7.15. 東京)
13. 和泉雄一：現代歯周治療のスタンダード、平成23年度鎌倉市歯科医師会第1回学術講演会、(2011.7.16. 大船)
14. 和泉雄一：歯周治療の新スタンダード、平成23年度東京都歯科医師会卒後研修会、(2011.7.21. 東京)
15. 和泉雄一：歯周環境の整備と全身とのかかわり、いま求められる歯科医療―国民の生活を支える歯科医療―　日本歯科医学会平成23年度学術講演会、(2011.7.31. 鹿児島)
16. 渡辺　久：歯周治療への光触媒による光殺菌法の応用.科学技術振興機構 JSTイノーベーションブランチ茨城主催　新技術説明会in 浜松　招待講演　(2011.8.5. 浜松)
17. Watanabe H：Application of laser for periodontal treatment. Invited lecture（ Mahidol University, Bangkok, 2011.12.13)
18. Watanabe H： Laser application for periodontal surgery-basis and clinic. Invited lecture

(Chulalongkorn University, Bangkok, 2011.12.14)
19. 荒川真一：オゾンナノバブル水・酸素ナノバブル水-歯科治療応用への可能性- オゾンナノバブル水講演会、、(2011.7.10. 本学)
20. 青木 章.Er：YAGレーザーによる歯石除去と歯周ポケット治療.日本レーザー歯学会認定医講習講演.第63回日本口腔科学会学術集会 (2011.4.21. 東京)
21. Aoki A. Use of lasers in periodontal therapy. 1 3th International Biennial IAP Congress, Lviv, Ukraine, June 16-18, 2011.
22. Aoki A. Clinical Application of the Er：YAG laser in periodontal and peri-implant surgery. The 3 4th Annual Scientific Meeting of the Association for Dental Sciences of the Republic of China, Chung Shan Medical University, Taichung, Taiwan, Aug 26-28, 2011.
23. 片桐さやか.糖尿病と歯周病の関わり.北海道医療大学病院 北海道医療大学歯周歯内治療学分野セミナー 特別講演 (2011. 2. 18. 北海道)

16) 主催学会

1. 和泉雄一：第41回グローバルCOE海外研究者講演会 , Dr. Neil S. Norton, PhD, Associate Professor, Department of Oral Biology, School of Dentistry, Creighton University, Omaha, USA： Review of anatomic features using cone beam CT imaging. (2011.2.28. 本学)
2. 和泉雄一,渡辺 久：第48回グローバルCOE海外研究者講演会, Dr. Andreas F. Bindl and Dr. Lutz Ritter：Digital dentistry with CAD/CAM and cone beam computed tomography and their applications in implantology. (2011.10.11. 本学)

17) 新聞、雑誌、TV報道

1. 和泉雄一：歯周病が妊婦さんに与える影響. 東京医師歯科医師協同組合 TMDC MATE p.25
2. 和泉雄一：重い歯周病、動脈疾患5倍.読売新聞 2011年7月31日
3. 和泉雄一：買い物案内おとなの歯の磨き方と道具.暮らしの手帖. 51.4-5号p.113-115
4. 和泉雄一：職場の予防医学歯周病. 経営情報 p.15-16
5. 和泉雄一：歯周病の治療 早期治療で歯の喪失は防げる 再生医療の選択肢も. エコノミスト 2011,3/22 p.82-83
6. 和泉雄一：Q&A和泉雄一先生にここが聞きたい!,日本歯科評論 5月号 p.13-15
7. 和泉雄一, 長谷川梢, 古市保志、野口和行：妊婦トラブル対策は歯周病の予防•治療から,オーラルヘルスと全身の健康 改訂版2011 p.12-13
8. 和泉雄一：Q&Aでわかる「いい歯医者」2012 歯周病, 週刊朝日BOOK p.96-111
9. 和泉雄一, 片桐さやか：糖尿病医療連携診療支援ツール. 北多摩北部医療圏医療機能連携協議会 東京都多摩小平保健所 3月, 2011
10. 渡辺 久：歯周治療にレーザー応用 痛み少なく早期治癒 宮崎日日新聞 2011.1.4
11. 渡辺 久：歯科で広がる レーザー応用 歯周治療に保険初適用 下野新聞 2011.1.8
12. 渡辺 久：広がるレーザー治療 痛み少なく殺菌効果も 福島民報 2011.1.9
13. 渡辺 久：歯周治療 レーザー応用広がる 新潟日報 2011.1.9
14. 渡辺 久：レーザー歯周治療に 南日本新聞 2011.1.11
15. 渡辺 久：広がる歯科のレーザー応用 埼玉新聞 2011.1.12
16. 渡辺 久：歯科で広がるレーザー応用 山形新聞 2011.1.14
17. 渡辺 久：痛み少なく歯石を除去 熊本日日新聞 2011.1.15
18. 渡辺 久：歯科,広がるレーザー治療 岐阜新聞 2011.1.17
19. 渡辺 久：歯科のレーザー治療拡大 京都新聞 2011.1.18
20. 渡辺 久：広がる歯科レーザー応用 静岡新聞(夕刊) 2011.1.21
21. 渡辺 久：歯周治療にレーザーが有効 山梨日日新聞 2011.1.27
22. 渡辺 久：広がる歯科のレーザー利用 山陰中央新報 2011.2.3
23. 渡辺 久：歯周病治療にレーザー 信濃毎日新聞 2011.2.11
24. 渡辺 久：歯科用レーザー応用広がる 山陽新聞(夕刊) 2011.3.8
25. 渡辺 久：口内炎の特徴、病因、治療法“生島ひろしの朝だ元気だ”TBSラジオ am5：20-25 , 2011.1.24～1.28
26. 小田 茂,須田智也：学生と健康 若者のためのヘル

スリテラシー　国立大学法人 保健管理施設協議会/監修　南江堂　2011年4月

27. 小田　茂,須田智也：正しいカルテ記載マスターガイド 湯島保険診療研究会編　クインテッセンス出版株式会社　2011年8月10日
28. 谷口威夫, 和泉雄一, 中川孝男, 赤羽正治：重新思考牙周病. GC CIRCLE No.17 p.4-10, 2011
29. 荒川真一.　医療新世紀　極微小の泡で歯周病治療　強い殺菌力と高い安全性　オゾンナノバブル水.共同通信、静岡新聞　2011.11.30
30. 荒川真一.オゾンナノバブル水・酸素ナノバブル水 - 歯科治療応用への可能性- ナノバブル研究会　医学部附属病院16階大会議室 2011.12.2

18）教室、分野や講座の准教授、講師、助教、特別研究員、ポスドク、指導を受けた大学院生の名前

准教授　渡辺　久
講　師　萩原　さつき
　　青木　章
助　教　荒川　真一
　　小林　宏明
　　竹内　康雄
　　秋月　達也
　　片桐　さやか
大学院　小柳　達郎
　　○鈴木　允文
　　谷口　陽一
　　○南原　弘美
　　早雲　彩絵
　　姫野　彰子
　　○Aslam AL Mehdi
　　○GA Rajakaruna
　　○Bharti Pariksha
　　高橋　茉莉香
　　○妻沼　有香
　　澤辺　正規
　　○山田　梓
　　小林　奈穂
　　藤原　香
　　花谷　智哉
　　伊藤　康夫
　　江尻　健一郎
　　○Chui Chanthoel
　　吉田　明日香
　　池田　裕一
　　木村　康之
　　遠藤　亜希子
　　清水　揚子
　　○芦垣　紀彦
　　丸山　緑子
　　○荻田　真弓
　　津野　顕子
　　芝　多佳彦
　　○Supreda Suphanantachat
　　○葉　暢暢
　　小沼　邦葉
　　前川　祥吾
　　松浦　孝典
　　星　嵩

○はAISS

19）GCOE活動についての感想、コメント、改善を望む点

若手研究者の育成には大いなる成果が認められ、また、国際交流の点でも徐々に成果を上げつつある。ただ、日頃の研究資金の増額を望みたい。

Biochemical and Biophysical Research Communications 417 (2012) 765–770

Contents lists available at SciVerse ScienceDirect

Biochemical and Biophysical Research Communications

journal homepage: www.elsevier.com/locate/ybbrc

Structural differences in the osteocyte network between the calvaria and long bone revealed by three-dimensional fluorescence morphometry, possibly reflecting distinct mechano-adaptations and sensitivities

Akiko Himeno-Ando [a,b,c], Yuichi Izumi [b,c], Akira Yamaguchi [a,c,*], Tadahiro Iimura [a,c,*]

[a] Section of Oral Pathology, Graduate School of Medical and Dental Sciences, Tokyo Medical and Dental University, Japan
[b] Section of Periodontology, Graduate School of Medical and Dental Sciences, Tokyo Medical and Dental University, Japan
[c] Global Center of Excellence (GCOE) Program, International Research Center for Molecular Science in Tooth and Bone Diseases, Tokyo Medical and Dental University, Japan

ARTICLE INFO

Article history:
Received 30 November 2011
Available online 16 December 2011

Keywords:
Osteocyte
Fluorescence imaging
Morphometry
Shear stress

ABSTRACT

The structural features of osteocytes and their cellular process network are thought to allow for mechanotransduction from the bone tissue to these cells. This study applied three-dimensional fluorescence microscopy to fixed and decalcified bone specimens to quantitatively compare the osteocytes and their networks between mouse parietal bone and tibia that are physiologically enforced by distinct mechanical loads. The subsequent morphometric analysis by the surface rendering of osteocyte cell bodies revealed the tibia to have relatively enriched cytoplasm in the osteocyte cell body in comparison to the parietal bone. Furthermore, quantitative tracing of the cellular processes *in silico* demonstrated that the numbers of the cellular processes and their bifurcation points per osteocyte in the tibia were significantly higher than those in the parietal bone. Though the total length of the processes per osteocyte in the tibia was two times longer, its total surface area and total volume were smaller than those in the parietal bone, due to its thinner diameter. These architectural differences in the osteocytes and their networks are thus implicated in the adaptation to physiologically different loading, and may also induce distinct mechanosensitivities.

© 2011 Elsevier Inc. All rights reserved.

1. Introduction

Osteocytes are embedded in the hard bone matrix of the lacunae, and form an intercellular network by extending slender cellular processes within narrow bony tubes of the canaliculi [1–4]. This structure ensures intercellular communication among bone cells including osteoblasts and osteoclasts. Osteocytes account for 90–95% of all bone cells and they are thought to sense mechanical loads and accordingly transmit the signals to osteoblasts and osteoclasts through the osteocyte network, and thus regulate bone remodeling [5–10]. Osteocytes also play a key role in phosphate metabolism by producing an endocrine factor, fibroblast growth factor 23 (FGF23), whose target organ is the kidney [11].

How osteocytes sense external loads remains unknown; however, the mechano-transduction of physical loads to the bone tissue must be tightly influenced by the structural features of bone including the lacunocanalicular and osteocyte network. Loading-induced fluid flow through the canalicular network has been thought to result in a fluid shear stress on the surface of osteocyte processes [12]. The interaction of the pericellular matrix and the osteocyte cellular process could amplify the physiological amplitude of loads to the bone tissue, thus producing sufficient levels of force to induce cellular response [13–16].

The skeletal system contains bones that are inherently loaded by distinct mechanical force patterns [17,18]. Long bones are loaded predominantly along the longitudinal direction with much higher amplitude than flat bones such as calvariae that are loaded radially and tangentially by intracranial pressure and mastication. The human fibula is estimated to have a load that is nearly twice that of the skull bone [19]. Extracellular mechanical forces are coupled to the intracellular organization of the cytoskeleton that regulates cellular connections to other cells and the extracellular matrix, thus affecting cell shape and functional outputs [20,21]. This suggests that the morphology of osteocytes, the patterning of the osteocyte network and their function are determined by external loading whose directional patterns and amplitudes are physiologically different in each bone. It is, therefore, relevant and intriguing to quantitatively manifest the structural differences of osteocytes and the osteocyte networks in distinct bones such as parietal bone and tibia.

* Corresponding authors. Address: Section of Oral Pathology, Graduate School of Medical and Dental Sciences, Tokyo Medical and Dental University, 1-5-45 Yushima, Bunkyo-ku, Tokyo 113-8549, Japan. Fax: +81 3 5803 0188.
E-mail addresses: akira.mpa@tmd.ac.jp (A. Yamaguchi), iimura.gcoe@tmd.ac.jp (T. Iimura).

0006-291X/$ - see front matter © 2011 Elsevier Inc. All rights reserved.
doi:10.1016/j.bbrc.2011.12.031

This study applied three-dimensional fluorescence microscopy to fixed and decalcified bone specimens followed by surface rendering of osteocyte cell bodies and tracing of osteocyte cellular processes *in silico* for better imaging acquisition of the osteocyte network to compare the mouse parietal bone and tibia. These morphometric analyses revealed significant quantitative architectural differences in the osteocytes and their networks in these bones.

2. Materials and methods

2.1. Animals and preparation of skeletal tissues

Mice (laboratory strain C57BL6J) were purchased from a local distributor. The parietal bones and tibiae were dissected from 8-week-old mice after anesthetizing the animals with 0.1% ethylanthranilate. Bone specimens were fixed in 4% paraformaldehyde for 4 °C. The specimens were washed with phosphate-buffered saline, and decalcified in 20% ethylenediaminetetraaceticacid (EDTA) for 14 days for 4 °C. The decalcified specimens were embedded in an optimal cutting temperature (OCT) compound (Sakura Finetek, Tokyo, Japan) to obtain cryosections. Frontal sections of the parietal bones and longitudinal sections of tibiae (10–20 μm) were prepared, respectively. The subsequent observations were focused on the outer cortical plates of parietal bones and the diaphysis of tibiae.

2.2. Staining for actin filaments with fluorescent dye-conjugatedphalloidin

The specimens were stained with phalloidin AlexaFluor 488 (Invitrogen, Carlsbad, CA, USA) for visualizing actin-rich cell bodies and cellular processes, and BOBO-3 (Invitrogen) for counter staining of nuclear DNA with 20 μg/ml of RNAaseI (Invitrogen) at room temperature for 2 h, as previously described [22].

2.3. Confocal laser scanning images

Confocal optical sectioning was performed with a system of LSM5 Pascal5 confocal laser scanning microscopy (Carl Zeiss, Oberkochen, Germany) with a PlanFluor objective (63×, N.A. = 1.4). Two laser lines, 488 nmand 543 nm were used. The theoretical *xy*- and *z*-axes resolutions were 0.178 and 0.700 μm, respectively. The refraction index correction was 0.934. The frame size of the image was 146.2 × 146.2 μm with 512 × 512 pixels and 8-bit color depth. Pixel size was 0.286 μm. Confocal images were taken with a 0.29 μm step size for voxel sampling and then were processed four times with Kalman averaging.

2.4. Three-dimensional (3D) reconstruction followed by the morphometry of osteocytes and the cellular network tracing in silico

The 3D structure of the osteocyte network was constructed from a z-series of CLS images using IMARIS software (Bitplane, Zürich, Switzerland). The diameters of the osteocyte cell body and point-to-point distances between osteocytes were measured using the Measurement Pro function of IMARIS by rotating the 3D-reconstructed images. The surface area and volume of single osteocytes were measured by surface rendering using the Surface function of IMARIS. The threshold for the surface rendering of osteocytes was determined by super imposing the surface images to the 3D-reconstructed images until these two images overlapped. Any cellular processes measuring less than 0.5 μm in diameter were excluded in this rendering to separate the cell body and cell processes. The Filament Tracer function of IMARIS was originally developed to analyze neurite morphology and designed to reconstruct 3D dendritic tree models. This software package was employed to obtain dendritic tree models of the osteocyte network and to quantitate the pattern of the osteocyte cellular processes by measuring the numbers of endpoints, branching points, segments between a branching point to another branching point, and the diameter, surface area and volume of each segment. The beginning point at each osteocyte was set in the 3D-reconstructed images to trace the cellular processes radiating from single osteocytes, and the endpoints of the cellular process were set in several different sizes of the diameter (0.2, 0.3, 0.4 and 0.5 μm). The average total length of the processes, the average surface area, the average volume, the average number of endpoints, the average number of branching points and the average number of segments per osteocyte were calculated by dividing each total value by the number of osteocytes analyzed.

2.5. Statistics

The mean values of the morphometric parameters were statistically analyzed using paired *t*-test. Differences were considered to be significant if $p < 0.01$.

3. Results

The decalcified parietal bones and tibiae of the 8-week-old mice stained by a fluorescent dye-conjugated phalloidin were scanned by the high-resolution optical slices of the confocal z-series, which clearly showed the presence of the intercellular osteocyte networks in parietal bone and tibia (Fig. 1A and B, respectively). The 3D reconstitution and the surface rendering of the osteocytes obtained from the confocal z-series images revealed the morphology of the osteocyte cell body in the parietal bone and tibia (Fig. 1C and D, respectively). The morphology of the osteocytes in the parietal bone appeared relatively spherical or oval shaped, whereas those in the tibia were elongated and spindle-shaped. This morphological distinction was quantitatively confirmed by determining the longest and shortest diameters in the 3D-reconstructed images (Table 1). The diameters of the osteocyte cell bodies in the parietal bone and tibiae ranged from 6.46 ± 0.39 to10.78 ± 0.37 μm, and from 5.71 ± 0.30 to 15.52 ± 0.92 μm, respectively. Though the shortest diameter showed no significant difference, the longest diameter of the osteocyte cell body in the tibia was 44% longer than that in the parietal bone. The ratio of the longest to the shortest diameter obviously demonstrated that the osteocytes in the tibia were more elongated than those in the parietal bones. The distances between neighboring osteocytes in the two types of bone showed no significant differences (Table 1). This study next analyzed the volume and the surface area of the osteocyte cell bodies (Table 1). The volume and the surface area of the tibial osteocytes were significantly higher than those of the parietal osteocytes. There was no significant difference in the nuclear volumes of both groups of the osteocytes (Fig. 1E and F), thus the ratios of the cellular volume was compared to the nuclear volume. This comparison demonstrated that the cytoplasmic volume in the tibial osteocytes was nearly 50% larger than that in the parietal osteocytes.

The osteocyte cellular processes were traced using the Filament Tracer function to quantitatively compare the intercellular osteocyte networks in the parietal bone and tibia. The beginning point at each single osteocyte was set in the 3D-reconstituted images, and the endpoint diameter of the cellular process was set in several different sizes (Fig. 2). Preliminary manual measurements of 3D-reconstructed images revealed the size of the cellular processes originating from the cell surface to range from approximately 0.8–0.5 μm in diameter, and that the size of recognizable slender

A. Himeno-Ando et al. / Biochemical and Biophysical Research Communications 417 (2012) 765–770

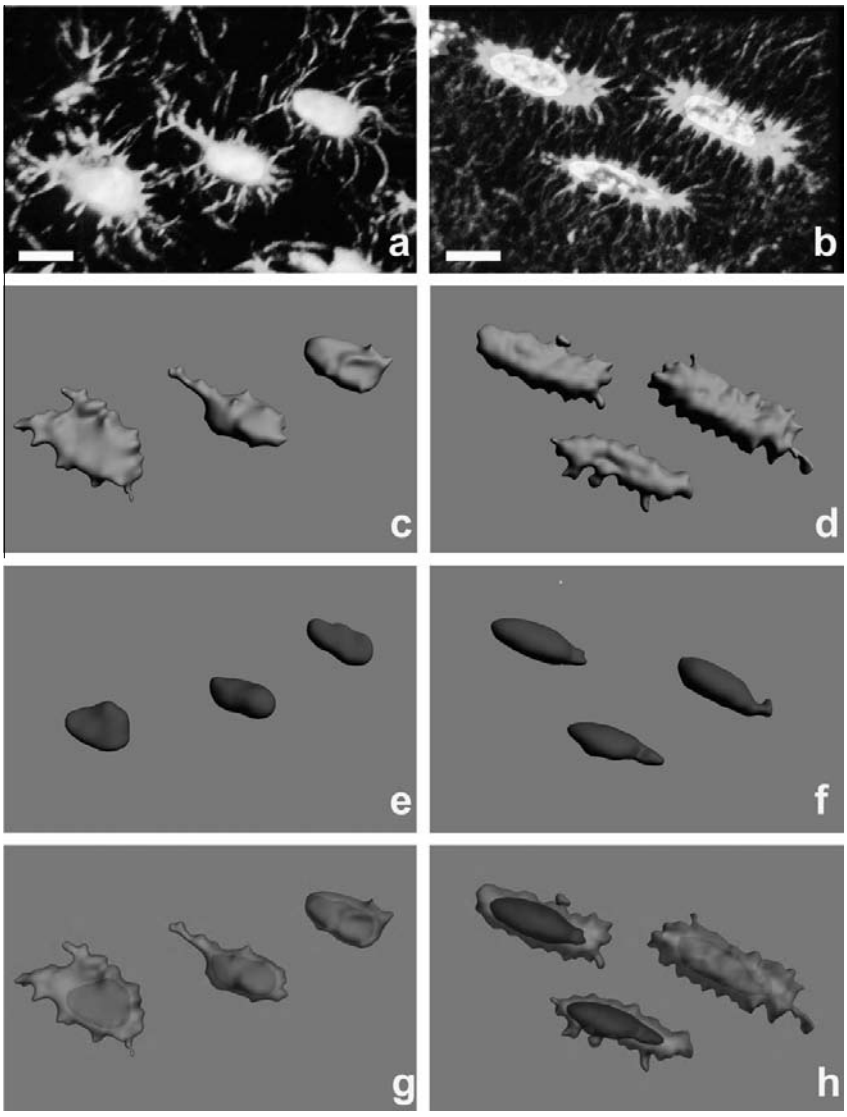

Fig. 1. Three dimensional (3D) reconstitution and surface rendering of osteocytes in the parietal bone (A, C, E and G) and tibia (B, D, F and H). The actin-rich cell body and cellular processes of osteocytes are visualized by a fluorescent dye-conjugated phalloidin (Pallioidin AlexaFluor 488) in green. Nuclei were conterstained by a cyanine nucleic acid dye (BOBO-3) in red. (A, B) Representative 3D-reconstituted images of the confocal z-series slices from parietal bone (A) and tibia (B) show osteocytes and theircellular process networks. Bar, 10 μm. (C, D) Surface renderings of osteocyte cell bodies of parietal bone (C) and tibia (D) from the 3D-reconstituted images (A and B, respectively) enable morphometric analyses (see Table 1). (E, F) Surface renderings of osteocyte nuclei of parietal bone (E) and tibia (F) from the 3D-reconstituted images (A and B, respectively) are shown. (G, H) Merged images (G and H) of the surface renderings of cell bodies and nuclei (C–E and D–F, respectively) are shown with 50% transparency of the cell bodies to visualize relative position of nucleus in cell body. (For interpretation of the references to colour in this figure legend, the reader is referred to the web version of this article.)

cellular processes forming the intercellular network and connections was nearly 0.2 μm in diameter. Therefore, the endpoints were set at 0.2, 0.3, 0.4 and 0.5 μm in diameter. Fig. 2 shows the dendritic tree models in different settings of the endpoint diameter. These tree models demonstrated that increasing number of the cellular processes and their bifurcations and more intensive and detailed appearances of the network were observed as the endpoint diameter setting got smaller in diameter. However, the settings of 0.2 and 0.3 μm in diameter revealed that the detailed rough surfaces of the osteocyte cell bodies that did not participate in the intercellular network were traced as the cellular processes. Furthermore, quite a few of the traced networks did not fit into the recognizable osteocyte network in the 3D-reconstructed images with connecting small separated fluorescence signals. Consistently, the quantification and statistical data at these settings often showed unreasonably small values in comparison to the actual

Table 1
Morphometric data of the osteocytes in mouse parietal bone and tibia.

	Parietal bone	Tibia
Shortest diameter (μm)	6.46 ± 0.39	5.71 ± 0.30
Longest diameter (μm)	10.78 ± 0.37	15.52 ± 0.92*
Diameter ratio, long/short	1.67	2.67
Cell-cell distance (μm)	22.09 ± 1.30	21.06 ± 1.20
Cell volume (μm^3)	242.93 ± 21.63	413.25 ± 41.69*
Cell surface area (μm^2)	279.41 ± 24.91	458.26 ± 53.60*
Nuclear volume (μm^3)	115.74 ± 7.60	135.54 ± 11.94
Volume ratio, cell/nucleus	2.1	3.05

The values are the mean ± SEM of 20 osteocytes in each bone.
* $P < 0.01$.

resolution of this microscopy system and image processing (data not shown). Therefore, the osteocyte network was further evaluated by the endpoint setting at 0.4 μm in diameter.

This *in silico* tracing of the cellular processes by Filament Tracer function was used to calculate the average length, the average volume, the average surface area and the average diameter of each segment (Table 2). All the values exhibited significant differences indicating that the tibia has a thinner cellular process network with a higher branching rate, in comparison to the parietal bone. The numbers of endpoints, branching points and segments per osteocyte in the tibia revealed higher scores than those in the parietal bones, suggesting more a comprehensive network in the tibia (Table 3). The total length of the cellular processes per osteocyte

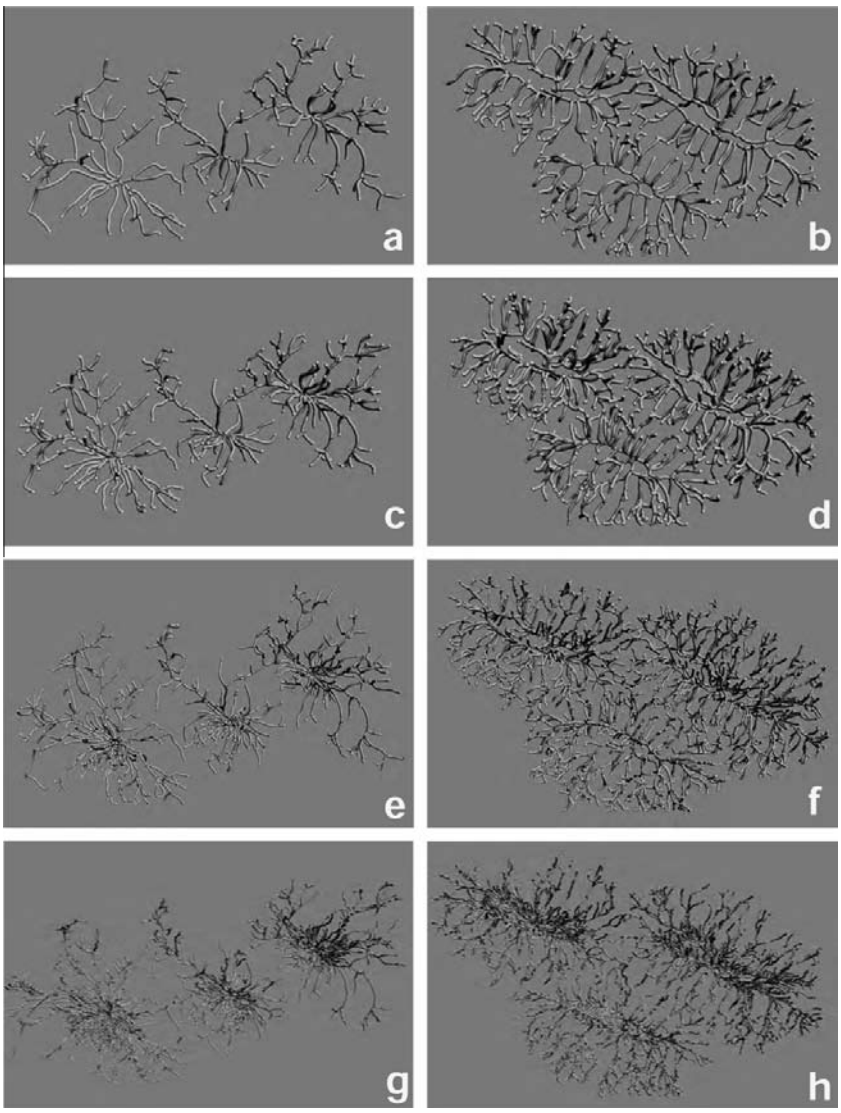

Fig. 2. Dendritic tree models of the osteocyte cellular processes in parietal bone (A, C, E and G) and tibia (B, D, F and H) from the 3D-reconstituted images (Fig. 1A and B, respectively). Dendritic tree models with different endpoint diameter settings at 0.5 μm (A and B), 0.4 μm (C and D), 0.3 μm (E and F) and 0.2 μm (G and H) are shown. Green dots, red dots and white bars indicate end points branching points and cellular process segments, respectively (see Tables 2 and 3). (For interpretation of the references to colour in this figure legend, the reader is referred to the web version of this article.)

Table 2
Morphometric values of the osteocyte networks in mouse parietal bone and tibia.

	Parietal bone	Tibia
Average length (μm)	2.57 ± 0.10	2.04 ± 0.05*
Average volume (μm^3)	2.39 ± 0.18	0.36 ± 0.02*
Average surface area (μm^2)	6.07 ± 0.35	2.26 ± 0.08*
Average diameter (μm)	0.95 ± 0.05	0.39 ± 0.01*

Average values per segment with the endpoint diameter setting at 0.4 μm are shown. A segment is defined as a cellular process segment from a branching point to another branching point or an endpoint. The values are the mean ± SEM.
* $P < 0.01$.

Table 3
Morphometric data of the osteocyte networks in mouse parietal bone and tibia (Total values of cellular processes per single osteocyte).

	Parietal bone	Tibia
Total length (μm)	311.06	637.67
Total volume (μm^3)	288.87	112.49
Total surface area (μm^2)	734.63	708.49
Total endpoints	64.00	162.00
Total branching point	58.00	152.33
Total segments	121.00	313.33

Total average values of cellular processes per single osteocyte were calculated from the values shown in Table 3.

was longer than that in the parietal bones. However, the total volume and the total surface area of the cellular processes per osteocyte in the tibia revealed lower scores than those in the parietal bone, due to the thinner diameter of the cellular process in the tibia. These findings indicated that the tibia has a longer and thinner intercellular network than that in the parietal bone.

4. Discussion

Vatsa et al. reported the morphometric differences in osteocytes and lacunae between the fibula and calvaria by combinatorial scanning of live bone fragments from 3 to 6-month-old mice using confocal microscopy and nano-computed tomography [23]. This revealed that osteocytes in the fibula had a spindle shape and stretched along the longitudinal axis of the principal loading direction, whereas those in the calvaria were spherical without any particular alignment in direction. The current study conducted two-color fluorescence morphometry by using three-dimensional confocal scanning followed by surface rendering of the osteocyte cell bodies and nuclei. This analysis revealed that the average volume and surface area of single osteocytes in the tibia was significantly larger than those in the parietal bone, which was mainly due to more cytoplasm in the tibial osteocytes. Cells engaging in active functions such as secretion and absorption tend to have relatively large volumes of cytoplasm probably due to their well-developed cell organelles. Therefore, the significant difference in the cytoplasmic volume of osteocytes between the tibia and parietal bone suggests a functional diversity in these cells to modulate bone metabolism.

A line of studies by Sugawara et al. performed quantitative morphometry for the cellular processes of osteocytes and provided a method to calculate the average length of the cellular processes per single osteocyte [24,25]. The current study attempted to measure and compare the sizes of the cellular processes of osteocytes in the parietal bone and tibia by tracing the cellular processes *in silico*. Considering the theoretical resolution of the microscopy system and the voxel size of the 3D reconstituted images, measurement of structures smaller than 0.4 μm was not expected to provide trust worthy data. In fact, the *in silico* tracings achieved by setting the endpoint at 0.3 and 0.2 μm did not fit for the visually recognizable network of the cellular process in the 3D reconstituted images. These settings revealed artificial connections of fluorescence signals that affected reasonable measurements. Though some part of the recognizable network smaller than 0.4 μm in diameter was not entirely traced, the morphometric analysis of the cellular processes revealed significant differences in the architectures of the osteocyte networks between the parietal bone and tibia.

The analysis revealed that osteocytes in the tibia radiate a significantly larger number of the cellular processes and branches in comparison to the parietal bone. Furthermore, the surface area and volume of each segment of the cellular process in the tibia was significantly smaller than those in the parietal bone, due to its smaller diameter. These data possibly indicate that tibia developed a more comprehensive and detailed osteocyte intercellular network in comparison to the parietal bone. Mechanical forces on cells influence their cytoskeletal structure, and thus their cellular shape and connection to the surrounding cells [20,21]. Immature osteocytes possibly align themselves and develop their intercellular network in response to distinct loading patterns during bone development, when they are being embedded in osteoid. The osteocyte cell body plays a key role for initial mechano-sensing during this process, as discussed by Vatsa et al. [23]. Hirose et al. reported a gradual arrangement and flattening of cortical osteocytes along the longitudinal axis of long bone with age [26]. Therefore, the architectural differences in the osteocytes and their cellular process networks between the parietal bone and tibia are probably adaptations to the physiologically different loading patterns. In our previous work, zebrafish have a poorly developed osteocyte lacunocanalicular network, whereas amphibians, reptiles and mammals all show well-developed lacunocanalicular systems, which could be intriguing because such osteocytic adaption to the mechanical loads might be involved in the phylogenetic diversity of bone [22].

The architectural differences in the network of osteocyte cellular processes may transduce extraosseous loads to cellular responses with distinct efficiency. The ultrastructure of osteocyte processes, the pericellular matrix and the encasing canaliculi provides the basic elements for fluid flow-based theoretical models [13,15,16]. Physical dynamics predicts that the extraosseous load could cause a shear strain and a hoop strain on the surface of the processes [12,13]. These two strains are in inverse proportion to the surface area and the inner diameter, respectively, in each basic physical model. Therefore, the surface area and the diameter of the cellular process could provide critical values with the mechanosensitivity of osteocytes. On the other hand, there is little view available regarding how the other quantitative values, such as the length, the number and the branching rate of the cellular processes affect the mechanosensitivity. These values also possibly reflect the comprehensiveness of the intercellular network system rather than simply the local ultrastructure. Therefore, these factors are likely to influence the cellular and intercellular flow of molecules associated with mechanosensitivity and biological functions [27]. The current findings collectively provoke views for the architectural differences in the osteocyte networks as the systems of molecular transduction and mechanotransduction, which may be associated with the functional diversity of the osteocyte itself.

In conclusion, our quantitative analyses based on the three-dimensional fluorescence microscopy revealed significant differences in the structural architecture of the osteocyte networks in the parietal bone and tibia. These morphometric differences in the osteocyte networks between flat bone and long bone probably reflect adaptations to different physiological loading patterns to these bones, and suggest different activities of the networks. The current analysis is therefore considered to provide new insights

into the physiological, pathological and phylogenetic mechanisms of mechanosensing and metabolism in bone [28,29].

Acknowledgments

The authors express sincere thanks to Ms. Kayoko Suenaga at Carl Zeiss MicroImaging Co., Ltd. for her valuable expertise on microscopy and image processing, and Drs Mayu Sugiyama and Hiroshi Kurokawa for their constructive comments on this work. The current work was supported by a grant from the Ministry of Education, Culture, Sports, Science, and Technology (MECSST), Global Center of Excellence (GCOE) Program, "International Research Center for Molecular Science in Tooth and Bone Diseases" to all the authors, a Grant-in-Aid for Scientific Research on Innovative Areas "Fluorescence Live imaging" (No. 22113002) of MECSST to T.I., and the Naito Foundation Subsidy for Promotion of Specific Research Projects (Osteobiology). A.Y. and T.I. were supported by a Grant-in-Aid for Scientific Research from the Japan Society for the Promotion of Science (JSPS). T. I. was also supported in part by the Takeda Science Foundation, the Mochida Memorial Foundation for Medical and Pharmaceutical Research, Yamada bee farm support project for honeybee research, and Grants H21-nanchi-097 and H22-nanchi-ippan157 from the Ministry of Health, Labor and Welfare.

References

[1] L.F. Bonewald, Osteocyte messages from a bony tomb, Cell Metab. 5 (2007) 410–411.
[2] L.F. Bonewald, Osteocytes as dynamic multifunctional cells, Ann. NY Acad. Sci. 1116 (2007) 281–290.
[3] L.F. Bonewald, The amazing osteocyte, J. Bone Miner Res. 26 (2011) 229–238.
[4] L.F. Bonewald, M.L. Johnson, Osteocytes, mechanosensing and Wnt signaling, Bone 42 (2008) 606–615.
[5] S. Tatsumi, K. Ishii, N. Amizuka, M. Li, T. Kobayashi, K. Kohno, M. Ito, S. Takeshita, K. Ikeda, Targeted ablation of osteocytes induces osteoporosis with defective mechanotransduction, Cell Metab. 5 (2007) 464–475.
[6] S.C. Cowin, L. Moss-Salentijn, M.L. Moss, Candidates for the mechanosensory system in bone, J. Biomech. Eng. 113 (1991) 191–197.
[7] E.H. Burger, J. Klein-Nulend, Mechanotransduction in bone-role of the lacuno-canalicular network, FASEB J. 13 Suppl (1999) S101–S112.
[8] T. Nakashima, M. Hayashi, T. Fukunaga, K. Kurata, M. Oh-Hora, J.Q. Feng, L.F. Bonewald, T. Kodama, A. Wutz, E.F. Wagner, J.M. Penninger, H. Takayanagi, Evidence for osteocyte regulation of bone homeostasis through RANKL expression, Nat. Med. 17 (2011) 1231–1234.
[9] J. Xiong, M. Onal, R.L. Jilka, R.S. Weinstein, S.C. Manolagas, C.A. O'Brien, Matrix-embedded cells control osteoclast formation, Nat. Med. 17 (2011) 1235–1241.
[10] C. Lin, X. Jiang, Z. Dai, X. Guo, T. Weng, J. Wang, Y. Li, G. Feng, X. Gao, L. He, Sclerostin mediates bone response to mechanical unloading through antagonizing Wnt/beta-catenin signaling, J. Bone Miner. Res. 24 (2009) 1651–1661.
[11] S. Fukumoto, T.J. Martin, Bone as an endocrine organ, Trends Endocrinol. Metab. 20 (2009) 230–236.
[12] K. Piekarski, M. Munro, Transport mechanism operating between blood supply and osteocytes in long bones, Nature 269 (1977) 80–82.
[13] Y. Han, S.C. Cowin, M.B. Schaffler, S. Weinbaum, Mechanotransduction and strain amplification in osteocyte cell processes, Proc. Natl. Acad. Sci. USA 101 (2004) 16689–16694.
[14] E.J. Anderson, S. Kaliyamoorthy, J. Iwan, D. Alexander, M.L. Knothe Tate, Nano-microscale models of periosteocytic flow show differences in stresses imparted to cell body and processes, Ann. Biomed. Eng. 33 (2005) 52–62.
[15] L. You, S.C. Cowin, M.B. Schaffler, S. Weinbaum, A model for strain amplification in the actin cytoskeleton of osteocytes due to fluid drag on pericellular matrix, J. Biomech. 34 (2001) 1375–1386.
[16] L.D. You, S. Weinbaum, S.C. Cowin, M.B. Schaffler, Ultrastructure of the osteocyte process and its pericellular matrix, Anat. Rec. A Discov. Mol. Cell Evol. Biol. 278 (2004) 505–513.
[17] M. Petrtyl, J. Hert, P. Fiala, Spatial organization of the haversian bone in man, J. Biomech. 29 (1996) 161–169.
[18] R. Hillam, M. Jackson, A. Goodship, and T. Skerry, Comparison of physiological strains in the human skull and tibia, Bone 19 (1) (1996) 686-686.
[19] K.L. Lambert, The weight-bearing function of the fibula. A strain gauge study, J. Bone Joint. Surg. Am. 53 (1971) 507–513.
[20] N. Wang, J.P. Butler, D.E. Ingber, Mechanotransduction across the cell surface and through the cytoskeleton, Science 260 (1993) 1124–1127.
[21] C.S. Chen, J. Tan, J. Tien, Mechanotransduction at cell-matrix and cell-cell contacts, Annu. Rev. Biomed. Eng. 6 (2004) 275–302.
[22] L. Cao, T. Moriishi, T. Miyazaki, T. Iimura, M. Hamagaki, A. Nakane, Y. Tamamura, T. Komori, A. Yamaguchi, Comparative morphology of the osteocyte lacunocanalicular system in various vertebrates, J. Bone Miner. Metab. (2011).
[23] A. Vatsa, R.G. Breuls, C.M. Semeins, P.L. Salmon, T.H. Smit, J. Klein-Nulend, Osteocyte morphology in fibula and calvaria – is there a role for mechanosensing?, Bone 43 (2008) 452–458
[24] Y. Sugawara, R. Ando, H. Kamioka, Y. Ishihara, T. Honjo, N. Kawanabe, H. Kurosaka, T. Takano-Yamamoto, T. Yamashiro, The three-dimensional morphometry and cell-cell communication of the osteocyte network in chick and mouse embryonic calvaria, Calcif. Tissue Int. 88 (2011) 416–424.
[25] Y. Sugawara, H. Kamioka, T. Honjo, K. Tezuka, T. Takano-Yamamoto, Three-dimensional reconstruction of chick calvarial osteocytes and their cell processes using confocal microscopy, Bone 36 (2005) 877–883.
[26] S. Hirose, M. Li, T. Kojima, P.H. de Freitas, S. Ubaidus, K. Oda, C. Saito, N. Amizuka, A histological assessment on the distribution of the osteocytic lacunar canalicular system using silver staining, J. Bone Miner. Metab. 25 (2007) 374–382.
[27] T. Adachi, Y. Aonuma, K. Taira, M. Hojo, H. Kamioka, Asymmetric intercellular communication between bone cells: propagation of the calcium signaling, Biochem. Biophys. Res. Commun. 389 (2009) 495–500.
[28] T. Iimura, A. Nakane, M. Sugiyama, H. Sato, Y. Makino, T. Watanabe, Y. Takagi, R. Numano, A. Yamaguchi, A fluorescence spotlight on the clockwork development and metabolism of bone, J. Bone Miner. Metab. (2011).
[29] R.P. van Hove, P.A. Nolte, A. Vatsa, C.M. Semeins, P.L. Salmon, T.H. Smit, J. Klein-Nulend, Osteocyte morphology in human tibiae of different bone pathologies with different bone mineral density – is there a role for mechanosensing?, Bone 45 (2009) 321–329

硬組織病態生化学分野

柳下 正樹

医歯学総合研究科・生体支持組織学系専攻
硬組織病態生化学・教授

1）研究の課題名

歯周病学分野とのイノベーション研究

和文：歯周組織炎症部位におけるスフィンゴシン-1-リン酸シグナルの役割

Roles of sphingolipid-signaling at the inflammation site of periodontal diseases

歯周病は歯周病原菌の感染による歯周組織の炎症を特徴とする慢性炎症性疾患で、日本人における歯周病罹患率は非常に高く45歳以上では40%を越えている（厚生労働省の平成17年歯科疾患実態調査）。歯周病の進行とともに歯周ポケットは深さを増し、ポケット内に嫌気性菌を中心として歯周病原菌が増加する。これに反応して歯周炎局部には様々な免疫応答が惹起され結果的に歯周組織の破壊が生じ、最後には歯の喪失に至る。また歯周疾患の炎症部位に由来する細菌由来成分や炎症性サイトカインが血流を介して全身に作用し糖尿病、心臓血管病、低体重児出産・早産、呼吸疾患、骨粗しょう症などの疾患の誘発に関与すると考えられている。歯周病および歯周病と関連する全身疾患の治療や予防のためには原因となる炎症部位の特殊性、すなわち「嫌気性細菌が繁殖する場となる低酸素領域（歯周ポケット）に隣接していること」の意味を明らかにすることが不可欠である。

本研究では歯周ポケットに嫌気性菌が感染した際にみられる局所細胞の病態生理学的変化を細胞レベルで明らかにしようとするものである。本年までの我々の研究で、転写因子/late inflammatory mediatorであるHMGB（high-mobility group box）1タンパク質が嫌気性菌に直接暴露されるjunctional epitheliumと細菌侵襲の少ない口腔部位の上皮ではその細胞内分布が大きく異なることを発見した（添付パワーポイントファイル）。これはHMGB1が口腔内粘膜免疫に大きく関与している可能性を示唆した。また、歯周病原菌から放出される内毒素（LPS）、外毒素、短鎖脂肪酸などはin vitroの実験系において細胞内の活性酸素産生を引き起こす。LPSに対して組織から放出される炎症性サイトカインも組織自身に作用して活性酸素産生を促進する。また歯周ポケット内が低酸素状態であることにより隣接する歯周組織の活性酸素産生が亢進する可能性がある。そこで歯周疾患の炎症部位は歯周ポケットに存在する細菌の種類や繁殖状況および免疫系、循環系の状態などの複数の因子の寄与を反映した酸化ストレスの状況を呈すると考えられる。しかし現在までに歯周疾患の病態と炎症部位の酸化ストレス状態とを直接結びつける知見はほとんど報告されていない。

本年度に得られた新知見としては、歯周病の炎症部位の酸化ストレスの実験系として歯肉癌由来細胞株を用い酪酸刺激をストレス状態とした実験系を解析したところ、ストレス刺激により放出されるHMGB1には有意に酸化型と考えられる分子が増加していた（項目12、学会発表）。酸化型HMGB1はToll-like受容体活性化機構が還元型のものとは明らかに異なることが予測されており、細菌性歯周炎の慢性化機構の解明に大きな意義をもつと考えられる。来年度はこの点に関してさらに精査を進める。

2）

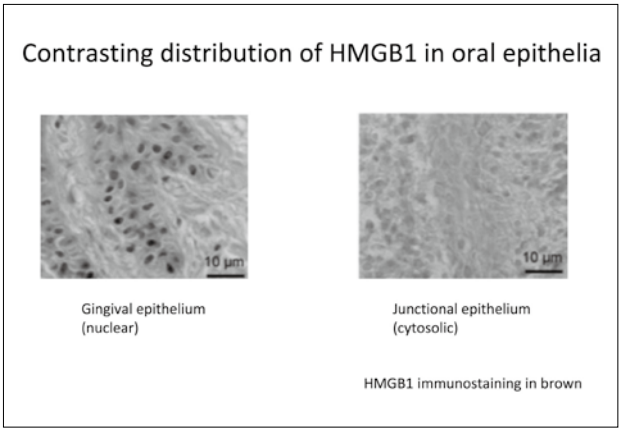

3）発表の研究内容についての英文要約

We have been studying roles of HMGB（high-mobility group box）1 eliciting chronic inflammation in bacterial gingivitis. During the years of 2011, we set up an experimental system representing oral epithelium under oxidative stress of bacterial infection, using a gingiva-derived cancer cell line under stimulation with butyric acid. Analysis was focused on the release of HMGB1 in vitro and its oxidative status upon stimulation with butyric acid. Results indicated that the secretion of HMGB1 by the cell was enhanced by the stimulation and the released molecule contained oxidized HMGB1. Since the activation mechanism of Toll-like receptors（of inflammatory cells）by oxidized HMGB1 differs from that by the one in reduced form, modulation of chronic inflammatory responses of gingival epithelium by HMGB1 may play an important role. This will clarify factors involved in initiation and continuation of immunological responses、especially those involving HMGB1, toward bacterial infection in periondontium.
We also continued our study identifying the presence of a molecular complex on the cell surface involving heparan sulfate proteoglycans, and the role of heparan sulfate chains on the integrity of membrane raft structure. Biochemical properties of heparan sulfate proteoglycans point to the presence of intimate molecular interactions in specialized domains of cell surface and their importance in the cellular signaling mechanisms. Research results, using isolation procedures of plasma membrane and identification of several membrane proteins together with heparan sulfate proteoglycans, indicated that cholesterol-rich, cell surface microdomains constitute one of specialized functional units of the plasma membrane and are associated with a species of cell surface heparan sulfate proteoglycan, syndecan-4. Biological significance of heparan sulfate proteoglycans in specialized membrane domains will be further investigated.

4）本事業に関連して世界的な研究拠点形成に向けて、以下の点で改善・整備等されたこと

A（研究拠点体制）

異なる分野のInnovationの確立する研究「歯周組織炎症部位におけるスフィンゴシン-1-リン酸シグナルの役割」を提案。採択を受け研究計画を遂行。

B（研究教育環境）

活発なシンポジウム、セミナーなどの開催、GCOE総合講義参加

C（人材確保）

大学院生（AISS）への奨学金授与、大学院生セミナーの開催

D（人材育成）

国際シンポジウム開催、国際セミナーへの参加、発表。

5）GCOE事業を推進するに当たって力を入れた点

若手研究者を軸とした分野間での共同研究体制、大学院生への教育活動に参加することを心がけた。

6）英文原著論文

1. ◎N. Ebe, M. Hara-Yokoyama, K. Iwasaki, S. Iseki, K. Terasawa, K. A. Podyma-Inoue, M. Yanagishita and Y. Izumi, Periodontal pockets as the pathological setting for HMGB1 release, J. Dental Res.（2011）90：235-240
2. Katarzyne A. Podyma-Inoue, Miki Yokoyama, Tomoko Kimura and Masaki Yanagishita, Syndecans are Residing in Sphingomyelin-enriched Low Density Fractions of the Plasma membrane Isolated from a Parathyroid Cell Line, PLOS ONE, submitted.

7）平成23年度までの自己評価

若手研究者を軸とした分野間での共同研究体制確立に努力した。その他の活動内容のうちで私の参加できる主な項目としては大学院生、GCOE教官に対する評価関連の活動および、大学院生に対するセミナーシリーズでの司会であった。これらの活動はGCOE事業全体からすると微力とは思いますが、可能な限り参加させていただきました。

8）学会発表（英文）

1. S. Takehara, M. Yanagishita, K. A. Podyma-Inoue, M. Ueno, K. Shinada and Y. Kawaguchi, Proteolytic Degradation of Human Salivary MUC5B and MUC7, Annual Meeting of International Association for Dental Research, March 16-19, San Diego
2. Miki Yokoyama, Membrane Dynamics and Lipid Biology [II]：Domains, Droplets and Diseases、第30回内藤コンファレンス、2011年6月28日 - 7月1日、北海道
3. Katarzyne A. Podyma-Inoue, Miki Yokoyama and Masaki Yanagishita, Characterization of Membrane Rafts Enriched in Cell Surface Haparan Sulfate Proteoglycans Isolated from a Rat Parathyroid Cell Line. 第84回日本生化学大会、2011年9月21日 - 24日、京都
4. S. Takehara, M. Yanagishita, K. A. Podyma-Inoue, M. Ueno, K. Shinada and Y. Kawaguchi, Proteolytic Degradation of Human Salivary MUC5B and MUC7, Symposium “Toward networking dental professionals in Asia”, October 6, 2011, Tokyo

9）学会発表（和文）

1. 横山三紀、新野睦子、寺澤和恵、橋井則貴、蛭田葉子、川崎ナナ、脇山素明、白水美香子、横山茂之、柳下正樹、リンパ球表面抗原CD38の4量体化を反映したN型糖

鎖プロセシング、第30回日本糖質学会、2011年7月11 - 13日、長岡

2. 横山三紀、市野瀬志津子、市野瀬省三、多田晃弘、寺澤和恵、吉垣純子、只野-有冨桂子、古川鋼一、柳下正樹、岩渕和久、GM2/GD2合成酵素欠損マウスにおける血液-精巣関門の異常、第84回日本生化学会、2011年9月21-24日、京都
3. 江部典子、横山三紀、寺澤和恵、柳下正樹、和泉雄一、酪酸による酸化ストレス誘導時に放出されるHMGB1の解析、日本歯科保存学会、2011年10月20-21日、大阪

10）外部資金の獲得状況

（受託研究）
糖質科学研究所、「グリコサミノグリカンオリゴ糖の生理活性解析と医薬応用」、期間：平成17年 -平成23年、総額：945万円
（受託研究）
ヒアルロン酸研究所、「異なる分子量のヒアルロン酸の大腸細胞株に対する影響」、期間：平成22年 - 平成23年、84万円

11）主催学会

第18回プロテオグライカンフォーラム、「結合組織細胞外マトリックス形成の制御」2011年2月19日、東京

12）教室、分野や講座の准教授、講師、助教、特別研究員、ポスドク、指導を受けた大学院生の名前

准 教 授　横山　三紀
講　　師　粂井　康宏
助　　教　井上-Podyma Katarzyna Anna
大学院生　Anupama Rajapakshe,
　　○江部　典子（歯周病学分野より）
○はAISS

13）GCOE活動についての感想、コメント、改善を望む点

執行上の細かい決定に了承を求める必要はないと思います。

RESEARCH REPORTS
Clinical

N. Ebe[1,3], M. Hara-Yokoyama[2,3]*, K. Iwasaki[1,4], S. Iseki[5], S. Okuhara[5], K.A. Podyma-Inoue[2,3], K. Terasawa[2], A. Watanabe[6], T. Akizuki[1], H. Watanabe[1], M. Yanagishita[2,3], and Y. Izumi[1,3]

[1]Section of Periodontology and [2]Section of Biochemistry, Department of Hard Tissue Engineering, Biochemistry, Division of Bio-Matrix, Graduate School, Tokyo Medical and Dental University, 1-5-45 Yushima, Bunkyo, Tokyo 113-8549, Japan; [3]Global Center of Excellence (GCOE) Program, International Research Center for Molecular Science in Tooth and Bone Diseases, Tokyo Medical and Dental University, 1-5-45 Yushima, Bunkyo, Tokyo 113-8549, Japan; [4]Department of Oral Maxillofacial Surgery, Tokyo Women's Medical University, Tokyo, Japan; [5]Department of Molecular Craniofacial Embryology, Graduate School, Tokyo Medical and Dental University, 1-5-45 Yushima, Bunkyo, Tokyo 113-8549, Japan; and [6]The Institute of Biomaterial and Bioengineering, Tokyo Medical and Dental University, 1-5-45 Yushima, Bunkyo, Tokyo 113-8549, Japan; *corresponding author, m.yokoyama.bch@tmd.ac.jp

J Dent Res 90(2):235-240, 2011

Pocket Epithelium in the Pathological Setting for HMGB1 Release

ABSTRACT

High-mobility group box-1 (HMGB1) protein acts as a transcription factor in the nucleus and also as a pro-inflammatory cytokine when released into extracellular fluids. The presence of higher levels of HMGB1 is reported in the gingival crevicular fluid from periodontal patients. Since the proliferation of bacteria within the periodontal pocket is closely involved in the exacerbation of periodontal disease, it is hypothesized that the periodontal pocket causes the release of HMGB1. Immunohistochemical staining of inflamed gingiva revealed that HMGB1 is exclusively dislocated from the nucleus to the cytoplasm in the pocket epithelium, whereas it is mainly present in the nucleus in the gingival epithelium. Butyric acid, an extracellular metabolite from periodontopathic bacteria populating the periodontal pocket, induced the passive release of HMGB1 as a result of eliciting necrosis in the human gingival epithelial cell line. Thus, the periodontal epithelium may provide a unique pathological setting for HMGB1 release by bacterial insult. *Abbreviations*: HMGB1, high-mobility group box-1; TNF-α, tumor necrosis factor-α; CHX, cycloheximide; PI, propidium iodide; ROS, reactive oxygen species; HDAC, histone deacetylase.

KEY WORDS: HMGB1, pocket epithelium, butyric acid.

DOI: 10.1177/0022034510385688

Received February 4, 2010; Last revision May 17, 2010; Accepted June 3, 2010

A supplemental appendix to this article is published electronically only at http://jdr.sagepub.com/appendix.

© International & American Associations for Dental Research

INTRODUCTION

High-mobility group box-1 (HMGB1) is one of the most abundant nuclear non-histone proteins (Bianchi and Beltrame, 1998). In the nucleus, HMGB1 acts as a DNA chaperone that facilitates the rate-limiting DNA distortion during nucleosome sliding and regulates transcription (Bonaldi *et al*., 2002). In contrast, HMGB1 acts as a cytokine when released into the extracellular milieu upon tissue injury or inflammation (Bianchi and Manfredi, 2007). Extracellular HMGB1 induces the migration and/or proliferation of stem cells in muscle (Palumbo *et al*., 2004) and heart (Limana *et al*., 2005), and enhances the immune response by facilitating dendritic cell maturation (Messmer *et al*., 2004; Yang *et al*., 2007), as well as the accumulation of neutrophils (Orlova *et al*., 2007) and the activation of monocytes/macrophages (Scaffidi *et al*., 2002). Thus, HMGB1 triggers tissue repair and immunological defense programs.

However, HMGB1 could also induce maladaptive or exaggerated autoimmune responses, and become pathogenic when released chronically, regardless of the presence of infection (Bianchi and Manfredi, 2007). HMGB1 was originally identified as a late mediator of endotoxin lethality in mice (Wang *et al*., 1999). A pathogenic role of HMGB1 has been suggested in the development of arthritis (Andersson and Erlandsson-Harris, 2004). Consistently, the administration of antibodies to HMGB1 attenuates the endotoxin lethality (Wang *et al*., 1999) and ameliorates collagen-induced arthritis (Andersson and Erlandsson-Harris, 2004).

Inflammatory periodontal disease is caused mainly by Gram-negative bacteria populating the gingival sulcus and periodontal pocket. The pathogenesis of periodontitis is characterized by complex interactions between pathogens and host responses, through cytokines and inflammatory mediators in periodontal tissues (Page, 1991). Recently, Morimoto *et al*. reported the presence of higher levels of HMGB1 in the gingival crevicular fluid from periodontal patients (Morimoto *et al*., 2008), and suggested the role of HMGB1 in inflammatory periodontal diseases. In the present study, we investigated a possibility that the periodontal pocket elicits a pathogenic potential of HMGB1. Therefore, we observed the distribution of HMGB1 around the periodontal pocket by immunohistochemistry. Furthermore, we focused on butyric acid, a virulent factor generated in the periodontal pocket (Kurita-Ochiai *et al*., 1995), and evaluated its effect on the release of HMGB1 *in vitro*.

MATERIALS & METHODS

Reagents

Butyric acid was purchased from Wako Pure Chemical Industries (Osaka, Japan). Eagle's minimum essential medium (MEM), fetal bovine serum, and

Downloaded from jdr.sagepub.com at TOKYO IKASHIKA UNIVERSITY on January 6, 2012 For personal use only. No other uses without permission.

© 2011 International & American Associations for Dental Research

cycloheximide (CHX) were from Sigma-Aldrich (St. Louis, MO, USA). z-VAD-fmk was purchased from the Peptide Institute (Osaka, Japan). Recombinant human tumor necrosis factor-α (TNF-α) was from R&D Systems (Minneapolis, MN, USA).

Preparation of Gingival Tissues

Gingival tissues were collected from two healthy volunteers (a 51- and a 30-year-old women, pocket depth, 2 mm) and four patients with chronic periodontitis (a 30-year-old man, pocket depth, 6 mm; a 51-year-old man, pocket depth, 13 mm; a 67-year-old woman, pocket depth, 12 mm; and a 65-year-old-woman, pocket depth, 5 mm) during periodontal flap surgery. Informed consent was obtained according to guidelines approved by the Ethics Committee of Tokyo Medical and Dental University. The excised tissues were immediately fixed in 4% formalin and embedded in paraffin.

Immunohistochemistry

Paraffin-embedded sections (5 μm in thickness) of gingival tissues were deparaffinized in xylene and rehydrated through a series of decreasing concentrations of ethanol. For hematoxylin and eosin (H.E.) staining, sections were stained with 1% EosinY solution and Mayer's Hematoxylin (Muto-Kagaku, Tokyo, Japan). To detect HMGB1, we treated the sections with 1% H_2O_2 in methanol for 15 min to inhibit intrinsic peroxidase activity and with 5% skimmed milk for 30 min to prevent non-specific antibody binding. The pre-treated sections were incubated overnight at room temperature with affinity-purified rabbit anti-HMGB1 antibody or rabbit IgG at a concentration of 5 μg/mL (SHINO-TEST Corporation, Kanagawa, Japan) or a control polyclonal rabbit IgG (DAKO, Glostrup, Denmark). We visualized the site of immunoreaction by incubating the sections successively with biotinylated anti-rabbit antibody (CHEMICON, Temecula, CA, USA) at 1:200 dilution for 30 min, avidin-biotinylated peroxidase complex (ABC Elite Kit; Vector Laboratories, Burlingame, CA, USA) for 30 min, and 0.05% solution of 3-diaminobenzidine (SIGMA) in the presence of 0.01% H_2O_2 for 10 min. Sections were counterstained with 1% methyl green. The sections were subjected to observation under a Leica DM 5000B microscope. The immunoreactivity was not observed with control IgG.

Cell Culture and Evaluation of Cell Viability

A human gingival epithelial cell line (Ca9-22) was obtained from the Japanese Collection of Research Bioresources (JCRB, Osaka, Japan), and was maintained in Eagle's MEM supplemented with 10% fetal bovine serum (F6178, Sigma-Aldrich, St. Louis, MO, USA), penicillin (50 U/mL), and streptomycin (50 μg/mL) at 37°C in 5% CO_2. After cells were cultured for 16 hrs (1 x 10^5 cells/mL, 0.1 mL/well in 96-well tissue culture plate), the culture medium was replaced with fresh medium containing butyric acid (0.3-20 mmol/L), TNF-α (10 ng/L), CHX 10 μg/L), or z-VAD (5 μmol/L). The concentrations were chosen based on the results as shown in Appendix Fig. 1. Then the cells were cultured further for 48 hrs. For the time-course experiments, the replacement of medium was delayed for 24 or 40 hrs. Cell viability was evaluated by means of a Cell Counting Kit-8 (Dojindo, Kumamoto, Japan). The absorbance at a 450-nm wavelength, due to the reaction of water-soluble tetrazolium salt (WST-8), was measured.

Evaluation of Cell Death and Generation of Reactive Oxygen Species (ROS) by Flow Cytometry

After the culture (2-4 x 10^5 cells/mL, 0.4 mL/well in 24-well tissue culture plate), the floating cells were combined with the adherent cells that were detached from the substratum by 0.05% trypsin-EDTA (GIBCO), and the cells were collected by centrifugation. To evaluate cell death or the generation of ROS, we stained the cells with 1 μg/mL propidium iodide (PI) or 4 μmol/L dihydroethidium (Invitrogen, Carlsbad, CA, USA), respectively. *N*-acetylcysteine (Tokyo Chemical Industry, Japan) and 1,2-dihydroxy-3,5-benzenedisulfonic acid (Tiron; Dojindo) were added together with butyric acid. The percentage of cells with high fluorescence intensity due to oxidization of dihydroethidium was identified as the ROS-producing cells. The cells were analyzed by flow cytometry with a FACSCaliber (BD Bioscience, Mountain View, CA, USA).

Statistical Analysis

Differences between mean values were assessed by a Student's *t* test. A p value < 0.05 or < 0.01 was considered statistically significant.

RESULTS

HMGB1 is Dislocated from the Nucleus in the Pocket Epithelium

Gingival tissues from chronic periodontal patients (Fig. 1, Appendix Fig. 2) and healthy volunteers (Appendix Fig. 3) were stained by an anti-HMGB1 antibody. In hematoxylin and eosin (H.E.) staining, all the samples showed infiltration of inflammatory cells in pocket epithelium, and the magnitude of the infiltration was consistent with the clinical periodontal condition. Regarding the localization of HMGB1, it was predominantly stained more in epithelial cells than in connective tissues, which is consistent with results from the previous study (Morimoto *et al*., 2008). Moreover, in the gingival epithelium, HMGB1 was mainly localized in the nucleus and was partly dislocated from the nucleus. In contrast, in the pocket epithelium, the localization of HMGB1 was exclusively cytoplasmic in all of these tissue samples.

Butyric Acid Induces HMGB1 Release in Ca9-22 Cells

Butyric acid is a metabolite of periodontopathic bacteria and a virulence factor common to *Porphyromonas gingivalis, Prevotella loescheii*, and *Fusobacterium nucleatum* (Kurita-Ochiai *et al*., 1995). The concentration of butyric acid was previously shown to reach 14-20 mmol/L in subgingival plaque at periodontal sites (Margolis *et al*., 1988). We examined the effect of butyric acid on the release of HMGB1, using a human gingival epithelial cell

Downloaded from jdr.sagepub.com at TOKYO IKASHIKA UNIVERSITY on January 6, 2012 For personal use only. No other uses without permission.

© 2011 International & American Associations for Dental Research

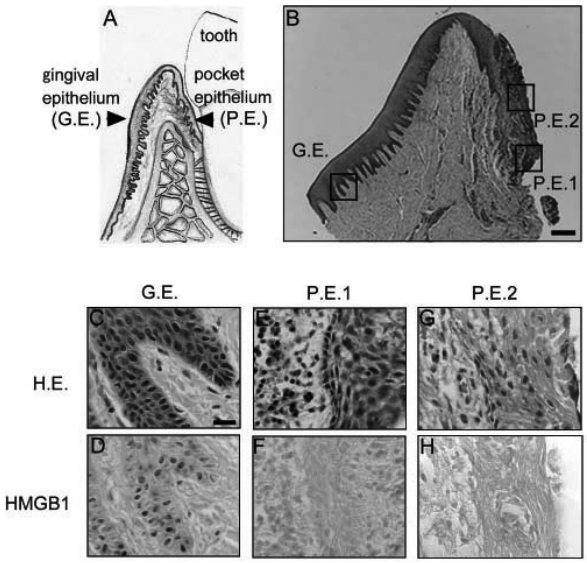

Figure 1. Immunohistochemical localization of HMGB1 in gingival tissue from a patient with chronic periodontitis. (**A**) Schematic presentation of periodontal tissues. (**B-H**) The section was stained with hematoxylin and eosin (H.E.) (B,C,E,G) or anti-HMGB1 antibody (HMGB1) (D,F,H). Areas corresponding to gingival epithelium (C,D) and pocket epithelium (E-H) were magnified. Scale bar: B, 200 μm; C-H, 20 μm.

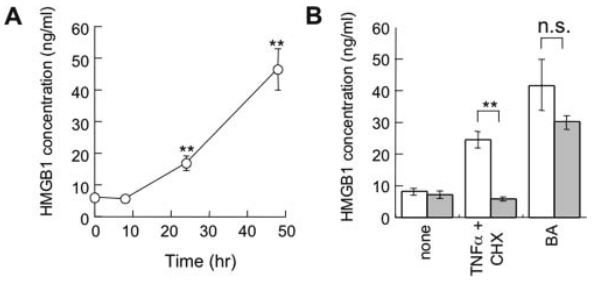

Figure 2. Butyric acid induces HMGB1 release in Ca9-22 cells. Ca9-22 cells (2 x 10^5 cells/mL, 0.4 mL/well in a 24-well tissue culture plate) were incubated with butyric acid at concentrations of 10 mmol/L for 0-48 hrs (**A**), or without (white) and with (gray) 5 μmol/L z-VAD for 48 hrs in the absence or presence of 10 ng/mL TNF-α with 10 μg/mL CHX or 10 mmol/L butyric acid (**B**). Conditioned media were passed through a GHP Acrodisc Syringe Filter with a 0.2 μm GHP Membrane (PALL, Ann Arbor, MI, USA). The amount of HMGB1 in the filtrates was measured with the use of an HMGB1 ELISA Kit (SHINO-TEST Corporation, Kanagawa, Japan). (A) Values are means ± SD (n = 4). The result is a representative of 4 independent experiments. (B) Values are means ± SD (n = 3). Essentially the same result was obtained in an independent experiment. Significant differences between z-VAD-treated and untreated conditions are indicated: ** $p < 0.01$.

line, Ca9-22. The release of HMGB1 was detected after 24 hrs in the presence of 10 mmol/L butyric acid (Fig. 2A).

Butyric Acid Induces Necrotic Cell Death in Ca9-22 Cells

The viability of Ca9-22 cells decreased in the presence of butyric acid (Figs. 3A, 3B). Cell death was observed after 24 hrs and was still evident after 48 hrs in the presence of 10 mmol/L butyric acid. A dose-response effect of butyric acid on cell death was coincident with that on HMGB1 release (Appendix Fig. 4).

The induction of cell death caused by a combination of TNF-α and CHX, which leads to apoptosis, was appreciably suppressed in the presence of a pan-caspase inhibitor, z-VAD (Fig. 3C). In contrast, butyric-acid-induced cell death was not significantly suppressed by z-VAD, although it was partly suppressed in the presence of 10 mmol/L butyric acid. Similarly, the release of HMGB1, induced by a combination of TNF-α and CHX, was almost undetectable in the presence of z-VAD, whereas the substantial release of HMGB1 by butyric acid was observed in the presence of z-VAD (Fig. 2B).

After the treatment with butyric acid, Ca9-22 cells were slightly swollen (Appendix Fig. 5). The morphological changes were further monitored by transmission electron microscopy. Most of the floating cells were enucleated (Appendix Fig. 6), whereas the released nuclei remained attached to the substratum and revealed the homogeneous staining in the nucleoplasm (Fig. 3F). In contrast, chromatin condensation and cell shrinkage were clearly observed when Ca9-22 cells were treated with TNF-α and CHX.

Butyric Acid Promotes the Generation of ROS in Ca9-22 Cells

The population of Ca9-22 cells producing ROS was increased by incubation with butyric acid (Fig. 4). The production of ROS was detected after 12 hrs. The addition of ROS scavengers failed to suppress the butyric-acid-dependent ROS production and cell death (Appendix Fig. 7).

DISCUSSION

Changes in the intracellular localization of HMGB1 have been observed in biopsy specimens from patients with rheumatoid arthritis (Kokkola *et al*., 2002) and systemic lupus erythematosus (Popovic *et al*., 2005). In gingival tissues from patients with chronic periodontitis, the occasional translocation of HMGB1 from the nucleus to the cytoplasm has been reported (Morimoto *et al*., 2008). In the present study, we demonstrated that HMGB1 is exclusively present in the cytoplasm of pocket epithelium cells close to the infiltrated inflammatory cells. It should be noted that the infiltration was observed in the pocket epithelium even without apparent periodontal diseases, which is possibly caused by indigenous bacterium in the pocket. In contrast, HMGB1 is preferentially present in the nucleus in the gingival epithelium. This clear contrast suggests the involvement of HMGB1 in the pocket-mediated processes.

One of the virulent factors generated in the periodontal pocket is butyric acid. It has been demonstrated that butyric acid

Downloaded from jdr.sagepub.com at TOKYO IKASHIKA UNIVERSITY on January 6, 2012 For personal use only. No other uses without permission.

© 2011 International & American Associations for Dental Research

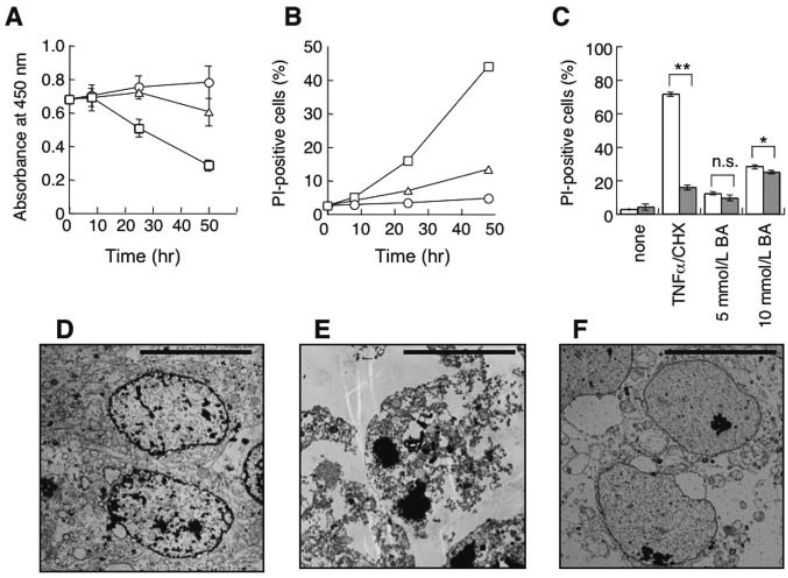

Figure 3. Butyric acid induces necrotic cell death in Ca9-22 cells. Ca9-22 cells were incubated with butyric acid at concentrations of 1.25 mmol/L (○), 5 mmol/L (Δ), and 10 mmol/L (□) for indicated times, and cell viability (**A**) and cell death (**B**) were evaluated. The result is a representative of 3 independent experiments. (**C**) Ca9-22 cells were incubated without (white) and with (gray) 5 μmol/L z-VAD for 48 hrs in the absence or presence of 10 ng/mL TNF-α with 10 μg/mL CHX or 10 mmol/L butyric acid, and cell death was evaluated. Values are means ± SD (n = 3). Significant differences between z-VAD-treated and untreated conditions are indicated: ** $p < 0.01$; * $p < 0.05$. A similar result was obtained in an independent experiment. (**D-F**) Transmission electron micrographs. Ca9-22 cells (4×10^6 cells in 10-cm tissue culture dish) were cultured in the absence (**D**) or presence of 10 ng/mL TNF-α and 10 μg/mL CHX (**E**) or 10 mmol/L butyric acid (**F**) for 48 hrs. Cells were scraped from the substratum, collected by centrifugation, and then fixed in 2.5% glutaraldehyde in 100 mmol/L phosphate buffer (pH 7.4) overnight at 4°C. After the fixative was changed to 100 mmol/L phosphate buffer (pH 7.4), the samples were post-fixed with 2% osmium tetroxide for 2 hrs and then dehydrated. The samples were finally embedded in Epon mixture. Ultra-thin sections (80 nm thick) were prepared with a HERZ ultramicrotome. The specimens were stained with lead citrate and uranyl acetate and examined with a HITACHI H-7100 transmission electron microscope, at an accelerating voltage of 75 kV. Typical morphology of the nuclei is shown. The result is a representative of 3 independent experiments. The bar denotes 10 μm.

induces apoptosis in murine and human T- and B-cells (Kurita-Ochiai *et al*., 1997, 1998, 2001) and in fibroblasts isolated from inflamed periodontal lesions of human adults with periodontitis (Kurita-Ochiai *et al*., 2008). In the present study, we demonstrated that butyric acid induces the release of HMGB1 in a human gingival epithelial cell line (Ca9-22). Previous studies reported the release of HMGB1 from gingival epithelial cells by TNF-α (Morimoto *et al*., 2008) and from gingival fibroblasts by lipopolysaccharide (Feghali *et al*., 2009). In addition to these factors, butyric acid can be a causative factor for HMGB1 release in gingival tissues.

HMGB1 is either secreted from activated monocytes and macrophages through secretory lysosomes, or passively leaked from cells when the integrity of the plasma membrane is disrupted during necrosis (Bianchi and Manfredi, 2007). In contrast, in the case of apoptosis, HMGB1 is retained in the nucleus by association with condensed chromatin, and therefore the release of HMGB1 does not occur even when plasma membranes are compromised after secondary necrosis (Scaffidi *et al*., 2002). However, some contradictory results have been presented (Bell *et al*., 2006; Jiang *et al*., 2007), suggesting that the release of HMGB1 from apoptotic cells is context-dependent. In Ca9-22 cells, the release of HMGB1 and the induction of cell death were observed in parallel. The butyric-acid-dependent cell death was not fully suppressed by a pan-caspase inhibitor and did not cause chromatin condensation, a sign of apoptosis. In addition, cell swelling was observed. These results suggested that butyric acid induced the release of HMGB1 as a result of necrosis. Butyric-acid-induced necrosis has been reported in murine colonic epithelial cell MCE301 (Matsumoto *et al*., 2006).

Although the mechanism of butyric-acid-induced necrosis in Ca9-22 cells remains to be elucidated, electron microscopic observation revealed the presence of a bulging intracellular organelle, suggesting oxidative stress. Butyric acid is known as a histone deacetylase (HDAC) inhibitor (Davie, 2003) and is able to induce transcriptional changes (Pajak *et al*., 2007). The homogeneous staining of nucleoplasm is probably caused by the hyperacetylation of nuclear proteins. Thus, further studies are needed to elucidate butyric-acid-induced gene expression related to ROS production.

Several mechanisms are known to promote the relocation of HMGB1 from the nucleus to the cytoplasm, such as the acetylation (Bonaldi *et al*., 2003; Carneiro *et al*., 2009) and phosphorylation (Youn and Shin, 2006) of HMGB1, and the destabilized association of HMGB1 with chromatin (Ditsworth *et al*., 2007) or a nuclear import protein (Youn and Shin, 2006). HMGB1 is reportedly a substrate of histone acetylase, and HDAC inhibitors induce the relocation of HMGB1 from the nucleus to the cytoplasm (Bonaldi *et al*., 2003; Carneiro *et al*., 2009). The effect of the HDAC-inhibiting activity of butyric acid in the relocation of HMGB1 remains to be elucidated.

Immunohistochemical staining revealed that HMGB1 is exclusively localized in the cytoplasm in the inflamed pocket epithelium. Cytoplasmic HMGB1 is destined for release to the extracellular space, either actively or passively, when the cells receive an appropriate second signal. Butyric acid was shown to induce the release of HMGB1 as a result of necrosis in the gingival epithelial cell line Ca9-22. Thus, it is considered that the pocket epithelium, which is continuously challenged by

Downloaded from jdr.sagepub.com at TOKYO IKASHIKA UNIVERSITY on January 6, 2012 For personal use only. No other uses without permission.

© 2011 International & American Associations for Dental Research

periodontopathic bacteria, is in a unique pathological setting for HMGB1 release. Since HMGB1 potentiates the action of lipopolysaccharide (Qin *et al*., 2009), HMGB1 could exaggerate the outcome of bacterial insult.

ACKNOWLEDGMENTS

We are grateful to Dr. Shigeru Oda, Dr. Akira Aoki, Dr. Motohiro Komaki, Dr. Shinichi Arakawa, Dr. Hidehiro Shioyama, Dr. Sae Hayakumo, and Dr. Youichi Taniguchi for the preparation of gingival tissues and to Dr. Shizuko Ichinose for the electron microscopy at Tokyo Medical and Dental University. This work was supported by Grants-in-Aid for the Global Center of Excellence (GCOE) Program to Tokyo Medical and Dental University and for Scientific Research 22592060 (to M.Y.) from the Ministry of Education, Culture, Sports, Science, and Technology, Japan.

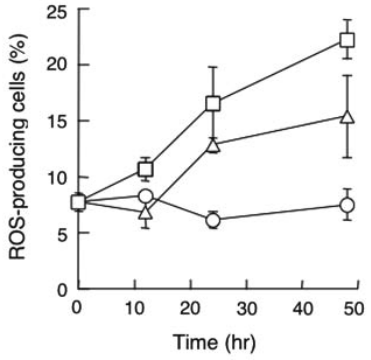

Figure 4. Butyric acid promotes the generation of ROS in Ca9-22 cells. Ca9-22 cells were incubated with butyric acid at concentrations of 1.25 mmol/L (○), 5 mmol/L (Δ), and 10 mmol/L (□) for the indicated times. Cells were stained with dihydroethidium and analyzed by flow cytometry. Values are means ± SD (n = 3). Essentially the same result was obtained in an independent experiment.

REFERENCES

Andersson U, Erlandsson-Harris H (2004). HMGB1 is a potent trigger of arthritis. *J Intern Med* 255:344-350.

Bell CW, Jiang W, Reich CF 3rd, Pisetsky DS (2006). The extracellular release of HMGB1 during apoptotic cell death. *Am J Physiol Cell Physiol* 291:C1318-C1325.

Bianchi ME, Beltrame M (1998). Flexing DNA: HMG-box proteins and their partners. *Am J Hum Genet* 63:1573-1577.

Bianchi ME, Manfredi AA (2007). High-mobility group box 1 (HMGB1) protein at the crossroads between innate and adaptive immunity. *Immunol Rev* 220:35-46.

Bonaldi T, Langst G, Strohner R, Becker PB, Bianchi ME (2002). The DNA chaperone HMGB1 facilitates ACF/CHRAC-dependent nucleosome sliding. *EMBO J* 21:6865-6873.

Bonaldi T, Talamo F, Scaffidi P, Ferrera D, Porto A, Bachi A, *et al*. (2003). Monocytic cells hyperacetylate chromatin protein HMGB1 to redirect it towards secretion. *EMBO J* 22:5551-5560.

Carneiro VC, de Moraes Maciel R, de Abreu da Silva IC, da Costa RF, Paiva CN, Bozza MT, *et al*. (2009). The extracellular release of *Schistosoma mansoni* HMGB1 nuclear protein is mediated by acetylation. *Biochem Biophys Res Commun* 390:1245-1249.

Davie JR (2003). Inhibition of histone deacetylase activity by butyrate. *J Nutr* 133(7 Suppl):2485S-2493S.

Ditsworth D, Zong WX, Thompson CB (2007). Activation of poly(ADP)-ribose polymerase (PARP-1) induces release of the pro-inflammatory mediator HMGB1 from the nucleus. *J Biol Chem* 282:17845-17854; *erratum* in *J Biol Chem* 284:22500, 2009.

Feghali K, Iwasaki K, Tanaka K, Komaki M, Machigashira M, Ishikawa I, *et al*. (2009). Human gingival fibroblasts release high-mobility group box-1 protein through active and passive pathways. *Oral Microbiol Immunol* 24:292-298.

Jiang W, Bell CW, Pisetsky DS (2007). The relationship between apoptosis and high-mobility group protein 1 release from murine macrophages stimulated with lipopolysaccharide or polyinosinic-polycytidylic acid. *J Immunol* 178:6495-6503.

Kokkola R, Sundberg E, Ulfgren AK, Palmblad K, Li J, Wang H, *et al*. (2002). High mobility group box chromosomal protein 1: a novel pro-inflammatory mediator in synovitis. *Arthritis Rheum* 46:2598-2603.

Kurita-Ochiai T, Fukushima K, Ochiai K (1995). Volatile fatty acids, metabolic by-products of periodontopathic bacteria, inhibit lymphocyte proliferation and cytokine production. *J Dent Res* 74:1367-1373.

Kurita-Ochiai T, Fukushima K, Ochiai K (1997). Butyric acid-induced apoptosis of murine thymocytes, splenic T cells, and human Jurkat T cells. *Infect Immun* 65:35-41.

Kurita-Ochiai T, Ochiai K, Fukushima K (1998). Volatile fatty acid, metabolic by-product of periodontopathic bacteria, induces apoptosis in WEHI 231 and RAJI B lymphoma cells and splenic B cells. *Infect Immun* 66:2587-2594.

Kurita-Ochiai T, Ochiai K, Fukushima K (2001). Butyric acid-induced T-cell apoptosis is mediated by caspase-8 and -9 activation in a Fas-independent manner. *Clin Diagn Lab Immunol* 8:325-332.

Kurita-Ochiai T, Seto S, Suzuki N, Yamamoto M, Otsuka K, Abe K, *et al*. (2008). Butyric acid induces apoptosis in inflamed fibroblasts. *J Dent Res* 87:51-55.

Limana F, Germani A, Zacheo A, Kajstura J, Di Carlo A, Borsellino G, *et al*. (2005). Exogenous high-mobility group box 1 protein induces myocardial regeneration after infarction via enhanced cardiac C-kit+ cell proliferation and differentiation. *Circ Res* 97:e73-83.

Margolis HC, Duckworth JH, Moreno EC (1988). Composition and buffer capacity of pooled starved plaque fluid from caries-free and caries-susceptible individuals. *J Dent Res* 67:1476-1482.

Matsumoto T, Hayasaki T, Nishimura Y, Nakamura M, Takeda T, Tabuchi Y, *et al*. (2006). Butyrate induces necrotic cell death in murine colonic epithelial cell MCE301. *Biol Pharm Bull* 29:2041-2045.

Messmer D, Yang H, Telusma G, Knoll F, Li J, Messmer B, *et al*. (2004). High mobility group box protein 1: an endogenous signal for dendritic cell maturation and Th1 polarization. *J Immunol* 173:307-313.

Morimoto Y, Kawahara KI, Tancharoen S, Kikuchi K, Matsuyama T, Hashiguchi T, *et al*. (2008). Tumor necrosis factor-alpha stimulates gingival epithelial cells to release high mobility-group box 1. *J Periodontal Res* 43:76-83.

Orlova VV, Choi EY, Xie C, Chavakis E, Bierhaus A, Ihanus E, *et al*. (2007). A novel pathway of HMGB1-mediated inflammatory cell recruitment that requires Mac-1-integrin. *EMBO J* 26:1129-1139.

Page RC (1991). The role of inflammatory mediators in the pathogenesis of periodontal disease. *J Periodontal Res* 26(3 Pt 2):230-242.

Pajak B, Orzechowski A, Gajkowska B (2007). Molecular basis of sodium butyrate-dependent proapoptotic activity in cancer cells. *Adv Med Sci* 52:83-88.

Palumbo R, Sampaolesi M, De Marchis F, Tonlorenzi R, Colombetti S, Mondino A, *et al*. (2004). Extracellular HMGB1, a signal of tissue damage, induces mesoangioblast migration and proliferation. *J Cell Biol* 164:441-449.

Popovic K, Ek M, Espinosa A, Padyukov L, Harris HE, Wahren-Herlenius M, *et al*. (2005). Increased expression of the novel proinflammatory cytokine high mobility group box chromosomal protein 1 in skin lesions of patients with lupus erythematosus. *Arthritis Rheum* 52: 3639-3645.

Qin YH, Dai SM, Tang GS, Zhang J, Ren D, Wang ZW, *et al*. (2009). HMGB1 enhances the proinflammatory activity of lipopolysaccharide

Downloaded from jdr.sagepub.com at TOKYO IKASHIKA UNIVERSITY on January 6, 2012 For personal use only. No other uses without permission.

© 2011 International & American Associations for Dental Research

by promoting the phosphorylation of MAPK p38 through receptor for advanced glycation end products. *J Immunol* 183:6244-6250.

Scaffidi P, Misteli T, Bianchi ME (2002). Release of chromatin protein HMGB1 by necrotic cells triggers inflammation. *Nature* 418:191-195.

Wang H, Bloom O, Zhang M, Vishnubhakat JM, Ombrellino M, Che J, *et al*. (1999). HMG-1 as a late mediator of endotoxin lethality in mice. *Science* 285:248-251.

Yang D, Chen Q, Yang H, Tracey KJ, Bustin M, Oppenheim JJ (2007). High mobility group box-1 protein induces the migration and activation of human dendritic cells and acts as an alarmin. *J Leukoc Biol* 81:59-66.

Youn JH, Shin JS (2006). Nucleocytoplasmic shuttling of HMGB1 is regulated by phosphorylation that redirects it toward secretion. *J Immunol* 177:7889-7897.

Downloaded from jdr.sagepub.com at TOKYO IKASHIKA UNIVERSITY on January 6, 2012 For personal use only. No other uses without permission.

© 2011 International & American Associations for Dental Research

口腔病理学分野

山口　朗

医歯学総合研究科・口腔機能再構築学系専攻
口腔病理学・教授

1）研究の課題名

光メージングと分子生物学の融合によるオステオネットワークの解明を目指したフロンティア研究拠点

New frontier of osteonetwork research by combinational approaches of optical imaging and molecular biology

イノベーション研究

（共同研究者：高柳広、飯村忠浩、中島友紀）

研究内容

1. 骨芽細胞分化および骨再生過程における細胞・分子間相互作用

Cellular and molecular interactions in osteoblast differentiation and bone regeneration

本研究では、骨芽細胞分化および骨再生過程における細胞・分子間の相互作用を解析し、骨再生の統合的理解を深め、優れた骨再生療法を確立するための分子基盤を構築することを目的とする。今年度は以下の研究を行った。

1）骨再生におけるCCN3の役割：我々はCCN3がBMP, Notchの分子間相互作用により骨芽細胞分化を抑制することを報告した。そのため、骨芽細胞特異的にCCN3を過剰発現するトランスジェニックマウスおよびCCN3ノックアウトマウスにおける骨再生過程を解析し、CCNノックアウトマウスでは骨形成が促進することを明らかにした。

2）イヌ口腔粘膜を利用した骨再生療法の開発：現在までに、骨髄間葉系幹細胞、筋肉、骨膜細胞などが骨再生の細胞移植療法に用いられているが、これらの細胞は歯科医師にとって簡便に採取できる細胞ソースではない。そのため、本研究ではイヌ口腔粘膜線維芽細胞が骨再生の細胞移植量療法に利用できるか、検討した。成犬の口腔粘膜より採取した線維芽細胞にGFPを導入し、BMP-2とともにヌードマウスに移植した所、GFPとALPの両者が陽性の細胞が異所性骨形成部に観察された。そのため、口腔粘膜線維芽細胞はBMPの作用により、in vivoでも骨芽細胞に分化でき、歯科領域の骨精製療法の開発に有用な細胞源と考えられた（論文投稿中）。現在、BMP-2遺伝子を導入したイヌ口腔粘膜線維芽細胞による骨形成能を検討中である。

2. 口腔癌による顎骨破壊の分子メカニズム

Molecular mechanism of bone destruction by oral cancer

口腔癌はその解剖学的構造に依存して、容易に顎骨に直接浸潤するという特徴をもち、顎骨浸潤はその予後を規定する重要な要因の一つである。そのため、歯肉癌の顎骨浸潤の予防あるいは顎骨浸潤の進展を阻止することができれば、今後の歯肉癌治療に大きく貢献できる。この目的を達成するために、我々は口腔癌による顎骨破壊の分子メカニズムの解析を行なっている。

1）口腔癌の骨浸潤におけるCXCL2の役割：口腔癌が産生する間質細胞のRANKL発現誘導因子の同定を試みた。HSC3口腔癌細胞から単一細胞に由来するクローン化細胞を13種類分離し、各々の培養上清がST2細胞のRANKL発現に与える影響を検討した。その結果、HSC3-C13細胞株がST2細胞におけるRANKL発現を最も効率的に上昇させ、HSC3-C17細胞がその活性能が一番低いことが明らかとなった。そのため、HSC3-C13とHSC30C17細胞間での遺伝子発現の相違をmicroarray解析で検討し、CXCL2がHSC3-C13細胞で高発現していることを見いだした。さらに、HSC3-C13細胞の培養上清が誘導する破骨細胞形成はCXCL2中和抗体で有意に抑制することを明らかにした。以上の結果より、CXCL2は口腔癌細胞が産生する破骨細胞性骨吸収促進因子の一つであると考えられた。現在、論文投稿中。

2）口腔癌による骨吸収過程における間質細胞と癌細胞の産生するRANKLの役割：我々は口腔癌の骨浸潤過程では、癌：骨の境界に存在する線維芽細胞様細胞が産生するRANKLが重要な役割を担っていることを報告した。近年、口腔癌細胞が自らRANKLを

産生していることが報告されているが、間質細胞の産生するRANKLと癌細胞の産生するRANKLがどのように骨破壊に関与しているのか明らかにされていない。そのため、本研究では、抗マウスRANKL特異的中和抗体と抗ヒトRANKL特異的中和抗体を用いた実験を行った。口腔癌細胞株をヌードマウス頭蓋部皮下に移植して、マウスRANKL特異的中和抗体とヒトRANKL特異的中和抗体を単独、または併用で投与した。その結果、各抗体を単独で投与すると骨破壊が抑制されたが、両抗体を同時に投与すると骨破壊抑制効果は相加的に抑制された。この実験系では、間質細胞の産生するRANKLはマウス由来で、癌細胞の産生するRANKLはヒト由来であるため、マウスとヒトのRANKLを特異的に中和する抗体を用いることにより、骨吸収過程で間質細胞と癌細胞の産生するRANKLの機能を区別化できた。本研究の結果より、間質細胞と癌細胞で産生される両方のRANKLが口腔癌における骨吸収に関与していることが明らかとなり、RANKL中和抗体が口腔癌における骨破壊の抑制に有効であることが示唆された。現在、論文投稿準備中。

3. 骨細胞形態の定量的解析法の基盤構築と機能の解析

骨細胞は、骨基質中に存在し周囲の骨細胞や、骨芽細胞、破骨細胞とも細胞突起を介してネットワークを形成し、多細胞複合体として細胞間コミュニケーションを通じて機能している。したがって、骨細胞の機能解析をする際には、骨細胞の細胞突起を介した3次元的な解析が重要である。そこで、本研究グループでは、高解像度の3次元蛍光イメージングと画像解析により、骨細胞突起の立体的構造を解析した。その結果、非荷重骨である頭蓋冠と荷重骨である長管骨では骨細胞の3次元的構造に差異がみられることを明らかにした（Ando-Himeno et al. BBRC in press）。また、脊椎動物の進化の過程における骨細胞の形態学的変化を明らかにする目的で、魚類、両生類、爬虫類、哺乳類の骨細胞の形態を解析し、魚類では骨細胞と骨細胞突起の発達が悪いが、両生類以上の脊椎動物では骨細胞の形態に大きな差がないことを明らかにした（Cao etal.J Bone Miner Res 2011）。これらの結果は、骨細胞の微細構造は力学的負荷によって異なる可能性を示唆するとともに、今後の骨細胞の定量的形態計測の基盤となると考えられた。

最近、骨細胞と破骨細胞の相互作用が注目されている。本研究では、骨細胞に特異的にジフテリア毒素受容体を発現するトランスジェニックマウス（DTR-Tg）にジフテリア毒素を投与することにより、特異的に骨細胞を死滅させることが可能なマウスを用いて矯正的歯牙移動時における骨細胞の役割を解析した。その結果、骨細胞を死滅させることにより、歯牙圧迫側の破骨細胞数が減少し、歯の移動量も少ないことを明らかにした。本研究の結果より、矯正的歯の移動における骨吸収過程では骨細胞が重要な役割を担っていることを初めて実証した（論文投稿準備中）。

4. 骨の代謝と疾患におけるケモカイン受容体シグナルの役割に関する研究

ケモカインのいくつかは、骨吸収性の関節炎やがん細胞の骨転移部位で発現が上昇することが報告されており、骨代謝への機能が注目されている。本研究グループは、国際医療センター研究所との共同研究で、ケモカイン受容体ノックアウトマウス（KO）の骨の表現型の解析をすすめている。ケモカイン受容体のひとつであるCCR1欠損マウスは骨芽細胞の機能分化と破骨細胞の分化が阻害され、骨減少症を示すことを昨年報告した。今年度はCCR5欠損マウスの骨の表現型を解析し、骨形成の促進と骨吸収の抑制により、骨量増加を示すことを明らかにした。CCR5はHIVのco-receptorであるため、本研究はAIDS患者における骨動態の理解にも役立つものである。現在、投稿論文準備中。

2）

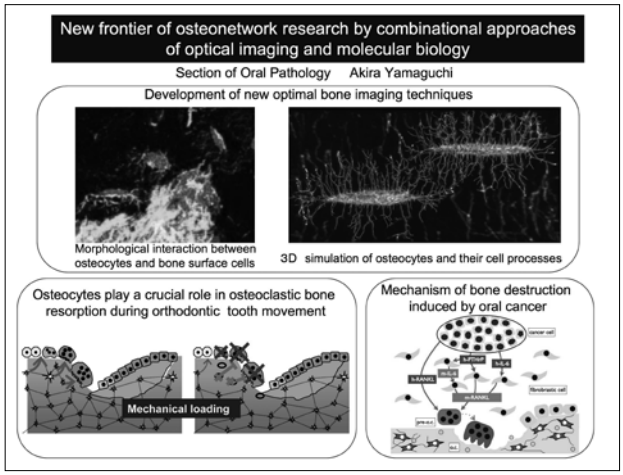

3）発表の研究内容についての英文要約

1. Erika Oue, Ji-Won Lee, Kei Sakamoto, Tadahiro Iimura, Kazuhiro Aoki, Kou Kayamori, Yasuyuki Michi, Masashi Yamashiro, Akira Yamaguchi：CXCL2 is involved in bone destruction induced by oral cancer.（submitted）To explore the mechanism of bone destruction

associated with oral cancer, we identified factors that stimulate osteoclastic bone resorption in oral squamous cell carcinoma. Two clonal cell lines, HSC3-C13 and HSC3-C17, were isolated from the maternal oral cancer cell line, HSC3. The conditioned medium from HSC3-C13 cells showed the highest induction of Rankl expression in the mouse stromal cell lines ST2 and UAMS-32 as compared to that in maternal HSC3 cells and HSC3-C17 cells. The conditioned medium from HSC3-C13 cells significantly increased the number of osteoclasts in a co-culture with mouse bone marrow cells and UAMS-32 cells. Xenograft tumors generated from HSC3-C13 cells caused extensive bone destruction and a significant increase in osteoclast numbers. CXCL2 gene was highly expressed in HSC3-C13 cells as compared to HSC3-C17 cells. The increase in osteoclast numbers induced by the HSC3-C13-conditioned medium was dose-dependently inhibited by addition of anti-human CXCL2-neutralizing antibody. These results indicate that CXCL2 is involved in bone destruction induced by oral cancer. This is the first report showing the role of CXCL2 in cancer-associated bone destruction.

2. Khanom R, Sakamoto K, Pal SK, Shimada Y, Morita K-i, Omura K, Miki Y, Yamaguchi A：Expression of basal cell keratin 15 and keratin 19 in oral squamous cell carcinoma represent diverse phthophysiologies. Histol Histopathol（in press）
The basal cells of oral epithelium express keratin 5（K5）, K14, K15 and K19, but their alterations in tumors are unclear. To address this issue and to seek for possible diagnostic application, we examined the expression of these keratins in oral squamous cell carcinoma（OSCC）and squamous intraepithelial neoplasm（SIN）. cDNA microarray analysis of 43 OSCC revealed slight upregulation of KRT14, downregulation of KRT15 and KRT19, and unaltered KRT5 expression. KRT15 was positively correlated with differentiation-related keratin, KRT13. K5 and K14 were ubiquitously expressed in all 50 OSCC and 50 SIN examined. K15 and K19 were generally downregulated, but were considerably retained in about half of the cases and showed diverse expression patterns. K15-positive cancers tended to show a well-differentiated phenotype, and K19-positive cancers tended to show more invasive tumor fronts. Most K19-positive cancers appeared to develop with little associating SIN. K19 was consistently downregulated in SIN, while K15 was downregulated mainly in high grade SIN. In summary, K15 and K19, unlike K5 or K14, are expressed variably in each SIN and OSCC, which reflects the differences in their pathogenesis and biological behaviors, suggesting their prospective applications as markers for subclassifying OSCC and SIN.

3. Sakamoto K, Fujii T, Kawachi H, Miki Y, Omura K, Morita K, Kayamori K, Khanom R, Katsube K, Yamaguchi A：Reduction of NOTCH1 expression pertains to maturation abnormalities of keratinocytes in squamous neoplasms. Lob Invest（in press）
We examined the expression in 56 cases of oral squamous intraepithelial neoplasm（SIN）or squamous cell carcinoma（OSCC）and 57 cases of cervical intraepithelial neoplasm（CIN）or squamous cell carcinoma（CSCC）. NOTCH1 expression was significantly reduced in most cases of SIN and OSCC, and tended to be downregulated in CIN and CSCC. Knockdown experiments using normal keratinocytes revealed that reduced NOTCH1 expression resulted in alteration of keratin subtype expression; namely the downregulation of keratin 13, that is associated with terminal differentiation of non-cornified epithelium, and the upregulation of keratin 17, that is associated with regeneration, suggesting that aberrant NOTCH1 expression leads to maturation abnormality of keratinocytes. Activation of Notch signaling may not have a major contribution to progression from intraepithelial neoplasm to cancer. Instead, reduced NOTCH1 expression closely associates with abnormal keratinocyte differentiation, and may play an essential role in development of dysplasia that is invariably recognized as immature epithelium.

4. Himeno-Ando A, Izumi Y, Yamaguchi A, Iimura T：Structural differences in the osteocyte network between the calvaria and long bone revealed by three-dimensional fluorescence morphometry, possibly reflecting distinct mechano-adaptations and sensitivities. Biochem Bioph Res Co, in press
The structural features of osteocytes and their cellular process network are thought to allow for mechanotransduction from the bone tissue to these cells. This study applied three-dimensional fluorescence microscopy to fixed and decalcified bone specimens to quantitatively compare the osteocytes and their networks between mouse parietal bone and tibia that are physiologically enforced by distinct mechanical loads. The subsequent morphometric analysis by the surface rendering of osteocyte cell bodies revealed the tibia to have relatively enriched cytoplasm in the osteocyte cell body in comparison to the parietal bone. Furthermore, quantitative tracing of the cellular processes in silico demonstrated that the numbers of the cellular processes and their bifurcation points per osteocyte in the tibia were significantly higher than those in the parietal bone. Though the total length

of the processes per osteocyte in the tibia was two times longer, its total surface area and total volume were smaller than those in the parietal bone, due to its thinner diameter. These architectural differences in the osteocytes and their networks are thus implicated in the adaptation to physiologically different loading, and may also induce distinct mechanosensitivities.

5. Cao L, Moriishi T, Miyazaki T, Iimura T, Tamamura S, Komori T, Yamaguchi A：Comparative morphology of osteocytes in aquatic and land vertebrates. J Bone Miner Metab 29：662-670,2011
Osteocytes are believed to be essential for the maintenance of bone homeostasis because they regulate mechanical sensing and mineral metabolism in mammalian bones. However, osteocyte morphology in other vertebrates has not been well documented. We conducted a comparative study on the morphology of osteocytes and the lacunocanalicular system of the following vertebrates：two teleost fishes [medaka（Oryzias latipes）, and zebrafish（Danio rerio）], three amphibians [African clawed frog（Xenopus laevis）, black-spotted pond frog（Rana nigromaculata）, and Japanese fire-bellied newt（Cynops pyrrhogaster）], two reptiles [four-toed tortoise（Testudo horsfieldii）and green iguana（Iguana iguana）], and two mammals（laboratory mouse C57BL6 and human）. The distribution of the osteocyte lacunocanalicular system in all these animals was investigated using the modified silver staining and the fluorescein-conjugated phalloidin staining methods. Bones of medaka had few osteocytes（acellular bone）. Bones of zebrafish contained osteocytes（cellular bone）but with a poorly developed osteocyte lacunocanalicular system. Bones of Xenopus laevis, a freshwater species, and of other amphibians, reptiles, and mammals contained numerous osteocytes and a well-developed lacunocanalicular system. The present study indicates that development of the osteocyte lacunocanalicular system differs between teleost fishes and land vertebrates, but this pattern is not directly related to aquatic habitat.

6. Sakamoto K, Aragaki T, Morita K, Kawachi H, Kayamori K, Nakanishi S, Omura K, Miki Y, Okada N, Katsube K, Takizawa T, Yamaguchi A.：Down-regulation of keratin 4 and keratin 13 expression in oral squamous cell carcinoma and epithelial dysplasia：a clue for histopathogenesis. Histopathology. 58：531-542,2011.
This study aimed to identify relevant keratin subtypes that may associate with the pathogenesis of oral epithelial neoplasms. Expression of all the keratin subtypes was examined by cDNA microarray analysis of 43 oral squamous cell carcinoma（OSCC）cases. Immunohistochemical expression of the major keratins was examined in 100 OSCC and oral epithelial dysplasia（OED）cases. Many changes in keratin expression were observed and, significantly, consistent down-regulation of keratin 4（K4）and K13 expression was observed. Aberrant expression of K4 and K13 was associated with morphological changes in the affected oral epithelium. Experiments with cell cultures transfected with various keratin subtypes suggested that alterations in keratin subtype expression can cause changes in cell shape and movement. Aberrant expression of K4 and K13, which are the dominant pair of differentiation-related keratins in oral keratinocytes, indicates dysregulation of epithelial differentiation in OSCC and OED. These keratins, especially K4, may be useful for pathological diagnosis. We propose that the aberrant expression of K4 and K13 and concomitant up-regulation of the other keratins may be one of the causative factors for morphological alterations in the affected epithelium.

7. Kihara K, Ichikawa S, Yonezawa T, Lee JW, Akihisa T, Woo JT, Michi Y, Amagasa T, Yamaguchi A：Acerogenin A, a natural compound isolated from Acer nikoense Maxim,stimulates osteoblast differentiation through bone morphogenetic protein action. Biochem Bioph Res Co 406：211-217,2011
We investigated the effects of acerogenin A, a natural compound isolated from Acer nikoense Maxim, on osteoblast differentiation by using osteoblastic cells. Acerogenin A stimulated the cell proliferation of MC3T3-E1 osteoblastic cells and RD-C6 osteoblastic cells（Runx2-deficient cell line）. It also increased alkaline phosphatase activity in MC3T3-E1 and RD-C6 cells and calvarial osteoblastic cells isolated from the calvariae of newborn mice. Acerogenin A also increased the expression of mRNAs related to osteoblast differentiation, including Osteocalcin, Osterix and Runx2 in MC3T3-E1 cells and primary osteoblasts：it also stimulated Osteocalcin and Osterix mRNA expression in RD-C6 cells. The acerogenin A treatment for 3 days increased Bmp-2, Bmp-4, and Bmp-7 mRNA expression levels in MC3T3-E1 cells. Adding noggin, a BMP specific-antagonist, inhibited the acerogenin A-induced increase in the Osteocalcin, Osterix and Runx2 mRNA expression levels. These results indicated that acerogenin A stimulates osteoblast differentiation through BMP action, which is mediated by Runx2-dependent and Runx2-independent pathways.

4）本事業に関連して世界的な研究拠点形成に向けて、以下の点で改善・整備等されたこと

A（研究拠点形成）

我々が従来行なってきた骨生物学的研究を基盤として、骨再生、癌による骨浸潤などの骨疾患の病態、治療法に関連する研究計画を立案し、「歯と骨の分子疾患科学の国際教育研究拠点」に相応しい研究を推進することとした。

B（研究教育環境）

In vivo imagingの研究を効率的に推進するために、既存の共焦点顕微鏡をグレードアップし、研究の促進を図った。

C（人材確保）

臨床系分野からの大学院生を受入、本研究を推進している。

D（人材育成）

大学院生の研究レベルを向上させるために、各大学院生には分野内で特定の指導教官を配置し、指導体制をとっている。

E（国際化）

国際学会での発表を目指すよう指導し、国内における外国人の講演への積極的に参加させている。

5）GCOE事業を推進するに当たって力を入れた点

現在までに我々が行なってきた骨細胞生物学の研究を基盤として、インージングの手法も取り入れて骨疾患の病態解析、治療法の開発へ向けた研究を推進するようにしている。

6）英文原著論文

1. Sakamoto K, Aragaki T, Kawachi H, Katsube K, Miki Y, Takizawa T, Omura K, Morita K, Okada N, Yamaguchi A：Down-regulation of keratin 4 and keratin 13 expression in oral squamous cell carcinoma and epithelial dysplasia：a clue for histopathogenesis.. Histopathol 58：531-542,2011
2. Kihara K, Ichikawa S, Yonezawa T, Lee JW, Akihisa T, Woo JT, Michi Y, Amagasa T, Yamaguchi A：Acerogenin A, a natural compound isolated from Acer nikoense Maxim,stimulates osteoblast differentiation through bone morphogenetic protein action. Biochem Bioph Res Commun 406：211-217,2011
3. Cao L, Moriishi T, Miyazaki T, Iimura T, Tamamura S, Komori T, Yamaguchi A：Comparative morphology of osteocytes in aquatic and land vertebrates. J Bone Miner Metab 29：662-670,2011
4. Horiguchi K, Sakamoto K, Koinuma D, Semba K, Inoue A, Inoue S, Fujii H, Yamaguchi A, Miyazawa K, Miyazono K, Saitoh M：TGF-β drives epithelial-mesenchymal transition through δEF1-mediated downregulation of ESRP. Oncogene（in press）
5. Sakamoto K, Fujii T, Kawachi H, Miki Y, Omura K, Morita K, Kayamori K, Khanom R, Katsube K, Yamaguchi A：Reduction of NOTCH1 expression pertains to maturation abnormalities of keratinocytes in squamous neoplasms. Lob Invest（in press）
6. Khanom R, Sakamoto K, Pal SK, Shimada Y, Morita K-i, Omura K, Miki Y, Yamaguchi A：Expression of basal cell keratin 15 and keratin 19 in oral squamous cell carcinoma represent diverse phthophysiologies. Histol Histopathol（in press）
7. Himeno-Ando A, Izumi Y, Yamaguchi Y, Iimura T：Structural differences in the osteocyte network between the calvaria and long bone revealed by three-dimensional fluorescence morphometry, possibly reflecting distinct mechano-adaptations and sensitivities. Biochem Bioph Res Commun（in press）

7）総説ならびに著書

1. Iimura T, Sugiyama M, Makino Y, Nakane A, Watanabe T, Yamaguchi A：Illumination of vertebrate development by fluorescence live imaging. Cytometry Research 21：57-63,2011
2. Iimura T, Nakane A, Sugiyama M, Sato H, Makino Y, Watanabe T, Takagi Y, Numano R, Yamaguchi A：A fluorescence spotlight on the clockwork development and metabolism of bone. J Bone Miner Metab. 2011 Jul 16. [Epub ahead of print]
3. 飯村忠浩、中根綾子、姫野彰子、杉山真由、山口 朗：骨の形態的解析法の進歩;骨のIn vivo 蛍光イメージングの現状と展望．骨形態計測学会雑誌 21：17-24,2011
4. 中根綾子、沼野利佳、佐藤博己、高木裕三、山口 朗、飯村忠浩：骨の成長と代謝における概日リズムの働きー蛍光イメージングによるアプローチと展望—. 骨形態計測学会雑誌 21：41-50,2011
5. 佐藤　潔、栢森　高、小村　健、山口 朗：IL-6の骨代謝に対する作用、骨粗鬆症治療 10：20-24,2011

8）平成23年度までの自己評価

我々は長年、骨形成の分子メカニズムの研究を中心として骨生物学の基礎研究を推進してきた。本GCOEプログラムでは、現在までの基礎研究を継続するとともに、

骨再生、癌の骨破壊、顎骨の疾患などの研究を推進し、「骨の分子疾患科学」に相応しい研究を推進した。特に、癌により顎骨浸潤のメカニズム、in vivo imagingによる骨の解析に概ね順調に推進することができたと考えている。しかし、骨再生の研究がやや予定より遅れているので、反省点として上げられる。

9）学会発表（英文）

1. Matsumoto T, Moriyama K, Yamaguchi A：Osteocytes are involved in osteoclastic bone resorption induced by mechanical loading during orthodontic tooth movement. 3rd Joint Meeting of the European Calcified Tissue Society & International Bone and Mineral Society, May 10, 2011, Athens, Greece
2. MakinoY, Takahashi Y, Tanabe R, Hata K, Goseki-Sone, Kanno J, Saga Y, Kaneko K, Yamaguchi A, Iimura T：Analysis of axial skeleton development in Type 2 Spondylocostal Dysostosis model Mesp2（-/-）mouse, suggesting an essential role of the segmentation clock output for proper alternate arrangement of vertebral bodies and intervertebral discs. 2nd Asia-Pacific Osteoporosis and Bone Meeting, Gold Coast, Australia, September 4-8、2011
3. Watanabe T,, Nakane A, Hoshino K, Makino Y, Yamaguchi A, Iimura T：Involvement of changes in subcellular localization of Runx2 and Osterix in osteoblast differentiation revealed by 3-dimensional fluorescencemorphometry The American Society for Bone and Mineral Research 2011 Annual Meeting, San Diego, California, USA, September 16-20, 2011

10）学会発表（和文）

1. 木原翼、道泰之、天笠光雄、山口 朗：骨芽細胞分化に及すアセロゲニンの作用、
第65回日本口腔科学会学術集会、2011年4月15日、タワーホール船堀、東京
2. 渡辺高、天笠光雄、山口 朗、飯村忠浩：骨芽細胞分化と骨形成における骨芽細胞特異的転写因子の細胞内局在—蛍光イメージングによる解析—、第65回日本口腔科学会学術集会、2011年4月15日、タワーホール船堀、東京
3. サミール　パル、坂本啓、天笠光雄、山口 朗：The role of thrombospondin-1（TSP1）in invasion of oral cancer、第65回　日本口腔科学会学術集会、2011年4月16日、タワーホール船堀、東京
4. 大上えりか、天笠光雄、山口 朗：口腔扁平上皮癌が産生する破骨細胞性骨吸収制御因子同定の基盤構築、第65回　日本口腔科学会学術集会、2011年4月16日、タワーホール船堀、東京
5. 坂本啓、山口 朗：NOTCH1の口腔癌の病態における意義、第100回日本病理学会総会、2011年4月29日、パシフィコ横浜
6. 松本　力、飯村忠浩、山口 朗：強制力による歯の移動における骨細胞の役割、第31回日本骨形態計測学会、2011年5月20日、長良川国際会議場、岐阜
7. 渡部　高、天笠光雄、山口 朗、飯村忠浩：定量的in situ蛍光イメージングによる骨芽細胞特異的転写因子の骨組織内での分布と細胞内局在の変化の観察、第31回日本骨形態計測学会、2011年5月21日、長良川国際会議場、岐阜
8. 星野昭芳、飯村忠浩、山本健二、山口 朗：骨代謝におけるケモカイン受容体（CCR1）の機能解析、第28回日本骨代謝学会学術集会、東京（京王プラザホテル）、2011年7月21日
9. 相澤怜、山田篤、鈴木大、山本剛、飯村忠浩、山口朗、山本松男、上條竜太郎：Cdc42は四肢形成における軟骨形成と肢芽指間域のアポトーシスを制御する（優秀ポスター賞）、第53回歯科基礎医学会学術大会、2011年9月30日、長良川国際会議場、岐阜
10. 佐藤潔、坂本啓、栢森高、山口朗：口腔扁平上皮癌による骨破壊予防治療法の開発（優秀ポスター賞）、第53回歯科基礎医学会学術大会、2011年9月30日、長良川国際会議場、岐阜

11）外部資金の獲得状況

1. 厚生労働省科学研究費金（再生医実用化事業）

研究課題：実験的再生歯の臨床応用に関する研究
研究代表者：山口　朗
期間：平成21－23年
研究費総額：2600万円（平成21-23年）

2. 科学研究費補助金基盤研究（A）

研究課題：オステオネットワークの維持と破綻：顎顔面骨疾患の病態解明を目指した基盤研究
研究代表者：山口　朗
期間：平成22年－平成24年3月
研究費総額：3700万円

3. 科学研究費補助金（挑戦的萌芽研究）

研究課題：オステオネットワーク獲得機構の解明を目指した挑戦的研究
研究代表者：山口　朗
期間：平成23－24年
研究費総額：300万円

12）特別講演、招待講演、シンポジウム

1. Yamaguchi A：Molecular mechanism of bone destruction by oral squamous cells carcinoma, The First international Oral Pathology Update Symposium, Taipei, 2011, Mar 27
2. 山口 朗：ビスホスホネート関連顎骨壊死（骨髄炎）、（シンポジウム：難治性骨髄炎の治療戦略）、第65回日本口腔科学会学術集会、2011年4月14日（東京）
3. 山口 朗：骨再生の分子基盤（シンポジウム：骨の再生医療）、第65回日本口腔科学会学術集会、2011年4月15日（東京）
4. 山口 朗：ビスフォスフォネート関連顎骨壊死（骨髄炎）の病理学的所見、シンポジウム、第31回日本骨形態計測学会、2011年5月20日（岐阜）
5. 山口 朗：血管石灰化と骨・軟骨関連因子、シンポジウム：CDKにおける異所性石灰化：基礎と臨床、第56回日本透析医学会学術総会、2011年6月18日（横浜）
6. Yamaguchi A：Histopathological characteristics of bisphosphonate-related osteomyelitis (osteonecrosis) of jaw. Keynote Lecture. 5th Meeting of Asian Society of Oral and Maxillofacial Pathology. Fukuoka, August 24, 2011
7. Yamaguchi A：Role of BMP, Notch, and CCN3 in osteoblast differentiation and bone regeneration. Lecture. International Summer Program 2011, Tokyo Medical and Dental University, Tokyo, August 30, 2011
8. 山口 朗：オステオネットワークの構築・維持・破壊、第41回骨・カルシウム代謝研究会（特別講演）、2011年10月14日、ホテルグランビィア京都
9. 山口 朗：口腔癌による骨破壊の分子メカニズム. 口腔三学会合同シンポジウム、第56回日本口腔外科学会総会、2011年10月22日（大阪）

13）教室、分野や講座の准教授、講師、助教、特別研究員、ポスドク、指導を受けた大学院生の名前

分野のスタッフ

特任准教授　飯村（GCOEシャペロン教官）
講　師　勝部　憲一
助　教　坂本　啓
特任助教　玉村　禎宏

指導を受けた大学院生

○ 松本　力（顎顔面矯正学）（4年）
○ Samir Kumar Pal（4年）
○ 大上　えりか（顎顔面外科学）（4年）
○ 渡辺　高（顎顔面外科学）（4年）
○ 佐藤　潔（顎口腔外科）（4年）
○ Rumana Khanom（3年）
○ 島田（顎口腔外科）（3年）
松下　祐樹（顎顔面外科学）（3年）
Xhao Xin（2年）

指導を受けた大学院特別研究学生

牧野　祐司
（順天堂大学医学部整形外科）（3年）

○はAISS

Laboratory Investigation (2012), 1–15
© 2012 USCAP, Inc All rights reserved 0023-6837/12 $32.00

Reduction of NOTCH1 expression pertains to maturation abnormalities of keratinocytes in squamous neoplasms

Kei Sakamoto[1], Takuma Fujii[2], Hiroshi Kawachi[3], Yoshio Miki[4], Ken Omura[5], Kei-ichi Morita[6], Kou Kayamori[7], Ken-ichi Katsube[1] and Akira Yamaguchi[1]

Notch is a transmembrane receptor functioning in the determination of cell fate. Abnormal Notch signaling promotes tumor development, showing either oncogenic or tumor suppressive activity. The uncertainty about the exact role of Notch signaling, partially, stems from inconsistencies in descriptions of Notch expression in human cancers. Here, we clarified basal-cell dominant expression of NOTCH1 in squamous epithelium. NOTCH1 was downregulated in squamous neoplasms of oral mucosa, esophagus and uterine cervix, compared with the normal basal cells, although the expression tended to be retained in cervical lesions. NOTCH1 downregulation was observed even in precancers, and there was little difference between cancers and high-grade precancerous lesions, suggesting its minor contribution to cancer-specific events such as invasion. In culture experiments, reduction of NOTCH1 expression resulted in downregulation of keratin 13 and keratin 15, and upregulation of keratin 17, and *NOTCH1* knockdown cells formed a dysplastic stratified epithelium mimicking a precancerous lesion. The NOTCH1 downregulation and the concomitant alterations of those keratin expressions were confirmed in the squamous neoplasms both by immunohistochemical and cDNA microarray analyses. Our data indicate that reduction of NOTCH1 expression directs the basal cells to cease terminal differentiation and to form an immature epithelium, thereby playing a major role in the histopathogenesis of epithelial dysplasia. Furthermore, downregulation of NOTCH1 expression seems to be an inherent mechanism for switching the epithelium from a normal and mature state to an activated and immature state, suggesting its essential role in maintaining the epithelial integrity.
Laboratory Investigation advance online publication, 13 February 2012; doi:10.1038/labinvest.2012.9

KEYWORDS: epithelial dysplasia; esophagus; Notch1; oral mucosa; squamous cell carcinoma; uterine cervix; keratin

Notch is a transmembrane receptor that regulates cell proliferation and differentiation in various tissues. Notch is constitutively processed and is tethered on the plasma membrane as a heterodimeric protein, and the signal is transduced by the Notch intracellular domain (NICD) produced by ligand-induced cleavage,[1,2] which translocates to the nucleus and directly induces the transcription of downstream targets by forming a transactivation complex with several cofactors.[3] In humans, there are four *Notch* homologs (*NOTCH1*, *2*, *3*, *4*) and they exhibit diverse patterns of expression, suggesting different contributions in each tissue.

The expression of Notch1, Notch2 and Notch3 in mouse skin and hair follicles has been documented,[4–7] and Notch signaling seems to have important roles in the regulation of epidermal differentiation. Conditional knockout of *Notch1* in skin results in epidermal and corneal hyperplasia.[8] Overexpression of constitutively active Notch1 in basal cells leads to hyperplastic epidermis and abnormal hair development.[4,9] In contrast, deletion of *Notch2*, *Notch3* and *Notch4* does not cause significant changes in the epidermis.[6,10,11] These results indicate the significance of Notch1 in epidermal differentiation.

Abnormal Notch signaling can promote tumor development. The first indication that Notch has a role in carcinogenesis was obtained from a mouse mammary tumor virus integration assay in which four genes were identified as candidates that associate with tumor progression, the third of which (int-3) turned out to be a truncated form of *Notch4*.[12]

[1]Section of Oral Pathology, Tokyo Medical and Dental University, Tokyo, Japan; [2]Department of Obstetrics and Gynecology, Keio University School of Medicine, Tokyo, Japan; [3]Section of Human Pathology, Tokyo Medical and Dental University, Tokyo, Japan; [4]Section of Molecular Genetics, Medical Research Institute, Tokyo Medical and Dental University, Tokyo, Japan; [5]Section of Oral and Maxillofacial Surgery, Tokyo Medical and Dental University, Tokyo, Japan; [6]Department of Advanced Molecular Diagnosis and Maxillofacial Surgery, Hard Tissue Genome Research Center, Tokyo Medical and Dental University, Tokyo, Japan and [7]Section of Diagnostic Oral Pathology, Tokyo Medical and Dental University, Tokyo, Japan
Correspondence: Dr K Sakamoto, Section of Oral Pathology, Tokyo Medical and Dental University, Yushima 1-5-45, Tokyo 113-0034, Japan.
E-mail: s-kei.mpa@tmd.ac.jp

Received 29 August 2011; revised 25 November 2011; accepted 15 December 2011; published online 13 February 2012

Gain of function mutation of *NOTCH1* was detected in many cases of T-cell acute lymphoblastic leukemia,[13] and this finding gave rise to the concept of treatment by inhibiting the formation of Notch transactivation complex.[14] In cervical cancer, the upregulation of NOTCH1[15,16] and NOTCH2,[16] and an increase in nuclear localization of NICD[17] were documented. On the basis of these observations, activation of Notch signaling is thought to be associated with the development of cervical cancer.[18] However, promotion of carcinogenesis by Notch signal activation seems contradictory to the phenotypes observed in the *Notch1* knockout mouse, which exhibits an increase in the incidence of papilloma and chemical-induced skin cancer,[8] and the transgenic mouse of the pan-Notch inhibitor, dominant-negative *Mastermind-like 1*, which shows dysplasia and SCC of skin.[19] In fact, expression of NOTCH1 is decreased in skin cancer,[20,21] suggesting that *NOTCH1* acts as a tumor suppressor. To solve the discrepancy of the proposed role of Notch, accurate knowledge of its expression is crucial. To assess its contribution in cancer, the Notch expression should be evaluated in comparison with the normal cells from which the cancer cells originated. However, it appears that the expression of Notch in human cancers has not been properly evaluated along this line. Even the localization of Notch proteins in normal adult tissue is unclear, partially, because of the difficulty of detection.

To address this issue, we have engaged in an examination of Notch expression in adult human tissues. In this study, we first demonstrate that NOTCH1 is predominantly expressed in the basal cells of normal squamous epithelium. Then we expand the examination to neoplasms that have originated from squamous epithelium and show that Notch1 expression is downregulated in these lesions. Cell culture experiments indicate that reduction of NOTCH1 expression associates with abnormal differentiation represented by alteration of keratin subtype expression. Our data suggest that aberrant epithelial differentiation in squamous neoplasms is caused by the reduction of NOTCH1 expression, which in turn unveils its essential function in the maintenance of normal epithelial integrity.

MATERIALS AND METHODS

Clinical Specimens

A total of 56 specimens of oral lesions (epithelial dysplasia and squamous cell carcinoma) were collected at the Dental Hospital of Tokyo Medical and Dental University. Pharyngeal cancers were excluded; the case summaries are shown in Supplementary Material 1. A total of 20 specimens of esophageal lesions (squamous cell carcinoma) and normal tissues were collected at Medical Hospital of Tokyo Medical and Dental University; the case summaries are shown in Supplementary Material 2. A total of 57 specimens of uterine cervical lesions (intraepithelial neoplasm and squamous cell carcinoma) were collected at Keio University Hospital; the case summaries are shown in Supplementary Material 3. The tissues were fixed in formalin and embedded in paraffin according to the routine laboratory protocol. HPV genotyping was performed as previously described[22] from the conventional cytology specimens. All experiments were approved by the ethics committees of both universities.

cDNA Microarray Analysis

Oral squamous cell carcinoma (OSCC) cells were taken from surgically excised specimens by laser capture microdissection and were subjected to cDNA microarray analysis, as previously described.[23]

Immunostaining and *In Situ* Hybridization

Immunohistochemical staining was performed using the Sequenza (Thermo Fisher Scientific, MA, USA). For antigen retrieval, the sections were autoclaved in alkaline buffer (10 mM Tris (pH = 9.0) and 1 mM EDTA) at 120 °C for 20 min. The primary antibodies used in this study were anti-Notch1 (EP1238Y, Epitomics, CA, USA); cleaved Notch1 (Val1744; D3B8, Cell Signaling, MA, USA) Notch2 (D67C8, Cell Signaling); Notch3 (D11B8, Cell Signaling); Hes1 (EPR4226, Epitomics); Hey1 (polyclonal, Millipore, MA, USA); keratin 5 (K5; EPR1600Y, Epitomics); K13 (EPR3671, Epitomics); K13 (alternative antibody, KS-1A3, Leica Microsystems, Wetzlar, Germany); K15 (EPR1614Y, Epitomics); K17 (D73C7, Cell Signaling); K17 (alternative antibody, E3, Dako, Glostrup, Denmark); K18 (DC10, Dako); pan-Keratin (AE1/AE3, Dako); Vimentin (SP20, Epitomics); E-cadherin (36/E-Cadherin, BD transduction laboratories, CA, USA); Desmoglein3 (3G133, Santa Cruz, CA, USA); p63 (4A4, Dako); β-tubulin (9F3, Cell Signaling) and β-actin (C-2, Santa Cruz). EnVision Dual Link (Dako) was used as the secondary antibody. Coloration was done in DAB substrate. For immunofluorostaining, Alexa Fluor 488 anti-rabbit IgG (Invitrogen, CA, USA) and DAPI were used. *In situ* hybridization to mouse E18.5 embryos was conducted as previously described.[24] Antibody adsorption test was performed as follows. HEK293 cells were transfected with *Notch1* or *NOTCH3* and were fixed 48 h after transfection. The anti-NOTCH1 or anti-NOTCH3 antibody (diluted 1/500) was applied to the fixed cells, respectively, and incubated for 1 h. The adsorbed supernatants were collected and used for immunohistochemical staining. The immunostaining results were compared with that using the antibody adsorbed to mock-transfected cells.

Protein Extraction from Formalin-Fixed Paraffin-Embedded Specimens

Formalin-fixed paraffin-embedded specimens were sectioned at 10 μm thick and deparaffinized. Tissues were manually dissected under a microscope. The collected tissues were heated at 95 °C for 1 h and then at 60 °C for 4 h in the protein extraction buffer (50 mM Tris (pH = 8.0), 5 mM EDTA, 2% SDS).

Genes

Mouse *Notch1* was provided by Dr J. Nye and constitutive active *Notch1* were previously described.[25] Notch extracellular domain (NECD) was created by ligating the PCR amplified *Notch1* extracellular and transmembrane regions (1 M to 1755G) into *pAcGFP1-C2* (Clontech). Human *Notch3* was provided by Dr A. Joutel. *Rbpj* cDNA was provided by the RIKEN BioResource Center (Ibaraki, Japan) courtesy of Dr T. Honjo and cloned into *pCMV-Tag4* (Stratagene, CA, USA), and dominant-negative *Rbpj (R218H)* was created by PCR mutagenesis. Dominant-negative *Dll1* (chick) was previously described.[26] Human *TP63α(TA)* was purchased from Invitrogen. *TP63α(ΔN)* was created as follows. A plasmid (*pBK-CMV-dN*) was made, which contained the sequence corresponding to the *TP63α(ΔN)*-specific N-terminal region by ligating annealed oligoniculeotides into *pBK-CMV* (Stratagene). As the N-terminal *TP63α(TA)*-specific region incidentally coincides to 5′ of MSC1 site, the N-terminal region was deleted from *TP63α(TA)* by MSC1 digestion, and the fragment was ligated into *pBK-CMV-dN*. The resulting plasmid was confirmed by DNA sequencing to carry *TP63α(ΔN)* identical to the wild type. Human *KRT13* and *KRT15* promoters were cloned by PCR from the BAC clone RP11-156A24, and human *KRT17* promoter was cloned from the BAC clone RP13-415G19, both of which were provided by the BACPAC Resources Center (CA, USA). The sequences of the PCR primers used in the cloning procedures will be provided on request. Stealth RNAs for human *NOTCH1* were purchased from Invitrogen. The sequence of the plus strand of the dsRNA is 5′-UCGCAUUGACCAUUCAAACUGGUGG-3′.

Cell Culture Experiments

GE-1, Ca9-22, HeLa and CaSki cells were provided by the RIKEN BioResource Center. HSC-3 and 293 cells were provided by the Japanese Collection of Research Bioresources (Osaka, Japan). Human foreskin (HFS) cells were purchased from Kurabo (Osaka, Japan). Transfections were performed using Lipofectamine 2000 (Invitrogen) or by calcium phosphate method. Cell proliferation was evaluated using a Cell Counting Kit (Dojindo, Kumamoto, Japan). Cells were lysed in RIPA buffer and the concentration of the protein was measured using a BCA Protein Assay Kit (Thermo Fisher Scientific, MA, USA). Western blot analysis and RT-PCR were performed according to standard protocols.[27] Three-dimensional culture was conducted using Millicell Culture Inserts (Millipore). Real-time RT-PCR was performed using a Lightcycler (Roche, Basel, Switzerland). The PCR primer sequences are as follows: hN1-5865F, 5′-CAACATCCAGGACAACATGG-3′; hN1-6093R, 5′-GGACTTGCCCAGGTCATCTA-3′; hN2-7187F, 5′-ATGCTTCCTCAAATGCTGCT-3′; hN2-7513R, 5′-TCATTTCTCTCCCGGATGAC-3′; hN3-7275F, 5′-GTCTGGGACCTCCTTCTTCC-3′; hN3-7628R, 5′-CCAAGGGTGCCTACTTGGTA-3′; hN4-6444F, 5′-TGCAGGCATATGGGATGTAA-3′; hN4-6665R, 5′-CATCCCCACAGTGGAGTTCT-3′; HES1-468F, 5′-GCGGACATTCTGGAATGACA-3′; HES1-594R, 5′-CGTTCATGCACTCGCTGAAG-3′; HEY1-485F, 5′-GATGACCGTGGATCACCTGAA-3′; HEY1-584R, 5′-CCGAAATCCCAAACTCCGATAG-3′; GAPDH-275F, 5′-GCACCGTCAAGGCTGAGAAC-3′; GAPDH-417R, 5′-ATGGTGGTGAAGACGCCAGT-3′.

Luciferase Activity Assay

KRT13, *KRT15* and *KRT17* promoter fragments were cloned as described in the Genes section, and ligated into *pGL4.10.* (Promega, WI, USA). The promoter construct of 0.1 μg, 0.1 μg of the *Notch1* construct and 0.01 μg of the *Renilla* luciferase standardization plasmid were transfected into GE-1 cells on 48-well plates and the luciferase activity was measured 48 h after transfection using a Dual-Luciferase Reporter Assay System (Promega). All transfections were done in triplicate and the experiments were repeated at least twice.

RESULTS

Expression of NOTCH1 in Basal Cells of Squamous Epithelium

In the pilot study, we screened for optimal antibodies that clearly detect an endogenous level of Notch in western blot analysis. The selected antibodies revealed that NOTCH1, NOTCH2 and NOTCH3 were expressed in primary HFS cells and HEK293 cells, whereas NOTCH4 was not detected (data not shown). This result was confirmed by RT-PCR analysis, which revealed expression of *NOTCH1*, *NOTCH2* and *NOTCH3* but not *NOTCH4* (data not shown). These (anti-NOTCH1 and anti-NOTCH3) antibodies reacted with recombinant Notch1 (mouse) and NOTCH3 (human), respectively, which were overexpressed in HEK293 cells as well as with the endogenous proteins, as revealed both by western blot analysis and immunofluorescent staining, validating their specific reactions (Supplementary Material 4A, B). We then examined their immunohistochemical expression in various human adult tissues. Distinct expression of NOTCH1 was observed in the basal cells of squamous epithelium (Figure 1a). This was consistent with the result of *in situ* hybridization, which exhibited basal-cell expression of *Notch1* in an embryonic mouse skin (Figure 1b). The NOTCH1 protein was detected mainly on the plasma membrane, which is consistent with its function as a transmembrane receptor (Figure 1a). Nuclear staining was rarely observed. Antibody adsorption test showed significantly reduced staining when the antibody was absorbed to *Notch1*-transfected cells, validating the usability in immunohistochemical detection (Supplementary Material 4C). Both cornified- and non-cornified squamous epithelia expressed NOTCH1. The expression in the esophagus and vagina appeared weaker than that in the skin and oral mucosa (Figure 1c), suggesting that the epithelium of ectodermal origin (skin, oral mucosa) expresses NOTCH1 more than that of endodermal origin (esophagus, vagina). Basal (myoepithelial) cells in the secretory glands were weakly

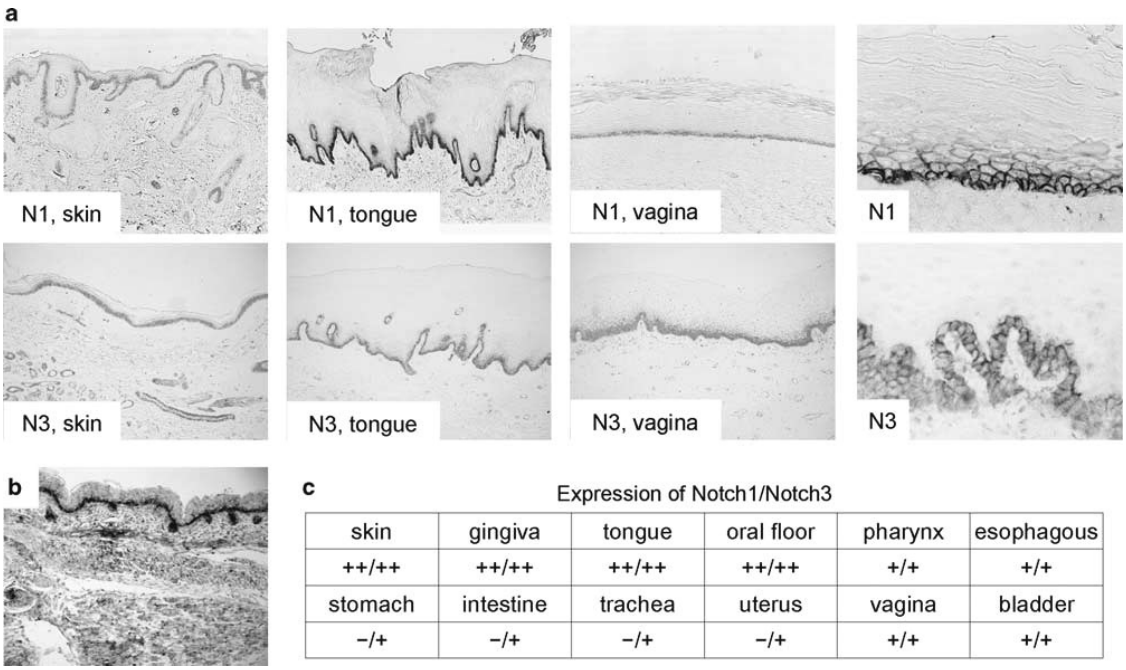

Expression of Notch1/Notch3

skin	gingiva	tongue	oral floor	pharynx	esophagous
++/++	++/++	++/++	++/++	+/+	+/+
stomach	intestine	trachea	uterus	vagina	bladder
−/+	−/+	−/+	−/+	+/+	+/+

Figure 1 Expression of NOTCH1 and NOTCH3 in various tissues. (**a**) Immunohistochemical staining of adult human skin, tongue and vagina shows distinct expression in the basal cells. Membrane staining pattern is obvious (right). (**b**) *In situ* hybridization on the skin of mouse E18.5 embryo, using *Notch1* RNA probe. (**c**) Simplified summary of the expression in the epithelium of each tissue.

positive for NOTCH1 (data not shown). In the uterus, the columnar epithelium, including subcolumnar reserve cells, was almost negative for NOTCH1. In the digestive tract, NOTCH1 was detected faintly only in the basal crypts (data not shown). In the subepithelial tissue, NOTCH1 was detected weakly in the vascular endothelial cells (data not shown). NOTCH3 was also expressed in the basal cells of squamous epithelium, showing membranous localization (Figure 1a). The staining pattern of NOTCH3 was a little different from that of NOTCH1, showing weak ubiquitous cytoplasmic staining also in glandular cells (data not shown). This staining in glandular cells seemed nonspecific because it did not decrease when the adsorbed antibody was used, whereas the staining in the basal cells weakened (data not shown). The NOTCH2 antibody was not applicable to immunohistochemical detection, showing no staining in any tissues (data not shown). In summary, NOTCH1 and NOTCH3 were expressed mainly in the basal cells of squamous epithelium.

NOTCH1 Expression Is Downregulated in Squamous Neoplasms

As the anti-NOTCH3 antibody yielded some nonspecific staining that would hamper correct evaluation, we determined to focus on NOTCH1 in this study and expanded our investigations to neoplasms. Because the squamous epithelia were dominant sites of NOTCH1 expression, we chose squamous neoplasms that develop at these sites and investigated whether the expression is upregulated, downregulated or unchanged. For this purpose, we collected surgical specimens of squamous cell carcinoma (cancer). To assess the contribution of NOTCH1 in cancer progression, surgical specimens of intraepithelial neoplasm (precancer) were also collected. To compensate for the organ-specific differences, specimens were collected from three different tissue sources—oral mucosa, esophagus and uterine cervix.

First we examined the NOTCH1 expression in 56 cases of oral epithelial neoplasm, including OSCC and oral intraepithelial neoplasm (OIN). We randomly collected specimens that contained normal epithelium, and the expression was evaluated by the staining intensity in individual tumor cells in comparison with that in normal basal cells within the same specimen. The distinct staining pattern with abrupt changes at the interface between normal epithelium and neoplasm enabled us to adopt this methodology. The expression was scored as being at one of five levels: level 4, upregulated expression compared with the normal basal cells; level 3, expression level similar to the normal basal cells (equivalent to '+ +' in Figure 1c); level 2, expression level less than the normal basal cells; level 1, stained only faintly

(stained at least more than fibroblasts); or level 0, undetected (equivalent to '−' in Figure 1b). NOTCH1 expression was significantly downregulated in most cases of OSCC and OIN (Figures 2a–d, Supplementary Material 1). The downregulation was observed even in the precancerous lesions with minimum histopathological changes (OIN1) and was apparent in most of the precancerous lesions with moderate histological alterations (OIN2), the lesions with prominent histological alterations (OIN3), and OSCC (Figure 2d). There were no cases showing an increase of NOTCH1 expression. No significant correlation was observed between the level of NOTCH1 expression and the histological variations of OIN or the histological differentiation grade of OSCC. To confirm the immunohistochemical evaluation, we dissected normal tissues and cancers separately from the sections, extracted proteins and conducted western blot analysis. In all, 4 out of 10 cases were informative, all of which showed reduced NOTCH1 expression in cancer, normalized to keratin 5 (Figure 2e). This result is consistent with the immunohistochemical observations. Proteins of sufficient amount and quality were not obtained from the other six specimens, probably due to the fixation period. The downregulation of *NOTCH1* in OSCC was also confirmed by cDNA microarray analysis of 41 OSCC *vs* 7 normal oral epithelia ($P<0.001$), with the average expression in OSCC reduced to 0.43-fold compared with the normal control (Figure 2f). The cDNA microarray showed that *NOTCH2* and *NOTCH3* were also downregulated in OSCC to 0.78-fold and 0.83-fold, respectively (data not shown).

Next, we examined the immunohistochemical expression of NOTCH1 in squamous cell carcinoma of esophagus (ESCC; Supplementary Material 2 and 5). Downregulation was evident in 17 out of 20 cases while weak expression remained. The remaining three cases retained a considerable expression, but there were no cases with NOTCH1 upregulation.

Next, we examined the immunohistochemical expression of NOTCH1 in uterine cervical lesions (Supplementary Material 3, 6). NOTCH1 expression tended to be downregulated in cervical intraepithelial neoplasm (CIN) and cervical squamous cell carcinoma (CSCC). However, more than 50% of the cases retained considerable expression (Supplementary Material 6). More cases showed NOTCH1 downregulation in precancerous lesions with little tendency of differentiation (CIN3 and CSCC), compared with precancerous lesions with some tendency of differentiation (CIN1 or CIN2). No significant difference was observed between CIN3 and CSCC (Supplementary Material 6). There was not a single case showing apparent NOTCH1 upregulation in the individual cancer cells. Indistinct nuclear staining was occasionally observed, but most of the neoplastic cells exhibited a membranous or cytoplasmic staining. No significant correlation was observed between the level of NOTCH1 expression and the type of HPV detected in the lesion (Supplementary Material 3).

In summary, the NOTCH1 expression was downregulated both in precancer and cancer of non-cornified squamous epithelium.

NOTCH1 Regulates the Differentiation of Squamous Epithelium

The fact that NOTCH1 was downregulated not only in cancer but also in precancer suggests that aberrant NOTCH1 expression associates with changes of epithelial properties observed both in precancers and cancers. The essential properties that discriminate cancer from precancer are invasion and resultant metastasis, and our data suggest that the downregulation of NOTCH1 may not contribute to these cancer-specific events. In contrast, dysregulation of differentiation is a common feature observed both in cancer and precancer, appearing as abnormality of cell alignment, stratification and keratinization. Considering that Notch governs cell-to-cell signaling, we hypothesized that reduction of Notch signaling might affect the cell-to-cell-based regulation of epithelial differentiation. To test this hypothesis, we conducted cell culture experiments. First, we examined Notch expression in cell lines derived from cervical cancers (HeLa, CaSki), oral cancers (BHY, Ca9-22, HSC-3) and primary HFS cells. Western blot analysis revealed that both NOTCH1 and NOTCH3 were expressed most abundantly in the normal cells, and variably, but at much lower levels, in the cancer cell lines (Figure 3a), which is a finding consistent with the observation that NOTCH1 expression was downregulated in squamous neoplasms. NOTCH2 was considerably expressed in Ca9-22 and HFS cells, and also in HeLa cells more strongly (Figure 3a). To assess the possible correlation between NOTCH1 and differentiation, we examined the expression of epithelial markers in these cells (Figure 3b). In normal non-cornified squamous epithelium, the basal cells express NOTCH1, K15, K19, CDH1, DSG3 and TP63, whereas K16 and K17 expression is weak, and K18 and vimentin are not expressed (data not shown). HFS cells mimicked this expression pattern. The cancer cell lines showed various expression patterns, reflecting the diversities in differentiation states of each cell line (Figure 3b). When we compared the two cervical cancer cell lines, CaSki expressed more NOTCH1 and exhibited a phenotype more similar to normal epithelium than to HeLa. When we compared the three oral cancer cell lines, Ca9-22 that expressed a significantly higher level of NOTCH1 than BHY and HSC-3 exhibited the phenotype very similar to normal epithelium. When the cells were cultured at a high density, HFS and Ca9-22 cells spontaneously differentiated, showing scattered cells positive for K13, a keratin in terminally differentiated keratinocytes (Figure 3c). The other cancer cells showed little potential to express K13. These results suggest that NOTCH1 expression may associate with differentiation of non-cornified epithelium. Cervical cancer cells, which do not fit into this hypothesis, will be discussed in the Discussion section.

Notch1 in squamous neoplasms
K Sakamoto *et al*

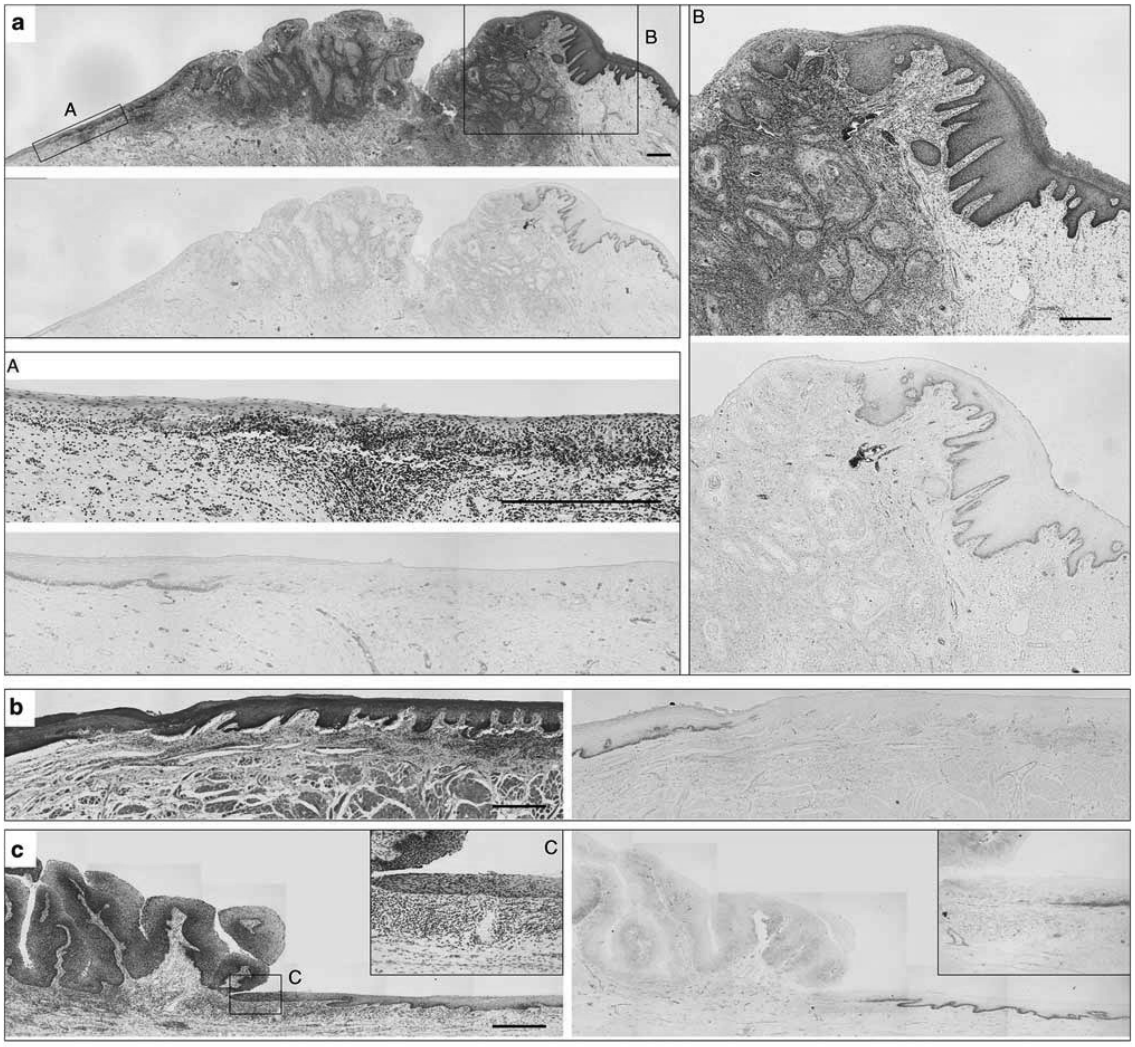

d

OIN		
OIN1	OIN2	OIN3
8/10 (80%)	12/13 (92%)	10/10 (100%)
OSCC		
G1	G2	G3
14/16 (88%)	8/8 (100%)	2/3 (67%)

e

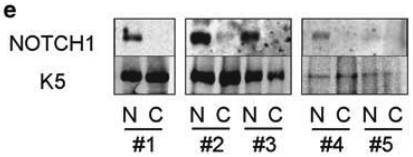

f

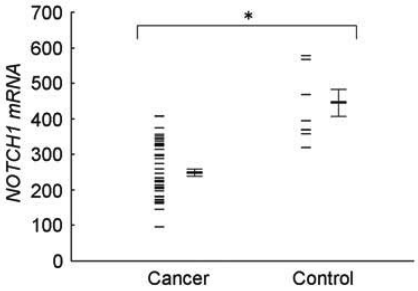

As Ca9-22 mimicked well the phenotype of normal epithelium, and Ca9-22 cells were easily transfected, we thought that they served as a good cell model for assessing differentiation. Accordingly, we examined the effects of Notch signaling in Ca9-22 cells. We treated Ca9-22 cells with gamma-secretase inhibitor (DAPT), which blocks the Notch signaling, and examined K13, K15 and K17 expression after 72 h. These keratins are expressed variably in physiological and pathological conditions, and represent distinct cellular states; K13 represents keratinocytes under terminal differentiation, K15 represents basal cells and K17 represents activated keratinocytes such as those appearing in regenerative epithelium and cancer. DAPT treatment led to reduced expression of a putative downstream target of Notch signaling, HES1, and K13 expression, whereas K15 and K17 levels were largely unchanged (Figure 3d), suggesting that Notch signaling is necessary for terminal differentiation. Next the cells were transfected with various constructs (Figure 3e). Constitutively, active Notch1 (NICD) upregulated HES1 and suppressed K13, suggesting that sustained, high-level Notch signaling inhibits terminal differentiation. Knockdown of *NOTCH1* by siRNA led to a decrease of HEY1, another putative target of Notch signaling, K13 and K15, and an increase of K17. *Rbpjm*, which is a mutant *Rbpj* with a single amino-acid replacement (R218H), and *dnDl*, which is a deletion mutant of *Dll1*, are both known to pose a dominant-negative effect on Notch signaling. Both constructs led to a decrease of HEY1 and an increase of K13. These results indicate that proper expression of NOTCH1 and its signaling are necessary for terminal differentiation, and either the absence of its signaling or its untimely activation results in abnormal differentiation. It should be noted that the phenotype observed in *NOTCH1* knockdown differed from that in the autonomous inhibition of Notch signaling.

We examined the correlation of TP63, a transcription factor that regulates keratinocyte differentiation, with NOTCH1. Among different isoforms, the most abundant TA- and ΔN-isoforms were examined. In uterine cervical cells, TP63(ΔN) acts as a transcriptional repressor of *NOTCH1*, which results in maintenance of self-renewing capacity.[28] In Ca9-22 cells, transfection of *TP63(ΔN)* only slightly decreased NOTCH1 expression and *TP63(TA)* did not have a significant effect on NOTCH1. Both *TP63(TA)* and *TP63(ΔN)* decreased K13 expression (Figure 3f). *NICD* overexpression and *NOTCH1* knockdown both led to downregulation of TP63(ΔN) and K13 (Figure 3g). These results indicate that TP63(ΔN) inhibits differentiation partially by repressing NOTCH1 expression, whereas Notch signaling also mediates TP63(ΔN) expression.

To further investigate the contribution of Notch signaling in regulation of keratin subtype expression, we conducted promoter analysis of the keratin genes using GE-1 cells that were established from normal mouse gingival epithelium. We co-transfected the cells with *Notch1*, *NICD* or *NECD*, and the luciferase reporter constructs for *KRT13*, *KRT15* or *KRT17* promoters. NECD is a membrane-tethered Notch1 extracellular domain whose intracellular domain was replaced by AcGFP. Notch1 increased the *KRT13* promoter activity while NICD decreased it. NECD decreased the *KRT15* promoter activity and slightly increased the *KRT17* promoter activity (Figure 3h). These results suggest that NOTCH1-expressing cells have more potential to differentiate, but Notch signaling itself autonomously inhibits differentiation and directs the cell to maintain basal-cell phenotype.

Next we examined the effect of *NOTCH1* knockdown in normal epithelial cells using the primary HFS cells. The knockdown efficiency was more than 90% as revealed by western blot analysis (Figure 4a). *NOTCH1* knockdown significantly suppressed the expression of *HEY1*, whereas *HES1* showed only slight (20%) reduction, as revealed by real-time PCR (Figure 4b, real-time PCR data are not shown). Cell proliferation was not altered by *NOTCH1* knockdown (data not shown). The total amount of keratin protein was unchanged, and vimentin was not induced by *NOTCH1* knockdown (Figure 4c). *NOTCH1* knockdown led to downregulation of K13 and K15, and upregulation of K17. Immunocytostaining using the anti-K13 antibody revealed that *NOTCH1* knockdown resulted in a decrease both of the staining intensity in individual cells and of the number of stained cells (Figure 4d). The expression of CDH1 (E-cadherin), DSG3 (desmoglein 3) and TP63 was not significantly altered (Figure 4c). In a three-dimensional culture, the *NOTCH1*-knockdown cells formed a stratified epithelium that exhibited a thickened cell layer and a disarray of stratification (Figure 4e), which are reminiscent of the histological features of precancer. These results suggest that reduced

Figure 2 Expression of NOTCH1 in oral squamous cell carcinoma (OSCC, cancer) and oral intraepithelial neoplasm (OIN, precancer). (**a**) OSCC associated with OIN. Low-magnification view and the highlighted borders of the lesion (A, B). NOTCH1 expression is significantly reduced in OIN (A) and OSCC (B). Clear demarcations of NOTCH1 expression are seen, which coincides with the border of the lesion. Scale bar, 0.5 mm. (**b**) OIN1 (mild epithelial dysplasia). NOTCH1 is significantly downregulated even in this lesion with minimum histological change, and the border of NOTCH1 expression coincides with the border of the lesion. Scale bar, 0.5 mm. (**c**) Papillary-type OSCC. Low-magnification view with the highlighted border of the lesion (C). Downregulation of NOTCH1 is evident. Scale bar, 0.5 mm. (**d**) Numbers of cases (and percentage) with reduction of NOTCH1 expression. G1, well-differentiated; G2, moderately differentiated; G3, poorly differentiated OSCCs. (**e**) Western blot analysis using surgical specimens. Formalin-fixed paraffin-embedded tissues were separately dissected from normal (N) and cancer (C) tissues, and the proteins were extracted. A sufficient amount of protein was obtained from 4 out of 10 cases, in which NOTCH1 expression was reduced in cancer (Case #1 to #4). Keratin 5 (K5) was used for standardization. Case #5 is shown as an example of a non-informative case. (**f**) cDNA microarray analysis of 41 OSCC and 7 normal control epithelia. Vertical axis corresponds to globally normalized signal intensity of *NOTCH1* mRNA expression. *NOTCH1* is significantly downregulated in OSCC compared with normal epithelium (*$P<0.001$). Short bars, expression in each case; long bars, mean; error bars, s.e.

NOTCH1 expression results in conversion from a differentiated epithelium to an immature or hyperplastic epithelium represented by K17 expression.

Correlation Between NOTCH1 and Keratin Subtype Expression in Tissue

To validate the results obtained by cell culture experiments, we immunohistochemically examined the keratin expression in cancer and precancer of oral mucosa, esophagus and uterine cervix. NOTCH1 and K13 were concomitantly downregulated along with downregulation of K15 and upregulation of K17 in most oral and esophageal lesions (Figure 5a). In cervical lesions, a similar tendency was observed. However, there were also cases with considerably retained NOTCH1 expression, and NOTCH1-retained lesions showed a different keratin pattern, namely, K15-positive basaloid cell

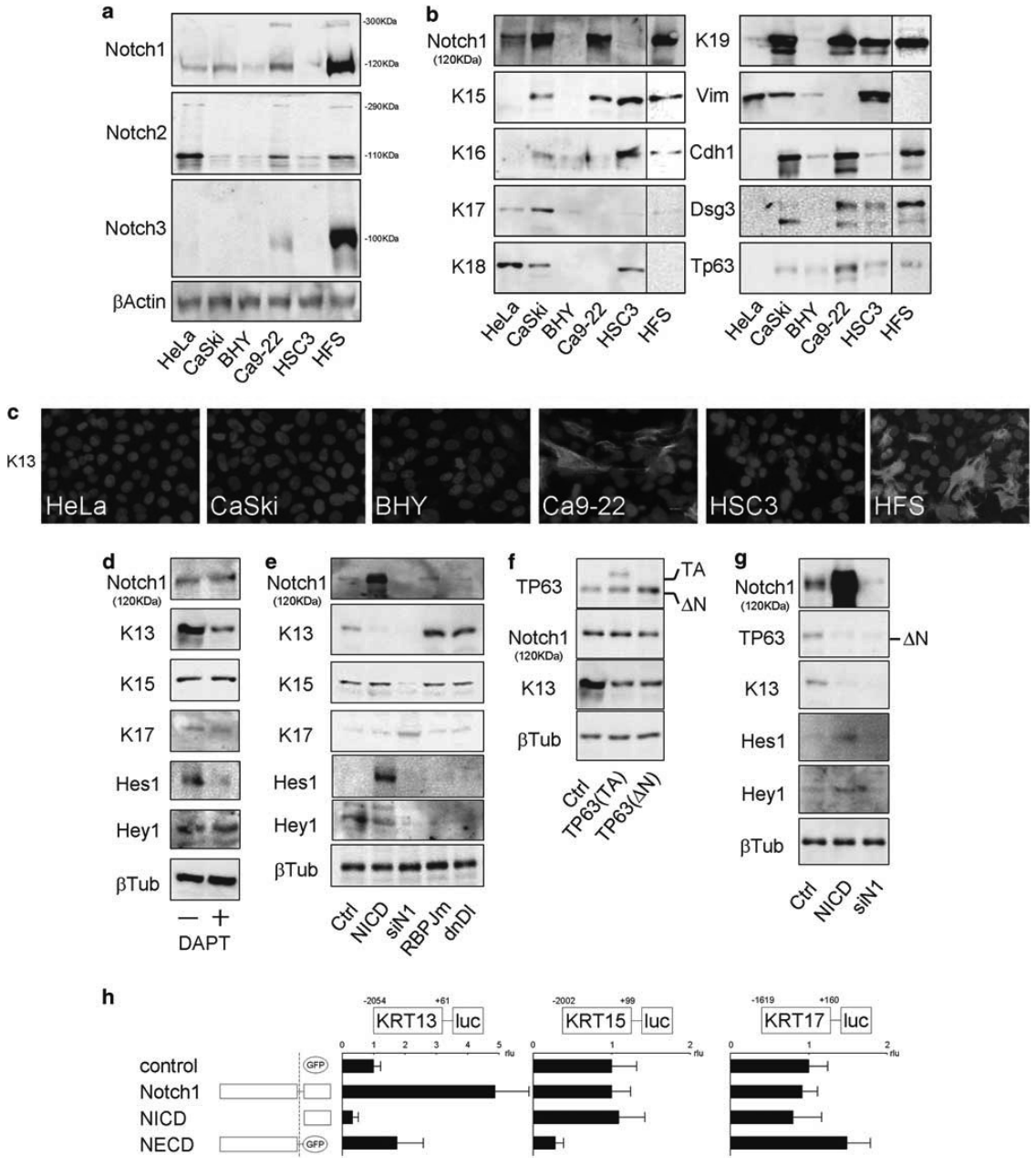

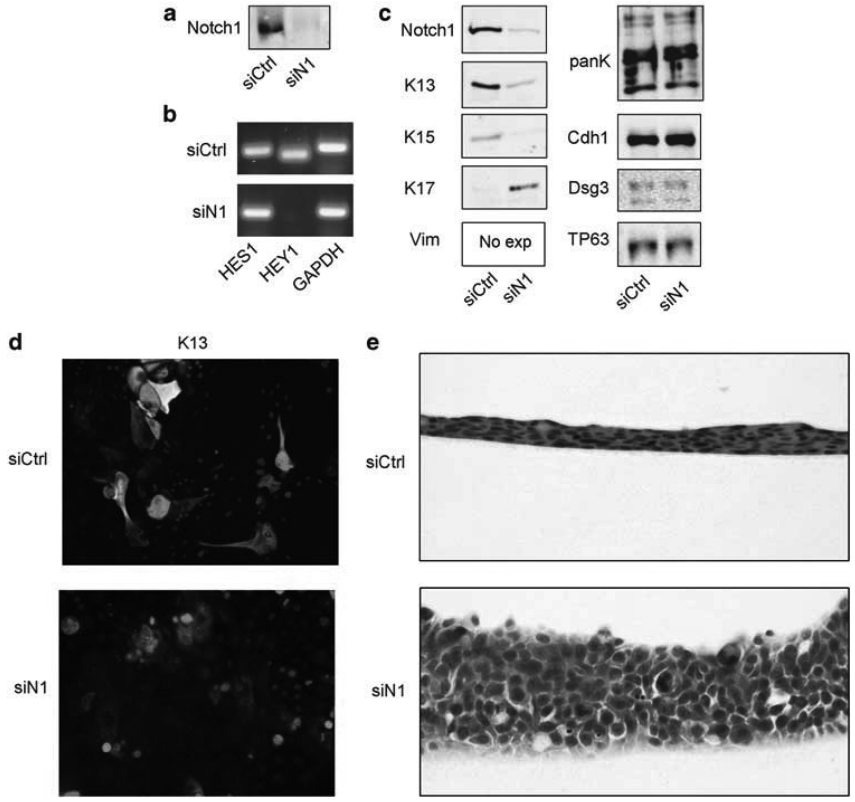

Figure 4 Notch1 knockdown in primary foreskin (HFS) cells results in immature epithelium. (**a**) Efficiency of *NOTCH1* knockdown. HFS cells were transfected with negative control siRNA (*siCtrl*) or siRNA for *NOTCH1* (*siN1*) were incubated for 7 days and subjected to western blot analysis. (**b**) Effect of *NOTCH1* knockdown on the target genes. Real-time RT-PCR revealed that *HEY1* was almost completely suppressed, whereas *HES1* was downregulated only by 20% (data not shown). The post-real-time PCR samples were diluted and amplified for an additional two cycles in order to make them visible on gel electrophoresis. Thus this figure actually shows conventional RT-PCR. (**c**) The effect of *NOTCH1* knockdown on the expression of keratinocyte differentiation markers. K, keratin; Vim, vimentin; panK, pan-keratin; Cdh1, E-cadherin; Dsg3, desmoglein 3; No exp, no expression. (**d**) Expression of K13 in HFS cells transfected with *siCtrl* or *siN1* 7 days after transfection, revealed by immunofluorostaining. The fluorescence intensity in the individual cells and the number of positively stained cells decreased in the siN1-transfected cells. (**e**) Vertical sections of three-dimensionally cultured HFS cell layers, stained with hematoxylin and eosin. Cells were transfected and seeded in Millicell culture inserts and cultured for 10 days.

Figure 3 NOTCH1 regulates keratin expression. (**a**) Expression of NOTCH1, NOTCH2 and NOTCH3 in cervical cancer cell lines (HeLa, CaSki), oral cancer cell lines (BHY, Ca9-22, HSC-3) and primary human foreskin (HFS) cells, as revealed by western blot. All the antibodies recognize an epitope in the intracellular domain. Most proteins were detected as a furin-cleaved form containing the transmembrane and intracellular domains. A small amount of full-length protein was also detected. Gamma-secretase-cleaved C-terminal fragment (NICD) was not observed in NOTCH1 and NOTCH3 blots. (**b**) Expression of various keratins (K), vimentin (Vim), E-cadherin (Cdh1), desmoglein 3 (Dsg3) and TP63 in various cells, as revealed by western blot. As the full-length NOTCH1 was observed at a much weaker intensity and in proportion to the intensity of the 120 kDa protein, only the 120 kDa protein of NOTCH1 is shown. (**c**) K13 expression in Ca9-22 and HFS cells cultured at a high density. Immunofluorostaining was conducted using the secondary antibody labeled by Alexafluor 488. The nuclei were counterstained by DAPI. K13-expressing cells appear in a scattered manner. HeLa, CaSki, BHY and HSC-3 showed no K13 expression. (**d**) Ca9-22 cells were treated with only DMSO or 2.5 μM DAPT at 80% confluency and were cultured for 72 h. An equal amount of protein was subjected to western blot analysis for keratins (K), HES1, HEY1 and β-tublin (βTub). (**e**) Ca9-22 cells were transfected at 30% confluency with an empty plasmid (Ctrl), NICD, dominant-negative RBPJ (R218H, RBPJm), dominant-negative Dll1 (dnDl) or siRNA for *NOTCH1* (*siN1*) and were cultured for 72 h. (**f**) Ca9-22 cells were transfected with *TP63(TA)* or *TP63(ΔN)* and were incubated for 72 h. Western blot analysis revealed the endogenous expression of TP63 (ΔN), but not TP63 (TA). NOTCH1 was only slightly downregulated by TP63 (ΔN). K13 was downregulated both by TP63 (TA) and TP63 (ΔN). (**g**) Ca9-22 cells were transfected with *NICD* or siRNA for *NOTCH1* and were incubated for 72 h. Both *NICD* and *siN1* downregulated TP63 and K13. (**h**) Luciferase reporter assay for human *KRT13*, *KRT15* and *KRT17* promoters. The promoter construct plus of 0.1 μg and 0.1 μg of the Notch1 construct and 0.01 μg of the *Renilla* luciferase standardization plasmid (*pEF-RL*). Transfections were done into GE-1 cells on 48-well plates and the luciferase activity was measured 48 h after transfection using Dual-Luciferase Reporter Assay System (Promega). The error bars denote standard errors. rlu; relative luciferase unit.

Notch1 in squamous neoplasms
K Sakamoto *et al*

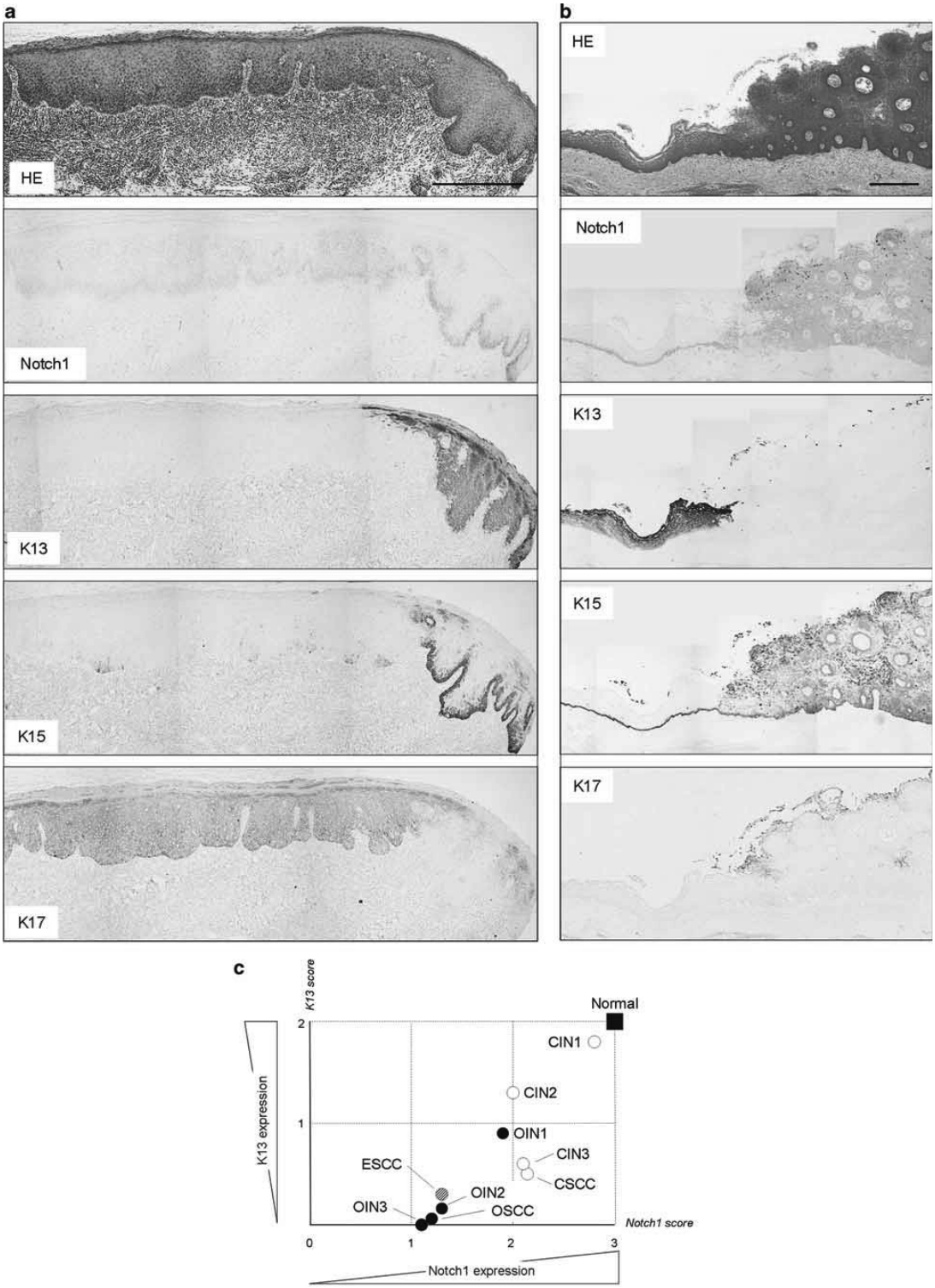

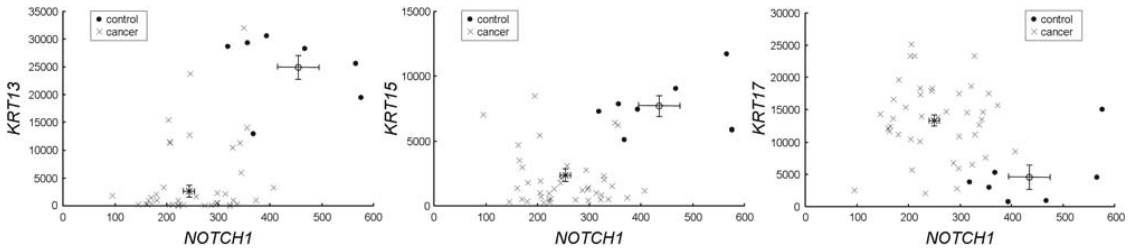

Figure 6 Correlation of *NOTCH1* and *KRT13*, *KRT15* or *KRT17* expression. cDNA microarray analysis of 41 OSCC and 7 normal controls. Globally normalized hybridization intensity data of each sample were scatterplotted. The filled circles represent normal controls and the crosses represent OSCC cases. The blank circle represents the mean of the normal controls. The large cross represents the mean of OSCC. The error bars represent standard errors.

expansion with minimum induction of K17 (Figure 5b). We scored the K13 expression either as being at level 2 (unaffected, almost uniform expression), level 1 (apparent downregulation but patchy expression remaining) or level 0 (almost complete loss of expression), and analyzed the correlation of these three expression levels with the NOTCH1 scores. Loss of K13 expression was observed in accordance with NOTCH1 downregulation (Figure 5c). The average scores of K13 and NOTCH1 decreased in accordance with the grades of OIN and CIN, although the high-grade lesions (OIN2, OIN3, CIN3) showed scores similar to those of OSCC or CSCC (Figure 5c), indicating that these precancers and cancers in each site are essentially the same lesions in the context of NOTCH1 and K13 expression. The cervical lesions, especially low-grade CIN, tended to show more NOTCH1 and K13 expression. Correlation between NOTCH1 expression and keratin expression was further assessed in oral cancers using microarray data. Scatter plots revealed that the downregulation of NOTCH1 in cancer correlated with downregulation of K13 and K15, and upregulation of K17 (Figure 6).

Asymmetric Activation of NOTCH1

In tissue, NOTCH1 was dominantly observed on the cell membrane, and nuclear staining was rarely seen. To gain an insight into when and how NOTCH1 is activated, its cellular localization was further investigated in HFS cells. NOTCH1 was detected on the cell membrane of culture cells, showing accumulation at the cell-cell interface (Figure 7a). No NOTCH1 accumulation was observed on the free surfaces. Western blot analysis, using cleaved NOTCH1-specific antibody, failed to detect activated NOTCH1 (data not shown), probably due to low expression. Still, immunostaining showed distinct nuclear expression of activated NOTCH1, but only in a very few ($<1\%$) cells (Figure 7b). This suggests that NOTCH1 protein is tethered to the cell membrane and is dormant in most cells, and that it is activated only in a limited population or on infrequent occasions. We further assessed nuclear translocation of NOTCH1. As the endogenous level of NOTCH1 expression was not sufficient for clear visualization, we overexpressed *Notch1* by transfection and examined cellular localization of the protein. Again, cells whose nuclei were positive for Notch1 were rare but were definitely observed. Interestingly, nuclear localization of Notch1 was occasionally observed in one of two neighboring cells, which appeared as postmitotic daughter cells (Figure 7c).

DISCUSSION

We demonstrated that NOTCH1 is expressed predominantly in the basal cells of normal squamous epithelium. Contrary to our findings, previous reports had documented the expression in both basal and suprabasal layers of the skin[4,21] and in the uterine cervix,[15,16] as well as in the suprabasal layer of the cornea,[29] but we believe the present study correctly demonstrates the basal-cell dominant NOTCH1 expression in human squamous epithelium and its neoplasms. The most prominent feature that supports the validity of our immunohistochemical examination is the sharp demarcation of NOTCH1 expression that matched to the border between normal and neoplastic epithelia, which would never be observed in nonspecific staining.

Although elevated Notch signaling has been suggested in tumor development,[13,30–32] neither an increase of NOTCH1

Figure 5 Immunohistochemical expression of NOTCH1, K13, K15 and K17 in squamous neoplasms. (**a**) In this OIN case, the lesion shows concomitant downregulation of NOTCH1, K13 and K15, with complimentarily induced expression of K17. Scale bar, 0.5 mm. (**b**) In this CIN case showing condylomatous proliferation, the level of NOTCH1 expression in the individual cells is retained, and basaloid cells expressing NOTCH1 and K15 expand in the whole layer. K17 induction is faint. Scale bar, 0.5 mm. (**c**) Schematic summary of the immunohistochemical expression of NOTCH1 and K13 in various squamous neoplasms. Each group of the lesions is plotted by the average scores of NOTCH1 and K13 expression. OIN, oral intraepithelial neoplasm; OSCC, squamous cell carcinoma of the oral cavity; ESCC, squamous cell carcinoma of the esophagus; CIN, cervical intraepithelial neoplasm; CSCC, squamous cell carcinoma of the cervix.

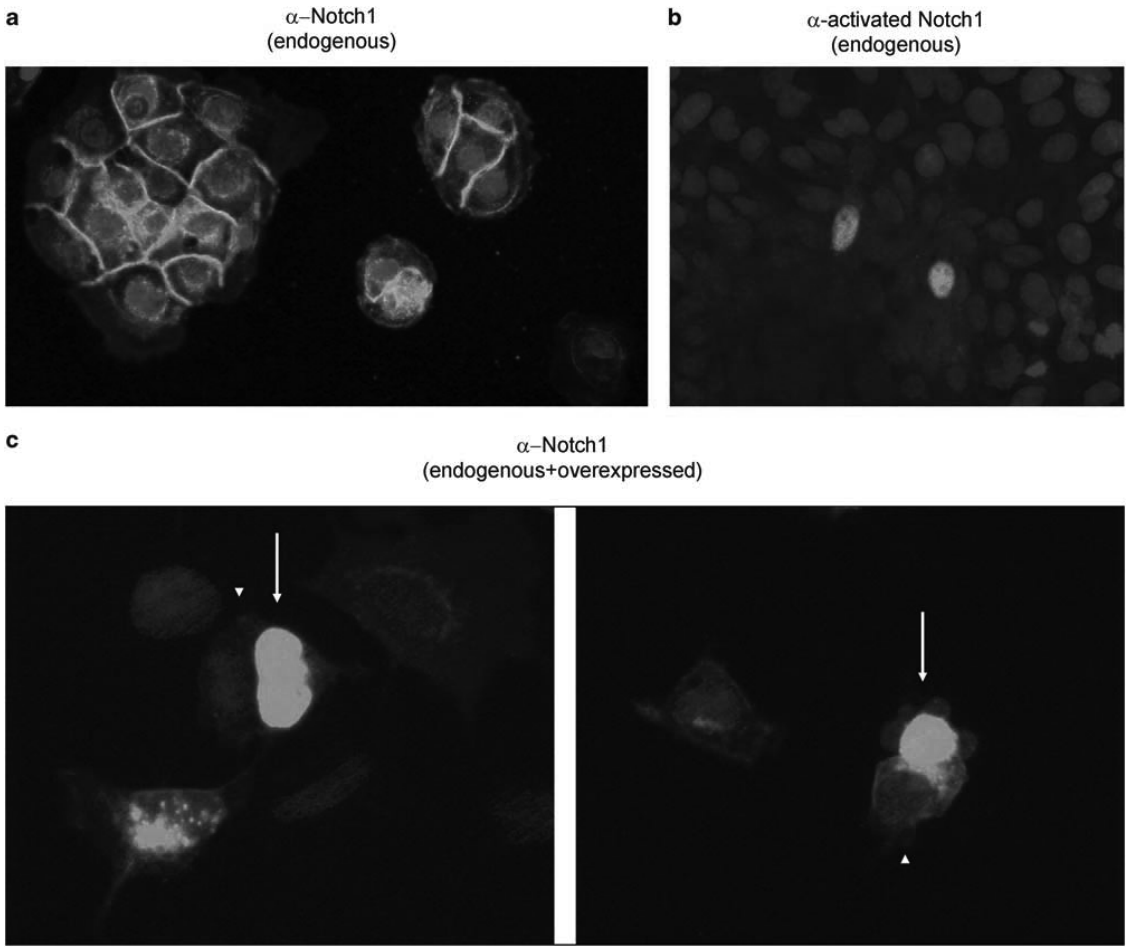

Figure 7 Nuclear translocation of NOTCH1 is rare, and it occasionally occurs asymmetrically in cultured keratinocytes. (**a**) Immunofluorostaining of HFS cells using the anti-NOTCH1 antibody. NOTCH1 protein accumulates at the cell–cell interface. Little protein was detected on the free surface or in the nuclei. (**b**) Immunofluorostaining of HFS cells using the anti-cleaved NOTCH1(Val1744) antibody. This activated form of intracellular domain of NOTCH1 is detected in the nuclei, but only in a very few cells—far $<1\%$ of the total population. (**c**) Immunofluorostaining of Ca9-22 cells transfected with wild-type mouse Notch1 using the anti-NOTCH1 antibody. The antibody crossreacts with mouse Notch1. Endogenous expression of NOTCH1 is observed as fine membranous or cytoplasmic staining. The transfected cells exhibit much stronger expression, facilitating detection. Nuclear localization of the NOTCH1 is observed in one of two neighboring cells, which appear as postmitotic daughter cells. Arrow: postmitotic cell with nuclear NOTCH1; arrowhead: postmitotic cell without nuclear NOTCH1.

expression nor its nuclear translocation was observed in the cases we examined. The cDNA microarray of OSCC showed that neither *NOTCH2* nor *NOTCH3* was upregulated in OSCC, suggesting that quantitative compensation is unlikely. These results indicate that upregulation of Notch-dependent signaling may not make a major contribution to the development and progression of squamous cell carcinoma. Conversely, consistent reduction of NOTCH1 expression in squamous neoplasms was evident. Also, *NOTCH1* has recently been shown to be mutated in 11–15% of head and neck cancer, and about 40% of the mutations were predicted to generate truncated NOTCH1 proteins, whereas no apparent activating mutation was found.[33,34] These results suggest that NOTCH1 may function as a tumor suppressor gene rather than as an oncogene in squamous neoplasms.

We demonstrated that impaired Notch1 signaling led to abnormal differentiation represented by alterations of keratin subtype expression, which was commonly observed not only in cancers but also in precancers. The role of Notch in regulation of squamous epithelium differentiation has also been suggested by studies using cultured cervical[28] and esophageal keratinocytes.[35] Collectively, these results indicate that

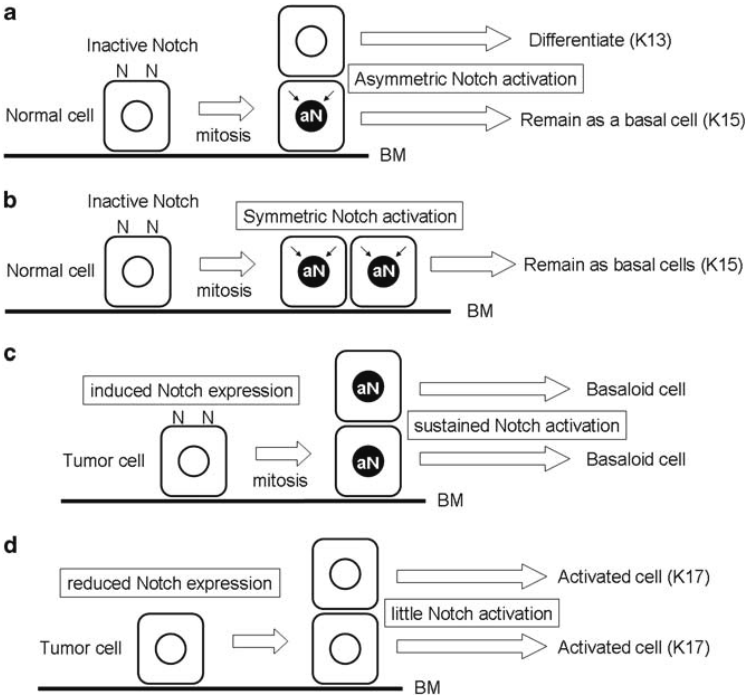

Figure 8 Proposed model of Notch-mediated mechanism of non-cornified squamous epithelium differentiation. (**a**) NOTCH1 is selectively activated in the basal cell (K15+) when the sister cell divides basoapically, and directs it to remain as a basal cell (K15+), whereas the apical daughter cell without Notch signal input differentiates (K13+). (**b**) When the sister cells divide symmetrically, Notch is activated in both cells, which remain as basal cells (K15+). (**c**) If the asymmetric Notch signaling is impaired and both basal and apical daughter cells undergo Notch activation, both remain as basaloid cells (K15+). (**d**) The cells with reduced NOTCH1 expression convert to activated cells (K17+) that lead to a hyperplastic phenotype.

reduced NOTCH1 expression affects the terminal differentiation, thus highlighting the essential role of NOTCH1 in maintaining normal epithelial integrity. In addition, we examined five cases of traumatic ulcer and found that NOTCH1 was downregulated in the regenerative epithelium, accompanied with loss of K13 expression and robust induction of K17 (K.S., unpublished observations). This suggests that the downregulation of NOTCH1 expression level is an inherent mechanism for switching the epithelium from a normal and mature state to an activated and immature state.

Cervical cancers tended to retain NOTCH1 expression compared with oral and esophageal cancers. We evaluated the expression in the cervical cancer cells in comparison with the neighboring vaginal squamous epithelium. However, this evaluation method might be misleading because cervical cancers arise from the reserve cells beneath the columnar epithelium of endocervix,[36] and the vaginal epithelium is not the origin of cervical cancers. As the reserve cells are almost negative for NOTCH1, it can also be said that NOTCH1 expression is increased in cervical cancer compared with its original cell type.

We hypothesized that strong NOTCH1 expression may correlate with a tendency for differentiation toward squamous epithelium. To check this hypothesis, we additionally examined five specimens of squamous metaplasia caused by obstruction of the minor salivary gland duct. As expected, NOTCH1 was significantly induced in ducts, which show ectopic K13 induction and squamous metaplasia (Supplementary Material 7). HPV infection to metaplastic epithelium in the transformation zone initiates progression to CIN or CSCC,[37] and *NOTCH1* is upregulated by HPV E6 and E7 oncoproteins, which are almost uniformly expressed in cervical cancer.[38] Virally induced NOTCH1 expression would tend to be maintained in CIN and CSCC, but would be no more upregulated. In this context, upregulation of NOTCH1 may have an essential role only in generation of metaplastic epithelium.

HPV has been detected only in a minority of OSCC cases, excluding pharyngeal cancer[39] and ESCC.[40] This is probably attributable to the difference in the NOTCH1 expression pattern between oro-esophageal and cervical cancers. The NOTCH1 expression patterns seem to underlie their histopathological differences. Expansion of a basaloid cell population is usually observed in CIN, whereas this finding is exceptional in OIN, whose basaloid cells are usually limited to the lower part of the epithelium. Remaining NOTCH1

expression appears to autonomously direct the cell to maintain the basaloid phenotype.

In our series of cell culture experiments, Notch signaling exhibited seemingly diverse effects. For example, both activation of Notch signaling and downregulation of NOTCH1 expression inhibited differentiation. To better understand such diverse effects, we have developed the following model, which is consistent with the experimental and histopathological findings, and also with the self-organizing nature of stratified epithelium. NOTCH1 is selectively activated in the basal cell when the sister cell divides basoapically, and acts to direct the basal cell to remain as a basal cell, whereas the apical daughter cell without Notch signal input is directed to differentiate (Figure 8a). When the sister cell divides laterally, Notch is activated in both cells, which directs them both to be basal cells (Figure 8b). If asymmetric Notch signaling is impaired, and both basal and apical daughter cells undergo Notch activation, both would remain as basaloid cells (Figure 8c), causing expansion of the basal-cell layer. Cells with reduced NOTCH1 expression convert to activated cells that lead to a hyperplastic phenotype (Figure 8d). In either case, impaired Notch signaling causes an immature epithelium. Although future research is required to confirm this model, it is consistent with the results of genetically engineered mouse experiments.[8,35]

Besides its role as a receptor, Notch is considered to have a function as a modulator of cell adhesion.[7] The NOTCH1 accumulation on the plasma membranes between neighboring cells and the rare observation of the activated form support this notion. Reduced Notch expression may facilitate the cell dissociation and movement that are required for regenerative epithelium and cancer invasion.

Altogether, we assume that NOTCH1 functions in two ways: it mediates the balance between populations of basal cells and differentiated cells in normal epithelium by symmetric and asymmetric activation; and in pathological conditions, such as wound healing, precancer and cancer, its expression is reduced, which converts the cells into an activated and immature state.

Impaired asymmetric cell division affects epidermal Notch signaling and results in defects in stratification and differentiation, suggesting that Notch is an effector of asymmetric cell division.[41] The mechanism of asymmetric Notch activation is unclear. JAG1, one of the canonical ligands, was expressed in the suprabasal layers (K.S., unpublished observations), which suggests that the signal is directionally transmitted from an apical cell to a basal cell because of these localizations of ligand- and receptor-expressing cells. However, JAG1 was also expressed in the basal cells, and the significance of the co-expression of receptors and ligand in the basal cells is yet to be elucidated. Accumulating evidence indicates that the canonical Notch ligands also act as a cell-autonomous repressor of Notch signaling,[26,42–46] suggesting that JAG1 expression in the basal cells may inhibit the signaling. Another possible mechanism of the asymmetric activation is the suppression of Notch signaling by protein degradation mediated by Numb, which is distributed differentially in the daughter cells and governs asymmetric cell division.[47,48]

The transcription of *NOTCH1* gene is suppressed by TP63(ΔN) in cervical keratinocytes,[28] and TP63(ΔN) inhibits differentiation in the oropharyngeal SCC cell line.[49] Our findings using Ca9-22 cells are consistent with these results, suggesting that the interplay between NOTCH1 and TP63(ΔN) in differentiation is common in non-cornified epithelia of various sites. In addition, we found that TP63(ΔN) expression was affected by Notch signaling, suggesting a feedback relationship between these factors. It should be noted that this hypothetical NOTCH1-TP63 interplay does not resemble the expression patterns of these factors in cancer tissues, in which TP63 is uniformly expressed in both basal and suprabasal layers of normal epithelium and cancer (data not shown). Thus, the NOTCH1-TP63 interplay is merely one of many mechanisms that govern the epithelial cell behaviors.

In summary, NOTCH1 is expressed predominantly in the basal cells of squamous epithelium, and it is generally downregulated in squamous neoplasms, even at early stages. Reduction of NOTCH1 expression directs the basal cells to cease terminal differentiation, resulting in an immature epithelium, which may have an essential role in the histopathogenesis of dysplastic features commonly observed in precancerous epithelium. These findings suggest that normal epithelial integrity is autonomously maintained by this evolutionarily conserved cell-to-cell signaling system.

Supplementary Information accompanies the paper on the Laboratory Investigation website (http://www.laboratoryinvestigation.org)

ACKNOWLEDGEMENT
This work was supported by a Grant-in-Aid for Scientific Research (C) (No. 21592320).

DISCLOSURE/CONFLICT OF INTEREST
The authors declare no conflict of interest.

1. Blaumueller CM, Qi H, Zagouras P, *et al.* Intracellular cleavage of Notch leads to a heterodimeric receptor on the plasma membrane. Cell 1997;90:281–291.
2. Logeat F, Bessia C, Brou C, *et al.* The Notch1 receptor is cleaved constitutively by a furin-like convertase. Proc Natl Acad Sci USA 1998;95:8108–8112.
3. Bray SJ. Notch signalling: a simple pathway becomes complex. Nat Rev Mol Cell Biol 2006;7:678–689.
4. Blanpain C, Lowry WE, Pasolli HA, *et al.* Canonical notch signaling functions as a commitment switch in the epidermal lineage. Genes Dev 2006;20:3022–3035.
5. Favier B, Fliniaux I, Thelu J, *et al.* Localisation of members of the notch system and the differentiation of vibrissa hair follicles: receptors, ligands, and fringe modulators. Dev Dyn 2000;218:426–437.
6. Pan Y, Lin MH, Tian X, *et al.* Gamma-secretase functions through Notch signaling to maintain skin appendages but is not required for their patterning or initial morphogenesis. Dev Cell 2004;7:731–743.
7. Watt FM, Estrach S, Ambler CA. Epidermal Notch signalling: differentiation, cancer and adhesion. Curr Opin Cell Biol 2008; 20:171–179.

8. Nicolas M, Wolfer A, Raj K, *et al.* Notch1 functions as a tumor suppressor in mouse skin. Nat Genet 2003;33:416–421.
9. Estrach S, Ambler CA, Lo Celso C, *et al.* Jagged 1 is a beta-catenin target gene required for ectopic hair follicle formation in adult epidermis. Development 2006;133:4427–4438.
10. Krebs LT, Xue Y, Norton CR, *et al.* Notch signaling is essential for vascular morphogenesis in mice. Genes Dev 2000;14:1343–1352.
11. Krebs LT, Xue Y, Norton CR, *et al.* Characterization of Notch3-deficient mice: normal embryonic development and absence of genetic interactions with a Notch1 mutation. Genesis 2003;37:139–143.
12. Robbins J, Blondel BJ, Gallahan D, *et al.* Mouse mammary tumor gene int-3: a member of the notch gene family transforms mammary epithelial cells. J Virol 1992;66:2594–2599.
13. Weng AP, Ferrando AA, Lee W, *et al.* Activating mutations of NOTCH1 in human T cell acute lymphoblastic leukemia. Science 2004; 306:269–271.
14. Moellering RE, Cornejo M, Davis TN, *et al.* Direct inhibition of the NOTCH transcription factor complex. Nature 2009;462:182–188.
15. Veeraraghavalu K, Pett M, Kumar RV, *et al.* Papillomavirus-mediated neoplastic progression is associated with reciprocal changes in JAGGED1 and manic fringe expression linked to notch activation. J Virol 2004;78:8687–8700.
16. Zagouras P, Stifani S, Blaumueller CM, *et al.* Alterations in Notch signaling in neoplastic lesions of the human cervix. Proc Natl Acad Sci USA 1995;92:6414–6418.
17. Daniel B, Rangarajan A, Mukherjee G, *et al.* The link between integration and expression of human papillomavirus type 16 genomes and cellular changes in the evolution of cervical intraepithelial neoplastic lesions. J Gen Virol 1997;78(Pt 5):1095–1101.
18. Maliekal TT, Bajaj J, Giri V, *et al.* The role of Notch signaling in human cervical cancer: implications for solid tumors. Oncogene 2008; 27:5110–5114.
19. Proweller A, Tu L, Lepore JJ, *et al.* Impaired notch signaling promotes *de novo* squamous cell carcinoma formation. Cancer Res 2006; 66:7438–7444.
20. Lefort K, Mandinova A, Ostano P, *et al.* Notch1 is a p53 target gene involved in human keratinocyte tumor suppression through negative regulation of ROCK1/2 and MRCKalpha kinases. Genes Dev 2007; 21:562–577.
21. Panelos J, Tarantini F, Paglierani M, *et al.* Photoexposition discriminates Notch 1 expression in human cutaneous squamous cell carcinoma. Mod Pathol 2008;21:316–325.
22. Yoshikawa H, Kawana T, Kitagawa K, *et al.* Detection and typing of multiple genital human papillomaviruses by DNA amplification with consensus primers. Jpn J Cancer Res 1991;82:524–531.
23. Tomioka H, Morita K, Hasegawa S, *et al.* Gene expression analysis by cDNA microarray in oral squamous cell carcinoma. J Oral Pathol Med 2006;35:206–211.
24. Sakamoto K, Tamamura Y, Katsube K, *et al.* Zfp64 participates in Notch signaling and regulates differentiation in mesenchymal cells. J Cell Sci 2008;121(Pt 10):1613–1623.
25. Minamizato T, Sakamoto K, Liu T, *et al.* CCN3/NOV inhibits BMP-2-induced osteoblast differentiation by interacting with BMP and Notch signaling pathways. Biochem Biophys Res Commun 2007.
26. Sakamoto K, Ohara O, Takagi M, *et al.* Intracellular cell-autonomous association of Notch and its ligands: a novel mechanism of Notch signal modification. Dev Biol 2002;241:313–326.
27. Taylor GP. Current Protocols in Molecular Biology. Wiley, 1987.
28. Yugawa T, Narisawa-Saito M, Yoshimatsu Y, *et al.* DeltaNp63alpha repression of the Notch1 gene supports the proliferative capacity of normal human keratinocytes and cervical cancer cells. Cancer Res 2010;70:4034–4044.
29. Ma A, Boulton M, Zhao B, *et al.* A role for notch signaling in human corneal epithelial cell differentiation and proliferation. Invest Ophthalmol Vis Sci 2007;48:3576–3585.
30. Hu C, Dievart A, Lupien M, *et al.* Overexpression of activated murine Notch1 and Notch3 in transgenic mice blocks mammary gland development and induces mammary tumors. Am J Pathol 2006; 168:973–990.
31. Park JT, Chen X, Trope CG, *et al.* Notch3 overexpression is related to the recurrence of ovarian cancer and confers resistance to carboplatin. Am J Pathol 2010;177:1087–1094.
32. Zhang Z, Wang H, Ikeda S, *et al.* Notch3 in human breast cancer cell lines regulates osteoblast-cancer cell interactions and osteolytic bone metastasis. Am J Pathol 2010;177:1459–1469.
33. Agrawal N, Frederick MJ, Pickering CR, *et al.* Exome sequencing of head and neck squamous cell carcinoma reveals inactivating mutations in NOTCH1. Science 2011;333:1154–1157.
34. Stransky N, Egloff AM, Tward AD, *et al.* The mutational landscape of head and neck squamous cell carcinoma. Science 2011;333:1157–1160.
35. Ohashi S, Natsuizaka M, Yashiro-Ohtani Y, *et al.* NOTCH1 and NOTCH3 coordinate esophageal squamous differentiation through a CSL-dependent transcriptional network. Gastroenterology 2010; 139:2113–2123.
36. Christopherson WM. Dysplasia, carcinoma *in situ*, and microinvasive carcinoma of the uterine cervix. Hum Pathol 1977;8:489–501.
37. Reid R. Genital warts and cervical cancer. II. Is human papillomavirus infection the trigger to cervical carcinogenesis? Gynecol Oncol 1983;15:239–252.
38. Weijzen S, Zlobin A, Braid M, *et al.* HPV16 E6 and E7 oncoproteins regulate Notch-1 expression and cooperate to induce transformation. J Cell Physiol 2003;194:356–362.
39. Machado J, Reis PP, Zhang T, *et al.* Low prevalence of human papillomavirus in oral cavity carcinomas. Head Neck Oncol 2010;2:6.
40. Syrjanen KJ. HPV infections and oesophageal cancer. J Clin Pathol 2002;55:721–728.
41. Williams SE, Beronja S, Pasolli HA, *et al.* Asymmetric cell divisions promote Notch-dependent epidermal differentiation. Nature 2011; 470:353–358.
42. del Alamo D, Schweisguth F. Notch signalling: receptor cis-inhibition to achieve directionality. Curr Biol 2009;19:R683–R684.
43. Klein T, Brennan K, Arias AM. An intrinsic dominant negative activity of serrate that is modulated during wing development in *Drosophila*. Dev Biol 1997;189:123–134.
44. Li Y, Baker NE. The roles of cis-inactivation by Notch ligands and of neuralized during eye and bristle patterning in Drosophila. BMC Dev Biol 2004;4:5.
45. Micchelli CA, Rulifson EJ, Blair SS. The function and regulation of cut expression on the wing margin of Drosophila: Notch, Wingless and a dominant negative role for Delta and Serrate. Development 1997;124:1485–1495.
46. Miller AC, Lyons EL, Herman TG. cis-Inhibition of Notch by endogenous Delta biases the outcome of lateral inhibition. Curr Biol 2009; 19:1378–1383.
47. McGill MA, Dho SE, Weinmaster G, *et al.* Numb regulates post-endocytic trafficking and degradation of Notch1. J Biol Chem 2009; 284:26427–26438.
48. Zhong W, Jiang MM, Weinmaster G, *et al.* Differential expression of mammalian Numb, Numblike and Notch1 suggests distinct roles during mouse cortical neurogenesis. Development 1997;124: 1887–1897.
49. Boldrup L, Coates PJ, Gu X, *et al.* DeltaNp63 isoforms regulate CD44 and keratins 4, 6, 14 and 19 in squamous cell carcinoma of head and neck. J Pathol 2007;213:384–391.

顎顔面矯正学分野

森山 啓司

医歯学総合研究科・顎顔面頚部機能再構築学系専攻
顎顔面矯正学・教授

1）研究の課題名

頭蓋早期癒合症のモデルマウスの解析と可溶型 FGFR2 の効果

Analysis of a model mouse of craniosynostosis and the effect of soluble FGFR2

Apert症候群は、頭蓋冠縫合部の早期癒合症と四肢の合指症を主症状とする常染色体優性遺伝性の先天疾患で、著しい中顔面部の劣成長による重篤な反対咬合、開咬および叢生を呈する。Apert型点変異はほぼ100%がFGFR2の2つの変異部位（ S252W / P253R ）に限局しており, この変異によってリガンド特異性の喪失,およびリガンド親和性の上昇によってFGFR2はgain of functionとなることが知られているが、この現象が本疾患の病態成立機序にどのように関わっているかは不明である。研究者らは過去に骨芽細胞の異常分化亢進が本疾患病態成立機序に関与する事、またApert型変異を含む可溶型FGFR2が骨芽細胞の異常分化亢進を阻害することを報告している。これらをふまえ本研究は、Apert症候群モデルマウス（以下Apマウスと表記する）頭蓋冠組織培養系にて縫合部におけるより詳細な病態成立機序の解明を目指し、かつ生体親和性の高いナノゲルを可溶型FGFR2投与の足場として利用した非侵襲的かつ疾患特異的な治療法確立への基礎的知見を得ることを目的とした。

頭蓋冠縫合部の発生におけるHedgehogシグナルの機能解析

Analysis of the role of Hedgehog signaling in the calvaria suture development

頭蓋冠縫合部は、隣接する頭蓋骨を結合する線維性組織であり、頭蓋冠の成長に重要な役割を果たす。頭蓋冠縫合部早期癒合症（Craniosynostosis）は、縫合部が早期に閉鎖する先天性の骨系統疾患であり、重篤な不正咬合を呈する事が多い。GLI3変異は、頭蓋の変形や多指症を主症状とするGreig Cephalopolysyndactyly Syndromeの原因となることが知られている。Gli3欠損マウス（$Gli3^{Xt-J/Xt-J}$）がラムダ状縫合に早期石灰化を呈することに着目し、Craniosynostosisに対する治療法の開発に向けての基礎的な研究を行ってきた。

野生型（Wt）頭蓋冠において、Gli3 mRNAは、ラムダ状縫合および前頭縫合に接するosteogenic frontで限局的に認められた。$Gli3^{Xt-J/Xt-J}$ラムダ状縫合ではPatched1, Runx2-II, 及びDlx5等の明らかな発現上昇、およびTwist1の発現低下が観察され、骨芽細胞分化の亢進が確認された。BrdU取り込み実験によって$Gli3^{Xt-J/Xt-J}$では縫合部中央部の間葉系細胞で有意な細胞増殖亢進が認められた。FGF2除放ビーズを$Gli3^{Xt-J/Xt-J}$ラムダ状縫合に適応したところ、ビーズ周囲にTwist1発現が誘導され、同部位における早期癒合を阻止した。最後に、Gli3/Runx2複合変異マウスを作成したところ、$Gli3^{Xt-J/Xt-J}$ $Runx2^{+/-}$マウスではラムダ状縫合の開存が全例で認められた。以上より、頭蓋冠縫合部の適切な発生には、Gli3が重要な働きをすることが示唆され、Runx2の機能抑制により、縫合部における早期石灰化が阻止されることが示された。以上の結果は、将来RNAi等を利用したcraniosynostosisに対する非外科的治療法開発へのヒントとなることが期待される。

リラクシン含有磁性リポソームを利用した顎顔面領域の縫合部拡大制御法の開発

Development of the strategy for expansion of craniofacial suture with magnetized liposome containing Relaxin

ペプチドホルモンの一種であるリラクシン（RELAXIN;RLN）は哺乳類の出産時に卵巣黄体より血中に分泌され、恥骨結合の弛緩と軟化、子宮頸部の軟化等を惹起する。この作用機序として、RLN2がマトリックスメタロプロテアーゼ（Mmp）の発現を誘導し、Mmpの阻害因子であるTimp1発現を抑制する事で細胞

外マトリックスの分解を引き起こす事が報告され、内因性リラクシンは細胞外基質の分解に重要な働きを担うことが示唆される。一方、破骨細胞の分化・成熟に必須のRANKL-OPGシステムを調節することが報告されている。本研究は、リラクシンの骨基質分解促進作用と破骨細胞機能亢進機構作用を頭蓋顎顔面領域の縫合部に生体親和性磁性リポソームを用いて適用し、その局所的骨代謝調節作用を利用することで縫合部の拡大を含めた顎顔面骨格の三次元的位置制御を目指すものである。研究代表者らは、予備実験として、胎生15.5～18.5日齢ラット胎児における内因性Rxfp1の免疫組織学的検索を行い、主に上皮系組織にその局在を認めた。また、蛍光物質（Cy3）とナノ磁性体内包、リラクシン結合型リポソームを作成し、ラット頭蓋冠（胎生18.5日齢）器官培養系に投与後、磁性ワイヤーを用いてリポソームの局在をコントロールすることに成功している。今後、マウス胎児頭蓋冠由来骨芽細胞様細胞およびマウス胎児口蓋器官培養系においてその安全性と至適条件を決定後、リラクシン磁性リポソームをラット正中口蓋縫合およびラット頭蓋冠矢状縫合部に注入後、矯正用拡大装置にて側方拡大を行う。磁気を帯びたステンレススチール線を装着し、リポソームの作用領域のコントロールを行い、至適条件下で縫合部の拡大を行い、拡大効率に与える影響について検討する。

ペリオスチンノックアウトマウスを用いた歯および歯周組織の生物学的特性の解明

Phenotypic and functional analysis of tooth and periodontal tissues found in periostin null mice

ペリオスチンは特に骨外膜、歯根膜、心臓弁に特異的に局在する細胞外基質（ECM）タンパクであり、細胞接着、コラーケン線維形成・架橋形成への関与、線維芽細胞の遊走・活性化促進に重要であると考えられている。ペリオスチンを欠失させたマウス（ノックアウトマウス）を解析した以前の報告では、咬合力に対抗して歯周組織を健全に維持する機能にペリオスチンが関与していることが示唆されていた。本研究では、マウスの歯の発育時に咬合力のような機械的な力が付加された際、ペリオスチンの有無がどのような影響を果たしているかを解析した。詳細な発現解析により歯髄内の象牙芽細胞、象牙芽細胞下細胞層、およびエナメル芽細胞にペリオスチン発現が確認された。咬合力が負荷された切歯において、ペリオスチンノックアウトマウスは野生型に比して象牙質形成が有意に増加していた。一方、ノックアウトマウスには切歯臼歯ともエナメル質の石灰化低下が確認された。切歯の象牙質にみられる非コラーゲン性タンパク（DSPP, DMP1, BSP, OPN）の発現がノックアウトマウスにおいて変化していた。また、切歯を切除して咬合力を取り除いたモデルにおける切歯象牙質形成速度は、野生型マウスは減少したが、ノックアウトマウスでは増加した。象牙芽細胞様細胞の培養実験や、TGF-beta1を過剰発現するトランスジェニックマウスとの比較から、これらの変化にはTGF-beta1によって直接制御されているペリオスチンの発現量が関与している可能性が示された。現在は、咬合力や歯の移動時に引き起こされる歯周組織における細胞死とペリオスチンの関連について、解析を行なっている。

先天性多数歯欠損家系におけるPAX9変異解析

Non-syndromic Oligodontia with a Novel Mutation of PAX9

歯の喪失や欠損が多数歯は、咀嚼、発音、摂食といった口腔機能に重大な障害を引き起こし、患者のQOLに深刻な影響を与える。歯の再生に対するreverse geneticなアプローチとして本課題では、6本以上の多数歯欠損が家族性にみられ、非症候群性に発症するケース（Familial oligodontia）の遺伝子解析を行ってきた。遺伝子解析の結果、この家系においてFamilial oligodontiaを示す3名に、動物実験より歯の発生における機能が既に報告されている転写因子PAX9に、フレームシフト型の遺伝子変異（321_322insG）を同定した。この変異は様々な種間で保存され、DNA 結合能を持つpaired domainに存在した。この家系内でFamilial oligodontiaを伴わない方からもDNA試料を提供いただき、遺伝子解析を行った結果、321_322insGは見られなかった。321_322insGの変異遺伝子機能をin vitroで解析した。この変異遺伝子をCOS-7に遺伝子導入した結果、野生型タンパクと異なり、321_322insGは分解されやすく、タンパクの安定性に劣ることが示唆された。

眼・顔面・心臓・歯症候群における歯根形成を制御する遺伝子BCORの役割の解明

Molecular Characterization of Human BCOR Mutations in OFCD syndrome

矯正治療や歯の再植・移植といった治療や炎症により、歯根吸収が惹起され、動揺や脱落といった転帰をたどるケースは少なくない。歯根形成のメカニズムを解明することは一端吸収が進んだ歯根の再生や歯根吸収の抑制といった治療法の開発に向けて期待されるテーマである。眼・顔面・心臓・歯（OFCD）症候群はまれな遺伝性疾患で、特異的な頭蓋顔面を呈し、心臓および眼の異常が

みられ、長い歯根を呈する疾患である。近年、BCL-6 co-repressor（BCOR）の変異により、OFCD症候群を引き起こすことが報告されたが、歯根形成におけるBCORの機能は明らかにされていない。そこで、分子生物学的、遺伝学的ならびにバイオインフォマティクスの手法を統合して、OFCD症候群を引き起こすBCORの機能を解析し、トランスレーショナルリサーチを目指した歯根形成のメカニズムを解明することを目的とした。研究代表者が担当しているOFCD症候群患者の矯正歯科治療のため便宜抜歯した小臼歯より、歯髄間葉細胞ならびに歯根膜細胞を単離し、ゲノムDNAを抽出し、BCORの変異解析を行ったこころフレームシフト型の遺伝子変異を同定した。

口蓋裂症例における合併症状に関する検討

Examination of associated malformations in cases with isolated cleft palates

口唇裂・口蓋裂は発生頻度の高い先天性疾患のひとつである。その中でも口蓋裂が単独で生じる場合、全身的な合併症状を伴うことが多いとされているが、詳細な検討はいまだ少ない。そこで、当分野に来院した口蓋裂症例に合併する口腔内および全身症状について検討を行ったので報告する。昭和52年から平成23年に当分野を受診した口唇裂、顎裂を伴わない完全口蓋裂患者226名（男性74名、女性152名、平均年齢11歳4か月）を対象とし、初診時調査用紙を用いて合併する1）口腔内および2）全身症状について検討した。1）永久歯の先天性欠損が54.4%で最も多かった。矮小歯は13.3%にみられ、その多くは上顎側切歯であった。またエナメル質減形成が12.8%でみられ、1歯のみから全歯におよぶものまで様々であった。舌においては舌小帯強直症が16.8%にみられた。2）眼の異常では内眼角贅皮が19.9%と最も多く、次いで両眼隔離が10.2%にみられ、また視力障害が19.5%、白内障も1.8%認めた。耳の異常として、耳介形成異常が14.2%、次いで耳介低位が9.3%にみられ、聴力障害も18.6%認めた。また斜頸や、手足においては指の彎曲がみられた。外胚葉系ではアトピー性皮膚炎や爪の形成不全がみられた。呼吸器系疾患では喘息が7.1%、循環器系疾患では不整脈・心雑音が2.7%、心室中隔欠損が2.2%にみられた。また、精神発達遅滞は7.1%、運動発達遅滞も5.8%にみられた。家族性に口蓋裂を発症している家系が13.7%に認められた。症候性の口蓋裂症例は18.1%にみられ、その中でPierre Robin症候群が4.0%と最も多く、次いでStickler症候群が1.8%であった。口蓋裂に合併する症状を歯科的見地からも詳細に検討することは、他科との連携をとるうえで重要な情報を提供するものと考えられる。

コーンビームCT 3D画像より作成した光造形ステントを使いた矯正用ミニスクリューの植立精度について

Accuracy of orthodontic miniscrew implantation guided by stereolithographic surgical stent based on cone-beam CT derived 3D images

近年、矯正治療において歯を移動する際の矯正力の固定源として矯正用インプラントアンカーが使用されている。そのうち特にミニスクリュータイプが多用されているものの、その安定性（成功率）に問題があり、精度の高い植立方法の確立もなされていない。よって本研究では、より精度の高いミニスクリュー植立方法の確立と安定性向上を目指し、ファントームモデルのコーンビームCT（CBCT）3D画像より光造形ステントを作成し、その正確性と有用性を検討した。 3つのX線撮影用ファントームモデルをCBCT撮影し、ミニスクリュー植立シミュレーションを30箇所についてコンピュータソフト上で行った。うち2画像のシミュレーションから光造形ステント10個（20箇所：スクリュー20本分）を作成した。ステントを使用してミニスクリューを植立した群（ステント群：N=20）と、事前シミュレーションに基づきフリーハンドで植立した群（フリーハンド群：N=10）におけるミニスクリューの植立精度を、事前シミュレーション画像と植立後再度CBCT撮影した画像の重ねあわせにより比較した。スクリューヘッド・スクリュー先端における垂直的・近遠心的距離、および垂直的・近遠心的角度における誤差の、すべての計測項目において、ステント群の植立精度は、フリーハンド群と比較して有意に精度が高かった。また、フリーハンド群では、歯根に接触したスクリューが4本あったのに対し、ステント群では全く歯根への接触がみられなかった。よって、コーンビームCT 3D画像より作成した光造形ステントは、臨床において正確なミニスクリュー植立に有用であるものと考えられた。

下顎頭軟骨形成メカニズムの生物学的解析

Biological analysis of mechanism for condylar cartilage formation

下顎頭軟骨は他の軟骨組織とは異なり顎顔面領域の成長中心の一つとして働き、さらに成長終了後は永久関節軟骨として下顎頭の表層に存在するという、「成長」と「関節機能」という2つの機能を一つの組織で担っている。このように頭蓋顎顔面の形態形成や顎関節機能に大きな影響を及ぼすことが知られている。近年下顎頭の退行性に変形するCondylar Resorptionが下顎後退による閉塞型

睡眠時無呼吸症や種々の顎変形症、不正咬合を惹起することが周知のこととなりつつある。下顎頭軟骨に代表される二次軟骨はType I、II、Xコラーゲンを同時に発現する特徴的な細胞外マトリックスを持っている。またその出現時期は骨組織が形成された後に付随的に形成され、下顎頭軟骨においては下顎骨が形成された後にその後縁に出現する。骨組織を完全に欠損しているRunx2 KO miceでは下顎頭軟骨を欠損していることからその形成機構においては骨との関連性が示唆されている。このRunx2 KO miceの下顎頭原基をBMP2存在下で培養すると二次軟骨形成が認められることから、下顎頭軟骨形成には骨芽細胞由来のBMP2が重要である可能性が示唆された。本研究では今後プロテオグリカン合成阻害薬であるβ-xylocidを用いた器官培養の実験系を用いて、下顎頭軟骨の形態形成における発現遺伝子の解析を考案している。

口唇閉鎖不全に対する筋機能療法の効果：マルチモダリティ解析

Effect of muscle function therapy on lips imperfect close：Multimodality analysis

口唇閉鎖不全を伴う、上下顎骨の前後的・垂直的位置関係の不調和が著しい不正咬合においては、矯正歯科治療単独での咬合の改善や顔貌の調和を図ることが困難である。このような場合に併用される筋機能療法のエビデンスには不明な点が多い。そこで、「口唇閉鎖不全患者における口輪筋収縮訓練に伴うオトガイ筋および口輪筋の血流量・筋活動の経時的変化における相互関連を探り、顎態および歯列に与える影響を解明するとともに、新たな口唇閉鎖不全患者に対する筋機能療法の評価法を確立する」ことを本研究の具体的な目的として遂行する。本研究では、口唇閉鎖時および口輪筋収縮訓練時におけるオトガイ筋・口輪筋の血流量と筋活動を同時計測し、健常者群（対照群）、口唇閉鎖不全患者群（実験群）に、2種類の異なる口輪筋収縮訓練課題（低負荷・長時間課題および高負荷・短時間課題）を施行し、その効果に関する機能的評価を行うとともに、顎態および歯列の形態計測による形態的評価を行う。この過程で、対照群と実験群を横断的比較するとともに、実験群において課題の持続効果を縦断的に比較する。

下顎側方偏位症例における大臼歯の頬舌的位置および角度と口腔内圧の関連

Association between intraoral pressure and molar position and inclination in subjects with facial asymmetry

上下顎骨の前後的、垂直的あるいは水平的な位置関係の不調和が著しい骨格性不正咬合においては、矯正治療単独での咬合の改善や顔貌の調和を図ることが困難である。このような場合には、外科的矯正治療が併用されることになる。外科的矯正治療においては、顔貌における審美性の改善、上下顎の位置関係および咬合の改善による個性正常咬合の確立、生理的な口腔機能の回復、心理的障害の排除と社会適応性の向上などを目標とする。以上の治療目標の達成および確立された咬合の維持には、歯や歯列を取り巻く口腔周囲の機能的安定が不可欠である。そこで、「顔面非対称患者における安静時口腔内圧と下顎の側方偏位との関連を解析する」ことを本研究の具体的な目的として遂行する。

習慣性咀嚼側に依存した舌の2点弁別能および舌触覚による大脳皮質賦活

Preferred-chewing-side-dependent two-point discrimination and cortical activation of tactile tongue sensation

咀嚼は両側で均等に行われるとは限らず、無意識下での咀嚼の側性は習慣性咀嚼側（Preferred Chewing Side：PCS）とよばれている。これまでPCSと非習慣性咀嚼側（non- PCS）との間での左右差に関して、機能的・形態学的観点から様々な検討が行われてきた。しかし、咀嚼運動中のフィードバックに関与する舌の触覚とPCSとに関連があるのか、中枢神経機構に差異があるのかは不明である。そこで本研究は、PCSを評価した上で2点弁別試験を行い、機能的磁気共鳴画像法（fMRI）を用いて触覚刺激に伴う一次体性感覚野の賦活領域を比較することで、PCSと舌の触覚および脳機能との関連を検討することを目的とした。その結果、2点弁別閾値は、前歯から犬歯、さらに臼歯相当部へと後方へ進むにしたがって増大した。また、PCSとnon-PCSの比較では、前歯相当部では有意差は認められなかったが、犬歯および臼歯相当部においては、PCSの方がnon-PCSよりも有意に小さかった。脳賦活に関しては、刺激と対側の一次体性感覚野は、PCS刺激時の方がnon-PCS刺激時に比べ有意に広い領域が賦活した。さらに側性の相互関連に関しては、末梢における咀嚼・舌感覚と中枢における脳賦活間に、それぞれ有意な正の相関を認めた。これらの結果から、PCSは末梢感覚である舌の触覚とその投射を受ける中枢機能に関与することが示唆された。PCSにおける舌感覚の鋭敏さは、咀嚼運動の円滑な遂行に重要な役割を担っていることが示唆される。

咬みしめに伴う上肢筋の促通とそれに同期した脳賦活パタン

Upper-limb facilitation by teeth clenching and its brain activation pattern

歯科やスポーツ生理学の分野において、随意的な咬みしめに伴って全身運動機能が促通されることが数多く報告されている。そこで我々は、咬みしめが上肢筋筋力に与える影響について非侵襲的脳機能計測法のひとつである機能的磁気共鳴画像法（fMRI）を用いて検討した。個性正常咬合を有する健康成人19名において、行動生理学的実験と神経生理学的実験を行った。前者に関しては、MR室外にて、1）咬みしめ時における最大握力、および2）下顎安静位における最大握力を、それぞれ利き手において測定した。後者に関しては、1.5TのMR装置を用いて1）咬みしめと握りしめを同時に施行（Clenching during Gripping：CG）、2）咬みしめのみ施行（Clenching：C）、3）握りしめのみ施行（Non-clenching during Gripping：NcG）の3条件下でfMRIデータを採得した。握りしめに関連する関心領域を設定し、statistical parametric mapping（SPM）5を用いてBlood oxygenation level dependent（BOLD）信号強度を解析した。咬みしめ時における最大握力は、下顎安静位における最大握力に比べ有意に大きかった。また、握りしめ動作に関連する大脳皮質一次感覚運動野（Primary sensorimotor cortex：SMC）、補足運動野（Supplementary motor area：SMA）、および小脳におけるBOLD信号強度は、CG条件下の方がNcG条件下に比べ有意に大きかった。さらに小脳に関しては最大握力の増加率とBOLD信号強度の増加率との間に有意な正の相関が認められた。これらの結果から、咬みしめに伴う上肢筋の促通には、SMC、SMAおよび小脳が関与していることが示唆され、さらに小脳によってその促通が調節されている可能性が示唆された。

CLP患者の言語想起時および発音時における言語障害に依存した脳機能

Misarticulation-dependent Brain Activations During Covert/Overt Speech In Cleft-lip-and palate Patients

口唇口蓋裂（CLP）患者は、手術により末梢器官の改善が図られているにも関わらず、構音障害を有する場合が散見される。CLP患者における構音障害の有無と中枢神経機能の関連を知る目的で機能的磁気共鳴画像法（fMRI）を用いて、軟口蓋破裂音（/k/）発音[内言語（言語想起）および外言語（言語発音）]時における脳賦活パタンを解析した。被験者は、健常成人6名と術後成人口唇口蓋裂患者6名（片側性2名および両側性4名、うち両側性の1名のみ軟口蓋音に構音障害あり）であった。その結果、内言語発音時には、CLPの有無にかかわらず言語関連領域が賦活した。一方、外言語発音時には、健常者ならびに構音障害を有しないCLP患者においては運動前野、一次感覚運動野および小脳が賦活したが、構音障害を有するCLP患者においては後帯状回が賦活した。これらの結果から、言語想起時においては、健常者とCLP患者の脳賦活パタンに差異は存在しないが、言語発音時においては、構音障害の有無に依存した中枢神経機能が存在し、構音障害と中枢神経機能が相互に関連していることが示唆された。

声門破裂音聴取時の聴覚連合野の賦活パタン

Brain activation patterns in auditory association area for glottalstop perception

音声は、言語情報や感情情報などを同時に伝えることが可能な基本的かつ効率的な情報伝達手段である。ヒトの社会的生存に必須である音声言語は、構音器官の巧妙な協調運動により生成され、また、生命維持に必要な呼気を利用することでほかの身体活動（たとえば労働など）と同時に遂行可能であるため、ヒト同士のコミュニケーションを容易に成立させている。しかし、構音器官の重要な構成要素である口蓋に先天的に器質的障害を有する口唇口蓋裂（CLP）患者のなかには代償性構音（compensatory misarticulations：CMAs）を呈することが少なくない。従来、長期的に残存する構音障害の原因は末梢の構音器官に限局したものであると考えられてきたが、近年の研究から脳機能と構音障害との関連性が推測されてきている。CMAsのひとつに声門破裂音（glottal stop：GS）があるが、これは聞きなれない者にとっては聞き取りにくい構音である。GSを聴取した際、高次中枢としての脳がそれをどのように認識しているのかは、CMAsを有するCLP患者自身のみならず健常者においても未だ明らかにされていない。そこで今回我々は、行動実験ならびに機能的脳機能画像法（fMRI）を用いて健常者におけるGS聴取時脳賦活パタンを解析した。その結果、正常構音（normal articulation：NA）聴取時と比較してGS聴取時では構音の識別に時間を要し、また高次の音声認識に関与している上側頭回（ブロードマンエリア22）が両側でより強く賦活することが示された。以上より、GSはNAよりも複雑な音声であることが脳科学的見地から示唆された。今後はGSを有する患者においても同様の実験を行い、結果を比較検討する

ことで長期的な代償性構音が高位中枢に与える影響について解明していく。さらに、本アプローチは、神経的反応や概念に基づいた言語治療の効果を評価する方法を確立し、新たな理論的基盤の構築に有用であると考えられる。

下顎骨後方移動術が上気道開存性に及ぼす影響

Effects of mandibular setback surgery on the upper airway

顎変形症や頭蓋顔面の形成異常等に代表される骨格性不正咬合は患者の社会心理的影響に大きく関与するとともに咀嚼、発音などの機能的問題が生じる。骨格性不正咬合患者は、矯正治療単独での咬合の改善や顔貌の調和を図ることが困難であり、外科的矯正治療を適応する。特に下顎骨後方移動術は顔貌および咬合状態の劇的な改善、適切な口腔機能の獲得が期待できるが、口腔内容積が減少し、舌房が狭くなることにより睡眠呼吸障害を発症する可能性が指摘される一方、下顎骨後方移動術と睡眠呼吸障害は関連性がないとの報告も散見される。そこで、我々は外科的矯正治療前後での硬組織の大きさと軟組織量との解剖学的バランス（Anatomical Balance）の変化と睡眠時呼吸機能との関連性を解明し、そしてAnatomical Balanceの変化が形態的、機能的に安定した外科的矯正治療の立案の指標となり得るかを検討した。Anatomical Balanceは下顔面硬組織（LFC）の大きさに対する軟組織（TG）の割合（TG/LFC）と定義し計測したところ、外科的矯正治療前後での統計学的な有意差を認めなかったことから外科的矯正治療適応により成体では何らかの補償機構によりTG/LFCが維持され、睡眠時の生理呼吸機能が保たれている可能性が示唆された。今後は周囲組織の動態についても解析して行く予定である。

卒前歯学教育における遺伝医学教育の現状

Status of Genetics Education in Japanese Dental Schools

先天異常疾患はその約70%において頭蓋顔面領域に何らかの奇形を示すといわれている。口唇裂・口蓋裂のように口腔領域に明らかな異常を認めるもの以外でも、歯列や顎骨に何らかの異常が認められ、形態的、機能的障害をきたす先天異常疾患は多く、そのような患者の診断、包括的治療を行っていくうえで、我々歯科の分野において遺伝医学の知識は不可欠であるといえる。また、近年ヒトゲノムの全容が解明され、一般医療の場で個人の遺伝情報が取り扱われる機会も増加し、遺伝情報の個人差に基づく健康維持や医療が現実化しようとしており、遺伝情報は特別な家系だけでなく、健康維持やより良い医療を望むすべての人々に必要な情報になっていくことを鑑みると、歯学教育における遺伝医学教育の重要性は今後更に増していくことが予想される。

H13年に「歯学教育モデル・コア・カリキュラム（コアカリ）-教育内容ガイドライン-」が策定されて以来、コアカリは全ての歯学部学生が卒業時までに共通して修得すべき必須の教育内容とされ、各大学はこのコアカリをもとにシラバス（教育要綱）を作成している。改訂されたH22年度のコアカリにおける遺伝学に関する項目は、大きく分けると「遺伝子の構造と機能および遺伝の基本的機序の理解」、「口唇・口腔・顎顔面領域の先天異常疾患の特徴と病因および診断・治療の基本的概念の理解」の二つである。つまり遺伝学の基礎、顎顔面領域に関連する先天異常疾患の知識に関して学ぶことができる一方で、遺伝情報を臨床の場でどのように収集し、どのように提供していくかという視点での臨床遺伝教育はまだ十分とはいえない。

本学における遺伝医学教育の概要を紹介し、さらに全国歯学部や海外における遺伝医学教育の実態などから、卒前歯学教育における遺伝医学教育の現状をまとめ、今後の遺伝医学教育の普及に役立てる。

先天異常診断エキスパートシステムのための三次元バーチャルフェイス合成

Evaluation of the three-demensional-virtual-face for diagnosis of congenital anomalies

当分野は国内の矯正歯科で最も多くの先天異常患者を有し、長年蓄積してきたデータを広く社会に発信し、先天異常患者の診断・治療に役立てたいと考え、以前から診断・矯正治療を支援する先天異常診断エキスパートシステムを構築し、仮想外来システムの実現を進めてきた。先天異常疾患の約70%に頭蓋顔面領域の異常を認め、本システムのさらなる発展のためには、顔貌の視覚情報を組み込むことが必須であると考えるが、個人情報保護の観点から公開は極めて困難である。本システムに個人情報保護対策を取り入れた視覚的な頭蓋顔面情報を取り入れるため、先天異常患者の頭蓋顔面領域の三次元情報から、先天異常疾患の特徴を有し、個人として特定できない三次元バーチャルフェイスを作成し、本システムに組み込むことを本研究課題の目的とした。3Dデジタイザを用いて、先天異常疾患の複数患者の三次元顔データの計測を行い、所定のデータ形式に変換後、顔画像へのワイヤーフレームのフィッティングを行い、三次元先天異常バーチャルフェイスを作成した。平成24年度は、バーチャルフェイスの先天異常疾患としての妥当性の評価

を行い、アンケート結果集計・解析し、バーチャルフェイスの個人としての異同評価を行い、総合判定とする。平成25年度はさらに種類を増やし、当分野の先天異常診断エキスパートシステムに三次元バーチャルフェイスを組み込み、社会に発信する第一段階として、本学で導入しているe-learning上で本システムを公開、学生講義・卒後教育で利用し、その効果を評価をおこなう。

Le Fort I 型骨切り術を併用し上下顎移動術を行った骨格性下顎前突症例の外鼻形態変化に対する三次元的検討

Three-Dimensional Analysis of External Nasal Morphology Changes Undergoing Two-Jaw Surgery Combined with Le Fort I Osteotomy for Skeletal Class III Patients

今回我々は、三次元CT画像を用いて上下顎移動術を適用した骨格性下顎前突症患者の術前後の外鼻形態の変化について検討を行った。三次元形状解析ソフトを用い術前後の硬組織三次元CT画像を重ね合わせ、さらに、軟組織三次元CT画像を構築し鼻形態に関して、左右の鼻翼最下点（Bi）、鼻尖（Prn）、鼻小柱の最突出点（Cm）、鼻下点（Sn）の3次元座標の変化、各計測点間の距離、および角度計測を行い術前後の変化について検討した。軟組織では、7症例共通の所見として左右のBiの前方移動、2点間の距離の増加、そして左右のBiとPrnを結ぶ直線がなす角度の増加を認めた。外鼻孔面積に関しては術後、優位な増加が認められた。今回の結果より、個々の症例における鼻口唇軟組織性状の多様性やLe Fort I 型骨切り術による上顎骨の移動方向・量の違い等により軟組織の変化も一様でない可能性が考えられることから、その変化に影響を与える要因を今後より詳細に解明する必要があると考えられる。

2）

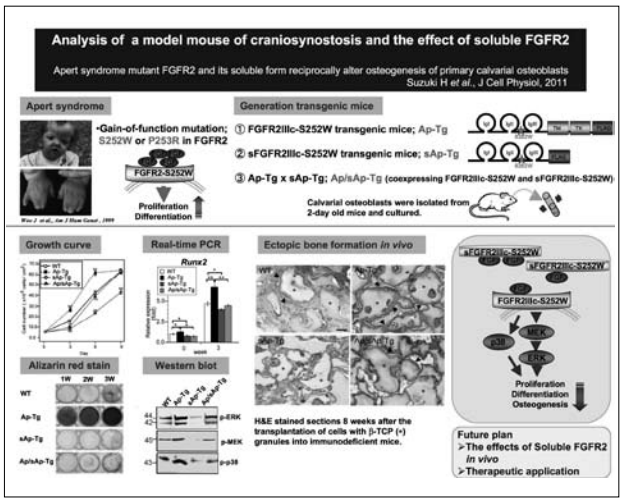

3）発表の研究内容についての英文要約

Apert syndrome mutant FGFR2 and its soluble form reciprocally alter osteogenesis of primary calvarial osteoblasts. Suzuki H, Suda N, Shiga M, Kobayashi Y, Nakamura M, Iseki S, Moriyama K. J Cell Physiol.（in press）

Apert syndrome is an autosomal dominant disease characterized by craniosynostosis and bony syndactyly associated with point mutations（S252W and P253R）in the fibroblast growth factor receptor（FGFR）2 that cause FGFR2 activation. Osteoblastic cells derived from Apert patients with the S252W mutation showed more prominent alkaline phosphatase activity, osteocalcin and osteopontin mRNA expression, and mineralized nodule formation compared with the control osteoblastic cells derived from syndromic patients. The enhanced osteoblastic marker gene expression and mineralized nodule formation was inhibited by the soluble FGFR2IIIcS252W. These results show that the S252W mutation in the FGFR2 gene enhances the osteoblast phenotype in human osteoblasts and that a soluble FGFR2 with the S252W mutation controls osteoblast differentiation induced by the S252W mutation through a dominant negative effect on FGFR2 signaling in Apert syndrome. The researchers try to figure out the mechanism of craniosynostosis and develop the novel treatment method using the soluble FGFR2 with the S252W mutation with nanogel.

Analysis of the role of Hedgehog signaling in the calvaria suture development

Mutations in the gene encoding the zinc-finger transcription factor GLI-Kruppel family Member 3（GLI3）have been identified in patients with Grieg cephalopolysyndactyly syndrome in which premature fusion of calvaria suture（craniosynostosis）is an infrequent but important feature. Here we show that Gli3 acts as a repressor in the developing murine calvaria and that Dlx5, Runx2 type II isoform（Runx2-II）and Bmp2 are ectopically expressed in the calvarial mesenchyme which results in aberrant osteoblastic differentiation in Gli3-deficient mouse（$Gli3^{Xt\text{-}J/Xt\text{-}J}$）and resulted in craniosynostosis. At the same time, enhanced activation of phospho-Smad1/5/8（p-Smad1/5/8）, which is a downstream mediator of canonical Bmp signaling, is observed. Therefore, we generated Gli3; Runx2 compound mutant mice to study the effects of decreasing Runx2 dosage in a $Gli3^{Xt\text{-}J/Xt\text{-}J}$ background. $Gli3^{Xt\text{-}J/Xt\text{-}J}$ $Runx2^{+/-}$ mice have neither craniosynostosis nor additional ossification centers and displayed a normalization of Dlx5, Runx2-II, and p-Smad1/5/8 expression as well as sutural mesenchymal cell proliferation. These findings suggest a novel role for Gli3 in regulating calvarial suture development by controlling canonical Bmp-Smad signaling which integrates

a Dlx5/Runx2-II cascade. We propose that targetting Runx2 might provide an attractive way of preventing craniosynostosis in patients.

Accuracy of orthodontic miniscrew implantation guided by stereolithographic surgical stent based on cone-beam CT derived 3D images. Qiu L, Haruyama N, Suzuki S, Yamada D, Obayashi N, Kurabayashi T, Moriyama K. Angle Orthod. (in press)

The purposes of this research were to develop surgical stents for cone-beam computed tomography (CBCT) 3-dimensional (3D) image-based stent-guided orthodontic miniscrew implantation and to evaluate its accuracy. Ten surgical stents were fabricated with stereolithographic appliances (SLAs) according to 3D CBCT image-based virtual implantation plans. Thirty self-drilling miniscrews were implanted at the maxillary or mandibular posterior arches in 3 phantoms; 20 guided by 10 surgical stents in 2 phantoms (stent group) and 10 guided freehand in 1 phantom (freehand group). Six parameters (mesiodistal and vertical deviations at the corona and apex, and mesiodistal and vertical angular deviations) were measured to compare variations between the groups. No root damage was found in the stent group, while 4 of 10 miniscrews contacted with roots in the freehand group. In the stent group, deviations in the mesiodistal and vertical directions were 0.15 ± 0.09 and 0.19 ± 0.19 mm at the corona, and 0.28 ± 0.23 and 0.33 ± 0.25 mm at the apex, respectively; angular deviations in the mesiodistal and vertical directions were 1.47 ± 0.92° and 2.13 ± 1.48°, respectively. In the freehand group, the corresponding results were 0.48 ± 0.46 mm, 0.94 ± 0.87 mm, 0.81 ± 0.61 mm, 0.78 ± 0.49 mm, 7.49 ± 6.09°, and 6.31 ± 3.82°. Significant differences were found in all 6 parameters between the 2 groups (Student's t-test, $P<.05$). These results indicated that the 3D CBCT image-based SLA-fabricated surgical stents can provide a safe and accurate method for miniscrew implantation.

Fibroblast growth factor 10 regulates Meckel's cartilage formation during early mandibular morphogenesis in rats. Terao F, Takahashi I, Mitani H, Haruyama N, Sasano Y, Suzuki O, Takano-Yamamoto T. Dev Biol. 350 (2) : 337-47, 2011.

Fibroblast growth factors (FGF) are pluripotent growth factors that play pivotal roles in the development of various organs. During mandibular organogenesis, Meckel's cartilage, teeth, and mandibular bone differentiate under the control of various FGF. In the present study, we evaluated the role of FGF10 in rat mandibular chondrogenesis and morphogenesis using mandibular organ culture and mandibular cell micromass culture systems. The overexpression of Fgf10 induced by the electroporation of an FGF10 expression vector not only altered the size and shape of Meckel's cartilage, but also upregulated the expression of the cartilage characteristic genes Col2a1 and Sox9 in a mandibular organ culture system. Meckel's cartilage was deformed, and its size was increased when Fgf10 was overexpressed in the lateral area of the mandible. Meanwhile, no effect was found when Fgf10 was overexpressed in the medial portion. In the mandibular cell micromass culture, recombinant FGF10 treatment enhanced chondrogenic differentiation and endogenous ERK (extracellular signal-regulated kinase) phosphorylation in cells derived from the lateral area of the mandible. On the other hand, FGF10 did not have significant effects on mandibular cell proliferation. These results indicate that FGF10 regulates Meckel's cartilage formation during early mandibular morphogenesis by controlling the cell differentiation in the lateral area of the mandibular process in rats.

A novel role of Periostin in postnatal tooth formation and mineralization. Ma D, Zhang R, Rios HF, Haruyama N, Sun Y, Xie Y, Kulkarni AB, Qin C, Feng JQ. J Biol Chem, 11;286 (6) : 4302–09, 2011.

Periostin plays multiple functions during development. Our previous work showed critical roles of this disulfide-linked cell adhesion protein in maintenance of periodontium integrity in response to occlusal load. In this study we attempted to address whether this mechanical response molecule played direct roles in postnatal tooth development. Our key findings are 1) periostin is expressed in subodontoblasts, and odontoblasts; and the periostin-null incisor displayed massive increases in dentin formation after mastication; 2) periostin is also expressed in the ameloblast cells, and an enamel defect is identified in both the adult-null incisor and molar; 3) deletion of periostin leads to changes in expression profiles of many non-collagenous protein such as DSPP, DMP1, BSP and OPN in incisor dentin; 4) the removal of the biting force leads to reduction of mineralization, which is partially prevented in periostin-null mice; and 6) both in vitro and in vivo data revealed direct regulation of periostin by TGF-beta1 in dentin formation. In conclusion, periostin plays direct roles in controlling postnatal tooth formation, which is required for the integrity of both enamel and dentin.

Non-syndromic Oligodontia with a Novel Mutation of PAX9. Suda N, Ogawa T, Kojima T, Saito C, Moriyama K. J Dent Res. 90 (3) : 382-6, 2011.

Agenesis of the permanent teeth is a congenital anomaly that is frequently seen in humans. Oligodontia is a severe type of tooth agenesis involving 6 or more congenitally missing teeth, excluding the third molars. Previous studies have indicated that mutations in the homeobox gene MSX1, paired domain transcription factor PAX9, and EDA are

associated with non-syndromic oligodontia. This study reports a Japanese family (eight of 14 family members affected) with nonsyndromic oligodontia who preferentially lacked molar teeth. In this family, a novel frameshift mutation (321_322insG) was identified in the paired domain of PAX9. The frameshift mutation caused altered amino acids in the paired domain and premature termination of translation by 26 amino acids. When transfected into COS-7 cells, the mRNA expression of 321_322insG PAX9 was comparable with that of wild-type PAX9. However, the mRNA of 321_322insG PAX9 was more unstable than that of wild-type PAX9. This mRNA instability caused a marked decrease in protein production, as evaluated by Western blot analysis and immunostaining. These findings suggest that the 321_322insG mutation causes insufficient function of PAX9 protein and haploinsufficiency as a genetic model of familial non-syndromic oligodontia with a PAX9 mutation.

Clinical survey on associated anomalies in cases with isolated cleft palate

It has been known that isolated cleft palate (CP) is frequently associated with other congenital anomalies. However, the prevalence and types of CP-associated anomalies vary amongst previous studies and it has not been well established whether CP is conclusively related to other birth defects. The aim of this study was to survey the anomalies associated with CP at our dental hospital. Across 226 individuals with CP, the incidence rate of recognized syndromes was 18.1%. Among them, Pierre Robin sequence was the most frequently seen condition (4.0%), followed by Stickler syndrome (1.8%). The prevalence of associated anomalies in female was twice higher than those in male (Male：74, Female：152). As for dental malformations, congenital missing of one or more teeth was observed in 54.6%, followed by conical teeth in 13.3% and enamel hypoplasia in 12.8%. Regarding malformations of eyes and ears, inner epicantic folds were seen in 19.9%, hypertelorism in 10.2%, auricular malformations in 14.2% and low set ear in 9.3%. Anomalies of the cardiovascular system and the respiratory system were observed in 9.7% and in 8.8%, respectively. Furthermore, mental retardation was found in 7.1% and motor retardation in 5.8%. CP seems to be associated with other congenital anomalies in a high prevalence.

Prevalence and gender comparison of malocclusion among Japanese adolescents：A population-based study

The lack of studies on the prevalence of malocclusion, including gender comparison, has precluded an efficient dental health policy in Japan. We aimed to describe the prevalence and perform gender comparison of malocclusion requiring orthodontic treatment in Japan. By using the modified version of the Index of Orthodontic Treatment Need, occlusal characteristics of a population-based sample of adolescents aged 12–15 yea¬rs were evaluated by orthodontists. A total of 963 adolescents participated. The prevalence of malocclusion was 49.3%. Multivariate logistic regression showed that girls were 1.4 times more likely to develop upper and lower crowding and anterior crossbite than boys. This population-based study showed that approximately half of the Japanese adolescents had malocclusion, especially girls. This study may provide reliable baseline data on the orthodontic treatment needs of the Japanese adolescent population.

Effect of muscle function therapy on lips imperfect close：Multimodality analysis

Although the visual inspection of muscular tension of the mental region and the electromyographic (EMG) activity of the perioral muscles are commonly used to evaluatelip incompetence, it is difficult to make quantitative evaluation usinga contactless method. It has been reported that the blood flow (BF) and EMG activity of the extremity muscles increased in parallel with an exercise load. However, the relationship between the change in BF and EMG activity in the orofacial region remains to be elucidated. Therefore, the purpose of this study was to examine the influence of lip-sealing on perioral muscles and establish a new method for evaluatinglip incompetence using laser Doppler perfusion imaging.

Association between intraoral pressure and molar position and inclination in subjects with facial asymmetry. Jun-ichi Takada, Takashi Ono, Jun J Miyamato, Toshiaki Yokota, Keiji Moriyama.
Eur J Orthod. 33 (3)：243-9, 2011.

Although it has been suggested that an imbalance in buccolingual pressure may play a role in dental compensation of the molars and asymmetry in the dental arch of the mandible in subjects with facial asymmetry, it is still unclear whether buccolingual pressure is associated with this phenomenon. Thus, the purpose of this study was to test the null hypothesis that there were no differences in cheek and tongue pressures between the shifted and non-shifted sides in 12 subjects with facial asymmetry that was defined to have 4 mm or more deviation of the midline in the mandibular incisors on a posteroanterior cephalogram. The resting buccolingual pressure on the bilateral mandibular first molars was simultaneously measured using four miniature pressure sensors. Moreover, a posteroanterior cephalometric radiograph was used to determine the buccolingual positions and the inclination of the mandibular first molars. The present findings did support the null hypothesis. The imbalance in buccolingual pressure in subjects with facial asymmetry appears to be related to dental compensation of the molars and

asymmetry in the mandibular arch.

Preferred-chewing-side-dependent two-point discrimination and cortical activation of tactile tongue sensation

The purpose of this study was to investigate whether the sensory threshold of the tongue differed according to the side, and whether the pattern of hemispheric cortical activation by tactile tongue stimulation differed, with special attention to the preferred chewing side (PCS). The mean thresholds of the two-point discrimination (TPD) of the anterior, canine and posterior regions on both sides of the tongue in behavioral study, and those between PCS and non-PCS in each region were statistically compared. Moreover, tactile stimulation was delivered to the either side of the tongue with acrylic balls via a mandibular splint in functional magnetic resonance imaging study. The threshold of TPD was significantly smaller on the PCS than the non-PCS in both the canine and posterior regions. The activated voxel numbers in the primary-somatosensory-cortex (S1) contralateral to the PCS was significantly greater than that in S1 contralateral to the non-PCS. The present study shows that the PCS is associated with the asymmetric tactile sensation and cortical activation of the tongue. The sensory acuity of the tongue on the PCS may be a functional coupling to maximize the efficiency of coordinated movement between the jaw and tongue.

Upper-limb facilitation by teeth clenching and its brain activation pattern

In the field of dentistry and sports physiology, there are many reports that voluntary teeth clenching facilitates human motor function. The purpose of this study was to investigate the facilitatory effect of teeth clenching on upper-limb and its brain activation pattern by using functional magnetic resonance imaging (fMRI) technique. Nineteen healthy right-handed subjects participated in this study. The subjects were asked to exert maximal right-hand-grip force with clenching during gripping (CG) and non-clenching during gripping (NcG). During fMRI scanning, subjects performed the following three tasks; CG, NcG, and only clenching (C). The regions of interests were defined in the activated areas during NcG and measured % signal change. The maximal grip force in task-CG was significantly larger than that in task-NcG. In the primary sensorimotor cortex (SMC), the supplementary motor area (SMA), and the cerebellum, % signal change in task-CG was significantly stronger than that in task-NcG. In the cerebellum, especially, a significant correlation was found between the increasing ratio of the maximal grip force and that of % signal change. The findings suggest that the SMC, SMA and the cerebellum are involved in the upper-limb facilitation by voluntary teeth clenching and the cerebellum might regulate its facilitation.

Brain activation patterns in auditory association area for glottalstop perception

Patients with cleft lip and/or palate (CLP) often show compensatory misarticulations (CMAs). Glottal stop (GS) is one of the characteristic CMAs in CLP patients and is known to be difficult to distinguish it for those who are unfamiliar with it. Moreover, the neural processing for the perception of GS remains to be clarified in not only CLP patients but also healthy subjects. Therefore, the purpose of this study was to investigate the perception of GS compared to normal articulation (NA) in both the behavioral and functional magnetic resonance imaging (fMRI) studies to clarify the brain activation patterns in healthy adults, using auditory stimuli of natural words with and without GS. As a result, the reaction time for the perception of GS was significantly longer than that for NA. Additionally, the bilateral superior temporal gyrus (Brodmann area 22) which were involved in the higher-level processing of auditory speech signals were activated stronger during listening to GS than NA. Our results suggested the possibility that GS might be more complex sounds than NA for the subjects without GS. Further studies should be conducted in CLP subjects with GS for comparison of neural processing between subjects with/without CMAs.

Misarticulation-dependent Brain Activations During Covert/Overt Speech In Cleft-lip-and palate Patients

Objectives：The speech-related central nervous system (CNS) might be subdivided into motor imaginary and execution for articulatory subsystems. The purpose of this study is to compare the cortical activation for each subsystem between subjects with and without cleft lip and palate (CLP) using functional magnetic resonance imaging (fMRI). Methods：Two unilateral CLP (UCLP), four bilateral CLP (BCLP) and six healthy subjects participated in this study, and only one BCLP subject showed CMA. The subjects were instructed to produce the syllable /ka/ in a normal tone (Overt-task) or generate it in their mind (Covert-task) during fMRI acquisition. Results：In the Covert-task, similar activation patterns were shown in subjects with and without CLP. In the Overt-task, the motor-related areas which were the premotor and primary sensorimotor cortices and the cerebellum were activated in subjects with healty, UCLP, and BCLP without CMA subjects. On the other hand, the posterior cingulate gyrus was activated in the BCLP subject with CMA. Conclusions：It appears that the CNS for motor imaginary of articulation between subjects with and without CLP might be similar. However, the CNS for execution of articulation between subjects with and without CMA might differ irrespective of the presence of CLP.

Dental and maxillofacial characteristics in six Japanese individuals with ectrodactyly-ectodermal dysplasia-clefting（EEC）syndrome. Okamura E, Suda N, Baba Y, Fukuoka H, Ogawa T, Ohkuma M, Ahiko N, Shiga M, Tsuji M, Moriyama K. Cleft Palate Craniofac J. 2011（in press）.
Ectrodactyly-ectodermal dysplasia-clefting（EEC）syndrome is a congenital anomaly characterized by ectodermal dysplasia, ectrodactyly, cleft lip and palate, and lacrimal duct anomalies. Because this syndrome is frequently accompanied by a congenital lack of teeth, narrow palate, and malocclusion, comprehensive orthodontic intervention is required. To highlight the specific dental and maxillofacial characteristics of EEC syndrome, 6 Japanese individuals diagnosed with EEC are described here. Their conditions included ectodermal dysplasia, cleft lip and/or palate, and ectrodactyly. Cephalograms, panoramic X-rays, and dental casts were taken; systemic complications were recorded at the first visit to our dental hospital. All individuals had severe oligodontia with 9 to 18 missing teeth. The missing teeth were mainly maxillary and mandibular incisors and second bicuspids, arranged in a symmetrical manner. Cephalometric analysis showed retruded and short maxilla due to cleft lip and/or palate. Interestingly, all individuals showed a characteristically shaped mandibular symphysis with a retruded point B. It is likely that this unusual symphyseal morphology is due to the lack of mandibular incisors. This study demonstrates the presence of severe oligodontia in the incisal and premolar regions and describes a characteristic maxillary and mandibular structure.

Three-Dimensional Analysis of External Nasal Morphology Changes Undergoing Two-Jaw Surgery Combined with Le Fort I Osteotomy for Skeletal Class III Patients
In this study, by using 3-dimentional computed tomography（3D-CT）, we examined the changes of external nasal morphology of the patients who had undergone two-jaw surgery to correct mandibular protrusion. 3D-CTs of pre-operative stage and post-operative stage were superimposed by 3D analysis software. After superimposition, soft tissue images of 3D-CT were reconstructed and changes of external nasal morphology were three-dimentionally analyzed. 3D geographical analysis, linear and angular measurements were performed in regard to the most inferior points on the nasal alar（LBi,RBi）on bilateral sides, the most anterior point on the nose（Prn）, the most anterior point on the columella of the nose（Cm）, the most posterior superior point on the nasolabial curvature（Sn）. LBi and RBi moved anterior according to the anterior movement of point A. Increase in distance of both LBi and RBi and angle of LBi-Prn-RBi were observed. We found significant increase in the area of external nasal aperture. Our result implies that it is necessary to investigate more details of the factors that influence changes of facial morphology since the changes may not be uniform due to the individual variety of soft tissue characterization, and direction and amount of maxillary movement by Le Fort I osteotomy.

4）本事業に関連して世界的な研究拠点形成に向けて、以下の点で改善・整備等されたこと

A（研究拠点体制）

昨年度に引き続き、GCOEの他の事業推進者や成育医療センターならびに、国際医療研究センターとの連携をさらに強化し、疾患に関わる情報を幅広く得られる基盤を確立した。

B（研究教育環境）

当分野では疾患に即した研究グループ分けが行われており、各グループにおいて、その疾患の原因の解明、検査診断や治療法の改良を目的とした研究が行われている。各大学院生は各研究グループに所属しており、そこで定期的にミーティングを行うなど、グループを基盤とした教育体制の充実化を図っている。また大学院生を含めた新人教育の一環として、先天性疾患をテーマにあげ、疾患の成因から臨床的な側面を含めた幅広い内容を求めた発表を課している。

C（人材確保）

本年度、大学院生が6人新たに加わり、各々GCOEのテーマである歯と骨の疾患の分子病態成立のメカニズムの解明を目指した研究だけでなく、当分野の特色である疾患を有する患者の咬合機能の回復のための治療法の開発にも携わっている。

D（人材育成）

GCOEプログラムでは、シャペロン制度やスーパースチューデント制度を創設して、若手研究者の人材の育成に取り組んでいるが、当分野において、本年度6名の大学院生がこの制度を利用している研究に携わっている。当分野の特色である臨床研究と基礎研究の橋渡しが出来る幅広い視野を持った研究者の育成が期待される。

E（国際化）

積極的に海外の学会発表や学術誌に投稿し、成果を発表した。さらに、タイ、ホンジュラスならびに中国とさまざまな国からの留学生を受け入れている。

5）GCOE事業を推進するに当たって力を入れた点

GCOEのテーマである歯と骨の疾患の分子病態成立のメカニズムを明らかにするには、ヒトから得られる情報を多角的に集積することが非常に大切であると思われる。そこで昨年度に引き続き、成育医療センターや国際医療

研究センターとも連携することで、さらに多くの疾患に関わる情報を幅広く得られる基盤を確立した。

6）英文原著論文

1. Kuroda S, Watanabe K, Ishimoto K, Nakanishi H, Moriyama K, Tanaka E. Long-term stability of LeFort III distraction osteogenesis with a rigid external distraction device in a patient with Crouzon syndrome. Am J Orthod Dentofacial Orthop. 140（4）：550-61, 2011.
2. Kawafuji A, Suda N, Ichikawa N, Kakara S, Suzuki T, Baba Y, Ogawa T, Tsuji M, Moriyama K. Systemic and maxillofacial characteristics of patients with Beckwith-Wiedemann syndrome not treated with glossectomy. Am J Orthod Dentofacial Orthop. 139（4）：517-25, 2011.
3. ◎Ng IW, Ono T, Inoue-Arai MS, Honda E, Kurabayashi T, Moriyama K. Application of MRI movie for observation of articulatory movement during a fricative /s/ and a plosive /t/. Angle Orthod. 81（2）：237-44, 2011.
4. ◎Suda N, Ogawa T, Kojima T, Saito C, Moriyama K. Non-syndromic oligodontia with a novel mutation of PAX9. J Dent Res. 90（3）：382-6, 2011.
5. ◎Takada J, Ono T, Miyamato JJ, Yokota T, Moriyama K. Association between intraoral pressure and molar position and inclination in subjects with facial asymmetry. Eur J Orthod. 33（3）：243-9, 2011.
6. ◎Terao F, Takahashi I, Mitani H, Haruyama N, Sasano Y, Suzuki O, Takano-Yamamoto T. Fibroblast growth factor 10 regulates Meckel's cartilage formation during early mandibular morphogenesis in rats. Dev Biol. 15;350（2）：337-47, 2011.
7. Ma D, Zhang R, Rios HF, Haruyama N, Sun Y, Xie Y, Kulkarni AB, Qin C, Feng JQ. A novel role of Periostin in postnatal tooth formation and mineralization. J Biol Chem. 11;286（6）：4302–09, 2011.
8. Suda N, Tominaga N, Niinaka Y, Amagasa T, Moriyama K. Orthognathic treatment for a patient with facial asymmetry associated with unilateral scissors-bite and a collapsed mandibular arch. Am J Orthod Dentofacial Orthop. 141（1）：94-104, 2012.
9. ◎Suzuki H, Suda N, Shiga M, Kobayashi Y, Nakamura M, Iseki S, Moriyama K. Apert syndrome mutant FGFR2 and its soluble form reciprocally alter osteogenesis of primary calvarial osteoblasts. J Cell Physiol.（in press）
10. ◎Okamoto N, Hayashi S, Masui R, Kosaki R, Oguri I, Hasegawa T, Imoto I, Makita Y, Hata A, Moriyama K, Inazawa J. Deletion at chromosome 10p11.23-p12.1 defines characteristic phenotypes with marked midface retrusion. J Hum Genet.（in press）
11. ◎Ng IW, Ono T, Inoue-Arai MS, Honda EI, Kurabayashi T, Moriyama K. Differential articulatory movements during Japanese /s/ and /t/ as revealed by MR image sequences with tooth visualization. Arch Oral Biol.（in press）
12. ◎Qiu L, Haruyama N, Suzuki S, Yamada D, Obayashi N, Kurabayashi T, Moriyama K. Accuracy of orthodontic miniscrew implantation guided by stereolithographic surgical stent based on cone-beam CT-derived 3D images. Angle Orthod.（in press）
13. ◎Okamura E, Suda N, Baba Y, Fukuoka H, Ogawa T, Ohkuma M, Ahiko N, Shiga M, Tsuji M, Moriyama K. Dental and maxillofacial characteristics in six Japanese individuals with ectrodactyly-ectodermal dysplasia-clefting（EEC）syndrome. Cleft Palate Craniofac J.（in press）

7）総説ならびに著書

（英文）

・Haruyama N, Hatakeyama J, Moriyama K, Kulkarni AB. Amelogenins：Multi-functional enamel matrix proteins and their binding partners.
J Oral Biosci. 2011 Aug;53（3）：257-66. Review.

（和文）

・辻美千子：ターナー女性特有の歯について. わかばの会15周年記念誌「わかばの会」、18-20、2011.
・辻美千子、松崎愛子：口唇口蓋裂患児の口腔ケア. 小児看護、第34巻12号、1613-1618、へるす出版、2011.

8）平成23年度までの自己評価

研究面においては、基礎研究の成果と臨床的要素を融合した研究を遂行することが可能であったとともに、公衆衛生の分野にも裾野を広げることで、疾患に関連した情報を幅広く得られる基盤を確立することができた。さらに、各々の大学院生が積極的に海外を含めた学会等で発表するとともに、発表した学術大会で受賞している大学院生も多数見られ、教育面でも充実化が図られた。

9）和文原著論文

河野郁子、川元龍夫、森山啓司. 歯科矯正治療と歯科補綴治療により咬合の改善を図った片側性口唇口蓋裂2症例. 日本口蓋裂学会誌、36（3）;213-226, 2011.

10）学会発表（英文）

1. ◎Takada J, Miyamoto JJ, Yokota T, Ono T, Moriyama K. Mandibular hinge axis in skeletal class III posterior unilateral crossbite patients. The 87th Congress of the European Orthodontic Society, Istanbul, June 19-3, 2011.

2. ◎Matsumoto T, Moriyama K, Yamaguchi A. Osteocytes are involved in osteoclastic bone resorption induced by mechanical loading during orthodontic tooth movement. The 3rd Joint Meeting of ECTS & IBMS, Athens, May 7-11, 2011.
3. ◎Uezono M, Takakuda K, Suzuki S, Moriyama K. Bone Forming Capability Around Novel Subperiosteal Anchorage Device for Orthodontic Treatment. Joint Conference of STAC5 and AMDI2. Yokohama, Japan. June 22-24 2011.
4. Kataoka K, Ogawa T, Baba Y, Higashihori N, Suzuki S, Moriyama K. Ultrasonographic monitoring for bony healing after maxillary distraction osteogenesis in an adult cleft lip and palate case. The 9th European Craniofacial Congress, Salzburg, September 14-17, 2011.
5. Ogawa T, Ohya A, Sato M, Baba Y, Moriyama K. Clinical surveys on associated anomalies in cases with isolated cleft palate. The 9th European Craniofacial Congress, Salzburg, September 14-17, 2011.
6. ◎Watanabe C, Morita M, Ezura T, Nakamoto T, Hayata T, Hemmi H, Notomi T, Moriyama K, Yamamoto T, Noda M. Cnot3, a crucial factor of mRNA stability, controls osteoblastic differentiation. The American Society for Bone and Mineral Research 2011 Annual Meeting, San Diego, September 16-20, 2011.
7. ◎Tsuji K, Koga T, Moriyama K, Takayanagi H. The Transcriptional Repressor LRF Regulates Osteoclastogenesis. The 59th Japanese Association for Dental Research, Hiroshima, October 8-9, 2011.
8. Hikita R, Ono T, Miyamoto JJ, Honda E, Kurabayashi T, Moriyama K. Brain activation patterns in auditory association area for glottal-stop perception. The 59th Japanese Association for Dental Research, Hiroshima, October 8-9, 2011.
9. Kawakubo N, Ono T, Miyamoto JJ, Katsuyama N, Taira M, Honda E, Kurabayashi T, Moriyama K. Upper-limb facilitation by teeth clenching and its brain activation pattern. The 59th Japanese Association for Dental Research, Hiroshima, October 8-9, 2011.
10. Komazaki Y, Fujiwara T, Kosaki R, Ogawa T, Moriyama K. The Methods of Three-Dimentional Anthropometric Measurements for Infants / Toddlers Face With Minor Anomalies. The 52nd Annual Meeting of the European for Paediatric Research, Newcastle, October 14-17, 2011.
11. ◎Haruyama N, Qiu L, Suzuki S, Yamada D, Obayashi N, Kurabayashi T, Moriyama K. Accuracy of miniscrew implantation guided by cone-beam CT based stereolithographic stent. The 4th International Congress & The 70th Annual meeting of the Japanese Orthodontic Society, Nagoya, October 17-20, 2011.

11）学会発表（和文）

1. 疋田理奈、小野卓史、宮本順、誉田栄一、倉林亨、森山啓司. 口蓋裂言語聴取時における聴覚連合野の脳賦活パタンfMRIを用いた研究. 第35回日本口蓋裂学会総会、新潟、平成23年5月25-26日.
2. 片岡恵一、小川卓也、馬場祥行、東堀紀尚、鈴木聖一、森山啓司. 上顎骨延長法適用後に超音波画像を用い延長部硬組織の治癒過程を経時的に観察した口唇口蓋裂の一症例. 第35回日本口蓋裂学会総会、新潟、平成23年5月25-26日.
3. 中久木康一、三島木節、村嶋真由子、高田潤一、佐藤豊、森山啓司、天笠光雄. 成人になってあらわれた口唇の裂の一例. 第35回日本口蓋裂学会総会、新潟、平成23年5月25-26日.
4. 北村良平、川元龍夫、宮本順、樺沢勇司、小村健、黒原一人、天笠光雄、森山啓司. 馬蹄形骨切り併用Le Fort I型骨切り術と下顎枝矢状分割術を施行した骨格性下顎前突症例の術後の顎態変化について. 第21回日本顎変形症学会総会・30周年記念国際シンポジウム、東京、平成23年6月16-17日.
5. 中川史彦、松下文彦、薗田直志、森山啓司. 上顎前歯部歯槽骨切り術による硬・軟組織の形態変化. 第21回日本顎変形症学会総会・30周年記念国際シンポジウム、東京、平成23年6月16-17日.
6. 志賀百年、馬場祥行、山田大輔、金沢英恵、徳山英二郎、金子剛、森山啓司、金田一純子. 成長期に顔面非対称が顕著となり外科的矯正治療を適用した1症例. 第21回日本顎変形症学会総会・30周年記念国際シンポジウム、東京、平成23年6月16-17日.
7. 岡村絵里花、川元龍夫、山田大輔、東堀紀尚、森山啓司. 顔面非対称を伴う骨格性下顎前突患者における顎矯正手術前後の硬軟組織変化に対する三次元的解析. 第21回日本顎変形症学会総会・30周年記念国際シンポジウム、東京、平成23年6月16-17日.
8. 中山友美子、川元龍夫、鈴木一史、東堀紀尚、森山啓司. 下顎枝矢状分割術を施行した骨格性下顎前突症例の長期術後経過からみた咬合安定性に関する検討. 第21回日本顎変形症学会総会・30周年記念国際シンポジウム、東京、平成23年6月16-17日.
9. 中久木康一、園田格、鈴木美保、鈴木剛史、黒原一人、儀武啓幸、細木美佐、森山啓司、天笠光雄.. 顎矯正手術後に一過性に顔面の異常運動を呈した1例. 第21回日本顎変形症学会総会・30周年記念国際シンポジウム、東京、平成23年6月16-17日.

10. 天願俊泉、比嘉努、新垣敬一、新崎章、砂川元、森山啓司、桃原均、古堅信、山内昌浩、崎原盛貴、上運修. 顎変形症の市民公開講座におけるアンケート. 第21回日本顎変形症学会総会・30周年記念国際シンポジウム、東京、平成23年6月16-17日.
11. 川元龍夫、鈴木剛史、岡村絵里花、中山友美子、茂木和久, 山田大輔、東堀紀尚、森山啓司. 東京医科歯科大学顎顔面矯正学分野における31年間の顎変形症治療に関する検討. 第21回日本顎変形症学会総会・30周年記念国際シンポジウム、東京、平成23年6月16-17日.
12. 鉄村明美、樺沢勇司、佐藤 昌、高楠 旻、川元龍夫、小村 健、倉林 亨. 顎関節MRIにおける矯正装置の影響. 日本歯科放射線学会 第213回関東地方会・第31回北日本地方会・第19回合同地方会、新潟、平成23年7月9日.
13. 出井彩乃、辻美千子、森山啓司.前歯部歯槽骨切りおよび自家腸骨海綿骨移植術を併用して咬合の改善を図った片側性口唇口蓋裂症例. 第70回東京矯正歯科学会、東京、平成23年7月21日.
14. 茂木和久、川元龍夫、東堀紀尚、森山啓司. 東京医科歯科大学歯学部附属病院顎顔面矯正学分野を受診し下顎頭変形を認めた不正咬合患者に関する臨床統計学的検討. 第24回日本顎関節学会総会・学術大会、広島、平成23年7月23－24日.
15. 松本力、飯村忠浩、山口朗. 矯正力による歯の移動における骨細胞の役割. 第29回日本骨形態計測学会、岐阜、平成23年5月20－22日.
16. 渡辺千穂、森田斉弘、江面陽一、中元哲也、早田匡芳、辺見弘明 、納富拓也、森山啓司、山本雅、野田政樹. mRNA制御因子であるCnot3 は骨量制御に関与する. 第29回日本骨代謝学会、大阪、平成23年7月28－30日.
17. 寺尾文恵、高橋一郎、三谷英稔、春山直人、笹野泰之、鈴木治、山本照子. 胎生期下顎形成期におけるFGF10によるメッケル軟骨形態の制御. 第29回日本骨代謝学会、大阪、平成23年7月28－30日.
18. 川久保直美、小野卓史、宮本順、誉田栄一、倉林亨、森山啓司. 咬みしめに伴う上肢筋の促通とそれに同期した脳賦活パタン　fMRIを用いた研究. 第70回日本矯正歯科学会＆第4回国際会議、名古屋、平成23年10月17－20日.
19. 湊亜紀子、宮本順、小野卓史、誉田栄一、倉林亨、森山啓司. 舌触覚刺激に対する2点弁別および大脳皮質賦活パタンにおける習慣性咀嚼側の関与. 第70回日本矯正歯科学会＆第4回国際会議、名古屋、平成23年10月17－20日.
20. 出井彩乃、宮本順、高田潤一、小野卓史、森山啓司.口輪筋訓練における口輪筋筋活動および血流量の同時計測の有用性. 第70回日本矯正歯科学会＆第4回国際会議、名古屋、平成23年10月17－20日.
21. 小林起穂、ヴァイスティネン・ロッタ、ライス・デビッド、森山啓司. Runx2発現抑制によるGli3Xt-J/Xt-Jマウス頭蓋冠縫合部早期癒合症発症の予防効果. 第70回日本矯正歯科学会＆第4回国際会議、名古屋、平成23年10月17－20日.
22. 松本力、山口朗、森山啓司. 矯正学的歯の移動における骨細胞の役割. 第70回日本矯正歯科学会＆第4回国際会議、名古屋、平成23年10月17－20日.
23. 大宅彩、小川卓也、阿彦希、佐藤麻緒、片岡恵一、井口隆人、小林起穂、東堀紀尚、春山直人、馬場祥行、森山啓司. 当分野の口蓋裂症例における合併症状に関する検討. 第70回日本矯正歯科学会＆第4回国際会議、名古屋、平成23年10月17－20日.
24. 佐藤智美、澤田紘美、志賀百年、吉崎正子、大隈瑞恵、辻美千子、佐藤麻緒、馬場祥行、金田一純子、小川卓也、森山啓司. Russell-Silver症候群の頭部X線規格写真を用いた顎顔面形態に関する検討. 第70回日本矯正歯科学会＆第4回国際会議、名古屋、平成23年10月17－20日.
25. 柘植理紗、小川卓也、上園将慶、丸岡亮、大隈瑞恵、志賀百年、辻美千子、須田直人、小崎健次郎、森山啓司. 当分野を受診したRussell-Silver症候群患者の臨床症状に関する検討. 第70回日本矯正歯科学会＆第4回国際会議、名古屋、平成23年10月17－20日.
26. 辻美千子、小川卓也、岡村絵里花、鈴木尋之、志賀百年、鈴木聖一、森山啓司. 当分野における先天異常患者の実態調査と当該患者に対するカウンセリングの概要について. 第70回日本矯正歯科学会＆第4回国際会議、名古屋、平成23年10月17－20日.
27. 丸岡亮、茂木和久、疋田理奈、駒崎裕子、小林起穂、川元龍夫、森山啓司. 上顎犬歯埋伏とエナメル上皮腫を伴う骨格性下顎前突症に対して自家歯牙移植と外科的矯正治療を行った一例. 第70回日本矯正歯科学会＆第4回国際会議、名古屋、平成23年10月17－20日.
27. 志賀百年、馬場祥行、金沢英恵、佐藤麻緒、森山啓司、堀川玲子、金田一純子. 国立成育医療研究セン

ターを受診したラッセル・シルバー症候群患者3例に対する歯科矯正治療. 第70回日本矯正歯科学会＆第4回国際会議、名古屋、平成23年10月17－20日.

29. 丸岡亮、辻美千子、小崎健次郎、森山啓司. 神経線維腫症I型患者に歯科矯正治療を行った2治験例. 第3回日本レックリングハウゼン病学会、東京、平成23年11月13日.
30. 岡村絵里花、川元龍夫、東堀紀尚、森山啓司. 顔面非対称症例における顎矯正手術前後の硬軟組織変化に対する三次元的解析. 第29回日本頭蓋顎顔面外科学会学術集会、東京、平成23年11月24-25日.
31. 松本力、森山啓司、山口朗. 矯正学的歯の移動における骨細胞の役割. 第76回口腔病学会学術大会、東京、平成23年12月10日.

12）受賞

1. 小林起穂、ヴァイスティネン・ロッタ、ライス・デビッド、森山啓司. Runx2発現抑制によるGli3Xt-J/Xt-Jマウス頭蓋冠縫合部早期癒合症発症の予防効果. 第70回日本矯正歯科学会＆第4回国際会議・優秀発表賞、名古屋、平成23年10月17－20日.
2. 出井彩乃、宮本順、高田潤一、小野卓史、森山啓司.口輪筋訓練における口輪筋筋活動および血流量の同時計測の有用性. 第70回日本矯正歯科学会＆第4回国際会議・優秀発表賞、名古屋、平成23年10月17－20日.
3. 湊亜紀子、宮本順、小野卓史、誉田栄一、倉林亨、森山啓司. 舌触覚刺激に対する2点弁別および大脳皮質賦活パタンにおける習慣性咀嚼側の関与. 第70回日本矯正歯科学会＆第4回国際会議・優秀発表賞、名古屋、平成23年10月17－20日.
4. 松本力、山口朗、森山啓司. 矯正学的歯の移動における骨細胞の役割. 第70回日本矯正歯科学会＆第4回国際会議・優秀発表賞、名古屋、平成23年10月17－20日.
5. 川久保直美、小野卓史、宮本順、誉田栄一、倉林亨、森山啓司. 咬みしめに伴う上肢筋の促通とそれに同期した脳賦活パタンfMRIを用いた研究. 第70回日本矯正歯科学会＆第4回国際会議・優秀発表賞、名古屋、平成23年10月17－20日.

13）外部資金の獲得状況

科学研究費補助金、基盤B

研究題目：ゲノム・ナノサイエンスを応用した顎顔面先天異常に対する分子標的治療開発の基盤創成
代表：森山啓司
期間：平成23年－平成25年
研究費総額：1,480万円

科学研究費補助金、挑戦的萌芽

研究題目：リラクシン含有磁気制御型リポソームを応用した新規骨縫合部改造法の開発
代表：森山啓司
期間：平成23年－平成24年
研究費総額：280万円

厚生労働科学研究費補助金、難治性疾患克服研究事業

研究題目：進行性下顎頭吸収の診断基準策定とその治療に関する研究
分担：森山啓司
期間：平成22年－平成23年
研究費総額：100万円

科学研究費補助金、基盤C

研究題目：骨延長統合モニタリングシステムの開発
代表：鈴木聖一
期間：平成21年－平成23年
研究費総額：370万円

科学研究費補助金、基盤C

研究題目：上顎歯槽部骨延長への歯の移動と移植に高気圧酸素療法が与える影響
代表：川元龍夫
期間：平成21年－平成23年
研究費総額：350万円

科学研究費補助金、基盤C

研究題目：骨延長術により上顎側方偏位を改善する際の牽引力の解析
代表：馬場祥行
期間：平成23年－平成25年
研究費総額：390万円

科学研究費補助金、基盤C

研究題目：ペリオスチンに着目した歯根膜弾性線維の機能解析
代表：志賀百年
期間：平成23年－平成25年
研究費総額：390万円

科学研究費補助金　若手（B）

研究題目：　象牙質細胞外マトリクスによる骨代謝制御医薬の新規開発
代表：　春山直人
期間：　平成22年－24年
研究費総額：　310万円

科学研究費補助金、若手B
研究題目：眼・顔面・心臓・歯症候群における歯根形成を制御する遺伝子BCORの役割の解明
代表：小川卓也
期間：平成22年－平成24年
研究費総額：300万円

科学研究費補助金、若手B
研究題目：ヒト脳機能の咀嚼運動制御の解明：脳機能画像と咀嚼筋活動・咬合力との同時計測の試み
代表：宮本順
期間：平成22年－平成25年
研究費総額：320万円

科学研究費補助金、若手B
研究題目：頭蓋冠縫合部早期癒合症に関与する細胞群の同定とその分化制御に関する研究
代表：小林起穂
期間：平成22年－平成24年
研究費総額：330万円

科学研究費補助金、若手B
研究題目：上皮間葉転換に関わる転写因子発現のエピジェネティクス制御機構
代表：大隈瑞恵
期間：平成22年－平成23年
研究費総額：260万円

科学研究費補助金、若手B
研究題目：口唇閉鎖不全に対する筋機能療法の効果：マルチモダリティ解析
代表：高田潤一
期間：平成22年－平成24年
研究費総額：300万円

科学研究費補助金、若手B
研究題目：上顎骨延長法における牽引力と軟組織変化の同時モニタリングシステムの開発
代表：南綾
期間：平成22年－平成23年
研究費総額：150万円

科学研究費補助金、研究活動スタート支援
研究題目：口唇裂発症時におけるエピジェネティックな変化
代表：東堀 紀尚
期間：平成22年－平成23年
研究費総額：229万

科学研究費補助金、研究活動スタート支援
研究題目：口唇形成術後の瘢痕組織への触覚刺激に伴う一次体性感覚野の賦活パタンの解析
代表：湊亜紀子
期間：平成22年－平成24年
研究費総額：250万

14）特別講演、招待講演、シンポジウム

1. Keiji Moriyama：New biological insights of tooth movement in response to mechanical stress, 23rd annual conference of the Taiwan Association of Orthodontists, Taichung, Taiwan, December 10, 2011
2. Keiji Moriyama："An orthodontic perspective of long-term care for cleft patients", Special lecturer, The 15th Congress of Korean Cleft Lip and Palate Association（KCLPA 2011）, Seoul, KOREA, June 25, 2011.
3. Keiji Moriyama：" Some considerations on dentofacial growth in cleft patients", the Symposium, he 15th Congress of Korean Cleft Lip and Palate Association（KCLPA 2011）Seoul, KOREA, June 25, 2011.
4. Keiji Moriyama："Growth and Development of Cleft Patients", the Symposium, the 15th Congress of Korean Cleft Lip and Palate Association（KCLPA 2011）Seoul, KOREA, June 25, 2011.
5. Keiji Moriyama：Accuracy of Orthodontic TAD Implantation Guided by Surgical Stent Based on Cone Beam Images. The Angle Society East Component Meeting, Providence, Rhode Island, U.S.A., March 24-27, 2011.
6. 小林起穂：頭蓋冠縫合部の発生におけるHedgehogシグナルの役割. 第4回硬組織疾患ゲノムセンターシンポジウム. 東京医科歯科大学、平成23年1月31日.
7. 森山啓司：顎顔面先天異常に対する矯正歯科的対応とその課題. 第4回硬組織疾患ゲノムセンターシンポジウム. 東京医科歯科大学、平成23年1月31日.
8. 辻美千子：ターナー症候群の歯科的問題について. 第12回関東甲信越ターナー講演会、東京、平成23年4月9日.
9. 森山啓司：顎顔面矯正学がめざすもの. 第70回東京矯正歯科学会、東京、平成23年7月21日.
10. 森山啓司：歯科技工士が知っておきたい歯科矯正治療の基礎知識. 全都講習会. 東京医科歯科大学、平成23年9月10日.

11. 森山啓司：矯正歯科治療における診査・診断～3Dシュミレーションの可能性～　第3回国際歯科シンポジウム. 平成23年10月23日.
12. 辻美千子：“顔”と歯の関係を探る～歯ならびで口元はどのように変わるのか?「知っているようで知らない顔のナゾ～顔学入門」講座、名古屋、平成23年10月27日.
13. 辻美千子、森山啓司：卒前歯学教育における遺伝医学教育の現状と課題. 第56回日本人類遺伝学会・第11回東アジア人類遺伝学会シンポジウム4「遺伝医学教育」、千葉、平成23年11月10日.

15）主催学会

第21回日本顎変形症学会総会・30周年記念国際シンポジウム、東京、平成23年6月16-17日.

16）GCOE総合講義

歯の形成期におこる石灰化現象は、生体内で起こる石灰化（バイオミネラリゼーション）の例のなかでもユニークで、多くの細胞外マトリクス（ECM）タンパクやその分解酵素が関与していることが判明している。ヒトにおける、歯に特異的なECMタンパクや分解酵素をコードする遺伝子異常の発見と、それらの遺伝子欠損マウスモデルの作出・解析により、近年各々のタンパク役割がより明確にされつつあり、従来臨床像に基づいて分類されていた非症候群性の「エナメル質形成不全症」および「象牙質形成不全症」について、疾患原因に基づいた分類が提唱されるようになってきた。今回の講義では、エナメル質・象牙質の石灰化におけるECMタンパクやその分解酵素の役割に関する最新の知見と、そこから提唱される石灰化モデルを紹介すると共に、「エナメル質形成不全症」および「象牙質形成不全症」の最新分類について述べる。

17）教室、分野や講座の准教授、講師、助教、特別研究員、ポスドク、指導を受けた大学院生の名前

准教授　鈴木　聖一
講　師　川元　龍夫
助　教　辻　美千子
小川　卓也
東堀　紀尚
宮本　順
福岡　裕樹
GCOE特任講師：春山　直人
硬組織疾患ゲノムセンター特任助教：小林　起穂
大学院生　岡本　奈那
○辻　香織
疋田　理奈
○松本　力
伊藤　洋介
川久　保直美
○森田　淳平
駒崎　裕子
○渡辺　千穂
上園　将慶
丸岡　亮
吉崎　正子
○Carolina Duarte
Paveenarat Aukkarasongsup
梅沢　峻之
小倉　健司
村本　慶子
山本　直
劉　世頴
Thunyaporn Surapornsawasd
外国人特別研究員：井上　マリステラ小百合
○はAISS

18）GCOE活動についての感想、コメント、改善を望む点

本年度においても、昨年度に整備したGCOE事業推進者との研究体制をさらに強化することができた。各研究分野でトップを走る他の事業推進者と連携して研究を進めていくことができる環境は、いち早く最先端の情報を得られることでき、今後の研究の展開に大変有意義であると思われた。

RESEARCH REPORTS
Clinical

N. Suda[1,2]*, T. Ogawa[1,2], T. Kojima[3], C. Saito[3], and K. Moriyama[1,2]

[1]Maxillofacial Orthognathics, Department of Maxillofacial Reconstruction and Function, Division of Maxillofacial/Neck Reconstruction, Graduate School of Medical and Dental Sciences, Tokyo Medical and Dental University, 1–5-45 Yushima, Bunkyo-ku, Tokyo, 113–8510, Japan; [2]Global Center of Excellence (GCOE) Program, International Research Center for Molecular Science in Tooth and Bone Diseases, Tokyo, Japan; and [3]Division of Reconstructive Surgery for Oral and Maxillofacial Region, Department of Tissue Regeneration and Reconstruction, Niigata University Graduate School of Medical and Dental Sciences, Niigata, Japan; *corresponding author, n-suda.mort@tmd.ac.jp

J Dent Res 90(3):382-386, 2011

Non-syndromic Oligodontia with a Novel Mutation of *PAX9*

ABSTRACT

Agenesis of the permanent teeth is a congenital anomaly that is frequently seen in humans. Oligodontia is a severe type of tooth agenesis involving 6 or more congenitally missing teeth, excluding the third molars. Previous studies have indicated that mutations in the homeobox gene *MSX1*, paired domain transcription factor *PAX9*, and *EDA* are associated with non-syndromic oligodontia. This study reports a Japanese family (eight of 14 family members affected) with non-syndromic oligodontia who preferentially lacked molar teeth. In this family, a novel frameshift mutation (321_322insG) was identified in the paired domain of *PAX9*. The frameshift mutation caused altered amino acids in the paired domain and premature termination of translation by 26 amino acids. When transfected into COS-7 cells, the mRNA expression of 321_322insG *PAX9* was comparable with that of wild-type *PAX9*. However, the mRNA of 321_322insG *PAX9* was more unstable than that of wild-type *PAX9*. This mRNA instability caused a marked decrease in protein production, as evaluated by Western blot analysis and immunostaining. These findings suggest that the 321_322insG mutation causes insufficient function of PAX9 protein and haploinsufficiency as a genetic model of familial non-syndromic oligodontia with a *PAX9* mutation.

KEY WORDS: oligodontia, *PAX9*, tooth, gene mutation, RNA stabilization.

DOI: 10.1177/0022034510390042

Received June 23, 2010; Last revision October 18, 2010; Accepted October 18, 2010

© International & American Associations for Dental Research

INTRODUCTION

Agenesis of the permanent teeth is an anomaly that is frequently seen in humans. The prevalence of agenesis of 1 or 2 teeth (excluding the third molars) is from 1.6% to 9.6% (Symons *et al*., 1993; Vastardis, 2000). Oligodontia is a severe type of tooth agenesis involving 6 or more congenitally missing teeth, excluding the third molars (Schalk-van der Weide *et al*., 1992; Stockton *et al*., 2000). In a study on Danish schoolchildren, 0.16% of the children were found to have oligodontia (Rølling and Poulsen, 2001). To date, 3 genes, namely, the homeobox gene *MSX1*, paired domain transcription factor *PAX9*, and *EDA*, have been associated with non-syndromic oligodontia (Vastardis *et al*., 1996; Stockton *et al*., 2000; Tao *et al*., 2006).

Familial non-syndromic oligodontia associated with *PAX9* mutation preferentially affects molar formation (Stockton *et al*., 2000; Frazier-Bowers *et al*., 2002; Kapadia *et al*., 2006). To date, 10 gene mutations have been identified in the DNA-binding paired domain of *PAX9* (Nieminen, 2009; Wang *et al*., 2009). One is a frameshift mutation (219_220insG) (Stockton *et al*., 2000; Mensah *et al*., 2004), one is a nonsense mutation (A340T) (Nieminen *et al*., 2001), and 8 are point mutations (Das *et al*., 2003; Lammi *et al*., 2003; Mostowska *et al*., 2003; Jumlongras *et al*., 2004; Kapadia *et al*., 2006; Ogawa *et al*., 2006; Wang *et al*., 2009).

In this study, a novel frameshift mutation of *PAX9* (321_322insG) was identified in a Japanese family with non-syndromic oligodontia. The purpose of this study was to clarify the aberrant function of this gene mutation. We hypothesized that this *PAX9* mutation caused abnormal mRNA and/or protein expression.

MATERIALS & METHODS

Family with Oligodontia

The proband was a 37-year-old female (III:3) in a Japanese family with oligodontia treated in Niigata University Hospital (Fig. 1A). IV:1 (an 18-year-old female) was also treated for oligodontia in the hospital, and their panoramic radiographs were used for the diagnosis. Oral examinations and interviews were performed on II:3 and III:2. An interview was performed by phone on I:1, II:5, III:4, and III:5, who lived far from the Dental Hospital of Tokyo Medical and Dental University and Niigata University Hospital. This

Downloaded from jdr.sagepub.com at TOKYO IKASHIKA UNIVERSITY on March 22, 2012 For personal use only. No other uses without permission.

© 2011 International & American Associations for Dental Research

was carried out by identification of the normal numbers and shapes of permanent teeth of each person. The extraction and loss of any teeth after eruption were carefully queried for each family member. Each individual with more than 6 congenitally missing teeth, excluding the third molars, was diagnosed as having oligodontia for the purposes of this study (Schalk-van der Weide *et al*., 1992; Stockton *et al*., 2000). The experimental protocol was approved by the Ethical Review Committee of the Tokyo Medical and Dental University and the Niigata University Graduate School of Medical and Dental Sciences.

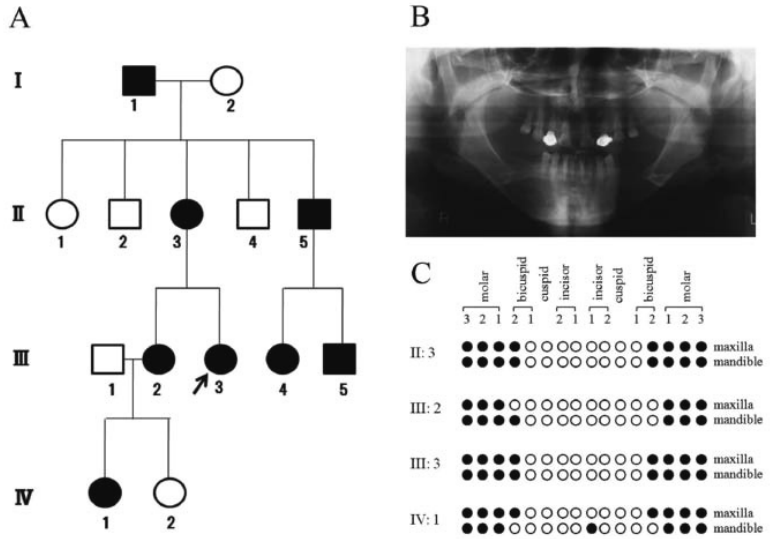

Figure 1. A Japanese family with non-syndrome oligodontia. **(A)** Pedigree of the Japanese family with non-syndromic oligodontia. The arrow indicates the proband. **(B)** Panoramic radiograph of III:3. **(C)** Summary of the permanent tooth agenesis in the present pedigree. Each tooth agenesis is denoted by a black circle.

Mutational Analysis

For mutational analysis, we obtained genomic DNA from individuals whose informed consent was obtained. Genomic DNA was isolated from nail samples of II:3, III:2, III:3, IV:1, and IV:2. The isolated DNA was amplified by polymerase chain-reaction in a GeneAmp PCR System 9700 and specific primers for *PAX9* (Das *et al*., 2003). The amplified products were sequenced with a PRISM® 3100 Genetic Analyzer and a BigDye Terminator v.3.1 Cycle Sequencing Kit (Applied Biosystems, Foster City, CA, USA).

Plasmid Construct

The human *PAX9* cDNA (NM_006194.2) was subcloned in-frame with a C-terminal Myc-tag downstream of the cytomegalovirus (CMV) promoter into the pReceiver-M09 empty vector (termed EX-NEG; GeneCopoeia, Rockville, MD, USA). Site-directed mutagenesis was carried out with the QuickChange mutagenesis kit (Stratagene, La Jolla, CA, USA), as previously reported (Wang *et al*., 2009). The entire coding sequence of the mutant construct was verified by a PRISM® 3100 Genetic Analyzer and a BigDye Terminator v.3.1 Cycle Sequencing Kit.

Transfection of Cultured Cells

COS-7 cells were cultured in Dulbecco's modified Eagle's medium (Wako, Tokyo, Japan) supplemented with 10% fetal bovine serum (Biowest, Nualle, France). All cultures were maintained in a humidified, 5% CO_2 atmosphere at 37°C. Transient transfection was performed with the Fugene 6 Transfection Reagent (Roche, Basal, Switzerland), according to the manufacturer's instructions.

Western Blot Analysis

COS-7 cells transfected with wild-type or mutant *PAX9* underwent lysis in buffer containing 50 mM Tris-HCl (pH 7.4), 125 mM NaCl, 0.1% Nonident P-40 (Sigma-Aldrich, St. Louis, MO, USA), and 1 mM each of EDTA (Wako) and phenylmethylsulfonyl fluoride (Sigma-Aldrich), followed by sonication, as described previously (Shiga *et al*., 2008). Western blot analysis was performed with cell lysates at 12 and 48 hrs after transfection. Briefly, a 20-μg quantity of protein was separated by 10% SDS-PAGE under reducing conditions and transferred electrophoretically to a Hybond-P polyvinylidene difluoride (PVDF) membrane (Amersham, Buckinghamshire, UK). The membrane was probed with an anti-Myc monoclonal antibody (Santa Cruz Biotechnology, Inc., Santa Cruz, CA, USA). The bound antibody was detected by ECL plus Western blotting detection reagents (Amersham), according to the manufacturer's instructions.

Immunohistochemistry

Transfected COS-7 cells were fixed with methanol for 10 min and stained with the anti-Myc monoclonal antibody. After being washed with PBS, the cells were incubated with a fluorescein isothiocyanate (FITC)-conjugated secondary antibody (Santa Cruz Biotechnology, Inc.). After the washing, fluorescence was observed by fluorescence microscopy (AF6000, Leica, Wetzlar, Germany).

RNA Preparation

COS-7 cells were transfected with wild-type or mutated *PAX9*. At 12 hrs after the transfection, total RNA was isolated from the cells with ISOGEN (Nippon Gene, Tokyo, Japan), according to the manufacturer's instructions. DNase treatment was performed with TURBO DNA-*free* (Ambion Inc., Austin, TX, USA). cDNA was synthesized from 1 μg of the total RNA with

Downloaded from jdr.sagepub.com at TOKYO IKASHIKA UNIVERSITY on March 22, 2012 For personal use only. No other uses without permission.

© 2011 International & American Associations for Dental Research

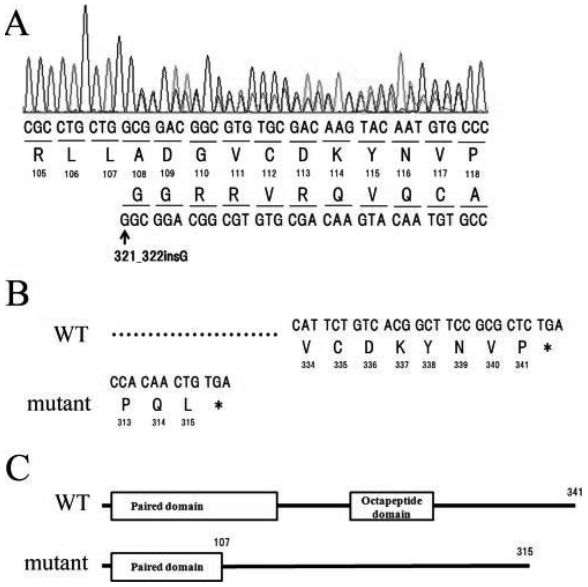

Figure 2. A novel mutation in a Japanese family with non-syndrome oligodontia. **(A)** Nucleotide sequence and amino acid alignment of *PAX9* in affected members (II:3, III:2, III:3, and IV:1) of the pedigree. The small numbers denote the order of the amino acids. The position of the 321_322insG mutation is indicated by the arrow. **(B)** C-termini of wild-type (WT) and 321_322insG (mutant) PAX9. The small numbers denote the order of the amino acids. Each asterisk denotes the terminal codon. **(C)** Constructs of wild-type (WT) and 321_322insG (mutant) PAX9 showing the premature termination of translation by 26 amino acids in the mutant protein. The small numbers denote the order of the amino acids.

a QuantiTect Reverse Transcription Kit (Qiagen, Valencia, CA, USA).

Real-time PCR and Examination of mRNA Stability

Each cDNA was used as a template for quantitative analysis of *PAX9* mRNA with a 7300 Real Time PCR system (Applied Biosystems). The real-time PCR amplifications were performed with TaqMan gene expression assays (Applied Biosystems), according to the manufacturer's instructions. The primers and TaqMan probe used were as follows: forward primer, 5′-GGCATCCGACCGTGTGA-3′, reverse primer, 5′-TCCTGG CAAGATCGAGCC-3′, TaqMan probe, 5′-ATCCTGGCGCGA TAC-3′. These primers and the probe corresponded to the N-terminus of the paired domain and upstream of the 321st nucleotide. The expression of human *PAX9* was normalized by the amplification of eukaryotic 18S rRNA (product number 4331182; Applied Biosystems).

To examine the mRNA stability, we similarly transfected COS-7 cells with wild-type or mutated *PAX9*. At 12 hrs after transfection, 1 μg/mL of actinomycin D (Wako) was added to the culture. Total RNA was isolated from the cells at 3 and 6 hrs after the actinomycin D addition. After treatment with TURBO DNA-*free* and cDNA synthesis with the QuantiTect Reverse Transcription Kit, quantitative analysis of *PAX9* mRNA was carried out in the 7300 Real-time PCR System. The mRNA stability was represented as the *PAX9* mRNA remaining after normalization by eukaryotic 18S rRNA (100% remaining *PAX9* mRNA denoted the value without actinomycin D treatment).

Statistical Evaluations

We used Student's *t* test to examine the differences in the relative expression levels of *PAX9*/18S rRNA and the decay of *PAX9* mRNA following addition of actinomycin D, between wild-type and 321_322insG *PAX9*. The statistical analyses were carried out with StatView (SAS Institute, Cary, NC, USA). Values of $P < 0.05$ were considered to indicate statistical significance.

RESULTS

The Family with Non-syndromic Oligodontia

The pedigree of the present family with oligodontia is shown in Fig. 1A. Eight (I:1, II:3, II:5, III:2, III:3, III:4, III:5, and IV:1) of 14 family members had oligodontia. In the regular health examinations, the family members had no medical history of abnormalities in their sweat glands, skin, hair, or nails, indicating the non-syndromic type of oligodontia. A panoramic radiograph of the proband (III:3; 37-year-old female) is shown in Fig. 1B. She had tooth agenesis of the upper and lower second premolars and all molars (agenesis of 12 permanent teeth in total, excluding the third molars) (Figs. 1B, 1C). Based on the oral examinations, interviews, and panoramic radiographs, the positions of the missing permanent teeth in this family are summarized in Fig. 1C. Four members (II:3, III:2, III:3, and IV:1) showed tooth agenesis of the premolars and molars, and the agenesis was also seen in the lower central incisor of IV:1.

DNA Sequence Analysis of the *PAX9* Gene

Since this family preferentially lacked teeth in the molar region, the DNA sequence of *PAX9* was examined in II:3, III:2, III:3, IV:1, and IV:2. II:3, III:2, III:3, and IV:1 had the same heterozygous insertion of G after the 321st nucleotide according to NM_006194.2 (Fig. 2A). This mutation was not seen in IV:2, who was a healthy control without oligodontia. The 321st nucleotide corresponded to an amino acid in the paired domain (Fig. 2B). This mutation caused a heterozygous frameshift mutation, resulting in premature termination of translation by 26 amino acids (Figs. 2B, 2C).

Characteristics of the 321_322insG Mutation in the *PAX9* Gene

Next, we transfected the 321_322insG mutated construct into COS-7 cells to examine the characteristics of the mutant protein. Expression was faintly seen at 12 hrs and clearly seen at 48 hrs after the transfection. A band of the expected size (40 kDa) was seen in the cell lysates of wild-type and mutated *PAX9* transfected COS-7 cells, but not in the lysate of the empty vector-transfected cells (Fig. 3A). The protein level was much lower in the mutated *PAX9*-transfected COS-7 cells than in the wild-type *PAX9*-transfected cells. This finding was also noted in the

Downloaded from jdr.sagepub.com at TOKYO IKASHIKA UNIVERSITY on March 22, 2012 For personal use only. No other uses without permission.

© 2011 International & American Associations for Dental Research

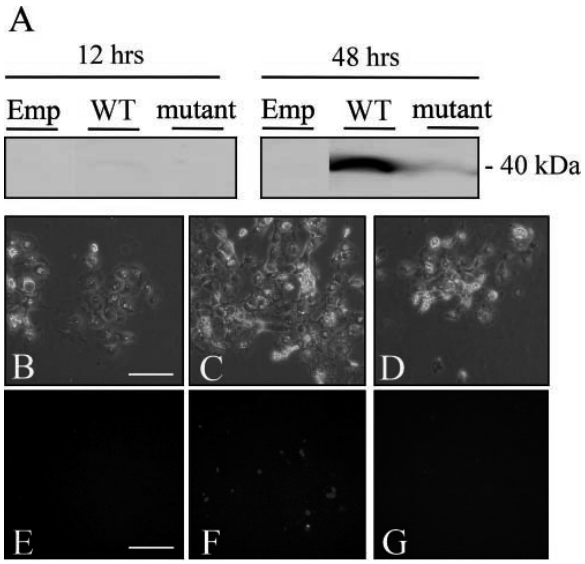

Figure 3. The protein expression of 321_322insG *PAX9*. **(A)** Western blot analysis with an anti-Myc monoclonal antibody. Cell lysates from COS-7 cells transfected with EX-NEG (Emp), wild-type *PAX9* (WT), or 321_322insG *PAX9* (mutant) for 12 or 48 hrs were analyzed. **(B-D)** Phase-contrast microscopic observations of COS-7 cells transfected for EX-NEG (B), wild-type *PAX9* (C), or 321_322insG *PAX9* (D) for 48 hrs. **(E-G)** Immuno-histochemistry with the anti-Myc monoclonal antibody. Fluorescence microscopic images of COS-7 cells transfected with EX-NEG (E), wild-type *PAX9* (F), or 321_322insG *PAX9* (G) for 48 hrs are shown.

immunostaining of COS-7 cells with the same antibody (Figs. 3B-3G). Positive staining was seen in the nuclei of COS-7 cells transfected with wild-type *PAX9* (Figs. 3C, 3F), but was scarcely seen in the COS-7 cells transfected with the mutant construct (Figs. 3D, 3G). Positive staining was not seen in the empty vector-transfected cells (Figs. 3B, 3E).

To clarify the mechanism for the decreased level of the mutant protein, we examined the mRNA expressions of the wild-type and 321_322insG *PAX9*. First, the mRNA expressions were examined by amplification of the N-terminus region of the paired domain. The results showed that the mRNA expression of 321_322insG *PAX9* did not differ significantly from that of wild-type *PAX9* at 12 hrs after transfection (Fig. 4A). Next, the mRNA stabilities of wild-type and 321_322insG *PAX9* were examined. At 12 hrs after transfection, the cells were treated with actinomycin D, an inhibitor of transcription (Fig. 4B). The mRNA levels were decreased for both wild-type and 321_322insG *PAX9* at 3 and 6 hrs after the actinomycin D addition. The mRNA of 321_322insG *PAX9* was significantly more unstable than the mRNA of wild-type P*AX9* during the examined time-course (Fig. 4B).

DISCUSSION

In this study, a novel frameshift mutation of *PAX9* (321_322insG) was identified in a Japanese family with non-syndromic oligodontia.

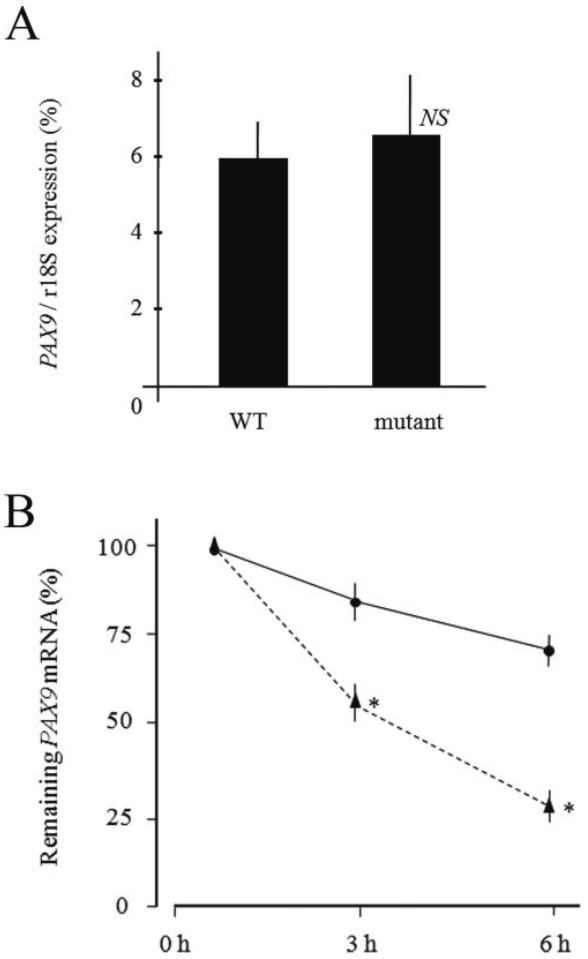

Figure 4. mRNA expression of 321_322insG *PAX9*. **(A)** Relative expression levels of *PAX9*/18S rRNA at 12 hrs after transfection. The expression of *PAX9* mRNA in COS-7 cells transfected with wild-type (WT) or 321_322insG (mutant) *PAX9* is shown. Expression is represented by the percentage (%) of *PAX9* mRNA expression relative to eukaryotic 18S rRNA (18S) expression. All data are expressed as means ± SE (n = 4). *NS*, not significant *vs.* wild-type *PAX9*. **(B)** Decay of *PAX9* mRNA following addition of actinomycin D. The decay of wild-type (solid line) and 321_322insG (dotted line). Each value is represented by the remaining *PAX9* mRNA after normalization by the eukaryotic 18S rRNA (100% remaining *PAX9* mRNA denotes the value without actinomycin D treatment). Data at 0, 3, and 6 hrs after the actinomycin D treatment are shown. All the data are expressed as means ± SE (n = 4). $^*P < 0.05$, significant difference *vs.* wild-type *PAX9*.

The family showed permanent tooth agenesis preferentially in the molar region. *In vitro* analyses revealed instability of the mRNA of the mutated *PAX9*, resulting in lower protein production.

The present family had tooth agenesis mainly of the molars. Since I:1, II:5, III:4, and III:5 did not live close to our universities, it was not possible to determine their tooth agenesis directly by oral examination or panoramic radiograph. However, the interview provided us with sufficient information that they had

Downloaded from jdr.sagepub.com at TOKYO IKASHIKA UNIVERSITY on March 22, 2012 For personal use only. No other uses without permission.

© 2011 International & American Associations for Dental Research

tooth agenesis in the molar region. In addition to the molars, II:3, III:2, III:3, and IV:1 had tooth agenesis of the premolars. This type of tooth agenesis was first reported in a family with a mutation in the paired domain of *PAX9* (Stockton *et al*., 2000). The reported family also showed missing second premolars and mandibular central incisors. Interestingly, tooth agenesis of the mandibular central incisor was also seen in one member of the present family (IV:1). The 321_322insG *PAX9* mutation was identified in this family. Ten different gene mutations have been identified in the paired domain of *PAX9* to date (Nieminen, 2009; Wang *et al*., 2009), but no previous studies have reported the present frameshift mutation.

It has been reported that 219_220insG *Pax9* (frameshift mutation in the paired domain) abrogates translocation of the protein from the cytoplasm to the nucleus (Wang *et al*., 2009). However, the total protein expression (including both the nuclear and cytoplasmic fractions) of this mutated mouse *Pax9* was comparable with that of mouse wild-type *Pax9*. In contrast to this mouse study, the protein expression of the present human mutated *PAX9* was much lower than that of human wild-type *PAX9*, and the mRNA of 321_322insG *PAX9* was significantly more unstable compared with that of the wild-type gene. The results for these mouse and human mutated proteins were obtained by experiments with the same COS-7 cells and mutagenesis kit. Therefore, it is likely that these two frameshift mutations have different gene functions from one another.

Further studies are required to clarify the instability of 321_322insG *PAX9* mRNA. Degradation of mRNA is an important mechanism for controlling gene expression, and eukaryotic mRNAs are primarily degraded by removal of the 3′ poly(A) tail (deadenylation) and cleavage of the 5′ cap structure (decapping) (Mitchell and Tollervey, 2000; Wilusz *et al*., 2001). In mammalian cells, it has been reported that PAN2 and CCR4 are the major poly(A) nucleases active in cytoplasmic deadenylation, and that DCP2-mediated de-capping is required after deadenylation (Yamashita *et al*., 2005). To clarify the mechanism of the mRNA instability, it is essential that we examine the activities of these molecules in the degradation process of the 321_322insG *PAX9* mRNA.

The discovery of one oligodontia family with a deletion encompassing the *PAX9* locus has suggested haploinsufficiency (not a dominant-negative effect) as a cause of non-syndromic oligodontia with mutations of this gene (Das *et al*., 2002). The present study showed that the 321_322insG mutation impaired the mRNA stability of *PAX9*, resulting in lower protein expression. These findings support the model of haploinsufficiency of *PAX9* as a cause of non-syndromic oligodontia.

ACKNOWLEDGMENTS

This study was supported by Grants-in-Aid for Scientific Research from the Ministry of Education, Culture, Sports, Science, and Technology of Japan (19659547, 21390546), and for the Supporting Project for Strategic Research of Nihon University School of Dentistry at Matsudo by the Ministry of Education, Culture, Sports, Science, and Technology of Japan. The authors thank Professor Hayato Ohshima (Niigata University Graduate School of Medical and Dental Sciences) for recruiting study participants.

REFERENCES

Das P, Stockton DW, Bauer C, Shaffer LG, D'Souza RN, Wright T, *et al*. (2002). Haploinsufficiency of PAX9 is associated with autosomal dominant hypodontia. *Hum Genet* 110:371-376.

Das P, Hai M, Elcock C, Leal SM, Brown DT, Brook AH, *et al*. (2003). Novel missense mutations and a 288-bp exonic insertion in PAX9 in families with autosomal dominant hypodontia. *Am J Med Genet A* 118(A):35-42.

Frazier-Bowers SA, Guo DC, Cavender A, Xue L, Evans B, King T, *et al*. (2002). A novel mutation in human PAX9 causes molar oligodontia. *J Dent Res* 81:129-133.

Jumlongras D, Lin JY, Chapra A, Seidman CE, Seidman JG, Maas RL, *et al*. (2004). A novel missense mutation in the paired domain of PAX9 causes non-syndromic oligodontia. *Hum Genet* 114:242-249.

Kapadia H, Frazier-Bowers S, Ogawa T, D'Souza RN (2006). Molecular characterization of a novel PAX9 missense mutation causing posterior tooth agenesis. *Eur J Hum Genet* 14:403-409.

Lammi L, Halonen K, Pirinen S, Thesleff I, Arte S, Nieminen P (2003). A missense mutation in PAX9 in a family with distinct phenotype of oligodontia. *Eur J Hum Genet* 11:866-871.

Mensah JK, Ogawa T, Kapadia H, Cavender AC, D'Souza RN (2004). Functional analysis of a mutation in PAX9 associated with familial tooth agenesis in humans. *J Biol Chem* 279:5924-5933.

Mitchell P, Tollervey D (2000). mRNA stability in eukaryotes. *Curr Opin Genet Dev* 10:193-198.

Mostowska A, Kobielak A, Biedziak B, Trzeciak WH (2003). Novel mutation in the paired box sequence of PAX9 gene in a sporadic form of oligodontia. *Eur J Oral Sci* 111:272-276.

Nieminen P (2009). Genetic basis of tooth agenesis. *J Exp Zool B Mol Dev Evol* 312(B):320-342.

Nieminen P, Arte S, Tanner D, Paulin L, Alaluusua S, Thesleff I, *et al*. (2001). Identification of a nonsense mutation in the PAX9 gene in molar oligodontia. *Eur J Hum Genet* 9:743-746.

Ogawa T, Kapadia H, Feng JQ, Raghow R, Peters H, D'Souza RN (2006). Functional consequences of interactions between Pax9 and Msx1 genes in normal and abnormal tooth development. *J Biol Chem* 281:18363-18369.

Rølling S, Poulsen S (2001). Oligodontia in Danish schoolchildren. *Acta Odontol Scand* 59:111-112.

Schalk-van der Weide Y, Steen WH, Bosman F (1992). Distribution of missing teeth and tooth morphology in patients with oligodontia. *ASDC J Dent Child* 59:133-140.

Shiga M, Saito M, Hattori M, Torii C, Kosaki K, Kiyono T, *et al*. (2008). Characteristic phenotype of immortalized periodontal cells isolated from a Marfan syndrome type I patient. *Cell Tissue Res* 331: 461-472.

Stockton DW, Das P, Goldenberg M, D'Souza RN, Patel PI (2000). Mutation of PAX9 is associated with oligodontia. *Nat Genet* 24: 18-19.

Symons AL, Stritzel F, Stamation J (1993). Anomalies associated with hypodontia of the permanent lateral incisors and second premolar. *J Clin Pediatr Dent* 17:109-111.

Tao R, Jin B, Guo SZ, Qing W, Feng GY, Brooks DG, *et al*. (2006). A novel missense mutation of the EDA gene in a Mongolian family with congenital hypodontia. *J Hum Genet* 51:498-502.

Vastardis H (2000). The genetics of human tooth agenesis: new discoveries for understanding dental anomalies. *Am J Orthod Dentofacial Orthop* 117:650-656.

Vastardis H, Karimbux N, Guthua SW, Seidman JG, Seidman CE (1996). A human MSX1 homeodomain missense mutation causes selective tooth agenesis. *Nat Genet* 13:417-421.

Wang Y, Groppe JC, Wu J, Ogawa T, Mues G, D'Souza RN, *et al*. (2009). Pathogenic mechanisms of tooth agenesis linked to paired domain mutations in human *PAX9*. *Hum Mol Genet* 18:2863-2874.

Wilusz CJ, Wormington M, Peltz SW (2001). The cap-to-tail guide to mRNA turnover. *Nat Rev Mol Cell Biol* 2:237-246.

Yamashita A, Chang TC, Yamashita Y, Zhu W, Zhong Z, Chen CY, *et al*. (2005). Concerted action of poly(A) nucleases and decapping enzyme in mammalian mRNA turnover. *Nat Struct Mol Biol* 12:1054-1063.

Downloaded from jdr.sagepub.com at TOKYO IKASHIKA UNIVERSITY on March 22, 2012 For personal use only. No other uses without permission.

© 2011 International & American Associations for Dental Research

整形外科学分野

大川　淳

医歯学総合研究科・先端医療開発学専攻
整形外科学・教授

1）研究の課題名

ビタミンEは破骨細胞の細胞融合を亢進させることで骨量を減少させる

Vitamin E decreases bone mass by stimulating osteoclast fusion

ビタミンE輸送タンパクであるα TTPを欠損したマウスの解析を通して、骨代謝におけるビタミンEの意義を明らかにするために本研究を行った。

まず、ビタミン 欠損のモデルマウスであるα TTP欠損マウスが、骨吸収低下に伴う骨量増加を示すことを発見した。このマウスはビタミンE添加食により骨量が回復することから、血中のビタミンE濃度が骨量に影響している可能性が考えられた。マウス骨髄由来の破骨細胞培養系にビタミンEを添加すると、破骨細胞の融合、多核化が促進すること、その際に破骨細胞多核化に必須の遺伝子であるDC-STAMPの発現が亢進することを発見した。この系はDC-STAMPの上流であるp38とMitf のリン酸化を解することを示した。

さらにin vivoでのビタミンEの骨量に対する効果を確認するため、野生型マウス、ラットにビタミンE添加食を投与したところ、骨吸収が増加し骨量が減少することを発見した。

この研究により、ビタミンEは生体内で破骨細胞融合を促進し、骨量減少を引き起こすことを明らかにし、ビタミンE摂取が骨粗鬆症を惹起する可能性を示唆した。

（現在進めている研究）

骨髄由来間葉系細胞（MSC）の質-骨形成抑制因子の同定-

The significance of the quality of the human bone marrow mesenchymal cells（hMSCs）in the bone formation

サルの骨髄間葉系細胞（MSCs）を用いた骨再生研究において、長期継代細胞（Passage5：P5）を、短期継代細胞（Passage1：P1）に加えて多孔質人工骨に導入、筋肉内移植すると、それを加えずにP1単独で移植したものより骨形成量が50%程度低下した（n=4）。即ちP5細胞は骨形成能を有してはいるが、同時に骨形成能を低下させる負の因子をも含んでいるということを意味し、この因子を除去すれば骨形成能を促進することができる可能性が示唆された。マイクロアレイによる抑制因子の絞り込み：P1と比較してP5で増加する（Log2値>1）遺伝子に着目すると、30近くの候補が列挙された。その中でも、MSCに発現するチロシンキナーゼ型受容体であるEphAsのうちEphA5のみ継代培養と共に発現が増加しており、前述の骨芽細胞のマーカーであるALPのmRNA発現との逆相関を認めた。今後は、EphA5が実際にMSCsの骨芽細胞分化に関与（抑制）しているかの検討を進めていく。

2）

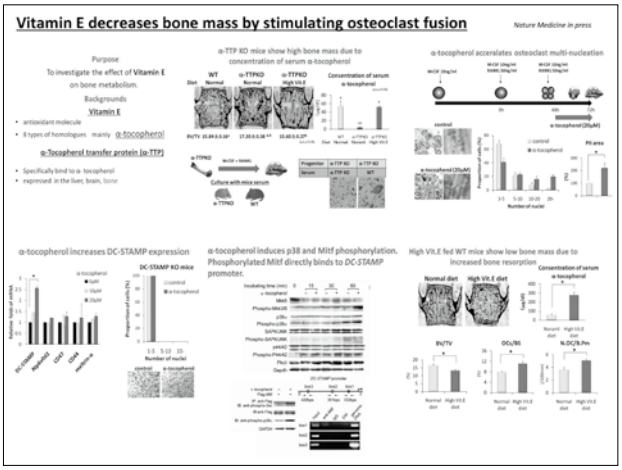

3）発表の研究内容についての英文要約

Bone homeostasis is maintained by the balance between osteoblastic bone formation and osteoclastic bone resorption. Osteoclasts are multinucleated cells formed by mononuclear preosteoclast fusion. Fat-soluble vitamins such as vitamin D are pivotal in maintaining skeletal integrity. However, the role of vitamin E（VitE）in bone remodeling remains unknown. Here, we show that α-tocopherol transfer

protein-deficient（Ttpa−/−）mice, a mouse model of genetic VitE deficiency6, have high bone mass due to a decrease in bone resorption. Cell-based assays indicated that α-tocopherol stimulated osteoclast fusion, independently of its antioxidant capacity, by inducing the expression of dendritic cell-specific transmembrane protein（DC-STAMP）, an essential molecule for osteoclast fusion, through p38 and microphthalmia-associated transcription factor activation and its direct recruitment to Tm7sf4（a gene encoding DC-STAMP）promoter7-9. Indeed, the bone abnormality of Ttpa−/− mice was rescued by Tm7sf4 transgene. Moreover, wild-type mice or rats fed a α-tocopherol-supplemented diet, which contains comparable amount of α-tocopherol to the supplement consumed by many people, lost bone mass. These results demonstrate that serum VitE is a determinant of bone mass through its regulation of osteoclast fusion.

（現在進めている研究）

On the basis of our previous in vivo experiment, we postulated that the long-term passaged cells contained some inhibitor of the short-term cultured cells' potential of bone formation.Our purpose is to identify the factors which are involved in the deterioration of the differentiation capability.The microarray analysis identified many genes in P5 cells that were upregulated compared to P1 cells. The characteristic of hMSCs was altered by repeating passages. We noticed EphA5 as a candidate of the inhibitor, because the expression patterns of this gene and ALP（well established osteogenic marker）are correlated inversely. The aim of our ongoing studies is to investigate how EphA5 is involved in osteogenic differentiation of MSCs.

4）本事業に関連して世界的な研究拠点形成に向けて、以下の点で改善・整備等されたこと

A（研究拠点体制）

・大学外との連携を図り、また研究環境（設備など）を整備することによって、研究拠点の基礎を立ち上げた（物質材料研究機構、産業技術総合研究所）。

・また、大学内連携を図り、他分野と共同で研究を行った。（生体材料工学研究所・有機材料分野、難治研究所・分子薬理学）

・企業との連携（オリンパス、HOYA、ストライカー）により、研究設備の充実を図るとともに、基礎と臨床との橋渡し研究領域を充実させた。

・研究専門部門として寄附講座を運営

B（研究教育環境）

・週に3回、論文の抄読会や研究報告会を実施することにより、分子生物学、骨・軟骨組織学、骨再生学の研究、教育体制を確立した。

・科学研究費補助金やその他研究助成金、企業との共同研究により外部資金を得ることによって、研究環境を整備し得た。

C（人材確保）

・寄付講座を開設・運営し、研究に専念できる人材を確保した。

D（人材育成）

・10名の大学院生（内留学生3名、他分野大学院生4名）に対して、骨・軟骨に関する研究教育、指導を行った。

・3名の学部生（医学部医学科）に対し、それぞれ5か月間、骨・軟骨に関する研究教育、指導を行った。

E（国際化）

・5名の留学生に研究教育、指導を行った。

・1名の大学院生と1名の大学院卒業生が米国に留学中である。

5）GCOE事業を推進するに当たって力を入れた点

・企業を含む大学内外との連携を強化するなどして、骨・軟骨に関する基礎領域だけでなく、臨床応用を目指した研究にも重点を置いた。

・分野内で研究経過・成果に関するdiscussionを重ねるとともに、外部への研究成果の発表の機会を増やすよう努力した。

6）英文原著論文

1. Kusano K, Enomoto M, Hirai T, Wakabayashi Y, Itoh S, Ichinose S, Okabe S, Shinomiya K, Okawa A. Enhancement of sciatic nerve regeneration by adenovirus-mediated expression of dominant negative RhoA and Rac1. Neurosci Lett. 492（1）：64-9. 2011
2. Sugata Y, Sotome S, Yuasa M, Hirano M, Shinomiya K, Okawa A. Effects of the systemic administration of alendronate on bone formation in a porous hydroxyapatite/collagen composite and resorption by osteoclasts in a bone defect model in rabbits. J Bone Joint Surg Br. 93（4）：510-6. 2011
3. Effects of the systemic administration of alendronate on bone formation in a porous hydroxyapatite/collagen composite and resorption by osteoclasts in a bone defect model in rabbits. J Bone Joint Surg Br. 93（4）：510-6. 2011
4. Okawa A, Sakai K, Hirai T, Kato T, Tomizawa S, Enomoto M, Kawabata S, Takahashi M, Shinomiya K.

Risk factors for early reconstruction failure of multilevel cervical corpectomy with dynamic plate fixation.
Spine（Phila Pa 1976）. 36（9）：E582-7. 2011
5. Yoshii T, Dumas JE, Okawa A, Spengler DM, Guelcher SA.
Synthesis, characterization of calcium phosphates/polyurethane composites for weight-bearing implants.
J Biomed Mater Res B Appl Biomater. 100（1）：32-40. 2012
6. ◎Koji Fujita, Makiko Iwasaki, Hiroki Ochi, Toru Fukuda, Chengshan Ma, Takeshi Miyamoto, Kimitaka Takitani, Takako Negishi-Koga, Satoko Sunamura, Tatsuhiko Kodama, Hiroshi Takayanagi, Hiroshi Tamai, Shigeaki Kato, Hiroyuki Arai, Kenichi Shinomiya, Hiroshi Itoh, Atsushi Okawa and Shu Takeda
Vitamin E decreases bone mass by stimulating osteoclast fusion
Nature medicine（in press）
7. Nimura A, Kato A, Yamaguchi K, Mochizuki T, Okawa A, Sugaya H, Akita K.
The superior capsule of the shoulder joint complements the insertion of the rotator cuff.
J Shoulder Elbow Surg. 2011 Aug 3. [Epub ahead of print]（in press）
8. Hirai T, Kato T, Kawabata S, Enomoto M, Tomizawa S, Yoshii T, Sakaki K, Shinomiya
Adhesive Arachnoiditis with Extensive Syringomyelia and Giant Arachnoid Cyst Following Spinal and Epidural Anesthesia：A Case Report.
Spine（Phila Pa 1976）. 2011 Jul 5. [Epub ahead of print]（in press）
9. ◎Yamada T, Yoshii T, Sotome S, Yuasa M, Kato T, Arai Y, Kawabata S, Tomizawa S, Sakaki K, Hirai T, Shinomiya K, Okawa A.
Hybrid Grafting using Bone Marrow Aspirate combined with Porous β-Tricalcium Phosphate and Trephine Bone for Lumbar Posterolateral Spinal Fusion：A Prospective, Comparative Study -Versus Local Bone Grafting-
Spine（Phila Pa 1976）. 2011 Jun 13. [Epub ahead of print]（in press）
10. Sakai K, Okawa A, Takahashi M, Arai Y, Kawabata S, Enomoto M, Kato T, Hirai T, Shinomiya K.
5-year Follow-up Evaluation of Surgical Treatment for Cervical Myelopathy Caused by Ossification of the Posterior Longitudinal Ligament：A Prospective Comparative Study of Anterior Decompression and Fusion with Floating Method Versus Laminoplasty.
Spine（Phila Pa 1976）. 2011 May 2. [Epub ahead of print]（in press）
11. Hirai T, Kawabata S, Enomoto M, Kato T, Tomizawa S, Sakai K, Yoshii T, Sakaki K, Shinomiya K, Okawa A.
Presence of Anterior Compression of the Spinal Cord Following Laminoplasty Inhibits Upper Extremity Motor Recovery in Patients with Cervical Spondylotic Myelopathy.
Spine（Phila Pa 1976）. 2011 May 2. [Epub ahead of print]（in press）
12. Hirai T, Okawa A, Arai Y, Takahashi M, Kawabata S, Kato T, Enomoto M, Tomizawa S, Sakai K, Torigoe I, Shinomiya K.
Middle-term results of a prospective comparative study of anterior decompression with fusion and posterior decompression with laminoplasty for the treatment of cervical spondylotic myelopathy.
Spine（Phila Pa 1976）. 2011 Nov 1;36（23）：1940-7.（in press）

7）総説ならびに著書

1. 草野和生, 榎本光裕, 平井高志, 大川淳
分子レベルからみた整形外科疾患（シリーズIX）
Small G protein制御による末梢神経再生促進（解説）
「整形・災害外科」 2ページ、2011
大川淳
整形外科医に求められる医療安全のコンセプト（解説）
「日本整形外科学会雑誌」8ページ、2011
2. 早乙女進一, 生駒俊之
最新用語解説　基礎（第35回）　ハイドロキシアパタイト（解説）
「骨粗鬆症治療」3ページ、2011

8）特許取得、特許申請

1. 「骨移植片製造装置」発明者：四宮謙一、早乙女進一他、特許番号4545015、特許取得日2010年7月9日
2. 「生体内薬物徐放材料の製造方法」発明者：早乙女進一、四宮謙一他、特許番号4204772、特許取得日2008年10月24日
3. 「多孔質複合材料の製造方法」発明者：早乙女進一、四宮謙一他、国内：特許番号3727059、特許取得日2005年10月7日、アメリカ合衆国：特許番号7163965、特許取得日2007年1月16日
4. 「複合生体材料」発明者：早乙女進一、四宮謙一他、特許番号3770555、特許取得日2006年2月17日　アメリカ合衆国：特許番号7494664、特許取得日2009年2月24日　カナダ：特許番号2467252、特許取得日2008年12月2日

9）平成23年度までの自己評価

平成23年末に藤田の論文がNature Medicineにaccept

されるなど、基礎研究に関しては順調に成果を上げられ、また臨床との橋渡し研究、臨床研究においても満足できる数の論文の上梓ができたと考えている。しかし、2005年に特許を取得した多孔質複合材料の認可が遅れ、臨床研究に進めなかったたことは次年度以後の課題である。

資金面において、寄附講座である整形外科先端治療開発学の出資元との複数年契約が達成できず、研究者の身分を安定化できていない点も改善の余地があると考えている。

10）和文原著論文

1. 佐々木真一, 江幡重人, 折井久弥, 沼野藤希, 鳥越一郎, 友利正樹, 吉田裕俊, 佐藤浩一, 大川淳, 四宮謙一
   腰椎変性疾患に対する内視鏡下筋肉温存型椎弓間除圧術変法（ME-MILD変法）の試み
   Journal of Spine Research　巻8号 Page1358-1361、2011
2. 鳥越一郎, 江幡重人, 佐藤浩一, 吉田裕俊, 折井久弥, 大川淳
   腰椎椎間板ヘルニアに対するLove法と内視鏡下ヘルニア摘出術（MED法）の中期成績の比較検討
   Journal of Spine Research 2巻8号 Page1338-1341、2011

11）学会発表（和文）

1. 竹田秀, 藤田浩二, 大川淳, 四宮謙一, 伊藤裕
   骨代謝調節研究の進展と臨床展開 ビタミンEは破骨細胞の多核化を促進し、骨粗鬆症を惹起する（シンポジウム）
   第84回日本内分泌学会学術総会、神戸市、2011年4月21-23日
2. 大川淳, 川端茂徳, 加藤剛, 富澤将司, 吉井俊貴
   骨粗鬆症椎体骨折に対する局麻下経皮的椎体形成術
   第60回東日本整形災害外科学会、つくば市、2011年9月16-17日
3. 正岡智和, 湯浅将人, 山田剛史, 大川淳, 森田定雄, 早乙女進一
   β-TCP/bone marrow hybridの骨形成能に対するdexamethasoneの効果
   第26回日本整形外科学会基礎学術集会、高崎市、2011年10月20-21日
4. 早乙女進一, 湯浅将人, 山田剛史, 正岡智和, 吉井俊貴, 四宮謙一, 大川淳
   骨髄間葉系細胞を用いた骨再生法の大型骨欠損再生に対する有効性　サル大腿骨大欠損モデルを用いた検討
   第26回日本整形外科学会基礎学術集会、高崎市、2011年10月20-21日
5. 榎本光裕, 請川円, 平井高志, 早乙女進一, 四宮謙一, 大川淳
   脊髄の再生 ハニカムコラーゲンスポンジと骨髄間葉系細胞移植を併用した損傷脊髄の再建（パネルディスカッション）
   第26回日本整形外科学会基礎学術集会、高崎市、2011年10月20-21日
6. 早乙女進, 阿江啓介, 若林良明, 四宮謙一, 大川淳, 平野昌弘, 石突正文, 森岡秀夫, 松本誠一, 中村孝志, 阿部哲士, 別府保男
   多孔質ハイドロキシアパタイト・コラーゲン複合体（HAp/Col）の開発……基礎研究から臨床応用へ（シンポジウム）
   第33回日本バイオマテリアル学会大会、京都市、2011年11月21-22日
7. 吉井俊貴（東京医科歯科大学 大学院整形）, 加藤剛, 川端茂徳, 富澤将司, 早乙女進一, 四宮謙一, 大川淳
   人工骨と経皮的採取海綿骨（hybrid）移植による頸椎前方除圧固定術　椎体亜全摘症例への適応
   第84回日本整形外科学会学術総会、Web開催、2011年
8. 大川淳（東京医科歯科大学 大学院整形）, 加藤剛, 富澤将司
   整形外科の有害事象に関する合併症の判断と回避可能性
   第84回日本整形外科学会学術総会、Web開催、2011年
9. 吉井俊貴（東京医科歯科大学 大学院整形）, 山田剛, 加藤剛, 川端茂徳, 富澤将司, 四宮謙一, 早乙女進一, 大川淳
   経皮的採取海綿骨、新鮮骨髄穿刺液人工骨を用いた腰椎側方固定術
   第84回日本整形外科学会学術総会、Web開催、2011年
10. 骨移植治療の歴史と進歩 多孔質ハイドロキシアパタイト・コラーゲン複合体（HAp/Col）の開発と臨床応用（シンポジウム）
    早乙女進一（東京医科歯科大学 大学院整形先端治療開発）, 阿江啓介, 若林良明, 四宮謙一, 平野昌弘, 石突正文, 森岡秀夫, 松本誠一, 中村孝志, 阿部哲士, 別府保男
    第84回日本整形外科学会学術総会、Web開催、2011年

12）外部資金の獲得状況

1. 厚生労働科学研究費補助金（長寿科学総合研究事業）
研究題目：骨粗鬆症椎体骨折に対する低侵襲治療法の開発
代表：四宮　謙一
期間：平成21年－平成24年
研究費総額：¥82,635,000.-（間接経費¥11,419,000.-）
2. 厚生労働科学研究費補助金（難治性疾患克服研究事業）
研究題目：脊柱靭帯骨化症に関する調査研究
分担：大川　淳
期間：平成20年－平成22年
研究費総額：¥2,500,000.-
3. 厚生労働科学研究費補助金（地域医療基盤開発推進研究事業）
研究題目：医療事故にかかわった医療従事者の支援体制に関する研究
分担：大川　淳
期間：平成22年－平成24年
研究費総額：¥900,000.-
4. 厚生労働科学研究費補助金（長寿科学総合研究事業）
研究題目：骨粗鬆症椎体骨折に対する低侵襲治療法の開発
分担：大川　淳
期間：平成21年－平成24年
研究費総額：¥5,700,000.-
5. 科学研究費補助金（基盤研究B）
研究題目：骨髄間葉系幹細胞を利用した巨大骨組織再生のための基礎技術の確立
代表：四宮　謙一
期間：平成21年－平成24年
研究費総額：¥13,400,000.-（間接経費¥4,020,000.-）
6. 科学研究費補助金（基盤研究C）
研究題目：末梢神経刺激-脊髄誘発磁界測定を用いた完全に非侵襲的脊髄機能診断の開発
代表：川端　茂徳
期間：平成22年－平成24年
研究費総額：¥3,400,000.-（間接経費¥1,020,000.-）
7. 科学研究費補助金（基盤研究C）
研究題目：マイクロRNAによる骨芽細胞・骨細胞分化調節機構の解明
代表：早乙女　進一
期間：平成21年－平成23年
研究費総額：¥3,500,000.-（間接経費¥1,050,000.-）
8. 科学研究費補助金（基盤研究C）
研究題目：注入硬化型生体吸収性人工骨補填材の開発と評価
代表：阿江　啓介
期間：平成23年度－平成25年度
研究費総額：¥5,200,000.-（間接経費¥1,200,000.-）
9. 科学研究費補助金（基盤研究C）
研究題目：神経栄養因子と上皮成長因子（EGF）受容体制御による末梢神経再生
代表：若林　良明
期間：平成23年－平成25年
研究費総額：¥3,800,000.-（間接経費¥1,140,000.-）
10. 科学研究費補助金（基盤研究C）
研究題目：脊髄損傷慢性期での細胞移植を併用した再髄鞘化と運動機能再建
代表：榎本　光裕
期間：平成21年－平成23年
研究費総額：¥4,160,000.-（間接経費¥987,000.-）
11. 科学研究費補助金（基盤研究C）
研究題目：関節軟骨代謝における老化制御因子SIRT1の機能解析
代表：麻生　義則
期間：平成21年度－平成23年度
研究費総額：¥4,550,000.-（間接経費¥1,050,000.-）
12. 科学研究費補助金（基盤研究C）
研究題目：関節軟骨細胞に発現する破骨細胞分化制御因子の機能に関する研究
代表：古賀　大介
期間：平成21年度－平成23年度
研究費総額：¥4,550,000.-（間接経費¥1,050,000.-）
13. 科学研究費補助金（基盤研究C）
研究題目：高気圧酸素療法を応用した新しい歯牙再植法の開発
分担：加藤　剛
期間：平成22年度－平成24年度
研究費総額：¥200,000.-
14. 挑戦的萌芽研究
研究題目：骨と血圧調節機構のクロストークの解明
代表：大川　淳
期間：平成23年度－24年度
研究費総額：¥3,640,000.-（間接経費¥840,000.-）
15. 挑戦的萌芽研究
研究題目：骨代謝における活性酸素シグナルの解明
代表：森田　定雄
期間：平成23年度－平成24年度

研究費総額：¥3,640,000.-（間接経費¥840,000.-）

16. 若手研究B
研究題目：miRNAによる骨軟部腫瘍の発生・進展における分子制御機構
代表：木村　文子
期間：平成23年度－平成25年度
研究費総額：¥3,200,000.-

17. 研究活動スタート支援
研究題目：注入型多孔質ポリウレタンscaffoldを使用した骨再生
代表：吉井　俊貴
期間：平成22年度－平成23年度
研究費総額：¥3,068,000.-（間接経費¥708,000.-）

18. 研究活動スタート支援
研究題目：骨モデリングにおけるマイクロRNAの生理的意義の解明
代表：　猪瀬　弘之
期間：平成23年度－平成24年度
研究費総額：¥2,500,000.-

19. 共同研究費（キッコーマン株式会社）
研究題目：関節軟骨代謝に対するプロアントシアニジンとオリゴヒアルロン酸の作用に関する研究
代表：麻生　義則
期間：平成21年度－平成23年度
研究費総額：¥2,727,273.-（間接経費¥272,727.-）

20. 助成金　社団法人　日本損害保険協会
研究題目：骨誘導性注入型骨補填剤の開発および難治性骨折への応用
代表：早乙女　進一
期間：平成21年度－平成23年度
研究費総額：¥4,000,000.-

21. 助成金　社団法人　日本損害保険協会
研究題目：SIP30遺伝子の制御による脊髄神経伝達効率をターゲットにした治療法の開発
代表：平井　高志
期間：平成22年度－24年度
研究費総額：¥2,000,000.-

22. 助成金　社団法人　日本損害保険協会
研究題目：新規薬剤を用いた末梢神経側枝発芽促進の試み
代表：榎本　光裕
期間：平成22年度－平成23年度
研究費総額：¥1,000,000.-

23. 助成金　社団法人　日本損害保険協会
研究題目：自家骨髄由来細胞濃縮法と自己血漿、人工骨を組み合わせた骨再生の可能性
代表：吉井　俊貴
期間：平成22年度－平成23年度
研究費総額：¥1,000,000.-

24. 助成金　社団法人　日本損害保険協会
研究題目：Qdotを用いた局所組織ラベリングによる骨形成タンパクによる異所性骨化のメカニズムの解明とその効率化に関する検討
代表：湯浅　将人
期間：平成22年度－平成23年度
研究費総額：¥1,000,000.-

25. 助成金　社団法人　日本損害保険協会
研究題目：骨髄由来間葉系細胞（MSC）の骨形成抑制因子の同定
代表：山田　剛史
期間：平成22年度－平成23年度
研究費総額：¥1,000,000.-

26. 助成金　社団法人　日本損害保険協会
研究題目：骨髄間葉系幹細胞を用いたﾊﾟｽﾂｰﾙ法の骨髄炎治療への応用
代表：小柳　広高
期間：平成22年度－平成23年度
研究費総額：¥1,000,000.-

27. 助成金　財団法人　整形災害外科学研究助成財団
代表：榎本　光裕
期間：平成22年度
研究費総額：¥1,000,000.-

13）特別講演、招待講演、シンポジウム

1. 第36回二豊会フォーラム
骨粗鬆症性脊椎圧迫骨折の治療上の課題
2011.8.26（金）　大分

2. 東京医科歯科大学公開講座
なぜ腰は曲がるのか?
2011.10.12（水）　東京

3. 杉並中野区整形外科医会
高齢者の腰痛ー病態と診断治療のポイント
2011.10.14（金）　東京

14）GCOE総合講義

Clinically Unsolved Problems related to Osteoporosis and Bone Atrophy in Orthopaedic Surgery

Mechanisms of bone metabolism have been illuminated gradually, but some clinical problems still left unsettled. In this lecture these problems and questions in the orthopaedic field will be illustrated. Topics dealt in the lecture are as follows：

1. Non-union of vertebral fracture
2. Lumbar Kyphosis due to spinal alignment change by multiple fractures
3. Insufficient fracture around pelvis
4. Bone atrophy caused by stress shielding or implant debris
5. Bone atrophy in relation with complex regional pain syndrome（ reflex sympathetic dystrophy）

Non-union of vertebral fracture
For osteoporotic patients newly developed drugs such as bisphonates and a recombinant form of parathyroid hormone became available in Japan, but treatment of vertebral fractures has not standardized yet. Some patients suffer non-union of the vertebral facture, in which the shape of the vertebra changes in response to posture. Bone cement（poly methyl methacrylate）is injected percutaneously into the cavity of the vertebral body and pain-relief achieved shortly. However, fracture of the adjacent segment occurs one or two months later and again severe pain comes back.

Lumbar Kyphosis due to spinal alignment change
Patient with thoracolumbar multiple fractures cannot walk long without aid such as a cane or so-called “silver cart” . A fracture spontaneously heals in a few months, but profile change（round back）shifts the center of gravity to more anterior of the body. In some cases one compression fracture of the thoracolumbar spine induces another new fractures in succession.

Insufficient fracture around pelvis
In oldest-old patient insufficient facture around pelvis occur, which cannot be detected by routine x-rays other than MRI. Pain of the unknown origin continues in several weeks, resulting in decrease of their activity of daily living.

Bone atrophy caused by stress shielding or implant's debris
In a spinal surgery mobile spinal segments are intentionally fused to correct spinal deformity. An artificial joint replacement also induces bone atrophy around the inserted solid implant. These bone atrophy sometimes provide a new fracture.

Bone atrophy in relation with complex regional pain syndrome
Complex regional pain syndrome（CRPS）is a disorder of the extremities that is characterized by pain, swelling, limited range of motion, vasomotor instability, skin changes, and patchy bone demineralization. Plain radiographs often demonstrate osteopenia and scintigraphy using technetium may reveal increased uptake in the involved extremity. The severe local osteopenia sometimes is hard to be treated.

In the lecture clinical features will be presented in detail.

15）教室、分野や講座の准教授、講師、助教、特別研究員、ポスドク、指導を受けた大学院生の名前

（整形外科学分野）

教　授	大川　淳
助　教	若林　良明
	川端　茂徳
	阿江　啓介
	加藤　剛
	古賀　大介
	富沢　将司
	澤村　千草
大学院生	岩崎　牧子
	小柳　広高
	石井　宣一
	山内　裕樹
	正岡　智和
	榊経　平
	平井　高志
	湯浅　将人
	○山田　剛史
	請　川大
	○許　レン
	○馬　成山
	○徐　成
	請　川円
	谷山　崇

（整形外科先端治療開発学講座）

寄付講座准教授：早乙女　進一
寄付講座講師：麻生　義則

○はAISS

16）GCOE活動についての感想、コメント、改善を望む点

整形外科は臨床科であり、骨、軟骨に関する基礎手研究の他に、トランスレーショナルリサーチも積極的に推進していきたいと考えている。

17）その他　研究教育活動について特記する点

数多くの留学生だけでなく学部学生のプロジェクト・セメスターでは学内随一の応募者5名に対して積極的な研究指導を行っている。

LETTERS

nature medicine

Vitamin E decreases bone mass by stimulating osteoclast fusion

Koji Fujita[1,2], Makiko Iwasaki[1], Hiroki Ochi[3], Toru Fukuda[3], Chengshan Ma[1,2], Takeshi Miyamoto[4], Kimitaka Takitani[5], Takako Negishi-Koga[6], Satoko Sunamura[3], Tatsuhiko Kodama[7], Hiroshi Takayanagi[6], Hiroshi Tamai[5], Shigeaki Kato[8], Hiroyuki Arai[9], Kenichi Shinomiya[1], Hiroshi Itoh[3], Atsushi Okawa[1] & Shu Takeda[3]

© 2012 Nature America, Inc. All rights reserved.

Bone homeostasis is maintained by the balance between osteoblastic bone formation and osteoclastic bone resorption[1–3]. Osteoclasts are multinucleated cells that are formed by mononuclear preosteoclast fusion[1,2,4,5]. Fat-soluble vitamins such as vitamin D are pivotal in maintaining skeletal integrity. However, the role of vitamin E in bone remodeling is unknown. Here, we show that mice deficient in α-tocopherol transfer protein (*Ttpa*$^{-/-}$ mice), a mouse model of genetic vitamin E deficiency[6], have high bone mass as a result of a decrease in bone resorption. Cell-based assays indicated that α-tocopherol stimulated osteoclast fusion, independent of its antioxidant capacity, by inducing the expression of dendritic-cell–specific transmembrane protein, an essential molecule for osteoclast fusion, through activation of mitogen-activated protein kinase 14 (p38) and microphthalmia-associated transcription factor, as well as its direct recruitment to the *Tm7sf4* (a gene encoding DC-STAMP) promoter[7–9]. Indeed, the bone abnormality seen in *Ttpa*$^{-/-}$ mice was rescued by a *Tm7sf4* transgene. Moreover, wild-type mice or rats fed an α-tocopherol–supplemented diet, which contains a comparable amount of α-tocopherol to supplements consumed by many people, lost bone mass. These results show that serum vitamin E is a determinant of bone mass through its regulation of osteoclast fusion.

Bone mass is maintained constant from puberty until menopause by a balance between osteoblastic bone formation and osteoclastic bone resorption, a process called bone remodeling[1–3]. Osteoclasts are multinucleated polykaryons that develop from monocyte-lineage hematopoietic precursors through sequential steps: an initial phase of proliferation and a late phase of differentiation and maturation[1,2,10,11]. Hormones and cytokines have pivotal roles in osteoclast development. Specifically, macrophage colony-stimulating factor (M-CSF) and receptor activator of NF-κB ligand (RANKL) are indispensable for the proliferation of preosteoclasts and the differentiation and maturation of osteoclasts, respectively[1–3,12]. Among the fat-soluble vitamins A, D and K are well known for their ability to affect the skeleton[13,14], however, vitamin E was not examined well in the aspect of bone remodeling.

Vitamin E is a lipid-soluble antioxidant that inhibits lipid peroxidation by scavenging reactive oxygen species and is believed to be protective against arteriosclerotic change and the aging process[15]. Indeed, vitamin E is one of the most popular supplements in the United States; more than 10% of adults in the United States currently take vitamin E daily[16]. Vitamin E, which is a mixture of tocopherols and tocotrienols, is absorbed from food and is transported to the liver, where α-tocopherol transfer protein (α-TTP) mediates the selective transfer of α-tocopherol into lipoproteins[6]. Accordingly, α-tocopherol is the most predominant isoform of vitamin E in the body. Mice deficient in α-TTP (*Ttpa*$^{-/-}$ mice) show ataxia and infertility as a result of reduced serum α-tocopherol concentrations (**Fig. 1a**), which can be rescued by dietary supplementation with α-tocopherol[6,17].

To address the role of vitamin E in bone remodeling, we first studied *Ttpa*$^{-/-}$ mice. The *Ttpa*$^{-/-}$ mice developed a high–bone-mass phenotype in both their vertebrae and long bones as a result of a lower bone resorption compared to wild-type (WT) mice, as evidenced by a lowering of osteoclast surface and deoxypyridinoline, a bone resorption marker (**Fig. 1b–e** and **Supplementary Fig. 1**)[18]. In contrast, the amount of bone formation was unchanged in *Ttpa*$^{-/-}$ mice compared to WT mice. (**Fig. 1d**). This high–bone-mass phenotype was attributed to reduced serum concentrations of vitamin E (**Fig. 1a**) rather than the α-TTP deficiency in the body, as supplementation with α-tocopherol in the diet, which normalized the serum concentrations of α-tocopherol in *Ttpa*$^{-/-}$ mice (**Fig. 1f**), rescued the bone abnormality seen in *Ttpa*$^{-/-}$ mice (**Fig. 1g** and **Supplementary Fig. 2**). In line with this observation, *Ttpa*$^{+/-}$ mice, whose serum concentrations of α-tocopherol are between those of WT and *Ttpa*$^{-/-}$ mice[17], also had an

[1]Department of Orthopedic Surgery, Tokyo Medical and Dental University, Tokyo, Japan. [2]Global Center of Excellence (GCOE) Program, International Research Center for Molecular Science in Tooth and Bone Diseases, Tokyo Medical and Dental University, Tokyo, Japan. [3]Section of Nephrology, Endocrinology and Metabolism, Department of Internal Medicine, School of Medicine, Keio University, Tokyo, Japan. [4]Department of Orthopedic Surgery, School of Medicine, Keio University, Tokyo, Japan. [5]Department of Pediatrics, Osaka Medical College, Osaka, Japan. [6]Department of Cell Signaling, Graduate School of Medical and Dental Sciences, Tokyo Medical and Dental University, Tokyo, Japan. [7]Laboratory for Systems Biology and Medicine, University of Tokyo, Tokyo, Japan. [8]Institute of Molecular and Cellular Biosciences, University of Tokyo, Tokyo, Japan. [9]Department of Health Chemistry, Graduate School of Pharmaceutical Sciences, University of Tokyo, Tokyo, Japan. Correspondence should be addressed to S.T. (shu-tky@umin.ac.jp).

Received 14 July 2011; accepted 1 January 2012; published online 4 March 2012; doi:10.1038/nm.2659

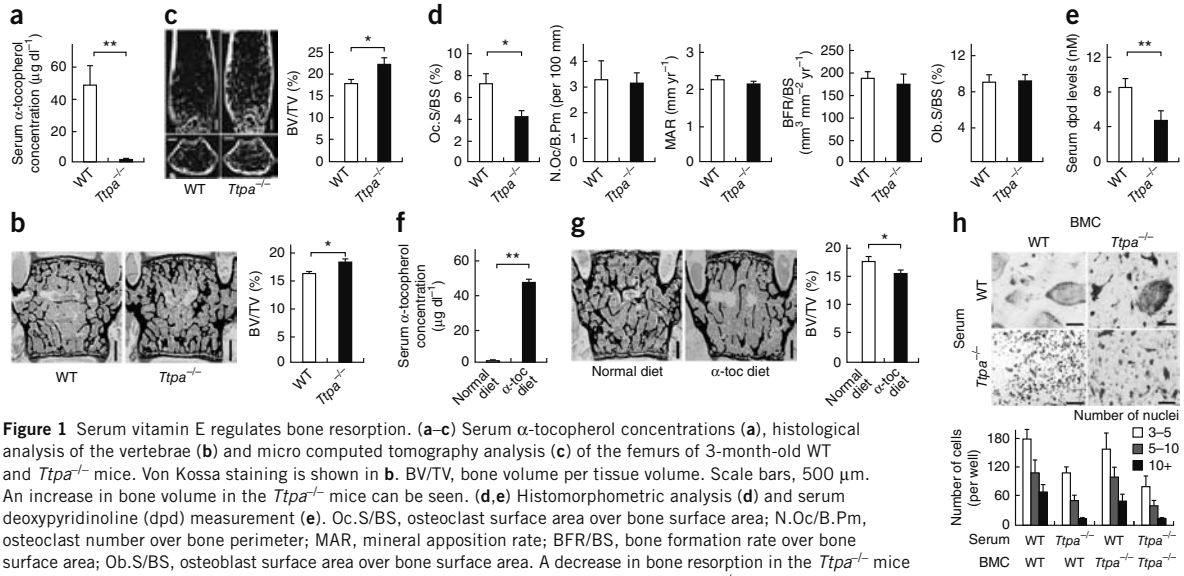

Figure 1 Serum vitamin E regulates bone resorption. (**a**–**c**) Serum α-tocopherol concentrations (**a**), histological analysis of the vertebrae (**b**) and micro computed tomography analysis (**c**) of the femurs of 3-month-old WT and *Ttpa*$^{-/-}$ mice. Von Kossa staining is shown in **b**. BV/TV, bone volume per tissue volume. Scale bars, 500 μm. An increase in bone volume in the *Ttpa*$^{-/-}$ mice can be seen. (**d**,**e**) Histomorphometric analysis (**d**) and serum deoxypyridinoline (dpd) measurement (**e**). Oc.S/BS, osteoclast surface area over bone surface area; N.Oc/B.Pm, osteoclast number over bone perimeter; MAR, mineral apposition rate; BFR/BS, bone formation rate over bone surface area; Ob.S/BS, osteoblast surface area over bone surface area. A decrease in bone resorption in the *Ttpa*$^{-/-}$ mice can be seen. (**f**,**g**) Serum α-tocopherol concentrations (**f**) and histological analysis (**g**) in *Ttpa*$^{-/-}$ mice fed a diet supplemented with α-tocopherol (α-toc diet). Von Kossa staining is shown in **g**. Scale bars, 500 μm. A decrease in bone volume as a result of the α-toc diet can be seen. (**h**) Serum α-tocopherol affects osteoclast differentiation. BMCs from the femurs of WT or *Ttpa*$^{-/-}$ mice were differentiated into osteoclasts in the presence of serum from WT or *Ttpa*$^{-/-}$ mice without addition of FBS. TRAP staining (left) and the number of osteoclasts (right) are shown. Scale bars, 50 μm. A decrease in the number of osteoclasts from WT BMCs with *Ttpa*$^{-/-}$ serum can be seen, whereas *Ttpa*$^{-/-}$ BMCs differentiated into osteoclasts normally with WT serum. $^{*}P < 0.05$, $^{**}P < 0.01$ by Tukey-Kramer testing (**b**) or Student's *t* test (**a**, **c**–**g**). All data are means ± s.e.m.

© 2012 Nature America, Inc. All rights reserved.

intermediate bone mass (**Supplementary Fig. 1b**). Moreover, osteoclast development *in vitro* was hampered when WT bone-marrow cells (BMCs) were cultured with the serum from *Ttpa*$^{-/-}$ mice (**Fig. 1h**), and this defect was ameliorated when this serum was supplemented with α-tocopherol or when serum from WT mice was used for the culture (**Fig. 1h** and **Supplementary Fig. 3**). In contrast, *Ttpa*$^{-/-}$ BMCs differentiated into osteoclasts normally when cultured with FBS or serum from WT mice (**Fig. 1h** and **Supplementary Fig. 3**). Thus, serum vitamin E regulates bone mass *in vivo* by affecting bone resorption.

Next, to examine the role of vitamin E in osteoclast development, we treated osteoclasts that were derived from WT BMCs and stimulated by RANKL with α-tocopherol *in vitro*. α-tocopherol stimulated osteoclast differentiation in a dose-dependent manner, as shown by an increase in the number of tartrate-resistant acid phosphatase (TRAP)-positive multinucleated osteoclasts (**Fig. 2a**), whereas the proliferation of osteoclast precursors and the survival of mature osteoclasts were unchanged by treatment with α-tocopherol (**Fig. 2b**,**c**). Osteoblastic differentiation and proliferation were not altered by α-tocopherol treatment (**Fig. 2d** and **Supplementary Fig. 4**), further indicating that vitamin E affects bone mass through osteoclasts rather than osteoblasts. Notably, α-tocopherol not only increased the generation of TRAP-positive multinucleated osteoclasts but also markedly increased the proportion of larger osteoclasts compared to the total osteoclasts (**Fig. 2e**), which indicated that vitamin E stimulated osteoclast maturation. As a result, α-tocopherol increased bone resorption by inducing the formation of additional mature osteoclasts (**Fig. 2f**).

Notably, α-tocopherol treatment administered only during the osteoclast maturation phase significantly increased osteoclast size and the number of nuclei per osteoclast (**Fig. 2e**), whereas α-tocopherol treatment administered at any other period did not have these effects (**Fig. 2e**), further indicating that vitamin E specifically affects late osteoclast maturation (that is, osteoclast fusion). Moreover, vitamin E also stimulated the generation of foreign-body giant cells, which are developed through macrophage fusion (**Fig. 2g**), further suggesting that vitamin E stimulates cell fusion. Indeed, the sizes of the TRAP-positive osteoclasts were smaller in the *Ttpa*$^{-/-}$ mice, which is in agreement with our *in vitro* observations (**Supplementary Fig. 2**). Taken together, the results suggest that vitamin E stimulates osteoclast fusion.

Because vitamin E is well known as an antioxidant[15], we next studied whether the antioxidant properties of vitamin E were indispensable for its ability to stimulate osteoclast fusion. With the exception of α-tocopherol, none of the isoforms of vitamin E, including α-tocotrienol, which is 100-fold stronger in antioxidant activity than α-tocopherol[15], stimulated osteoclast fusion (**Fig. 2h**). Moreover, except for α-tocopherol, none of the antioxidants tested, including ascorbic acid, which is the primary water-soluble antioxidant[19–22], stimulated osteoclast fusion (**Fig. 2i** and **Supplementary Fig. 5**). In line with these observations, hydrogen peroxide did not affect osteoclast fusion when it was present at a concentration that did not affect cell viability (**Supplementary Fig. 5**). Taken together, these results clearly show that, unlike other vitamin E isoforms and antioxidants, α-tocopherol specifically regulates osteoclast fusion independent of its antioxidant activity.

To address the molecular mechanism of the α-tocopherol–specific ability to stimulate osteoclast fusion, we analyzed the molecular markers of osteoclast differentiation after treatment with α-tocopherol. Among the many genes involved in osteoclast differentiation, only the expression of the differentiation marker genes, such as *Trap* and *Ctsk*[1,2,4,12], was increased, whereas the expression of other genes key for osteoclast differentiation, such as *Nfatc1* (nuclear factor of activated T cells c1)[1,2,4,12], was unchanged (**Fig. 3a**). We focused on

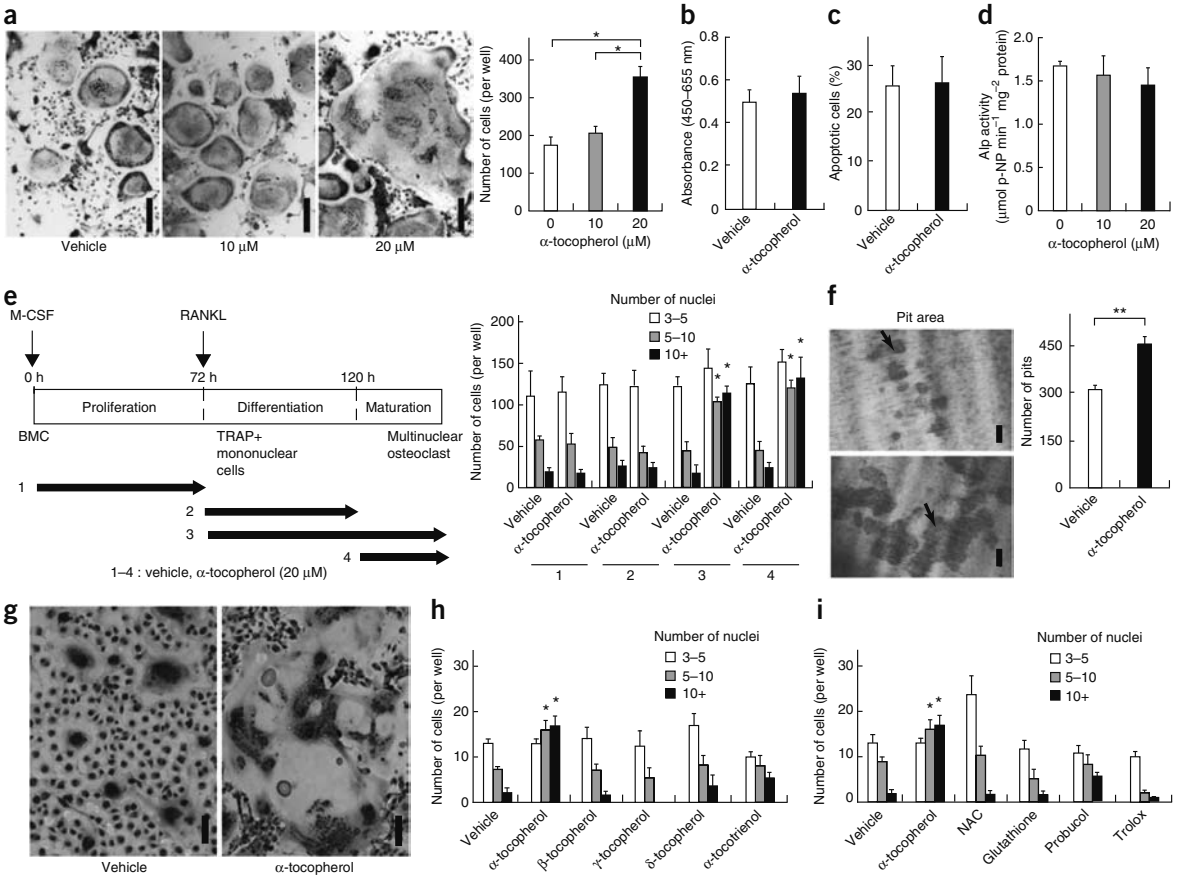

Figure 2 Vitamin E stimulates osteoclast fusion independent of its antioxidant activity. (**a**–**c**) The effect of α-tocopherol on osteoclast differentiation, proliferation and apoptosis. (**a**) BMCs were cultured with M-CSF, RANKL and 10% FBS. TRAP-stained cells (left) and the number of cells with more than three nuclei (right) are shown. An increase in osteoclasts after α-tocopherol treatment can be seen. (**b**) BrdU assay. BMCs were cultured with M-CSF, 10% FBS and α-tocopherol. (**c**) TUNEL assay. BMCs were cultured with M-CSF, RANKL and 10% FBS. (**d**) The effect of α-tocopherol on osteoblasts. An alkaline phosphatase (Alp) assay is shown. p-NP, p-nitrophenol. (**e**) The effect of α-tocopherol on osteoclast fusion. BMCs were cultured with M-CSF and RANKL, and α-tocopherol was added in the proliferation (1), differentiation (2 and 3) or maturation (3 and 4) phase. An increase in the proportion of multinucleated osteoclasts (3 and 4) can be seen. (**f**) The effect of α-tocopherol on bone resorption. A pit formation assay is shown. The eroded area (arrows, left) and the number of pits (right) are shown. BMCs were cultured on dentin with M-CSF and RANKL. α-tocopherol was added later. An increase in bone resorption can be seen. (**g**) Giant-cell progenitors from bone marrow were treated with α-tocopherol. (**h**,**i**) BMCs were cultured with M-CSF and RANKL. Vitamin E isoforms and antioxidants were added later. $^{*}P < 0.05$, $^{**}P < 0.01$ by Tukey-Kramer testing (**a**) or Student's *t* test (**f**,**h**,**i**). Scale bars, 50 μm. All data are means ± s.e.m.

© 2012 Nature America, Inc. All rights reserved.

dendritic-cell–specific transmembrane protein (DC-STAMP), a molecule essential for osteoclast fusion, because among the osteoclast-fusion–related genes[4,5], the gene encoding DC-STAMP (*Tmsf4*) was the only one whose expression was induced by α-tocopherol treatment (**Fig. 3a**). Notably, none of the other vitamin E isoforms induced *Tm7sf4* expression (**Fig. 3b**). Conversely, *Tm7sf4* expression was significantly decreased in *Ttpa*$^{-/-}$ mice, whereas expression of other fusion-related genes was unchanged, with the exception of osteoclast stimulatory transmembrane protein, which is another important molecule that is involved in osteoclast fusion (**Fig. 3c**)[23,24]. Next, to clarify the functional role of DC-STAMP in α-tocopherol–induced osteoclast fusion, we performed four sets of gain- and loss-of-function experiments for DC-STAMP. First, overexpression of *Tm7sf4* in RANKL-induced osteoclasts derived from WT mice markedly increased osteoclast fusion even in the absence of α-tocopherol (**Fig. 3d**). Conversely, although knockdown of *Nfatc1* in BMCs derived from WT mice eliminated the appearance of TRAP-positive mononuclear and multinuclear cells, knockdown of *Tm7sf4* only reduced the multinucleation of osteoclasts (that is, osteoclast fusion) (**Fig. 3e** and **Supplementary Fig. 6**), even in the presence of α-tocopherol. Moreover, osteoclast precursors isolated from *Tm7sf4*$^{-/-}$ mice did not differentiate into multinucleated osteoclasts in the presence of α-tocopherol (**Fig. 3f**). Furthermore, *Tm7sf4* transgenic mice[25] rescued the bone abnormality of the *Ttpa*$^{-/-}$ mice, as shown by a decreased bone volume accompanied by an increased bone resorption in the transgenic mice (**Fig. 3g** and **Supplementary Fig. 7**), which is consistent with the hypothesis that vitamin E induces osteoclast fusion through DC-STAMP. Taken together, these results indicate that the induction of DC-STAMP is necessary and sufficient for α-tocopherol to stimulate osteoclast fusion *in vitro* and *in vivo*.

LETTERS

Next, to gain insight into the molecular pathway of the induction of DC-STAMP by α-tocopherol, we examined whether α-tocopherol activates signaling pathways crucial for osteoclast differentiation. Among the pathways we studied, only the p38 pathway was specifically activated by α-tocopherol, as shown by the increase in phosphorylation of p38α, together with mitogen-activated protein kinase kinases 3 and 6 (Mkk3/6), a molecule that is upstream of p38α (**Fig. 4a** and **Supplementary Fig. 8**)[26]. Stimulation of p38α results in the downstream activation of the transcriptional regulator microphthalmia-associated transcription factor (Mitf)[27], an essential molecule for osteoclast maturation and fusion[1], and, indeed, treatment with α-tocopherol increased Mitf phosphorylation (**Fig. 4b**). Moreover, an antibody against Mitf immunoprecipitated the region containing the putative Mitf binding site in the *Tm7sf4* promoter (**Fig. 4c**), showing that Mitf binds to this site *in vivo*. To address the functional role of p38α and Mitf activation in α-tocopherol–induced osteoclast fusion, we knocked down *Tm7sf4* or *Mitf* in osteoclasts derived from WT mice. Knockdown of *Mapk14* (a gene encoding p38) or *Mitf* abolished the stimulatory effect of α-tocopherol on osteoclast fusion (**Fig. 4d**) and *Tm7sf4* induction (**Supplementary Fig. 6**). Conversely, overexpression of *Mapk14* significantly stimulated

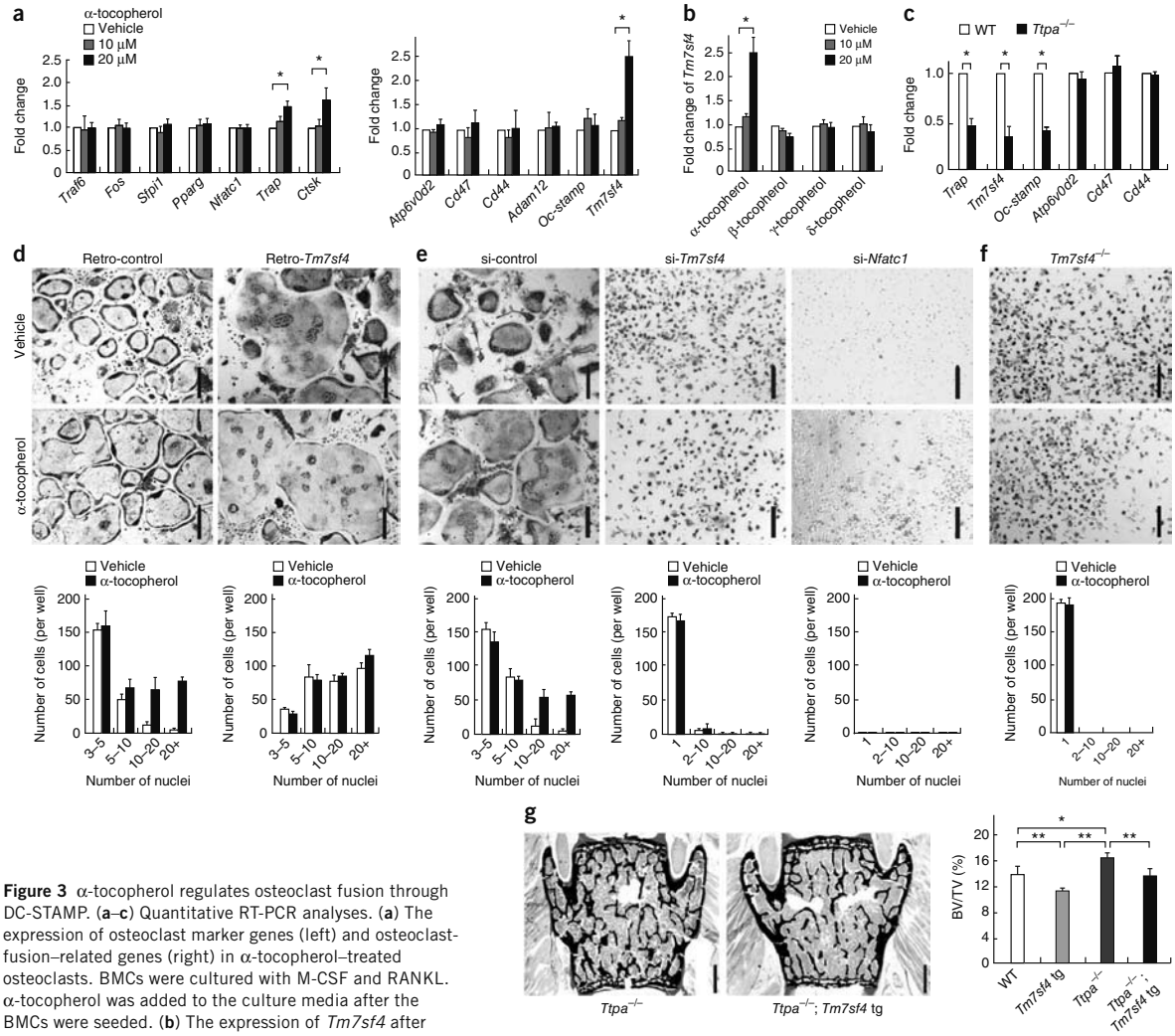

Figure 3 α-tocopherol regulates osteoclast fusion through DC-STAMP. (**a**–**c**) Quantitative RT-PCR analyses. (**a**) The expression of osteoclast marker genes (left) and osteoclast-fusion–related genes (right) in α-tocopherol–treated osteoclasts. BMCs were cultured with M-CSF and RANKL. α-tocopherol was added to the culture media after the BMCs were seeded. (**b**) The expression of *Tm7sf4* after treatment with various isoforms of vitamin E. (**c**) Expression of osteoclast-marker genes in WT and *Ttpa*$^{-/-}$ femurs. A decrease of the expression of *Tm7sf4* among the osteoclast-fusion–related genes can be seen. (**d**–**f**) DC-STAMP is essential for α-tocopherol–induced osteoclast fusion. (**d**) Retroviral overexpression of DC-STAMP. An increase in osteoclast fusion by DC-STAMP in the absence of α-tocopherol can be seen. Retro-*Tm7sf4*, retroviral overexpression of *Tm7sf4*; retro-control, retroviral overexpression of control vector. (**e**,**f**) The effect of α-tocopherol on siRNA-treated BMCs (**e**) and *Tm7sf4*$^{-/-}$ BMCs (**f**). si-control, non-targeting siRNA; si-*Tm7sf4*, siRNA to *Tm7sf4*; si-*Nfatc1*, siRNA to *Nfatc1*. A decrease in osteoclast fusion even in the presence of α-tocopherol can be seen. BMCs from WT (**d**,**e**) and *Tm7sf4*$^{-/-}$ (**f**) mice were cultured with M-CSF and RANKL. α-tocopherol was added to culture media after the BMCs were seeded. Scale bars, 50 μm. (**g**) Histological analysis of the vertebrae from WT, *Tm7sf4* transgenic (*Tm7sf4* tg), *Ttpa*$^{-/-}$ and *Ttpa*$^{-/-}$; *Tm7sf4* tg mice. Scale bars, 500 μm. $^{*}P < 0.05$, $^{**}P < 0.01$ by Tukey-Kramer testing (**a**,**b**,**g**) or Student's *t* test (**c**). All data are means ± s.e.m.

© 2012 Nature America, Inc. All rights reserved.

osteoclast fusion in the absence of α-tocopherol (**Fig. 4e**). These results clearly show that α-tocopherol regulates osteoclast fusion through p38α, Mitf and DC-STAMP. Currently, the molecular mechanism by which α-tocopherol induces p38α activation is unknown. A report showing that α-tocopherol succinate, which is a redox-silent analog of α-tocopherol, induces the activation of mitogen-activated protein kinase kinase kinase 5 (Ask-1)[28], which is an upstream protein kinase in the Mkk3/6-p38α pathway, suggests that α-tocopherol may use this same pathway in an antioxidant-independent manner.

Finally, to address the clinical relevance of our observations, we fed WT mice for 8 weeks with a diet containing an amount of α-tocopherol that is comparable to that found in supplements consumed by many people (**Fig. 4f**)[29]. WT mice fed a α-tocopherol–supplemented diet showed a 20% decreased bone mass after 8 weeks, with a concomitant increase in bone resorption and osteoclast size (**Fig. 4g,h** and **Supplementary Figs. 2** and **9**). Moreover, WT rats fed the same α-tocopherol–supplemented diet also had a 20% loss of bone mass after 8 weeks (**Fig. 4i** and **Supplementary Fig. 10**), showing that excessive intake of vitamin E is deleterious to maintaining bone mass in rodents. Notably, when WT mice were fed a diet supplemented with δ-tocopherol or antioxidants, we observed no bone loss (**Supplementary Fig. 9**), further indicating that α-tocopherol decreases bone mass independent of its antioxidant activity.

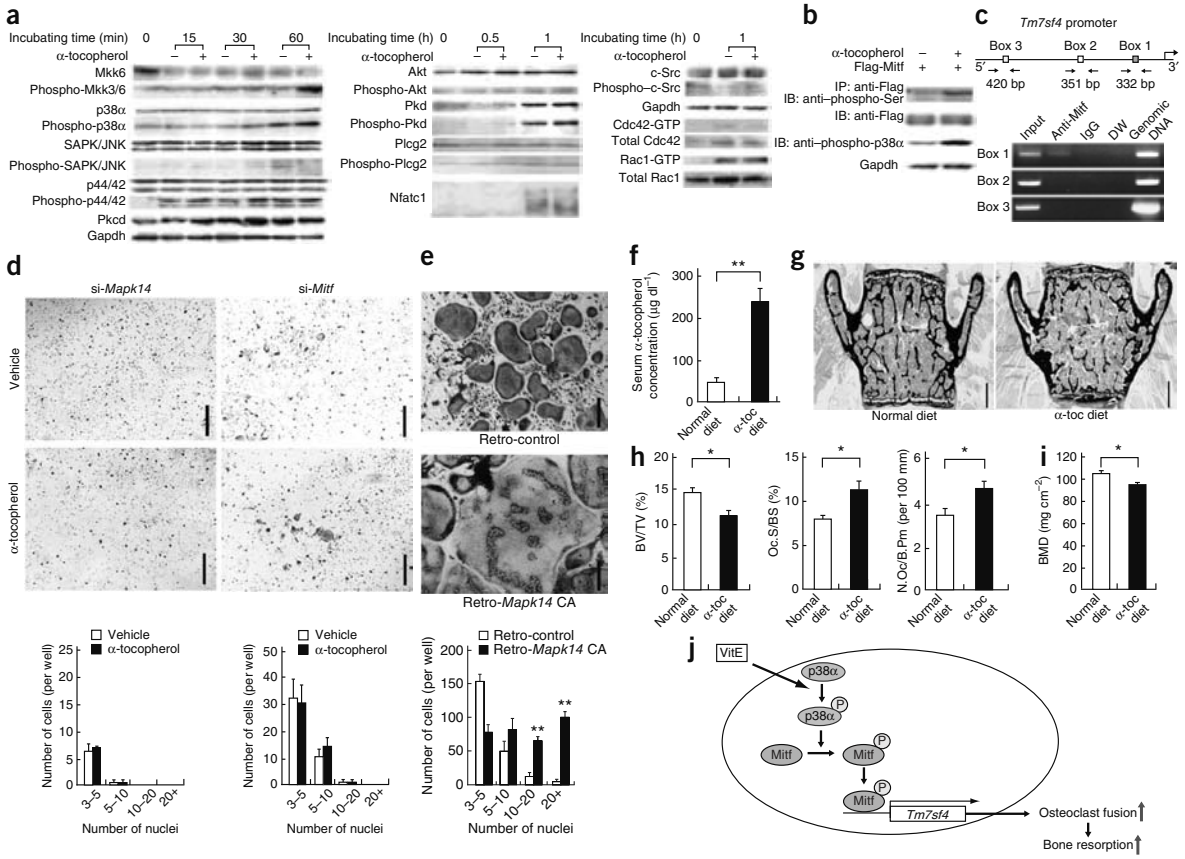

Figure 4 α-tocopherol decreases bone mass through p38α and Mitf. (**a**) Protein analysis of the α-tocopherol–treated osteoclasts. BMCs cultured with M-CSF only (left, middle) or mature osteoclasts that were induced by M-CSF and RANKL (right) were stimulated with α-tocopherol (20 μM) (– or +) and RANKL (middle right). Phospho-, phosphorylated; SAPK/JNK, mitogen-activated protein kinase 9 or mitogen-activated protein kinase 8; p44/42, mitogen-activated protein kinase 3 or cyclin-dependent kinase 20; Pkcd, protein kinase C, δ; Gapdh, glyceraldehyde-3-phosphate dehydrogenase; Akt, thymoma viral proto-oncogene 1; Pkd, protein kinase D; Plcg2, phospholipase C, γ 2; Nfatc1, nuclear factor of activated T cells, cytoplasmic, calcineurin dependent 1; c-Src, Rous sarcoma oncogene. (**b**) Immunoprecipitation analysis. An increase in the phosphorylation of p38α after treatment with α-tocopherol in p38α-expressing HEK293 cells can be seen. (**c**) Chromatin immunoprecipitation assay. Three potential binding sites (boxes 1–3) in the *Tm7sf4* promoter are shown (above). An antibody against Mitf (anti-Mitf) specifically immunoprecipitated the region containing the box 1 site of the *Tm7sf4* promoter. IgG, immunoglobulin G; DW, distilled water. (**d**,**e**) Gene knockdown (**d**) and retroviral overexpression (**e**) in osteoclasts. BMCs derived from WT mice were cultured with M-CSF and RANKL. α-tocopherol was added later. Scale bars, 50 μm. A decrease in osteoclast fusion even in the presence of α-tocopherol in BMCs treated with siRNA to *Mapk14* (si-*Mapk14*) (encoding p38α) or siRNA to *Mitf* (si-*Mitf*) (**d**) and an increase in osteoclast fusion in the absence of α-tocopherol in constitutively active p38α (*Mapk14*CA)-expressing BMCs (**e**) can be seen. (**f**–**h**) Analyses of WT mice and rats fed an α-tocopherol–supplemented diet. Serum α-tocopherol concentrations in these animals (**f**) and histological (**g**) and histomorphometric analyses (**h**). Scale bars, 500 μm. AA decrease in bone mass and an increase in bone resorption after α-tocopherol treatment can be seen. (**i**) Dual-energy X-ray absorptiometry analysis. A decrease in bone mineral density resulting from a α-tocopherol–supplemented diet. (**j**) The proposed mechanism of vitamin E (VitE)-induced osteoclastic fusion. P, phosphorylated. $^{*}P < 0.05$, $^{**}P < 0.01$ by Student's *t* test. All data are means ± s.e.m.

© 2012 Nature America, Inc. All rights reserved.

In summary, we show that vitamin E stimulates bone resorption and decreases bone mass by inducing osteoclast fusion (**Fig. 4j**). Moreover, we provide evidence that serum vitamin E is a determinant of bone mass. In contrast with our results, several reports have indicated that vitamin E participates in bone anabolism and that 6-hydroxy-2,5,7,8-tetramethylchroman-2-carboxylic acid (trolox), which is a vitamin E analog, inhibits inflammation-induced osteoclast differentiation[30–33]. In our experiments, trolox mildly inhibited osteoclast differentiation when we added it during the early osteoclast differentiation period (**Supplementary Fig. 11**), but it did not induce osteoclast fusion when we added it during the maturation phase (**Fig. 2i**). Alternatively, differences in the methodologies or the ages of the animals that were used in the previous compared to the present analyses may explain the discrepant results. In addition, several reports have shown the beneficial effects of α-tocopherol on human bone, which probably occur by reducing oxidative stress[21,34,35]. Nevertheless, most of these studies used a small sample size and were not well controlled. Given the widespread use of vitamin E, and especially α-tocopherol, as a supplement in humans, a larger, controlled study that addresses its effects on human bone is warranted.

METHODS

Methods and any associated references are available in the online version of the paper at http://www.nature.com/naturemedicine/.

Note: Supplementary information is available on the Nature Medicine website.

ACKNOWLEDGMENTS

We thank G. Karsenty, R. Baron and S. Tanaka for discussions; Y. Hotta, K. Miyamoto, H. Inose, S. Sato, A. Kimura, R. Xu and C. Xu for technical assistance; and T. Kitamura (Divisions of Cellular Therapy and Hematopoietic Factors, The Institute of Medical Science, The University of Tokyo, Tokyo, Japan) and I. Takada (Department of Microbiology and Immunology, Keio University School of Medicine, Tokyo, Japan) for plasmids. This work was supported by the Funding Program for Next Generation World-Leading Researchers (NEXT Program), grant-in-aid for scientific research from the Japan Society for the Promotion of Science, a grant for Global Center of Excellence Program from the Ministry of Education, Culture, Sports, Science and a Takeda Scientific Foundation grant.

AUTHOR CONTRIBUTIONS

K.F. conducted most of the experiments. M.I., H.O. and C.M. conducted mice analyses. T.F. and S.S. conducted *in vitro* experiments. T.M. provided DC-STAMP–related mice. K.T. and H. Tamai conducted the analyses of vitamin E serum concentrations. T.N.-K. performed western blots. H.A. provided *Ttpa*$^{-/-}$ mice. T.K. and H. Takayanagi conducted gene expression analyses. S.T., K.S., A.O. and H.I. designed the project. S.T. supervised the project and wrote most of the manuscript. S.K. designed the project.

COMPETING FINANCIAL INTERESTS

The authors declare no competing financial interests.

Published online at http://www.nature.com/naturemedicine/.
Reprints and permissions information is available online at http://www.nature.com/reprints/index.html.

1. Teitelbaum, S.L. & Ross, F.P. Genetic regulation of osteoclast development and function. *Nat. Rev. Genet.* **4**, 638–649 (2003).
2. Horne, W.C., Sanjay, A., Bruzzaniti, A. & Baron, R. The role(s) of Src kinase and Cbl proteins in the regulation of osteoclast differentiation and function. *Immunol. Rev.* **208**, 106–125 (2005).
3. Karsenty, G., Kronenberg, H.M. & Settembre, C. Genetic control of bone formation. *Annu. Rev. Cell Dev. Biol.* **25**, 629–648 (2009).
4. Lorenzo, J., Horowitz, M. & Choi, Y. Osteoimmunology: interactions of the bone and immune system. *Endocr. Rev.* **29**, 403–440 (2008).
5. Zou, W. & Teitelbaum, S.L. Integrins, growth factors, and the osteoclast cytoskeleton. *Ann. NY Acad. Sci.* **1192**, 27–31 (2010).
6. Yokota, T. *et al.* Delayed-onset ataxia in mice lacking α-tocopherol transfer protein: model for neuronal degeneration caused by chronic oxidative stress. *Proc. Natl. Acad. Sci. USA* **98**, 15185–15190 (2001).
7. Wagner, E.F. & Nebreda, A.R. Signal integration by JNK and p38 MAPK pathways in cancer development. *Nat. Rev. Cancer* **9**, 537–549 (2009).
8. Weilbaecher, K.N. *et al.* Linkage of M-CSF signaling to Mitf, TFE3, and the osteoclast defect in Mitf(mi/mi) mice. *Mol. Cell* **8**, 749–758 (2001).
9. Yagi, M. *et al.* DC-STAMP is essential for cell-cell fusion in osteoclasts and foreign body giant cells. *J. Exp. Med.* **202**, 345–351 (2005).
10. Vignery, A. Macrophage fusion: the making of osteoclasts and giant cells. *J. Exp. Med.* **202**, 337–340 (2005).
11. Bruzzaniti, A. & Baron, R. Molecular regulation of osteoclast activity. *Rev. Endocr. Metab. Disord.* **7**, 123–139 (2006).
12. Takayanagi, H. Osteoimmunology and the effects of the immune system on bone. *Nat. Rev. Rheumatol.* **5**, 667–676 (2009).
13. Kato, S. *et al.* The function of nuclear receptors in bone tissues. *J. Bone Miner. Metab.* **21**, 323–336 (2003).
14. Cockayne, S. *et al.* Vitamin K and the prevention of fractures: systematic review and meta-analysis of randomized controlled trials. *Arch. Intern. Med.* **166**, 1256–1261 (2006).
15. Azzi, A. *et al.* Specific cellular responses to α-tocopherol. *J. Nutr.* **130**, 1649–1652 (2000).
16. Radimer, K. *et al.* Dietary supplement use by US adults: data from the National Health and Nutrition Examination Survey, 1999–2000. *Am. J. Epidemiol.* **160**, 339–349 (2004).
17. Jishage, K. *et al.* α-tocopherol transfer protein is important for the normal development of placental labyrinthine trophoblasts in mice. *J. Biol. Chem.* **276**, 1669–1672 (2001).
18. Sato, S. *et al.* Central control of bone remodeling by neuromedin U. *Nat. Med.* **13**, 1234–1240 (2007).
19. Le Nihouannen, D., Barralet, J.E., Fong, J.E. & Komarova, S.V. Ascorbic acid accelerates osteoclast formation and death. *Bone* **46**, 1336–1343 (2010).
20. Ragab, A.A., Lavish, S.A., Banks, M.A., Goldberg, V.M. & Greenfield, E.M. Osteoclast differentiation requires ascorbic acid. *J. Bone Miner. Res.* **13**, 970–977 (1998).
21. Ruiz-Ramos, M., Vargas, L.A., Fortoul Van der Goes, T.I., Cervantes-Sandoval, A. & Mendoza-Nunez, V.M. Supplementation of ascorbic acid and α-tocopherol is useful to preventing bone loss linked to oxidative stress in elderly. *J. Nutr. Health Aging* **14**, 467–472 (2010).
22. Tsuneto, M., Yamazaki, H., Yoshino, M., Yamada, T. & Hayashi, S. Ascorbic acid promotes osteoclastogenesis from embryonic stem cells. *Biochem. Biophys. Res. Commun.* **335**, 1239–1246 (2005).
23. Yang, M. *et al.* Osteoclast stimulatory transmembrane protein (OC-STAMP), a novel protein induced by RANKL that promotes osteoclast differentiation. *J. Cell. Physiol.* **215**, 497–505 (2008).
24. Kim, M.H., Park, M., Baek, S.H., Kim, H.J. & Kim, S.H. Molecules and signaling pathways involved in the expression of OC-STAMP during osteoclastogenesis. *Amino Acids* **40**, 1447–1459 (2011).
25. Iwasaki, R. *et al.* Cell fusion in osteoclasts plays a critical role in controlling bone mass and osteoblastic activity. *Biochem. Biophys. Res. Commun.* **377**, 899–904 (2008).
26. Greenblatt, M.B. *et al.* The p38 MAPK pathway is essential for skeletogenesis and bone homeostasis in mice. *J. Clin. Invest.* **120**, 2457–2473 (2010).
27. Steingrimsson, E. *et al.* Mitf and Tfe3, two members of the Mitf-Tfe family of bHLH-Zip transcription factors, have important but functionally redundant roles in osteoclast development. *Proc. Natl. Acad. Sci. USA* **99**, 4477–4482 (2002).
28. Zu, K., Hawthorn, L. & Ip, C. Up-regulation of c-Jun–NH2-kinase pathway contributes to the induction of mitochondria-mediated apoptosis by α-tocopheryl succinate in human prostate cancer cells. *Mol. Cancer Ther.* **4**, 43–50 (2005).
29. Miller, E.R. III *et al.* Meta-analysis: high-dosage vitamin E supplementation may increase all-cause mortality. *Ann. Intern. Med.* **142**, 37–46 (2005).
30. Lee, J.H. *et al.* Trolox prevents osteoclastogenesis by suppressing RANKL expression and signaling. *J. Biol. Chem.* **284**, 13725–13734 (2009).
31. Arjmandi, B. *et al.* Vitamin E improves bone quality in the aged but not in young adult male mice. *J. Nutr. Biochem.* **13**, 543 (2002).
32. Mehat, M.Z., Shuid, A.N., Mohamed, N., Muhammad, N. & Soelaiman, I.N. Beneficial effects of vitamin E isomer supplementation on static and dynamic bone histomorphometry parameters in normal male rats. *J. Bone Miner. Metab.* **28**, 503–509 (2010).
33. Shuid, A.N., Mehat, Z., Mohamed, N., Muhammad, N. & Soelaiman, I.N. Vitamin E exhibits bone anabolic actions in normal male rats. *J. Bone Miner. Metab.* **28**, 149–156 (2010).
34. Chuin, A. *et al.* Effect of antioxidants combined to resistance training on BMD in elderly women: a pilot study. *Osteoporos. Int.* **20**, 1253–1258 (2009).
35. Ostman, B. *et al.* Oxidative stress and bone mineral density in elderly men: antioxidant activity of α-tocopherol. *Free Radic. Biol. Med.* **47**, 668–673 (2009).

© 2012 Nature America, Inc. All rights reserved.

ONLINE METHODS

Animals. We purchased the C57BL/6J mice from the Charles River Laboratory and Oriental Yeast, and we purchased the Wister rats from CLEA Japan. *Ttpa*$^{-/-}$, *Tm7sf4*$^{-/-}$ and *Tm7sf4* transgenic mice were previously described[6,9,25]. We crossed *Ttpa*$^{-/-}$ and *Tm7sf4* transgenic mice to obtain *Ttpa*$^{-/-}$; *Tm7sf4* transgenic mice. We fed the mice a diet supplemented with α-tocopherol (600 mg per kg^{1} of body weight; Sigma) from 4–12 weeks of age, and we fed the rats the same diet from 6–14 weeks of age. The α-tocopherol–supplemented diet was made by CLEA Japan. We analyzed seven or eight mice in each group. We maintained all animals under a 12-h light-dark cycle with *ad libitum* access to food and water. All animal experiments were performed with the approval of the Animal Study Committee of Tokyo Medical and Dental University and conformed to the relevant guidelines and laws.

Dual X-ray absorptiometry analyses. We measured the bone mineral density of the femurs of all animals by DCS-600 (ALOKA), as previously described[18]. We examined at least eight mice for each group.

Histological and histomorphometric analyses. We injected mice with calcein (25 mg per kg of body weight; Sigma) and stained the undecalcified sections of the lumbar vertebrae using von Kossa and TRAP, as previously described[18,36]. We performed static and dynamic histomorphometric analyses using the OsteoMeasure Analysis System (OsteoMetrics); the Oc.S/BS and N.Oc/B.pm values were calculated for the slices that stained positive for TRAP. We analyzed seven or eight mice in each group.

Cell culture. *In vitro* osteoclast differentiation was accomplished as previously described[18]. Briefly, BMCs of 6–8-week-old mouse femurs were cultured in minimum essential medium α supplemented with FBS in the presence of human M-CSF (10 ng ml^{-1}; R&D Systems) for 3 d and then differentiated into osteoclasts using human RANKL (50 ng ml^{-1}; PeproTech) and M-CSF for 3 d. The osteoclast culture using mouse serum is decribed in detail in the **Supplementary Methods**. The pit formation assay, BrdU assay and TUNEL assay were performed as previously described[18], and the details are described in the **Supplementary Methods**. The foreign-body giant-cell culture was established as previously described[37]. Briefly, BMCs were collected in DMEM (Sigma) with 10% FBS. Cells were stimulated with interleukin-4 (IL-4) (10 ng ml^{-1}) for 48 h, fixed and stained with May-Grünwald-Giemsa for evaluation. The *in vitro* primary osteoblast culture was established as previously described[38,39] (**Supplemntary Methods**). α-tocopherol was added to the culture media at 20 μM or at the indicated concentrations. Other vitamin E isoforms were added at 20 μM, N-acetylcysteine was added at 2 mM, glutathione was added at 5 mM, probucol was added at 5 μM and trolox was added at 200 μM. We cultured all cells in triplicate or quadruplicate wells and repeated each experiment more than three times. Additional details are given in the **Supplementary Methods**.

Transfection and retroviral infection. A total of 20 nM siRNA (Invitrogen) was transfected into BMCs derived from the femurs of WT mice using HiPerFect (QIAGEN). After transfection, cells were cultured using the same methods as those used for the osteoclast differentiation. Complementary DNA (cDNA) of *Tm7sf4* was cloned from osteoclasts using PCR. The constitutively active form of p38α was obtained from Addgene. Retrovirus was produced by the retroviral vector pMXs-IRES-GFP system, which was based on Moloney murine leukemia virus, as previously described[40]. Briefly, we collected the virus produced by packaging cells after 2 d of transfection. BMCs were infected with the retrovirus for 2 d in the presence of M-CSF. After 2 d of infection, cells were stimulated by RANKL to differentiate into osteoclasts. The details are described in the **Supplementary Methods**.

Quantitative RT-PCR analyses. To acquire RNA from mouse bones, we flushed bone marrow out of the femurs with PBS and used the bones as previously described[18]. RNA was extracted using TRIzol (Invitrogen), and reverse transcription was performed for cDNA synthesis using a High Capacity cDNA Reverse Transcription Kit (Applied Biosystems). We performed quantitative analyses of gene expression using the Mx3000P Real-Time PCR System (Stratagene). We examined the gene expressions in triplicate or quadruplicate individually and repeated each experiment more than three times.

Protein analyses. We collected cell lysate protein using radioimmunoprecipitation assay buffer with a phosphatase inhibitor cocktail (Nacalai) and the Complete Mini protease inhibitor cocktail (Roche). To detect RAS-related C3 botulinum substrate 1 (Rac1) and cell division cycle 42 (Cdc42) expression, we used Active GTPase Pull-Down and Detection kits (Thermo Scientific). For detecting the phosphorylation of Mitf, we used Anti-Flag M2 Affinity beads (Sigma), horseradish peroxidase–conjugated M2 antibody to Flag (1:1,000; Sigma) and antibody to phopshorylated serine (1:1,000; Millipore). Further details are given in the **Supplementary Methods**. We examined the expressions individually and repeated each experiment more than three times.

Chromatin immunoprecipitation (ChIP). We used ChIP-IT Express Chromatin Immunoprecipitation Kits (Active Motif), following the manufacturer's instructions. Briefly, we cultured BMCs from WT mice for 2 d. Cells were crosslinked with 0.4% formaldehyde, and the reaction was stopped by adding glycine. Fixed cells were resuspended in lysis buffer and sonicated for 5 min (with cycles of 30 s on and 30 s off). The supernatant was used immediately for ChIP experiments.

Statistical analyses. We performed statistical analyses using Tukey-Kramer testing for multiple comparisons and Student's *t* tests for two-group comparisons. Values were considered statistically significant at $P < 0.05$. All data are means ± s.e.m. Results are representative of more than four individual experiments.

Additional methods. Detailed methodology is described in the **Supplementary Methods**.

36. Kimura, A. *et al.* Runx1 and Runx2 cooperate during sternal morphogenesis. *Development* **137**, 1159–1167 (2010).
37. McNally, A.K., Macewan, S.R. & Anderson, J.M. Foreign body-type multinucleated giant cell formation requires protein kinase C β, δ, and ζ. *Exp. Mol. Pathol.* **84**, 37–45 (2008).
38. Ducy, P. *et al.* Leptin inhibits bone formation through a hypothalamic relay: a central control of bone mass. *Cell* **100**, 197–207 (2000).
39. Inose, H. *et al.* A microRNA regulatory mechanism of osteoblast differentiation. *Proc. Natl. Acad. Sci. USA* **106**, 20794–20799 (2009).
40. Kitamura, T. *et al.* Retrovirus-mediated gene transfer and expression cloning: powerful tools in functional genomics. *Exp. Hematol.* **31**, 1007–1014 (2003).

© 2012 Nature America, Inc. All rights reserved.

doi:10.1038/nm.2659

膠原病・リウマチ内科学分野

宮坂 信之

医歯学総合研究科・生体環境応答学系専攻
膠原病・リウマチ内科学・教授

1）研究の課題名

A; 新規関節炎治療法の開発及び作用機序解析

Development of new anti-rheumatic drugs and analysis of their mechanisms of actions

【TREM-1リガンド同定による関節炎治療法の開発】

TREM-1阻害はマウスコラーゲン誘導関節炎（CIA）を改善するだけではなく、細菌感染の危険性が少ない治療法となりうることが示唆されている。TREM-1阻害法として以前報告した可溶型TREM-1を用いる方法以外に、未知であったマウスTREM-1リガンドを同定し、同分子に対する抗体投与によりCIAを改善することに成功した。感染という副作用の少ない抗リウマチ薬への応用にむけてヒトTREM-1リガンドの同定を試みている。

【microRNAを標的とした関節リウマチの新規治療法の開発】

microRNAの阻害剤libraryを用いて、滑膜線維芽細胞の活性化や細胞増殖を抑制する阻害剤のスクリーニングを行い、治療標的となりうるmicroRNAの同定を行った。これらのmicroRNAの滑膜線維芽細胞における作用機序を明らかにし、関節炎における新規治療標的としての可能性について検討を進めている。（本研究は、歯と骨のグローバルCOE拠点内における異なる分野のInnovationを確立する研究である）

【関節炎における病的滑膜線維芽細胞の起源の同定】

関節炎の主病態は炎症性滑膜線維芽細胞の過剰な増殖と活性化であり、このような病的滑膜線維芽細胞の起源と、分化・活性化を制御する因子を同定することにより、新たな関節リウマチの治療戦略を開発することを目的に検討を行っている。

【CDK阻害剤の関節炎改善効果機序解析】

細胞周期を制御するサイクリン依存性キナーゼ（CDK）の活性を抑制することで滑膜線維芽細胞（RASF）の増殖を抑制し、CIAを改善させることをこれまでに報告した。この機序を検討中、CDK4/6阻害薬存在下では、TNF-αとIL-1β刺激に対するRASFからのMMP-3産生が抑制された一方、IL-6産生は影響を受けないことが判明した。このCDK4/6阻害薬が炎症抑制御にも働く機序をEMSAやTransAM kitを用いて解析している。

B：多発性筋炎・皮膚筋炎（PM/DM）の病態解析と新規治療法開発

【PM/DMにおける自然免疫活性化の研究】

我々は、独自に開発したPM/DMマウスモデルを用いて自己反応性T細胞ばかりでなく、筋組織における自然免疫活性化が、筋炎発症にかかわっていることを見いだし、前者を種、後者を土壌に例え、自己免疫のseed and soil modelを提唱した。このうち、自然免疫の活性化には、筋線維の再生過程もが関与していることを見いだし、筋炎への関与や制御法について研究している。

【PM/DMにおける自己反応性T細胞活性化の研究】

上記の通り、自己反応性T細胞活性化の制御も治療法開発の鍵を握る。しかしながら、副作用防止の観点からは、広範なT細胞抑制よりも病態特異的な抑制法が望ましい。そこれ、PMではキラーT細胞が病態に重要であることを考慮し、キラーT細胞の細胞傷害機能に重要なDNAM-1分子や活性化T細胞機能発現に重要なCD28のPMモデルマウスにおける関与について検討し、その重要性を確認した。

2)

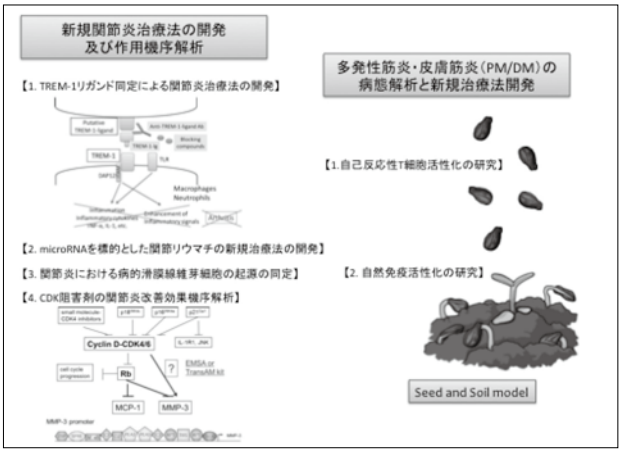

C. オートタキシン/リゾフォスファチジン酸受容体を標的とした関節リウマチの新規治療法開発

Autotaxin and lysophosphatidic acid receptors：potential target molecules in new therapies for rheumatoid arthritis

リゾフォスファチジン酸（LPA）は生理活性を有する脂質メディエーターであり、オートタキシン（ATX）により合成され、LPA受容体（$LPA_{1\text{-}6}$）を介して作用する。関節リウマチ（RA）滑膜組織では、変形性関節症と比較してATX、$LPA_{1\text{-}4}$の発現上昇がみられた。In vitroにおいてLPAはRA線維芽細胞様滑膜細胞（FLS）のサイトカイン産生、細胞増殖を亢進させた。また、脂質フリーの血清を用いて末梢血単球をRANKL + M-CSF刺激する際に、LPAを加えることにより破骨細胞分化が促進した。一方、BrP-LPA（ATXおよび汎LPA受容体の阻害薬）はマウスコラーゲン関節炎（CIA）、並びに移入した$CD11b^{+}$細胞のCIAマウス滑膜組織への浸潤を抑制した。さらに治療標的を絞るためATX活性阻害薬、LPA_1阻害薬のCIAマウスへの効果を解析した。ATX、LPA_1それぞれの阻害によりCIAの関節炎スコア、滑膜への炎症細胞浸潤、骨破壊が抑制された。さらにコラーゲン刺激したCIA脾臓T細胞からのIL-17産生がATX、LPA_1阻害により低下した。LPAはFLS活性、破骨細胞分化、炎症細胞浸潤、Th17分化に寄与し、その阻害がRAの新規治療となることが示唆された。

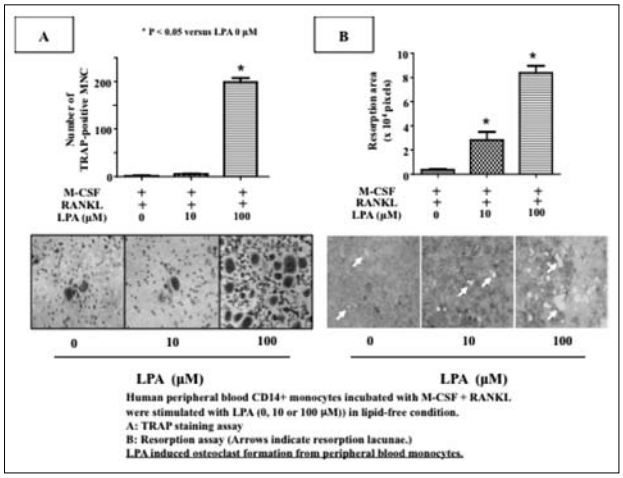

D. カンナビノイドによる関節炎抑制作用

Agonist for cannabinoid receptor 2（CB2）ameliorates murine collagen-induced arthritis

カンナビノイド（CB：cannabinoid）は大麻の主成分であるが、その受容体であるCB_1は主に中枢神経系に、CB_2は免疫系細胞に発現しているため、CB_2特異的リガンドは中枢神経への作用がなく、免疫系へ作用することが推測される。内在性のCBは近年免疫系への関与が注目されている脂質メディエーターである。本研究では、関節リウマチ（RA）におけるCBの治療への有用性とその機序を検討した。RA滑膜組織でのCB_2発現を免疫染色にて解析したところ、RA滑膜組織において、変形性関節症と比較し発現の亢進がみられた。蛍光二重染色ではCD68陽性マクロファージ、CD4陽性Tリンパ球、CD21陽性Bリンパ球、vimentin陽性線維芽細胞様滑膜細胞（FLS）にCB_2との共染性を認めた。CB_2選択的アゴニストであるJWH133をコラーゲン関節炎（CIA）マウスに投与し、関節炎抑制効果を解析した。関節炎発症前より投与したところ、関節炎スコア、滑膜組織への炎症細胞浸潤、骨破壊の程度が有意に抑制された。関節炎発症後の投与においてもスコアの抑制効果を認めた。In vitroにおいて、末梢血単球からのRANKL + M-CSF刺激による破骨細胞分化、およびFLSからのIL-6産生への、JWH133による影響を解析した。その結果、いずれもJWH133による有意な抑制効果を認めた。今回我々はCB_2選択的アゴニストによる関節炎抑制効果を見出し、その機序として破骨細胞分化の抑制や、FLSからのサイトカイン産生抑制が寄与している可能性が示唆された。

E. CCL18による関節リウマチ線維芽細胞様滑膜細胞の活性化

Stimulation with CCL18 enhanced production of IL-6, MCP-1 and MMP-3 by fibroblast-like synoviocytes from patients with rheumatoid arthritis

CCL18は樹状細胞、単球/マクロファージから産生され、リンパ球、単球および樹状細胞に対する遊走能を持つケモカインである。変形性関節症（OA）と比べてCCL18が関節リウマチ（RA）の関節液中で発現上昇していることが報告されている。本研究では、RAにおけるCCL18の病態形成への関与を解析することを目的とした。RA滑膜組織では、OAと比較してCCL18の発現は増強し、マクロファージ、血管内皮細胞、線維芽細胞様滑膜細胞（FLS）にCCL18の発現を認めた。In vitroでFLSをCCL18で刺激すると、IL-6、MCP-1、MMP-3の発現が亢進し、その刺激はG蛋白共役受容体（GPCR）阻害剤である百日咳毒素によって阻害された。また、CCL18刺激によりAkt、ERK1/2のリン酸化を認めた。RA滑膜にてCCL18の機能的受容体であるPITPNM3の発現を免疫染色で解析したところ、マクロファージ、樹状細胞、B細胞、FLSに発現がみら

れた。FLSについてはRT-PCRとWestern Blot法でもPITPNM3の発現を確認した。以上より、CCL18はRA滑膜に発現し、PITPNM3を介して、Akt、ERK1/2のリン酸化を誘導し、FLSからの炎症性サイトカイン等の発現を亢進させると考えられた。CCL18はRA FLSの活性化によりRAの病態形成に関与しており、CCL18、PITPNM3はRAの新たな治療ターゲットとなりうることが示唆された。

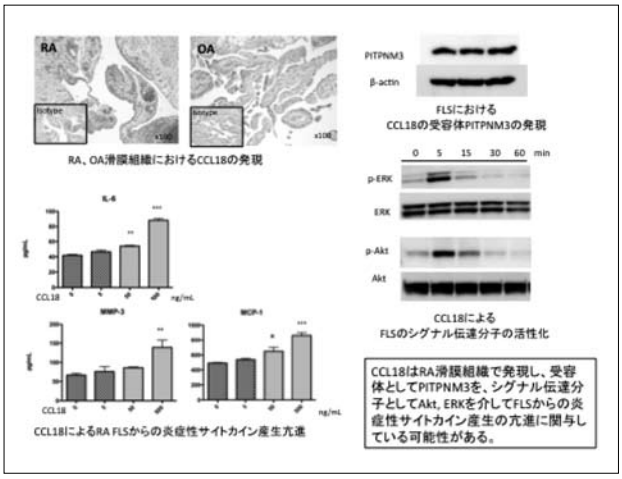

F. 関節リウマチに対する生物学的製剤の安全性に関する多角的解析

生物学的製剤の安全性を評価するため、三つの研究を行った。第一に、「日本における生物学的製剤使用関節リウマチ患者に関する疫学研究（REAL研究）」では、TNF阻害薬開始から3年までの重篤感染症リスクを検討し、リスクが1年目は高く、その後は時間依存性に低下することを示した。第二に、「生物学的製剤使用関節リウマチ患者の長期安全性研究（SECURE研究）」を設立し、生物学的製剤使用患者17000例のデータベースを作成し、生物学的製剤使用が、RA患者の発癌リスク（固形癌および悪性リンパ腫）を上昇させないことを明らかにした。第三に、諸外国に比較して我が国のTNF阻害薬投与RA患者に高頻度に発現するニューモシスチス肺炎に関する症例・対照研究などを行い、発症予測因子を同定した。今年度から、RA患者で高頻度に合併する間質性肺炎・気道病変などの肺合併症に着目し、肺合併症を有するRA患者と有さないRA患者についての治療内容・安全性の比較を開始した。また、RA患者の平均年齢が日本よりも10歳若年の韓国のRA患者コホートとREALコホートの比較研究を開始した。これらの研究は来年度以降も継続する予定である。

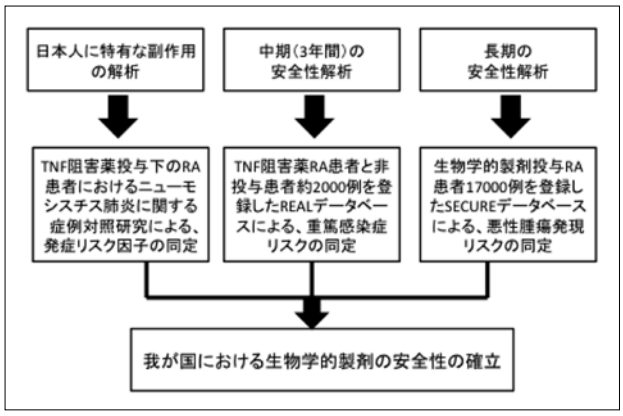

3）発表の研究内容についての英文要約

A. Arthritis research

【Identification of the TREM-1 ligand as a therapeutic target of arthritis】

TREM-1 blockade is reported to suppress pathological inflammation with maintaining inflammatory cytokine production for physiological protection against microbes. We identified the TREM-1 ligand molecule and generated blocking anti-TREM-1-ligand monoclonal antibody. Administration of this antibody ameliorated collagen-induced arthritis of mice. The TREM-1 blockade in Rheumatoid Arthritis patients will be a new anti-rheumatic therapy that is less associated with a risk of infection than the current treatments.

【Identification of crucial microRNA in rheumatoid arthritis】

We analyzed the role of 954 kinds of microRNAs in the proliferation and activation of synovial fibroblasts derived from rheumatoid arthritis by using microRNA inhibitor library. We identified the crucial microRNAs in the pathogenesis of rheumatoid arthritis. We are now analyzing the mechanisms of each microRNAs in the pathogenesis of rheumatoid arthritis.

【Identification of the origin of the pathogenic synovial fibroblast in rheumatoid arthritis】

Pathogenesis of rheumatoid arthritis is characterized by the

proliferation and activation of inflamed synovial fibroblasts. We are investigating the origin of the pathogenic synovial fibroblast and trying to identify the molecules to regulate the differentiation and activation of the pathogenic synovial fibroblasts in rheumatoid arthritis.

B. Myositis research

【Activation of innate immunity in polymyositis and dermatomyositis (PM/DM)】

Based on our previous observation in clinical practice as well as on murine polymyositis model we developed, we propose that activation of muscle-specific T cells and activation of innate immunity in the target muscles need to act in concert for development of myositis. We call this as seed and soil model, regarding T cells as seeds and muscles as soil. A series of research studies were conducted to elucidate the activation od muscle innate immunity.

【Activation of autoaggressive T cells in PM/DM】

Control of autoaggressive T cells is another obvious target in treatment of PM, in which killer T cells are important in the pathology. Instead of suppressing all T cells, we have explored suppressing subset of T cells expressing molecules that are important for killer T cell activity. In vivo and in vitro experiments have showen promising results.

C. Pathogenic Role of Lysophosphatidic Acid on Rheumatoid Arthritis

Lysophosphatidic acid (LPA) is a bioactive lipid and binds to cell surface G coupled-protein receptors (LPAR1-5), which is generated by autotaxin (ATX). In this study, we analyzed expression of ATX and LPA receptors (LPAR1-5) in rheumatoid arthritis (RA), and examined the pathogenic role in RA. ATX and LPAR1-5 were expressed in the RA synovium. Stimulation with LPA upregulated expression of IL-6, MCP-1, and MMP-3 by fibroblast-like synoviocytes (FLS) from RA. LPA also induced migration and proliferation on FLS from RA. We induced murine collagen-induced arthritis (CIA) by immunization with bovine type II collagen at days 1 and 22. Treatment with BrP-LPA (antagonist for ATX and LPAR) from day 22 significantly reduced clinical arthritis score and radiographic bone destruction of the CIA. Moreover, IFN-γ and IL-17 production by collagen-stimulated splenocytes from BrP-LPA-treated mice were lower than that from vehicle-treated mice. Treatment with BrP-LPA after onset of arthritis also ameliorated clinical arthritis score. These results indicate that LPA plays an important role for activation of FLS, and could be a new target for RA therapy.

D. Agonist for cannabinoid receptor 2 (CB2) ameliorates murine collagen-induced arthritis

Cannabinoids (CBs) are chemical compounds included in marijuana. Its receptor CB_1 is predominantly expressed in the brain, whereas the cells of immune system express CB_2. Therefore, CB_2-specific agonist should affect on immune cells but not on central nervous system. Endogenous CB is one of the lipid mediators, which exhibit immunosuppressive properties. In this study, we investigated therapeutic effect of CB on arthritis. Expression of CB_2 in the rheumatoid arthritis (RA) synovium was analyzed by immunohistochemistry. Effect of JWH133, CB_2-specific agonist, on murine collagen-induced arthritis (CIA) was evaluated. Osteoclastogenesis from peripheral blood monocyte incubated with RANKL + M-CSF was analyzed by TRAP staining. IL-6 production was measured by ELISA. CB_2 was highly expressed in the RA synovium compared to osteoarthritis, which was expressed on macrophages, T cells, B cells and fibroblast-like synoviocytes (FLS). JWH133 reduced arthritis score, inflammatory cell infiltration and bone destruction on CIA mice. JWH133 also inhibited osteoclast formation from monocyte and IL-6 production by FLS in vitro. Present study suggests that CB_2-specific agonist could be new therapy for RA by inhibiting osteoclast differentiation and cytokine production.

E. Stimulation with CCL18 enhanced production of IL-6, MCP-1 and MMP-3 by fibroblast-like synoviocytes from patients with rheumatoid arthritis

CCL18 is a chemokine expressed by dendritic cells (DCs) and monocytes/macrophages, and induces chemotactis for lymphocytes, monocytes and DCs. It was reported that CCL18 was abundantly expressed in synovial fluid from rheumatoid arthritis (RA) compared to osteoarthritis (OA). The aim of this study is to explore novel functions of CCL18 on RA. CCL18 was highly expressed in the RA synovial tissue compared to OA. CCL18 was expressed on macrophages, endothelial cells and fibroblast-like synoviocytes (FLSs) in the synovium. Stimulation with CCL18 increased production of IL-6, MCP-1 and MMP-3 from RA FLSs in vitro, which was blocked by pertussis toxin, a Gi-coupled receptor inhibitor. Moreover, CCL18 induced phosphorylation of Akt and ERK1/2 of FLSs. Next, we analyzed the expression of PITPNM3, a functional receptor for CCL18. PITPNM3 was expressed on macrophages, DCs, B cells and FLSs in the RA synovial tissue. PITPNM3 was also expressed in vitro cultured FLSs. These results suggest that CCL18 might play an important role on FLS stimulation in the RA synovium, probably via PITPNM3 with phosphorylation of Akt and ERK1/2. Interaction with CCL18 and PITPNM3 could be a new therapeutic target for RA.

4）本事業に関連して世界的な研究拠点形成に向けて、以下の点で改善・整備等されたこと

A.（研究拠点体制）

当GCOEの中の研究者相互の交流が密になった。

B.（教育研究環境）

その結果、協同研究がやりやすくなった。

C.（人材育成）

研究に専念できるポストの提供が可能となった。

D.（国際化）

英語での講義プレゼン、質疑応答によって、研究者の英語へのアフィニティが強まった。

5）英文原著論文

1. ◎Nakashioya H, Nakano K, Watanabe N, Miyasaka N, Matsushita S, Kohsaka H. Therapeutic effect of D1-like dopamine receptor antagonist on collagen- induced arthritis of mice. Mod Rheumatol 21（3）：260-266, 2011.
2. ◎Toyomoto M, Ishido S, Miyasaka N, Sugimoto H, Kohsaka H. Anti-arthritic effect of E3 ubiquitin ligase, c-MIR, expression in the joints. Int Immunol 23（3）, 177-183, 2011.
3. ◎Okiyama N, Kitajima T, Ito Y, Yokozeki H, Miyasaka N, Kohsaka H. Addition of the collagen binding domain of fibronectin potentiates the biochemical availability of hepatocyte growth factor for cutaneous wound healing J Dermatol Sci 61（3）, 215-217, 2011
4. Honne K, Kohsaka H, Kaneko H, Komano Y, Nakanishi S, Kitagawa M, Miyasaka N. A case of Behçet's disease with widespread perforating enteric ulcers preceded by a long history of peripheral gangrene. Mod Rheumatol 21（6）：651-654, 2011
6. ◎Kaneko K, Miyabe Y, Takayasu A, Fukuda S, Miyabe C, Ebisawa M, Yokoyama W, Watanabe K, Imai T, Muramoto K, Terashima Y, Sugihara T, Matsushima K, Miyasaka N, Nanki T. Chemerin Activates Fibroblast-like Synoviocytes in Patients with Rheumatoid Arthritis. Arthritis Res Ther 13（5）：R158, 2011
7. Sakai R, Komano Y, Tanaka M, Nanki T, Koike R, Nakajima A, Atsumi T, Tanaka Y, Saito K, Toma S, Fujii T, Ihata A, Tamura N, Kawakami A, Sugihara T, Ito S, Miyasaka N, Harigai M, for the REAL Study Group. The REAL database reveals no significant risk for serious infection during treatment with methotrexate over 8 mg/week in patients with rheumatoid arthritis. Mod Rheumatol 21（4）：444, 2011
8. Nonomura Y, Miyabe Y, Tanaka M, Tsubata R, Nanki T, Harigai M, Miyasaka N. Prominent splenic microcalcifications in a patient with systemic lupus erythematosus complicated by antiphospholipid syndrome. J Clin Rheumatol 17（5）：288, 2011
9. Komano Y, Tanaka M, Nanki T, Koike R, Sakai R, Kameda H, Nakajima A, Saito K, Takeno M, Atsumi T, Tohma S, Ito S, Tamura N, Fujii T, Sawada T, Ida H, Hashiramoto A, Koike T, Ishigatsubo Y, Eguchi K, Tanaka Y, Takeuchi T, Miyasaka N, Harigai M, for the REAL Study Group. Incidence and risk factors for serious infection in patients with rheumatoid arthritis treated with tumor necrosis factor inhibitors：a report from the Registry of Japanese Rheumatoid Arthritis Patients for Longterm Safety. J Rheumatol 38（7）：1258, 2011
10. ◎Koike R, Tanaka M, Komano Y, Sakai F, Sugiyama H, Nanki T, Ide H, Jodo S, Katayama K, Matsushima H, Miwa Y, Morita K, Nakashima H, Nakamura H, Natsumeda M, Sato Y, Semba S, Tateishi M, Miyasaka N, Harigai M. Tacrolimus-induced pulmonary injury in rheumatoid arthritis patients. Pulm Pharmacol Ther 24（4）：401, 2011
11. Yamazaki H, Nanki T, Miyasaka N, Harigai M. Methotrexate and trimethoprim-sulfamethoxazole for pneumocystis pneumonia prophylaxis. J Rheumatol 38（4）：777, 2011
12. Koike T, Harigai M, Inokuma S, Ishiguro N, Ryu J, Takeuchi T, Tanaka Y, Yamanaka H, Fujii K, Yoshinaga T, Freundlich B, Suzukawa M. Postmarketing surveillance of safety and effectiveness of etanercept in Japanese patients with rheumatoid arthritis. Mod Rheumatol. 21（4）：343-51, 2011
13. Tanaka Y, Harigai M, Takeuchi T, Yamanaka H, Ishiguro N, Yamamoto K, Miyasaka N, Koike T, Kanazawa M, Oba T, Yoshinari T, Baker D, and the GO-FORTH Study Group. Golimumab in combination with methotrexate in Japanese patients with active rheumatoid arthritis：results of the GO-FORTH study. Ann Rheum Dis.
14. Koike T, Harigai M, Inokuma S, Ishiguro N, Ryu J, Takeuchi T, Takei S, Tanaka Y, Ito K, Yamanaka H.Postmarketing surveillance of tocilizumab for rheumatoid arthritis in Japan：interim analysis of 3881 patients. Ann Rheum Dis. 70（12）：2148-51, 2011.
15. Hashimoto J, Garnero P, van der Heijde D, Miyasaka N, Yamamoto K, Kawai S, Takeuchi T, Yoshikawa H, Nishimoto N. Humanized anti-interleukin-6-receptor antibody（tocilizumab）monothearapy is more effective in slowing radiographic progression in patients with rheumatoid arthritis at high baseline risk for structural damage evaluated with levels of biomarkers, radiography, and BMI：data from the SAMURAI study. Mod. Rheumatol. 21（1）：10-15, 2011
16. Takenaka K, Takada K, Kobayashi D, Moriguchi M, Harigai M, Miyasaka N. A case of IgG4-related disease with features of Mikulicz' s disease, and retroperitoneal fibrosis and lymphadenopathy mimicking Castleman's

disease. Mod. Rheumatol. 21（4）：410-414, 2011
17. Kawai S, Takeuchi T, Yamamoto K, Tanaka Y, Miyasaka N. Efficacy and safety of additional use of tacrolimus in patients with early rheumatoid arthritis with inadequate response to DMARDs —a multicenter, double-blind, parallel-group trial. Mod. Rheumatol. 21（5）：458-468, 2011
18. Takeuchi T, Miyasaka N, Tatsuki Y, Yano T, Yoshinari T, Abe T, Koike T. Baseline tumour necrosis factor alpha levels predict the necessity for dose escalation of infliximab therapy in patients with rheumatoid arthritis. Ann. Rheum. Dis. 70（7）：1208-1215, 2011
19. Miyasaka N, Hara M, Koike T, Saito E, Yamada M, Tanaka Y; Additional Members of the GB-0998 Study Group. Effects of intravenous immunoglobulin therapy in Japanese patients with polymyositis and dermatomyositis resistant to corticosteroids：a randomized double-blind placebo-controlled trial. Mod. Rheumatol. 2011 Oct5.[Epub ahead of print]
20. Kobayashi S, Harigai M, Mozaffarian N, Pangan AL, Sharma S, Brown LS, Miyasaka N. A multicenter, open-label, efficacy, pharmacokinetic, and safety study of adalimumab in Japanese patients with ankylosing spondylitis. Mod. Rheumatol. 2011 Dec29 [Epub ahead of print]
21. ◎Komano Y, Yagi N, Onoue I, Kaneko K, Miyasaka N, Nanki T. Arthritic joint-targeting small interfering RNA-encapsulated liposome：Implication for treatment strategy for rheumatoid arthritis. J Pharmacol Exp Ther 340（1）：109, 2012
22. Harigai M, Tanaka Y, Maisawa S. Safety and Efficiency of Various Dosages of Ocrelizumab in Japanese Rheumatoid Arthritis Patients with an Inadequate Response to Methotrexate Therapy：A Placebo-controlled, Double-blind, Parallel-group Study. J. Rheumatol. in press.
23. Koike T, Harigai M, Inokuma S, Ishiguro N, Ryu J, Takeuchi T, Tanaka Y, Yamanaka H, Fujii K, Yoshinaga T, Freundlich B, Suzukawa M. Safety and effectiveness of switching from infliximab to etanercept in patients with rheumatoid arthritis：results from a large Japanese postmarketing surveillance study. Rheumatol Int. in press.
24. Koike T, Harigai M, Inokuma S, Ishiguro N, Ryu J, Takeuchi T, Tanaka Y, Yamanaka H, Fujii K, Yoshinaga T, Freundlich B, Suzukawa M. Safety and effectiveness responses to etanercept for rheumatoid arthritis in Japan：a sub-analysis of a post-marketing surveillance study focusing on the duration of rheumatoid arthritis. Rheumatol Int. in press.
25. Koike T, Harigai M, Ishiguro N, Inokuma S, Takei S, Takeuchi T, Yamanaka H, Tanaka Y.Safety and effectiveness of adalimumab in Japanese rheumatoid arthritis patients：postmarketing surveillance report of the first 3,000 patients. Mod Rheumatol. In press
26. ◎Harigai M, Takeuchi T, Tanaka Y, Matsubara T, Yamanaka H, Miyasaka N, for the BRIGHT study investigators group. Discontinuation of adalimumab treatment in rheumatoid arthritis patients after achieving low disease activity. Mod Rheumatol. In press

6）総説ならびに著書

1. 杉原毅彦、上阪　等　多発性筋炎モデルの治療法開発における有用性　リウマチ科　45（2）; 158-163. 2011
2. 豊本雅康、上阪　等　ユビクチンリガーゼによる炎症性サイトカインの産生抑制　臨床免疫・アレルギー科　55（2）：160-166,2011
3. 上阪　等　CD28　最新医学 66（2）, 252-257, 2011
4. 上阪　等　膠原病の新しい風　内科　107（4）, 562-564, 2011
5. 上阪　等、Peter Shane、亀田秀人、渥美達也　膠原病診療の現在と未来 –ステロイド・ファーストからステロイド・フリーへ–　107（4）, 687-699, 2011
6. 上阪　等　多発性筋炎と皮膚筋炎　ドクターサロン　55（4）, 294-297, 2011
7. 上阪　等　三科の診る多発性筋炎・皮膚筋炎　医学のあゆみ　239（1）1-5, 2011
8. 上阪　等　ここまでわかった自己免疫疾患　多発性筋炎/皮膚筋炎　臨床検査　55（11）, 1150-1155, 2011
9. 上阪　等　生物学的製剤　T細胞活性化阻害薬　日本内科学会雑誌100（10）, 2979-2984, 2011
10. 上阪　等 炎症性筋疾患の病態と治療「序」 炎症と免疫 20（1）, 32-33, 2011
11. 木村直樹、上阪　等　多発性筋炎モデル動物による病態解析　炎症と免疫20（1）, 56-63, 2011
12. 溝口史高. 関節リウマチにおけるmicroRNAの役割 .リウマチ科, 46（5）, 575-580, 2011.
13. 南木敏宏。関節リウマチにおけるマクロファージの役割。リウマチ科。44（1）：100-104、2010。科学評論社。
14. 松島綱治、横地祥司、上羽悟史、南木敏宏.関節リウマチ（第2版）-寛解を目指す治療の新時代-、関節リウマチの成因と病態生理、炎症メディエーター、主なサイトカイン、インターロイキン8ファミリー、ケモカイン。日本臨牀 増刊号p123-132、2010。日本臨牀社。

15. 南木敏宏。製剤ごとの感染症とその頻度について教えて下さい。ファーマナビゲーターリウマチ～生物学的製剤編～。竹内勤編。p128-131、2010。メディカル・レビュー社。
16. 針谷正祥：日本の生物学的製剤使用ガイドライン（特集 世界のリウマチガイドラインをみわたす）。分子リウマチ治療4（2）：27（77）-30（80）,2011.
17. 針谷正祥：日常臨床とファーマコビジランス（薬害監視）（特集　全身性疾患と腎障害）。綜合臨床60（6）：1451-1452,2011.6
18. 針谷正祥：治療目標-目標達成に向けた治療（Treat to Target）のエビデンスと実際。別冊・医学のあゆみ（関節リウマチ”治癒をめざす”最新治療コンセンサス）：14-19,2011.
19. 針谷正祥、野々村美紀、酒井良子：REALコホートにおける検証。（特集2010関節リウマチ新分類基準を検証する）。分子リウマチ治療、先端医学社4（4）：15-18（193-196）,2011.
20. 渡部香織、針谷正祥：関節リウマチ患者が妊娠した場合に生物学的製剤は継続すべきか中止すべきか?（特集）内科診療における論点。内科107（6）：1411-1416,2011.6
21. 山村昌弘、佐田憲映、針谷正祥、藤井隆夫、有村義宏、槇野博史：RemIT-JAV研究：わが国のANCA関連血管炎の診察実態の把握を目指して。脈管学51（1）：79-85,2011.
22. 萩山裕之、針谷正祥：抗体療法の副作用対策。医学のあゆみ238（6）637-642,2011.8.
23. 長坂憲治、針谷正祥：生物学的製剤の利点と欠点（特集 ここまでわかった自己免疫疾患）。臨床検査（増刊号）、医学書院55（11）：1349-1358,2011.10.
24. 山崎隼人、針谷正祥：エタネルセプトは週1回投与が可能。（特集：生物学的製剤時代の関節リウマチ最新治療戦略）、Mebio（Graphic Medical Magazine）、メディカルビュー29（1）：47-53,2012.
25. アメリカリウマチ学会（ACR）/ヨーロッパリウマチ学会（EULAR）合同関節リウマチ分類基準の考え方.宮坂信之　成人病と生活習慣病　41（1）：28-32, 2011
26. 関節炎の鑑別診断.宮坂信之　日本内科学会雑誌「関節炎の鑑別：診断と治療の進歩　99（10）：1-3,2010
27. 巻頭言ここまでわかった自己免疫疾患.宮坂信之　臨床検査　55（11）：1044-1045, 2011
28. 関節リウマチ治療における光と影.宮坂信之　日本医事新報プラタナス
29. 関節リウマチの治療は変わった！　宮坂信之　週刊朝日臨時増刊号「新名医の再診治療　完全読本」
30. 関節リウマチの治癒は可能か？　宮坂信之　内科109（4）：
31. ステロイド療法の実際—関節リウマチ—.高村聡人、宮坂信之 「臨床と研究」 88（1）：6-10,2011
32. パンヌス形成における cadherin 11 の役割.金子佳代子、宮坂信之　　リウマチ科44（5）：601-606, 2011
33. 全身性エリテマトーデス.宮坂信之 「Guideline　膠原病・リウマチ」小池隆夫、住田孝之編
34. 免疫グロブリン製剤の適応疾患と治療.宮坂信之 「静注免疫グロブリン製剤ハンドブック」正岡　徹監修
35. 針谷正祥：多発性筋炎・皮膚筋炎。薬局増刊号病気と薬パーフェクトBook 2011、南山堂62（4）：850-852、2011.
36. 針谷正祥：Ⅵ.生物学的製剤のリスクマネジメントとインフォームドコンセントとは?。インフォームドコンセントのための図説シリーズ・関節リウマチ生物学的製剤の正しい使い方とは?、宮坂信之編、医薬ジャーナル社、66-73、2011.10

7）特許取得、特許申請

1. 国内　p21Cip1リウマチ治療剤 特許登録（2011/2/18）特許第4684512号

8）平成23年度までの自己評価

関節リウマチ、筋炎を初めとする膠原病・リウマチ内科疾患について、病態形成の分子機構の解明、新規治療法の開発に努めた。その過程を通じて、大学院生にこの研究分野の進歩に貢献させることができた。

9）学会発表（英文）

1. M.Tanaka, Y.Tanaka, M. Doi, et al. Life Prognosis of Patients with Pheumatic Diseases with Respiratory Involvements- A Retrospective, Multi-center Study of 887 Cases. 2011 Symposium of the Asia Pacific League of Associations for Rheumatology,示説, Taipei, 2011.04
2. Sakai R, Komano Y, Tanaka M, Nonomura Y, Nanki T, Koike R, Miyasaka N, Harigai M. Incidence and risk factors of serious infections in the long-term in patients with rheumatoid arthritis（RA）receiving tumor necrosis factor（TNF）antagonists using the REAL database in Japan.ヨーロッパリウマチ学会。Roma, Italy, 2010年6月。
3. Y. Tanaka, M. Harigai, T. Takeuchi, et al. Golimumab, a

human anti-TNF α monoclonal antibody administered subcutaneously every four weeks in patients with active rheumatoid arthritis despite methotrexate therapy：24-week results of clinical and radiographic assessments. The European League Against Rheumatism（EULAR）2011, 口頭, London, 2011.06

4. Y. Tanaka, M. Harigai, T. Takeuchi, et al. Golimumab, a human anti-TNF α monoclonal antibody administered subcutaneously every four weeks as monotherapy in patients with active rheumatoid arthritis despite DMARD therapy：24-week results of clinical and radiographic assessments. The European League Against Rheumatism（EULAR）2011, 口頭, London, 2011.06
5. T. Takeuchi, M. Harigai, S. Inokuma, et al. Postmarketing surveillance of tocilizumab for rheumatoid arthritis I Japan interim analysis of 6424 patients –poster tours. The European League Against Rheumatism（EULAR）2011, 示説, London, 2011.06
6. M. Harigai. Clinical characteristics of and risk factors for Pneumocystis jirovecii pneumonia in patients with rheumatoid arthritis receiving TNF antagonists. The European League Against Rheumatism（EULAR）2011, 示説, London, 2011.06
7. Kaneko K, Watanabe K, Miyasaka N, Nanki T. Chemerin and ChemR23 Expression in Rheumatoid Arthritis：The Therapeutic Implication of the Pathway. 第14回国際免疫学会。神戸、2010年8月。
8. Morio T, Terada N, Nanki T, Miyasaka N, Kobata T, Matsumoto K, Azuma M, Mizutani S. Impaired CD4 and CD8 Effector Function and Decreased Memory T-cell Populations in ICOS-deficient Patients. 第14回国際免疫学会。神戸、2010年8月。
9. Mizoguchi F, Miyasaka N, Kohsaka H. MiRNA-31 Controls Osteoclast Formation and Bone Resorption by Targeting RhoA. The 4th East Asian Group of Rheumatology. Tokyo. 2011年10月15日.口頭発表
10. M. Harigai, T. Nanki, R. Koike, et al. Biological agents in rheumatoid arthritis and risk of malignancy -results from the nation-wide cohort study in Japan, アメリカリウマチ学会、示説, Chicago, 2011.11
11. F Mizoguchi , H Kohsaka , N Miyasaka,MiRNA-31 Controls Osteoclast by Targeting RhoA.Keystone symposia.Rheumatoid Arthritis：Molecular and Clinical Insights（A4）,Santa Fe, USA.2012年1月19-24日.口頭発表
12. H Iwai , T Hosoya , H Kohsaka , N Miyasaka , Y Murakami,Identification of the TREM-1 ligand as a therapeutic target of arthritis,Keystone symposia. Rheumatoid Arthritis：Molecular and Clinical Insights（A4）,Santa fe, USA.2012年1月19-24日.口頭発表

10）学会発表（和文）

1. 針谷正祥、南木敏宏、田中みち、酒井良子、野々村美紀、駒野有希子、小池竜司、宮坂信之。生物学的製剤使用日本人関節リウマチ患者における発癌リスクの検討-SECURE研究。第54回日本リウマチ学会総会。神戸、2010年4月。
2. 酒井良子、駒野有希子、田中みち、野々村美紀、南木敏宏、小池竜司、宮坂信之、針谷正祥。REALを用いた関節リウマチ患者における生物学的製剤の長期完全性に関する検討。第54回日本リウマチ学会総会。神戸、2010年4月。
3. 野々村美紀、酒井良子、田中みち、南木敏宏、小池竜司、宮坂信之、針谷正祥。REALデータベースからみた2009ACR/EULAR RA分類基準（2009ACR/EULAR）の検証。第54回日本リウマチ学会総会。神戸、2010年4月。
4. 横山和佳、野々村美紀、河野宏、溝口史高、南木敏宏、針谷正祥、宮坂信之、濱田啓一、中久木康一、天笠光雄。結節性紅斑を合併した下顎骨原発の無菌性骨髄炎の一例。関東リウマチ。東京、2010年6月。
5. 酒井良子、駒野有希子、田中みち、野々村美紀、南木敏宏、小池竜司、宮坂信之、針谷正祥。REALを用いた関節リウマチ患者における生物学的製剤の長期安全性に関する検討。第31回日本炎症・再生医学会。東京、2010年8月。
6. Fumitaka Mizoguchi, Nobuyuki Miyasaka, Hitoshi Kohsaka miR-3 1 contributes to bone resorption by osteoclasts　第55回日本リウマチ学会学術集会　神戸　2011年7月17-20日（ポスター発表）
7. Shinya Hirata, Naoki Kimura, Nobuyuki Miyasaka and Hitoshi Kohsaka Chemokines expressed by the regenerating muscle cells in murine myositis model. 第55回日本リウマチ学会学術集会　神戸　2011年7月17-20日（ポスター発表）
8. 竹内勤、針谷正祥、田中良哉、他.DMARD治療抵抗性関節リウマチに対するゴリムマブ（GLM：ヒト抗TNF αモノクローナル抗体）　単剤療法;52週までの有効性・安全性の解析結果.第55回日本リウマチ学会総会・学術集会第20回国際リウマチシンポジウム、口頭、神戸、2011.07
9. 田中良哉、針谷正祥、竹内　勤、他.MTX治療抵抗性関節リウマチに対するゴリムマブ（GLM：ヒト抗TNF αモノクローナル抗体）MTX併用療法：52週までの有効性・安全性の解析結果.第55回日本リウ

マチ学会総会・学術集会第20回国際リウマチシンポジウム、 口頭、神戸、2011.07

10. 田中良哉、針谷正祥.MTX抵抗性RA患者を対象としたヒト化抗CD20抗体オクレリズマブの用量反応性試験.第55回日本リウマチ学会総会・学術集会第20回国際リウマチシンポジウム、 口頭、神戸、2011.07
11. 山崎隼人、酒井良子、渡部香織、他.REALデータベースにおけるACR/EULAR新RA寛解基準の検討.第55回日本リウマチ学会総会・学術集会第20回国際リウマチシンポジウム、 口頭、神戸、2011.07
12. 田中みち、酒井良子、駒野有希子、他.リウマチ性疾患の肺合併症の診断および治療法に関する後ろ向き研究.第55回日本リウマチ学会総会・学術集会第20回国際リウマチシンポジウム、 口頭、神戸、2011.07
13. 土屋尚之、伊東郁恵、古川宏、他.日本人集団におけるANCA関連血管炎BLKとの関連.第55回日本リウマチ学会総会・学術集会第20回国際リウマチシンポジウム、 口頭、神戸、2011.07
14. 渡部香織、小池竜司、酒井良子、他.アダリムマブ使用関節リウマチ患者におけるニューモシスチス肺炎.第39回日本臨床免疫学会、示説、東京、2011.09
15. 加勢優子、久保佳史、柏原純一、結城隆、藤井明啓、中江孝、宮坂信之、上阪等　免疫グロブリン製剤によるCタンパク誘導性筋炎の抑制とT細胞活性化に及ぼす影響　第23回日本神経免疫学会　平成23年9月15-17日　東京（口頭発表）
16. 上阪　等、木村直樹、沖山奈緒子、宮坂信之　多発性筋炎における抗サイトカイン治療の標的－Seed and Soil Model－　第39回日本臨床免疫学会　平成23年9月15-17日　東京（口頭発表）
17. 岩井秀之、細矢　匡、村上洋介、宮坂信之、上阪等　TREM-1リガンドの同定とモノクローナル抗体による新規関節炎治療法の開発　第39回日本臨床免疫学会　平成23年9月15-17日　東京（ポスター発表）
18. 溝口史高、宮坂信之、上阪　等　miR-31はRhoAを標的とし細胞骨格を制御することにより破骨細胞機能を調節する　第39回日本臨床免疫学会　平成23年9月15-17日　東京（ポスター発表）
19. 中里洋子、溝口史高、針谷正祥、上阪　等、宮坂信之、側頭動脈病変を呈した顕微鏡的多発血管炎の三症例　第39回日本臨床免疫学会　平成23年9月15-17日　東京（ポスター発表）
20. 横田 雅也、鈴木 浩太郎、中込 大樹、岩田 有史、常世田 好司、中山 俊憲、上阪 等、中島 裕史　多発性筋炎マウスモデルにおける肥満細胞の役割の解析　第40回日本免疫学会学術集会　平成23年11月27-29日　幕張（ポスター発表）
21. HARADA Masaya、KAMIMURA Daisuke、OKUYAMAYuko、NAKATSUJI Yuji、KOHSAKA Hitoshi、MIYASAKA Nobuyuki、HIRANO Toshio、MURAKAMI Masaaki Enhancement of IL-6 amplifier activation by a soluble factor, SFX, which accelerates the development of autoimmune diseases　第40回日本免疫学会学術集会　平成23年11月27-29日　幕張（口頭発表）
22. 岩井秀之、細矢　匡、村上洋介、宮坂信之、上阪等　関節炎治療標的としてのB細胞上のTREM-1リガンドの同定　第40回日本免疫学会学術集会　平成23年11月27-29日　幕張（口頭発表）

11）受賞

1. 溝口史高.第55回日本リウマチ学会総会・学術集会.ポスター賞。神戸.2011年7月18日
2. 溝口史高.第39回日本臨床免疫学会総会・学術集会.優秀演題賞。東京.2011年9月17日
3. 岩井秀之.第39回日本臨床免疫学会総会・学術集会.優秀演題賞。東京.2011年9月17日
4. 岩井秀之.The 4th East Asian Group of Rheumatology. Young Investigator award Tokyo. 2011年10月15日.
5. 平田真哉　.第39回日本臨床免疫学会総会・学術集会.優秀演題賞。東京.2011年9月17日

12）外部資金の獲得状況

【上阪　等】

1. 文部科学省科学研究費補助金　基盤A
   研究題目：　新しいメカニズムによる次世代抗リウマチ療法の開発
   代表：上阪　等
   期間：　平成21年－平成23年
   研究費総額：7,800万円
2. 文部科学省科学研究費補助金　挑戦的萌芽研究
   研究題目：　炎症性疾患克服に向けた線維芽細胞病理学開拓への挑戦
   代表：上阪　等
   期間：　平成23年
   研究費総額：3,000万円
3. 戦略的創造研究推進事業CRES

慢性炎症に伴う臓器線維化の分子・細胞基盤[研究代表：松島綱治]
主たる共同研究者：上阪　等
8,000千円

4. 二国間交流事業　韓国との共同研究
新規治療法開発に向けた多発性筋炎にかかわるサイトカインの研究
代表：上阪　等
400千円

5. 二国間交流事業　韓国との共同研究
多発性筋炎の治療標的としての自然免疫細胞の研究
代表：上阪　等
800千円

6. 厚生労働科学研究費補助金（難治性疾患克服研究事業）
自己免疫疾患に関する調査研究[主任研究者：住田孝之]
多発性筋炎・皮膚筋炎分科会長：上阪　等
6,000千円

7. 共同研究
多発性筋炎・皮膚筋炎などの難病に対する人免疫グロブリン療法の作用機序の解明
担当：上阪　等
1,000千円

8. 共同研究
マウス筋炎モデル（CIMモデル）を用いた薬効評価研究
担当：上阪　等
2,620千円

9. 共同研究
関節リウマチ滑膜細胞及び血清の細胞周期調整因子、細胞活性化因子、細胞遊走因子、細胞成長因子の解析
担当：上阪　等
1,000千円

10. 共同研究
TREM1リガンドの創薬可能性評価
担当：上阪　等
420千円

【溝口史高】

1. 平成23年度金原一郎記念医学医療振興財団　第26回基礎医学医療研究助成金
関節リウマチにおける病的滑膜線維芽細胞の起源の同定と新規治療法開発の検討
代表：溝口史高
400千円

2. 2011年イーライリリー研究助成
骨代謝におけるmicroRNAの働きの解明と治療応用の検討
代表：溝口史高
1,000千円

【岩井秀之】

1. 文部科学省科学研究費　若手研究（B）
新規細胞表面分子TREM1リガンド及び細胞周期阻害による新規関節炎治療法の開発
岩井秀之
800千円

2. GCOE競争的研究費
新規細胞表面分子TREM-1-TREM-1リガンド修飾及び細胞周期阻害剤による新規関節炎治療法の開発
岩井秀之
1,000千円

3. 日本リウマチ財団奨学寄付金
新規細胞表面分子TREM1リガンド及び細胞周期阻害による新規関節炎治療法の開発
岩井秀之
1,000千円

【針谷正祥】

1. 文部科学省科学研究費基盤研究（C）〈一般〉（H23～H25）
生物学的製剤及び分子標的薬投与下の重篤感染症、日和見感染症に関する薬剤疫学的研究
針谷正祥
100千円

2. 厚生労働科学研究費補助金・免疫アレルギー疾患等予防・治療研究事業・平成22年度-24年度
関節リウマチに対する生物学的製剤の作用機序、投与方法、治療効果等に関する研究（竹内　勤）
針谷正祥
2,000千円

3. 厚生労働科学研究費補助金・免疫アレルギー疾患等予防・治療研究事業・平成23年度-25年度
我が国における関節リウマチ治療の標準化に関する多層的研究（宮坂信之）
針谷正祥
1,500千円

4. 厚生労働科学研究費補助金（難治性疾患克服研究事業）平成23年度-25年度
難治性血管炎に関する調査研究
針谷正祥

920千円

【南木敏宏】

1. 科学研究費補助金、基盤研究C
   研究題目：フラクタルカイン阻害による血管炎症候群に対する新規治療法の開発
   代表：南木敏宏
   期間：平成20年-平成22年度
   研究費総額：468万円
2. 科学研究費補助金、基盤研究B
   研究題目：関節リウマチにおける生物学的製剤の長期安全性と副作用リスク因子に関する疫学研究
   分担：南木敏宏（代表：針谷正祥）
   期間：平成21年-平成22年度
   研究費総額：65万円
3. （財）武田科学振興財団、医学系研究奨励
   研究題目：脂質メディエーターを標的とした関節リウマチの新規治療の開発
   代表：南木敏宏
   期間：平成22年度
   研究費総額：300万円
4. エーザイ（株）との共同研究
   研究題目：ケモカイン・接着分子等の関節リウマチなどの自己免疫疾患における役割の研究
   代表：南木敏宏
   期間：平成17年-平成22年度
   研究費総額：600万円

【宮坂信之】

1. 免疫アレルギー疾患等予防・治療研究事業　指定研究「我が国における関節リウマチ治療の標準化に関する多層的研究」研究代表者
   39,000千円
2. 免疫アレルギー疾患等予防・治療研究事業「関節リウマチの関節破壊の解明と関節破壊ゼロを目指す治療指針の確立に関する研究」研究分担者
   2,000千円
3. 治験推進事業「多発性筋炎・皮膚筋炎に合併する間質性肺炎に対するタクロリムスの臨床試験」の調整・管理に関する研究　研究代表者
   16,814千円

13）特別講演、招待講演、シンポジウム

1. 上阪　等　自己免疫疾患と抗サイトカイン療法　北関東甲信越タクロリムス関節リウマチ治療講演会　平成23年2月5日　東京
2. 宮坂信之：「生物学的製剤の有効性と安全性を最大限に発揮するためには?」第4回埼玉Biologics研究会　平成23年5月7日　埼玉
3. 針谷正祥　医師主導臨床研究を成功させるために.第23回日本アレルギー学会春季臨床大会、2011.05、幕張
4. 宮坂信之：「リウマチ治療における生物学的製剤の使い分け」第25回城南リウマチ会　平成23年6月4日　東京
5. 上阪　等　関節リウマチの新しい治療　名古屋市立大学膠原病内科セミナー　平成23年6月4日　名古屋
6. 宮坂信之：「関節リウマチ治療にみられたパラダイムシフトとは－分子標的療法の光と影」第54回日本腎臓学会学術総会　教育講演　平成23年6月15日　横浜
7. 宮坂信之：「リウマチ診療のABC」土浦協同病院・OB合同セミナー　平成23年6月22日　土浦
8. 針谷正祥 T2T Initiativeの背景と日本における展開に向けて.香川GOAL研究会　関節リウマチにおける Treat to Target（T2T）.2011.06、香川
9. 宮坂信之：「関節リウマチの治療はこう変わった」第1回市民公開講座　平成23年7月2日　静岡
10. 上阪 等、細矢 匡、岩井 秀之、宮坂 信之　関節リウマチのサイクリン依存症キナーゼ4/6阻害療法　第55回日本リウマチ学会学術集会　神戸　2011年7月17-20日
11. 宮坂信之：「自己免疫疾患－その病態解明と治療の進歩」第35回阿蘇シンポジウム　平成23年7月29日　阿蘇
12. 針谷正祥 T2T Initiativeの背景と日本における展開に向けて.神奈川GOAL研究会　運営検討会.2011.07、横浜
13. 針谷正祥 生物学的製剤のリスク評価とその対応.第20回札幌臨床免疫アレルギーの集い、2011.07、札幌
14. 針谷正祥 T2T Initiativeの背景と日本における展開に向けて.徳島GOAL研究会　関節リウマチにおける Treat to Target（T2T）.2011.07、徳島
15. 針谷正祥 国内5コホートを用いた2010ACR/EULAR RA新分類基準検証結果のまとめ.第55回日本リウマチ学会総会・学術集会.2011.07、神戸
16. 針谷正祥 内科的立場から見たRA患者周術期の薬物治療管理.第55回日本リウマチ学会総会・学術集会.2011.07、神戸
17. 針谷正祥 MTXの副作用に対する対策-開始時、使用時の注意点と副作用発生時の対処法-.第55回日本リウマチ学会総会・学術集会.2011.07、神戸
18. 針谷正祥　ヒュミラ全例調査結果報告　-安全性の観点から-.HUMIRA National Symposium 2011、2011.07、京都
19. 宮坂信之：「関節リウマチ治療における生物学的製剤

の有用性について」生物学的製剤クリニカルアップデートミーティング　平成23年9月3日　東京
20. 上阪　等　膠原病内科医が診た多発性筋炎・皮膚筋炎　第73回　金沢皮膚研究会学術講演　平成23年9月12日　金沢
21. 上阪　等、細矢　匡、岩井秀之、村上洋介、宮坂信之　リウマチ治療の新戦略を求めて　第39回日本臨床免疫学会　2011年9月15-17日　東京
22. 上阪　等　多発性筋炎・皮膚筋炎の病態生理とその治療　第23回　日本神経免疫学会学術集会　平成23年9月15-17日　東京
23. 上阪　等、杉原毅彦、沖山奈緒子、宮坂信之　膠原病内科医の診る筋炎：免疫動態からのアプローチ　第23回　日本神経免疫学会学術集会　平成23年9月15-17日　東京
24. 上阪　等　関節リウマチ治療の現在とこれからの治療標的　技術情報協会講演会　平成23年9月27日　東京
25. 針谷正祥　抗リウマチ薬のリスクマネージメント.第3回川崎南部リウマチUp Date 研究会、2011.09、川崎
26. 上阪　等　膠原病とT細胞　–多発性筋炎・皮膚筋炎のSeeds and Soilモデル–　第63回日本皮膚科学会西部支部学術大会　平成23年10月8-9日　沖縄
27. 宮坂信之：「ここまで進んだリウマチ治療」第5回二豊リウマチフォーラム　平成23年10月15日　大分
28. Hideyuki Iwai, Tadashi Hosoya, Yousuke Murakami, Nobuyuki Miyasaka, Hitoshi Kohsaka Identification of the TREM-1 ligand as a therapeutic target of arthritis. 4th East Asian Group of Rheumatology Meeting October 15, 2011, Tokyo
29. 上阪　等　多発性筋炎・皮膚筋炎の基礎と臨床　Meet the Expert 平成23年10月21日　富山
30. 針谷正祥　関節リウマチの診断と治療の進歩.第1回さいたまRA治療戦略セミナー、2011.10、さいたま市
31. 上阪　等　進歩の激流にある膠原病治療　第5回川島腎糸球体カンファレンス　平成23年11月19-20日　各務原
32. 針谷正祥　関節リウマチにおける生物学的製剤の薬剤疫学.薬剤疫学セミナー、2011.11、東京
33. 針谷正祥　関節リウマチ分類基準の進歩（関節リウマチの診療の革新的進歩）.第61回日本アレルギー学会秋季学術集会、2011.11、東京
34. 針谷正祥　リウマチ治療　知っておきたい最新情報（特別講演）.第7回常陸リウマチ治療研究会　市民公開講座、2011.11、水戸
35. 針谷正祥　関節リウマチの診断と治療の新潮流.茂原市長生郡医師会　学術講演会.2011.11、茂原
36. 宮坂信之：「高用量MTX時代を迎えて－その対策とは？－」第65回北九州・筑豊リウマチ懇話会　平成23年11月24日　北九州
37. 宮坂信之：「関節リウマチ治療における抗TNF療法の有用性について」Biologics Users Forum on RA～抗TNF療法の最適化を目指して～　平成23年12月18日　東京
38. 宮坂信之：「リウマチ・アレルギー疾患について、その正しい情報の普及を図る」平成23年度リウマチ・アレルギー相談員養成研修会　平成23年12月20日　東京
39. 針谷正祥　リウマチ医から見た肺疾患を有する関節リウマチ患者の治療.第26回日本臨床リウマチ学会.2011.12、横浜
40. 宮坂信之：「MTX高用量時代を迎えたリウマチ治療」第9回リウマチとTNF-α北海道フォーラム　平成24年1月21日　札幌
41. Hitoshi Kohsaka Lessons from a new animal model of polymyositis Autoimmunity Congress Asia November 17-19, 2012 Singapore

14）教室、分野や講座の准教授、講師、助教、特別研究員、ポスドク、指導を受けた大学院生の名前

准教授　　上阪　　等
GCOE特任講師：岩井　秀之
助　教　　溝口　史高
助　教　　高村　聡人
助　教　　長谷川　久紀
薬害監視学講座
准教授　　南木　敏宏
助　教　　田中　みち
　　渡部　香織
大学院生　酒井　良子
　　○宮部　斉重
　　細矢　　匡
　　木村　直樹
　　福田　　真
　　○鈴木　晶子
　　松尾　祐介
　　横山　和佳
　　中里　洋子
　　山崎　隼人

○はAISS

朝日新聞 2011年(平成23年)1月20日 木曜日 13版 生活 30

関節リウマチ すぐ診断

欧米の分類基準で早期治療

医療

関節に腫れや痛みが続く関節リウマチ＝。より早く治療を始めるために、診断（分類）基準が2009年に欧米で変わった。国内の臨床現場でも新しい基準を使う医師が増えており、日本リウマチ学会も近く基準を変更する。治療薬の開発が進み、早期に治療すれば症状を無くすこともできるようになってきた。（大岩ゆり）

関節リウマチ

自分の免疫の仕組みに異常が生じて起きる病気だが、詳しい原因はわかっていない。全身の関節に炎症が起こり、とくに手足の関節に起きやすい。患者は推計で約70万人。30～59歳が多く、女性の患者は男性の約3倍とされる。主な治療は抗リウマチ薬などによる薬物療法。より効果が高い生物学的製剤も次々と出ている。運動などリハビリテーションも大切。重症化して関節が変形した場合、人工関節を入れるなどの手術をすることも。

東京都内に住む会社員の男性(32)は昨年初め、左手の親指の腫れと痛みに悩まされるようになった。関節は倍近くに腫れ赤紫色になって熱を帯びた。仕事は装飾品の手作りのため、当初は「手を酷使しすぎたのかな」と思った。

2週間以上たっても親指の関節の腫れと痛みは治まらず、人さし指も腫れ、他の指の関節や手首も痛くなった。水道の蛇口をひねるのも一苦労。朝は手をついて起きると手首に激痛が走り、ひじを使わざるを得なくなった。

近所の外科を皮切りに、3カ所の診療所を受診。痛み止めや湿布、電気刺激によるリハビリも受けたが、症状は治まらなかった。親指の関節が腫れ始めてから半年以上たっていた。

男性は中学時代にけがで入院したことがある慶応大学病院の整形外科を受診。リウマチ内科に行くよう言われた。

リウマチ内科の竹内勤教授は手などの関節を診ながら、男性が腫れを自覚していた関節以外についても次々と腫れがあると指摘。男性は関節リウマチと診断され、抗リウマチ薬のリウマトレックス（一般名メトトレキサート）の服用を始めた。

これ以前に診療所で受けた血液検査でリウマチの疑いは否定されたことなどから、男性は当初、診断に半信半疑だった。が、薬を飲み始めて2週間もしないうちに親指の腫れがひき始め、診断に納得した。薬の服用から2カ月ほどすると、たまに痛みを感じるほかは症状は無くなった。

男性は慶応大学病院を受診する際、原因が何であれ重症に違いないと覚悟していた。しかし竹内さんから「まだ軽いうちに診断がついて良かったですね」と言われ、驚いた。

「2009年に欧米のリウマチ学会が作った新しい診断基準を使ったので、この男性の診断が早くつきました。従来の基準では、まだ診断できなかったと思います」と竹内さんは言う。

日本版 年内にも制定

1987年にできた従来の基準は、朝の関節のこわばりが1時間以上続くことや、3カ所以上の関節の腫れなど7項目のうち4項目以上が当てはまれば関節リウマチと診断する、としている。

会社員の男性の場合、当てはまるのは3項目だけで従来なら診断されなかった恐れがあった。

竹内さんが使った欧米の新基準＝チャート＝は、エックス線検査で滑膜炎（骨びらん）などの有無などを確かめる。そのうえで、腫れている関節の数や、リウマチの場合に血中に増えることが多い物質「抗CCP抗体」「CRP」などを調べ、該当する点数を合算する。

日本リウマチ学会理事長の宮坂信之東京医科歯科大学教授によると、従来の基準は患者約260人の症状を基に作られたが、リウマチを患う平均罹患期間は7・7年で症状は早期のものではなかった。このため早期診断しにくいという問題点があった。

リウマチ学会は昨春、「新基準検証小委員会」を作り、国内向けに新基準をどう導入するか検討中だ。委員長の竹内さんらが早期リウマチ患者の初診時データを従来基準と新基準で診断したところ、従来基準で診断できたのは半数程度だったのが、新基準では75％が診断できた。

ただ、竹内さんは「国内では、リウマチの専門医以外が最初に診察することが多い。このため、関節リウマチ以外の病気ではないかどうか鑑別する基準の最初のステップが一番の関門となると予想される」と指摘する。

小委ではリウマチと鑑別が難しい病気をリストアップする作業などを進めており、欧米の新基準に追加情報を加える形で、年内にも国内向けの新基準を発表する予定だ。

早期発見が強調されるようになったのは最近10年ほど。治療薬の選択肢が増え、早く治療を始めれば症状がほとんど無い「寛解」と呼ばれる状態になる患者も出ている。

「以前はいい薬が少なく、早期診断のメリットがあまりなかった。今は効くスピードも効果も格段に良くなった薬がそろい、早く治療を始めるメリットは大きい。少しでもリウマチを疑ったら専門医を受診して欲しい」と宮坂さんは強調する。リウマチを疑う最初の症状は「痛みを伴う関節の腫れ」という点は新基準も同じだという。

欧米の関節リウマチの新診断（分類）基準

関節の腫れがある
- はい → 関節リウマチ以外の病気ではない
- いいえ → 別の病気

関節リウマチ以外の病気ではない
- はい → エックス線検査でリウマチに典型的な骨びらん
- いいえ → 別の病気

エックス線検査でリウマチに典型的な骨びらん
- 関節リウマチ ← はい
- いいえ → 下記の症状に応じた点数の合計が6点以上

腫れている関節の数	
□ 大小関係なく1カ所	0点
□ 大きな関節が2カ所以上10カ所未満	1点
□ 小さな関節が1～3カ所	2点
□ 小さな関節が4～10カ所	3点
□ 大小関係なく11カ所以上	5点
血液検査（リウマトイド因子や抗CCP抗体の値）	
□ 両方とも陰性	0点
□ どちらかが正常値上限～3倍まで	2点
□ どちらかが正常値上限の3倍超	3点
症状の継続期間	
□ 6週間未満	0点
□ 6週間以上	1点
急性炎症たんぱく質検査（CRPまたは血沈検査）	
□ 正常	0点
□ 異常	1点

はい → 関節リウマチ　いいえ → 別の病気

The Asahi Shimbun

11 くらしナビ 統12版 2011年(平成23年)8月16日(火) 毎日新聞

関節リウマチ治療薬の投与量上限引き上げ 厚労省

厚生労働省はこのほど、関節リウマチの主要な治療薬「メトトレキサート」の週間投与量の上限を、8ミリグラムから16ミリグラムに倍増することを認めた。投与前の検査で副作用が起こりやすい人を調べることもでき、日本リウマチ学会は、医師に適正使用を呼びかけている。

関節リウマチは手足などの関節に炎症が起こり、骨や軟骨を破壊する進行性の病気。国内患者は約70万人と推定され、約7割が女性。30～50歳代に発症する人が多い。

メトトレキサートは関節リウマチの炎症を抑える作用があり、学会が出した医師向けガイドラインは、第1選択薬として使うことを認めている。学会理事長の宮坂信之・東京医科歯科大学医学部付属病院長は、従来の投与量で十分効果がなかった人に「週8ミリグラム以上使えば3割以上の人に効果がある」と話す。

一方、白血球や血小板減少、間質性肺炎などの副作用が出ることがある。ガイドラインでは、副作用の起こりやすい人を割り出すため投与前の血液検査や肝炎ウイルス検査などを勧めている。処方後は、副作用を防ぐため葉酸製剤の並行投与が有効だという。

Question 01
脳
SLE脳症

脳梗塞を起こしSLE脳症と診断。意識が戻らない

44歳の妻のことで相談します。妻は全身性エリテマトーデスの治療中ですが、脳梗塞で倒れました。脳梗塞治療と並行した検査の結果、SLE脳症と診断されました。ステロイドの大量点滴治療中、3週間点滴し、今週は中断しています。主治医から「薬遺から治療を再開する。それで意識回復がなければ難しい」とのこと。この治療しかないのでしょうか。SLEが進行しているのですが、今後の経過はどうでしょうか。（千葉県 I・C）

Answer

脳梗塞とSLEの治療を続けて様子を見るしかない

全身性エリテマトーデス（以下SLEと表記）では中枢神経症状を起こすことがあり、中枢神経（CNS）ループスと呼ばれます。SLE脳症もその中の一つです。早期発見・早期治療が必要不可欠ですが、重症になることも珍しくありません。

最も多く見られる症状は、けいれんや意識障害（せん妄、昏睡、抑うつ状態、不眠など）です。頑固な頭痛や髄膜炎なども現れることもあります。

これらの症状の多くは、SLEの活動性に関連しています。しかし、一般にSLEの診断指標として用いられる「抗dsDNA抗体」や「血清補体価」などと必ずしも一致するわけではありません。また、これらの病態はステロイド投与後に誘発されることがありますので、ステロイドによる精神障害（ステロイド精神病）との鑑別が重要になります。

診断には、髄液検査、脳波、CT（コンピューター断層撮影）検査、MRI（磁気共鳴画像）検査、SPECT（※1）検査などが用いられます。特に髄液検査では、「インターロイキン（※2）-6」の上昇や「IgGインデックス（※3）」の増加が特徴的です。

治療としては、ステロイドの大量投与やシクロホスファミド水和物（エンドキサン）、パルス療法などが行われます。

今までに中枢神経症状がなかったのに新たに現れたということでしたら、やはりSLEが進行したと考えられます。

必ずしも脳梗塞とSLEが関連し合うわけではない

ご相談の方のように、脳血管障害が起こることもあれば、一過性脳虚血発作や脳梗塞、脳出血など多様な病態が現れることもあります。

特に脳梗塞は抗リン脂質抗体症候群を伴っていることが多く、必ずしもSLEの疾患活動性との相関があるわけではありません。ほかの感染症などで誘発される場合もあります。ちなみに、動脈硬化のリスクの低い若年例の脳梗塞では、抗リン脂質抗体症候群に関連した場合がほとんどです。脳梗塞は単発性の場合もありますが、多発性のこともあります。

検査所見としては、活性化部分トロンボプラスチン時間（APTT）の延長や、抗β2GPI抗体やループスアンチコアグラントの陽性などが見られます。

急性期にはヘパリンやウロキナーゼなどによる抗凝固療法を行います。慢性期、または維持療法ではワーファリン※3が用いられます。症状がひどいときには、ステロイド大量投与やシクロホスファミドなどの免疫抑制薬や血漿交換療法も用いられますが、有効性は必ずしも証明されていません。

ご相談の方の状態が詳しくわからないのでなんとも言えませんが、脳梗塞とSLEの治療を並行して続けるしかないと思われます。脳梗塞の治療が一段落しても意識が戻らないようなら、治療は難しくなるかもしれません。

私が回答します
東京医科歯科大学
膠原病・リウマチ内科 教授
宮坂信之
〒113-8519
東京都文京区湯島1-5-45
TEL.03-3813-6111
http://www.tmd.ac.jp/

※1…単一光子放射断層撮影（single photon emission computed tomography）
※2…細胞から分泌され、自由球間の情報伝達を担う
※3…中枢神経系における炎症性タンパク「免疫グロブリン」の指標

ドは、承認後5年を目覚ましい成果を上げ、3割以上の患者を寛解（症状が治まった状態）に導き、9割以上の患者に関節破壊の進行を抑制する効果があるという結果が出ている。ただし、感染症などの副作用があるので、専門医のところで注意して使う必要がある。

また、05年に承認されたエンブレル（エタネルセプト）も同様に、8割以上の患者に有効であるとの結果が出ている。週に1、2回の自己皮下注射が必要だが、抗リウマチ薬としても単独で使える。

さらに08年4月には二つの、10年7月には一つの生物学的製剤が承認され、治療の可能性が広がっている（コラム参照）。

10年に承認されたオレンシア（アバタセプト）は、従来の生物学的製剤とは異なる作用で免疫細胞を抑える働きがあるため、ほかの薬で治療効果を得られなかったり、効かなくなったりした患者に対するリウマチ薬を併用せず単独でも使え、2～4週に1回、30分の点滴投与と負担も少ない。

「生物学的製剤によって、関節リウマチは根本療法が可能になってきました。そのため、治療目的がこれまでと大きく変わっています。目標は三つありますが、一つは、腫れも痛みもない寛解。二つ目は、関節破壊の進行を完全に抑えること。三つ目は、完治の状態。早期の患者さんなら骨びらん（骨の変形）も回復し、薬をやめられる可能性も出てきたのです」（田中医師）

新薬の登場によって治療法が飛躍的に向上した関節リウマチだが、症状によっては手術が必要な場合がある。

群馬県在住の主婦・清水幸恵さん（仮名・58歳）は、40代になったころからおもに両ひざの関節の腫れや痛みを感じながらも、放置していた。やがて、ひざは90度近くで曲がったままの状態にまで進行。約10年前、とうとう我慢できずに地元の病院に駆け込んだ。そこで薬物治療を受けたが、治療開始が遅かったのと、当時は新薬が承認されていなかったこともあり、その後ひざは伸びないままだった。

この状態での治療法は手術しか残っておらず、しかも手術の難易度が高いため、地元の病院のすすめで実績のある日本大学板橋病院を紹介された。

新薬登場で可能性拡大 副作用を恐れすぎない

「この病気は関節に起こった『火事』のようなものです。その火事が今までの治療法や薬だとなかなかうまく消せませんでした。ところが、抗リウマチ薬のリウマトレックスを十分使い、生物学的製剤を併用することで、従来消えなかった関節の火事を消せるようになったのです」

こう話す東京医科歯科大学病院膠原病・リウマチ内科診療科長の宮坂信之医師によると、2008年は、日本の関節リウマチ関係者にとって画期的な年になったという。生物学的製剤は今までこしなかったが、新たにアクテムラ（トシリズマブ）と、ヒュミラ（アダリムマブ）の2製剤が承認され、強力な武器になったからだ。

新薬の一つ、アクテムラは、もともとキャッスルマン病というリンパ節の病気に使われていた薬だが、関節リウマチにも効果があることが認められ、適用拡大で承認された。持病などの問題でほかの生物学的製剤を使えなかったり、効かなかったりする患者にも使えるようになったのが大きな利点。エンブレルと同様に単独で使え、臨床試験では高い有効性と安全性が確認されている。

もう一方のヒュミラの特徴は、レミケードと同等の高い効果が期待できることと、レミケードがヒトとマウスの2種類のたんぱく質由来であるのに対し、ヒュミラはヒト由来のものなので

みやさか のぶゆき
宮坂信之医師
東京医科歯科大学病院
膠原病・リウマチ内科診療科長
東京都文京区湯島1-5-45
☎03-3813-6111

2011年2月28日(月)/11月5日 土曜日 13版 12

【特集】 読売新聞広告特集

主催：読売新聞社
後援：厚生労働省、東京都、日本リウマチ学会、東京都医師会
東京都薬剤師会、東京都看護協会、日本リウマチ友の会
協賛：ブリストル・マイヤーズ株式会社

最新の薬物療法と手術療法

紙上採録 関節リウマチ市民セミナー

関節の痛みや腫れが続き、日常生活に不自由をきたす関節リウマチ。近年、その治療法は大きく進歩したといわれています。9月19日、日本教育会館一ツ橋ホール（東京）にて開催された市民セミナーでは、最新の薬物療法と手術療法について専門医による解説が行われました。関節リウマチ患者の支援を行っている社団法人日本リウマチ友の会の代表からは、患者の実態調査の結果が報告され、参加者は熱心に耳を傾けていました。

－開会挨拶－
東京医科歯科大学大学院 膠原病・リウマチ内科診療科 教授 宮坂 信之 先生

講演1「関節リウマチの診断・薬物療法」
東京慈恵会医科大学 リウマチ内科 教授 竹内 勤 先生

講演2「関節リウマチの手術療法」
埼玉医科大学 整形外科 教授 織田 弘美 先生

講演3「リウマチ患者の現状 ～ペパウマチ白書より～」
社団法人日本リウマチ友の会 会長 長谷川 三枝子 氏

質疑応答
事前までのから多数に寄せられた質問に対して会場入りされました。

Q 関節リウマチの治療は、どのようなものですか？
A 関節リウマチの治療は、薬物療法と手術療法に大別されます。

Q 関節リウマチの治療は、どのようなものですか？
A 関節リウマチの治療は、薬物療法と手術療法に大別されます。

Q 関節リウマチの治療は、どのようなものですか？
A 関節リウマチの治療は、薬物療法と手術療法に大別されます。

Q 関節リウマチの治療は、どのようなものですか？
A 関節リウマチの治療は、薬物療法と手術療法に大別されます。

生物学的製剤の種類と特徴

	インフリキシマブ	エタネルセプト	トシリズマブ	アダリムマブ	ゴリムマブ	アバタセプト
皮下注射		週2回	2週1回	週2回	週2回	2週1回
点滴	8週ごと～2週ごと		4週ごと			4週ごと
単独	必要でない	必要でない	必要でない	必要でない	必要でない	必要でない
併用	必要	必要でない	必要でない	必要でない	必要でない	必要でない

みんなで支えるリウマチのページ リウマチTearoom http://www.bms.co.jp/ra/

関節リウマチ

薬物治療が基本だが手術という選択肢も

早期発見が最も重要

関節リウマチは、外敵から体を守る免疫の仕組みに異常が起こって関節に炎症が生じる病気だ。朝の指のこわばり、関節の腫れや強い痛みなどの症状が出る。進行すると、関節が傷んで変形し、歩くのが困難になることもある。患者数は30～60歳代を中心に約70万人とされ、女性が約7割を占める。

関節は、骨と骨の間のクッションの役割を果たす軟骨、関節を包む薄い膜である滑膜などから成る。関節リウマチは、関節に免疫細胞が集まり、滑膜を攻撃し、炎症が起こる。滑膜が厚く増殖し、骨が破壊され、関節が変形する。

最近の研究では、発病から1年間における関節破壊が、それ以降より激しいことが分かってきた。東京医科歯科大学医学部付属病院病院長で膠原病・リウマチ内科教授の宮坂信之さんは「病気をできるだけ早く発見し、患者に合った最適な治療を行うことが、関節破壊や寝たきりを防ぐことにつながる。やはり、治療実績が豊富な病院で、最初に診てもらうことが大切だ」と話す。

治療の基本は薬物治療だ。免疫の働きを抑えるメトトレキサート（MTX）などの「抗リウマチ薬」の飲み薬を最初に使う。しかし、効果には個人差があり、効果があっても数年後には効かなくなることもある。

抗リウマチ薬で病気の進行が抑えられない場合には、炎症を起こす物質の働きを妨げる薬「生物学的製剤」による治療を行う。従来の薬では不可能だった、関節破壊を止める効果もある。

生物学的製剤は現在、6種類ある。投与方法、投与間隔が異なり、患者が自分の生活に合わせて選ぶことができる。読売新聞が日本リウマチ学会の教育施設に対して調査を行った2008年時点では、生物学的製剤は4種類だった。調査では、生物学的製剤の治療を受けた患者数は施設により、850～0人と差があった。

東京医科歯科大学病院
病院長
宮坂信之さん

みやさか のぶゆき / 1973年、東京医科歯科大学卒業。カリフォルニア大学留学などを経て2001年から同大学膠原病・リウマチ内科教授。日本リウマチ学会理事長、日本炎症・再生医学会副理事長など。

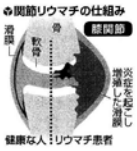

生物学的製剤の特徴を説明する。

①**レミケード**（一般名インフリキシマブ） 承認は03年で、最も治療実績がある。MTXと併用する必要がある。点滴薬で治療時間は2時間ほど。2回目の治療は、初回の2週間後。3回目は2回目の4週間後。4回目以降は8週間に1度の治療となる。09年7月から、効果が不十分な場合、投与量の増量や投与間隔の短縮ができるようになった。

②**エンブレル**（一般名エタネルセプト） 承認は05年。1週間に2回、皮下注射をする。医師の許可を受けると、自宅で、自分で注射することもできる。

③**ヒュミラ**（一般名アダリブマブ） 承認は08年。2週間に1回、皮下注射する。医師の許可を受けると、自宅で、自分で注射することもできる。

④**アクテムラ**（一般名トシリズマブ） 承認は08年。日本で開発された薬だ。点滴治療だが、レミケードのようにMTXを併用する必要がない。4週間に1回点滴し、1回の点滴に約1時間かかる。

⑤**オレンシア**（一般名アバタセプト） 承認は10年。4週間に1回点滴し、1回の点滴に約30分かかる。

⑥**シンポニー**（一般名ゴリムマブ） 承認は11年。4週間に1回、皮下注射する。

内科、外科、リハビリの連携で

生物学的製剤は、免疫反応を抑えてしまうため、肺炎や結核などの感染症にも注意が必要だ。承認から数年たつとレミケードとエンブレルによる肺炎の発病率は、投与者の1～2％ほどだ。感染の未経験が必要で、実績のある病院のほうが信頼が置ける。

生物学的製剤は高額で、3割の自己負担だと、年40万～60万円ほどかかり、ずっと使い続けなければならない。ただし、身体障害者手帳を持っていると、医療費の助成が受けられる。

症状が進んだ場合には手術が行われる。そのうちの一つが「滑膜切除術」だ。関節に小さな穴を開け、炎症が起きている滑膜を専用の内視鏡でのぞきながら取り除く。痛みを和らげ、症状の進行を抑える効果はあるが、関節の変形を治すことはできない。

関節破壊が進んだ場合には、「人工関節手術」を行う。破壊された骨や軟骨を削り、金属やポリエチレンなどでできた人工関節に置き換える手術だ。関節がなめらかに動くようになり、痛みも減る。08年の調査では、膝関節が56％で最も多く、股関節が25％、指や肩などその他の関節が19％だった。医療機関によって、得意な手術が異なることがある。

関節リウマチの治療は、①薬物治療を担当する内科医（若年性関節リウマチを治療する小児科医を含む）②人工関節手術などを行う整形外科医③曲がったり、破壊されたりした関節を動きやすくするリハビリテーション医――が連携して行うのが理想だ。

日本リウマチ学会では、学会が認定した教育施設などで通算5年以上のリウマチの臨床研修を行ったことなどの条件をクリアした医師を、専門医に認定している。内科医、整形外科医、リハビリ医ともに認定が受けられる。

一方、日本整形外科学会も独自にリウマチ認定医を認めている。専門医が多い医療機関は一般的には重症患者などの治療も上手に行うことができるので、病院の実力を知るための一つの指標となる。

患者の役に立つ情報を得たいなら、頼り頼りになるのは患者団体で、「社団法人 日本リウマチ友の会」がある。〒101－0047 東京都千代田区内神田2の7の7 新内神田ビル3階。（平日午前9時半～午後4時半。土・日・祝日休 ☎03・3258・6565）

（宮上 博）

Kaneko *et al. Arthritis Research & Therapy* 2011, **13**:R158
http://arthritis-research.com/content/13/5/R158

arthritis research&therapy

RESEARCH ARTICLE Open Access

Chemerin activates fibroblast-like synoviocytes in patients with rheumatoid arthritis

Kayoko Kaneko[1], Yoshishige Miyabe[1], Aiko Takayasu[1], Shin Fukuda[1], Chie Miyabe[1], Masashi Ebisawa[1], Waka Yokoyama[1], Kaori Watanabe[1], Toshio Imai[2], Kenzo Muramoto[3], Yuya Terashima[4], Takahiko Sugihara[5], Kouji Matsushima[4], Nobuyuki Miyasaka[1] and Toshihiro Nanki[1*]

Abstract

Introduction: Chemerin is a chemotactic agonist identified as a ligand for ChemR23 that is expressed on macrophages and dendritic cells (DCs). In this study, we analyzed the expression of chemerin and ChemR23 in the synovium of rheumatoid arthritis (RA) patients and the stimulatory effects of chemerin on fibroblast-like synoviocytes (FLSs) from RA patients.

Methods: Chemerin and ChemR23 expression in the RA synovium was ascertained by immunohistochemistry and Western blot analysis. Chemerin expression on cultured FLSs was analyzed by ELISA. ChemR23 expression on FLSs was determined by immunocytochemistry and Western blot analysis. Cytokine production from FLSs was measured by ELISA. FLS cell motility was evaluated by utilizing a scrape motility assay. We also examined the stimulating effect of chemerin on the phosphorylation of mitogen-activated protein kinase (MAPK), p44/42 mitogen-activated protein kinase (ERK1/2), p38MAPK, c-Jun N-terminal kinase (JNK)1/2 and Akt, as well as on the degradation of regulator of NF-κB (IκBα) in FLSs, by Western blot analysis.

Results: Chemerin was expressed on endothelial cells and synovial lining and sublining cells. ChemR23 was expressed on macrophages, immature DCs and FLSs and a few mature DCs in the RA synovium. Chemerin and ChemR23 were highly expressed in the RA synovium compared with osteoarthritis. Chemerin and ChemR23 were expressed on unstimulated FLSs. TNF-α and IFN-γ upregulated chemerin production. Chemerin enhanced the production of IL-6, chemokine (C-C motif) ligand 2 and matrix metalloproteinase 3 by FLSs, as well as increasing FLS motility. The stimulatory effects of chemerin on FLSs were mediated by activation of ERK1/2, p38MAPK and Akt, but not by JNK1/2. Degradation of IκB in FLSs was not promoted by chemerin stimulation. Inhibition of the ERK1/2, p38MAPK and Akt signaling pathways significantly suppressed chemerin-induced IL-6 production. Moreover, blockade of the p38MAPK and Akt pathways, but not the ERK1/2 pathway, inhibited chemerin-enhanced cell motility.

Conclusions: The interaction of chemerin and ChemR23 may play an important role in the pathogenesis of RA through the activation of FLSs.

Introduction

Rheumatoid arthritis (RA) is a chronic inflammatory disease characterized by synovial hyperplasia, joint destruction and infiltration of the synovium by immunocytes, including lymphocytes, macrophages and dendritic cells (DCs) [1-3]. In addition to these cells, fibroblast-like synoviocytes (FLSs) play a major role in the pathogenesis of RA [4,5] in that they produce a variety of cytokines, chemokines and matrix-degrading enzymes that mediate interaction with neighboring inflammatory and endothelial cells and are responsible for the progressive inflammation in the joints and destruction of the articular cartilage and bone [6-8].

Chemerin is the ligand protein for ChemR23, a G protein-coupled receptor expressed on macrophages, DCs and natural killer cells (NK cells) [9-11]. Chemerin is

* Correspondence: nanki.rheu@tmd.ac.jp
[1]Department of Medicine and Rheumatology, Graduate School of Medical and Dental Sciences, Tokyo Medical and Dental University, 1-5-45, Yushima, Bunkyo-ku, Tokyo, 113-8519, Japan
Full list of author information is available at the end of the article

BioMed Central

© 2011 Kaneko et al.; licensee BioMed Central Ltd. This is an open access article distributed under the terms of the Creative Commons Attribution License (http://creativecommons.org/licenses/by/2.0), which permits unrestricted use, distribution, and reproduction in any medium, provided the original work is properly cited.

characterized as a strong chemoattractant factor for ChemR23-expressing cells and acts at subnanomolar concentrations [9,12]. Chemerin is synthesized as an inactive precursor protein, prochemerin, which binds ChemR23 with low affinity [9,13]. It can be rapidly converted into a full ChemR23 agonist by the proteolytic removal of the last six or seven amino acids by neutrophil-derived proteases (elastase and cathepsin G), mast cell products (tryptase), proteases of the coagulation cascade [14,15] and certain bacterial proteases [16] at the inflammatory site.

Investigators in recent studies have reported that the expression of chemerin correlates with ChemR23-positive cell recruitment in human skin inflammatory diseases, such as systemic lupus erythematosus, oral lichen planus and psoriasis [10,12,17]. Moreover, it has been reported that chemerin and ChemR23 are expressed by human articular chondrocytes [18] and endothelial cells [19,20]. The interaction of chemerin with ChemR23 is assumed to play an important role not only in the migration of macrophages and DCs to the sites of inflammation but also in the mediating inflammatory signaling to articular chondrocytes and endothelial cells. However, there is little information on the expression and function of chemerin in the RA synovium.

In the present study, we analyzed the expression of chemerin and ChemR23 in the RA synovium and evaluated the function of chemerin in cultured FLSs isolated from the synovium of RA patients to explore a possible role of chemerin and ChemR23 interaction in the pathogenesis of RA.

Materials and methods

Specimens

Synovial tissue samples were obtained from nine RA patients who fulfilled the American College of Rheumatology diagnostic criteria for RA [21] and from four patients with osteoarthritis (OA) who underwent total knee joint replacement surgery. Signed consent forms were obtained before the operations. All patients with RA and OA were female. In RA patients, the mean age (± SEM) was 71.0 ± 3.7 years, mean disease duration (± SEM) was 10.75 ± 3.5 years, and their mean C-reactive protein concentration (± SEM) was 0.33 ± 0.17 mg/dl. Among the patients with RA, seven patients were seropositive for rheumatoid factor and five were positive for anticitrullinated protein antibodies. Two of the patients with RA were receiving prednisolone, one was being treated with bucillamine (an analogue of D-penicillamine), one was receiving methotrexate monotherapy, one was being treated with methotrexate and etanercept and three were was taking tocilizumab. Three patients were receiving no medication at the surgery. The experimental protocol was approved by the Ethics Committee of Tokyo Medical and Dental University.

Immunohistochemistry

Immunohistochemical analysis was conducted on OCT compound-embedded sections of frozen synovial tissues. Briefly, 8-μm-thick cryostat sections were fixed in cold acetone (stored at -20°C) for three minutes. Endogenous peroxidase activity was blocked by incubation in 2% H_2O_2 in methanol for 15 minutes, and then nonspecific binding was blocked with 10% normal goat serum in PBS for 40 minutes. Serial sections were then incubated for two hours at 4°C with 1 μg/ml rabbit anti-chemerin pAb (affinity-purified from rabbit serum immunized with glutathione *S*-transferase-chemerin (E^{21}-S^{157}) fusion protein; provided by KAN Research Institute, Kobe, Japan), 1 μg/ml rabbit anti-ChemR23 pAb (Acris Antibodies, Herford, Germany) or normal rabbit immunoglobulin G (IgG) (Sigma-Aldrich, St Louis, MO, USA) as an isotype control. Antibody binding was detected using the EnVision+ Kit (DakoCytomation, Carpinteria, CA, USA).

For immunofluorescence double-staining with CD68, CD1a, DC-LAMP or vimentin, and ChemR23, nonspecific binding was blocked with 1% blocking reagent (Roche, Manheim, Germany) in PBS, and then the sections were incubated overnight at 4°C with rabbit anti-ChemR23 pAb or normal rabbit IgG (control) at 1 μg/ml. The samples were then incubated with Alexa Fluor 568-conjugated goat anti-rabbit IgG (4 μg/ml; Invitrogen, Carlsbad, CA, USA) for one hour at room temperature. Next the sections were incubated overnight with 2.35 μg/ml mouse anti-CD68 mAb (KP1; DakoCytomation), 10 μg/ml mouse anti-CD1a mAb (BL6; Immunotech, Marseille, France), 10 μg/ml mouse anti-DC-LAMP mAb (104.G4; Immunotech) or 1 μg/ml mouse anti-vimentin mAb (V9; DakoCytomation) at 4°C. Subsequently, the samples were incubated with 4 μg/ml Alexa Fluor 488-conjugated goat anti-mouse IgG2a (Invitrogen) or anti-mouse IgG1 (Invitrogen) for one hour at room temperature. The slides were examined using a Biozero Fluorescence Microscope (Keyence, Tokyo, Japan).

For whole-mount staining, human synovial tissues from RA patients were washed vigorously in ice-cold PBS, then fixed and permeabilized with a BD Cytofix/Cytoperm Kit (BD Biosciences, San Jose, CA, USA). The whole-mount specimens of synovial tissues were then stained with rabbit anti-ChemR23 pAb or rabbit IgG as an isotype control, followed by secondary antibodies conjugated with Alexa Fluor 488-conjugated goat anti-rabbit IgG (BD Biosciences). The specimens were further stained with Alexa Fluor 633-labeled phalloidin (BD Biosciences). The specimens were embedded in a

Kaneko *et al. Arthritis Research & Therapy* 2011, **13**:R158
http://arthritis-research.com/content/13/5/R158

30% solution of glycerol in PBS and analyzed with a DM IRE2 confocal laser scanning microscope (Leica Microsystems, Wetzlar, Germany).

Cell cultures

Synovial tissues from RA patients were minced and incubated with 0.5 mg/ml collagenase (Sigma-Aldrich) for one hour at 37°C, then pressed through a metal screen to obtain single-cell suspensions. The harvested cells were plated in cell culture plates and incubated with DMEM (Sigma-Aldrich) supplemented with 10% FCS (Sigma-Aldrich). Adherent cells were maintained in the medium as FLSs and used after five passages [22] in the experiments that followed.

For immunofluorescence double-staining of cultured FLSs with ChemR23 and vimentin, FLSs were incubated on eight-well chamber slides (4×10^4 cells/well) (IWAKI, Tokyo, Japan) at 37°C overnight. The adherent cells were fixed in cold acetone for three minutes. Nonspecific binding was blocked with 10% normal goat serum in PBS, then the cells were incubated overnight at 4°C with rabbit anti-ChemR23 pAb or normal rabbit IgG at 1 μg/ml. Next the cells were incubated with Alexa Fluor 568-conjugated goat anti-rabbit IgG (4 μg/ml) for one hour at room temperature. After that step, the cells were incubated overnight with 1 μg/ml mouse anti-vimentin mAb at 4°C, followed by incubation with 1 μg/ml Alexa Fluor 488-conjugated goat anti-mouse IgG1 for one hour at room temperature. The slides were examined using a Biozero Fluorescence Microscope (Keyence).

ELISA for chemerin and inflammatory mediators produced by cultured fibroblast-like synoviocytes

FLSs were cultured overnight in 96-well plates (2×10^4 cells/well) in DMEM with 10% FCS and then incubated with or without recombinant human TNF-α (0.1, 1 or 10 ng/ml) or IFN-γ (1, 10 or 100 ng/ml) (both from R&D Systems, Minneapolis, MN, USA) at 37°C for 48 hours. The concentration of chemerin in culture supernatant was measured with an ELISA kit (R&D Systems) according to the instructions provided by the manufacturer.

To determine the effects of chemerin on the production of IL-6, chemokine (C-C motif) ligand 2 (CCL2) and matrix metalloproteinase 3 (MMP-3) by FLSs, the cells were cultured separately overnight in 96-well plates (4×10^4 cells/well), then incubated with or without recombinant bioactive human chemerin (2, 10 or 50 nM; R&D Systems) in FCS-free DMEM at 37°C for 24 and 48 hours. The protein levels of IL-6, CCL2 and MMP-3 in the supernatant were assessed using ELISA kits (R&D Systems) according to the manufacturer's instructions. To block the signaling pathway through p44/42 mitogen-activated protein kinase (ERK1/2), p38 mitogen-activated protein kinase (p38MAPK) or Akt, FLSs (4×10^4 cells/well) were pretreated with specific inhibitors, including a mitogen-activated protein kinase kinase (MEK) inhibitor (10 μM PD98059; Calbiochem, Merck KgaA, Germany), a p38MAPK inhibitor (10 μM SB203580; Calbiochem) or phosphoinositide 3-kinase (PI3K) inhibitor (10 μM LY294002; Cell Signaling Technology, Danvers, MA, USA) for 30 minutes before stimulation with 50 nM chemerin. To confirm the lack of a significant amount of endotoxin in the stimulation procedure, FLSs were incubated with 50 μg/ml polymyxin B in addition to 50 nM chemerin.

Scrape motility assay

RA FLSs were plated at a density of 1×10^5 cells/ml in 12-well plates (22.1-mm diameter) in DMEM with 10% FCS. After overnight incubation, the tip of a plastic pipette was drawn across the center of the well to produce a scraped area [23]. The culture wells were washed twice with PBS, and free cells were removed. Then the cells were pretreated with or without pertussis toxin (PTX) (0.5 μg/ml), PD98059 (10 μM), SB203580 (10 μM) or LY294002 (10 μM) for 30 minutes, followed by incubation with 2 or 10 nM of chemerin and CCL2 in FCS-free medium. Immediately after scraping (zero hours) as well as after 24-hour incubation, the process of two-dimensional FLS migration into the cell-free area at the center of the well was photographed with a Nikon TE2000U inverted microscope (Nikon Instruments, Tokyo, Japan) and printed. Cells that migrated into the scraped area after 24 hours were counted by an observer blinded to the study design. The fold increase in the cells was calculated (number of cells with chemerin with or without signal inhibitor per number of cells without treatment).

Western blot analysis

Synovial tissues from patients with RA and OA were lysed with radioimmunoprecipitation assay (RIPA) buffer (Millipore, Temecula, CA, USA) containing protease inhibitor (Roche) and phosphatase inhibitor cocktail (Sigma-Aldrich) for 30 minutes at 4°C. RA FLSs (3×10^5 cells/well) were cultured overnight in 60-mm dishes in DMEM with 10% FCS, then the medium was replaced with FCS-free DMEM. This step was followed by incubation with or without recombinant human TNF-α (10 ng/ml), IFN-γ (100 ng/ml), transforming growth factor-β1 (TGF-β1; 1 ng/ml), IL-1β (5 ng/ml) or IL-6 (20 ng/ml) (all from R&D Systems) at 37°C for 24 hours. After incubation, cells were collected and lysed with the RIPA buffer containing protease inhibitor and phosphatase inhibitor cocktail for 30 minutes at 4°C.

Kaneko *et al. Arthritis Research & Therapy* 2011, **13**:R158
http://arthritis-research.com/content/13/5/R158

A total of 20 μg of protein were boiled in the presence of SDS sample buffer and separated on a 10% SDS-polyacrylamide gel (ATTO, Tokyo, Japan). Proteins were then electrotransferred onto a polyvinylidene fluoride microporous membrane (Millipore) in a semidry system. The membrane was blocked with 5% skim milk for one hour at room temperature, then the immunoblots were incubated overnight with rabbit anti-chemerin pAb (1:1, 000 dilution; Phoenix Pharmaceuticals, Burlingame, CA, USA) or rabbit anti-ChemR23 pAb (1:500 dilution; Abcam, Cambridge, UK) in Can Get Signal Immunoreaction Enhancer Solution (Toyobo Co, Ltd, Tokyo, Japan) at 4°C. Peroxidase-conjugated goat anti-rabbit IgG pAb (GE Healthcare, Birmingham, UK) was used as the secondary antibody.

To detect phosphorylated and total ERK1/2, p38MAPK, c-Jun N-terminal kinase (JNK)1/2 or Akt, cells were incubated in a medium supplemented with 10 nM human recombinant chemerin prior to lysis for 5, 15 or 30 minutes. A total of 7.5 μg of protein was boiled in the presence of SDS sample buffer and separated on 10% SDS-polyacrylamide gel. After blotting, the membranes were blocked with Block Ace blocking solution (Snow Brand Milk Products Co, Ltd, Tokyo, Japan) for one hour at room temperature, then the immunoblots were incubated overnight with rabbit anti-phospho-ERK1/2 pAb (1:1, 000 dilution), rabbit anti-pan-ERK1/2 pAb (1:1, 000 dilution), rabbit anti-phospho-p38MAPK pAb (1:1, 000 dilution), mouse anti-pan-p38MAPK mAb (1:1, 000 dilution) (all from Cell Signaling Technology), mouse anti-phospho-JNK mAb (1:300 dilution; Santa Cruz Biotechnology, Santa Cruz, CA, USA), rabbit anti-pan-JNK pAb (1:1, 000 dilution), rabbit anti-phospho-Akt pAb (1:2, 000 dilution) or rabbit anti-pan-Akt pAb (1:1, 000 dilution) (all from Cell Signaling Technology) in Tris-buffered saline (TBS) containing 0.1% Tween 20 at 4°C. To detect the expression of the regulator of NF-κB, (IκBα), and β-actin, the immunoblots were incubated overnight with rabbit anti-IκBα pAb (1:1, 000 dilution; Santa Cruz Biotechnology) at 4°C or with mouse anti-β-actin mAb (1:5, 000 dilution; Sigma-Aldrich) for one hour at room temperature in TBS containing 0.1% Tween 20. Peroxidase-conjugated goat anti-rabbit IgG pAb (GE Healthcare), rabbit anti-mouse IgG pAb (SouthernBiotech, Birmingham, AL, USA), goat anti-mouse IgG pAb (Promega, Madison, WI, USA) or donkey anti-rabbit IgG pAb (GE Healthcare) was used as the secondary Ab. ECL Plus detection reagent and the ImageQuant LAS 4000 Mini Biomolecular Imager (both from GE Healthcare) were used in conjunction with MultiGauge software (Fujifilm, Tokyo, Japan) to detect and quantitate the bands.

Statistical analysis

Data are presented as means ± SEM. Student's *t*-tests were applied to compare two groups, and one-way analysis of variance and Dunnett's multiple comparison tests were used to compare three or more groups. $P < 0.05$ was considered statistically significant.

Results

Expression of chemerin and ChemR23 in the rheumatoid arthritis synovium

Strong immunohistochemical staining for chemerin was noted on endothelial cells and synovial lining and sublining cells in the RA synovium (Figure 1A). In contrast, chemerin expression in the OA synovium was minimal (Figure 1B).

Widespread immunostaining for ChemR23 was noted in all RA samples, with dense staining observed on the sublining cells (Figure 2A). On the other hand, staining in OA samples was much weaker (Figure 2B). Double-staining analysis showed the presence of ChemR23 immunoreactivity on most of the $CD68^+$ macrophages (Figures 2C through 2E), on $CD1a^+$ immature DCs [24,25] (Figures 2F through 2H) and on a few of DC-$LAMP^+$ mature DCs [26] (Figures 2I through 2K). Interestingly, ChemR23 was also expressed on $vimentin^+$ FLSs (Figures 2L through 2N). Furthermore, we performed whole-mount immunostaining of synovial tissues with anti-ChemR23 pAb. The expression of ChemR23 was observed in infiltrated cells in the tissue (Figure

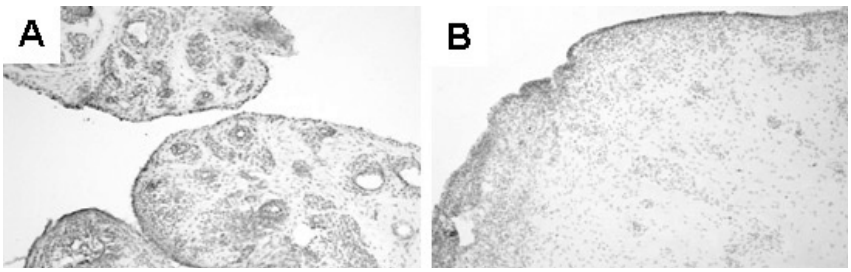

Figure 1 Expression of chemerin in rheumatoid arthritis and osteoarthritis synovial tissue samples. Chemerin expression in synovial tissue samples obtained from five RA patients **(A)** and three OA patients **(B)** examined by immunohistochemistry. All sections were counterstained with hematoxylin. OA = osteoarthritis; RA = rheumatoid arthritis.

Kaneko *et al. Arthritis Research & Therapy* 2011, **13**:R158
http://arthritis-research.com/content/13/5/R158

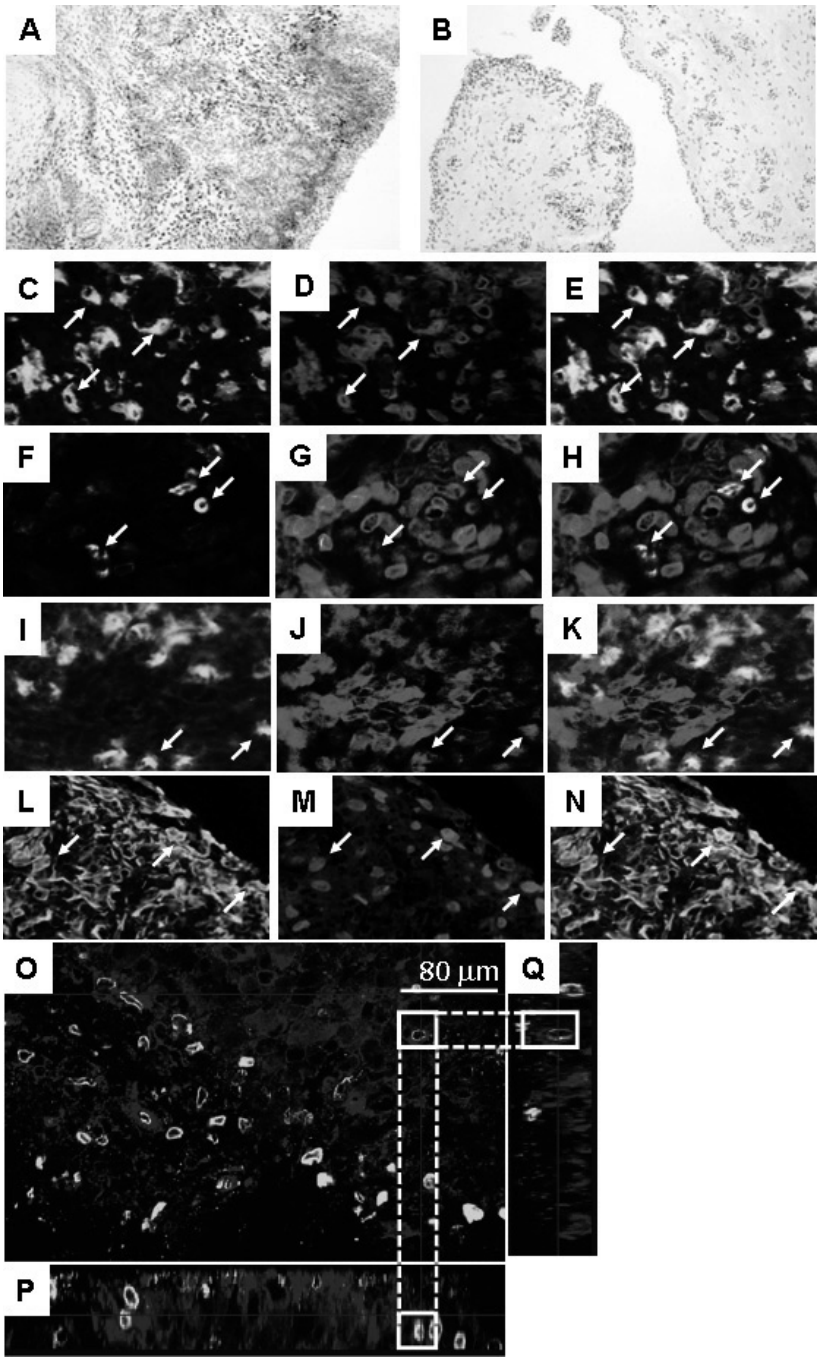

Figure 2 Expression of ChemR23 in rheumatoid arthritis and osteoarthritis synovial tissue samples. ChemR23 expression in synovial tissue samples examined by immunohistochemistry that were obtained from five rheumatoid arthritis (RA) patients **(A)** and three osteoarthritis (OA) patients **(B)**. All sections were counterstained with hematoxylin. Sections of RA synovial tissues were also double-stained with CD68, CD1a, DC-LAMP or vimentin, and ChemR23 and were analyzed by fluorescence microscopy as follows: **(C)** CD68, **(D)** ChemR23, **(E)** merged image of (C) and (D), **(F)** CD1a, **(G)** ChemR23, **(H)** merged image of (F) and (G), **(I)** DC-LAMP, **(J)** ChemR23, **(K)** merged image of (I) and (J), **(L)** vimentin, **(M)** ChemR23 and **(N)** merged image of (L) and (M). Arrows indicate double-positive cells. Original magnification ×100 in (A) and (B) and ×400 in (C) through (N). Whole-mount specimens obtained from RA patients were stained with anti-ChemR23 pAb (green) or phalloidin (blue) and then analyzed by confocal laser-scanning microscopy. **(O)** *x-y* view of synovial tissue sectioning. *x-z* image **(P)** and *y-z* image **(Q)** of synovial tissue sectioning are displayed below and to the right of the *x-y* view in (O). Scale bars = 80 μm. White straight line boxes indicate identical cell in each direction (O-Q). Dashed line connects the boxes.

Kaneko *et al. Arthritis Research & Therapy* 2011, **13**:R158
http://arthritis-research.com/content/13/5/R158

2O). No signal was observed on specimens stained with an isotype-matched IgG control of irrelevant specificity (data not shown). In addition, the *x-z* and *y-z* sectioning images obtained by confocal microscopic analysis indicated that ChemR23 was expressed on the surface of the infiltrated cells (Figures 2P and 2Q).

Next we compared the expression of chemerin and ChemR23 in RA and OA synovial tissues by Western blot analysis. Expression of chemerin by RA synovium was higher than that of OA synovium (Figure 3A). The relative amount of chemerin protein to β-actin in RA was significantly higher than that in OA (Figure 3B). ChemR23 expression by RA synovial tissue was also significantly upregulated compared with OA (Figures 3C and 3D).

Expression of chemerin and ChemR23 in cultured rheumatoid arthritis fibroblast-like synoviocytes

The expression of chemerin on cultured FLSs isolated from the RA synovium was analyzed by ELISA. Chemerin was produced by unstimulated FLSs, and the production was significantly upregulated by stimulation with TNF-α and IFN-γ ($P < 0.05$) (Figures 4A and 4B). IL-1β, IL-6 and TGF-β1 did not show any effect on chemerin production (data not shown).

ChemR23 expression on FLSs was determined by immunocytochemical analysis and Western blot analysis. Double-staining revealed that cultured FLSs expressed both ChemR23 and vimentin (Figures 4C through 4E). The use of a specific ChemR23 Ab also showed its expression in RA FLSs on Western blots (Figure 4F). Stimulation with TNF-α, IFN-γ, TGF-β, IL-1β and IL-6 did not show any effect on the expression of ChemR23 in RA FLSs.

Chemerin enhances IL-6, CCL2 and MMP-3 production by fibroblast-like synoviocytes

We next evaluated the effects of chemerin on the production of inflammatory mediators by RA FLSs. The cells were stimulated with chemerin for 24 and 48 hours, and the concentrations of IL-6 in the culture supernatant were measured by ELISA. After stimulation with chemerin for 24 hours, IL-6 production from FLSs was moderately increased, although it was not statistically significant. The incubation for 48 hours showed significant upregulation of chemerin-induced IL-6 production from FLSs ($P < 0.05$) (Figure 5A). The expression of CCL2 and MMP-3 from FLSs was also enhanced by incubation with chemerin for 48 hours in a dose-dependent manner ($P < 0.05$) (Figures 5B and 5C).

Chemerin enhances cell motility of rheumatoid arthritis fibroblast-like synoviocytes

In the RA synovium, the migration of RA FLSs into the cartilage and bone is considered important for pannus development [27]. Therefore, by using a scrape motility assay, we investigated whether chemerin could directly alter the migratory behavior of these cells. As shown in Figures 6A and 6B, exogenously added chemerin significantly increased the number of cells that migrated to the scraped area ($P < 0.05$). Moreover, incubation with PTX significantly suppressed chemerin-induced FLS motility (Figures 6A and 6B). Since PTX was previously

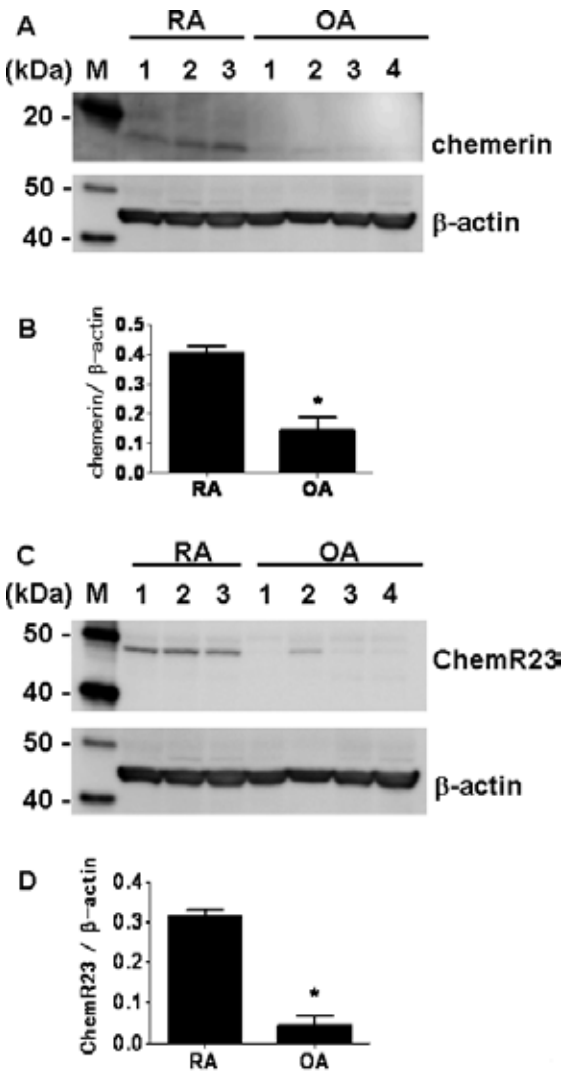

Figure 3 Expression of chemerin and ChemR23 in rheumatoid arthritis and osteoarthritis synovial tissue samples. **(A)** Western blots of chemerin protein expression in three rheumatoid arthritis (RA) and four osteoarthritis (OA) synovial tissues. M, protein molecular weight marker. **(B)** Relative protein expression of chemerin to β-actin in RA and OA synovial tissues. *$P < 0.05$ relative to RA synovial tissue. **(C)** Western blots of ChemR23 protein expression in three RA and four OA synovial tissues. M, protein molecular weight marker. **(D)** Relative expression of ChemR23 protein to β-actin. *$P < 0.05$ relative to RA synovial tissue.

Kaneko *et al. Arthritis Research & Therapy* 2011, **13**:R158
http://arthritis-research.com/content/13/5/R158

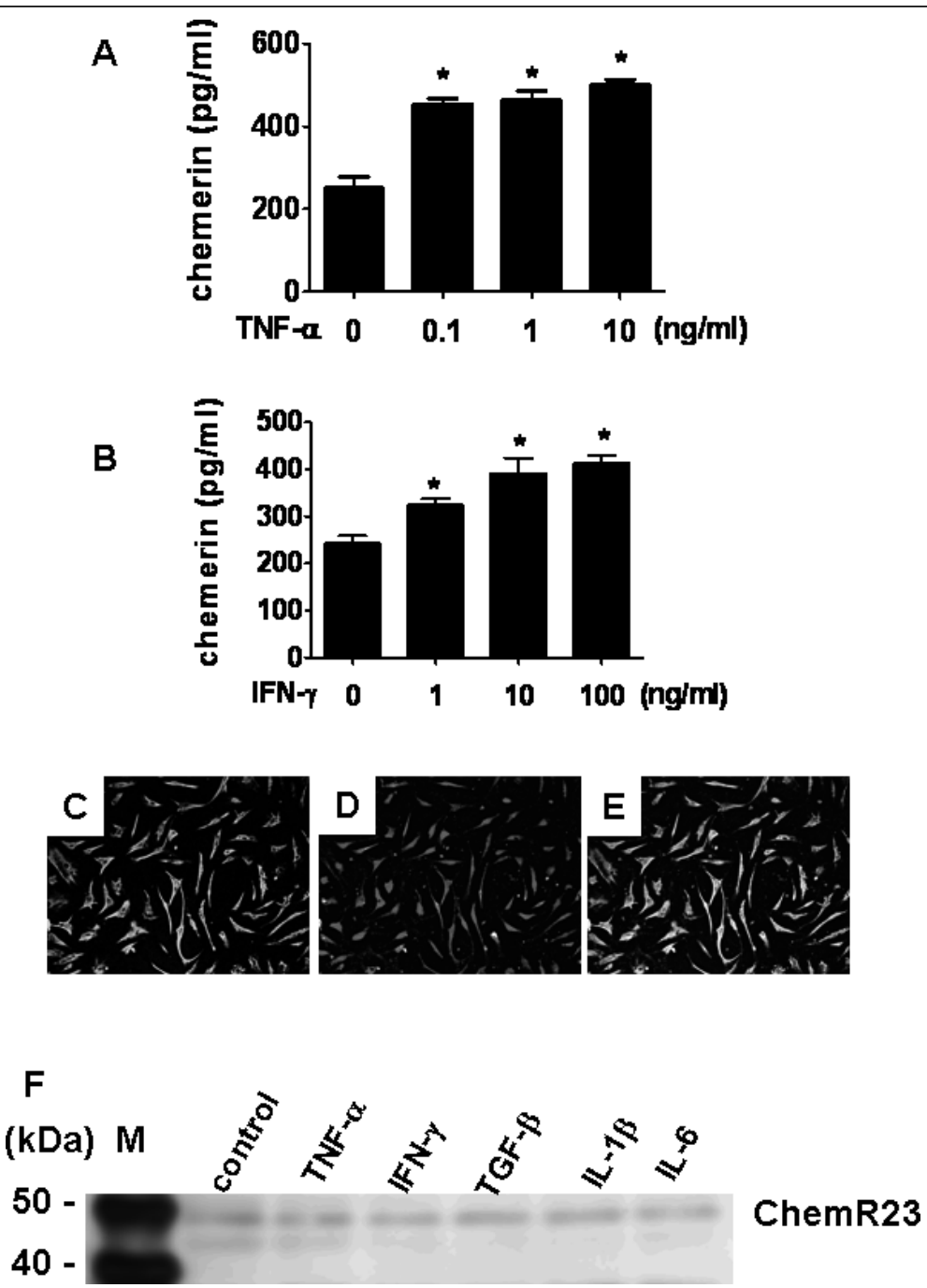

Figure 4 Expression of chemerin and ChemR23 by rheumatoid arthritis fibroblast-like synoviocytes. **(A)** and **(B)** Chemerin expression stimulated by TNF-α **(A)** or IFN-γ **(B)** and evaluated by ELISA using supernatants of cultured fibroblast-like synoviocytes (FLSs) isolated from synovial tissue samples taken from rheumatoid arthritis (RA) patients (n = 4). FLSs (2×10^4 cells/well) were stimulated at 37°C for 48 hours with TNF-α (0.1, 1 or 10 ng/ml) (A) or IFN-γ (1, 10 or 100 ng/ml) (A). Data in (A) and (B) are presented as means (± SEM) of one of four independent experiments analyzed in triplicate. *P < 0.05 relative to control. **(C)** through **(E)** Immunocytochemistry showing double-staining of cultured RA FLSs with **(C)** vimentin **(D)** ChemR23 and **(E)** a merged image of (C) and (D). **(F)** Western blot of ChemR23 protein expression in RA FLSs following TNF-α (10 ng/ml), IFN-γ (100 ng/ml), transforming growth factor (TGF)-β1 (1 ng/ml), IL-1β (5 ng/ml) or IL-6 (20 ng/ml) stimulation at 37°C for 24 hours.

Kaneko *et al. Arthritis Research & Therapy* 2011, **13**:R158
http://arthritis-research.com/content/13/5/R158

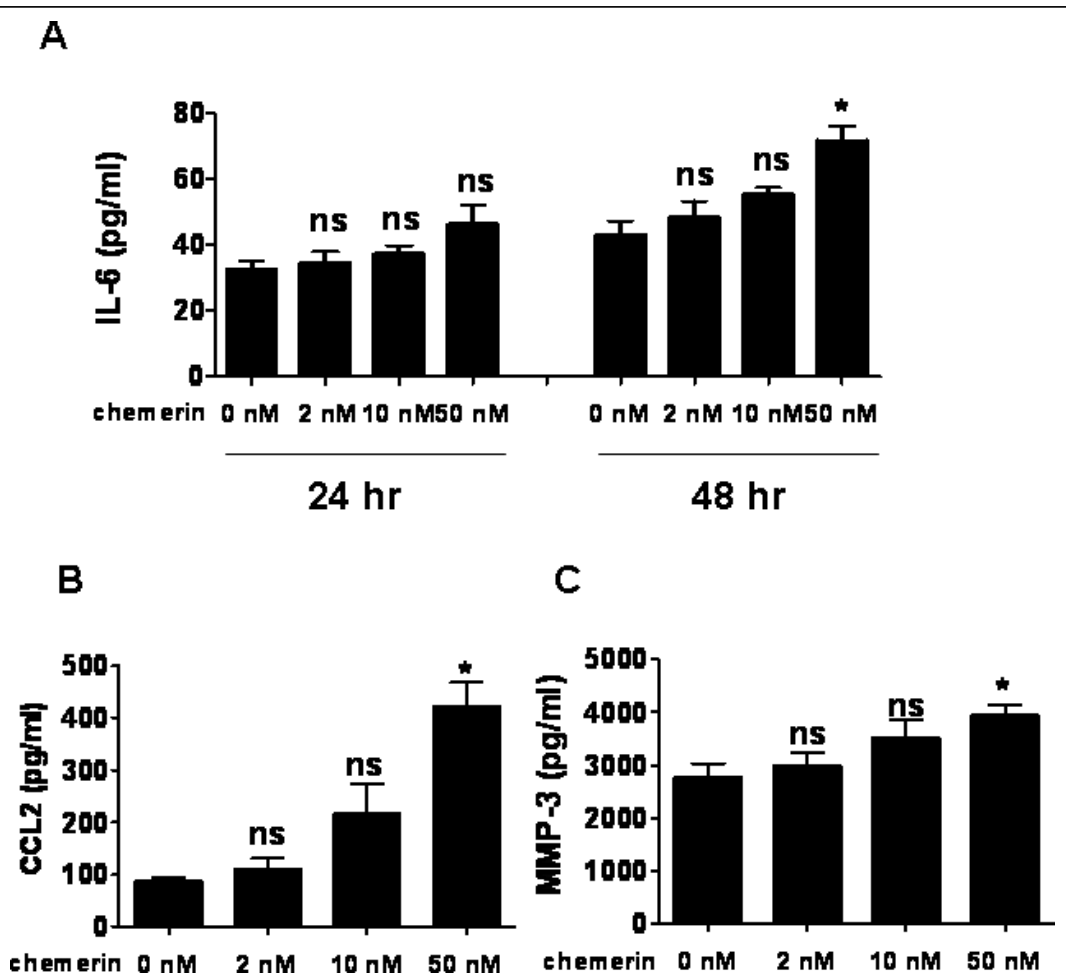

Figure 5 Chemerin enhances IL-6, chemokine (C-C motif) ligand 2 and matrix metalloproteinase 3 production by rheumatoid arthritis fibroblast-like synoviocytes. IL-6 **(A)**, chemokine (C-C motif) ligand 2 (CCL2) **(B)** and matrix metalloproteinase 3 (MMP-3) **(C)** expression levels were measured by ELISA using supernatants of cultured fibroblast-like synoviocytes isolated from the synovium of four patients with rheumatoid arthritis. FLSs (4×10^4 cells/well) were stimulated with 2, 10 or 50 nM recombinant chemerin at 37°C for 24 and 48 hours. Data are presented as means (± SEM) of one of four independent experiments analyzed in quadruplicate. *$P < 0.05$ relative to samples not treated with chemerin. ns = not significant.

reported to inhibit signal transduction in ChemR23$^+$ cells by ribosylation of the α_i subunits of the heterotrimeric G protein of ChemR23 [9], our result suggested the involvement of ChemR23 with chemerin-induced FLS motility. We also evaluated the effect of CCL2 on FLS migration. Incubation with CCL2 (2 or 10 nM) did not promote cell motility of FLSs (Figure 6C).

Chemerin induces activation of ERK1/2, p38MAPK and Akt of fibroblast-like synoviocytes

To determine the signaling pathway of chemerin-induced stimulation of FLSs, we stimulated FLSs with 10 nM chemerin for various time periods and performed Western blot analysis with phospho-specific Abs against ERK1/2, p38MAPK, JNK1/2 and Akt. Unstimulated FLSs showed only minimal phosphorylation of ERK1/2 (at zero minutes), whereas a marked increase in phosphorylation was detected after five minutes of stimulation with chemerin (Figures 7A and 7G). Cell lysates were also examined for chemerin-induced phosphorylation of other MAP kinases, including p38MAPK and JNK1/2. The addition of chemerin augmented the phosphorylation of p38MAPK at 5 to 15 minutes compared with unstimulated RA FLSs, but the level decreased at 30 minutes (Figures 7B and 7H), whereas phosphorylation of JNK1/2 was not promoted by chemerin stimulation (Figures 7C, D, I and 7J). Next, Akt activation, which is linked to regulation of proinflammatory cytokine production by RA FLSs

Kaneko *et al. Arthritis Research & Therapy* 2011, **13**:R158
http://arthritis-research.com/content/13/5/R158

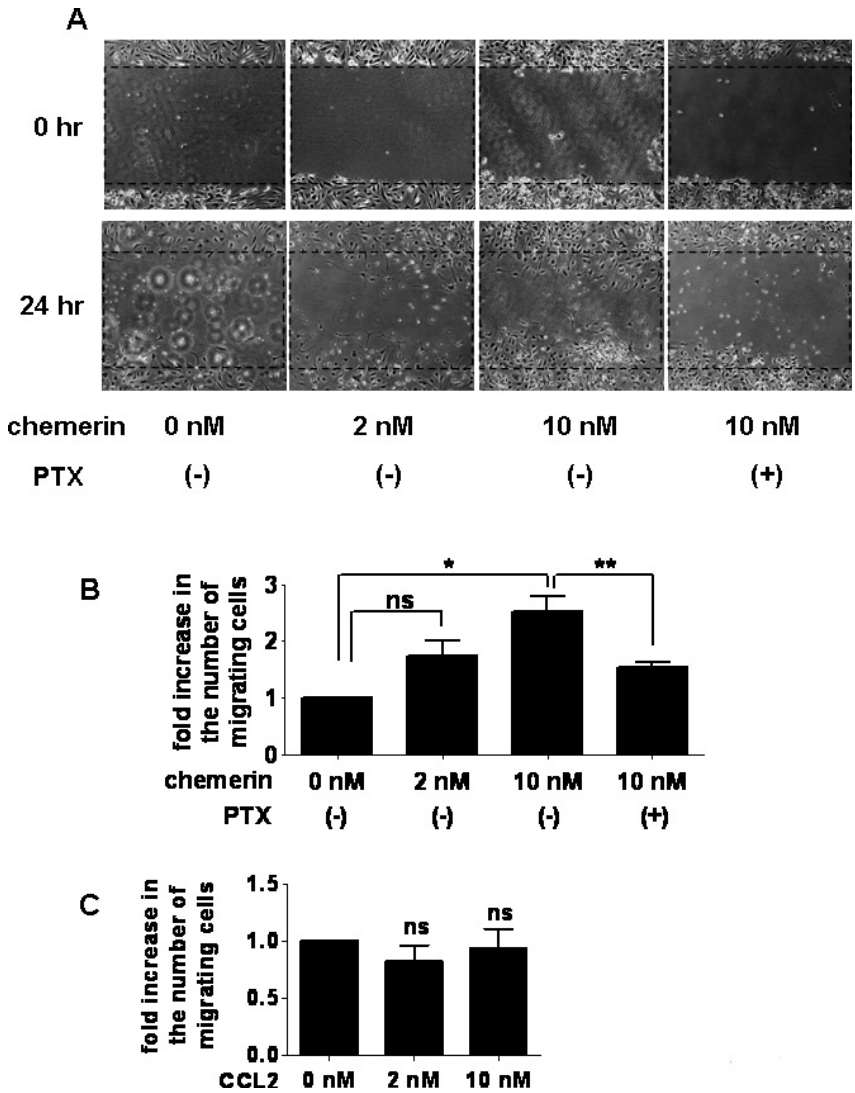

Figure 6 Chemerin promotes cell motility of rheumatoid arthritis fibroblast-like synoviocytes. **(A)** A scraped cell-free area was created on a monolayer of fibroblast-like synoviocytes (FLSs). After incubation with serum-free DMEM containing chemerin (2 or 10 nM) with or without pertussis toxin (PTX) (0.5 μg/ml), the process of two-dimensional FLS migration into the cell-free area at the center of the well was photographed with an inverted microscope at 0 and 24 hours. Representative photographs of three separate experiments are shown **(A)**. The number of the cells in the scraped area was counted. Data are fold increases in the number of migrating cells at 24 hours (number of cells that migrated after chemerin stimulation compared to the number of cells without stimulation) **(B)**. Data are presented as means (± SEM) of one of three independent experiments analyzed in triplicate. $^{*}P < 0.05$ relative to samples not treated with chemerin. $^{**}P < 0.05$ relative to samples not treated with PTX; ns, not significant. **(C)** Fold increase in the number of migrating cells when FLS were stimulated with 2 or 10 nM of chemokine (C-C motif) ligand 2 (CCL2) for 24 hours is shown; ns = not significant.

[28], was examined. Figures 7E and 7K show that stimulation of RA FLSs with 10 nM chemerin resulted in enhanced phosphorylation of Akt, with a peak level occurring at five minutes.

IκBα is one of the regulatory proteins of NF-κB, a transcriptional factor which induces various proinflammatory cytokines, including TNF-α and IL-6 [29,30]. When the cells were stimulated for NF-κB activation, IκBα was degraded and the amount of the protein was decreased [31]. Therefore, we analyzed the effect of chemerin on the degradation of IκBα in FLSs to clarify whether NF-κB is involved in chemerin-induced FLS activation. Figures 7F and 7L indicate that chemerin does not induce IκBα degradation in FLSs.

Kaneko *et al. Arthritis Research & Therapy* 2011, **13**:R158
http://arthritis-research.com/content/13/5/R158

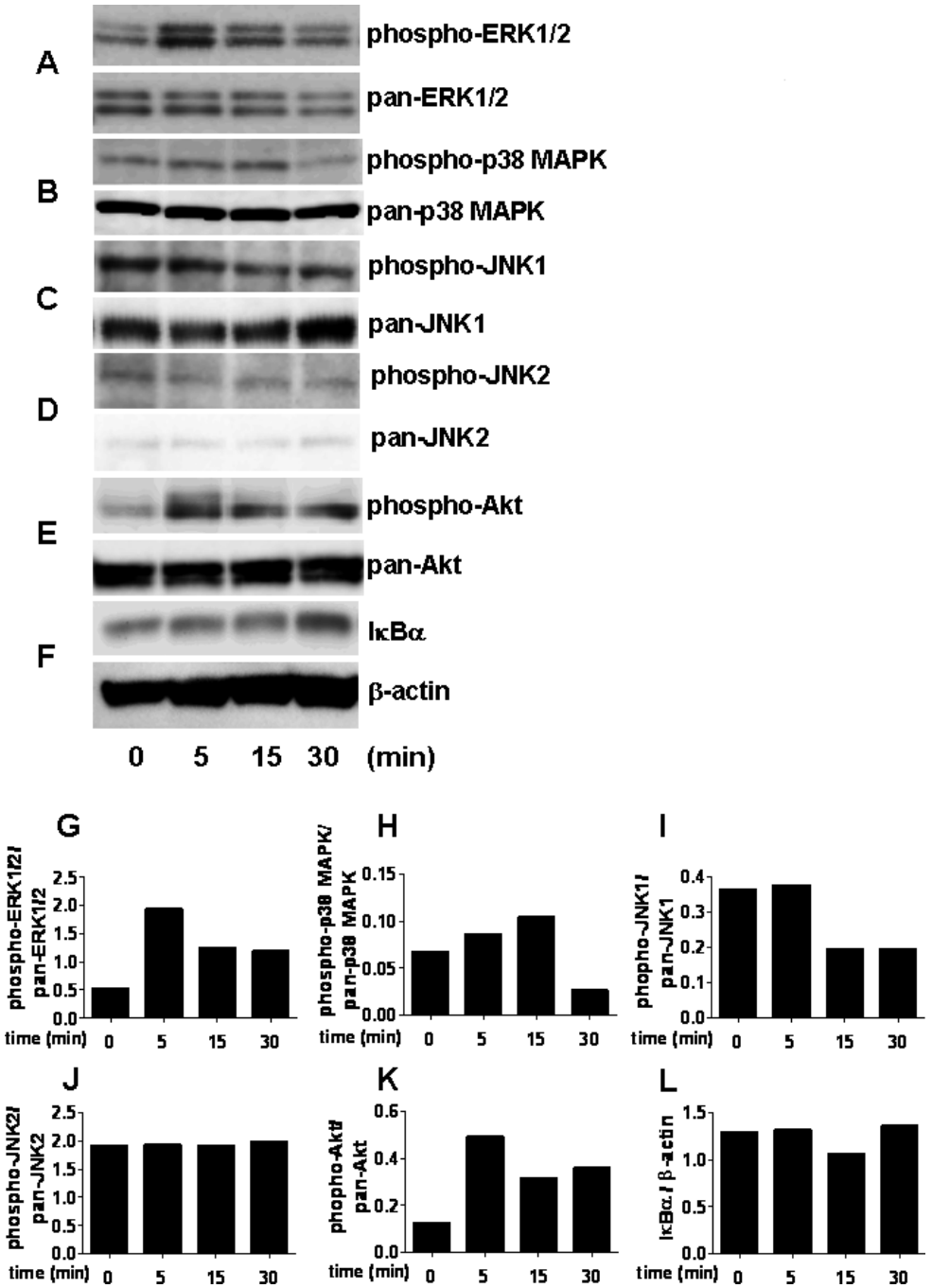

Figure 7 Chemerin activates p44/42 mitogen-activated protein kinase, p38 mitogen-activated protein kinase and Akt in rheumatoid arthritis fibroblast-like synoviocytes. Rheumatoid arthritis (RA) fibroblast-like synoviocytes (FLSs) were left unstimulated (zero minutes) or stimulated with 10 nM chemerin for 5 to 30 minutes. Cell lysates were examined by Western blot analysis with anti-phospho-p44/42 mitogen-activated protein kinase (anti-phospho-ERK1/2) and pan-ERK1/2 **(A)**, phospho-p38 mitogen-activated protein kinase (phospho-p38MAPK) and pan-p38MAPK **(B)**, phospho-c-Jun N-terminal kinase (pan-JNK)1/2 and pan-c-pan-JNK1/2 **(C)** and **(D)**, phospho-Akt and pan-Akt **(E)** and regulator of NF-κB (IκBα), and β-actin **(F)**. Shown are band intensity (expressed in arbitrary units) of phospho-ERK1/2 **(G)**, p38MAPK **(H)**, JNK1 **(I)**, JNK2 **(J)** and Akt **(K)** normalized to pan-ERK1/2, p38MAPK, JNK1, JNK2 and Akt, respectively. Relative expression of IκBα protein to β-actin is also shown **(L)**. The results are representative of three different experiments performed using RA FLSs from three different patients.

Kaneko *et al. Arthritis Research & Therapy* 2011, **13**:R158
http://arthritis-research.com/content/13/5/R158

Involvement of ERK1/2, p38MAPK and Akt pathways in chemerin-induced IL-6 production and cell motility of fibroblast-like synoviocytes

Next we examined the effects of signal blockade on IL-6 production and cell motility of FLSs to evaluate the involvement of signal transduction in chemerin-induced FLS activation. PD98059 (MEK, upstream of ERK1/2, inhibitor [32]), SB203580 (p38MAPK inhibitor [33]) and LY294002 (PI3K, upstream of Akt, inhibitor [34]) were used to block each signaling pathway. Pretreatment with 10 μM PD98059, SB203580 and LY294002 significantly inhibited chemerin-induced IL-6 production by RA FLSs ($P < 0.05$) (Figure 8A). The chemerin-induced enhancement of IL-6 production was not inhibited by polymyxin B, suggesting the lack of a significant amount of endotoxin in this procedure. Furthermore, chemerin-enhanced cell motility was inhibited by SB203580 and LY294002, but not by PD98059 (Figures 8B and 8C).

Discussion

In this study, we have shown that chemerin and ChemR23 are highly expressed in RA synovium. Chemerin enhanced the production of IL-6, CCL2 and MMP-3 from RA FLSs and promoted cell motility. These results suggest that chemerin activates FLSs in the RA synovium and is probably involved in the pathogenesis of RA.

Our results show upregulation of chemerin and accumulation of ChemR23$^+$ cells in RA synovium. We found that chemerin was expressed on synovial lining and sublining cells and on endothelial cells. Moreover, our study shows that FLSs isolated from RA synovium also produce chemerin *in vitro* and that this production is upregulated by stimulation with TNF-α and IFN-γ, which characterize the inflammatory environment in the RA synovium. In this regard, it was reported that the concentration of chemerin in the synovial fluid was much higher in RA than that in OA (358 ng/ml vs < 1 ng/ml) [9]. ChemR23 was expressed on most macrophages, CD1a$^+$ immature DCs and FLSs in RA synovium. A few DC-LAMP$^+$ mature DCs also expressed ChemR23. It was previously reported that ChemR23 was expressed on immature DCs derived from peripheral blood and that the expression was downregulated by maturation induced by lipopolysaccharide or CD40L [9].

The unique pathway of activation of the chemerin precursor, prochemerin, has been well-investigated [13-15,35,36]. Prochemerin is considered to be activated through C-terminal six- or seven-amino acid processing by protease and to be produced by neutrophils and mast cells at inflammatory sites. Neutrophils and mast cells are known to release protease-rich granules and to secrete immune mediators to activate themselves and other immune cells, triggering positive regulatory feedback that leads to acute or chronic RA inflammation [37-39]. Considered together, our data suggest that chemerin is produced at high levels by FLSs in RA synovium and that extracellular protease is produced by preexistent neutrophils and mast cells converted from inactive prochemerin into bioactive chemerin, which have powerful chemoattractant properties for migration of macrophages and DCs into the RA synovium.

The present results reveal that the expression of ChemR23 on RA FLSs and chemerin itself activate FLSs to enhance the production of IL-6 and CCL2. IL-6 is considered to have pleiotropic functions, including the regulation of maturation and activation of T and B cells, macrophages, osteoclasts, chondrocytes and endothelial cells in RA [40,41]. Clinically, tocilizumab, a humanized mAb specific for IL-6R, has outstanding anti-inflammatory effects, including suppression of disease activity and erosive progression in patients with RA that is resistant to traditional disease-modifying antirheumatic drugs [42]. CCL2 is known as a prototype chemokine that attracts monocytes, T cells, NK cells and basophils into the RA synovium [43]. Therefore, our results indicate that chemerin may be involved in the enhancement of local proinflammatory cytokine and chemokine production by RA FLSs, leading to persistent amplification of inflammation in the RA synovium, possibly in an autocrine or paracrine manner.

The present results indicate that chemerin enhances the cell motility of RA FLSs, whereas CCL2 does not promote FLS migration by this examination procedure. These data suggest that the effect of chemerin for FLS mobility is not affected by inducing the production of CCL2. In the RA joints, the pannus tissue migrates and invades the cartilage and bone, which contribute to damaging these structures [44]. FLSs are the predominant cell type in pannus tissue, especially at the pannus-cartilage junction [45]. FLSs retrieved from synovial tissues directly cause cartilage degradation when cocultured with macrophages *in vitro* [46], suggesting that FLS migration and invasion play a central role in pannus tissue-related cartilage degradation in RA. Moreover, our results show that chemerin enhances MMP-3 production from RA FLSs, which is a proteolytic enzyme with cartilage degradation properties. Collectively, our results suggest that chemerin plays an important role in cartilage destruction through FLS activation.

The present results show that chemerin enhances the activation of ERK1/2, p38MAPK and Akt, but not of JNK1/2 and NF-κB, in FLSs. Moreover, pretreatment with a specific inhibitor of MEK, p38MAPK, and PI3K suppressed chemerin-induced IL-6 production, and p38 MAPK and PI3 kinase inhibitor reduced RA FLS cell motility. These results suggest the involvement of both the MAPK (including MEK-ERK1/2 and p38MAPK) and

Kaneko *et al. Arthritis Research & Therapy* 2011, **13**:R158
http://arthritis-research.com/content/13/5/R158

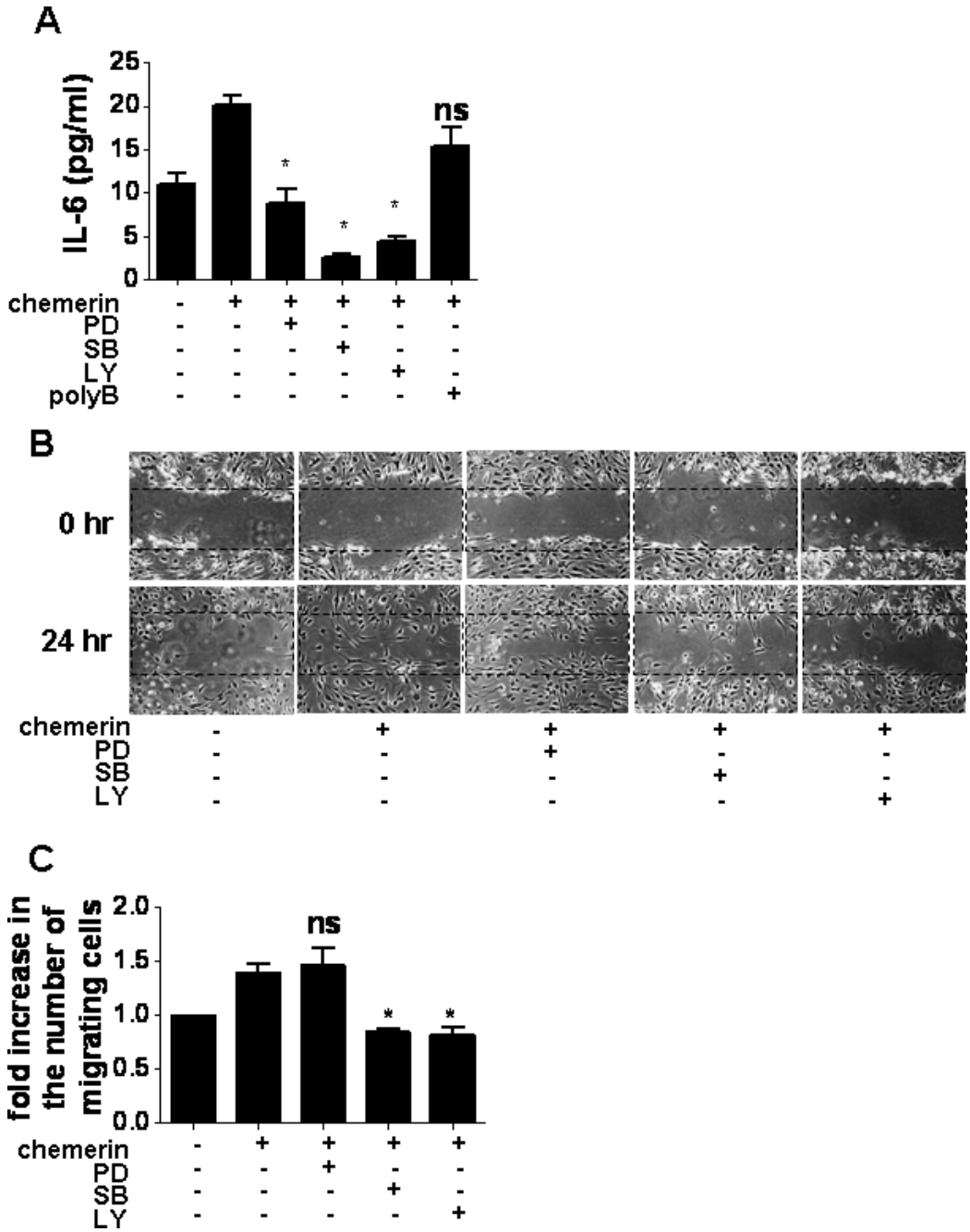

Figure 8 Involvement of mitogen-activated protein kinase and phosphoinositide 3-kinase-Akt pathways in chemerin-induced fibroblast-like synoviocyte activation. **(A)** Rheumatoid arthritis (RA) fibroblast-like synoviocytes (FLSs) were pretreated for 30 minutes with PD98059 (mitogen-activated protein kinase kinase inhibitor, 10 μM), SB203580 (p38 mitogen-activated protein kinase inhibitor, 10 μM), LY294002 (phosphoinositide 3-kinase inhibitor, 10 μM), or polymyxin B (50 μg/ml) before stimulation with or without 50 nM chemerin for 48 hours. IL-6 production in the supernatant was measured by ELISA. Data are presented as means ± SEM of one of four independent experiments analyzed in quadruplicate. LY = LY294002; PD = PD98059; polyB = polymyxin B; SB = SB203580. *$P < 0.05$ relative to treatment with 50 nM chemerin; ns, not significant. **(B)** and **(C)** Effects of PD98059, SB203580 and LY294002 on FLS motility were assessed by scrape motility assay. Representative two-dimensional photographs of FLS migratory process into the scraped cell-free area (0 and 24 hours) are shown in (B). The number of migrating cells in the scraped area was counted. Data represent the fold increase in the number of migrating cells, shown in (C). Data are presented as means ± SEM of one of four independent experiments analyzed in triplicate. *$P < 0.05$ relative to samples not treated with inhibitor; ns, not significant.

PI3K-Akt pathways in chemerin-induced IL-6 production by RA FLSs. The p38MAPK and PI3K-Akt pathways are also involved in cell motility induced by chemerin. Chemerin activated macrophage adhesion to fibronectin by activation of p38MAPK and PI3K-Akt signaling pathway [47]. These results suggest that chemerin activates macrophages as well as FLSs in RA synovium.

Conclusions

Our results identify the important role of chemerin in the activation of FLSs in RA synovium, suggesting that chemerin and ChemR23 interaction might play a role in the pathogenesis of RA.

Abbreviations

CCL2: chemokine (C-C motif) ligand 2; DC: dendritic cell; DMEM: Dulbecco's modified Eagle's medium; ELISA: enzyme-linked immunosorbent assay; ERK1/2: p44/42 mitogen-activated protein kinase; FCS: fetal calf serum; FLS: fibroblast-like synoviocyte; IFN: interferon; IL: interleukin; JNK: c-Jun N-terminal kinase; mAb: monoclonal antibody; MAPK: mitogen-activated protein kinase; MEK: mitogen-activated protein kinase kinase; MMP: matrix metalloproteinase; NF-κB: nuclear factor κB; NK cells: natural killer cells; OA: osteoarthritis; pAb: polyclonal antibody; PBS: phosphate-buffered saline; PI3K: phosphoinositide 3-kinase; PTX: pertussis toxin; RA: rheumatoid arthritis; TBS: Tris-buffered saline; TGF-β1: transforming growth factor β1; TNF-α: tumor necrosis factor α.

Acknowledgements

We thank Aya Sato for excellent technical support and Timothy Sullivan and Thomas J Schall (ChemoCentryx, Inc, Mountain View, CA, USA) for critical advice. This work was supported in part by Grants-in-Aid for Scientific Research from the Ministry of Health, Labor and Welfare and the Ministry of Education, Culture, Sports, Science, and Technology, Japan, and by the Japanese Ministry of Education, Global Center of Excellence (GCOE) Program, the International Research Center for Molecular Science in Tooth and Bone Diseases, and the Mitsui Life Social Welfare Foundation.

Author details

[1]Department of Medicine and Rheumatology, Graduate School of Medical and Dental Sciences, Tokyo Medical and Dental University, 1-5-45, Yushima, Bunkyo-ku, Tokyo, 113-8519, Japan. [2]KAN Research Institute, 3F, Kobe MI R&D Center, 6-7-3, Minatojima-minamimachi, Chuo-ku, Kobe, 650-0047, Japan. [3]Tsukuba Research Laboratories, Eisai Co, Ltd, 5-1-3, Toukoudai, Tsukuba, 300-2635, Japan. [4]Department of Molecular Preventive Medicine, Graduate School of Medicine, University of Tokyo, 7-3-1, Hongo, Bunkyo-ku, Tokyo, 113-0033, Japan. [5]Department of Medicine and Rheumatology, Tokyo Metropolitan Geriatric Hospital, 35-2, Sakae-cho, Itabashi-ku, Tokyo, 173-0015, Japan.

Authors' contributions

KK participated in the design of the study, carried out the experiments and statistical analysis and drafted the manuscript. YM, AT, SF, CM, WY, ME and KW assisted with carrying out the experiments and collecting data. TI, KMu, YT and KMa assisted in data interpretation and manuscript preparation. TS collected the clinical material. TN and NM conceived the study, participated in its design and coordination and helped to draft the manuscript. All authors read and approved the final manuscript for publication.

Competing interests

KMu is an employee of Eisai Co, Ltd. The authors declare that they have no competing interests.

Received: 9 March 2011 Revised: 5 May 2011
Accepted: 29 September 2011 Published: 29 September 2011

References

1. Lundy SK, Sarkar S, Tesmer LA, Fox DA: **Cells of the synovium in rheumatoid arthritis: T lymphocytes.** *Arthritis Res Ther* 2007, **9**:202.
2. Kinne RW, Stuhlmüller B, Burmester GR: **Cells of the synovium in rheumatoid arthritis: macrophages.** *Arthritis Res Ther* 2007, **9**:224.
3. Lebre MC, Jongbloed SL, Tas SW, Smeets TJM, McInnes IB, Tak PP: **Rheumatoid arthritis synovium contains two subsets of CD83$^-$DC-LAMP$^-$ dendritic cells with distinct cytokine profiles.** *Am J Pathol* 2008, **172**:940-950.
4. Huber LC, Distler O, Tarner I, Gay RE, Gay S, Pap T: **Synovial fibroblasts: key players in rheumatoid arthritis.** *Rheumatology (Oxford)* 2006, **45**:669-675.
5. Bartok B, Firestein GS: **Fibroblast-like synoviocytes: key effector cells in rheumatoid arthritis.** *Immunol Rev* 2010, **233**:233-255.
6. Nakano K, Okada Y, Saito K, Tanaka Y: **Induction of RANKL expression and osteoclast maturation by the binding of fibroblast growth factor 2 to heparan sulfate proteoglycan on rheumatoid synovial fibroblasts.** *Arthritis Rheum* 2004, **50**:2450-2458.
7. Takayanagi H, Iizuka H, Juji T, Nakagawa T, Yamamoto A, Miyazaki T, Koshihara Y, Oda H, Nakamura K, Tanaka S: **Involvement of receptor activator of nuclear factor kappaB ligand/osteoclast differentiation factor in osteoclastogenesis from synoviocytes in rheumatoid arthritis.** *Arthritis Rheum* 2000, **43**:259-269.
8. Gravallese EM: **Bone destruction in arthritis.** *Ann Rheum Dis* 2002, **61(Suppl 2)**:ii84-ii86.
9. Wittamer V, Franssen JD, Vulcano M, Mirjolet JF, Le Poul E, Migeotte I, Brézillon S, Tyldesley R, Blanpain C, Detheux M, Mantovani A, Sozzani S, Vassart G, Parmentier M, Communi D: **Specific recruitment of antigen-presenting cells by chemerin, a novel processed ligand from human inflammatory fluids.** *J Exp Med* 2003, **198**:977-985.
10. Parolini S, Santoro A, Marcenaro E, Luini W, Massardi L, Facchetti F, Communi D, Parmentier M, Majorana A, Sironi M, Tabellini G, Moretta A, Sozzani S: **The role of chemerin in the colocalization of NK and dendritic cell subsets into inflamed tissues.** *Blood* 2007, **109**:3625-3632.
11. Meder W, Wendland M, Busmann A, Kutzleb C, Spodsberg N, John H, Richter R, Schleuder D, Meyer M, Forssmann WG: **Characterization of human circulating TIG2 as a ligand for the orphan receptor ChemR23.** *FEBS Lett* 2003, **555**:495-499.
12. Vermi W, Riboldi E, Wittamer V, Gentili F, Luini W, Marrelli S, Vecchi A, Franssen JD, Communi D, Massardi L, Sironi M, Mantovani A, Parmentier M, Facchetti F, Sozzani S: **Role of ChemR23 in directing the migration of myeloid and plasmacytoid dendritic cells to lymphoid organs and inflamed skin.** *J Exp Med* 2005, **201**:509-515.
13. Wittamer V, Grégoire F, Robberecht P, Vassart G, Communi D, Parmentier M: **The C-terminal nonapeptide of mature chemerin activates the chemerin receptor with low nanomolar potency.** *J Biol Chem* 2004, **279**:9956-9962.
14. Wittamer V, Bondue B, Guillabert A, Vassart G, Parmentier M, Communi D: **Neutrophil-mediated maturation of chemerin: a link between innate and adaptive immunity.** *J Immunol* 2005, **175**:487-493.
15. Zabel BA, Allen SJ, Kulig P, Allen JA, Cichy J, Handel TM, Butcher EC: **Chemerin activation by serine proteases of the coagulation, fibrinolytic, and inflammatory cascades.** *J Biol Chem* 2005, **280**:34661-34666.
16. Kulig P, Zabel BA, Dubin G, Allen SJ, Ohyama T, Potempa J, Handel TM, Butcher EC, Cichy J: **Staphylococcus aureus-derived staphopain B, a potent cysteine protease activator of plasma chemerin.** *J Immunol* 2007, **178**:3713-3720.
17. Albanesi C, Scarponi C, Pallotta S, Daniele R, Bosisio D, Madonna S, Fortugno P, Gonzalvo-Feo S, Franssen JD, Parmentier M, De Pità O, Girolomoni G, Sozzani S: **Chemerin expression marks early psoriatic skin lesions and correlates with plasmacytoid dendritic cell recruitment.** *J Exp Med* 2009, **206**:249-258.
18. Berg V, Sveinbjörnsson B, Bendiksen S, Brox J, Meknas K, Figenschau Y: **Human articular chondrocytes express ChemR23 and chemerin: ChemR23 promotes inflammatory signalling upon binding the ligand chemerin$^{21-157}$.** *Arthritis Res Ther* 2010, **12**:R228.
19. Kaur J, Adya R, Tan BK, Chen J, Randeva HS: **Identification of chemerin receptor (ChemR23) in human endothelial cells: chemerin-induced endothelial angiogenesis.** *Biochem Biophys Res Commun* 2010, **391**:1762-1768.
20. Bozaoglu K, Curran JE, Stocker CJ, Zaibi MS, Segal D, Konstantopoulos N, Morrison S, Carless M, Dyer TD, Cole SA, Goring HH, Moses EK, Walder K,

Cawthorne MA, Blangero J, Jowett JB: **Chemerin, a novel adipokine in the regulation of angiogenesis.** *J Clin Endocrinol Metab* 2010, **95**:2476-2485.
21. Arnett FC, Edworthy SM, Bloch DA, McShane DJ, Fries JF, Cooper NS, Healey LA, Kaplan SR, Liang MH, Luthra HS, Medsger TA Jr, Mitchell DM, Neustadt DH, Pinals RS, Schaller JG, Sharp JT, Wilder RL, Hunder GG: **The American Rheumatism Association 1987 revised criteria for the classification of rheumatoid arthritis.** *Arthritis Rheum* 1988, **31**:315-324.
22. Nanki T, Nagasaka K, Hayashida K, Saita Y, Miyasaka N: **Chemokines regulate IL-6 and IL-8 production by fibroblast-like synoviocytes from patients with rheumatoid arthritis.** *J Immunol* 2001, **167**:5381-5385.
23. Zhao C, Fernandes MJ, Prestwich GD, Turgeon M, Di Battista J, Clair T, Poubelle PE, Bourgoin SG: **Regulation of lysophosphatidic acid receptor expression and function in human synoviocytes: implications for rheumatoid arthritis?** *Mol Pharmacol* 2008, **73**:587-600.
24. Caux C, Vanbervliet B, Massacrier C, Dezutter-Dambuyant C, de Saint-Vis B, Jacquet C, Yoneda K, Imamura S, Schmitt D, Banchereau J: **CD34+ hematopoietic progenitors from human cord blood differentiate along two independent dendritic cell pathways in response to GM-CSF+TNFα.** *J Exp Med* 1996, **184**:695-706.
25. Rivollier A, Mazzorana M, Tebib J, Piperno M, Aitsiselmi T, Rabourdin-Combe C, Jurdic P, Servet-Delprat C: **Immature dendritic cell transdifferentiation into osteoclasts: a novel pathway sustained by the rheumatoid arthritis microenvironment.** *Blood* 2004, **104**:4029-4037.
26. de Saint-Vis B, Vincent J, Vandenabeele S, Vanbervliet B, Pin JJ, Aït-Yahia S, Patel S, Mattei MG, Banchereau J, Zurawski S, Davoust J, Caux C, Lebecque S: **A novel lysosome-associated membrane glycoprotein, DC-LAMP, induced upon DC maturation, is transiently expressed in MHC class II compartment.** *Immunity* 1998, **9**:325-336.
27. Pap T, Gay S: **Fibroblasts and fibroblast-like synoviocytes.** In *Kelly's Textbook of Rheumatology. Volume 1.*. 8 edition. Edited by: Firestein GS, Budd RC, Harris ED Jr, McInnes IB, Ruddy S, Sergent JS. Philadelphia: Saunders Elsevier; 2008:201-214.
28. Hwang SY, Kim JY, Kim KW, Park MK, Moon Y, Kim WU, Kim HY: **IL-17 induces production of IL-6 and IL-8 in rheumatoid arthritis synovial fibroblasts via NF-κB- and PI3-kinase/Akt-dependent pathways.** *Arthritis Res Ther* 2004, **6**:R120-R128.
29. Georganas C, Liu H, Perlman H, Hoffmann A, Thimmapaya B, Pope RM: **Regulation of IL-6 and IL-8 expression in rheumatoid arthritis synovial fibroblasts: the dominant role for NF-κB but not C/EBPβ or c-Jun.** *J Immunol* 2000, **165**:7199-7206.
30. Ozes ON, Mayo LD, Gustin JA, Pfeffer SR, Pfeffer LM, Donner DB: **NF-κB activation by tumour necrosis factor requires the Akt serine-threonine kinase.** *Nature* 1999, **401**:82-85.
31. Huang TT, Kudo N, Yoshida M, Miyamoto S: **A nuclear export signal in the N-terminal regulatory domain of IκBα controls cytoplasmic localization of inactive NF-κB/IκBα complexes.** *Proc Natl Acad Sci USA* 2000, **97**:1014-1019.
32. Alessi DR, Cuenda A, Cohen P, Dudley DT, Saltiel AR: **PD 098059 is a specific inhibitor of the activation of mitogen-activated protein kinase kinase *in vitro* and *in vivo*.** *J Biol Chem* 1995, **270**:27489-27494.
33. Cuenda A, Rouse J, Doza YN, Meier R, Cohen P, Gallagher TF, Young PR, Lee JC: **SB 203580 is a specific inhibitor of a MAP kinase homologue which is stimulated by cellular stresses and interleukin-1.** *FEBS Lett* 1995, **364**:229-233.
34. Vlahos CJ, Matter WF, Hui KY, Brown RF: **A specific inhibitor of phosphatidylinositol 3-kinase, 2-(4-morpholinyl)-8-phenyl-4H-1-benzopyran-4-one (LY294002).** *J Biol Chem* 1994, **269**:5241-5248.
35. Zabel BA, Zuniga L, Ohyama T, Allen SJ, Cichy J, Handel TM, Butcher EC: **Chemoattractants, extracellular proteases, and the integrated host defense response.** *Exp Hematol* 2006, **34**:1021-1032.
36. Du XY, Zabel BA, Myles T, Allen SJ, Handel TM, Lee PP, Butcher EC, Leung LL: **Regulation of chemerin bioactivity by plasma carboxypeptidase N, carboxypeptidase B (activated thrombin-activable fibrinolysis inhibitor), and platelets.** *J Biol Chem* 2009, **284**:751-758.
37. Eklund KK: **Mast cells in the pathogenesis of rheumatic diseases and as potential targets for anti-rheumatic therapy.** *Immunol Rev* 2007, **217**:38-52.
38. Maruotti N, Crivellato E, Cantatore F, Vacca A, Ribatti D: **Mast cells in rheumatoid arthritis.** *Clin Rheumatol* 2007, **26**:1-4.
39. Cascão R, Rosário HS, Souto-Carneiro MM, Fonseca JE: **Neutrophils in rheumatoid arthritis: more than simple final effectors.** *Autoimmun Rev* 2010, **9**:531-535.
40. Brennan FM, McInnes IB: **Evidence that cytokines play a role in rheumatoid arthritis.** *J Clin Invest* 2008, **118**:3537-3545.
41. Kishimoto T: **Interleukin-6: from basic science to medicine: 40 years in immunology.** *Annu Rev Immunol* 2005, **23**:1-21.
42. Nishimoto N, Hashimoto J, Miyasaka N, Yamamoto K, Kawai S, Takeuchi T, Murata N, van der Heijde D, Kishimoto T: **Study of active controlled monotherapy used for rheumatoid arthritis, an IL-6 inhibitor (SAMURAI): evidence of clinical and radiographic benefit from an *x* ray reader-blinded randomised controlled trial of tocilizumab.** *Ann Rheum Dis* 2007, **66**:1162-1167.
43. Iwamoto T, Okamoto H, Toyama Y, Momohara S: **Molecular aspects of rheumatoid arthritis: chemokines in the joints of patients.** *FEBS J* 2008, **275**:4448-4455.
44. Firestein GS: **Etiology and pathogenesis of rheumatoid arthritis.** In *Kelly's Textbook of Rheumatology. Volume 1.*. 8 edition. Edited by: Firestein GS, Budd RC, Harris ED Jr, McInnes IB, Ruddy S, Sergent JS. Philadelphia: Saunders Elsevier; 2008:1035-1086.
45. Bromley M, Woolley DE: **Histopathology of the rheumatoid lesion: identification of cell types at sites of cartilage erosion.** *Arthritis Rheum* 1984, **27**:857-863.
46. Scott BB, Weisbrot LM, Greenwood JD, Bogoch ER, Paige CJ, Keystone EC: **Rheumatoid arthritis synovial fibroblast and U937 macrophage/monocyte cell line interaction in cartilage degradation.** *Arthritis Rheum* 1997, **40**:490-498.
47. Hart R, Greaves DR: **Chemerin contributes to inflammation by promoting macrophage adhesion to VCAM-1 and fibronectin through clustering of VLA-4 and VLA-5.** *J Immunol* 2010, **185**:3728-3739.

doi:10.1186/ar3475
Cite this article as: Kaneko *et al.*: Chemerin activates fibroblast-like synoviocytes in patients with rheumatoid arthritis. *Arthritis Research & Therapy* 2011 **13**:R158.

Submit your next manuscript to BioMed Central and take full advantage of:

- **Convenient online submission**
- **Thorough peer review**
- **No space constraints or color figure charges**
- **Immediate publication on acceptance**
- **Inclusion in PubMed, CAS, Scopus and Google Scholar**
- **Research which is freely available for redistribution**

Submit your manuscript at
www.biomedcentral.com/submit

BioMed Central

運動器外科学分野
軟骨再生学分野

宗田　大

医歯学総合研究科・生体支持組織学系専攻
運動器外科学・教授

1）研究の課題名

（1）前十字靱帯（ACL）損傷膝の問題の解決

Solution of ACL injured knee related problems

スポーツ傷害の代表である前十字靱帯（ACL）損傷とその治療法の発展を長年のテーマとして取り組んでいる。内側ハムストリング腱を移植腱として用いる2重束再建術を開発し、臨床的に取り組んできた。本年は2束の初期張力についての経験のまとめ（1）、さらに術中のNAVIやTension meterを用いた研究が出版された（2）。今後このトピックについて世界的な情報発信をしていく予定である。

ACL損傷を放置すると外傷性関節症を発症する。手術前後の血清グルコサミン値と患者背景の相関が認められ、そのまとめを行っている。発症素因について患者の検体を用いたマイクロアレイ解析により、重要な遺伝子を明らかにし関節症治療に結びつける取り組みを行っている。

ACL損傷患者は遺伝子的な背景を持つ。マイクロアレイ解析、患者の形態評価（3）、動作解析を行うことにより損傷の予防に効果的な術前、術後の指導法を開発している。またACL受傷の動作解析を留学先でスタッフのKoga Hが行った（4,5）。その結果を踏まえてACL損傷予防の取り組みにも多方面で関わっている（6）。

1. Muneta T, et al. Sports Med Arthrosc Rehabil Ther Technol. 2011 28;3：15.
2. Koga H, Muneta T, et al. Am J Sports Med. 2011 Nov 22. [Epub ahead of print]
3. Yamazaki J, Muneta T, et al. Am J Sports Med. 2011 Feb;39（2）：410-4.
4. Koga H, et al. Am J Sports Med. 2010 38（11）：2218-25
5. Koga H, et al. Clin J Sport Med. 2011 21（3）：271-4.

（2）そのほかの関節疾患についての臨床的取組み

Solution of Problems in Orthopaedic Surgery besides ACL injury related surgery

運動器外科学では主に下肢関節疾患の治療を扱っているが、膝関節手術として確立している人工膝関節や人工股関節の成績向上の臨床的意義は大きい。人工膝関節のデザイン上後十字靱帯（PCL）を温存するか否かで、コンセプトが異なり、両者の優劣は得られていない。我々は両膝同時置換例で無作為に双方の使い分け、左右の成績の検討を行いPCLを切除するデザインの成績が良好であることを報告した（6）。

十字靱帯損傷に合併する内側の動揺性に対して独自に開発した方法で10数年来行ってきた。今回成績のまとめを出版する機会を得た（7）。

6.Yagishita K, Muneta T, et al. J Arthroplasty. 2011 Jun 14. [Epub ahead of print]
7.Koga H, Muneta T, et al.　Knee Surg Sports Traumatol Arthrosc. 2012 20（1）：88-94.

（3）骨、軟骨の形成、ホメオスタシスおよび造血微小環境の制御における骨形成因子BMPの生理機能の解析

Roles of BMPs 2, 4, and 7 during skeletal development, in postnatal bone homeostasis, and in intramedullary hematopoiesis

骨形成因子（BMP）ファミリーの中でBMP2, 4, 7は、胎生期の骨格ならびに生後の骨組織にオーバーラップして発現が観察される分子である。私たちは、コンディショナルノックアウトマウスの解析から、BMP2は生後の骨のホメオスタシスにおいて必須の分子であり、その欠損により、骨折後の骨修復の過程が完全に阻害されることを明らかとしてきた（Tsuji et al., Nature Genetics, 2006）。これに対して、BMP4及びBMP7のコンディショナルノックアウトマウスでは、X線による解析では、明らかな骨折は確認できず、骨折後の組織修復過程も明らかな遅延は観察されなかった。生後の骨組織で発現しているBMPの中でBMP2のみが重要な生理機能を持っている理由は未だ不明である。一方、BMP4、BMP7を同時に欠損したマウスにおいては、胎生期の骨形成は生じるが、生後の骨形成に重篤な障害が生じることが明ら

かとなった。このことは、BMP4、BMP7の分子機能は互いに補完しあう関係にあることを示唆している。本研究では、BMP2, 4, 7の機能的分担をより詳細に検討することで、それぞれの骨、軟骨のホメオスタシスにおける生理機能を明らかとしていくことを目的としている。BMP4、BMP7を同時に欠損したコンディショナルノックアウトマウスの機能解析とBMP7のコンディショナルノックアウトマウスに強制ランニングを加えることによりin vivoでの軟骨ホメオスターシスに対するBMP7の役割を明らかにしつつある。

近年、骨芽細胞が造血微小環境の主要なコンポーネントである事が示され、その維持にBMPシグナルが関与する可能性が示唆されている。造血系のホメオスタシスにおけるBMP分子の生理機能を検討するため、骨髄におけるBMPコンディショナルノックアウトマウスの作成を行い、その表現型の解析をおこなった。骨髄でBMP4を欠損したマウスでは、赤芽球、T細胞、B細胞、単球のポピュレーションに変化はなかったが、造血幹細胞を含む未分化細胞のポピュレーションであるLSK（Lin-ScaI+c-kit+）細胞分画は、有為に減少していた。この事は、BMP4の活性が、骨髄微小環境の維持に必要である可能性を示唆している。さらにBMP2コンディショナルノックアウトマウスの作成を共同研究で行う予定である。

またin vivoの動物実験でザイモサン誘発関節炎モデルで関節炎をコントロールするとともに軟骨代謝を改善することを示した（8）。またBMP7が腱に注射を行うことによって軟骨分化を起こし、力学的な性質が変化する可能性を示し、同時に再生半月を促進する可能性が示唆されている。

8.Takahashi T, Muneta T, Sekiya I, et al. Cell Tissue Res. 2011 344（2）：321-32.

（4）関節症発症及び病態の進行の分子メカニズムの解析および非侵襲性のマウス関節症モデルの確立

Identification and characterization of the genes in the pathogenesis of osteoarthritis and a new model of osteoarthritis by forced running in mice

本研究は、変形性関節症の発症及び進行に関与する遺伝子の同定及び生理機能の解析を通じて病態の分子メカニズムを明らかとすることを目的としている。ヒト変形性関節症において、人工膝関節置換術を行った患者の了承のもと、滑膜サンプルにおける遺伝子発現パターンの網羅的解析を行った。その結果、骨棘形成の多寡と相関する遺伝子として、オステオポンチン及びその翻訳後修飾に関与する酵素であるプロトロンビナーゼを同定した。まずオステオポンチン並びにトロンビン切断型オステオポンチンの生理機能の解析を膝前十字靱帯の患者からの関節液と臨床症状を対象として、炎症への関与と治癒における役割に分けて解析している（ORS2012で発表予定）。関節症研究の展開を広げるため強制的走行機械を用いたマウスの関節症発症モデルを開発中である。マウスの種類、卵巣摘出の有無、走行距離などをパラメター―として、マウスの非侵襲性の関節症発症モデルを開発中（ORS2012で発表予定）である。

（5）間葉幹細胞による再生医療の開発

Repair of intraarticular tissue injury by synovial mesenchymal stem cells

私たちのこれまでの解析によると、正常膝関節液中の間葉幹細胞はわずかにしか存在しないが、前十字靭帯損傷や軟骨損傷を有する膝の関節液中には100倍以上の間葉幹細胞が存在する。また、前十字靭帯、半月板、滑膜等の関節内組織由来の間葉幹細胞は、骨髄液、皮下脂肪、骨格筋等の関節外組織由来の間葉幹細胞と比較し、互いに遺伝子プロファイルが類似する。さらに滑膜由来の間葉幹細胞を関節内に投与すると、損傷組織部位に接着し、修復に寄与する。関節軟骨、半月板、靭帯等の関節内組織損傷により、間葉幹細胞が滑膜から関節液中に動員され、損傷部位に接着し、組織修復に貢献する機序の存在が予測される。しかし、実際には動員または損傷部位に接着する幹細胞の数が限られるため、自然治癒には限界があるものと推察される。より軟骨欠損モデルを用いて、より効率の良い滑膜幹細胞の移植法を工夫している。

私たちは、これまでの基礎研究の成果を踏まえ、滑膜の間葉幹細胞を体外で自己血清を使用して増殖させ、人工素材を使用せずに、関節鏡視下で、軟骨欠損部に移植する、関節軟骨の再生医療を開始している。家兎の椎間板変性モデルに対する滑膜幹細胞移植の有用性を検討した（9）。

本年は関節症変化の重要な構造である半月板の再生促進法を種々の動物（ラット、家兎、ミニブタ）で行ってきた。内側半月板の前方2分の1の切除モデルを用いて、滑膜幹細胞を移植することにより有意に半月板再生を促進することを認めている。ミニブタを用いた研究がCytotherapy にアクセプトされた。治癒促進法についてさらに細かい具体的な検討を重ねている（ORS2012で発表予定）。

一方将来の企業化を見据えて、同種の滑膜幹細胞移植の研究も進めている。ラット半月板欠損モデルを用いた結果としては、minor mismatchの移植では自家移植と遜色ない再生促進が得られるが、major mismatchではコントロールと同様の効果しか得られていない（ORS2012で発表予定）。

歯学部とのイノベーション研究もまとめの段階に入った。歯肉の間葉幹細胞の増殖能・多分化能は、歯髄、歯根膜細胞よりも優れ、特に骨分化能は将来の臨床的な応用も考慮できることを見出している。

2）

3）発表の研究内容についての英文要約

Bere T, Florenes TW, Krosshaug T, Koga H, Nordsletten L, Irving C, Muller E, Reid RC, Senner V, Bahr R. Mechanisms of anterior cruciate ligament injury in world cup alpine skiing：a systematic video analysis of 20 cases. Am J Sports Med 39（7）：1421-9, 2011.

This study was undertaken to qualitatively describe the mechanisms of anterior cruciate ligament injury in World Cup alpine skiing. Three main categories of injury mechanisms were identified：slip-catch, landing back-weighted, and dynamic snowplow. The slip-catch mechanism accounted for half of the cases（n = 10）, and all these injuries occurred during turning, without or before falling. The skier lost pressure on the outer ski, and while extending the outer knee to regain grip, the inside edge of the outer ski caught abruptly in the snow, forcing the knee into internal rotation and valgus. The same loading pattern was observed for the dynamic snowplow（n = 3）. The landing back-weighted category included cases（n = 4）where the skier was out of balance backward in flight after a jump and landed on the ski tails with nearly extended knees. The suggested loading mechanism was a combination of tibiofemoral compression, boot-induced anterior drawer, and quadriceps anterior drawer. Based on this video analysis of 20 injury situations, the main mechanism of anterior cruciate ligament injury in World Cup alpine skiing appeared to be a slip-catch situation where the outer ski catches the inside edge, forcing the outer knee into internal rotation and valgus.

Gamer, L.W., Tsuji, K., Cox, K., Capelo, L.P., Lowery, J., Beppu, H., and Rosen, V. BMPR-II is dispensable for formation of the limb skeleton. Genesis 49：719, 2011

Initiation of BMP signaling is dependent upon activation of Type I BMP receptor by constitutively active Type II BMP receptor. Three Type II BMP receptors have been identified; Acvr2a and Acvr2b serve as receptors for BMPs and for activin-like ligands whereas BMPR-II functions only as a BMP receptor. As BMP signaling is required for endochondral ossification and loss of either Acvr2a or Acvr2b is not associated with deficits in limb development, we hypothesized that BMPR-II would be essential for BMP signaling during skeletogenesis. We removed BMPR-II from early limb mesoderm by crossing BMPR-II floxed mice with those carrying the Prx1-Cre transgene. Mice lacking limb expression of BMPR-II have normal skeletons that could not be distinguished from control littermates. From these data, we conclude that BMPR-II is not required for endochondral ossification in the limb where loss of BMPR-II may be compensated by BMP utilization of Acvr2a and Acvr2b.

Kokabu, S., Gamer, L., Cox, K., Lowery, J., Tsuji, K., Raz, R., Economides, A., Katagiri, T., and Rosen, V. BMP3 Suppresses Osteoblast Differentiation of Bone Marrow Stromal Cells via Interaction with Acvr2b. Mol Endocrinol 26：87, 2012.

Enhancing bone morphogenetic protein（BMP）signaling increases bone formation in a variety of settings that target bone repair. However, the role of BMP in the maintenance of adult bone mass is not well understood. Targeted disruption of BMP3 in mice results in increased trabecular bone formation, whereas transgenic overexpression of BMP3 in skeletal cells leads to spontaneous fracture, consistent with BMP3 having a negative role in bone mass regulation. Here we investigate the importance of BMP3 as a mediator of BMP signaling in the adult skeleton. We find that osteoblasts（OBL）and osteocytes are the source of BMP3 in adult bone. Using in vitro cultures of primary bone marrow stromal cells, we show that overexpression of BMP3 suppresses OBL differentiation, whereas loss of BMP3 increases colony-forming unit fibroblasts and colony-forming unit OBL. The ability of BMP3 to affect OBL differentiation is due to its interaction with activin receptor type 2b（Acvr2b）because knockdown of endogenous Acvr2b in bone marrow stromal cells reduces

the suppressive effect of BMP3 on OBL differentiation. These findings best fit a model in which BMP3, produced by mature bone cells, acts to reduce BMP signaling through Acvr2b in skeletal progenitor cells, limiting their differentiation to mature OBL. Our data further support the idea that endogenous BMPs have a physiological role in regulating adult bone mass.

Koga H, Bahr R, Myklebust G, Engebretsen L, Grund T, Krosshaug T. Estimating anterior tibial translation from model-based image-matching of a noncontact anterior cruciate ligament injury in professional football：a case report. Clin J Sport Med 21（3）：271-4, 2011.
Although video analysis is the only method available to extract kinematic data from real injury situations to clarify the mechanisms for noncontact anterior cruciate ligament（ACL）injury, most studies have been limited to simple visual inspection, the accuracy of which has been shown to be limited. As an alternative, a model-based image-matching（MBIM）technique has been developed to extract joint kinematics from uncalibrated video recordings. This technique has been validated in noninjury situations in a laboratory environment and has also been found to be feasible for use in actual ACL injury situations. This study presents a noncontact ACL injury situation in a male footballer recorded during a television broadcast using 4 high-definition cameras from different views, including 2 high-speed recordings. We have used the MBIM technique to describe the detailed joint kinematics, including tibial translations.

Koga H, Muneta T, Yagishita K, Ju YJ, Sekiya I. Surgical management of grade 3 medial knee injuries combined with cruciate ligament injuries. Knee Surg Sports Traumatol Arthrosc 20（1）：88-94, 2012.
Although various surgical procedures have attempted to restore valgus stability in medial knee injuries, so far none has achieved satisfactory results. The purpose of this study was to assess clinical outcome for patients with grade 3 valgus instability who were treated according to our surgical management strategy.

Koga H, Muneta T, Yagishita K, Ju YJ, Sekiya I. The Effect of Graft Fixation Angles on Anteroposterior and Rotational Knee Laxity in Double-Bundle Anterior Cruciate Ligament Reconstruction：Evaluation Using Computerized Navigation. Am J Sports Med（in press）.
One of the main differences affecting outcome between single-bundle and double-bundle anterior cruciate ligament（ACL）reconstructions may be graft fixation angles and initial force settings; however, there has been little research to investigate these effects in either technique. In this in vivo laboratory model, double-bundle ACL reconstruction with fixation of AMB（anteromedial bundle）at 20° and PLB（posterolateral bundle ）at 20° or 45° restored better stability than single AMB or single PLB reconstruction in which the graft was of smaller size.

◎Sekiya I, Ojima M, Suzuki S, Yamaga M, Horie M, Koga H, Tsuji K, Miyaguchi K, Ogishima S, Tanaka H, Muneta T. Human mesenchymal stem cells in synovial fluid increase in the knee with degenerated cartilage and osteoarthritis. J Orthop Res（in press）.
We investigated whether mesenchymal stem cells（MSCs）in synovial fluid（SF）increased in the knee with degenerated cartilage and osteoarthritis. SF was obtained from the knee joints of 22 patients with anterior cruciate ligament（ACL）injury during ACL reconstruction, and cartilage degeneration was evaluated arthroscopically. SF was also obtained from the knee joints of 6 healthy volunteers, 20 patients with mild osteoarthritis, and 26 patients with severe osteoarthritis, in which the grading was evaluated radiographically. The cell component in the SF was cultured for analyses. Synovium（SYN）and bone marrow（BM）were also harvested during total knee arthroplasties. The MSC number in SF was correlated with the cartilage degeneration score evaluated by arthroscopy. The MSC number in the SF was hardly noticed in normal volunteers, but it increased in accordance with the grading of osteoarthritis. Though no significant differences were observed regarding surface epitopes, or differentiation potentials, the morphology and gene profiles in SF MSCs were more similar to those in SYN MSCs than in BM MSCs. We listed 20 genes which were expressed higher in both SYN MSCs and SF MSCs than in BM MSCs, and 3 genes were confirmed by quantitative RT-PCR. MSCs in SF increased along with degenerated cartilage and osteoarthritis.

Takahashi, T., Muneta, T., Tsuji, K., and Sekiya, I. BMP-7 inhibits cartilage degeneration through suppression of inflammation in rat zymosan-induced arthritis. Cell Tissue Res 344：321, 2011.
Bone morphogenetic protein-7（BMP-7）regulates cartilage metabolism and promotes matrix synthesis. However, the effect of BMP-7 on inflammatory arthritis remains unknown. We investigated the effect and mechanism of exogenous BMP-7 on cartilage and synovium in vivo in rat zymosan-induced arthritis. Zymosan was injected into the left knees of Wistar rats. Phosphate-buffered saline or BMP-7 at 10, 100, or 1000 ng per joint was injected into the left knee every 2 days. Normal joints acted as normal controls. The knee joints were analyzed histologically and immunohistologically at 14 days. Joint swelling was evaluated by measuring the transverse diameter of the knee joints. Synovial lysates were collected, and the

concentrations of interleukin-1 β（IL-1 β）, IL-6, and IL-10 were measured by enzyme-linked immunosorbent assay. Intra-articular injection of zymosan resulted in acute inflammation and was followed by cartilage degeneration. Local administrations of BMP-7 inhibited this loss of cartilage matrix in a dose-dependent manner. Immunohistochemical analysis demonstrated enhanced type II collagen levels in cartilage and enhanced BMP-7 levels in cartilage and synovium after exogenous BMP-7 treatment. Joint swelling and cell infiltration into synovium were significantly reduced by BMP-7 injections. Administration of BMP-7 decreased IL-1 β production significantly and increased IL-10 production in the synovium. Thus, intra-articular injections of BMP-7 had a protective effect on cartilage degeneration in the inflammatory arthritis model by enhancing levels of BMP-7 in cartilage and suppressing the production of IL-1 β in synovium.

Muneta T, Koga H, Ju YJ, Yagishita K, Sekiya I.　Effects of different initial bundle tensioning strategies on the outcome of double-bundle ACL reconstruction：a cohort study.　Sports Med Arthrosc Rehabil Ther Technol. 2011 Jul 28;3：15.

This study was performed to investigate the effects of different strategies and initial tension applied to each one of the bundles, antero-medial（AM）and postero-lateral（PL）, on clinical outcome in double bundle（DB）ACL reconstruction.

One hundred fifty-one primary unilateral DB ACL reconstructions performed by a single surgeon from 1994 through 2002 were included in the study with a follow-up of at least 24 months. They were divided in the following 3 groups：Group I - Higher initial tension applied manually in the AM bundle compared to PL. II - Higher tension applied in the PL bundle compared to AM. III - The 2 bundles were attempted to be equally tensioned. All fixations were performed in 30 degrees of flexion. Clinical outcome was retrospectively evaluated by use of knee range of motion, manual knee laxity tests, KT-1000, Lysholm knee scale, subjective recovery scale and sports performance recovery scale. Group I showed a significant extension deficit compared with groups II and III. ANOVA revealed a significant difference of anterior laxity measured by the KT-1000（average KT difference of 2.1, 2.1 and 1.2 mm in Group I, II and III, respectively）. A statistical difference was found among the three groups regarding subjective and sports performance recovery scales with Group II showing higher scores in recovery than Group I.

The current clinical study does not recommend manual maximum of initial tension applied to the anteromedial or posterolateral bundles with graft tension imbalance at 30 degrees of flexion in double-bundle ACL reconstruction to achieve a better clinical outcome.

Yagishita K, Muneta T, Ju YJ, Morito T, Yamazaki J, Sekiya I. High-flex Posterior Cruciate-Retaining vs Posterior Cruciate-Substituting Designs in Simultaneous Bilateral Total Knee Arthroplasty A Prospective, Randomized Study. J Arthroplasty（in press）.

The superiority between the posterior cruciate-retaining and the posterior cruciate-substituting designs still remains controversial. We performed a prospective, randomized control study for evaluation of the superiority of these designs. This study investigated 58 knees in 29 patients with simultaneous bilateral total knee arthroplasty, in which the high-flex CR design was randomly implanted in one knee and the high-flex PS design was implanted in the other knee. The follow-up duration averaged 5.0 years, with a minimum duration of 3 years. Postoperatively, Knee Score and pain points in Knee Score resulted in no significant differences between the 2 designs. However, postoperative arc of range of motion, patient satisfaction, and posterior knee pain at passive flexion in the PS design were significantly superior to that of the CR design.

Yamazaki J, Muneta T, Koga H, Sekiya I, Ju YJ, Morito T, Yagishita K. Radiographic description of femoral tunnel placement expressed as intercondylar clock time in double-bundle anterior cruciate ligament reconstruction. Knee Surg Sports Traumatol Arthrosc. 2011 Mar;19（3）：418-23.

The purpose of this study was to propose an objective description of femoral tunnel position expressed as time of the intercondylar clock in ACL reconstruction using a simple radiograph for the sake of objective discussion and technical improvement. The reproducibility of the method was evaluated in double-bundle（DB）reconstructions.

The o'clock descriptions of femoral tunnel placement resulted in noon 40 min（standard deviation（SD）：10 min）for the AM bundle and one o'clock 40 min（SD：20 min）for the PL bundle on average in the "isometric" reconstruction. In the "anatomic" reconstruction, the time descriptions of femoral tunnel placement were one o'clock 20 min（SD：10 min）for the AM bundle and two o'clock 20 min（SD：20 min）for the PL bundle on average. With the intra-examiner reproducibility assessment in the "anatomic" reconstruction, the differences between first and second assessments averaged 10 min（SD：7 min）for femoral tunnel placement of the AM bundle and 12 min（SD：9 min）of the PL bundle. Regarding the inter-examiner reproducibility, the differences between two examiners averaged 9 min（SD：6 min）for femoral tunnel placement of the AM bundle and 14 min（SD：9 min）of the PL bundle.

This simple radiographic assessment is reproducible and reliable for clinical use, and useful for the evaluation of ACL reconstructive procedures.

Yamazaki J, Muneta T, Ju YJ, Morito T, Okuwaki T, Sekiya I. Hip acetabular dysplasia and joint laxity of female anterior cruciate ligament-injured patients. Am J Sports Med. 2011 Feb;39（2）：410-4.

It has been noted that some female anterior cruciate ligament-injured patients have complaints of both coxalgia and joint laxity. To know if these are due to acetabular dysplasia and generalized joint laxity, we performed cohort analyses.

Hip radiographs of 100 female anterior cruciate ligament-injured patients and 40 female athletes without any hip joint complaints or history of anterior cruciate ligament injury were evaluated by measuring their center-edge angle（CEA）. In addition, generalized joint laxity tests using 8 items were performed for anterior cruciate ligament-injured patients. Anterior-posterior（A-P）tibiofemoral translation of the uninjured knee was measured using a KT-1000 knee arthrometer to evaluate joint laxity under anesthesia before anterior cruciate ligament reconstruction.

The average（± standard deviation）CEA of female anterior cruciate ligament-injured patients was 25.5° ± 5.3°（uninjured side）and 25.8° ± 4.8°（injured side）, and that of the control group was 28.2° ± 4.2°（right side）and 29.2° ± 5.7°（left side）, both $P < .05$. Among the 100 patients with anterior cruciate ligament tears, both the generalized joint laxity score and A-P tibiofemoral translation of the group with acetabular dysplasia（CEA of <25°, n = 37）were significantly greater than that of the normal group（CEA of ≧25°, n = 63）. There was a negative correlation between the CEA of female anterior cruciate ligament-injured patients and both the generalized joint laxity score and A-P tibiofemoral translation.

The CEA of female anterior cruciate ligament-injured patients was significantly smaller than that of the control group. Statstical analysis showed a moderate negative correlation between the CEA and generalized joint laxity score. Female athletes with an anterior cruciate ligament injury had an increased prevalence of acetabular dysplasia and generalized joint laxity.

4）本事業に関連して世界的な研究拠点形成に向けて、以下の点で改善・整備等されたこと

A（研究拠点体制）

間葉幹細胞を用いた新規治療：これまで教室のメインテーマとして滑膜幹細胞の細胞移植による関節軟骨欠損の治療を臨床応用まで高めた。さらに性能の良い修復法を検討し、microsphere法を次のステップ候補として研究している（ORS2012で発表予定）。また適切なサイズや細胞数についても詳細に検討を進めている

滑膜幹細胞の臨床応用を米国の施設とも共同して臨床応用を進めていく計画が進んでいる。また関節軟骨欠損の治療ばかりでなく、他の関節構造、特に変形性関節症の進展の主要素の1つと考えられる半月板の再建に滑膜幹細胞を応用する基礎的研究が進んでいる。

各種BMPの機能解析と新規治療法の開発：各種BMPを発生過程さらに生後の必要な時期にノックアウト、ノックダウンする技術を駆使して研究をしてきた研究者をGCOEの国際シャペロン教官として教室に得た。M・Dタワーに教室が移転し、ノックアウトマウスの飼育スペースも確保され、BMP4, BMP7のコンディショナルノックアウトマウスの作成に成功した。現在解析中である。Harvard大学との共同研究も引き続いて行われている。

膝前十字靱帯損傷治療などの主要関節手術の成績改善：高い臨床治療実績、長年のACL研究、解剖学的研究に基づいた再建手術の最適化に加えて、バイオメカ研究によってACL損傷患者の特徴を明らかにしつつある。またフィールドスタディも進みつつある。その他人工関節手術の向上のために臨床研究を主体として取り組んでいる。

B（研究教育環境）

M・Dタワーへの引っ越しにより教室の研究面積が3倍増した。新しい動物実験設備も完備し、遺伝子組み換え実験室も整った。GCOE事業担当分野間の共同研究も複数進行している。教育スタッフの増員によって大学院生各人に対する個別教育の時間が増し、同時に複数の研究テーマを扱うことを大学院生のルーチンにしている。昨年10月に再生医療ハイウェープログラムに滑膜幹細胞を用いた半月板再生が採択され、10年のグラントを得ることができ、研究費が飛躍的に充実した。

C（人材確保）

国際シャペロンの分野への採用により研究の幅が広がり、教育の充実化が図られた。毎年3,4人の大学院生を受け入れ、国外からの留学生も慎重な選択のもとに受け入れている。

D（人材育成）

週3回の早朝カンファランスと勉強会により、研究基盤として最新研究に遅れないように留意している。海外の著名な研究者や新進の研究者に積極的に依頼し、セミナーを適時開催している。セミナーの前後に大学院生に個別の指導を依頼し、実施している。国際シャペロンの分野への採用により教育の充実化が図られた。

E（国際化）

国際シャペロンとの関係からHarvard大学歯学部との2つの共同研究プロジェクトを立ち上げた。滑膜幹細胞を用いた関節軟骨細胞治療の臨床研究が米国テキサス州の病院と進みつつある。

大学院生卒業生が米国とノルウェーに留学し業績を挙げている。大学院卒業生の留学率が増加している。

5）GCOE事業を推進するに当たって力を入れた点

GCOEにより新たに教室に加わった国際シャペロン教官による各種改変マウスを駆使したBMP研究の推進。シャペロン教官による大学院生の個別教育の充実。滑膜幹細胞を用いた治療法の臨床応用の推進と間葉幹細胞研究の対象の広域化。国際的な共同研究の推進。事業者間の共同研究の立ち上げ。

6）英文原著論文

1. Bere T, Florenes TW, Krosshaug T, Koga H, Nordsletten L, Irving C, Muller E, Reid RC, Senner V, Bahr R. Mechanisms of anterior cruciate ligament injury in world cup alpine skiing：a systematic video analysis of 20 cases. Am J Sports Med 39（7）：1421-9, 2011.
2. Gamer, L.W., Tsuji, K., Cox, K., Capelo, L.P., Lowery, J., Beppu, H., and Rosen, V. BMPR-II is dispensable for formation of the limb skeleton. Genesis 49：719, 2011
3. ◎Takahashi, T., Muneta, T., Tsuji, K., and Sekiya, I. BMP-7 inhibits cartilage degeneration through suppression of inflammation in rat zymosan-induced arthritis. Cell Tissue Res 344：321, 2011.
4. Yamazaki J, Muneta T, Ju YJ, Morito T, Okuwaki T, Sekiya I. Hip acetabular dysplasia and joint laxity of female anterior cruciate ligament-injured patients. Am J Sports Med. 2011 Feb;39（2）：410-4.
5. Yamazaki J, Muneta T, Koga H, Sekiya I, Ju YJ, Morito T, Yagishita K. Radiographic description of femoral tunnel placement expressed as intercondylar clock time in double-bundle anterior cruciate ligament reconstruction. Knee Surg Sports Traumatol Arthrosc. 2011 Mar;19（3）：418-23.
6. Muneta T, Koga H, Ju YJ, Yagishita K, Sekiya I. Effects of different initial bundle tensioning strategies on the outcome of double-bundle ACL reconstruction：a cohort study.　Sports Med Arthrosc Rehabil Ther Technol. 2011 Jul 28;3：15.
7. Kokabu, S., Gamer, L., Cox, K., Lowery, J., Tsuji, K., Raz, R., Economides, A., Katagiri, T., and Rosen, V. BMP3 Suppresses Osteoblast Differentiation of Bone Marrow Stromal Cells via Interaction with Acvr2b. Mol Endocrinol 26：87, 2012.
8. Koga H, Bahr R, Myklebust G, Engebretsen L, Grund T, Krosshaug T. Estimating anterior tibial translation from model-based image-matching of a noncontact anterior cruciate ligament injury in professional football：a case report. Clin J Sport Med 21（3）：271-4, 2011.
9. Koga H, Muneta T, Yagishita K, Ju YJ, Sekiya I. Surgical management of grade 3 medial knee injuries combined with cruciate ligament injuries. Knee Surg Sports Traumatol Arthrosc 20（1）：88-94, 2012.
10. Koga H, Muneta T, Yagishita K, Ju YJ, Sekiya I. The Effect of Graft Fixation Angles on Anteroposterior and Rotational Knee Laxity in Double-Bundle Anterior Cruciate Ligament Reconstruction：Evaluation Using Computerized Navigation. Am J Sports Med（in press）.
11. ◎Sekiya I, Ojima M, Suzuki S, Yamaga M, Horie M, Koga H, Tsuji K, Miyaguchi K, Ogishima S, Tanaka H, Muneta T. Human mesenchymal stem cells in synovial fluid increase in the knee with degenerated cartilage and osteoarthritis. J Orthop Res（in press）.
12. ◎Nakamura T, Sekiya I, Muneta T, Hatsushika D, Horie M, Tsuji K, Kawarasaki T, Watanabe A, Hishikawa S, Fujimoto Y, Tanaka H, Kobayashi E. Arthroscopic, histological, and MRI analyses of cartilage repair after a minimally invasive method of transplantation of allogeneic synovial mesenchymal stem cells into cartilage defects in pigs. Cytotherapy（in press）.
13. Yagishita K, Muneta T, Ju YJ, Morito T, Yamazaki J, Sekiya I. High-flex Posterior Cruciate-Retaining vs Posterior Cruciate-Substituting Designs in Simultaneous Bilateral Total Knee Arthroplasty A Prospective, Randomized Study. J Arthroplasty（in press）.

7）総説ならびに著書

池田浩夫

主な疾患の診療の進め方　前十字靱帯以外の膝靭帯単独損傷、整形外科臨床パサージュ7 下肢のスポーツ外傷と障害、222-233、2011

古賀英之

バスケットボールにおけるACL損傷時のビデオ分析、復帰を目指すスポーツ整形外科、p123-124、2011。

神野哲也

変形性股関節症.運動器の痛み　プライマリケア　股関節の痛み.　菊地臣一編集、pp181-190、2011,　南江堂

神野哲也

関節痛,四肢痛.小児の治療薬の選び方と使い方.土井庄三郎編集,pp438-443,2011,羊土社

神野哲也：ストレスシールディング.特集：THAの合併症対策.関節外科,2012.1刊行予定.

古賀英之、宗田　大、関矢一郎

膝十字靱帯損傷に合併した3度膝内側側副靱帯損傷に対するつり上げ修復法

Bone Joint Nerve 2012

古賀英之
IOC World Conference on Prevention of Injury & Illness in Sport報告記
臨床スポーツ医学28（9）：1052-1055, 2011.

小林英司、関矢一郎、山本博徳
外科医のためのトランスレーショナルリサーチ
～ブタを用いた研究に夢をのせて～
Medical Torch　p31-37 Vol.7 No.1 2011

朱　寧進、宗田　大
柔道・相撲における膝前十字靭帯損傷の診断と治療
復帰をめざすスポーツ整形外科539-543 Medical View社2011.4.10

朱　寧進、宗田　大
半月板・靭帯障害特集：運動器の痛み –その診断と治療-, 牛田享宏編
Monthly Book Orthopaedics 24,（5）：75-82, 2011、全日本病院出版会

関矢一郎、宗田　大
滑膜間葉幹細胞を使った軟骨再生
再生医療叢書 第6巻　骨格系
朝倉書店　2012

関矢一郎、宗田　大
滑膜間葉幹細胞の役割と低侵襲な軟骨再生への応用
雑誌整形外科　2012　整形トピックス

関矢一郎、宗田　大
変形性膝関節症をめぐる進歩
滑膜由来の幹細胞による再生医療
Bone Joint Nerve 2012

関矢一郎、宗田大
再生医学のいま　基礎研究から臨床への展開に向けて
滑膜幹細胞を用いた関節軟骨再生
治療　2011

関矢一郎
滑膜間葉幹細胞を用いた関節軟骨再生
クリニカルカルシウム　p83-93 Vol.21 No.6 2011

関矢一郎
軟骨再生の概要と応用の可能性
医事新報 p59-61 No. 4548　2011

関矢一郎・宗田　大
半月板の再生医療
臨床整形外科 p42-45 Vol. 46 No.1 2011

仁賀定雄、池田浩夫
サッカーにおけるハムストリング肉離れの診断と治療.復帰を目指すスポーツ整形外科.メジカルビュー社（宗田大編集）387-393, 2011.

仁賀定雄
骨盤・股関節のスポーツ外傷・障害の特性.新版スポーツ整形外科.南江堂（中嶋寛之監修）231-233、2011

仁賀定雄
鼠径部痛症候群.新版スポーツ整形外科.南江堂（中嶋寛之監修）237-243、2011

仁賀定雄
骨盤・股関節周囲の外傷（恥骨結合炎）.コーチとプレーヤーのためのサッカー医学テキスト.金原出版.160-162、2011

仁賀定雄
鼠径部痛症候群.コーチとプレーヤーのためのサッカー医学テキスト.金原出版.166-171、2011

仁賀定雄
スポーツ選手の鼠径部痛.下肢のスポーツ外傷と障害（整形外科パサージュ7）.中山書店（中村耕三総監修、宗田大専門編集）164-177、2011

林　将也、宗田　大、関矢　一郎
BMP7による変形性関節症の予防
Bone Joint Nerve 2012

宗田　大
膝ACL最前線。整形外科リハビリテーション学会誌13：27-30, 2010

宗田　大
変形性関節症の診断と治療。医学の歩み「ロコモティブシンドローム」中村耕三企画。236（5）：494 - 500,2011.1.29

宗田　大
変形性膝関節症の診断と治療。医学のあゆみVol.236 No.5：494-500, 2011.1.29

川口浩、宗田　大、出家正隆、戸山芳昭
変形性膝関節症治療の現状と将来。HUMAN SCIENCE APRIL 2011, 4-12

宗田　大
屈筋腱を用いる前十字靱帯再建術。整形外科Surgical Technique 1：29-46, 2011

宗田　大
変形性膝関節症を予防・克服するための運動療法
CLINICIAN 11 No.603：1269-1274

宗田　大（専門編集）中村耕三（総編集）
下肢のスポーツ外傷と障害。整形外科臨床パサージュ7.中山書店　2011.3.25

宗田　大
スポーツ選手の伸展機構障害以外の膝の障害。宗田大（専門編集）中村耕三（総編集）：下肢のスポーツ外傷と障害。整形外科臨床パサージュ7.中山書店 2011.3.25　P.269-281

宗田　大
復帰をめざすスポーツ整形外科。メジカルビュー社、2011.4.10

宗田　大
バレーボールにおける手関節肘関節外傷・障害の診断と治療。復帰をめざすスポーツ整形外科。メジカルビュー社、p.162-165, 2011.4.10

宗田　大
バレーボールにおけるひざ前十字靱帯損傷の診断と治療。復帰をめざすスポーツ整形外科。メジカルビュー社、p.166-172, 2011.4.10

宗田　大
運動器の部位別にみた痛みの発生源と主な疼痛性疾患「膝関節」。山下敏彦（専門編集）中村耕三（総編集）：運動器のペインマネジメント。整形外科臨床パサージュ8.中山書店　2011.4.25　P.88-104

宗田　大
前十字靱帯再再建術。膝関節の手術。専門編集 黒坂昌弘。中山書店　2011.9.20、P.94-101.

宗田　大、水田博志
「変形性膝関節症の介入研究の短期成績」序文　第83回日本整形外科学術総会シンポジウム、日整会誌85：731-732, 2011

柳下和慶
高気圧酸素治療による再建ACLの治癒促進.特集ACL再建術後のスポーツ復帰.関節外科30（1）：35, 2011

柳下和慶
【高気圧酸素治療の基礎知識　安全な治療のために】高気圧酸素治療で知っておきたい副作用と注意点（解説／特集）. Clinical Engineering. 22（3）：216, 2011.

柳下和慶
わが国において高気圧酸素療法による医療水準の底上げは可能か? 外保連活動による診療報酬改定活動の報告と今後の方向性.日本高気圧環境・潜水医学会雑誌 46（3）：128, 2011.

8）平成23年度までの自己評価

GCOEの国際シャペロンが教室に加わったことにより基礎的研究と教育の密度が増し、新しい研究が芽生えつつある。教室も活気を増した。新棟に引っ越し研究環境も改善した。しかし本年度の基礎研究論文数は少なく、来年度の飛躍が待たれる。

一方10年のグラントを得て、研究費がふんだんに用いることができる環境になったことは非常に大きな収穫だった。これをもとに研究の質をあげ大動物研究を増加させる計画が実現しつつある。臨床面での滑膜幹細胞を用いた軟骨治療に対する一層の改善と発展が求められる。

9）和文原著論文

酒井朋子, 柳下和慶
人工膝関節抜去時の人工関節型カスタムメイドセメントスペーサーの有効性.整形外科 62（7）：627, 2011.

朱　寧進、宗田　大、山賀美賀、柳下和慶、古賀英之、関矢一郎、大川　淳
変形性膝関節症に対する積極的膝伸展・屈曲訓練介入研究の短期成績
日整会誌740-744, 85（10）2011

中川 裕介、浅野浩司、中村 香織
前十字靭帯及び後十字靱帯付着部剥離骨折の1例
JOSKAS（in press）.

仁賀定雄
ACL再建術後のスポーツ復帰（プロサッカー）、関節外科、Vol.30 No1, 86-93, 2011

仁賀定雄
サッカーによる神経系障害.神経内科 Vol.75 No.5, 444-449, 2011

結城新、仁賀定雄、池田浩夫、吉村英哉、岩澤大輔、林将也、中川裕介
プロサッカー選手に生じた大腿直筋肉近位腱断裂の2例
日本整形外科スポーツ医学会　VOL.31 NO.3 267-273

10）学会発表（英文）

1. Otabe K,Regenerative Property of Mesenchymal Stem Cells in Oral Tissues. Orthopedic Research Society Annual Meeting、Poster presentation、Long Beach、January 2011
2. Koga H, Bahr R, Myklebust G, Engebretsen L, Muneta T, Sekiya I, Krosshaug T. A New Hypothesis for ACL Injury Mechanisms based on Video Analysis using Model-Based Image-Matching Technique. International

Symposium on Ligaments & Tendons - XI, Oral, Long Beach, CA, USA, 2011.1.12

3. Koga H, Bahr R, Myklebust G, Engebretsen L, Grund T, Muneta T, Sekiya I, Krosshaug T. The First Ever Video Analysis of Anterior Tibial Translation in a Non-contact ACL Injury Situation Using Model-based Image-matching Technique. 57th Annual Meeting of the Orthopaedic Research Society, Poster, Long Beach, CA, USA, 2011.1.13-16
4. Takahashi T, Muneta T, Tsuji K, Sekiya I. BMP-7 inhibits cartilage degeneration through suppression of inflammation in rat zymosan-induced arthritis. 57th Annual Meeting of the Orthopaedic Research Society, Poster, Long Beach, CA, USA, 2011.1.13-16
5. Nakamura T, Sekiya I, Hatsushika D, Horie M, Tsuji K, Muneta T, Kawarasaki T, Watanabe A, Hishikawa S, Fujimoto Y, Tanaka H, Kobayashi E. Synovial Mesenchymal Stem Cells Transplantation Contributes to Cartilage Regeneration in Porcine Model. Orthopaedic Research Society 2011, Poster, Long Beach, CA, 2011.1.13-16
6. Miyatake, K; Yamaga, M　Sekiya, I　Muneta, T and Tsuji, K. Human chitinase 3-like protein 2（YKL39）; an osteoarthritis-associated gene which enhances adipogenic differentiation of synovial fibroblasts. Orthopaedic Research Society 2011, Poster, Long Beach, CA, 2011.1.13-16
7. Koga H, Bere T, Bahr R, Krosshaug T. Kinematics of a slip-catch mechanism for　anterior cruciate ligament injury in World Cup alpine skiing. IOC World Conference on Prevention of Injury & Illness in Sport, Oral, Monaco, 2011.4.7-9
8. Jinno T, Koga D, Yamauchi Y, Asou Y, Taniguchi N, Hasegawa S, Matsubara M, Morita S, Okawa A, Muneta T：Effects of hydroxyapatite-coating for acetabular components on radiographical results of total hip arthroplasty. 84th Annual Meeting of Japanese Orthopaedic Association, Oral（Web開催）, Yokohama, 2011.5.12-15
9. Okazaki F, Yagishita K, Togawa S, Kato T, Kojima Y, Niwa Y, Mano Y. Hyperbaric oxygen therapy for radiation-induced hemorrhagic cystitis and proctitis. The 44th Undersea and Hyperbaric Medical Society（UHMS）Annual Scietific Meeting（2011年6月16日、Fort-Worth, Texas, USA）
10. Watanabe T, Banks S, Kreuzer S, Leffers K, Dunbar N, Iorgulescu A, Jones J, Conditt M. Deep Flexion Kinematics with Robotic Modular Knee Arthroplasty. 11th　Annual meeting of International Society for Computer Assisted Orthopaedic surgery（CAOS）, Podium, London, 2011/6/17
11. Yamaga M, Tsuji K, Miyatake K, Yamada J, Sekiya I, Muneta T. OSTEOPONTIN LEVEL IN SYNOVIAL FLUID IS ASSOCIATED WITH THE SEVERITY OF KNEE JOINT PAIN. 2011　OARSI,　Oral, San Diego, CA, 2011.9.15
12. Tsuji K., Sekiya I., Muneta T. BMP4 Regulates the Hematopoietic Stem Cell Niche Size in Bone Marrow. American Society for Bone and Mineral Research, Oral, San Diego, CA USA, September 16-20, 2011
13. Toshifumi Watanabe; Michael Conditt; Scott Banks; Stefan Kreuzer; Kevin Leffers; Takeshi Muneta; Jennifer Jones. Deep Flexion Kinematics With Robotic Modular Knee Arthroplasty
International Society For Technology in arthroplasty（ISTA）2011, Poster, Brugge, 2011/9/20-23
14. Koga H, Muneta T, Sekiya I. Effect of graft fixation angles on knee kinematics, graft tension curves and load sharing in double-bundle anterior cruciate ligament reconstruction. International Symposium on Ligaments & Tendons - XII, Oral, San Francisco, CA, USA, 2012.2.3
15. Watanabe, T; Ishizuki, M; Muneta, T; Dunbar, N; Iorgulescu, A; Banks, S A. Kinematic comparison of fixed-and mobile-bearing total knee arthroplasty in vivo, Orthopaedic Research Society（ORS）2012, Poster, San Francisco, 2012/2/4-5
16. Watanabe, T; Kreuzer, S; Leffers, K; Conditt, M; Jones, J; Dunbar, N; Iorgulescu, A, Banks, SA. Is Cruciate-Ligament Functionality Retained in Partial and Multicompartmental Knee Arthroplasty? Orthopaedic Research Society（ORS）2012, Poster, San Francisco, 2012/2/4-5
17. Koga H, Muneta T, Sekiya I. Effect of Graft Fixation Angles on Knee Kinematics in Double-bundle Anterior Cruciate Ligament Reconstruction. 58th Annual Meeting of the Orthopaedic Research Society, Oral, San Francisco, CA, USA, 2012.2.4-7
18. Suzuki S, Sekiya I, Tsuji K, Muneta T. Properties and effectiveness of aggregated synovial mesenchymal stem cells for cartilage regeneration. ORS 2012 Annual Meeting, Poster, San Francisco, California,2012.2.4-7
19. Miyatake, K; Yamaga, M　Sekiya, I　Muneta, T and Tsuji, K. Human chitinase 3-like protein 2（YKL39）is a novel secreted protein which supports cell proliferation　and chondrocytic differentiation of ATDC5.
ORS 2012 Annual Meeting, Poster, San Francisco, California,2012.2.4-7
20. Hatsushika D. Intraarticular injection of synovial stem cells promotes meniscal regeneration in rabbit massive meniscal defect. 58th Annual Meeting of the Orthopaedic Research Society, Oral, San Francisco, CA, USA, 2012.2.4-7
21. Yamaga M, Tsuji K, Miyatake K, Sekiya I, Muneta T. Osteopontin level in synovial fluid is transiently upregulated after joint injury and associated with the severity of knee joint pain. 58th Annual Meeting of the

Orthopaedic Research Society, Poster, San Francisco, CA, USA, 2012.2.4-7

22. Yamada, J. Miyatake, K. Yamaga, M. Sekiya, I. Muneta, T. Tsuji, K. Follistatin alleviates articular cartilage degradation induced by carrageenan. 58th Annual Meeting of the Orthopaedic Research Society, Poster, San Francisco, CA, USA, 2012.2.4-7
23. Watanabe, T; Ishizuki, M; Muneta, T; Dunbar, N; Iorgulescu, A; Banks, S A. Knee Kinematics in ACL Substituting Arthroplasty With or Without PCL. Orthopaedic Research Society（ORS）2012, Podium, San Francisco, 2012/2/7

11）学会発表（和文）

浅野浩司

CR型人工膝関節置換術における軟部組織の緊張と術後の可動域との関係

日本人工関節学会　那覇 2011.2.25

浅野浩司

PS型とCR型人工膝関節置換術後の術後成績の比較

第3回　JOSKAS　札幌 2011.6.17

池田浩夫、林将也、望月智之、吉村英哉、塩崎彰、島谷雅之、塚田幸行、大原敏之、星野明穂、仁賀定雄

プロサッカー選手に行った鏡視下半月板部分切除術後の臨床成績、第48回埼玉県医学会総会、浦和、2011/2/20

岡崎史紘, 柳下和慶, 外川誠一郎, 加藤剛, 小島泰史, 小宮正久, 芝山正治, 丹羽康江, 眞野喜洋.

放射線治療に起因する晩期有害事象である膀胱炎、および直腸炎に対する高気圧酸素治療.第21回日本臨床工学技士会総会（2011年5月21日、別府）

小田邉浩二

歯周組織の間葉幹細胞による硬組織再生、日本整形外科学会基礎学術集会、前橋、2011年10月20日

北浜純、小谷野岳、冨岡秀樹、上杉幸二、橋本敬史、鈴木幹雄

抗生剤含有骨セメントでコーティーングした横止め髄内釘による感染性骨折の治療

第17回救急外傷シンポジウム　札幌　2011年3月11日

古賀英之、宗田大、柳下和慶、朱寧進、森戸俊行、山崎順也、清水禎則、関矢一郎

二重束ACL再建術における移植腱固定角度が膝キネマティクスに与える影響、3rd JOSKAS、

札幌、2011.6.16-18。

加藤剛, 柳下和慶, 榎本光裕, 岡崎史紘, 川嶌眞人, 大川淳.

神経 脊髄神経疾患に対する高気圧酸素療法の効果.第46回日本高気圧環境・潜水医学会学術総会（2011年10月29日、東京）

古賀英之、Tone Bere、Roald Bahr、宗田大、関矢一郎、Tron Krosshaug

Model-based image-matching technique を用いたアルペンスキーにおけるACL損傷メカニズムのビデオ解析、日本整形外科学会基礎学術集会、前橋、2011.10.20-21。

古賀英之、宗田大

Model-based image-matching technique を用いた非接触性膝前十字靱帯損傷における股関節キネマティクスの解析、日本臨床スポーツ医学会、青森、2011.11.5-6。

古賀英之、宗田大、柳下和慶、朱寧進、望月智之、堀江雅史、中村智祐、関矢一郎

二重束ACL再建術における移植腱固定角度が制動性及び張力変化に与える影響、日本臨床バイオメカニクス学会、京都、2011.11.18-19。

古賀英之

ワールドカップアルペンスキーにおけるACL損傷のビデオ解析、第17回御茶ノ水膝スポーツ懇話会、東京、2011.12.1。

島谷雅之、星野明穂、池田浩夫、吉村英哉、高橋徹、塚田幸行、小松秀郎、尾辻正樹、仲津留恵日、塩田幹夫

人工膝関節再置換術の術後成績、日本人工関学会、那覇、2012.2.23-24

島谷雅之、池田浩夫、吉村英哉、望月智之、林将也、塩崎彰、塚田幸行、大原敏之、星野明穂、仁賀定雄

膝屈筋腱多重折りを用いたACL再建術後の膝屈曲筋力低下の自覚とFlexion Lagの関連、JOSKAS、札幌、6月17日

島谷雅之、星野明穂、池田浩夫、大原敏之、塚田幸行、塩崎彰、林将也、望月智之、吉村英哉

CCK型大腿骨componentを使用した人工膝関節置換術の術後成績、日本人工関節学会、東京、2月26日

朱　寧進、宗田　大、柳下和慶、清水禎則、古賀英之、森戸俊行、山崎順也、関矢一郎

人工膝関節置換術における大腿骨後顆骨切り量が伸展・屈曲ギャップに与える影響

第41回　日本人工関節学会、東京、2011年2月25-26.日

朱　寧進、宗田　大、柳下和慶、清水禎則、古賀英之、森戸俊行、山崎順也、関矢一郎

人工膝関節置換術における脛骨インプラント設置方法の術後回旋に関する検討：3Dテンプレートを用いた研究
第41回　日本人工関節学会、東京、2011年2月25-26.日

朱　寧進、宗田　大、柳下　和慶、清水　禎則、古賀英之、森戸　俊行、山崎　順也、関矢　一郎
人工膝関節置換術における脛骨インプラント設置方法の術後回旋に関する検討：3Dテンプレートを用いた研究
第84回　日本整形外科学会総会、横浜、2011年5月12-15.日

朱　寧進、関矢一郎、柳下和慶、古賀英之、宗田　大
内側型変形性膝関節症における大腿骨外反角の検討-CT, XP間の比較
第3回日本関節鏡・膝・スポーツ整形外科学会（JOSKAS）、札幌、2011年6月16-18.日

神野哲也,古賀大介, 山内裕樹, 谷口直史, 大川淳,宗田大
髄腔占拠型ハイドロキシアパタイトコーティング・ストレートステムの術後長期成績.第41回日本人工関節学会,口頭,東京,2011年2月25日

神野哲也,古賀大介, 山内裕樹, 谷口直史, 大川淳
関節リウマチに対するセメントレス人工股関節全置換術のX線成績と術後合併症.日本リウマチ学会学術集会,口頭,神戸,2011年7月19日

神野哲也,古賀大介,麻生義則,山内裕樹,森田定雄,長谷川清一郎,松原正明,大川淳,宗田大
髄腔占拠型近位ハイドロキシアパタイトコーティング・ストレートステム周囲の長期骨リモデリング.第38回日本股関節学会,口頭,鹿児島,2011年10月7日

神野哲也,古賀大介, 谷口直史, 麻生義則,森田定雄,大川淳,宗田大
近位HAコーティングステム：髄腔占拠型かtapered wedge型か.第38回日本股関節学会,口頭,鹿児島,2011年10月8日

神野哲也、古賀大介、麻生義則、小谷野岳,高田ちさと,森田定雄、大川淳,宗田大
前方および後方進入による人工股関節置換術における術前後の股関節回旋可動域.第42回日本人工関節学会,口頭,沖縄,2012年2月24日

鈴木志郎　関矢一郎　辻邦和　荻島創一　大川淳　宗田大
滑膜間葉幹細胞の軟骨分化を制御するMicroRNAの発現解析
第26回日本整形外科学会基礎学術集会
口演前橋, 群馬　2011年10月20,21日

鈴木志郎　関矢一郎　辻邦和　宗田大
滑膜間葉幹細胞集合体による軟骨再生
第25回日本軟骨代謝学会
名古屋, 愛知　2012年3月9,10日

関矢一郎
膝軟骨損傷に対する関節鏡視下の滑膜幹細胞移植術
日本整形外科学会総会（横浜）
2011/5/15

芝山正治, 柳下和慶, 外川誠一郎, 小島泰史, 加藤剛, 榎本光裕, 岡崎史紘, 小宮正久, 眞野喜洋.
レクリエーショナルダイバーの減圧症予防対策に関する安全停止の意識とナイトロックス利用の現状.第46回日本高気圧環境・潜水医学会学術総会（2011年10月29日、東京）

鈴木直子, 柳下和慶, 椎塚詰仁, 外川誠一郎, 加藤剛, 小島泰史, 榎本光裕, 芝山正治, 山本和雄, 眞野喜洋.
レジャータイバーの減圧症発症誘因　ダイビング地域毎の検討.第46回日本高気圧環境・潜水医学会学術総会（2011年10月29日、東京）

外川誠一郎, 柳下和慶, 榎本光裕, 眞野喜洋.
調査科学潜水の安全.第46回日本高気圧環境・潜水医学会学術総会（2011年10月29日、東京）

谷山崇, 榎本光裕, 加藤剛, 柳下和慶, 岡崎史紘, 外川誠一郎, 小島泰史, 眞野喜洋.
高気圧酸素治療により著明な神経症状の回復を認めた脊髄型減圧症の1例.第46回日本高気圧環境・潜水医学会学術総会（2011年10月29日、東京）

中川 裕介　浅野 浩司　立石 智彦
陳旧性坐骨結節剥離骨折に手術を施行した一例　第19回よこはまスポーツフォーラム 横浜　2011年6月12日

中川 裕介 浅野 浩司 中村香織　北原 建彰 品田春生　三宅 論彦　小森 博達　四宮 謙一　宗田 大
前十字・後十字靭帯付着部剥離骨折の1例　第3回JOSKAS　札幌　2011年6月16日

中川 裕介 浅野　浩司　中村 香織　北原 建彰 品田 春生　三宅　論彦 小森　博達　四宮　謙一
踵骨関節内骨折に対する外側小切開及び顆粒状β-TCPを使用した観血的整復固定術の治療成績　第37回骨折治療学会　横浜　2011年7月1日

中川 裕介 浅野 浩司 中村 香織 小森 博達　宗田 大
大腿骨顆部Hoffa骨折に対してプレートを使用し観

血的整復固定術を施行した1例　第52回関東災害整形外科 横浜 2012年3月22日

中村智祐、関矢一郎、田中穂積、小林英司、大川淳、宗田大

ブタ軟骨欠損モデルにおける同種滑膜幹細胞移植
第26回日本整形外科学会基礎学術集会
群馬（前橋）2011年10月21日

仁賀定雄

「スポーツ選手の鼠径部痛症候群に対するアスレティックリハビリテーションの成績」
第3回日本関節鏡・膝・スポーツ整形外科学会（JOSKAS）札幌、2011年6月17日

仁賀定雄

「プロサッカークラブにおける鼠径周辺部痛に対する治療と予防の経験」
第37回日本整形外科スポーツ医学会
福岡、2011年9月23日

仁賀定雄

「スポーツ選手の鼠径周辺部痛の治療と予防」
第60回　日大スポーツ医学勉強会
東京、2012年1月14日

林将也

前十字靱帯損傷に合併する内側半月板損傷の保存療法の短期成績、JOSKAS、札幌、2011年6月17日

林将也

Jones骨折術後に骨髄炎をきたした症例に行ったサルベージ手術の報告、日本臨床スポーツ医学会、青森、2011年11月5日

林将也

人工膝関節置換術の術後成績を評価するには何年間の経過観察を要するか?、日本人工関節学会、沖縄、2012年2月24日

堀江雅史、関矢一郎、宗田大

滑膜間葉間細胞の局所投与は半月板再生を促進する-ウサギ半月板部分欠損モデルを用いた検討
日整会基礎
群馬県前橋　2010年10月20日

宮武　和正、山賀　美芽、関矢　一郎、宗田　大、辻　邦和

変形性関節症に伴い滑膜で発現が増大する遺伝子YKL39（chitinase 3-like protein 2）の分子機能の解析
ポスター発表　2011　第24回軟骨代謝学会　福岡
2011年3月4日

宮武 和正　辻 邦和　山田 淳　片桐 洋樹　山賀 美芽　大川 淳　関矢 一郎　宗田 大

関節内処置を必要としないマウスの膝関節軟骨変性モデル
- 卵巣摘出と強制走行の影響-
ポスター発表　2011　第26回 日本整形外科学会基礎学術集会 群馬　2011年10月21日

宮武　和正 辻　邦和　山田　淳　Kahaer Abula 松倉　遊 関矢　一郎 宗田　大

変形性関節症（OA）発症における卵巣摘出と強制走行の影響
ポスター発表　2012　第25回軟骨代謝学会　名古屋
2012年3月9日

柳下和慶、榎本光裕、堀江正樹、下田学、今井智子、渡部厚一、入江一憲、宮川俊平.

高強度運動負荷後の疲労回復に対する高気圧酸素環境の影響.第22回日本臨床スポーツ医学会学術集会（2011年11月6日、青森）

山賀　美芽、辻　邦和、宮武和正、山田淳、片桐洋樹、関矢一郎、宗田大

関節液中のオステオポンチン量は膝関節痛の程度に相関する
口演発表　2011　第24回軟骨代謝学会　福岡　2011年3月4日

山賀　美芽、辻　邦和、宮武和正、山田淳、片桐洋樹、関矢一郎、宗田大

関節液中オステオポンチンの関節痛における役割
口演発表　2011　第26回 日本整形外科学会基礎学術集会 群馬　2011年10月21日

山田　淳,辻　邦和,宮武　和正,Kahaer Abula, 松倉　遊, 関矢　一郎, 宗田　大

Carrageenan誘導性の関節炎においてFollistatinは軟骨の退行変性を抑制する
ポスター発表　2012　第25回軟骨代謝学会　名古屋
2012年3月9日

結城新、宗田大、関矢一郎、古賀英之

Model-based image-matching techniqueをもちいたpivot shift testの解析
日本臨床バイオメカニクス学会第38回学術集会
神戸ポートピアホテル南館　2011年11月18日

12）受賞

堀江雅史

Implantation of Allogenic Synovial Stem Cells Promotes Meniscal Regeneration in a Rabbit Meniscal Defect Model

東京医科歯科大学整形外科同門会　研究奨励賞
2011年12月23日
Toshifumi Watanabe; Michael Conditt; Scott Banks; Stefan Kreuzer; Kevin Leffers; Takeshi Muneta; Jennifer Jones
Deep Flexion Kinematics With Robotic Modular Knee Arthroplasty
International Society For Technology in arthroplasty（ISTA）2011
Best poster award
Brugge
2011/9/20-23

13）外部資金の獲得状況

文部科学省委託　国家基幹研究開発推進事業
「再生医療の実現化プロジェクト　再生医療の実現化ハイウェイ」
研究課題：「滑膜幹細胞による膝半月板再生」
代表：関矢一郎
期間：平成23年―平成33年
研究総額：10億円

厚生労働科学研究費　再生医療実用化研究事業
研究課題：「幹細胞による次世代の低侵撃軟骨再生治療の開発と臨床応用」
代表：関矢一郎
期間：平成23年―平成25年
研究総額：1億6千万円

科学研究費補助金、基盤C
研究題目：「滑膜幹細胞を用いた新しい低侵襲骨関節疾患治療の臨床応用の発展のための大動物研究」
代表：宗田　大
期間：平成21年―平成23年
研究総額：340万円

科学研究費補助金、 基盤C
研究題目：「軟骨損傷に対する滑膜幹細胞浮遊液静置療法において細胞接着効率を向上させる為の検討」
代表：関矢一郎
期間：平成21年―平成23年
研究費総額：340万円

科学研究費補助金、基盤研究C
研究題目：「骨形成因子BMPシグナルによる造血微小環境のホメオスタシスの制御」
代表：辻邦和
平成22年度―平成24年度
研究費総額：405万円

科学研究費補助金、基盤研究C
研究題目：「変形性膝関節症における疼痛の分子メカニズムの解析　」
代表：　朱寧進
平成22年度―平成24年度
研究費総額：382万円

科学研究費補助金、基盤研究C
研究題目：「変形性関節症の発症機構解明の為の新規動物モデルの確立と間接組織の初期病変の解析」
代表：神野哲也
平成23年度―平成25年度
研究費総額：450万円

14）特別講演、招待講演、シンポジウム

池田浩夫
変形性膝関節症 - 中高年の膝の痛み - 、鳩ケ谷市民公開講座、2011/9/15、鳩ヶ谷駅市民センター
岡崎史紘, 柳下和慶, 外川誠一郎, 加藤剛, 小島泰史, 丹羽康江
シンポジウム「放射線障害に対するHBO　evidenceとcommon sense、社会的展開」放射線治療に起因する膀胱炎、および直腸炎に対する高気圧酸素治療.第46回日本高気圧環境・潜水医学会学術総会（2011年10月28日、東京）

古賀英之
A new hypothesis for ACL injury mechanisms, based on video analysis. Presented in the Symposium：Solving the mystery of non-contact ACL injuries - how do they happen? IOC World Conference on Prevention of Injury & Illness in Sport, Monaco, 2011.4.

古賀英之
Model-Based image-matching techniqueを用いた動作解析。日本リハビリテーション医学会、2011年11月2日千葉

古賀英之
ACL損傷メカニズムの新たな仮説の提唱-Model-based image-matching techniqueを用いた解析-。日本臨床スポーツ医学会、2011年11月6日、青森

古賀英之
Model-based image-matching法によるビデオ解析に基づいた非接触性ACL損傷の新たな受傷メカニズムの提唱。埼玉アスレチックリハビリテーション研究会、2011年11月12日さいたま

古賀英之
ACL損傷-ビデオ映像を用いた損傷メカニズムの解明-。スポーツ傷害フォーラム、2012年1月28日大阪

古賀英之
A new hypothesis for ACL injury mechanisms -based on video analysis using model-based image-matching technique. 傷害予防セミナー、2012年2月26日、東京

下田学, 柳下和慶, 榎本光裕, 堀江正樹, 今井智子, 渡部厚一, 宮川俊平.
シンポジウム「スポーツ外傷、コンディショニングに対するHBO」高気圧酸素負荷による運動後の回復における影響と高気圧酸素負荷の安全性評価　酸化・抗酸化マーカーによる検討.第46回日本高気圧環境・潜水医学会学術総会（2011年10月28日、東京）

神野哲也,古賀大介,森田定雄,長谷川清一郎,松原正明,宗田大
シンポジウム　股関節骨切り術の成績向上を目指して.変形性股関節症に対する骨盤側骨切り術の適応と術式.第39回日本関節病学会,2011年11月12日、横浜

神野哲也
骨インプラント界面のバイオロジーとセメントレス人工股関節周囲の骨反応.第2 回取手・守谷地区運動器疾患学術講演会,2011年11月10日守谷

神野哲也
股関節待機手術における静脈血栓塞栓症対策.第59回日本職業・災害医学会学術大会,
2011年11月11日,東京

関矢一郎
Mesenchymal stem cells derived form synovium：their properties and clinical application for cartilage regeneration
Morehouse college（Atlanta）　2011/1/18

関矢一郎
Cartilage regeneration with synovial stem cells
The International Symposium of Global Center of Excellence Program
Clinical Researches and Experiences for Cartilage Regeneration Therapy
Tokyo Medical and Dental University　2011/2/3

関矢一郎
滑膜幹細胞による軟骨再生医療
日本再生医療学会シンポジウム（新宿）
2011年3月2日

関矢一郎
滑膜間葉幹細胞を用いる低侵襲軟骨再生医療におけるマグネシウムの細胞接着促進効果
日本軟骨代謝学会シンポジウム（博多）
2011年3月5日

関矢一郎
滑膜幹細胞を関節鏡視下で移植する軟骨再生医療
東京整形外科画像診断研究会（神田）
2011年6月11日

関矢一郎
再生医療を利用した半月板損傷の治療への挑戦
JOSKASシンポジウム（札幌）2011年6月18日

関矢一郎
Mesenchymal stem cells derived form synovium：their properties and clinical application for cartilage regeneration
The 3rd International Cartilage and Osteoarthritis Symposium（ICOA 2011）（Suwon, Korea）2011/7/4

関矢一郎
幹細胞の観点から半月板損傷の病態と治療を考える
山口県関節外科症例検討会（山口）2011年7月9日

関矢一郎
滑膜間葉幹細胞による軟骨再生
日本骨代謝学会シンポジウム（大阪）2011年7月28日

関矢一郎
関節液中の幹細胞と関節内組織損傷
日本骨代謝学会シンポジウム（大阪）2011年7月30日

関矢一郎
Mesenchymal stem cells derived form synovium：their properties and clinical application for cartilage regeneration
International Summer Program 2011
Tokyo Medical and Dental University　2011/8/30

関矢一郎
滑膜幹細胞の視点から膝関節疾患の病態と構造体の再生を考える
第10回鹿児島サイトカイン制御療法研究会
2011年9月21日

関矢一郎
Mesenchymal stem cells derived form synovium：their properties and clinical application for cartilage regeneration
BioKorea（Seoul）2011/9/30

関矢一郎
滑膜幹細胞による軟骨・半月板再生
信州運動器診療フォーラム（松本）2011年10月1日

関矢一郎
Roles of stem cells in synovial fluid and clinical applications of stem cells from synovium
Singapore Orthopaedic Association　2011/10/13

関矢一郎
滑膜幹細胞の役割と低侵襲な軟骨再生への応用
日本整形外科学会 第26回基礎学術集会　ランチョンセミナー　2011年10月20日
関矢一郎
幹細胞による軟骨再生―現状と展望―
日本臨床スポーツ医学会シンポジウム（青森）
2011年11月6日
関矢一郎
モーラステープ貼付後の筋肉・筋膜組織中ケトプロフェン濃度の推移
モーラステープ記念講演会（両国）　2011年11月22日
関矢一郎
二次性（外傷性）膝関節症の病態：主に生化学的な観点から
膝関節フォーラム（高田馬場）2011年12月3日
関矢一郎
滑膜幹細胞による軟骨再生
東京大学　再生医療カンファレンス　2012年2月16日
関矢一郎
滑膜幹細胞による半月板再生
東京大学　再生医療カンファレンス　2012年2月16日
関矢一郎
滑膜幹細胞による膝半月板再生
再生医療の実現化ハイウェイ・キックオフ・シンポジウム
東京医科歯科大学　2012年2月28日
関矢一郎
滑膜幹細胞による膝半月板再生
再生医療の実現化ハイウエイ第1回公開シンポジウム
東京国際フォーラム　2012年3月4日
関矢一郎
Cartilage regeneration with synovial stem cells
The 9th International Symposium for Orthopaedic Sports Medicine
Chang Gung Memorial Hospital - Keelung, Taiwan
2012年3月24日
仁賀定雄
“ACTIVE ATHLETIC TRAINING IMPROVES AND PREVENTS GROIN PAIN SYNDROME”
IOC World Conference on Prevention of Injury & Illness in Sport in Monaco, April 7, 2011
仁賀定雄
第5回高知整形外科スポーツ医学研究会
「プロサッカー選手のスポーツ障害」（日整会教育研修講演）
高知市、2011年10月15日
丹羽康江, 出水祐介, 藤井收, 寺嶋千貴, 美馬正幸, 橋本直樹, 金東村, 阿部光幸, 村上昌雄, 柳下和慶.
シンポジウム「放射線障害に対するHBO　evidence と common sense、社会的展開」放射線晩期障害に対するHBOの適応に関するアンケート調査.第46回日本高気圧環境・潜水医学会学術総会（2011年10月28日、東京）
辻邦和
Roles of BMPs during skeletal development and in postnatal bone homeostasis
The 3rd International Conference on Oral Biology (TICOB)
May 26-27, 2011, Bangkok, Thailand
辻邦和
歯と骨のGCOE拠点　総合プレゼンテーション　3月5日、東京医科歯科大学
堀江正樹, 榎本光裕, 下田学, 今井智子, 渡部厚一, 入江一憲, 宮川俊平, 柳下和慶.
シンポジウム「スポーツ外傷、コンディショニングに対するHBO」高気圧酸治療が高強度運動負荷後の疲労回復に与える影響についての検討.第46回日本高気圧環境・潜水医学会学術総会2011年10月28日、東京
宗田　大
スポーツ選手に対する痛点ストレッチ。第15回フィールドケア21。
2010年110日　都市センターホテル
宗田　大
膝関節障害：加齢とロコモ。ロコモティブシンドローム講演会in鹿児島。
2011年2月10日　鹿児島大学　小宮節郎教授
宗田　大
Remnant Preserving Double-bundle ACL Reconstruction.7th PCL Symposium in Seoul 2011.2.12
Prof. Jung Young-Bok
宗田　大
骨関節のスポーツ障害に対するヒアルロン酸製剤注射治療。第48回サッカードクターセミナー。
2011年2月26日　福林徹医科学委員長　時の棲
宗田　大
Remnant preserving double-bundle ACL reconstruction by transtibial technique. Debate：Remnant Preservation in ACL Reconstruction：Is it Worth Doing?
ISAKOS 2011, Rio de Janeiro, May 15, 15：00 – 15：30

KNEE –ACL RECONSTRUCTION

宗田　大

17- year experience of 4-strand semitendinosus double-bundle ACL
reconstruction ICL：ACL Reconstruction - Single vs. Double Bundle. ISAKOS 2011, Rio de Janeiro, May 16, 7：30 – 9：00

宗田　大

Treatment for knee osteoarthritis before Total Knee - Biologic resurfacing options for osteochondral defects of the knee -. ICL：Treatment of Knee Osteoarthritis：What are the Options Before Total Knee? ISAKOS 2011, Rio de Janeiro, May 16, 7：30 – 8：30

宗田　大

What's going on in the section of Orthopedic Surgery, Graduate School of Medicine, Tokyo Medical and Dental University? Mini Symposium, 2011 5 20 @ Gary J. Miller PhD Orthopedic Biomechanics Laboratory, Gainesville, FL

宗田　大

17- year experience of 4-strand semitendinosus double-bundle ACL reconstruction. Grand Rounds in Orthopaedics & Rehabilitation, OHSU, May 23, 7:30 – 8:30, 2011

宗田　大

Anatomic double-bundle ACL reconstruction using 4-strand semitendinosus tendon. 1 st Jishuitan Sports Medicine Summit in Beijin. 2011.6.10, President Dr. Feng, Hua

宗田　大

Medial patellofemoral reconstruction in various patellar instability. 1 st Jishuitan Sports Medicine Summit in Beijin. 2011.6.11, President Dr. Feng, Hua

宗田　大

Physiological background of ACL injured patients. 1 st Jishuitan Sports Medicine Summit in Beijin. 2011.6.12, President Dr. Feng, Hua

宗田　大

4つ折りの半腱様筋腱を用いた2重束再建術の進歩と課題。第3回JOSKAS　特別シンポジウム。2011年6月16日　北海道大学　安田　和則　会長

宗田　大

膝関節の障害に対する保存療法と手術療法の位置づけ。エルムセミナー10　第3回JOSKAS　2011年6月17日　北海道大学　安田　和則　会長

宗田　大

複合靱帯損傷に対する治療のコツとピットフォール。第3回JOSKASセミナー
2011年6月18日　北海道大学　安田　和則　会長

宗田　大

小児・思春期の膝スポーツ外傷と障害。立山セミナー。富山大学　木村友厚教授

宗田　大

膝の痛みと外来での対応。兵庫医大開講記念学術講演会。
2011年9月10日　吉矢晋一教授

宗田　大

2重束再建術のピットフォールとリハビリの工夫。主題18　ACL再建術　診断からリハビリテーション
2011年9月16日　第60回東日本整災第51回関東整災合同学会　会長　落合直之教授

宗田　大

前十字靱帯損傷患者に学んできたこと。日本スポーツ整形外科医学会　ランチョンセミナー
会長　岩本幸英　教授

宗田　大

膝の痛みの診断と治療。第11回茨城県骨・関節フォーラム。
2011年10月28日　石突正文先生座長

宗田　大

バイオメカニクスからみた2重束再建術とリハビリテーションの工夫。第38回日本臨床バイオメカニクス学会。会長　黒坂昌弘教授　2011年11月19日

宗田　大

市民公開講座「痛みのエキスパートに聞く」「膝の痛みとうまく付き合う方法」 第4回日本運動器疼痛学会　2011年11月20日

森山雄吉, 小森恵子, 櫻庭直達, 岸則和, 堀猛史, 春田良雄, 菅田塁, 鎌田桂, 堀義里, 柳下和慶.

パネルディスカッション「大地震災害における高気圧酸素治療と安全対策」東日本大震災におけるHBO治療施設の被害状況と安全管理　アンケート調査報告.第46回日本高気圧環境・潜水医学会学術総会
2011年10月29日、東京

柳下和慶

パネルディスカッション「診療報酬点数適正化への展開」2012年度診療報酬点数改定作業と外保連での活動報告.第46回日本高気圧環境・潜水医学会学術総会
2011年10月28日、東京

柳下和慶

シンポジウム「高気圧酸素療法の再評価と将来展望」晩期放射線障害に対する高気圧酸素治療―総論―.日

本放射線腫瘍学会第24回学術大会（2011年11月18日、神戸）

柳下和慶

コンパートメント症候群・スポーツ傷害に対する高気圧酸素治療について.第12回九州高気圧酸素スポーツ医学研究会環境医学会　市民公開講座.

2011月7月2日、大分県中津市

柳下和慶

スポーツ領域における高気圧酸素治療.第5回日本高気圧環境・潜水医学会北海道地方会2011年10月2日、札幌

15）主催学会

大学院特別講義

日時：2011年10月14日（金）18：30～

東海大学整形外科教授

持田　譲治先生

椎間板変性抑制の為の細胞移植療法

第24回運動器外科セミナー

日時：2011年7月11日（月）18：00～

東京医科歯科大学MDタワー13F大学院講義室2

第25回運動器外科セミナー

日時：2011年7月25日（月）18：30～19：30

東京医科歯科大学MDタワー13F大学院講義室2

臨床解剖学　教授

秋田恵一　先生

第26回運動器外科学セミナー

日時：2011年11月7日（月）午後5：30～7：00

場所：東京医科歯科大学医学部附属病院地下1階

臨床講堂1

第27回運動器外科学セミナー

日時：2012年　3月12日（月）

Dr. A. Hari Reddi

Professor Ellison Chair of Orthopaedic Research

Orthopedics

UC Davis School of Medicine

第5回スポーツリハビリテーションワークショップ

日時：2011年1月22日（土）午後4：30～21：00

場所：東京医科歯科大学

第6回スポーツリハビリテーションワークショップ

日時：2011年10月29日（土）午後17：00～21：00

場所：東京医科歯科大学

第11回膝と歩む会

第8回お茶の水間接症研修会

日時：2012年1月20日（金）午後19：00～21：00

場所：東京医科歯科大学

16）新聞、雑誌、TV報道

新聞

2011年1月7日　産経新聞朝刊

「膝の半月板自身の細胞で再生」

2011年3月4日　読売新聞朝刊

「かけた軟骨幹細胞で修復」

2011年12月13日　朝日新聞朝刊

「痛む膝の半月板再生」

TV

11月20日　日曜日　朝　7時～

TBS系列　「カラダのキモチ」

17）教室、分野や講座の准教授、講師、助教、特別研究員、ポスドク、指導を受けた大学院生の名前

運動器外科	教　授	宗田　　大
軟骨再生学	教　授	関矢　一郎
GCOE	講　師	辻　　邦和
運動器外科	助　教	朱　　寧進
軟骨再生学	助　教	古賀　英之
軟骨再生学	助　教	谷口　直史
間接機能再建学	准教授	望月　智之
運動器外科	医　員	中村　智祐
運動器外科	医　員	堀江　雅史
運動器外科	大学院生	鈴木　志郎
運動器外科	大学院生	山賀　美芽
運動器外科	大学院生	宮武　和正
運動器外科	大学院生	初鹿　大祐
運動器外科	大学院生	小田邉　浩二
運動器外科	大学院生	片桐　洋樹
運動器外科	大学院生	山田　　淳
運動器外科	大学院生	結城　　新
運動器外科	大学院生	大関　信武
運動器外科	大学院生	奥野　真起子
運動器外科	大学院生	中川　祐介
運動器外科	大学院生	松倉　　遊
運動器外科	大学院生	○アブラ・カハル
運動器外科	非常勤講師	山本　晴康
運動器外科	非常勤講師	松原　正明
運動器外科	非常勤講師	森戸　俊行
運動器外科	非常勤講師	八木　茂典

○はAISS

18）GCOE活動についての感想、コメント、改善を望む点

GCOEによる研究の活発化や業績の評価は高い。しかし臨床分野の一人の事業担当者としてみるとGCOEのメリットはあまり大きいとはいえない。メリットに対する報告書作成に必要な労力、拘束時間は少ないとはいえない。国際シンポジウムの開催について、この機会に海外の研究者を招聘できることは魅力があるが、GCOE予算の使い勝手の悪さは上記同様であり、時間および神経の浪費が大きかった。

19）その他　研究教育活動について特記する点

2011.2.世話人としてGCOE国際シンポジウムを開催した。軟骨再生医療の実践してきた日本の3人の講師と海外からの3名の著名な研究者を招聘し、熱心に討議が行われた。シンポジウム翌日の大学院のプレゼンテーションに対して英語での熱心な質疑が行われ、国際的な教育指導が展開された

海外からの3名の著名な研究者を定期的に招聘し、英語によるプレゼンテーション、討論、講演を行っている。

また留学経験者の話やトラベリングフェローの経験を聞く機会を設け、留学に対する前向きな姿勢を養うことに努力している。

産経新聞
平成23年(2011)日刊24458号
1|7[金]
発行所 ©産業経済新聞東京本社2011
〒100－8077東京都千代田区大手町1-7-2
☎東京(03)3231-7111（大代表）

膝の半月板 自身の細胞で再生

東京医科歯科大 研究グループ

軟骨で成果 世界初、臨床応用へ

激しい痛みや腫れを伴う変形性膝関節症の原因になる半月板損傷について、自分の膝の滑膜の幹細胞を取り出して培養し、それを注入して半月板を再生させる医療が東京医科歯科大学の関矢一郎准教授（軟骨再生学）の研究グループによって実用化されることになった。半月板再生の臨床応用は世界初という。厚生労働省によると、自覚症状のある変形性膝関節症の患者数は約1千万人と推定され、半月板再生医療に注目が集まりそうだ。

半月板は膝の骨と骨の間で衝撃を和らげるクッションの役目を果たす軟骨組織。過度のスポーツによる損傷や加齢によって、摩耗したり変形した場合は治りにくく、これまでは糸で縫合したり、傷ついた箇所を切除するなどの治療が行われてきた。

関矢准教授のグループは、滑膜が軟骨などの損傷が起きると傷を治そうと関節液中に幹細胞を増加させ、損傷した箇所を自己修復しようとする機能に着目。滑膜を取り出し、患者の血液で分離した血清によって増やした幹細胞組織を注射で複数回、損傷箇所に注入することにした。

関矢准教授らは平成20年から膝の軟骨が損傷、欠損した20～51歳の患者12人にこの治療を施したところ、7割で軟骨が再生した。これを半月板の再生に応用する方針。関矢准教授は「滑膜幹細胞は年齢にほぼ関係なく、体外で増やせる。まずは外傷性の半月板損傷の患者を対象にし、加齢による変形などの患者にも応用したい」としている。

朝日新聞　2011年12月13日

半月板再生に新治療

滑膜の幹細胞移植

一度傷つくと再生が難しいひざの半月板を、自分のひざの滑膜という組織からとった幹細胞で再生させる治療法を、東京医科歯科大の関矢一郎教授（軟骨再生学）が開発し、来年4月にも臨床研究を始める。半月板の損傷は、全国に2500万人という変形性膝関節症につながる。歩きづらいひざの痛みに苦しむ患者には朗報になりそうだ。

半月板は関節軟骨に挟まれた軟骨組織で、クッションの役目をする。加齢などですり切れると、手術で縫い合わせたりするが、手術できない場合も多い。

新しい治療法では、患者のひざの状態を内視鏡で確認するとき、半月板の近くにある滑膜の一部を採取。2週間培養して増やした幹細胞を、注射器で半月板の損傷部に移植して再生させる。同大で3年間で20人ほどの患者を対象に臨床研究を行ったあと、他の病院にも広げて臨床試験を行う。

関矢教授は、同じ手法でひざの関節軟骨の再生治療をしている。2008年以降、滑膜幹細胞を移植して半年以上たった18人のうち14人で軟骨が再生していることが確認された。当面は手術とセットで行う。

軟骨の再生医療に詳しい京都大学iPS細胞研究所の戸口田淳也教授（整形外科）は「滑膜は手術前に通常行う検査で採れるのが利点。半月板が動きに耐えうる強度を確保することが大事で、うまくいけば画期的な治療になる」と話す。

（下司佳代子）

読売新聞　2011年3月4日

医療ルネサンス　No.5033　再生医療　3/7

欠けた軟骨 幹細胞で修復

関節にかかる衝撃を和らげる「軟骨」。栄養を届ける血管が通っていないため、一度すり減ったり欠けたりすると元に戻らないとされる。しかしいま、その常識は覆されつつある。

神奈川県の男性会社員Bさん(40)は2009年3月、ランニング中に転び、左膝を痛めた。歩く際に激痛が走るようになり、4か月後、総合病院で膝関節内の軟骨の切れ端などを取り除く手術を受けた。

しかし、関節鏡という小型カメラで関節内を見ると、大腿骨側の軟骨が縦1・6ミリ、横0・8ミリほど欠け、骨がむき出しになっていた。これが痛みの原因だった。

「現状では、軟骨を元に戻す治療法はない」と医師に言われ、太ももの筋力を強化するリハビリに取り組んだ。しかし、2か月たっても多少歩きにくさが改善しただけで、激痛は消えない。そのうち、以前は1時間で済んだ通勤に1時間半かかるようになった。

幹細胞注入で膝関節軟骨が再生した例の関節鏡画像。傷ついて荒れた関節軟骨の表面（上）が、11か月後には滑らかになった（下）（関矢一郎さん提供）

そこでインターネットで調べて知ったのが、東京医科歯科大（東京都文京区）で研究中の「軟骨再生」だった。体の様々な組織に変化する「幹細胞」を使うという。「痛みを感じずに歩きたい」と、臨床研究への参加を希望し、昨年春、この再生治療を受けた。

同大軟骨再生学准教授の関矢一郎さんによると、患者の膝関節を取り巻く軟骨と滑膜は、同じ幹細胞が分化してできており、滑膜から採取した幹細胞を、軟骨の欠けた部位に入れると軟骨に変化するという。

まず、関節鏡で関節内を見ながら、滑膜組織を0・5ミリ・グラム採取。その中の幹細胞を2週間、自分の血液で5000万個まで培養し、軟骨が欠けた部分に注射器で入れる。

Bさんは1週間で退院し、最初の1か月半は松葉づえで生活、3か月後には職場復帰した。「日に日に良くなり、今は歩いても痛まない」と喜ぶ。膝への負担が大きいランニングは無理だが、週末には5キロのウオーキングをする。

関矢さんらの研究では、軟骨を損傷し半年以上たった患者12人（20～51歳）にこの治療を行うと、9人で軟骨が増えた。ただし、強度が十分になるまで2年以上かかるとみられ、激しい運動は避けた方がよい。

対象は当面、直径2ミリ程度までの狭い範囲の欠損だが、関矢さんは「将来は、加齢に伴い軟骨がすり減って起こる変形性膝関節症に応用したい」と話す。

軟骨再生の研究は他の施設でも進んでおり、患者から取った軟骨細胞を増やし、欠損部分に縫いつける方法なども試みられている。

2011年(平成23年)12月13日　火曜日　朝日新聞

朝日新聞

2011年(平成23年)
12月13日
火曜日

経済6・8面
国際11・13面
金融情報16・17面
文化18面
小説18面／生活22・25面
スポーツ26・27面
囲碁・将棋30面
地域32・33面
TV・ラジオ29・30・40面

朝日新聞大阪本社
発行所:〒530-8211大阪市北区中之島3-2-4
電　話:06-6231-0131　www.asahi.com

痛むひざ半月板再生

東京医科歯科大、臨床研究へ

幹細胞採り注射

一度傷つくと再生が難しいひざの半月板を、自分のひざの滑膜（かっまく）という組織からとった幹細胞で再生させる治療法を、東京医科歯科大の関矢一郎教授（軟骨再生学）が開発し、来年4月にも臨床研究を始める。

半月板損傷は、全国に2500万人という変形性膝（しつ）関節症につながる。歩きづらいひざの痛みに苦しむ患者には朗報になりそうだ。

半月板は関節軟骨に挟まれた軟骨組織で、クッションの役目をする。加齢などですり切れると、縫い合わせて補強したりするが、手術できない場合も多い。

新しい治療法では、患者のひざの状態を内視鏡で確認するとき、半月板の近くにある滑膜の一部を採取。2週間培養して増やした幹細胞を、注射器で半月板の損傷部に移植して再生させる。同大で3年間で20人ほどの患者を対象に臨床研究を行ったあと、他の病院にも広げて臨床試験を行う。

幹細胞を使う再生医療では骨髄の幹細胞がよく使われるが、お年寄りでは採りにくいことがある。

関矢教授は、同じ手法でひざの関節軟骨の再生治療をしている。2008年以降、滑膜幹細胞を移植して半年以上たった18人のうち14人で軟骨が再生していることが確認された。14人は移植の翌日には松葉杖で、6週間後には自力で歩けるようになったといい、半月板でも同じペースでの回復を見込む。「まずは、従来の手術のみで治癒させるのが難しい半月板の断裂を対象にしたい」といい、当面は手術とセットで行う。

軟骨の再生医療に詳しい京都大学iPS細胞研究所の戸口田淳也教授（整形外科）は「滑膜は手術前に通常行う検査で採れるのが利点。ひざの動きに耐えうる強度を確保することが大事で、うまくいけば画期的な治療になる」と話す。半月板の損傷に悩むスポーツ選手も多く、昨年のサッカーW杯で活躍した本田圭佑選手やプロ野球阪神の城島健司選手らがいる。（下司佳代子）

ひざの構造

Human Mesenchymal Stem Cells in Synovial Fluid Increase in the Knee with Degenerated Cartilage and Osteoarthritis

Ichiro Sekiya,[1] Miyoko Ojima,[2] Shiro Suzuki,[2] Mika Yamaga,[2] Masafumi Horie,[2] Hideyuki Koga,[1] Kunikazu Tsuji,[3] Ken Miyaguchi,[4] Soichi Ogishima,[4] Hiroshi Tanaka,[4] Takeshi Muneta[2]

[1]Section of Cartilage Regeneration, Graduate School, Tokyo Medical and Dental University, Tokyo, Japan, [2]Section of Orthopedic Surgery, Graduate School, Tokyo Medical and Dental University, Tokyo, Japan, [3]Global Center of Excellence Program, International Research Center for Molecular Science in Tooth and Bone Diseases, Tokyo Medical and Dental University, Tokyo, Japan, [4]Department of Bioinformatics, Medical Research Institute, Tokyo Medical and Dental University, Tokyo, Japan

Received 11 January 2011; accepted 17 November 2011
Published online in Wiley Online Library (wileyonlinelibrary.com). DOI 10.1002/jor.22029

ABSTRACT: We investigated whether mesenchymal stem cells (MSCs) in synovial fluid (SF) increased in the knee with degenerated cartilage and osteoarthritis. SF was obtained from the knee joints of 22 patients with anterior cruciate ligament (ACL) injury during ACL reconstruction, and cartilage degeneration was evaluated arthroscopically. SF was also obtained from the knee joints of 6 healthy volunteers, 20 patients with mild osteoarthritis, and 26 patients with severe osteoarthritis, in which the grading was evaluated radiographically. The cell component in the SF was cultured for analyses. Synovium (SYN) and bone marrow (BM) were also harvested during total knee arthroplasties. The MSC number in SF was correlated with the cartilage degeneration score evaluated by arthroscopy. The MSC number in the SF was hardly noticed in normal volunteers, but it increased in accordance with the grading of osteoarthritis. Though no significant differences were observed regarding surface epitopes, or differentiation potentials, the morphology and gene profiles in SF MSCs were more similar to those in SYN MSCs than in BM MSCs. We listed 20 genes which were expressed higher in both SYN MSCs and SF MSCs than in BM MSCs, and 3 genes were confirmed by quantitative RT-PCR. MSCs in SF increased along with degenerated cartilage and osteoarthritis. © 2011 Orthopaedic Research Society. Published by Wiley Periodicals, Inc. J Orthop Res

Keywords: mesenchymal stem cells; synovial fluid; cartilage degeneration; osteoarthritis; synovium

Mesenchymal stem cells (MSCs) can be defined as being derived from mesenchymal tissue and having the functional capacity for self-renewal, commonly identified by colony-forming unit fibroblast assay[1] and generation of a number of differentiated progeny.[2] We previously reported that MSCs in synovial fluid (SF) from anterior cruciate ligament (ACL) injury patients were 100 times more in number than those from healthy volunteers, and that the MSC number was positively correlated with post-injury period.[3] During ACL reconstruction, cartilage degeneration was also observed at high rates,[4] and ACL transection is one of the most widely used animal models for cartilage degeneration.[5] Therefore, there seems to be three intercorrelations among three conditions; ACL injury, cartilage degeneration, and MSCs in SF. The first purpose of this study was to investigate a direct relation between the number of MSCs in SF and cartilage degeneration in the ACL injured knees.

The existence of MSCs in SF of osteoarthritis knees was first reported by Jones et al.[6] They further reported in 2008 that MSCs in SF numerically increased in early osteoarthritis.[7] This review is of value because it shed light on the roles of MSCs in SF of osteoarthritis knees. However, the design of their study seemed to be inappropriate. All SF examined was obtained from patients with unexplained knee pain and from those who underwent arthroscopy. Furthermore, the nonosteoarthritis group they studied consisted of individuals with meniscal tears in addition to individuals without damage to the articular cartilage. Our second purpose was to investigate more strictly whether MSCs in SF increased in the knee with osteoarthritis.

MSCs can be obtained from various tissues, and they contain common features. However, an increasing number of reports have described variant properties dependent on cell sources.[8–11] In ACL injured knees, the gene profile of SF MSCs was more similar to that of synovium (SYN) MSCs than to that of bone marrow (BM) MSCs,[3] however, different pathological conditions may have led to different properties of synovial MSCs. Our third purpose was to perform patient-matched quantitative comparisons of the properties of SF MSCs, synovial MSCs, and BM MSCs. The properties examined included cell morphology, surface epitopes, chondrogenic, adipogenic, and osteogenic differentiation potentials, and gene profiles.

MATERIALS AND METHODS

Synovial Fluid Derived from ACL Injury Patients

The study was approved by an institutional review board, and informed consents were obtained from all study subjects. SF was obtained from the knee joints of 22 patients with ACL injury of the knees during ACL reconstruction under spinal anesthesia. The average age was 26 years, and the range was 12–45 years. During the operation, 6 areas consisting of medial femoral condyle, medial tibial plateau, lateral femoral condyle, lateral tibial plateau, patella, and femoral groove of cartilage were evaluated arthroscopically as 1 (normal), 2 (softening), 3 (fissure), 4 (more than half

Ichiro Sekiya and Miyoko Ojima contributed equally to this study.

Correspondence to: Ichiro Sekiya (T: +81-3-5803-4020; F: +81-3-5803-4020; E-mail: sekiya.orj@tmd.ac.jp)

© 2011 Orthopaedic Research Society. Published by Wiley Periodicals, Inc.

cartilage thickness), 5 (less than half cartilage thickness), 6 (full thickness cartilage defect), or 7 (bone defect), respectively, and the total number[6–28] was calculated for the cartilage degeneration score.

Synovial Fluid Derived from Osteoarthritis Patients

Synovial fluid was obtained from the knee joints of 6 healthy volunteers, 35-year old on average, ranging from 30 to 45, and from 20 patients with osteoarthritis of the knee at Grades 1 and 2 of Kellgren–Lawrence at our outpatient clinic. The patients were 50-year old on average, ranging from 40 to 60. SF was also obtained from the knee joints of 26 patients with osteoarthritis of the knee at Grades 3 and 4 of Kellgren–Lawrence during total knee arthroplasty under spinal anesthesia. The patients were 75-year old on average, ranging from 65 to 85. Kellgren–Lawrence grading was evaluated by radiographs of weight bearing posterior–anterior view at 45° of flexion of the knee.[12]

Cultures of Colony-Forming Cells in Synovial Fluid

Synovial fluid was diluted with phosphate-buffered saline (PBS), filtered through a 70 μm nylon filter (Becton Dickinson, Franklin Lakes, NJ) to remove debris, and plated in six culture dishes of 60 cm^2 (Nalge Nunc International, Rochester, NY) in complete culture medium: α-modified essential medium (α-MEM; Invitrogen, Carlsbad, CA) containing 10% fetal bovine serum (Invitrogen), 100 U/ml penicillin, 100 μg/ml streptomycin, and 250 ng/ml amphotericin B (Invitrogen). The dishes were incubated at 37°C with 5% humidified CO_2. After 24 h, the adherent cells were washed with PBS. Fourteen days after initial plating, three dishes were stained with 0.5% crystal violet (Wako, Osaka, Japan) in 4% paraformaldehyde for 5 min, and the number of colonies was counted. Colonies less than 2 mm in diameter and faintly stained colonies were ignored. The other three dishes were harvested with 0.25% trypsin and 1 mM EDTA (Invitrogen; Passage 0), replated at 500 cells/cm^2 in a 145-cm^2 culture dish (Nalge Nunc International) and cultured for 14 days for further analyses.

In Vitro Differentiation Assay

For chondrogenesis, 250,000 cells were placed in a 15 ml polypropylene tube (Becton-Dickinson, Franklin Lakes, NJ), centrifuged at 450*g* for 10 min, and cultured in chondrogenesis medium containing 1,000 ng/ml BMP-7 (Stryker Biotech, Hopkinton, MA), 10 ng/ml transforming growth factor-β3 (R&D Systems, Minneapolis, MN), and 100 nM dexamethasone (Sigma–Aldrich Corp., St. Louis, MO) for 14 days. For microscopy, the pellets were embedded in paraffin, cut into 5 μm sections, and stained with toluidine blue.[13]

For adipogenesis, cells were cultured in adipogenic medium which consisted of complete medium supplemented with 100 nM dexamethasone (Sigma–Aldrich Corp.), 0.5 mM isobutyl-methylxanthine (Sigma–Aldrich Corp.), and 50 μM indomethacin (Wako) for 21 days. The adipogenic cultures were fixed in 4% paraformaldehyde and then stained with fresh oil red-O solution.[14] For quantification, isopropyl alcohol was added to the stained culture dish. After 5 min, the absorbance of the extract was assayed by a spectrophotometer at 510 nm after dilution to a linear range.[15]

For osteogenesis, cells were cultured in osteogenesis medium that comprised complete medium consisting of 1 nM dexamethasone, 10 mM β-glycerol phosphate (Wako), and 50 μg/ml ascorbate-2-phosphate (Sigma–Aldrich Corp.) for 21 days. The dishes were stained with 0.5% alizarin red solution.[16] For alkaline phosphatase activity (ALP), the cells were harvested with lysis buffer (0.1 M Tris–HCl, 5 mM $MgCl_2$, 2% Triton-X 100, and 1 mM phenylmethylsulfonyl fluoride) and sonicated. An aliquot (10 μl) of supernatant was added into 100 μl 50 mM *p*-nitrophenylphosphatase hexahydrate containing 1 mM $MgCl_2$, and the mixture was incubated at 37°C for 30 min. The absorption at 405 nm was measured with a spectrophotometer. ALP activity represented millimoles of *p*-nitrophenol release after 30 min of incubation at 37°C.[16]

Isolation and Culture of Synovium and Bone Marrow MSCs

During total knee arthroplasty, SYN and BM were also collected. SYN was harvested from the bony side of the suprapatellar pouch, digested in a 3 mg/ml collagenase D solution (Roche Diagnostics, Mannheim, Germany) for 3 h. BM was aspirated from the tibia, and the nucleated cells were separated with a Ficoll density gradient (Ficoll-Paque; Pharmacia Biosystems, Uppsala, Sweden). Nucleated cells from SYN and BM were plated in a 60-cm^2 dish and cultured in a similar method as described earlier.

Epitope Profile

One million cells were resuspended in 200 μl PBS containing 20 μg/ml antibody. After incubation for 30 min at 4°C, the cells were washed with PBS and re-suspended in 1 ml PBS for flowcytometric analysis. Fluorescein isothiocyanate (FITC)- or phycoerythrin (PE)-coupled antibodies against CD34, CD45, CD90, and CD146 (BD), CD44 (eBioscience, San Diego, CA), CD105, CD166 (Ancell, Bayport, MN), and CXCR4 (R&D Systems) were used. For STRO-1 staining, the cells were incubated for 30 min with an antibody against STRO-1 (mouse IgM; Genzyme-Techne Minneapolis, MN). The cells were then incubated with a secondary antibody (fluorescein-conjugated goat anti-mouse IgM; Vector Laboratories, Burlingame, CA) for 30 min. For D7-FIB staining, the cells were incubated for 30 min with an antibody against D7-FIB (mouse IgG; Serotec, Kidlington, UK). The cells were then incubated with a secondary antibody (fluorescein-conjugated rabbit anti-mouse IgG; Serotec) for 30 min. The cells were also incubated with a secondary antibody (fluorescein-conjugated rabbit anti-goat IgG; Southern Biotech, Birmingham, AL) for 30 min. For isotype control, FITC- or PE-coupled nonspecific mouse immunoglobulin G (IgG; BD) was substituted for the primary antibody. Cell fluorescence was evaluated by flow cytometry using a FACSCalibur instrument (BD). The data were analyzed using CellQuest software (BD).

Microarray Analysis

Three samples in each group were analyzed. Human genome-wide gene expression was examined on a total 28,000 genes with the Human Gene 1.1 ST Array (GeneChip; Affymetrix, Santa Clara, CA). Total RNA was prepared from colony-forming cells (Passage 1) derived from SYV, SF, and BM using TRIzol solution (Invitrogen). Sense-strand cDNA probes for hybridization were synthesized using the WT Expression Kit for Affymetrix GeneChip Whole Transcript Expression Arrays (Ambion, Foster City, CA). The microarray data were analyzed using the Robust Multichip Average method[17] (Bioconductor, http://www.bioconductor.org). A heatmap was constructed by hierarchical clustering on highly differentially expressed genes which show >5.0- or

<0.2-fold changes in any pairs of samples (SYV/SF, SYV/BM, and SF/BM). To identify the genes showing (1) high expressions in both SYV and SF, and (2) low expressions in BM, expression values in triplicates were averaged and filtered by the following threshold for fold changes; SYV/BM > 5 and SF/BM > 5; and listed in descending order of SYV/BM.

Quantitative Real-Time PCR

First-strand cDNAs were synthesized using a Transcriptor First-strand cDNA synthesis kit (Roche Applied Sciences, Indianapolis, IN), and Q-PCR analyses were performed using a LightCycler 480 Probe Master system (Roche). β-Actin was used as an internal control. Relative mRNA expression levels were calculated as described by Niikura et al.[18] PCR primers were as follows: SMOC2 5′-AAGGAAGTATACCCAGG AGCAA-3′ (forward), 5′-GTGTAGCTGTGACACTGGACCT-3′ (reverse); GPR133 5′-TATACGCGGGACAATTCCAT-3′ (forward), 5′-AAATAGGACATGAGTCCAA TAGGG-3′ (reverse); SFRP4 5′-GCCTGAAGCCATCGTCAC-3′ (forward), 5′-CCATCATGTCTGGTGTGATGT-3′ (reverse); β-actin 5′-ATTGGCAATGAGC GGTTC-3′ (forward), 5′-TGAAGGTAGTTTCGTGGATGC-3′ (reverse).

RESULTS

Synovial Fluid MSCs and Cartilage Degeneration

A large number of colonies consisting of spindle shaped cells were observed after 14 days culturing of cell components in SF of the knee with ACL injury (Fig. 1A). The colony-forming cells differentiated into chondrocytes, adipocytes, and calcified when cultured in the differentiation medium (Fig. 1B). These findings indicate that colony-forming cells, which originally existed in syonvial fluid, had characteristics of MSCs. The MSC number in the SF was correlated to the cartilage degeneration score evaluated with arthroscopy (Fig. 1C).

Synovial Fluid MSCs and Osteoarthritis

Representative culture dishes indicated that the colony number of SF MSC increased according to the radiological osteoarthritis grading by Kellgren–Lawrence (Fig. 2A). Comparing the normal (Grade 0), mild (Grades 1 and 2), and severe (Grades 3 and 4) osteoarthritis groups, the MSC number in the SF increased along with the grading of the osteoarthritis (Fig. 2B).

Comparison among Synovium MSCs, Synovial Fluid MSCs, and Bone Marrow MSCs from Osteoarthritis Patients

Morphologically, SF MSCs appeared to be closer to SYN MSCs than to BM MSCs, in that SYN MSCs and SF MSCs were narrower, and their nuclei were more obvious (Fig. 3A). For surface epitopes, 3 populations of MSCs were positive for CD44, CD90, CD105, and negative for CD34, CD45. These results were identical to those of distinctive MSCs, and there were no significant differences of surface epitopes among the 3 populations (Fig. 3B). After MSC pellets were cultured in chondrogenic medium, they became cartilage pellets whose matrix appeared as purple from toluidine blue staining in the 3 populations (Fig. 3C). There were no significant differences of pellet weights, an indicator of cartilage matrix synthesis, among the 3 populations (Fig. 3D). After culturing in adipogenic medium, lipids showing red by oil red-O staining were observed in the 3 populations (Fig. 3E). There were no significant differences of absorbance at 510 nm for extraction of oil red-O among the 3 populations (Fig. 3F). In addition, there were no significant differences of ALP activity among the 3 populations of MSCs both when MSCs were cultured in osteogenesis medium containing 10 mM β-glycerol phosphate and in osteogenesis medium containing 20 mM β-glycerol phosphate (Fig. 3G).

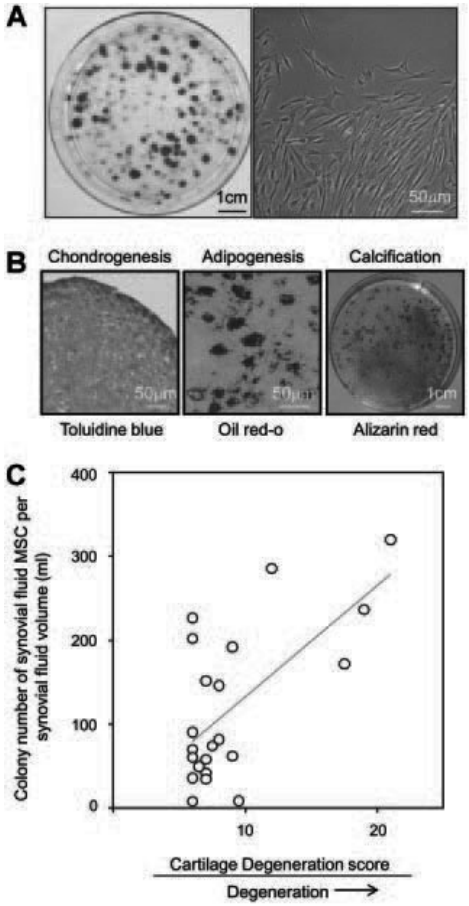

Figure 1. Colony-forming cells in synovial fluid derived from ACL injury patients. (A) Representative cell colonies stained with crystal violet and cell morphology. (B) Multidifferentiation potential. (C) Relationship between cartilage degeneration score and colony number of synovial fluid MSCs per synovial fluid volume (ml; $r^2 = 0.64$, $P = 0.002$ by correlation analysis).

Comparison of the Gene Expression Profiles among Synovium MSCs, Synovial Fluid MSCs, and Bone Marrow MSCs from Osteoarthritis Patients

Hierarchical clustering analysis demonstrated that gene profiles in SF MSCs were more similar to those in SYN MSCs than to those in BM MSCs (Fig. 4A). To demonstrate specific genes which were expressed higher in both SYN MSCs and SF MSCs than in BM

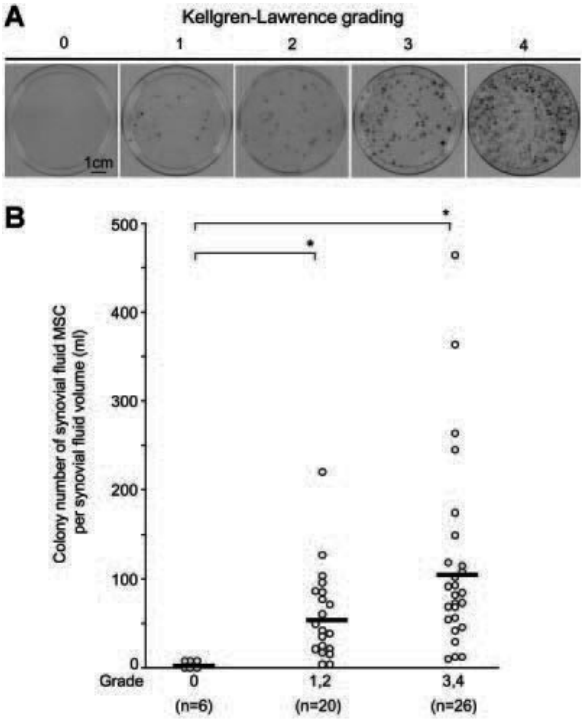

Figure 2. MSCs in synovial fluid derived from osteoarthritis patients. (A) Representative dishes for colonies of synovial fluid MSCs according to the Kellgren–Lawrence grading system. (B) Relationship between the osteoarthritis grading and the colony number of synovial fluid MSCs per synovial fluid volume (ml). Average values are shown as bars ($P = 0.002$ by Kruskal–Wallis test; $^{*}P < 0.05$ by Steel–Dwass test).

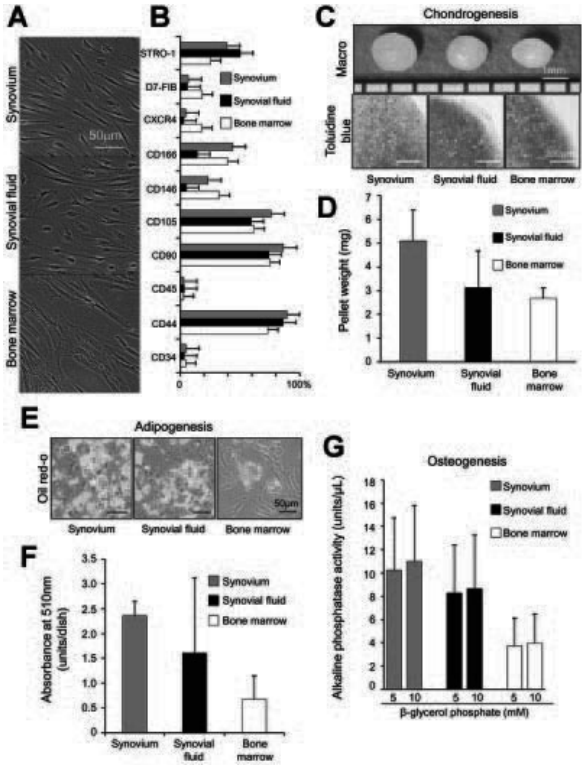

Figure 3. Comparison among synovium MSCs, synovial fluid MSCs, and bone marrow MSCs from osteoarthritis patients. (A) Representative morphologies. (B) Surface epitopes of MSCs. Positive expression rates are displayed as the average and standard deviation ($n = 5$). (C) Chondrogenesis. (D) Wet weight of the cartilage pellets. (E) Adipogenesis. (F) Quantification of adipogenesis by absorbance at 510 nm for extraction of oil red-O. (G) Alkaline phosphatase activity. MSCs were cultured in osteogenesis medium containing 5 and 10 mM β-glycerol phosphate.

MSCs, 20 genes are listed in Table 1. For SMOC2, GPR 133, and SFRP4 genes, which are listed as the top 3, quantitative RT-PCR analyses were performed in five other donors with osteoarthritis, and expressions of these genes were much higher in SYN MSCs and SF MSCs than in BM MSCs (Fig. 4B).

DISCUSSION

In this study, we directly demonstrated a correlation between number of MSCs in SF and cartilage degeneration in the ACL injured knees. However, variability still seems to exist in a population with a minimum cartilage degeneration score which is shown in Figure 1C. The number of SF MSCs per volume was 119 ± 92 in ACL injured knees, while it was 60 ± 52 in Grade 1, 2 osteoarthritis knees, and 115 ± 109 in Grade 3, 4 osteoarthritis knees. Though the degree of cartilage degeneration was much higher in Grade 3, 4 osteoarthritis knees, the number of SF MSCs per volume was similar between ACL injured knees and Grade 3, 4 osteoarthritis knees. This will be due to that ACL injury itself affected the number of SF MSCs in addition to the cartilage degeneration.[3] More detailed analysis will be of value in the same population from the standpoints of post-injury period, stability of the knee, appearance of ACL remnants, and so on.

Though the existence of MSCs in SF from the knee with osteoarthritis patients was previously reported,[6,7] we first demonstrated that the MSC number in SF increased along with radiological osteoarthritis grading. Our previous study showed that autologous SF enhanced expansion of MSCs in tissue culture of SYN from osteoarthritis patients.[19] These results suggest one mechanism by which SF derived from osteoarthritis promotes mobilization of SYN MSCs into SF. Similar to ACL injured knees, variability also still seems to exist in the mild and severe osteoarthritis groups, respectively. A future study to analyze osteoarthritis of the same grade from the standpoints of spur formation, SYN conditions, subjective scores, and so on would be important.

Here, SF MSCs were more similar to SYN MSCs than to BM MSCs from the morphological and gene profile views. However, similar characteristics between SF MSCs and SYN MSCs may be due to the environmental cues; both kinds of MSCs are constantly exposed to the same cytokines and growth factors in the knee joint, the environment of both kinds of MSCs is

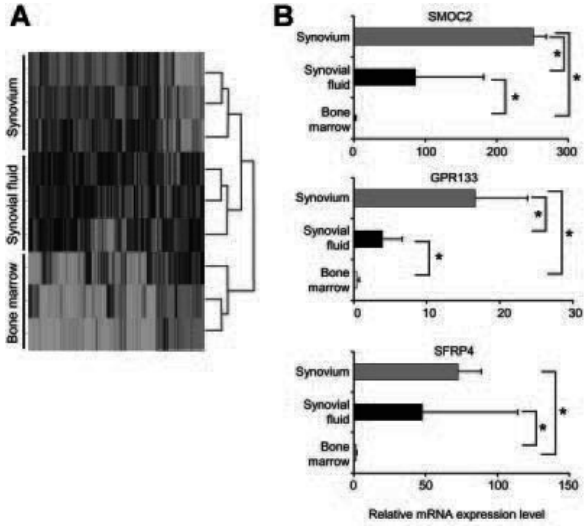

Figure 4. Comparison of the gene expression profiles among synovium MSCs, synovial fluid MSCs, and bone marrow MSCs from osteoarthritis patients. (A) Hierarchical clustering analysis ($n = 3$). (B) Quantitative RT-PCR analysis for the top three genes shown in Table 1. Relative amount of PCR products to that in bone marrow MSCs are displayed as the average and standard deviation ($n = 5$; $^{*}P < 0.05$ by Steel–Dwass test). The tissues were harvested from five donors in addition to the donor analyzed in the microarray.

quite different from that of BM, and, thus resulting in a similar gene expression pattern. The gene expression pattern of MSCs that are recruited from BM through systemic circulation may change after they are sent to SF. It would be quite interesting to examine whether BM MSCs which incubate in SF resemble the phenotypes as they do in SYN MSCs.

There were no significant differences of surface epitopes among SYN MSCs, SF MSCs, and BM MSCs. One of the surface epitopes we examined was D7-FIB, whose antigen is a fibroblast-specific molecule of unknown function. According to Jones et al.,[20] D7-FIB is a marker of BM MSCs, and $CD45^{low}D7\text{-}FIB^{+}LNGFR^{+}$ BM cells express classic markers of cultured MSCs CD73/SH3, CD105/SH2, and CD106/VCAM.[21] In our results, the positive rate for D7-FIB was less than 20% in the 3 populations of MSCs.

In SF MSCs, the differentiation potentials were not correlated to the cartilage degeneration score and to the MSC number in SF. In 10 donors we examined, SF MSCs differentiated into all three lineages, though the quantitative values varied. SF MSCs had common properties in all donors, however, each property varied individually.

The volume of SF taken from the patients was 9.9 ± 6.9 ml in Grade 1, 2 osteoarthritis knees, and 11.1 ± 9.5 ml in Grade 3, 4 osteoarthritis knees. There

Table 1. Specific Genes Which Were Expressed Higher in Both Synovium MSCs (SYB) and Synovial Fluid MSCs (SF) Than in Bone Marrow MSCs (BM)

				Fold Ratio of Expression		
No.	GenBank No.	Gene Name	Symbol	SYV/BM	SF/BM	SYV/SF
1	NM_022138	SPARC-related modular calcium binding 2	**SMOC2**	13.4	13.8	1.0
2	NM_198827	Secreted frizzled-related protein 4	**GPR133**	13.1	10.5	1.2
3	NM_003014	Peptidase inhibitor 16	**SFRP4**	11.9	8.5	1.4
4	NM_153370	Transmembrane and tetratricopeptide repeat containing 1	PI16	9.8	8.2	1.2
5	NM_175861	Calcium channel, voltage-dependent, beta 4 subunit	TMTC1	9.0	6.1	1.5
6	NR_030672	KIAA1324-like	KIAA1324L	8.9	8.1	1.1
7	NM_000726	Calcium channel, voltage-dependent, beta 4 subunit	CACNB4	8.5	6.2	1.4
8	NR_002196	H19, imprinted maternally expressed transcript	H19	8.4	6.6	1.3
9	BC006141	Erythrocyte membrane protein band 4.1-like 3	EPB41L3	7.8	6.1	1.3
10	BC101809	Prostaglandin I2 (prostacyclin) synthase	PTGIS	7.8	8.8	0.9
11	NR_001284	Tenascin XA	TNXA	7.7	10.3	0.7
12	NM_004753	Dehydrogenase/reductase (SDR family) member 3	DHRS3	7.6	6.2	1.2
13	NM_020858	Sema domain, transmembrane domain (TM), and cytoplasmic domain (semaphorin), 6D	SEMA6D	6.5	5.5	1.2
14	NM_198148	Carboxypeptidase X (M14 family), member 2	CPXM2	6.4	4.8	1.3
15	NM_001276	Chitinase 3-like 1 (cartilage glycoprotein-39)	CHI3L1	6.3	5.5	1.1
16	NM_002214	Integrin, beta 8	ITGB8	6.2	5.0	1.2
17	NM_015419	Matrix-remodeling associated 5	MXRA5	6.2	5.7	1.1
18	NM_000062	Serpin peptidase inhibitor, clade G (C1 inhibitor), member 1	SERPING1	6.0	4.4	1.4
19	NM_005807	Proteoglycan 4	PRG4	5.6	8.4	0.7
20	NM_001354	Aldo-keto reductase family 1, member C2	AKR1C2	5.3	5.2	1.0

The genes are listed in descending order of SYV/BM. Genes in bold were confirmed by real-time PCR.

was a weak tendency between SF volume and synovial MSC number per SF volume in the osteoarthritis knees (data not shown). In this study, only SF with translucency viewed with naked eyes were analyzed, and the blood test for CRP was negative in most cases. However, the volume of SF is one of the indexes for inflammation in the osteoarthritis knee. Mild inflammation undetectable with our examinations might have affected the number of SF MSCs in the osteoarthritis knees.

The volume of SF taken from the patients was 3.8 ± 3.1 ml in ACL injured knee, and there was no tendency between SF volume and synovial MSC number per SF volume. In ACL injury knees, several other factors in addition to cartilage degeneration, as mentioned above, might have affected SF MSCs and negated the factor of SF volume.

We demonstrated that the MSC number in SF increased along with the radiological grading of osteoarthritis as shown in Figure 2B. The age distribution of the three groups was different; the average age was 35 in the normal group, 50 in the mild group, and 75 in the severe osteoarthritis group. This may have influenced the data because several studies have reported that aging affects properties of MSCs derived from several kinds of mesenchymal tissues, though the subjects diagnosed were elderly people with osteoarthritis or osteoporosis in most of the previous studies.[22,23] To remove the factor of aging, normal control groups at the same age are required, however, it is practically difficult to collect SF from elderly people with normal knees.

We showed 20 specific genes whose expression was higher in both SYN MSCs and SF MSCs in comparison to that in BM MSCs. We further confirmed expressions of the top three genes by RT-PCR. SMOC2 stands for SPARC-related modular calcium binding 2. SPARC (secreted protein acidic and rich in cysteine) is highly expressed during embryogenesis, and its expression becomes more restricted in adult tissues.[24] SMOC-2 is expressed highly in the heart, muscle tissue, spleen, and ovary.[25] Only the function of SMOC2 reported previously involves stimulation of endothelial cell proliferation.[26] In comparison with normal cartilage, SMOC-2 mRNA expression was higher in osteoarthritis cartilage.[27] GPR133 encodes a G-protein-coupled receptor (GPCR). GPCRs are involved in osteoclast function and regulation of bone mineral density and cell growth.[28] A genome-wide association study recently demonstrated that genetic variation in GPR133 was associated with body height.[29] SFRP4 stands for secreted frizzled-related protein 4. Secreted frizzled-related protein is one of the regulators for the Wnt signaling pathway, which regulates various normal and pathological developmental processes of many organs. Some studies reported that SFRP4 is a negative regulator of peak bone mineral density.[30] In most genes listed in Table 1, including the three genes mentioned above, their relationships to SYN or SF remains unknown, however, these genes would be interesting as signatures in that they distinguish the SYN and SF MSCs from BM MSCs. This knowledge would be greatly helpful to clarify the mechanisms of treatment for osteoarthritis. For example, we would be able to answer the question about the tissue origin of the MSCs, which appear in the degenerated site of articular cartilage induced by abrasion arthroplasty.

What is the role of MSCs in SF? MSCs are postulated to participate in tissue homoeostasis, remodeling, and repair by ensuring the replacement of mature cells lost to physiological turnover, senescence, injury, or disease. Stem cell populations are found in most adult tissues, and in general, their differentiation potential may reflect the local cell population.[8,9] Developmentally, intraarticular tissues are differentiated from common progenitors, referred to as common interzone cells.[31] SYN MSCs have a high chondrogenic potential[8–10]; intraarticular injection of SYN MSCs promoted cartilage regeneration in rabbit cartilage defect model[32]; and intraarticular injection of SYN MSCs contributed to meniscal regeneration in a rat meniscus defect model.[33] We speculate that synovial tissue may serve as a reservoir of stem cells that mobilize following intraarticular tissue diseases and migrate to the site to participate in the repair response.

Why is the number of SF MSCs increased in accordance with the degree of cartilage degeneration? In the adult cartilage, because of enzymatic activities and the mechanical stress imposed onto the joints, cartilage damage always occurs. In normal circumstances, this is compensated by the turnover of the matrix components synthesized by chondrocytes. Thus, in normal adult articular cartilage, there is an equal balance between anabolism and catabolism. In osteoarthritis, catabolism becomes stronger than the anabolic capacities of chondrocytes, the cartilage matrix degenerates, and the joint cartilage gets damaged.[34] We speculate that MSCs were mobilized from SYN through SF toward degenerative cartilage. Seemingly, the number of mobilized MSCs is limited, therefore osteoarthritis progresses in its natural course. Our next step is to investigate whether intraarticular injection of SYN MSCs can inhibit the progression of osteoarthritis.

In conclusion, the MSC number in SF was correlated to cartilage degeneration evaluated with arthroscopy in the ACL injured knees. The MSC number in SF increased along with the radiological grading of osteoarthritis. SF MSCs were more similar to SYN MSCs than to BM MSCs from the morphological and gene profile views.

ACKNOWLEDGMENTS

The present study was supported by grants from the Japanese Ministry of Education Global Center of Excellence Program, International Research Center for Molecular Science in Tooth and Bone Diseases to T.M., from the Japan Society for the Promotion of Science (16591478), and from Health and Labor Sciences Research Grant, Research on

Regenerative Medicine for Clinical Application to I.S. Recombinant human BMP-7 was distributed by Stryker Biotech. We thank Izumi Nakagawa for management of our laboratory.

REFERENCES

1. Friedenstein AJ. 1976. Precursor cells of mechanocytes. Int Rev Cytol 47:327–359.
2. Horwitz EM, Le Blanc K, Dominici M, et al. 2005. Clarification of the nomenclature for MSC: The International Society for Cellular Therapy position statement. Cytotherapy 7:393–395.
3. Morito T, Muneta T, Hara K, et al. 2008. Synovial fluid-derived mesenchymal stem cells increase after intra-articular ligament injury in humans. Rheumatology (Oxford) 47:1137–1143.
4. Asano H, Muneta T, Ikeda H, et al. 2004. Arthroscopic evaluation of the articular cartilage after anterior cruciate ligament reconstruction: a short-term prospective study of 105 patients. Arthroscopy 20:474–481.
5. Hayashi M, Muneta T, Ju YJ, et al. 2008. Weekly intra-articular injections of bone morphogenetic protein-7 inhibits osteoarthritis progression. Arthritis Res Ther 10:R118.
6. Jones EA, English A, Henshaw K, et al. 2004. Enumeration and phenotypic characterization of synovial fluid multipotential mesenchymal progenitor cells in inflammatory and degenerative arthritis. Arthritis Rheum 50:817–827.
7. Jones EA, Crawford A, English A, et al. 2008. Synovial fluid mesenchymal stem cells in health and early osteoarthritis: detection and functional evaluation at the single-cell level. Arthritis Rheum 58:1731–1740.
8. Sakaguchi Y, Sekiya I, Yagishita K, et al. 2005. Comparison of human stem cells derived from various mesenchymal tissues: superiority of synovium as a cell source. Arthritis Rheum 52:2521–2529.
9. Yoshimura H, Muneta T, Nimura A, et al. 2007. Comparison of rat mesenchymal stem cells derived from bone marrow, synovium, periosteum, adipose tissue, and muscle. Cell Tissue Res 327:449–462.
10. Koga H, Muneta T, Nagase T, et al. 2008. Comparison of mesenchymal tissues-derived stem cells for in vivo chondrogenesis: suitable conditions for cell therapy of cartilage defects in rabbit. Cell Tissue Res 333:207–215.
11. Segawa Y, Muneta T, Makino H, et al. 2009. Mesenchymal stem cells derived from synovium, meniscus, anterior cruciate ligament, and articular chondrocytes share similar gene expression profiles. J Orthop Res 27:435–441.
12. Rosenberg TD, Paulos LE, Parker RD, et al. 1988. The forty-five-degree posteroanterior flexion weight-bearing radiograph of the knee. J Bone Joint Surg Am 70:1479–1483.
13. Shimaya M, Muneta T, Ichinose S, et al. 2010. Magnesium enhances adherence and cartilage formation of synovial mesenchymal stem cells through integrins. Osteoarthritis Cartilage 18:1300–1309.
14. Sekiya I, Larson BL, Vuoristo JT, et al. 2004. Adipogenic differentiation of human adult stem cells from bone marrow stroma (MSCs). J Bone Miner Res 19:256–264.
15. Sekiya I, Larson BL, Smith JR, et al. 2002. Expansion of human adult stem cells from bone marrow stroma: conditions that maximize the yields of early progenitors and evaluate their quality. Stem Cells 20:530–541.
16. Sakaguchi Y, Sekiya I, Yagishita K, et al. 2004. Suspended cells from trabecular bone by collagenase digestion become virtually identical to mesenchymal stem cells obtained from marrow aspirates. Blood 104:2728–2735.
17. Irizarry RA, Bolstad BM, Collin F, et al. 2003. Summaries of Affymetrix GeneChip probe level data. Nucleic Acids Res 31:e15.
18. Niikura T, Hak DJ, Reddi AH. 2006. Global gene profiling reveals a downregulation of BMP gene expression in experimental atrophic nonunions compared to standard healing fractures. J Orthop Res 24:1463–1471.
19. Zhang S, Muneta T, Morito T, et al. 2008. Autologous synovial fluid enhances migration of mesenchymal stem cells from synovium of osteoarthritis patients in tissue culture system. J Orthop Res 26:1413–1418.
20. Jones EA, Kinsey SE, English A, et al. 2002. Isolation and characterization of bone marrow multipotential mesenchymal progenitor cells. Arthritis Rheum 46:3349–3360.
21. Jones EA, English A, Kinsey SE, et al. 2006. Optimization of a flow cytometry-based protocol for detection and phenotypic characterization of multipotent mesenchymal stromal cells from human bone marrow. Cytometry B Clin Cytom 70:391–399.
22. Mochizuki T, Muneta T, Sakaguchi Y, et al. 2006. Higher chondrogenic potential of fibrous synovium- and adipose synovium-derived cells compared with subcutaneous fat-derived cells: distinguishing properties of mesenchymal stem cells in humans. Arthritis Rheum 54:843–853.
23. Murphy JM, Dixon K, Beck S, et al. 2002. Reduced chondrogenic and adipogenic activity of mesenchymal stem cells from patients with advanced osteoarthritis. Arthritis Rheum 46:704–713.
24. Porter PL, Sage EH, Lane TF, et al. 1995. Distribution of SPARC in normal and neoplastic human tissue. J Histochem Cytochem 43:791–800.
25. Vannahme C, Gosling S, Paulsson M, et al. 2003. Characterization of SMOC-2, a modular extracellular calcium-binding protein. Biochem J 373:805–814.
26. Rocnik EF, Liu P, Sato K, et al. 2006. The novel SPARC family member SMOC-2 potentiates angiogenic growth factor activity. J Biol Chem 281:22855–22864.
27. Wu J, Liu W, Bemis A, et al. 2007. Comparative proteomic characterization of articular cartilage tissue from normal donors and patients with osteoarthritis. Arthritis Rheum 56:3675–3684.
28. Hsiao EC, Boudignon BM, Chang WC, et al. 2008. Osteoblast expression of an engineered Gs-coupled receptor dramatically increases bone mass. Proc Natl Acad Sci USA 105:1209–1214.
29. Tonjes A, Koriath M, Schleinitz D, et al. 2009. Genetic variation in GPR133 is associated with height: genome wide association study in the self-contained population of Sorbs. Hum Mol Genet 18:4662–4668.
30. Nakanishi R, Akiyama H, Kimura H, et al. 2008. Osteoblast-targeted expression of Sfrp4 in mice results in low bone mass. J Bone Miner Res 23:271–277.
31. Archer CW, Dowthwaite GP, Francis-West P. 2003. Development of synovial joints. Birth Defects Res C Embryol Today 69:144–155.
32. Koga H, Shimaya M, Muneta T, et al. 2008. Local adherent technique for transplanting mesenchymal stem cells as a potential treatment of cartilage defect. Arthritis Res Ther 10:R84.
33. Horie M, Sekiya I, Muneta T, et al. 2009. Intra-articular injected synovial stem cells differentiate into meniscal cells directly and promote meniscal regeneration without mobilization to distant organs in rat massive meniscal defect. Stem Cells 27:878–887.
34. Aigner T, Soeder S, Haag J. 2006. IL-1beta and BMPs—interactive players of cartilage matrix degradation and regeneration. Eur Cell Mater 12:49–56, discussion 56.

分子細胞遺伝学分野

稲澤 譲治

難治疾患研究所
分子細胞遺伝学・教授

1）研究の課題名

癌と遺伝子疾患の個別化医療に向けたゲノム・エピゲノム解析研究

Integrative genomics and epigenomics for personalized medicine in cancer and genetic disorders

1. **Okamoto N, Hayashi1,3, Ayako Masui4, Rika Kosaki5, Izumi Oguri6, Tomoko Hasegawa7, Issei Imoto8, Yoshio Makita9, Akira Hata10, Keiji Moriyama2,3 and Johji InazawaDeletion at chromosome 10p11.23-p12.1 defines characteristic phenotypes with marked midface retrusion. J Hum Genet （in press）**
   Approximately 3% of the live-born infants have major dysmorphic features, and about two-thirds of which are observed in the maxillofacial region; however, in many cases, the etiology of the dysmorphic features remains uncertain. Recently, the genome-wide screening of large patient cohorts with congenital disorders has made it possible to discover genomic aberrations corresponding to the pathogenesis. In our analyses of more than 536 cases of clinically undiagnosed multiple congenital anomalies and mental retardation（MR）by microarray-based comparative genomic hybridization, we detected two non-consanguineous unrelated patients with microdeletions at 10p11.23-p12.1, which overlapped for 957 kb, including four protein-coding genes：ARMC4, MPP7, WAC and BAMBI. As the two patients had similar phenotypes; for example, MR and multiple maxilla- facial abnormalities including midface retrusion, wide mouth and large tongue, we assessed the phenotypes in detail to define the common features, using quantitative evaluations of the maxillofacial dysmorphism. The concordance of the genetic and phenotypic alterations is a good evidence of a new syndrome. Although an interstitial deletion of 10p is rare, the current study is the first trial to examine precisely the craniofacial characteristics of patients with a heterozygous deletion at 10p11.23-p12.1, and presents good evidence to diagnose potential patients with the same genetic cause.
   10p11.23-p12.1欠失を有する精神遅滞症例2例を対象に、欠失の詳細なゲノム解析と特徴的表現型である顎顔面異常の数量的検討を行い、本領域の欠失が新規症候群として定義される可能性を示した。

2. **Ono H, Imoto I, Kozaki K, Tsuda H, Matsui T, Kurasawa Y, Muramatsu T, Sugihara K, Inazawa J：SIX1 promotes epithelial-mesenchymal transition in colorectal cancer through ZEB1 activation. Oncogene.（in press）**
   The epithelial-mesenchymal transit　ion（EMT）plays a major role in cancer progression as well as normal organ development and human pathology such as organ fibrosis and wound healing. Here, we performed a gene expression array specialized in EMT of colorectal cancer（CRC）. From a comprehensive gene expression analysis using epithelial- and mesenchymal-like CRC cell lines and following the ontology（GO）analysis, SIX1 gene was identified to be an EMT-related gene in CRC. Using SW480 cells stably transfected with SIX1 expression construct and their control counterparts, we demonstrated that SIX1 overexpression represses CDH1 expression and underwent EMT in CRC. SIX1-induced CDH1 repression and EMT in CRC cells was correlated at least in part with posttranscriptional ZEB1 activation and miR-200 family transcriptional repression. In primary tumors of CRC, in accord with the functional findings, aberrant expression of SIX1 in cancer cells was observed at the disruption of basement membrane and at the tumor invasive front, where tumor cells underwent EMT in vivo. Taken together, SIX1 overexpression is suggested to be occurred in carcinogenesis, and contribute to repress CDH1 expression and promote EMT partly through repressing miR-200 family expression and activating ZEB1 in CRC.
   大腸癌（CRC）細胞株における網羅的発現解析結果等からSIX1に注目し、SIX1による上皮-間葉転換（epithelial-mesenchymal transition, EMT）誘導が既

報のmiR-200-ZEB1-CDH1経路を介する事、CRC症例での基底膜破壊部や浸潤先端部のEMT様細胞でSIX1が強発現する事を明らかにした。

3. **Bai H, Inoue J, Kawano T, Inazawa J：A transcriptional variant of the LC3A gene is involved in autophagy and frequently inactivated in human cancers. Oncogene.（in press）**
Microtubule-associated protein 1 light chain 3（MAP1LC3：LC3）has an important role in autophagy. The human LC3 gene family has five members, LC3A（variant-1：v1 and -2：v2）, LC3B, LC3B2, and LC3C. While a form of LC3B modified by phosphatidylethanolamine（PE）（form-II）is localized in autophagosomes, it is not clear whether other LC3 proteins also function in autophagy. Here, we examined the association between autophagy and human LC3 proteins during starvation- or p53-induced autophagy in Saos-2 cells. In an analysis of the intracellular distribution of each LC3 protein fused with GFP, GFP-LC3Av1 was frequently localized in autophagosomes with a punctate pattern, similar to GFP-LC3B. Further, endogenous LC3Av1 generated form-II and mostly localized in LC3B-positive autophagosomes during the induced autophagy. Interestingly, we found that LC3Av1, not LC3B, was frequently inactivated at the transcriptional level in various human cancer cell lines（111/244 cell lines, 45.5%）and its inactivation was due to aberrant DNA methylation in esophageal squamous cell carcinoma（ESCC）cell lines and primary tumors. These results suggest that LC3Av1, not only LC3B, functions in autophagy and further, LC3Av1 may be crucial in tumor suppression.
MAP1LC3は、オートファジーにおいて重要な役割を果たしており、ヒトでは、LC3遺伝子ファミリーとして、LC3A（variant-1：v1 and -2：v2）, LC3B, LC3B2, LC3Cの5種類が存在する。様々な癌種由来細胞株および食道癌臨床検体において、LC3Av1の発現が高頻度に低下しており（111/244 cell lines, 45.5%）、その発現低下の機序はDNAメチル化によるものであった。そして、LC3Av1が発現していない食道癌細胞株（KYSE170）におけるLC3Av1の安定発現は、in vivoでの細胞増殖を抑制した。これらの結果は、LC3Av1はオートファジーに関与しており、癌形質の抑制に寄与する可能性が示唆している。

4. **Honda S, Satomura S, Hayashi S, Imoto I, Nakagawa E, Goto Y, Inazawa J：Concomitant microduplications of MECP2 and ATRX in male patients with severe mental retardation. J Hum Genet. in press**
Investigations of chromosomal rearrangements in patients with mental retardation（MR）are particularly informative in the search for genes involved in MR. Here we report a family with concomitant duplications of methyl CpG binding protein 2（MECP2）at Xq28 and ATRX（the causative gene for X-linked alpha thalassemia/mental retardation）at Xq21.1 detected by array-comparative genomic hybridization. The alterations were observed in a 25-year-old man who inherited them from his mother, who showed a normal phenotype and completely skewed X-chromosome inactivation, and also in his cousin, a 32-year-old man. The proband and his cousin showed severe MR, muscular hypotonia, recurrent respiratory infections and various other features characteristic of MECP2 duplication syndrome. However, the proband also had cerebellar atrophy never reported before in MECP2 duplication syndrome, suggesting that his phenotypes were modified through the ATRX duplication in an additive or epistatic manner.
X連鎖性精神発達遅滞のアレイCGH解析においてATRX, MECP2両領域の重複例を検出した。MECP2単独重複に比べて小脳萎縮などの特徴が見られ、ATRX重複による表現型修飾の可能性が示唆された。

5. **Ishihara T, Inoue J, Kozaki K, Imoto I, Inazawa J：The HECT-type ubiquitin ligase ITCH targets lysosomal-associated protein multispanning transmembrane 5（LAPTM5）and prevents LAPTM5-mediated cell death. J Biol Chem. 286：44086-94. 2011**
LAPTM5（lysosomal-associated protein multispanning transmembrane 5）is a membrane protein on the intracellular vesicles. We have previously demonstrated that the accumulation of LAPTM5-positive vesicles was closely associated with the programmed cell death occurring during the spontaneous regression of neuroblastomas. Although the accumulation of LAPTM5 protein might occur at the post-translational level, the molecular mechanism has been unclear. Here, we found that the level of LAPTM5 protein is regulated negatively by the degradation through ubiquitination by ITCH, an E3 ubiquitin ligase. ITCH directly binds to the PPxY motif of LAPTM5 via its WW domains and promotes ubiquitination through a HECT-type ligase domain. Overexpression of ITCH led to the degradation of LAPTM5 protein, and conversely, knockdown of ITCH by siRNA resulted in the stabilization of LAPTM5 protein. In addition, the inhibition of ITCH enhanced the cell death occurred by accumulation of LAPTM5 in neuroblastoma cells. These findings suggest that LAPTM5 is a novel substrate in terms of degradation

by the ubiquitin ligase ITCH, and this system might act as a negative regulator in the spontaneous regression of neuroblastomas by preventing LAPTM5-mediated cell death.

LAPTM5（lysosomal-associated protein multispanning transmembrane 5）は、細胞内小胞に局在する膜タンパク質である。今回の研究において、LAPTM5がITCHによるタンパク質分解の新規基質であり、そして、このタンパク質分解制御は、LAPTM5を介した細胞死を抑制することにより、神経芽腫の自然退縮を負に制御している可能性を示唆した。

6. **Kurasawa Y, Kozaki K, Pimkhaokham A, Muramatsu T, Ono H, Ishihara T, Uzawa N, Imoto I, Amagasa T, Inazawa J：Stabilization of phenotypic plasticity through mesenchymal-specific DNA hypermethylation in cancer cells. Oncogene.（in press）**

The epithelial-mesenchymal transition（EMT）has a crucial role in normal and disease processes including tumor progression. In this study, we first classified epithelial-like and mesenchymal-like oral squamous cell carcinoma（OSCC）cell lines based on expression profiles of typical EMT-related genes using a panel of 18 OSCC cell lines. Then, we performed methylation-based and expression-based analyses of components of the Wnt signaling pathway, and identified WNT7A and WNT10A as genes silenced by mesenchymal-specific DNA hypermethylation in OSCCs. A significant association was revealed between some clinicopathological findings and the DNA methylation status of WNT7A（normal vs tumor, P=0.007; T1-2 vs T3-4, P=0.040; I-III vs IV, P=0.016）and WNT10A（N0-N1 vs N2-N3, P=0.046）in the advanced stages of OSCC. Moreover, we found that E-cadherin expression in cancer cells may be positively regulated by WNT7A, whose expression is negatively regulated by mesenchymal-specific DNA hypermethylation or ZEB1 in mesenchymal-like OSCC cells. Our findings indicate that epithelial-specific gene silencing through mesenchymal-specific DNA hypermethylation may stabilize the phenotypic plasticity of cancer cells during EMT/MET.

口腔扁平上皮癌（OSCC）細胞株におけるEMT関連遺伝子群の解析から、間葉系特異的DNA過剰メチル化により発現抑制されるWNT7AとWNT10Aを見出し、OSCC症例でのDNAメチル化異常と臨床病理学的悪性度との相関性や既報のmiR-200-ZEB1-CDH1経路とは独立したmiR-200-ZEB1-WNT7A-CDH1経路を明らかにするとともに、間葉系特異的DNAメチル化異常による遺伝子サイレンシングが間葉系癌細胞の可塑性を抑制し、細胞形質を安定化させている事を示した。

7. **Tsuruta T, Kozaki K, Uesugi A, Furuta M, Hirasawa A, Imoto I, Susumu N, Aoki D, Inazawa J：miR-152 is a tumor suppressor microRNA that is silenced by DNA hypermethylation in endometrial cancer. Cancer Res. 71：6450-62. 2011**

The etiology and development of human cancers that remain little understood might be enlightened by defining tumor suppressor microRNAs（TS-miRNA）. In this study, we identified TS-miRNAs silenced by aberrant DNA hypermethylation in endometrial cancer. Functional screening of 327 synthetic miRNAs in an endometrial cancer cell proliferation assay identified 103 miRNAs that inhibited cell growth. We then determined the sequence, DNA methylation status, and expression levels of these miRNAs in endometrial cancer cell lines and primary tumors. These determinations led to the identification of miR-152 as a candidate TS-miRNA gene in endometrial cancer. Epigenetic silencing documented in miR-152 was consistent with its location at 17q21.32 in intron 1 of the COPZ2 gene, which is also silenced often in endometrial cancer by DNA hypermethylation, and also with evidence that miR-152 targets the DNA methyltransferase DNMT1. Notably, restoration of miR-152 expression in endometrial cancer cell lines was sufficient to inhibit tumor cell growth in vitro and in vivo. We identified E2F3, MET, and Rictor as novel candidate targets of miR-152, suggesting how its epigenetic silencing can drive endometrial carcinogenesis. Our findings define a central role for miR-152 in endometrial cancer, and they also suggest its use in new therapeutic strategies to treat this cancer.

新規癌抑制遺伝子型miRNA（TS-miRNA）の同定を目的に、子宮体癌（EC）細胞株での細胞増殖抑制効果を指標とする機能的スクリーニングを試み、327種類のmiRNA配列から腫瘍特異的DNA過剰メチル化により発現抑制されるmiR-152を同定し、その新規標的分子であるE2F3、MET、Rictorを同定した。さらに、EC症例ではDNA過剰メチル化によりmiR-152が高頻度に発現抑制されている事、EC細胞株移植SCIDマウスへの合成二本鎖RNA投与実験から、miR-152による新規癌RNA創薬の可能性を示した。

8. **Uesugi A, Kozaki K, Tsuruta T, Furuta M, Morita K, Imoto I, Omura K, Inazawa J：The tumor suppressive microRNA miR-218 targets the mTOR component Rictor and inhibits AKT phosphorylation in oral cancer. Cancer Res. 71：5765-78. 2011**

The incidence of oral squamous cell carcinoma（OSCC）

is rising rapidly in developed countries, posing a growing challenge due to the poor management of this type of malignancy at present. In this study, we profiled tumor suppressive microRNAs（miRNAs）that are silenced by DNA hypermethylation in OSCC using a function-based screening approach. This approach employed a cell proliferation assay for 327 synthetic miRNAs in two OSCC cell lines. Among the 110 miRNAs identified in this set that exhibited inhibitory properties, we compared DNA methylation and expression status in a wider panel of OSCC cell lines and primary tumor tissues, resulting in the identification of miR-218 and miR-585 as functionally significant miRNA genes that are frequently silenced in OSCC by DNA hypermethylation. Ectopic expression of miR-218 and miR-585 in OSCC cells lacking endogenous expression reduced cell growth in part through caspase-mediated apoptosis. Notably, miR-218 reduced levels of the rapamycin-insensitive component of mTOR, Rictor, in a manner associated with a suppression of Akt S473 phosphorylation. Together our findings define miR-585 as a tumor suppressive function that is often epigenetically silenced in OSCC, and they identify Rictor as a novel target of miR-218, suggesting that activation of the mTOR-Akt signaling pathway induced by Rictor contributes centrally to oral carcinogenesis.

新規癌抑制遺伝子型miRNA（TS-miRNA）の同定を目的に、口腔扁平上皮癌（OSCC）細胞株での細胞増殖抑制効果を指標とする機能的スクリーニングを行い、327種類のmiRNA配列から腫瘍特異的DNA過剰メチル化により発現抑制されるmiR-218とmiR-585を同定した。さらに、miR-218はRictorを標的分子とし、Aktの不活性化を介して細胞増殖を負に制御する事を明らかにした。

9. Hayashi S, Okamoto N, Chinen Y, Takanashi J, Makita Y, Hata A, Imoto I, Inazawa J：Novel intragenic duplications and mutations of CASK in patients with mental retardation and microcephaly with pontine and cerebellar hypoplasia（MICPCH）. Hum Genet. 131：99-110. 2012

The CASK gene encoding a member of the membrane-associated guanylate kinase protein family is highly expressed in the mammalian nervous system of both adults and fetuses, playing several roles in neural development and synaptic function. Recently, CASK aberrations caused by both mutations and deletions have been reported to cause severe mental retardation（MR）, microcephaly and disproportionate pontine and cerebellar hypoplasia（MICPCH）in females. Here, mutations and copy numbers of CASK were examined in ten females with MR and MICPCH, and the following changes were detected：nonsense mutations in three cases, a 2-bp deletion in one case, mutations at exon-intron junctions in two cases, heterozygous deletions encompassing CASK in two cases and interstitial duplications in two cases. Except for the heterozygous deletions, each change including the intragenic duplications potentially caused an aberrant transcript, resulting in CASK null mutations. The results provide novel mutations and copy number aberrations of CASK, causing MR with MICPCH, and also demonstrate the similarity of the phenotypes of MR with MICPCH regardless of the CASK mutation.

小脳脳幹部低形成・小頭症を伴う発達遅滞（MR/MICPCH）を有する女性10例を対象にCASK遺伝子を解析し、全例において多様なゲノム異常がCASKヌル変異の原因となっていることを示した。

10. Muramatsu T, Imoto I, Matsui T, Kozaki K, Haruki S, Sudol M, Shimada Y, Tsuda H, Kawano T, Inazawa J：YAP is a candidate oncogene for esophageal squamous-cell carcinoma. Carcinogenesis. 32：389-98. 2011

Yes-associated protein（YAP）, the nuclear effector of the Hippo pathway, is a key regulator of organ size and a candidate human oncogene located at chromosome 11q22. Since we previously reported amplification of 11q22 region in esophageal squamous cell carcinoma（ESCC）, in this study we focused on the clinical significance and biological functions of YAP in this tumor. Frequent overexpression of YAP protein was observed in ESCC cells including those with a robust amplicon at position 11q22. Overexpression of the YAP protein was frequently detected in primary tumors of ESCC as well. Patients with YAP-overexpressing tumors had a worse overall rate of survival than those with non-expressing tumors, and YAP positivity was independently associated with a worse outcome in the multivariate analysis. Further analyses in cells in which YAP was either overexpressed or depleted confirmed that cell proliferation was promoted in a YAP isoform-independent but YAP expression level-dependent manner. YAP depletion inhibited cell proliferation mainly in the G（0）-G（1）phase and induced an increase in CDKN1A/p21 transcription but a decrease in BIRC5/survivin transcription. Our results indicate that YAP is a putative oncogene in ESCC and it represents a potential diagnostic and therapeutic target.

食道扁平上皮癌（ESCC）の11q22増幅領域に座位するHippo経路構成分子Yes-associated protein（YAP）に注目し、ESCCにおけるYAP発現が細胞株や症例

で高頻度に増大している事、YAP高発現患者群は低発現患者群に比して有意に予後不良であり、YAP発現がESCCの予後規定因子となりえる事を明らかにした。一方、ESCC細胞株の増殖能がYAP発現依存的に制御される事、YAP発現の抑制によりG0-G1期の細胞が蓄積し、p21の発現上昇とsurvivinの発現低下を生じる事等を示した。

11. Hayashi S, Imoto I, Aizu Y, Okamoto No, Mizuno S, Kurosawa K, Okamoto Na, Honda S, Araki S, Mizutani S, Numabe H, Saitoh S, Kosho T, Fukushima Y, Mitsubuchi H, Endo F, Chinen Y, Kosaki R, Okuyama T, Ohki H, Yoshihashi H, Ono M, Takada F, Ono H, Yagi M, Matsumoto H, Makita Y, Hata A, Inazawa J：Clinical application of array-based comparative genomic hybridization by two-stage screening for 536 patients with mental retardation and multiple congenital anomalies. J Hum Genet. 56：110-24. 2011

Recent advances in the analysis of patients with congenital abnormalities using array-based comparative genome hybridization（aCGH）have uncovered two types of genomic copy-number variants（CNVs）; pathogenic CNVs（pCNVs）relevant to congenital disorders and benign CNVs observed also in healthy populations, complicating the screening of disease-associated alterations by aCGH. To apply the aCGH technique to the diagnosis as well as investigation of multiple congenital anomalies and mental retardation（MCA/MR）, we constructed a consortium with 23 medical institutes and hospitals in Japan, and recruited 536 patients with clinically uncharacterized MCA/MR, whose karyotypes were normal according to conventional cytogenetics, for two-stage screening using two types of bacterial artificial chromosome-based microarray. The first screening using a targeted array detected pCNV in 54 of 536 cases（10.1%）, whereas the second screening of the 349 cases negative in the first screening using a genome-wide high-density array at intervals of approximately 0.7 Mb detected pCNVs in 48 cases（13.8%）, including pCNVs relevant to recently established microdeletion or microduplication syndromes, CNVs containing pathogenic genes and recurrent CNVs containing the same region among different patients. The results show the efficient application of aCGH in the clinical setting.

原因不明である多発奇形を伴う精神遅滞536例を収集し、診断型・全ゲノム型BACアレイを用いた2段階スクリーニングを行い、それぞれ10.1%, 13.8%に疾患に関連するゲノムコピー数変化を検出した。

2）

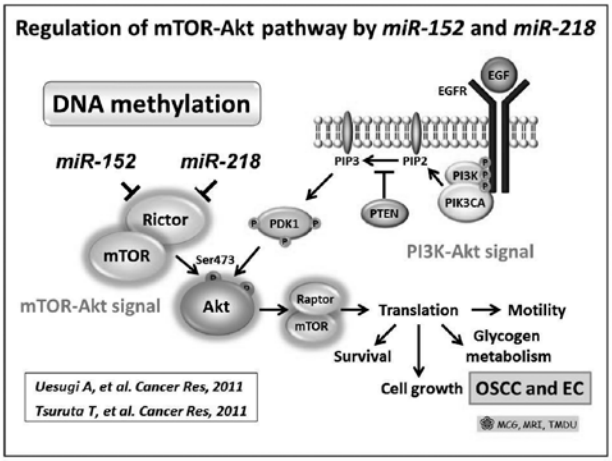

3）発表の研究内容についての英文要約

Innovative techniques for detection of genomic and epigenomic aberrations underlying the pathogenesis in cancer and genetic diseases have been developed and using those techniques numerous disease-related genes or disease-related genomic alterations have been successfully identified during the course of the research program.
In particular, we identified many novel cancer-related genes including tumor suppressor microRNAs in various types of cancers including oral squamous cell carcinoma（OSCC）. Furthermore, we constructed a consortium with 23 medical institutes and hospitals in Japan, and recruited 536 patients with clinically uncharacterized MCA/MR, whose karyotypes were normal according to conventional cytogenetics, for two-stage screening using two types of bacterial artificial chromosome-based microarray. The first screening detected pCNV in 69 of 646 cases（10.7%）, whereas the second screening of the 515 cases negative in the first screening detected pCNVs in 61 cases（11.8%）. Through the project, a possible new syndrome of congenital abnormality has been identified in two independent cases with de novo deletion at 10p11.23-12.1 and characteristic phenotypes with marked midfacial hypoplasia.

4）本事業に関連して世界的な研究拠点形成に向けて、以下の点で改善・整備等されたこと

A（研究拠点体制）

1. 難治性硬組織疾患の病態オミックス先端研究拠点（Advanced Omics Research for Intractable Hard-Tissue Diseases）オミックス解析の成果とナノサイエンス技術の統合化を図り、成果に基づく難治性硬組織疾患トランスレーショナルリサーチを推進し、当該疾患の克服に向けたオミックス医科学の実現、ならびに教育・人材育成の充実・強化を目指したオミックス研究の先

端拠点を構築する。

【参加教授】野田政樹、小村 健、森山啓司、宮坂信之、三木義男、稲澤譲治

【分担研究者】江面陽一、小崎健一、津田 均、森田圭一、阿江啓介、上阪 等、佐々木善浩、林深

【研究協力】四宮謙一（横浜みなと赤十字病院・院長）、秋吉一成（京大・院工・教授）

2. 口腔がんの国際共同研究拠点：タイ王国チュラロンコン大学Atiphan Pimkamkam博士と「口腔癌のゲノム・エピゲノム解析」に関する国際共同研究体制を構築
3. 先天異常症の病態解明・診断法開発研究拠点：国内23医療機関（大学病院・国立成育医療センターなど）とコンソーシアムを形成し先天異常症の新規診断法開発と病因性CNV探索研究体制を構築
4. 口腔扁平上皮癌、食道扁平上皮癌の異時性・同時性発症のコンセプトとなるfield cancerizationの分子病態解明プロジェクトの組織構築

【参加教授】小村 健、稲澤譲治

【分担研究者】河野辰幸、江石義信、小崎健一、森田圭一、井上　純

B（研究教育環境）

・毎月曜日セミナーにて国際一流誌原著論文、総説論文の抄読会を実施。
・毎土曜日研究進捗状況報告会を実施。
・各研究者は半年に一度、Research in progress報告を行い研究進捗の確認・助言。

C（人材確保）

1. 慶應大学・院・医学研究科より大学院特別研究生を受け入れた。
2. 京都府立医大・院・医学研究科より大学院特別研究生を受け入れた。
3. ブラジル国サンパウロ大学より国費博士課程学生（平成23年度・専攻生）
4. フィリピン国St Lukes Medical Centerより国費博士課程学生（平成23年度・専攻生）
5. 谷本幸介が平成23年度4月1日付けでゲノム解析室助教に着任した。

D（人材育成）

1. 平成23年度は以下の17名の大学院生が在籍して研究を実施している。そのうち5名は歯科医師（下線）である。坂本宙子、白　樺、村松智輝、古田繭子、小野宏晃、山本（岡本）奈那、遠藤寛則、宮脇　豊、原園陽介、山本信祐、李慧、Nuylan Michelle Loyola、Daniela Tiaki Uehara、永田啓明、岩舘怜子、長縄光代、與子田一輝
2. 春木茂男（大学院医歯学総合研究科博士課程平成21年度卒業）が第12回田中道子がん研究奨励賞を受賞した.
3. 村松智輝が平成22年度「難治疾患の研究」を重点課題とする研究助成に採択された.
4. 小野宏晃が平成22年度大学院生・若手研究者研究発表会で大学院生部門1位（ベストプレゼンテーション賞）を受賞した.
5. 本田尚三が平成22年度大学院生・若手研究者研究発表会で大学院生部門2位を受賞した.
6. 村松智輝が平成22年度大学院生・若手研究者研究発表会で難治疾患研究賞を受賞した.
7. 古田繭子が平成22年度大学院生・若手研究者研究発表会で萌芽賞を受賞した.
8. 古田繭子が東京医科歯科大学グローバルCOE（GCOE）スーパースチューデント（SS）研究発表で優秀賞「Excellent Award」を受賞した.
9. 元ポスドク研究員の石原孝也さんが平成23年12月1日付で久留米大学分子生命科学研究所高分子化学研究部門の助教に就任した.

E（国際化）

1. 本田尚三が米国Cedars-Sinai Medical Centerに博士研究員として採用された。
2. ブラジル国サンパウロ大学より国費博士課程学生（平成23年度・専攻生）
3. フィリピン国St Lukes Medical Centerより国費博士課程学生（平成23年度・専攻生）を受け入れた。
4. 古田繭子が文部科学省科学研究費新学術領域研究がん研究分野の特性等を踏まえた支援活動・平成23年度日仏がんワークショップの公募に採択されフランスに派遣された.
5. 村松智輝が平成23年度東京医科歯科大学大学院学生研究奨励賞を受賞し,海外研修に派遣され、Weis Center for Researchにて研究発表を行った

5）GCOE事業を推進するに当たって力を入れた点

基礎研究成果が医療貢献するよう研究成果の出口を具体的かつ明確に設定してこれを達成するよう努力した。

6）英文原著論文

1. ◎ Tsuruta T, Kozaki K, Uesugi A, Furuta M, Hirasawa A, Imoto I, Susumu N, Aoki D, Inazawa J：miR-152 is a tumor suppressor microRNA that is silenced by DNA

hypermethylation in endometrial cancer. Cancer Res. 71：6450-62. 2011
2. Niihori T, Aoki Y, Okamoto N, Kurosawa K, Ohashi H, Mizuno S, Kawame H, Inazawa J, Ohura T, Arai H, Nabatame S, Kikuchi K, Kuroki Y, MiuraM, Tanaka T, Ohtake A, Omori I, Ihara K, Mabe H, Watanabe K, Niijima S, Okano E, Numabe H, Matsubara Y：HRAS mutants identified in Costello syndrome patients can induce cellular senescence：possible implications for the pathogenesis of Costello syndrome. J Hum Genet. 56：707-15. 2011
3. Miyake K, Hirasawa T, Soutome M, Itoh M, Goto YI, Endoh K, Takahashi K, Kudo S, Nakagawa T, Yokoi S, Taira T, Inazawa J, Kubota T：The protocadherins, PCDHB1 and PCDH7, are regulated by MeCP2 in neuronal cells and brain tissues：Implication for the pathogenesis of Rett syndrome. BMC Neurosci. 12：81.2011
4. ◎ Uesugi A, Kozaki K, Tsuruta T, Furuta M, Morita K, Imoto I, Omura K, Inazawa J：The tumor suppressive microRNA miR-218 targets the mTOR component Rictor and inhibits AKT phosphorylation in oral cancer. Cancer Res. 71：5765-78. 2011
5. ◎ Hayashi S, Okamoto N, Chinen Y, Takanashi J, Makita Y, Hata A, Imoto I, Inazawa J：Novel intragenic duplications and mutations of CASK in patients with mental retardation and microcephaly with pontine and cerebellar hypoplasia（MICPCH）. Hum Genet. 2011[Epub ahead of print]
6. ◎ Matsui T, Miyamoto K, Kubo A, Kawasaki H, Ebihara T, Hata K, Tanahashi S, Ichinose S, Imoto I, Inazawa J, Kudoh J, Amagai M：SASPase regulates stratum corneum hydration through profilaggrin-to-filaggrin processing. EMBO Mol Med. 3：320-33. 2011
7. Arai E, Wakai-Ushijima S, Fujimoto H, Hosoda F, Shibata T, Kondo T, Yokoi S, Imoto I, Inazawa J, Hirohashi S, Kanai Y：Genome-wide DNA methylation profiles in renal tumors of various histological subtypes and non-tumorous renal tissues. Pathobiology. 78：1-9.2011
8. Gotoh M, Arai E, Wakai-Ushijima S, Hiraoka N, Kosuge T, Hosoda F, Shibata T, Kondo T, Yokoi S, Imoto I, Inazawa J, Kanai Y：Diagnosis and prognostication of ductal adenocarcinomas of the pancreas based on genome-wide DNA methylation profiling by bacterial artificial chromosome array-based methylated CpG island amplification. J Biomed Biotechnol. 2011：780836. 2011
9. Nishiyama N, Arai E, Nagashio R, Fujimoto H, Hosoda F, Shibata T, Tsukamoto T, Yokoi S, Imoto I, Inazawa J, Kanai Y：Copy number alterations in urothelial carcinomas：Their clinicopathological significance and correlation with DNA methylation alterations. Carcinogenesis. 32：462-9.2011
10. ◎ Muramatsu T, Imoto I, Matsui T, Kozaki K, Haruki S, Sudol M, Shimada Y, Tsuda H, Kawano T, Inazawa J：YAP is a candidate oncogene for esophageal squamous-cell carcinoma. Carcinogenesis. 32：389-98. 2011
11. ◎ Hayashi S, Imoto I, Aizu Y, Okamoto No, Mizuno S, Kurosawa K, Okamoto Na, Honda S, Araki S, Mizutani S, Numabe H, Saitoh S, Kosho T, Fukushima Y, Mitsubuchi H, Endo F, Chinen Y, Kosaki R, Okuyama T, Ohki H, Yoshihashi H, Ono M, Takada F, Ono H, Yagi M, Matsumoto H, Makita Y, Hata A, Inazawa J：Clinical application of array-based comparative genomic hybridization by two-stage screening for 536 patients with mental retardation and multiple congenital anomalies. J Hum Genet. 56：110-24. 2011
12. ◎ Okamoto N, Hayashi1,3, Ayako Masui4, Rika Kosaki5, Izumi Oguri6, Tomoko Hasegawa7, Issei Imoto8, Yoshio Makita9, Akira Hata10, Keiji Moriyama2,3 and Johji InazawaDeletion at chromosome 10p11.23-p12.1 defines characteristic phenotypes with marked midface retrusion. J Hum Genet（in press）
13. ◎ Ono H, Imoto I, Kozaki K, Tsuda H, Matsui T, Kurasawa Y, Muramatsu T, Sugihara K, Inazawa J：SIX1 promotes epithelial-mesenchymal transition in colorectal cancer through ZEB1 activation. Oncogene.（in press）
14. ◎ Bai H, Inoue J, Kawano T, Inazawa J：A transcriptional variant of the LC3A gene is involved in autophagy and frequently inactivated in human cancers. Oncogene.（in press）
15. ◎ Honda S, Satomura S, Hayashi S, Imoto I, Nakagawa E, Goto Y, Inazawa J：Concomitant microduplications of MECP2 and ATRX in male patients with severe mental retardation. J Hum Genet. 2011（in press）
16. ◎ Ishihara T, Inoue J, Kozaki K, Imoto I, Inazawa J：The HECT-type ubiquitin ligase ITCH targets lysosomal-associated protein multispanning transmembrane 5（LAPTM5）and prevents LAPTM5-mediated cell death. J Biol Chem. 2011（in press）
17. ◎ Kurasawa Y, Kozaki K, Pimkhaokham A, Muramatsu T, Ono H, Ishihara T, Uzawa N, Imoto I, Amagasa T, Inazawa J：Stabilization of phenotypic plasticity through mesenchymal-specific DNA hypermethylation in cancer cells. Oncogene. 2011（in press）

7）総説ならびに著書

［総説］

1. 小野宏晃、稲澤譲治：DNAミスマッチ修復遺伝子.（株）日本臨牀社.日本臨牀増刊号.大腸癌.69巻増刊号3（通巻997号）：77-83, 2011（2011/4/20）（7P）
2. 宮脇豊、稲澤譲治：がんにおけるゲノムコピー数異常とその解析.最新医学社.最新医学.66巻9号：69-

75,2011（2011/9/10）（7P）

［著書］

1. （分担）稲澤譲治：中国・日本科学最前線-研究の現場から- 2011年版.独立行政法人科学技術振興機構中国総合研究センター（東京）.2011,3,15（603P）

8）平成23年度までの自己評価

我が国において、はじめて集学的な通常の染色体検査で衣装を検出することのない先天異常症を対象に536例において自作BACアレイによる集学的なゲノム異常スクリーニングを実施した。その結果、約24%の症例に病因性のある微細染色体コピー数異常（copy number variation, CNV）を検出した。これらの中で、小頭症、小脳脳幹部低形成を症状とする疾患群にCASK遺伝子の重複を見出すなど、幾つかの新しい疾患単位となる病態を同定した点において特筆すべき成果が上がった。

9）学会発表（英文）

1. ◎ Hayashi S, Imoto I, Makita Y, Hata A, Inazawa J：Pathogenic CNVs and causative genes detected by two-stage screening in 647 patients with mental retardation and multiple congenital anomalies of unknown etiology. The 12th International Congress of Human Genetics/ The American Society of Human Genetics 61th annual meeting, Montreal, Canada. Octber11-15, 2011（Poster）
2. Niihori T, Aoki Y, Okamoto N, Kurosawa K, Ohashi H, Mizuno S, Kawame H, Inazawa J, Ohura T, Arai H, Nabatame S, Kikuchi K, Kuroki Y, Miura M, Tanaka T, Ohtake A, Omori I, Ihara K, Mabe H, Watanabe K, Niijima S, Okano E, Numabe H, Matsubara Y：HRAS mutants identified in Costello syndrome patients have the ability to induce cellular senescence：Possible association with the pathogenesis of Costello syndrome. The 12th International Congress of Human Genetics/ The American Society of Human Genetics 61th annual meeting, Montreal, Canada. Octber11-15, 2011（Poster）

10）学会発表（和文）

1. 林深、稲澤譲治：先天異常疾患の原因となるゲノム異常の網羅的探索.国立大学法人東京医科歯科大学第四回硬組織疾患ゲノムセンター・シンポジウム.東京医科歯科大学講堂.東京.2011年1月31日
2. 原園陽介、小崎健一、村松智輝、倉沢泰浩、天笠光雄、稲澤譲治：膵癌細胞株におけるE-cadherinの発現変化を指標とした機能的スクリーニングによるEMT関連microRNAの探索.第70回日本癌学会学術総会.名古屋国際会議場.愛知.2011年10月3日
3. 宇野雅哉、斉藤愛記、井本逸勢、稲澤譲治、山岡昇司：卵巣癌細胞における恒常的NF-κB活性化と足場非依存性増殖能に対するNIKの寄与.第70回日本癌学会学術総会.名古屋国際会議場.愛知.2011年10月3日
4. 小野宏晃、井本逸勢、小崎健一、津田均、杉原健一、稲澤譲治：大腸癌においてSIX1はZEB1を介し上皮間葉転換を誘導する.第70回日本癌学会学術総会.名古屋国際会議場.愛知.2011年10月3日
5. 宮脇豊、井本逸勢、春木茂男、小崎健一、河内洋、嶋田裕、河野辰幸、稲澤譲治：食道扁平上皮癌において高頻度に発現抑制される新規癌関連プロトカドヘリン遺伝子の同定.第70回日本癌学会学術総会.名古屋国際会議場.愛知.2011年10月4日
6. 井上純、白樺、河野辰幸、稲澤譲治：癌におけるオートファジー関連遺伝子LC3Avariant-1の不活性化.第70回日本癌学会学術総会.名古屋国際会議場.愛知.2011年10月4日
7. 小西博貴、井上純、市野瀬志津子、津田均、河野辰幸、市川大輔、大辻英吾、井本逸勢、稲澤譲治：食道癌におけるオートファジーATG7の不活性化.第70回日本癌学会学術総会.名古屋国際会議場.愛知.2011年10月4日
8. 細田文恵、新井康仁、宮本正之、北川敬之、片井均、谷口浩和、柳原五吉、井本逸勢、稲澤譲治、大木操、柴田龍弘：胃がんにおける新規がん遺伝子グリオキサラーゼIの機能解析.第70回日本癌学会学術総会.名古屋国際会議場.愛知.2011年10月4日
9. 遠藤寛則、小崎健一、古田繭子、天笠光雄、稲澤譲治：腫瘍特異的DNA過剰メチル化によって発現抑制される口腔扁平上皮癌抑制遺伝子型microRNAの探索.第70回日本癌学会学術総会.名古屋国際会議場.愛知.2011年10月4日
10. 上杉篤史、小崎健一、鶴田智彦、古田繭子、井本逸勢、小村健、稲澤譲治：機能的スクリーニングとDNAメチル化解析による口腔癌関連新規癌抑制遺伝子型microRNAの探索.第70回日本癌学会学術総会.名古屋国際会議場.愛知.2011年10月4日
11. 村松智輝、小崎健一、稲澤譲治：膵臓がん細胞株Panc1を用いた自発的転移モデルの構築と検証.第70回日本癌学会学術総会.名古屋国際会議場.愛知.2011年10月3日
12. 松村聡、井本逸勢、小崎健一、松井毅、古田繭子、田中真二、坂元亨宇、有井滋樹、稲澤譲治：統合的アレイ解析による肝細胞癌の新規がん抑制遺伝子候

補PACAPの同定.第70回日本癌学会学術総会.名古屋国際会議場.愛知.2011年10月5日

13. 田中真二、藍原有弘、茂櫛薫、落合高徳、ヤセン・マハムット、稲澤譲治、田中博、有井滋樹：肝癌再発を予測するオミックス解析と分子標的治療への応用.第70回日本癌学会学術総会.名古屋国際会議場.愛知.2011年10月5日
14. 古田繭子、小崎健一、田中真二、有井滋樹、井本逸勢、稲澤譲治：Functionalスクリーニングを用いた肝細胞癌抑制性microRNAの同定.第70回日本癌学会学術総会.名古屋国際会議場.愛知.2011年10月5日
15. 藍真澄、神田英一郎、小笹由香、二井奈保子、大坂瑞子、稲澤 譲治、吉田雅幸：遺伝子解析研究とバイオリソースバンクに関する医療者の意識調査.日本人類遺伝学会第56回大会/第11回東アジア人類遺伝学会.幕張メッセ.千葉.2011年11月10日
16. 林深、長縄光代、チアキ・ウエハラ・ダニエラ、井本逸勢、稲澤譲治：BACアレイ・SNPアレイを用いた日系ブラジル人100家系のトリオ解析による日本人健常者CNVデータベースの構築.日本人類遺伝学会第56回大会/第11回東アジア人類遺伝学会.幕張メッセ.千葉.2011年11月10日
17. 林深、チアキ・ウエハラ・ダニエラ、長縄光代、井本逸勢、蒔田芳男、羽田明、稲澤譲治：オリゴアレイ・SNPアレイを用いた先天異常疾患症例におけるゲノム異常評価とアレイポテンシャルの比較.日本人類遺伝学会第56回大会/第11回東アジア人類遺伝学会.幕張メッセ.千葉.2011年11月10日
18. 岡本伸彦、山本悠斗、大町和美、林深、稲澤譲治：Pitt-Hopkins症候群を考える4例.日本人類遺伝学会第56回大会/第11回東アジア人類遺伝学会.幕張メッセ.千葉.2011年11月11日
19. 醍醐弥太郎、三木大樹、久保充明、角田達彦、鎌谷直之、茶山一彰、高橋隆、稲澤譲治、中村祐輔：Genome-wide association study of lung cancer：Association of variation in TP6 3 with lung adenocarcinoma susceptibility. 日本人類遺伝学会第56回大会/第11回東アジア人類遺伝学会.幕張メッセ.千葉.2011年11月11日

11）受賞

1. 春木茂男（大学院医歯学総合研究科博士課程平成21年度卒業）が第12回田中道子がん研究奨励賞を受賞.
2. 村松智輝が平成22年度「難治疾患の研究」を重点課題とする研究助成に採択.
3. 小野宏晃が平成22年度大学院生・若手研究者研究発表会で大学院生部門1位（ベストプレゼンテーション賞）を受賞.
4. 本田尚三が平成22年度大学院生・若手研究者研究発表会で大学院生部門2位を受賞.
5. 村松智輝が平成22年度大学院生・若手研究者研究発表会で難治疾患研究賞を受賞.
6. 古田繭子が平成22年度大学院生・若手研究者研究発表会で萌芽賞を受賞.
7. 古田繭子が東京医科歯科大学グローバルCOE（GCOE）スーパースチューデント（SS）研究発表で優秀賞「Excellent Award」を受賞.
8. 井上純が川野小児医学奨学財団の研究助成に採択.
9. 村松智輝が平成23年度東京医科歯科大学大学院学生研究奨励賞を受賞.
10. 古田繭子が文部科学省科学研究費新学術領域研究がん研究分野の特性等を踏まえた支援活動・平成23年度日仏がんワークショップの公募に採択.（フランスに派遣）

12）外部資金の獲得状況

科学研究費補助金、新学術領域
　研究題目：がんの統合的ゲノム・エピゲノム解析と治療標的分子シーズの探索
　代表：稲澤 譲治
　期間：平成22年－平成26年
　研究費総額40,700,000 円

科学研究費補助金、基盤A
　研究題目：がんのゲノム・エピゲノム解析に基づく個性診断法の開発
　代表：稲澤　譲治
　期間：平成22年－平成24年
　研究費総額：12,300,000 円

科学研究費補助金、基盤B
　研究題目：癌抑制遺伝子型microRNAの統合的スクリーニングと核酸医薬への応用
　代表：小崎 健一
　期間：平成23年－平成25年
　研究費総額：6,100,000 円

科学研究費補助金、若手B
　研究題目：神経芽腫における腫瘍自然退縮の分子メカニズムの解明
　代表：井上　純

期間：平成22年－平成23年
研究費総額：1,400,000 円
科学研究費補助金、若手B
研究題目：共通のゲノム異常に基因する新規症候群の定義と病態解析
代表：林　深
期間：平成23年－平成24年
研究費総額：1,700,000 円
科学研究費補助金、基盤A
研究題目：難治性消化器癌における転移・再発の分子診断と分子標的治療の開発
代表：有井　滋樹
期間：平成20年－平成23年
研究費総額：1,000,000 円
科学研究費補助金、新学術領域
研究題目：領域の研究方針の策定
代表：宮野　悟
期間：平成22年－平成23年
研究費総額：100,000 円
受託研究費
（独立行政法人新エネルギー・産業技術総合開発機構）
研究課題：個別化医療の実現のための技術融合ﾊﾞｲｵ診断技術開発／染色体解析技術開発
代表：稲澤 譲治
期間：平成18年-平成23年
研究費総額：64,051,000円
国立精神・神経センター（精神・神経疾患研究委託費）
研究課題：精神・神経疾患のバイオリソース・レポジトリーの構築及び病因病態の解明に関する研究
代表：後藤 雄一
期間：平成23年
研究費総額：1,500,000円
厚生労働省科学研究費
研究課題：網羅的なゲノム異常解析と詳細な臨床情報に基づく、ヒトがんの多様な多段階発がん過程の分子基盤の解明とその臨床応用に関する研究
代表：横田 淳
期間：平成23年
研究費総額：5,000,000円
文部科学省（科学技術試験研究委託事業）
研究課題：ゲノム網羅的解析情報を基盤とするオーダーメイドがん医療
代表：稲澤 譲治
期間：平成23年
研究費総額：5,000,000 円
受託研究費（ロシュ・ダイアグノスティックス株式会社）
研究課題：CGH解析用オリゴヌクレオチドマイクロアレイの臨床的有用性の検討に関する研究
代表：稲澤 譲治
期間：平成23年
研究費総額：475,000円

13）特別講演、招待講演、シンポジウム

1. Inazawa J：Copy-number variation（CNV）in Japanese patients with multiple congenital anomalies and mental retardation（MCA/MR）by array-based comparative genomic hybridization analysis. Taiwan Association of Obstetrics and Gynecology.台湾産婦人科学会学会第50回大会. The Grand Hi Lai Hotel（Taipei, Taiwan）13/March/2011
2. Inazawa J：Function-based screening of tumor-suppressor microRNAs silenced by DNA hypermethylation in cancer. The 8th Nikko International Symposium 2011. Jichi Medical University.
Tochigi. Japan. 21/ October/2011
3. 稲澤譲治：「パーソナルゲノム医療の時代は既に始まっている」.2011年度東京医科歯科大学オープンキャンパス.M&Dタワー2階共用講義室2.東京.2011年7月28日
4. 小崎健一、稲澤譲治：がん細胞においてDNA過剰メチル化により発現抑制される癌抑制遺伝子型microRNAの機能的スクリーニング.第70回日本癌学会学術総会.名古屋国際会議場.愛知.2011年10月4日
5. 稲澤譲治：がんの統合的ゲノム・エピゲノム解析の最近の進歩.第70回日本癌学会学術総会.名古屋国際会議場.愛知.2011年10月5日
6. 三木大樹、久保充明、角田達彦、鎌谷直之、茶山一彰、高橋隆、稲澤譲治、中村祐輔、醍醐弥太郎：日本人と韓国人の肺腺癌発症に関連するTP63の一塩基多型の同定.第70回日本癌学会学術総会.名古屋国際会議場.愛知.2011年10月5日
7. 小崎健一、稲澤譲治：DNA過剰メチル化により発現抑制される癌抑制遺伝子型microRNAの機能的スクリーニング.日本人類遺伝学会第56回大会／第11回東アジア人類遺伝学会.幕張メッセ.千葉.2011年11月10日
8. 稲澤譲治：がんの統合的ゲノム・エピゲノム解析.日本人

類遺伝学会第56回大会/第11回東アジア人類遺伝学会.幕張メッセ.千葉.2011年11月11日

9. 稲澤譲治:がんのテーラーメイド医療 -診断、治療、予防の最前線-. 平成23年度国立大学附置研究所・センター長会議第2部会(医学・生物学)シンポジウム.東京医科歯科大学5号館4階講堂.東京.2011年11月18日

14)新聞、雑誌、TV報道

1. 医科歯科Bloom! Jan 2011 No.12 掲載

15)教室、分野や講座の准教授、講師、助教、特別研究員、ポスドク、指導を受けた大学院生の名前

准教授	小崎 健一
特任講師	谷本 幸介
助 教	井上 純
特任講師	林 深
研究補佐員	高橋 綾子
研究補佐員	森 留美
大学院生	○白 樺
大学院生	○古田 繭子
大学院生	村松 智輝
大学院生	鶴田 智彦
大学院生	倉沢 泰浩
大学院生	上杉 篤史
大学院生	小野 宏晃
大学院生	岡本 奈那
大学院生	小西 博貴
大学院生	遠藤 寛則
大学院生	宮脇 豊
大学院生	原園 陽介
大学院生	山本 信祐
大学院生	前田 誠
大学院生	大森 逸美
大学院生	坂本 宙子
大学院生	永田 啓明
大学院生	岩舘 怜子
大学院生	長縄 光代
大学院生	Nuylan Michielle Loyola
大学院生	Daniela Tiaki Uehara
大学院生	李 慧
大学院生	與子田 一輝

○はAISS

Published OnlineFirst August 25, 2011; DOI:10.1158/0008-5472.CAN-11-0364

Cancer Research

Molecular and Cellular Pathobiology

miR-152 Is a Tumor Suppressor microRNA That Is Silenced by DNA Hypermethylation in Endometrial Cancer

Tomohiko Tsuruta[1,4], Ken-ichi Kozaki[1,3], Atsushi Uesugi[1], Mayuko Furuta[1,2], Akira Hirasawa[4], Issei Imoto[1], Nobuyuki Susumu[4], Daisuke Aoki[4], and Johji Inazawa[1,2,3]

Abstract

The etiology and development of human cancers that remain little understood might be enlightened by defining tumor suppressor microRNAs (TS-miRNA). In this study, we identified TS-miRNAs silenced by aberrant DNA hypermethylation in endometrial cancer. Functional screening of 327 synthetic miRNAs in an endometrial cancer cell proliferation assay identified 103 miRNAs that inhibited cell growth. We then determined the sequence, DNA methylation status, and expression levels of these miRNAs in endometrial cancer cell lines and primary tumors. These determinations led to the identification of *miR-152* as a candidate TS-miRNA gene in endometrial cancer. Epigenetic silencing documented in *miR-152* was consistent with its location at 17q21.32 in intron 1 of the *COPZ2* gene, which is also silenced often in endometrial cancer by DNA hypermethylation, and also with evidence that *miR-152* targets the *DNA methyltransferase DNMT1*. Notably, restoration of *miR-152* expression in endometrial cancer cell lines was sufficient to inhibit tumor cell growth *in vitro* and *in vivo*. We identified *E2F3*, *MET*, and *Rictor* as novel candidate targets of *miR-152*, suggesting how its epigenetic silencing can drive endometrial carcinogenesis. Our findings define a central role for *miR-152* in endometrial cancer, and they also suggest its use in new therapeutic strategies to treat this cancer. *Cancer Res; 71(20); 6450–62. ©2011 AACR.*

Introduction

MicroRNAs (miRNA) are endogenous small nonprotein-coding RNAs of 19–22 nucleotides. These single-stranded RNAs are considered to play crucial roles in many normal cellular processes (1–4) and the multistep processes of carcinogenesis (5, 6). Among various mechanisms of cancer-related gene silencing in an epigenetic manner, DNA hypermethylation of CpG sites within CpG islands is known to lead to the inactivation of many tumor suppressor genes (TSG; ref. 7) and several tumor-suppressive miRNAs (TS-miRNA; ref. 8). Recently, in fact, DNA methylation–mediated downregulation of miRNAs by proximal CpG islands has been described by a number of groups, including ours (9–11), and further identification of remaining targets for methylation may clarify the specific molecular events involved in endometrial cancer progression, enabling the prevention, diagnosis, and treatment of endometrial cancer to be approached at a molecular level.

Endometrial cancer is the most common malignancy of the female genital tract, and is the fourth most common malignancy in women in the United States after breast, lung, and colon cancers. In 2009, it is estimated that 42,160 American women were diagnosed with endometrial cancer (6% of new cancer cases), and 7,780 women died of the disease (3% of all cancer deaths). Worldwide, endometrial cancer is the seventh most common cancer in women, being newly diagnosed in an estimated 226,000 women in 2007 (12). Endometrial cancer is generally considered to arise through the progressive accumulation of multiple genetic abnormalities, which may activate oncogenes and inactivate TSGs. Recently, genome-wide screenings of altered DNA methylation for exploring endometrial cancer–associated TSGs have been reported (13), though there are few reports about epigenetic alterations of miRNA genes in endometrial cancer.

Here, we identified a novel TS-miRNA frequently silenced through tumor-specific DNA methylation in endometrial cancer and its multiple targets by function-based screening with a cell proliferation assay for 327 synthetic miRNAs in HEC-1A cell line and an approach with a series of sequential analyses of DNA methylation and expression analysis in endometrial cancer cell lines and primary cases. The function-based screening makes it possible to analyze the biological effects of a large number of double-stranded RNAs (dsRNA) on cancer cells directly. In addition, this approach has already proved successful in the exploration of dsRNAs having oncogenic or tumor-suppressive effects on cancer cells (14, 15).

Authors' Affiliations: [1]Department of Molecular Cytogenetics, Medical Research Institute and School of Biomedical Science, [2]Global Center of Excellence (GCOE) Program for International Research Center for Molecular Science in Tooth and Bone Diseases, and [3]Department of Genome Medicine, Hard Tissue Genome Research Center, Tokyo Medical and Dental University; and [4]Department of Obstetrics and Gynecology, Keio University School of Medicine, Tokyo, Japan

Note: Supplementary data for this article are available at Cancer Research Online (http://cancerres.aacrjournals.org/).

Corresponding Author: Johji Inazawa, Department of Molecular Cytogenetics, Medical Research Institute, Tokyo Medical and Dental University, 1-5-45 Yushima, Bunkyo-ku, Tokyo 113-8510, Japan. Phone: 03-5803-5820; Fax: 03-5803-0244; E-mail: johinaz.cgen@mri.tmd.ac.jp

doi: 10.1158/0008-5472.CAN-11-0364

©2011 American Association for Cancer Research.

Published OnlineFirst August 25, 2011; DOI:10.1158/0008-5472.CAN-11-0364

Consequently, a possible endometrial cancer–associated TS-miRNA, *miR-152*, and novel candidates for its putative targets were identified in our study. This study is the first to show clearly that the tumor-suppressive activity of *miR-152* is epigenetically silenced in endometrial cancer and that its multiple targets are *E2F3*, *MET*, and *Rictor*.

Materials and Methods

Cell lines and primary tumor samples

A total of 13 human endometrial cancer cell lines—HEC-1, HEC-1A, HEC-1B, HEC-50B, HEC-59, HEC-108, HEC-151, HEC-251, HEC-265, HHUA, HOOUA, Ishikawa, and SNG-M—were obtained from RIKEN BioResource Center, and authenticated at our laboratory by in-house BAC/PAC-based arrays for array-CGH analyses (unpublished data) in December 2009. All cell lines were maintained in Dulbecco's modified Eagle's medium, supplemented with streptomycin (100 μg/mL), penicillin (100 units/mL), 2 mmol/L glutamine, and 10% FBS. To analyze the restored expression of genes of interest, cells were cultured with or without 10 μmol/L of 5-aza 2′-deoxycytidine (5-aza-dCyd) for 5 days. A total of 70 frozen primary samples were obtained from endometrial cancer patients (stage I, 38 cases; stage II, 8 cases; stage III, 21 cases; and stage IV, 3 cases; Supplementary Table S1) and 6 normal endometria from patients with endometriosis or leiomyoma treated at KEIO University with written consent from each patient and after approval by the local ethics committee. The International Federation of Gynecology and Obstetrics (FIGO) classification was used.

Transfection with synthetic miRNAs and siRNAs

Endometrial cancer cells were seeded at 10,000 cells per well in 24-well plates the day before transfection. dsRNA (10 nmol/L) mimicking human mature miRNAs or control nonspecific miRNA (Ambion; Thermo Scientific Dharmacon) and 20 nmol/L of Stealth RNAi siRNA for *Rictor* or control nonspecific siRNA (Invitrogen) were transfected individually into endometrial cancer cells, using Lipofectamine RNAiMAX (Invitrogen) according to the manufacturer's instructions. The suitable concentration of dsRNAs was decided on the basis of the result of *in vitro* cell proliferation assay beforehand. Representative results of those were shown in Supplementary Fig. S1A and B. The function-based screening was done by Pre-miR miRNA Precursor Library-Human V2 (Ambion) in duplicate. The numbers of viable cells were assessed by the colorimetric water-soluble tetrazolium salt (WST) assay (Cell counting kit-8; Dojindo Laboratories). Results were normalized to the cell numbers among control cells transfected with nonspecific miRNA. The cell cycle was evaluated by a fluorescence-activated cell sorting (FACS) analysis as described elsewhere (16).

Methylation analysis

Each gene and CpG island was searched in miRBase database (release April 17, 2011; ref. 17), UCSC Genome Browser on Human February 2009 Assembly (hg19; ref. 18), and PubMed (19). Genomic DNA was treated with sodium bisulfite and subjected to PCR, using primer sets designed to amplify regions of interest (Supplementary Table S2). The combined bisulfite restriction analysis (COBRA) and the bisulfite-sequencing analysis were carried out as described elsewhere (9).

Real-time reverse transcription PCR

Real-time reverse transcription PCR (RT-PCR) was carried out as described elsewhere (9). Relative expression levels of miRNAs and a host gene were quantified in comparison with *RNU6B* and *GAPDH* mRNA, respectively.

In vivo analysis of effects of synthetic miRNAs on tumor growth in SCID mice

Four-week-old female SCID mice were purchased from the Oriental Yeast Co. Ltd and maintained under specific pathogen-free conditions. A total of 1.0×10^7 cells in 100 μL of Matrigel (BD Biosciences) were injected in the subcutaneous (s.c.) tissue of the left abdominal wall of 7-week-old SCID mice. Tumor-bearing SCID mice treated with 1 nmol of dsRNAs (Ambion) in 100 μL of AteroGene (KOKEN) were administrated into the s.c. spaces around the tumors 3 times every week from day 14. At the end of the experiment, mice were sacrificed by cervical dislocation under deep anesthesia, and the resected s.c. tumors were weighed.

miRNA target predictions, Western blotting, and luciferase activity assay

Predicted targets for candidate miRNAs and their target sites were analyzed by using miRanda (20), TargetScan (21), and PicTar (22).

The protein levels of predicted targets in transfectants were analyzed by Western blotting, using anti-Akt, anti-phospho-Akt (Ser-473), anti-MET, anti-PCNA, anti-Rictor (Cell Signaling Technology), anti-E2F3 (Abcam), anti-DNMT1 (Santa Cruz Biotechnology) rabbit polyclonal antibodies, and anti-β-actin monoclonal antibodies (Sigma).

Luciferase constructs were made by ligating oligonucleotides containing the 3′-UTR target sites downstream of luciferase gene in pMIR-REPORT luciferase vector (Ambion). Luciferase activities were measured as described elsewhere (9).

Statistical analysis

Differences between subgroups were tested with the Mann–Whitney *U* test.

Results

Function-based screening of TS-miRNAs in endometrial cancer cell lines

To identify TS-miRNAs silenced by DNA hypermethylation in endometrial cancer, we first conducted function-based screening, in which the proliferation-inhibitory effect was made an index, using HEC-1A cell line and 327 synthetic miRNAs at 10 nmol/L. The strategy and partial results of this study are shown in Figure 1A. Relative cell growth ratios in Figure 1B and Supplementary Table S3 indicate effects of each miRNA 5 days after transfection. In this first screening,

Published OnlineFirst August 25, 2011; DOI:10.1158/0008-5472.CAN-11-0364

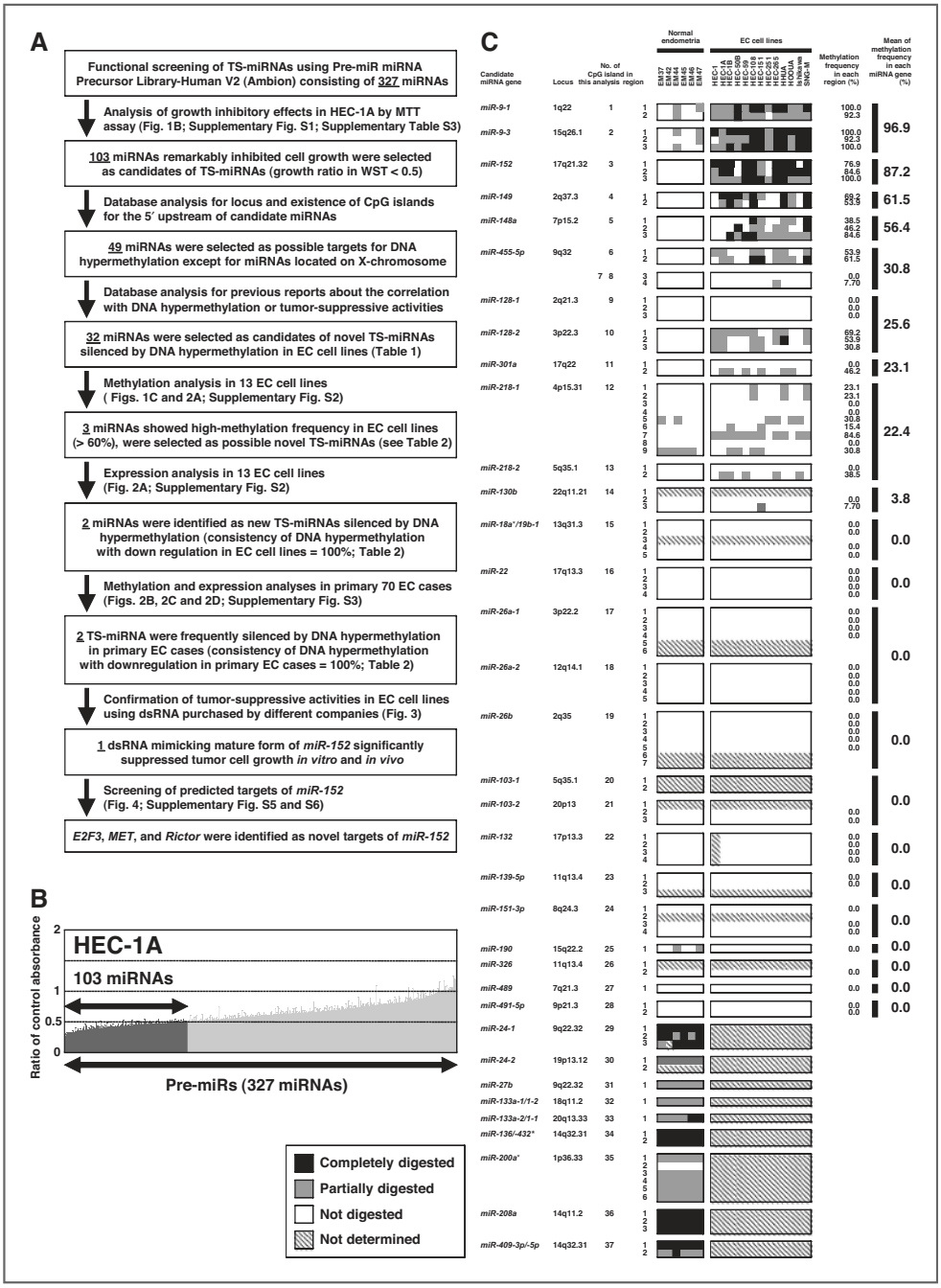

Figure 1. HEC-1A cell line. A, strategy for identifying epigenetically silenced TS-miRNAs in endometrial cancer. B, results of function-based screening of TS-miRNAs in HEC-1A cells, using Pre-miR miRNA Precursor Library-Human V2 (Ambion). The closed arrow at the bottom indicates 327 miRNAs examined in this screening, and the closed arrow at the top indicates 103 miRNAs which showed marked growth inhibitory effects (growth ratio < 0.5; Supplementary Table S3). C, summary of DNA methylation status of CpG islands around 32 mature sequences of miRNAs located at 37 loci in 13 endometrial cancer cell lines and 6 normal endometria determined by COBRA. PCR products used for COBRA were digested with *Bst*UI, *Taq*I, or *Hha*I (Fig. 2A; Table 1; Supplementary Table S2), and electrophoresed (Fig. 2B; Supplementary Fig. S2B; data not shown). Black, gray, white, and slant boxes indicate complete, partial, no digestion, and not determined, respectively. EC, endometrial cancer.

Published OnlineFirst August 25, 2011; DOI:10.1158/0008-5472.CAN-11-0364

Table 1. Summary of 32 miRNA genes selected as candidates of new TS-miRNAs silenced by DNA hypermethylation in function-based screening

	miRNA	miRNA gene	Locus	Host gene	Clustered miRNA	No. of CpG island in this analysis	Distance between 3′ end of CpG island and the most 5′ pre-miRNA sequence (bp)	Distance between 3′ end of CpG island and the most 5′ host gene sequence (bp)	Methylation frequency (total %)
1	*hsa-miR-9*	*hsa-miR-9-1*	1q22:	*C1orf61*	-	1	183	−16,349	96.9
		hsa-miR-9-3	15q26.1	-	-	2	0	-	
2	*hsa-miR-152*	*hsa-miR-152*	17q21.32	*COPZ2*	-	3	0	−93	87.2
3	*hsa-miR-149*	*hsa-miR-149*	2q37.3	*GPC1*	-	4	0	−20,134	61.5
4	*hsa-miR-148a*	*hsa-miR-148a*	7p15.2	-	-	5	407	-	56.4
5	*hsa-miR-455-5p*	*hsa-miR-455*	9q32	*COL27A1*	-	6	54,692	1,209	30.8
						7	53,696	213	
						8	53,192	79	
6	*hsa-miR-128*	*hsa-miR-128-1*	2q21.3	*R3HDM1*	-	9	133,333	0	25.6
		hsa-miR-128-2	3p22.3	*ARPP-21*	-	10	104,340	3,339	
7	*hsa-miR-301a*	*hsa-miR-301a*	17q22	*FAM33A*	*miR-454*	11	3,274	944	23.1
8	*hsa-miR-218*	*hsa-miR-218-1*	4p15.31	*SLIT2*	-	12	273,030	0	22.4
		hsa-miR-218-2	5q35.1	*SLIT3*	*miR-585/218-2*	13	532,170	0	
9	*hsa-miR-130b*	*hsa-miR-130b*	22q11.21	-	*miR-301b/130b*	14	545	-	3.8
10	*hsa-miR-18a**	*hsa-miR-18a**	13q31.3	*C13orf25*	*miR-17/18a/19a/20a/19b-1/92a-1*	15	1,564	0	0.0
11	*hsa-miR-19b*	*hsa-miR-19b-1*	13q31.3	*C13orf25*	*miR-17/18a/19a/20a/19b-1/92a-1*	15	2,005	0	0.0
12	*hsa-miR-22*	*hsa-miR-22*	17p13.3	*C17orf92*	-	16	1,924	0	0.0
13	*hsa-miR-26a*	*hsa-miR-26a-1*	3p22.3	*CTDSPL*	-	17	106,932	0	0.0
		hsa-miR-26a-2	12q14.1	*CTDSP2*	-	18	20,366	0	
14	*hsa-miR-26b*	*hsa-miR-26b*	2q35	*CTDSP1*	-	19	1,889	0	0.0
15	*hsa-miR-103*	*hsa-miR-103-1*	5q35.1	*PANK3*	-	20	18,121	0	0.0
		hsa-miR-103-2	20p13	*PANK2*	-	21	27,571	0	
16	*hsa-miR-132*	*hsa-miR-132*	17p13.3	-	*miR-212/132*	22	0	-	0.0
17	*hsa-miR-139-5p*	*hsa-miR-139*	11q13.4	PDE2A	-	23	27,049	0	0.0
18	*hsa-miR-151-3p*	*hsa-miR-151-3p*	8q24.3	*PTK2*	-	24	267,689	0	0.0
19	*hsa-miR-190*	*hsa-miR-190*	15q22.2	*TLN2*	-	25	126,715	50,405	0.0
20	*hsa-miR-326*	*hsa-miR-326*	11q13.4	*ARRB1*	-	26	15,995	650	0.0
21	*hsa-miR-489*	*hsa-miR-489*	7q21.3	*CALCR*	*miR-489/653*	27	90,755	0	0.0
22	*hsa-miR-491-5p*	*hsa-miR-491*	9p21.3	*KIAA1797*	-	28	31,468	−25,718	0.0

(Continued on the following page)

Published OnlineFirst August 25, 2011; DOI:10.1158/0008-5472.CAN-11-0364

Table 1. Summary of 32 miRNA genes selected as candidates of new TS-miRNAs silenced by DNA hypermethylation in function-based screening (Cont'd)

	miRNA	miRNA gene	Locus	Host gene	Clustered miRNA	No. of CpG island in this analysis	Distance between 3′ end of CpG island and the most 5′ pre-miRNA sequence (bp)	Distance between 3′ end of CpG island and the most 5′ host gene sequence (bp)	Methylation frequency (total %)
23	*hsa-miR-24*	*hsa-miR-24-1*	9q22.32	*C9orf3*	*miR-23b/27b/24-1*	29	0	−359,190	ND
		hsa-miR-24-2	19p13.12	-	*miR-23a/27a/24-2*	30	6,050	-	
24	*hsa-miR-27b*	*hsa-miR-27b*	9q22.32	*C9orf3*	*miR-23b/27b/24-1*	31	36,455	−359,190	ND
25	*hsa-miR-133a*	*hsa-miR-133a-1*	18q11.2	*MIB1* (reverse)	*miR-1-2/133a-1*	32	71,107	-	ND
		hsa-miR-133a-2	20q13.33	*C20orf166*	*miR-1-1/133a-2*	33	14,332	0	ND
26	hsa-miR-1-2	has-miR-1-2	18q11.2	*MIB1* (reverse)	*miR-133a-1/1-2*	32	71,107	-	ND
	has-miR-1-1	has-miR-1-1	20q13.33	*C20orf166*	*miR-133a-2/1-1*	33	14,332	0	ND
27	*hsa-miR-136*	*hsa-miR-136*	14q32.31	*RTL1* (reverse)	*miR-665/431/433/127/432/136*	34	1,179	-	ND
28	*hsa-miR-432**	*hsa-miR-432**	14q32.31	*RTL1* (reverse)	*miR-337/665/431/433/127/432/136*	34	960	-	ND
29	*hsa-miR-200a**	*hsa-miR-200a**	1p36.33	-	*miR-200b/200a/429*	35	2,659	-	ND
30	*hsa-miR-208a*	*hsa-miR-208a*	14q11.2	*MYH6*	-	36	1,482	−8,158	ND
31	*hsa-miR-409-3p*	*hsa-miR-409-3p*	14q32.31	-	*miR-485/453/154/496/377/541/409/412/369/410/656*	37	0	-	ND
32	*hsa-miR-409-5p*	*hsa-miR-409-5p*	14q32.31	-	*miR-485/453/154/496/377/541/409/412/369/410/656*	37	0	-	ND

NOTE: These data were searched in miRBase database (release April 17, 2011), UCSC Genome Browser on Human February 2009 Assembly (hg19), and PubMed.
Abbreviation: ND, not determined.

Published OnlineFirst August 25, 2011; DOI:10.1158/0008-5472.CAN-11-0364

103 miRNAs, including known TS-miRNAs such as *miR-124* (23), *miR-126* (24), *miR-137* (9), and *miR-491* (14), showed remarkable inhibitory effects on cell growth (relative growth ratio < 0.5). Then we enrolled miRNAs with CpG islands in the 5′ upstream region and excluded miRNAs previously reported to show a correlation between DNA hypermethylation and tumor-suppressive activity. Consequently, 32 miRNAs emerged as candidates for new TS-miRNAs silenced by DNA hypermethylation in endometrial cancer cell lines (Table 1).

Methylation and expression analyses of candidates in endometrial cancer cell lines and primary cases

Next, we explored DNA methylation status of CpG islands around 32 mature sequences of miRNAs located at 37 loci in a panel of 13 endometrial cancer cell lines and 6 normal endometria determined by COBRA (Fig. 1C). As multiple copies of some mature miRNAs, as listed in Table 1, are transcribed from different loci, the number of mature forms of miRNAs is smaller than the number of genomic loci. On the basis of a comparison of mean methylation frequencies in each region examined, frequent DNA hypermethylation (>60% of endometrial cancer lines) was found in only 3 of 32 miRNAs, that is, *miR-9* (96.9%), *miR-152* (87.2%), and *miR-149* (61.5%), although a few normal endometria were found to have hypermethylated CpG islands on/around these miRNAs (Fig. 2A; Supplementary Fig. S2A and B). Notably, DNA hypermethylation within region 1 in *miR-9-1* (1q22), region 1 and 3 in/around *miR-9-3* (15q26.1), and region 3 in *miR-152* (17q21.32) was observed in all endometrial cancer cell lines. Therefore, we focused on these 3 miRNAs. We next determined the correlation between the DNA methylation status of these miRNAs and their expression patterns in 13 endometrial cancer cell lines and 6 normal endometria. Frequencies of translational downregulation of *miR-9*, *miR-152*, and *miR-149* in endometrial cancer cell lines (<0.5-fold expression) were 61.5% (8 of 13), 100% (13 of 13), and 15.4% (2 of 13), respectively (Fig. 2A; Supplementary Fig. S2C and D), whereas 3 miRNAs were detected in all normal endometria. Furthermore, the expressions of *miR-9* and *miR-152* were also restored by demethylation with 10 μmol/L 5-aza-dCyd at a high frequency in endometrial cancer cells lacking their expressions (Fig. 2A; Supplementary Fig. S2C), strongly suggesting that DNA methylation around CpG islands on *miR-9* and *miR-152* suppressed their expressions in endometrial cancer cell lines. Additionally, as shown in Table 2, the downregulation of *miR-9*, *miR-152*, and *miR-149* expression correlated with DNA hypermethylation in 61.5% (8 of 13), 100% (13 of 13), and 0% (0 of 9) of endometrial cancer cell lines, respectively. These findings indicate that *miR-152* is the only miRNA showing a complete consistency in the correlation between DNA methylation status and expression pattern in a panel of endometrial cancer cell lines.

To determine the correlation between DNA methylation status and expression patterns of *miR-152* in 70 primary endometrial cancer tumors, we carried out COBRA and real-time RT-PCR analysis, respectively. In these analyses, aberrant DNA methylation in region 3 containing *pre-miR-152*

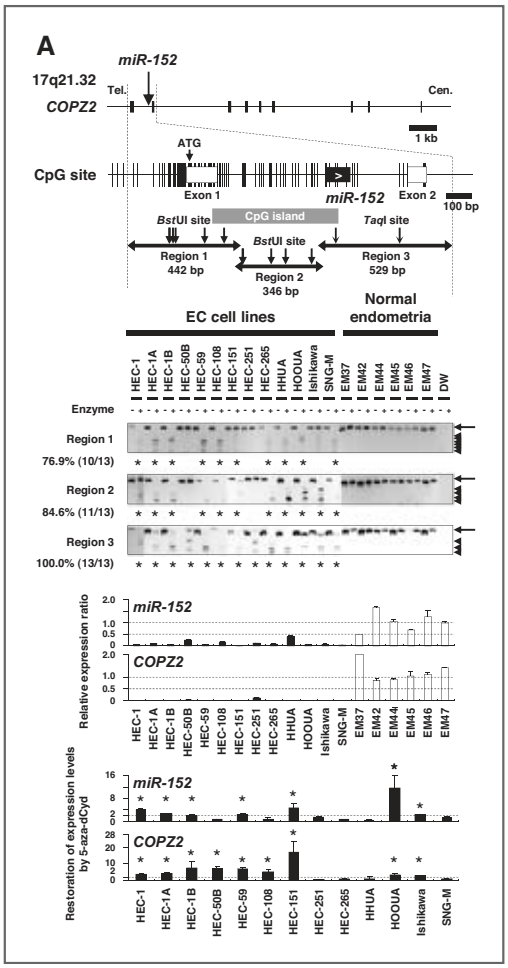

Figure 2. Correlation between methylation and expression status of *miR-152* and its host gene, *COPZ2*, in endometrial cancer cell lines and primary cases. A, analysis for *miR-152* and *COPZ2* in 13 endometrial cancer cell lines and 6 normal endometria. A map (top) shows *miR-152*, *COPZ2*, CpG island, CpG sites, and PCR products used for COBRA and bisulfite sequencing. White boxes, exons of *COPZ2*; black box, *pre-miR-152*; gray box, CpG island; closed arrows, PCR products (primers, Supplementary Table S2); vertical tick marks, CpG sites; vertical arrows, restriction enzyme sites. In results of COBRA (middle), arrows, arrowheads, and black stars indicate unmethylated alleles, methylated alleles, and samples in which the aberrant hypermethylation of CpG islands was detected, respectively. In the results of quantitative real-time RT-PCR (bottom), expression levels of *miR-152* and *COPZ2* were based on the amount of target message relative to *RNU6B* and *GAPDH*, respectively, to normalize the initial input of total RNA. Bar graphs show the ratio of the expression level in each cell line and primary case to the mean value in 6 normal endometria. Bar graphs for restoration of expression levels after treatment with 10 μmol/L 5-aza-dCyd for 5 days in 13 endometrial cancer cell lines show the ratio of the expression level in treated cells to that in untreated cells. White stars indicate endometrial cancer cell lines in which a remarkable restoration of expression (>2-fold expression) was observed after treatment with 5-aza-dCyd.

Published OnlineFirst August 25, 2011; DOI:10.1158/0008-5472.CAN-11-0364

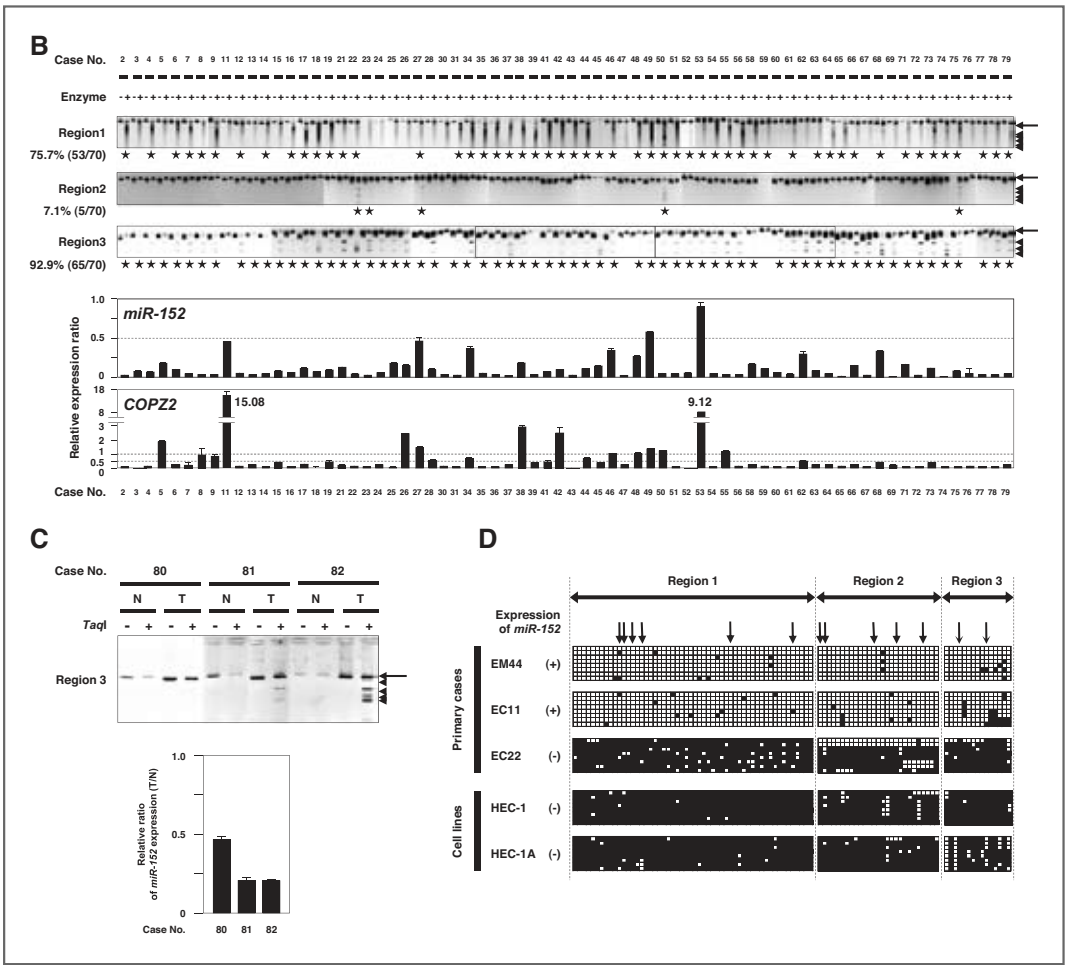

Figure 2. (*Continued*) B, analysis for *miR-152* and *COPZ2* in 70 primary samples and 6 normal endometria. C, representative results of methylation and expression analyses for *miR-152* in primary endometrial cancer tumors (T) and their corresponding normal endometria (N). D, representative results of bisulfite sequencing of CpG islands on *pre-miR-152* and *COPZ2* in normal endometrium (EM44), primary endometrial cancer tumors (endometrial cancer11 and endometrial cancer22), and endometrial cancer cell lines (HEC-1 and HEC-1A) with (+) or without (−) *miR-152* expression in regions within/around *miR-152*. Closed arrows, PCR products used for COBRA and bisulfite sequencing; vertical arrows, restriction enzyme sites (Fig. 2A). Open and filled squares represent unmethylated and methylated CpG sites, respectively, and each row represents a single clone.

and deregulation of its expression were detected in 92.9% (65 of 70) and 97.1% (68 of 70) of endometrial cancer cases, respectively, and consistency in DNA hypermethylation of region 3 and silencing of *miR-152* expression was found in 100.0% (65 of 65) of endometrial cancer cases (Fig. 2B), whereas such consistencies found in *miR-152* were not observed in *miR-9* (Table 2; Supplementary Fig. S3A and B). Moreover, both tumor-specific DNA hypermethylation and downregulated expression of *miR-152* were observed in 66.7% (2 of 3) of paired samples from primary endometrial cancer tumors and their corresponding normal endometria (Fig. 2C). The DNA hypermethylation of this CpG island was also confirmed by bisulfite sequencing of selected positive cell lines and cases (Fig. 2D). These results suggest that *miR-152* is the most likely TS-miRNA frequently silenced through tumor-specific hypermethylation in endometrial cancer. Thus, hereafter we focused on *miR-152* as a prime candidate.

Tumor-suppressive effects of ectopic *miR-152* expression on tumor cell growth *in vitro* and *in vivo*

To confirm the effects of *miR-152* on tumor cell growth, we introduced the dsRNA mimicking mature *miR-152* into

Published OnlineFirst August 25, 2011; DOI:10.1158/0008-5472.CAN-11-0364

Table 2. Frequencies of endometrial cancer cell lines and primary cases, in which DNA hypermethylation accorded with downregulation of miRNA expression

miRNA gene	Region in COBRA	endometrial cancer cell lines		endometrial cancer cases	
		Methylation frequency (%)[a]	Consistency of methylation with downregulation (%)[b]	Methylation frequency (%)[a]	Consistency of methylation with downregulation (%)[b]
miR-9-1	1	100.0 (13/13)	61.5 (8/13)	60.0 (42/70)	21.4 (9/42)
miR-9-3	1	100.0 (13/13)	61.5 (8/13)	84.3 (59/70)	23.7 (14/59)
miR-9-3	3	100.0 (13/13)	61.5 (8/13)	35.7 (25/70)	24.0 (6/25)
miR-152	3	100.0 (13/13)	100.0 (13/13)	92.9 (65/70)	100.0 (65/65)
miR-149	1	69.2 (9/13)	0.0 (0/9)	ND	ND

Abbreviation: ND, not determined.

[a]Frequency of cell lines or primary cases, in which DNA hypermethylation were detected by COBRA (Figs. 1C, 2B and E; Supplementary Figs. S2 and S3).

[b]Frequency of cell lines or primary cases, in which downregulation was consistent with DNA hypermethylation (Fig. 2C and F; Supplementary Figs. S2 and S3).

endometrial cancer cell lines, HEC-1 and HEC-1A, lacking its expression, *in vitro* and *in vivo*. Although *miR-152* overexpression significantly inhibited cell growth *in vitro*, potential dose-dependent effects of this dsRNA on cell proliferation *in vitro* were not observed in these cell lines (Supplementary Fig. S1A). On the contrary, expression levels of *miR-152* were remarkably increased in endometrial cancer cells transfected with this dsRNA (<0.005 nmol/L) as compared with untreated endometrial cancer cells and normal endometria (Supplementary Fig. S1B). Then 2 synthetic miRNAs purchased from Ambion and Thermo Scientific Dharmacon were used in consideration of off-target effects of dsRNAs. Consistent with the results of function-based screening, restoring *miR-152* expression significantly reduced cell proliferation in all endometrial cancer cell lines tested (Fig. 3A), confirming the tumor-suppressive function of *miR-152*; note that a large number of *miR-152* transfectants were rounded and floating compared with their control counterparts (Fig. 3A). Because such apoptotic changes were more remarkable in HEC-1 than HEC-1A under the phase-contrast microscope at 5 days after transfection, we carried out FACS analysis and Western blot analysis for caspase-mediated apoptosis, using endometrial cancer cell lines 72 hours after the transfection. In FACS analysis, overexpression of *miR-152* induced the accumulation of cells in sub-G_1 phase or G_2–M phase to HEC-1 or HEC-1A cell lines, respectively (Fig. 3A). The results of Western blotting, moreover, showed that the ectopic expression of *miR-152* remarkably increased levels of caspase-3, cleaved caspase-3, and cleaved PARP in HEC-1 cells, whereas only caspase-3 was increased in HEC-1A (Fig. 3B). These findings suggest *miR-152* to be associated with cell cycle arrest at both the G_1–S and G_2–M checkpoints in endometrial cancer cells, leading us to further investigate the potential of dsRNA mimicking *miR-152* as a therapeutic agent. Therefore, we examined whether *miR-152* could suppress tumor growth *in vivo*, and consequently significant reduction of s.c. tumors of HEC-1 cells could be observed by treatment with *miR-152* (Fig. 3C).

Coexpression of intronic miRNA, *miR-152*, and its host gene, *COPZ2*

Interestingly, the *miR-152* gene is located at 17q21.32 and within intron 1 of the *coatomer protein complex, subunit zeta 2* (*COPZ2*) gene (Fig. 2A). In real-time PCR analysis using endometrial cancer cell lines and primary cases, the expression pattern of these 2 transcripts seemed to be similar (Fig. 2A and B); note that the frequencies of downregulation of *COPZ2* in endometrial cancer cell lines and primary cases (<0.5-fold expression) were 100% (13 of 13) and 75.7% (53 of 70), respectively. The correlation between the DNA methylation status of *COPZ2* in region 3 in COBRA and its expression patterns was 100% (13 of 13) in endometrial cancer cell lines and 75.4% (49 of 65) in endometrial cancer cases. To investigate the relationship between DNA hypermethylation in this CpG island and the downregulation of *miR-152* and *COPZ2* expression, we treated endometrial cancer cell lines with 5-aza-dCyd. The expression of intronic *miR-152* gene and the host gene, *COPZ2*, was restored to a similar pattern in endometrial cancer cell lines 5 days after treatment with 5-aza-dCyd (concordance rate at 2-fold increased restoration between downregulation and restoration of *COPZ2* expression = 69.2%, 9 of 13; Fig. 2A), strongly suggesting that DNA methylation around CpG islands on *miR-152* also suppressed the expression of *COPZ2* in cell lines. To determine whether COPZ2, as well as *miR-152*, had a potent tumor-suppressive function, we also carried out colony-formation assays using the full coding sequence of *COPZ2* with Myc-tags cloned into a mammalian expression vector (pCMV-3Tag4A-*COPZ2*) and 2 endometrial cancer cell lines lacking the expression of *COPZ2* (Supplementary Fig. S4A). However, the number of large colonies produced by *COPZ2*-transfected HEC-1 cells significantly decreased compared with those produced by empty vector-transfected counterparts 2 weeks after the transfection and subsequent selection of drug-resistant colonies, such findings were not observed in *COPZ2*-transfected HEC-1A cells (Supplementary Fig. S4B). Further detailed analyses will be necessary to prove that *COPZ2* is a TSG.

Published OnlineFirst August 25, 2011; DOI:10.1158/0008-5472.CAN-11-0364

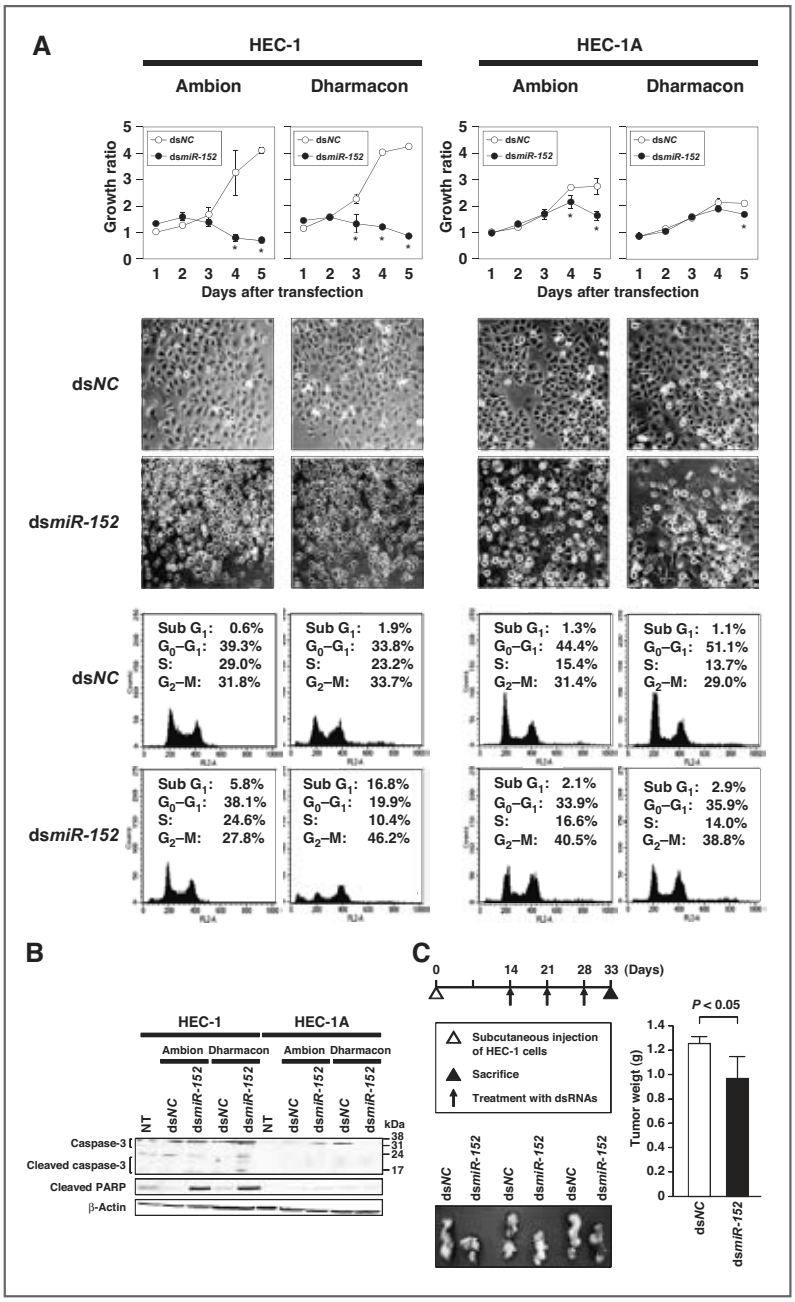

Figure 3. *In vitro* and *in vivo* analyses of tumor-suppressive effects of *miR-152* on endometrial cancer cell lines lacking their expression. A, the results of *in vitro* growth curves (top), phase-contrast micrographs (middle, 5 days after transfection of dsRNAs), and FACS analysis (bottom, 72 hours after transfection of dsRNAs) of HEC-1 and HEC-1A in which 10 nmol/L of dsRNA mimicking *miR-152* or control nonspecific miRNA (Ambion and Dharmacon) was transfected. The numbers of viable cells after transfection were assessed by WST assay. Each data point represents the mean of triplicate determinations (bars, SD) in these experiments. *, $P < 0.01$, statistical analysis with the Mann–Whitney *U* test. B, the results of Western blotting of caspase-3, cleaved caspase-3, and cleaved PARP in endometrial cancer cell lines 48 hours after transfection of dsRNAs. C, effects of *miR-152* on tumor growth *in vivo*. A schema indicates the protocol of *in vivo* analysis. Photograph shows features of s.c. tumors derived from HEC-1 cells treated with dsRNAs (Ambion). Bar graph shows the mean value of tumor weight in 3 SCID mice.

Screening of predicted targets for *miR-152* in endometrial cancer cells

To explore oncogenic targets of *miR-152* in endometrial cancer cells, we searched for potential genes involved in tumorigenesis, using algorithms such as miRanda, TargetScan, and Pictar, and identified *DNA methyltransferase 1* (*DNMT1*), *E2F transcription factor 3* (*E2F3*), *MET*, and *rapamycin-insensitive companion of mTOR* (*Rictor*). DNMT1 had

Published OnlineFirst August 25, 2011; DOI:10.1158/0008-5472.CAN-11-0364

already been described as a target of *miR-152* (25). We first carried out Western blot analysis of these predicted targets in HEC-1 and HEC-1A cells 48 hours after the transfection of 2 kinds of dsRNAs mimicking *miR-152* (Fig. 4A), and observed that protein levels were reduced in the transfectants compared with their control counterparts, although the reductions were not remarkable. To further determine whether the predicted target sites for *miR-152* in the 3′-UTR of the mRNAs of *DNMT1*, *E2F3*, *MET*, and *Rictor* (Fig. 4B) were responsible for the translational regulation by dsRNA, we next carried out luciferase assays with vectors containing these 3′-UTR target sites downstream of the luciferase reporter gene. The reporter construct containing the *miR-152* binding site within the 3′-UTR of *DNMT1* was used as a positive control. In endometrial cancer cells transfected with dsRNAs mimicking *miR-152* purchased from Ambion, a statistically significant reduction in luciferase activity was observed in *DNMT1*, *MET*, and *Rictor*, but

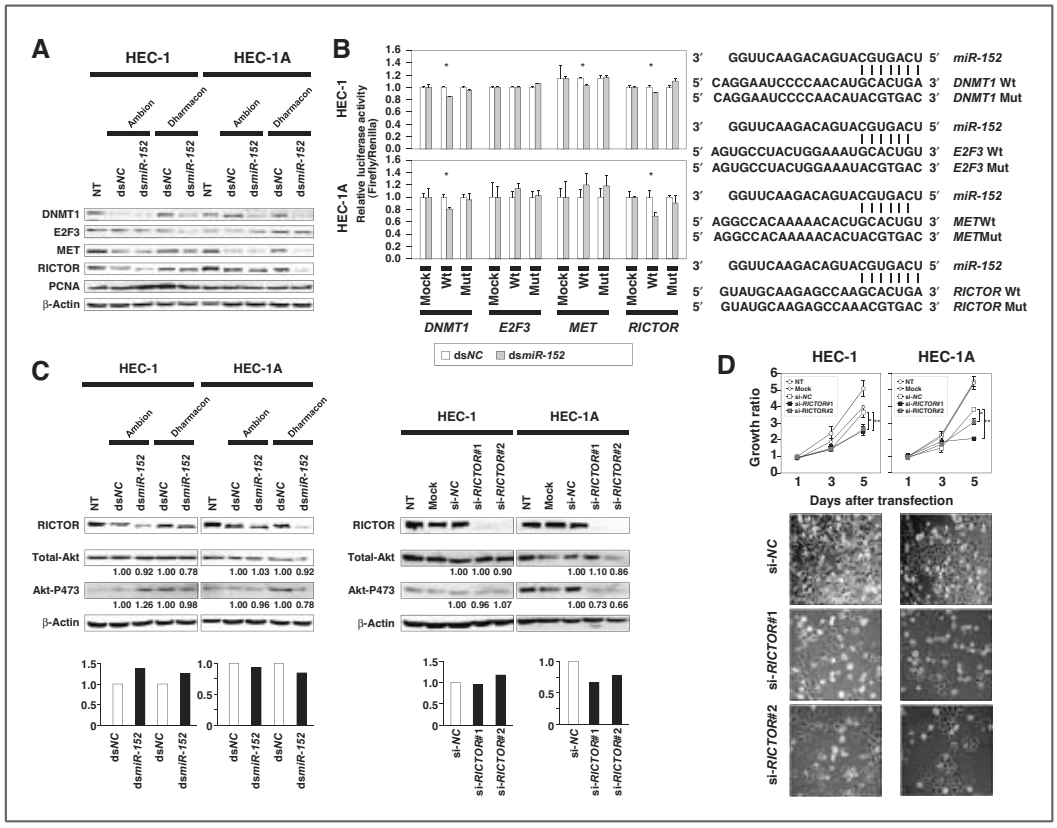

Figure 4. Screening of predicted targets of *miR-152*. A, the results of Western blotting of predicted targets for miR-152 in endometrial cancer cell lines 48 hours after transfection of dsRNA mimicking *miR-152* or control nonspecific miRNA. B, luciferase reporter assay. Left, results of luciferase assays in endometrial cancer cell lines 48 hours after cotransfection of pMIR-REPORT luciferase vectors containing wild type (Wt) or mutated (Mut) 3′-UTR target sites of *DNMT1*, *E2F3*, *MET*, and *Rictor* for *miR-152*, dsRNA mimicking *miR-152* or control nonspecific miRNA (Ambion), and pRL-CMV internal control vector using Lipofectamine 2000 (Invitrogen). *, $P < 0.05$ versus vehicle-treated cells, statistical analysis with the Mann–Whitney *U* test. Right, putative binding site of *miR-152* in the 3′-UTR region of their targets. These target sites were analyzed by miRanda (20), TargetScan (21), and PicTar (22). C, comparison of Rictor protein expression levels and AKT activation in endometrial cancer cell lines by Western blot analysis. Western blot analysis for the phosphorylation of Akt at Ser-473 in endometrial cancer cell lines 48 hours after the transfection of 2 kinds of dsRNA mimicking *miR-152* or control nonspecific miRNA (left) and 2 kinds of *Rictor*-specific siRNA (si-*Rictor* #1 and si-*Rictor* #2; Sigma) or control nonspecific siRNA (right). To determine the increased phosphorylation of Akt, total Akt levels in the same samples were evaluated. The quantification of each protein band was done by using LAS-3000 with MultiGauge software (Fujifilm). D, effects of downregulation of *Rictor* protein expression on cell proliferation in endometrial cancer cell lines. Growth curves (top) and phase-contrast micrographs (bottom) of HEC-1 and HEC-1A cells in which 20 nmol/L of si-*Rictor* #1, si-*Rictor* #2, or nonspecific siRNA was transfected. The numbers of viable cells after transfection were assessed by WST assay. Each data point represents the mean of triplicate determinations (bars, SD) in these experiments. *, $P < 0.05$; **, $P < 0.01$, statistical analysis with the Mann–Whitney *U* test. Phase-contrast micrographs show endometrial cancer cells 5 days after transfection.

Published OnlineFirst August 25, 2011; DOI:10.1158/0008-5472.CAN-11-0364

not in their mutant constructs (Fig. 4B), although synthetic *miR-152* purchased from Thermo Scientific Dharmacon markedly decreased the luciferase activities in all of 4 targets, including *E2F3* (Supplementary Fig. S5). On the contrary, expressions of *DNMT1*, *E2F3*, *MET*, and *Rictor* were upregulated in 47.1% (33 of 70), 28.6% (20 of 70), 1.5% (1 of 70), and 20% (14 of 70) of endometrial cancer cases, respectively (Supplementary Fig. S6). Taken together, these findings suggested that *DNMT1* and *Rictor* might be the most likely targets for *miR-152* in endometrial cancer.

Rictor, together with the mTOR kinase, forms mTOR complex 2 (mTORC2), and the Rictor–mTOR complex directly regulates the phosphorylation of Akt at Ser-473, resulting in cell growth (26). To investigate whether Rictor participates in the growth inhibitory effects of *miR-152* in endometrial cancer cells, we analyzed the phosphorylation of Akt and proliferation in HEC-1 and HEC-1A cells transfected with or without 2 dsRNAs mimicking *miR-152* or 2 specific siRNAs for *Rictor*. Levels of Rictor protein and phosphorylation of Akt at Ser-473 were weakly decreased in HEC-1A cells 48 hours after the transfection of *miR-152* compared with those in the control transfectants, whereas levels of phosphorylated Akt showed no reduction in HEC-1 cells (Fig. 4C). The transient transfection of specific siRNA for *Rictor* clearly decreased levels of the transcripts (data not shown) and protein of Rictor (Fig. 4C) and inhibited cell growth (Fig. 4D) in both cell lines. Forty-eight hours after the knockdown of *Rictor*, similar to the results for *miR-152*, a marked reduction in the phosphorylation of Akt was detected in HEC-1A cells, but not in HEC-1 cells (Fig. 4C), suggesting Akt to be significantly activated and phosphorylated by another pathway, for example, phosphatidylinositol 3-kinase (PI3K)-Akt signaling, different from TOR-Akt signaling for the silencing of *miR-152* through DNA hypermethylation in HEC-1A cells.

Discussion

In this study, we carried out function-based screening by using 327 dsRNA mimicking mature human miRNAs as the first screening of TS-miRNAs having remarkable inhibitory effects on the growth of endometrial cancer cell lines although expression-based or DNA methylation–based screening had been successfully performed in our previous studies in oral squamous cell carcinoma (9) and hepatocellular carcinoma (10). Actually, several known TS-miRNAs, such as *miR-124* (10, 23), *miR-126* (27), *miR-137* (9), and *miR-491* (14), were identified through similar screening processes, strongly suggesting the function-based approach presented here to be a powerful tool for exploring dsRNAs having tumor-suppressive effects, including TS-miRNAs and siRNAs, as therapeutic agents for several types of cancer cells. The tumor-suppressive function of a candidate miRNA eventually identified in our study was reexamined by using 2 kinds of dsRNA purchased from independent companies to take account of off-target effects by dsRNA. Although such effects have been known to complicate the interpretation of phenotypic effects in gene-silencing experiments using siRNAs (28), dsRNAs mimicking miRNAs can potentially cause these unwanted actions. These unpredictable target-independent effects should be addressed during data interpretation in all dsRNA-based studies related with functional genomics, drug target discovery and validation, and dsRNA therapeutics. However, dsRNAs including miRNAs and siRNAs have commonly been used so far at 1.0 to 50.0 nmol/L in dsRNA-based studies, remaining the possibility that overexpressions above their physiologic conditions may lead to biologically toxic effects.

We have considered that the hypermethylation of CpG islands on/around miRNA genes is a good marker to explore novel epigenetically silenced TS-miRNAs, similar to classic TSGs in several types of human cancers, and have already reported *miR-137*, *miR-193a*, *miR-124*, and *miR-203* as TS-miRNAs (9, 10). This study showed that the second screening, combining DNA methylation and expression analyses in endometrial cancer cell lines and primary cases, resulted in the identification of *miR-152* as a prime candidate for a TS-miRNA silenced by DNA hypermethylation in endometrial cancer. Because tumor-suppressive effects of *miR-152* have not been described to date, we carried out detailed analyses of *miR-152*. Recently, in *MLL*-rearranged acute lymphoblastic leukemia, aberrant DNA methylation of *miR-152* CpG islands was reported to correlate with a poor clinical outcome (29). Altered expression of *miR-152* was shown in gastrointestinal cancer (30) and cholangiocarcinoma (25). Our data showed that DNA hypermethylation and downregulation of *miR-152* were frequently observed in endometrial cancer cell lines and primary tumors, and that treatment with 5-aza-dCyd restored the expression of *miR-152* in endometrial cancer cell lines lacking it. In addition, the correlation between DNA methylation status around *miR-152* and expression pattern was 100% (13 of 13) in a panel of 13 endometrial cancer cell lines and 100% (65 of 65) in endometrial cancer cases, suggesting that DNA hypermethylation around the CpG island of *miR-152* seemed to deregulate its expression in endometrial cancer. Moreover, we successfully showed for the first time that dsRNA mimicking *miR-152*, in its administration with atelocollagen for the drug delivery in mice, suppressed *in vivo* growth of an endometrial cancer cell line. The finding led us to consider the possibility that *miR-152* might have some benefit as therapeutic agents. This miRNA is located at 17q21.32 in intron 1 of the host gene *COPZ2*. COPZ2 was described as a coat protein (COP) and to form part of a COPI complex which transports vesicles from the Golgi apparatus to endoplasmic reticulum (31). In addition, a recent study showed that COPI was required for early endosomal maturation in autophagy, whereas the biological function of COPZ2 remains uncharacterized (32). Our data showed that DNA hypermethylation–mediated silencing of *miR-152* and *COPZ2* was a relatively frequent molecular event in endometrial cancer and inhibited cell growth in endometrial cancer cell lines, suggesting the epigenetic silencing of these genes to contribute to endometrial carcinogenesis, although further experiments will be needed to confirm that the coexpression has tumor suppressor effects in this disease.

In this study, we successfully identified possible direct targets of *miR-152* other than *DNMT1* (25), such as *E2F3*,

Published OnlineFirst August 25, 2011; DOI:10.1158/0008-5472.CAN-11-0364

MET, and *Rictor* (Supplementary Fig. S7). E2F3 is a transcriptional repressor of the E2F family, and its potential oncogenic capacity was also shown recently (33). MET is already well known as an oncogene and the cell-surface receptor for hepatocyte growth factor (34). These previous studies as well as our own results suggest that the altered expression of these targets caused by the downregulation of *miR-152* expression through CpG island hypermethylation may contribute to the tumorigenesis through the activation of target oncogenic pathways in endometrial cancer. Rictor is a component of the mTOR-containing complex, mTORC2, which directly regulates the phosphorylation of Akt at Ser-473 (26), and has already been reported the correlation with the molecular mechanisms in cancer cells (35, 36). These results including our findings support the hypothesis that the silencing of *miR-152* through CpG methylation may contribute to carcinogenesis and cancer progression at least partly through the activation of mTORC2-Akt signaling in endometrial cancer. However, knockdown of *Rictor* was reported to induce G_1 arrest in the breast cancer cell line MCF7 and prostate cancer cell line PC3 (37), and inhibition of the Akt-mTOR pathway was shown to induce G_2–M arrest and autophagy in the breast cancer cell line MDA-MB-231 (38). On the contrary, we showed here that ectopic *miR-152* expression reduced cell proliferation and induced the accumulation of cells into sub-G_1 phase or G_2–M phase in HEC-1 or HEC-1A cell lines, respectively. Cell cycle progression of *miR-152* transfectants may be affected by its targets other than *Rictor*, considering that miRNAs regulate target gene expression through imperfect pairing with target messenger RNAs. Although Akt signaling pathways were also described to play a key role in both G_1–S and G_2–M transitions (39), these differences in effects on cell cycle progression remain largely unknown.

In conclusion, we describe here the identification of a TS-miRNA, *miR-152*, frequently silenced by DNA hypermethylation in endometrial cancer, using function-based screening and a series of sequential analyses. Moreover, we identified *E2F3*, *MET*, and *Rictor* as potential targets of *miR-152*, suggesting that the epigenetic silencing of *miR-152* and consequent activation of its multiple targets may contribute to endometrial carcinogenesis, and that *miR-152* and targeting *E2F3*, *MET*, and *Rictor* may provide a novel treatment strategy for endometrial cancer, although further studies *in vivo* will be needed to confirm that dsRNA mimicking *miR-152* can work as a TS-miRNA in this disease.

Disclosure of Potential Conflicts of Interest

No potential conflicts of interest were disclosed.

Acknowledgments

We thank Ayako Takahashi and Rumi Mori for technical assistance.

Grant Support

This study was supported in part by Grant-in-Aid for Scientific Research (A), (B), and (C), and Scientific Research on Priority Areas and Innovative Areas, and a Global Center of Excellence (GCOE) Program for International Research Center for Molecular Science in Tooth and Bone Diseases from the Ministry of Education, Culture, Sports, Science, and Technology, Japan; a Health and Labour Sciences Research Grant by the Ministry of Health, Labour and Welfare, Japan; and a grant from the New Energy and Industrial Technology Development Organization (NEDO). This work was also supported by the Joint Usage/Research Program of Medical Research Institute, Tokyo Medical and Dental University.

The costs of publication of this article were defrayed in part by the payment of page charges. This article must therefore be hereby marked *advertisement* in accordance with 18 U.S.C. Section 1734 solely to indicate this fact.

Received February 4, 2011; revised August 19, 2011; accepted August 19, 2011; published OnlineFirst August 25, 2011.

References

1. Bartel DP. MicroRNAs: genomics, biogenesis, mechanism, and function. Cell 2004;116:281–97.
2. He L, Hannon GJ. MicroRNAs: small RNAs with a big role in gene regulation. Nat Rev Genet 2004;5:522–31.
3. Miska EA. How microRNAs control cell division, differentiation and death. Curr Opin Genet Dev 2005;15:563–8.
4. Harfe BD. MicroRNAs in vertebrate development. Curr Opin Genet Dev 2005;15:410–5.
5. Esquela-Kerscher A, Slack FJ. Oncomirs - microRNAs with a role in cancer. Nat Rev Cancer 2006;6:259–69.
6. Osada H, Takahashi T. MicroRNAs in biological processes and carcinogenesis. Carcinogenesis 2007;28:2–12.
7. Herman JG, Baylin SB. Gene silencing in cancer in association with promoter hypermethylation. N Engl J Med 2003;349:2042–54.
8. Chuang JC, Jones PA. Epigenetics and microRNAs. Pediatr Res 2007;61:24R–29R.
9. Kozaki K, Imoto I, Mogi S, Omura K, Inazawa J. Exploration of tumor-suppressive microRNAs silenced by DNA hypermethylation in oral cancer. Cancer Res 2008;68:2094–105.
10. Furuta M, Kozaki K, Tanaka S, Arii S, Imoto I, Inazawa J. miR-124 and miR-203 are epigenetically silenced tumor-suppressive microRNAs in hepatocellular carcinoma. Carcinogenesis 2009;31:766–76.
11. Iorio MV, Piovan C, Croce CM. Interplay between microRNAs and the epigenetic machinery: an intricate network. Biochim Biophys Acta 2010;1799:694–701.
12. Dizon DS. Treatment options for advanced endometrial carcinoma. Gynecol 2010;117:373–81.
13. Murayama-Hosokawa S, Oda K, Nakagawa S, Ishikawa S, Yamamoto S, Shoji K, et al. Genome-wide single-nucleotide polymorphism arrays in endometrial carcinomas associate extensive chromosomal instability with poor prognosis and unveil frequent chromosomal imbalances involved in the PI3-kinase pathway. Oncogene 2010;29:1897–908.
14. Nakano H, Miyazawa T, Kinoshita K, Yamada Y, Yoshida T. Functional screening identifies a microRNA, miR-491 that induces apoptosis by targeting Bcl-X(L) in colorectal cancer cells. Int J Cancer 2010;127:1072–80.
15. Levy C, Khaled M, Iliopoulos D, Janas MM, Schubert S, Pinner S, et al. Intronic miR-211 assumes the tumor suppressive function of its host gene in melanoma. Mol Cell 2010;40:841–9.
16. Suzuki E, Imoto I, Pimkhaokham A, Nakagawa T, Kamata N, Kozaki K, et al. PRTFDC1, a possible tumor-suppressor gene, is frequently silenced in oral squamous-cell carcinomas by aberrant promoter hypermethylation. Oncogene 2007;26:7921–32.
17. miRBase database (Release 17 April 2011). Available from: http://www.mirbase.org/index.shtml.
18. UCSC Genome Browser on Human February 2009 Assembly (hg19). Available from: http://genome.ucsc.edu/cgi-bin/hgGateway.
19. PubMed. Available from: http://www.ncbi.nlm.nih.gov/pubmed.
20. miRanda. Available from: http://microrna.sanger.ac.uk/sequences/index.shtml.

Published OnlineFirst August 25, 2011; DOI:10.1158/0008-5472.CAN-11-0364

21. TargetScan. Available from: http://www.targetscan.org/.
22. PicTar. Available from: http://pictar.mdc-berlin.de/.
23. Pierson J, Hostager B, Fan R, Vibhakar R. Regulation of cyclin dependent kinase 6 by microRNA 124 in medulloblastoma. J Neurooncol 2008;90:1–7.
24. Sun Y, Bai Y, Zhang F, Wang Y, Guo Y, Guo L. miR-126 inhibits non-small cell lung cancer cells proliferation by targeting EGFL7. Biochem Biophys Res Commu 2010;391:1483–9.
25. Braconi C, Huang N, Patel T. MicroRNA-dependent regulation of DNA methyltransferase-1 and tumor suppressor gene expression by interleukin-6 in human malignant cholangiocytes. Hepatology 2010;51: 881–90.
26. Hresko RC, Mueckler M. mTOR.RICTOR is the Ser473 kinase for Akt/protein kinase B in 3T3-L1 adipocytes. J Biol Chem 2005;280:40406–16.
27. Saito Y, Friedman JM, Chihara Y, Egger G, Chuang JC, Liang G. Epigenetic therapy upregulates the tumor suppressor microRNA-126 and its host gene EGFL7 in human cancer cells. Biochem Biophys Res Commun 2009;379:726–31.
28. Svoboda P. Off-targeting and other non-specific effects of RNAi experiments in mammalian cells. Curr Opin Mol Ther 2007;9:248–57.
29. Stumpel DJ, Schotte D, Lange-Turenhout EA, Schneider P, Seslija L, de Menezes, et al. Hypermethylation of specific microRNA genes in MLL-rearranged infant acute lymphoblastic leukemia: major matters at a micro scale. Leukemia 2010;25:429–39.
30. Chen Y, Song Y, Wang Z, Yue Z, Xu H, Xing C, et al. Altered expression of MiR-148a and MiR-152 in gastrointestinal cancers and its clinical significance. J Gastrointest Surg 2010;14:1170–9.
31. Lee C, Goldberg J. Structure of coatomer cage proteins and the relationship among COPI, COPII, and clathrin vesicle coats. Cell 2010;142:123–32.
32. Razi M, Chan EY, Tooze SA. Early endosomes and endosomal coatomer are required for autophagy. J Cell Biol 2009;185: 305–21.
33. Chen HZ, Tsai SY, Leone G. Emerging roles of E2Fs in cancer: an exit from cell cycle control. Nat Rev Cancer 2009;9:785–97.
34. Trusolino L, Bertotti A, Comoglio PM. MET signalling: principles and functions in development, organ regeneration and cancer. Nat Rev Mol Cell Biol 2010;11:834–48.
35. Roulin D, Cerantola Y, Dormond-Meuwly A, Demartines N, Dormond O. Targeting mTORC2 inhibits colon cancer cell proliferation in vitro and tumor formation in vivo. Mol Cell 2010;9:57.
36. Guertin DA, Stevens DM, Saitoh M, Kinkel S, Crosby K, Sheen JH, et al. mTOR complex 2 is required for the development of prostate cancer induced by Pten loss in mice. Cancer Cell 2009; 15:148–59.
37. Hietakangas V, Cohen SM. TOR complex 2 is needed for cell cycle progression and anchorage-independent growth of MCF7 and PC3 tumor cells. BMC Cancer 2008;8:282.
38. Kuo PL, Hsu YL, Cho CY. Plumbagin induces G2-M arrest and autophagy by inhibiting the AKT/mammalian target of rapamycin pathway in breast cancer cells. Mol Cancer Ther 2006;5: 3209–21.
39. Liang J, Slingerland JM. Multiple roles of the PI3K/PKB (Akt) pathway in cell cycle progression. Cell Cycle 2003;2:339–45.

分子遺伝分野

三木 義男
難治疾患研究所
分子遺伝・教授

1）研究の課題名

①骨肉腫におけるP53によって誘導されるアポトーシス関連遺伝子の解析

（Discovery of pro-apoptotic genes induced by p53 in osteosarcoma）

骨肉腫は、小児～青春期において発症する。がん抑制遺伝子p53の変異は、骨肉腫を含むヒトがんの中で最も高頻度に検出される。p53は、DNA損害に反応してアポトーシスを制御し、p53の転写活性や選択性は主にその翻訳後修飾に依存する。特に、p53セリン-46（Ser46）のリン酸化は、プロアポトーシス遺伝子群を活性化するために必須である。我々はヒト骨肉腫細胞において、p53 Ser46のリン酸化によって活性化される新しいproapoptoticな遺伝子を同定するために、マイクロアレイ解析とクロマチン免疫沈降（ChIP）解析を行った。マイクロアレイ解析では、変異型p53 Ser46（p53S46A）では遺伝子発現に変化なく、野生型p53（wt-p53）で高発現が認められた296遺伝子を同定した。ChIP解析では、p53S46Aは結合せず、wt-p53が結合する領域を有する9294遺伝子を同定した。これら両方のデータから、p53 Ser46のリン酸化により活性化される候補遺伝子68遺伝子を同定した。これらの遺伝子について、RT-PCRによりさらに詳細に解析した結果、脂質のアンカーであるparalemminタンパクファミリーのmRNA発現が、wt-p53特異的に増加することを突き止めた。我々は、このp53によって誘導されるプロアポトーシス遺伝子の発見が骨肉腫治療のために重要な情報を提供するものと考えている。

②新規プロラインキナーゼCδ（PKCδ）アポトーシス標的分子Evi-1の同定

（Identification of Evi-1 as a novel PKCδ Apoptosis Regulatory Target）

PKCδはDNA損傷に応答して様々なシグナル伝達機構を制御することから、本研究ではPKCδによって引き起こされる細胞死誘導に重要な新規下流制御因子の同定を目標とした。PKCδによって誘導されるアポトーシス制御機構を明らかにするために、ChIP-cloning法とMicroarray解析を組み合わせたスクリーニングを行い、PKCδの新規標的転写因子を探索した。候補転写因子はMicroarray法と同様にin silico解析によって選出した。そして本スクリーニングによって、新規PKCδ標的分子として白血病の癌遺伝子Evi-1を同定することに成功した。また、PKCδがDNA損傷に応答してEvi-1によるPLZFの活性化を制御していることを見出した。更に、Evi-1がDNA損傷性ストレスによるアポトーシス誘導に関与すること明らかにした。これらの結果より、我々は新規PKCδ標的因子Evi-1がDNA損傷下においてPLZFを活性化し、細胞死を誘導することを明らかにした。

2）

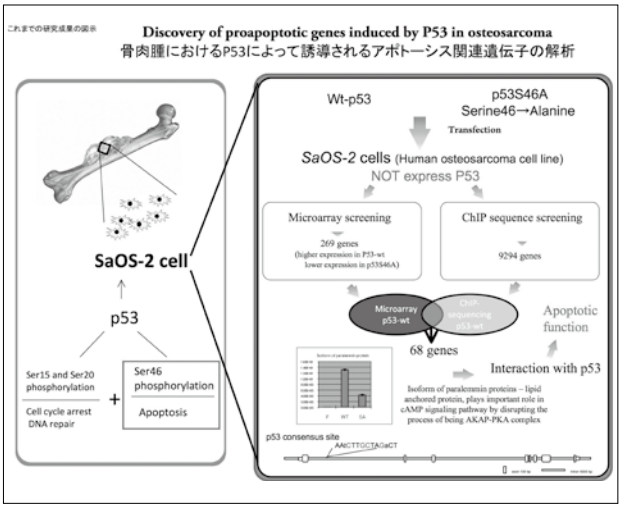

3）発表の研究内容についての英文要約

1. Discovery of the pro-apoptotic genes induced by p53 in osteosarcoma

The genetic alterations in p53 are one of the most frequently mutated tumor suppressor gene in human cancer including osteosarcoma. The tumor suppressor gene p53 regulates apoptosis in response to DNA damage. Promoter selectivity of p53 depends mainly on its post-translational modification. Notably, the phosphorylation at serine-46（Ser46）of p53 is essential to promote pro-apoptotic genes. However, little is known about pro-apoptotic genes induced by Ser46 phosphorylation. Recently, microarray analysis became common tool in molecular biology research, we intended to compare microarray analysis with chromatin immunoprecipitation（ChIP）sequencing assay to discover novel proapoptotic genes promoted by p53 phosphorylation at Ser46 in human osteosarcoma cells. In the microarray analysis, 24970 genes were probed and 296 genes were upregulated in expression of wild type p53（wt-p53）, but not in mutant p53 at Ser46（p53S46A）. p53 binding regions of 9294 genes were isolated in wt-p53 by the ChIP sequencing assay. Sixty eight genes which are specific in p53S46A were successfully extracted by comparing the genes isolated from the microarray analysis and the ChIP sequencing assay. From them, the genes strongly elicited by the phosphorylation of Ser46 of p53 were clarified by quantitative real time RT-PCR. mRNA level of the paralemmin protein family, lipid-anchoring was significantly increased in wt-p53 but not in p53S46A. The DNA binding site of p53 of isoform of paralemmin protein was found in intron 1 region. We hope that the discovery of pro-apoptotic gene induced by p53 will convey important information for osteosarcoma therapy.

2. Identification of Evi-1 as a novel PKC δ Apoptosis Regulatory Target

The projects aim to identify PKC δ downstream regulatory substrates that are responsible for the cell death machinery. We sought to uncover transcription factor targets of PKC δ by devising a screening strategy that utilizes ChIP-cloning and microarray analysis. As a result, we have discovered a novel regulation of Evi-1, which transactivates PLZF, by PKC δ to induce cell death by genotoxic stress. We hope that the achievement of this project will bring about new knowledge for the understanding of how PKC δ regulates apoptosis.

4）本事業に関連して世界的な研究拠点形成に向けて、以下の点で改善・整備等されたこと

A（研究拠点体制）

研究室におけるスペースの確保、機器の整備および補充、研究推進のためのスケジュール等を作成し研究室内部の体制の整備を継続するとともに、整形外科、口腔外科等の臨床グループと立案した共同研究計画を進めるなど、総合的に研究拠点体制の継続に努めた。

B（研究教育環境）

ジャーナルクラブ、研究進捗ミーティング、GCOEセミナー等研究教育環境の整備を継続した。

C（人材確保）

大学院生２名（うち１名がSS）がGCOE研究を遂行した。

D（人材育成）

新たに入学する大学院生を含め上記体制で人材育成に努めている。

E（国際化）

GCOEプログラムの中で国際セミナーへの参加、海外招聘研究者との議論等を通して国際化を図った。

5）GCOE事業を推進するに当たって力を入れた点

GCOE推進研究者間で立案した共同研究計画を積極的に進め、特に臨床グループとの共同研究で患者臨床検体を用いたゲノム研究推進体制の構築及びその継続に努めた。

6）英文原著論文

1. Hew HC, Liu H, Miki Y, Yoshida K. PKCdelta regulates Mdm2 independently of p53 in the apoptotic response to DNA damage. Mol Carcinog 50：719-731, 2011
2. Hew HC, Liu H, Lu ZG, et al. Identification of Evi-1 as a novel effector of PKCdelta in the apoptotic response to DNA damage. Biochim Biophys Acta 1809：285-294, 2011
3. ◎ Wang HF, Takenaka K, Nakanishi A, Miki Y. BRCA2 and nucleophosmin coregulate centrosome amplification and form a complex with the Rho effector kinase ROCK2. Cancer Res 71：68-77, 2011
4. Ito Y, Nagasaki K, Miki Y, et al. Prospective randomized phase II study determines the clinical usefulness of genetic biomarkers for sensitivity to primary chemotherapy with paclitaxel in breast cancer. Cancer Sci 102：130-136, 2011
5. Kimura J, Kudoh T, Miki Y, Yoshida K. Identification of dihydropyrimidinase-related protein 4 as a novel target of the p53 tumor suppressor in the apoptotic response to DNA damage. Int J Cancer 128：1524-1531, 2011

6. Sakamoto K, Aragaki T, Morita K, et al. Down-regulation of keratin 4 and keratin 13 expression in oral squamous cell carcinoma and epithelial dysplasia：a clue for histopathogenesis. Histopathology 58：531-542, 2011;
7. Iyevleva AG, Kuligina ES, Mitiushkina NV, et al. High level of miR-21, miR-10b, and miR-31 expression in bilateral vs. unilateral breast carcinomas. Breast Cancer Res Treat 2011 [epub ahead of print]
8. Wang L, Tsutsumi S, Kawaguchi T, et al. Whole-exome sequencing of human pancreatic cancers and characterization of genomic instability caused by MLH1 haploinsufficiency and complete deficiency. Genome Res 2011 [epub ahead of print]
9. Taira N, Mimoto R, Kurata M, Yamaguchi T, Kitagawa M, Miki Y, Yoshida K. DYRK2 phosphorylation of human c-Jun and c-Myc controls tumor progression by monitoring the G1/S transition. J Clin Invest, in press

7）総説ならびに著書

和文：

1. 三木 義男; 染色体 BRCA2とヌクレオホスミン. 生体の科学 62巻5号, 474-475,（2011）
2. 三木 義男; 遺伝性乳癌・卵巣癌の遺伝子診断および研究の現状. 産科と婦人科 78巻9号, 1050-1055,（2011）
3. 斉藤 広子, 三木 義男; PARP阻害剤と癌治療. 癌と化学療法 38巻1号, 12-18,（2011）

8）平成23年度までの自己評価

GCOE プログラムに参加し、骨軟部腫瘍（骨肉腫、軟骨肉腫、歯肉癌など）を中心に、ゲノム科学を応用した研究を進めてきた。一方、骨肉腫におけるp53 Ser46のリン酸化により活性化されるプロアポトーシス分子として、paralemminタンパクファミリーの同定に成功した。今度は、臨床系グループとの共同研究体制を維持し臨床検体収拾システムを作製、順次癌組織の収集を促進し遺伝子発現プロファイル解析を進める。また、教育等には大きく貢献できたと判断している。

9）学会発表（英文）

1. Miki Y, Takenaka K, Nakanishi A. New insights into the cellular function of BRCA2. 70th Annual Meeting of the Japanese Cancer Association,（oral presentation）Nagoya, Japan, October 3-5, 2011

10）学会発表（和文）

1. 新井正美, 瀧景子, 須貝幸子, 小松美樹, 佐藤友理, 西村誠一郎, 岩瀬拓士, 横山士郎, 権藤延久, 三木義男; BRCA遺伝子検査により診断が困難であった症例への取り組み. 第17回日本家族性腫瘍学会学術集会、京都市、2011年6月16-19日
2. 近藤裕道, 堀井理絵, 岩瀬拓士, 秋山太, 三木義男, 野田哲生, 冨田章弘; in situにおける半定量的遺伝子発現解析技術. 第52回日本組織細胞化学会総会学術集会、金沢市、2011年9月24-25日
3. 三本麗, 平直江, 鷹橋浩之, 内田賢, 三木義男, 吉田清嗣; DYRK2はsnail/E-cadherin系を介して癌の浸潤を制御する． 第70回日本癌学会学術総会、名古屋市、2011年10月3-5日
4. 平直江, 三本麗, 倉田盛人, 北川昌伸, 三木義男, 吉田清嗣; DYRK2によるc-Jun/c-Mycのリン酸化は細胞周期G1/S期の進行を制御する. 第70回日本癌学会学術総会、名古屋市、2011年10月3-5日
5. ダシゼウェゲ ヌルマ, 平直江, 木村純子, 三木義男, 吉田清嗣; 癌抑制遺伝子産物p53によるアポトーシス関連遺伝子の探索. 第70回日本癌学会学術総会、名古屋市、2011年10月3-5日
6. 高岡美帆, 斉藤広子, 中西啓, 三木義男; 細胞質分裂におけるミッドボディでのBRCA2とⅡ型ミオシンⅡCの役割． 第70回日本癌学会学術総会、名古屋市、2011年10月3-5日
7. 木村仁美, 中西啓, 三木義男; 中心体の大きさと微小管形成はプロテオームによって制御されている． 第70回日本癌学会学術総会、名古屋市、2011年10月3-5日
8. 須貝幸子, 奥村栄, 坂尾幸則, 文敏景, 小松美樹, 尾本大輔, 大仲悟, 石川雄一, 佐藤之俊, 中川健, 三木義男; 原発性非小細胞肺癌切除時の胸腔内洗浄液におけるTRC法によるCEAmRNAとCK19mRNAの迅速的検出の検討. 第70回日本癌学会学術総会、名古屋市、2011年10月3-5日
9. 古田玲子, 秋山太, 杉山裕子, 宇津木久仁子, 竹島信宏, 須貝幸子, 三木義男, 石川雄一, 北川知行; 子宮頸部神経内分泌癌とHPV18型の強い関連． 第70回日本癌学会学術総会、名古屋市、2011年10月3-5日
10. 奥喜全, 瀧藤克也, 堀田司, 横山省三, 松田健司, 那須亨, 田村耕一, 家田淳司, 山本直之, 岩本博光, 三木義男, 山上裕機; 大腸癌先進部脱分化をもたらす遺伝子機能ネットワーク. 第66回日本大腸肛門病学会学術集会、東京都、2011年11月25-26日

11）外部資金の獲得状況

1. 文部科学省科学技術試験研究・委託業務
   研究題目：分子プロファイリングによる新規標的同定を通じた難治がん治療法開発
   代表：三木義男
   期間：平成23年
   研究費総額：1,400万円
2. 文部科学省科学技術試験研究・委託業務
   研究題目：ゲノム網羅的解析情報を基盤とするオーダーメイドがん医療
   代表：稲澤　譲治
   期間：平成20年～平成23年
   研究費総額：2,000万円
3. 科学研究費補助金、 基盤C
   研究題目：細胞アレイによる卵巣癌抗癌剤効果予測システムの構築と分子標的薬の探索
   代表：津田　浩史
   期間：平成22～23年
   研究費総額：234万円
4. 科学研究費補助金、 挑戦的萌芽研究
   研究題目：MT1-MMPの中心体制御を介した新規がん形質転換機構の解明
   代表：三木　義男
   期間：平成23～24年
   研究費総額：280万円
5. 新学術領域研究、公募研究
   研究題目：乳癌の分子サブタイプ分類と個別化抗癌剤治療の開発
   代表：三木　義男
   期間：平成23～24年
   研究費総額：1600万円

12）特別講演、招待講演、シンポジウム

1. 三木義男; 遺伝性乳がん卵巣がんの臨床　BRCA1/2遺伝子検査と薬物療法 BRCA1/2研究の現状と展望 基礎から臨床. 第17回日本家族性腫瘍学会学術集会、シンポジウム、京都市、2011年6月16-19日
2. 三木義男; 遺伝性乳がん・卵巣がん症候群の分子遺伝. 第47回北九州乳腺カンファレンス、特別講演、北九州市、2011年11月11日
3. 三木義男; 乳がんはなぜおこるの?-遺伝子の異常と乳がん-. 乳がん講演会、徳島市、2011年11月19日
4. 三木義男; BRCA1/2遺伝子の分子生物学-遺伝子の発見から今、そして今後の展望-. 日本家族性腫瘍学会・第14回家族性腫瘍セミナー、東大阪市、2011年8月26-28日

13）教室、分野や講座の准教授、講師、助教、特別研究員、ポスドク、指導を受けた大学院生の名前

准教授	吉田　清嗣
助教	竹中　克也
特任助教	平　直江
D4	高岡 美帆
D3	Wali Nadila（瓦力 娜迪拉）
D3	Mariku Sadiya（真利久 サディヤ）
○ D2	Dashzeveg Nurmaa（ダシュゼウェゲ　ヌルマ）
M2	Guo Tiantian（郭　甜甜）
M2	加賀美裕也
M2	鈴木　一穂
M1	木村　仁美
M1	滝沢　涼子
M1	中澤　和也
M1	山本　武徳
M1	和田　匠太

○はAISS

14）GCOE活動についての感想、コメント、改善を望む点

GCOEプログラムに参加した学生の教育、研究推進は大きな前進が認められ、このような活動が財政的支援とともに継続されることを強く希望する。

Biochimica et Biophysica Acta 1809 (2011) 285–294

Contents lists available at ScienceDirect

Biochimica et Biophysica Acta

journal homepage: www.elsevier.com/locate/bbagrm

Identification of Evi-1 as a novel effector of PKCδ in the apoptotic response to DNA damage

Hoi Chin Hew, Hanshao Liu, Zheng-Guang Lu, Junko Kimura, Yoshio Miki *, Kiyotsugu Yoshida **

Department of Molecular Genetics, Medical Research Institute, Tokyo Medical and Dental University, Tokyo 113-8510, Japan

ARTICLE INFO

Article history:
Received 10 August 2010
Received in revised form 10 February 2011
Accepted 22 February 2011
Available online 27 February 2011

Keywords:
PKCδ
Evi-1
PLZF
DNA damage
Apoptosis

ABSTRACT

Protein kinase C delta (PKCδ), a PKC family isoform, regulates diverse signal transduction pathways during DNA damage to induce apoptosis. To explore the apoptosis mechanism that PKCδ modulates, we sought to uncover transcription factor targets of PKCδ by devising a screening strategy that utilizes ChIP-cloning and microarray analysis. Transcription factor candidates were generated with the application of public access data-mining tools and this resulted in the identification of Evi-1 as a novel PKCδ-mediated DNA damage responsive molecule. The results demonstrated that PKCδ is constitutively associated with Evi-1. PKCδ regulated Evi-1 to activate PLZF transcription upon genotoxic stress. Furthermore, both Evi-1 and PLZF were associated with DNA damage-stimulated apoptosis. Taken together, we have discovered a novel regulation of Evi-1, which transactivates PLZF, by PKCδ to induce cell death in response to genotoxic stress.

© 2011 Elsevier B.V. All rights reserved.

1. Introduction

Protein kinase C (PKC) family of serine/threonine kinases plays an essential role in signal transduction pathways of diverse cellular processes including cell proliferation, differentiation, migration, and apoptosis. Protein kinase C δ (PKCδ) belongs to the novel PKCs and was the first novel PKC isozyme discovered [1]. PKCδ undergoes self-phosphorylation and is further phosphorylated on different sites depending on the stimuli [2]. While pro-survival aspect of PKCδ has been described, it is generally conceived that PKCδ is a pro-apoptotic molecule as evidenced from experiments in a variety of cell types in response to different death stimuli [3,4]. PKCδ-mediated induction of apoptosis upon genotoxic stress involves its breaking up into a 40 kDa protein catalytic domain that can be translocated into the mitochondria and nucleus by proteolysis with caspase-3 [5,6]. Association of PKCδ with the c-Abl tyrosine kinase is also important for the apoptotic response since PKCδ and c-Abl are found to be activated by inter-phosphorylation each other [7,8].

DNA damage triggers PKCδ to maneuver apoptosis events by targeting a vast spectrum of substrates such as DNA-dependent protein kinase [9], phospholipid scamblase 1 [10], lamin B [11], or Rad9 [12]. In particular, it is interesting to note that those effectors reported include TP53, a transcription factor central to DNA damage defend mechanism. TP53 Ser46 phosphorylation is regulated by PKCδ in response to DNA damage signal [13,14]. More surprisingly, PKCδ transactivates TP53 by interacting with the death promoting domain Btf, which itself is also a transcription factor to promote apoptosis [15]. Taken together, these findings indicate that transcription factors belong to one of the target categories that contribute to the PKCδ apoptotic mechanism.

In view of this, we intended to uncover unknown PKCδ regulated, directly or indirectly, transcription factors induced by genotoxic damage. For this purpose, we have developed a strategy that utilizes chromatin immunoprecipitation (ChIP)-sequencing and microarray. The strategy presented here makes the use of the public access bioinformatics tools to predict transcription factors from the data generated by two screens. By comparing the occurrence of the in silico-predicted transcription factors, the data revealed Evi-1 as a top candidate. Further experiments showed that Evi-1 transactivates promyotic leukemic zinc finger (PLZF), a previously reported downstream target of Evi-1 [16], in response to DNA damage.

2. Materials and methods

2.1. Cell culture

U2OS cells (human osteosarcoma cells expressing wild type p53 and Rb) were cultured in RPMI1640 medium containing 10% (v/v) heat-inactivated fetal bovine serum (FBS) and antibiotics. Cells were treated with 5 μM rottlerin (PKCδ inhibitor; Sigma-Aldrich), 2 μg/ml adriamycin (ADR; Sigma-Aldrich), or 10 μM etoposide (ETO; Sigma-Aldrich).

Abbreviations: ChIP, chromatin immunoprecipitation; HSC, haematopoietic stem cells; PKCδ, protein kinase C δ; PLZF, promyotic leukemic zinc finger

* Corresponding author.
** Correspondence to: K. Yoshida, Department of Molecular Genetics, Medical Research Institute, Tokyo Medical and Dental University, 1-5-45 Yushima, Bunkyo-ku, Tokyo 113-8510, Japan. Tel.: +81 3 5803 5826; fax: +81 3 5803 0242.
E-mail address: yos.mgen@mri.tmd.ac.jp (K. Yoshida).

1874-9399/$ – see front matter © 2011 Elsevier B.V. All rights reserved.
doi:10.1016/j.bbagrm.2011.02.004

2.2. Construction of plasmids

PKCδ cDNA was cloned as described previously [17,18]. Evi-1 cDNA was amplified from U2OS cDNA using polymerase Pfu Ultra (Stratagene) and was cloned into pFLAG-CMV-5a (Sigma-Aldrich) and pEGFP-C1 (Clontech). Plasmids for luciferase assay were constructed as mentioned previously [16]. Briefly, the PLZF promoter region was first amplified by using the following primer set: 5′-AAAGTGGCATCTTCTCCCCAAA-3′ and 5′-TGGCTGCACAGCAGTTTGATAA-3′. P2 and P1 from the promoter region were then amplified by nested-PCR using the template obtained with the previous primer set. The nested-PCR was performed with the following forward primers: for P2 5′-GGCAGGTACCCGCGAGAGATT-GAGTATT-3′ and 5′-GTTTCTCGAGCCCAGATAAAGCAGCAGC-3′; for P1 5′-CTCTGGTACCTTTCCATCCTGCTTGTTT-3′, 5′-GTTTCTCGAGCCCAGA-TAAAGCAGCAGC-3′. These amplified DNA fragments were cloned into pGL3-Basic vector (Promega) resulting in P2-Luc and P1-Luc, respectively.

2.3. Cell transfection

Plasmid DNA was transfected by using FuGENE 6 transfection reagent (Roche). Validated PKCδ gene-specific siRNAs (short-interfering RNAs) and Evi-1 stealth siRNAs were purchased from Invitrogen (Stealth RNAi). The RNAi sequences are as follows:

PKCδ siRNA: 5′-CCAUCCACAAGAAAUGCAUCGACAA-3′,
Evi-1 siRNA: 5′-AUUGAAGCCAGAUUCUGAAGAGGGC-3′,
Evi-1 siRNA-a: 5′-AAUCAUUCACAGCUCCUGACACCGC-3′,
Evi-1 siRNA-b: 5′-UUUCGAGGCUCAGUCAGCUUUGUCC-3′.

Transfection of 50 nM siRNAs was performed using Lipofectamine RNAi MAX (Invitrogen) as according to the manufacturer's protocol.

2.4. Semi-quantitative RT-PCR analysis

Isolation of total RNA from cells was performed using TRIsure (Nippon Gene) according to the manufacturer's protocol. Total RNA (400 ng) was amplified using SuperScript III One Step RT-PCR System with Platinum Taq Kit (Invitrogen) according to the manufacturer's instruction.

2.5. Immunoblotting and immunoprecipitation

Cell lysates were prepared as described elsewhere [19,20]. Briefly, cultured cells were washed once with chilled PBS and resuspended in lysis buffer [50 mM Tris/HCl, pH 7.6, containing 150 mM NaCl, 10 mM NaF, 1 mM Na_3VO_4, 1 mM PMSF, 1 mM DTT (dithiothreitol), 10 μg/ml aprotinin, 1 μg/ml leupeptin, 1 μg/ml pepstatin A, and 1% (v/v) Tergitol NP-40]. Cell lysates were centrifuged at 12,500*g* for 10 min at 4 °C. Immunoprecipitation was performed by mixing cell lysates with Flag-tagged agarose (Sigma-Aldrich) or GFP-tagged agarose (Nacalai Tesque) for overnight with rotation at 4 °C. Western blotting was carried out by SDS/PAGE separation of the denatured cell lysates and transferred onto nitrocellulose membranes. The membranes were incubated with anti-Evi-1 (Santa Cruz Biotechnology), anti-PLZF (Santa Cruz Biotechnology), anti-tubulin (Sigma-Aldrich), anti-GFP (Nacalai Tesque), or anti-FLAG (Sigma-Aldrich) for 1–4 h at room temperature. After washing, the membranes were incubated with anti-rabbit or anti-mouse IgG–peroxidase conjugate (Santa Cruz Biotechnology). The antigen–antibody complexes were visualized by chemiluminescence (PerkinElmer).

2.6. In vitro luciferase assay

Luciferase activities were measured at 48 h post-transfection using the Bright-Glo Luciferase assay system (Promega) according to the manufacturer's protocol. The relative increase in activity compared with cells transfected with pGL-3 basic vector was determined as described [14,21].

2.7. Chromatin immunoprecipitation (ChIP) assay

ChIP was performed as previously described [15]. Briefly, 1–5 × 10^7 cells were fixed and sonicated. Sonicated cell mixture (50 μl) was used as input. Immunoprecipitation was performed with anti-PKCδ (Santa Cruz Biotechnology) or anti-Evi-1 (Cell Signaling) for 2 h or overnight at 4 °C before incubation with 30 μl of Protein A–Sepharose beads (Amersham) for 1 h at 4 °C. The beads were washed and chromatin complexes were eluted. DNA recovered from ChIP was blunt-ended with T4 DNA polymerase (Takara) before cloning into pBluescript SK vector. Sequencing was performed with T7 promoter and T3 promoter primers. For ChIP analysis, quantitative real-time PCR was performed by using SYBR Green PCR Master Mix (Applied Biosystems) according to the instruction manual. The data was normalized for the level of input control. Primer sequences are listed in Table 1.

2.8. Microarray analysis

Total RNA was isolated from cells using an RNeasy kit (Qiagen). Total RNA (5 μg) was used to start the protocol of One-Cycle cDNA Synthesis and to label cDNA, following the manufacturer's protocol (Affymetrix). Before making a cocktail solution, 20 μg of biotin-labeled cDNA was fragmented to 35–200 bases, and 15 μg of cDNA fragment was used to prepare the cocktail solution. The solution was applied into a GeneChip Human Genome U133 plus 2.0 array (Affymetrix) and hybridized for 16 h at 45 °C. After hybridization, the arrays were washed and stained using Fluidic station 450 according to the manufacturer's protocol, EukGE-WS2v5_450, and were then scanned using the Affymetrix GeneChip Scanner 3000. Analysis of the data was performed as previously described [22]. The complete expression datasets have been submitted to the online data repository ArrayExpress (http://www.ebi.ac.uk/microarray-as/ae/), under accession E-MEXP-2643.

2.9. Terminal deoxynucleotidyltransferase-mediated dUTP nick-end labeling (TUNEL) assays

Cells cultured in poly-D-lysine-coated eight-well chamber slides, at 5,000 cells per well, were transfected with siRNAs and then treated with ETO. Apoptotic cells were detected with DeadEnd Fluorometric TUNEL System (Promega) according to the manufacturer's instruction.

3. Results

3.1. Identification of Evi-1 as a PKCδ downstream target

In an attempt to identify transcription factors that are regulated by PKCδ, we embarked upon the ChIP-based cloning and sequencing

Table 1
Primers used for RT-PCR and ChIP assays.

	Primer sequences
GAPDH	Forward: 5′-AAGGCTGTGGGCAAGGTCATCCCT-3′ Reverse: 5′-TTACTCCTTGGAGGCCATGTGGGC-3′
Evi-1	Forward: 5′-TTCCTTCCGGCTTGTACCACAGGC-3′ Reverse: 5′-ACTTTCCAGATCAGAGCCGAGG-3′
PKCδ	Forward: 5′-ACGGCGCTGGAGAAATACG-3′ Reverse: 5′-CCTCTTTGGCTTCCTCACT-3′
PLZF	Forward: 5′-AGGCTGACGCTGTATTGAGC-3′ Reverse: 5′-TCTCAGCCGCAAACTATCCAG-3′
PLZFp (ChIP assay)	Forward: 5′-ACTGATACCCAGGTTTCCCTTAAA-3′ Reverse: 5′-AGAGCTATGTCCTTGGGTCCTG-3′
PLZFp-CR (ChIP assay)	Forward: 5′-AGCCACCACCTCCCAGGTT-3′ Reverse: 5′-AACTCCAGATTGCCACTGG-3′

approach (Fig. 1). Untreated or ADR-treated U2OS cells were harvested for ChIP assays performed with anti-PKCδ. Seventy-nine clones were sequenced and 58 unique sequences were obtained. To elicit molecular mechanism of PKCδ regulation in response to DNA damage, we examined PKCδ-mediated transcriptional control by microarray analysis (Fig. 1). U2OS cells were transfected with scrambled siRNA or PKCδ siRNA, then left untreated or treated with ADR. Total RNA was extracted and mRNA expression was analyzed with GeneChip system. The experiments set 4 conditions, i.e. I. scrambled siRNA-transfected cells; II. scrambled siRNA-transfected cells treated with ADR; III. siPKCδ-transfected cells; and IV. siPKCδ-transfected cells treated with ADR. To minimize the background noise and to amplify the true signals, expression data of transcripts from (II) was divided by that of (I) (II versus I in Fig. 1B). By applying 1.5 fold change as the cutoff value, 735 transcripts that were up-regulated by ADR treatment were discovered. Similarly, microarray data from (IV) was divided with that from (III) (IV versus III in Fig. 1), and resulted in 867 transcripts after selecting those with > 1.5 fold change. These transcripts represent that those were stimulated by ADR but not modulated by PKCδ. Comparison of the transcripts from II vs. I and IV vs. III revealed that, according to the gene ontology grouping of the genes, the molecules involved in a number of important pathways, particularly apoptosis, cell cycle and transcription factor activity were affected by ADR treatment in cells expressing PKCδ. The abundance of transcripts discovered here suggests that many molecules are regulated at transcriptional level in response to genotoxic stress. On the other hand, knocking down PKCδ alone altered gene expression in 527 transcripts when compared to the scrambled siRNA control sample (III versus I, Fig. 1), reflecting the importance of PKCδ in cellular homeostasis.

In order to map out PKCδ-mediated transcriptional control in apoptosis induction, we chose to focus on transcripts in apoptosis pathway. By eliminating PKCδ regulated apoptotic transcripts prior to ADR treatment, i.e. III vs. I, and non-PKCδ regulated apoptotic transcripts in response to DNA damage, i.e. IV vs. III, from ADR-stimulated apoptotic transcripts, i.e. II vs. I, we obtained 44 candidates from II vs. I–III vs. I–IV vs. III (Table 2). These represent PKCδ-mediated apoptosis associated genes identified upon DNA damage. Sequences of all the 44 genes obtained from microarray screen (I vs. II–I vs. III–III vs. IV) were entered into the database of Transcription Start Sites (DBTSS) (http://www.dbtss.hgc.jp), by using *H. sapiens* matrices, to predict the transcription start sites. The sequence from 1000 bp upstream to 200 bp downstream at the transcription start site of each gene was extracted as the promoter region. To search for potential transcription factors, promoter regions of 44 genes predicted from the microarray screen as well as the ChIP-sequence are served as binding sites in a quest for identification of candidate transcription factors. To achieve this, the sequences were compared to the transcription factor binding sites in the TRANSFAC database (http://www.biobaseinternational.com/pages/index.php?id=transfac) using MATCH program (http://www.gene-regulation.com/pub/program.html). The vertebrate matrices and the built-in matrix profile, with cutoff values adjusted to minimize false positives, were used here in the detection of the sites. The accumulative occurring counts for each of the putative transcription factors are listed in Table 3.

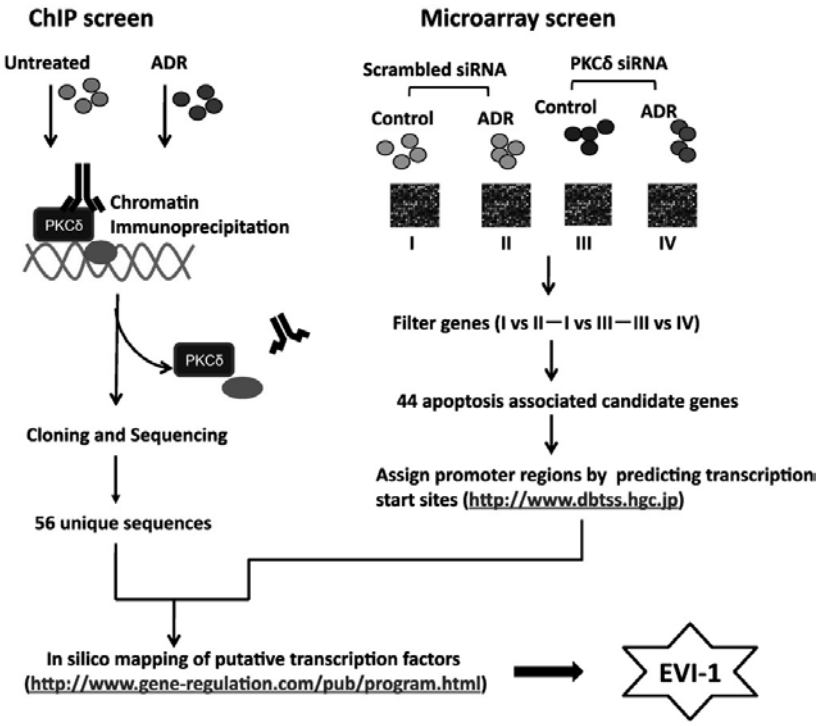

Fig. 1. Schematic representation of the screening strategy devised for uncovering PKCδ modulated transcription factors. ChIP was carried out from two pools of cells: untreated U2OS or ADR-treated U2OS cells. Immunoprecipitated DNA was treated for blunt-end to clone into pBluescript SK vector, yielding 58 clones with unique sequences. A total of 4 GeneChips were performed in microarray analysis, i.e. I. scrambled siRNA-transfected U2OS; II. scrambled siRNA-transfected and ADR-treated U2OS; III. PKCδ siRNA-transfected U2OS; IV. PKCδ siRNA-transfected and ADR-treated U2OS. The data indicate the means from three independent experiments, each performed in triplicate. Promoter regions of transcripts identified from I vs. II–I vs. III–III vs. IV were extracted from DBTSS database. For identification of PKCδ regulated transcription factor candidates, promoter regions extracted from DBTSS database as well as ChIP sequences were entered into TRANSFAC-Gene Transcription Factor Database for transcription factor prediction.

Table 2
Apoptotic genes identified from the microarray screen.

No.	Genes
1	SCIN: scinderin
2	STAT1: Signal transducer and activator of transcription 1, 91 kDa
3	PPP1R15A: protein phosphatase 1, regulatory (inhibitor) subunit 15A
4	CTNNAL1: catenin (cadherin-associated protein), alpha-like 1
5	BAG5: BCL2-associated athanogene 5
6	DAPK3: death-associated protein kinase 3
7	IFI6: interferon, alpha-inducible protein 6
8	APAF1: apoptotic peptidase activating factor
9	CD40: CD40 molecule, TNF receptor superfamily member 5
10	NRG2: neuregulin 2
11	GADD45B: growth arrest and DNA damage-inducible, beta
12	SNRK: SNF related kinase
13	TP53: tumor protein p53 (Li-Fraumeni syndrome)
14	CFLAR: CASP8 and FADD-like apoptosis regulator
15	BAG1: BCL2-associated athanogene
16	CD40: CD40 molecule, TNF receptor superfamily member 5
17	PPP1R13B: protein phosphatase 1, regulatory (inhibitor) subunit 13B
18	MRPS30: mitochondrial ribosomal protein S30
19	TNFRSF21: tumor necrosis factor receptor superfamily, member 21
20	FASTKD3: FAST kinase domains 3
21	CARD9: caspase recruitment domain family, member 9
22	IFT57: intraflagellar transport 57 homolog (Chlamydomonas)
23	NTN1: Netrin 1
24	SEC14L2: SEC14-like 2 (S. cerevisiae)
25	ANXA4: Annexin A4
26	APP: Amyloid beta (A4) precursor protein (peptidase nexin-II, Alzheimer disease)
27	SNRK: SNF related kinase
28	JMY: junction-mediating and regulatory protein
29	PSEN1: Presenilin 1 (Alzheimer disease 3)
30	BRE: Brain and reproductive organ-expressed (TNFRSF1A modulator)
31	HSPA9B: heat shock 70 kDa protein 9B (mortalin-2)
32	ATP2B4: ATPase, Ca++ transporting, plasma membrane 4
33	TRIAD3: TRIAD3 protein
34	CARD4: caspase recruitment domain family, member 4
35	BCAP29: B-cell receptor-associated protein 29
36	CASP2: caspase 2, apoptosis-related cysteine peptidase (neural precursor cell expressed, developmentally down-regulated 2)
37	37 EFHC1: EF-hand domain (C-terminal) containing 1
38	PRKCE: protein kinase C, epsilon
39	ATG5: ATG5 autophagy related 5 homolog (S. cerevisiae)
40	ZNF346: zinc finger protein 346
41	CCAR1: Cell division cycle and apoptosis regulator 1
42	ABP1: Amiloride binding protein 1 (amine oxidase (copper-containing))
43	TXNL1: Thioredoxin-like 1
44	RAF1: V-raf-1 murine leukemia viral oncogene homolog 1

Table 3
Transcription factors identified from ChIP-sequencing and microarray analysis.

Transcription factors predicted from ChIP analysis				Transcription factors predicted from microarray analysis		
Ranking	Transcription factor	Control*	ADR*	Ranking	Transcription factor	Count*
1	Oct-1	13	21	1	Pax-4	41
2	Evi-1	6	20	2	Oct-1	18
3	HNF-1	3	10	3	Nkx2-5	16
4	HNF-4	2	7	4	FOXD3	12
5	FOXJ2	5	6	5	Evi-1	11
6	FOXD3	9	6	6	Pax-6	10
7	Nkx2-5	1	6	7	COMP1	9
8	COMP-1	2	5	8	Elk-1	9
9	Pax-6	13	5	9	USF	8
10	Cart-1	0	4	10	v-Myb	7
11	v-Maf	0	4	11	Hand1/E4	6
12	CDP CR1	1	4	12	HNF-1	6
13	NF-Y	0	3	13	HNF-3beta	6
14	AP-1	2	3	14	HNF-4	6
15	Hand1/E4	2	3	15	YY1	5
16	HNF-3beta	2	3	16	c-Ets-1	4
17	Pax-4	5	3	17	c-Rel	4
18	CCAAT	0	2	18	FOXJ2	4
19	GATA-3	0	2	19	MyoD	4
20	Gfi-1	0	2	20	v-Maf	4
21	MyoD	0	2	21	CCAAT box	3
22	USF	0	2	22	CDP CR1	3
23	Myogenin	1	1	23	CREB	3
24	NF-kappa	2	0			
25	C/EBP	3	0			

* The numbers indicate the accumulative counts for each transcription factor listed.

Based on these results, Oct-1 was revealed as an attractive candidate since it was ranked top in the ChIP list and 2nd in the microarray list. However, Evi-1, though ranked 5th in the microarray screen, emerged as the most promising candidate because the in silico mining of the ChIP screen revealed that accumulative appearance count of Evi-1 was as many as 20 times from ADR-treated samples, in contrast to only 6 times from untreated samples (Table 3).

3.2. DNA damage triggers PKCδ activation of Evi-1 to increase transcription of PLZF

To verify the screening results, we first conducted luciferase reporter assay to study the mode of PKCδ regulation on transcription of Evi-1. Evi-1 has been previously reported to activate transcription of PLZF [16]. We utilized 128 and 158 bp upstream of the PLZF promoter region to generate two reporter constructs and denoted them as P1-Luc and P2-Luc, respectively (Fig. 2A). P1-Luc but not P2-Luc lacks the Evi-1 like promoter binding region, which shares 8 out of 10 matches to the Evi-1 consensus, GACAAGATAA [16,23]. U2OS cells were co-transfected with the luciferase reporter constructs, P1-Luc, P2-Luc or a vector control with Flag-Evi-1. DMSO or rottlerin pretreated U2OS cells were left untreated or treated with ADR for 8 h before the luciferase activities of the promoters were measured. Expression of Evi-1 was significantly associated with the increase the promoter activity in response to DNA damage (Fig. 2B). Consistent with our finding that PKCδ plays a role in

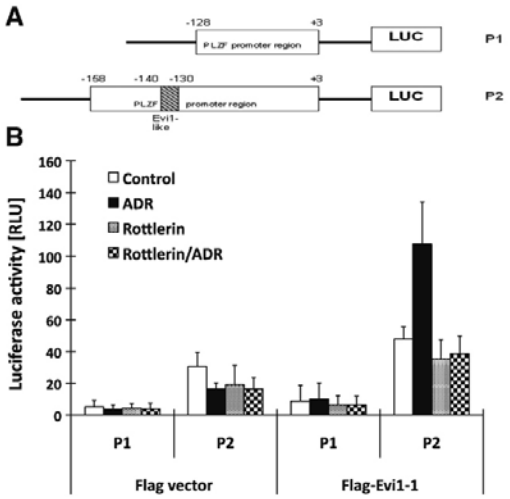

Fig. 2. PKCδ up-modulates Evi-1 activation to transactivate PLZF after DNA damage. (A) Schematic depiction of the PLZF promoter-driven luciferase reporter constructs, P1 and P2. (B) U2OS cells transiently co-transfected with Flag vector or Flag-Evi-1 and the luciferase vector pGL3, or the luciferase reporter constructs P1 or P2, as described in (A), for 48 h. Cells were then pretreated with rottlerin for 1 h followed by ADR for 8 h. Luciferase activity was measured and averaged from three independent experiments performed. The relative fold increase in luciferase activity (RLU; relative light unit) was calculated by dividing the luciferase readings of the transfected or treated cells to those of mocked-control cells.

activation of Evi-1 transcription activity upon induction of DNA damage, the luciferase promoter activities were markedly suppressed in rottlerin-treated cells. These results suggest that PKCδ kinase activity is required for Evi-1 to transactivate PLZF and this transcription is stimulated by DNA damage caused by ADR treatment. The specificity of the 158 bp PLZF promoter clone, P2-Luc, in which the Evi-1-like promoter binding site can be located, is evidenced because, in concert to reported finding, the P1-Luc showed little activity because it does not contain relevant binding site. Note that the difference of the luciferase promoter activity profile in the vector-transfected cells compared to the Evi-1-overexpressing cells is most probably due to unspecific promoter activity caused by genes other than the endogenous Evi-1 in the cells. ChIP screening results also indicate that PKCδ might interact directly with Evi-1. Indeed, the immunoprecipitation performed in U2OS expressing Flag-tagged PKCδ and GFP-tagged Evi-1 confirmed the binding of PKCδ and Evi-1, both in undisturbed and ADR-stimulated cells (Fig. 3A).

To further ascertain that Evi-1 is a bona fide PKCδ regulatory substrate, we investigated the in vivo transcription activity of Evi-1 through ChIP assay on the PLZF at the Evi-1-like promoter site. U2OS was transiently transfected with scrambled siRNA or PKCδ siRNA and either left untreated or treated with ADR. The chromatin–protein complexes were then immunoprecipitated with anti-Evi-1 or control IgG antibody at 4 °C overnight. Immunoprecipitated DNA was collected, denatured and analyzed by real-time PCR using primer set that amplifies the Evi-1-like promoter region. In accordance with the luciferase reporter assay results, quantification of ChIP performed with anti-Evi-1 clearly demonstrates, in contrast to the untreated cells, a substantial increase in occupancy of Evi-1to the Evi-1-like promoter region in PLZF following DNA damage (Fig. 3B). Moreover, the binding of Evi-1 to the PLZF promoter region was suppressed in ADR-treated cells silenced for PKCδ, less than half of that found in ADR-treated mock cells, demonstrating that PKCδ is required for the Evi-1 to transcriptionally control PLZF expression in response to ADR. While anti-IgG ChIP and control region (CR) enrichments were higher in ADR and si-PKCδ /ADR cells compared to their respective untreated controls, it is conceivable that the anti-Evi-1 ChIP enrichments in those cells were profound enough to suggest that the elevation of Evi-1 binding to the PLZF promoter is significant. Subsequently, as PKCδ and Evi-1 form a protein complex, we also investigated PKCδ binding

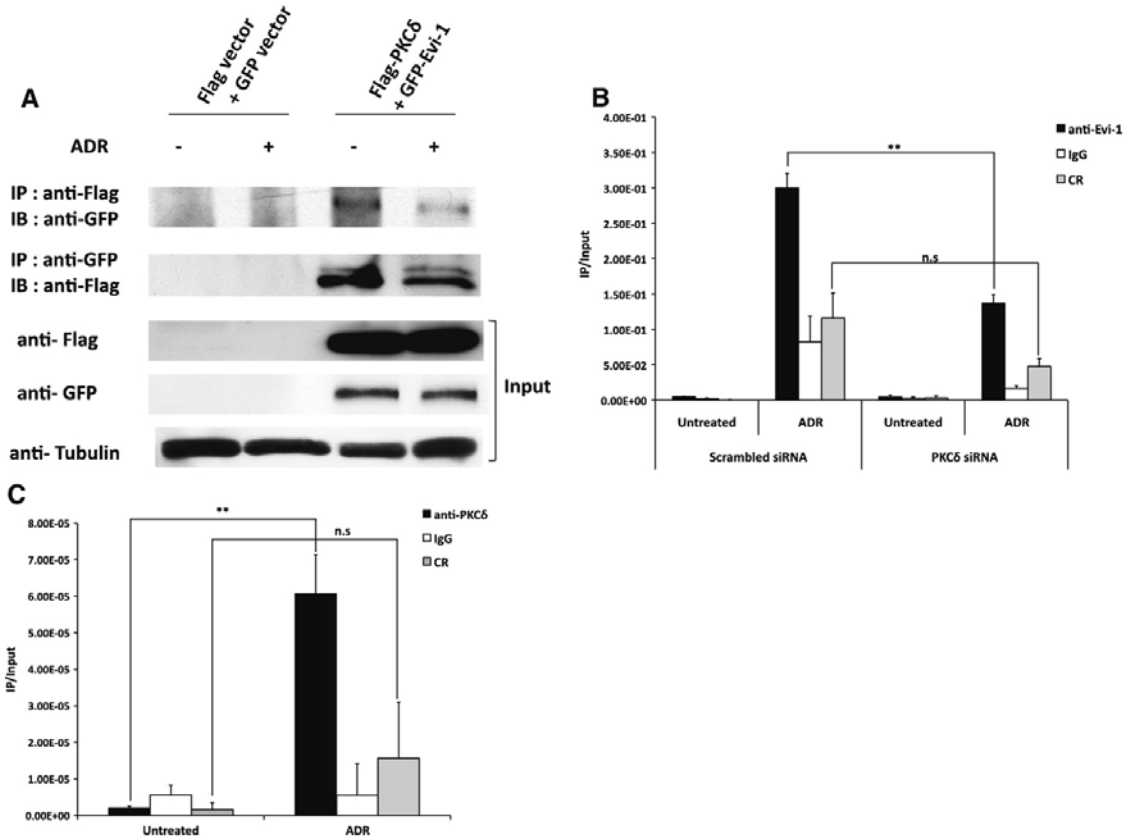

Fig. 3. Evi-1 transcription control on PLZF is elevated by PKCδ upon DNA damage induction. (A) GFP-Evi-1 and Flag-PKCδ were ectopically expressed in U2OS cells. Cell lysates from untreated or ADR-treated cells were immunoprecipitated with anti-GFP or anti-Flag agarose. The pull-down beads were examined with SDS-PAGE for immunoblotting with anti-GFP, anti-Flag, or anti-tubulin. (B) U2OS cells treated with scrambled siRNA or siPKCδ and were left untreated, or were treated with 10 μg/mL ADR for 8 h. Cells were harvested, fixed, and sonicated. ChIP was performed with anti-Rabbit Evi-1 or anti-Rabbit IgG and quantification of ChIP by was carried out by real-time PCR analysis. Primer pair used in real-time PCR was designed as according to [16] to amplify −264 to −36 from PLZF promoter region that contains the Evi-1like promoter sequence. A negative control region of the Evi-1 promoter (CR; −1203 to −899 upstream of PLZF promoter) was also examined. IP/Input is calculated as a ratio of the real-time PCR amplifications from the ChIP products to the real-time PCR expression level of the inputs, which represent amplification of total chromatin before immunoprecipitation. Results are representative of three experiments each performed in triplicate. $^{**}P<0.05$, n.s. not significant. (C) U2OS cells were left untreated or treated with ADR and ChIP with anti-PKCδ was performed as described above.

to the promoter region of PLZF. Anti-PKCδ ChIP in Fig. 3C indicates stimulated binding of PKCδ to the Evi-1 like promoter in PLZF after genotoxic stress induction, whereas neither the IgG ChIP nor amplification of CR exhibited similar trends. Consequently, these results strongly argue that Evi-1 is recruited to the Evi-1-like binding site on the PLZF promoter only when PKCδ is fully functional and DNA damage is incurred.

3.3. PLZF is up-regulated by PKCδ acting through EVI-1 upon DNA damage

We first tested Evi-1 siRNA for its specificity by comparing the knockdown efficiency of Evi-1 siRNA with two other Evi-1 siRNAs, Evi-1 siRNA-a, and Evi-1 siRNA-b. As demonstrated in Fig. 4A, Evi-1siRNA attenuated Evi-1 expression significantly compared to the other two siRNAs. Importantly, the PLZF mRNA changes are parallel to the reduction of Evi-1 expression caused by different siRNA, suggesting that Evi-1 specifically regulates PLZF expression. To further clarify whether Evi-1transactivates PLZF, U2OS cells were transfected with scrambled siRNA or Evi-1 siRNA. Cells were then treated with rottlerin for 1 h followed by ADR for 8 h. PLZF mRNA decreased in Evi-1-depleted cells, proving that knockdown of Evi-1 affects PLZF transcription (Fig. 4B). In contrast, ADR-stimulated mRNA expression of PLZF in both mock and si-Evi-1 cells. Inhibiting PKCδ affects Evi-1 expression as both Evi-1 mRNA and protein levels declined (Fig. 4B and C), denoting PKCδ-dependent regulatory control on Evi-1. Intriguingly, Evi-1 mRNA changes did not coincide well with the alterations in protein abundance, except in rottlerin/ADR cells, in which both mRNA and protein expressions were significantly down-regulated. Specifically, the gain in Evi-1 mRNA caused by addition of ADR was not reflected in the protein. To determine whether knocking down PKCδ also affects Evi-1 transcriptional control of PLZF in the same way as rottlerin, we examined mRNA of Evi-1 in cells by transfecting U2OS with scrambled siRNA or PKCδ siRNA and treating them with or without ADR for 8 h. The analysis of RT-PCR demonstrated that, in accordance to our luciferase reporter and ChIP assays, PLZF mRNA is up-regulated after ADR exposure (Fig. 4C). This indicates that PLZF is transactivated in response to ADR. ADR or ETO administration resulted in PLZF protein augmentation (Fig. 4C). Furthermore, incurring DNA damage in PKCδ-silenced cells led to repression of PLZF protein expression. Taken together, these findings strongly demonstrate that the PKCδ-dependent PLZF regulation by Evi-1 is a specific pathway that is geared towards DNA damage response.

3.4. PKCδ administers apoptosis through activation of Evi-1 transcription acting on PLZF upon DNA damage

As apoptotic role for PKCδ on DNA damage has been well established in U2OS cells [15], we proposed that Evi-1 is a PKCδ-modulated substrate that is involved in PKCδ-mediated cell death. U2OS cells transfected with scrambled siRNA or PKCδ siRNA were co-transfected with Flag vector or Flag-Evi-1. The cells were also left untreated or treated with ETO, a DNA damage agent that works similarly to ADR, for 24 h. As expected, depletion of PKCδ significantly abrogated DNA damaged incurred apoptosis (Fig. 5A). More importantly, cells co-transfected with PKCδ siRNA and Flag-Evi-1exhibited almost 4-fold reduction in number of TUNEL positive cells when compared to the percent apoptosis found in cells overexpressing Flag- Evi-1 alone (Fig. 5A). This impairment on apoptosis implies that PKCδ activity is required for Evi-1 to maneuver cell death events. Apoptosis percentage in cells expressing ectopic Evi-1 increased to nearly two-fold in the control cells, signifying a role for Evi-1 in apoptosis regulation. Thus these results strongly suggest that Evi-1 is the effector involved in PKCδ-incurred apoptosis mechanism in response to genotoxic stress. To define further the functional significance of PKCδ on Evi-1 transcription regulation, we sought to investigate apoptotic event in Evi-1-silenced cells following DNA damage. TUNEL assays were performed on U2OS cells transiently transfected with scrambled siRNA or Evi-1 siRNA, followed by treatment with or without ETO for 24 h. The results demonstrated that depletion of Evi-1 greatly suppressed induction of apoptosis to about 8 fold compared to that found in ETO-treated mock cells (Fig. 5B). As an attempt to clarify the biological role of PLZF up-regulation in response to genotoxin, PLZF was ectopically expressed in U2OS cells. TUNEL assay was carried out after ETO treatment for 24 h. PLZF overexpression led to two-fold increment in DNA damage triggered apoptosis (Fig. 5C). This observation strongly indicates that PLZF enhances genotoxic stress-induced apoptosis.

4. Discussion

ChIP assay is a powerful tool used widely to uncover transcription targets [24]. In addition to ChIP, microarray analysis can be also used to search for potential transcriptional regulated molecule by examining gene expressions. Both ChIP and microarray use a whole genome-wide analysis approach that yields such an abundance of data so that data mining becomes a necessity. We had made use of the bioinformatics tools available on the web to mine the data that generated from ChIP and microarray screens in order to identify the true target of PKCδ in response to DNA damage induced apoptosis. In addition, the strategy here involved the comparison of both screening results to add confidence to the final target examined such as Evi-1.

Evi-1 is a nuclear transcription factor that encodes 1051 amino acids [25]. It is comprised of 10 zinc finger motifs in 2 zinc finger domains, with 7 located at the N-terminal domain while the other 3 at the C-terminal domain. It can act as transcription activator or repressor, both through its conserved GACAAGATA DNA binding sequence [23,26]. Deviant overexpression due to chromosomal rearrangement of Evi-1, t(3;21)(q26;q22), was found in human acute myeloid leukemia, myelodysplastic syndrome, and chronic myelogenous leukemia. In this context, it has been labeled as a proto-oncogene [27]. Furthermore, several reports have narrated role of Evi-1 as an important regulator in embryogenesis and differentiation [28–30]. In contrast to studies that showed that Evi-1 confers proliferative and survival advantages, our results have demonstrated Evi-1 as an apoptotic molecule. However, our report is not unique since accelerated apoptosis was observed in murine bone marrow 10–12 months after ectopic expression of Evi-1 [31]. Furthermore, forced expression of Evi-1 has been also demonstrated to elevate cell death in human myeloid cells [32]. Subsequently, Goyama and co-workers had noted that deletion of Evi-1 increased cell death in haematopoietic stem cells (HSC) from fetal liver but HSC from bone marrow of mice displayed no change in apoptosis after knocking out Evi-1 [28]. This data thus strongly argues that exhibition of apoptotic role for Evi-1 is context-dependent. More importantly, recent published work has illustrated that overexpressed Evi-1 in Rat1 fibroblast stimulated apoptosis upon treatment with H_2O_2 by suppressing carbonic anhydrase III transcription, while conferring resistance to paclitaxel-induced apoptosis [33]. This suggests that, depending on the nature of the stimuli, Evi-1 can response to DNA damage as a positive cell death regulator. Apoptosis was markedly impaired in Evi-1 silenced ETO-treated cells (Fig. 5B), whereas ectopic Evi-1 expression aggravated the apoptotic events in ETO affected cells (Fig. 5A). Collectively, these inspections propose an apoptotic role of Evi-1 in U2OS cells.

Our findings also manifest a PKCδ-dependent Evi-1 transactivation of PLZF (Figs. 3B and 4). Interestingly, Evi-1 enrichment in PKCδ knocked down cells is higher than expected (Fig. 3B). The Evi-1 amplification in si-PKCδ transfected cells probably reflects the activity of the residual PKCδ in the cells. However, it is highly plausible that this excessive Evi-1 enrichment in PKCδ depleted cells suggests the presence of a PKCδ-independent Evi-1 activation mechanism in response to ADR stress.

H.C. Hew et al. / Biochimica et Biophysica Acta 1809 (2011) 285–294 291

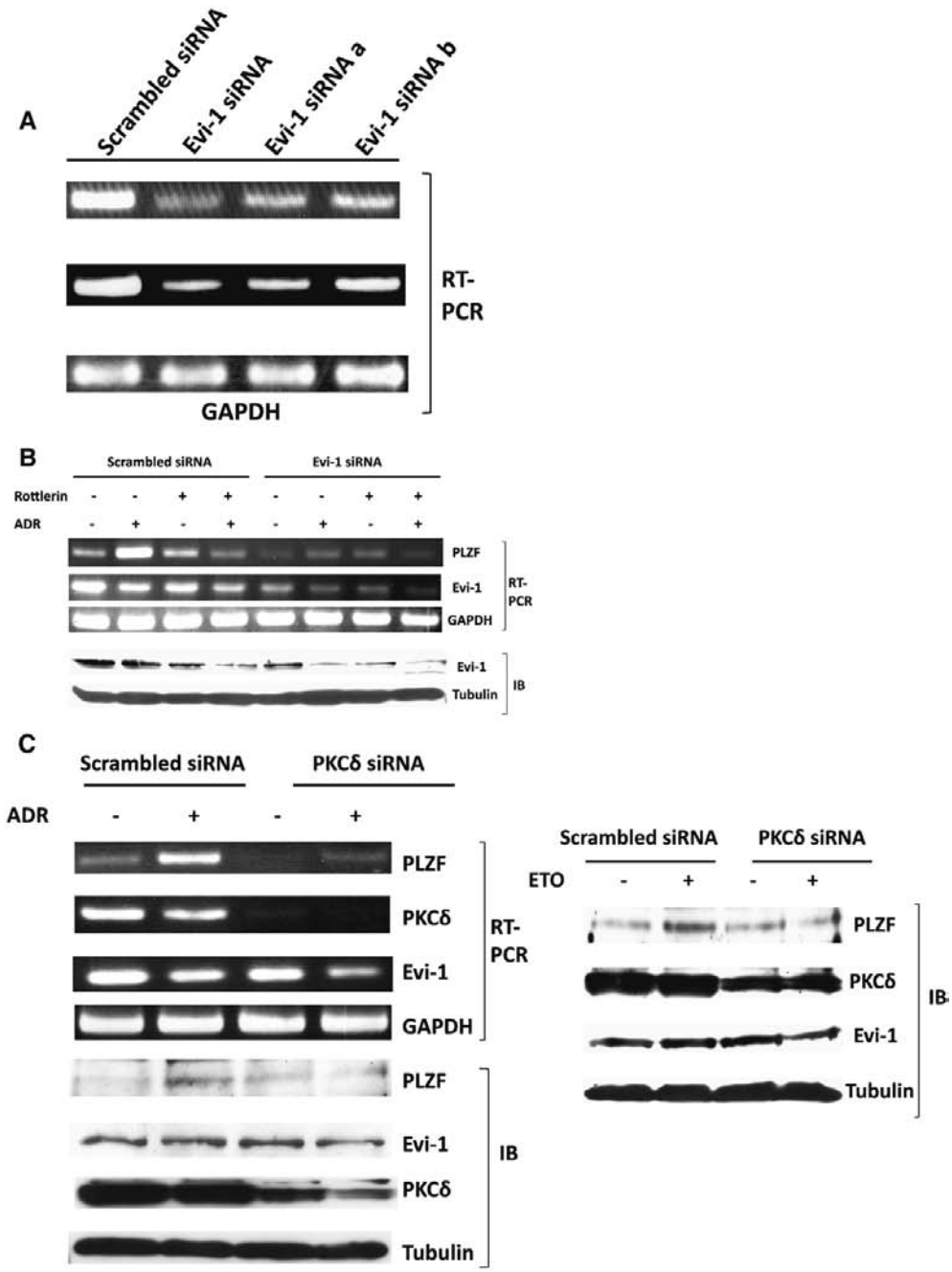

Fig. 4. PLZF transcription increases due to PKCδ regulated Evi-1 activation in response to DNA damage. (A) U2OS cells transfected with Evi-1 siRNA, Evi-1 siRNA-a, or Evi-1 siRNA-b were collected for RT-PCR with PLZF and GAPDH primers. (B) U2OS cells were transiently transfected with scrambled siRNA or Evi-1 siRNA. Cells were pretreated with or without rottlerin for 1 h and left untreated or treated with ADR for 8 h. Cells were collected for RT-PCR with PLZF and GAPDH primers or subjected to SDS-PAGE examined with anti-Evi-1 and anti-tubulin. (C) U2OS was transfected with scrambled siRNA or PKCδ siRNA and left untreated or treated with ADR (right panels) or ETO (left panels) for 8 h. Cells were harvested for Western blot analyzed with anti-Evi-1, anti-PKCδ, anti-PLZF, and anti-tubulin or were extracted for total RNA for RT-PCR using PLZF, PKCδ and GAPDH primer pairs (left panels).

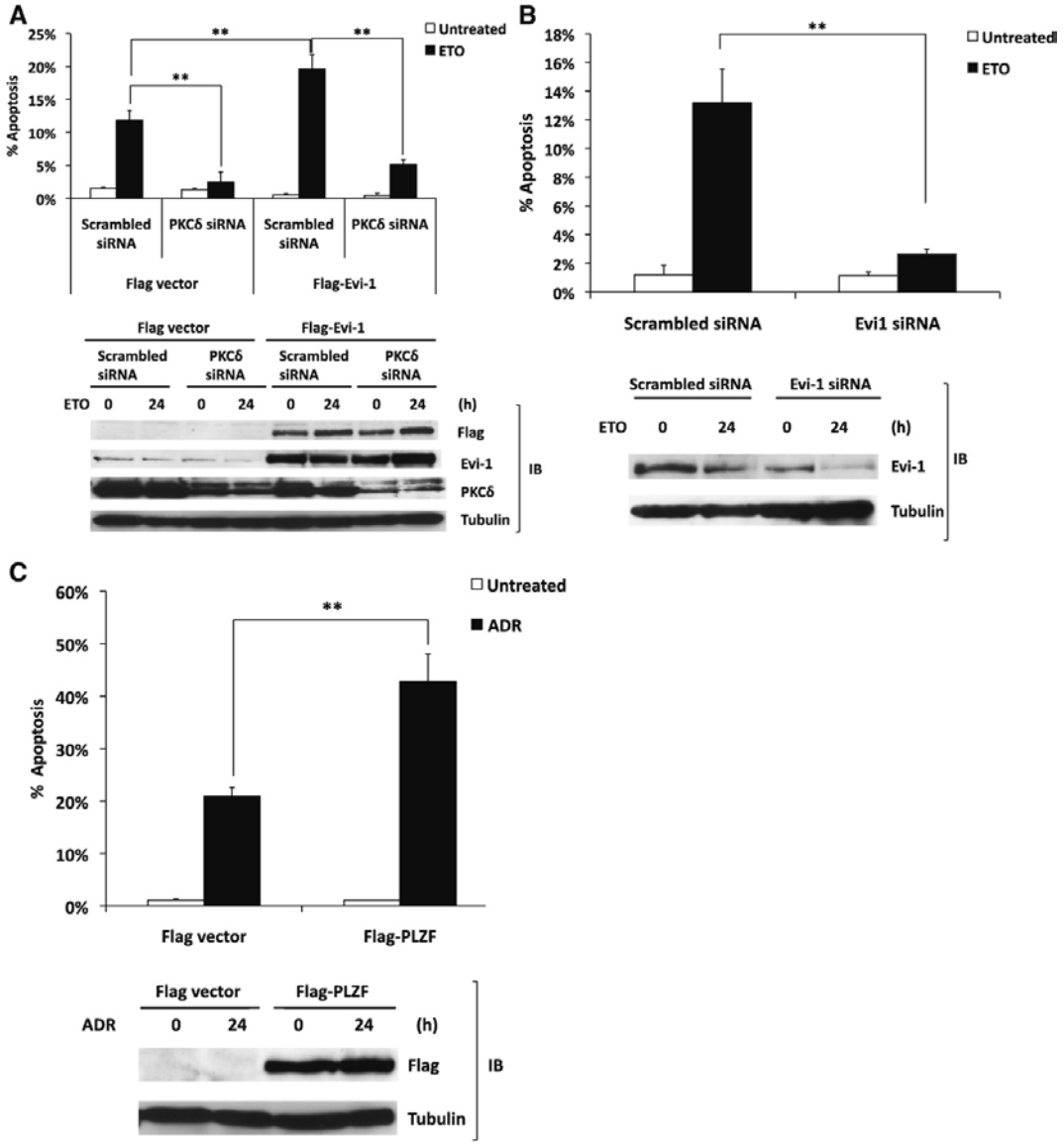

Fig. 5. Evi-1 and PLZF induces DNA damage dependent apoptosis. U2OS cells were transfected with scrambled siRNA or PKCδ siRNA together with Flag vector or Flag-Evi-1 (A); scrambled siRNA or Evi-1 siRNA (B); Flag vector or Flag-PLZF (C) and were then left untreated or were treated with 10 μM ETO for 24 h. The percentage of apoptotic cells was determined by TUNEL assays. The results are represented as means ± S.D. obtained from three fields of 100–300 cells each conducted three independent experiments. $^{**}P<0.05$. Cell lysates were applied in Western blot analyses with indicated antibodies.

PLZF, a transcription repressor, is a member of the poxvirus and zinc finger (POZ)-zinc finger proteins, with an N-terminal POZ, also known as Broad complex/Tramtrack/Bric-a-brac domain, and nine C2-H2 zinc finger motifs at the C-terminal [34]. The chromosomal translocation of PLZF at t(11;17)(q23;q21) results in the formation of PLZF-RARα complex, which has been accounted for carcinogenesis of acute promyelocytic leukemia [34,35]. This fusion product was found to stimulate transcription of cyclin A2, a PLZF target gene, to allow transformation of NIH3T3 cells [36]. PLZF has been implicated in cell differentiation and proliferation as well as stem cells maintenance [37–41]. Importantly, the apoptotic role of PLZF has been reported [42–44]. Suppression of PLZF expression in melanoma, B-cell chronic lymphocytic leukemia and mesothelioma implies tumor-suppressing function for PLZF [42–44]. In addition, PLZF interacts and represses cyclin A2 transcription, inhibiting growth in myeloid cells, while PLZF-RARα induces transformation of NIH3T3 cells [36]. Moreover,

observation from PLZF$^{-/-}$ mice suggests that severe limb and skeleton deformations was the consequence of dysregulation of apoptosis due to absence of PLZF, hereby affecting bone development during embryogenesis [41]. Finally, overexpression of PLZF incurred growth inhibition in 32Dcl3 cells [45], U937 cells [46], and Jurkat cells [47]. Regulation of PLZF by Evi-1 was previously manifested in leukemic cells by investigating transcriptional modulation of Evi-1 on PLZF through EMSA, ChIP, and reporter assays [16]. However, the authors did not detect corresponded transcriptional change of PLZF mRNA caused by Evi-1 regulation. In contrast to their finding, we showed for the first time that PLZF mRNA expression is induced accordingly by Evi-1 transcriptional activation. As Evi-1 protein expression did not alter in control or ADR-treated cells (Fig. 4B and C), we deduce that PKCδ most likely plays a key role in post-translational modification of Evi-1 to initiate PLZF transcription.

As depicted in Fig. 6, we have identified a novel apoptosis mechanism regulated by PKCδ that involves Evi-1 transactivation of PLZF to trigger DNA damage apoptosis. As Evi-1 is a nuclear transcription factor, it is thus conceivable that generation of PKCδ catalytic fragment by after DNA damage is required for Evi-1 to transactivate PLZF. Evi-1 mRNA was slightly suppressed by either the inhibition or knockdown of PKCδ in non-treated cells (Fig. 4B and C). While ADR down-regulated Evi-1 transcription, depletion of PKCδ induced further repression of Evi-1 mRNA upon ADR treatment. Collectively, these observations suggest that PKCδ might exert certain degree of transcriptional regulation on Evi-1. Intriguingly, Evi-1 mRNA alterations in both ADR-treated cells and PKCδ-depleted cells were not reflected in their corresponded Evi-1 protein expressions. A plausible explanation is that Evi-1 could have undergone post-translational modification change, which then affects its detection by the antibody. Given that Evi-1 acetylation by PCAF or CREB (cAMP-response element-binding protein) binding protein had been demonstrated before [48] and possible Evi-1 phosphorylation of Evi-1 by ATM or ATR due to DNA damage signal had also been previously reported [49], PKCδ might activate Evi-1-PLZF transcription through protein modification. Interestingly, PKCδ is capable of phosphorylating p300, which associates with PCAF, to impair p300 histone acetyltransferase activity. Consequently, unraveling the interactions among these players would provide insights to how PKCδ directs the regulation of Evi-1 in response to DNA damage.

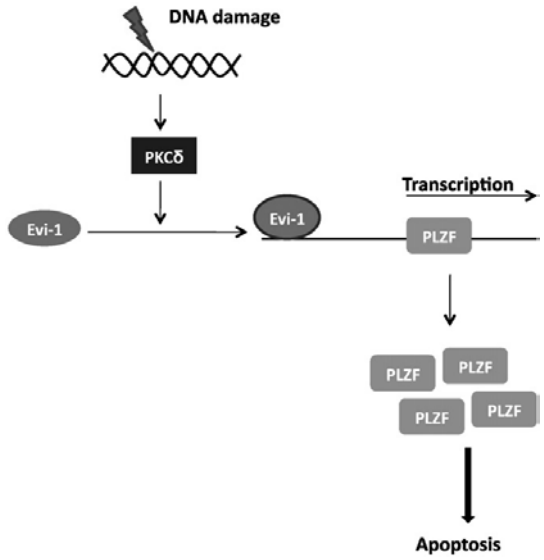

Fig. 6. Proposed model for PKCδ regulation of Evi-1. Upon DNA damage, PKCδ is activated by various modifications such as tyrosine phosphorylation or proteolytic cleavage. PKCδ activates Evi-1 to transactivate PLZF. Genotoxic stress-induced Evi-1 functions as an apoptotic factor to enhance apoptotic cell death.

Acknowledgements

We would like to thank Dr. Takashi Ueda for his help. This work was supported by grants from the Ministry of Education, Science and Culture of Japan (to K.Y. and Y.M.), Takeda Science Foundation (to K.Y.), Kowa Life Science Foundation (to K.Y.), Sankyo Foundation of Life Science (to K.Y.), Sato Memorial Foundation for Cancer Research (to K.Y.), and The Ichiro Kanehara Foundation (to K.Y.).

References

[1] M. Gschwendt, Protein kinase C delta, Eur. J. Biochem. 259 (1999) 555–564.
[2] W. Li, H. Mischak, J.C. Yu, L.M. Wang, J.F. Mushinski, M.A. Heidaran, J.H. Pierce, Tyrosine phosphorylation of protein kinase C-delta in response to its activation, J. Biol. Chem. 269 (1994) 2349–2352.
[3] D.N. Jackson, D.A. Foster, The enigmatic protein kinase Cdelta: complex roles in cell proliferation and survival, FASEB J. 18 (2004) 627–636.
[4] S.F. Steinberg, Distinctive activation mechanisms and functions for protein kinase Cdelta, Biochem. J. 384 (2004) 449–459.
[5] Y. Emoto, Y. Manome, G. Meinhardt, H. Kisaki, S. Kharbanda, M. Robertson, T. Ghayur, W.W. Wong, R. Kamen, R. Weichselbaum, et al., Proteolytic activation of protein kinase C delta by an ICE-like protease in apoptotic cells, EMBO J. 14 (1995) 6148–6156.
[6] T. Ghayur, M. Hugunin, R.V. Talanian, S. Ratnofsky, C. Quinlan, Y. Emoto, P. Pandey, R. Datta, Y. Huang, S. Kharbanda, H. Allen, R. Kamen, W. Wong, D. Kufe, Proteolytic activation of protein kinase C delta by an ICE/CED 3-like protease induces characteristics of apoptosis, J. Exp. Med. 184 (1996) 2399–2404.
[7] Z.M. Yuan, T. Utsugisawa, T. Ishiko, S. Nakada, Y. Huang, S. Kharbanda, R. Weichselbaum, D. Kufe, Activation of protein kinase C delta by the c-Abl tyrosine kinase in response to ionizing radiation, Oncogene 16 (1998) 1643–1648.
[8] X. Sun, F. Wu, R. Datta, S. Kharbanda, D. Kufe, Interaction between protein kinase C delta and the c-Abl tyrosine kinase in the cellular response to oxidative stress, J. Biol. Chem. 275 (2000) 7470–7473.
[9] A. Bharti, S.K. Kraeft, M. Gounder, P. Pandey, S. Jin, Z.M. Yuan, S.P. Lees-Miller, R. Weichselbaum, D. Weaver, L.B. Chen, D. Kufe, S. Kharbanda, Inactivation of DNA-dependent protein kinase by protein kinase Cdelta: implications for apoptosis, Mol. Cell. Biol. 18 (1998) 6719–6728.
[10] J. Liu, J. Chen, Q. Dai, R.M. Lee, Phospholipid scramblase 3 is the mitochondrial target of protein kinase C delta-induced apoptosis, Cancer Res. 63 (2003) 1153–1156.
[11] T. Cross, G. Griffiths, E. Deacon, R. Sallis, M. Gough, D. Watters, J.M. Lord, PKC-delta is an apoptotic lamin kinase, Oncogene 19 (2000) 2331–2337.
[12] K. Yoshida, H.G. Wang, Y. Miki, D. Kufe, Protein kinase Cdelta is responsible for constitutive and DNA damage-induced phosphorylation of Rad9, EMBO J. 22 (2003) 1431–1441.
[13] K. Yoshida, H. Liu, Y. Miki, Protein kinase C delta regulates Ser46 phosphorylation of p53 tumor suppressor in the apoptotic response to DNA damage, J. Biol. Chem. 281 (2006) 5734–5740.
[14] T. Yamaguchi, Y. Miki, K. Yoshida, Protein kinase C delta activates IkappaB-kinase alpha to induce the p53 tumor suppressor in response to oxidative stress, Cell. Signal. 19 (2007) 2088–2097.
[15] H. Liu, Z.G. Lu, Y. Miki, K. Yoshida, Protein kinase C delta induces transcription of the TP53 tumor suppressor gene by controlling death-promoting factor Btf in the apoptotic response to DNA damage, Mol. Cell. Biol. 27 (2007) 8480–8491.
[16] S. Takahashi, J.D. Licht, The human promyelocytic leukemia zinc finger gene is regulated by the Evi-1 oncoprotein and a novel guanine-rich site binding protein, Leukemia 16 (2002) 1755–1762.
[17] K. Yoshida, D. Kufe, Negative regulation of the SHPTP1 protein tyrosine phosphatase by protein kinase C delta in response to DNA damage, Mol. Pharmacol. 60 (2001) 1431–1438.
[18] K. Yoshida, T. Yamaguchi, H. Shinagawa, N. Taira, K.I. Nakayama, Y. Miki, Protein kinase C delta activates topoisomerase IIalpha to induce apoptotic cell death in response to DNA damage, Mol. Cell. Biol. 26 (2006) 3414–3431.
[19] K. Yoshida, S. Kharbanda, D. Kufe, Functional interaction between SHPTP1 and the Lyn tyrosine kinase in the apoptotic response to DNA damage, J. Biol. Chem. 274 (1999) 34663–34668.
[20] K. Yoshida, Y. Miki, D. Kufe, Activation of SAPK/JNK signaling by protein kinase Cdelta in response to DNA damage, J. Biol. Chem. 277 (2002) 48372–48378.
[21] T. Yamaguchi, J. Kimura, Y. Miki, K. Yoshida, The deubiquitinating enzyme USP11 controls an IkappaB kinase alpha (IKKalpha)-p53 signaling pathway in response to tumor necrosis factor alpha (TNFalpha), J. Biol. Chem. 282 (2007) 33943–33948.
[22] J. Kimura, S.T. Nguyen, H. Liu, N. Taira, Y. Miki, K. Yoshida, A functional genome-wide RNAi screen identifies TAF1 as a regulator for apoptosis in response to genotoxic stress, Nucleic Acids Res. 36 (2008) 5250–5259.

[23] K. Morishita, K. Suzukawa, T. Taki, J.N. Ihle, J. Yokota, EVI-1 zinc finger protein works as a transcriptional activator via binding to a consensus sequence of GACAAGATAAGATAAN1-28 CTCATCTTC, Oncogene 10 (1995) 1961–1967.
[24] P. Collas, The current state of chromatin immunoprecipitation, Mol Biotechnol, 45:87–100.
[25] K. Morishita, D.S. Parker, M.L. Mucenski, N.A. Jenkins, N.G. Copeland, J.N. Ihle, Retroviral activation of a novel gene encoding a zinc finger protein in IL-3-dependent myeloid leukemia cell lines, Cell 54 (1988) 831–840.
[26] S. Buonamici, S. Chakraborty, V. Senyuk, G. Nucifora, The role of EVI1 in normal and leukemic cells, Blood Cells Mol. Dis. 31 (2003) 206–212.
[27] K. Mitani, S. Ogawa, T. Tanaka, H. Miyoshi, M. Kurokawa, H. Mano, Y. Yazaki, M. Ohki, H. Hirai, Generation of the AML1-EVI-1 fusion gene in the t(3;21)(q26;q22) causes blastic crisis in chronic myelocytic leukemia, EMBO J. 13 (1994) 504–510.
[28] S. Goyama, G. Yamamoto, M. Shimabe, T. Sato, M. Ichikawa, S. Ogawa, S. Chiba, M. Kurokawa, Evi-1 is a critical regulator for hematopoietic stem cells and transformed leukemic cells, Cell Stem Cell 3 (2008) 207–220.
[29] P.R. Hoyt, C. Bartholomew, A.J. Davis, K. Yutzey, L.W. Gamer, S.S. Potter, J.N. Ihle, M.L. Mucenski, The Evi1 proto-oncogene is required at midgestation for neural, heart, and paraxial mesenchyme development, Mech. Dev. 65 (1997) 55–70.
[30] H. Kazama, T. Kodera, S. Shimizu, H. Mizoguchi, K. Morishita, Ecotropic viral integration site-1 is activated during, and is sufficient for, neuroectodermal P19 cell differentiation, Cell Growth Differ. 10 (1999) 565–573.
[31] S. Buonamici, D. Li, Y. Chi, R. Zhao, X. Wang, L. Brace, H. Ni, Y. Sauntharajah, G. Nucifora, EVI1 induces myelodysplastic syndrome in mice, J. Clin. Invest. 114 (2004) 713–719.
[32] T.A. Konrad, A. Karger, H. Hackl, I. Schwarzinger, I. Herbacek, R. Wieser, Inducible expression of EVI1 in human myeloid cells causes phenotypes consistent with its role in myelodysplastic syndromes, J. Leukoc. Biol. 86 (2009) 813–822.
[33] P. Roy, E. Reavey, M. Rayne, S. Roy, M. Abed El Baky, Y. Ishii, C. Bartholomew, Enhanced sensitivity to hydrogen peroxide-induced apoptosis in Evi1 transformed Rat1 fibroblasts due to repression of carbonic anhydrase III, FEBS J. 277 (2009) 441–452.
[34] Z. Chen, N.J. Brand, A. Chen, S.J. Chen, J.H. Tong, Z.Y. Wang, S. Waxman, A. Zelent, Fusion between a novel Kruppel-like zinc finger gene and the retinoic acid receptor-alpha locus due to a variant t(11;17) translocation associated with acute promyelocytic leukaemia, EMBO J. 12 (1993) 1161–1167.
[35] A. Parrado, C. Chomienne, R.A. Padua, Retinoic acid receptor alpha (RAralpha) mutations in human leukemia, Leuk. Lymphoma 39 (2000) 271–282.
[36] P.L. Yeyati, R. Shaknovich, S. Boterashvili, J. Li, H.J. Ball, S. Waxman, K. Nason-Burchenal, E. Dmitrovsky, A. Zelent, J.D. Licht, Leukemia translocation protein PLZF inhibits cell growth and expression of cyclin A, Oncogene 18 (1999) 925–934.
[37] J.A. Costoya, R.M. Hobbs, M. Barna, G. Cattoretti, K. Manova, M. Sukhwani, K.E. Orwig, D.J. Wolgemuth, P.P. Pandolfi, Essential role of Plzf in maintenance of spermatogonial stem cells, Nat. Genet. 36 (2004) 653–659.
[38] F.W. Buaas, A.L. Kirsh, M. Sharma, D.J. McLean, J.L. Morris, M.D. Griswold, D.G. de Rooij, R.E. Braun, Plzf is required in adult male germ cells for stem cell self-renewal, Nat. Genet. 36 (2004) 647–652.
[39] M. Barna, T. Merghoub, J.A. Costoya, D. Ruggero, M. Branford, A. Bergia, B. Samori, P.P. Pandolfi, Plzf mediates transcriptional repression of HoxD gene expression through chromatin remodeling, Dev. Cell 3 (2002) 499–510.
[40] J.A. Costoya, P.P. Pandolfi, The role of promyelocytic leukemia zinc finger and promyelocytic leukemia in leukemogenesis and development, Curr. Opin. Hematol. 8 (2001) 212–217.
[41] M. Barna, N. Hawe, L. Niswander, P.P. Pandolfi, Plzf regulates limb and axial skeletal patterning, Nat. Genet. 25 (2000) 166–172.
[42] F. Felicetti, L. Bottero, N. Felli, G. Mattia, C. Labbaye, E. Alvino, C. Peschle, M.P. Colombo, A. Care, Role of PLZF in melanoma progression, Oncogene 23 (2004) 4567–4576.
[43] A. Parrado, M.E. Noguera, A. Delmer, S. McKenna, J. Davies, I. Le Gall, P. Bentley, J.A. Whittaker, F. Sigaux, C. Chomienne, R.A. Padua, Deregulated expression of promyelocytic leukemia zinc finger protein in B-cell chronic lymphocytic leukemias does not affect cyclin A expression, Hematol. J. 1 (2000) 15–27.
[44] M. Cheung, J. Pei, Y. Pei, S.C. Jhanwar, H.I. Pass, J.R. Testa, The promyelocytic leukemia zinc-finger gene, PLZF, is frequently downregulated in malignant mesothelioma cells and contributes to cell survival, Oncogene (2009).
[45] R. Shaknovich, P.L. Yeyati, S. Ivins, A. Melnick, C. Lempert, S. Waxman, A. Zelent, J.D. Licht, The promyelocytic leukemia zinc finger protein affects myeloid cell growth, differentiation, and apoptosis, Mol. Cell. Biol. 18 (1998) 5533–5545.
[46] M.J. McConnell, N. Chevallier, W. Berkofsky-Fessler, J.M. Giltnane, R.B. Malani, L.M. Staudt, J.D. Licht, Growth suppression by acute promyelocytic leukemia-associated protein PLZF is mediated by repression of c-myc expression, Mol. Cell. Biol. 23 (2003) 9375–9388.
[47] M.V. Bernardo, E. Yelo, L. Gimeno, J.A. Campillo, A. Parrado, Identification of apoptosis-related PLZF target genes, Biochem. Biophys. Res. Commun. 359 (2007) 317–322.
[48] S. Chakraborty, V. Senyuk, S. Sitailo, Y. Chi, G. Nucifora, Interaction of EVI1 with cAMP-responsive element-binding protein-binding protein (CBP) and p300/CBP-associated factor (P/CAF) results in reversible acetylation of EVI1 and in co-localization in nuclear speckles, J. Biol. Chem. 276 (2001) 44936–44943.
[49] S. Matsuoka, B.A. Ballif, A. Smogorzewska, E.R. McDonald 3rd, K.E. Hurov, J. Luo, C.E. Bakalarski, Z. Zhao, N. Solimini, Y. Lerenthal, Y. Shiloh, S.P. Gygi, S.J. Elledge, ATM and ATR substrate analysis reveals extensive protein networks responsive to DNA damage, Science 316 (2007) 1160–1166.

エピジェネティクス分野

石野 史敏

難治疾患研究所
エピジェネティクス・教授

1）研究の課題名

レトロトランスポゾン由来の哺乳類特異的遺伝子群の個体発生・生殖機構における役割

Functions of mammalian-specific retrotransposon-derived genes in mammalian development and reproduction

哺乳類を構成する真獣類、有袋類、単孔類の3つのグループのなかで、胎生の生殖機構を採用している前二者にのみ存在しているレトロトランスポゾン由来の内在性遺伝子の機能の体系的解析を進めている。以前にPeg10（Ono et al. Genomics 2001, Nat Genet 2006）およびPeg11/Rtl1（Sekita et al. Nat Genet 2008）が胎盤形成や機能に必須の役割をはたすことを報告してきた。

真獣類には、この他にこれらと同じsushi-ichiレトロトランスポゾンに由来する9個のSirh family（sushi-ichi retrotransposon homologues）遺伝子が存在する。現在、東海大学の金児－石野研と共同でSirh3、Sirh4-6、Sirh7、Sirh11のノックアウトマウスの解析を進めている。これらは個体の致死性には影響しないが、例えばSirh7では胎盤の3層構造の形成に必須な機能をもつことがわかっている（Naruse et al. 論文準備中）。その他の遺伝子についても、どのような哺乳類特異的機能に関係するかを解析している。さらに有袋類特異的なSIRH12遺伝子を同定し報告した（Ono et al. DNA Res 2011）。

X染色体不活性化の制御により体細胞クローニングの成功率をあげる

X chromosome inactivation regulation leads to successful somatic cloning in mice.

体細胞クローン技術はiPS細胞作製技術とならんで将来の再生医療を大きく変える可能性を秘めている。昨年、理化学研究所バイオリソースセンターの小倉淳郎室長のグループとの共同研究で、この低い成功率の原因が性染色体であるX染色体の全域に渡る遺伝子発現低下にあることを明らかにした（Inoue et al. Science 2010）。今回、より効率的なクローン作製技術としてXist ノックダウンとトリコスタチン処理を組み合わせた方法を開発した（Inoue et al. PNAS 2011）。これにより体細胞クローン技術の成功率は20 %を超えるところまで改善された。

顕微授精は遺伝子発現に影響をあたえる

Intracytoplasmic sperm injection induces transcriptome perturbation.

現在、ヒトにおける不妊治療の一つとして広く用いられている顕微授精技術（ICSI：intracaytoplasmic sperm injection）の影響をマウスをモデルに解析した。体外受精（IVF：in vitro fertilization）では全く影響が見られないのに対し、ISCIでは全発現遺伝子の5%に発現量の増減が確認された（図）。この影響は胎児、新生児の各種臓器で見られるが、生後8ヶ月では消失した。幸いなことに、有性生殖で産まれた次世代のマウスには全く影響はないことが確認された（Kohda et al. BBRC 2011）。

2）

図：ICSIによる遺伝子発現の変化

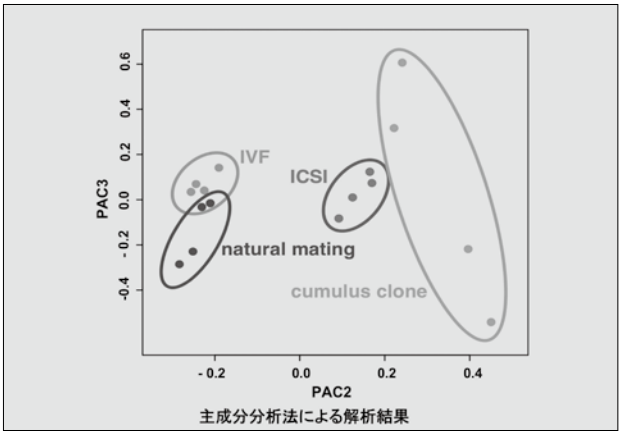

説明：新生仔の肝臓における全遺伝子発現の主成分分析による解析を示した。有性生殖（natural mating：青）とIVF（緑）、

ICSI（赤）および体細胞クローン（cumulus clone：オレンジ）の間で比較をすると、IVFは正常の有性生殖に近いパターン、ICSIはより体細胞クローンに近い遺伝子発現パターンを取っていることがわかる。

3）発表の研究内容についての英文要約

1. Characterisation of the marsupial PHLDA2 reveals eutherian specific acquisition of imprinting

Genomic imprinting causes parent-of-origin specific gene expression by differential epigenetic modifications between two parental genomes. We previously reported that there is no evidence of genomic imprinting of CDKN1C in the KCNQ1 domain in the placenta of an Australian marsupial, the tammar wallaby（Macropus eugenii）whereas wallaby IGF2 and H19, located adjacent to the KCNQ1 imprinted domain in eutherian mammals, are imprinted. We have now identified and characterized the marsupial orthologue of PHLDA2, another gene in the KCNQ1 domain（also known as IPL or TSSC3）that is imprinted in eutherians. In mice, Phlda2, like Cdkn1c for embryonic growth, is a dose-sensitive negative regulator of placental growth. Wallaby PHLDA2 is highly expressed in the yolk sac placenta compared with other fetal tissues, confirming a similar expression pattern to that of the mouse Phlda2. However, wallaby PHLDA2 is biallelically expressed in both the fetus and yolk sac placenta, so it is not imprinted. The lack of imprinting in wallaby PHLDA2 demonstrates that the acquisition of genomic imprinting of the KCNQ1 domain, accompanied with gene dosage reduction, occurred only in the evolution of the eutherian linage. Our results confirm the idea that acquisition of genomic imprinting to the KCNQ1 domain occurred specifically in the eutherian lineage after the divergence of marsupials, but that imprinting of the adjacent H19-IGF2 domain arose before the marsupial-eutherian split.

2. Identification of SIRH12, a retrotransposon-derived gene specific to marsupial mammals.

In humans and mice, there are 11 genes derived from sushi-ichi related retrotransposons, some of which are known to play essential roles in placental development. Interestingly, this family of retrotransposons was thought to exist only in eutherian mammals, indicating their significant contributions to the eutherian evolution, but at least one, PEG10, is conserved between marsupials and eutherians. Here we report a novel sushi-ichi retrotransposon-derived gene, SIRH12, which is specific to marsupials. In the tammar wallaby, an Australian marsupial species of the kangaroo family, SIRH12 encodes a protein highly homologous to the sushi-ichi retrotransposon Gag protein, while SIRH12 in the South American short-tailed grey opossum is a pseudogene degenerated by accumulation of multiple nonsense mutations. This suggests that SIRH12 retrotransposition occurred only in the marsupial lineage but acquired and retained some as yet unidentified novel function, at least in the tammar wallaby.

3. Intracytoplasmic sperm injection induces transcriptome perturbation without any transgenerational effect.

Faithful transcriptome regulation is important in development and also crucial for applications in reproductive and regenerative medicine. Intracytoplasmic sperm injection（ICSI）, one of the human assisted reproductive technologies（ART）, has long raised concerns about its influence on development. No clear consensus has been reached, however, in spite of many cohort studies carried out in the last two decades on the children conceived by ICSI and/or in vitro fertilization（IVF）. In this study, the pre- and postnatal effects of ICSI were assessed using comprehensive transcriptome and phenotypic analyses in mice under strict conditions. Here we demonstrate that, in contrast to IVF, ICSI induces distinct long-lasting transcriptome change that remains at the neonatal stage. Importantly, no remarkable differences were observed in the ICSI adults in either the gene expression or phenotypic profiles, and there was no indication of transmission to the next generation via natural mating. Our results suggest there are no lifelong or transgenerational effects of ICSI, but the ICSI effects during neonatal period remain to be evaluated.

4. RNAi-mediated knockdown of Xist can rescue the impaired postimplantation development of cloned mouse embryos

Cloning mammals by somatic cell nuclear transfer（SCNT）is highly inefficient. Most SCNT-generated embryos die after implantation because of unidentified, complex epigenetic errors in the process of postimplantation embryonic development. Here we identify the most upstream level of dysfunction leading to impaired development of clones by using RNAi against Xist, a gene responsible for X chro- mosome inactivation（XCI）. A prior injection of Xist-specific siRNA into reconstructed oocytes efficiently corrected SCNT-specific aberrant Xist expression at the morula stage, but failed to do so thereafter at the blastocyst stage. However, we found that shortly after implan- tation, this aberrant XCI status in cloned embryos had been corrected autonomously in both embryonic and extraembryonic tissues, prob- ably through a newly established XCI control for postimplantation embryos. Embryo transfer experiments revealed that siRNA-

treated embryos showed 10 times higher survival than controls as early as embryonic day 5.5 and this high survival persisted until term, result- ing in a remarkable improvement in cloning efficiency（12% vs. 1% in controls）. Importantly, unlike control clones, these Xist-siRNA clones at birth showed only a limited dysregulation of their gene expression, indicating that correction of Xist expression in preimplantation em- bryos had a long-term effect on their postnatal normality. Thus, con- trary to the general assumption, our results suggest that the fate of cloned embryos is determined almost exclusively before implantation by their XCI status. Furthermore, our strategy provides a promising breakthrough for mammalian SCNT cloning, because RNAi treatment of oocytes is readily applicable to most mammal species.

5. **The evolution of mammalian genomic imprinting was accompanied by the acquisition of novel CpG islands**
Parent-of-origin-dependent expression of imprinted genes is mostly associated with allele- specific DNA methylation of the CpG islands（CGIs）called germline differentially methylated regions（gDMRs）. Whilst the essential role of gDMRs for genomic imprinting has been well established, little is known about how they evolved. In several imprinted loci the CGIs forming gDMRs may have emerged with the insertion of a retrotransposon or retrogene. To examine the generality of the hypothesis that the CGIs forming gDMRs were novel CGIs recently acquired during mammalian evolution, we reviewed the time of novel CGI emergence for all the maternal gDMR loci, using the novel data analysed in this study combined with the data from previous reports. The comparative sequence analyses using mouse, human, dog, cow, elephant, tammar, opossum, platypus and chicken genomic sequences were carried out for Peg13, Meg1/Grb10, Plagl1/Zac1, Gnas and Slc38a4 imprinted loci to obtain comprehensive results. The combined data showed that emergence of novel CGIs occurred universally in the maternal gDMR loci at various time points during mammalian evolution. Furthermore, the analysis of Meg1/Grb10 locus provided evidence that gradual base-pair-wise sequence change was involved in the accumulation of CpG sequence, suggesting the mechanism of novel CGI emergence is more complex than the suggestion that CpG sequences originated solely by insertion of GC-rich transposable elements. We propose that acquisition of novel CGIs was a key genomic change for the evolution of imprinting, and that it usually occurred in the maternal gDMR loci.

6. **Gene expression profile normalization in cloned mice by trichostatin A treatment**
Cloning mammals by somatic cell nuclear transfer（SCNT）has become an established procedure, but the success rate remains low and gene expression abnormalities are also observed. In addition, SCNT pups exhibited an abnormal gene expression profile with a high degree of heterogeneity among individuals. Recently, we reported that somatic clones treated with trichostatin A（TSA）exhibited a significantly improved success rate, probably due to its effects on chromatin remodeling and histone modification in early embryos. Here we show that the TSA treatment also improves the long-term consistency of genome-wide gene expression regulation：the total number of genes commonly exhibiting up- or down-regulation in the TSA clone pups decreased to half of the conventional SCNT pups, and the variation among individuals observed in the SCNT pups was also reduced to the level of the pups produced by the intracytoplasmic sperm injection（ICSI）method. Interestingly, the total gene expression profile of the TSA clones came to resemble that of the ICSI pups.

4）本事業に関連して世界的な研究拠点形成に向けて、以下の点で改善・整備等されたこと

A（研究拠点体制）

拠点を形成することで関連研究を行う他の研究室での研究内容をより深く理解し、共同研究などを通じて自分の研究に新たな展開を盛り込む事が可能になった。

B（研究教育環境）

独立した研究者をめざす優秀なポスドク（GCOE特任講師）が研究室におり頑張っている姿をみせることは、大学院生に自分の将来を考える上で重要なロールモデルとなっている。英語での総合プレゼンテーションも参加したメンバーに対しての教育効果は高いと考えている。

C（人材確保）

将来性の高い研究者をGCOE特任講師として採用できた。さきがけ研究にも選ばれており、若い大学院生に良い影響をあたえている。

D（人材育成）

採用したGCOE特任講師には、施設、機器などの利用に便宜をはかり、自身の研究に専念してもらえる環境を提供している。また、将来、独立して研究室を運営できるよう、研究の将来構想や学生の指導法や研究室運営の仕方などについても相談にのっている。

E（国際化） 博士課程の大学院生には、国際共同研究で1－3ヶ月海外に滞在して研究できる機会を与えている。相手国からも大学院生を受け入れており、大学院生のと

きから海外の研究者との交流をもたせている。本拠点には外国人大学院生が多くいるため、国際化はスムーズに展開できるようになると考えている。

5）GCOE事業を推進するに当たって力を入れた点

指導している大学院生にとって自分の研究者としての将来を考える上で良い経験を得られる環境を作ること。大学院生のそれぞれの個性を伸ばすため、個別研究指導をすることは当然として、研究者としての経歴にはいろいろな選択肢が存在することを理解させる事は重要である。本制度GCOEのポスドク、研究所独自のテニュアトラックのポスドク、大型研究費によるポスドクなどが、研究所内にいることで、大学の正規の助教ポストだけでなく自分の将来の選択の幅を知ることが可能になった。

6）英文原著論文

1. Ono, R., Kuroki, Y., Naruse, M., Ishii, M., Iwasaki, S., Toyoda, A., Fujiyama, A., Shaw, G., Renfree, M. B., Kaneko-Ishino, T. and Ishino, F. Identification of SIRH12, a retrotransposon-derived gene specific to marsupial mammals. DNA Research 18（4）, 211-219（2011）.
2. Kohda, T., Ogonuki, N., Inoue, K., Furuse, T., Kaneda, H., Suzuki, T., Kaneko-Ishino, T., Wakayama, T., Wakana, S., Ogura, A. and Ishino, F. Intracytoplasmic sperm injection induces transcriptome perturbation without any transgenerational effect. Biochem Biophys Res Commun 410（2）, 282-288（2011）.
3. Suzuki, S., Shaw, G., Kaneko-Ishino, T., Ishino, F. and Renfree, M. B. Characterisation of marsupial PHLDA2 reveals eutherian specific acquisition of imprinting. BMC Evol Biol. 11（1）, 244（2011）.
4. Matoba, S.*, Inoue, K.*, Kohda, T.*, Sugimioto, M.*, Mizutani, E., Ogonuki, N., Nakamura, T., Abe, K., Nakano, T., Ishino, F. and Ogura, A. RNAi-mediated knockdown of Xist can rescue the impaired postimplantation development of cloned mouse embryos Proc Natl Acad Sci U. S. A. 108（51）, 20621-20626（2011）.
5. Suzuki, S., Shaw, G., Kaneko-Ishino, T., Ishino, F. and Renfree, M. B. The evolution of mammalian genomic imprinting was accompanied by the acquisition of novel CpG islands. Genome Biology and Evolution 3, 1276-1283（2011）.
6. Kohda, T., Kishigami, S., Kaneko-Ishino, T., Wakayama T. and Ishino F. Gene expression profile normalization in cloned mice by trichostatin A treatment. Cellular Reprogramming（in press）.

7）平成23年度までの自己評価

哺乳類の個体発生に影響をあたえたレトロトランスポゾン由来の遺伝子群の機能解析は、ノックアウトマウス解析から新たな発見があり着実に成果はあがっている。骨格形成異常に関係するPeg11/Rtl1の機能解析もmiRNAの制御というユニークな展開になって来ている。哺乳類特異的ゲノム機能はヒトの個体発生にも確実に影響を与えているため、医学研究への展開は重要であると認識している。体細胞クローニングやICSIという発生工学技術におけるエピジェネティック異常の研究は、社会に還元するものとして重要なものであると考えている。

8）学会発表（英文）

1） Fumitoshi Ishino and Tomoko Kaneko-Ishino Evolution of genomic imprinting in mammals, On the critical issues in EvoDevo, 44th JSDB Annual Meeting, Invited speaker, May 21, 2011, Okinawa Convention Center（Okinawa, Japan）.
2） Fumitoshi Ishino, Ryuichi Ono, Sunsuke Suzuki, Yoichi Sekita, Mie Naruse, Takashi Kohda and Tomoko Kaneko-Ishino Role of retrotransposons in mammalian evolution -Domesticated genes for mammalian-specific functions-, US-Japan Conference：Inflamation, Diabetes and Cancer, Invited speaker, August 4, 2011, Beckman Research Institute of City of Hope（California, USA）.
3） Sawa Iwasaki, Takashi Kohda, Tomoko Kaneko-Ishino and Fumitoshi Ishino. Genomic impirinting status of retrotransposon-derived PNMA family genes, ICC on Genomic Imprinting and Beyond 2011, Poster, September 21-23, 2011（Barcelona, Spain）.
4） Fumitoshi Ishino and Tomoko Kaneko-Ishino Evolution of viviparity and genomic imprinting in mammals by retrotransposons, 15th Evolutionary Biology Meeting in Marseilles, Invited speaker, September 27-30, 2011（Marseilles, France）.
5） Fumitoshi Ishino Retrotransposon-derived genes in mammalian development and evolution. From Early Universe to Evolution of Life, Germany-Japan Round Table, Invited speaker, December 3, 2011, Heidelberg University,（Heidelberg, Germany）.
6） Fumitoshi Ishino, Ryuichi Ono, Mie Naruse, Masahito Irie, Sawa Iwasaki, Masayuki Ishii and

Tomoko Kaneko-Ishino Role of domesticated genes fromretrotransposons in mammalian evolution. Symposium "Mobile elements and its biological functions" The 34th Annual Meeing of the Molecular Biology Society of Japan, organizer, December 13-16, PcificoYokohama（Yokohama, Japan）.

7） Sawa Iwasaki, Geoff Shaw, Ryuichi Ono, Shunsuke Suzuki, Marilyn Renfree, Tomoko Kaneko-Ishino, Fumitoshi Ishino, Identification of PNMA-MS1, a retrotransopson-derived gene specific to marsupial mammals. The 34th Annual Meeing of the Molecular Biology Society of Japan, poster, December 13-16, PcificoYokohama（Yokohama, Japan）.

8） Takashi Kohda, Narumi Ogonuki, Kimiko Inoue, Tamio Furuse, Hideki Kaneda, Tomohiro Suzuki, Tomoko Kaneko-Ishino, Teruhiko Wakayama, Shigeharu Wakana, Atsuo Ogura, Fumitoshi Ishino Transcriptome perturbation by intracytospermatic sperm injection in the mouse. The 34th Annual Meeing of the Molecular Biology Society of Japan, talk, December 13-16, PcificoYokohama（Yokohama, Japan）.

9）Ryuichi Ono, Yoko Kuroki, Mie Naruse, Masayuki Ishii, Sawa Iwasaki, Atsushi Toyoda, Asao Fujiyama, Geoff Shaw, Marilyn Renfree, Tomoko Kaneko-Ishino, Fumitoshi Ishino. Identification of SIHR12, a retrotransposon-derived gene specific to marsupial mammals. The 34th Annual Meeing of the Molecular Biology Society of Japan, poster, December 13-16, PcificoYokohama（Yokohama, Japan）.

10）Masazumi Nishimoto, Miyuki Katano, Toshiyuki Yamagishi, Tomoaki Hishida, Masayoshi Kamon, Yoko Nabeshima, Yo-ichi Nabeshima, Yoko Kuroki, Ryuichi Ono, Fumitoshi Ishino, Hidemasa Kato, Akihiko Okuda Eutheria-specific UTF1 gene is critical for the placental growth. The 34th Annual Meeing of the Molecular Biology Society of Japan, talk, December 13-16, PcificoYokohama（Yokohama, Japan）.

9）学会発表（和文）

1）石野史敏　哺乳類の個体発生におけるエピジェネティクスーゲノムインプリンティングと体細胞クローンについて―　エピジェネティクスから探る発生から疾患までの制御―　第25回環境ホルモン学会、招待講演、2011年6月16日　東京大学山上会議所

2）石野史敏、小野竜一、成瀬美衣、入江将仁、黒木陽子、石井雅之、岩崎佐和、幸田尚、Marilyn Renfree、金児―石野知子　レトロトランスポゾン由来の哺乳類特異的遺伝子群　　シンポジウム「転移因子の新たな機能と制御」 第84回日本生化学会大会シンポジウム、オーガナイザー、2011年9月23日　京都国際会議場

3）成瀬美衣、日野敏昭、赤塚明、幸田尚、中村健司、横山峯介、小野竜一、金児―石野知子、石野史敏　レトロトランスポゾン由来の遺伝子Sirh7 KOマウスの胎盤の解析　第34回日本分子生物学会年会　2011年12月13日-16日　パシフィコ横浜、横浜）

4）入江将仁、成瀬美衣、幸田尚、小野竜一、石野史敏、金児―石野知子　Sushi-ishiレトロトランスポゾン由来の遺伝子Sirh3の機能解析　第34回日本分子生物学会年会　2011年12月13日-16日　パシフィコ横浜、横浜）

5）及川真実、幸田尚、石野史敏　マイクロアレイ解析のためのcDNA増幅法の改良　第34回日本分子生物学会年会　2011年12月13日-16日　パシフィコ横浜、横浜）

6）山口佑季、幸田尚、金児－石野知子、石野史敏　成体体細胞におけるインプリント領域のDNAメチル化解析　第34回日本分子生物学会年会　2011年12月13日-16日　パシフィコ横浜、横浜）

7）小野由美子、渡辺久子、幸田尚、石野史敏、入江将仁、金児―石野知子　胎児への低栄養暴露が与える遺伝子発現への影響　第34回日本分子生物学会年会　2011年12月13日-16日　パシフィコ横浜、横浜）

8）高橋沙央里、鈴木俊介、小野竜一、幸田尚、金児－石野知子、石野史敏　新規インプリンティング遺伝子スクリーニング方法の開発　第34回日本分子生物学会年会　2011年12月13日-16日　パシフィコ横浜、横浜）

10）外部資金の獲得状況

1. 科学研究費基盤研究（S）
研究課題「哺乳類特異的ゲノム機能の解析」
研究期間　平成23年度～平成27年度（5年間）
総額　165,200千円　　平成23年度分34,000千円

2. 日本学術振興会　日豪二国間共同研究
研究課題「有袋類におけるゲノムインプリンティングの進化」
研究期間　平成23年度～平成24年度（2年間）
平成23年度分　2,450千円

11）特別講演、招待講演、シンポジウム

1）Fumitoshi Ishino and Tomoko Kaneko-Ishino Evolution of genomic imprinting in mammals, On the critical issues in EvoDevo, 44th JSDB Annual Meeting, May 21, 2011, Okinawa Convention Center（Okinawa, Japan）.

2）石野史敏　哺乳類の個体発生におけるエピジェネティクスーゲノムインプリンティングと体細胞クローンについて―　エピジェネティクスから探る発生から疾患までの制御―　第25回環境ホルモン学会、2011年6月16日　東京大学山上会議所

3）Fumitoshi Ishino, Ryuichi Ono, Sunsuke Suzuki, Yoichi Sekita, Mie Naruse, Takashi Kohda and Tomoko Kaneko-Ishino Role of retrotransposons in mammalian evolution -Domesticated genes for mammalian-specific functions-, US-Japan Conference：Inflamation, Diabetes and Cancer, August 4, 2011, Beckman Research Institute of City of Hope（California, USA）.

4）石野史敏、小野竜一、成瀬美衣、入江将仁、黒木陽子、石井雅之、岩崎佐和、幸田尚、Marilyn Renfree、金児―石野知子　レトロトランスポゾン由来の哺乳類特異的遺伝子群　　シンポジウム「転移因子の新たな機能と制御」 第84回日本生化学会大会シンポジウム、2011年9月23日　京都国際会議場

5）Fumitoshi Ishino and Tomoko Kaneko-Ishino Evolution of viviparity and genomic imprinting in mammals by retrotransposons, 15th Evolutionary Biology Meeting in Marseilles, Invited speaker, September 27-30, 2011（Marseilles, France）.

6）Fumitoshi Ishino Retrotransposon-derived genes in mammalian development and evolution. From Early Universe to Evolution of Life, Germany-Japan Round Table, December 3, 2011（Heidelberg University, Germany）.

7）Fumitoshi Ishino, Ryuichi Ono, Mie Naruse, Masahito Irie, Sawa Iwasaki, Masayuki Ishii and Tomoko Kaneko-Ishino Role of domesticated genes fromretrotransposons in mammalian evolution. Symposium “Mobile elements and its biological functions” The 34th Annual Meeing of the Molecular Biology Society of Japan, December 13-16, PcificoYokohama（Yokohama, Japan）.

12）主催学会

The 8th Okazaki Biology Conference "Speciation and Adaptation II - Environment and Epigenetics -" March 18-23, Institute of Basic Biology, Okazaki, Aichi.

13）新聞、雑誌、TV報道

毎日新聞朝刊 2011年7月2日
　　顕微授精 遺伝子働きに乱れ
朝日新聞朝刊 2011年7月18日
　　顕微授精 遺伝子5%に影響

14）教室、分野や講座の准教授、講師、助教、特別研究員、ポスドク、指導を受けた大学院生の名前

准教授	幸田	尚
助教	小野	竜一
非常勤講師	小林	慎
GCOE特任講師	李	知英
特任助教	遠藤	大輔（5月末まで）
特任助教	成瀬	美衣
大学院生D3	松本	和也
大学院生D3	岩崎	佐和
大学院生D3	石井	雅之
大学院生D2	○山口	祐季
大学院生D1	及川	真実
大学院生D1	高橋	沙央里
大学院生M1	北澤	萌絵
大学院生M1	押本	彩夏

○はAISS

15）GCOE活動についての感想、コメント、改善を望む点

英語での講義が、日本人大学院生にはまだ負担になっているように思うが、英語でのプレゼンテーションの演習などが準備されたことにより、積極的に関わっている学生には良い環境が整ってきたと感じている。また、若手研究者支援としてGCOEで雇用した特任講師の将来のキャリアーについては、今後充分考えて行く必要があると考えている。

RNAi-mediated knockdown of *Xist* can rescue the impaired postimplantation development of cloned mouse embryos

Shogo Matoba[a,1], Kimiko Inoue[a,b,1,2], Takashi Kohda[c,1], Michihiko Sugimoto[a,1], Eiji Mizutani[a], Narumi Ogonuki[a], Toshinobu Nakamura[d,3], Kuniya Abe[a], Toru Nakano[d], Fumitoshi Ishino[c,2], and Atsuo Ogura[a,b,e,2]

[a]RIKEN BioResource Center, Tsukuba, Ibaraki 305-0074, Japan; [b]Graduate School of Life and Environmental Science, University of Tsukuba, Tsukuba, Ibaraki 305-8572, Japan; [c]Department of Epigenetics, Medical Research Institute, Tokyo Medical and Dental University, Tokyo 113-8510, Japan; [d]Graduate School of Frontier Bioscience, Osaka University, Suita, Osaka 565-0871, Japan; and [e]Center for Disease Biology and Integrative Medicine, Faculty of Medicine, University of Tokyo, Tokyo 113-0033, Japan

Edited by R. Michael Roberts, University of Missouri, Columbia, MO, and approved October 12, 2011 (received for review August 5, 2011)

Cloning mammals by somatic cell nuclear transfer (SCNT) is highly inefficient. Most SCNT-generated embryos die after implantation because of unidentified, complex epigenetic errors in the process of postimplantation embryonic development. Here we identify the most upstream level of dysfunction leading to impaired development of clones by using RNAi against *Xist*, a gene responsible for X chromosome inactivation (XCI). A prior injection of *Xist*-specific siRNA into reconstructed oocytes efficiently corrected SCNT-specific aberrant *Xist* expression at the morula stage, but failed to do so thereafter at the blastocyst stage. However, we found that shortly after implantation, this aberrant XCI status in cloned embryos had been corrected autonomously in both embryonic and extraembryonic tissues, probably through a newly established XCI control for postimplantation embryos. Embryo transfer experiments revealed that siRNA-treated embryos showed 10 times higher survival than controls as early as embryonic day 5.5 and this high survival persisted until term, resulting in a remarkable improvement in cloning efficiency (12% vs. 1% in controls). Importantly, unlike control clones, these *Xist*-siRNA clones at birth showed only a limited dysregulation of their gene expression, indicating that correction of *Xist* expression in preimplantation embryos had a long-term effect on their postnatal normality. Thus, contrary to the general assumption, our results suggest that the fate of cloned embryos is determined almost exclusively before implantation by their XCI status. Furthermore, our strategy provides a promising breakthrough for mammalian SCNT cloning, because RNAi treatment of oocytes is readily applicable to most mammal species.

somatic cell cloning | RNA FISH | DNA micro array | Tsix | trichostatin A

Somatic cell nuclear transfer (SCNT) is a unique technology for endowing the somatic cell genome with totipotency by genomic reprogramming (1). This technique has a distinct advantage over other similar biotechnologies, such as generating induced pluripotent stem cells, because a single somatic cell can give rise to a new individual with exactly the same genome as that of the donor cell (2, 3). Therefore, SCNT could become an invaluable tool with a broad range of applications including biological drug manufacturing, regenerative medicine, endangered species preservation, and commercial animal breeding. However, the success rate of cloning mammals by SCNT is low, predominantly because of the developmental arrest of cloned embryos after embryo transfer (1, 4).

Our recent in-depth gene expression analysis of cloned mouse blastocysts revealed ectopic expression of the noncoding RNA *Xist*—responsible for X chromosome inactivation (XCI) in female cells (5)—from the active X chromosome in both male and female clones (6). This ectopic expression of *Xist* had a global adverse effect on the gene expression of cloned embryos, because normalization of *Xist* expression by genetic knockout remarkably improved the expression patterns of not only X-linked genes but also a number of autosomal genes in the cloned embryos. As a result, many of the knockout-cloned embryos survived to term, resulting in an eight- to ninefold increase in overall cloning efficiency (6). These findings indicate that many, if not all, of the mechanisms that compromise the development of clones can be attributed to ectopic expression of the *Xist* gene in mice. The *XIST* gene is also known to be aberrantly expressed in bovine and pig SCNT-derived embryos and is implicated in their prenatal death (7–9). Thus, correction of X-linked gene expression is one of the most promising strategies now conceivable for improving the efficiency of mammalian SCNT.

Despite its potential efficacy, the *Xist*-knockout approach is impractical because it causes irreversible modification of the donor genome. Furthermore, gene targeting is still difficult for animal species other than mouse because of the difficulty in establishment of germ line-competent embryonic stem cells and the low cost-effectiveness of designed nucleases (10). In addition, it is still unclear from knockout studies how and when the ectopic expression of *Xist* affects the development of cloned embryos. The most probable solution to overcome these problems might be RNA interference (RNAi)-mediated gene knockdown, which works transiently and does not alter genomic DNA sequences (11–13). This strategy is easily applicable to many mammalian species and could provide us with clues to understanding the critical period of gene expression that might allow cloned embryos to survive to term. In this study, we examined whether RNAi-mediated knockdown against *Xist* could ameliorate the poor development of cloned mouse embryos by injecting a short interfering RNA (siRNA) into reconstructed embryos. As exact quantitative adjustment by conventional RNAi is technically difficult, we primarily focused on the silencing of *Xist* RNA in male cloned embryos with only a single X chromosome.

Results

Injected *Xist*-siRNA Repressed Ectopic *Xist* Expression at the Morula Stage but Not Later in Cloned Embryos. First, we examined the validity of an siRNA construct using parthenogenetic embryos, which express the *Xist* gene from the morula stage onward (14).

Author contributions: S.M., K.I., and A.O. designed research; S.M., K.I., T.K., M.S., E.M., N.O., and A.O. performed research; T. Nakamura contributed new reagents/analytic tools; T.K., K.A., T. Nakano, and F.I. analyzed data; and A.O. wrote the paper.

The authors declare no conflict of interest.

This article is a PNAS Direct Submission.

Freely available online through the PNAS open access option.

Data deposition: The microarray data reported in this paper have been deposited in the Gene Expression Omnibus (GEO) database, www.ncbi.nlm.nih.gov/geo (accession no. GSE33208).

[1]S.M., K.I., T.K., and M.S. contributed equally to this work.

[2]To whom correspondence may be addressed. E-mail: inoue@rtc.riken.jp, fishino.epgn@mri.tmd.ac.jp, or ogura@rtc.riken.go.jp.

[3]Present address: Department of Animal Bio-Science, Nagahama Institute of Bio-Science and Technology, Nagahama, Shiga 526-0829, Japan.

This article contains supporting information online at www.pnas.org/lookup/suppl/doi:10.1073/pnas.1112664108/-/DCSupplemental.

DEVELOPMENTAL BIOLOGY

We found that the siRNA treatment effectively decreased the *Xist* RNA level in the resulting blastocysts when injected into oocytes at 6 h postactivation (Fig. S1). As parthenogenetic embryos arrest their development at midgestation, we next injected the *Xist*-siRNA into in vitro fertilization (IVF)-derived embryos to determine whether the knockdown of *Xist* would affect normal postimplantation development. After embryo transfer, 44% of the siRNA-injected embryos reached term, showing a nearly 1:1 sex ratio, with no significant difference from that of control embryos ($P > 0.05$ by Fisher's exact test) (Table S1). This result indicates that *Xist*-siRNA did not affect the normal development of embryos of either sex. Therefore, in the next series of experiments, the same regimen was used for male SCNT embryos reconstructed using nuclei from neonatal Sertoli cells. Quantitative reverse transcription–PCR (RT-PCR) analyses revealed that *Xist* transcripts were first detected at the four-cell stage in cloned embryos and reached a steady level at the morula and blastocyst stages (Fig. 1*A*). When cloned embryos were pretreated with *Xist*-siRNA (hitherto termed *Xist*-siRNA embryos), the *Xist* level was reduced significantly compared with control siRNA embryos at the morula stage but not at the blastocyst stage (Fig. 1*A*). The effect of RNAi on ectopic *Xist* expression was further examined with *Xist* RNA fluorescent in situ hybridization (RNA FISH). At the morula stage, a clustered *Xist* RNA signal, referred to as a "cloud," was found in the majority of nuclei in control siRNA-treated embryos (Fig. 1 *B* and *C*), as has been reported previously (6). By contrast, in *Xist*-siRNA–treated embryos, most blastomeres showed regionally restricted "pinpoint" signals, which presumably represented nascent *Xist* RNA on the X chromosome. This confirmed massive degradation of *Xist* induced by the injected *Xist*-siRNA (Fig. 1 *B* and *C*). At the blastocyst stage, the ectopic *Xist* expression spread as a cloud in some of the blastomeres of *Xist*-siRNA embryos, showing a pattern indistinguishable from that in control siRNA embryos (Fig. 1 *B* and *C*). We also investigated the XCI status of cloned blastocysts by staining for trimethylated histone H3 at lysine 27 (H3K27me3), a marker for repressed chromatin state in the inactive X chromosome (15). In blastocysts of both *Xist*-siRNA–treated and control embryos, the majority (>65%) of inner cell mass cells and trophectoderm cells were positive for punctate H3K27me3 staining (Fig. 1*D*), confirming the findings by RNA-FISH analysis (Fig. 1*B*). These results collectively indicate that the injected *Xist*-siRNA was effective up to about 72 h of embryo development but that the efficacy diminished thereafter.

Injected *Xist*-siRNA Normalized Global Gene Expression of Cloned Embryos at the Morula Stage. We then examined the effect of *Xist*-siRNA injection on the gene expression pattern of cloned embryos by DNA microarray analysis using single embryos (6). When relative expression levels of control cloned morulae were plotted on the positions of the X chromosome, X-linked genes were largely down-regulated over the entire chromosome (Fig. 2*A*) because of the high ectopic *Xist* expression at this stage, as shown in Fig. 1. By contrast, in cloned *Xist*-siRNA embryos, the relative expression levels were elevated considerably in a chromosome-wide manner, indicating that the repression of ectopic *Xist* had a profound effect on the correction of X-linked gene expression. Indeed, the number of down-regulated X-linked genes was reduced from 80 in control embryos to 56 in *Xist*-siRNA embryos (Fig. 2*B*). Interestingly, the number of down-regulated autosomal genes was also reduced by 52.1% (1,045 to 501) compared with control cloned embryos, indicating that the *Xist*-siRNA treatment had a genome-wide effect on the gene expression in cloned embryos (Fig. 2*B*).

At the blastocyst stage, by contrast, cloned embryos from the two siRNA groups did not differ in their X-linked gene expression (Fig. 2*A*) or in the number of down-regulated genes (Fig. 2*B*), most likely because of the reappearance of ectopic *Xist*

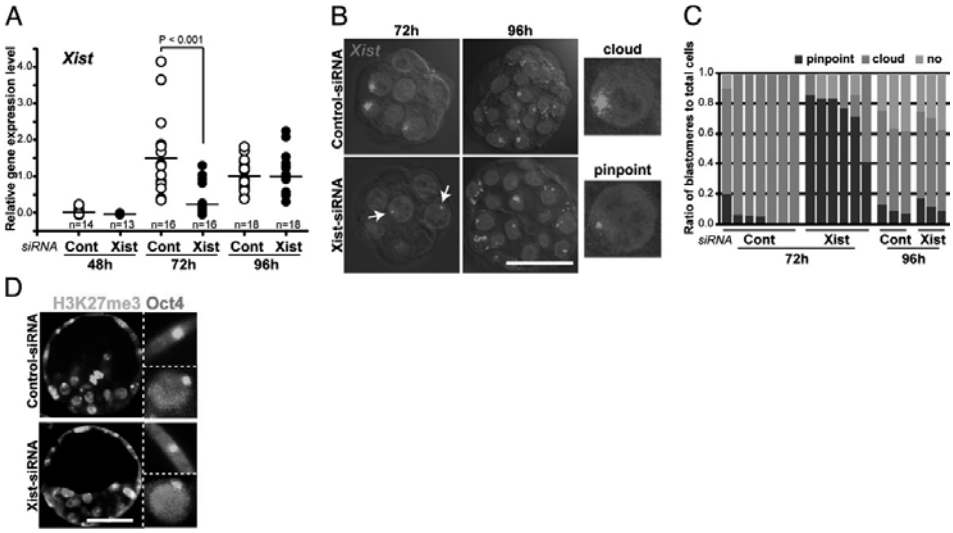

Fig. 1. Transient repression of ectopic *Xist* in SCNT-generated embryos by *Xist*-siRNA injection. (*A*) Quantitative RT-PCR of *Xist* in cloned embryos injected with control or *Xist*-siRNA and cultured for 48 h (four-cell), 72 h (morula), or 96 h (blastocyst). The expression levels of *Xist* were significantly decreased by *Xist*-siRNA at 72 h ($P < 0.001$ by Student's *t* test), whereas no significant difference was observed at 48 or 96 h. (*B*) RNA-FISH analyses of *Xist* in siRNA-injected cloned embryos. After 72 h in culture (morula), ectopic *Xist* expression was observed as a cloud pattern in most nuclei of the control cloned embryos, whereas it was detected as small pinpoint signals in *Xist*-siRNA–treated cloned embryos (arrows). At 96 h (blastocyst), the majority of nuclei showed cloud signals of *Xist* RNA in both groups. (Scale bar, 50 μm.) (*C*) The ratios of blastomeres classified according to the cloud or pinpoint expression patterns of *Xist* analyzed by RNA FISH. Each column represents a single embryo. It is apparent that the siRNA against *Xist* strongly repressed spreading of the *Xist* RNA over the X chromosome at 72 h but not at 96 h. (*D*) Immunostaining for H3K27me3 (green) and Oct4 (red) in control or *Xist*-siRNA–treated cloned embryos at 96 h. Strong punctate signals of H3K27me3 were observed in more than 65% of trophectoderm cells (Oct4-negative; *Upper Inset*) and inner cell mass cells (Oct4-positive; *Lower Inset*) in both siRNA-treated groups. (Scale bar, 50 μm.)

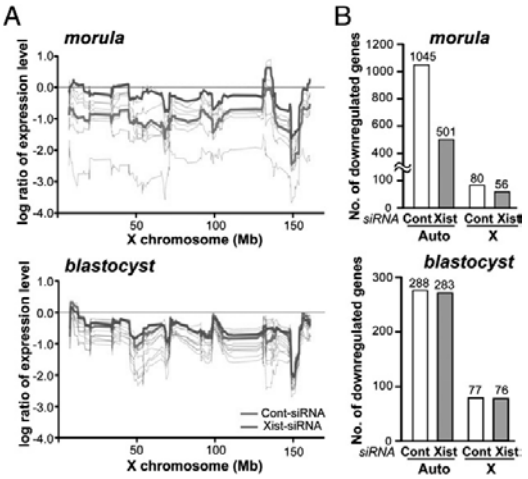

Fig. 2. Effects of *Xist*-siRNA injection on the global gene expression patterns of cloned embryos. (*A*) Relative expression levels of X-linked genes plotted on the X chromosome position in cloned embryos compared with IVF embryos at 72 h in culture (morula stage) and at 96 h (blastocyst stage) ($n = 4$ for each group). At the morula stage, X-linked genes were largely down-regulated over the entire chromosome in control cloned embryos (red), and the majority of them were increased in their expression levels by *Xist*-siRNA injection (green). By contrast, in blastocyst embryos, X-linked genes were down-regulated over the entire chromosome in both siRNA groups. Dotted lines represent a single embryo, and solid lines indicate their mean values. (*B*) Numbers of down-regulated genes (fold change >10) in cloned embryos compared with conventional IVF-generated embryos. At the morula stage, gene numbers were reduced by the injection of *Xist*-siRNA for genes not only on the X chromosome but also on autosomes, whereas they did not differ between the two groups at the blastocyst stage.

expression in *Xist*-siRNA embryos. However, despite such aberrant XCI status, there was a significant up-regulation of several developmentally important genes (e.g., *Fras1*, *Car2*, and *Tet3*) in *Xist*-siRNA blastocysts (Table S2). As implicated from the public database Mouse Genome Informatics (http://www.informatics.jax.org), these genes might play important roles in the cross-talk between the embryonic and extraembryonic parts of the conceptus that is a prerequisite for subsequent normal fetal development (16).

***Xist*-siRNA Increased the Birth Rates of Male Clones.** Next, we sought to explore whether the injection of reconstructed oocytes with *Xist*-siRNA could improve their subsequent development in vitro and in vivo. After a 96-h culture in vitro, 66% (53/80 embryos cleaved) of *Xist*-siRNA cloned embryos developed into blastocysts (Table S1). This efficiency was not statistically different from that of embryos injected with control siRNA (52%, 44/84; $P > 0.05$ by Fisher's exact test). The number of blastomeres per embryo did not differ between the groups either: 15 ± 2 ($n = 7$) and 16 ± 1 ($n = 6$) at the morula stage and 74 ± 4 ($n = 3$) and 73 ± 3 ($n = 3$) at the blastocyst stage, respectively. Thus, the *Xist*-siRNA injection seemed to have no effect on the development of cloned embryos during preimplantation stages.

We then performed embryo transfer experiments to assess the postimplantation developmental ability of the siRNA-injected cloned embryos. At embryonic day (E)5.5, there was no effect of siRNA on the implantation rate, as determined by the endometrial decidual reaction and the embryo recovery rate (Table S1). However, the typical morphology of embryos retrieved from the implantation sites (Fig. 3*A*) was improved remarkably: 75% (9/12) of *Xist*-siRNA embryos showed normal morphology with distinct embryonic and extraembryonic compartments, whereas only 5% (1/20) of the control group showed normal morphology (Fig. 3*B*; $P < 0.005$ by Fisher's exact test). These rates corresponded to 16% and 1% of the embryos transferred in *Xist*-siRNA and control groups, respectively (Fig. 3*B* and Table S1). The remaining embryos showed some developmental retardation or various developmental defects in embryonic and/or extraembryonic regions (Fig. 3*A*), as reported for embryos cloned from embryonic stem cells (17). The distribution of Oct4-positive cells, which normally show exclusive localization to the epiblast, was also dysregulated (Fig. 4 *A* and *C*). We then allowed the recipient females to deliver young at term. The resultant birth rate was greatly improved: up to 12% of the *Xist*-knockdown embryos developed to normal-looking pups, attaining a more than 10-fold increase in birth rate compared with that of the control siRNA-treated group (1%; $P < 0.005$ by Fisher's exact test; Fig. 3*B* and Table S1). It is interesting to note that the rates of normal development examined at E5.5 and E19.5 (term) were not significantly different within the same group (16% vs. 12% in *Xist*-siRNA embryos and 1% vs. 1% in controls; $P > 0.05$ by Fisher's exact test). This clearly indicates that the developmental fate of cloned embryos is largely determined as early as E5.5, an early stage after implantation. Importantly, this birth rate could be further improved to about 20% by combining *Xist*-siRNA with 50 nM trichostatin A (TSA) treatment (Fig. 3 *B* and *C* and Table S1). TSA is a potent histone deacetylase inhibitor that is known to promote the in vitro and in vivo development of cloned embryos by relaxing the histone-related repression of the donor chromatin at the time of genomic reprogramming (18). This finding indicates that TSA treatment and *Xist* knockdown had synergistic effects on the development of cloned embryos. This is consistent with the finding that TSA had no corrective effect on the aberrant X chromosome inactivation in SCNT embryos (6). To our knowledge, this is the highest birth rate ever reported for mouse SCNT cloning since the first success by Wakayama et al. (19).

We also examined the gene expression patterns of the cloned neonates by microarray analysis, because we have previously shown that neonatal cloned mice had considerable diversity in their gene expression patterns despite their normal appearance and genetic identity (20). The number of transcripts commonly exhibiting a more than twofold up-regulation in the four Sertoli clone pups was 547, and the number exhibiting down-regulation was 1,752. In the siRNA-injected clone pups, the numbers of transcripts exhibiting more than twofold up- or down-regulation were 131 and 132, respectively. The gene expression profile was largely normalized, and the variation between clone individuals was also reduced in *Xist*-siRNA–injected clones (Fig. 3*D* and Fig. S2). These findings indicate that the SCNT-associated aberration in the gene expression patterns at birth can be corrected largely by injection of *Xist*-siRNA into early embryos. Thus, correction of XCI status in the preimplantation stage not only increased the cloning efficiency remarkably but also improved the epigenetic status of clones at birth.

Ectopic *Xist* Expression in Cloned Embryos Was Corrected Autonomously After Implantation in both Embryonic and Extraembryonic Regions. That *Xist*-siRNA embryos surviving at E5.5 showed a distinctively normal phenotype might suggest the importance of the short peri-implantation period for the survival of cloned mouse embryos. However, this seemed contradictory, because XCI aberration was suggested by the presence of the *Xist* RNA cloud and H3K27me3 signal in cloned blastocysts, which corresponded to around E4.5 (Fig. 1 *B* and *D*). Therefore, we investigated the XCI status of cloned embryos at E5.5 by localization of *Xist* RNA and H3K27me3. In both the embryonic (epiblast) and extraembryonic regions of cloned embryos, there were only a few cells with a *Xist* RNA signal, irrespective of siRNA treatment (Fig. 4 *A* and *B*). Consistent with this, the positive punctate signals for H3K27me3 were also rarely observed in cloned embryos in both regions (Fig. 4 *C* and *D*). These findings clearly suggest that the ectopic *Xist* expression found in

DEVELOPMENTAL BIOLOGY

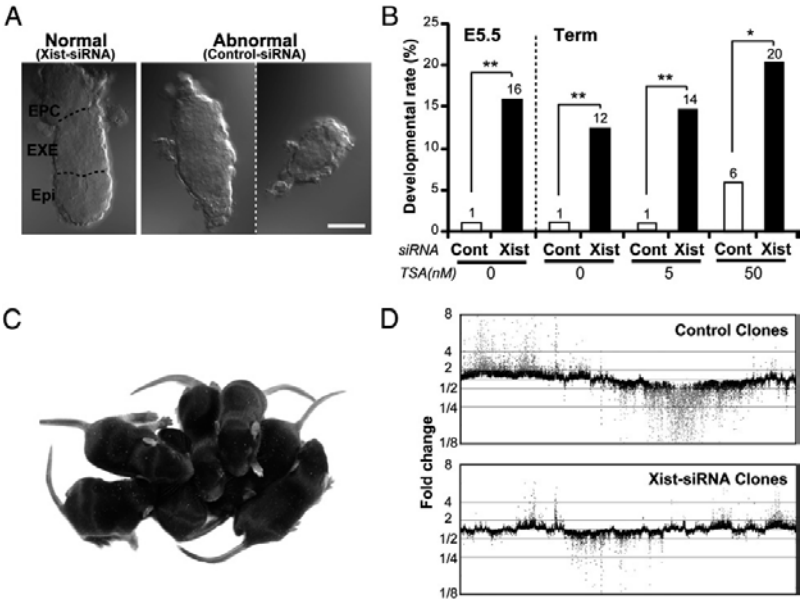

Fig. 3. Effects of *Xist*-siRNA on the postimplantation development of cloned embryos. (*A*) Representative photomicrographs of siRNA-treated cloned embryos recovered at E5.5. Most *Xist*-siRNA embryos showed normal morphology (*Left*) with a distinct embryonic epiblast region (Epi) and extraembryonic ectoderm (EXE) or an ectoplacental cone (EPC), whereas most control siRNA-treated embryos showed abnormal morphology such as developmental retardation or ambiguous embryonic and extraembryonic regions (*Center* and *Right*). (Scale bar, 50 μm.) (*B*) The developmental rate of embryos assessed at E5.5 and at term. In some experiments, TSA was added at 5 or 50 nM in the culture medium. The numbers at the top of the bars indicate the rates of normal-shaped embryos (E5.5) and full-term births per embryos transferred. $^{*}P < 0.05$, $^{**}P < 0.001$ by Fisher's exact test. (*C*) A litter of cloned pups produced by SCNT from Sertoli cell nuclei, obtained following treatment with *Xist*-siRNA and 50 nM TSA. They were born at the best efficiency we observed in this series: Seven pups were born from 23 embryos transferred (30%) to a single recipient mother. (*D*) Gene expression profiles of livers in neonatal mice generated by SCNT with or without *Xist*-siRNA injection. The values indicate the mean fold changes from the control IVF level (=1). Red dots represent genes of which expression levels exceeded a twofold change in all of the individual clones. *Xist*-siRNA clones showed much fewer dysregulated genes compared with control clones. For data on each individual clone, see Fig. S2.

cloned blastocysts was corrected autonomously shortly after implantation in both embryonic and extraembryonic tissues.

Discussion

The present study provides unequivocal evidence that the ectopic expression of *Xist* in SCNT-generated embryos could be mitigated by conventional siRNA, leading to more than a 10-fold increase in the birth rate of male clones. Although in our previous study we showed a remarkable improvement in SCNT by genetic deletion of *Xist* (6), we thought initially that conventional knockdown would not bring about such a high cloning efficiency. The results obtained in this study were beyond our expectations in three respects.

First, it is generally accepted that nuclear long noncoding RNA molecules such as *Xist* RNA are less amenable to conventional siRNA-knockdown techniques because RNAi-mediated RNA degradation occurs predominantly in the cytoplasm (11–13). This study reports successful knockdown of *Xist* using a specific siRNA, giving a remarkable improvement in cloning efficiency. Although we do not know the exact kinetics of the injected siRNA in the cloned embryos, it is possible that siRNA degraded *Xist* RNA molecules in embryonic cells at the metaphase stage, as has been reported in an RNAi experiment targeting meiotic proteins in metaphase II oocytes (21). In human cell lines, exogenous siRNA was reported to degrade nuclear RNA, as evidenced by the presence of nuclear RNA-induced silencing complexes (22). By contrast, the *Xist*-independent down-regulation of X-linked genes in cloned embryos reported previously (6, 23) was not corrected by RNAi treatment (*SI Text*, Fig. S3, and Table S3), indicating that RNAi strategies are not always effective for improving SCNT outcomes.

Second, unlike a genetic knockout approach, siRNA-mediated knockdown has inherent temporal and quantitative limitations. Indeed, under our experimental conditions, the ectopic *Xist* expression was down-regulated only at the morula stage, and it reappeared at the blastocyst stage. The repression itself was also incomplete, and there was still a modest *Xist* expression at this stage (Fig. 1 *A* and *B*). However, this temporal and incomplete repression of *Xist* resulted in considerable reactivation not only of X-linked genes but also of many autosomal genes. We could not exclude the possibility that *Xist*-siRNA might have also affected *Tsix*, an antisense repressor RNA of *Xist*, and thereby indirectly altered *Xist* expression levels. Thus, despite such inherent limitations and technical ambiguity in the use of siRNA, knockdown of *Xist* had a remarkable genome-wide effect on the expression of its downstream genes and could rescue severe impairment associated with clone development.

Third, we initially assumed that the ectopic *Xist* expression in early-stage cloned embryos would be transmitted, at least in part, to postimplantation cloned embryos because the imprinted XCI in female embryos is normally maintained in the trophectoderm lineage (24, 25) and the same was true for female SCNT embryos (26). However, contrary to our expectation, the eventual disappearance of the XCI markers in male cloned conceptuses suggested that the clone-specific ectopic *Xist* expression was corrected autonomously in both embryonic and extraembryonic tissues (Fig. 4). Although the exact molecular basis remains to be determined, this was likely caused by the initiation of another XCI mechanism that works specifically in postimplantation embryos. This mechanism primarily depends on *Tsix*, which is the antisense transcript from the *Xist* locus and ensures maintenance of the active X chromosome by repressing *Xist in cis* (27). In extraembryonic tissues, *Tsix* plays a particularly important role in both male and female embryos, as revealed by gene knockout studies (27, 28). The same mechanism might have worked in male cloned embryos and erased the aberrant *Xist* expression that had been imposed in earlier stages. Indeed, our RNA-FISH analysis for *Tsix* confirmed that *Tsix* was transcribed in most (>80%) cells of both embryonic and extraembryonic tissues in all E5.5 cloned embryos we examined (Fig. S4).

Taken together with the results we obtained, we can assume that the severely impaired development of SCNT mouse embryos might be largely attributed to an ectopic *Xist* expression from the active X chromosome that can be confined to a narrow stage before implantation. Thus, *Xist* knockdown (and knockout,

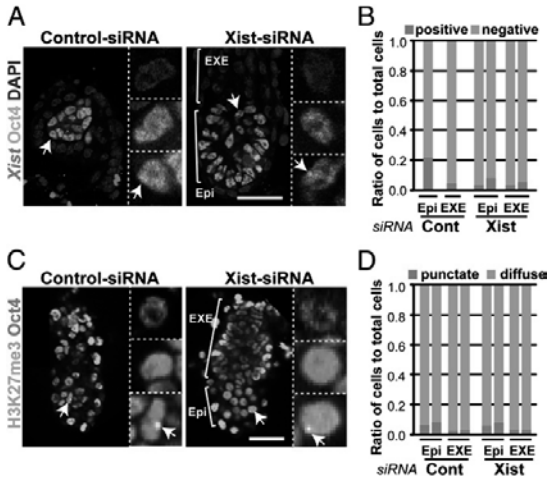

Fig. 4. The XCI status of cloned embryos at E5.5. (*A*) RNA-FISH analyses of *Xist* (red) combined with immunostaining for Oct4 (green) in control or *Xist*-siRNA–injected cloned embryos. There were very few *Xist* signals in either Oct4-positive epiblast (Epi) (*Middle Inset*) or Oct4-negative extraembryonic ectoderm (EXE) (*Top Inset*) in either siRNA group. In these micrographs, only one *Xist*-positive cell was found within the epiblast (arrow; *Bottom Inset*, higher magnification). (Scale bar, 50 μm.) (*B*) Ratios of *Xist*-positive cells in the epiblast or extraembryonic ectoderm region analyzed by RNA FISH. Each column represents a single embryo. Only a few *Xist*-positive cells were observed in the regions irrespective of siRNA treatment. (*C*) Immunostaining for H3K27me3 (green), another marker for XCI, and Oct4 (red) in control or *Xist*-siRNA–treated cloned embryos. There were very few punctate H3K27me3 signals in either epiblast (*Middle Inset*) or extraembryonic ectoderm (*Top Inset*) in either siRNA group. The nuclei of some EXE cells showed relatively weak and diffuse staining for H3K27me3, which does not represent XCI. In these micrographs, only a single cell within the epiblast showed a punctate H3K27me3 signal (arrow; *Bottom Inset*). (Scale bar, 50 μm.) (*D*) Ratios of cells classified according to the punctate or diffuse patterns of H3K27me3 signals. Each column represents a single embryo. Consistent with the results of *Xist* RNA FISH, the punctate signals for H3K27me3 were rarely observed in cloned embryos in either group.

too) probably exerted its greatest effect in rescuing cloned embryos during this very short period, leading to the remarkable improvements in cloning efficiency. A schematic representation of this assumption, together with the putative survival curve of clones, is shown in Fig. 5.

In addition to its scientific significance, our study also has an important implication for the practical applications of mammalian cloning. Because injecting siRNA into mammalian oocytes or embryos is technically feasible, our *Xist*-knockdown strategy should be readily applicable to other mammalian species such as bovines and pigs. Moreover, *Xist* knockdown had a synergistic effect with TSA, resulting in a birth rate of as high as 20% per embryo transferred. This combination would be a promising strategy for large-animal cloning, where histone deacetylase inhibitors have also proved effective for promoting the development of clones (29, 30). Unlike cloning mice, cloning domestic species by SCNT has often been associated with stillbirth or early neonatal death, which is also one of the major obstacles of SCNT that hamper its broad practical application (1). Although the underlying etiologies of these perinatal abnormalities are not yet understood, dysregulation of the *XIST* gene, in terms of its expression level and promoter hypomethylation, is associated with the neonatal death of clones in bovines and pigs (7–9). In mice, although most clones are alive and look normal at birth, there are also many aberrations in global gene expression patterns in their tissues (20). Interestingly, the present study with *Xist*-siRNA newborn clones revealed that they showed

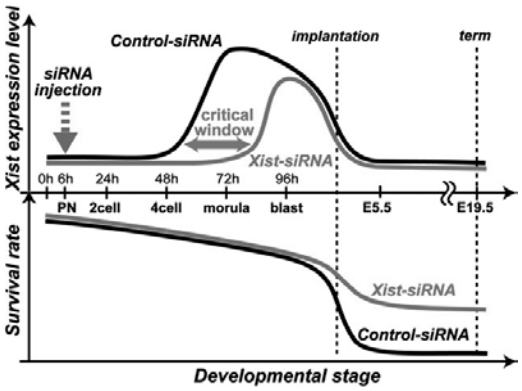

Fig. 5. Schematic representation of siRNA-mediated *Xist* repression and its effect on the survival of male SCNT-generated embryos. (*Upper*) In control cloned embryos, ectopic *Xist* expression increased rapidly from 48 h through 72 h and maintained a high level until 96 h (black line; see also ref. 6). Injection of *Xist*-siRNA into pronuclear (PN)-stage cloned embryos at 6 h (dotted arrow) resulted in repression of the *Xist* level over 48–72 h, but this became ineffective at 96 h (magenta line). Thereafter, around implantation, ectopic *Xist* expression diminished spontaneously from all embryonic tissues in *Xist*-siRNA and control embryos. (*Lower*) Repression of *Xist* by siRNA had a remarkable effect on the survival of cloned embryos. As early as E5.5, more than 10 times as many *Xist*-siRNA embryos survived compared with control embryos, and this high survival persisted until term. These results suggest that the adverse effects of ectopic *Xist* expression in cloned embryos are confined to a short critical time window in the preimplantation period and that this can be reversed very efficiently by injecting *Xist*-siRNA into SCNT-derived embryos.

only a limited dysregulation of their gene expression (Fig. 3*D*), indicating that correction of *Xist* expression in preimplantation embryos might have long-term effects on their development and postnatal growth. If this is also the case with domestic species, we may expect that more clones would be born healthy at term following SCNT with a *XIST*-knockdown approach. This might realize the long-awaited breakthrough for SCNT technology in mammals, as it holds great potential in commercial animal breeding, producing gene-modified animals for medical and bioindustrial uses, and generating stem cells for regenerative medicine.

Methods

Animal Experiments. All animal experiments described here were approved by the Animal Experimentation Committee at the RIKEN Tsukuba Institute and were performed in accordance with the committee's guiding principles.

Preparation of siRNAs and mRNAs. Synthetic siRNA duplexes were designed by Stealth Designer (Life Technologies Japan) as follows. For *Xist*, 5′-AUAACAGUAAGUCUGAUAGAGGACA-3′ and 5′-UGUCCUCUAUCAGACUUACUGUUAU-3′; for negative control, 5′-UUACUCAUGUGUCAUAACACAGGUG-3′ and 5′-CACCUGUGUUAUGACACAUGAGUAA-3′. Primers MSS201293 and MSS293979 were used for *G9a* (*Ehmt2*) and *Glp* (*Ehmt1*), respectively. siRNA duplex mixtures were prepared as 200 μM stock solutions and stored at –80 °C until use. mRNAs for *Jhdm2a* were synthesized by a T7 mMESSAGE mMACHINE Kit (Ambion) and dissolved in water to a final concentration of 100 pg/mL.

Preparation of Donor Sertoli Cells. Testicular masses of 1- to 9-d-old (C57BL/6 × DBA/2) F1 (BDF1) male mice were treated with 0.1 mg/mL collagenase (Sigma-Aldrich) for 30 min at 37 °C, followed by 0.2 mg/mL trypsin (Sigma-Aldrich) for 5 min at 37 °C (31). The cell suspension was washed with PBS containing 4 mg/mL BSA and used for nuclear transfer.

Nuclear Transfer. Nuclear transfer was carried out as described (19, 31). Briefly, recipient oocytes were collected from BDF1 female mice by superovulation and enucleated in Hepes-buffered potassium modified simplex optimization medium (KSOM) containing 7.5 μg/mL cytochalasin B. Thereafter, the donor Sertoli

cell nuclei were injected into enucleated oocytes using a Piezo-driven micromanipulator (PMM-150FU; Prime Tech). After 1 h of culture, the SCNT-treated oocytes were activated with 2.5 mM $SrCl_2$ for 1 h. The reconstructed embryos were cultured in KSOM containing 5 μg/mL cytochalasin B for 5 h, followed by further culture in KSOM. In some experiments, trichostatin A (Sigma-Aldrich) was added to each medium (5 and 50 nM final concentrations) from the beginning of oocyte activation for 6 and 8 h in total, respectively.

siRNA and mRNA Injection. Microinjection of siRNA or mRNA was carried out by using a Piezo-driven micropipette (Prime Tech). To examine the time schedule of siRNA injection, siRNAs (5 mM final concentration) were injected into BDF1 oocytes before and after parthenogenetic activation with $SrCl_2$ (Fig. S1). SCNT-generated or IVF embryos were injected with siRNA 6–7 h after activation, corresponding to the pronuclear (one-cell) stage (Fig. 3). In some experiments, injections of mRNA (1–100 pg/mL) into oocytes were performed just before SCNT.

Embryo Transfer and Recovery. Embryos at the two-cell stage were transferred into the oviducts of ICR strain recipient mice at day 1 of pseudopregnancy. On day 20, the recipient females were examined for the presence of term fetuses. Some recipients were killed on day 6, corresponding to E5.5, and the implanted embryos were recovered carefully from the uteri.

RNA Amplification and Microarray Analyses. Total RNA was extracted with TRIzol (Invitrogen) from single embryos generated by nuclear transfer or IVF (32). They were subjected to linear amplification using TargetAmp Two-Round Aminoallyl-aRNA Amplification Kits (Epicentre Biotechnologies). Amplified RNA was labeled with Cy3 dye (GE Healthcare) and hybridized to a whole mouse genome oligo DNA microarray (4 × 44 K; Agilent Technologies) for 17 h at 65 °C. The scanned images of microarray slides were processed using Feature Extraction software (Agilent Technologies). All raw data were loaded into Gene Spring GX 11 (Agilent Technologies) and transformed by quantile normalization. For analyzing gene expression patterns on the X chromosome, signal intensities with mean values of more than 50 units in IVF embryos were chosen, and the mean values of 20 genes were plotted in accordance with their chromosomal locations.

For the examination of gene expression in neonatal mice, total RNA was also prepared using TRIzol (Invitrogen) and further purified using an RNeasy Mini Kit (Qiagen). The probe for hybridization was synthesized according to the manufacturer's protocol (Agilent Technologies). Data were analyzed using the R package (http://www.r-project.org/) with Bioconductor (http://www.bioconductor.org/) and Cluster 3.0 (http://bonsai.hgc.jp/~mdehoon/software/cluster/software.htm).

Quantitative RT-PCR. cDNAs of single embryos were synthesized with Cell to cDNAII Kits (Ambion). Quantitative PCR was performed using QuantiTect SYBR Green PCR Kits (Qiagen) and the Prism 7900HT System (Applied Biosystems). All PCR runs were performed at an annealing temperature of 60 °C for 50 cycles. The primer sequences were as follows. For *Xist*, 5′-GTCAGCAAGAGCCTT-GAATTG-3′ and 5′-TTTGCTGAGTCTTGAGGAGAATC-3′; for *Gapdh*, 5′-CAACAG-CAACTCCCACTCTTC-3′ and 5′-CCTGTTGCTGTAGCCGTATTC-3′.

Immunofluorescence. Embryos were fixed with 4% paraformaldehyde overnight at 4 °C. After permeabilization with PBST (0.5% Triton X-100 in PBS), they were incubated in a mixture of rabbit anti-H3K27me3 antibody (1:100 dilution; Millipore) and goat anti-Oct4 antibody (1:100 dilution; Santa Cruz Biotechnology) overnight at 4 °C. Immunostaining was revealed with Alexa Fluor-488- and -546-conjugated secondary antibodies (Invitrogen) and observed using a confocal scanning laser microscope (Digital Eclipse C1; Nikon).

RNA FISH. A probe to detect *Xist* RNA was prepared by nick translation with Cy3-dCTP (GE Healthcare) from a *Xist* genomic clone encompassing a 7.5-kb fragment of exon 1. An antisense single-strand DNA probe for detecting *Tsix* RNA was labeled with Cy3-dCTP by random-primed reverse transcription from in vitro transcribed *Tsix* RNA. A plasmid containing a 9.2-kb *Tsix* genomic fragment encompassing exons 2 and 3 of *Tsix* was used as a template for synthesizing sense-strand *Tsix* RNA. Embryos were incubated in PBST for 10 s on ice and fixed with 4% paraformaldehyde for 10 min at room temperature. Hybridization was carried out at 37 °C overnight. The nuclei of embryos were stained with TO-PRO-3 (Invitrogen). In some experiments, immunostaining against Oct4, as described above, was followed by *Xist* RNA FISH.

Statistical Analysis. Developmental rates of embryos were compared between groups using Fisher's exact test. The relative transcription levels determined by quantitative RT-PCR were analyzed by Student's *t* test for comparing group means. The microarray datasets were analyzed using fold-change analyses (cutoff >10) or one-way ANOVA followed by Tukey's post hoc test, and $P < 0.05$ was considered statistically significant.

ACKNOWLEDGMENTS. This research was supported by grants from the Ministry of Education, Culture, Sports, Science and Technology (Japan) (to S.M., K.I., and A.O.), Joint Usage/Research Program of Medical Research Institute Tokyo Medical and Dental University (T.K. and A.O.), and the Novartis Foundation (Japan) for the Promotion of Science (to K.I.).

1. Meissner A, Jaenisch R (2006) Mammalian nuclear transfer. *Dev Dyn* 235:2460–2469.
2. Gurdon J, Murdoch A (2008) Nuclear transfer and iPS may work best together. *Cell Stem Cell* 2(2):135–138.
3. Yamanaka S, Blau HM (2010) Nuclear reprogramming to a pluripotent state by three approaches. *Nature* 465:704–712.
4. Thuan NV, Kishigami S, Wakayama T (2010) How to improve the success rate of mouse cloning technology. *J Reprod Dev* 56(1):20–30.
5. Okamoto I, Heard E (2009) Lessons from comparative analysis of X-chromosome inactivation in mammals. *Chromosome Res* 17:659–669.
6. Inoue K, et al. (2010) Impeding *Xist* expression from the active X chromosome improves mouse somatic cell nuclear transfer. *Science* 330:496–499.
7. Xue F, et al. (2002) Aberrant patterns of X chromosome inactivation in bovine clones. *Nat Genet* 31:216–220.
8. Jiang L, et al. (2008) Expression of X-linked genes in deceased neonates and surviving cloned female piglets. *Mol Reprod Dev* 75:265–273.
9. Su JM, et al. (2011) Expression and methylation status of imprinted genes in placentas of deceased and live cloned transgenic calves. *Theriogenology* 75:1346–1359.
10. Gama Sosa MA, De Gasperi R, Elder GA (2010) Animal transgenesis: An overview. *Brain Struct Funct* 214(2-3):91–109.
11. Scherr M, Eder M (2007) Gene silencing by small regulatory RNAs in mammalian cells. *Cell Cycle* 6:444–449.
12. Siomi H, Siomi MC (2009) On the road to reading the RNA-interference code. *Nature* 457:396–404.
13. Ketting RF (2011) The many faces of RNAi. *Dev Cell* 20(2):148–161.
14. Nesterova TB, Barton SC, Surani MA, Brockdorff N (2001) Loss of *Xist* imprinting in diploid parthenogenetic preimplantation embryos. *Dev Biol* 235:343–350.
15. Plath K, et al. (2003) Role of histone H3 lysine 27 methylation in X inactivation. *Science* 300(5616):131–135.
16. Ang SL, Constam DB (2004) A gene network establishing polarity in the early mouse embryo. *Semin Cell Dev Biol* 15:555–561.
17. Jouneau A, et al. (2006) Developmental abnormalities of NT mouse embryos appear early after implantation. *Development* 133:1597–1607.
18. Kishigami S, et al. (2006) Significant improvement of mouse cloning technique by treatment with trichostatin A after somatic nuclear transfer. *Biochem Biophys Res Commun* 340(1):183–189.
19. Wakayama T, Perry AC, Zuccotti M, Johnson KR, Yanagimachi R (1998) Full-term development of mice from enucleated oocytes injected with cumulus cell nuclei. *Nature* 394:369–374.
20. Kohda T, et al. (2005) Variation in gene expression and aberrantly regulated chromosome regions in cloned mice. *Biol Reprod* 73:1302–1311.
21. Amanai M, Shoji S, Yoshida N, Brahmajosyula M, Perry AC (2006) Injection of mammalian metaphase II oocytes with short interfering RNAs to dissect meiotic and early mitotic events. *Biol Reprod* 75:891–898.
22. Robb GB, Brown KM, Khurana J, Rana TM (2005) Specific and potent RNAi in the nucleus of human cells. *Nat Struct Mol Biol* 12(2):133–137.
23. Fukuda A, et al. (2010) Identification of inappropriately reprogrammed genes by large-scale transcriptome analysis of individual cloned mouse blastocysts. *PLoS One* 5: e11274.
24. Huynh KD, Lee JT (2003) Inheritance of a pre-inactivated paternal X chromosome in early mouse embryos. *Nature* 426:857–862.
25. Sado T, Ferguson-Smith AC (2005) Imprinted X inactivation and reprogramming in the preimplantation mouse embryo. *Hum Mol Genet* 14(Spec No 1):R59–R64.
26. Eggan K, et al. (2000) X-chromosome inactivation in cloned mouse embryos. *Science* 290:1578–1581.
27. Sado T, Wang Z, Sasaki H, Li E (2001) Regulation of imprinted X-chromosome inactivation in mice by Tsix. *Development* 128:1275–1286.
28. Ohhata T, Hoki Y, Sasaki H, Sado T (2006) Tsix-deficient X chromosome does not undergo inactivation in the embryonic lineage in males: Implications for Tsix-independent silencing of Xist. *Cytogenet Genome Res* 113:345–349.
29. Wang YS, et al. (2011) Production of cloned calves by combination treatment of both donor cells and early cloned embryos with 5-aza-2/-deoxycytidine and trichostatin A. *Theriogenology* 75:819–825.
30. Zhao J, et al. (2009) Significant improvement in cloning efficiency of an inbred miniature pig by histone deacetylase inhibitor treatment after somatic cell nuclear transfer. *Biol Reprod* 81:525–530.
31. Ogura A, et al. (2000) Production of male cloned mice from fresh, cultured, and cryopreserved immature Sertoli cells. *Biol Reprod* 62:1579–1584.
32. Mochida K, et al. (2005) Birth of mice after in vitro fertilization using C57BL/6 sperm transported within epididymides at refrigerated temperatures. *Theriogenology* 64(1): 135–143.

分子細胞生物学分野

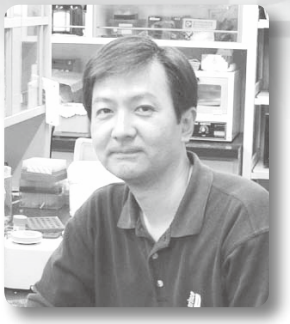

澁谷 浩司

医歯学総合研究科・器官システム制御学系専攻
分子細胞生物学・教授

1）研究の課題名

p38-NLK経路によるXenopus前頭部形成の制御機序

NLKがツメガエルの頭部前方領域の形成に関与していることが示唆されていたことから、前頭部の形成におけるNLKの機能を検討するために、NLKと相互作用する分子群を検索し、MAPキナーゼファミリーの一つであるp38を単離した。ツメガエルにおいて、NLKに関してはこれまでに知られていたNLK（xNLK1）以外にxNLK2（ほ乳類のNLKにより相同性が高い）が存在すること、p38に関してはp38 α、p38 βが頭部形成に関する機能の相違が確認されたことを含めて、下記のような新たな知見を得ることができた。

1）ツメガエル胚において、神経形成期でのxNLK1、xNLK2、p38 α、p38 βの4つの遺伝子の発現は全て頭部前方領域において重なっており、MOを用いてそれぞれの遺伝子の機能を消失させると、xNLK1、xNLK2、p38 βの3つの遺伝子に関して頭部前方領域の形成不全が確認された。p38 αの機能消失は頭部形成に影響を与えなかった。

2）p38 βはxNLK1のN末端付近のセリン残基をリン酸化していたが、xNLK2ではほ乳類のNLKと同様にC末端付近のセリン残基を特異的にリン酸化した。p38 βの機能消失による表現型は、野生型xNLK1と同様に、xNLK2の強制発現では回復されたが、p38 βによるリン酸化部位をアラニンに置換した変異型xNLK2では回復されなかった。

3）xNLK1の機能消失による表現型は、野生型xNLK2の強制発現で、xNLK2の機能消失による表現型は、野生型xNLK1の強制発現で回復された。xNLK1とxNLK2の機能の重複が確認された。

今回得られた新たな知見は、ツメガエルに存在するxNLK1及びxNLK2の両遺伝子のp38 βによるリン酸化修飾を介した機能制御が頭部前方領域の形成過程に重要であることを示唆した。

NLK, an essential effector of anterior formation, functions downstream of p38 MAP kinase

Nemo-like kinase（NLK）is known to function as a mitogen-activated protein kinase（MAPK）-like kinase. However, the upstream molecules and molecular mechanisms that regulate NLK activity remain unclear. In the present study, we identified p38 MAPK as an upstream kinase and activator of NLK. p38 regulates the function of NLK via phosphorylation, and this modification can be abrogated by depletion of endogenous p38. In Xenopus embryos, depletion of either p38 β or NLK by antisense morpholino oligonucleotides results in a severe defect in anterior development and impaired expression of endogenous anterior markers. It is notable that morphants of Xenopus p38 α, another isoform of the p38 MAPK family, exhibited no obvious defects in anterior development. Defects in head formation or expression of anterior marker genes caused by suppression of endogenous p38 β expression could be rescued by expression of wild-type NLK, but not mutant NLK lacking the p38 β phosphorylation site. In contrast, defects in head formation or expression of anterior marker genes caused by suppression of endogenous NLK expression could not be rescued by expression of p38. These results provide the first evidence that p38 specifically regulates NLK function required for the anterior formation in Xenopus development.

2）

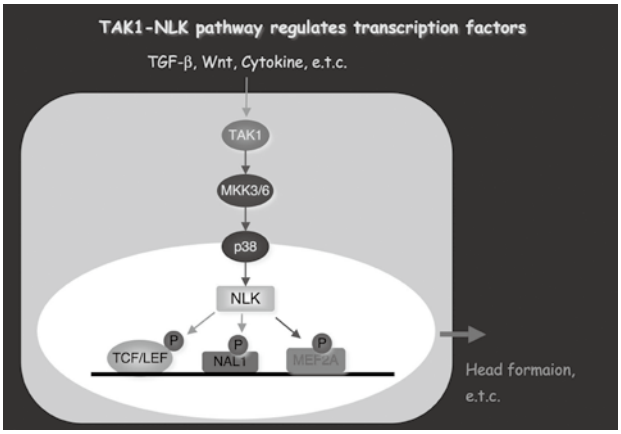

3）発表の研究内容についての英文要約

Leucine-rich repeat kinase LRRK1 regulates endosomal trafficking of the EGF receptor

Activation of the epidermal growth factor receptor（EGFR）initiates multiple signal transduction pathways, including the MAP kinase（MAPK）pathway, but also triggers trafficking events that relocalize the receptors from the cell surface to intracellular endocytic compartments. Here we demonstrate that leucine-rich repeat kinase LRRK1, which contains a MAPKKK-like kinase domain, forms a complex with activated EGFR through an interaction with Grb2. Subsequently, LRRK1 and EGF are internalized and colocalized in early endosomes. LRRK1 regulates EGFR transport from early to late endosomes and regulates the motility of EGFcontaining early endosomes in a manner dependent on its kinase activity. Furthermore, LRRK1 serves as a scaffold facilitating the interaction of EGFR with the ESCRT-0 complex, thus enabling efficient sorting of EGFR to the inner vesicles of multivesicular bodies. Our findings provide the first evidence that a MAPKKK-like protein regulates the endosomal trafficking of EGFR.

4）本事業に関連して世界的な研究拠点形成に向けて、以下の点で改善・整備等されたこと

A（国際化）

分野内でのセミナーを英語で実施している。

5）GCOE事業を推進するに当たって力を入れた点

将来の優秀な研究者に成るべく大学院生の育成

6）英文原著論文

Hanafusa, H., Ishikawa, K., Kedashiro, S., Saigo, T., Iemura, S., Natsume, T., Komada, M., Shibuya, H., Nara, A. and Matsumoto, K.（2011）. Leucine-rich repeat kinase LRRK1 regulates endosomal trafficking of the EGF receptor. Nat Commun. 2, 158.

7）平成23年度までの自己評価

着実に研究が進行し、論文としてまとまりつつある状況である。また、本GCOE国際PIシャペロン教員であった後藤利保を准教授に迎え、研究の質も向上し、今後、数年以内で良い研究成果が得られるものと思われる。

8）学会発表（和文）

A new downstream molecule, Awh is involved in the WNK signaling.

Atsushi Sato, Hiroshi Shibuya

第34回日本分子生物学会年会2011年12月13日、横浜。

9）外部資金の獲得状況

科学研究費補助金、 基盤B

研究題目： WNKシグナルによる発生制御機構の解明

代表： 澁谷浩司

期間： 平成23年―平成25年

研究費総額：1520万円

10）教室、分野や講座の准教授、講師、助教、特別研究員、ポスドク、指導を受けた大学院生の名前

准教授	後藤 利保
助 教	佐藤 淳
大学院生	清水 幹容
	松澤 純平
	大熊 祐一

nature COMMUNICATIONS

OPEN

ARTICLE

Received 26 Aug 2010 | Accepted 8 Dec 2010 | Published 18 Jan 2011

DOI: 10.1038/ncomms1161

Leucine-rich repeat kinase LRRK1 regulates endosomal trafficking of the EGF receptor

Hiroshi Hanafusa[1], Kouki Ishikawa[1], Shin Kedashiro[1], Tsukasa Saigo[1], Shun-ichiro Iemura[2], Tohru Natsume[2], Masayuki Komada[3], Hiroshi Shibuya[4], Atsuki Nara[5] & Kunihiro Matsumoto[1]

Activation of the epidermal growth factor receptor (EGFR) not only initiates multiple signal-transduction pathways, including the MAP kinase (MAPK) pathway, but also triggers trafficking events that relocalize receptors from the cell surface to intracellular endocytic compartments. In this paper, we demonstrate that leucine-rich repeat kinase LRRK1, which contains a MAPKKK-like kinase domain, forms a complex with activated EGFR through an interaction with Grb2. Subsequently, LRRK1 and epidermal growth factor (EGF) are internalized and co-localized in early endosomes. LRRK1 regulates EGFR transport from early to late endosomes and regulates the motility of EGF-containing early endosomes in a manner dependent on its kinase activity. Furthermore, LRRK1 serves as a scaffold facilitating the interaction of EGFR with the endosomal sorting complex required for transport-0 complex, thus enabling efficient sorting of EGFR to the inner vesicles of multivesicular bodies. Our findings provide the first evidence that a MAPKKK-like protein regulates the endosomal trafficking of EGFR.

[1] Department of Molecular Biology, Graduate school of Science, Nagoya University, Chikusa-ku, Nagoya 464-8602, Japan. [2] National Institutes of Advanced Industrial Science and Technology, Biological Information Research Center (JBIRC), Kohtoh-ku, Tokyo 135-0064, Japan. [3] Department of Biological Sciences, Graduate school of Bioscience and Biotechnology, Tokyo Institute of Technology, 4259-B-16 Nagatsuta, Midori-ku, Yokohama 226-8501, Japan. [4] Department of Molecular Cell Biology, Medical Research Institute, Tokyo Medical and Dental University, Chiyoda-ku, Tokyo 101-0062, Japan. [5] Faculty of Bioscience, Nagahama Institute of Bio-Science and Technology, Nagahama, Shiga 526-0829, Japan. Correspondence and requests for materials should be addressed to K.M. (email: g44177a@nucc.cc.nagoya-u.ac.jp).

© 2011 Macmillan Publishers Limited. All rights reserved.

Binding of epidermal growth factor (EGF) to its cell surface receptor (EGFR) results in the activation of numerous cell signalling pathways essential for cellular proliferation, survival and differentiation. Activation of EGFR also initiates events leading to its endocytosis[1,2]. Receptors, once internalized, are delivered to the endosomal system, from where they are either recycled to the cell surface or sorted to lysosomes for degradation[3–5]. Endocytic trafficking serves as an important determinant of the intensity and duration of EGFR signalling.

Recent studies have shown that the endosomal sorting complexes required for transport, ESCRT-0, -I, -II and -III, are involved in the endosomal sorting of ubiquitinated EGFR to lysosomes through multivesicular bodies (MVBs)[6–10]. The ESCRT-0 complex, which is composed of hepatocyte growth factor-regulated substrate (Hrs) and signal-transducing adaptor molecule (STAM), is believed to initiate the process by which EGFR is targeted to lysosomes at the early endosome stage. This targeting involves the clustering of ubiquitinated EGFR underneath a clathrin microdomain by recruiting the ESCRT-I complex to the surface of endosomes. Binding of ESCRT-I to the surface of endosomes leads to the sequential recruitment of ESCRT-II and ESCRT-III complexes. These complexes function sequentially in the formation of MVB vesicles and in the sorting of EGFR into the MVB pathway. Thus, the recognition of EGFR by the ESCRT-0 complex is a critical step in the sorting of EGFR to lysosomes.

Human LRRK1 and LRRK2 belong to the ROCO family of proteins and contain a Roc (Ras in complex proteins) domain together with a MAPKKK-like kinase domain and several protein–protein interaction domains. Recently, LRRK2 has been reported to be involved in the pathogenesis of familial Parkinson's disease[11,12]. However, the functions of LRRK1 and LRRK2 remain unknown.

In this study, we identified Grb2, which is known to be essential for EGFR signalling and endocytosis[1,13–16], as an LRRK1-interacting protein. We demonstrate that LRRK1 participates in the intracellular trafficking of EGFR through an interaction with Grb2. Our findings indicate that LRRK1 regulates transport and sorting of EGFR in a manner dependent on and independent of its kinase activity, respectively.

Results

LRRK1 forms a complex with activated EGFR via Grb2. To investigate the physiological roles of LRRK1, we attempted to identify molecules with which it interacts. We used liquid chromatography-coupled tandem mass spectrometry (LC–MS/MS)[17], and identified multiple peptides (Supplementary Table S1). Among the proteins identified, we focused on the Grb2 protein. To confirm the association between LRRK1 and Grb2, COS7 cells were co-transfected with Flag-LRRK1 and HA-Grb2. As seen in Figure 1a, Flag-LRRK1 associated with HA-Grb2. This association was specific for LRRK1, because LRRK2 did not interact with Grb2 (Fig. 1a).

Grb2 contains a single SH2 domain flanked by two SH3 domains[14]. We examined whether the SH2 or SH3 domain is required for interaction with LRRK1. Mutations in the amino (N)-terminal SH3 (P49L) or SH2 (S90N) domain of Grb2 had no effect on its interaction with LRRK1 (Fig. 1a). In contrast, a mutation in its carboxy (C)-terminal SH3 domain (G203R) resulted in the loss of detectable binding to LRRK1 (Fig. 1a). Thus, interaction of Grb2 with LRRK1 requires the C-terminal SH3 domain of Grb2. We next examined which region of LRRK1 is required for its association with Grb2. We constructed several deletion mutants of LRRK1 (Fig. 1b) and analysed their binding to Grb2. C-terminal-deleted mutants LRRK1(1–1163) and LRRK1(1–595), but not the N-terminal-deleted mutant LRRK1(1164–1989), bound to Grb2 (Supplementary Fig. S1). It is known that the SH3 domain of Grb2 binds to the proline-based motif PXXP[14]. As the LRRK1(1–595) fragment contains two PXXP motifs, which are located at residues 88–91 and 119–122 (Fig. 1b), we examined whether these sites are responsible for Grb2 association. We found that mutation of the Pro residues in both PXXP motifs to Ala (mutant LRRK1(P88A/P91A/P119A/P122A); LRRK1(4PA)) eliminated binding to Grb2 (Fig. 1c). These results indicate that LRRK1 associates with Grb2 through an interaction between the PXXP motifs of LRRK1 and the C-terminal SH3 domain of Grb2. Using a polyclonal anti-LRRK1 antibody that we generated (Supplementary Fig. S2), we also investigated the interaction of endogenously expressed LRRK1 and Grb2. We found that endogenous LRRK1 was able to associate with endogenous Grb2 in a ligand-independent manner (Fig. 1d).

Because Grb2 functions as an adaptor protein facilitating the association of several factors with activated EGFR[14,15], we examined whether LRRK1 forms a complex with EGFR in response to EGF stimulation. COS7 cells were transfected with GFP-LRRK1. We found that GFP-LRRK1 bound to EGFR in a stimulus-dependent manner (Fig. 1e). In contrast, the Grb2-binding-defective mutant GFP-LRRK1(4PA) was unable to associate with EGFR after EGF stimulation (Fig. 1e), suggesting that Grb2 mediates the interaction between LRRK1 and EGFR. We also found that endogenous LRRK1 was able to form a complex with EGFR following EGF stimulation (Fig. 1f). Furthermore, when cells were depleted of Grb2 by transfection with small interfering RNA (siRNA), LRRK1 was unable to interact with EGFR in response to EGF stimulation, regardless of where endogenous or overexpressed LRRK1 was used (Fig. 1f; Supplementary Fig. S3). Taken together, these results demonstrate that LRRK1 forms a complex with EGFR in response to EGF stimulation in a Grb2-dependent manner.

LRRK1 co-localizes with EGF in early endosomes. To investigate the role of LRRK1 in EGFR signalling, we examined the subcellular localization of LRRK1. Because our polyclonal anti-LRRK1 antibody did not provide a sensitive enough detection of the endogenous protein by immunostaining, we used an epitope-tagged LRRK1. We expressed GFP-LRRK1 in HeLa cells and assessed LRRK1 localization by immunofluorescence under basal and EGF-stimulated conditions, together with a fluorescently labelled rhodamine-conjugated EGF (EGF-Rh). LRRK1 was diffusely distributed in cells not treated with EGF-Rh (Fig. 2a). When cells were stimulated with EGF-Rh for 15 min, GFP-LRRK1 became distributed in a fine, punctate pattern that co-localized with EGF-Rh. A large portion of GFP-LRRK1 overlapped with the early endosomal marker autoantigen 1 (EEA1) receptor (Fig. 2b; Supplementary Fig. S4).

We next analysed the ability of Grb2 to affect the intracellular localization of LRRK1 in EGF-stimulated cells. When Grb2 was depleted from HeLa S3 cells using siRNA, EGF-induced localization of LRRK1 in EEA1-positive early endosomes was greatly decreased (Fig. 2c,d; Supplementary Fig. S5a). This suggests that Grb2 is required for the EGF-induced translocation of LRRK1 to early endosomes. Consistent with this, LRRK1(4PA), which is defective for Grb2 binding, failed to localize to early endosomes in response to EGF stimulation (Fig. 2e; Supplementary Fig. S5b). Thus, EGF-induced localization of LRRK1 to early endosomes is dependent on Grb2-mediated complex formation with activated EGFR.

LRRK1 regulates EGFR transport from early to late endosomes. Given the EGF-dependent association of LRRK1 with the early endosome, we reasoned that LRRK1 might function by affecting the endocytic trafficking of EGFR. To test this idea, we monitored the endocytic movement of EGF in cells depleted of LRRK1 by siRNA. HeLa S3 cells incubated with LRRK1 siRNA had a much lower expression of LRRK1 (Supplementary Fig. S6). HeLa S3 cells treated with control or LRRK1 siRNA were stimulated with fluorescent EGF (Alexa 647-EGF) briefly, followed by washing to remove labelled EGF from the medium. Under these conditions, the fluorescence detected in cells was due to endocytosed EGFR bound to

© 2011 Macmillan Publishers Limited. All rights reserved.

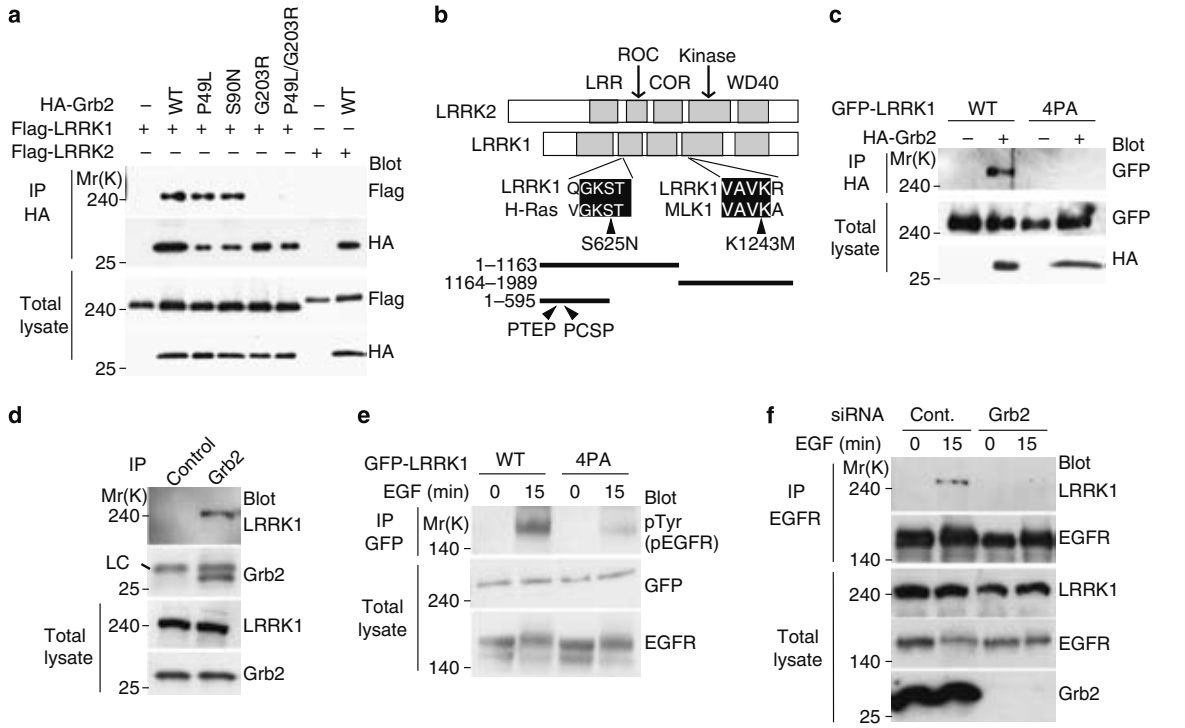

Figure 1 | LRRK1 forms a complex with EGFR via Grb2 in response to EGF stimulation. (**a**) Interaction of LRRK1 with Grb2. COS7 cells were co-transfected with Flag-LRRK1, Flag-LRRK2 and HA-Grb2 (wild type (WT), P49L, S90N, G203R and P49L/G203R mutants), as indicated. Complex formation was detected by immunoprecipitation (IP) with anti-HA antibodies, followed by immunoblotting (Blot) with anti-Flag antibodies. (**b**) Comparison of LRRK1 and LRRK2 structures. Schematic diagrams of human LRRK1 and LRRK2 proteins are shown. Domains are shown as follows: leucine-rich repeats (LRR), a Roc domain, a Cor domain, a MAPKKK-like kinase domain and WD40 repeats. The sequence alignment of LRRK1 and H-Ras in the Roc domain and of LRRK1 and mixed-lineage kinase 1 (MLK1) in the kinase domain are shown. Identical residues are highlighted with black shading. Arrowheads indicate amino-acid substitutions used in this study. Deletion constructs of LRRK1 are shown below. Two PXXP motifs within LRRK1(1–595) are shown by the arrowheads. (**c**) Effect of the 4PA mutation on the interaction of LRRK1 with Grb2. COS7 cells were co-transfected with GFP-LRRK1 (wild type and the 4PA mutant) and HA-Grb2, as indicated. Complex formation was detected by immunoprecipitation (IP) with anti-HA antibodies, followed by immunoblotting (Blot) with anti-GFP antibodies. (**d**) Interaction of endogenous LRRK1 with endogenous Grb2. Complex formation in HEK293 cells was detected by immunoprecipitation (IP) with anti-Grb2 antibodies, followed by immunoblotting (Blot) with anti-LRRK1 antibodies. LC, light chain. (**e**) Effect of the 4PA mutation on the interaction of LRRK1 with activated EGFR. COS7 cells were transfected with GFP-LRRK1 (wild type and the 4PA mutant). After 16 h of serum starvation, cells were stimulated with 100 ng per ml of EGF. Complex formation was detected by immunoprecipitation (IP) with anti-GFP antibodies, followed by immunoblotting (Blot) with anti-phospho-tyrosine (pTyr) antibodies. (**f**) Interaction of endogenous LRRK1 with endogenous EGFR. HEK293 cells treated with control or Grb2 siRNA were serum starved and stimulated with 100 ng per ml of EGF. Complex formation was detected by immunoprecipitation (IP) with anti-EGFR antibodies, followed by immunoblotting (Blot) with anti-LRRK1 antibodies.

labelled growth factor. In LRRK1-depleted cells, the initial localization of EGF to clathrin-coated pits occurred normally, similar to control cells (Supplementary Fig. S7). Thus, depletion of LRRK1 has little obvious effect on the internalization of EGF/EGFR.

Because it is known that Rab5 and Rab7 primarily associate with early and late endosomes, respectively, we coexpressed GFP-Rab5 and DsRed-Rab7 in HeLa S3 cells to visualize early and late endosomes. In this experiment, we used the monomer version of DsRed. Most of the Rab5-positive endosomes were distributed in the cell periphery, whereas Rab7-positive endosomes were more common in the perinuclear region (Fig. 3a–d). In control siRNA-transfected cells, at 10 min after a brief pulse of Alexa 647-EGF stimulation, most of the EGF was found in early endosomes, as evidenced by their co-localization with Rab5 (Fig. 3a,e; Supplementary Fig. S8a). After 15 min, EGF dissociated from the early endosomes, as illustrated by decreased co-localization with Rab5. Remarkably, this decreased co-localization with Rab5 was accompanied by an increase in the co-localization with Rab7 (Fig. 3b,e and f; Supplementary Fig. S8b), suggesting the progression of EGFR to the late-endosomal compartments. In LRRK1-depleted cells, the early endosomal localization of EGF occurred normally, as in control cells (Fig. 3c,e; Supplementary Fig. S8c). However, after 15 min of stimulation, Alexa 647-EGF remained associated with Rab5-positive structures and Rab7 co-localization did not increase (Fig. 3d–f; Supplementary Fig. S8d). This suggests that the transport of EGFR towards late endosomes is inhibited in LRRK1-deficient cells. Thus, LRRK1 is required for the progression of EGFR from early to late endosomes.

LRRK1 regulates the motility of EGF-early endosomes. Because maturation of early to late endosomes is accompanied by the movement of endosomes towards the cell centre[18–20], we examined the effect of LRRK1 knockdown on the movement of EGF-containing early endosomes. Using time-lapse confocal fluorescence microscopy, movement of EGF-containing early endosomes was followed in cells expressing GFP-Rab5 at 15 min after a brief pulse of

© 2011 Macmillan Publishers Limited. All rights reserved.

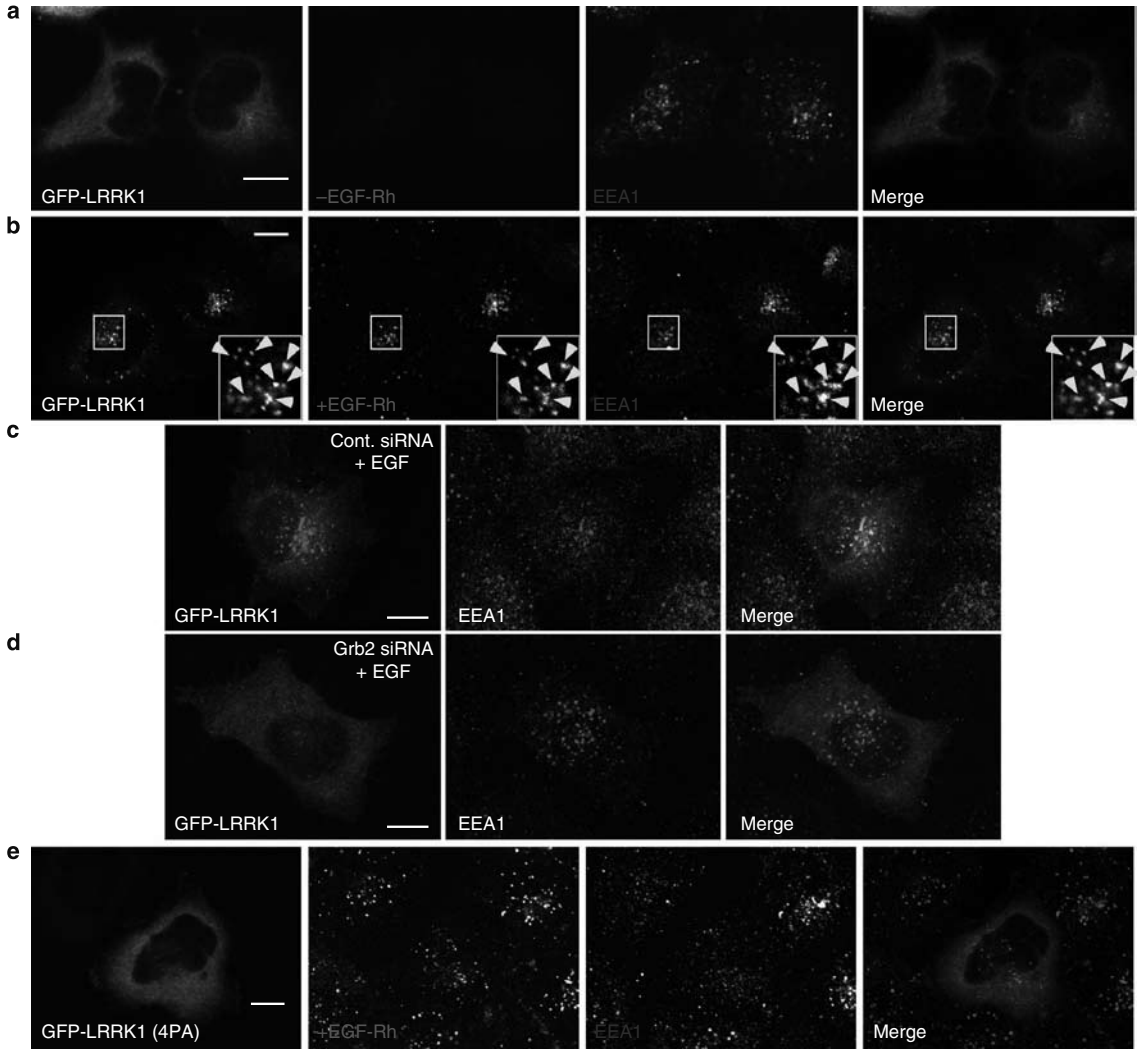

Figure 2 | LRRK1 co-localizes with EGF in early endosomes. (**a**,**b**) Co-localization of LRRK1 with EGF in EEA1-labelled early endosomes. HeLa cells were transfected with GFP-LRRK1. After 16 h of serum starvation, cells were incubated without (**a**) or with (**b**) 50 ng per ml of EGF-Rh (red) for 45 min at 4°C, followed by warming for 15 min at 37°C, and stained with anti-EEA1 antibodies (blue). All cells were imaged by confocal microscopy. The boxed regions are magnified in insets. Examples of co-localization of GFP-LRRK1, EGF-Rh and EEA1 are indicated with arrowheads (Supplementary Fig. S4). Scale bar, 10 μm. (**c**, **d**) Effect of Grb2 depletion on LRRK1 localization in early endosomes. HeLa S3 cells treated with control (**c**) or Grb2 siRNA (**d**) were transfected with GFP-LRRK1. After 16 h of serum starvation, cells were stimulated with 100 ng per ml of EGF for 15 min. The cells were fixed, stained with anti-EEA1 antibodies and imaged by confocal microscopy. Yellow colour in the merged images indicates co-localization. Scale bar, 10 μm. (**e**) Effect of 4PA mutation on LRRK1 localization. HeLa cells were transfected with GFP-LRRK1(4PA). After 16 h of serum starvation, cells were incubated with 50 ng per ml of EGF-Rh (red) for 45 min at 4°C, followed by warming for 15 min at 37°C, and stained with anti-EEA1 antibodies (blue). All cells were imaged by confocal microscopy. Scale bar, 10 μm.

Alexa647-EGF. In addition to short-range movement, long-range rapid movement of EGF-positive early endosomes from the periphery to the centre was frequently observed (Fig. 4a,b). When LRRK1 was knocked down by siRNA, long-range rapid movement of EGF-containing early endosomes was remarkably disrupted (Fig. 4c,d). In control cells, 39.7% of GFP-Rab5- and Alexa 647-EGF-double-positive endosomes moved more than 3.0 μm during the imaging time (35 s), but this fraction decreased to only 2.4% in LRRK1-depleted cells (Fig. 4e). We further confirmed this effect of knocking down LRRK1 on the frequency of long-range movement of EGF using a different LRRK1 siRNA in different HeLa cell lines (Supplementary Fig. S9). These observations suggest that LRRK1 is required for the motility of EGF-containing early endosomes.

The role of Roc and kinase domains in EGFR trafficking. Ras proteins switch between an inactive GDP-bound state and an active GTP-bound state and only the latter interacts with its downstream effectors. Among the best characterized downstream effectors of Ras are the MAPKKKs[21]. Members of the ROCO protein family contain a Ras GTPase-like (Roc) domain and a MAPKKK domain (Fig. 1b). The Roc domain likely serves as a molecular switch, regulating kinase activity by cycling between GDP-bound and

© 2011 Macmillan Publishers Limited. All rights reserved.

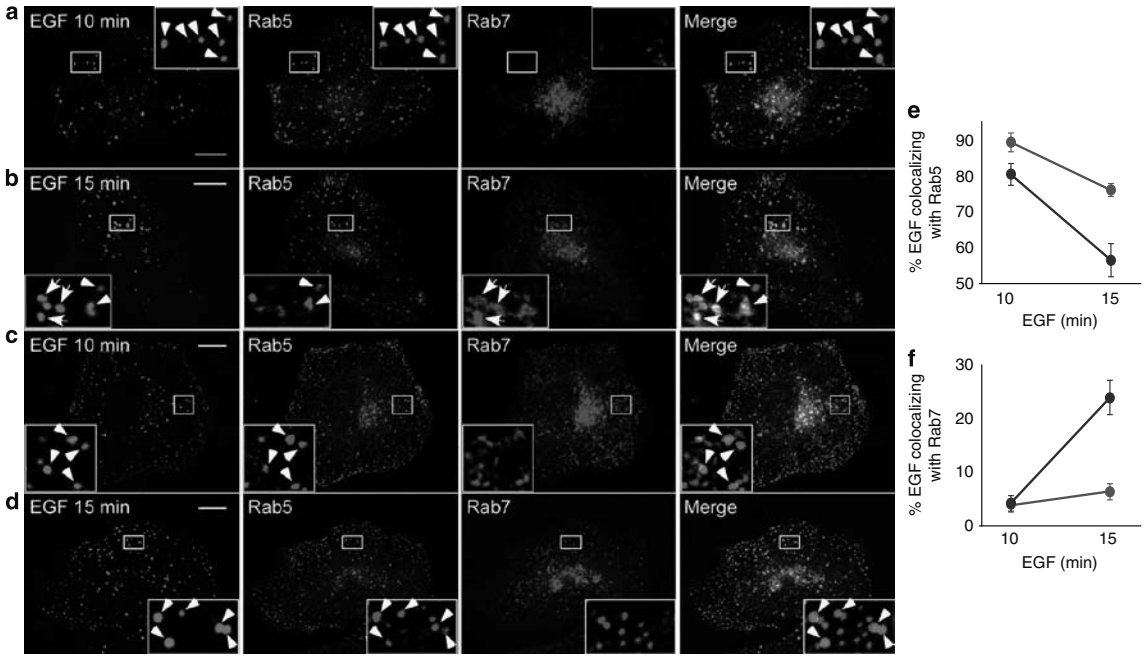

Figure 3 | Depletion of LRRK1 inhibits EGFR transport from early to late endosomes. (**a**, **b**) HeLa S3 cells treated with control siRNA were co-transfected with GFP-Rab5 and DsRed-Rab7. After 16 h of serum starvation, cells were stimulated with 100 ng per ml of Alexa 647-EGF for 3 min at 37°C, followed by washing to remove labelled EGF from the medium. The cells were fixed at 10 min (**a**) and 15 min (**b**) after the initial exposure to Alexa 647-EGF and imaged by confocal microscopy. The boxed regions are magnified in insets. Arrowheads and arrows indicate co-localization of Alexa 647-EGF with GFP-Rab5 and DsRed-Rab7, respectively (Supplementary Fig. S8). Scale bar, 10 μm. (**c**, **d**) Effect of LRRK1 depletion on EGFR transport from early to late endosomes. HeLa S3 cells treated with LRRK1 siRNA (Stealth#1) were co-transfected with GFP-Rab5 and DsRed-Rab7. After 16 h of serum starvation, cells were stimulated with 100 ng per ml of Alexa 647-EGF for 3 min at 37°C, followed by washing to remove labelled EGF from the medium. The cells were fixed at 10 min (**c**) and 15 min (**d**) after the initial exposure to Alexa 647-EGF and imaged by confocal microscopy. The boxed regions are magnified in insets. Arrowheads indicate co-localization of Alexa 647-EGF with GFP-Rab5 (Supplementary Fig. S8). Scale bar, 10 μm. (**e**, **f**) Quantification of co-localization of EGFR with Rab5 (**e**) and Rab7 (**f**). Cells treated with control (blue) or LRRK1 siRNA (Stealth#1) (red) were co-transfected with GFP-Rab5 and DsRed-Rab7. After 16 h of serum starvation, cells were stimulated with 100 ng per ml of Alexa 647-EGF for 3 min at 37°C, followed by washing to remove labelled EGF from the medium. The cells were fixed at 10 min and 15 min after the initial exposure to Alexa 647-EGF. Data are presented as percentages of Rab5-labelled (**e**) or Rab7-labelled (**f**) Alexa647-EGF-containing vesicles out of the total number of Alexa647-EGF-containing vesicles per cell. Values reflect the mean s.d. of three independent experiments, with an average of ten cells scored per experiment.

GTP-bound states[22–24]. To test whether the Roc domain of LRRK1 also regulates its kinase activity, we generated LRRK1(S625N) (Fig. 1b), in which Ser-625 in the Roc domain of LRRK1 has been mutated to Asn, on the basis of homology to Ras[25]. We confirmed that the LRRK1(S625N) form lost the ability to bind to GTP sepharose (Supplementary Fig. S10a) and was defective in kinase activity, similar to a kinase-inactive LRRK1(K1243M) (Fig. 1b; Supplementary Fig. S10b). These results are consistent with a model wherein the Roc domain regulates the activity of the kinase domain.

We next examined whether LRRK1(K1243M) or LRRK1(S625N) could rescue the defect in EGFR trafficking caused by LRRK1 knockdown. A large fraction of EGF dissociated from early endosomes 20 min after EGF-Rh stimulation in control siRNA-treated cells (Supplementary Fig. S11a), whereas the EGF remained localized in early endosomes in LRRK1 siRNA-treated cells (Supplementary Fig. S11b), as evidenced by their co-localization with EEA1. Expression of siRNA-resistant wild-type GFP-LRRK1 in LRRK1-depleted cells decreased co-localization of EGF with EEA1 and somewhat enhanced the transport of EGF towards the cell centre at 20 min after EGF-Rh stimulation (Supplementary Fig. S11c), suggesting that EGF was localized in late endosomes. When siRNA-resistant GFP-LRRK1(K1243M) or GFP-LRRK1(S625N) was reintroduced into LRRK1-depleted cells, most of the EGF remained co-localized with EEA1 even after a chase of 20 min (Supplementary Fig. S11d,e). Furthermore, we found that siRNA-resistant wild-type GFP-LRRK1, but not GFP-LRRK1(K1232M), was able to rescue the movement of EGF in LRRK1-depleted cells (Supplementary Fig. S12). These results suggest that the kinase function of LRRK1 is required for the transport of EGF/EGFR from early to late endosomes.

The relationship between LRRK1 and the ESCRT-0 complex. Trafficking of EGF/EGFR in early endosomes is initiated by the interaction of ubiquitinated EGFR with components of the ESCRT-0 complex, STAM and Hrs[6–10]. To determine whether the effect of LRRK1 on EGFR trafficking involves these endosomal sorting components, we examined the interaction of LRRK1 with STAM and Hrs. COS7 cells were transfected with GFP-LRRK1 and stimulated with EGF. Coimmunoprecipitation experiments revealed that LRRK1 associated with endogenous STAM1 and that this interaction was increased by EGF stimulation (Fig. 5a). Furthermore, we found that endogenous LRRK1 was coimmunoprecipitated with endogenous Hrs in an EGF stimulation-dependent manner (Fig. 5b). These results demonstrate that LRRK1 interacts with the ESCRT-0 complex in response to EGF stimulation.

To determine which regions are responsible for the LRRK1–STAM1 interaction, we constructed several deletion mutants of

© 2011 Macmillan Publishers Limited. All rights reserved.

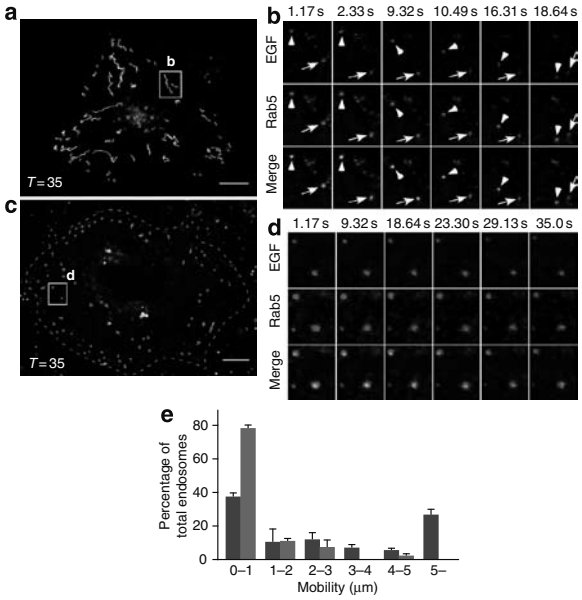

Figure 4 | Depletion of LRRK1 inhibits the motility of EGF-containing early endosomes. (**a**) Images representing GFP-Rab5-positive endosomes containing Alexa 647-EGF (red circles) and tracks (yellow). HeLa S3 cells treated with control siRNA were transfected with GFP-Rab5, pulse-labelled with Alexa 647-EGF. Movement of GFP-Rab5-positive endosomes containing Alexa 647-EGF was observed by time-lapse confocal fluorescence microscopy and analysed using the 'Manual Tracking' Image J plug-in. Imaging started at 15 min after the initial exposure to Alexa 647-EGF, with frames captured at 1.165 s intervals for 35 s. Scale bar, 10 μm. (**b**) Stills from control cells (the boxed region in **a**). Arrowheads and arrows indicate the movement of GFP-Rab5-positive endosome containing Alexa 647-EGF. (**c**) Images representing GFP-Rab5-positive endosomes containing Alexa 647-EGF (red circles) and tracks (yellow). HeLa S3 cells treated with LRRK1 siRNA (Stealth#1) were transfected with GFP-Rab5, pulse-labelled with Alexa 647-EGF. Movement of GFP-Rab5-positive endosomes containing Alexa 647-EGF was observed by time-lapse confocal fluorescence microscopy and analysed using the 'Manual Tracking' Image J plug-in. Imaging started at 15 min after the initial exposure to Alexa 647-EGF, with frames captured at 1.165 s intervals for 35 s. Scale bar, 10 μm. (**d**) Stills from LRRK1-depleted cells (the boxed region in **c**). (**e**) A mobility histogram of randomly selected Rab5- and EGF-double-positive endosomes from control (blue) or LRRK1-depleted cells (red). Mobility is defined as the distance of the trajectory of endosomes during the 35 s observation period, quantified using the 'Manual Tracking' Image J plug-in. Values reflect the mean s.d. of five independent experiments, with an average of 30 Rab5- and EGF-double-positive endosomes scored per experiment.

STAM1 (Fig. 5c). Coimmunoprecipitation assays showed that the coiled-coil domain of STAM1 was important for its interaction with LRRK1 (Fig. 5d). We next tested whether the kinase function of LRRK1 would affect its interaction with STAM1. We found that Flag-STAM1 coimmunoprecipitated with GFP-LRRK1(K1243M) (Fig. 5e), indicating that LRRK1 kinase activity is not required for its association with STAM1. In addition, the Grb2-binding-defective mutant GFP-LRRK1(4PA) was also able to associate with STAM1 (Fig. 5e), suggesting that different regions of LRRK1 interact with Grb2 and STAM1. We next examined whether LRRK1, EGFR and STAM1 exist in the same complex. Flag-STAM1 and Myc-LRRK1 or Myc-LRRK1(K1243M) were coexpressed in COS7 cells and ternary complex formation was investigated via two-step immunoprecipitation. Both Myc-LRRK1 and Myc-LRRK1(K1243M) were able to form a ternary complex with EGFR and STAM1 in response to EGF stimulation (Fig. 5f), indicating that LRRK1 kinase activity is not required for formation of this ternary complex. Given the results showing that LRRK1 interacts with EGFR and the ESCRT-0 complex, we reasoned that loss of LRRK1 should also result in decreased EGFR–ESCRT-0 complex formation. When cells were treated with LRRK1 siRNA, we observed a reduction in the EGF-dependent interaction of activated EGFR with Flag-STAM1 (Fig. 5g). Taken together, these results suggest that LRRK1, by interacting with both Grb2 and the Hrs–STAM1 complex simultaneously, functions as a scaffolding protein linking activated EGFR to the ESCRT-0 complex.

To further evaluate the interaction between LRRK1 and STAM, we examined the potential co-localization of LRRK1 and STAM1 in early endosomes. Previous studies have revealed that Hrs accumulates in restricted microdomains on the endosome membrane, strongly co-localizing with clathrin[26–29]. By contrast, EEA1-containing regions of the endosome membrane are largely devoid of Hrs and clathrin. To study these endosomal microdomains, HeLa S3 cells were transfected with a constitutively active form of Rab5(Q79L), to increase the fusion rate of endosomes[30]. High Rab5 activity results in enlarged early endosomes on which microdomains can be easily distinguished by confocal immunofluorescence microscopy[26,27,29,31]. STAM1 co-localized strongly with clathrin on the enlarged endosomes (Supplementary Fig. S13a), whereas there was little co-localization of STAM1 and EEA1 (Supplementary Fig. S13b). These results suggest that STAM1 participates together with Hrs in the sorting of ubiquitinated cargo in clathrin-coated microdomains of early endosomes. GFP-LRRK1 was mainly distributed to the cytosol in the absence of EGF stimulation (Fig. 6a). However, LRRK1 localization was restricted to the enlarged endosomes of EGF-treated cells, and we could detect a certain degree of localization of GFP-LRRK1 to STAM1-positive microdomains (Fig. 6b). We also found that EGFR co-localized with STAM1 on Rab5(Q79L)-induced enlarged endosomes after EGF stimulation (Fig. 6c). To investigate whether LRRK1 is important for the recruitment of EGFR into STAM1-positive microdomains, we set out to study the relative localizations of EGFR and STAM1 in LRRK1-depleted cells. In such LRRK1-depleted cells, both EGFR and STAM1 could still be detected on endosomes. Interestingly, however, LRRK1-depleted endosomes appeared to show decreased co-localization of EGFR and STAM1 (Fig. 6d). Furthermore, this co-localization gradually increased at the later phase of EGF stimulation (Fig. 6e), indicating that LRRK1 depletion delays EGFR-STAM1 co-localization. We confirmed the effect of LRRK1 depletion on the co-localization of Alexa 647-EGF and STAM1 by three-dimensional reconstruction of confocal Z-stack images (Supplementary Fig. S14). These results suggest that LRRK1 determines the efficiency of recruitment by serving as a scaffolding function on the endosomal membrane to restrict EGFR localization to STAM-positive microdomains.

LRRK1 modulates the ubiquitination status of STAM1. The sorting of ubiquitinated EGFR is initiated by the recognition of EGFR ubiquitin (Ub) moieties by the Ub-interacting motifs (UIMs) within Hrs and STAM[10,32]. Hrs and STAM themselves are also ubiquitinated[32,33], and a recent study has suggested that intramolecular binding between UIMs and Ub prevents Hrs from binding in *trans* to ubiquitinated EGFR[32]. We therefore examined the effect of LRRK1 knockdown on the ubiquitination status of STAM1. We co-transfected HeLa S3 cells with Flag-STAM1 and HA-Ub. In control siRNA cells, we could detect weak ubiquitination of STAM1 and this ubiquitination was enhanced by EGF stimulation (Fig. 7a). Depletion of LRRK1 resulted in hyper-ubiquitination of STAM1 (Fig. 7a). Thus, depletion of LRRK1 results in the enhancement of Ub

© 2011 Macmillan Publishers Limited. All rights reserved.

NATURE COMMUNICATIONS | DOI: 10.1038/ncomms1161

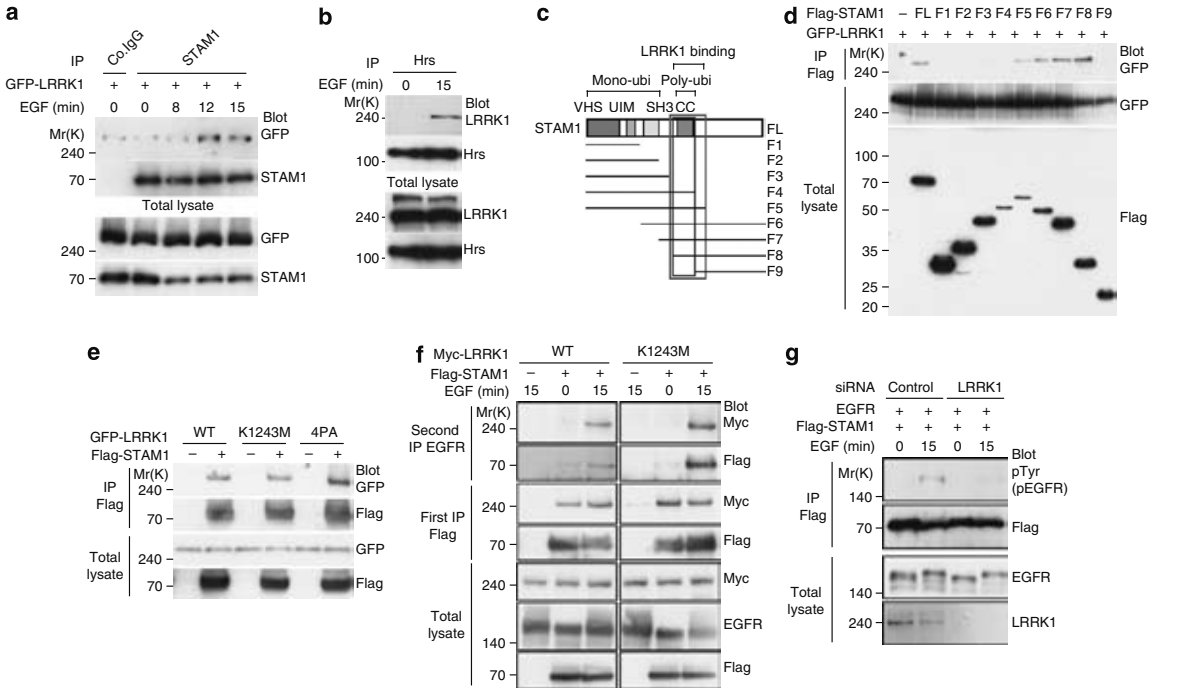

Figure 5 | LRRK1 interacts with the ESCRT-0 complex in response to EGF stimulation. (**a**) Association of LRRK1 with STAM1. COS7 cells were transfected with GFP-LRRK1, and stimulated with 100 ng per ml of EGF. Complex formation was detected by immunoprecipitation (IP) with anti-STAM1 antibodies, followed by immunoblotting (Blot) with anti-GFP antibodies. (**b**) Association of LRRK1 with Hrs. After 16 h of serum starvation, COS7 cells were stimulated with 100 ng per ml of EGF. Complex formation was detected by immunoprecipitation (IP) with anti-Hrs antibodies, followed by immunoblotting (Blot) with anti-LRRK1 antibodies. (**c**) Schematic diagram of STAM1 protein. Deletion constructs of STAM1 are shown below. (**d**) Interaction of STAM1 fragments with LRRK1. COS7 cells were co-transfected with Flag-STAM1 and GFP-LRRK1, as indicated. Complex formation was detected by immunoprecipitation (IP) with anti-Flag antibodies, followed by immunoblotting (Blot) with anti-GFP antibodies. (**e**) Interaction of STAM1 with LRRK1 variants. COS7 cells were co-transfected with GFP-LRRK1 (wild type, K1243M and 4PA mutants) and Flag-STAM1, as indicated. Complex formation was detected by immunoprecipitation (IP) with anti-Flag antibodies, followed by immunoblotting (Blot) with anti-GFP antibodies. (**f**) Both wild-type LRRK1 and LRRK1(K1243M) form a ternary complex with EGFR and STAM1 in response to EGF stimulation. COS7 cells were co-transfected with Myc-LRRK1 (wild type and the K1243 mutant) and Flag-STAM1, as indicated, stimulated with 100 ng per ml of EGF, and collected for the first immunoprecipitation (IP) with anti-Flag antibody-conjugated agarose. Thereafter, the immunocomplexes were eluted by 3xFlag peptide and subjected to the second immunoprecipitation (IP) with anti-EGFR antibodies, followed by immunoblotting (Blot) with anti-Myc and anti-Flag antibodies. (**g**) LRRK1 is required for the interaction between EGFR and STAM1. HeLa S3 cells treated with control or LRRK1 siRNA (Stealth#1) were co-transfected with EGFR and Flag-STAM1, and stimulated with 100 ng per ml of EGF. Complex formation was detected by immunoprecipitation (IP) with anti-Flag antibodies, followed by immunoblotting (Blot) with anti-phospho-tyrosine (pTyr) antibodies.

modification in STAM1. We then examined the effect of LRRK1 overexpression on the ubiquitination status of STAM1. We found that overexpression of LRRK1 inhibited ubiquitination of STAM1 (Fig. 7b). In addition, overexpression of kinase-negative LRRK1(K1243M) was able to inhibit STAM1 ubiquitination (Fig. 7b), suggesting that LRRK1 kinase activity is not necessary for this reaction.

We next attempted to narrow down the region(s) where STAM1 is ubiquitinated, using various deletion mutants of STAM1 (Fig. 5c). Ubiquitination assays revealed that the N-terminal Ub-binding domains (VHS and UIM) and the SH3 domain of STAM1 are important for monoubiquitination, and that the coiled-coil domain contains the majority of polyubiquitination sites in STAM1 (Fig. 7c). Thus, the coiled-coil domain of STAM1 is involved in both its interaction with LRRK1 and its ubiquitination, raising the possibility that LRRK1 inhibits STAM1 ubiquitination by associating with its coiled-coil domain.

The coiled-coil domain in STAM1 has five lysine residues (Fig. 7d). To confirm the importance of the coiled-coil domain for STAM1 ubiquitination, we generated STAM1(5KR), in which all these five lysines have been mutated to arginines. STAM1(5KR) was impaired in polyubiquitination but not in monoubiquitination (Fig. 7d). These results suggest that the lysine residues in the coiled-coil domain of STAM1 are polyubiquitinated. The above results suggested that LRRK1 affects the interaction between EGFR and STAM1 by modulating the ubiquitination status of STAM1. Consistent with this, STAM1(5KR) showed an increase in its interaction with activated EGFR compared with wild-type STAM1 (Fig. 7e). Taken together, these results suggest that LRRK1 functions as a scaffolding protein linking activated EGFR to the ESCRT-0 complex by suppressing the polyubiquitination of STAM1.

LRRK1 regulates sorting of EGF/EGFR into intraluminal vesicles of MVBs. EGFR localized in clathrin-coated microdomains on endosomes is sorted into intraluminal vesicles (ILVs) within MVBs and delivered to lysosomes for degradation. We therefore examined whether LRRK1 knockdown affects the sorting of EGFR into ILVs of enlarged endosomes using three-dimensional reconstructions. In control siRNA-transfected cells, Alexa 647-EGF was translocated

© 2011 Macmillan Publishers Limited. All rights reserved.

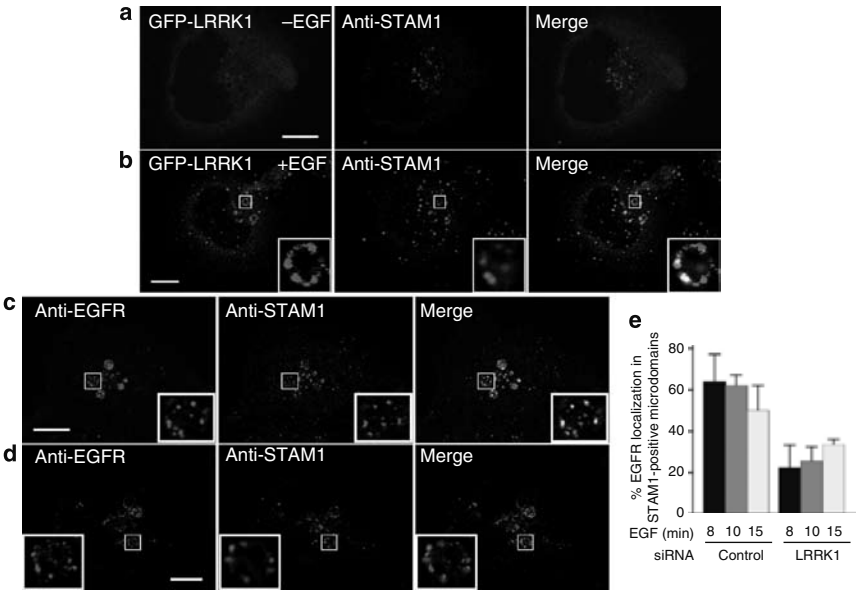

Figure 6 | Localization of LRRK1 and EGFR on STAM1-positive microdomains of early endosomes. (**a**, **b**) Localization of LRRK1 and STAM1 on enlarged endosomes. HeLa S3 cells were co-transfected with DsRed-Rab5(Q79L) and GFP-LRRK1, and stimulated without (**a**) or with (**b**) 100 ng per ml of EGF for 10 min. The cells were fixed and stained with anti-STAM1 antibodies and imaged by confocal microscopy. Experiments were conducted three times with similar results. Scale bar, 10 μm. (**c**, **d**) Effect of LRRK1 depletion on EGFR localization to STAM-positive microdomains of early endosomes. HeLa S3 cells treated with control (**c**) or LRRK1 siRNA (Stealth#1) (**d**) were transfected with GFP-Rab5(Q79L) and stimulated with 100 ng per ml of EGF for 10 min. The cells were fixed, stained with anti-EGFR and anti-STAM1 antibodies and imaged by confocal microscopy. The boxed regions indicate the Rab5(Q79L)-induced enlarged endosomes and are magnified in the inset. Scale bar, 10 μm. (**e**) Quantification of EGFR localization to STAM-positive microdomains of early endosomes. HeLa S3 cells treated with control or LRRK1 siRNA (Stealth#1) were transfected with GFP-Rab5(Q79L), and stimulated with 100 ng per ml of EGF for the indicated times. The cells were fixed, and stained with anti-EGFR and anti-STAM1 antibodies. Data show the percentage of STAM1-labelled EGFR-positive microdomains per endosomes. Values reflect the mean s.d. of three independent experiments, with an average of 15 cells (total 80 endosomes) scored per experiment.

from the limiting membrane to ILVs of Rab5(Q79L)-induced enlarged endosomes at 30 min after EGF stimulation (Fig. 8a). In contrast, depletion of LRRK1 reduced the intraluminal transport of Alexa 647-EGF into enlarged endosomes (Fig. 8b). Line intensity profiles of individual endosomes clearly showed that most of the EGF was localized within the inner membranes in control cells (Fig. 8c), but were retained in the limiting membrane in LRRK1-depleted cells (Fig. 8d). Quantification of EGF labelling showed that about 66.2% of the labelling was localized to the inner membranes in cells treated with control siRNA, whereas only 16.7% showed this localization in cells treated with LRRK1 siRNA (Fig. 8e). These results demonstrate that LRRK1 is needed for sorting of EGF/EGFR into ILVs of MVBs. When siRNA-resistant, wild-type GFP-LRRK1 was expressed in LRRK1-depleted cells, the defect in the intraluminal transport of Alexa 647-EGF was partially rescued (Fig. 8e). However, expression of the siRNA-resistant, kinase-negative GFP-LRRK1(K1243M) was able to rescue the defect in EGF sorting in LRRK1-depleted cells (Fig. 8e), suggesting that LRRK1 kinase activity is not essential for this step. Thus, LRRK1 functions as a scaffold in this process, independent of its kinase activity.

We confirmed the above immunofluorescence data by electron microscopy. Silver-enhanced gold particles revealed the presence of endogenous EGFR associated with both the limiting membrane and ILVs of MVBs in control cells, whereas most of the EGFR was still located on the limiting membrane of MVBs in LRRK1-depleted cells (Fig. 8f). We next asked whether LRRK1 could also affect EGFR degradation. Although EGF stimulation normally causes the degradation of EGFR, we observed stabilization of activated EGFR in cells treated with LRRK1 siRNA (Fig. 8g). These results suggest that LRRK1 is required for EGFR sorting into the degradative pathway.

Discussion

EGFR targeted for lysosomal degradation is delivered to MVBs by a highly specialized process that begins with receptor ubiquitination and sequestration by elements of the ESCRT complex on the surface of early endosomes[6–10]. Endosomal sorting of ubiquitinated EGFR is initiated by ESCRT-0, which is composed of Hrs and STAM[6–10]. It has been proposed that Hrs and STAM can concentrate ubiquitinated cargo on clathrin-coated microdomains of early endosomes and link the cargo with the subsequent ESCRT machinery that is required for proper sorting[27,29,31]. In this study, we show that LRRK1 is required for EGFR transport from early to late endosomes. Our results demonstrate that LRRK1 forms a complex with EGFR via Grb2 and associates with STAM and Hrs in response to ligand stimulation. Furthermore, we find that knockdown of LRRK1 disrupts the recruitment of EGFR to STAM1-positive microdomains of early endosomes, leading to the inhibition of EGFR sorting to the inner vesicles of MVBs. LRRK1 may function as a scaffolding protein between ubiquitinated EGFR and the Hrs–STAM1 complex. Consistent with this possibility, EGFR, LRRK1 and STAM1 can form a ternary complex in response to EGF stimulation, and knockdown of LRRK1 disrupts the interaction of EGFR with STAM1. In addition, our data suggest a mechanism whereby LRRK1 modulates the ubiquitination status of STAM1 by direct interaction. It is likely that ubiquitination of STAM1, which leads to intramolecular binding within STAM1, inhibits its ability to interact with ubiquitinated

© 2011 Macmillan Publishers Limited. All rights reserved.

NATURE COMMUNICATIONS | DOI: 10.1038/ncomms1161

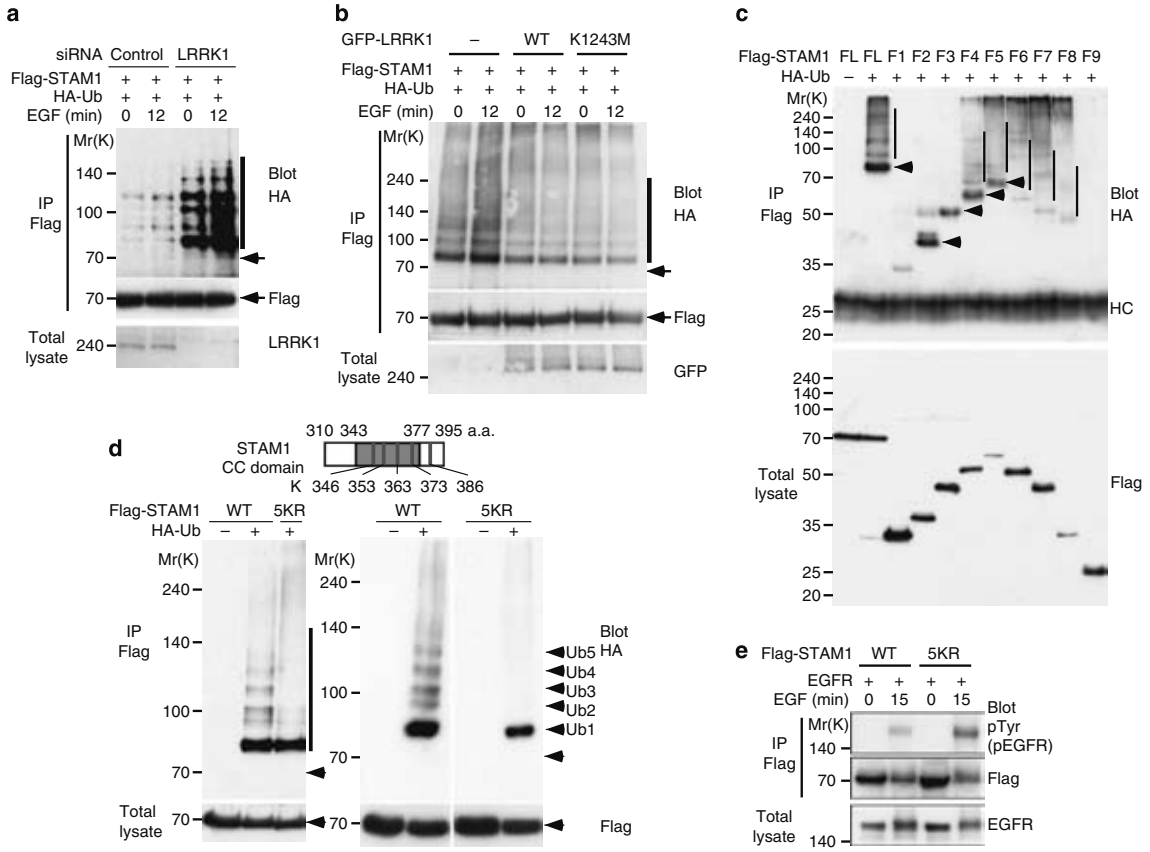

Figure 7 | LRRK1 modulates the ubiquitination status of STAM1. (**a**) Effect of LRRK1 depletion on the ubiquitination of STAM1. HeLa S3 cells treated with control or LRRK1 siRNA (Stealth#1) were co-transfected with Flag-STAM1 and HA-Ub, and stimulated with 100 ng per ml of EGF. Complexes immunoprecipitated (IP) with anti-Flag antibody were immunoblotted (Blot) with anti-HA antibodies. Arrows and line indicate the positions of the unmodified and ubiquitinated forms of Flag-STAM1, respectively. (**b**) Effect of LRRK1 overexpression on the ubiquitination of STAM1. COS7 cells were co-transfected with GFP-LRRK1 (wild type and the K1243 mutant), Flag-STAM1 and HA-Ub as indicated. Complexes immunoprecipitated (IP) with anti-Flag antibody were immunoblotted (Blot) with anti-HA antibodies. Arrows and line indicate the positions of the unmodified and ubiquitinated forms of Flag-STAM1, respectively. (**c**) Ubiquitination of STAM1. COS7 cells were co-transfected with Flag-STAM1 and HA-Ub as indicated. Complexes immunoprecipitated (IP) with anti-Flag antibodies were immunoblotted (Blot) with anti-HA antibodies. Arrowheads and lines indicate the positions of the monoubiquitinated and polyubiquitinated forms of Flag-STAM1, respectively. HC represents heavy chain. (**d**) Ubiquitination sites in STAM1. The lysine residues around the STAM1 coiled-coil domain (green) are shown. COS7 cells were co-transfected with Flag-STAM1 (wild type and the 5KR mutant) and HA-Ub as indicated. Complexes immunoprecipitated (IP) with anti-Flag antibodies were immunoblotted (Blot) with anti-HA antibodies. Arrows and line indicate the positions of the unmodified and ubiquitinated forms of Flag-STAM1, respectively. (**e**) Interaction between EGFR and STAM1(5KR). COS7 cells were co-transfected with Flag-STAM1 (wild type and the 5KR mutant) and EGFR as indicated, and stimulated with 100 ng per ml of EGF. Complex formation was detected by immunoprecipitation (IP) with anti-Flag antibodies, followed by immunoblotting (Blot) with anti-phospho-tyrosine (pTyr) antibodies.

EGFR. Therefore, LRRK1 promotes complex formation between activated EGFR and STAM1 by decreasing the ubiquitination of STAM1. Our findings suggest that LRRK1 might function as a cargo-specific factor that efficiently links the activated EGFR to the ESCRT machinery.

Remarkably, we find that the motility of EGF-containing early endosomes is diminished dramatically by LRRK1 knockdown. We demonstrate that LRRK1 kinase activity is required for the transport of EGFR-containing early endosomes from the periphery to the centre. Recent studies have shown that early endosomes move towards the cell centre as they mature[18,20]. The movement of early endosomes is mediated by cytoplasmic dynein, a minus end-directed microtubule motor[19,34]. LRRK1 might thus be involved in the regulation of dynein-dependent transport of EGF-containing early endosomes. Interestingly, in a screen for LRRK1-binding proteins, we have identified NudC and CLIP-170, which are involved in dynein-mediated processes[35,36]. Thus, LRRK1 might regulate the motility of EGF-containing early endosomes by phosphorylating these candidates.

Because excessive or inappropriate signalling by activated EGFR is associated with the development of a broad range of human cancers, the spatiotemporal regulation of EGFR trafficking by LRRK1 is likely to be important for the maintenance of cellular homoeostasis. Identification of specific LRRK1 targets involved in the regulation of EGFR trafficking in early endosomes will be necessary. Further analysis of LRRK1 function may shed new light on the molecular mechanisms regulating the intracellular trafficking of EGFR, and thus the spatiotemporal control of EGFR signalling.

© 2011 Macmillan Publishers Limited. All rights reserved.

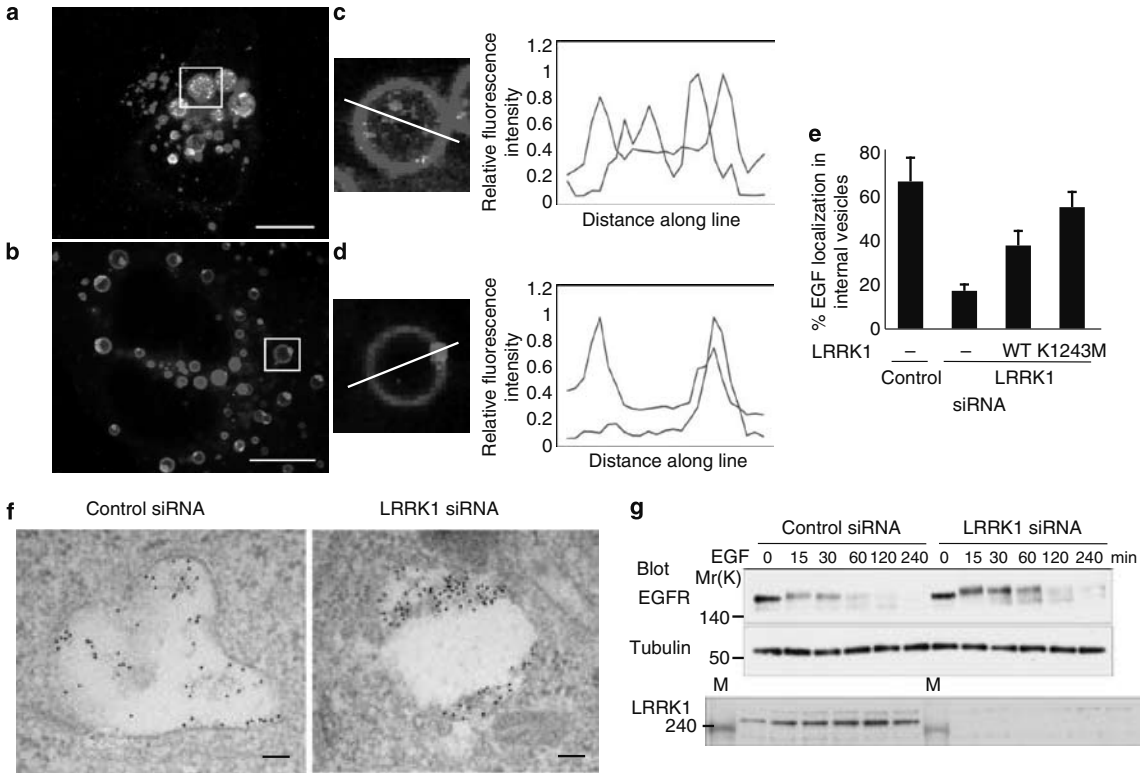

Figure 8 | Effects of LRRK1 depletion on localization of EGFR in MVBs and EGFR degradation. (**a**, **b**) Effect of LRRK1 depletion on EGFR sorting into the lumen of Rab5(Q79L)-induced enlarged endosomes. HeLa S3 cells treated with control (**a**) or LRRK1 siRNA (Stealth#1) (**b**) were transfected with DsRed-Rab5(Q79L) and stimulated with 100 ng per ml of Alexa 647-EGF for 30 min. The cells were fixed and imaged by confocal microscopy. Images are three-dimensional reconstructions from a series of confocal Z-stack images (0.3 μm-thick sections). Scale bar, 10 μm. (**c**, **d**) Confocal images from control (**c**; the boxed region in **a**) or LRRK1-depleted cells (**d**; the boxed region in **b**) show individual enlarged endosomes. Areas of co-localization are shown by line intensity profiles. (**e**) Quantification of Alexa 647-EGF localization into the lumen of Rab5(Q79L)-induced enlarged endosomes. Cells treated with control or LRRK1 siRNA (Stealth#1) were co-transfected with DsRed-Rab5(Q79L) and siRNA-resistant GFP-LRRK1 (wild type and the K1243 M mutant), as indicated. Cells were stimulated with 100 ng per ml of Alexa 647-EGF for 30 min and then fixed. Data are presented as percentages of Alexa 647-EGF localization into the lumen of enlarged endosomes out of the total number of Rab5(Q79L)-induced enlarged endosomes (diameter; >1 μm). Values reflect the mean s.d. of three independent experiments, with an average of 15 cells (total 100 endosomes) scored per experiment. (**f**) HeLa S3 cells were treated with control or LRRK1 siRNA (Stealth#1). After 16 h of serum starvation, cells were incubated with anti-EGFR antibodies (LA-22) for 2 h at 37°C, followed by goat anti-mouse IgM antibodies conjugated to 10 nm gold for 1 h at 37°C. After washing to remove antibodies from the medium, the cells were stimulated with EGF for 10 min and then fixed. The localization of EGFR was examined by silver-enhanced immunogold electron microscopy. Scale bar, 100 nm. (**g**) HeLa S3 cells treated with control or LRRK1 siRNA (Stealth#1) were transfected with EGFR. After 16 h of serum starvation, cells were stimulated with 100 ng per ml of EGF. Cell lysates were immunoblotted with indicated antibodies. Tubulin serves as a loading control.

Methods

Plasmids and mutations. Human LRRK1 cDNA was subcloned into vector pGFP-C1 (Clontech), pCMV or pCS2. LRRK1(4PA), LRRK1(K1243M) and LRRK1(S625N) were generated using the QuickChange Site-Directed Mutagenesis Kit according to the manufacturer's protocol (Stratagene). siRNA-resistant LRRK1 was generated by mutating the target sequence of the LRRK1 siRNA (5′-GCAG GAACAGGAAAGTCACCATTTA-3′) into 5′-GTCGAAATCGAAAAGTCAC CATTTA-3′. Human LRRK2 (Park8) cDNA was subcloned into vector pCMV. HA-Grb2(P49L), HA-Grb2(S90N), HA-Grb2(G203R) and HA-Grb2(P49L/G203R) were generated using the mutagenesis kit described above and subcloned into vector pSRα[37]. Human Rab5 and Rab7 were subcloned into vector pGFP-C1 or pDsRed-C1 (Clontech; catalogue number 632466), and Rab5(Q79L) was generated using the mutagenesis kit described above. pDsRed-C1 produces the monomer form of DsRed. Deletion constructs of STAM1 were generated by PCR-based mutagenesis and subcloned into pCMV-Flag.

Antibodies and reagents. Rabbit antibodies against LRRK1 were produced by MBL (Medical and Biological Laboratories) by injecting rabbits with synthetic peptides corresponding to residues 1767–1783 and 1848–1865 of LRRK1 coupled to keyhole limpet haemocyanin. Antibodies and their suppliers were as follows: anti-HA (16B12, Babco); anti-Flag (M2, Sigma); anti-Myc (9E10, Santa Cruz Biotechnology); anti-GFP (JL-8 or Full-length polyclonal antibody, Clontech); anti-phospho-Tyr (4G10, Upstate Biotechnology); anti-EGFR (SC-03, Santa Cruz Biotechnology, LA22, Upstate Biotechnology or 6F1, MBL); anti-Grb2 (SC-23, Santa Cruz Biotechnology); anti-EEA1 (Clone 14, BD Transduction Laboratories); anti-STAM1 (H-175, Santa Cruz Biotechnology); anti-Hrs (A-5, Alexis Biochemicals); anti-clathrin (clone 23, BD Transduction Laboratories); anti-Tubulin (B-5-1-2, Sigma); Goat anti-mouse IgM conjugated to 10 nm gold (BBinternational). EGF-Rh and Alexa647-EGF were purchased from Molecular Probes and human recombinant EGF from TOYOBO.

Cell cultures and transfections. HeLa, HeLa S3, HEK293 and COS7 cells were cultured in Dulbecco's modified Eagle's medium containing 10% fetal bovine serum. These cells were split on 35-mm, 60-mm or 100-mm dishes at 2×10^5, 5×10^5 or 2×10^6 cells per dish, respectively. After 19 h, cells were transfected using RNAi MAX (Invitrogen) or FuGENE 6 reagent (Roche Applied Science) according to the manufacturer's protocol.

Immunoprecipitation. For immunoprecipitation, cells were lysed in RIPA buffer containing 50 mM Tris-HCl (pH 7.4), 150 mM NaCl, 0.25% deoxycholic acid, 1% NP-40, 1 mM EDTA, 2 mM dithiothreitol, 1 mM phenylmethylsulphonyl fluoride,

© 2011 Macmillan Publishers Limited. All rights reserved.

phosphatase inhibitor cocktail 2 (Sigma) and protease inhibitor cocktail (Sigma), followed by centrifugation at 15,000 *g* for 15 min. The supernatant was added to 10 µl (bed volume) of protein G sepharose beads (GE Healthcare) or Dynabeads protein G (Invitrogen) with the indicated antibodies and rotated for 2 h at 4°C or for 10 min at room temperature. The beads were washed three times with ice-cold phosphate-buffered saline and subjected to immunoblotting or kinase assays.

Immunoblotting. After the extracts were subjected to SDS–polyacrylamide gel electrophoresis (SDS–PAGE), proteins were transferred to polyvinylidene difluoride membrane (Hybond-P, GE Healthcare). Membranes were incubated with indicated antibodies using the SNAP i.d. system (Millipore). Immunoreactive bands were detected by an HRP chemiluminescent substrate reagent kit (Novex ECL, Invitrogen).

***In vitro* autophosphorylation assay**. Immunocomplex kinase reactions of GFP-LRRK1, GFP-LRRK1(K1243M) or GFP-LRRK1(S625N) were performed in a final volume of 20 µl containing 20 mM Tris-HCl (pH7.4), 5 mM EGTA, 15 mM $MgCl_2$, 5 µCi of [γ-^{32}P]ATP. Samples were incubated for 20 min at 30°C. Reactions were terminated by the addition of Laemmli sample buffer and boiling. GFP-LRRK1, GFP-LRRK1(K1243M) or GFP-LRRK1(S625N) was resolved by SDS–PAGE. Autophosphorylation of LRRK1 was detected by autoradiography.

RNA interference. siRNA targeted against human LRRK1, human Grb2 and negative control siRNAs were purchased from Invitrogen and Ambion. Stealth siRNA (Stealth#1) for human LRRK1 (target sequence: 3165gcaggaacaggaaagt caccattta TT), Silencer Validated siRNA (Ambion#1) for human LRRK1 (target sequence: 5493ggaatcactcactgactac TT) and Custom siRNA for human Grb2 (target sequence: 607catgtttccccgcaattat TT)[15] were used. Annealed siRNAs were transfected using RNAiMAX (Invitrogen). The transfected cells were analysed 72 h after transfection. For immunofluorescence experiments, cells were transfected with control siRNA, Grb2 siRNA or LRRK1 siRNA using RNAiMAX, incubated overnight and then transfected with GFP-LRRK1, GFP-Rab5, DsRed-Rab7, GFP-Rab5(Q79L) or DsRed-Rab5(Q79L) in the indicated combinations, using FuGENE 6 reagent (Roche Applied Science).

GTP-binding studies. Cells were lysed at 48 h post transfection in lysis buffer G (100 mM Tris-HCl pH 7.5, 50 mM KCl, 1 mM EDTA, 0.1 mM dithiothreitol, 5 mM $MgCl_2$, 1% Triton X-100) containing phosphatase inhibitor cocktail and protease inhibitor cocktail (Sigma) for 10 min on ice, and lysates were clarified by centrifugation at 15,000 *g* for 10 min at 4°C. Supernatants were incubated with 20 µl of GTP-sepharose bead suspension (Sigma) by rotating at 4°C for 2 h and then sequentially pelleted and washed three times with 1 ml PBS. For guanine nucleotide competition experiments, GTP (Sigma) was added to a final concentration of 2 mM, and incubation was continued for a further 60 min at 4°C followed by washing. Precipitated proteins were resolved by SDS–PAGE and immunoblotted with anti-GFP antibodies.

Fluorescence microscopy. For immunofluorescence microscopy, cells grown on coverslips were treated, as indicated, and then fixed in 4% paraformaldehyde, permeabilized in 0.5% Triton X-100 and incubated with primary and secondary antibodies. Primary antibodies were anti-EEA1 at 1:100, anti-EGFR at 1:100, anti-STAM1 at 1:250 and anti-clathrin at 1:100. Secondary antibodies were Alexa-Fluor 647 goat anti-mouse IgG, Alexa-Fluor 555 goat anti-mouse IgG and Alexa-Fluor 488 goat anti-mouse IgG (Molecular Probes). Confocal microscopy was performed using an Olympus FV1000 microscope. For live-cell fluorescence microscopy, cells were grown in 35-mm plastic-bottomed dishes. Time-lapse images were obtained with a laser scanning confocal microscope (FV1000; Olympus). Tracking of GFP-Rab5- and A647-EGF-positive endosomes was conducted using the 'Manual Tracking' Image J plug-in (National Institutes of Health).

Conventional electron microscopy. Conventional electron microscopy was performed as described previously[38]. In brief, cells were fixed in 2.5% glutaraldehyde in 0.1 M sodium phosphate buffer at pH 7.4 for 20 min. The specimens were postfixed in buffer containing 1% OsO_4, dehydrated in a series of graded ethanol solutions and embedded in epoxy resin. Ultrathin sections were collected and stained with uranylacetate and lead citrate and observed under an H7600 transmission electron microscope (Hitachi).

References

1. Wang, Z. & Moran, M. F. Requirement for the adaptor protein GRB2 in EGF receptor endocytosis. *Science* **272,** 1935–1939 (1996).
2. Vieira, A. V., Lamaze, C. & Schmid, S. L. Control of EGF receptor signaling by clathrin-mediated endocytosis. *Science* **274,** 2086–2089 (1996).
3. Maxfield, F. R. & McGraw, T. E. Endocytic recycling. *Nat. Rev. Mol. Cell Biol.* **5,** 121–132 (2004).
4. Soldati, T. & Schliwa, M. Powering membrane traffic in endocytosis and recycling. *Nat. Rev. Mol. Cell Biol.* **7,** 897–908 (2006).
5. Mukhopadhyay, D. & Riezman, H. Proteasome-independent functions of ubiquitin in endocytosis and signaling. *Science* **315,** 201–205 (2007).
6. Katzmann, D. J., Odorizzi, G. & Emr, S. D. Receptor downregulation and multivesicular-body sorting. *Nat. Rev. Mol. Cell Biol.* **3,** 893–905 (2002).
7. Nickerson, D. P., Russell, M. R. & Odorizzi, G. A concentric circle model of multivesicular body cargo sorting. *EMBO Rep.* **8,** 644–650 (2007).
8. Williams, R. L. & Urbe, S. The emerging shape of the ESCRT machinery. *Nat. Rev. Mol. Cell Biol.* **8,** 355–368 (2007).
9. Hurley, J. H. ESCRT complexes and the biogenesis of multivesicular bodies. *Curr. Opin. Cell Biol.* **20,** 4–11 (2008).
10. Raiborg, C. & Stenmark, H. The ESCRT machinery in endosomal sorting of ubiquitylated membrane proteins. *Nature* **458,** 445–452 (2009).
11. Paisan-Ruiz, C. *et al.* Cloning of the gene containing mutations that cause PARK8-linked Parkinson's disease. *Neuron* **44,** 595–600 (2004).
12. Zimprich, A. *et al.* Mutations in *LRRK2* cause autosomal-dominant parkinsonism with pleomorphic pathology. *Neuron* **44,** 601–607 (2004).
13. Schlessinger, J. Cell signaling by receptor tyrosine kinases. *Cell* **103,** 211–225 (2000).
14. Pawson, T. Specificity in signal transduction: from phosphotyrosine-SH2 domain interactions to complex cellular systems. *Cell* **116,** 191–203 (2004).
15. Jiang, X., Huang, F., Marusyk, A. & Sorkin, A. Grb2 regulates internalization of EGF receptors through clathrin-coated pits. *Mol. Biol. Cell* **14,** 858–870 (2003).
16. Waterman, H. *et al.* A mutant EGF-receptor defective in ubiquitylation and endocytosis unveils a role for Grb2 in negative signaling. *EMBO J.* **21,** 303–313 (2002).
17. Natsume, T. *et al.* A direct nanoflow liquid chromatography-tandem mass spectrometry system for interaction proteomics. *Anal. Chem.* **74,** 4725–4733 (2002).
18. Rink, J., Ghigo, E., Kalaidzidis, Y. & Zerial, M. Rab conversion as a mechanism of progression from early to late endosomes. *Cell* **122,** 735–749 (2005).
19. Driskell, O. J., Mironov, A., Allan, V. J. & Woodman, P. G. Dynein is required for receptor sorting and the morphogenesis of early endosomes. *Nat. Cell Biol.* **9,** 113–120 (2007).
20. Woodman, P. G. & Futter, C. E. Multivesicular bodies: co-ordinated progression to maturity. *Curr. Opin. Cell Biol.* **20,** 408–414 (2008).
21. Chang, L. & Karin, M. Mammalian MAP kinase signalling cascades. *Nature* **410,** 37–40 (2001).
22. Smith, W. W., Pei, Z., Jiang, H., Dawson, V. L., Dawson, T. M. & Ross, C. A. Kinase activity of mutant LRRK2 mediates neuronal toxicity. *Nat. Neurosci.* **9,** 1231–1233 (2006).
23. Ito, G. *et al.* GTP binding is essential to the protein kinase activity of LRRK2, a causative gene product for familial Parkinson's disease. *Biochem.* **46,** 1380–1388 (2007).
24. Weiss, B. ROCO kinase activity is controlled by internal GTPase function. *Sci. Signal.* **1,** pe27 (2008).
25. Bourne, H. R., Sanders, D. A. & McCormick, F. The GTPase superfamily: conserved structure and molecular mechanism. *Nature* **349,** 117–127 (1991).
26. Raiborg, C., Bache, K. G., Mehlum, A., Stang, E. & Stenmark, H. Hrs recruits clathrin to early endosomes. *EMBO J.* **20,** 5008–5021 (2001).
27. Raiborg, C., Bache, K. G., Gillooly, D. J., Madshus, I. H., Stang, E. & Stenmark, H. Hrs sorts ubiquitinated proteins into clathrin-coated microdomains of early endosomes. *Nat. Cell Biol.* **4,** 394–398 (2002).
28. Urbe, S. *et al.* The UIM domain of Hrs couples receptor sorting to vesicle formation. *J. Cell Sci.* **116,** 4169–4179 (2003).
29. Raiborg, C., Wesche, J., Malerod, L. & Stenmark, H. Flat clathrin coats on endosomes mediate degradative protein sorting by scaffolding Hrs in dynamic microdomains. *J. Cell Sci.* **119,** 2414–2424 (2006).
30. Stenmark, H., Parton, R. G., Steele-Mortimer, O., Lutcke, A., Gruenberg, J. & Zerial, M. Inhibition of rab5 GTPase activity stimulates membrane fusion in endocytosis. *EMBO J.* **13,** 1287–1296 (1994).
31. Bache, K. G., Raiborg, C., Mehlum, A. & Stenmark, H. STAM and Hrs are subunits of a multivalent ubiquitin-binding complex on early endosomes. *J. Biol. Chem.* **278,** 12513–12521 (2003).
32. Hoeller, D. *et al.* Regulation of ubiquitin-binding proteins by monoubiquitination. *Nat. Cell Biol.* **8,** 163–169 (2006).
33. Polo, S. *et al.* A single motif responsible for ubiquitin recognition and monoubiquitination in endocytic proteins. *Nature* **416,** 451–455 (2002).
34. Aniento, F., Emans, N., Griffiths, G. & Gruenberg, J. Cytoplasmic dynein-dependent vesicular transport from early to late endosomes. *J. Cell Biol.* **123,** 1373–1387 (1993).
35. Yamada, M. *et al.* mNUDC is required for plus-end-directed transport of cytoplasmic dynein and dynactins by kinesin-1. *EMBO J.* **29,** 517–531 (2010).
36. Lomakin, A. J. *et al.* CLIP-170-dependent capture of membrane organelles by microtubules initiates minus-end directed transport. *Dev. Cell* **17,** 323–333 (2009).
37. Hanafusa, H., Torii, S., Yasunaga, T. & Nishida, E. Sprouty1 and Sprouty2 provide a control mechanism for the Ras/MAPK signalling pathway. *Nat. Cell Biol.* **4,** 850–858 (2002).
38. Hayashi-Nishino, M., Fujita, N., Noda, T., Yamaguchi, A., Yoshimori, T. & Yamamoto, A. A subdomain of the endoplasmic reticulum forms a cradle for autophagosome formation. *Nat. Cell Biol.* **11,** 1433–1437 (2009).

© 2011 Macmillan Publishers Limited. All rights reserved.

Acknowledgments
We thank A. Yamamoto and N. Hisamoto for helpful discussion and K. Tanaka and T. Yamamoto for providing materials. This research was supported by grants from the Ministry of Education, Culture, Sports, Science and Technology of Japan (to K.M. and H.H.), as well as from the Nakajima Foundation, the Uehara Memorial Foundation and the Kato Memorial Bioscience Foundation (to H.H.).

Author contributions
H.H., K.I., S.K., T.S. and M.K. conducted the experiments. S.-I.L. and T.N. performed the LC–MS/MS. H.S. isolated and mutated the LRRK1 cDNA. A.N. performed the electron microscopy analysis. H.H. and K.M. designed the experiments and wrote the paper.

Additional information
Supplementary Information accompanies this paper at http://www.nature.com/naturecommunications

Competing financial interests: The authors declare no competing financial interests.

Reprints and permission information is available online at http://npg.nature.com/reprintsandpermissions/

How to cite this article: Hanafusa, H. *et al.* Leucine-rich repeat kinase LRRK1 regulates endosomal trafficking of the EGF receptor. *Nat. Commun.* 2:158 doi: 10.1038/ncomms1161 (2011).

License: This work is licensed under a Creative Commons Attribution-NonCommercial-Share Alike 3.0 Unported License. To view a copy of this license, visit http://creativecommons.org/licenses/by-nc-sa/3.0/

© 2011 Macmillan Publishers Limited. All rights reserved.

分子代謝医学分野

小川 佳宏

医歯学総合研究科・器官システム制御学系専攻
分子代謝医学・教授

1）研究の課題名

我々は既に、肥満に伴って肥大化脂肪細胞から過剰放出される飽和脂肪酸が、TLR4を介して脂肪組織マクロファージを活性化し、脂肪組織炎症の増悪に繋がることを明らかにした。本研究では、肥満脂肪組織における新たな炎症調節分子の同定を目的として、cDNAマイクロアレイ法を用いて、脂肪細胞とマクロファージの共培養により発現が亢進する遺伝子の探索を行った。共培養により発現が増加し、マクロファージ選択的に発現する遺伝子群よりmacrophage-inducible C-type lectin（Mincle）に注目した。TLR4シグナルを欠損するマクロファージでは、飽和脂肪酸や共培養によるMincle発現誘導が著しく阻害された。骨髄マクロファージを用いた培養系において、MincleはM1マクロファージに選択的に発現した。遺伝性および食餌誘導性肥満マウスの脂肪組織においてMincleの著明な発現亢進を認めたが、TLR4シグナル欠損マウスでは有意な上昇を認めなかった。ヒト皮下脂肪組織においても、Mincle遺伝子発現はBMIと正の相関を示した（r=0.598）。脂肪細胞とマクロファージの共培養系を用いて、脂肪組織マクロファージにおける新たな炎症調節分子としてMincleを同定した。Mincleは真菌や結核菌に対する病原体センサーとして機能するため、脂肪組織炎症の病態形成への関与が示唆された。

2）

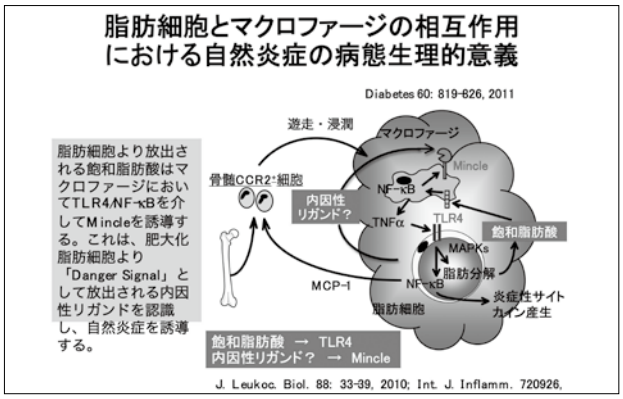

3）発表の研究内容についての英文要約

We have provided evidence that saturated fatty acids, which are released from adipocytes via macrophage-induced adipocyte lipolysis, serve as a naturally occurring ligand for the TLR4 complex in macrophages, thereby aggravating obesity-induced adipose tissue inflammation. We performed a cDNA microarray analysis of coculture of 3T3-L1 adipocytes and RAW264 macrophages. Cultured adipocytes and macrophages and the adipose tissue of obese mice and humans were used to examine mRNA and protein expression. We found that macrophage-inducible C-type lectin（Mincle）, a type II transmembrane C-type lectin, is induced selectively in macrophages during the interaction between adipocytes and macrophages. Treatment with palmitate, a major saturated fatty acid released from 3T3-L1 adipocytes, induced Mincle mRNA expression in macrophages at least partly through the TLR4/NF-kB pathway. Mincle mRNA expression was increased in parallel with macrophage markers in the adipose tissue of obese mice and humans. The obesity-induced increase in Mincle mRNA expression was markedly attenuated in C3H/HeJ mice with defective TLR4 signaling relative to control C3H/HeN mice. Notably, Mincle mRNA was expressed in bone-marrow cell（BMC）-derived proinflammatory M1 macrophages rather than in BMC-derived anti-inflammatory M2 macrophages in vitro. Our data suggest that Mincle is induced in adipose tissue macrophages in obesity at least partly through the saturated fatty acid/TLR4/NF-kB pathway, thereby suggesting its pathophysiologic role in obesity-induced adipose tissue inflammation.

4）本事業に関連して世界的な研究拠点形成に向けて、以下の点で改善・整備等されたこと

A（研究拠点体制）

新しく寄附研究部門を設置することにより研究活動の充実を図った。

B（研究教育環境）

新しく寄附研究部門を設置することにより教育活動の

充実を図った。

C（人材確保）

卒業研究生が本学医歯学総合研究科修士課程に進学することとなった。

D（人材育成）

関連学会において教室員が研究奨励賞、若手研究奨励賞（菅波、伊藤）を受賞した。

E（国際化）

多くの海外研究者（Theodore W. Kurtz教授、Jae Bum Kim教授、Philipp E. Scherer教授、Domenico Accili教授）の訪問を受けて、当教室における研究について議論する機会を得た。

5）GCOE事業を推進するに当たって力を入れた点

多くの海外研究者の訪問を受けて国際化に力を入れた。

6）英文原著論文

1. H. Nambu, M. Fukushima, H. Hikichi, T. Inoue, N. Nagano, Y. Tahara, T. Nambu, J. Ito, Y. Ogawa, S. Ozaki, and H. Ohta. Characterization of metabolic phenotypes of mice lacking GPR61, an orphan G-protein coupled receptor. Life Sci. 89：765-772, 2011.
2. ◎M. Itoh, T. Suganami, N. Nakagawa, M. Tanaka, Y. Yamamoto, Y. Kamei, S. Terai, I. Sakaida, and Y. Ogawa. Melanocortin-4 receptor-deficient mice as a novel mouse model of non-alcoholic steatohepatitis. Am. J. Pathol. 179：2454-2463, 2011.
3. ◎M. Tanaka, T. Suganami, M. Kim-Saijo, C. Toda, M. Tsuiji, K. Ochi, Y. Kamei, Y. Minokoshi, and Y. Ogawa. Role of central leptin signaling in the starvation-induced alteration of B cell development. J. Neurosci. 31：8373-8380, 2011.
4. ◎S. Sugita, Y. Kamei, F. Akaike, T. Suganami, S. Kanai, M. Hattori, Y. Manabe, N. Fujii, T. Takai-Igarashi, M. Tadaishi, J. Oka, H. Aburatani, T. Yamada, H. Katagiri, S. Kakehi, Y. Tamura, H. Kubo, K. Nishida, S. Miura, O. Ezaki, and Y. Ogawa. Increased systemic glucose tolerance with increased muscle glucose uptake in transgenic mice overexpressing RXR γ in skeletal muscle. PLoS ONE 6：e20467, 2011.
5. ◎M. Ichioka, T. Suganami, N. Tsuda, I. Shirakawa, Y. Hirata, N. Satoh-Asahara, Y. Shimoda, M. Tanaka, M. Kim-Saijo, Y. Miyamoto, Y. Kamei, M. Sata, and Y. Ogawa. Increased expression of macrophage-inducible C-type lectin in adipose tissue of obese mice and humans. Diabetes 60：819-826, 2011.

7）総説ならびに著書

M. Itoh, T. Suganami, R. Hachiya, and Y. Ogawa. Adipose tissue remodeling as homeostatic inflammation. Int. J. Inflamm. 720926, 2011.

8）平成23年度までの自己評価

以前より継続している生活習慣病における慢性炎症の病態生理的意義に関する研究に関して英文論文を複数発表することができた点は評価できると考えている。

9）学会発表（英文）

1. Y. Ogawa：Adipose tissue remodeling homeostatic inflammation：2011 Seoul Symposium on obesity & Diabetes, 2011.4.9, Seoul
2. Y. Ogawa：Epigenetic Modifications Underlying Insulin Resistance：THE ENDOCRINE SOCIETY’S 93RD ANNUAL MEETING & EXPO（ENDO2011）,2011.6.4-7,Boston
3. Y. Ogawa：Homeostatic inflammation：A molecular basis underlying metabolic diseases：International Symposium on Inflammation and Disease：2011.9.8-9,Academia Sinica,台湾

10）学会発表（和文）

1. 小川佳宏：「肥満症治療と慢性炎症」：第32回日本肥満学会,2011.9.23-24,兵庫
2. 菅波孝祥、小川佳宏：「病原体センサーと慢性炎症」：第32回日本肥満学会,2011.9.23-24,兵庫
3. 伊藤美智子、菅波孝祥、田中都、亀井康富、寺井崇二、坂井田功、小川佳宏：「NASHの発症・進展と脂肪組織炎症―新しいNASHモデル・MC4R欠損マウスを用いて―」：第32回日本肥満学会,2011.9.23-24,兵庫
4. 江原達弥、亀井富康、金井沙綾香、高橋真由美、袁勲梅、菅波孝祥、小川佳宏：「グリセロール3リン酸アシル基転移酵素（GPAT1）遺伝子のDNAメチル化による発現制御」：第32回日本肥満学会,2011.9.23-24,兵庫
5. 田中都、菅波孝祥、西條美佐、筑地信、越智梢、亀井康富、小川佳宏：「骨髄Bリンパ球分化に及ぼす中枢レプチンシグナルの作用機序の解明」：第32回日本肥満学会,2011.9.23-24,兵庫
6. 亀井康富、杉田聡、赤池史子、菅波孝祥、金井沙綾香、服部真季、眞鍋康子、藤井宣晴、三浦進司、江崎治、小川佳宏：「骨格筋における核内受容体RXRY

の糖代謝促進作用」：第32回日本肥満学会,2011.9.23-24,兵庫

7. 岩崎順博、菅波孝祥、蜂屋瑠見、白川伊吹、西條美佐、袁勲梅、亀井康富、小川佳宏：「飽和脂肪酸による新たな炎症性サイトカイン転写制御機構の検討」：第32回日本肥満学会,2011.9.23-24,兵庫
8. 天野直子、鬼頭浩史、蜂屋瑠見、鳴海覚志、小川佳宏、西村玄、長谷川奉延：「Maroteaux型遠位中間肢異形成症に新規NPR2 変異を同定した1例」：第45回日本小児内分泌学会学術集会,2011.10.6-8,さいたま

11）受賞

1. 菅波孝祥　日本肥満学会学術奨励賞「肥満の脂肪組織における慢性炎症の分子機構の解明と医学応用」
2. 伊藤美智子　日本肥満学会若手研究奨励賞「NASHの発症・進展と脂肪組織炎症－新しいNASHモデル・MC4R欠損マウスを用いて－」
3. 小川佳宏　日本糖尿病・肥満動物学会研究賞「糖尿病・肥満における慢性炎症の分子機構に関する研究」

12）外部資金の獲得状況

新学術領域研究（研究領域提案型）

研究題目：メタボリックシンドロームにおける内因性リガンドと病原体センサーの機能的意義の解明
代表：小川　佳宏
期間：平成21年―平成25年
研究費総額：10520万円

科学研究費補助金基盤研究（B）

研究題目：DNAメチル化に着目したメタボリックメモリーの分子機構の解明と医学応用
代表：小川　佳宏
期間：平成23年―平成25年
研究費総額：1490万円

科学研究費補助金挑戦的萌芽研究

研究題目：骨格筋におけるDNAメチル化標的遺伝子の同定と医学応用
代表：小川　佳宏
期間：平成23年―平成25年
研究費総額：300万円

難治性疾患克服研究事業

研究題目：中枢性摂食異常症に関する調査研究
代表：小川　佳宏
期間：平成23年―平成25年
研究費総額：923万円

13）特別講演、招待講演、シンポジウム

1. 菅波孝祥、伊藤美智子、小川佳宏：「メタボリックシンドロームの臓器相関における脂肪組織マクロファージの意義」：第84回日本内分泌学会,2011.4.21-23,神戸
2. 小川佳宏：「生活習慣病とDNAメチル化」：ネスレ栄養科学会議,2011.5.14,東京
3. 小川佳宏：「エピジェネティスク機構による細胞制御と病態」：ネスレ栄養科学会議,2011.5.14,東京
4. 伊藤美智子、菅波孝祥、小川佳宏：「EPAとメタボリックシンドローム」：第54回日本糖尿病学会年次学術集会,2011.5.19-21,札幌
5. 菅波孝祥、小川佳宏：「脂肪組織の慢性炎症」：第54回日本糖尿病学会年次学術集会,2011.5.19-21,札幌
6. 小川佳宏：「メタボリックシンドロームと慢性炎症」：第11回日本抗加齢医学総会,2011.5.27-29,京都
7. 小川佳宏：「メタボリックシンドロームと慢性炎症」：熊本大学最先端・次世代研究開発プログラム　キックオフシンポジウム特別講演,2011.6.30,熊本
8. 小川佳宏：「糖尿病合併症と炎症」座長：第26回日本糖尿病合併症学会,2011.10.14-15,さいたま
9. 津田直人、菅波孝祥、市岡誠之、田中都、白川伊吹、平田陽一郎、佐藤哲子、西條美佐、宮本恵宏、亀井康富、佐田政隆、小川佳宏：「脂肪組織マクロファージにおける新たな炎症調節分子の探索」：第25回日本糖尿病・肥満動物学会年次学術集会,2011.11.5,東京
10. 小川佳宏：「栄養環境によるエピゲノム変化と医学応用」：日本人類遺伝学会第56回大会,第11回東アジア人類遺伝学会,2011.11.9-12,千葉
11. 小川佳宏：「慢性炎症からみたメタボリックシンドローム」：日本薬理学会第39回薬物活性シンポジウム,2011.11.21-22,福岡
12. 小川佳宏：「Obesity and Adipose Tissue Inflammation」：第19回日本血管生物医学会学術集会,2011.12.8-10,東京
13. 小川佳宏：「Chronic inflammation,a molecular basis underlying the metabolic syndrome」：第34回日本分子生物学会年会,2011.12.13-16,横浜
14. 菅波孝祥、小川佳宏：「Obesity and adipose tissue inflammation」：第34回日本分子生物学会年会,2011.12.13-16,横浜

14）新聞、雑誌、TV報道

2011年7月9日（土） PM7：56 ～ PM8：54

世界一受けたい授業

「痩せていても危ない!日本人を蝕む第3の脂肪」

（日本テレビ）

http：//www.ntv.co.jp/sekaju/onair/110709.html?st=3

15）教室、分野や講座の准教授、講師、助教、特別研究員、ポスドク、指導を受けた大学院生の名前

亀井　康富　（特任教授）
菅波　孝祥　（准教教）
澤田　直樹　（特任講師）
西條　美佐　（特任助教）
袁　　勲梅　（特任助教）
高橋　真由美（特任助教）
白川　伊吹　（特任助教）
田中　　都　（特任助教）
伊藤　美智子（特任助教）
蜂屋　瑠見　（特別研究員）
市岡　誠之　（社会人大学院生）
江原　達弥　（社会人大学院生）
滝沢　文彦　（大学院生）
津田　直人　（社会人大学院生）
南部　宏英　（社会人大学院生）
池田　賢司　（大学院生）
岩崎　順博　（大学院生）
青山　千賀子（社会人大学院生）
櫻井　俊之　（社会人大学院生）
小沼　邦葉　（大学院生）
服部　真季　（大学院生）
笠原　知美　（卒業研究生）
田村江梨奈　（卒業研究生）

OPEN ACCESS Freely available online PLoS one

Increased Systemic Glucose Tolerance with Increased Muscle Glucose Uptake in Transgenic Mice Overexpressing RXRγ in Skeletal Muscle

Satoshi Sugita[1], Yasutomi Kamei[1]*, Fumiko Akaike[1,2], Takayoshi Suganami[1], Sayaka Kanai[1], Maki Hattori[1,2], Yasuko Manabe[3], Nobuharu Fujii[3], Takako Takai-Igarashi[4], Miki Tadaishi[5,6], Jun-Ichiro Oka[2], Hiroyuki Aburatani[7], Tetsuya Yamada[8], Hideki Katagiri[8], Saori Kakehi[9], Yoshifumi Tamura[9,10], Hideo Kubo[11], Kenichi Nishida[11], Shinji Miura[5], Osamu Ezaki[5], Yoshihiro Ogawa[1,12]

1 Department of Molecular Medicine and Metabolism, Medical Research Institute, Tokyo Medical and Dental University, Tokyo, Japan, **2** Laboratory of Pharmacology, Faculty of Pharmaceutical Sciences, Tokyo University of Science, Chiba, Japan, **3** Graduate School of Human Health Sciences, Tokyo Metropolitan University, Tokyo, Japan, **4** Department of Bioinformatics, Graduate School of Biomedical Science, Tokyo Medical and Dental University, Tokyo, Japan, **5** Nutritional Science Program, National Institute of Health and Nutrition, Tokyo, Japan, **6** Department of Nutritional Science, Faculty of Applied Bioscience, Tokyo University of Agriculture, Tokyo, Japan, **7** Research Center for Advanced Science and Technology, University of Tokyo, Tokyo, Japan, **8** Department of Metabolic Diseases, Center for Metabolic Diseases, Tohoku University Graduate School of Medicine, Miyagi, Japan, **9** Department of Medicine, Metabolism and Endocrinology, School of Medicine, Juntendo University, Tokyo, Japan, **10** Sportology Center, Juntendo University, Tokyo, Japan, **11** Daiichi-Sankyo Co., Ltd., Tokyo, Japan, **12** Global Center of Excellence Program, International Research Center for Molecular Science in Tooth and Bone Diseases, Medical Research Institute, Tokyo Medical and Dental University, Tokyo, Japan

Abstract

Background: Retinoid X receptor (RXR) γ is a nuclear receptor-type transcription factor expressed mostly in skeletal muscle, and regulated by nutritional conditions. Previously, we established transgenic mice overexpressing RXRγ in skeletal muscle (RXRγ mice), which showed lower blood glucose than the control mice. Here we investigated their glucose metabolism.

Methodology/Principal Findings: RXRγ mice were subjected to glucose and insulin tolerance tests, and glucose transporter expression levels, hyperinsulinemic-euglycemic clamp and glucose uptake were analyzed. Microarray and bioinformatics analyses were done. The glucose tolerance test revealed higher glucose disposal in RXRγ mice than in control mice, but insulin tolerance test revealed no difference in the insulin-induced hypoglycemic response. In the hyperinsulinemic-euglycemic clamp study, the basal glucose disposal rate was higher in RXRγ mice than in control mice, indicating an insulin-independent increase in glucose uptake. There was no difference in the rate of glucose infusion needed to maintain euglycemia (glucose infusion rate) between the RXRγ and control mice, which is consistent with the result of the insulin tolerance test. Skeletal muscle from RXRγ mice showed increased Glut1 expression, with increased glucose uptake, in an insulin-independent manner. Moreover, we performed *in vivo* luciferase reporter analysis using *Glut1* promoter (*Glut1*-Luc). Combination of RXRγ and PPARδ resulted in an increase in *Glut1*-Luc activity in skeletal muscle *in vivo*. Microarray data showed that RXRγ overexpression increased a diverse set of genes, including glucose metabolism genes, whose promoter contained putative PPAR-binding motifs.

Conclusions/Significance: Systemic glucose metabolism was increased in transgenic mice overexpressing RXRγ. The enhanced glucose tolerance in RXRγ mice may be mediated at least in part by increased Glut1 in skeletal muscle. These results show the importance of skeletal muscle gene regulation in systemic glucose metabolism. Increasing RXRγ expression may be a novel therapeutic strategy against type 2 diabetes.

Citation: Sugita S, Kamei Y, Akaike F, Suganami T, Kanai S, et al. (2011) Increased Systemic Glucose Tolerance with Increased Muscle Glucose Uptake in Transgenic Mice Overexpressing RXRγ in Skeletal Muscle. PLoS ONE 6(5): e20467. doi:10.1371/journal.pone.0020467

Editor: Massimo Federici, University of Tor Vergata, Italy

Received March 15, 2011; **Accepted** April 26, 2011; **Published** May 31, 2011

Copyright: © 2011 Sugita et al. This is an open-access article distributed under the terms of the Creative Commons Attribution License, which permits unrestricted use, distribution, and reproduction in any medium, provided the original author and source are credited.

Funding: This work was supported in part by a Grant-in-Aid for scientific research KAKENHI from the Japanese Ministry of Education, Culture, Sports, Science and Technology (MEXT, Tokyo, Japan), research grants from the Japanese Ministry of Health, Labor and Welfare, and by the joint research program of the Institute for Molecular and Cellular Regulation, Gunma University. S. Sugita is a Research Fellow of the Japan Society for the Promotion of Science. The funders had no role in study design, data collection and analysis, decision to publish, or preparation of the manuscript.

Competing Interests: HK and KN are currently employed by the commercial company Daiichi-Sankyo Co., Ltd. HK and KN were non-commercially involved in this study. This does not alter the authors' adherence to all the PLoS ONE policies on sharing data and materials. Therefore, HK and KN do not have competing interests to disclose.

* E-mail: kamei.mmm@mri.tmd.ac.jp

Introduction

The skeletal muscle, known as the largest organ in the human body, plays an important role in exercise, energy expenditure, and glucose metabolism. It is a major site of glucose disposal [1,2]. In type 2 diabetic subjects, glucose uptake in the skeletal muscle is impaired [2]. Blood glucose is taken up by the skeletal muscle via insulin-dependent and independent glucose transporters (Glut4

and Glut1, respectively) [3], where it is converted into glycogen. Increasing capacity of glucose uptake in the skeletal muscle is considered beneficial for the prevention and treatment of type 2 diabetes [3,4]. On the other hand, glucose metabolism in the skeletal muscle may affect the whole body metabolism; the skeletal muscle-specific inactivation of *Glut4* has resulted in defect in insulin action in the adipose tissue (glucose uptake) and liver (suppression of gluconeogenesis) [5]. Thus, identification of the molecular mechanisms involved in skeletal muscle glucose metabolism should help clarify the pathophysiology of diabetes.

Nuclear receptors are part of a large superfamily of transcription factors that includes receptors for steroids, retinoic acid, and thyroid hormones [6]. RXRs are heterodimeric partners of many nuclear receptors, such as retinoic acid receptors (RARs), thyroid hormone receptors (T3Rs), liver X receptors (LXRs), peroxisome proliferator activated receptors (PPARs), and RXRs themselves [6]. Among RXR heterodimer partners, activation of PPARδ in the skeletal muscle increases insulin sensitivity [7]. The RXR subfamily consists of RXRα, RXRβ, and RXRγ [6,8]. Although RXRγ is preferentially expressed in the skeletal muscle, its functional role is poorly understood. We have recently found that expression of retinoid X receptor γ (RXRγ) is changed in the skeletal muscle under nutritional conditions; RXRγ mRNA expression is down-regulated by fasting and recovered by refeeding [9]. In an attempt to explore the role of RXRγ in the skeletal muscle, we established transgenic mice overexpressing RXRγ in the skeletal muscle (RXRγ mice) and found that they exhibit increased triglyceride contents in the skeletal muscle as a result of increased expression of sterol regulatory element binding protein 1c (SREBP1c), a transcriptional master regulator of lipogenesis [9]. Indeed, RXRγ has been shown to enhance SREBP1c gene expression in C2C12 myocytes *in vitro* at least in part by heterodimerization with LXR [9]. On the other hand, we also found that blood glucose levels are lower in RXRγ mice than in control mice [9]. These observations, taken together, suggest that RXRγ plays a critical role in glucose and lipid metabolism in the skeletal muscle. However, the molecular mechanism involved in RXRγ regulation of glucose metabolism in the skeletal muscle and how it affects systemic glucose metabolism are poorly understood.

Here, we demonstrate enhanced glucose metabolism with increased Glut1 expression and glucose uptake in RXRγ mice. This study suggests that activation of the skeletal muscle RXRγ is a novel therapeutic strategy to treat or prevent type 2 diabetes.

Methods

Animals

C57BL6 mice were purchased from Charles River Japan (Yokohama, Japan). Generation of RXRγ mice under the control of the human α-actin promoter was described previously [9]. They were allowed free access to food (CRF-1; Charles River) and water, unless otherwise stated. All animal experiments were approved by Institutional Animal Care and Use Committee of Tokyo Medical and Dental University (approval ID: No. 0090041).

Blood analysis

Serum samples were obtained from mice, when fed *ad libitum*. Serum glucose levels were measured by the blood glucose test meter (Glutest PRO R; Sanwa-Kagaku, Nagoya, Japan). Serum concentrations of insulin were determined by the enzyme-linked immunosorbent assay (ELISA) kits (Morinaga Institute of Biological Science, Inc., Yokohama, Japan).

Glucose and insulin tolerance tests

For glucose tolerance test, D-glucose (1 mg/g of body weight, 10% (w/v) glucose solution) was administered by intraperitoneal injection after an overnight fast. For insulin tolerance test, human insulin (Humulin R; Eli Lilly Japan K.K., Kobe, Japan) was injected intraperitoneally (0.75 mU/g of body weight), when fed *ad libitum*.

Hyperinsulinemic-euglycemic clamp studies

We analyzed as described previously [10–12] with slight modification. Two days before the clamp studies, a catheter was inserted into the right jugular vein for infusion under general anesthesia with sodium pentobarbital. Studies were performed on mice under conscious and unstressed conditions after a 4-h fast. The clamp study began with a prime (4 mg/kg for 5 min) of [6,6-^{2}H] glucose (Cambridge Isotope Laboratories, Inc, Andover, MA) followed by continuous infusion at a rate of 0.5 mg/kg per minute for 2 hr to assess the basal glucose turnover. After the basal period, hyperinsulinemic-euglycemic clamp was conducted for 120 min with a primed/continuous infusion of human insulin (25 mU/kg prime for 5 min, 5 mU/kg/min infusion) and variable infusion of 20% glucose to maintain euglycemia (approximately 100 mg/dl). The 20% glucose was enriched with [6,6-^{2}H] glucose to approximately 2.5% as previously described [12]. To determine the enrichment of [6,6-^{2}H]glucose in plasma at basal and insulin stimulated state, samples were deproteinized with trichloroacetic acid and derivatized with *p*-aminobenzoic acid ethyl ester. The atom percentage enrichment of glucose$_{m+2}$ was then measured by high-performance liquid chromatography with LTQ-XL-Orbitrap mass spectrometer (Thermo Scientific, CA). The glucose$_{m+2}$ enrichment was determined from the m/z ratio 332.2: 330.2. The hepatic glucose production was calculated by using the rate of infusion of [6,6-^{2}H]glucose over the atom percent excess in the plasma minus the rate of glucose being infused. The insulin-stimulated whole-body glucose uptake was calculated by adding the total glucose infusion rate plus the hepatic glucose production [12].

Quantitative real-time PCR. Quantitative real-time PCR was performed as described [9]. Total RNA was prepared using Sepazol (Nacalai Tesque, Kyoto, Japan). cDNA was synthesized from 5 μg of total RNA using Superscript II reverse transcriptase (Invitrogen Inc., Carlsbad, CA) with random primers. Gene expression levels were measured with an ABI PRISM 7700 using SYBR Green PCR Core Reagents (Applied Biosystems, Tokyo, Japan). The primers used were as follows, RXRγ: Fw: 5′-CAC-

Table 1. Body and dissected tissue weight and blood glucose level in RXRγ mice (4-3 line).

	Wild-type	RXRγ
Body weight (g)	26.4±0.3	26.5±0.4
Epididymal fat mass (g)	0.138±0.004	0.156±0.090
Gastrocnemius muscle weight (g)	0.282±0.004	0.238±0.008**
Liver weight (g)	1.290±0.029	1.321±0.033
Glucose (mg/dL) basal	170.0±9.4	145.6±4.9*
Glucose (mg/dL) fasting	74.4±1.7	67.0±0.6**

Mice were males 12 weeks of age. The number of animals used was 6 for both wild-type control and RXRγ mice.
* $P<0.05$;
** $P<0.01$, compared with wild-type control.
Values are the means ± SE. These samples were also used in Fig 2*A*, *B*, and *D*.
doi:10.1371/journal.pone.0020467.t001

Table 2. Body and dissected tissue weight and blood glucose level in RXRγ mice (5-3 line).

	Wild-type	RXRγ
Body weight (g)	36.0±1.8	31.9±1.2
Epididymal fat mass (g)	1.030±0.191	0.861±0.134
Gastrocnemius muscle weight (g)	0.305±0.016	0.214±0.020**
Liver weight (g)	1.375±0.119	1.320±0.066
Glucose (mg/dL) basal	142.5±8.6	117.3±8.2
Glucose (mg/dL) fasting	67.2±1.6	53.3±2.5**

Mice were males 38 weeks of age. The number of animals used was 6 for both wild-type control and RXRγ mice.
** $P<0.01$, compared with wild-type control.
Values are the means ± SE.
doi:10.1371/journal.pone.0020467.t002

CCTGGAGGCCTATACCA-3′, Rv: 5′-AAACCTGCCTGG-CTGTTCC-3′, Glut1: Fw: 5′-CCAGC TGGGA ATCGT CG-TT-3′, Rv: 5′-CAAGT CTGCA TTGCC CATGAT-3′, Glut4: Fw: 5′-TCTGTGGGTGGCATGATCTCT-3′, Rv: 5′-GCCCT-TTTCCTTCCCAACC-3′, glucose phosphate isomerase 1: Fw: 5′-AGCGCTTCAACAACTTCAGCT-3′, Rv: 5′-CAGAATAT-GCCCATGGTTGGT-3′, phosphoglycerate mutase 1: Fw: 5′-TCCTGAAACATCTGGAAGGTATCTC-3′, Rv: 5′-CAGTG-GGCAGAGTGATGTTGAT-3′, fructose bisphosphatase 2: Fw: 5′-TGAATGCAATCCTGTGGCC-3′, Rv: 5′-TGGTTGCCA-TACCTCCTGCT-3′, pyruvate dehydrogenase kinase isoenzyme 1: Fw: 5′-GGACTTCTATGCGCGCTTCT-3′, Rv: 5′-CTGA-CCCGAAGTCCAGGAAC-3′, glycogen synthase 2: Fw: 5′-AG-GATCATTCAGAGGAACCGC-3′, Rv: 5′-CCAGTCCAGGA-GATCTGAGAGC-3′.

Tissue sampling for analysis of Glut1 and Glut4 protein levels

Skeletal muscles were homogenized in ice-cold buffer containing 250 mmol/L sucrose, 20 mmol/L 2-[4-(2-hydroxyethyl)-1-piperadinyl] ethonsulforic acid (HEPES) (pH 7.4), and 1 mmol/L EDTA, and centrifuged at 1200 g for 5 minutes. The supernatant was centrifuged at 200 000 g for 60 minutes at 4°C [13]. The resulting pellet was solubilized in Laemmli sample buffer containing dithiothreitol. Samples were subjected to Western blotting as described [14]. Antibodies used were those against Glut1 (#07-1401, Millipore, Temecula, CA), and Glut4 (SC-1606, Santa Cruz Biotechnology Inc., Santa Cruz, CA).

Muscle incubation and glucose transport

Glucose transport was measured as described [15]. Mice were fasted overnight and killed. The extensor digitorum longus (EDL) muscles were rapidly removed, each of which was mounted on the incubation apparatus and preincubated in Krebs-Ringer bicarbonate (KRB) buffer containing 2 mmol/l pyruvate for 30 min. The muscles were then incubated in KRB buffer in the absence or presence of 50 mU/ml insulin for 10 min. The buffers were kept at 37°C throughout the experiment and gassed continuously with 95% O_2 and 5% CO_2. Immediately after incubation, the muscle was transferred to KRB buffer containing 1 mmol/l 2-[^{3}H]-deoxy-d-glucose (1.5 μCi/ml) and 7 mmol/l d-[^{14}C]-mannitol (0.3 μCi/ml).

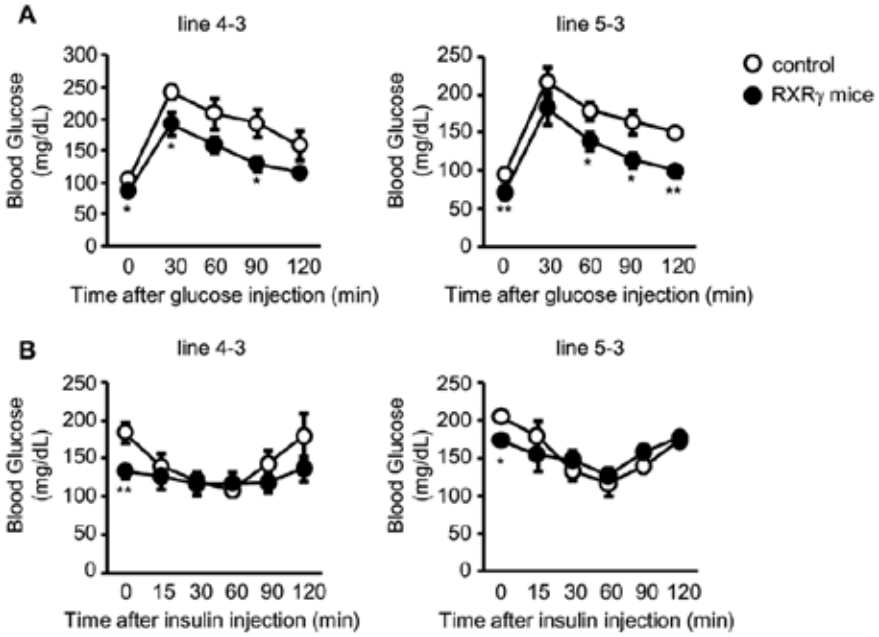

Figure 1. Glucose tolerance and insulin tolerance tests on RXRγ mice. (*A*, *B*) In A and B, male mice, 5 months of age, were used. The number of animals used was 6 for both control (open circles) and RXRγ (filled circles) mice of line 4-3, and 5 for both control (open circles) and RXRγ (filled circles) mice of line 5-3. * $P<0.05$ and ** $P<0.01$ compared with respective control.
doi:10.1371/journal.pone.0020467.g001

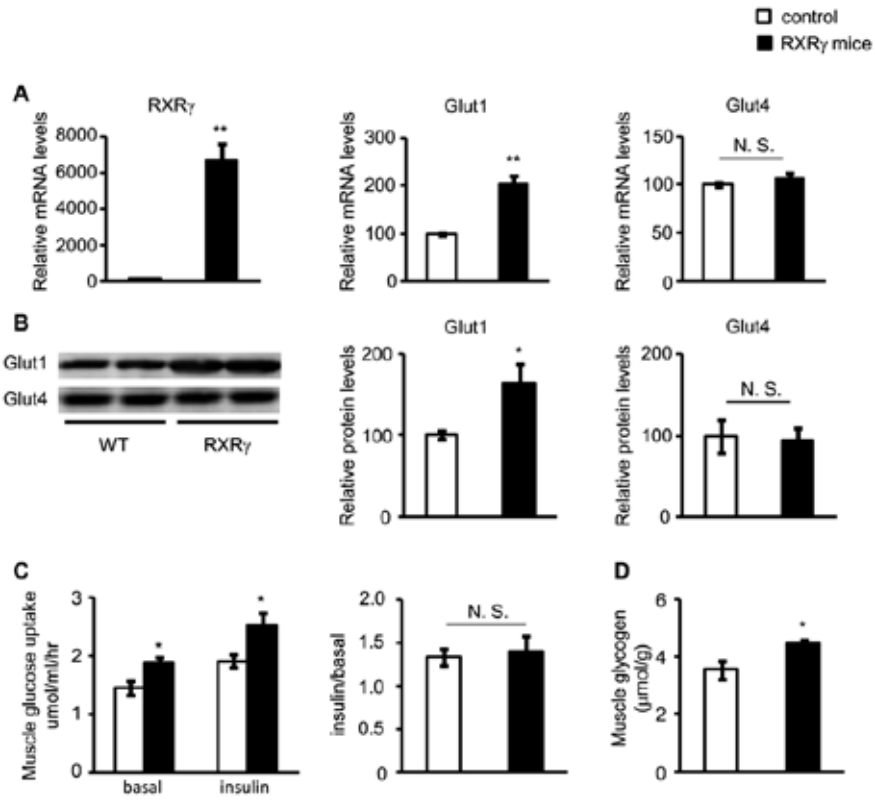

Figure 2. Levels of Glut 1 and Glut4, and glucose uptake in the skeletal muscle of RXRγ mice. (*A*) Gene expressions of *RXRγ*, *Glut1*, and *4* were examined by quantitative real-time PCR. The value for wild-type (littermates of line 4-3) mice was set at 100, and relative values are shown. (*B*) Protein levels of Glut1 and Glut4 were examined by Western blotting. Results of relative densitometric signal for Glut1 and 4 are shown. (*C*) Glucose uptake in the absence or presence of insulin and (*D*) glycogen content were increased in the skeletal muscle of RXRγ mice. Ratio of enhanced glucose uptake in the presence of insulin (insulin/basal) was similar in control and RXRγ mice. In *A*, *B* and *D*, the same samples were used. Mice were males of 12 weeks of age. The number of animals was 6 for both control (open bars) and RXRγ (filled bars) mice. These samples were also used in Table 1. In *C*, mice were males of 24–27 weeks of age. The number of animals was 6 for both control (open bars) and RXRγ (filled bars) mice. * $P<0.05$ and ** $P<0.01$ compared with respective control. N. S., not significant.
doi:10.1371/journal.pone.0020467.g002

Measurement of skeletal muscle glycogen

The skeletal muscle glycogen content was measured as glycosyl units after acid hydrolysis [16]. The skeletal muscle samples were minced, 50 mg of which was added to 1 ml of 0.3 M percholic acid and homogenized on ice. One ml of 1 N HCl was added and incubated for 2 h at 100°C, thereafter, 1 ml of 1 N NaOH was added at room temperature. Glucose content was examined using the F-kit glucose (Roche Diagnostics, Mannheim, Germany).

Plasmids

The coding region of mouse RXRγ and PPARδ cDNA were subcloned into a mammalian expression plasmid, pCMX [9]. The 1.5-kb 5′-flanking region of the mouse *Glut1* promoter was obtained by PCR with mouse genomic DNA (RefSeqs number: NC_000070). The PCR primers used were: Fw: 5′-GTGGTG-CGCGCCTGTAGTCC-3′ and Rv: 5′-GGCGCACTCCACG-GATGCCG-3′. The fragment was subcloned into the pGL3-basic luciferase vector (Promega Corporation, Madison, WI). The promoter regions used were: -1500 to +75, -647 to +75, and -152 to +75, counting the transcription start site as +1.

Electroporation and *in vivo* luciferase reporter analysis

In vivo electroporation was performed according to the modified method of Aihara and Miyazaki [17]. Under the pentobarbital anesthesia (30 mg/kg), bilateral quadriceps muscles from C57BL6

Table 3. Body weight, blood glucose and plasma insulin levels in RXRγ mice in clamp study.

		Wild-type	RXRγ
	Body weight (g)	24.1±1.2	23.4±0.3
Basal period	Glucose (mg/dL)	141.8±15.3	106.6±5.5*
	Insulin (ng/mL)	0.55±0.08	0.44±0.07
Clamp period	Glucose (mg/dL)	92.5±3.8	96.7±3.6
	Insulin (ng/mL)	2.60±0.20	2.38±0.33

Mice were males 13–16 weeks of age. The number of animals used was 6 for wild-type control mice and 7 for RXRγ mice.
* $P<0.05$, compared with wild-type control.
Values are the means ± SE. These mice were also used in Fig 3.
doi:10.1371/journal.pone.0020467.t003

mice (male, 12 weeks of age) were injected with 80 μg of plasmid DNA (25 μl) by using a 29-gauge needle attached to a 0.5-ml insulin syringe (Terumo Corporation, Tokyo, Japan). Square-wave electrical pulses (160 V/cm) were applied six times with an electrical pulse generator (CUY21EDIT, Nepa Gene Co. Ltd., Chiba, Japan) at a rate of one pulse per second, with each pulse being 20 ms. in duration. The electrodes were a pair of stainless steel needles inserted into the quadriceps muscles and fixed 5 mm apart. Seven days after gene delivery, the muscles were removed and subjected to analysis. Frozen muscle tissues were homogenized in ice-cold passive lysis buffer from Promega. The homogenate was centrifuged at 10,000 g for 10 min at 4°C. The supernatant was reserved for luciferase assay using Promega's dual luciferase assay kit. The luciferase activity was calculated as the ratio of firefly to Renilla (internal control) luciferase activity and represented as the average of triplicate experiments.

Computer-based DNA sequence motif search

We used MATCH software [18] (BIOBASE GmbH, Wolfenbuettel, Germany) to investigate transcriptional binding sites in the mouse *Glut1* promoter. We investigated mouse genome in the region of -1500 to +100 relative to transcription start of *Glut1* (Chr.4 11878131(+)).

cDNA microarray analysis

RNA was isolated from the skeletal muscle of sex- and age-matched RXRγ mice (line 4-3) and non-transgenic control mice

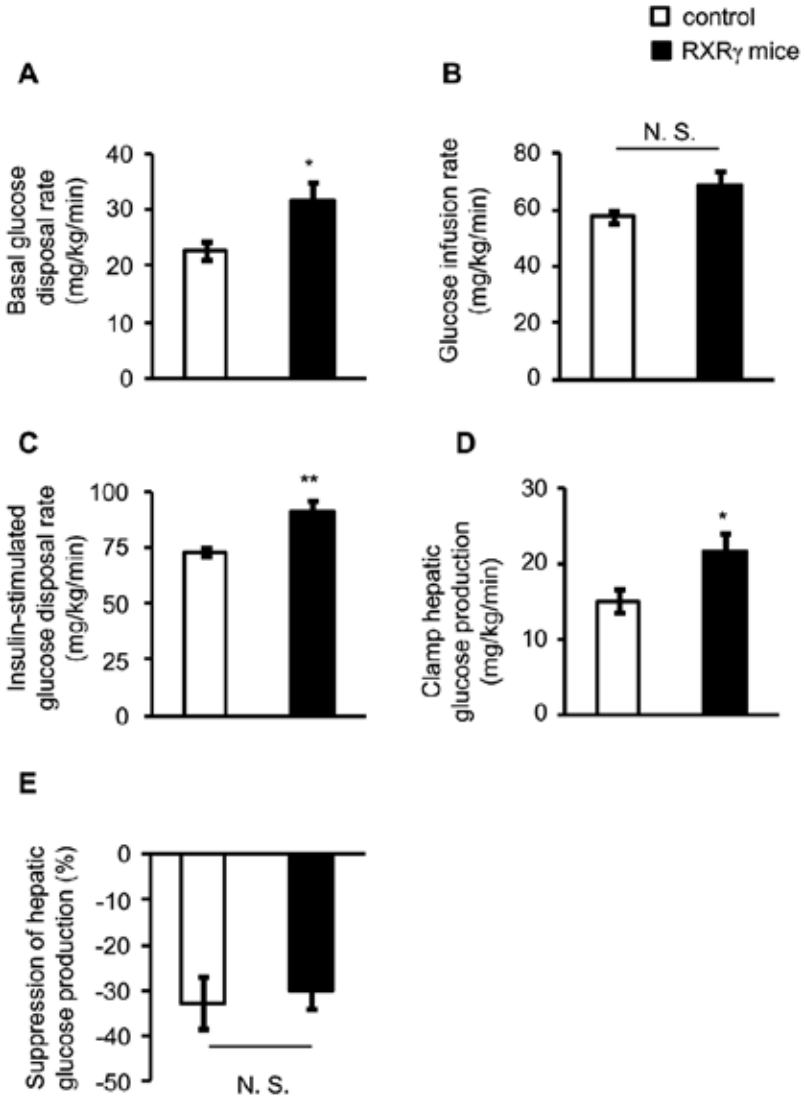

Figure 3. Hyperinsulinemic-euglycemic clamp test in RXRγ mice, fed a chow diet. (*A*) Basal glucose disposal rate, (*B*) glucose infusion rate needed to maintain euglycemia, (*C*) insulin-stimulated glucose disposal rate and (*D*) clamp hepatic glucose production (hepatic glucose production during the clamp period) (*E*) suppression of hepatic glucose production during the clamp period in RXRγ mice. Male mice, 13~16 weeks of age, were used. The number of animals used was 6 for control mice (open bars) and 7 for RXRγ mice (filled bars). * $P<0.05$ and ** $P<0.01$ compared with respective control. N. S., not significant.
doi:10.1371/journal.pone.0020467.g003

(females at 4 months of age, five samples from each group were combined). Each of the combined samples was hybridized to the Affymetrix MG430 microarray, which contains 45,102 genes, including expressed sequence tags (ESTs), and analyzed with the software Affymetrix Gene Chip 3.1. Of the 45,102 genes including ESTs analyzed, 8,054 (non-transgenic control mice) and 8,083 (transgenic) were expressed at a substantial level (absolute call is present and average difference is above 150). In order of fold changes in gene expression levels in skeletal muscle from RXRγ mice relative to control mice, genes whose expression was increased more than $2^{0.4}$-fold in RXRγ mice were listed (Dataset S1). Fold changes were calculated as an indication of the relative change of each transcript represented on the probe array. Differentially expressed genes were identified using the following criteria; 'absolute call' is present, and 'average difference' was above 250. 'Absolute call', which was calculated with this software using several markers, is an indicator of the presence or absence of each gene transcript. The 'average difference' value is a marker of the abundance of each gene, obtained by comparing the intensity of hybridization to 20 sets of perfectly matched 25-mer oligonucleotides relative to 20 sets of mismatched oligonucleotides using Affymetrix Gene Chip 3.1 software. All data of microarray is MIAME compliant and that the raw data has been deposited in a MIAME compliant database (GEO), whose accession number is GSE28448.

Gene Ontology Analysis

We used DAVID v6.7 [19] for gene ontology (GO) analysis. DAVID is a web application providing a comprehensive set of functional annotation tools to understand the biological meaning behind a large list of genes. Functional Annotation Clustering of DAVID was applied to the genes whose gene expression increased in RXRγ mice. Our GO analysis produced 62 GO terms from gene sets from RXRγ mice with increased expression compared to the wild-type mice, under the condition of $P<0.05$ (P value from Fisher's Exact Test). The obtained GO terms contained many similar functional concepts. In order to group similar GO terms, we applied the Functional Annotation Clustering tool provided by DAVID [19,20]. Twenty-three clusters were produced with genes showing increased expression. We showed one GO term of the lowest P value of all the members of an individual cluster.

Transcriptional factor binding sites analysis

We used MATCH software [18] with BKL TRANSFAC 2010.3 Release (BIOBASE GmbH, Worfenbuettel, Germany) to investigate transcriptional binding sites in the promoter regions of genes. The F-Match algorithm compares the number of sites found in a query sequence set against the background set. It is assumed, if a certain transcription factor (or factor family), alone or as a part of a *cis*-regulatory module, plays a significant role in the regulation of the considered set of promoters, then the frequency of the corresponding sites found in these sequences should be significantly higher than expected by random chance. We investigated the mouse genome in the region of -1000 to +100 relative to the transcription start of an individual gene. Statistical hypothesis testing was evaluated against housekeeping genes of mice. We investigated promoter regions of 15 genes: that is 14 'glucose metabolic process' genes with increased expression in RXRγ mice, plus Glut1. In the GO analysis, Glut1 was categorized as a 'transporter' not 'glucose metabolic process' gene.

Statistical analysis

Statistical analysis was performed using the Student's t test and analysis of variance (ANOVA) followed by Scheffe's test. Data were expressed as the mean ± SE. $P<0.05$ was considered statistically significant.

Results

Increased glucose metabolism in RXRγ mice

In our previous study, we established two lines of RXRγ mice (named lines 4-3 and 5-3) with similar expression levels of the *RXRγ* transgene and protein specifically in the skeletal muscle [9]. There was no significant difference in body weight, adipose tissue,

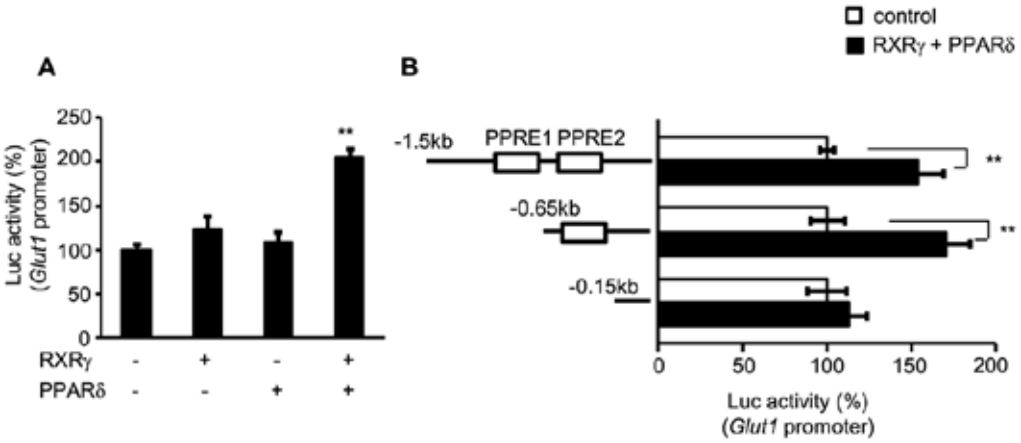

Figure 4. Transient transfection-reporter assay of the effect of RXRγ on *Glut1* promoter. (*A*) *Glut1*-Luc plasmid, with or without RXRγ and/or PPARδ expression vectors, was transfected into the quadriceps muscle of C57BL6 mice. Activation of the luciferase reporter gene was measured in relative light units and normalized to dual luciferase activity. Mean values from experiments (n = 5) are shown as fold induction, where the activity in the absence of RXRγ is the reference value (set at 100). (*B*) Schematic representations of serial deletion of *Glut1* promoter constructs are shown in the figure. Squares denote the putative PPAR/RXR binding sites. Open bars; *Glut1*-Luc without RXRγ and PPARδ expression vectors, and filled bars; *Glut1*-Luc with RXRγ and PPARδ expression vectors. The activity in the absence of RXRγ and PPARδ in each experiment for different *Glut1*-Luc construct in the reference value (set at 100). ** $P<0.01$, compared with the value of wild-type promoter in the absence of RXRγ/PPARδ.
doi:10.1371/journal.pone.0020467.g004

and liver weight between RXRγ and control mice in both lines 4-3 and 5-3, although the skeletal muscle weight was slightly lower in RXRγ mice than in control mice (Tables 1 and 2). In this study, blood glucose in RXRγ mice was lower than in control mice (fasting state, $P<0.01$ in lines 4-3 and 5-3; basal state, $P<0.05$ in line 4-3 and $P=0.06$ in line 5-3), which is consistent with our previous report [9].

To elucidate the role of the skeletal muscle RXRγ in systemic glucose metabolism, we performed glucose and insulin tolerance tests in RXRγ mice. The glucose tolerance test revealed increased glucose disposal in RXRγ mice relative to control mice (Fig. 1*A*). On the other hand, there was no significant difference in the insulin-induced hypoglycemic response between genotypes (Fig. 1*B*). These observations suggest that RXRγ mice have a higher capacity for glucose disposal with no change in insulin sensitivity.

Increased Glut1 expression and glucose uptake in the skeletal muscle of RXRγ mice

As both lines of RXRγ mice showed increased glucose metabolism, for the following experiments, we only utilized the line 4-3 of RXRγ mice (hereafter just RXRγ mice). Interestingly, mRNA expression of *Glut1* was increased in the skeletal muscle from RXRγ mice relative to control mice ($P<0.01$), whereas that of *Glut4* was unchanged (Fig. 2*A*). We also observed that Glut1 is significantly increased in RXRγ mice at the protein level ($P<0.05$), with no significant difference in Glut4 between genotypes (Fig. 2*B*). Consistently, we also found increased glucose uptake in the skeletal muscle from RXRγ mice relative to control mice ($P<0.05$), which was not further enhanced in the presence of insulin (Fig. 2*C*). We also observed increased glucose glycogen content in the skeletal muscle from RXRγ mice relative to control mice ($P<0.05$, Fig. 2*D*).

Table 4. Gene Ontology Analysis.

GO ID	GO Term	P value
GO:0060537	muscle tissue development	6.91E-05
GO:0006461	protein complex assembly	6.78E-05
GO:0008104	protein localization	1.18E-04
GO:0051146	striated muscle cell differentiation	6.06E-04
GO:0030334	regulation of cell migration	8.04E-04
GO:0006886	intracellular protein transport	0.002367379
GO:0019220	regulation of phosphate metabolic process	0.00312153
GO:0048514	blood vessel morphogenesis	0.00172443
GO:0045859	regulation of protein kinase activity	0.00563927
GO:0006915	apoptosis	0.007513423
GO:0006006	glucose metabolic process	0.002958786
GO:0006917	induction of apoptosis	0.005257921
GO:0042981	regulation of apoptosis	0.014518039
GO:0043066	negative regulation of apoptosis	0.022995692
GO:0006633	fatty acid biosynthetic process	0.012664127
GO:0032956	regulation of actin cytoskeleton organization	0.027565775
GO:0043388	positive regulation of DNA binding	0.021966247
GO:0006469	negative regulation of protein kinase activity	0.045894089
GO:0016477	cell migration	0.045248711
GO:0030521	androgen receptor signaling pathway	0.027402985
GO:0055003	cardiac myofibril assembly	0.020081231
GO:0000165	MAPKKK cascade	0.032045331
GO:0046825	regulation of protein export from nucleus	0.027402985

738 genes up-regulated in RXRγ mice compared with wild-type mice by microarray (Listed in Dataset S1) were classified into GO functional annotations, as described in Methods.
doi:10.1371/journal.pone.0020467.t004

Increased basal glucose disposal rate of RXRγ mice

To gain further insight into the glucose metabolism in RXRγ mice, we performed a hyperinsulinemic-euglycemic clamp study. Plasma insulin concentrations during the basal period were similar between genotypes (Table 3). The basal glucose disposal rate was significantly increased in RXRγ mice than in the controls ($P<0.05$, Fig. 3*A*), supporting that an insulin-independent increase in glucose uptake occurred, as observed in Fig. 2*C*. Meanwhile, we observed that the rate of glucose infusion needed to maintain euglycemia (glucose infusion rate) was similar between genotypes (Fig. 3*B*), which is consistent with the result of the insulin tolerance test (Fig. 1*B*). On the other hand, insulin-stimulated glucose disposal rate was higher in RXRγ mice than in the controls ($P<0.01$, Fig. 3*C*), which probably reflects the increased basal glucose disposal rate (Fig. 3*A*). Also, the clamp hepatic glucose production (hepatic glucose production during the clamp period) was higher in RXRγ mice than in the controls ($P<0.05$, Fig. 3*D*). Meanwhile, hepatic glucose production was similarly suppressed by insulin in both genotypes (Fig. 3*E*). Together, these data support the idea that Glut1, an insulin-independent glucose transporter, is involved in the increased glucose disposal in the skeletal muscle of RXRγ mice.

Activation of the *Glut1* promoter by combination of RXRγ and PPARδ in the skeletal muscle *in vivo*

To examine whether RXRγ directly activates mRNA expression of *Glut1*, we performed the *in vivo* luciferase reporter analysis

Table 5. List of 'glucose metabolic process' genes.

Gene Symbol	Gene description
Atf3	Activating transcription factor 3
Bpgm	2-3-bisphosphoglycerate mutase
Dcxr	Dicarbonyl L-xylulose reductase
Fbp2	Fructose bisphosphatase 2
Gbe1	Glucan branching enzyme 1
Gpd1l	Glycerol-3-phosphate dehydrogenase 1-like
Gpi1	Glucose phosphate isomerase 1
Gys2	Glycogen synthase 2
Igf2	Insulin-like growth factor 2
Mat2b	Methionine adenosyltransferase II, beta
Nisch	Nischarin; an imidazoline receptor
Pdk1	Pyruvate dehydrogenase kinase isoenzyme 1
Pgam1	Phosphoglycerate mutase 1
Pgd	Phosphogluconate dehydrogenase
Pgm2l1	Phosphoglucomutase 2-like 1
Phkb	Phosphorylase kinase beta

Up-regulated genes in RXRγ mice in the microarray, classified as 'glucose metabolic process' genes by GO analysis, as described in Method. Genes are listed in alphabetic order of gene symbol. Glut1, which appeared in the up-regulated list in the microarray (Dataset S1), is not included in this list, as it was classified 'transporter' in the GO analysis.
doi:10.1371/journal.pone.0020467.t005

using *Glut1* promoter (*Glut1*-Luc). In this study, the activity of *Glut1*-Luc was marginally enhanced by RXRγ alone (Fig. 4*A*). Moreover, we found no significant activation of the *Glut1*-Luc by PPARδ, an important regulator of glucose as well as lipid metabolism in the skeletal muscle [7]. Interestingly, combination of RXRγ and PPARδ resulted in significant increase in *Glut1*-Luc activity in the skeletal muscle *in vivo* ($P<0.01$) (Fig. 4*A*). Motif search analysis revealed two putative PPAR-responsive elements (PPRE1 and PPRE2) (−657/−645 and −520/−508, respectively) in the mouse *Glut1* promoter. A series of deletion mutant analysis showed that combination of RXRγ and PPARδ activates the regions of −1500/+75, and −647/+75, but not the region of −152/+75 in the *Glut1* promoter (Fig. 4*B*), suggesting that the second putative PPRE (−520/−508) is involved in the RXRγ/PPARδ-induced *Glut1* promoter activation.

Microarray and bioinformatics analyses of up-regulated gene in RXRγ mice

In order to gain insight into the gene expression change in RXRγ mice, we performed microarray analysis. As shown in Dataset S1, 738 genes were up-regulated in the analysis. As expected, Glut1 expression was increased in the microarray data. Also, SREBP1c expression, which we previously reported [9], was increased in the microarray data. Using the data, we performed GO analysis to determine if genes, up-regulated in RXRγ mice, are associated with particular biological processes. Our GO analysis revealed genes with increased expression in the RXRγ mice in various categories (Table 4), including 'glucose metabolic process' genes and 'fatty acid biosynthetic process' genes, which indicated that overexpression of RXRγ affects the expression of many genes. The up-regulated genes categorized as glucose metabolism genes in GO term are listed in Table 5. Among them, we confirmed enhanced gene expression by quantitative real time PCR (Fig. 5), supporting the microarray data reliable. Moreover, we calculated the ratio of putative transcription factor binding motifs in glucose metabolism genes, which were up-regulated in RXRγ mice. In the sample, several motifs showed statistical significance (Table 6) ($P<0.05$), including PPAR responsive elements. These data suggest that glucose metabolism genes up-regulated in RXRγ mice are possible target genes of the RXRγ and PPAR heterodimer.

Discussion

RXRγ is a nuclear receptor-type transcription factor that is expressed abundantly in the skeletal muscle and is regulated by nutritional conditions. Treatment of obese and diabetic mice with RXR pan-agonists (agonists for all the RXR isoforms) has improved glucose metabolism in mice [21–23], suggesting the beneficial effect of RXR on diabetes. However, which RXR isoform(s) are involved and where they work to improve diabetes

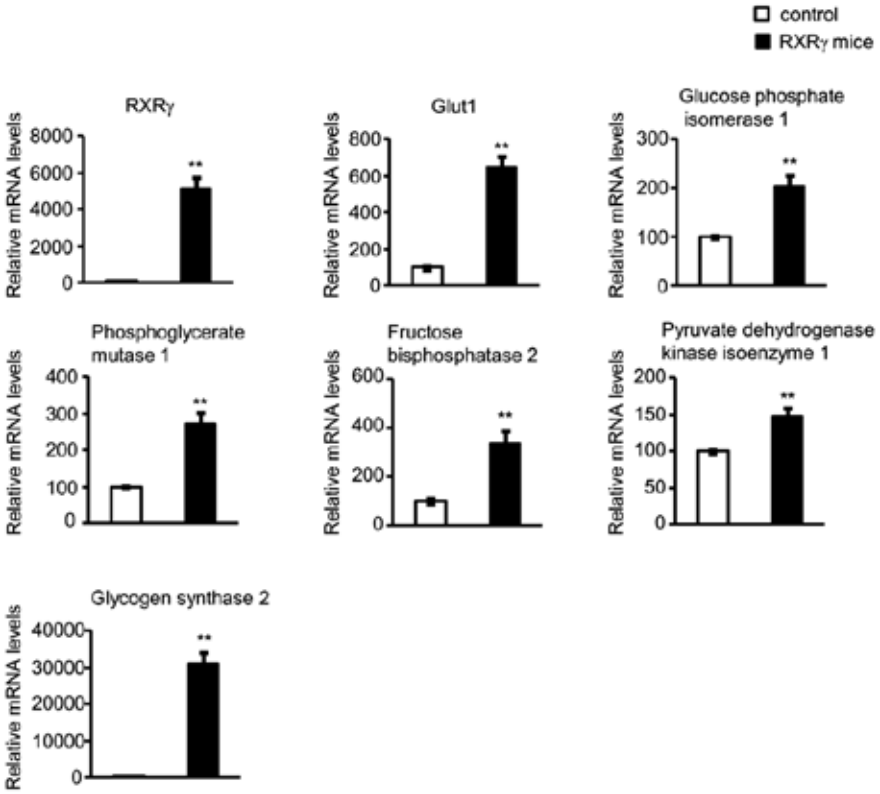

Figure 5. Levels of 'glucose metabolic process' gene expression in the skeletal muscle of RXRγ mice. Representative gene expressions of 'glucose metabolic process genes' analyzed by microarray and GO analysis (Table 5) were examined by quantitative real-time PCR. The value for wild-type (littermates of line 4-3) mice was set at 100, and relative values are shown. Mice were females of 4 months of age. The number of animals was 6 for both control (open bars) and RXRγ (filled bars) mice. These samples were also used in microarray analysis (Dataset S1). * $P<0.05$ and ** $P<0.01$ compared with respective control. N. S., not significant.
doi:10.1371/journal.pone.0020467.g005

Table 6. Possible transcription factor binding sites in the 'glucose metabolic process' gene up-regulated in RXRγ mice.

Transcription factors	Matrix name	P-value
WT1, WT1 -KTS, WT1 I, WT1 I -KTS	WT1_Q6	6.98E-04
HNF-4, HNF-4alpha	HNF4ALPHA_Q6	0.0013
PPARalpha	PPARA_01	0.0017
c-Myb, c-Myb-isoform1	VMYB_02	0.0026
PPARalpha, PPARdelta, PPARgamma	PPAR_DR1_Q2	0.003
CART1, CART1, CART1	CART1_01	0.0036
COUP-TF1, COUP-TF2, HNF-4, HNF-4alpha	COUP_DR1_Q6	0.0036
CP2, CP2-isoform1	CP2_02	0.0055
NRF1-isoform1, NRF1-isoform2, NRF1-xbb1	TCF11_01	0.0057
SZF1	SZF11_01	0.0057
PPARgamma	PPARG_01	0.0057
COUP-TF1, COUP-TF2, HNF-4, HNF-4alpha, HNF4gamma	DR1_Q3	0.0057
BRCA1, BRCA1	BRCA_01	0.0065
HNF-3beta	HNF3B_01	0.007
Pax-2b, pax2	PAX2_01	0.007
C/EBPalpha, C/EBPbeta(LAP), C/EBPbeta(p20), C/EBPbeta(p20), C/EBPbeta(p34), C/EBPbeta(p35), C/EBPgamma, cebpe, CRP3, NF-IL6-1, NF-IL6-3	CEBP_Q3	0.007
MITF, MITF-M1, tcfec, TFEA, TFEA-xbb1, TFEA-xbb2, tfeb, tfeb-isoform1	TFE_Q6	0.007
AP-2alpha, AP-2beta, AP-2gamma	AP2_Q6_01	0.0077
Pax-4a, Pax-4c, Pax-4d, Pax4	PAX4_04	0.0079
c-Myc, deltaMax, max, max-isoform1, max-isoform2, N-Myc	MYCMAX_03	0.0093

The mouse genome in the region of −1000 to +100 relative to the transcription start of an individual gene classified as glucose metabolism gene by GO analysis (Table 5), was analyzed. Statistical hypothesis testing was evaluated against housekeeping genes of mice. Matrics names are based on the MATCH software (see **Methods**), which are listed in *P*-value order. Indicated binding sites of transcription factors appeared significantly more frequent occurrence in the promoter sets.
doi:10.1371/journal.pone.0020467.t006

has not been addressed. Here, we investigated glucose metabolism in RXRγ mice.

We demonstrated increased glucose metabolism in RXRγ mice relative to control mice, although there was no significant difference in the insulin-induced hypoglycemic effect between genotypes, based on insulin tolerance test and glucose clamp analysis. Because insulin level is similar between RXRγ mice and control mice, it is unlikely that increased insulin secretion is responsible for increased glucose tolerance in RXRγ mice. On the other hand, mRNA and protein expression of Glut1 is increased in the skeletal muscle from RXRγ mice relative to control mice, with increased glucose uptake and glycogen content. Because transgenic overexpression of Glut1 in the skeletal muscle has resulted in increased glucose uptake [24], glycogen content [25] and lowering of blood glucose [24], it is likely that enhanced glucose tolerance in RXRγ mice is mediated at least in part by increased Glut1 in the skeletal muscle.

As RXRγ is a nuclear receptor-type transcription factor that heterodimerizes with many nuclear receptors [6], we examined whether the *Glut1* gene is directly regulated by RXRγ. In an *in vivo* luciferase reporter analysis, combination of RXRγ and PPARδ activates the *Glut1* promoter activity, which is diminished by deletion of the putative PPREs. It is, therefore, RXRγ/PPARδ may activate *Glut1* expression in the skeletal muscle *in vivo*. In this regard, we found that overexpression of RXRγ or PPARδ alone or both in C2C12 myocytes *in vitro* does not induce *Glut1* gene expression (unpublished data). This may be because C2C12 cells lack other factor(s) that are present in the skeletal muscle *in vitro* and are required to activate *Glut1* transcription. Whether the increased *Glut1* gene in RXRγ mice is mediated by RXRγ/PPARδ should be confirmed by additional experiments using PPARδ knockout mice. Meanwhile, the transgene expression level in RXRγ mice was very high, and appeared to be beyond the physiological level. Nonetheless, if RXRγ can be enhanced in skeletal muscle, an increase in glucose metabolism can be expected.

We recently demonstrated that in addition to glycogen content, RXRγ mice exhibit increased triglyceride in the skeletal muscle as a result of increased SREBP1c gene expression [9]. In obese and diabetic subjects, intramuscular lipid is high with insulin resistance [26]. Moreover, in athletes, the skeletal muscle is also high in lipid but with high insulin sensitivity, which is known as the athlete paradox [27,28]. A partial explanation is an increased fatty acid load in obese and diabetic subjects, but not in athletes; increased intramuscular lipotoxic fatty acid metabolites, such as diacylglycerol and ceramide, cause insulin resistance in skeletal muscles [29,30]. Taken together with our previous report [9], this study demonstrates that RXRγ mice do not develop insulin resistance despite high intramuscular lipids, and appear to be protected against obesity-induced lipotoxicity in the skeletal muscle. Depositing glucose as both glycogen and triglycerides in the skeletal muscle may be effective in enhancing glucose metabolism.

Microarray analysis showed that various genes are up-regulated in the skeletal muscle of RXRγ mice. As RXRγ can heterodimerize several nuclear receptors, it is not surprising that expression of many genes was up-regulated by RXRγ overexpression. Concerning glucose metabolism genes, in the skeletal muscle of RXRγ mice, the expression levels of genes, such as glucose phosphate isomerase 1 and phosphoglycerate mutase 1 (stimulate glycolysis or gluconeogenesis), fructose bisphosphatase 2 (stimulates gluconeogenesis), pyruvate dehydrogenase kinase

isoenzyme 1 (suppresses glycolysis), glycogen synthase 2 (stimulates glycogen synthesis)[31,32], were markedly increased (Fig. 5), suggesting the anabolic reaction of glucose. This is consistent with the observation that the glycogen content of skeletal muscle is higher in RXRγ mice (Fig. 2C). It is of note that glycogen synthase 2 is a liver-type enzyme, not a skeletal muscle-type enzyme [32]. In addition, usually, gluconeogenesis is not considered to be a major metabolic pathway in skeletal muscle. Chronic transgenic overexpression of RXRγ may have caused a super-physiological gene expression change in the skeletal muscle. Meanwhile, our bioinformatics analysis showed that glucose metabolism genes up-regulated in RXRγ mice contain several transcription factor binding motifs including PPRE in their promoter region. These observations support the concept that the RXRγ/PPAR heterodimer contributes to activation of these gene sets, although this needs to be confirmed by further experiments.

In summary, we demonstrated enhanced glucose metabolism with increased Glut1 expression and glucose uptake in RXRγ mice. This study suggested that activation of the skeletal muscle RXRγ is a novel therapeutic strategy to treat or prevent type 2 diabetes.

Supporting Information

Dataset S1 List of genes up-regulated in RXRγ mice compared with wild-type control mice by microarray.
(XLS)

Acknowledgments

We thank Dr. Christopher K. Glass (University of California, San Diego) for discussion. We thank Dr. Kotaro Ishibashi (Daiichi-Sankyo Co., Ltd.) for assistance in animal experiments.

Author Contributions

Conceived and designed the experiments: JIO KN SS YK OE YO. Performed the experiments: SS YK FA TS SK (Sayaka Kanai) MH YM NF TTI MT HA TY HK (Hideki Katagiri) SK (Saori Kakehi) YT HK (Hideo Kubo) SM. Analyzed the data: SS YK FA TS SK (Sayaka Kanai) MH YM NF TTI HA TY HK (Hideki Katagiri) SK (Saori Kakehi) YT HK (Hideo Kubo) SM. Contributed reagents/materials/analysis tools: TTI HA JIO KN. Wrote the paper: SS YK OE YO.

References

1. Zurlo F, Larson K, Bogardus C, Ravussin E (1990) Skeletal muscle metabolism is a major determinant of resting energy expenditure. J Clin Invest 86: 1423–1427.
2. DeFronzo RA (1988) Lilly lecture 1987. The triumvirate: beta-cell, muscle, liver. A collusion responsible for NIDDM. Diabetes 37: 667–687.
3. Marshall BA, Hansen PA, Ensor NJ, Ogden MA, Mueckler M (1999) GLUT-1 or GLUT-4 transgenes in obese mice improve glucose tolerance but do not prevent insulin resistance. Am J Physiol 276: E390–E400.
4. Petersen KF, Dufour S, Savage DB, Bilz S, Solomon G, et al. (2007) The role of skeletal muscle insulin resistance in the pathogenesis of the metabolic syndrome. Proc Natl Acad Sci U S A 104: 12587–12594.
5. Kim JK, Zisman A, Fillmore JJ, Peroni OD, Kotani K, et al. (2001) Glucose toxicity and the development of diabetes in mice with muscle-specific inactivation of GLUT4. J Clin Invest 108: 153–160.
6. Shulman AI, Mangelsdorf DJ (2005) Retinoid x receptor heterodimers in the metabolic syndrome. N Engl J Med 353: 604–615.
7. Lee CH, Olson P, Hevener A, Mehl I, Chong LW, et al. (2006) PPARdelta regulates glucose metabolism and insulin sensitivity. Proc Natl Acad Sci U S A 103: 3444–3449.
8. Szanto A, Narkar V, Shen Q, Uray IP, Davies PJ, et al. (2004) Retinoid X receptors: X-ploring their (patho)physiological functions. Cell Death Differ 11: S126–S143.
9. Kamei Y, Miura S, Suganami T, Akaike F, Kanai S, et al. (2008) Regulation of SREBP1c gene expression in skeletal muscle: role of retinoid X receptor/liver X receptor and forkhead-O1 transcription factor. Endocrinology 149: 2293–2305.
10. Suzuki R, Tobe K, Aoyama M, Inoue A, Sakamoto K, et al. (2004) Both insulin signaling defects in the liver and obesity contribute to insulin resistance and cause diabetes in Irs2(-/-) mice. J Biol Chem 279: 25039–25049.
11. Uno K, Katagiri H, Yamada T, Ishigaki Y, Ogihara T, et al. (2006) Neuronal pathway from the liver modulates energy expenditure and systemic insulin sensitivity. Science 312: 1656–1659.
12. Erion DM, Yonemitsu S, Nie Y, Nagai Y, Gillum MP, et al. (2009) SirT1 knockdown in liver decreases basal hepatic glucose production and increases hepatic insulin responsiveness in diabetic rats. Proc Natl Acad Sci U S A 106: 11288–11293.
13. Tanaka S, Hayashi T, Toyoda T, Hamada T, Shimizu Y, et al. (2007) High-fat diet impairs the effects of a single bout of endurance exercise on glucose transport and insulin sensitivity in rat skeletal muscle. Metabolism 56: 1719–1728.
14. Ito A, Suganami T, Miyamoto Y, Yoshimasa Y, Takeya M, et al. (2007) Role of MAPK phosphatase-1 in the induction of monocyte chemoattractant protein-1 during the course of adipocyte hypertrophy. J Biol Chem 282: 25445–25452.
15. Fujii N, Ho RC, Manabe Y, Jessen N, Toyoda T, et al. (2008) Ablation of AMP-activated protein kinase alpha2 activity exacerbates insulin resistance induced by high-fat feeding of mice. Diabetes 57: 2958–2966.
16. Lowry OH, Passonneau JV (1972) A flexible system of enzymatic analysis. Academic Press London 1-291.
17. Aihara H, Miyazaki J (1998) Gene transfer into muscle by electroporation in vivo. Nat Biotechnol 16: 867–870.
18. Kel AE, Gossling E, Reuter I, Cheremushkin E, Kel-Margoulis OV, et al. (2003) MATCH: A tool for searching transcription factor binding sites in DNA sequences. Nucleic Acids Res 31: 3576–3579.
19. Huang da W, Sherman BT, Lempicki RA (2009) Systematic and integrative analysis of large gene lists using DAVID bioinformatics resources. Nat Protoc 4: 44–57.
20. Carbon S, Ireland A, Mungall CJ, Shu S, Marshall B, Lewis S (2009) AmiGO: online access to ontology and annotation data. Bioinformatics 25: 288–289.
21. Mukherjee R, Davies PJ, Crombie DL, Bischoff ED, Cesario RM, et al. (1997) Sensitization of diabetic and obese mice to insulin by retinoid X receptor agonists. Nature 386: 407–410.
22. Davies PJ, Berry SA, Shipley GL, Eckel RH, Hennuyer N, et al. (2001) Metabolic effects of rexinoids: tissue-specific regulation of lipoprotein lipase activity. Mol Pharmacol 59: 170–176.
23. Shen Q, Cline GW, Shulman GI, Leibowitz MD, Davies PJ (2004) Effects of rexinoids on glucose transport and insulin-mediated signaling in skeletal muscles of diabetic (db/db) mice. J Biol Chem 279: 19721–19731.
24. Marshall BA, Ren JM, Johnson DW, Gibbs EM, Lillquist JS, et al. (1993) Germline manipulation of glucose homeostasis via alteration of glucose transporter levels in skeletal muscle. J Biol Chem 268: 18442–18445.
25. Ren JM, Marshall BA, Gulve EA, Gao J, Johnson DW, et al. (1993) Evidence from transgenic mice that glucose transport is rate-limiting for glycogen deposition and glycolysis in skeletal muscle. J Biol Chem 268: 16113–16115.
26. Goodpaster BH, Wolf D (2004) Skeletal muscle lipid accumulation in obesity, insulin resistance, and type 2 diabetes. Pediatr Diabetes 5: 219–226.
27. Stannard SR, Johnson NA (2004) Insulin resistance and elevated triglyceride in muscle: more important for survival than "thrifty" genes? J Physiol 554: 595–607.
28. Goodpaster BH, He J, Watkins S, Kelley DE (2001) Skeletal muscle lipid content and insulin resistance: evidence for a paradox in endurance-trained athletes. J Clin Endocrinol Metab 86: 5755–5761.
29. Schenk S, Horowitz JF (2007) Acute exercise increases triglyceride synthesis in skeletal muscle and prevents fatty acid-induced insulin resistance. J Clin Invest 117: 1690–1698.
30. Liu L, Zhang Y, Chen N, Shi X, Tsang B, et al. (2007) Upregulation of myocellular DGAT1 augments triglyceride synthesis in skeletal muscle and protects against fat-induced insulin resistance. J Clin Invest 117: 1679–1689.
31. Kaslow HR, Lesikar DD, Antwi D, Tan AW (1985) L-type glycogen synthase. Tissue distribution and electrophoretic mobility. J Biol Chem 260: 9953–9956.
32. Salway JG (1999) Metabolism at a glance. London: Blackwell Science Ltd.

細胞生理学分野

水島　昇

医歯学総合研究科・器官システム制御学系専攻
細胞生理学・教授

1）研究の課題名

オートファジーの分子機構と生理的意義の研究

Molecular mechanism and physiological roles of autophagy

哺乳類細胞でのオートファゴソーム形成に関わるAtg因子群の遺伝学的階層構造を調べ、それをもとにオートファゴソーム形成場所の解析を行った。さらに、オートファジーの選択的基質であるp62がどのステップでオートファジー関連構造体にリクルートされるかを検討した。従来はp62がオートファゴソーム膜のLC3と直接結合することがその認識機構であると考えられてきたが、今回の解析からp62はLC3を含むほとんどのAtg因子に非依存的にオートファゴソーム形成部位に集積しうることが明らかとなった。

パーキンソン病原因因子のひとつであるパーキンは、オートファジーによる不良ミトコンドリアの除去を行うことが知られているが、この作用に加えてパーキンはミトコンドリア外膜タンパク質の広範な分解を担っていることがわかった。これはプロテアソーム依存的であった。従って、パーキンはタンパク質レベルでのミトコンドリア外膜の修復と、オルガネラレベルでのミトコンドリア丸ごとの分解の両方を制御していると考えられた。また、オートファジー因子によるミトコンドリアの認識については、これまでp62がミトコンドリアとオートファゴソーム膜に存在するLC3の間を仲介するアダプターと考えられてきた。しかし、脱分極したミトコンドリアの認識にはp62もLC3も必要なく、最初のステップでULK1複合体とAtg9Aを小胞が互いに非依存的にミトコンドリアに局在し、両者がクラスIII PI3キナーゼ複合体やその下流因子のリクルートに重要であることが示された。LC3はミトコンドリアの初期認識ではなく、ミトコンドリアを適切にオートファゴソーム内に隔離する過程で重要であると考えられた。

オートファジーの生理的意義の解析としては、Atg5全身モザイク欠損マウスの長期間観察によって、オートファジー欠損は肝の多発性腫瘍を誘発することを明らかにした。このマウスの肝細胞では、腫脹した不良ミトコンドリアが集積し、過剰な酸化ストレス応答やゲノム傷害応答が観察された。従って、オートファジーによるミトコンドリアの品質管理が、腫瘍の自然発生を抑制する上で重要であることが示唆された。

2）

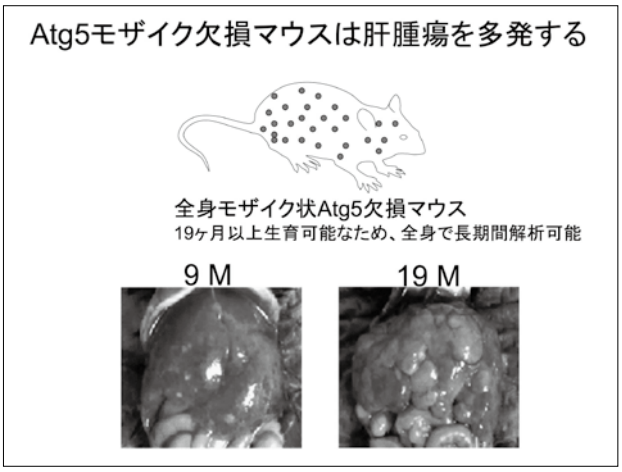

3）発表の研究内容についての英文要約

Autophagy is an intracellular degradation process, through which cytosolic materials are delivered to the lysosome. We examined the hierarchical relationships among mammalian Atg proteins. The protein complex including ULK1 and FIP200 is the most upstream unit and is required for puncta formation of the Atg14-containing PI3-kinase complex. Upstream Atg proteins such as ULK1 and Atg14 localize to the ER-associated autophagosome formation sites. We also found that the autophagy-selective substrate p62 can localize to the autophagosome formation site.
We also analyzed the long-term effect of defects in autophagy in vivo using a new mouse model with systemic mosaic deletion of Atg5, in which only a small population of cells were autophagy-defective in every tissue. These mice are viable for more than 19 months and develop multiple tumors only in the liver. Mitochondrial swelling, p62 accumulation, and oxidative stress and genomic damage responses were observed in these tumors. This new model

provides evidences suggesting that autophagy is important for suppression of spontaneous tumorigenesis, particularly in the liver.

4）本事業に関連して世界的な研究拠点形成に向けて、以下の点で改善・整備等されたこと

A（研究拠点体制）

国内でオートファジー研究会を開催。

B（人材確保）

助教1名、メディカルフェロー1名を採用。

C（国際化）

カンファレンスOrganizerとしてオートファジーに関するZing Conference on Autophagyをメキシコで開催

5）GCOE事業を推進するに当たって力を入れた点

インド人大学院生2名、ベトナム人大学院生1名を引き続き指導するとともに、専攻生として受け入れていた中国人留学生1名を新たに大学院生として指導し、国際性を維持。

6）英文原著論文

1. Velikkakath, A.K.G,, Nishimura, T., Oita, E., Ishihara, O., Mizushima, N. Mammalian Atg2 proteins are essential for autophagosome formation and important for regulation of size and distribution of lipid droplets. Mol. Biol. Cell [Epub ahead of print]
2. Itakura, E., Kishi-Itakura, C., Koyama-Honda, I., Mizushima, N. Structures containing Atg9A and the ULK1 complex independently target depolarized mitochondria at initial stages of Parkin-mediated mitophagy. J. Cell Sci. in press
3. Katayama, H., Kogure, T., Mizushima, N., Yoshimori, T., Miyawaki, A. A sensitive and quantitative technique for detecting autophagic events based on lysosomal delivery. Chem. Biol. 18：1042-1052（2011）.
4. Yoshii, S.R., Kishi, C., Ishihara, N., Mizushima, N. Parkin mediates proteasome-dependent protein degradation and rupture of the outer mitochondrial membrane. J. Biol. Chem. 286：19630-19640（2011）.
5. Asano, T., Komatsu, M., Yamaguchi-Iwai, Y., Ishikawa, F., Mizushima, N., Iwai, K. Distinct mechanisms of ferritin delivery to lysosomes in iron depleted and iron-replete cells. Mol. Cell Biol. 31, 2040-52（2011）
6. Takamura, A., Komatsu, M., Hara, T., Sakamoto, A., Kishi, C., Waguri, S., Eishi, Y., Hino, O., Tanaka, K., Mizushima, N. Autophagy-deficient mice develop multiple liver tumors. Genes Dev. 25：795-800（2011）.
7. Itakura, E., Mizushima, N. p62 targeting to the autophagosome formation site requires self-oligomerization but not LC3 binding. J. Cell Biol. 192：17-27（2011）.

7）総説ならびに著書

1. Mizushima, N., Komatsu, M. Autophagy：renovation of cells and tissues. Cell 147：728-41（2011）.
2. Klionsky, D.J., Baehrecke, E.H., Brumell, J.H., Chu, C.T., Codogno, P., Cuervo, A.M., Debnath, J., Deretic, V., Elazar, Z., Eskelinen, E.L., Finkbeiner, S., Fueyo-Margareto, J., Gewirtz, D., Jäättelä, M., Kroemer, G., Levine, B., Melia, T.J., Mizushima, N., Rubinsztein, D.C., Simonsen, A., Thorburn, A., Thumm, M., Tooze, S.A. A comprehensive glossary of autophagy-related molecules and processes（2nd edition）. Autophagy 7：1273-1294（2011）.
3. Mizushima, N. Autophagy in Protein and Organelle Turnover. Cold Spring Harb. Symp.Quant. Biol. 2011 Aug 3.
4. Mizushima, N., Yoshimori, T., Ohsumi, Y. The Role of Atg Proteins in Autophagosome Formation. Annu. Rev. Cell Dev. Biol. 27：107-32（2011）.
5. Stappenbeck, T.S., Rioux, J.D., Mizoguchi, A., Saitoh, T., Huett, A., Darfeuille-Michaud, A., Wileman, T., Mizushima, N., Carding, S., Akira, S., Parkes, M., Xavier, R.J. Crohn disease：A current perspective on genetics, autophagy and immunity. Autophag. 7：1-20（2011）
6. Levine, B., Mizushima, N., Virgin, H.W. Autophagy in immunity and inflammation. Nature 469：323-335（2011）.

和　文

1. 北村圭、太田伸生、水島昇　原虫のオートファジー炎症と免疫　印刷中
2. 貝塚剛志、内藤貴子、水島昇　オートファジーの制御シグナル　内分泌・糖尿病・代謝内科　33, 365-370（2011）
3. 水島昇、上田泰己、上村匡、後藤由季子、白髭克彦、小林武彦、塩見美喜子　効率的なラボ運営法　オーサーシップについて考える　細胞工学　30, 652-655（2011）
4. 水島昇　効率的なラボ運営法　効率的に読んでもらえるノートの書き方　細胞工学　30, 424-427（2011）
5. 水島昇　効率的なラボ運営法　マテリアルリクエストへの対応　細胞工学　30, 202-206（2011）
6. 久万亜紀子、水島昇　哺乳動物におけるオートファジーの生理的役割　実験医学増刊号　29, 133-139（2011）
7. 貝塚剛志、水島昇　オートファジーを駆動するシグ

ナリング　実験医学増刊号 29, 127-132（2011）
8. 久万亜紀子、水島昇　飢餓におけるmTORの役割：オートファジー誘導とリソソーム生合成　実験医学 29, 877-882（2011）
9. 久万亜紀子、水島昇　飢餓における細胞応答：オートファジー　アディポサイエンス 7, 199-205（2011）
10. 塚本　智史、水島昇　オートファジーの受精卵発生における役割　Hormone Frontier in Gynecology 18, 53-58（2011）
11. 貝塚剛志、水島昇　オートファジーの分子機構と生理機能　血液内科　62, 127-134（2011）
12. 西村多喜、高村聡人、水島昇　オートファジーと癌抑制　実験医学　29, 236-241（2011）

著　書

1. Mizushima N. Autophagy in Protein and Organelle Turnover. Cold Spring Harb. Symp. Quant. Biol. 2011

和　文

1. 水島昇 「細胞が自分を食べる　オートファジーの謎」PHPサイエンス・ワールド　新書　2011
2. 久万亜紀子　水島昇　糖尿病イラストレイテッド「代謝とオートファジー」羊土社（印刷中）
3. 西村多喜　水島昇　がん生物学イラストレイテッド「オートファジー」羊土社　2011

8）平成23年度までの自己評価

オートファジーメカニズム研究と生理学的研究の双方は順調に進んでいる。疾患との関連ではParkinの新しい作用についても発見することができた。

9）学会発表（英文）

1. Taki Nishimura, Noboru Mizushima The role of autophagy-related proteins on lipid metabolism in the ER membrane　The 30th Naito Conference　示説　Sapporo　2011.6.28-7.1
2. Pham Nguyen Quy, Akiko Kuma, Noboru Mizushima　Autophagy is suppressed following denervation through proteasome-dependent mTOR activation　第84回日本生化学会大会 口頭および示説　京都　2011.9.21-24
3. Sahani Mayurbhai Himatbhai, Eisuke Itakura, Noboru Mizushima　Restoration of p62 expression during prolonged starvation depends on transcriptional upregulation and autophagy-derived amino acids　第84回日本生化学会大会　口頭および示説　京都　2011.9.21-24
4. Eisuke Itakura, Noboru Mizushima Mitophagosome Formation In Parkin Dependent Mitophagy　The second Japan-Sino autophagy symposium 口頭　Hayama　2011.10.5-8
5. Atsushi Tanaka, Richard J. Youle, Noboru Mizushima Proteasome and p97/ VCP Mediate Mitophagy and Degradation of Mitofusins Induced by Parkin EMBO conference series：Autophagy in health and disease 示説　Israel 2011.10.30-11.4
6. Taki Nishimura Mammalian Atg2 proteins are essential for autophagosome formation and important for regulation of size and distribution of lipid droplets Zing conference on autophagy 口頭および示説　Cancun, Mexico 2011.12.7-11

10）学会発表（和文）

1. 水島昇　Role of autophagy in tumorigenesis　第6回オートファジー研究会　口頭　掛川　2011.1.12-14
2. 岸千絵子、吉井紗織、石原直忠、水島昇　障害ミトコンドリアのオートファジーによる分解：ミトファジーの超微細構造解析/Ultrastructural analysis of Parkin-mediated mitophagy　日本顕微鏡学会第67回学術講演会　口頭　福岡　2011.5.16-18
3. Yuta Ogasawara, Eisuke Itakura, Noboru Mizushima, Tamio Mizukami, Akitsugu Yamamoto. Stearoyl-CoA desaturase inhibitor suppresses autophagosome formation 第63回日本細胞生物学会大会　示説　札幌　2011.6.27-29
4. 塚本智史、久万亜紀子、岸千絵子、Pham Nguyen Quy、太田有紀、西川哲、岡崎絵里子、南直治郎、水島昇　精子完成過程におけるオートファジーの生理機能の解析　第104回日本繁殖生物学会大会 示説　盛岡　2011.9.15-17
5. 田中敦、水島昇、Youle Richard J.　ユビキチンリガーゼParkinが制御する選択的マイトファジー　第84回日本生化学会大会　シンポジウム　京都　2011.9.21-24
6. 内藤貴子、久万亜紀子、水島昇　オートファジー制御におけるインスリンの役割　第84回日本生化学会大会口頭および示説　京都　2011.9.21-24
7. Yuta Ogasawara, Eisuke Itakura, Noboru Mizushima, Tamio Mizukami, Akitsugu Yamamoto

Is lipid chain unsaturation necessary for starvation-induced autophagy? 第84回日本生化学会大会　示説　京都　2011.9.21-24

8. Eisuke Itakura, Ikuko Koyama-Honda, Chieko Kishi, and Noboru Mizushima Analysis of mitophagosome formation during parkin-dependent mitophagy 第34回日本分子生物学会年会 示説　横浜　2011.12.13-16
9. Ikuko Koyama-Honda, Eisuke Itakura, Takahiro Fujiwara and Noboru Mizushima Temporal relationship of recruitment of mammalian Atg proteins to the autophagosome formation site 第34回日本分子生物学会年会 口頭　横浜　2011.12.13-16
10. 森下英晃、岸千絵子、水島昇　水晶体オルガネラ分解過程におけるリソソームの関与　第38回水晶体研究会 口頭　東京　2012.1.7-8
11. 西村多喜、水島昇　オートファジー関連因子による小胞体膜の膜動態制御機構の解析 第117回 日本解剖学会総会・全国学術集会 シンポジウム 甲府 2012.3.26-28

11）受賞

平成23年11月　武田医学賞受賞
　添付5（科学新聞　2011.10.07）

12）外部資金の獲得状況

最先端・次世代研究開発支援プログラム
　研究題目：オートファジーの分子機構と生理機能に関する分野横断型研究
　代表：水島　昇
　期間：平成22―25年
　研究費総額：13900万円

科学研究費補助金、 特定領域研究
　研究題目：オートファジーのダイナミクスと生理意義の解析（成果とりまとめ）
　代表：水島　昇
　期間：平成23年
　研究費総額：300万円

13）特別講演、招待講演、シンポジウム

1. 水島昇　オートファジーによる細胞内分解の生理的役割と分子機構 第2回 Cell Metabolism & Communication Conference　2011.1.15　東京
2. Noboru Mizushima Hierarchical Relationships among Mammalian Atg Proteins Keystone symposium on Autophagy 2011.3.27-4.1 Whistler, Canada
3. Noboru Mizushima Physiological role of autophagy in protein and organelle turnover LSI 10th Annual Symposium "Autophagy in Health & Disease" 2011.5.5 Ann Arbor, MI USA
4. Noboru Mizushima Quality control of proteins and organelles by autophagy IPSEN foundation symposium "Protein Quality Control in Neurodegenerative Diseases" 2011.5.9 Paris, France
5. 水島昇　オートファジーの生理的役割　日本分子生物学会第11回春季シンポジウム　2011.5.25-26　金沢
6. 水島昇　マウスを用いたオートファジー長期不全による影響の評価　第11回日本抗加齢医学会総会 2011.5.28　京都
7. Noboru Mizushima Role of autophagy in protein metabolism and tumor suppression The 76th Cold Spring Harbor Symposium "Metabolism & Disease" 2011.6.1-11 New York, NY USA
8. Noboru Mizushima Autophagy：the cytoplasm-to-lysosome pathway 2011 Tokyo Meeting on Lysosomal Storage Disease Screening　2011.8.4-6 東京
9. 水島昇　オートファジーの生理的役割　動脈硬化 Update2011 2011.9.3 神戸
10. Noboru Mizushima Molecular machinery and regulation of autophagy The EMBO Meeting 2011 2011.9.10-13 Vienna, Austria
11. Noboru Mizushima Regulation of autophagy through the mTOR pathway 第84回日本生化学会大会 2011.9.21-24 京都
12. 水島昇　オートファジーによる細胞内品質管理と腫瘍抑制作用　第70回日本癌学会学術総会　2011.10.3 名古屋
13. Noboru Mizushima Autophagy prevents spontaneous tumor development in the liver 第70回日本癌学会学術総会　2011.10.3　名古屋
14. Noboru Mizushima Mammalian Atg2 protein The second Japan-Sino autophagy symposium 2011.10.5-8 Hayama
15. Noboru Mizushima Physiological roles of autophagy The 16th Japan-Korea Symposium on Diabetes

Mellitus 2011.10.21 Urayasu
16. 水島昇　オートファジーが支える哺乳類の個体発生 第1回都医学研シンポジウム　2011.10.27　東京
17. Noboru Mizushima Mammalian Atg proteins in autophagosome formation EMBO conference series: Autophagy in health and disease 2011.10.30-11.4 Israel
18. Noboru Mizushima　オートファジーの分子機構と生理機能　第40回日本免疫学会学術集会　2011.11.28 幕張
19. Noboru Mizushima Formation of autophagosome and mitophagosome Zing conference on autophagy 2011.12.7-11 Cancun, Mexico
20. Noboru Mizushima Autophagy regulation in cells and whole organisms 2012 Senri Life Science International Symposium. "CuttingCutting-edge of Autophagy Study" 2012.1.20 大阪

14）主催学会

1. Zing conference on Autophagy. 2011.12.7-11 Cancun, Mexico（Organizer）
2. 第6回オートファジー研究会　2011.1.12-14　掛川

15）新聞、雑誌、TV報道

科学新聞
「オートファジーによる腫瘍抑制効果　マウスで解明」
2011.4.29　　添付6

化学工業日報
「オートファジーが腫瘍抑制　哺乳動物で初めて証明」
2011.4.18　　添付7

16）教室、分野や講座の准教授、講師、助教、特別研究員、ポスドク、指導を受けた大学院生の名前

助　教	久万　亜紀子
助　教	田中　敦
助　教	西村　多喜
メディカルフェロー	岸千　絵子
学振特別研究員	板倉　英祐
学振特別研究員	本田　郁子
大学院生D4	渡邉（浅野）　貴子
大学院生MD-PhD4	北村　圭
大学院生D4	Velikkakath, Anoop Kumar Gopi
大学院生D3	Sahani, Mayurbhai Himatbhai
大学院生D3	森下　英晃
大学院生D3	Pham Nguyen, Quy
大学院生D3	内藤　貴子
大学院生D2	貝塚　剛志
大学院生D2	山本　篤
大学院生D1	Jiang, Peidu

The Science News 科学新聞　2011年（平成23年）10月7日（金曜日）

武田医学賞決定

2型糖尿病解明 門脇孝氏
細胞内分解研究 水島昇氏

水島昇氏

門脇孝氏

武田科学振興財団は9月27日、2011年度武田医学賞を、門脇孝博士（東京大学教授）と水島昇博士（東京医歯大学教授）に授与することを決定した。同賞は、医学発展に顕著な業績を挙げ、医学・医療に貢献された2人の学者・研究者に毎年贈られる。授賞式は11月15日に東京都内で行われ、受賞者には賞状、顕彰盾、副賞1500万円が贈られる。

門脇博士の受賞テーマは「2型糖尿病の分子機構に関する研究―アディポネクチン受容体の発現と機能解析を中心に」。門脇博士は一貫して2型糖尿病の分子機構の解明に、特にインスリンシグナルとアディポネクチンシグナルを中心に取り組んできた。インスリン受容体遺伝子異常によるインスリン抵抗性糖尿病を世界に先駆けて同定。インスリン受容体基質IRS―1欠損マウスを作製することで、IRS―1がインスリンによる血糖降下作用に必須であることを突き止めた。またIRS―1、IRS―2などのように各臓器でインスリン作用の発揮を媒介しているかなどを明らかにした。さらに、脂肪細胞から分泌されるアディポネクチンがインスリン感受性を亢進させるアディポカインであることで、世界に衝撃・内臓脂肪蓄積に伴いアディポネクチンが低下すること、がインスリン抵抗性―メタボリックシンドローム―「2型糖尿病の主要な要因であること」を発見した。またアディポネクチン受容体（AdipoR1、AdipoR2）の同定に成功し、その構造や機能を明らかにした。

水島博士の受賞テーマは「オートファジーの分子機構と生理学的意義に関する研究」。水島博士は細胞内の分解系のひとつであるオートファジーについて、酵母から研究を開始し、その欠損マウスを作製することで、哺乳類へと展開した。哺乳類のオートファジーに必須の遺伝子を多数同定、この制御機構と分解の意義による病状解析（オートファゴソーム）の形成機構のモデルを提唱。全身の オートファゴソーム出現を観察することで、臓器におけるオートファジー活性の可視化を実現した。このマウスは400以上の国内外の研究者に使われ、世界のオートファジー研究を大きく加速させた。また、オートファジー関連欠損マウスを作製することで、オートファジーの生理的・病態生理的意義を個体レベルで強く示唆した。新たにマウスは巨大タンパク質の分解で得られるアミノ酸を利用することで出生に必要な栄養を供給していることを明らかにした。

2011年（平成23年）4月29日（金曜日）　第3338号
科学新聞
週刊（金曜日発行）
発行所　科学新聞社

オートファジーによる腫瘍抑制効果 マウスで解明
―水島・東医歯大教授ら成功―

オートファジー（自食作用）は細胞内を大掃除に分解する仕組みのひとつである。東京医科歯科大学大学院医歯学総合研究科の水島昇教授の研究グループは、東京都医学総合研究所、順天堂大学、福島県立医科大学と共同で、オートファジーによる細胞内分解機構が、細胞内浄化作用を通じて腫瘍の自然発生を抑えていることをつきとめた。

細胞が健全であるために、新しい状態に保つことが重要だ。オートファジーは、細胞の構成因子であるタンパク質や細胞内小器官を作るだけでなく、それらを適切に分解処理し、常に細胞内の大掃除分解をしているが、これまで生体内でのオートファジーの長期作用は調べられてはなかった。同研究グループは、全ての臓器の一部の細胞がオートファジーが不能となる全身性モザイク状オートファジー欠損マウス（Atg5モザイクマウス）を作製し、これを用いて初めてオートファジー欠損細胞の運命を長期間にわたって追跡した。

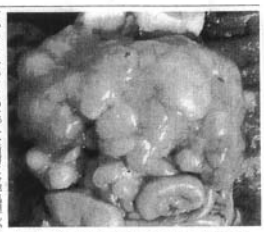
Atg5モザイク欠損マウスで発生した肝腫瘍

その結果、このマウスの全例で多発性肝腫瘍が発症した。腫瘍は肝臓特異的Atg5ノックアウトマウスでも再現された。これらの腫瘍細胞は異常に増殖したミトコンドリア（細胞内小器官のひとつ）や肝障害を起こしうるたんぱく質（P62）が蓄積した。Atg5ノックアウトP62を同時にノックアウトすると、腫瘍のみが発生しないことをつきとめた。

水島教授の話「オートファジーは常に細胞内のミトコンドリアやタンパク質をクリーンに保つことによって、細胞が腫瘍化することを抑制していることが示されました。これまで腫瘍発生はゲノム（核）の異常を中心に研究されてきましたが、これら腫瘍は肝臓特異的A異常も腫瘍形成のひとつの要因であることを実証したものです」

THE CHEMICAL DAILY
化學工業日報
2011年（平成23年）
4月18日 月曜日
第22080号（日刊、土・日・祝日除く）

医療／ライフ＆コンシューマー

オートファジーが腫瘍抑制

哺乳動物で初めて証明

東京医科歯科大など

水島東京医科歯科大教授

東京医科歯科大学大学院医歯学総合研究科の水島昇教授（細胞生理学分野）の研究グループは、細胞内のごくたん白質などを分解するオートファジーが腫瘍抑制システムとして機能することを解明した。オートファジーは、細胞内のたん白質などを分解し、細胞質成分を再利用する機構。オートファジー関連遺伝子Atg5ノックアウトマウスでは、乳動物で初めて証明された。オートファジーによる細胞質成分の1つの役割に依りうることが示され、新たな発がん機構の解明につながると期待される。

東京都臨床医学総合研究所、順天堂大学、福島県立医科大学との共同研究。

15日付の国際科学技ジャーナル「細胞代謝」に掲載された。

オートファジーには、細胞内のたん白質などを分解し、自給自足しながら、細胞内を浄化したりして神経変性疾患を抑制する働きがあることが知られている。腫瘍抑制作用も指摘されてきたが、動物を用いた証拠は得られていなかった。

水島教授らは、オートファジー関わる遺伝子Atg5がノックアウトマウスのうち、各臓器の一部の細胞だけがオートファジー不能となる「Atg5モザイク欠損」型マウスを作製、初めて長期間にわたってオートファジー不能細胞の影響を追跡することに成功した。19カ月齢まで追跡したところ、全例のマウスが9カ月齢までに肝腫瘍を発症。いずれも腫瘍ができたのは肝臓のみで、腫瘍細胞だった。また、太欠損したノックアウトマウスでは肝腫瘍を発症しない。

新たな発がん機構解明へ

来オートファジーにより分解される不良ミトコンドリアの蓄積、肥大が腫瘍発生、がんの発症に関与することも推察された。

研究ではオートファジーに腫瘍の発生を抑制する作用があり、腫瘍抑制にはオートファジーの促進が重要であることが明らかにされた。一方で、すでに発生した腫瘍に対してはオートファジーは腫瘍増殖を促進すると考えられ、海外ではマウリア抽出液のグロロキンを投与してオートファジーを抑制し、腫瘍増殖の抑制効果を検証する臨床試験が進められているという。

Downloaded from genesdev.cshlp.org on April 15, 2011 - Published by Cold Spring Harbor Laboratory Press

RESEARCH COMMUNICATION

Autophagy-deficient mice develop multiple liver tumors

Akito Takamura,[1,2,8] Masaaki Komatsu,[3,8] Taichi Hara,[1,9] Ayako Sakamoto,[3] Chieko Kishi,[1] Satoshi Waguri,[4] Yoshinobu Eishi,[5] Okio Hino,[6] Keiji Tanaka,[7] and Noboru Mizushima[1,10]

[1]Department of Physiology and Cell Biology, Tokyo Medical and Dental University, Tokyo 113-8519, Japan; [2]Department of Medicine and Rheumatology, Tokyo Medical and Dental University, Tokyo 113-8519, Japan; [3]Protein Metabolism Project, Tokyo Metropolitan Institute of Medical Science, Tokyo 156-8506, Japan; [4]Department of Anatomy and Histology, Fukushima Medical University School of Medicine, Hikarigaoka, Fukushima 960-1295, Japan; [5]Department of Human Pathology, Tokyo Medical and Dental University, Tokyo 113-8519, Japan; [6]Department of Pathology and Oncology, Juntendo University School of Medicine, Tokyo 113-8421, Japan; [7]Laboratory of Frontier Science, Tokyo Metropolitan Institute of Medical Science, Tokyo 156-8506, Japan

Autophagy is a major pathway for degradation of cytoplasmic proteins and organelles, and has been implicated in tumor suppression. Here, we report that mice with systemic mosaic deletion of Atg5 and liver-specific *Atg7*$^{-/-}$ mice develop benign liver adenomas. These tumor cells originate autophagy-deficient hepatocytes and show mitochondrial swelling, p62 accumulation, and oxidative stress and genomic damage responses. The size of the *Atg7*$^{-/-}$ liver tumors is reduced by simultaneous deletion of p62. These results suggest that autophagy is important for the suppression of spontaneous tumorigenesis through a cell-intrinsic mechanism, particularly in the liver, and that p62 accumulation contributes to tumor progression.

Supplemental material is available for this article.

Received December 23, 2010; revised version accepted March 2, 2011.

Macroautophagy (hereafter referred to as autophagy) is one of the major degradation pathways in the cell, along with the ubiquitin–proteasome system. In autophagy, intracellular components are sequestered by autophagosomes and then degraded upon fusion with lysosomes (Mizushima 2007). Genetic studies of yeast have identified >30 autophagy-related (*ATG*) genes that are essential for various types of autophagy (not only macroautophagy). Among them, *ATG* genes that are required for macroautophagy are highly conserved in higher eukaryotes (Yang and Klionsky 2010). Using reverse genetic approaches, many important roles of autophagy in mammals have been demonstrated, including adaptive response to starvation, quality control of intracellular proteins and organelles, preimplantation embryonic development, elimination of intracellular microbes, and presentation of cytoplasmic antigens (Rubinsztein 2006; Mizushima 2007; Cecconi and Levine 2008; Mizushima et al. 2008; Deretic and Levine 2009).

Evidence has suggested that autophagy is also involved in tumor suppression (Levine and Kroemer 2008; Chen and Debnath 2010; White et al. 2010). Possible tumor-suppressive mechanisms thus far proposed in cell culture and allografted tumor models include suppression of tumorigenic inflammation (Degenhardt et al. 2006), mitigation of metabolic stress and genomic damage (Karantza-Wadsworth et al. 2007; Mathew et al. 2007), and p62 (also called SQSTM1) degradation (Mathew et al. 2009). However, results from currently available in vivo models have been limited. Mice with heterozygous disruption of Beclin 1, the mammalian homolog of yeast Atg6, induce an increased frequency of spontaneous cancers, lung cancers, hepatocellular carcinomas, and lymphomas (Qu et al. 2003; Yue et al. 2003). Several Beclin 1-interacting proteins—including Ambra 1 (Fimia et al. 2007), Bif-1 (Takahashi et al. 2007), and UVRAG (Liang et al. 2006)—were also shown to have tumor-suppressive or anti-proliferation effects. However, these factors are not specific for autophagy and are considered to have multiple functions, such as involvement in the endocytic pathway (Funderburk et al. 2010; He and Levine 2010; Thoresen et al. 2010), which has many roles in tumorigenesis (Mosesson et al. 2008). Therefore, the suppressive role of autophagy in tumorigenesis in vivo should be further evaluated using a different model deficient for a factor more specific to autophagy. However, because systemic deletion of Atg3, Atg5, Atg7, Atg9, and Atg16L1 causes neonatal lethality (Kuma et al. 2004; Komatsu et al. 2005; Saitoh et al. 2008, 2009; Sou et al. 2008), the long-term effects of defects in autophagy have not been analyzed.

In this study, we analyzed a new mouse model in which the *ATG5* genes were mosaically deleted in various tissues. Our results showed that multiple benign tumors developed only in the liver, but not in other tissues. Swollen mitochondria and oxidative stress and genomic damage responses were detected in the hepatic tumor cells. Liver-specific *ATG7*-deficient mice also developed liver tumors, but their size was reduced by concomitant knockout of the *p62* gene. Our study suggests that continuous autophagy is important for suppression of tumorigenesis in the liver, and accumulation of p62 caused by autophagy deficiency contributes to tumor progression. Generation of only benign tumors, not cancers, also suggests that autophagy may be required for progression beyond the benign state.

Results and Discussion

Mosaic deletion of Atg5 causes multiple liver tumors

To overcome the lethal phenotype of *Atg5*$^{-/-}$ mice (Kuma et al. 2004), we analyzed mice with mosaic deletion of Atg5 (Hara et al. 2006). Originally, we intended to generate systemically deleted mice by crossing *Atg5*$^{flox/flox}$

[*Keywords*: autophagy; tumorigenesis; model mouse; oxidative stress]
[8]These authors contributed equally to this work.
[9]Present address: Laboratory of Molecular Traffic, Institute for Molecular and Cellular Regulation, Gunma University, Maebashi, Gunma 371-8512, Japan.
[10]Corresponding author.
E-MAIL nmizu.phy2@tmd.ac.jp; FAX 81-3-5803-0118.
Article is online at http://www.genesdev.org/cgi/doi/10.1101/gad.2016211.

Downloaded from genesdev.cshlp.org on April 15, 2011 - Published by Cold Spring Harbor Laboratory Press

mice with CAG-*Cre* transgenic mice in which Cre recombinase is ubiquitously expressed. However, the resultant *Atg5*$^{flox/flox}$;CAG-*Cre* mice showed only partial deletion of the *Atg5* gene in the liver, heart, skeletal muscle, and brain (Hara et al. 2006). This incomplete deletion was observed in all tissues as far as we examined; PCR analyses of genomic DNA extracted from various organs showed both recombinant (deleted) and flox (undeleted) alleles (Fig. 1A). In addition, real-time quantitative PCR analysis showed that, in most cases, ~60%–90% of cells in various organs of *Atg5*$^{flox/flox}$;CAG-*Cre* mice possessed the undeleted *Atg5* flox allele (Fig. 1B). Although the exact cause of the incomplete deletion is unknown, mosaic deletion occurred reproducibly. *Atg5*$^{flox/flox}$;CAG-*Cre* mice were viable and could survive >19 mo. With this mouse model, we were able to follow the fate of autophagy-deficient cells systemically and in a nonbiased manner for a long period.

Gross anatomy revealed severe hepatomegaly in *Atg5*$^{flox/flox}$;CAG-*Cre* mice within 6 mo after birth. By 6–9 mo, multiple small tumors were detected in the liver (Fig. 1C). These tumors increased in both size and number, and the liver was finally occupied by multiple tumors at 19 mo of age. Tumors were detected in all *Atg5*$^{flox/flox}$;CAG-*Cre* mice after 9 mo (n = 17), but not in *Atg5*$^{flox/+}$;CAG-*Cre* mice (n = 14) and *Atg5*$^{flox/flox}$ mice (n = 4). Tumor formation was so far observed only in the liver; there was no evidence of tumors or any other macroscopic abnormalities in other organs (Supplemental Fig. 1).

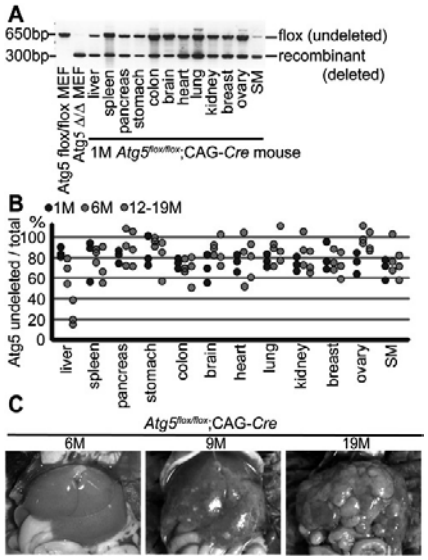

Figure 1. Mosaic deletion of Atg5 causes multiple liver tumors. (*A*) Genotyping of *Atg5*$^{flox/flox}$;CAG-*Cre* mouse organs by PCR at 1 mo. Positions of the Atg5 flox (undeleted) and recombinant (deleted) alleles are indicated. *Atg5*$^{\Delta/\Delta}$ mouse embryonic fibroblasts (MEFs) indicates *Atg5*$^{flox/flox}$ MEFs infected with the adenovirus vector coding Cre recombinase. (SM) Skeletal muscle. (*B*) Real-time quantitative PCR with the *Atg5* flox allele-specific primers. Genomic DNA is extracted from various tissues of *Atg5*$^{flox/flox}$;CAG-*Cre* mice and *Atg5*$^{flox/flox}$ mice at 1 mo (blue circles), 6 mo (red circles), and 12–19 mo (green circles) (n = 3). The relative DNA quantity of the Atg5 flox allele is normalized to that of Atg14. Ratio (percentage) of flox allele in Atg5$^{flox/flox}$;CAG-*Cre* organs to that in Atg5$^{flox/flox}$ organs is shown. (*C*) Representative gross anatomy of *Atg5*$^{flox/flox}$;CAG-*Cre* mice analyzed at 6 mo (n = 3), 9 mo (n = 6), and 18–19 mo (n = 9).

Histological findings of Atg5$^{flox/flox}$*;CAG-Cre mice*

Hematoxylin and eosin staining and silver impregnation staining revealed the focal expansive growth of abnormal cells in the *Atg5*$^{flox/flox}$;CAG-*Cre* mouse liver (Fig. 2A, Supplemental Fig. 2A). At high magnification, hepatocellular enlargement was observed in the *Atg5*$^{flox/flox}$;CAG-*Cre* liver at 6 mo (Supplemental Fig. 2B). Only slight lymphocytic infiltration and intracellular vacuolation were observed at 9 mo. These findings became clearer and were observed almost throughout the liver at 12–19 mo. At 19 mo, many foamy hepatocytes and a small number of necrotic cells were observed (Fig. 2B). However, no typical signs of malignancy—such as abnormal nuclear morphology, pleomorphism, and local invasion—were detected even at 19 mo. Thus, the histological diagnosis of the tumor was benign tumor (adenoma), not malignant cancer. Oil-red O staining revealed that the cytoplasmic vacuoles were lipid droplets (Supplemental Fig. 2C). There was no histological abnormality in the *Atg5*$^{flox/+}$;CAG-*Cre* liver (Fig. 2B). Abnormally swollen mitochondria were observed by electron microscopy in the cytoplasm of most of the *Atg5*$^{flox/flox}$;CAG-*Cre* hepatocytes at 19 mo (Fig. 2C). On the other hand, no morphologic abnormalities were observed by light microscopy in tissues other than the liver in *Atg5*$^{flox/flox}$;CAG-*Cre* mice (Supplemental Fig. 1).

Liver tumors originate from autophagy-deficient hepatocytes

Next, we examined the origin of these liver tumors in the mosaically deleted mice. Although a defect in autophagy could cause tumors by an intrinsic mechanism, it is also possible that tumors developed as a secondary result of inflammation, as suggested previously (Degenhardt et al. 2006). If the latter is the case, tumors could develop from Atg5-undeleted cells. To this end, we analyzed genotypes of cells obtained by laser capture microdissection of liver section samples. PCR analysis revealed that the tumor areas mostly contained the recombinant (deleted) allele, whereas the nontumor areas contained both flox (undeleted) and recombinant alleles (Fig. 3A). Small amounts of the flox allele were occasionally detected in the tumor areas, which may be derived from infiltrating lymphocytes. These data suggest that the liver tumors in *Atg5*$^{flox/flox}$;CAG-*Cre* mice originate from Atg5-deficient hepatocytes.

To confirm that the tumor cells are indeed autophagy-defective, we analyzed the formation of ubiquitin-positive aggregates because accumulation of ubiquitinated proteins/aggregates is one of the hallmarks of autophagy deficiency (Komatsu et al. 2005, 2006; Hara et al. 2006). In the tumor areas of the *Atg5*$^{flox/flox}$;CAG-*Cre* mouse liver, a significantly higher proportion of hepatocytes (85.4% ± 2.0%) showed ubiquitin aggregates than that in nontumor areas (24.6% ± 4.1%) (Fig. 3B). We also analyzed p62, which is a selective substrate of autophagy (Bjørkøy et al. 2005), and found a higher accumulation rate of p62-positive dots in the tumor areas (80.8% ± 1.8%) than in the nontumor areas (22.5% ± 2.3%) (Fig. 3B). These data

Downloaded from genesdev.cshlp.org on April 15, 2011 - Published by Cold Spring Harbor Laboratory Press

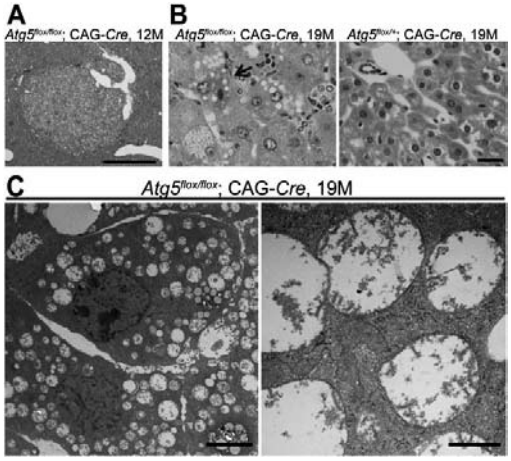

Figure 2. Histological findings of the liver in *Atg5*$^{flox/flox}$;CAG-*Cre* mice. (*A*) Hematoxylin and eosin (H&E) staining of *Atg5*$^{flox/flox}$;CAG-*Cre* (n = 2). Bar, 500 μm. (*B*) High-power-field images of H&E staining of the livers from *Atg5*$^{flox/flox}$;CAG-*Cre* mice (n = 4) and an *Atg5*$^{flox/+}$;CAG-*Cre* mouse (n = 4) at 19 mo. The arrow shows a necrotic hepatocyte observed in a *Atg5*$^{flox/flox}$;CAG-*Cre* mouse liver at 19 mo. Bar, 20 μm. (*C*) Electron micrographs of *Atg5*$^{flox/flox}$;CAG-*Cre* mouse hepatocytes (n = 2). (*Right*) Magnified image shows swollen mitochondria. Bars: *left*, 4 μm; *right*, 500 nm.

support the idea that the origin of these liver tumors is *ATG5*-deleted cells.

Time-course analysis revealed that liver DNA contents of the flox (undeleted) allele decreased and that of the recombinant (deleted) allele increased with age (Fig. 1B, Supplemental Fig. 3A). In addition, many hepatocytes in the tumor areas of the *Atg5*$^{flox/flox}$;CAG-*Cre* liver at 19 mo were positive for the cell proliferation marker Ki-67 (49.6% ± 1.3% in the tumor area vs. 2.7% ± 0.5% in the nontumor area, $P < 0.01$), and this was mostly negative in the *Atg5*$^{flox/+}$;CAG-*Cre* liver (Fig. 4A; Supplemental Fig. 3B). These data suggest that Atg5-deficient hepatocytes have a growth advantage over normal hepatocytes under long-term experimental conditions in vivo.

In other organs of 19-mo-old *Atg5*$^{flox/flox}$;CAG-*Cre* mice, a small population of cells showed high levels of diffuse and aggregated ubiquitin and p62 signals, which were not observed in *Atg5*$^{flox/+}$;CAG-*Cre* mice (Supplemental Fig. 4A,B). The data suggest that these organs indeed possess Atg5-deficient cells, even though they do not develop spontaneous tumors, at least by 19 mo.

Induction of the oxidative stress and DNA damage responses in the Atg5$^{flox/flox}$*;CAG-Cre mouse liver*

The presence of abnormally enlarged mitochondria in *Atg5*$^{flox/flox}$;CAG-*Cre* hepatocytes suggests that these cells might be affected by reactive oxygen species (ROS), which have been implicated in tumorigenesis. We performed immunostaining of 8-hydroxydeoxyguanosine (8-OHdG), which is considered to be an indicator of the oxidative stress (Cadet et al. 2003). In *Atg5*$^{flox/flox}$;CAG-*Cre* mice, most of the hepatocytes, especially in the tumor areas, were 8-OHdG-positive (41.8% ± 2.0% in the tumor area vs. 0.9% ± 0.1% in the nontumor area, $P < 0.01$), whereas those in *Atg5*$^{flox/+}$;CAG-*Cre* mice were mostly negative (Fig. 4B; Supplemental Fig. 3C). An increase in 8-OHdG staining was observed as early as 6 mo (Supplemental Fig. 3C). In addition, an increase in the levels of the detoxifying enzyme glutathione-S-transferase (GST), which is a typical oxidative stress-inducible protein, was observed in liver tumor areas, as reported previously (Supplemental Fig. 5; Matsumoto et al. 2008; Mathew et al. 2009). Moreover, part of the hepatocytes in the same liver expressed phospho-histone H2A.X in the nuclei (2.1% ± 0.4% in *Atg5*$^{flox/flox}$;CAG-*Cre* vs. 0.4% ± 0.1% in *Atg5*$^{flox/+}$;CAG-*Cre* hepatocytes, $P < 0.05$) (Fig. 4C). Because phosphorylation of the histone variant H2A.X is a rapid response to DNA damage, this result suggests that DNA damage response is promoted in *Atg5*$^{flox/flox}$;CAG-*Cre* hepatocytes. In contrast, 8-OHdG-positive and phospho-histone H2A.X-positive cells were mostly negative in other organs (Supplemental Fig. 6). These data are consistent with the recent in vitro and in vivo studies (Karantza-Wadsworth et al. 2007; Mathew et al. 2007).

Tumor progression in liver-specific ATG7-deficient mice was partially suppressed by p62 deletion

To test whether the tumor-suppressive function is specific to Atg5, we analyzed liver-specific *ATG7*-deficient mice (*Atg7*$^{flox/flox}$;Alb-*Cre*) (Komatsu et al. 2007). Although

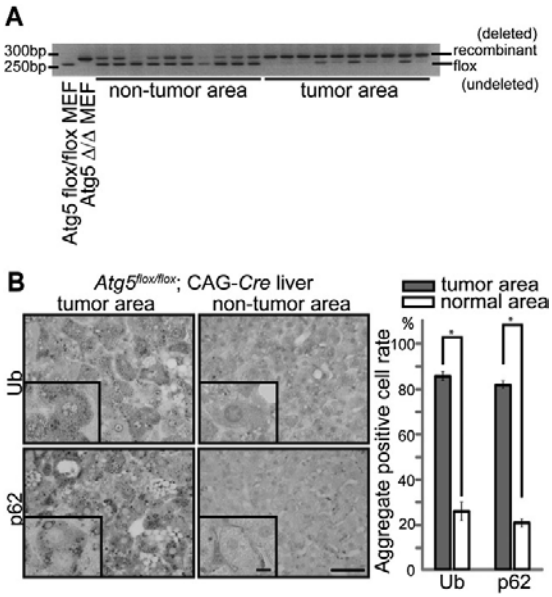

Figure 3. Liver tumors are derived from Atg5-deleted hepatocytes. (*A*) Genotyping of liver samples microdissected from the tumor and nontumor areas of 9-mo-old *Atg5*$^{flox/flox}$;CAG-*Cre* mice. Positions of the Atg5 flox (undeleted) and recombinant (deleted) alleles are indicated. *Atg5*$^{\Delta/\Delta}$ MEFs indicate *Atg5*$^{flox/flox}$ MEFs infected with the adenovirus vector coding Cre recombinase. (*B*) Immunohistochemical staining for ubiquitin and p62 of the tumor and nontumor areas of *Atg5*$^{flox/flox}$;CAG-*Cre* mouse livers. The graph shows the percentage of cells with ubiquitin- or p62-positive aggregates in the tumor (gray) and nontumor (white) areas. One-hundred hepatocytes in 10 tumor and nontumor areas (total 1000 cells for each) were analyzed at 9 mo. Data are mean ± SE values from four mice. (*) $P < 0.01$. Bars: 40 μm; *insets*, 10 μm.

Downloaded from genesdev.cshlp.org on April 15, 2011 - Published by Cold Spring Harbor Laboratory Press

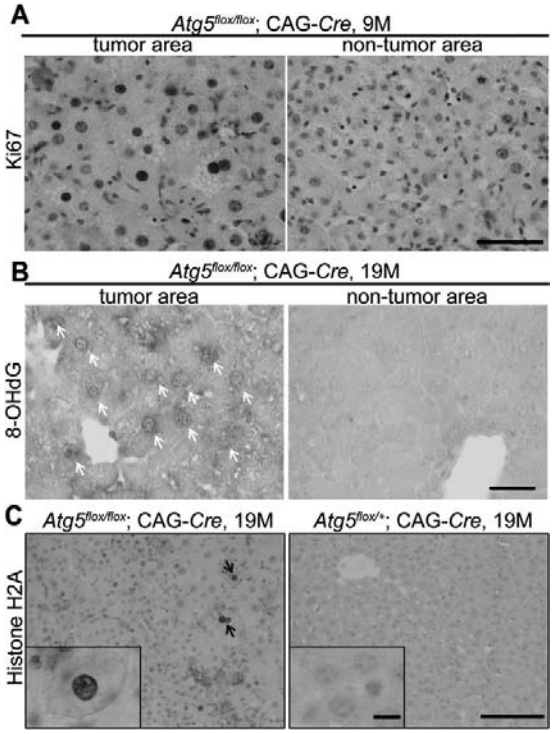

Figure 4. Induction of the oxidative stress and DNA damage responses in *Atg5*$^{flox/flox}$;CAG-*Cre* mouse livers. (*A*) Immunohistochemical analysis of the tumor and nontumor areas in *Atg5*$^{flox/flox}$;CAG-*Cre* mouse livers at 19 mo for Ki-67 expression. $n = 3$. Bar, 50 μm. (*B*) 8-OHdG staining of the tumor and nontumor areas in the liver of *Atg5*$^{flox/flox}$;CAG-*Cre* mice at 19 mo. White arrows indicate anti-8-OHdG antibody-positive nuclei ($n = 3$). Bar, 40 μm. (*C*) Phospho-histone H2A.X staining in the liver of *Atg5*$^{flox/flox}$;CAG-*Cre* ($n = 3$) and *Atg5*$^{flox/+}$;CAG-*Cre* ($n = 3$) mice at 19 mo. Black arrows indicate phospho-histone H2A.X-positive nuclei. Bars: 100 μm; *insets*, 10 μm.

sporadically some of these mice died due to liver dysfunction 3 mo after *ATG7* gene deletion (M. Komatsu, unpubl.), others survived for >1 yr and developed liver tumors, as observed in *Atg5*$^{flox/flox}$;CAG-*Cre* mice (Fig. 5A,B). Thus, tumor formation is the shared phenotype between Atg5 and Atg7 deficiency, and is not specific to Atg5 deletion.

Next, using this mouse model, we determined the relationship between tumor formation and p62 accumulation, as suggested previously (Mathew et al. 2009). The hepatic damage caused by Atg7 deficiency was ameliorated by simultaneous deletion of p62 (*Atg7*$^{flox/flox}$;Alb-*Cre, p62*$^{-/-}$) (Komatsu et al. 2007). In these double-knockout mice, tumors were still generated, but their size was much reduced (Fig. 5A,B). It has been shown that p62 accumulation traps and inactivates Keap1, a key regulator of the oxidative stress response, leading to activation of the transcription factor Nrf2 (Komatsu et al. 2010; Lau et al. 2010). Indeed, accumulation of Keap1 in a detergent-insoluble fraction and up-regulation of NAD(P)H dehydrogenase quinone 1 (Nqo1), an Nrf2-responsive factor were observed both in the tumor and nontumor areas in *Atg7*$^{flox/flox}$;Alb-*Cre* mice (Supplemental Fig. 7). Keap1 sequestration and Nqo1 induction were restored in *Atg7*$^{flox/flox}$;Alb-*Cre, p62*$^{-/-}$ mice (Supplemental Fig. 7). These data suggest that p62 accumulation due to autophagy suppression contributes to tumor formation, probably at the progression step.

In the present study, we determined the long-term effect of defects in autophagy in vivo for the first time and found that systemic mosaic deficiency of Atg5 leads to cell-type specific tumorigenesis; that is, benign tumor development only or at least preferentially in the liver. There were no apparent histological and physiological abnormalities in other organs except the accumulation of p62 and ubiquitinated proteins. Although neurodegeneration was observed in neural cell-specific Atg5- and Atg7-deficient mice (Hara et al. 2006; Komatsu et al. 2006), mosaically Atg5-deleted mice do not develop any neurological abnormality, which may be compensated by Atg5-undeleted neuronal cells. Liver tumors were observed also in liver-specific Atg7-deficient mice in the present study.

The pattern of tumor formation is different from that of Beclin 1-heterozygous mutant mice, in which malignant cancers develop in multiple organs, including the liver, lung, and lymphoid tissues (Qu et al. 2003; Yue et al. 2003). Beclin 1 is included in at least two different class III PI3-kinase complexes: the Beclin 1–Atg14–Vps34–Vps15 complex that is specifically required for autophagy, and the Beclin 1–UVRAG–Vps34–Vps15 complex that is involved in the endocytic pathway (Funderburk et al. 2010; He and Levine 2010; Thoresen et al. 2010). It is possible that the liver tumors that develop in Beclin 1 heterozygous mutant mice are caused by autophagy deficiency, but other tumors might be caused by loss of Beclin 1 functions other than in autophagy.

Regarding the underlying mechanism of tumor suppression by autophagy, several hypotheses have been proposed. Our observation that the hepatic tumors originated from Atg5-deficient cells even though intact cells (with undeleted *Atg5*^{flox} allele) remained supports the

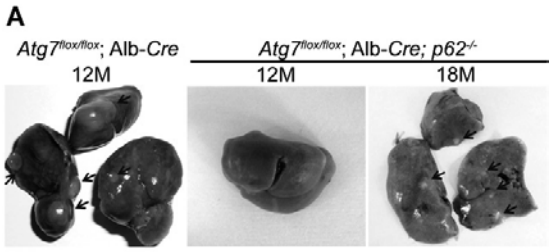

B

	tumorigenic mice / total	
	12M	18M
Atg7$^{flox/flox}$; Alb-*Cre*	10/11	1/1
Atg7$^{flox/flox}$; Alb-*Cre; p62*$^{-/-}$	*1/4	*3/3

*small tumors (<5mm)

Figure 5. Suppression of tumor progression in liver-specific *ATG7*-deficient mice by p62 deletion. (*A*) Representative gross anatomy of *Atg7*$^{flox/flox}$;Alb-*Cre* mice analyzed at 12 mo ($n = 11$) and *Atg7*$^{flox/flox}$;Alb-*Cre; p62*$^{-/-}$ mice analyzed at 12 mo ($n = 4$) and 18 mo ($n = 3$). Tumors are indicated by arrows. (*B*) Summary of tumor formation in *Atg7*$^{flox/flox}$;Alb-*Cre* and *Atg7*$^{flox/flox}$;Alb-*Cre; p62*$^{-/-}$ mice. (*) Small tumors (<5 mm).

Downloaded from genesdev.cshlp.org on April 15, 2011 - Published by Cold Spring Harbor Laboratory Press

hypothesis of an intrinsic mechanism rather than secondary tumorigenesis as a result of chronic inflammation. An interesting hypothesis is that p62 accumulation could cause tumorigenesis through enhancing oxidative stress and genomic instability (Mathew et al. 2009). Indeed, we observed a reduction in tumor size in *Atg7*$^{flox/flox}$;Alb-*Cre, p62*$^{-/-}$ mice. However, small tumors were still detected in the *Atg7*$^{flox/flox}$;Alb-*Cre, p62*$^{-/-}$ mouse liver, suggesting that p62 accumulation is important for the tumor progression step, rather than the initiation step. Activation of the Nrf2 pathway caused by p62 accumulation (Supplemental Fig. 7) can be important for progression of tumors and is consistent with reports that somatic mutations in either Keap1 or Nrf2 that cause constitutive Nrf2 activation have been found in human cancers (Padmanabhan et al. 2006; Shibata et al. 2008). Another possible mechanism is that p62 accumulation deregulates the canonical NF-κB pathway, which leads to activation of the noncanonical NF-κB pathway and tumorigenesis in the liver (Mathew et al. 2009). Further analysis of these downstream events may also answer the question of why tumors are generated only in the liver even though p62 accumulated in small populations of cells. Alternatively, lack of tumors in other organs may simply be because autophagy deficiency caused cell death or growth retardation.

Although we showed that autophagy is indeed a tumor suppressor, other studies have also suggested that autophagy could support tumor progression and survival (Levine and Kroemer 2008; Chen and Debnath 2010; White et al. 2010). These hypotheses are not mutually exclusive; generation of only benign tumors in our models suggests that autophagy may be important for progression beyond the benign state. This possibility needs to be further examined.

Materials and methods

Mice

Atg5$^{flox/flox}$ mice (Hara et al. 2006), CAG-*Cre* transgenic mice expressing Cre recombinase under the control of the CAG (CMV enhancer and chicken β-actin promoter) (Sakai and Miyazaki 1997), *Atg7*$^{flox/flox}$ mice (Komatsu et al. 2005), *p62*$^{-/-}$ mice (Okada et al. 2009), and *Atg7*$^{flox/flox}$;Alb-*Cre, p62*$^{-/-}$ mice (Komatsu et al. 2007) were described previously. Wild-type C57BL/6 mice were obtained from Japan SLC, Inc. All animal experiments were approved by the Institutional Animal Care and Use Committee of Tokyo Medical and Dental University and the Ethics Review Committee for Animal Experimentation of the Tokyo Metropolitan Institute of Medical Science.

Antibodies

A monoclonal antibody against ubiquitin (1B3) was purchased from Medical and Biological Laboratories (MBL) and used for immunohistochemistry. The following antibodies were also used: anti-p62 polyclonal antibody (PROGEN), anti-Ki67 monoclonal antibody (Thermo), anti-8-OHdG antibody (Japan Institute for the Control of Aging), phosphohistone H2A.X (Ser139) rabbit monoclonal antibody (Cell Signaling Technology), and anti-GST (B-14) monoclonal antibody (Santa Cruz Biotechnology). Anti-Atg7 (Komatsu et al. 2005), anti-Keap1 (Proteintech Group, Inc.), anti-Nqo1 (Abcam, Inc.), and anti-actin (MAB1501R, Chemicon International, Inc.) antibodies were used for immunoblotting.

Immunohistochemistry, electron microscopy, and laser capture microdissection

Detailed information of experimental procedures is provided in the Supplemental Material.

Statistics

Results are expressed as means ± SEM, and significance was determined by unpaired Student's *t*-test.

PCR

Tissue-genotyping PCR was performed with the following primers: check2 (5′-ACAACGTCGAGCACAGCTGCGCAAGG-3′) and short2 (5′-GTACTGCATAATGGTTTAACTCTTGC-3′) for the *Atg5* flox allele, and 5Long2 (5′-CAGGGAATGGTGTCTCCCAC-3′) and short2 for the recombinant allele. PCR analysis with laser capture microdissection samples were performed with the following primers: NR1 (5′-CCTCTT GCAAAACCACACTGCTCGACATTG-3′) and short2 for the Atg5 flox allele, and 5Long2 and short2 for the recombinant allele. For real-time PCR analysis, genomic DNA was extracted from paraffin-embedded tissues with a DEX-PAT system (TAKARA) or from nonembedded tissues with proteinase K treatment. Real-time PCR analysis was performed with the SYBR PrimeScript RT–PCR system (TAKARA) and specific primers as follows: NR1 and short2 for the *Atg5* flox allele, RecF (5′-GCCGCACG TCTAAGAAACC-3′) and short2 for the *Atg5* recombinant allele, and mAtg14 ex5 F′ (5′-GAAGCTTTACAGCCGAGCAC-3′) and mAtg14 ex3 R′ (5′-TCACTTCGTCGATTGGGAAT-3′) for *Atg14*.

Acknowledgments

We thank N. Miyasaka for his mentorship and encouragement. We also thank P.N. Quy, K. Uchida, A. Furukawa, and Y. Suzuki for technical assistance; J. Miyazaki for the kind donation of CAG-*Cre* transgenic mice; and T. Ishii for p62 knockout mice. This work was supported by Grants-in-Aid for Scientific Research on Priority Areas (to M.K. and N.M.), Grants-in-Aid for Young Scientist (S) (to M. K.), and Specially Promoted Research (to K. T.) from the Ministry of Education, Culture, Sports, Science, and Technology, Japan; Funding Program for Next Generation World-Leading Researchers (to M.K. and N.M.); Takeda Science Foundation; and Research Award Grant of Japanese Society of Anti-Aging Medicine (to N.M.).

References

Bjørkøy G, Lamark T, Brech A, Outzen H, Perander M, Øvervatn A, Stenmark H, Johansen T. 2005. p62/SQSTM1 forms protein aggregates degraded by autophagy and has a protective effect on huntingtin-induced cell death. *J Cell Biol* **171:** 603–614.

Cadet J, Douki T, Gasparutto D, Ravanat JL. 2003. Oxidative damage to DNA: formation, measurement and biochemical features. *Mutat Res* **531:** 5–23.

Cecconi F, Levine B. 2008. The role of autophagy in mammalian development: cell makeover rather than cell death. *Dev Cell* **15:** 344–357.

Chen N, Debnath J. 2010. Autophagy and tumorigenesis. *FEBS Lett* **584:** 1427–1435.

Degenhardt K, Mathew R, Beaudoin B, Bray K, Anderson D, Chen G, Mukherjee C, Shi Y, Gelinas C, Fan Y, et al. 2006. Autophagy promotes tumor cell survival and restricts necrosis, inflammation, and tumorigenesis. *Cancer Cell* **10:** 51–64.

Deretic V, Levine B. 2009. Autophagy, immunity, and microbial adaptations. *Cell Host Microbe* **5:** 527–549.

Fimia GM, Stoykova A, Romagnoli A, Giunta L, Di Bartolomeo S, Nardacci R, Corazzari M, Fuoco C, Ucar A, Schwartz P, et al. 2007. Ambra1 regulates autophagy and development of the nervous system. *Nature* **447:** 1121–1125.

Funderburk SF, Wang QJ, Yue Z. 2010. The Beclin 1–VPS34 complex—at the crossroads of autophagy and beyond. *Trends Cell Biol* **20:** 355–362.

Hara T, Nakamura K, Matsui M, Yamamoto A, Nakahara Y, Suzuki-Migishima R, Yokoyama M, Mishima K, Saito I, Okano H, et al. 2006. Suppression of basal autophagy in neural cells causes neurodegenerative disease in mice. *Nature* **441:** 885–889.

He C, Levine B. 2010. The Beclin 1 interactome. *Curr Opin Cell Biol* **22:** 140–149.

Karantza-Wadsworth V, Patel S, Kravchuk O, Chen G, Mathew R, Jin S, White E. 2007. Autophagy mitigates metabolic stress and genome damage in mammary tumorigenesis. *Genes Dev* **21:** 1621–1635.

Downloaded from genesdev.cshlp.org on April 15, 2011 - Published by Cold Spring Harbor Laboratory Press

Komatsu M, Waguri S, Ueno T, Iwata J, Murata S, Tanida I, Ezaki J, Mizushima N, Ohsumi Y, Uchiyama Y, et al. 2005. Impairment of starvation-induced and constitutive autophagy in Atg7-deficient mice. *J Cell Biol* **169:** 425–434.

Komatsu M, Waguri S, Chiba T, Murata S, Iwata JI, Tanida I, Ueno T, Koike M, Uchiyama Y, Kominami E, et al. 2006. Loss of autophagy in the central nervous system causes neurodegeneration in mice. *Nature* **441:** 880–884.

Komatsu M, Waguri S, Koike M, Sou YS, Ueno T, Hara T, Mizushima N, Iwata JI, Ezaki J, Murata S, et al. 2007. Homeostatic levels of p62 control cytoplasmic inclusion body formation in autophagy-deficient mice. *Cell* **131:** 1149–1163.

Komatsu M, Kurokawa H, Waguri S, Taguchi K, Kobayashi A, Ichimura Y, Sou YS, Ueno I, Sakamoto A, Tong KI, et al. 2010. The selective autophagy substrate p62 activates the stress responsive transcription factor Nrf2 through inactivation of Keap1. *Nat Cell Biol* **12:** 213–223.

Kuma A, Hatano M, Matsui M, Yamamoto A, Nakaya H, Yoshimori T, Ohsumi Y, Tokuhisa T, Mizushima N. 2004. The role of autophagy during the early neonatal starvation period. *Nature* **432:** 1032–1036.

Lau A, Wang XJ, Zhao F, Villeneuve NF, Wu T, Jiang T, Sun Z, White E, Zhang DD. 2010. A non-canonical mechanism of Nrf2 activation by autophagy deficiency: a direct interaction between Keap1 and p62. *Mol Cell Biol* **30:** 3275–3285.

Levine B, Kroemer G. 2008. Autophagy in the pathogenesis of disease. *Cell* **132:** 27–42.

Liang C, Feng P, Ku B, Dotan I, Canaani D, Oh BH, Jung JU. 2006. Autophagic and tumour suppressor activity of a novel Beclin1-binding protein UVRAG. *Nat Cell Biol* **8:** 688–699.

Mathew R, Kongara S, Beaudoin B, Karp CM, Bray K, Degenhardt K, Chen G, Jin S, White E. 2007. Autophagy suppresses tumor progression by limiting chromosomal instability. *Genes Dev* **21:** 1367–1381.

Mathew R, Karp CM, Beaudoin B, Vuong N, Chen G, Chen HY, Bray K, Reddy A, Bhanot G, Gelinas C, et al. 2009. Autophagy suppresses tumorigenesis through elimination of p62. *Cell* **137:** 1062–1075.

Matsumoto N, Ezaki J, Komatsu M, Takahashi K, Mineki R, Taka H, Kikkawa M, Fujimura T, Takeda-Ezaki M, Ueno T, et al. 2008. Comprehensive proteomics analysis of autophagy-deficient mouse liver. *Biochem Biophys Res Commun* **368:** 643–649.

Mizushima N. 2007. Autophagy: process and function. *Genes Dev* **21:** 2861–2873.

Mizushima N, Levine B, Cuervo AM, Klionsky DJ. 2008. Autophagy fights disease through cellular self-digestion. *Nature* **451:** 1069–1075.

Mosesson Y, Mills GB, Yarden Y. 2008. Derailed endocytosis: an emerging feature of cancer. *Nat Rev Cancer* **8:** 835–850.

Okada K, Yanagawa T, Warabi E, Yamastu K, Uwayama J, Takeda K, Utsunomiya H, Yoshida H, Shoda J, Ishii T. 2009. The α-glucosidase inhibitor acarbose prevents obesity and simple steatosis in sequestosome 1/A170/p62 deficient mice. *Hepatol Res* **39:** 490–500.

Padmanabhan B, Tong KI, Ohta T, Nakamura Y, Scharlock M, Ohtsuji M, Kang MI, Kobayashi A, Yokoyama S, Yamamoto M. 2006. Structural basis for defects of Keap1 activity provoked by its point mutations in lung cancer. *Mol Cell* **21:** 689–700.

Qu X, Yu J, Bhagat G, Furuya N, Hibshoosh H, Troxel A, Rosen J, Eskelinen E-L, Mizushima N, Ohsumi Y, et al. 2003. Promotion of tumorigenesis by heterozygous disruption of the *beclin 1* autophagy gene. *J Clin Invest* **112:** 1809–1820.

Rubinsztein DC. 2006. The roles of intracellular protein-degradation pathways in neurodegeneration. *Nature* **443:** 780–786.

Saitoh T, Fujita N, Jang MH, Uematsu S, Yang BG, Satoh T, Omori H, Noda T, Yamamoto N, Komatsu M, et al. 2008. Loss of the autophagy protein Atg16L1 enhances endotoxin-induced IL-1β production. *Nature* **456:** 264–268.

Saitoh T, Fujita N, Hayashi T, Takahara K, Satoh T, Lee H, Matsunaga K, Kageyama S, Omori H, Noda T, et al. 2009. Atg9a controls dsDNA-driven dynamic translocation of STING and the innate immune response. *Proc Natl Acad Sci* **106:** 20842–20846.

Sakai K, Miyazaki J. 1997. A transgenic mouse line that retains Cre recombinase activity in mature oocytes irrespective of the cre transgene transmission. *Biochem Biophys Res Commun* **237:** 318–324.

Shibata T, Ohta T, Tong KI, Kokubu A, Odogawa R, Tsuta K, Asamura H, Yamamoto M, Hirohashi S. 2008. Cancer related mutations in NRF2 impair its recognition by Keap1-Cul3 E3 ligase and promote malignancy. *Proc Natl Acad Sci* **105:** 13568–13573.

Sou YS, Waguri S, Iwata J, Ueno T, Fujimura T, Hara T, Sawada N, Yamada A, Mizushima N, Uchiyama Y, et al. 2008. The Atg8 conjugation system is indispensable for proper development of autophagic isolation membranes in mice. *Mol Biol Cell* **19:** 4762–4775.

Takahashi Y, Coppola D, Matsushita N, Cualing HD, Sun M, Sato Y, Liang C, Jung JU, Cheng JQ, Mul JJ, et al. 2007. Bif-1 interacts with Beclin 1 through UVRAG and regulates autophagy and tumorigenesis. *Nat Cell Biol* **9:** 1142–1151.

Thoresen SB, Pedersen NM, Liestol K, Stenmark H. 2010. A phosphatidylinositol 3-kinase class III sub-complex containing VPS15, VPS34, Beclin 1, UVRAG and BIF-1 regulates cytokinesis and degradative endocytic traffic. *Exp Cell Res* **316:** 3368–3378.

White E, Karp C, Strohecker AM, Guo Y, Mathew R. 2010. Role of autophagy in suppression of inflammation and cancer. *Curr Opin Cell Biol* **22:** 212–217.

Yang Z, Klionsky DJ. 2010. Mammalian autophagy: core molecular machinery and signaling regulation. *Curr Opin Cell Biol* **22:** 124–131.

Yue Z, Jin S, Yang C, Levine AJ, Heintz N. 2003. Beclin 1, an autophagy gene essential for early embryonic development, is a haploinsufficient tumor suppressor. *Proc Natl Acad Sci* **100:** 15077–15082.

Published January 10, 2011

JCB: Report

p62 targeting to the autophagosome formation site requires self-oligomerization but not LC3 binding

Eisuke Itakura and Noboru Mizushima

Department of Physiology and Cell Biology, Tokyo Medical and Dental University, Bunkyo-ku, Tokyo 113-8519, Japan

Autophagy is an intracellular degradation process by which cytoplasmic contents are degraded in the lysosome. In addition to nonselective engulfment of cytoplasmic materials, the autophagosomal membrane can selectively recognize specific proteins and organelles. It is generally believed that the major selective substrate (or cargo receptor) p62 is recruited to the autophagosomal membrane through interaction with LC3. In this study, we analyzed loading of p62 and its related protein NBR1 and found that they localize to the endoplasmic reticulum (ER)–associated autophagosome formation site independently of LC3 localization to membranes. p62 colocalizes with upstream autophagy factors such as ULK1 and VMP1 even when autophagosome formation is blocked by wortmannin or FIP200 knockout. Self-oligomerization of p62 is essential for its localization to the autophagosome formation site. These results suggest that p62 localizes to the autophagosome formation site on the ER, where autophagosomes are nucleated. This process is similar to the yeast cytoplasm to vacuole targeting pathway.

THE JOURNAL OF CELL BIOLOGY

Downloaded from jcb.rupress.org on January 10, 2011

Introduction

Macroautophagy (which we will simply refer to as autophagy) is an intracellular degradation system mediated by the autophagosome. A small portion of the cytoplasm is engulfed by an isolation membrane/phagophore, which results in the formation of an autophagosome. The outer membrane of autophagosome then fuses with the lysosome membrane, and materials inside the autophagosome are degraded by the lysosomal hydrolases together with the inner autophagosome membrane. Autophagy is involved in various physiological processes such as maintenance of the amino acid pool during starvation and preimplantation embryo development, intracellular quality control, antigen presentation, and killing of intracellular microorganisms (Rubinsztein, 2006; Mizushima, 2007; Cecconi and Levine, 2008; Mizushima et al., 2008; Deretic, 2009; Virgin and Levine, 2009). To date, >30 autophagy-related (*ATG*) genes have been identified in yeast, many of which are conserved in higher eukaryotes (Suzuki and Ohsumi, 2007; Xie and Klionsky, 2007; Longatti and Tooze, 2009).

Although autophagy has been considered to be a nonselective, bulk process (Kominami et al., 1983; Kopitz et al., 1990), recent studies have revealed that the autophagosome membrane can selectively recognize certain specific proteins and organelles (Yu et al., 2008; Kirkin et al., 2009b; Kraft et al., 2010). The prototype for selective autophagy is the yeast cytoplasm to vacuole targeting (Cvt) pathway (Wang and Klionsky, 2003; Lynch-Day and Klionsky, 2010). Two vacuolar enzymes, aminopeptidase 1 (Ape1) and α-mannnosidase (Ams1), lack typical signal sequences and are synthesized as precursor enzymes in the cytosol. prApe1 dodecamers form an Ape1 complex, which are assembled into a Cvt complex with Ams1 and Atg19, and are then sequestered into Cvt vesicles. The Cvt vesicles are reminiscent of autophagosomes but are smaller in size. The Cvt vesicles finally fuse with the vacuole, releasing the two proenzymes into the vacuolar lumen. Mitochondria can also be selectively degraded by autophagy, and a yeast cargo receptor on the mitochondrial membrane, Atg32, was recently identified (Kanki et al., 2009; Okamoto et al., 2009).

The best-known mammalian autophagy-specific substrate is p62/SQSTM1 (Bjørkøy et al., 2005; Pankiv et al., 2007). p62 has multiple functions in bone metabolism, obesity, caspase activation, inclusion body formation, and tumorigenesis (Wooten et al., 2006; Seibenhener et al., 2007; Moscat and Diaz-Meco, 2009).

Correspondence to Noboru Mizushima: nmizu.phy2@tmd.ac.jp

Abbreviations used in this paper: Cvt, cytoplasm to vacuole targeting; KO, knockout; LRS, LC3 recognition sequence; MEF, mouse embryonic fibroblast; mRFP, monomeric RFP; PAS, preautophagosomal structure; PI3-kinase, phosphatidylinositol 3-kinase; UBA, ubiquitin associated.

© 2011 Itakura and Mizushima This article is distributed under the terms of an Attribution–Noncommercial–Share Alike–No Mirror Sites license for the first six months after the publication date (see http://www.rupress.org/terms). After six months it is available under a Creative Commons License (Attribution–Noncommercial–Share Alike 3.0 Unported license, as described at http://creativecommons.org/licenses/by-nc-sa/3.0/).

Supplemental Material can be found at:
http://jcb.rupress.org/content/suppl/2011/01/10/jcb.201009067.DC1.html

The Rockefeller University Press $30.00
J. Cell Biol. Vol. 192 No. 1 17–27
www.jcb.org/cgi/doi/10.1083/jcb.201009067

Published January 10, 2011

Selective degradation of p62 by autophagy is physiologically important because accumulation of p62 is cytotoxic, at least in the liver (but not in the brain; Komatsu et al., 2007). It is also hypothesized that p62 functions as an adaptor or cargo receptor in degradation of ubiquitinated proteins, organelles such as peroxisomes and mitochondria (Kim et al., 2008; Kirkin et al., 2009b), and intracellular bacteria (Dupont et al., 2009; Yoshikawa et al., 2009; Zheng et al., 2009). Another structurally related protein, NBR1 (neighbor of BRCA1 gene 1), is also selectively incorporated into autophagosomes and degraded by autophagy (Kirkin et al., 2009a).

These selective substrates/adaptors such as Atg19, Atg32, p62, and NBR1 have an Atg8/LC3-interacting motif (WXXL/I) called the LC3 recognition sequence (LRS) or the LC3-interacting region (Noda et al., 2010). Atg8 and its mammalian homologue LC3 are present on both outer and inner membranes of the autophagosome. Direct binding to Atg8/LC3 allows the cargos to be selectively enclosed by autophagosomes. In yeast, Ape1, Ams1, and Atg19 are present on the preautophagosomal structure (PAS), where most Atg proteins gather and autophagosome are generated (Suzuki et al., 2001; Kim et al., 2002; Chang and Huang, 2007). Importantly, localization of the Cvt complex to the PAS requires Atg19 but does not absolutely depend on other Atg proteins including Atg8, suggesting that cargo recruitment can be achieved independently of the Atg8–cargo interaction (Cao et al., 2008). In contrast, how mammalian selective substrates or cargo receptors are loaded into autophagosomes remains to be determined. It is generally thought that the cargo proteins are recruited to the elongating isolation membrane in an LC3-dependent manner (Kirkin et al., 2009b; Lamark et al., 2009).

In this study, we examined how p62 and NBR1 are loaded onto autophagosomes and found that they are recruited to the autophagosome formation site, which may be equivalent to the yeast PAS. Localization of p62 to this site is dependent on self-oligomerization but independent of most Atg proteins, including LC3. LC3 seems to be critical for later enclosing steps. These results suggest that p62 and NBR1 are already present at autophagosome formation sites. Localization of these proteins may determine where autophagosomes are nucleated.

Results and discussion

p62 can localize to early autophagic structures in an LC3-PE–independent manner

To study p62 loading into the autophagosome, we first determined the requirement of LC3 in p62 association with the autophagic membrane using mouse embryonic fibroblasts (MEFs). When wild-type cells were starved, LC3 punctate structures representing isolation membranes and autophagosomes increased in number (Fig. 1 A). p62 also formed punctate structures, even under nonstarved conditions, although the number increased after starvation (Fig. 1 A). Most of the p62 puncta that were generated under starvation conditions would represent autophagosomes because p62 is incorporated into autophagosomes (Komatsu et al., 2007). The p62 puncta colocalized well with LC3 and Atg16L1 (Fig. 1, A and B), which represented isolation membrane (Mizushima et al., 2001).

Localization of LC3 to the autophagosome depends on conjugation of LC3 with phosphatidylethanolamine, or LC3–PE (LC3-II) formation, which requires Atg3 as a specific E2-like conjugation enzyme. Accordingly, in Atg3 knockout (KO) cells, both LC3–PE formation and LC3 membrane association were completely inhibited (Fig. 1 C; Sou et al., 2008). In these cells, however, Atg16L1-positive puncta were generated, which would represent intermediate structures lacking LC3 (Fig. 1 C; Sou et al., 2008). Unexpectedly, most p62 puncta still colocalized with Atg16L1, even in these Atg3 KO cells. This suggests that LC3 is not essential for the p62 recruitment to the autophagic structures, which is apparently inconsistent with the general idea that p62 recruitment is LC3 dependent (Fig. 1 C). However, the colocalization rate was not as high as in wild-type cells (Fig. 1 B). Approximately 87% and 35% of the Atg16L1 puncta were positive for p62 in wild-type and Atg3 KO cells, respectively. Thus, these results suggest that, although partially important, LC3 is not essential for p62 targeting to the autophagosome intermediates.

In yeast, the hierarchical relationship among the Atg proteins has recently been determined by a systematic analysis (Suzuki et al., 2007). We performed a similar comprehensive analysis using mammalian cells including higher eukaryote-specific factors (Itakura and Mizushima, 2010). The results indicate that the complex containing ULK1 (unc-51–like kinase 1), Atg13, FIP200 (focal adhesion kinase family interacting protein of 200 kD) and Atg101, the ULK1–Atg13–FIP200–Atg101 complex, functions at the most upstream position in the process. This is followed in turn by the Atg14–Beclin 1–Vps34–p150 phosphatidylinositol 3-kinase (PI3-kinase) complex, its putative effecters WIPI-1 (WD-repeat protein interacting with phosphoinosides 1) and DFCP1 (double FYVE domain-containing protein 1), the Atg12–Atg5–Atg16L1 complex, and LC3–PE. LC3 is the most downstream factor among these mammalian Atg proteins. Given this hierarchy, we sought to determine at which step p62 is recruited to the autophagy structures.

Atg5 is covalently attached to the ubiquitin-like protein, Atg12, and further associates with Atg16L1. Atg5 is also essential for LC3–PE formation and LC3 puncta formation (Mizushima et al., 2001). We tested the requirement of Atg5 for the recruitment of p62 to the autophagic membrane. In this assay, we used an upstream factor, WIPI-1, which is present on isolation membranes in a PI3-kinase activity dependent manner (Proikas-Cezanne et al., 2007; Itakura and Mizushima, 2010). Starvation treatment induced WIPI-1 punctate structures, which colocalized with p62 (Fig. 1, D and E). This colocalization was still observed in Atg5-deficient MEFs (Fig. 1, F and G), suggesting that Atg5 is also dispensable for p62 recruitment.

p62 localizes to the ER-associated autophagosome formation site

Autophagosome formation requires PI3-kinase activity; a PI3-kinase inhibitor, wortmannin, suppresses autophagic degradation (Blommaart et al., 1997) and isolation membrane formation (Kovács et al., 2000). Although wortmannin treatment indeed

Downloaded from jcb.rupress.org on January 10, 2011

Published January 10, 2011

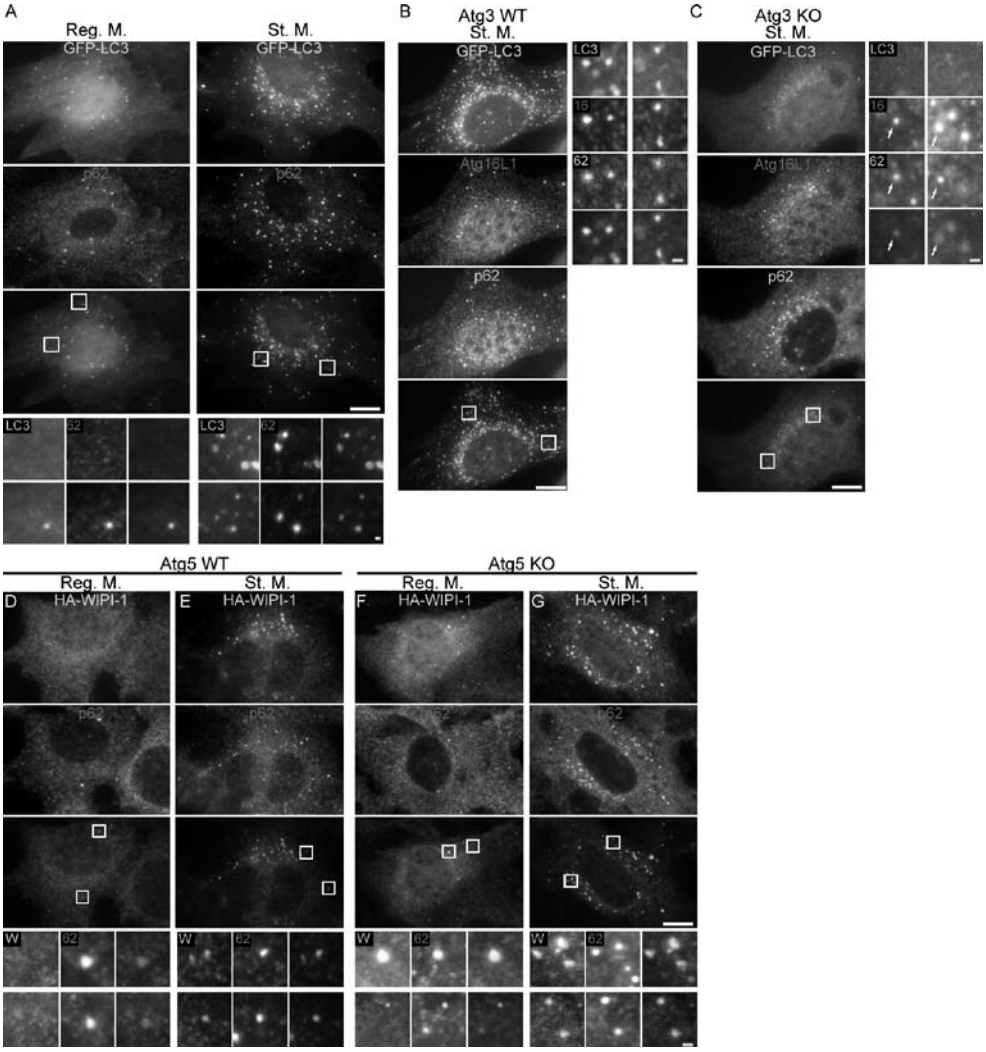

Figure 1. **Localization of p62 to the early autophagic structures is independent of LC3.** (A) MEFs stably expressing GFP-LC3 were cultured in regular medium or starvation medium for 1 h. Cells were stained with anti-p62 antibodies and analyzed by immunofluorescence microscopy. (B and C) Localization of p62 to the autophagic structures is independent of LC3 lipidation. Wild-type (B) and Atg3 KO MEFs (C) stably expressing GFP-LC3 were cultured in starvation medium for 2 h. Cells were stained with anti-Atg16L1 and anti-p62 antibodies. Structures positive for Atg16L1 and p62 but not for GFP-LC3 are indicated by arrows. (D–G) Localization of p62 to the autophagic structures is independent of Atg5. Wild-type (D and E) and Atg5 KO MEFs (F and G) stably expressing HA–WIPI-1 were cultured in regular (D and F) or starvation medium (E and G) for 2 h. Cells were stained with anti-HA and anti-p62 antibodies. Signal color is indicated by color of typeface. Reg. M., regular medium; St. M., starvation medium; WT, wild type. Bars: (white) 10 μm; (yellow) 1 μm.

suppresses puncta formation of downstream Atg proteins, such as WIPI-1, DFCP1, Atg5, Atg16L1, and LC3, it does not affect that of upstream Atg proteins such as ULK1 and Atg14 (Itakura and Mizushima, 2010). We proposed that the ULK1- and Atg14-positive structures observed in wortmannin-treated cells represent autophagosome formation sites. We therefore determined whether p62 could localize to these sites.

Under nutrient rich conditions, there were quite a few Atg14 puncta, and p62 dots were mostly negative for Atg14 (Fig. 2 A). After starvation treatment, Atg14 punctate structures were induced, most of which colocalized with p62 (Fig. 2 B). Notably, the wortmannin treatment, which should inhibit isolation membrane formation, did not disrupt the Atg14–p62 colocalization (Fig. 2 C). One concern was that the Atg14–p62 colocalization might simply represented cytoplasmic protein aggregates in which both Atg14 and p62 were incorporated. To address this possibility, we treated cells with puromycin, which is commonly used to increase the production of truncated

Downloaded from jcb.rupress.org on January 10, 2011

Published January 10, 2011

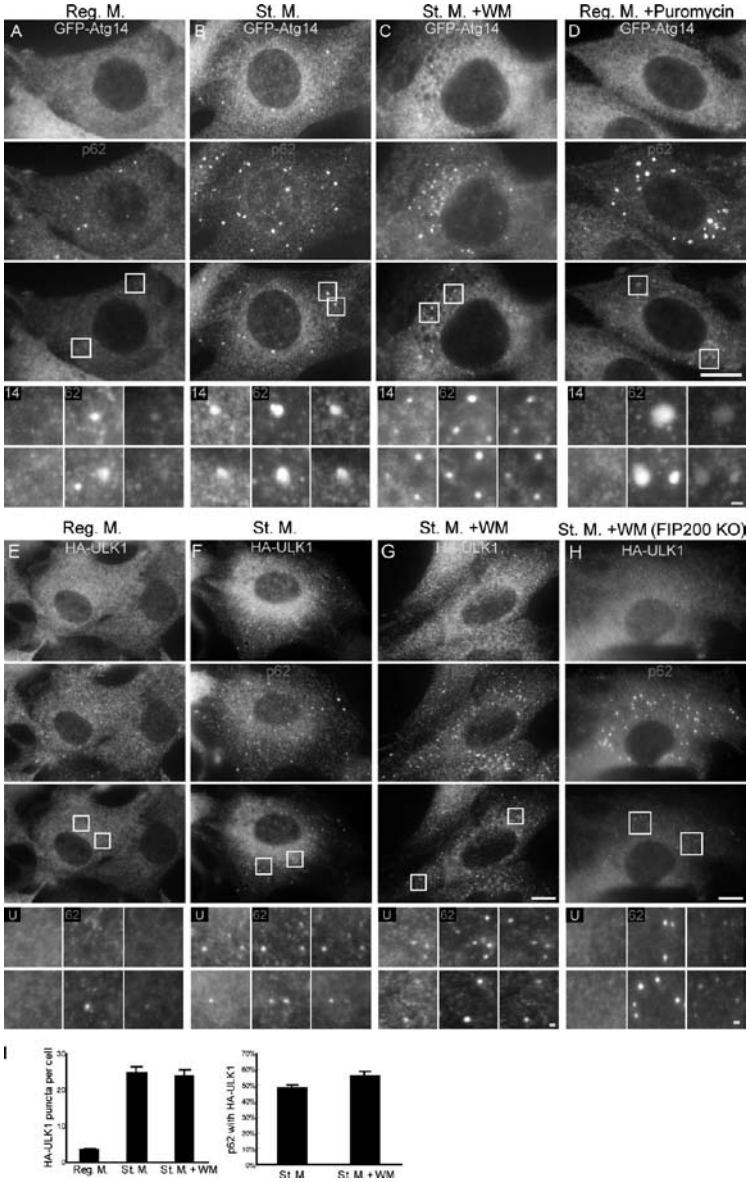

Figure 2. **p62 localizes to the autophagosome formation site.** (A–D) NIH3T3 cells stably expressing GFP-Atg14 were cultured in regular medium (A), starvation medium with (C) or without (B) 0.2 μM wortmannin for 1 h, or in regular medium containing 50 μg/ml puromycin for 2 h (D). Cells were analyzed by immunofluorescence microscopy using anti-GFP and anti-p62 antibodies. (E–H) Wild-type (E–G) and FIP200 KO MEFs (H) stably expressing HA-ULK1 were cultured in the indicated medium for 1 h. Cells were stained as described in Fig. 1. Signal color is indicated by color of typeface. (I) Quantification of HA-ULK1 puncta per cell (left) and HA-ULK1 positivity (%) of the p62 puncta (right) are shown. Data represent mean ± SEM of 30 images. Reg. M., regular medium; St. M., starvation medium; WM, wortmannin; WT, wild type. Bars: (white) 10 μm; (yellow) 1 μm.

and misfolded proteins, and thereby induce formation of cytoplasmic inclusions containing p62 (Szeto et al., 2006; Pankiv et al., 2007; Kirkin et al., 2009b). However, GFP-Atg14 was not incorporated into the puromycin-induced p62 aggregates (Fig. 2 D), suggesting that the Atg14–p62 colocalization is specific for autophagy induction, and does not simply represent protein aggregates.

We reported that Atg14 punctate structures are not formed in FIP200 KO cells and proposed that the ULK1-FIP200 complex is the most upstream unit among the autophagy core units (Itakura and Mizushima, 2010). We thus examined ULK1 and confirmed that the starvation-induced puncta of ULK1 colocalized with p62, even in the presence of wortmannin (Fig. 2, E–G and I). This colocalization was regulated by FIP200 because the ULK1 puncta disappeared in FIP200 KO cells, even though a large number of p62 structures were observed in these cells (Fig. 2 H). These data again argue that the ULK1–p62 colocalization does not represent nonspecific incorporation of ULK1 into p62 aggregates. The colocalization of p62 with ULK1 and Atg14 in wortmannin-treated cells suggests that p62 localizes to the autophagosome formation site independently of downstream factors.

Downloaded from jcb.rupress.org on January 10, 2011

Published January 10, 2011

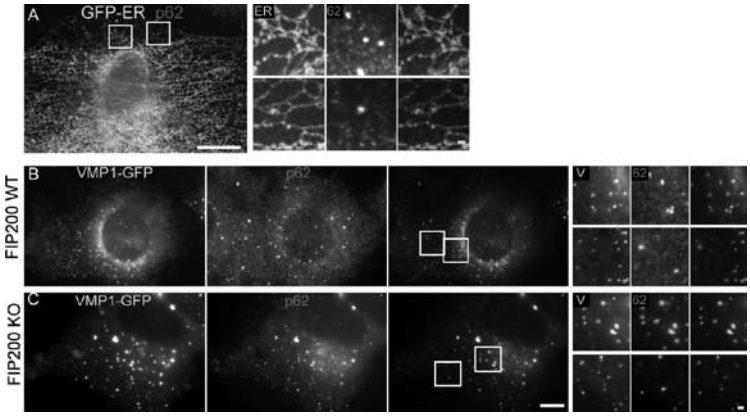

Figure 3. **p62 puncta associate with the ER independently of FIP200.** (A) MEFs stably expressing GFP-ER (GFP fused to cytochrome b5 residues 95–134) were cultured in starvation medium for 1 h. Cells were fixed, permeabilized, and subjected to immunofluorescence microscopy using anti-GFP and anti-p62 antibodies. (B and C) p62 puncta colocalize with VMP1 in FIP200 KO cells. Wild-type (B) and FIP200 KO MEFs (C) stably expressing VMP1-GFP were cultured in starvation medium for 1 h. Cells were stained with anti-p62 antibodies. Signal color is indicated by color of typeface. Bars: (white) 10 μm; (yellow) 1 μm.

p62 localizes to autophagy-related structures even in FIP200 KO cells

We have found that these ULK1 puncta tightly associate with the ER membrane (Itakura and Mizushima, 2010). Consistent with this observation, some of the p62 dots attached the ER networks and were moving together with the ER (Fig. 3 A and Video 1). The p62–ER association was also observed in the presence of wortmannin (Video 2). Collectively, these data suggest that p62 can accumulate at the ER-associated autophagosome formation site, where Atg proteins are recruited.

We further tested whether classical Atg proteins are required for generation of the ER-associated p62 punctate structures. We found in a separate study that most Atg proteins including ULK1, Atg14, Atg16L1, WIPI-1, DFCP1 and LC3 do not form puncta in FIP200 KO cells, whereas VMP1 puncta are constitutively generated in FIP200 KO cells (Itakura and Mizushima, 2010). VMP1 is an ER-associated protein required for autophagosome formation (Ropolo et al., 2007). VMP1 transiently associates with the ULK1 puncta and dissociates from them during autophagosome formation (Itakura and Mizushima, 2010). We therefore determined the requirement of FIP200 in targeting of p62 to the autophagosome formation site using VMP1 as a marker. In wild-type cells, only a few p62 puncta colocalized with the VMP1 puncta (Fig. 3 B). In contrast, almost all p62 puncta colocalized with the VMP1 puncta in FIP200 KO cells (Fig. 3 C). These results suggest that targeting of p62 to the autophagosome formation site on or close to the ER membrane is independent of the ULK1–FIP200 complex, and p62 seems to be trapped at the VMP1 structures when autophagosome formation is inhibited.

These results raised another possibility that VMP1 may be required for targeting of p62 to the autophagosome formation site. To this end, we performed siRNA-mediated silencing of VMP1 and analyzed p62 localization. As we previously reported (Itakura and Mizushima, 2010), ULK1 and DFCP1 puncta accumulated in VMP1 knockdown cells. Knockdown of VMP1 also led to accumulation of large p62 puncta, which colocalized with ULK1 and DFCP1, an ER-associated protein (Fig. S1). These results suggest that VMP1 is not necessary for the p62 recruitment to the ER-associated autophagosome formation site.

NBR1 localizes to the autophagosome formation site in a p62-independent manner

We also tested whether another autophagy selective substrate (or cargo receptor), NBR1, is also targeted to the autophagosome formation site in an LC3-independent manner. NBR1 is structurally similar to p62; it has a PB1 domain at the N terminus and a ubiquitin-associated (UBA) domain at the C terminus (Kirkin et al., 2009a). Moreover, NBR1 has an LRS-like sequence (YIII) which interacts with LC3, and is consequently selectively degraded by autophagy. Under nutrient rich conditions, NBR1 formed punctate structures, which colocalized with p62, but were mostly negative for ULK1 (Fig. S2 A). However, starvation treatment induced the ULK1 punctate structures, which colocalized with both p62 and NBR1 (Fig. S2 B). This colocalization was still maintained when cells were treated with wortmannin (Fig. S2 C), suggesting that NBR1 also targets to the autophagosome formation site independently of Atg factors downstream of the PI3-kinase complex, including LC3. This targeting is also independent of p62 because similar results were obtained when we used p62 KO MEFs (Fig. S2, D–F). These results suggest that localization to the autophagosome formation sites is not specific to p62, but may be a general feature of autophagy-selective substrates and cargo receptors.

The PB1 domain but not LRS of p62 is critical for its localization to the autophagosome formation site

p62 interacts with LC3 via the LRS, which is critical for p62 degradation (Pankiv et al., 2007; Ichimura et al., 2008; Noda et al., 2008). Interaction of LC3 with p62 was found to be severely reduced in the p62 LRS mutant 1 (L343A) and was virtually abolished in the p62 LRS mutant 2 (D337/D338/D339A; Ichimura et al., 2008). We analyzed colocalization of LC3 and mutant p62 proteins in p62-deficient cells to eliminate the effect of endogenous p62. To avoid aggregation caused by overexpression, we used stably transformants expressing GFP-tagged p62 mutants at approximately less than fivefold of the endogenous levels. Consistent with previous observations, colocalization of LC3, with the p62 LRS mutant 1, LRS mutant 2 and p62ΔC (lacking both LRS and the UBA domain) was profoundly

Downloaded from jcb.rupress.org on January 10, 2011

Published January 10, 2011

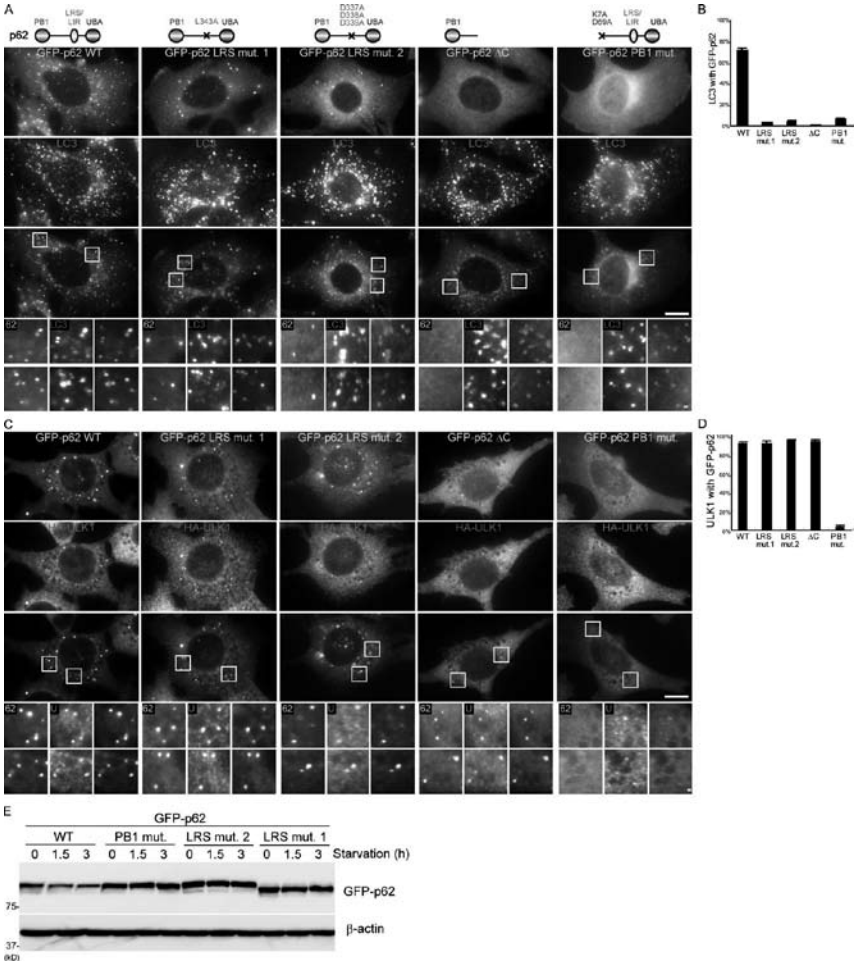

Figure 4. **The PB1 domain but not LRS of p62 is essential for localization to the autophagosome formation site.** (A and B) p62 KO MEFs stably expressing GFP-p62 wild type, GFP-p62 LRS mutant 1 (L343A), GFP-p62 LRS mutant 2 (D337A, D338A, and D339A), GFP-p62ΔC (1–265 amino acids), and PB1 mutant (K7A and D69A) were cultured in starvation medium for 1 h. Cells were analyzed by immunofluorescence microscopy using anti-LC3 antibodies. GFP-p62 positivity (%) of the LC3 puncta is shown in B. Data represent mean ± SEM of 30 images. (C and D) p62 KO MEFs stably coexpressing HA-ULK1 and one of the GFP-p62 described in A were cultured in starvation medium containing 0.2 μM wortmannin for 1 h. Cells were analyzed by immunofluorescence microscopy using anti-HA antibodies. GFP-p62 positivity (%) of the LC3 puncta is shown in D. Data represent mean ± SEM of 30 images. (E) p62 KO MEFs stably expressing the indicated GFP-p62 were cultured in regular or starvation medium for 1.5 and 3 h. Cell lysates were analyzed by immunoblot analysis with the anti-p62 and β-actin antibodies. Signal color is indicated by color of typeface. St. M., starvation medium; WM, wortmannin; WT, wild type. Bars: (white) 10 μm; (yellow) 1 μm.

inhibited compared with wild-type p62 under starvation conditions (Fig. 4, A and B).

We next determined whether these p62 mutants could localize to the autophagosome formation site by testing colocalization between ULK1 and p62 mutants in the presence of wortmannin to inhibit isolation membrane formation. GFP-p62 (wild type) colocalized with ULK1 after starvation in the presence of wortmannin, as did endogenous p62 (91% of HA-ULK1 puncta were positive for GFP-p62; Fig. 4, C and D). Although p62 LRS mutant 1 and LRS mutant 2 are defective in LC3 binding, almost all ULK1 puncta generated after starvation and wortmannin treatment colocalized with the p62 LRS mutants (92% and 95% of HA-ULK1 puncta were positive for GFP-p62 LRS mutant 1 and mutant 2, respectively; Fig. 4, C and D). Furthermore, GFP-p62ΔC could form puncta and colocalized with ULK1 (Fig. 4, C and D), although it seldom forms puncta without wortmannin (Fig. 4, A and B). These data suggest that the LRS domain can be dispensable for targeting to the autophagosome formation site, although it may be important for incorporation into LC3-positive mature autophagosomes.

We therefore determined whether the other domains in p62 are required for targeting to the autophagosome formation site.

Downloaded from jcb.rupress.org on January 10, 2011

Published January 10, 2011

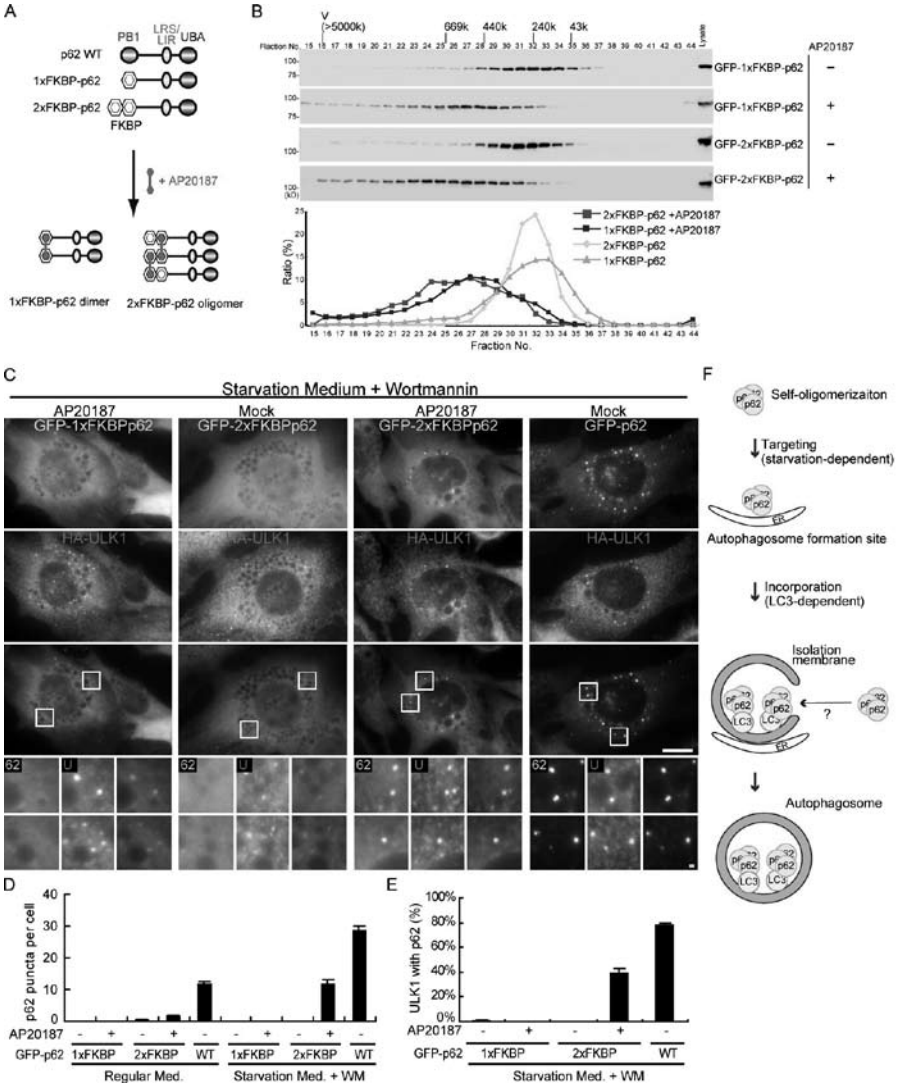

Figure 5. **Self-oligomerization of p62 is critical for its localization to the autophagosome formation site.** (A) Schematic representation of the artificial p62 oligomerization system using a FKBP domain. The PB1 domain of p62 was replaced by one FKBP or two tandem FKBP domains. The small ligand AP20187 chemically links two FKBP domains. (B) p62 KO MEFs stably expressing GFP-1xFKBP-p62 or GFP-2xFKBP-p62 were treated with ethanol (vehicle) or 0.1 μM AP20187 for 24 h. After homogenization and centrifugation, the resulting supernatant fractions were applied to a Superose 6 column. Each fraction was analyzed by immunoblotting using anti-p62 antibodies. Positions of the molecular mass standards (kD) are shown. (C–E) p62 KO MEFs stably expressing HA-ULK1 and either GFP-1xFKBP-p62 or GFP-2xFKBP-p62 were treated with ethanol (vehicle) or 0.1 μM AP20187 for 24 h and cultured in regular or starvation medium containing 0.2 μM wortmannin with or without 0.1 μM AP20187 for 1 h. Cells were analyzed by immunofluorescence microscopy using anti-HA antibodies. The number of p62 puncta per cell (D) and the ULK1 positivity (%) of the p62 puncta (E) are shown. Data represent mean ± SEM of 30 images. Signal color is indicated by color of typeface. AP, AP20187; WM, wortmannin. (F) Proposed model of p62 localization to autophagic structures. Bars: (white) 10 μm; (yellow) 1 μm.

p62 has a Phox and Bem1 (PB1) and UBA domains. We tested the effect of a PB1 mutation (K7A/D69A) in p62, which compromises the interaction surface of the PB1 domain and causes loss of p62 self-oligomerization activity (Ichimura et al., 2008). The PB1 mutant of GFP-p62 did not form any punctate structures even in the presence of wortmannin, although LC3- and ULK1-positive structures were generated normally in these cells (Fig. 4, A–D). Thus, the PB1 domain plays a critical role in p62 recruitment to the autophagosome formation site. We also confirmed that starvation-induced p62 degradation was suppressed in the PB1 domain mutant and in the LRS mutants (Fig. 4 E).

Downloaded from jcb.rupress.org on January 10, 2011

Published January 10, 2011

Collectively, these results suggest that the interaction with LC3 is not necessary for p62 association with early autophagic structures, but appears to be important to incorporate p62 inside these structures. In contrast, the PB1 domain is important for targeting of p62 to the early autophagic structure.

Self-oligomerization is required for localization of p62 to the autophagosome formation site

p62 is known to be self-oligomerized through the PB1 domain (Lamark et al., 2003; Wilson et al., 2003). We confirmed that p62 exists as oligomers irrespective of nutritional conditions (Fig. S3). To investigate the effect of p62 oligomerization through the PB1 domain, we developed an artificial self-oligomerization system using FK506-binding protein (FKBP) domain and a small ligand AP20187 (Amara et al., 1997; Clackson et al., 1998). This system is based on the binding between the FKBP domain and the small ligand AP20187, which can chemically link two FKBP domains. We replaced the PB1 domain of p62 with either one or two tandem FKBP domains, and generated p62 KO cells stably expressing GFP-1xFKBP-p62 or GFP-2xFKBP-p62 with HA-ULK1 (Fig. 5 A). After treatment of AP20187, two 1xFKBP-p62 molecules are linked to form a dimmer, whereas multiple 2xFKBP-p62 molecules are linked to form an oligomer. Gel filtration analysis confirmed that 1xFKBP-p62 moved to approximately twofold higher molecular weight fractions by treatment with AP20187 (Fig. 5 B). Treatment of cells expressing 2xFKBP-p62 causes broader shift to much higher molecular weight fractions, suggesting that 2xFKBP-p62 indeed formed oligomers (Fig. 5 B).

Using this system, we investigated the localization of these FKBP-p62 oligomers. Treatment of AP20187 did not induce p62 puncta formation in either 1xFKBP-p62– or 2xFKBP-p62–expressing cells cultured in regular medium (Fig. 5 D), suggesting that dimerization/oligomerization is not sufficient for puncta formation of p62. However, 2xFKBP-p62 formed puncta after treatment of AP20187 when cells were cultured in a starvation medium containing wortmannin (Fig. 5, C and D). Although starvation-induced puncta formation of 2xFKBP-p62 was less efficient than that of p62 (wild type), it was more efficient than that of 1xFKBP-p62 (Fig. 5, C and D). We also confirmed that these starvation-induced 2xFKBP-p62 puncta colocalized with ULK1 (Fig. 5, C and E). These results suggest that self-oligomerization of p62 through its PB1 domain is prerequisite to its localization to autophagosome formation sites.

Conclusion

It has been speculated that p62 is recruited to preexisting isolation membranes through interaction with LC3. However, our data suggest a completely different model of the p62 loading (Fig. 5 F). At the first step, oligomerized p62 targets to the autophagosome formation site. This step is clearly accelerated by starvation, but appears to be independent of LC3 and other classical Atg proteins. How p62 targets to the autophagosome formation site is currently unknown. One potential mechanism could be an interaction between p62 and ULK1 (Zhou et al., 2007), but we could not detect this interaction in our system (unpublished data). At the second step, the p62 oligomers are incorporated into autophagosomes probably in an LC3-dependent manner. Additional p62 molecules may be further recruited during autophagosome formation. This model is consistent with previous studies showing that the interaction with LC3 is not sufficient for efficient p62 degradation, and the PB1 domain is also important for its degradation (Ichimura et al., 2008; Lamark et al., 2009). We do not know the exact nature of p62 puncta that become enclosed by the autophagosome. They might be small protein aggregates or soluble oligomeric p62 associated with the autophagosome formation sites.

Because p62 is present on the autophagosome formation site, one might expect that p62 could serve in the machinery for autophagosome formation. However, ULK1 and Atg14 puncta formation are not affected in p62 KO cells (unpublished data), and starvation-induced autophagosome formation and degradation of long-lived proteins are normal in p62 KO cells (Komatsu et al., 2007). Nonetheless, it is still possible that p62 has the ability to recruit Atg proteins and to determine where autophagosome should be generated, although p62 is dispensable for autophagy induction. As p62 is also important for pexophagy (Kim et al., 2008) and elimination of bacteria (Yoshikawa et al., 2009), p62 may play a general role in recruiting Atg proteins to initiate autophagosome formation. It is also possible that other p62-like proteins such as NBR1 may function redundantly with p62 (Kirkin et al., 2009a).

Although the Cvt-specific genes are not conserved in mammals, p62 recruitment to the autophagosome formation site is reminiscent of the yeast Cvt pathway (Wang and Klionsky, 2003). After synthesis in the cytosol, precursors of Ape1 (prApe1) forms a homo-dodecamer and assembles into a Cvt complex. Atg19 serves as a receptor for prApe1 and recruits the Cvt complex to the PAS because Atg19 can also bind Atg8 and Atg11 (Scott et al., 2001; Shintani et al., 2002; Suzuki et al., 2002; Chang and Huang, 2007). An in vivo reconstitution experiment showed that prApe1, Atg19, and Atg11 are sufficient for cargo packaging and, at least in part, for cargo delivery to the PAS, which is the autophagosome/Cvt vesicle formation site in yeast (Cao et al., 2008). These processes may be similar to those of p62 targeting to the autophagosome formation site in mammalian cells. p62 could target to the site in an LC3-independent manner, and self-oligomerization of p62 through the PB1 domain is essential for the targeting (Figs. 4 and 5). The delivery of cargos and cargo receptors to the autophagosome/Cvt vesicle formation site would facilitate efficient incorporation of these cargos into autophagosomes and the Cvt vesicles.

Materials and methods

Cell culture and transfection

MEFs were cultured in DME supplemented with 10% FBS and 50 μg/ml penicillin and streptomycin (regular medium) in a 5% CO_2 incubator. NIH3T3 cells were maintained in DME containing 10% bovine calf serum and the antibiotics (regular medium). Atg5 KO (Kuma et al., 2004), Atg3 KO (Sou et al., 2008), FIP200 KO (Gan et al., 2006), and p62 KO (Ichimura et al., 2008) MEFs were generated as described previously. For starvation, cells were washed with PBS and incubated in amino acid–free DME without serum (starvation medium). FuGENE 6 reagent (Roche) was used for transfection. Wortmannin and puromycin were purchased from Sigma-Aldrich.

Downloaded from jcb.rupress.org on January 10, 2011

Published January 10, 2011

Plasmids
Mouse p62 cDNAs (WT and mutants) were provided by M. Komatsu (Tokyo Metropolitan Institute of Medical Science, Tokyo, Japan). An FLJ clone (GenBank accession no. D30756) encoding human NBR1 was obtained from Promega. To generate the pMXs-puro-GFP-p62 and pMXsIP-GFP-NBR1 plasmids, cDNAs were cloned into pMXs-puro or pMXs-IP (provided by T. Kitamura, University of Tokyo, Tokyo, Japan; Kitamura et al., 2003) together with EGFP (Takara Bio Inc.). pMXs-puro-HA-WIPI-1, pMXs-puro-VMP1-GFP, pMXs-IP-GFP-LC3, and pMXs-IP-GFP-Atg14 were described previously (Hara et al., 2008; Itakura et al., 2008; Itakura and Mizushima, 2010). To construct GFP-ER and monomeric RFP (mRFP)–ER, a cDNA of rat cytochrome b5 encoding residues 95–134 (provided by K. Mihara, Kyushu University, Fukuoka, Japan) was subcloned into pMXs-puro-GFP and pMXs-puro-mRFP (provided by R.Y. Tsien, University of California, San Diego, La Jolla, CA; Campbell et al., 2002). To generate the pMRX-IP-GFP-1xFKBP-p62 and pMRX-IP-GFP-2xFKBP-p62 plasmids, 1xFKBP and 2xFKBP amplified from pC_4-F_v1E or pC_4M-F_v2E (provided by ARIAD Pharmaceuticals; see http://www.ariad.com/wt/page/regulation_kits) were inserted into pMRX-IP (provided by S. Yamaoka, Tokyo Medical and Dental University, Tokyo, Japan) together with EGFP and p62.

Retroviral infections and generation of stable cell lines
Stable cell lines were generated using a retroviral expression system. pMXs and pMRX vectors were used to transfect Plat E cells to generate recombinant retroviruses. MEF and NIH3T3 cells were infected with recombinant retroviruses and selected in medium containing 1 µg/ml puromycin as previously described (Hara et al., 2008).

Antibodies
Mouse monoclonal anti-HA (16B12) antibodies were purchased from Covance. Rat monoclonal anti-GFP antibodies (GF090R) were purchased from Nacalai Tesque. Guinea pig polyclonal anti-p62 antibodies (for immunocytochemistry) were purchased from Progen. Rabbit polyclonal anti-p62 antibodies (for immunoblotting) were purchased from MBL International. The rabbit polyclonal antibodies against LC3 (SK2-6; Kabeya et al., 2000) and Atg16L1 (Mizushima et al., 2003) have been described previously. Mouse monoclonal anti–β-actin antibodies were purchased from Sigma-Aldrich.

Immunocytochemistry
Cells grown on coverslips were washed with PBS and fixed in 4% paraformaldehyde in PBS for 10 min at 4°C. Fixed cells were permeabilized with 50 µg/ml digitonin in PBS for 5 min, blocked with 3% BSA in PBS for 30 min, and incubated with primary antibodies for 1 h. After washing, cells were incubated with Alexa Fluor 488–conjugated goat anti–rat, anti–rabbit, or anti–mouse IgG, Alexa Fluor 564–conjugated goat anti–rabbit, anti–mouse, or anti–guinea pig IgG or Alexa Fluor 660–conjugated goat anti–guinea pig IgG secondary antibodies (Invitrogen) for 30 min and examined under a fluorescence microscope (IX81; Olympus) equipped with a charge-coupled device camera (ORCA-ER; Hamamatsu Photonics). A 60× 1.42 NA Plan Apo oil immersion lens (Olympus) was used. Images were acquired using MetaMorph image analysis software (version 7.0; MDS Analytical Technologies).

Time-lapse imaging
Cells were plated onto a glass-bottom dish and mounted in a chamber for live recording, and conditions were maintained with 5% CO_2 at 37°C. Data were analyzed using MetaMorph image analysis software.

Immunoprecipitation and immunoblotting
Cell lysates were prepared in a lysis buffer (50 mM Tris-HCl, pH 7.5, 150 mM NaCl, 1 mM EDTA, 1% Triton X-100, 1 mM phenylmethanesulfonyl fluoride, 1 mM Na_3VO_4, and protease inhibitor cocktail [Complete EDTA free; Roche]). The lysates were subjected to immunoprecipitation using specific antibodies in combination with protein G–Sepharose (GE Healthcare). Immunoblot analysis was performed with the indicated antibodies and visualized with SuperSignal West Pico Chemiluminescent substrate (Thermo Fisher Scientific; Itakura et al., 2008; Itakura and Mizushima, 2010).

Gel filtration analysis
Gel filtration analysis was performed as previously described (Hosokawa et al., 2009). Cells were scrapped from the dish with a rubber policeman and homogenized in hypotonic buffer (40 mM Tris-HCl, pH 7.5, and protease inhibitors cocktail) by repeated passage (30 times) through a 1-ml syringe with a 27-G needle. The 100,000 *g* supernatant fraction (1.6 mg protein in 800 µl) was applied to a Superose 6 column (GE Healthcare) and eluted at a flow rate of 0.5 ml/min with 40 mM Tris-HCl, pH 7.5, and 150 mM NaCl. 0.5-ml fractions were examined by immunoblotting. The column was calibrated with 669-kD thyrogloblin, 440-kD ferritin, 232-kD catalase, and 43-kD ovalbumin.

RNAi
Stealth RNAi oligonucleotides (Invitrogen) were used for siRNA experiments. The following sequences were used for VMP1 siRNA: human VMP1 siRNA antisense, 5′-UAUACGUUGCACAUACUGUUGAUGC-3′; and sense, 5′-GCAUCAACAGUAUGUGCAACGUAUA-3′ (Itakura et al., 2008; Itakura and Mizushima, 2010). For a negative control, a medium GC duplex of Stealth RNAi negative control duplexes (Invitrogen) was used. The Stealth RNAi oligonucleotides were transfected into cells using Lipofectamine RNAiMAX (Invitrogen) according to the manufacturer's protocols. After 2 d, the cells were again transfected with the same siRNA and cultured for an additional 3 d before analysis unless otherwise specified.

Online supplemental material
Fig. S1 shows that VMP1 knockdown does not affect p62 targeting. Fig. S2 shows that NBR1 localizes to the early autophagic structures independently of PI3K and p62. Fig. S3 shows that oligomerization of p62 is not promoted by starvation. Video 1 shows that p62 puncta are closely associated with the ER during starvation. Video 2 shows that p62 puncta are closely associated with the ER during starvation with wortmannin treatment. Online supplemental material is available at http://www.jcb.org/cgi/content/full/jcb.201009067/DC1.

We thank Dr. Masaaki Komatsu (Tokyo Metropolitan Institute of Medical Science) for providing Atg3 KO MEFs, p62 KO MEFs, and p62 cDNA constructs, Dr. Tetsuro Ishii (University of Tsukuba) for p62 KO MEFs, Dr. Roger Y. Tsien (University of California at San Diego) for mRFP cDNA, Dr. Katsuyoshi Mihara (Kyushu University) for rat cytochrome b5 cDNA, Dr. Toshio Kitamura (University of Tokyo) for the retroviral vectors and Plat-E cells, Dr. Shoji Yamaoka (Tokyo Medical and Dental University) for pMRX-IP plasmid, Dr. Jun-Lin Guan (University of Michigan) for FIP200 KO cells, and ARIAD Pharmaceuticals for providing AP20187 chemical dimerizer and the pC_4-F_v1E and pC_4M-F_v2E plasmids. We also thank Drs. Naotada Ishihara and Chieko Kishi for helpful discussions.

This work was supported in part by Grants-in-Aid for Scientific Research from the Ministry of Education, Culture, Sports, Science and Technology of Japan (to N. Mizushima) and by grants for research fellowships from the Japan Society for the Promotion of Science for Young Scientists (to E. Itakura), the Toray Science Foundation, and the Takeda Science Foundation (to N. Mizushima).

Submitted: 13 September 2010
Accepted: 7 December 2010

References

Amara, J.F., T. Clackson, V.M. Rivera, T. Guo, T. Keenan, S. Natesan, R. Pollock, W. Yang, N.L. Courage, D.A. Holt, and M. Gilman. 1997. A versatile synthetic dimerizer for the regulation of protein-protein interactions. *Proc. Natl. Acad. Sci. USA.* 94:10618–10623. doi:10.1073/pnas.94.20.10618

Bjørkøy, G., T. Lamark, A. Brech, H. Outzen, M. Perander, A. Øvervatn, H. Stenmark, and T. Johansen. 2005. p62/SQSTM1 forms protein aggregates degraded by autophagy and has a protective effect on huntingtin-induced cell death. *J. Cell Biol.* 171:603–614. doi:10.1083/jcb.200507002

Blommaart, E.F.C., U. Krause, J.P.M. Schellens, H. Vreeling-Sindelárová, and A.J. Meijer. 1997. The phosphatidylinositol 3-kinase inhibitors wortmannin and LY294002 inhibit autophagy in isolated rat hepatocytes. *Eur. J. Biochem.* 243:240–246. doi:10.1111/j.1432-1033.1997.0240a.x

Campbell, R.E., O. Tour, A.E. Palmer, P.A. Steinbach, G.S. Baird, D.A. Zacharias, and R.Y. Tsien. 2002. A monomeric red fluorescent protein. *Proc. Natl. Acad. Sci. USA.* 99:7877–7882. doi:10.1073/pnas.082243699

Cao, Y., H. Cheong, H. Song, and D.J. Klionsky. 2008. In vivo reconstitution of autophagy in *Saccharomyces cerevisiae. J. Cell Biol.* 182:703–713. doi:10.1083/jcb.200801035

Cecconi, F., and B. Levine. 2008. The role of autophagy in mammalian development: cell makeover rather than cell death. *Dev. Cell.* 15:344–357. doi:10.1016/j.devcel.2008.08.012

Chang, C.Y., and W.P. Huang. 2007. Atg19 mediates a dual interaction cargo sorting mechanism in selective autophagy. *Mol. Biol. Cell.* 18:919–929. doi:10.1091/mbc.E06-08-0683

Downloaded from jcb.rupress.org on January 10, 2011

Published January 10, 2011

Clackson, T., W. Yang, L.W. Rozamus, M. Hatada, J.F. Amara, C.T. Rollins, L.F. Stevenson, S.R. Magari, S.A. Wood, N.L. Courage, et al. 1998. Redesigning an FKBP-ligand interface to generate chemical dimerizers with novel specificity. *Proc. Natl. Acad. Sci. USA.* 95:10437–10442. doi:10.1073/pnas.95.18.10437

Deretic, V. 2009. Multiple regulatory and effector roles of autophagy in immunity. *Curr. Opin. Immunol.* 21:53–62. doi:10.1016/j.coi.2009.02.002

Dupont, N., S. Lacas-Gervais, J. Bertout, I. Paz, B. Freche, G.T. Van Nhieu, F.G. van der Goot, P.J. Sansonetti, and F. Lafont. 2009. *Shigella* phagocytic vacuolar membrane remnants participate in the cellular response to pathogen invasion and are regulated by autophagy. *Cell Host Microbe.* 6:137–149. doi:10.1016/j.chom.2009.07.005

Gan, B., X. Peng, T. Nagy, A. Alcaraz, H. Gu, and J.L. Guan. 2006. Role of FIP200 in cardiac and liver development and its regulation of TNFalpha and TSC-mTOR signaling pathways. *J. Cell Biol.* 175:121–133. doi:10.1083/jcb.200604129

Hara, T., A. Takamura, C. Kishi, S. Iemura, T. Natsume, J.L. Guan, and N. Mizushima. 2008. FIP200, a ULK-interacting protein, is required for autophagosome formation in mammalian cells. *J. Cell Biol.* 181:497–510. doi:10.1083/jcb.200712064

Hosokawa, N., T. Hara, T. Kaizuka, C. Kishi, A. Takamura, Y. Miura, S. Iemura, T. Natsume, K. Takehana, N. Yamada, et al. 2009. Nutrient-dependent mTORC1 association with the ULK1-Atg13-FIP200 complex required for autophagy. *Mol. Biol. Cell.* 20:1981–1991. doi:10.1091/mbc.E08-12-1248

Ichimura, Y., T. Kumanomidou, Y.S. Sou, T. Mizushima, J. Ezaki, T. Ueno, E. Kominami, T. Yamane, K. Tanaka, and M. Komatsu. 2008. Structural basis for sorting mechanism of p62 in selective autophagy. *J. Biol. Chem.* 283:22847–22857. doi:10.1074/jbc.M802182200

Itakura, E.M., and N. Mizushima. 2010. Characterization of autophagosome formation site by a hierarchical analysis of mammalian Atg proteins. *Autophagy.* 6:764–776. doi:10.4161/auto.6.6.12709

Itakura, E., C. Kishi, K. Inoue, and N. Mizushima. 2008. Beclin 1 forms two distinct phosphatidylinositol 3-kinase complexes with mammalian Atg14 and UVRAG. *Mol. Biol. Cell.* 19:5360–5372. doi:10.1091/mbc.E08-01-0080

Kabeya, Y., N. Mizushima, T. Ueno, A. Yamamoto, T. Kirisako, T. Noda, E. Kominami, Y. Ohsumi, and T. Yoshimori. 2000. LC3, a mammalian homologue of yeast Apg8p, is localized in autophagosome membranes after processing. *EMBO J.* 19:5720–5728. doi:10.1093/emboj/19.21.5720

Kanki, T., K. Wang, Y. Cao, M. Baba, and D.J. Klionsky. 2009. Atg32 is a mitochondrial protein that confers selectivity during mitophagy. *Dev. Cell.* 17:98–109. doi:10.1016/j.devcel.2009.06.014

Kim, J., W.-P. Huang, P.E. Stromhaug, and D.J. Klionsky. 2002. Convergence of multiple autophagy and cytoplasm to vacuole targeting components to a perivacuolar membrane compartment prior to de novo vesicle formation. *J. Biol. Chem.* 277:763–773. doi:10.1074/jbc.M109134200

Kim, P.K., D.W. Hailey, R.T. Mullen, and J. Lippincott-Schwartz. 2008. Ubiquitin signals autophagic degradation of cytosolic proteins and peroxisomes. *Proc. Natl. Acad. Sci. USA.* 105:20567–20574. doi:10.1073/pnas.0810611105

Kirkin, V., T. Lamark, Y.S. Sou, G. Bjørkøy, J.L. Nunn, J.A. Bruun, E. Shvets, D.G. McEwan, T.H. Clausen, P. Wild, et al. 2009a. A role for NBR1 in autophagosomal degradation of ubiquitinated substrates. *Mol. Cell.* 33:505–516. doi:10.1016/j.molcel.2009.01.020

Kirkin, V., D.G. McEwan, I. Novak, and I. Dikic. 2009b. A role for ubiquitin in selective autophagy. *Mol. Cell.* 34:259–269. doi:10.1016/j.molcel.2009.04.026

Kitamura, T., Y. Koshino, F. Shibata, T. Oki, H. Nakajima, T. Nosaka, and H. Kumagai. 2003. Retrovirus-mediated gene transfer and expression cloning: powerful tools in functional genomics. *Exp. Hematol.* 31:1007–1014.

Komatsu, M., S. Waguri, M. Koike, Y.S. Sou, T. Ueno, T. Hara, N. Mizushima, J.I. Iwata, J. Ezaki, S. Murata, et al. 2007. Homeostatic levels of p62 control cytoplasmic inclusion body formation in autophagy-deficient mice. *Cell.* 131:1149–1163. doi:10.1016/j.cell.2007.10.035

Kominami, E., S. Hashida, E.A. Khairallah, and N. Katunuma. 1983. Sequestration of cytoplasmic enzymes in an autophagic vacuole-lysosomal system induced by injection of leupeptin. *J. Biol. Chem.* 258:6093–6100.

Kopitz, J., G.O. Kisen, P.B. Gordon, P. Bohley, and P.O. Seglen. 1990. Nonselective autophagy of cytosolic enzymes by isolated rat hepatocytes. *J. Cell Biol.* 111:941–953. doi:10.1083/jcb.111.3.941

Kovács, A.L., G. Réz, Z. Pálfia, and J. Kovács. 2000. Autophagy in the epithelial cells of murine seminal vesicle in vitro. Formation of large sheets of nascent isolation membranes, sequestration of the nucleus and inhibition by wortmannin and 3-ethyladenine. *Cell Tissue Res.* 302:253–261. doi:10.1007/s004410000275

Kraft, C., M. Peter, and K. Hofmann. 2010. Selective autophagy: ubiquitin-mediated recognition and beyond. *Nat. Cell Biol.* 12:836–841. doi:10.1038/ncb0910-836

Kuma, A., M. Hatano, M. Matsui, A. Yamamoto, H. Nakaya, T. Yoshimori, Y. Ohsumi, T. Tokuhisa, and N. Mizushima. 2004. The role of autophagy during the early neonatal starvation period. *Nature.* 432:1032–1036. doi:10.1038/nature03029

Lamark, T., M. Perander, H. Outzen, K. Kristiansen, A. Øvervatn, E. Michaelsen, G. Bjørkøy, and T. Johansen. 2003. Interaction codes within the family of mammalian Phox and Bem1p domain-containing proteins. *J. Biol. Chem.* 278:34568–34581. doi:10.1074/jbc.M303221200

Lamark, T., V. Kirkin, I. Dikic, and T. Johansen. 2009. NBR1 and p62 as cargo receptors for selective autophagy of ubiquitinated targets. *Cell Cycle.* 8:1986–1990.

Longatti, A., and S.A. Tooze. 2009. Vesicular trafficking and autophagosome formation. *Cell Death Differ.* 16:956–965. doi:10.1038/cdd.2009.39

Lynch-Day, M.A., and D.J. Klionsky. 2010. The Cvt pathway as a model for selective autophagy. *FEBS Lett.* 584:1359–1366. doi:10.1016/j.febslet.2010.02.013

Mizushima, N. 2007. Autophagy: process and function. *Genes Dev.* 21:2861–2873. doi:10.1101/gad.1599207

Mizushima, N., A. Yamamoto, M. Hatano, Y. Kobayashi, Y. Kabeya, K. Suzuki, T. Tokuhisa, Y. Ohsumi, and T. Yoshimori. 2001. Dissection of autophagosome formation using Apg5-deficient mouse embryonic stem cells. *J. Cell Biol.* 152:657–668. doi:10.1083/jcb.152.4.657

Mizushima, N., A. Kuma, Y. Kobayashi, A. Yamamoto, M. Matsubae, T. Takao, T. Natsume, Y. Ohsumi, and T. Yoshimori. 2003. Mouse Apg16L, a novel WD-repeat protein, targets to the autophagic isolation membrane with the Apg12-Apg5 conjugate. *J. Cell Sci.* 116:1679–1688. doi:10.1242/jcs.00381

Mizushima, N., B. Levine, A.M. Cuervo, and D.J. Klionsky. 2008. Autophagy fights disease through cellular self-digestion. *Nature.* 451:1069–1075. doi:10.1038/nature06639

Moscat, J., and M.T. Diaz-Meco. 2009. p62 at the crossroads of autophagy, apoptosis, and cancer. *Cell.* 137:1001–1004. doi:10.1016/j.cell.2009.05.023

Noda, N.N., H. Kumeta, H. Nakatogawa, K. Satoo, W. Adachi, J. Ishii, Y. Fujioka, Y. Ohsumi, and F. Inagaki. 2008. Structural basis of target recognition by Atg8/LC3 during selective autophagy. *Genes Cells.* 13:1211–1218. doi:10.1111/j.1365-2443.2008.01238.x

Noda, N.N., Y. Ohsumi, and F. Inagaki. 2010. Atg8-family interacting motif crucial for selective autophagy. *FEBS Lett.* 584:1379–1385. doi:10.1016/j.febslet.2010.01.018

Okamoto, K., N. Kondo-Okamoto, and Y. Ohsumi. 2009. Mitochondria-anchored receptor Atg32 mediates degradation of mitochondria via selective autophagy. *Dev. Cell.* 17:87–97. doi:10.1016/j.devcel.2009.06.013

Pankiv, S., T.H. Clausen, T. Lamark, A. Brech, J.A. Bruun, H. Outzen, A. Øvervatn, G. Bjørkøy, and T. Johansen. 2007. p62/SQSTM1 binds directly to Atg8/LC3 to facilitate degradation of ubiquitinated protein aggregates by autophagy. *J. Biol. Chem.* 282:24131–24145. doi:10.1074/jbc.M702824200

Proikas-Cezanne, T., S. Ruckerbauer, Y.D. Stierhof, C. Berg, and A. Nordheim. 2007. Human WIPI-1 puncta-formation: a novel assay to assess mammalian autophagy. *FEBS Lett.* 581:3396–3404. doi:10.1016/j.febslet.2007.06.040

Ropolo, A., D. Grasso, R. Pardo, M.L. Sacchetti, C. Archange, A. Lo Re, M. Seux, J. Nowak, C.D. Gonzalez, J.L. Iovanna, and M.I. Vaccaro. 2007. The pancreatitis-induced vacuole membrane protein 1 triggers autophagy in mammalian cells. *J. Biol. Chem.* 282:37124–37133. doi:10.1074/jbc.M706956200

Rubinsztein, D.C. 2006. The roles of intracellular protein-degradation pathways in neurodegeneration. *Nature.* 443:780–786. doi:10.1038/nature05291

Scott, S.V., J. Guan, M.U. Hutchins, J. Kim, and D.J. Klionsky. 2001. Cvt19 is a receptor for the cytoplasm-to-vacuole targeting pathway. *Mol. Cell.* 7:1131–1141. doi:10.1016/S1097-2765(01)00263-5

Seibenhener, M.L., T. Geetha, and M.W. Wooten. 2007. Sequestosome 1/p62—more than just a scaffold. *FEBS Lett.* 581:175–179. doi:10.1016/j.febslet.2006.12.027

Shintani, T., W.P. Huang, P.E. Stromhaug, and D.J. Klionsky. 2002. Mechanism of cargo selection in the cytoplasm to vacuole targeting pathway. *Dev. Cell.* 3:825–837. doi:10.1016/S1534-5807(02)00373-8

Sou, Y.S., S. Waguri, J. Iwata, T. Ueno, T. Fujimura, T. Hara, N. Sawada, A. Yamada, N. Mizushima, Y. Uchiyama, et al. 2008. The Atg8 conjugation system is indispensable for proper development of autophagic isolation membranes in mice. *Mol. Biol. Cell.* 19:4762–4775. doi:10.1091/mbc.E08-03-0309

Suzuki, K., and Y. Ohsumi. 2007. Molecular machinery of autophagosome formation in yeast, *Saccharomyces cerevisiae. FEBS Lett.* 581:2156–2161. doi:10.1016/j.febslet.2007.01.096

Suzuki, K., T. Kirisako, Y. Kamada, N. Mizushima, T. Noda, and Y. Ohsumi. 2001. The pre-autophagosomal structure organized by concerted functions of

Downloaded from jcb.rupress.org on January 10, 2011

Published January 10, 2011

APG genes is essential for autophagosome formation. *EMBO J.* 20:5971–5981. doi:10.1093/emboj/20.21.5971

Suzuki, K., Y. Kamada, and Y. Ohsumi. 2002. Studies of cargo delivery to the vacuole mediated by autophagosomes in *Saccharomyces cerevisiae. Dev. Cell.* 3:815–824. doi:10.1016/S1534-5807(02)00359-3

Suzuki, K., Y. Kubota, T. Sekito, and Y. Ohsumi. 2007. Hierarchy of Atg proteins in pre-autophagosomal structure organization. *Genes Cells.* 12:209–218 . doi:10.1111/j.1365-2443.2007.01050.x

Szeto, J., N.A. Kaniuk, V. Canadien, R. Nisman, N. Mizushima, T. Yoshimori, D.P. Bazett-Jones, and J.H. Brumell. 2006. ALIS are stress-induced protein storage compartments for substrates of the proteasome and autophagy. *Autophagy.* 2:183–193.

Virgin, H.W., and B. Levine. 2009. Autophagy genes in immunity. *Nat. Immunol.* 10:461–470. doi:10.1038/ni.1726

Wang, C.-W., and D.J. Klionsky. 2003. The molecular mechanism of autophagy. *Mol. Med.* 9:65–76.

Wilson, M.I., D.J. Gill, O. Perisic, M.T. Quinn, and R.L. Williams. 2003. PB1 domain-mediated heterodimerization in NADPH oxidase and signaling complexes of atypical protein kinase C with Par6 and p62. *Mol. Cell.* 12:39–50. doi:10.1016/S1097-2765(03)00246-6

Wooten, M.W., X. Hu, J.R. Babu, M.L. Seibenhener, T. Geetha, M.G. Paine, and M.C. Wooten. 2006. Signaling, polyubiquitination, trafficking, and inclusions: sequestosome 1/p62's role in neurodegenerative disease. *J. Biomed. Biotechnol.* 2006:62079. doi:10.1155/JBB/2006/62079

Xie, Z., and D.J. Klionsky. 2007. Autophagosome formation: core machinery and adaptations. *Nat. Cell Biol.* 9:1102–1109. doi:10.1038/ncb1007-1102

Yoshikawa, Y., M. Ogawa, T. Hain, M. Yoshida, M. Fukumatsu, M. Kim, H. Mimuro, I. Nakagawa, T. Yanagawa, T. Ishii, et al. 2009. *Listeria monocytogenes* ActA-mediated escape from autophagic recognition. *Nat. Cell Biol.* 11:1233–1240. doi:10.1038/ncb1967

Yu, L., L. Strandberg, and M.J. Lenardo. 2008. The selectivity of autophagy and its role in cell death and survival. *Autophagy.* 4:567–573.

Zheng, Y.T., S. Shahnazari, A. Brech, T. Lamark, T. Johansen, and J.H. Brumell. 2009. The adaptor protein p62/SQSTM1 targets invading bacteria to the autophagy pathway. *J. Immunol.* 183:5909–5916. doi:10.4049/jimmunol.0900441

Zhou, X., J.R. Babu, S. da Silva, Q. Shu, I.A. Graef, T. Oliver, T. Tomoda, T. Tani, M.W. Wooten, and F. Wang. 2007. Unc-51-like kinase 1/2-mediated endocytic processes regulate filopodia extension and branching of sensory axons. *Proc. Natl. Acad. Sci. USA.* 104:5842–5847. doi:10.1073/pnas.0701402104

Downloaded from jcb.rupress.org on January 10, 2011

細菌感染制御学分野

中川 一路

医歯学総合研究科・口腔機能再構築学系専攻
細菌感染制御学・教授

1）研究の課題名

①細胞内侵入性細菌の認識機構と細胞内分解機構の解析

Molecular analysis of recognition system and inflammation responses against bacterial infection.

病原性細菌の病原性の発揮は,宿主組織への付着により生体組織に定着することから開始する.そのため,生体を広く覆う上皮や粘膜といった組織は,これらの菌の侵入を感知する最前線の組織であり,かつ重要な防御組織となっている.近年,多くの細菌種がこのような上皮組織の細胞内に侵入することが知られているが,その動態はほとんど明らかとされていない.本年度は、細胞内に侵入するA群レンサ球菌の動態を、特にエンドソームでの菌の動態を、細胞内の小胞輸送に関わるRabタンパク質について解析を行った.その結果、A群レンサ球菌の細胞内侵入に関わり、通常の飢餓状態で誘導されるオートファジーとは異なるRabタンパク質が菌体の排除に関わっていることが明らかとなった.

②比較ゲノム解析に基づく病原性細菌の外来性遺伝子獲得機構と進化の解析

Comparative genomics for bacterial gene acquisition and evolution systems.

病原性細菌は生体の防御機構に対抗するため,ゲノムの再構成や,外来性遺伝子の取り込みなど様々な方法を用いて進化してきたと考えられる.しかし、口腔内という特殊な環境にどのように適応して自らの生息域（ニッチ）を獲得したかというゲノム情報を元にした解析についてはほとんど行われていない.そこで日本で分離されたS. mutansの全ゲノム解析を行い比較ゲノム解析によりこれらの菌の特徴を新たな観点で明らかにすると同時に、重要な歯周病原性細菌であるP. gingivalis TDC60株の全ゲノム解析を終了した. また、レンサ球菌の進化過程における病原性獲得機能を明らかとするため、A群レンサ球菌では,ファージが外来遺伝子の獲得および再編成に重要な役割を果たしている一方で,S. mutansでは、ファージに対しての抵抗性を有し、CRISPRと呼ばれる防御機構が重要であることなどを明らかとした.さらに現在これらの53株についての比較ゲノム解析を進めている.また、比較ゲノム情報を充実させるため、S. mutans JL23株、S. pyogenes JRS4株の全ゲノム解析を終了した.

2）

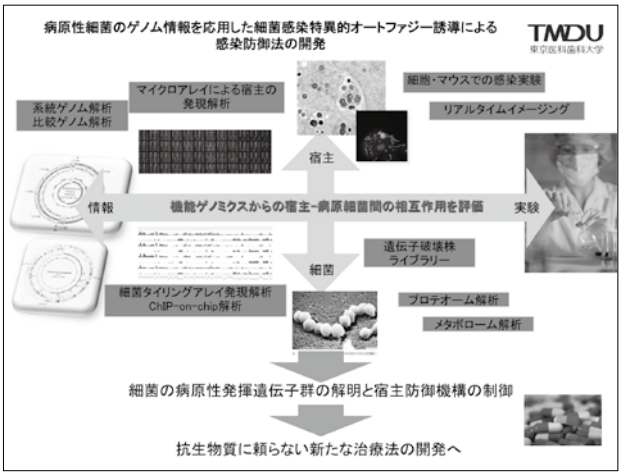

3）発表の研究内容についての英文要約

Streptococcus pyogenes（group A Streptococcus, GAS）, one of the most frequent pathogens of humans, attaches and invades into human pharyngeal or skin epithelial cells. We have previously reported that induction of apoptosis is associated with the GAS invasion, which induces mitochondrial dysfunction and apoptotic cell death. We demonstrated here that GAS-induced apoptosis is mediated by reactive oxygen species（ROS）production. These observations indicated that GAS invasion triggers ROS production through Rac1 activation, and generated ROS resulted in mitochondrial dysfunction leading to cellular apoptosis. We also performed the comparative genomics of S. pyogenes. S. pyogenes possesses clustered regularly

interspaced short palindromic repeats（CRISPR）/Cas systems that can restrict horizontal gene transfer（HGT）including phage insertion. Therefore, it was of interest to examine the relationship between CRISPR and acquisition of prophages in S. pyogenes. Our results suggested that limitations in CRISPR content could explain the characteristic acquisition of prophages and might contribute to strain-specific pathogenesis in S. pyogenes.

4）本事業に関連して世界的な研究拠点形成に向けて、以下の点で改善・整備等されたこと

A：東京医科歯科大学で大規模ゲノム配列解析施設を整えるため、高速シーケンサーIllumina GIIxの稼働を開始した.2011年までの問題点として、その配列解析を行うための計算サーバーが本大学に設営されていないため他大学から貸与していた.しかし、2011年度に入ってから震災の節電要請のため、9月まではほとんど稼働できない状況であった.そのため、細菌感染制御学分野としてDell PowerEdgeT410という省エネルギータイプの計算サーバーを3台導入し、解析を行える環境を整えた.また、シングルランだけではなく、現在イルミナ社と共同で、多サンプル同時解析のためのMultiplex解析法の開発を行い多数同時解析を可能とした.また

B：研究教育環境については昨年よりM&Dタワー8Fに移動が環境し、まだ本分野に次世代型高速シーケンサーRoche GSjuniorが導入されたことにより、分野内で微生物ゲノムの前配列決定、細菌叢解析などが可能となった.

C：人材確保については、高速シーケンサーの運用・稼働のため、ウェット・ドライ双方の研究が可能な人材として、東京工業大学出身の修士学生、また大阪大学微生物病研究所よりH24年3月より野澤孝志助教を採用した.

D：人材育成については、高速シーケンサーの運用・稼働のため、現在分野に所属するポスドク・大学院生でも運用可能になるように教育を行っている.現在では、高速シーケンサーの運用可能なスタッフ3名、大学院生3名となっている.

E：国際化：大学院生としてタイ国NIHよりAmonrattana Roobthaisongが大学院生として入学した.また、次世代型高速シーケンサーを用いた初めての解析として、タイ国NIHとの共同研究としての論文（文献2）を発表することができた.

5）GCOE事業を推進するに当たって力を入れた点

本分野は、大量のゲノム情報を扱うためのプラットフォームを確定することが、本事業での任務であると捉えているため、本年度はそのためのアプリケーションの開発・運営指導体制の確立を行ってきた.高速シーケンサーであるIllumina GIIxは、高速シーケンサーとしては現段階では世界的な標準となっているが、その性能上、短いDNA配列（約150bp）を大量に取得するため、ゲノム配列を決定するというよりもSNP解析やde noveでの配列確定に使われているのが現状である.そこで、本分野として通常のサンガー法と次世代型シーケンサーの中間的な性能をもつRoche GS juniorを導入し、補完関係を構築した.GIIxでは比較ゲノムに適した多数サンプルの同時解析を、GS juniorでは全ゲノム解析や細菌叢解析を分野内で解析できる体制を整えた.

6）英文原著論文

1. Nakano K, Hokamura K, Taniguchi N, Wada K, Kudo C, Nomura R, Kojima A, Naka S, Muranaka Y, Thura M, Nakajima A, Masuda K, Nakagawa I, Speziale P, Shimada N, Amano A, Kamisaki Y, Tanaka T, Umemura K, Ooshima T. The collagen-binding protein of Streptococcus mutans is involved in haemorrhagic stroke. Nat Commun. 27;2：485.（2011）
2. Nagahama M, Itohayashi Y, Hara H, Higashihara M, Fukatani Y, Takagishi T, Oda M, Kobayashi K, Nakagawa I, Sakurai J. Cellular vacuolation induced by Clostridium perfringens epsilon-toxin. FEBS J. 278（18）：3395-407.（2011）
3. ◎Watanabe T, Maruyama F, Nozawa T, Aoki A, Okano S, Shibata Y, Oshima K, Kurokawa K, Hattori M, Nakagawa I, Abiko Y. Complete genome sequence of the bacterium Porphyromonas gingivalis TDC60, which causes periodontal disease. J Bacteriol. 193（16）：4259-60.（2011）
4. Yamato K, Egawa N, Endo S, Ui-Tei K, Yamada T, Saigo K, Hyodo I, Kiyono T, Nakagawa I. Enhanced specificity of HPV16 E6E7 siRNA by RNA-DNA chimera modification. Cancer Gene Ther. 18：587-97（2011）
5. ◎Nozawa, T., Furukawa, N., Aikawa, C., Watanabe, T., Haobam, B., Kurokawa, K., Maruyama, F., Nakagawa, I., CRISPR inhibiton of prophage acquisition in Streptotoccus pyogenes. PLoS One. 6：6（5）：e19543.（2011）
6. ◎Okada K, Roobthaisong A, Nakagawa I, Hamada S, Chantaroj S. Genotypic and PFGE/MLVA analyses of Vibrio cholerae O1：geographical spread and temporal changes during the 2007-2010 cholera outbreaks in

Thailand. PLoS One. 7（1）：e30863.（2012）
7. Aoki A, Shibata Y, Okano S, Maruyama F, Amano A, Nakagawa I, Abiko Y. Transition metal ions induce carnosinase activity in PepD-homologous protein from Porphyromonas gingivalis. Microb Pathog. 52（1）：17-24.（2012）
8. ◎Aikawa C,, Furukawa N, Watanabe T, Minegishi K, Furukawa A, Eishi Y, Oshima K, Kurokawa K, Hattori M, Nakano K, Maruyama F, Nakagawa I, Ooshima T. Complete Genome Sequence of the serotype k Streptococcus mutans LJ23. J Bacteriol. In press.

7）平成23年度までの自己評価

平成22年5月より本GCOEに参加させていただき、高速シーケンサーを実稼働させた.多量の核酸サンプルを高精度に扱うスタッフの育成と、多量の情報処理を行うバイオインフォマティクスのウェットとドライ双方のスタッフの育成を行い、平成23年度では微生物全ゲノム解析を5株で終了し、そのうち2株については論文として発表することができた.現在解析を行っているものも5株あり引き続きその解析をおこなっていく.また、歯周病学分野との研究での口腔細菌叢解析についてもデータの取得を終了し、来年度に発表する予定である.

8）学会発表（英文）

1. Chihiro Aikawa, Takashi Nozawa, Takayasu Watanabe, Bijaya Haobam, Nayuta Furukawa, Fumito Maruyama and Ichiro Nakagawa. 2011. NLRX1 promotes the GAS induced-autophagy in epithelial cells. 111th General Meeting, American Society for Microbiology. 2011.5.21. New Orleans, Louisiana, USA

9）学会発表（和文）

1. 郷田 瑛, 野澤 孝志, 相川 知宏, 渡辺 孝康, Bijaya Haobam, 古川 那由太, 丸山 史人, 中川 一路. 2011. A群レンサ球菌感染誘導オートファジーにおけるユビキチンシステムの機能解析. 第5回細菌学若手コロッセウム. 2011.8.8. 高知大学農学部キャンパス（高知県）
2. 相川 知宏, 野澤 孝志, 郷田 瑛, 渡辺 孝康, Bijaya Haobam, 古川 那由太, 丸山 史人, 中川 一路. 2011. A群レンサ球菌感染によるオートファジーと細胞死の生理機能解析. 第5回細菌学若手コロッセウム. 2011.8.8. 高知大学農学部キャンパス（高知県）
3. Nayuta Furukawa, Takashi Nozawa, Chihiro Aikawa, Takayasu Watanabe, Bijaya Haobam, Akiko Endo, Fumito Maruyama, Ichiro Nakagawa. 2011. Antisense RNA from prophage inhibits prokaryotic acquired immunity in group A streptococci. International Union of Microbiological Societies 2011 Congress. 2011.9.6. Sapporo, Japan.
4. Chihiro Aikawa, Takashi Nozawa, Takayasu Watanabe, Bijaya Haobam, Nayuta Furukawa, Fumito Maruyama and Ichiro Nakagawa. 2011. NLRX1 promotes the GAS induced-autophagy in epithelial cells. International Union of Microbiological Societies 2011 Congress. 2011.9.6. Sapporo, Japan.
5. Takayasu Watanabe, Nayuta Furukawa, Takashi Nozawa, Chihiro Aikawa, Bijaya Haobam, Akiko Endo, Fumito Maruyama, Ichiro Nakagawa. 2011. Elucidation of diversification mechanism of periodontogenic bacterium Porphyromonas gingivalis by analyzing genomic and diversity features. International Union of Microbiological Societies 2011 Congress. 2011.9.6. Sapporo, Japan.
6. 細見晋吾. 2011. A群レンサ球菌ゲノムの種内多様性解析. 第5回日本ゲノム微生物学会若手の会研究会. 2011.9.29. ろうきん研究所富士センター（静岡県）
7. 相川 知宏, 野澤 孝志, 郷田 瑛, 渡辺 孝康, Bijaya Haobam, 古川 那由太, 丸山 史人, 中川 一路. 2011. A群レンサ球菌感染によるオートファジーと細胞死の生理機能解析. 第94回日本細菌学会関東支部会総会. 2011.10.6. 北里大学白金台キャンパス（東京）
8. 古川那由太, 野澤孝志, 相川知宏, 渡辺孝康, 郷田瑛, Bijaya Haobam, 遠藤亜希子, 丸山史人, 中川一路. 2011. プロファージ由来antisense RNAによる細菌の獲得免疫機構の抑制に関する研究. 第94回日本細菌学会関東支部会総会. 2011.10.6. 北里大学白金台キャンパス（東京）
9. 郷田 瑛, 野澤 孝志, 相川 知宏, 渡辺 孝康, Bijaya Haobam, 古川 那由太, 丸山 史人, 中川 一路. 2011. A群レンサ球菌感染誘導オートファジーにおけるユビキチンシステムの機能解析. 第94回日本細菌学会関東支部会総会. 2011.10.6. 北里大学白金台キャンパス（東京）
10. 渡辺孝康, 古川那由太, 野澤孝志, 相川知宏, Bijaya Haobam, 遠藤亜希子, 丸山史人, 中川一路. 2011. Porphyromonas gingivalis国内臨床分離株の比較ゲノム解析と発現解析. 第94回日本細菌学会関東支部会総会. 2011.10.6. 北里大学白金台キャンパス（東京）

10）外部資金の獲得状況

最先端次世代研究開発支援プログラム

「病原性細菌のゲノム情報を応用した細菌感染特異的オートファジー誘導による感染防御法の開発」

中川一路 期間：平成22年―平成24年 研究費総額：13,500万円

科学研究費補助金

基盤C 研究題目：　高解像度細菌叢解析による口腔微生物環境の恒常性維持メカニズムの解明 代表：丸山史人 期間：平成22年―平成24年 研究費総額：500万円

11）教室、分野や講座の准教授、講師、助教、特別研究員、ポスドク、指導を受けた大学院生の名前

准教授　丸山　史人

助教　野澤　孝志（平成24年3月1日より）
日本学術振興会特別研究員：相川知宏（東京大学メディカルゲノム専攻よりの委託）

大学院生　渡辺　孝康（博士課程3年）

大学院生　○Bijaya Haobam（博士課程2年）

大学院生　Amonrattana Roobthaisong
（博士課程1年）：平成23年9月入学（国費）

大学院生　古川那　由太（修士課程2年）

大学院生　細見　晋吾（修士課程1年）

○はAISS

12）GCOE活動についての感想、コメント、改善を望む点

2次世代型シーケンサーを用いた解析が、ようやく本分野内で完結できるようになったが、昨年の震災による節電要請のため、使用していた東京工業大学のサーバーが使用できなくなったため、急遽分野内で計算サーバーを導入し、秋口より解析を本格化することができた.昨年度もお願いしたが、できたら大学内で大容量の計算サーバーなどの環境を整えていただきたいと考えている.

OPEN ACCESS Freely available online

PLoS one

CRISPR Inhibition of Prophage Acquisition in *Streptococcus pyogenes*

Takashi Nozawa[1], Nayuta Furukawa[1], Chihiro Aikawa[2], Takayasu Watanabe[1], Bijaya Haobam[1], Ken Kurokawa[3], Fumito Maruyama[1]*, Ichiro Nakagawa[1]

1 Section of Bacterial Pathogenesis, Graduate School of Medical and Dental Sciences, Tokyo Medical and Dental University, Tokyo, Japan, **2** Department of Medical Genome Sciences, Graduate School of Frontier Sciences, The University of Tokyo, Kashiwa, Japan, **3** Division of Information Biotechnology, Department of Bioinformation Engineering, Tokyo Institute of Technology School and Graduate School of Bioscience and Biotechnology, Yokohama, Japan

Abstract

Streptococcus pyogenes, one of the major human pathogens, is a unique species since it has acquired diverse strain-specific virulence properties mainly through the acquisition of streptococcal prophages. In addition, *S. pyogenes* possesses clustered regularly interspaced short palindromic repeats (CRISPR)/Cas systems that can restrict horizontal gene transfer (HGT) including phage insertion. Therefore, it was of interest to examine the relationship between CRISPR and acquisition of prophages in *S. pyogenes*. Although two distinct CRISPR loci were found in *S. pyogenes*, some strains lacked CRISPR and these strains possess significantly more prophages than CRISPR harboring strains. We also found that the number of spacers of *S. pyogenes* CRISPR was less than for other streptococci. The demonstrated spacer contents, however, suggested that the CRISPR appear to limit phage insertions. In addition, we found a significant inverse correlation between the number of spacers and prophages in *S. pyogenes*. It was therefore suggested that *S. pyogenes* CRISPR have permitted phage insertion by lacking its own spacers. Interestingly, in two closely related *S. pyogenes* strains (SSI-1 and MGAS315), CRISPR activity appeared to be impaired following the insertion of phage genomes into the repeat sequences. Detailed analysis of this prophage insertion site suggested that MGAS315 is the ancestral strain of SSI-1. As a result of analysis of 35 additional streptococcal genomes, it was suggested that the influences of the CRISPR on the phage insertion vary among species even within the same genus. Our results suggested that limitations in CRISPR content could explain the characteristic acquisition of prophages and might contribute to strain-specific pathogenesis in *S. pyogenes*.

Citation: Nozawa T, Furukawa N, Aikawa C, Watanabe T, Haobam B, et al. (2011) CRISPR Inhibition of Prophage Acquisition in *Streptococcus pyogenes*. PLoS ONE 6(5): e19543. doi:10.1371/journal.pone.0019543

Editor: Eliane Namie Miyaji, Instituto Butantan, Brazil

Received February 8, 2011; **Accepted** March 31, 2011; **Published** May 6, 2011

Copyright: © 2011 Nozawa et al. This is an open-access article distributed under the terms of the Creative Commons Attribution License, which permits unrestricted use, distribution, and reproduction in any medium, provided the original author and source are credited.

Funding: This work was supported by Grants-in-Aids for Scientific Research (#21390487 and #22592032), and by the Japanese Ministry of Education, Global Center of Excellence (GCOE) Program, "International Research Center for Molecular Science in Tooth and Bone Diseases." The funders had no role in study design, data collection and analysis, decision to publish, or preparation of the manuscript.

Competing Interests: The authors have declared that no competing interests exist.

* E-mail: fumito-m.bac@tmd.ac.jp

These authors contributed equally to this work.

Introduction

During evolution, bacteria acquired new traits primarily by horizontal gene transfer (HGT) as a key driving force for expressing novel pathogenic properties, new colonization niches as well as metabolic adaptations [1,2,3,4,5]. Conjugation, transduction and transformation are the major mechanisms for HGT. The contributions and the impact of each mechanism are variable among species [6]. Of the three HGT mechanisms, transduction involving bacteriophage-mediated DNA transfer often provides the profound alteration in host bacterial genomes. This process can also convert a non-pathogenic strain into a pathogenic variety through prophage-encoded toxins, surface alterations, or increasing resistance to human immunity [7]. In addition, prophage insertion into the host genome often inactivates or alters the host genes [7,8].

In contrast, phages can cause lytic infection and phage infection is often a danger to host bacteria [7,9]. Therefore, phage infection can have divergent effects: new traits acquisition as an advantage and bacteriolysis as a disadvantage. To protect against the invading phages, bacteria have developed several defense mechanisms such as prevention of adsorption, blocking injection, cleaving phage nucleic acid, and aborting infection [10]. Recently, a novel defense system, clustered regularly interspaced short palindromic repeats (CRISPR) loci, has been identified as a form of acquired immunity against invading foreign DNA including bacteriophage and plasmid DNA [11,12,13]. CRISPR loci are found in almost all Archaea and approximately 40% of sequenced bacterial genomes. They composed of a short repeat sequence (21–47 bp) separated by a unique variable sequence called a spacer [14,15,16]. The repeat sequence is highly conserved within a particular CRISPR locus. In contrast, the spacers vary greatly and their sequences have similarity to phages and plasmids and sometimes to host chromosomal sequences [17]. Each CRISPR is commonly followed by a conserved AT-rich sequence known as a leader sequence. CRISPR-associated (*cas*) genes, essential components of the system, are located adjacent to the CRISPR loci [18]. Acquired immunity involving CRISPR/Cas systems can be divided into two stages: the acquisition stage for uptake of the foreign element as a spacer into the leader-proximal end of CRISPR, and the immunity stage involving interference with the

targeting of DNA in a sequence-specific manner [18,19]. This role was first demonstrated experimentally in a bacterium important in the dairy industry, *Streptococcus thermophilus*, in which CRISPR-harboring strains acquired resistance to infection by phages by incorporating novel spacers derived from the previously infected phages [11,20]. The CRISPR/Cas system was also reported to limit HGT in other bacteria such as staphylococci [12].

In addition to *S. thermophilus*, there are several other medically and economically important species in the genus Streptococcus such as *S. mutans*, *S. pneumoniae* and *S. pyogenes*. *S. mutans* is known to be principal aetiological agent of dental caries and *S. pneumoniae* is the most common cause of lobar pneumonia. *S. pyogenes* causes a wide range of infections, including pharyngitis, sepsis, toxic shock-like syndrome, and life-threatening necrotizing fasciitis [21]. In all of these species, HGT appears to have played an important role in their evolution. For example, the uptake of exogenous DNA by transformation apparently increased the diversity of *S. pneumoniae* and *S. sanguinis* while insertion sequences (IS) and transposons contribute to the genetic diversity of *S. mutans* [22,23,24,25,26,27]. Most notably, *S. pyogenes* is a unique species which has acquired strain-specific virulence genes by means of multiple prophages [28,29]. The sequences of 13 strain-specific genomes from *S. pyogenes* revealed the existence of 2–8 prophages and ~90% conserved genomic sequences (excluding exogenous genetic regions) [29,30] therefore suggesting that their diversity and disease causing capacity might be related to the acquisition of prophages [31]. Because of the predicted role of CRISPR in limiting HGT including phage insertions, it would be of significance to determine whether the CRISPR are involved in the acquisition of prophages in *S. pyogenes*. In this study, we examined 13 sequenced *S. pyogenes* strains and the relationship between CRISPR and the acquisition of prophages. In addition, we extended the analysis of the distribution of CRISPR and prophages by examining a total of 35 streptococcal strain sequences.

Results

S. pyogenes has two distinct CRISPR loci containing relatively few spacers

We determined the distributions of CRISPR loci and *cas* genes for all of the 13 sequenced *S. pyogenes* strains. 15 CRISPR were found and classified as two distinct loci (designated CRISPR1 and CRISPR2) based on their typical repeat sequences. Of the 13 strains, seven strains (SF370, MGAS5005, MGAS10270, MGAS2096, MGAS9429, MGAS6180, NZ131) had both CRISPR1 and CRISPR2, one strain (MGAS10750) possessed only the CRISPR2 locus, and the position of each one of the CRISPR loci was conserved across strains (Table 1, Fig. S1). In contrast, five strains (MGAS315, SSI-1, MGAS8232, Manfredo, MGAS10394) had no CRISPR loci. The typical repeat sequences of both CRISPR1 and CRISPR2 were highly conserved between the strains (Table S1). The typical repeat sequences of CRISPR1 and CRISPR2 belong to the repeat clusters 10 and 3 previously defined, respectively [32]. As is often the case, the terminal repeat sequences of CRISPR1 and CRISPR2 are relatively degenerate compared with their typical repeat sequences (Table S1) [20,33,34,35]. CRISPR1 is located between *hemN* and *lepA* while CRISPR2 is positioned between *valS* and *msrA* (Fig. S2). In MGAS10750, MGAS315, and SSI-1, one sequence that is similar to the CRISPR1 terminal repeat sequence but not remainder of CRISPR (i.e. not a cluster of repeat sequences) was found (Table S1). Although the CRISPR1 terminal repeat-like sequence of MGAS10750 is also located between *hemN* and *lepA*, those of MGAS315 and SSI-1 are distant by 39.5 kb from the CRISPR1 locus of the other strains (Fig. S1A, B). This interesting case is described more in detail below.

We next identified the *cas* genes in the *S. pyogenes* genome. *cas* gene sets are clustered into 8 subtypes based on the member of *cas* genes [36]. The CRISPR clusters 10 and 3 usually are associated with the Nmeni and Dvulg subtype *cas* genes, respectively [32]. Indeed, Nmeni and Dvulg subtype *cas* genes were found upstream

Table 1. Distribution of CRISPR loci and prophages in *S. pyogenes*.

Strain	M type	CRISPR1[a]	CRISPR1 location[b]	CRISPR2[a]	CRISPR2 location[b]	Prophage[c]	ICE[d]
SF370	1	7	1049–1050	4	1559–1561	4	1
MGAS5005	1	4	772–773	5	1284–1285	3	1
MGAS10270	2	3	889–890	4	1364–1365	5	2
MGAS315	3	(1)[e]	889–890	-	-	6	0
SSI-1	3	(1)[e]	937–737	-	-	6	0
MGAS10750	4	(1)[e]	736–737	6	1391–1392	4	2
Manfredo	5	-	-	-	-	5	0
MGAS10394	6	-	-	-	-	8	0
MGAS2096	12	3	846–847	7	1303–1304	2	2
MGAS9429	12	3	888–889	8	1278–1279	3	1
MGAS8232	18	-	-	-	-	5	0
MGAS6180	28	5	751–752	2	1288–1289	4	3
NZ131	49	5	827–828	6	1206–1207	3	0

[a]The number of repeats are shown.
[b]Gene numbers that located both side of CRISPR are shown.
[c]The number of prophage regions are shown.
[d]The number of ICE are shown.
[e](1) indicate that the presence of one terminal repeat-like sequence.
[f]- indicate the absence of CRISPR locus.
doi:10.1371/journal.pone.0019543.t001

from CRISPR1 and CRISPR2, respectively (Fig. S2). Not only the seven CRISPR1-harboring strains but MGAS10750 and MGAS315 also have Nmeni subtype *cas* genes at the same relative position as CRISPR1-harboring strains. Since the repeat sequence, the *cas* gene subsets and the location of CRISPR/*cas* loci were conserved among the strains, it is suggested that *S. pyogenes* harbored CRISPR/*cas* loci early in their evolution. Therefore, the absence of CRISPR may have been adaptive by allowing the integration of bacteriophages into genomes to acquire new traits like Enterococci, which could acquire antibiotic resistance genes for environmental adaptation [20,37].

As CRISPR/*cas* loci are widely distributed among streptococcal species, we compared the characteristics of CRISPR/*cas* among these species. The repeat sequence, repeat size, spacer size, and *cas* genes subtypes are very similar within the same repeat cluster (Table S2). Interestingly, we found a major difference in the number of spacers per locus. The mean number of repeats per genome within *S. pyogenes* was only 6.6, which was significantly fewer than for other streptococci ($P<0.01$) (Fig. 1). Because it was reported that there is a correlation between the numbers of spacers in a CRISPR locus and phage resistance [11,15], it is suggested that phage resistance in *S. pyogenes* is lower than that for other streptococci.

Spacer deletion and acquisition in *S. pyogenes* CRISPR

Since new spacers are regularly added at the end of the repeat cluster adjoining the leader sequence as a spacer-repeat unit [11,34,38,39,40], there is regularity in the alignment of the sequence of spacers. It has been established experimentally and computationally that the leader-proximal end of spacers are more diversified and the leader-distal end of spacers are more conserved among strains [20,41]. Indeed, in *S. mutans* and *S. thermophilus*, similar spacer structures were observed [20,42]. In contrast, *S. pyogenes* spacer structure was characteristic in that the spacers were variable between strains and the most conserved spacers were observed in only closely related strains (Fig. 2A, B). This suggests that the progenitor spacers were deleted and the existing spacers were obtained relatively recently after their diversification [43]. These observations indicate that both spacer acquisition and deletion are active in *S. pyogenes* CRISPR. Considering the location of deleted spacers, the deletions seem to occur randomly and is consistent with previous reports in *Mycobacterium tuberculosis* and *Yersinia pestis* [39,44].

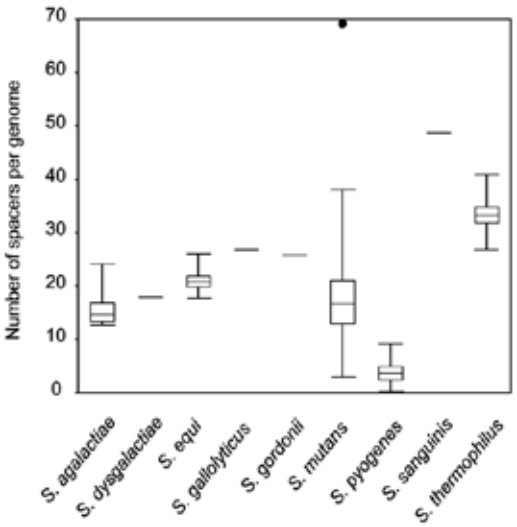

Figure 1. Box plot of the number of spacers in streptococcal CRISPR. The boxes indicate the medians and 25th–75th percentiles of the number of spacers per genome of streptococcal CRISPR. Whiskers indicate 5th to 95th percentiles and outliers are indicated by the closed circle.
doi:10.1371/journal.pone.0019543.g001

Despite the fact that *S. pyogenes* CRISPR appear to be active in spacer acquisition, the number of spacers is small. In the spacer acquisition stage, it is known that Cas1 functions to integrate novel spacers into the CRISPR loci [45]. Hence, small number of *S. pyogenes* CRISPR spacers may result from a mutation or inactivation of Cas1. In light of this, we examined the *cas1* gene sequences in *S. pyogenes*. However, the amino acid sequences of Cas1 were highly conserved (>96% identity) among strains, and the sequences exhibited high similarity with the sequence of *S. thermophilus* LMD-9 (79.6% identity) and *S. mutans* NN2025 (87.15% identity), whose CRISPR are thought to function in acquiring novel spacers [20,27]. The phylogenic tree for the *cas1* sequence was similar to the MLST tree of *S. pyogenes* suggesting that the CRISPR/*cas* loci were not acquired recently but may have existed in an early ancestor (data not shown).

S. pyogenes CRISPR inhibits phage insertion

To assess the functionality of *S. pyogenes* CRISPR, we examined their spacer sequences and defined their respective protospacers. It was previously shown that perfect identity between spacer and protospacer is required to provide immunity [11,46]. However, because of the rapid evolution of phage sequences, we compared the protospacers with a criteria of >95% identity. Of 41 distinct spacers, 27 spacers matched streptococcal phage genomes and one spacer matches one of its own chromosomal gene sequences with >95% identity (Table 2). The remaining 13 spacers (32%) did not match known sequences, which may reflect the small number of sequenced phages and the existence of unknown phages which have recently infected these strains. All spacers that matched streptococcal phages showed exact or approximate matches with the sequences of the prophage regions in various *S. pyogenes* strains (Fig. S3). For example, the most recently added spacer (i.e. the spacer adjacent to the leader sequence) in MGAS370 CRISPR1 matched the sequences within the prophage regions of MGAS10394, MGAS6180, MGAS8232 and SSI-1 (Fig. S3). This suggests that *S. pyogenes* has acquired the spacers following infection with similar streptococcal phages. Of note, despite the fact that all 26 spacers derived from streptococcal phages match the variable prophage regions in *S. pyogenes* genomes, there is no spacer which is homologous to a prophage region in its own genome (Table 2). This strongly suggests that *S. pyogenes* CRISPR are antagonistic to phage insertions.

A spacer similar to the sequence of the host gene *trcF* was observed in MGAS2096 and MGAS9429 (Fig. S3). However, the spacer has a one-base pair difference with the *trcF* gene sequence and the *trcF* sequence is conserved among *S. pyogenes* strains as well as in *S. dysgalactiae*. This suggests that the spacer sequence, but not *trcF*, was mutated and has a relatively low impact on the host.

The CRISPR/Cas system is thought to provide the host bacteria with resistance against not only phages but also various mobile genetic elements [12]. It is known that several exogenous integrated conjugative elements (ICEs) are present in the *S. pyogenes* genome and the ICEs contain various genes such as antibacterial resistance genes [29]. Therefore, we investigated whether *S.*

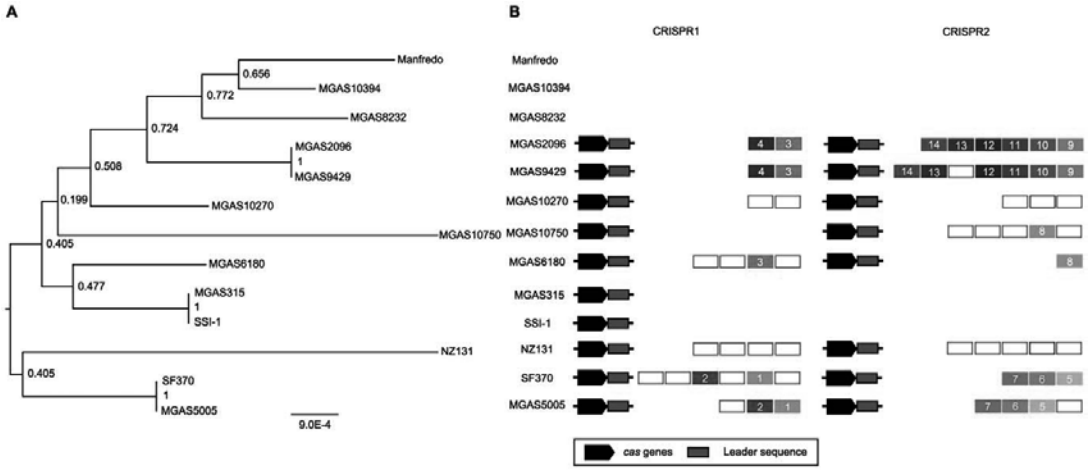

Figure 2. Phylogenetic relationship and spacers across the two CRISPR loci for *S. pyogenes* strains. (A) An MLST-based dendrogram of the 13 strains was generated using the *S. pyogenes* MLST database (see Materials and Methods). (B) Conserved spacers among strains were shown as colored boxes. Single spacers appear in white background; identical spacers are represented using a same color background and identical number. *cas* genes and leader sequences are represented by black and brown boxes, respectively.
doi:10.1371/journal.pone.0019543.g002

pyogenes CRISPR also contain spacers to counteract ICEs. In spite of the presence of 12 ICEs distributed in 13 sequenced strains, we could not find any spacers that showed similarity with the sequences of ICEs in *S. pyogenes* strains (data not shown).

Although all 13 *S. pyogenes* strains possess multiple prophages, five of them lack CRISPR/*cas* loci and the existing CRISPR have relatively few spacers. This implies that *S. pyogenes* CRISPR could not have functioned as an immunity system against invading phages. Instead, the spacer contents suggest that CRISPR appears to have functioned to inhibit phage insertions.

Inverse correlation of *S. pyogenes* prophages and the number of spacers in a CRISPR locus

To further confirm the function of *S. pyogenes* CRISPR, we investigated whether CRISPR-possessing strains have fewer prophages than those lacking CRISPR by a Wilcoxon rank sum test. We addressed the null hypothesis that there is no difference in the numbers of prophages between the CRISPR-positive and -negative strains and the null hypothesis could be rejected ($P<0.01$) indicating that the numbers of acquired prophages significantly differ between CRISPR-positive and -negative *S. pyogenes* strains. We next investigated whether a correlation exists between the number of spacers and prophages in each *S. pyogenes* genome. As shown Fig. 3A, we observed a clear inverse correlation between the total number of repeats per genome and the number of prophages within each genome ($R=-0.83$; $P<0.001$). These results strongly suggest that *S. pyogenes* CRISPR functions to inhibit phage incorporation into host genomes which depends on spacer number. Interestingly, although the correlation between the number of CRISPR2 repeats and the number of prophages was also clear ($R=-0.82$; $P<0.001$), the negative correlation between the number of CRISPR1 repeats and the number of prophages was relatively low ($R=-0.60$; $P<0.05$) (Fig. 3B, C), indicating that CRISPR2 may be more active than CRISPR1 in *S. pyogenes* genomes. Taken together, it was suggested that the absence of CRISPR/*cas* loci in five of the genomes and the low number of spacers in the seven strains with a functional CRISPR loci may explain the relatively high number of prophages in *S. pyogenes*.

Insertion of phages into the terminal repeat-like sequence of *S. pyogenes* MGAS315

As described above, in MGAS315 *cas* genes are located in the same locus as that of the other CRISPR harboring strains and a terminal repeat-like sequence was found about 39.5 kb from the *cas* genes (Fig. S1B). In SSI-1, the terminal repeat-like sequence is located at the same position as MGAS315, and *cas* genes are located far away from the loci of *cas* genes in other strains. Since it was reported that the location of all CRISPR adjacent to the *cas* genes is required for their role as an acquired immunity system [11], it was suggested that the CRISPR/Cas system was not functional in the two strains. The prophage region (Φ 315.1) was found in between a terminal repeat-like sequence and *cas* genes of MGAS315 and SSI-1 also has a prophage (Φ SPsP5) just downstream of the *cas* genes (Fig. S2). From further detailed analysis of sequences around the prophage insertion site and between the terminal repeat-like sequence and *cas* genes, we found a portion of a terminal repeat sequence (14 bp in length) upstream of the prophage (Fig. 4A). The sequence of the prophage (Φ 315.1) in MGAS315 is highly similar to the sequence of Phage 3396 and these two phages were designated as the Φ315.1-like family by Davies [47]. We investigated the Phage 3396 genome and found that a region of the Phage 3396 genome is identical to an upper 12 bp of the terminal repeat-like sequence in MGAS315 and is the region for an *att* site (Fig. 4B). It is suggested, therefore, that the *att* site sequence can be used for recombination and enables phage genomes to be incorporated into the host MGAS315 genome. As shown Figure 4B, if recombination between the 14 bp sequence at the *att* site of the phage (GAGCTATG) and the homologous terminal repeat sequence (GAGCTATG) occurred, a combined sequence (GTTTTAGAGCTATG) is formed upstream of the prophage and a chimeric sequence of the former part of *att* site and the latter part of the repeat is produced downstream of the

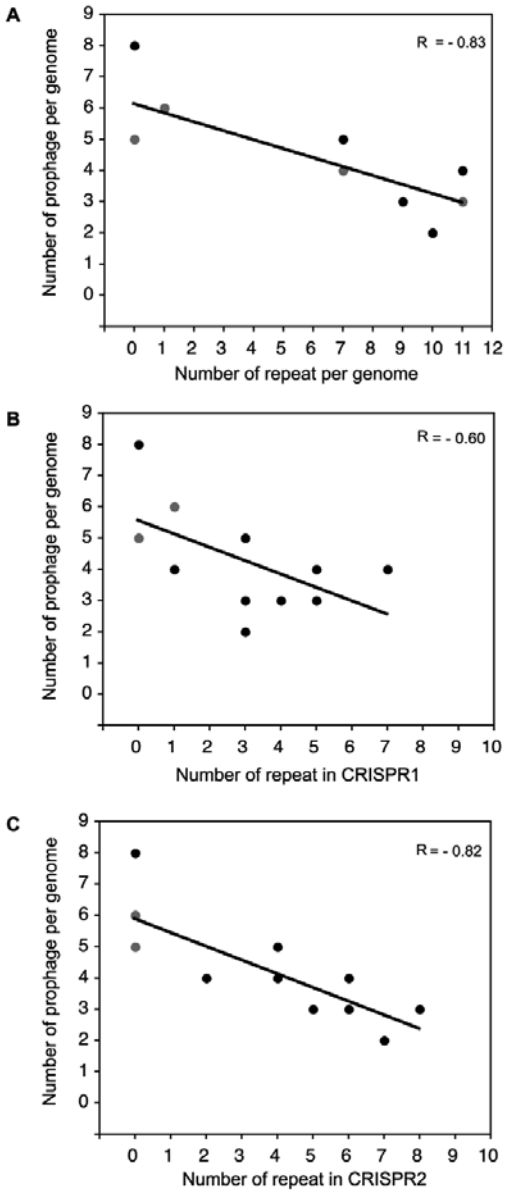

Figure 3. The relationship between the number of repeat sequences and prophages in *S. pyogenes*. (A), (B) and (C) show the number of prophages per genome versus the number of repeats per genome in CRISPR1 and CRISPR2, respectively. Red dots means overlapping of two dots.
doi:10.1371/journal.pone.0019543.g003

prophage (Fig. 4B). These observations could explain how the terminal repeat-like sequence of MGAS315, which is different by 2 bases from the typical terminal repeat sequence of CRISPR1, was produced after separation of the terminal sequence and *cas* genes by insertion of the phage into the MGAS315 genome.

We also compared the leader sequences among the strains and found that the leader sequence of MGAS315 was the same as those of other CRISPR1-harboring strains. This result suggests that the insertion of phages into the terminal repeat sequence of MGAS315 did not occur because of the impairment of the CRISPR system following mutation of the leader sequence.

Derivative strain, SSI-1, from MGAS315 by large-scale genomic recombination

As with MGAS315, the position of the terminal repeat sequence of SSI-1 is separated from the *cas* genes and the distance in SSI-1 is 187 kbp further than that of MGAS315. The average of Single Nucleotide Polymorphism (SNP) per gene comparing MGAS315 and SSI-1 is 0.05% and high similarity is recognized between these genomes [48]. Nevertheless, the relative position of the CRISPR sequence and *cas* genes in the MGAS315 genome is clearly distinct from SSI-1. This can be explained by large genomic rearrangements which have occurred during evolution of the two strains [48]. Genomic rearrangement is a phenomenon whereby a genome region is exchanged between homologous sequences [49]. Although it was showed that large-scale genomic recombinations occurred in MGAS315 or SSI-1 [48], which is the ancestral strain has not been determined. In this study, we showed that MGAS315 was generated from the ancestral strain following the insertion of phage, suggesting that MGAS315 is the progenitor of SSI-1 (Fig. 4C).

Distribution of prophages and CRISPR loci in other streptococci

To further examine the relationship between CRISPR/Cas systems and prophages in the genus Streptococcus, we expanded the analysis to an additional 35 bacterial sequenced streptococci. Prophage elements were widely distributed and observed in both CRISPR-harboring and CRISPR-lacking species (Fig. S4). To examine the impact of CRISPR on the acquisition of prophages for the genus of Streptococci, we evaluated whether CRISPR-possessing species have fewer prophages than those lacking CRISPR by a Wilcoxon rank sum test. We addressed the null hypothesis that there is no difference in the distributions of prophages between the CRISPR-positive and -negative species, and the null hypothesis could not be rejected ($P>0.05$). Similar results were obtained when the same analysis was performed with the 35 streptococci strains omitting the 13 *S. pyogenes* strains. Therefore, we could not conclude that CRISPR-lacking streptococci have acquired more prophages than CRISPR-harboring ones. However, it is possible that the influences of CRISPR on the acquisition of prophage vary among species. We then examined the distribution of prophages and CRISPR within each species though the number of sequenced strains per species was relatively small. *S. mutans*, *S. gordonii*, *S. sanguinis*, some *S. agalactiae*, and some *S. thermophilus* possess CRISPR loci and do not have any phage inserted into their genomes, whereas *S. mitis* and some strains of *S. pneumoniae* and *S. suis* do not have CRISPR locus and permitted insertion of phages into their genomes (Fig. S4). However, some *S. agalactiae*, *S. dysgalactiae*, *S. equi*, and *S. thermophilus* possess both CRISPR loci and prophage elements, and other *S. pneumoniae* strains have no prophage despite they lack the CRISPR locus (Fig. S4). These observations suggest that CRISPR may be involved in the inhibition of phage insertion even in streptococci other than *S. pyogenes* and the degree of contribution of CRISPR to the restriction of phage insertion varies among species. Further study is needed with more complete genome sequences to delineate more clearly the effects of CRISPR systems on genomic evolution.

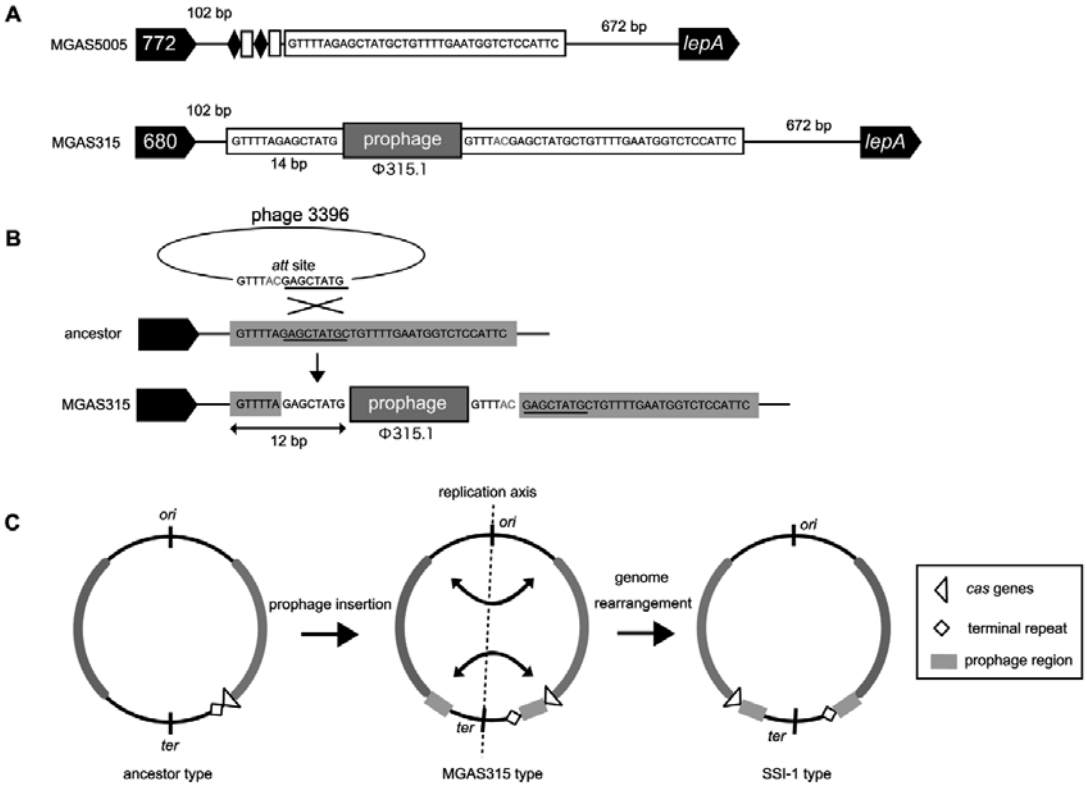

Figure 4. Phage insertion into the repeat sequences of MGAS315 and genome rearrangements. (A) The adjacent sequence of the Φ315.1 insertion site in the MGAS315 genome. (B) A scheme forΦ315.1 insertion into the repeat sequences of MGAS315. (C) Schematic diagram of the evolutionary relationship of MGAS315 and SSI-1 following phage insertion and genome rearrangement.
doi:10.1371/journal.pone.0019543.g004

Discussion

S. pyogenes strains are well-known to induce a variety of diseases and the sequences of 13 strains suggested that the prophage regions contain variable virulence genes and confer pathogenic capacities [31]. In this study, we examined all 13 sequenced *S. pyogenes* strains and evaluated the relationship between CRISPR and the acquisition of prophages in *S. pyogenes*. We found that five of 13 *S. pyogenes* strains lacked CRISPR/*cas* loci and the existing CRISPR in seven strains have essentially complete repeat sequences and *cas* gene systems. Furthermore, the number of spacers was fewer than that of other CRISPR-harboring streptococci. As the number of spacers is a reliable indicator of CRISPR activity [43], the activities of *S. pyogenes* CRISPR may be lower than for other streptococcal CRISPR.

Spacer content and arrays suggested that most spacers were deleted and the acquisition of new spacers is an ongoing process. It is known that the Cas1 protein is involved in a spacer-acquisition step dependent upon its endonuclease activity [18,50]. There is also a report that *S. mutans* UA159 has a truncating mutation in its *cas1* gene and its CRISPR contains only one spacer [42], supporting the importance of Cas1 in spacer acquisition. In our study, we could not find any apparent mutation in *S. pyogenes cas1*. Although it was recently reported that the divalent metal binding site of Cas1 are likely important for the function in *Pseudomonas aeruginosa* CRISPR [50], the *cas1* gene of *P. aeruginosa* varies greatly from that of *S. pyogenes* or other streptococci, and the active sites for streptococcal Cas1 activity have not yet been identified. So, we cannot exclude the possibility that *S. pyogenes* Cas proteins have undefined defect(s) such as a single amino-acid substitution in active site regions in some strains. In *S. thermophilus*, *csn2* (*cas7*) gene was shown to be involved in the spacer acquisition [11]. *csn2* is a member of the Nmeni subtype *cas* genes and widely harbored in Streptococcal genomes including *S. pyogenes*, and *S. pyogenes csn2* showed the high similarity with that of *S. thermophilus*. As well as the case of *cas1*, further detailed investigation of *cas* genes will be useful to determine whether the currently identified *S. pyogenes* Cas proteins have any defects.

The deletion of spacers is frequently observed in other bacteria, which is thought to be necessary to prevent over-inflation of the CRISPR locus [39,51,52]. The lacking of several spacers was observed among same M1 type *S. pyogenes* strains, indicating that spacer deletion frequently occurs in *S. pyogenes* CRISPR [35]. We also found evidence of frequent spacer deletion in *S. pyogenes* CRISPR. However, it is not clear whether such deletions occur actively or result from passive homologous recombination. Considering the irregularity of spacer deletion in *S. pyogenes*, the deletions may be a consequence of spontaneous homologous

Table 2. Characteristics of spacers in *S. pyogenes*.

	CRISPR1	CRISPR2
Spacer size (bp)	30 (30–31)	35 (33–36)
Number of spacers	23	33
Number of distinct spacers	18	23
Number of single spacers	14 (78%)	13 (57%)
Number of distinct spacers matched chromosome	1	0
Number of distinct spacers matched prophage	13	13
Number of distinct spacers matched own prophages	0	0

doi:10.1371/journal.pone.0019543.t002

recombination events. Therefore, one of the reasons for the small number of *S. pyogenes* CRISPR spacers may be that homologous recombinations have frequently occurred and/or the *S. pyogenes* CRISPR/Cas system is unable to acquire new spacers as efficiently as other streptococcal CRISPR due to unknown effect(s).

Despite the low number of spacers in *S. pyogenes* CRISPR, spacer contents and the relationship between the number of repeats and prophages showed that *S. pyogenes* CRISPR has rejected the phage insertion. Interestingly, the inverse correlation between number of spacers and phages is significant for CRISPR2 ($R = -0.82$; Fig. 3C), and less so for CRISPR1 ($R = -0.60$; Fig. 3B). We found that larger portion of spacers in CRISPR1 (82.6%; 19/23) showed high similarity to known sequences, whereas smaller portion of that in CRISPR2 (64.7%; 22/34) matched with known sequences. Among these spacers, 21.1% (4/19; in CRISPR1) and 45.5% (10/22; in CRISPR2) of spacers match prophages with >95% identity but not 100%. Since phages specifically mutated the proto-spacer to overcome CRISPR/Cas immunity [19], it may be suggested that spacers in CRISPR1 are acquired more recently than that in CRISPR2. This may be the reason why CRISPR1 showed less inverse correlation compared to CRISPR2.

Recently, there was a report that transcription of the *cas* genes and some CRISPR arrays is repressed by heat-stable nucleoid-structuring (H-NS) proteins in *Escherichia coli* [53], suggesting the existence of a CRISPR regulation system. Transmittable phages and plasmids contain unique genetic elements which could confer novel characteristics on the recipients. In addition, these characteristic contributions are thought to be important for host environmental adaptation. For example, lysogenic infection of *P. aeruginosa* with bacteriophage DMS3 inhibits biofilm formation and swarming motility and this inhibition requires the CRISPR region [54]. Based on this report, Papenfort also suggested that some pathogens might adapt CRISPR activity to control prophage-encoded genes for virulence [55]. More recently, it was reported that Enterococci have acquired antibiotic resistant genes through the loss of CRISPR/*cas* loci demonstrating an additional role for CRISPR/*cas* in HGT [37]. In the case of *S. pyogenes*, despite prophage-encoded genes providing important characteristics to the organism, CRISPR/*cas* is present in their genomes and appears to function in inhibiting phage insertions. This raises the possibility that *S. pyogenes* might have evolved its CRISPR activity for incorporation of beneficial phages into its own genome.

The CRISPR/Cas system was reported to have a potential for influencing genome-scale evolution involving spacers which are homologous to chromosomal genes in *Pelobacter carbinolicus* [56]. In *S. pyogenes* CRISPR, one spacer in MGAS2096 and MGAS9429 was similar to the sequence within *trcF*, a transcription repair coupling factor gene of *S. pyogenes*. TrcF has been well studied in *E. coli* and is known to be involved in the transcription coupled repair system for DNA which operates in tandem with transcription [57]. Therefore, there it is possible that the spacers could influence DNA repair systems. However, for *S. pyogenes*, the spacer sequence has a one-base difference from the *trcF* gene sequence and this later sequence is conserved among *S. pyogenes* strains as well as in *S. dysgalactiae*. This suggests that it has a relatively low impact on the host. To definitely determine the effects of the spacer on the host, further experimental studies will be necessary.

As for MGAS315 and SSI-1, because these strains have almost completely conserved genome sequences, it was difficult to determine which is the more primitive strain. In this study, we suggested that MGAS315 is the ancestral strain of SSI-1. Although the insertion of phages into the repeat sequences may be a random event, we propose the possibility that this event is a novel anti-CRISPR mechanisms which allow phages to subvert CRISPR antagonism and facilitate entry of more phages into the host genome. Of note, CRISPR have been identified within two prophages in *Clostridium difficile* [58]. When the prophages inserted into the CRISPR are deleted due to homologous recombination between the repeat sequences that are located external to the prophages, CRISPR-containing phages are produced. Therefore, the invasion of phages into the repeat sequences may be required not only for inactivation of the CRISPR/Cas system but also for the acquisition of CRISPR. However, the identification of CRISPR in prophage regions is still somewhat limited so additional comprehensive research may provide further interesting findings regarding the relationship between phages and CRISPR.

As a result of the analysis of an additional 35 streptococcal genomes, the influences of CRISPR loci on the distributions of prophages appeared to be species dependent. This could be explained by the presence of other anti-phage systems or unknown environmental effects. If these species have additional strict self-defense systems against invading phages or their habitats contain fewer phages, the CRISPR/*cas* locus may be unnecessary. Therefore, even in the same genus, the contribution of CRISPR to phage sensitivity seems to depend on the species and bacteria might have evolved their intrinsic self-defense systems depending on their environments. Prophage identification using prophage prediction tools such as Prophinder [59] is principally based on similarity searches, gene annotation and detection of conserved pairs of genes found in phage genomes. Moreover, where similar prophages are inserted into one genome, it is very difficult to identify the actual number of prophages [59]. Therefore, to understand the relationship between the CRISPR/Cas system and prophages, more complete genome sequences are required. We also showed the importance of comparative genome analysis in CRISPR research in previous studies [37,43]. However, experimental studies will also be indispensable to verify our findings.

The involvement of CRISPR in bacterial adaptation to their environments is suggested in enterococci which lack endogenous CRISPR/*cas* loci and can obtain new antibiotic resistance genes in antibiotic treated environments [37]. Likewise, *S. pyogenes* might have evolved limited CRISPR/Cas activity to enhance the acquisition of virulence genes, and this phenomenon might have contributed to the diverse strain-specific pathogenicities observed in this important pathogen. More generally, the absence of CRISPR could be one important survival strategy for human pathogens.

Materials and Methods

Genomes

The information for the complete genome sequences of streptococcal strains used in this study was derived from the

search results of the Gold genome online database (http://www.genomesonline.org/) as complete sequences as of October 20, 2010. These data include 13 strains of *S. pyogenes* (accession no. NC_002737, NC_007297, NC_003485, NC_007296, NC_004606, NC_011375, NC_006086, NC_009332, NC_008022, NC_008024, NC_008023, NC_004070, NC_008021), three strains of *S. agalactiae* (NC_007432, NC_004116, NC_004368), one strain of *S. dysgalactiae* (NC_012891), three strains of *S. equi* (NC_012471, NC_012470, NC_011134), one strain of *S. gallolyticus* (NC_013798), one strain of *S. gordonii* (NC_009785), one strain of *S. mitis* (NC_013853), two strains of *S. mutans* (NC_013928, NC_004350), 12 strains of *S. pneumoniae* (NC_011900, NC_012468, NC_010582, NC_008533, NC_011072, NC_010380, NC_012466, NC_012467, NC_003098, NC_012469, NC_014251, NC_003028), one strain of *S. sanguinis* (NC_009009), six strains of *S. suis* (NC_009442, NC_009443, NC_012926, CP_000837, NC_012925, NC_012924), three strains of *S. thermophilus* (NC_006449, NC_008532, NC_006448), and one strain of *S. uberis* (NC_012004). Each complete gene sequence was obtained from the NCBI (http://www.ncbi.nlm.gov) database.

CRISPR analysis

The CRISPR candidates were obtained with CRISPRfinder (http://crispr.u-psud.fr/Server/) [60]. The CRISPR candidates were confirmed manually by examining their adjacent sequences [34]. We added the CRISPR data for *S. mutans* and *S. thermophilus* from previous reports [20,27,42]. The classification of repeat clusters was based upon a previous study [32]. To investigate protospacers, the nucleotide sequence database was queried with each of the CRISPR spacers of *S. pyogenes* using Blastn of NCBI with default parameters for short input sequences [61]. Amino acid and nucleic acid sequence alignments were generated with ClustalW in DDBJ (http://clustalw.ddbj.nig.ac.jp/top-j.html) [62].

Prophage identification

To identify the distribution of prophages in streptococci, we used Prophinder (http://aclame.ulb.ac.be/Tools/Prophinder/) [59]. We submitted Genbank files of genome data obtained from NCBI to a query system of Prophinder and generated the results for prophage prediction.

Analysis of streptococcal CRISPR and prophage distribution

To test whether the numbers of acquired prophage elements differ in the presence or absence of CRISPR/loci, we performed the nonparameric Wilcoxon rank sum test.

Phylogenetic tree of *S. pyogenes*

Thirteen concatenated sequences were obtained from MLST.net [63] and aligned with the ClustalW-2.0.12 Software [62]. The MEGA4 program [64] was used to estimate nucleotide diversity and evolutionary distances as well as to build phylogenetic trees by the neighbor-joining method [65] using the Jukes-Cantor distances [66], which were selected for nucleotide substitutions using jModelTest, version 0.1.1 [67]. The reliability of clustering patterns in the phylogenetic trees was assessed by bootstrapping [68] and 1000 bootstrap pseudo-samples were used. Before conducting the phylogenetic analysis, we tested for recombination using the PHI test as implemented in the SplitsTree4 program [69] and no recombination events were detected (cutoff value: $P<0.05$). The data were mid-point-rooted and images were created using FigTree v1.3.1 [70].

Supporting Information

Figure S1 Position of the CRISPR/*cas* and exogenous elements loci in the chromosome. (A) The position of prophages, ICEs, and CRISPR/*cas* loci were shown. The position of prophages and ICEs were followed by Beres et al [28]. CRISPRs are indicated with diamond shapes, *cas* genes set with rectangles, prophages with triangles, and ICEs with circles. Stacked shapes indicate a common insertion site. Elements are color-coded to indicate the source strain. (B) Enlarged figure of the position of *cas* genes and terminal repeat-like sequence in MGAS315 and SSI-1 was shown.
(PDF)

Figure S2 *S. pyogenes* CRISPR locus overview. Nmeni *cas* subtype is characterized by the presence of 4 successive genes; *csn1*, *cas1*, *cas2*, and *csn2*. Dvulg *cas* subtype is characterized by 7 successive genes; *cas3*, *cas5*, *csd1*, *cds2*, *cas4*, *cas1*, and *cas2*. Repeat-spacer array are shown as white boxes. Same or homologous genes are represented by identical color boxes.
(PDF)

Figure S3 Graphic representation of spacers matched a known sequence. Repeats are not included. The spacers matched a known sequence are represented with colored box. The spacers does not match a known sequence are represented with white box. Names of prophage or bacterial chromosome gene sequences that are matched with the spacer were shown under the boxed (perfect identity: black character, >95% identity: colored character).
(PDF)

Figure S4 CRISPR and prophage distribution in all sequenced Streptococci. All 48 sequenced streptococci are listed. Possessing prophage is shown in blue, and CRISPR locus presence is shown in red. The number of prophage, CRISPR loci or repeats are shown.
(PDF)

Table S1 Repeat sequences of *S. pyogenes* CRISPR.
(PDF)

Table S2 Characteristics of CRISPR loci of Streptococci.
(PDF)

Author Contributions

Conceived and designed the experiments: FM KK IN. Performed the experiments: TN NF FM CA. Analyzed the data: TN NF FM TW. Wrote the paper: TN BH FM IN.

References

1. de la Cruz F, Davies J (2000) Horizontal gene transfer and the origin of species: lessons from bacteria. Trends Microbiol 8: 128–133.
2. Gogarten JP, Townsend JP (2005) Horizontal gene transfer, genome innovation and evolution. Nat Rev Microbiol 3: 679–687.
3. Ianeva OD (2009) Mechanisms of bacteria resistance to heavy metals. Mikrobiol Z 71: 54–65.
4. Dobrindt U, Chowdary MG, Krumbholz G, Hacker J (2010) Genome dynamics and its impact on evolution of *Escherichia coli*. Med Microbiol Immunol 199: 145–154.
5. Pal C, Papp B, Lercher MJ (2005) Adaptive evolution of bacterial metabolic networks by horizontal gene transfer. Nat Genet 37: 1372–1375.
6. Ochman H, Lawrence JG, Groisman EA (2000) Lateral gene transfer and the nature of bacterial innovation. Nature 405: 299–304.
7. Stephen Mcgrath DVS (2007) Bacteriophage: Genetics and Molecular Biology. Caister Academic Press. 343 p.
8. Canchaya C, Fournous G, Brussow H (2004) The impact of prophages on bacterial chromosomes. Mol Microbiol 53: 9–18.

9. Weinbauer MG (2004) Ecology of prokaryotic viruses. FEMS Microbiol Rev 28: 127–181.
10. Labrie SJ, Samson JE, Moineau S (2010) Bacteriophage resistance mechanisms. Nat Rev Microbiol 8: 317–327.
11. Barrangou R, Fremaux C, Deveau H, Richards M, Boyaval P, et al. (2007) CRISPR provides acquired resistance against viruses in prokaryotes. Science 315: 1709–1712.
12. Marraffini LA, Sontheimer EJ (2008) CRISPR interference limits horizontal gene transfer in staphylococci by targeting DNA. Science 322: 1843–1845.
13. Brouns SJ, Jore MM, Lundgren M, Westra ER, Slijkhuis RJ, et al. (2008) Small CRISPR RNAs guide antiviral defense in prokaryotes. Science 321: 960–964.
14. Sorek R, Kunin V, Hugenholtz P (2008) CRISPR-a widespread system that provides acquired resistance against phages in bacteria and archaea. Nat Rev Microbiol 6: 181–186.
15. Bolotin A, Quinquis B, Sorokin A, Ehrlich SD (2005) Clustered regularly interspaced short palindrome repeats (CRISPRs) have spacers of extrachromosomal origin. Microbiology 151: 2551–2561.
16. Godde JS, Bickerton A (2006) The repetitive DNA elements called CRISPRs and their associated genes: evidence of horizontal transfer among prokaryotes. J Mol Evol 62: 718–729.
17. Stern A, Keren L, Wurtzel O, Amitai G, Sorek R (2010) Self-targeting by CRISPR: gene regulation or autoimmunity? Trends Genet 26: 335–340.
18. Deveau H, Garneau JE, Moineau S (2010) CRISPR/Cas system and its role in phage-bacteria interactions. Annu Rev Microbiol 64: 475–493.
19. Horvath P, Barrangou R (2010) CRISPR/Cas, the immune system of bacteria and archaea. Science 327: 167–170.
20. Horvath P, Romero DA, Coute-Monvoisin AC, Richards M, Deveau H, et al. (2008) Diversity, activity, and evolution of CRISPR loci in *Streptococcus thermophilus*. J Bacteriol 190: 1401–1412.
21. Cunningham MW (2000) Pathogenesis of group A streptococcal infections. Clin Microbiol Rev 13: 470–511.
22. Tettelin H, Nelson KE, Paulsen IT, Eisen JA, Read TD, et al. (2001) Complete genome sequence of a virulent isolate of *Streptococcus pneumoniae*. Science 293: 498–506.
23. Glaser P, Rusniok C, Buchrieser C, Chevalier F, Frangeul L, et al. (2002) Genome sequence of *Streptococcus agalactiae*, a pathogen causing invasive neonatal disease. Mol Microbiol 45: 1499–1513.
24. Hiller NL, Ahmed A, Powell E, Martin DP, Eutsey R, et al. (2010) Generation of genic diversity among *Streptococcus pneumoniae* strains via horizontal gene transfer during a chronic polyclonal pediatric infection. PLoS Pathog 6: e1001108.
25. Xu P, Alves JM, Kitten T, Brown A, Chen Z, et al. (2007) Genome of the opportunistic pathogen *Streptococcus sanguinis*. J Bacteriol 189: 3166–3175.
26. Liu M, Siezen RJ, Nauta A (2009) In silico prediction of horizontal gene transfer events in *Lactobacillus bulgaricus* and *Streptococcus thermophilus* reveals protocooperation in yogurt manufacturing. Appl Environ Microbiol 75: 4120–4129.
27. Maruyama F, Kobata M, Kurokawa K, Nishida K, Sakurai A, et al. (2009) Comparative genomic analyses of *Streptococcus mutans* provide insights into chromosomal shuffling and species-specific content. BMC Genomics 10: 358.
28. Beres SB, Sylva GL, Barbian KD, Lei B, Hoff JS, et al. (2002) Genome sequence of a serotype M3 strain of group A Streptococcus: phage-encoded toxins, the high-virulence phenotype, and clone emergence. Proc Natl Acad Sci U S A 99: 10078–10083.
29. Beres SB, Musser JM (2007) Contribution of exogenous genetic elements to the group A Streptococcus metagenome. PLoS One 2: e800.
30. McShan WM, Ferretti JJ, Karasawa T, Suvorov AN, Lin S, et al. (2008) Genome sequence of a nephritogenic and highly transformable M49 strain of *Streptococcus pyogenes*. J Bacteriol 190: 7773–7785.
31. Fischetti VA (2007) In vivo acquisition of prophage in *Streptococcus pyogenes*. Trends Microbiol 15: 297–300.
32. Kunin V, Sorek R, Hugenholtz P (2007) Evolutionary conservation of sequence and secondary structures in CRISPR repeats. Genome Biol 8: R61.
33. Jansen R, van Embden JD, Gaastra W, Schouls LM (2002) Identification of a novel family of sequence repeats among prokaryotes. OMICS 6: 23–33.
34. Jansen R, Embden JD, Gaastra W, Schouls LM (2002) Identification of genes that are associated with DNA repeats in prokaryotes. Mol Microbiol 43: 1565–1575.
35. Hoe N, Nakashima K, Grigsby D, Pan X, Dou SJ, et al. (1999) Rapid molecular genetic subtyping of serotype M1 group A Streptococcus strains. Emerg Infect Dis 5: 254–263.
36. Haft DH, Selengut J, Mongodin EF, Nelson KE (2005) A guild of 45 CRISPR-associated (Cas) protein families and multiple CRISPR/Cas subtypes exist in prokaryotic genomes. PLoS Comput Biol 1: e60.
37. Kelli L, Palmer MSG (2010) Mulidrug-resistant Enterococci lack CRISPR-*cas*. mBio 1: e00227–00210.
38. Tang TH, Polacek N, Zywicki M, Huber H, Brugger K, et al. (2005) Identification of novel non-coding RNAs as potential antisense regulators in the archaeon *Sulfolobus solfataricus*. Mol Microbiol 55: 469–481.
39. Pourcel C, Salvignol G, Vergnaud G (2005) CRISPR elements in *Yersinia pestis* acquire new repeats by preferential uptake of bacteriophage DNA, and provide additional tools for evolutionary studies. Microbiology 151: 653–663.
40. Lillestol RK, Redder P, Garrett RA, Brugger K (2006) A putative viral defence mechanism in archaeal cells. Archaea 2: 59–72.
41. He J, Deem MW (2010) Heterogeneous diversity of spacers within CRISPR (clustered regularly interspaced short palindromic repeats). Phys Rev Lett 105: 128102.
42. van der Ploeg JR (2009) Analysis of CRISPR in *Streptococcus mutans* suggests frequent occurrence of acquired immunity against infection by M102-like bacteriophages. Microbiology 155: 1966–1976.
43. Touchon M, Rocha EP (2010) The small, slow and specialized CRISPR and anti-CRISPR of *Escherichia* and *Salmonella*. PLoS One 5: e11126.
44. van Embden JD, van Gorkom T, Kremer K, Jansen R, van Der Zeijst BA, et al. (2000) Genetic variation and evolutionary origin of the direct repeat locus of *Mycobacterium tuberculosis* complex bacteria. J Bacteriol 182: 2393–2401.
45. Makarova KS, Grishin NV, Shabalina SA, Wolf YI, Koonin EV (2006) A putative RNA-interference-based immune system in prokaryotes: computational analysis of the predicted enzymatic machinery, functional analogies with eukaryotic RNAi, and hypothetical mechanisms of action. Biol Direct 1: 7.
46. Deveau H, Barrangou R, Garneau JE, Labonte J, Fremaux C, et al. (2008) Phage response to CRISPR-encoded resistance in *Streptococcus thermophilus*. J Bacteriol 190: 1390–1400.
47. Davies MR, McMillan DJ, Van Domselaar GH, Jones MK, Sriprakash KS (2007) Phage 3396 from a *Streptococcus dysgalactiae* subsp. equisimilis pathovar may have its origins in *Streptococcus pyogenes*. J Bacteriol 189: 2646–2652.
48. Nakagawa I, Kurokawa K, Yamashita A, Nakata M, Tomiyasu Y, et al. (2003) Genome sequence of an M3 strain of *Streptococcus pyogenes* reveals a large-scale genomic rearrangement in invasive strains and new insights into phage evolution. Genome Res 13: 1042–1055.
49. Liu GR, Rahn A, Liu WQ, Sanderson KE, Johnston RN, et al. (2002) The evolving genome of *Salmonella enterica* serovar Pullorum. J Bacteriol 184: 2626–2633.
50. Wiedenheft B, Zhou K, Jinek M, Coyle SM, Ma W, et al. (2009) Structural basis for DNase activity of a conserved protein implicated in CRISPR-mediated genome defense. Structure 17: 904–912.
51. Aranaz A, Romero B, Montero N, Alvarez J, Bezos J, et al. (2004) Spoligotyping profile change caused by deletion of a direct variable repeat in a *Mycobacterium tuberculosis* isogenic laboratory strain. J Clin Microbiol 42: 5388–5391.
52. Tyson GW, Banfield JF (2008) Rapidly evolving CRISPRs implicated in acquired resistance of microorganisms to viruses. Environ Microbiol 10: 200–207.
53. Westra ER, Pul U, Heidrich N, Jore MM, Lundgren M, et al. (2010) H-NS-mediated repression of CRISPR-based immunity in *Escherichia coli* K12 can be relieved by the transcription activator LeuO. Mol Microbiol.
54. Zegans ME, Wagner JC, Cady KC, Murphy DM, Hammond JH, et al. (2009) Interaction between bacteriophage DMS3 and host CRISPR region inhibits group behaviors of *Pseudomonas aeruginosa*. J Bacteriol 191: 210–219.
55. Papenfort K, Vogel J (2010) Regulatory RNA in bacterial pathogens. Cell Host Microbe 8: 116–127.
56. Aklujkar M, Lovley DR (2010) Interference with histidyl-tRNA synthetase by a CRISPR spacer sequence as a factor in the evolution of *Pelobacter carbinolicus*. BMC Evol Biol 10: 230.
57. Deaconescu AM, Savery N, Darst SA (2007) The bacterial transcription repair coupling factor. Curr Opin Struct Biol 17: 96–102.
58. Sebaihia M, Wren BW, Mullany P, Fairweather NF, Minton N, et al. (2006) The multidrug-resistant human pathogen *Clostridium difficile* has a highly mobile, mosaic genome. Nat Genet 38: 779–786.
59. Lima-Mendez G, Van Helden J, Toussaint A, Leplae R (2008) Prophinder: a computational tool for prophage prediction in prokaryotic genomes. Bioinformatics 24: 863–865.
60. Grissa I, Vergnaud G, Pourcel C (2007) CRISPRFinder: a web tool to identify clustered regularly interspaced short palindromic repeats. Nucleic Acids Res 35: W52–57.
61. Altschul SF, Gish W, Miller W, Myers EW, Lipman DJ (1990) Basic local alignment search tool. J Mol Biol 215: 403–410.
62. Thompson JD, Higgins DG, Gibson TJ (1994) CLUSTAL W: improving the sensitivity of progressive multiple sequence alignment through sequence weighting, position-specific gap penalties and weight matrix choice. Nucleic Acids Res 22: 4673–4680.
63. Aanensen DM, Spratt BG (2005) The multilocus sequence typing network: mlst.net. Nucleic Acids Res 33: W728–733.
64. Tamura K, Dudley J, Nei M, Kumar S (2007) MEGA4: Molecular Evolutionary Genetics Analysis (MEGA) software version 4.0. Mol Biol Evol 24: 1596–1599.
65. Saitou N, Nei M (1987) The neighbor-joining method: a new method for reconstructing phylogenetic trees. Mol Biol Evol 4: 406–425.
66. Stewart CB (1993) The powers and pitfalls of parsimony. Nature 361: 603–607.
67. Posada D (2008) jModelTest: phylogenetic model averaging. Mol Biol Evol 25: 1253–1256.
68. Shearer AC, Johnson MS (1993) Confidence limits on the branching order of phylogenetic trees. Protein Sci 2: 1686–1696.
69. Huson DH, Bryant D (2006) Application of phylogenetic networks in evolutionary studies. Mol Biol Evol 23: 254–267.
70. Rambaut A (2010) FigTree v1.3.1. Institute of Evolutionary Biology, University of Edinburgh.

東京医科歯科大学

歯と骨の分子疾患科学 国際教育研究拠点

～デント・メドミクスのインテリジェンスハブ～

平成23年度 実績報告書